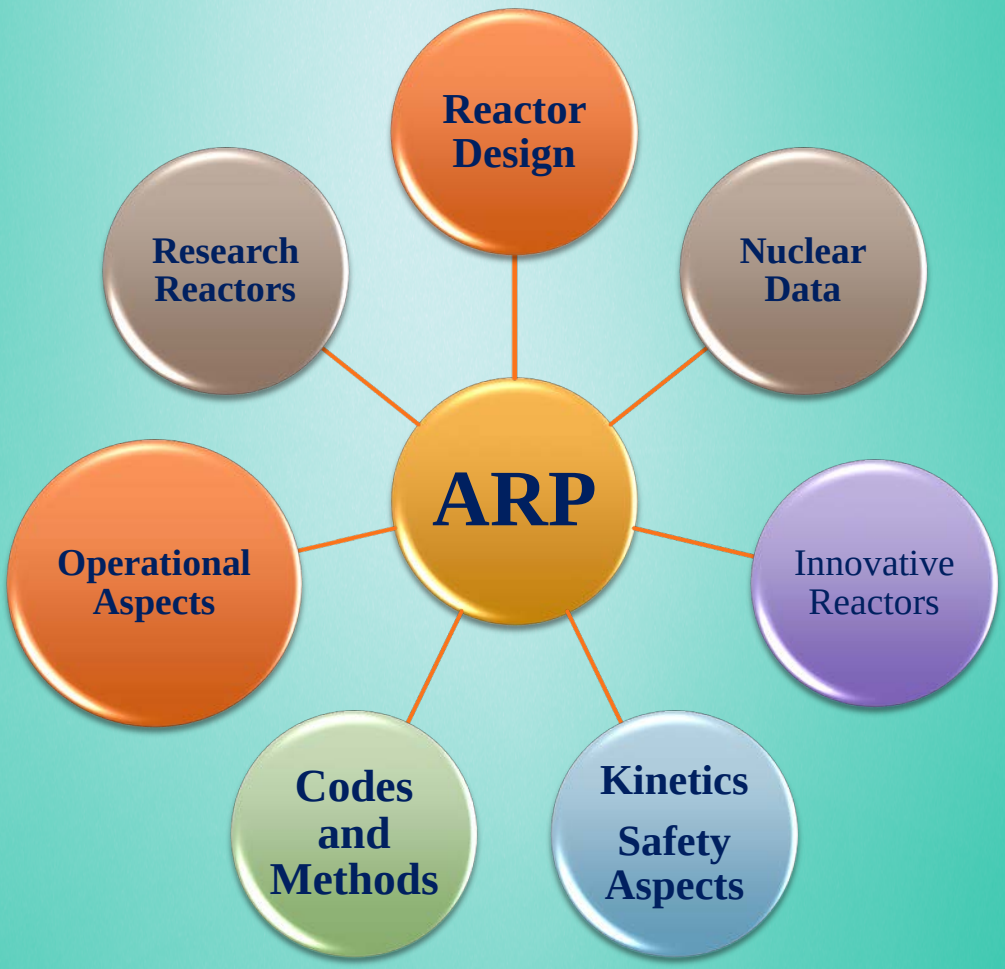
Proceedings of Advances in Reactor Physics 2022

18 – 21 May 2022



Click on Button to Navigate

Table of Contents

S. No:	Abstract No.	Contributed Papers	Paper No.
Invited Talks			
1	**IT-01**	**Physics of next generation reactors –Towards self-reliance in design, safety and operation** *Umasankari kannan*	15
2	**IT-02**	**Gaining a Mechanistic Understanding of Nuclear Fuel Material Performance by Combining Modelling and Experiment** *Simon Middleburgh*	16
3	**IT-03**	**Creating DRAGON5 Cross Section Databases for Neutronics-Thermal Hydraulics Coupled Canadian SCWR Simulations** *G. Marleau, U. Le Tennier*	16
4	**IT-04**	**High-Fidelity Reactor Core Physics Simulations for Identification of Irradiated Fuel Characteristics** *Sunil S. Chirayath*	17
5	**IT-05**	**Physics Design Studies of 500 MWe FBR1&2 Core** *K. Devan*	21
6	**IT-06**	**Model-Order Reduction of Neutronic Systems via POD-Galerkin Projection** *Jeremy Roberts*	21
7	**IT-07**	**Advances in Physics Design of Indian PHWRs** *M.P.S. Fernando*	22
Session A: Reactor Design and Analysis			
8	**AO-01**	**LHGR Estimation for IPWR Equilibrium Core using Pin-By-Pin Code HEXPIN** *Suhail Ahmad Khan and Umasankari Kannan*	23
9	**AO-02**	**Use of Artificial Neural Networks for AHWR Refueling Strategy** *Amit Thakur, Debasmit Sarkar, Vishal Bharti and Umasankari Kannan*	27
10	**AO-03**	**Development of a New Code MSDYN for Safety Analysis of Molten Salt Reactors (MSRS)** *Indrajeet Singh, Anurag Gupta and Umashankari Kannan*	31
11	**AO-04**	**Burnup Simulation Results from Upgraded McBurn and Comparison with Other Codes**	35

		Debasmit Sarkar, K. K. Gupta and K. P. Singh	
12	**AO-05**	**Analysis of AER MIDI CORE VVER-1000 Core Periphery Power Distribution Benchmark** *L. Thilagam, K. Obaidurrahman, and D. K. Mohapatra*	39
13	**AP-01**	**Estimation of Na-24 Activity for an Open Pool Type Research Reactor** *M. Hansda, A. Sharma and S. Sengupta*	43
14	**AP-02**	**Transient Analysis of VVER-1000 X2 benchmark with ARCH code** *Argala Srivastava, D.K. Dwivedi and Umasankari Kannan*	47
15	**AP-03**	**Methods & Techniques Developed in Code ARCH for 3D Core Transients of Pressurized Heavy Water Reactors** *Taresh Aggarwal, D.K. Dwivedi, Anurag Gupta, Umasankari K*	51
16	**AP-04**	**Estimate of Spatial Influence of Neutron Flux Monitoring with SPNDs in AHWR** *Anupreethi B., Umasankari Kannan and Anurag Gupta*	55
17	**AP-05**	**A Design Study for 500 MWe IPWR** *Suhail Ahmad Khan and Umasankari Kannan*	59
18	**AP-06**	**Analysis of VVER Lattice Benchmark Using DP1 Model of VISWAM** *Suhail Ahmad Khan and Umasankari Kannan*	63
19	**AP-07**	**Analysis of VVER-1000 Pin Cell Benchmarks using ν-TRAC with ENDF/B-VIII.0 Library** *Anmol Singh, Usha Pal, V. Harikrishnan and R. Karthikeyan*	67
20	**AP-08**	**A model for Quasi-Static Perturbation Analysis of 540MW (e) PHWR** *A. Alok Jha, B. S.Samanta*	71
21	**AP-09**	**Neutronic Investigation of Burnable Poison Materials for Long Life Reactor Cores** *Usha Pal, R. Karthikeyan and Ravindra Babu*	77
22	**AP-10**	**Effect of Temperature on Neutronic Behaviour of PHWR** *Khaidem Charanjit Singh, Manisha Misra, Shailesh Mahawar and Rajib Maji*	81
23	**AP-11**	**A Parametric Study of Multiplication Factor and Reactivity Coefficients in Light Water Spectrum** *Suhail Ahmad Khan and Umasankari Kannan*	85
24	**AP-12**	**Re-optimization of Worth of RRS in AHWR to Improve Core Power Distribution**	89

		Vishal Bharti, Baltej Singh &Umasankari Kannan	
25	**AP-13**	**Analysis of First Approach to Criticality (FAC) and Low Power PHASE-B Experiments of KAPP-3 using DRAGON and DONJON Code System** *L. Thilagam and D. K. Mohapatra*	93
26	**M-01**	**Estimation of Thermophysical Properties of Thorium Based MOX Fuel Using Classical Molecular Dynamics Simulation** *Arindam Chakraborty, Chandra Bhanu Basak and Umasakari Kannan*	97
Session B: Nuclear Data and Uncertainty			
27	**BO-01**	**Studies on the Variation of Reactor Kinetic Parameters with Latest ENDF-6 Nuclear Data Libraries** *Arun Stanley, Puspendu Hazra, T. Sathiyasheela, K. Devan*	101
28	**BO-02**	**Development of a New Neutron Multi-Group Cross Section Set in ABBN Format from the Latest ENDF-6 Files for Fast Reactors** *Puspendu Hazra, A. Riyas, K. Devan*	105
29	**BO-03**	**Quantification of Nuclear Data Contribution to Uncertainty in Fuel SA Decay Power** *G. Pandikumar and A. John Arul*	109
30	**BP-01**	**Estimation of Uncertainty in The Control Rod Worth in CANDU PHWR** *M. Mohideen Abdul Razak*	113
31	**BP-02**	**Dynamic Uncertainty Analysis in the Power Transient of CANDU PHWR** *M. Mohideen Abdul Razak*	116
32	**BP-03**	**Lattice Level Sensitivity Analysis of Indian PHWR** *Ishi Jain, Manish Raj, Sherly Ray and M.P.S. Fernando*	121
33	**BP-04**	**Nuclear Data Sensitivity of VVER-1000 Pin-Cell Benchmark** *V. Harikrishnan, Anek Kumar and Usha Pal*	125
34	**BP-05**	**Analysis of Doppler reactivity (Mosteller) benchmarks using ENDFB8GX library** *V. Harikrishnan, R. Karthikeyan and Usha Pal*	129
35	**BP-06**	**Stochastic Interpolation of Nuclides to Represent Doppler Broadened Data in Reactor Physics Calculation** *Rashbihari Rudra, Rashmi Rai, K. P. Singh and Umasankari Kannan*	133

36	**BP-07**	**Uncertainty and Sensitivity Analysis of Neutron Multiplication Factor in Candu Reactor** *M. Mohideen Abdul Razak, P. Ravindra Babu*	137
Session C: Innovative and Fast Reactor Physics			
37	**CO-01**	**Physics Design Optimization of Liquid Hydrogen based Cold Neutron Source in HFRR** *Dipankar Pal, Archana Sharma and Samiran Sengupta*	141
38.	**CO-02**	**Oxidation Resistant Iron Based Alloy as clad Material in LWRs** *Krishna Kumar Yadav, Usha Pal and R. Karthikeyan*	145
39.	**CO-03**	**Performance Analysis of various Tritium Breeding Solids in Fusion Reactor Blanket** *Aditi Ray*	149
40.	**CO-04**	**Reaction Rate Spectral Profiling for PFBR BOL Core Configuration Employing Mesh Tallywith Pin Level Heterogeneity** *Bilal Hassan Khan*	153
41.	**CO-05**	**Studies on Core Characteristics of the Proposed 40MWt FBTR Core** *Neethu Hanna Stephen, Rajesh Chandrakanth, Raghukumar.G, Manimaran.N, Shanmugam.G & Suresh Kumar. K. V*	157
42.	**CO-06**	**Development of a Power and Flow Transient Model for Sodium Cooled Fast Reactor Core** *Amandeep Singh, Obaidurrahman K. and H. P. Gupta*	162
43.	**CP-01**	**Development of a Coolant Dynamic Model for Sodium Cooled Fast Reactor Core** *Amandeep Singh, Obaidurrahman K and H. P. Gupta*	166
44.	**CP-02**	**Development of Monte Carlo Model of Tarapur Boiling Water Reactor to Estimate Number of Sb-Be Neutron Sources** *Indrajeet singh, Rashmi Rai, Pradeep Baraila, Arun Kumar Singh, Anurag Gupta, K.P. Singh and Umashankari Kannan*	170
45.	**CP-03**	**Shield Optimization for Offset Handling Machine of Future Fast Breeder Reactors** *Anupam Chakraborty, Anu Krishnan, D. Sunil Kumar, A. John Arul*	174
46.	**CP-04**	**Machine Learning Assisted k-infinity Prediction for Analysis of Molten Salt Reactor** *A. K. Srivastava, Anurag Gupta, Umasankari Kannan*	179

47.	**CP-05**	**Integration of DRAGON and ARCH with SARRA for Analysing the Neutronics Aspect of Refuelling and Reprocessing in MSR** *A. K. Srivastava, Anurag Gupta, Umasankari Kannan*	183
48.	**CP-06**	**Response Matrix of an Extended Bonner Sphere System using MCNP5** *Subhrojit Bagchi, A. John Arul*	187
49.	**CP-07**	**Tritium Production from Lithium under Irradiation of Molten Salt Fuel in a Nuclear Reactor** *Taresh Aggarwal, Indrajeet Singh, Anurag Gupta, Umasankari K*	191
50.	**CP-08**	**Isotopic Fission Rate and Power Distribution for PFBR BOL Core Employing Monte Carlo Transport** *Bilal Hassan Khan*	195
51.	**CP-09**	**Estimation of Shield Requirement for X-Ray Radiography Facility in FRFCF** *M. M. Shanthi, B. Sivakumar, D. Sunil Kumar, A. John Arul, G. Sivasankaran and S. Raghupathy*	199
52.	**CP-10**	**Development of Inverse Kinetics Module to Evaluate Control Rod Worths and Source Term Estimation** *Mainak Mallick, T. Sathiyasheela*	203
53.	**CP-11**	**Investigation of Homogenous Vs Heterogeneous Modelling Effects for OECD/NEA MOX-3600 Pin Cell, Fuel Assembly and Core Variants** *L. Thilagam and D. K. Mohapatra*	207
54.	**CP-12**	**Benchmark Analysis of Ebr-II Shutdown Heat Removal Tests** *S.S. Singh, R. Karthik and D.K. Mohapatra*	211
55.	**CP-13**	**Development of Initial Core Loading for 900 MW (e) IPWR** *Devesh Raj, Umasankari Kannan*	215
56.	**CP-14**	**Optimization Study of AHWR Equilibrium Core After Prolonged EMCCR** *Sandeep Singh, Arindam Chakraborty, Amit Thakur and Umasankari Kannan*	219
57.	**M-02**	**Optimization of Local Shield for IHX of FBR 1 & 2** *Rajeev Ranjan Prasad, D Sunil Kumar and A John Arul*	223
58.	**M-03**	**Concept of increasing core size with poison sub-assemblies and transition from 32 MWt core to 40 MWt core** *G. Raghu Kumar and E. Radha*	229

Session D: Reactor Safety and Regulatory aspects			
59.	**DO-01**	**Bifurcation Analysis of Large Pressurized Heavy Water Reactors** *Abhishek Chakraborty and M. P. S. Fernando*	232
60.	**DO-02**	**Nonlinear Stability Analysis of Boiling Water Reactor by Lyapunov Exponents** *S. S. Singh*	236
61.	**DO-03**	**Insights from Reactor Physics Design Review of IPHWR-700** *Susheel Kumar, Amandeep Singh, Soumen Koner, Obaidurrahman K. and Utkarsh S.C.*	240
62.	**DO-04**	**Loss of Regulation Scenario in AHWR Orificed Core** *A. Srivastava, A. D. Contractor and Rajesh Kumar*	244
63.	**DP-01**	**LORA Analysis of AHWR Equilibrium Core using Modal Kinetics Method** *Arindam Chakraborty, Debasmit Sarkar, Baltej Singh and Umasankari Kannan*	248
64.	**DP-02**	**Linear Stability Analysis of IPWR (900 MWe) Equilibrium Core** *Gopal Mapdar, Umasankari Kannan*	252
65.	**DP-03**	**Preliminary LORA Analysis for IPWR Equilibrium Core** *Gopal Mapdar, D K Dwivedi, U Kannan*	256
66.	**DP-04**	**Significance of Reactivity Induced Events at MCL for VVER-1000 Reactors Safety Analysis** *S. K. Shukla, Sanuj Chaudhary, P. Krishna Kumarand Y.K. Pandey*	260
67.	**DP-05**	**Stability Analysis of a Large PHWR** *Rakesh Kumar, Obaidurrahman K., Suneet Singh*	264
68.	**DP-06**	**Worth Computation of GEM Assembly in FFTF Core** *Abhitab Bachchan, Puspendu Hazra A. Riyas and K. Devan*	269
69.	**DP-07**	**Clad Relocation Dynamics for LMFBR ULOFA Analysis** *Anuraj V L, T. Sathiyasheela and K. Devan*	273
70.	**DP-08**	**Stability analysis of AHWR** *Amit Thakur and Umasankari Kannan*	277
71.	**DP-09**	**Study of ATWS Scenario with Passive Systems for VVER-1000 Reactors**	281

		Anirban Biswangri, Manish Mehta, P Krishna Kumar and Y K Pandey	
72.	**DP-10**	**Estimation of Critical Channel Powers in 700 MWe IPHWR for Independent Assessment of ROPS Design** *Vivek A. Kale and Obaidurrahman K.*	285
Session E: Reactor Kinetics and Multi-physics			
73.	**EO-01**	**Incorporation of Kinetic Module in WIMS** *Anindita Sarkar, Umasankari Kannan*	289
74.	**EO-02**	**Analysis of Unprotected Transients of Interruptions in Heat Removal in IMSR-5MW with Code PATH** *D.K. Dwivedi, Anurag Gupta and Umasankari K.*	293
75.	**EO-03**	**Space Time Monte Carlo Code KINMC for simulating Reactor Transients** *Argala Srivastava and K. P. Singh*	297
76.	**EP-01**	**Implementing Weighted Delta Tracking Method in Dynamic Monte Carlo Code KINMC** *Argala Srivastava, K. P. Singh and Umasankari Kannan*	301
77.	**EP-02**	**3D Multi-Physics analysis of Hot Start up Transients of Natural Circulation Cooled CHTR** *D.K. Dwivedi, Anurag Gupta and Umasankari K.*	305
78.	**EP-03**	**Exponential–Time Differencing Method for Solving Reactor Point Kinetics Equations with Temperature and Power Feedback and Its Validation by Analysing Thermal Reactor Benchmarks** *P. Ravindra Babu, Usha Pal, R.N. Sen and R. Karthikeyan*	309
79.	**EP-04**	**Extending the Capability of the Code "KINFIN" for Simulating Hexagonal Cores** *Debasmit Sarkar, Argala Srivastava and K .P. Singh*	314
80.	**EP-05**	**Stochastic Formulation of Reactor Kinetics-A Brief Survey** *Amritha Krishnan S, Anurag Gupta and Rajarshi Das*	318
81.	**EP-06**	**Physics & Thermal-Hydraulic Calculations for Core Power & Critical Power Ratio Estimation for Orificed AHWR Initial Core** *Vishal Bharti, D.K. Chandraker, Amit Thakur & Mukesh Kumar*	322
82.	**EP-07**	**Approach for Coupling of KKNPP System Thermal Hydraulics Computer code ATMIKA-LWR with 3D Kinetics Code** *Vivek Singla, Paresh Patra, Sanjay Singh, Hemant Kalra, Y.K. Pandey*	326

83.	**EP-08**	**A Condensed Overview of AERB Benchmark on Coupled Code Systems (ABCS)** *Obaidurrahman K., Santosh Kumar Pradhan*	331
84.	**EP-09**	**Development and Validation of Multi-Physics Capability in Code ARCH-TH for 3d Core Transients of Water Cooled Reactors** *D.K. Dwivedi, Anurag Gupta and Umasankari K.*	335
Session F: Reactor Codes and Methods			
85.	**FO-01**	**Brief Description of Lattice code 'ν-TRAC' and its validation for Square and Hexagonal lattices** *Anmol Singh, Usha Pal, R. Karthikeyan, and Amod Kishore Mallick*	339
86.	**FO-02**	**Development of Monte Carlo -Reaction Rates (Tally) Based Burnup Code and Its Validation through LWR Benchmark Exercises** *P RavindraBabu, Usha Pal, and R N Sen and R. Karthikeyan*	343
87.	**FO-03**	**Use of Bond Energy Clustering Algorithm for Optimisation of In-Core Detector locations in AHWR** *B. Anupreethi, Anurag Gupta, Umasankari Kannan and AkhilanandPati Tiwari*	347
88.	**FO-04**	**A Finite Volume Method based Multi Group Neutron Diffusion Model for Criticality Problems in 2D R-Z Geometry** *R. Kondala Rao, P. Mangarjuna Rao, K. Natesan and S. Raghupathy*	351
89.	**FO-05**	**Stability Analysis for Multi-group k-eigenvalue Iterations with Linear Prolongation CMFD Acceleration** *Lakshay Jain, P. Mohanakrishnan, R. Karthikeyan and Umasankari Kannan*	355
90.	**FO-06**	**Introduction of Hexagonal Lattice Core Analysis in NDIFF3D** *Arindam Chakraborty, Debasmit Sarkar, K P Singh and Umasankari Kannan*	359
91.	**FO-07**	**STEMPWR - A Neutron Transport Theory Code for PWR Type Geometries** *Kapil Deo*	363
92.	**FO-08**	**Solving Neutron Diffusion Equation using Machine Learning** *Saivirinchi P, Lakshay Jain and Kondayya Gundra*	367
93.	**FP-01**	**Implementation of a Model for Estimating Gaseous Fission Product Release from Fuel**	371

		G. Pandikumar and A. John Arul	
94.	**FP-02**	**New Empirical Formula for Evaluating Gamma Build-up Factor in Double-Layer Shield44 and its validation with FLUKA Code** *Avijit Das, Aditi Ray, Tej Singh*	376
95.	**FP-03**	**Extension of Pomraning's Simplified Spherical Harmonics Model to General N and Finite Medium** *Abhishek Mishra, Aditi Ray and Tej Singh*	380
96.	**FP-04**	**Analysis of KUCA-Atype Core using Deterministic Codes** *K.P.Singh and A.K. Singh*	384
97.	**FP-05**	**Development of Monte Carlo Code for the Assessment of Criticality of Fissile Systems** *Sachin Shet and K.V. Subbaiah*	388
98.	**FP-06**	**A Multi group Space Time Kinetics Code in 2d Rectangular and Cylindrical Geometries with Doppler Feedback** *Arun Stanley, T. Sathiyasheela*	392
99.	**FP-07**	**Nodal Integral Method for Solution of Time Dependent Neutron Diffusion Equation** *Manish Raj, Sherly Ray, M.P.S. Fernando and Suneet Singh*	396
100.	**FP-08**	**Development of Lattice and Core Models for PHWR in VISWAM Code System** *V. Jagannathan, S.Koner and Obaidurrahman K.*	401
101.	**FP-09**	**Development of Spiral Pin by Pin Finite Difference Model for Hexagonal Lattice Core** *V. Jagannathan*	405
102.	**FP-10**	**Monte Carlo Scheme for Computation of Dancoff Factor** *Amod Kishore Mallick, Argala Srivastava and Umasankari Kannan*	409
103.	**FP-11**	**Development of PATMOC – An Indigenous General-Geometry Multi-group Monte Carlo Code for Full Core Neutron Transport Simulations** *Amod Kishore Mallick, Anurag Gupta, Indrajeet Singh and Umasankari Kannan*	413
104.	**FP-12**	**Treatment of Convergence Instability in MOC Iterations with Large Negative Self-Scattering Cross Sections in DIAMOND** *Lakshay Jain, R. Karthikeyan and Umasankari Kannan*	417

105.	**FP-13**	**A Multigroup Neutron Diffusion Model for Space-Time Reactor Kinetics Problems in 2D Cartesian Geometry** *R. Kondala Rao, P. Mangarjuna Rao, K. Natesan and S. Raghupathy*	421
106.	**FP-14**	**Development of a Core Model for Real Time Flux Distribution Monitoring in PWR** *Mihir Naskar, Gopal Mapdar, S. K. Sen, Anurag Gupta, Umashankari Kannan*	425
107.	**FP-15**	**Development of MLIB - A 'Plug n Play' Module for Processing of WIMS-D Nuclear Data Library for Reactor Physics Simulations** *Amod Kishore Mallick, Lakshay Jain, Umasankari Kannan and R. Karthikeyan*	429
Session G: Research Reactors and Experimental Reactor Physics			
108.	**GO-01**	**Production of Ru-105 and Rh-105 through Proton Induced Reaction on Natural Uranium** *Najumunnisa T, M. M. Musthafa, C. V. Midhun, Alok Saxena, P. Surendran, J. P. Nair and Anil Shanbhag*	433
109.	**GO-02**	**Analysis of First Approach to Criticality (FAC) and Phase-B Experiments of KAPP-3 using VISWAM Code** *S.Koner, V. Jagannathan and Obaidurrahman K.*	437
110.	**GO-03**	**Noise Experiment in BRAHMMA Subcritical System using Accelerator based Neutron Source** *N K Ray, T Patel and P S Sarkar*	441
111.	**GO-04**	**Xenon Spatial Oscillation Experiments InKakrapar Atomic Power Project-3** *Amritha Krishnan S, Abhishek Chakraborthy, Rajarshi Das, M.P.S Fernando*	445
112.	**GO-05**	**Measurement of Critical Height with (Th-Pu) MOX Experimental cluster of different Enrichments in AHWR-CF Extended Core** *Sudipta Samanta, Amod Kishor Mallick, Deep Bhandari, Kapil Deo, Rajeev Kumar, Neelima Prasad and Umasankari Kannan*	449
113.	**GO-06**	**Irradiation of Thorium in PHWR Spectrum using In-House Code ADWITA** *Devesh Raj, Umasankari Kannan*	453
114.	**GO-07**	**Critical Calibration of Reactivity Devices in KAPP-3** *Rimpi, Himanshu Mishra, Satyendra Kr. Gautam and Rajarshi Das*	457

115.	**GP-01**	**Simulation of the Integral Experiments of AHWR Critical Facility with Diffusion based Monte Carlo Method** *Argala Srivastava, Deep Bhandari, K. P. Singh and Umasankari Kannan*	461
116.	**GP-02**	**Study of Variance in the Counting Statistics of Radiation Detectors** D.V.Subramanian, Adish Haridas and A.John Arul	465
117.	**GP-03**	**Performance Testing of New Modified Criticality Accident Dosimeter Badge Using AHWR Critical Facility** Deepa Sathian, A.K. Bakshi, Umasankari Kannan, B.K. Sapra	469
118.	**GP-04**	**A Study of Alpha-Induced Pre-Equilibrium Neutron Emission in Natural Titanium** Gokul Das H, MM Musthafa, Midhun C V, Swapna B, Vafiya T, Najmunnisa T, F S Shana, Rijin N T, S Dasgupta, J Datta, S Ganesan, S V Suryanarayana	473
119.	**GP-05**	**Design of a Short Beam Tube for Neutron TOF Facility based on 30MeV Electron Accelerator** Kapil Deo and Umasankari Kannan	477
120.	**GP-06**	**Monte Carlo Characterization of Neutron Spectrum at Irradiation Locations of APSARA-U Reactor** Amod Kishore Mallick, Rajeev Kumar and Umasankari Kannan	481
121.	**GP-07**	**Measurement of Neutron Flux Profile at Apsara-U for the Study of Neutron Transmutation Doping in Silicon** Amod Kishore Mallick, Rajeev Kumar, Sudipta Samanta, Deep Bhandari, Kapil Deo, Umasankari Kannan, Tej Sigh, Sajin Prasad S. and Ranjit Sharma	485
122.	**GP-08**	**Monte Carlo Characterization of Neutron Spectrum at Ion-Chamber Irradiation Locations of AHWR Critical Facility** Amod Kishore Mallick, Sudipta Samanta, Rajeev Kumar and Umasankari Kannan	489
123.	**GP-09**	**Analysis of the Extended Core of AHWR-CF with one Experimental Cluster by WIMS-ARCH code** Deep Bhandari, Amod Kishore Mallick, Sudipta Samanta, Rajeev kumar and Umasankari Kannan	493
124.	**GP-10**	**Validation of Multi-Group Diffusion Code NEM3D**	497

		Sandeep Singh, Arindam Chakraborty, Amit Thakur and Umasankari Kannan	
125.	**GP-11**	**Conceptual Design of Delayed Neutron Precursors (DNP) Flow Experiment in Apsara-U for MSR Program** Indrajeet Singh, Amod Kishore Mallick, Anurag Gupta and Umasankari Kannan	501
126.	**GP-12**	**Theoretical Calculation of Excitation Function of Proton Induced Reaction and Evaluation of Recommended data by TALYS – 1.95 and Empire – 3.2.2 Code** Sourav Mondal and Rebecca Lallunthluangi	505
Session H: Operational Reactor Physics			
127.	**HO-01**	**Neutron Monitoring of Kakrapar Atomic Power Project-3 Core during Extended Shutdown** Himanshu Mishra, Gaurav Agrawal and R. Das	509
128.	**HO-02**	**Supply of Co-60 from PHWR to meet the increasing demand for societal benefits in India** Surendra Mishra and Baltej Singh	513
129.	**HO-03**	**Flux Profile Measurements through Traveling In-Core Probe (Tip) Scan and LPFL Readings for various Reactivity Device Configurations** Surabhi, Amritha Krishnan S, Rajarshi Das, P. B. Kamble and Manojkumar Sonawani	517
130.	**HO-04**	**Estimation of Dynamic Characteristic of Inconel Detectors in KAPP-3** Suresh Kandpal, Rajarshi Das, M. P. S. Fernando	521
131.	**HP-01**	**Modified Slope Method Analysis of Delayed Neutron Data for Early Fuel Failure Identification** A. Chiranjit Ghosh, B. Alok Kumar Jha and C. Samiran Samanta	525
132.	**HP-02**	**Improvement in Fuel Follow-up Scheme using Online In-Core Vanadium Detector Readings of Flux Mapping System** Abhishek Chakraborty, Amritha Krishnan S, Rajarshi Das2, M. P. S. Fernando	529
133.	**HP-03**	**Fuel Management Techniques Adopted at RAPS-3&4** G. C. Chauthwani, Sumitra Kumari, L K Gupta	533
134.	**HP-04**	**Fuel Conservation during Pre-Equilibrium Core Operation of PHWR** Ravi Kumar Bansal, Amit Thakur,MPS Fernando	537

135.	**HP-05**	**Study of ATWS Mitigation for Cool Down and Heat Up Events for VVER-1000 Reactors** Manish Mehta, Anirban Biswangri, P Krishna Kumar and Y.K. Pandey	541
136.	**HP-06**	**Reactor Safety Analysis of Reactivity Excursion Event of Wrong Start-Up of Inactive Reactor Coolant Pump for VVER-1000 Reactors** Sanuj Chaudhary, S. K. Shukla, P. Krishna Kumar and Y.K. Pandey	545
137.	**HP-07**	**Operational Aspects of Loading of Cobalt-Natural Uranium (Co-NU) Bundle in KGS-3 Reactor** Hardeep Singh, Hari Ram, S. K. Subramanya and Ashok Bhatia	549
138.	**HP-08**	**Bulk Addition of Moderator and First Approach to Criticality (FAC) of Kakrapar Atomic Power Project-3** Himanshu Mishra, Rimpi, R. Das and Shankar Venkataramani	553
139.	**HP-09**	**Operating Experience of Single Channel Pulse Amplifier (Scpa) with Fission Counters in Kaps-1** G.Rajarao, R.Goutam, R.Padhy, R.Das and M.K.Sonavani	557
140.	**HP-10**	**Comparison of Theoretically Estimated Thermal Neutron Flux Profile with TIP Generated Profile during Phase-B of KAPP-3** Gaurav Agarwal and Sherly Ray	561
141.	**HP-11**	**Startup source calculation for Tarapur BWR using Monte-Carlo Methods** Pradeep Baraila, Rashmi Rai, A.K. Singh, K.P. Singh	565
142.	**M-04**	**Composite LOG-LINEAR Amplifier for Full Power Range Operation of Nuclear Reactors** A. Shivam Tripathi, B. DM Nikhare, C. SP Borkar and D. Sadhana Bhattacharya Xenon	569
143.	**M-05**	**Poison Measurements In APSARA-U Intermediate Core** Shantanab Banerjee, Paritosh Pandey and Tej Singh	574

Invited talk

Physics of next generation reactors –Towards self-reliance in design, safety and operation

Umasankari kannan
Bhabha Atomic Research Centre, Mumbai, India
e-mail –uma_k@barc.gov.in

Abstract

Nuclear energy will have to be the mainstay in today's green economy scenario and sustainability. There will have to be a mix of different innovative and revolutionary reactors as well as enhanced efficiency of current day reactor systems. Reactor physics will have to play a major role in design of these new energy systems which will have to cater to diverse needs. BARC has been engaged in the development of thorium fuel based Advanced Heavy Water Reactor (AHWR), enriched uranium based light water reactor (IPWR) and several newer reactor concepts such as High Temperature Reactor (HTR) and Molten Salt Reactor (MSR). The physics design of each one these are complex and require a radical approach. This talk will summarise the latest developments in the design of these thermal reactors and the neutronic codes and methods developed for their analysis.

There are several challenges right from basic nuclear reaction cross section data for advanced fuel and materials, optimisation for longer life cores, simulation for multi-physics and multi-scale phenomena, and detailed experimentation. The designs are being taken to a higher level of safety. While the reactor designs on the one hand are evolving, the solution strategies have also progressed from simple deterministic simulations to more precise probabilistic methods. The optimisation of the physics design of AHWR for deriving power from thorium, U-233 breeding and design of the fuel cluster for enhanced thermal margins, were some of the major challenges in the past few years. Experimentation for qualifying the fuel and safety parameters was another important activity taken up recently. Reactor physics experiments were performed with several thoria based fuel clusters in the zero enrgy AHWR Critical Facility which were used for extensive validation exercise. Another example of challenge in the design of Molten Salt reactors is the treatment of moving liquid dynamics and its impact on kinetics. Fuel inventory optimisation and fuel management for MSR requires dynamic online models.

Development efforts in diffusion and transport theory based 3D core neutronic codes for square and hexagonal geometries such as ARCH, FEMINA, TRIHEX-FA, pin-by-pin simulation tools HEXPIN, TRANPIN, modelling for heterogeneities etc. will be illustrated in this talk. Monte Carlo code development in M3C, PATMOC, McBURN will be presented along with their benchmark studies. Evolutional algorithms have been demonstrated for use in in-core fuel management and its use in design of loading patterns will be discussed. Indigenous efforts in fuel cycle analysis code ADWITA, its associated cross section generation and its use for the analysis if PHWR and AHWR will also be presented. Neutronics an thermal hydraulic coupling also has undergone transformation from simple external coupling to treatment of multi volumes for more accurate estimate of thermal margins.

This talk will give an overview of the current developments in the reactors of tomorrow and the self-reliance achieved in the designing these systems.

Invited talk

Gaining a Mechanistic Understanding of Nuclear Fuel Material Performance by Combining Modelling and Experiment

Simon Middleburgh
Bangor University, UK
email- s.middleburgh@bangor.ac.uk

Abstract

A range of advanced technology fuels (ATFs) are now being considered that aim to improve operational characteristics, such as residence times and reduction in centre-line temperatures, with accident tolerance providing an overall economic and viable fuel candidate for both light water reactors and reactors currently under development, including lead-cooled fast reactors and high temperature gas reactors. Here we present a range of recently published developments being undertaken to support ATF development with a focus on the manner in which modelling is guiding experiment and how experiment dictates the modelling required to develop a new fuel candidate - here the focus shall be on a UO2-based composite fuel systems and uranium borides.

Invited talk

Creating DRAGON5 Cross Section Databases for Neutronics-Thermal Hydraulics Coupled Canadian SCWR Simulations

G. Marleau, U. Le Tennier
Institut de génie nucléaire, Polytechnique Montréal
P.O. Box 6079, stn. CV, Montréal (QC), Canada
e-mail - guy.marleau@polymtl.ca, ulysse.le-tennier@polymtl.ca

Abstract

To analyze the safety behaviour of the most recent designs for the Canadian Super Critical Water Reactor (SCWR), coupled calculations of core neutronics and thermal hydraulics are required. Since core neutronics simulations are generally based on two groups diffusion calculations, a burnup and local properties dependent database containing diffusion coefficients as well as macroscopic cross section must first be built using a lattice code. Since our core neutronics calculations are to be performed by DONJON5 and CATHENA will be used for thermal hydraulics simulation, the obvious code to use for lattice calculations is DRAGON5. For a steady-state core under normal operation conditions, the reactor database built by DRAGON5 is designed to cope with a wide variety and range of cell properties. For the three different fuel enrichment found in the core, this should include the fuel temperature, the upward and downward coolant density and temperature as well as the global boron concentration in the moderator. This paper describes the procedure that was set up to generate and validate our three database (one for each enrichment) and some results we obtained using coupled DONJON5 and CATHENA simulations of the Canadian SCWR.

Invited talk

HIGH-FIDELITY REACTOR CORE PHYSICS SIMULATIONS FOR IDENTIFICATION OF IRRADIATED FUEL CHARACTERISTICS

Sunil S. Chirayath

Department of Nuclear Engineering, Texas A&M University, College Station, TX-77843-3133, USA.

e-mail: sunilsc@tamu.edu

Abstract

High-fidelity neutronics simulations were performed by developing nuclear reactor core models of a set of reactors with the goal of predicting fuel burnup, time since irradiation, and reactor-type of an unknown irradiated fuel sample. Monte Carlo N-Particle code, MCNP6.2 was used to perform the neutronics simulations, which included fuel burnup simulations in addition to estimating the values of effective neutron multiplication factor and the energy dependent neutron fluxes. The objective of these simulations was to build a database containing concentration of isotopes of interest that can be used to identify the characteristics of irradiated fuel. The information stored in the database was concentration of the following 14 isotopes: ^{133}Cs, ^{134}Cs, ^{135}Cs, ^{137}Cs, ^{154}Eu, ^{153}Eu, ^{136}Ba, ^{138}Ba, ^{149}Sm, ^{150}Sm, ^{152}Sm, ^{239}Pu, ^{240}Pu, ^{241}Pu, and ^{242}Pu. The isotopic information was stored as a function of fuel burnup and time since irradiation for each reactor core simulated. The information in the database was stored as ten intra-element isotopic ratios: ^{137}Cs/^{133}Cs, ^{154}Eu/^{153}Eu, ^{134}Cs/^{137}Cs, ^{135}Cs/^{137}Cs, ^{136}Ba/^{138}Ba, ^{150}Sm/^{149}Sm, ^{152}Sm/^{149}Sm, ^{240}Pu/^{239}Pu, ^{241}Pu/^{239}Pu, and ^{242}Pu/^{239}Pu. Storing as intra-element isotopic ratios in the database was found to be better amenable to characterize the irradiated fuel sample. Using this database, we were able to predict the characteristics of an unknown irradiated nuclear reactor fuel sample in two different ways; one using a maximum likelihood statistical method and another using a combination of machine learning methods.

1. Introduction

Methods development to characterize reactor type, fuel burnup, and time since irradiation (TSI) of irradiated nuclear fuel is needed to enable the prediction of these three parameters of an unknown irradiated fuel sample. High-fidelity neutronics simulations, including fuel burnup simulations of reactor cores are extremely important for such methods development. The radiation transport code, MCNP6.2 based on Monte Carlo stochastic method [1] was used to model reactor cores and perform neutronics simulations to estimate the resulting isotope concentrations in irradiated uranium fuel. The simulation results were used to create a reactor-dependent database of irradiated fuel isotope ratio values as a function of fuel burnup and TSI. Ratios of intra-element isotopes (fission product or actinide) are used as characteristics to determine a combination of reactor parameters of interest corresponding to the unknown irradiated nuclear fuel sample. The ten intra-element isotopic ratios used in this study were ^{37}Cs/^{133}Cs, ^{154}Eu/^{153}Eu, ^{134}Cs/^{137}Cs, ^{135}Cs/^{137}Cs, ^{136}Ba/^{138}Ba, ^{150}Sm/^{149}Sm, ^{152}Sm/^{149}Sm, ^{240}Pu/^{239}Pu, ^{241}Pu/^{239}Pu, and ^{242}Pu/^{239}Pu (Figure 1). The reason for selecting intra-element isotope ratios was because, in case if the unknown fuel sample has been reprocessed, we need not be concerned with the varying decontamination factors of different elements. The isotopes selected for the method development were based upon the initial criteria of isotope production yield in fuel and half-life; note that some of the isotopes selected are nonradioactive. Subsequently, intra-element isotope ratios were formed with the criterion that the ratio must have a functional dependence on at least one of the reactor parameters (reactor type, fuel burnup, and TSI) of interest. Our method compares the values

of reactor-dependent intra-element isotope ratios in the database developed to the same ratios of the unknown sample. We used two different strategies for developing the method; [a] maximum likelihood statistical analysis and [b] machine learning method to predict the reactor type, fuel burnup, and TSI of the unknown irradiated nuclear fuel sample. Both strategies were tested with intra-element ratios of pseudo unknown irradiated fuel samples.

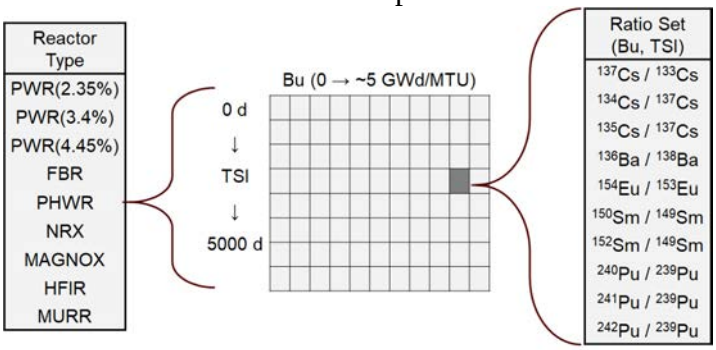


Figure 1: Reactor model burnup and time since irradiation dependent intra-element isotopic ratios set matrix (PWR: Pressurized Water Reactor with three different ^{235}U enrichments; FBR: Fast Breeder Reactor; PHWR: Pressurized Heavy Water Reactor; NRX: Canadian National Research Experimental research reactor; MAGNOX: Britain's Magnesium alloy—"magnox" cladded fuel reactor; HFIR: High Flux Isotope Reactor; MURR: Missouri University Research Reactor).

2. Correspondence of Intra-Element Isotopic Ratios to Reactor Parameters of Interest

The relationship of intra-element isotopic ratios to the three reactor parameters of interest (reactor-type, fuel burnup, TSI) are needed to be understood for a variety of such combinations that could be formed from the results of fuel burnup calculations using MCNP6.2 code. Based on this understanding of relationship of intra-element isotopic ratios and the reactor parameters of interest, selection of the ratios was made to incorporate in the database discussed in section 1. Even though the current database stores information of ten such intra-element isotopic ratios, for brevity only three of them are discussed here.

2.1 ^{150}Sm/^{149}Sm Ratio

The ^{150}Sm/^{149}Sm ratio can provide insight to the reactor-type, where the fuel was irradiated. The dependency is shown in figure 2. ^{150}Sm and ^{149}Sm are stable isotopes and their ratio increases with increasing fuel burnup with a large dependency on the neutron energy spectrum. This behaviour is due to the radiative capture cross-section of the well-known fission product neutron poison, ^{149}Sm, which has a very large reaction cross-section for thermal neutron absorption in a reactor. Other intra-element isotopic ratios which will contribute to determination of reactor-type of the irradiated fuel include ^{135}Cs/^{137}Cs, ^{136}Ba/^{138}Ba, ^{152}Sm/^{149}Sm, ^{240}Pu/^{239}Pu, ^{241}Pu/^{239}Pu, and ^{242}Pu/^{239}Pu.

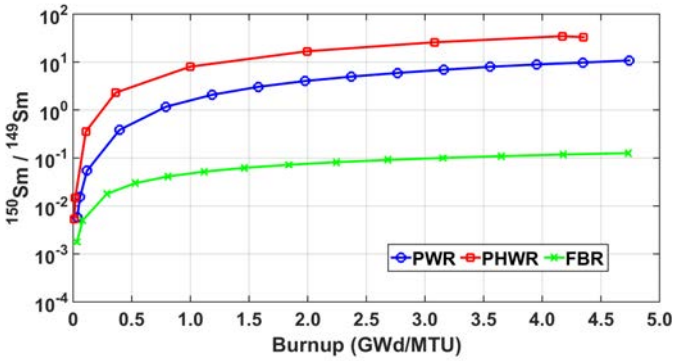


Figure 2: The ^{150}Sm/^{149}Sm ratio as a function of fuel burnup for three reactors in the database.

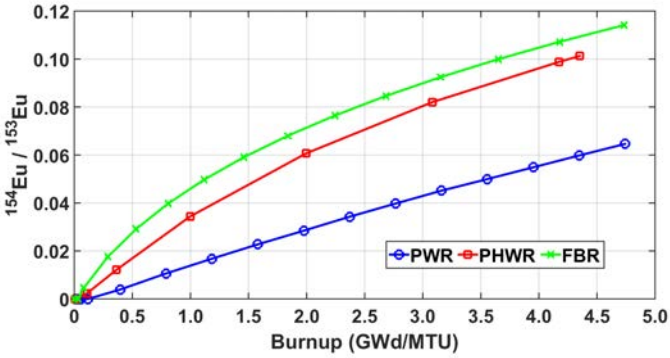


Figure 3: The ^{154}Eu/^{153}Eu ratio as a function of fuel burnup for three reactors in the database.

2.2 ^{154}Eu/^{153}Eu Ratio

^{153}Eu is a stable fission product. The primary production of ^{154}Eu is from radiative capture on ^{153}Eu. The radiative capture on ^{154}Eu serves as the primary loss mechanism of ^{154}Eu during irradiation. The ^{154}Eu(n,γ)^{155}Eu neutron reaction cross section is significantly larger than the ^{153}Eu(n,γ)^{154}Eu neutron reaction cross section at thermal neutron energies, but nearly equal at fast neutron energies. This leads to the ratio behaviour seen in figure 3 with the ^{154}Eu/^{153}Eu ratio being larger in the fast neutron spectrum reactor. Like many of the identified isotopic ratios, the ^{154}Eu/^{153}Eu ratio exhibits a dependency on all three parameters of interest: fuel burnup, TSI, and reactor-type, with a clear dependence on fuel burnup. All ten identified intra-element isotopic ratios used in the method with the exceptions of the ^{137}Cs/^{133}Cs and ^{135}Cs/^{137}Cs ratios are found to influence the determination of fuel burnup.

2.3 ^{137}Cs/^{133}Cs Ratio

The concentrations of both ^{137}Cs and ^{133}Cs in irradiated fuel contain information on fuel burnup, but the intra-element ratio of ^{137}Cs/^{133}Cs cancels out the fuel burnup dependence. Both ^{137}Cs and ^{133}Cs are produced with similar fission yields and have insignificant dependence on neutron energy. The isotope ^{133}Cs is stable while ^{137}Cs is radioactive, resulting in the ^{137}Cs/^{133}Cs ratio value decaying with a half-life of 30.08 y. Assuming no extended shutdowns during irradiation, this leads to the ratio quickly approaching an asymptotic value close to 1.0 with almost no dependence on fuel burnup or reactor type. The computed ratio values of ^{137}Cs/^{133}Cs are shown in figure 4 as a function of fuel burnup for the three reactor types in our database. With the ^{137}Cs/^{133}Cs ratio being relatively independent of burnup and reactor-type, a measured value of the ^{137}Cs/^{133}Cs ratio will indicate the TSI of the fuel. Other ratios identified as contributors to determining TSI include ^{154}Eu/^{153}Eu, ^{134}Cs/^{137}Cs, ^{135}Cs/^{137}Cs, and ^{241}Pu/^{239}Pu.

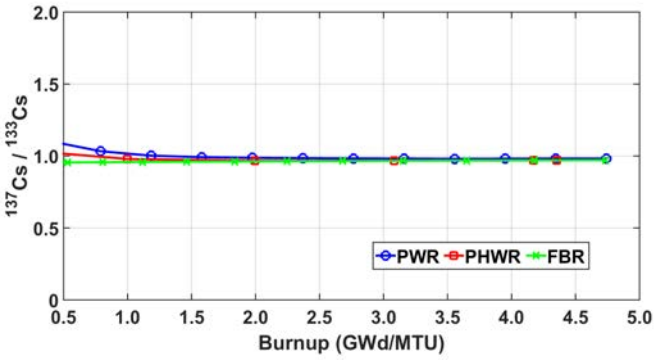


Figure 4: The ^{137}Cs/^{133}Cs ratio as a function of fuel burnup for three reactors in the database.

3. Results

Two methods (maximum likelihood and machine learning) were employed in identifying an unknown irradiated fuel sample's parameter of interest (reactor-type, fuel burnup, and TSI).

3.1 Maximum likelihood method

Maximum likelihood estimation is performed by taking the product of the likelihoods that each of the ten ratios of the experimental sample matches with the corresponding ratio for a point in the reference database. The model, *M*, matching the measured vector, r_{mes}, given by Eq. 1 is used to compute the likelihood and subsequently the log-likelihood values were estimated using Eq. 2 to avoid the computational overflow errors.

$$L(M|r_{mes}) \propto L(r_{mes}|M) = \prod_{j=1}^{n} \frac{1}{\sigma_{j,sim}\sqrt{2\pi}} exp\left\{-\frac{(r_{j,mes}-r_{j,sim})^2}{2\sigma_{j,sim}^2}\right\} \quad (1)$$

$$Log\ L(M|r_{mes}) = \sum_{j=1}^{n}\left[log\left(\frac{1}{\sigma_{j,sim}\sqrt{2\pi}}\right) - \frac{(r_{j,mes}-r_{j,sim})^2}{2\sigma_{j,sim}^2}\right] \quad (2)$$

where

$r_{j,mes}$ = j^{th} intra-element isotope ratio (for example $^{137}Cs/^{133}Cs$) in a vector of n measured intra-element ratios (in this paper n=10)

$r_{j,sim}$ = j^{th} intra-element isotope ratio in a vector of n simulated intra-element ratios from model, M, (database)

$\sigma_{j,sim}$ = uncertainty associated with the j^{th} intra-element ratio from vector, r_{sim}.

The calculated likelihood and loglikelihood values obtained are indicative of each reactor model, M, whether the measured material is from that reactor, with higher likelihood or loglikelihood values indicating a higher possibility of that reactor being the source of the material. The maximum likelihood calculations using equations 1 and 2 are conducted for every point in the database. The logarithmic-likelihood values can be mapped, creating a surface for each reactor-type of interest. The highest peak found across all the surfaces indicates the predicted reactor-type, fuel burnup, and TSI [3].

3.2 Machine learning method

The machine learning methods employed for reactor-type, fuel burnup, and TSI in a serial sequence were [a] support vector machine (SVM) classifier, [b] Gaussian process regression (GPR) algorithm, and [c] an analytic decay scheme, respectively [4].

Reactor Type	Method	Burnup (GWd/MTU)	TSI (days)
HFIR	Experimental	4.36 ± 0.28	1601
	Maximum Likelihood	4.29 ± 0.01	1834 ± 54
	Machine Learning (SVM-GPR)	4.20 ± 0.06	1820 ± 6
MURR	Experimental	0.973 ± 0.03	318
	Maximum Likelihood	1.01 ± 0.02	305 ± 83
	Machine Learning (SVM-GPR)	1.045 ± 0.03	315 ± 38

4. Conclusion

We have developed two methods to identify three parameters (reactor-type, fuel burnup, and TSI) of an unknown irradiated nuclear fuel. The methods are based on maximum likelihood statistical analysis and machine learning. The heart of both the methods is a database consisting of information on ten intra-element isotopic ratios: $^{137}Cs/^{133}Cs$, $^{154}Eu/^{153}Eu$, $^{134}Cs/^{137}Cs$, $^{135}Cs/^{137}Cs$, $^{136}Ba/^{138}Ba$, $^{150}Sm/^{149}Sm$, $^{152}Sm/^{149}Sm$, $^{240}Pu/^{239}Pu$, $^{241}Pu/^{239}Pu$, and $^{242}Pu/^{239}Pu$ of the irradiated fuel as a function of reactor-type, fuel burnup, and TSI. Neutronics simulations of several types of nuclear reactor cores were performed using MCNP6.2 code to create the database. Both methods were validated using “unknown” or characterized irradiated fuel samples and they were found to be successful in predicting three reactor parameters of interest. Work is in progress now to expand the machine learning method for mixed samples of irradiated fuel.

5. References

[1] C.J. Werner, “MCNP® User’s Manual: Code Version 6.2,”, *LA-UR-17-29981*, Los Alamos National Laboratory, 2017.

[2] J.M. Osborn et al., “Nuclear Forensics Methodology for Reactor-Type Attribution of Chemically Separated Plutonium”, *Nuclear Technology*, Vol. 201 (1), pp: 1-10, 2018.

[3] J.M. Osborn et al., “Experimental Validation of a Nuclear Forensics Methodology for Source Reactor-Type Discrimination of Chemically Separated Plutonium”, *Nuclear Engineering and Technology*, Vol. 51 (2), pp: 384-393, 2019.

[4] P. O’Neal, S.S. Chirayath, and Q. Cheng, “A Machine Learning Method for the Forensics Attribution of Separated Plutonium”, *Nuclear Science and Engineering*, in press, https://doi.org/10.1080/00295639.2021.2024037, 2022.

Invited talk

Physics Design Studies of 500 MWe FBR1&2 Core

K. Devan
email-devan@igcar.gov.in

Abstract

After PFBR, a road-map to construct two more 500 MWe MOX fuelled sodium-cooled fast breeder reactors (as twin unit) has been conceived by employing the design, R&D, safety review, construction and commissioning experiences of PFBR. This reactor (also known as FBR 1&2) design has to meet the evolving new safety criteria. In this lecture, various physics design studies made to arrive at an optimised core is discussed.

Invited talk

Model-Order Reduction of Neutronic Systems via POD-Galerkin Projection

Jeremy Roberts
Kansas State University, USA
e-mail-jaroberts@ksu.edu

Abstract

The pursuit of high-fidelity models for nuclear systems has been central to research around the world as the commercial, regulatory, and research communities explore next-generation reactors. Neutronic models can be classified as stochastic or deterministic, the latter of which are based on numerical discretization of the governing equations. Accurate predictions require a sufficiently resolved phase space, and the cost of analyses needing repeated simulations can become excessive. Presented here is the preliminary development of reduced-order models (ROMs) for steady-state and transient, neutronic applications based on both the diffusion and transport approximations. Proper-Orthogonal Decomposition
(POD) was used to define problem-specific bases for Galerkin projection of the full-order model (FOM) equations. For transient applications with nonlinear feedback, this projection can be expensive (with a cost proportional to the size of the FOM system). To overcome this expense, both "interpolate-then-project" and "project-then-interpolate" approximations were explored. For the former, variants of the Discrete Empirical Interpolation Method led to ROMs for transient diffusion models that reduce computational times by up to 50 and preserve accuracy to within 1% on localized powers for the problems studied. However, interpolation of the transport operators is impossible because the operators are not explicitly constructed. Instead, a simple, quasi-static-like update of projected operators was shown to yield similar accuracies and efficiencies for the problems studied. Because this latter technique requires only the "action" of the underlying operators, the method is trivially intrusive and should be easily incorporated in many large-scale transport codes under development.

Invited talk

Advances in Physics Design of Indian PHWRs

Dr. M.P.S. Fernando,
Associate Director (FPSS)
Nuclear Power Corporation of India Limited, Mumbai, India
e-mail – mpsfernando@npcil.co.in

Abstract

The Pressurized Heavy Water Reactor (PHWR) is a horizontal pressure-tube reactor which uses natural uranium (NU) as fuel and heavy water as moderator and coolant. India presently has 17 pressurized heavy water reactors (PHWRs) in operation. Out of these 17 PHWRs, 15 are 220 MWe PHWRs and the rest are 540 MWe PHWRs. The reactor core design of 540 MWe with 392 coolant channels and each channel having 37 element fuel bundles was uprated about 25 % to produce 700 MWe. The nominal maximum value of channel power and flux flattening was enhanced to achieve this. Partial boiling to the extent of 2 to 3 % quality at the exit of coolant channel is allowed at full power. Many first of its kind systems are provided for power measurement, reactor control and protection. The primary heat transport system consists of two coolant loops with interleaved feeder distribution, such that coolant void is uniformly distributed throughout the core region in the event of loss of coolant and thus improves the available safety margins. The steam generators and pressuriser are sized accordingly for heat removal.

KAPP-3, located at Kakrapar, Gujarat achieved its first criticality on July 22, 2020, is the first reactor of such design. It is currently undergoing extensive tests as it is a demonstration for the upcoming PHWRs in India. In addition, 3 units of 700MWe PHWR are in advanced stage of commissioning and are expected to be operational shortly. Ten more such units are sanctioned in the fleet mode by Government of India.

With the increase in core dimensions and power rating, PHWRs become neutronically loosely coupled and requires continuous monitoring and control of core power distribution. Degradation of spatial power control or non-uniform refuelling may result in zone powers, Channel Power Peaking Factors and bundle powers beyond their desired design values.

Extensive in-core instrumentation based on Self Powered Neutron Detectors is provided for control and protection purpose. Inconel SPND of 1 metre long Integral type is used for control and protection purpose. These detectors are prompt in response, low neutron absorption and have long operational life. These detectors are housed in Vertical Flux Units and Horizontal Flux Units penetrating the calandria vessel in vertical and horizontal direction, respectively. They are cooled and kept in dry environment with helium under pressure.

3D flux mapping is carried out at every cycle time of reactor regulating system (RRS) with the help 106 Vanadium SPNDS each of 30 cm length. They provide accurate zone power estimations for spatial power control, trims reactor power to ensure compliance to operating limit of channel and bundle powers and to provide enough operating margin. Two independent Regional Overpower Protection Systems based on fast responding Inconel SPNDs ensure fuel clad/coolant channel integrity during normal reactor operation, AOO and accidental conditions.

Initial Fuel Loading pattern with 258 DDU (0.28 weight % U-235) and rest NU bundles provide adequate flux flattening with all fresh fuel and full power operation is possible addressing all operational and safety aspects. In the equilibrium core, in addition to normal 8 Bundle shift scheme, 4 BSS is adopted in few central high-powered channels to maintain CPPF below 1.1.

In this talk, the advances made in 700MWe PHWR physics design starting from 220MWe and 540MWe PHWRs will be covered.

LHGR ESTIMATION FOR IPWR EQUILIBRIUM CORE USING PIN-BY-PIN CODE HEXPIN

Suhail Ahmad Khan and Umasankari Kannan
Bhabha Atomic Research Centre, Mumbai, India
email: - suhailak@barc.gov.in

Abstract

A 2700 MWth/900 MWe Indian Pressurized Water Reactor (IPWR) is being designed for developing indigenous capability to commercial light water technology. A fine mesh pin-by-pin analysis of equilibrium core of IPWR was performed using HEXPIN code system. The linear heat generation rate (LHGR) is an important safety parameter which decides the fuel rod durability during the reactor operation. The LHGR is not allowed to exceed the safety limit for safe operation. It is important to know the variation of LHGR with the cycle burnup. The LHGR variation with burnup has been estimated for the equilibrium core of IPWR using HEXPIN code system. The pin homogenised parametric cross section library generated by lattice burn up code EXCEL was used to perform this calculation. The present paper gives the detailed results and analysis of calculation procedure.

1. Introduction

The Indian Pressurized Water Reactor (IPWR) with operating power of 2700 MWTh/900 MWe is being designed to demonstrate the indigenous capability for designing PWRs [1]. The core follow up calculations for equilibrium core of IPWR was performed using the fine mesh 3D pin-by-pin code HEXPIN [2] and parameters like pin peaking factor and local peak factor distribution was estimated for equilibrium core.

The linear heat generation rate (LHGR) is an important safety parameter which determines the clad integrity and fuel rod durability for safe and efficient operation of the reactor. The limitations on the linear heat generation rate (typically called the limit curve) determine the level of possible values of the local linear heat rate under the conditions of normal or transient operation. These limits are primarily decided by the thermo-mechanical stress limits of the clad of the fuel rod. The limit on LHGR for the fuel rods which are seeing third cycle of operation should not be higher than the fuel rods which are under second operating cycle. Therefore, it is necessary to calculate and study the variation of LHGR with cycle burnup during rector operation. This calculation has been performed for the equilibrium core of IPWR using indigenous 3D pin-by-pin code HEXPIN. The present paper gives the details of calculation procedure. The brief description of the calculation tools is provided in Section 2. Section 3 presents results of calculations. Section 4 gives concluding remarks.

2. Calculation Tools

The calculations are performed using indigenous EXCEL-HEXPIN code system. The details of nuclear data used and calculation tools are described below.

2.1 Nuclear Data Library

The present calculations are performed using the high temperature library ‘HTEMPLIB’ [3], based on JEFF-3.1 nuclear data library. This library has cross section data for 185 nuclides in

172 energy groups. The burnup chain in HTEMPLIB library has been extended up to ^{252}Cf. The library has resonance tabulation for 48 nuclides. The resonance integral tables are available up to a temperature of 2500K. Equivalence relations are used for obtaining resonance self-shielded cross sections. Mutual shielding of a mixture of resonance nuclides is treated using Stammler's method.

2.2 EXCEL Code System

EXCEL is lattice burnup analysis code in hexagonal geometry. The EXCEL code system solves hexagonal lattice assembly cell by a combination of 1-D multigroup transport and 2-D few group diffusion theory. The fuel assembly cell consists of a number of heterogeneities like water rod, control rod or burnable absorber rod (BAR) cells. These heterogeneities are treated by supercell method in 1D cylindrical geometry using multigroup transport theory. Few group cross sections of distinct pincell, water or absorber cell types are obtained by weighting and collapsing with appropriate supercell spectra. The 2-D fuel assembly cell is treated by diffusion theory using few group homogenized cell cross sections. EXCEL writes the output of few group cross sections of both assembly cell and the individual fuel and non-fuel cells in the assembly. The former is used by TRIHEX-FA code and the latter by HEXPIN code. The few group lattice parametric database is generated for each fuel type considered in KK core as a function of burnup, boron, fuel and coolant temperatures, coolant density, saturated xenon for different heat rating levels and Sm loads.

2.3 HEXPIN Code System

The code HEXPIN has been developed for reactor core analysis with a pincell size mesh description up to pressure vessel in hexagonal geometry [4]. HEXPIN uses the centre mesh finite difference method to solve 3D diffusion equation in few groups. Currently HEXPIN is compatible with lattice parametric database of EXCEL code. The pin by pin description of the whole core is an arduous task. The description of fuel/non-fuel zones of each type of fuel assembly present in the core is considered by EXCEL code and is written in a file. The HEXPIN code reads this file for each fuel type.

At core level HEXPIN reads only the input of assembly type distribution in the core. The code superimposes the local distribution of fuel and non-fuel cells within each assembly with global assembly type distribution and derives the pin by pin description of entire core. In VVER type problems, there is a thin inter assembly water gap. In EXCEL code this region is expanded to half or 1/3rd hexagonal cells by using diluted water cross sections. In the present pin-by-pin model the two half hexagons of adjoining assemblies coalesce into a single integral hexagon. It was found that the core size gets expanded when the regular lattice pitch is considered. To avoid this problem, the lattice pin pitch in HEXPIN simulation is reduced to an equivalent pitch by preserving the area of each assembly as well as the core area [4]. The core external regions are alternate ring layers of steel and water up to pressure vessel. The hexagonal cells within a given radius are automatically identified by the code. Few group homogenized parameters of reflector is also provided by EXCEL. The 3D few group diffusion equation is solved using centre mesh finite difference method. HEXPIN calculates typical core parameters like k_{eff}, pinwise 3D power/burnup distribution of the whole core. Critical soluble boron search is possible.

The HEXPIN code has recently been refurbished and rewritten in FORTRAN 90. Some new models have been added to HEXPIN. This includes the five group perturbation model and a first

order perturbation method to calculate the reactivity coefficients using pin level cross sections. In the perturbation method, it is assumed that for small perturbations the direct and adjoint flux of the reference and perturbed state are nearly same. With this approximation, the reactivity change due to perturbation of any of the parmeters listed aboved can be determined from the expression:

$$\rho_{pert.} = \frac{\Delta k}{k} = \frac{\int dr \sum_{g=1}^{G} \phi_g^{\dagger} \left[\nabla . \Delta D^g \nabla \phi_0^g - \Delta \Sigma_t^g \phi_0^g + \sum_{g'=1}^{G} \Delta \Sigma^{g' \to g} \phi_0^{g'} + \frac{\chi^g}{k_0} \sum_{g'=1}^{G} \Delta \left(\nu \Sigma_{f0}^{g'} \right) \phi_0^{g'} \right]}{\int dr \sum_{g=1}^{G} \phi_g^{\dagger} \chi^g \sum_{g'=1}^{G} \nu \Sigma_{f0}^{g'} \phi_0^{g'}}$$

Here it should be noted that the few group cross sections used in the above expression are pin homogenised cross sections.

3. Results and Discussion

The detailed pin-by-pin analysis of IPWR equilibrium core had been completed earlier and the detailed description can be found in [2]. The details of pin homogenised parametric few group cross section library of the profiled IPWR FA required by HEXPIN and generated by the lattice burnup code EXCEL are given in [2]. These cross sections are generated for all identified fuel and non-fuel pin cells of the profiled FA for a set of reactor state parameters.

The core calculation for Cycle 1 is performed using fresh FAs and a pin wise burnup profile is generated. The core for subsequent cycles is reconstituted using the previous burnup profile and loading pattern. This calculation is repeated till a converged burnup profile is obtained for the equilibrium core.

HEXPIN gives the power fraction and burnup values for all axial and radial meshes during the core follow up calculation. An auxiliary processing program has been written to read and process the 3D power fractions and burnup outputs obtained from HEXPIN. The 3D pin level meshes of the core are identified according to burnup cycles seen by them. In order to obtain mesh wise LHGR, the power fraction of each mesh is multiplied by the nominal LHGR value of 159.6 W/cm. For LHGR protection set point, an engineering factor of 1.16 and an error in calculation of reactor thermal power of 1.04 are considered over and above the calculated values by HEXPIN. These factors are derived from previous experience of VVER-1000 MWe reactor calculation. The mesh burnup and LHGR value, thus, obtained for the mesh is written to separate files for three cycles. The LHGR values are plotted as a function of burnup for three cycles in Figs. 1 to 3 respectively. These three figures are combined in Fig. 4. It is seen from these figures that the maximum value of LHGR values for meshes seen by fuel pins of cycles 1, 2 and 3 (of 410 days each) are less than 375W/cm, 335W/cm and 310W/cm respectively. The maximum burnup seen by few meshes of cycle 3 is seen below 75MWD/Kg.

4. Conclusion

The 3D pin level mesh wise variation of LHGR with burnup is calculated with HEXPIN for equilibrium core of IPWR. The LHGR value for each pincell level mesh is sorted by the cycles seen by them using an auxiliary program. For LHGR protection set point, an engineering factor of 1.16 and an error in calculation of reactor thermal power of 1.04 are considered over and above the calculated values by HEXPIN. It is seen from that the maximum value of LHGR values for meshes seen by fuel pins of cycles 1, 2 and 3 are less than 375W/cm, 335W/cm and 310W/cm respectively. The maximum burnup seen by few meshes of cycle 3 is seen below 75MWD/Kg.

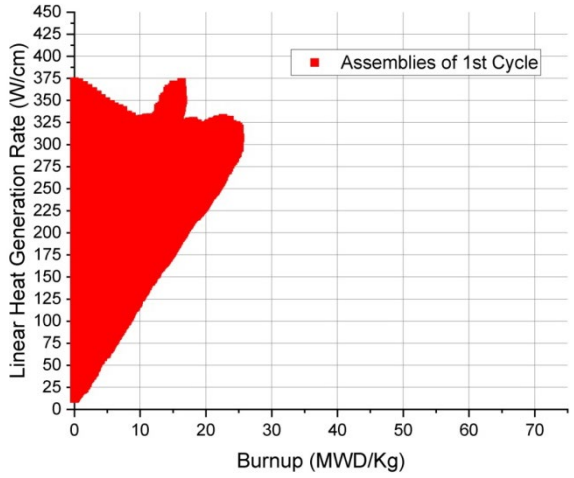


Fig. 1 Variation of LHGR with burnup for assemblies of Cycle 1

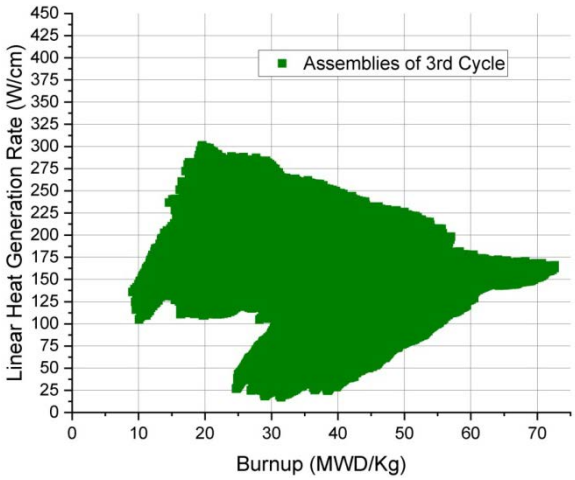


Fig. 3 Variation of LHGR with burnup for assemblies of Cycle 3

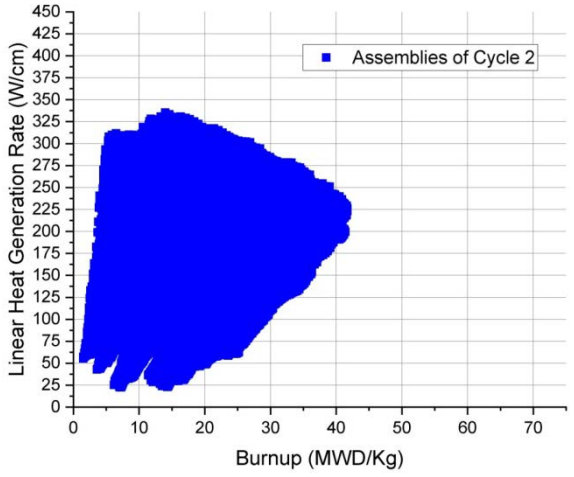


Fig. 2 Variation of LHGR with burnup for assemblies of Cycle 2

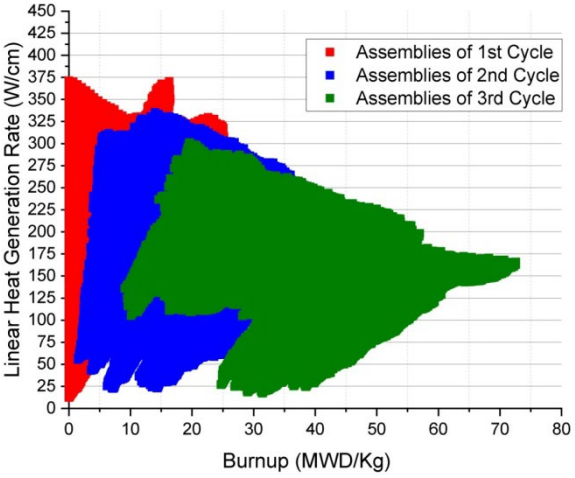


Fig. 4 Variation of LHGR with burnup for assemblies of three Cycles

5. References

1. IPWR Design Report, Chapter 3 Reactor Physics Design
2. Suhail Ahmad Khan and Umasankari Kannan, “Pin–by–Pin Analysis of IPWR”, RPDD/IPWR/85/2019, June, 27, 2019
3. Suhail Ahmad Khan, V. Jagannathan , U. Pal., R. Karthikeyan and A. Srivastava, “Need for High Temperature Nuclear Data Library for LWR Design Computations”, *Journal of the Korean Physical Society*, **59 (2)**, 1073 (2011)
4. Suhail Ahmad Khan and V. Jagannathan, “HEXPIN–A Pin–by–Pin 3D Core Diffusion Code with Space–Dependent Feedback Model”, *Proc. of ARP 2013–Advance in Reactor Physics: Simulation Techniques and Analysis Methodologies*, BARC Training School Hostel, Anushaktinagar, Mumbai, India, October 23–25, 2013 (2013)
5. W.M. Stacey, ‘Nuclear Reactor Physics’, WILEY-VCH Verlag GmbH & Co. KGaA, Weinheim, 2007

Use of Artificial Neural Networks for AHWR refuelling strategy

Amit Thakur[1], Debasmit Sarkar, Vishal Bharti and Umasankari Kannan
Bhabha Atomic Research Centre, Mumbai, India
[1]*e-mail: - thakur@barc.gov.in*

Abstract

The unique fuel cycle of Advanced Heavy Water Reactor (AHWR) has necessitated a requirement of special on-power refuelling scheme. A computer code CARS was developed for automatically selecting channels for refuelling and reshuffling at all stages and simulate the core for generating required operational data. Artificial neural networks (ANNs) are considered as efficient tools for providing solution to combinatorial optimization problems. In this manuscript a module based on ANNs has been developed and integrated in CARS. The AHWR refuelling scheme generated by modified code CARS-ANN has been found to be very efficient where, desired discharge burn-up is achieved along with safe and full power operation.

1. Introduction

The computer code CARS uses trial and error approach for developing AHWR refuelling scheme. In this approach, only a small number of possible combinations of channels are simulated at each refuelling and leaving out simulation of many good candidates of search space. The simulation of all the combinations at each refuelling is computationally costly in reasonable time scale due to vast search space. To make the code more efficient and fast, a different approach with ANNs [1,2] for estimation of operational parameters (excess reactivity and maximum channel power) at each stage of reactor operation has been considered.

2. Development of ANN module for CARS

The replica of biological neural network to an artificial model is through layers of neurons, with each connected to every other neurons in the subsequent layer. Figure 1 & 2 shows a biological neural network and a representative artificial neural network. An artificial neuron, calculates a weighted sum of inputs supplied from previous layer.

$$WS(j,k) = \sum_{i=1}^{n} x_{ji}^{k-1} W_{ji} + \theta_j \quad (1)$$

Here, $\boldsymbol{\theta}_j$ is bias. The activation function is applied on this weighted sum and output signal of this neuron is produced. The W's (weights) are adjusted during the learning phase of algorithm. We start with random weights and in Back propagation network learns by adjusting the weights such that error is minimized.

$$\frac{\partial E}{\partial W_{jk}} = 0 \quad (2)$$

The neural networks learn by refining their link weights which are guided by the error (the difference between actual output in training data and the predicted output). The error back propagation method is used to train the neural network and to estimate the weights between layers of the network. The working of artificial neuron is shown in Figure 3 and equation 1. The ANN has three important parts, input layer, hidden layers and output layer. For estimating the outputs of unknown cases with ANN, three things are required,

1) Training data set: In this set we have already simulated cases with known outputs for learning phase of algorithm and to generate/optimize weights of all the layers.

2) Test data set: this set is like training data set however it is not used for training purpose. This is used to predict the outputs and calculate the error.
3) Optimization of hidden layers and number of neurons in hidden layers based on training data set and test data set to minimize the error. This is basically, first two steps but with different number of hidden layers and different number of neurons in hidden layers.

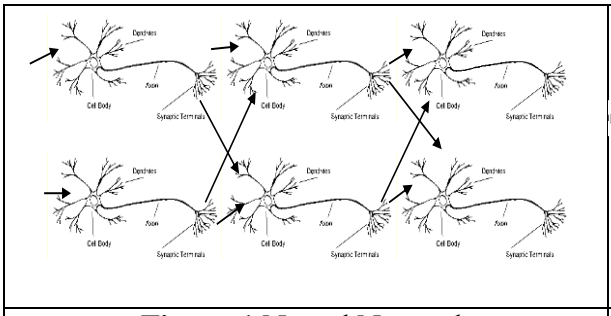


Figure 1 Neural Network

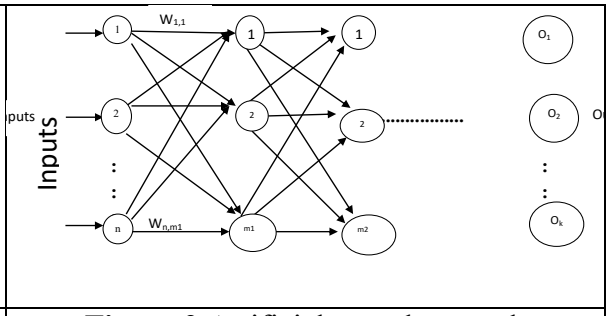


Figure 2 Artificial neural network

3. Data-set for ANN for AHWR fuel management problem

The AHWR core was mapped so that the individual lattice information is a single element of one vector (input layer). This will be the input to the ANN network and the corresponding core output parameters (output layer) in another single vector.

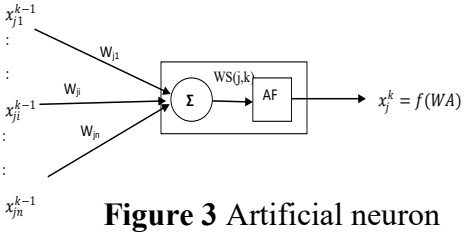


Figure 3 Artificial neuron

The output layer consists of core excess reactivity and maximum channel power (2-element vector). It was decided to prepare a vector of infinite multiplication factor (burnup dependent) of the clusters that can be used as input layer to ANN network. Also, since quarter core symmetry of the AHWR core is demanded, the whole core's information can be exhaustively modelled in a vector with quarter core information. As the quarter core of AHWR has 113 lattice locations, therefore, the input layer to ANN will consists of 113 k-infinity values. It was also decided to generate at least 112 inputs corresponding to fresh fuel in each lattice location. While putting fresh fuel in one lattice location, all the 112 reshuffling options were simulated. Therefore, the total number of simulations was 113 X 112 (or $^{113}P_2$). Diffusion equation for the corresponding core configuration is solved using 3D diffusion theory code FEMINA and corresponding reactivity and maximum channel powers were calculated. Each such case gave rise to one line (one training data) of the training data set file and 12656 different lines (training data) were prepared. To speed up in preparation of the training data set file, help of parallel architecture was used.

4. Training and prediction procedure for ANN

The AHWR core data generated in last section was used for training of neurons. The different cases considered for training to optimize the number of hidden layers and number of neurons in each hidden layers. Figure 4 and 5 shows the error in prediction for k-effective and maximum channel power for optimized ANN. The average error is 2.42 and 2.97 in k-effective and MCP respectively. It was also observed that more than 94% cases have an error of <10% for MCP and excess reactivity-effective as shown in table -1. The maximum error of remaining 6% cases is less than 15%.

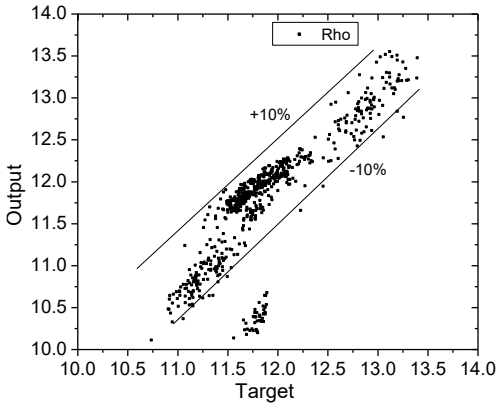


Figure 4: Predicted error in Rho

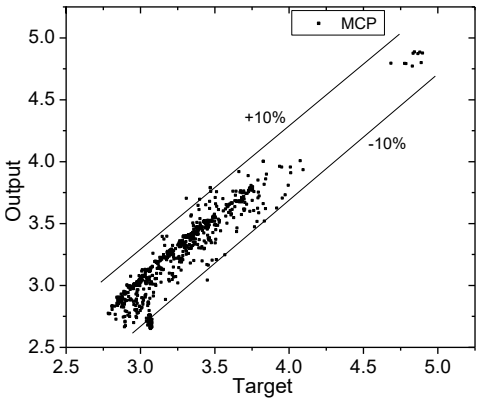


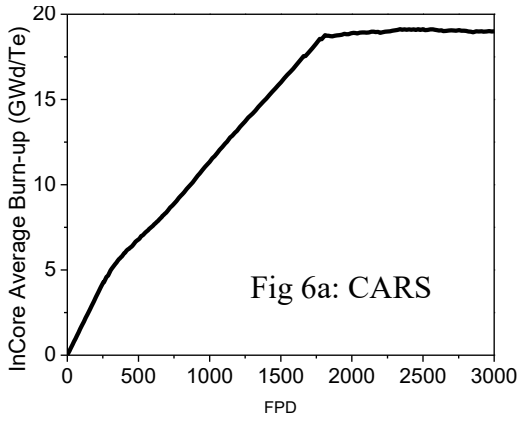
Figure 5: Predicted error in MCP

Table-1: Error percentage for unseen inputs for case-1					
Unseen data sets		Error			Av. error
		<5%	<10%	<15%	
650	MCP	541	613	650	2.97
	RHO	598	610	650	2.42

A new module was developed for incorporation of ANN in CARS. The module uses the weights file generated by the ANN as input and predicts the output of all the possible refueling and reshuffling combinations. The earlier method of choosing the refueling and reshuffling inputs was de-coupled. It was observed that the prediction of MCP and excess reactivity for all the cases at a particular refueling stage takes 1-3 minutes. It takes about 1-day time to simulate full core follow-up of AHWR.

5. Results and Discussion

The modified code CARS with ANN module was used for core follow-up studies of AHWR classical core from initial phase to transition phase. These studies have already been done with the previous version of CARS (without ANN). The results of both the studies have been compared in figures 6, 7 and 8. Fig 6a, 7a and 8a shows the in-core average burn-up, MCP and cumulative discharge burn-up of different clusters generated by CARS without ANN. While figures 6b , 7b and 8b shows the corresponding results for data generated by CARS-ANN.



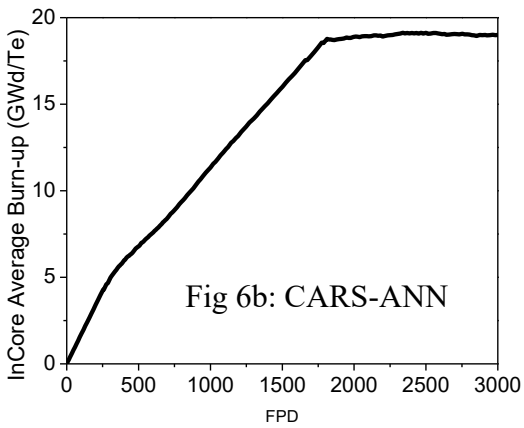


Fig 6: Average In-core burn-up vs. FPDs

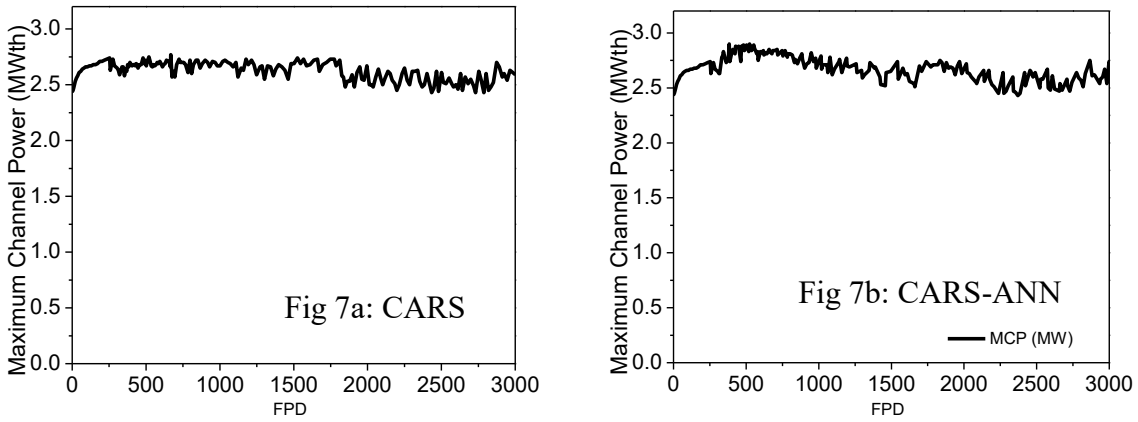


Fig 7: MCP vs. FPDs

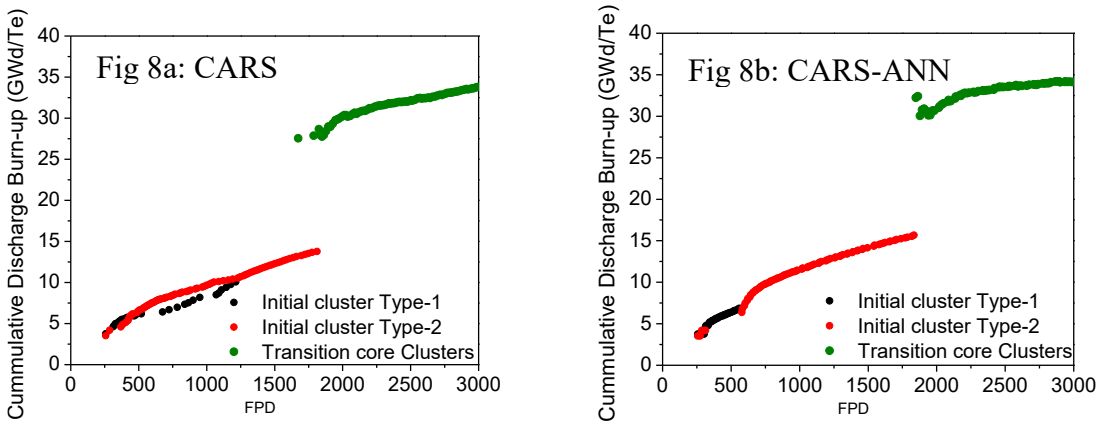


Fig 8: Cumulative discharge burn-up vs. FPDs

6. Conclusions

In this study, we have observed that by using ANN, the code CARS has become more fast and efficient. The refuelling scheme generated by CARS with ANN is better than the earlier generated refuelling scheme (without ANN). Overall for ~3000 days of operation, ~5% less fuel will be required if we use refuelling scheme generated by CARS-ANN than CARS without ANN. This is because, with ANN we get a good idea about excess reactivity and MCP generated at each refuelling for all the 113 X 112 (12656 cases) refuelling inputs at each refuelling in a short time of ~1-3 minutes. Therefore, only best cases are simulated actually which results in efficiency improvement and more economic refuelling scheme.

7. Referances

[1] Kim H. G., et al.., 1993, Pressurized Water reactor core parameter prediction using Artificial neural network, Nuclear Science and Engineering 113, pp 70-76

[2] Thakur A et al., "Development of in-core fuel management tool for AHWR using artificial neural networks", Annals of Nuclear Energy 150 (2021) 107869

DEVELOPMENT OF A NEW CODE MSDYN FOR SAFETY ANALYSIS OF MOLTEN SALT REACTORS (MSRs)

Indrajeet singh[1], Anurag Gupta[1] and Umashankari Kannan[1]
[1]Bhabha Atomic Research Centre Mumbai, India
[1]*e-mail: - jeet@barc.gov.in*

Abstract

Circulation of molten salt fuel through the reactor core to the heat exchanger characterizes the Molten Salt Reactors. As a consequence of fuel salt flow and the delayed neutron precursors (DNP) drift along the primary circuit, MSRs show unusual physical behaviour and dynamic behaviour becomes complex and highly non-linear in nature. In this paper, these peculiar characteristics of MSRs have been accounted in analyses of MSRE dynamics with the reference to the experimental data using a new safety analysis code, called **M**olten **S**alt Reactor **Dyn**amic (MSDyn). The new features include incorporation of model for the closed loop DNP circulation, 1D energy balance solution for core heat transfer, 5-regions lumped model of heat-exchanger with fuel salt in primary side and coolant salt in secondary sides, 4-regions lumped model of radiator. The new development also includes various transport delays of fluid flow in piping connections. Main aim of the present work is to validate working model of MSDyn for the simulation of a non-linear plant dynamics of the graphite moderated MSRs including core, heat exchanger and radiator.

1. Introduction

As compared to the traditional solid fuel reactors, MSRs are very different nuclear system having fuel in liquid state circulating throughout the primary circuit to remove heat produced via fission in the core. Consequence of heat transfer by fuel salt itself is that the dynamics of MSRs becomes complex and highly non-linear in nature [1]. The DNP drifts along the primary circuit diminishes the total delayed neutrons fractions (β) and their distribution in the core. This is because DNPs half-lives are such that there is finite probability to decay out of the core and few DNPs re-enter the core without emitting neutrons. In order to predict the accurate dynamic behaviour of MSRs by accounting the effect of fuel flow, a new non-linear plant dynamic code MSDyn is developed based on the modified point kinetics equations and thermal hydraulic equations [2]. It solves coupled 0/1D (DNP) equations and 1D energy balance equation in addition to the fully lumped models of neutronics and thermal hydraulic. In the present work, lumped models of the primary heat exchanger and the secondary heat exchanger (Radiator) have been augmented in MSDyn code to evaluate the average temperatures of fuel salt, coolant salt and air coolant. These new features of the code are validated with reference to the MSRE due to availability of the design and the experimental data [3]. However, it is challenging to gather appropriate reactor parameters at the time of experiments as various changes had been made during design and operation of the MSRE. The basic mathematical model adopted for the dynamic study of MSR in Section 2. In the next Section 3, results for the various transients are presented. This includes the step reactivity and fuel salt flow driven transients with temperature feedback. Finally, summary of results and conclusions are given in Section 4.

2. Theoretical model

The dynamic behaviour of a nuclear reactor is primarily depending on heat generation as a result of fission reaction and heat removal from the reactor core using coolant flow. The heat generation process in fission reaction is mathematically represented by point kinetics equation. In MSDyn-1, the energy balance equations are used to estimate fuel salt and graphite temperatures with fully lumped models. The

neutronics and thermal-hydraulics models used in the development of this code is explained in subsequent sub-sections.

2.1 Neutronics Equations: point kinetics(0D)

In this section, modified point kinetics model with six groups of delayed neutrons is adopted to obtain the reactor power in reactor safety analysis. The neutron power governing equation [Eq. (1)] is identical to that used in static fuel reactor. On the other hand, mathematical model for the DNP drift due to fuel flow need to be modified [3]. The precursors drift causes loss of DNP from the core. There is finite chance that these precursors decay outside the core before they re-enter the core. Thus, precursors balance equation consists of two extra terms in addition to the classical terms in 0-dimensional representation as given by Eq. (2)

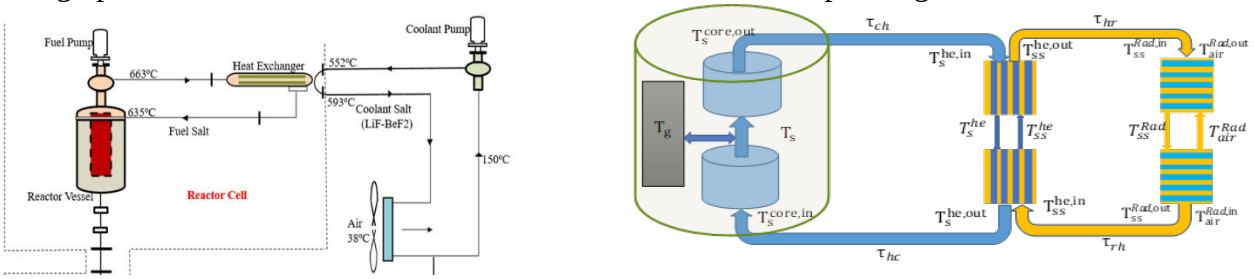
$$\frac{dn(t)}{dt} = \frac{(\rho - \beta)}{\Lambda} n(t) + \sum_{i=1}^{6} \lambda_i c_i \quad (1)$$

$$\frac{dc_i(t)}{dt} = \frac{\beta_i}{\Lambda} n(t) - \lambda_i c_i(t) - \frac{c_i(t)}{\tau_c} + \frac{c_i(t-\tau_l)}{\tau_c} e^{-\lambda_i \tau_l} \quad (2)$$

Eq. (2) is a delay differential equation and simple ODE solver cannot be used directly. The delay differential equation solvers are normally used to solve the coupled set of Eq. (1) and (2). In case of MSRs, unlike static fuel reactors the core reactivity in steady state is not zero i.e., reactor is sub-critical due to loss of delayed neutron as a result of fuel flow. This lumped model represents DNP decay outside the core and re-enter to the core after τ_l time spending into the external loop with survival probability $e^{-\lambda_i \tau_l}$. For U235 based fuel salt in MSRE, the loss of reactivity due to fuel circulation is 245pcm and for U-233 based fuel it is 112pcm at nominal flow rate with 8.5s and 16.5 s transit times of fuel salt in core and in external loop, respectively. MSDyn has capability to solve DNP Eqns. in one-dimension with convective term in a closed loop to accounts the limitations of fully lumped model.

2.2 Thermal Hydraulic Model of Reactor Core

To avoid the limitation of single lumped model of reactor core, two lump model of fuel salt and one lump for graphite is used in the present analysis. MSRE plant layout and model used is shown in Fig1(a) and Fig.1(b), respectively. The rate of change of salt temperatures in core consists of fuel-to-fuel heat transfer term, a fuel to graphite heat transfer term and a term for fraction of fission power generated in fuel salt.



(a) (b)

Figure 1 Schematic of (a) MSRE plant including reactor core, primary heat exchanger and radiator (b) and MSDyn model of the MSRE plant

$$\frac{dT_s^{out}(t)}{dt} = -\frac{2}{\tau_s}\left(T_s^{out}(t) - T_s(t)\right) + \frac{U_{s\to g}}{M_s C_{ps}}\left(T_g(t) - T_s(t)\right) + \frac{\gamma_s P}{M_s C_{ps}} \quad (3)$$

$$\frac{dT_s(t)}{dt} = -\frac{2}{\tau_s}\left(T_s(t) - T_s^{in}(t)\right) + \frac{U_{s\to g}}{M_s C_{ps}}\left(T_g(t) - T_s(t)\right) + \frac{\gamma_s P}{M_s C_{ps}} \quad (4)$$

$$\frac{dT_g(t)}{dt} = -\frac{U_{s\to g}}{M_g C_{pg}}\left(T_g(t) - T_s(t)\right) + \frac{\gamma_g P}{M_g C_{pg}} \quad (5)$$

The rate of change of graphite temperature has a fuel to graphite heat transfer term and a term for the fractional power generated in graphite lump [4]. These equations are given by Eqs. [3-5]

2.3 Thermal Hydraulic Model for Heat-Exchanger and Radiator

In heat transfer modelling of heat exchanger, the fuel salt in each side of the heat exchanger is divided in equal mass and two equations of energy balance is used. On shell side of heat exchanger, the rate of change of fuel salt temperature equation consists of a fuel-to-fuel lump heat transfer term and a fuel salt to coolant salt heat transfer term as represented by Eq. (6) and Eq. (7). [5]

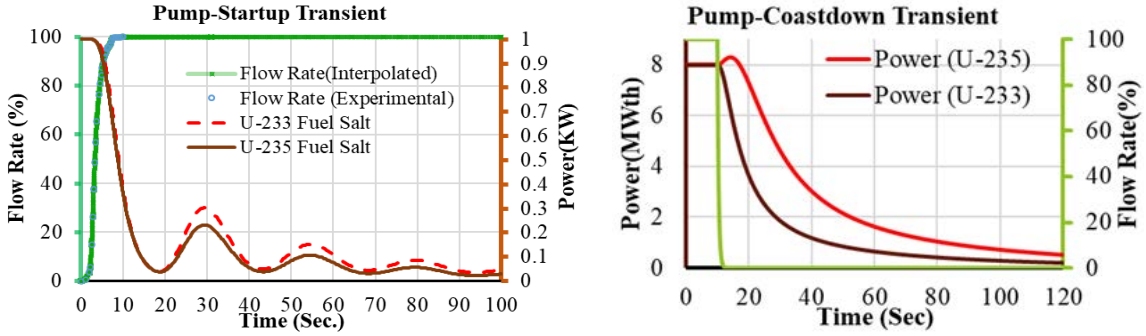
$$\frac{\mathrm{M}_s^{he} C_s}{2}\frac{dT_s^{he,out}}{dt} = -\dot{m}_s C_s\left(T_s^{he,out} - T_s^{he}\right) - \frac{U_{s\leftarrow \mathrm{ss}}}{2}\left(T_s^{he} - T_{ss}^{he}\right) \quad (6)$$

$$\frac{\mathrm{M}_s^{he} C_s}{2}\frac{dT_s^{he}}{dt} = -\dot{m}_s C_s\left(T_s^{he} - T_s^{he,in}\right) - \frac{U_{s\leftarrow \mathrm{ss}}}{2}\left(T_s^{he} - T_{ss}^{he}\right) \quad (7)$$

On tube side of heat exchanger, the rate of change of coolant salt temperature equation consists of a coolant-to-coolant lump heat transfer term and a fuel salt to coolant salt heat transfer term. The heat transfer model used for the radiator is similar to that of the primary heat exchanger. Here also, the contributions from two equal lumps are considered in the two energy balance equations on both side of radiator.

3. Results and Discussions

MSDyn code is specifically being developed for studying the dynamic behaviour of Circulating Fuel Reactors (CFRs). The new development is used to study the effect of DNP drift in core, in external loop, pump start-up and pump coast-down transients [2]. The pump start-up transient is induced by delayed neutron precursors (DNP) drift along with fuel flow. During the fuel pump is start-up, the DNP drift due to increasing fuel flow rate and results in net loss of reactivity from the core. Variations of reactor power and reactivity are calculated using MSDyn during the pump start-up experiment. It is evident that reactor shows damped power oscillation for both types of fuel salts i.e., U-235 and U233 based salts due to DNP recirculation in core through external loop as shown in Fig. 2(a).



(a) (b)

Figure 2 Variation of power during the pump startup transient when reactor was at low power (a) and variation of power during pump coast-down transient when reactor was at full power (b)

In case of pump-coast down transient, fuel salt circulation stops within 20s and there would not be any loss of delayed neutron which result in reactivity gain. The reactor power starts increasing if the temperature coefficient of reactivity is not sufficiently negative. For the U-235 based fuel salt in the MSRE, reactor power first increases to the maximum of 8.28 MWth and then starts decreasing due to negative temperature feedback. This is because U-235 fuel salt have less negative temperature co-efficient as compared to the U-233 base fuel salt and therefore gain in the reactivity during the first few seconds of the transient could not by compensated by rise in temperature as shown in Fig. 2b.

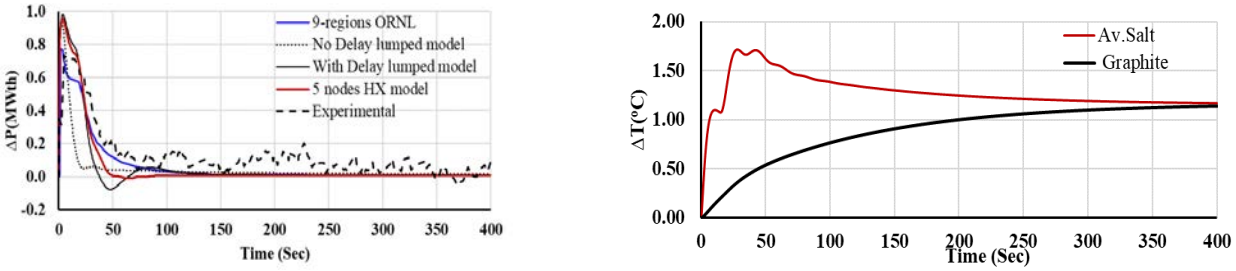


Figure 3 Dynamic response of MSRE at 5MWth for 19.6pcm reactivity insertion and variation of average fuel salt and graphite temperature during the transient.

The response of MSRE has been calculated for a step of 19.6pcm reactivity is inserted to MSRE when power was 5MWth [4]. Result is compared with experimental result obtained from the ORNL report [5-7]. It is evident from Fig 3 that reactor power sharply increases to peak value and quickly damps towards initial power level. This is due to the fact that rise in power is very sharp accompanied with increase in fuel salt temperature which gives negative feedback to counterbalance the inserted reactivity. A plateau is observed while power is decreasing from peak power. The inlet temperature of the fuel salt does not change as warmer fuel salt from the core outlet has to traverse through piping, heat exchanger and then again piping connection. It takes about 17s for salt to flow into the reactor core and thus inlet fuel salt temperature remains same as it was before the reactivity insertion.

4. Conclusion

In this work, a new development in MSDyn code is carried out to simulate the non-linear dynamics of MSRE type reactor plant. The development includes closed loop circulation of DNP, 5 nodes model of primary heat exchanger, 4 node model for secondary heat exchanger i.e., radiator with pure time delay model for fluid transport in piping connections between the core and the heat exchanger as well as between the heat exchanger and radiator. For validation of the new developments, time responses of MSRE have been calculated for step reactivity insertions at different power levels. Results of MSDyn model of MSRE have been compared with ORNL model and with the experimental results for U-235 and U-233 based fuel salts. It is found that the MSDyn model overestimate the power peak for all cases. However, longer time response and overall trend of the transient agrees well with the reference results. Moreover, MSDyn shows close agreement with the reference results based on same mathematical model.

5. References

[1] S. J, Ball, T.W. Kerlin, “Stability Analysis of the Molten-Salt Reactor Experiment”, Technical Report, *ORNL-TM-1070*, December-1965.

[2] Indrajeet Singh, Anurag Gupta and Umasankari Kannan, “A Program to Study the Molten Salt Reactor Dynamics: MSDyn-1”, Report No.: *RPDD/MSR/February-2020/37*

[3] R.C. Steffy, Jr. P. J. Wood, “Theoretical Dynamic Analysis of the MSRE with 233U Fuel” *ORNL-TM- 2571*, July 1969.

[4] Steffy Jr., R.C., “Experimental Dynamic Analysis of MSRE with ^{233}U Fuel”, *ORNLTM-2997*. Oak Ridge National Laboratory.

[5] Robertson, R.C., “MSRE Design and Operations Report Part I: Description of Reactor Design”, *ORNL-TM-0728*. Oak Ridge National Laboratory,1965.

[6] Vikram Singh et al., “Nonlinear dynamic model of Molten-Salt Reactor Experiment –Validation and operational analysis,” Annals of Nuclear Energy 113 (2018) 177–193.

[7] H. Guymon, “MSRE Systems and components performance”, Technical Report *ORNL-TM-3039*, 1973.

BURNUP SIMULATION RESULTS FROM UPGRADED MCBURN AND COMPARISON WITH OTHER CODES

Debasmit Sarkar[1], K. K. Gupta[2] and K. P. Singh
Bhabha Atomic Research Centre, Mumbai, India
e-mail: - [1]*debasmit@barc.gov.in*, [2]*kkgupta@barc.gov.in*

Abstract

Depletion code McBurn has been upgraded with the intent of large-scale deployment for practical purposes. The upgraded McBurn has been validated with different standard problems and international benchmarks. In this paper, McBurn results for NEA computational benchmark problem for VVER-1000 LEU Assembly is presented. Also, McBurn results for PHWR 37 pin bundle is compared with CP method based lattice code ITRAN. Infinite multiplication factor, concentration of important isotopes and power distribution estimated by McBurn are found to be in good agreement with the benchmark specified results as well as ITRAN estimated results.

1. Introduction

McBurn [1] is a depletion code which solves Bateman equations for a nuclear reactor fuel system. It is coupled with a Continuous Energy Monte Carlo (CEMC) particle transport code which simulates the transport of neutrons through the given system and estimates various nuclear reaction rates. From these known reaction rates and concentration of isotopes, McBurn estimates the new concentration of isotopes after a given burnup. It also prepares a new input for CEMC code with updated concentration of isotopes. This completes calculation of one burnup step of appropriate size and can be repeated any number of times for complete calculation for any given amount of fuel burnup. Flow chart of a burnup calculation using McBurn is shown in Figure 1.

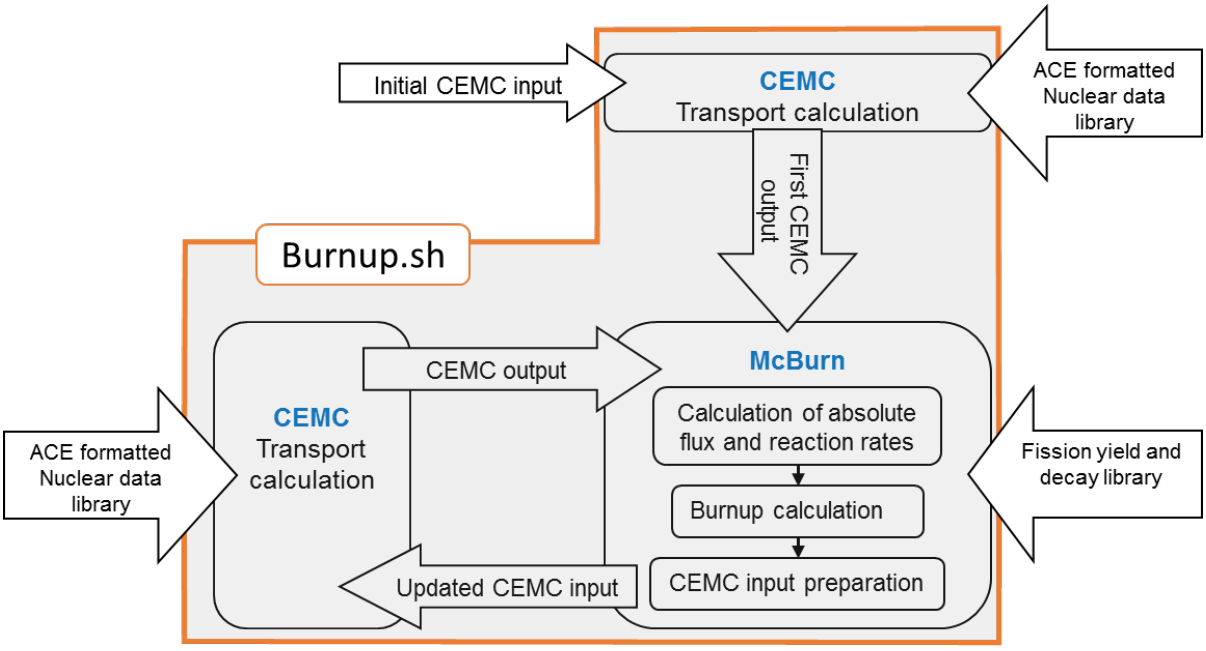


Figure 1 Flowchart of burnup calculation using McBurn.

McBurn was originally developed at Theoretical Physics Division, Bhabha Atomic Research Centre, Mumbai [1]. Coupled with CEMC transport code, it is a useful tool for performing burnup calculations for reactors where applicability of traditional deterministic neutron transport codes is limited. For calculations presented in this paper ENDF/B-6.8 nuclear data is used for CEMC based neutron transport code, while burnup library associated with McBurn consisting of Decay and Fission yield data are based on evaluations in Ref. [2].

2. Improvements in McBurn

McBurn has been recently upgraded with intent of large-scale deployment for practical purposes. Some of the major highlights of modifications made in the code are listed below:

- Modules responsible for reading the CEMC output have been modified with efficient algorithms.
- Bateman equations for different burnup zones are not coupled to each other. Hence they are solved simultaneously on different processors in parallel computing architecture. For inter-processor communication, MPICh-2.0 is used.
- Search algorithms of ~ O(N) has been replaced with that of ~ O(1) using a pointer based indexing technique.
- For identification and proper treatment of a nuclide at different temperatures, CEMC input format associates three characters (extension) along with ZAID of the nuclide. Provision has been included also in McBurn to consider these isotopes with different extensions separately during burnup.

Implementation of above features and modifications have significantly reduced the running time of McBurn and have enhanced its capability of handling practical problems. In subsequent sections, validation of McBurn against benchmarks and conventional codes are discussed.

3. VVER-1000 Assembly lattice Benchmark

VVER-1000 Assembly hot condition benchmark [3] was employed to validate the code McBurn. The benchmark problem assembly consists of 300 LEU pins of 3.7%eU, 12 IFBA pins of 3.6%eU and 4% Gd_2O_3. Light water containing 0.6g/kg of boron is used as moderator.

This problem was solved using McBurn and results were compared with benchmark values given in Ref [3]. In **Figure 2** a comparative plot of k-inf estimated by McBurn along with benchmark specified results are given. Standard deviation in all k-inf values estimated by CEMC code is ~10^{-4}. In **Figure 3**, isotopic concentrations of few major isotopes with burnup estimated by McBurn and benchmark values are plotted. All estimates from McBurn are well within the variance of benchmark specified results. Detailed analysis of the benchmark problem using McBurn can be found in

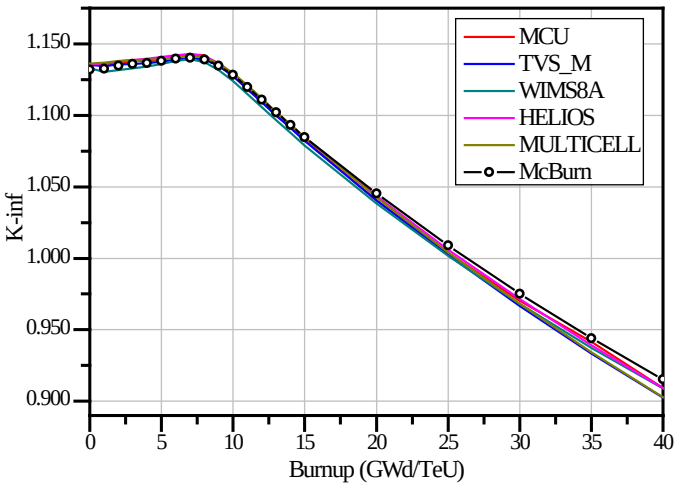


Figure 2 Comparison of k-inf estimated by McBurn with VVER-1000 assembly benchmark values

Ref [4].

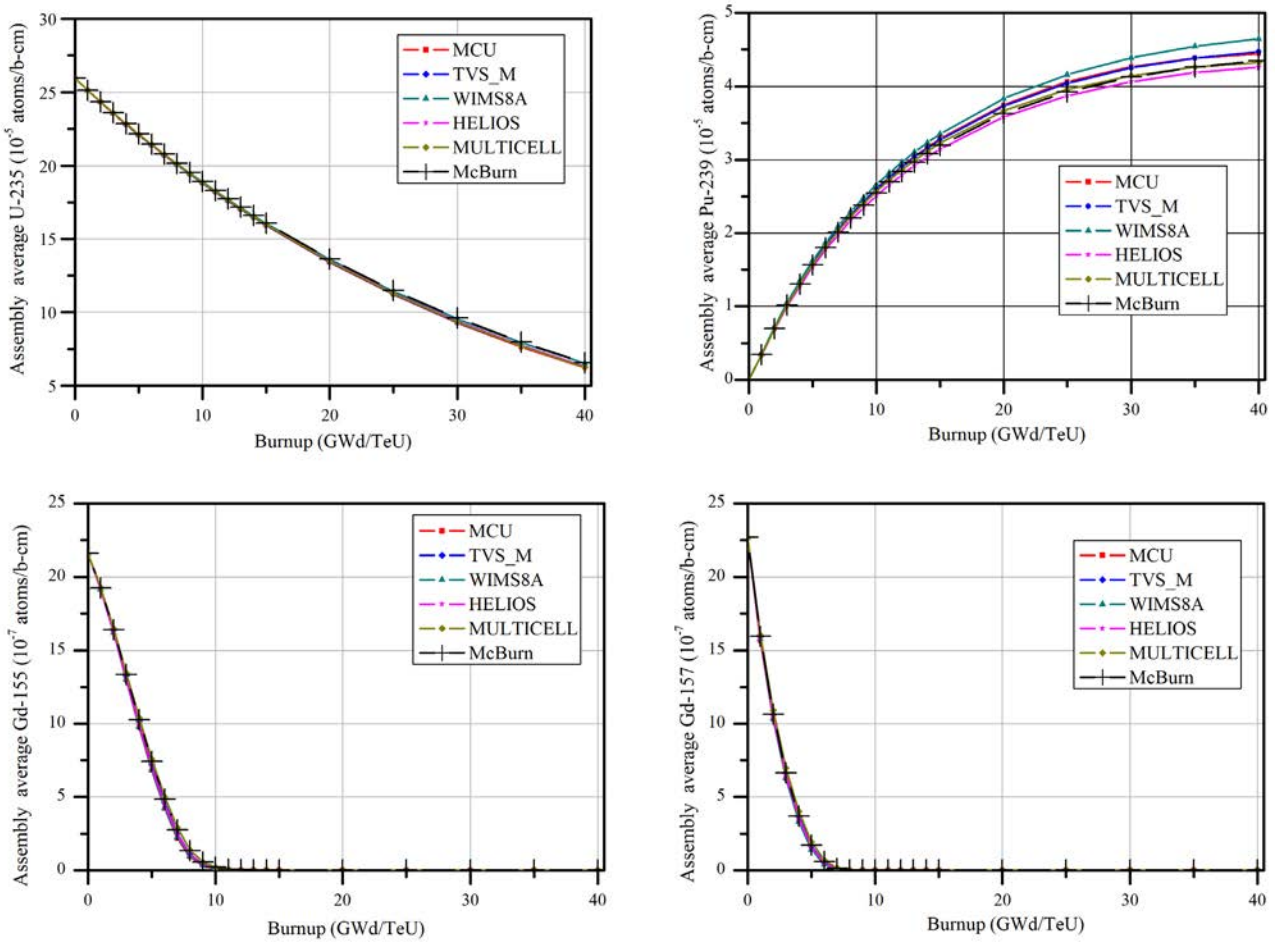


Figure 3 Comparison of assembly averaged inventory of major isotopes by various codes for VVER-1000 assembly

4. PHWR 37 pin bundle fuel lattice

Burnup of PHWR 37 pin bundle fuel lattice [6] consisting of 37 fuel pins was simulated in cold condition using McBurn and results were compared with code ITRAN [5]. ITRAN is a CP method based deterministic lattice burnup code, widely used for PHWR operations. ENDF/B-6 nuclear data library in WIMS 69 energy group format was used to generate results using ITRAN for comparative studies reported here. In **Figure 4** k-inf with burnup estimated by the two codes are plotted. Standard deviation in all k-inf values estimated by CEMC calculations is ~ 10^{-5}. At high burnup of ~11GWd/TeU, McBurn over estimates k-inf by ~0.3%.

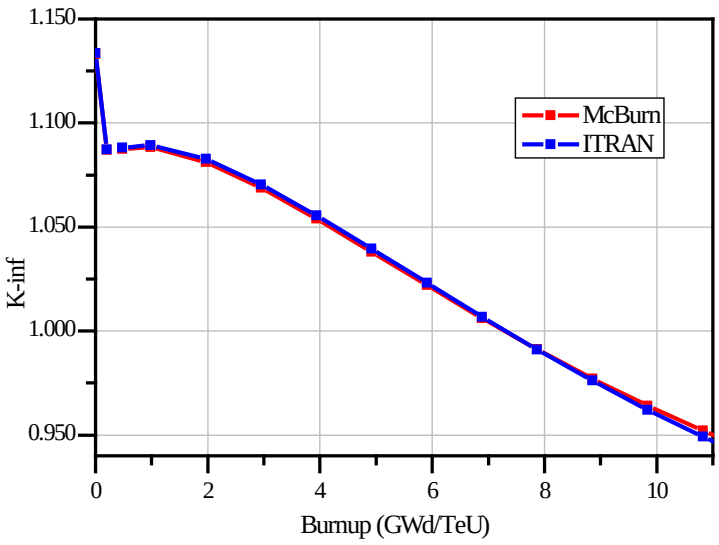


Figure 4 Comparison of k-inf estimated by McBurn with ITRAN for PHWR bundle

Ring power factor at the same burnup is shown in **Figure 5**. The max difference in ring power factor estimated by the two codes is less than 1.5%. Inventory of some important isotopes estimated by the two codes were compared and results are shown in **Table 1**. It can be seen that differences between McBurn results and that of ITRAN are within acceptable range.

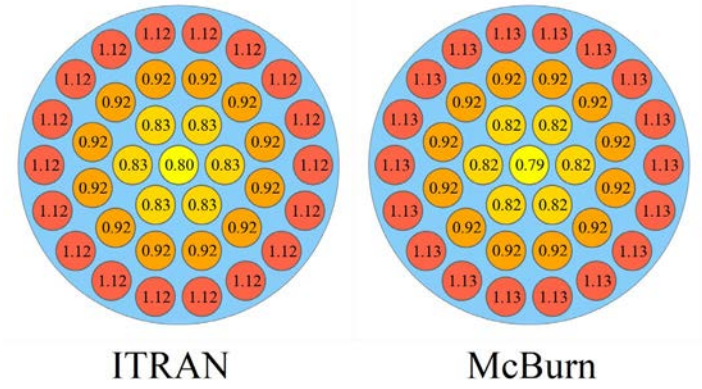


Figure 5 Ring power factor at ~11GWd/TeU

Table 1 Inventory of isotopes estimated by McBurn at ~11 GWd/TeU relative to ITRAN

Isotope	% Difference
Xe135	0.53
Rh105	-2.9
U235	-0.5
U238	0.5
Pu239	1.6
Pu240	-1.1
Pu241	-1.1
Pu242	-2.7

Comparison of McBurn results with other well established codes for few other fuel pins and reactor lattices are given in Ref. [6].

5. Conclusion

In this report a brief description of code McBurn and major highlights of modifications done in the code is given. VVER-1000 assembly NEA benchmark is employed to validate the code McBurn. Burnup of PHWR 37 pin bundle fuel lattice is simulated using McBurn and results are compared with code ITRAN. Integral and differential lattice parameters estimated by McBurn was found to be in satisfactory agreement with other codes. This report establishes the validity of the code McBurn.

6. References

[1] B. Ghosh and S. B. Degweker, "Physics of Accelerator Driven Sub-critical Systems & Development of a Monte Carlo Burnup Code **McBurn**", *ARP-S2-IT-04*.

[2] T. R. England and B. F. Rider, "Evaluation and Compilation of Fission Product Yields", *LA-UR-94-3106*, October 1994.

[3] OECD/NEA, "A VVER-1000 LEU and MOX Assembly Computational Benchmark", ISBN-92-64-18491-0.

[4] Debasmit Sarkar and K. P. Singh, "Validation of McBurn using VVER-1000 LEU Assembly benchmark problem", Technical Report No. : RPDD/RP/31, December 06, 2021

[5] P. D. Krishnani, "Input Preparation of the computer code ITRAN", Note No. RPDD/ RP/11, June 23, 2006.

[6] Kapil K. Gupta, Debasmit Sarkar and K.P. Singh, "Burnup simulation results from McBurn and comparison with other codes", Technical Report no. RPDD/GEN/56, March 21, 2022.

ANALYSIS OF AER MIDICORE VVER-1000 CORE PERIPHERY POWER DISTRIBUTION BENCHMARK

L. Thilagam[1], K. Obaidurrahman[2], and D. K. Mohapatra[1]
[1] Safety Research Institute, NSARG, Atomic Energy Regulatory Board, Kalpakkam, India
[2] Safety Research Institute, NSARG, Atomic Energy Regulatory Board, Mumbai, India

[1]*e-mail: - thilagam@igcar.gov.in*

Abstract

Prediction capability of open-source Monte Carlo (MC) code OpenMC is evaluated for Atomic Energy Research (AER) proposed MIDICORE VVER-1000 core periphery power distribution benchmark. The results like Infinite neutron multiplication factors (k_∞) at lattice level and the core physics parameters viz., effective neutron multiplication factors (K_{eff}), relative fuel assembly (FA) power distributions and relative pin power distributions are calculated and compared with the BM results and literature values. Comparison shows that the results of OpenMC code are at par with the other international state-of-the-art codes for all parameters of interest.

1. Introduction

The MIDICORE benchmark (BM) is a 2D theoretical benchmark [1] based on the VVER-1000 reactor core cold state geometry taking into the account explicit radial reflector modelling. It was proposed in the 20th symposium of Atomic Energy Research (AER) on VVER Reactor Physics and Reactor Safety by the working groups A&B of AER. The objective of this benchmark is to provide reference solution for validation of the codes for pin-by-pin power distribution in selected fuel assemblies (FA) that are present mainly at the peripheral regions of the VVER-1000 core. The present study is an effort to evaluate the prediction capability of OpenMC code [2] for MIDICORE VVER-1000 core periphery power distribution benchmark.

2. Description of AER MIDICORE VVER-1000 benchmark model

A brief description of the BM model is presented here. Detailed specification of the BM model, regarding the geometrical and material information, is available in AER symposium paper [1]. The horizonal cross-sectional view of the BM model, comprising of 10 fuel assemblies (FAs) in 1/6th symmetry, is shown in Figure 1. As shown in the figure, the BM model is a 2D model restricted only to a small part of the core at the basket near the periphery. It is based on the cold state geometry of the VVER-1000 reactor vessel. The inner edge of the reactor pressure vessel is the outer boundary of the BM model in the radial direction. The core segment with the FA mapping and numbering can also be seen in Figure 1 which shows that the BM model employs four different FA types: A200, A40E6, P36E9 and P40E9. Out of four FA types, three employ gadolinium oxide mixed uranium oxide (UGD) fuel pins as burnable absorber. Like all other VVER-1000 FA designs, the fuel pins within a FA are arranged in regular hexagonal lattice with a pitch of 1.275cm. Each FA has 331 lattice locations, where 312 locations are occupied by fuel pins, 18 locations by guide tubes, and 1 central channel for instrumentation. FA pitch in cold state is 23.6 cm. The core structure in an axial direction is assumed to be an infinitely uniform. In radial reflector regions, as shown in Figure1 there are several cylindrical water holes with the diameter of about 70 mm in the basket. The distances of the holes centre from the inner edge of basket are 75 mm and 150 mm, respectively. Additionally, a thin water gap of 3 mm thickness can be seen between the edge of core basket and the edge of peripheral FAs.

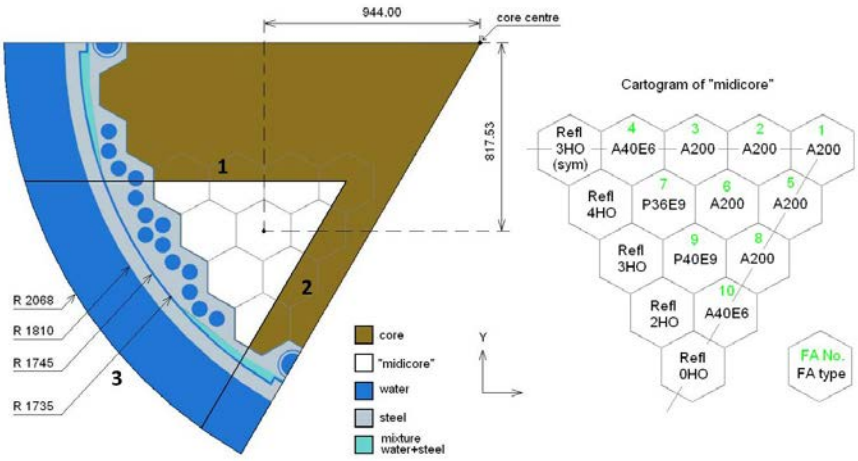


Figure 1 AER MIDICORE VVER-1000 Benchmark Model

Reference calculations were carried out using a MC code, MCNP with the following conditions: (1) 2D calculation with the reflection boundary conditions in axial directions and on the azimuthal surfaces numbered as 1 and 2 in Figure 1 and a vacuum boundary condition on the cylindrical outer boundary numbered as 3, (2) Temperature of all fuel and non-fuel materials is 600 K, (3) Cold state geometry and densities of materials except for coolant which is assumed a density 0.66108 g/cc at 600 K & 15.7 MPa, and (5) No Rod Cluster Controlled Assemblies (RCCA) are inserted in the guide tube locations.

3. Computational methodology

Open-source MC code OpenMC [2] developed by Computational Reactor Physics Group (CRPG) of Massachusetts Institute of Technology (MIT) is used in the present analysis. The code OpenMC can model complex geometries in full 3D detail employing continuous energy cross section in ACE format. Input is provided in XML (eXtensible Markup Language) format and output is written in either binary or HDF5 format, a Hierarchical Data Format (HDF). In OpenMC simulations, all FA variants with no symmetry and the MIDICORE VVER-1000 in $1/6^{th}$ symmetry are modelled in a similar way as described in the benchmark report [1]. All simulations have been carried out employing the lib80x, LANL released ENDF/B-VIII.0 based ACE data files. For S (α, β) treatment of hydrogen in water, thermal neutron scattering law data generated at the temperature 600 K is used. The KCODE option is used employing 400 million neutron histories (2050 active cycles with 200,000 neutrons each, and 50 discarded cycles for converging the source distribution), leading to statistical uncertainties as low as 7.0×10^{-5} in the multiplication factors and 1.0×10^{-3} in the pin power distributions on the 1σ level. Assumptions in the modelling are: (1) the water holes in the basket are modelled as per specification in the VVER-1000 MOX core benchmark [3] and the grooves are excluded from the modelling.

4. Results and discussions

The Infinite neutron multiplication factors (k_∞) calculated for different FA variants of MIDICORE BM are compared with the literature values [4] in Table 1 with the respective deviations. Comparison indicates that the k_∞ calculated using OpenMC are at par with the other literature values for all FA variants. The effective neutron multiplication factors (K_{eff}) calculated using OpenMC model is 1.03970 (ENDF/B-VIII) against the benchmark reported MCNP values of 1.04530

(ENDF/B-VI) and 1.03576 (JEFF-3.1). The deviation (OpenMC(ENDF/B-VIII) - MCNP(ENDF/B-VI)) % of OpenMC simulated K_{eff} with respect to the reference MCNP simulation is -0.56%.

Table 1 Infinite neutron multiplication factors (k∞) for various FA types of MIDICORE BM

FA Type	Infinite neutron multiplication factors (k_∞)		
	OpenMC / Deviation (OpenMC -MCNP(Ref.)) %	Literatures [4]	
		MCNP (Ref.)	MULTICELL
A200	1.07634 / -0.23	1.07861	1.07167
40E6	1.21519 / -0.76	1.22281	1.21420
36E9	1.15333 / -0.67	1.16005	1.15152
40E9	1.18252 / -0.80	1.19049	1.18061
Nuclear Data	ENDF/B-VIII	ENDF/B-VI	Unknown

OpenMC simulated relative FA power distribution with the respective percentage deviations from BM is given in Figure 2. Comparison shows good agreement with the BM results and the deviations observed are within ± 2.3% for relative FA power. Though the BM results on relative pin power distributions are available for three FAs viz., No. 6 (A200), No. 7 (36E9) and No. 9 (40E9), as a demonstration plot, the relative pin power distribution calculated by OpenMC is given in Figure 3 for peripheral FA No. 7 (36E9) with the respective percentage deviations. For FA No. 6 (A200), located away from the periphery, the deviations are found to be within -0.8 to 1.1 %. For peripheral FAs, No. 7 (36E9) and No. 9 (40E9) involving UGD fuel pin cells, slightly larger deviations are observed. For peripheral FA No. 7 (36E9), the deviations for non-UGD fuel pin cells are found to be within ±2.2% and larger up to -7.9% for UGD pin cells. Similarly, for peripheral FA No. 9 (40E9), the deviations for non-UGD fuel pin cells are found to be within ±3.1% and larger up to -7.8% for UGD pin cells.

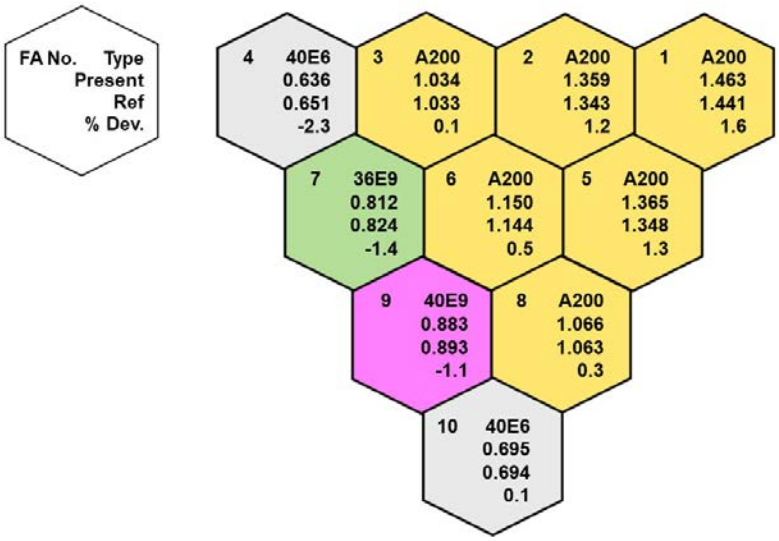


Figure 2 Comparison of relative FA power distributions for the MIDICORE VVER-1000 model

5. Conclusions

Analysis of AER MIDICORE VVER-1000 core periphery power distribution benchmark has been carried out using the open-source OpenMC code. The results like Infinite neutron multiplication factors (k_∞) at lattice level and the core physics parameters viz., effective neutron multiplication factors (K_{eff}), relative FA power distributions and relative pin power distributions are calculated and

compared with the benchmark results. The study in general demonstrates the good prediction capability of OpenMC code for such analysis of VVER-1000 core with complex heterogeneities.

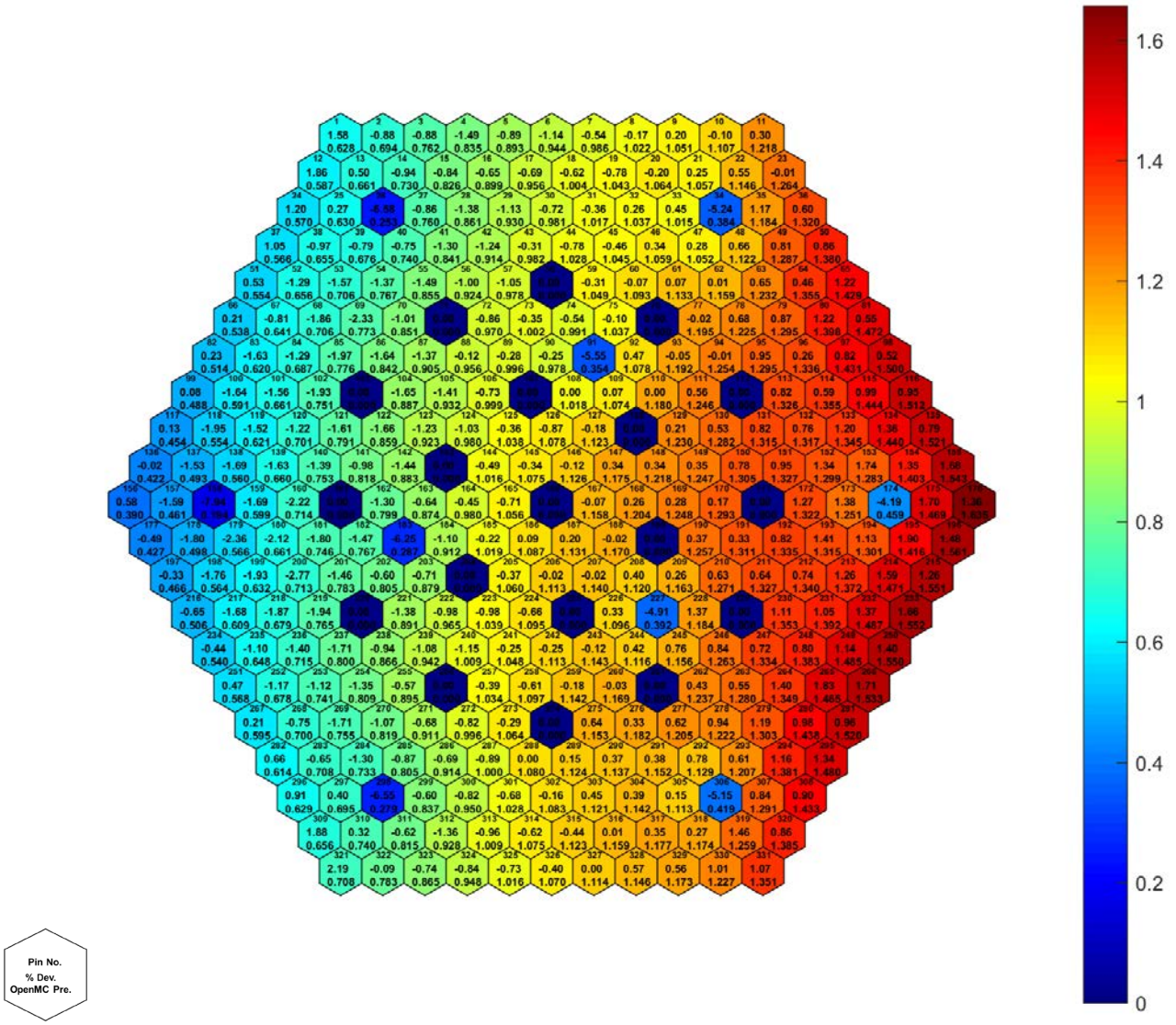


Figure 3 Comparison of Relative pin power distribution for peripheral FA No. 7 (36E9) (Reflector facing sides on left)

6. References

[1] Václav Krýsl *et al.*, "MIDICORE VVER-1000 Core Periphery Power Distribution Benchmark Proposal", 20th SYMPOSIUM of AER on VVER Reactor Physics and Reactor Safety, (2010).

[2] Paul K. Romano *et al.*, "OpenMC: A State-of-the-Art Monte Carlo Code for Research and Development," *Annals of Nuclear Energy*, 82, 90--97 (2015)

[3] NEA/NSC/DOC (17), "VVER-1000 MOX Core Computational Benchmark", OECD/NEA, (2005).

[4] Georgy *et al.*, "Calculations of a Postulated Stylized Small Region of a VVER-1000 Core by KARATE code and MCNP", 20th International Conference on Nuclear Energy for New Europe (2011).

Estimation of Na-24 Activity for An Open Pool Type Research Reactor

M. Hansda[1], A. Sharma[1] and S. Sengupta[1]
[1] Bhabha Atomic Research Centre, Mumbai, India
[1]*e-mail: - hansda@barc.gov.in*

Abstract

Open pool type research reactor is very much user friendly for the researchers because of its easy accessibility from the pool top for various irradiation experiments. However, the open pool type reactor design should ensure the pool top radiation field very low based on the ALARA (as low as reasonably achievable) principle. Hence assessment of pool top radiation field is essential for the design of this type of reactors. Out of all the radionuclides, Na-24 is the major contributor of radiation field at the pool top. Therefore, estimation of Na-24 activity in the reactor pool and the coolant system for open pool type nuclear research reactor is very important from the point of view of radiation safety. This paper presents the validation and verification of the theoretical modeling of estimating Na-24 activity in an open pool type research reactor. The saturation activity of Na-24 at different locations has been estimated and compared with measured data from the reactor.

1. Introduction

Coolant activity in an open pool-type research reactor is very important in view of operational and radiological safety considerations. As pool water acts as the shielding medium to minimize the radiation dose at the top of the reactor pool, an estimation of radionuclides in pool water is essential to establish the safety of the operating personnel and researchers working at the reactor pool top [1]. Na-24 ($T_{1/2}$=15.0 hrs) is one of the most significant radio-nuclides in terms of radiological safety during the normal operation and also after shutdown of any pool type nuclear research reactor. Na-24 is generated by the neutron activation of Al-27 in the reactor from $Al^{27}(n,\alpha)Na^{24}$ reaction [2]. In pool type research reactor, demineralized water is used as a primary coolant and aluminium is used as structural material and also fuel clad. The other radio-nuclides like Mg-27 ($T_{1/2}$= 9.46 m), Al-28 ($T_{1/2}$=2.31 m), N-16 ($T_{1/2}$=7.13 sec), N-17 ($T_{1/2}$=4.2 sec), O-19 ($T_{1/2}$=29.4 sec) etc. are also produced due to activation of aluminium and water. But among all these nuclides, only Na-24 is radiologically significant because it has relatively larger half-life. In an open tank pool type reactor, radiation field at the pool top where operational personnel may work frequently, is mainly governed by Na-24. The short-lived radio-nuclides viz N-16, N-17 and O-19 die out drastically in the delay tank as well as in the piping and cannot reach at the pool top. The radio-nuclides Mg-27 and Al-28 also will not reach at the pool top because there is sufficient float up delay in the reactor pool water. Hence, the estimation of Na-24 activity in this type of reactor is necessary to predict the pool top radiation level and also for the shielding requirement of the coolant system equipment room.

As an example, the estimation of Na-24 activity was done for Upgraded Apsara reactor (Apsara-U). The Apsara-U is a 2 MWt swimming pool type research reactor loaded with Low Enriched Uranium (LEU) in the form of U_3Si_2 dispersed in aluminium matrix as fuel, light water as coolant & moderator and Beryllium Oxide as reflector. The Apsara-U attained First Approach to Criticality (FAC) on 10th September, 2018. It uses aluminium as material of construction for fuel clad, reflector vessel and irradiation thimbles. In this paper, a theoretical estimation of Na-24 concentration in reactor pool water has been carried out. The calculation methodology has number of steps [3] which are mainly categorized into two viz., (i) Source term estimation in reactor core and (ii) Saturation activity estimation in pool water. To validate the theoretical modelling and assumptions, measurements of Na-24 activity were also carried out. The water samples were

collected from the core exit (before delay tank) and the hot water layer and the reactor pool. The theoretical results are compared with the measure data and show a very good agreement.

2. Source estimation of Na-24

The activation reaction $Al^{27}(n,\alpha)Na^{24}$ takes place where the fast neutron flux is sufficiently available, because it is a threshold reaction (>3.74 MeV neutron energy). The Na-24 source term is estimated by finding the activation reaction rates in the effective coolant volume of the reactor core. The activation reaction rate in volume V can be expressed as

$$S_c = N\sigma\phi V \tag{1}$$

where, N is the number density of the parent nuclide, ϕ is the total neutron flux and σ is the average microscopic cross section of activation reactions. The following subsections describes the calculation methodology of finding group wise neutron flux, spectral averaged cross sections and the effective volume of aluminum [4].

Step-1: Evaluation of neutron spectrum

Energy group wise neutron flux in aluminium clad is calculated by using the computer code WIMSD. Here 172 energy group of WIMS library is used for better resolution in the fast energy range.

Step-2: Spectrum averaged cross-sections

The threshold neutron energy for production of Na-24 is 3.74 MeV. So, the energy in the range from 3.74 MeV to 20 MeV (maximum energy of the incident neutron) is divided into 8 energy groups and in each group the flux average cross-section is calculated. The following expression is used for obtaining the flux averaged cross-section.

$$\bar{\sigma} = \frac{\sum_i \phi_i \sigma_i}{\sum_i \phi_i} \tag{2}$$

Where, ϕ_i and σ_i are the point wise neutron flux and the microscopic cross-section (obtained from ENDFB-VIII library) respectively.

Step-3: Effective volume of aluminium

Radionuclide Na-24 is produced in the aluminum clad and depending on their recoil kinetic energy and direction, it will come into the coolant. Total Na-24 produced in the whole volume of aluminium do not contribute to the activity of coolant. Only those Na-24 isotopes which traverse the aluminium clad thickness and reach the clad-coolant interface, contribute to the activity of coolant. This thickness is called Effective Thickness (ET) of aluminium in which the produced activation products have non-zero probability of passing to the coolant [5]. To calculate the ET, we need to find the kinetic energy of activation products, their range in aluminium and probability of their release into coolant based on solid angle. The expression of calculating the effective volume using ET is

Effective volume of aluminium (V) = *Total surface area of Al* x *Transmission Coeff.* x *ET* (3)

3. Theoretical Modelling to estimate Saturation activity in pool water based on coolant system flow scheme

The reactor core of Apsara-U is cooled by demineralized water which is flowing from top to bottom to minimize the radiation field at the pool top. The primary coolant system consists of delay tank which provides an average delay time of about 2 minutes. A tapping from the primary coolant circuit goes through the purification system for maintaining the pool water chemistry. Activity of Na-24 in pool water and coolant is estimated by modeling the nuclide balance equation of pool and coolant system. For simplification, uniform temperature throughout the pool water is assumed with reactor operating at constant power. The schematic diagram of primary cooling system of Apsara-U is shown in Fig.-1. The thermal hydraulic parameters used for the analysis is shown in Table-1.

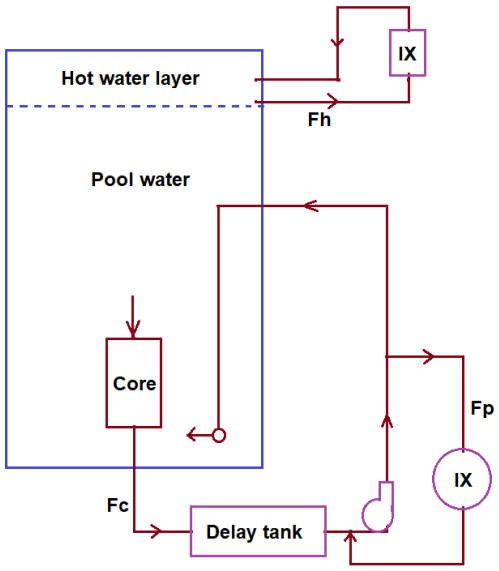


Figure 1: Schematic diagram of pool and coolant system

Table-1: Thermal hydraulic parameters of Apsara-U	
Parameters	***Value***
Volumetric flow rate through the core, F_c (lpm)	4900
Volumetric flow rate of purification system, F_p (lpm)	100
Volumetric flow rate of Hot Water layer (HWL) purification system, F_h (lpm)	200
Rate of Na-24 generations in the core, S (atoms/s)	3.21 E+10
Volume of pool water of Region-1, V_1 (cm^3)	2.28 E+08
Volume of the hot water layer, V_h (cm^3)	2.9 E+07
Clean up efficiency of ion-exchanger in HWL system, f_{hwl}	0.9
Clean up efficiency of ion-exchanger in Purification system, p_{ix}	0.9
Diffusion coefficient of Na-24, D (cm^2/s)	1.33 E-05
Diffusion thickness between region-1 and Hot Water Layer (HWL), Δz (cm)	10
Radioactive decay constant of Na-24, $\boldsymbol{\lambda}$ (s^{-1})	1.2833 E-05
Area of the pool, A (cm^2)	2.9 E+05
Total circulation time, t_p (sec)	120

According to this model pool water is divided into two regions like (i) Region-1 (pool with normal water) and (ii) Region-2 (1.0 m thick hot water layer region). If n_c, n_1 and n_h are the Na-24 concentrations at the core outlet, region-1 and hot water layer respectively, the time dependent nuclide balance equation in three regions can be expressed as

$$\text{Core exit}: n_c F_c = n_1 F_c + S \tag{4}$$

$$\text{Region-1: } V_1 \frac{dn_1}{dt} = n_c F_c (1 - f_{pcw}) e^{-\lambda t_p} - n_1 F_c - DA \frac{n_1 - n_h}{\Delta z} - V_1 n_1 \lambda$$

$$f_{pcw} = \frac{p_{ix} F_p}{F_c + p_{ix} F_p} \tag{5}$$

$$\text{HWL: } V_h \frac{dn_h}{dt} = DA \frac{n_1 - n_h}{\Delta z} - f_{hwl} n_h F_h - V_h n_h \lambda \tag{6}$$

The activity of Na-24 is estimated by solving the above coupled equations simultaneously using Euler method. The nomenclature of the above equations is given in Table-1.

4. Measurement of Na-24 activity

In order to measure the Na-24 activity, water samples were collected at the core exit before delay tank and at different height of the pool water at 2MW reactor operation. The Na-24 activity of the water samples were measured with the gamma ray spectroscopy as shown in Table-2.

5. Results and validation

The saturation activity of Na-24 at core exit, pool water and hot water layer have been estimated with theoretical modelling and compared with measured activity. The Table-2 shows very good agreement of the theoretical values with that of the measured data. The maximum deviation in results is less than 10% except in the hot water layer where the data cannot be quantified due to low value.

Table 2: Specific activity of Na-24

Location	Theoretical prediction (Bq/ml	Measured data (Bq/ml)
Core exit	91	100
Pool water (region-1)	88	86
Hot water layer	0.1	<1.5

6. Conclusion

A theoretical modelling was done to estimate the Na-24 activity in an open pool type research reactor. The modelling was based on assumptions (i) uniform temperature throughout the pool water with reactor operating at constant power, (ii) no convective flow mixing between pool water and hot water layer and (iii) homogeneous mixing of radio-nuclides within the pool water and also within the hot water layer. Measurements of activity were done from sample taken from core exit, pool water and hot water layer. Analysis methodology was validated by comparing the estimated value with the measured activity and good agreement was observed.

7. Acknowledgement

The authors wish to express their profound gratitude to Mr. C. G. Karhadkar, Director RG and Mr. Kunal Chakrabarty, Head ROD for their continuous support & expert guidance and Mr. Shibu Thomas, RS and Mr. Sanjit Pal, ARS of Apsara-U for providing necessary help & support for this study. Authors would also like to thank the technicians and operators of Apsara-U for their assistance to do the research work.

8. References

[1] "Modelling and simulation for coolant activity and dose rate estimation in a pool-type nuclear research reactor", V K Veluri, S Sengupta, S Mammen, S Bhattacharya, Nuclear Technology, 204 (2018) 227

[2] S. Glasstone & A. Sesonske, "Nuclear Reactor Engineering", 4th Edition, Vol.-1

[3] "Estimation of Primary Coolant and Pool water Activity in HFRR", BARC Report, BARC/2015/E/017

[4] James Wood, "Computational Method in Reactor Shielding", 1st Edition, 1982, eBook ISBN:9781483148137

[5] "Estimation of aluminium and argon activation sources in HANARO coolant", Byung Jin Jun, Byungchul Lee and Myong-Seop Kim; Nuc. Eng. Tech. 42 (2010) 434

Transient Analysis of VVER-1000 X2 benchmark with ARCH code

Argala Srivastava, D.K. Dwivedi and Umasankari Kannan
Bhabha Atomic Research Centre, Mumbai, India
e-mail: - argala@barc.gov.in

Abstract

This paper presents VVER-1000 X2 benchmark transient analysis carried out using 3D space-time code ARCH developed at BARC. The VVER-1000X2 benchmark with modern fuel assembly design was proposed for validating and verifying package of the codes and data libraries for steady-state and transient calculations. The benchmark includes fuel assembly modeling, fuel assembly data preparation, reactor core modeling and space-time simulations of the core. In this paper, we have analyzed the transient data obtained for the unit 2 of the NPP Khemelyntska with ARCH code. The data includes the variation of the reactor power with time due to scram for the reactor period of less than 10 s. The predicted results are compared and observed to be well in agreement with the experimental data.

I. Introduction

The work presented in this paper describes the transient analysis of an international VVER-1000 X2 Benchmark. This benchmark was proposed during the 19th and 20th AER symposium in2009 and 2010 [1]. The benchmark is based on theVVER-1000 operational data of the second unit of the KhmelnitskyNuclear Power Plant (NPP) located in Ukraine. The unit was operational in 2004 and was one of the first VVER-1000 units fully loadedwith fresh TVSA fuel type.Table 1 gives the core details of the benchmark.The benchmark comprises of several core loadings using TVSA assemblies with different enrichment as well as different pin numbers with burnable absorber and weight percentage of the burnable absorber material Gd_2O_3 mixed with different enriched UO_2 fuel.Table 2 gives the description of fuel types used in cycle 3 .The benchmark is divided into three parts:-1. Fresh core hot zero power (HZP) experiments;2. The depletion part containing core layouts and operational historyof the first four fuel cycles as well as measured power distributionsnapshots for selected time points of each cycle.3.The transient part contains documented information on theoperational transients that occurred at the unit during the third cyclesuch as reactor SCRAM, xenon oscillations, and a main coolantpump trip. This benchmark is useful for validating and verifying the whole system of codes and datalibraries for reactor physics calculations including fuel assembly modeling, fuelassembly data preparation, few group data parameterization and reactor core modeling for steady-state as well as in transient conditions. Several international lattice codes; HELIOS, WIMS, CASMO, and core codes; DYN3D, TRAPEZ, SERPENT, and BIPR have been used to perform the steady-state and transient analysis of this benchmark [1]. The paper aimsto assess the prediction capability of the space-time diffusion based code ARCH [2]forthe transient calculations, which are compared with the experimental data and with other international code systems.

2. Description of the ARCH Code

The neutronics code (**A**nalysis of **R**eactor Transients in **C**artesian and **H**exagonal Geometries) ARCH solves the multi-group diffusion equation discretised with the finite difference scheme in both space and time. For space, it uses the Finite Difference Method (FDM). For temporal variation, the code has a fully implicit (backward Euler differencing) based module, which is

unconditionally stable and simple in implementation in addition to a module based on an efficient IQS scheme. ARCH is capable of simulating the reactor core with both Rectangular and Hexagonal/Triangular-Z lattices. In the hexagonal option, user can choose to define number of triangles filling a hexagon and also fill materials in individual Triangular-Z meshes. The numbering scheme used for hexagonal modeling in ARCH code is shownin Fig. 1. The diffusion equation is solved over each mesh by accounting for flux continuity conditions between meshes. For the solution of generalized eigenvalue problems of the type $Ax = \lambda Bx$, where A and B are matrices, several options are available in ARCH: conventional Power Iterations, Orthomin, OrthoFS and CGNL. ARCH uses a cross-section data library for the reactor containing macroscopic cross-sections generated using a lattice transport code for each fuel type. This code can be used for analyzing the K-eigenvalue problem, External Source with/without Multiplying Medium, Reactor Transients, Xenon Spatial and Transient Effects, Core Depletion, Higher Eigenmodes, Time Average Computation and Thermal Hydraulics Feedback.

3. Reactor SCRAM due to signal Reactor Period < 10 s.

The transient related to VVER1000 X2 benchmark available are SCRAM, xenon oscillations, and a main coolant pump trip. The transient initiated by SCRAM is analyzed in this paper.
The reactor scram was actuated during the 3rd cycle at the moment 231.53 EFPD. The reactor state at the beginning of the transient was: Thermal power N_T = 2990 MW; Position of the working control group no. 10 is 90.3% of the core height, control groups 1-9 are in full out condition. Due to the automatic switch-off of the one feed water pump, the automatic power control actuated the load dump from full to 40-50% by dropping the respective control group no. 2. By that time thermal power was reduced to 75% of the full power. Then the necessary power level was adapted by the working group no. 10. Soon after that, the reactor protection system actuated a SCRAM due to the protection signal “Reactor period T < 10 sec.” Reactor power with time was recorded.

4. Results and Discussion

Five group condensed cross-sections for each fuel type were generated with EXCEL Code [3] for the simulation.The cross-sections of each fuel type and burnup profile are read by the code. Figure 2 gives the distribution of the fuel assemblies for cycle 3. Convergence criteria of 10^{-4} and 10^{-5} for flux and eigen value respectively are are used as iteration limits. The steady-state Keff for the cycle 3 at 231.53 EFPDwas estimated to be 1.0001. The IQS method is used for the transient simulations. The time steps used for simulating reactor SCRAM condition is 140 msec. Figure 3 shows the variation of the estimated neutron power with time for SCRAM transient. As can be from the figure there is drop in power up to 2 sec by dropping control group 2 and then power is raised by raising control group 10 up to 4 sec and it then followed by a SCRAM action due to reactor period less than 10 sec. The results are compared with the experimental data and with those reported by DYN3D simulation. There is a maximum deviation of 6% from the experimental value.

5. Conclusions

In this paper, we have analyzed the SCRAM transient data obtained for unit 2 of the NPP Khemelyntska with the ARCH code -. The data includes the variation of the reactor power with time due to scram for the reactor period of less than 10 s. The results are comparing well with the

experimental data within the 6 % deviation. In the future, other transients of the VVER-1000 X2 benchmark likexenon oscillations and a main coolantpump trip will be studied with the ARCH code.

References

1. T. Lotsch, V. Khalimonchuk, A. Kuchin, ‘ Corrections and additions to the propositions of a Benchmark for core burn up calculations for a VVER 1000 Reactor, Westendst, 199, 80686, Ukarine.
2. Gupta, Anurag, 2017. ARCH- A 3-D core simulations tool. Proceedings of 3rd DAE-BRNS Symposium on Advances in Reactor Physics (ARP-2017), Anushakti Nagar, Mumbai, India, Dec 06-09, 2017.
3. Lattice Analysis of VVER 1000 Benchmark using EXCEL Code System Argala Srivastava, R. Karthikeyan and Usha Pal, RPDD/LWRPS/005, 2021.

Table-1 – VVER 1000 X2 Core Details

Thermal Power	3000MWt; 1000MWe
Cycle length	~300 effective full power days
Fuel	Enriched UO_2
No. of FAs / Fuel Rods per FA	163 / 312
Core height & diameter	3.55m,
Coolant inlet temp	291°C
Coolant outlet temp	321°C
No. of CPSARs ($B_4C + Dy_2O_3.TiO_2$)	61 (cycles-1 to 4)

Table-2 – Description of the fuel types

FA	Enrichment w/o %)	No. of UO_2 pins/enrichment	No. of Gd Pins (w/o Gd_2O_3/U^{235})
22AU	2.2	312/2.20	--
30AV5	2.99	303/3.00	9(5.0/2.4)
39AWU	3.90	243/4.0 60/3.60	9(5.0/3.3)
390GO	3.90	240/4.00 66/3.60	6(5.5/3.3)
398GO	3.99	306/4.40	6(5.0/3.3)
430GO	4.30	240/4.40 66/4.00	6(5.0/3.6)
439GT	4.39	306/4.40	6(5.0/3.6)

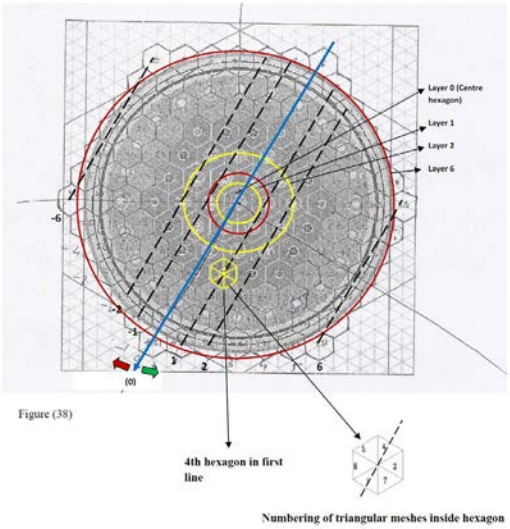


Figure 1 Modeling of Hexagonal Core in ARCH Code

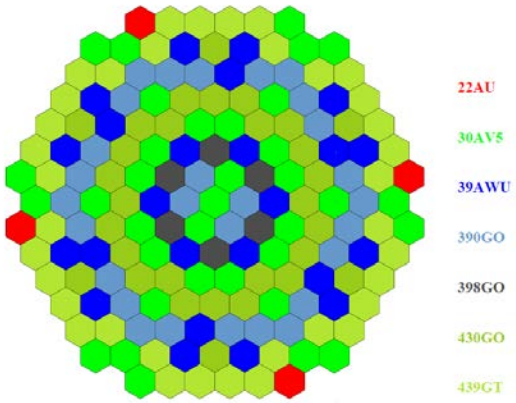


Figure 2 Distribution of fuel assemblies in Cycle-3

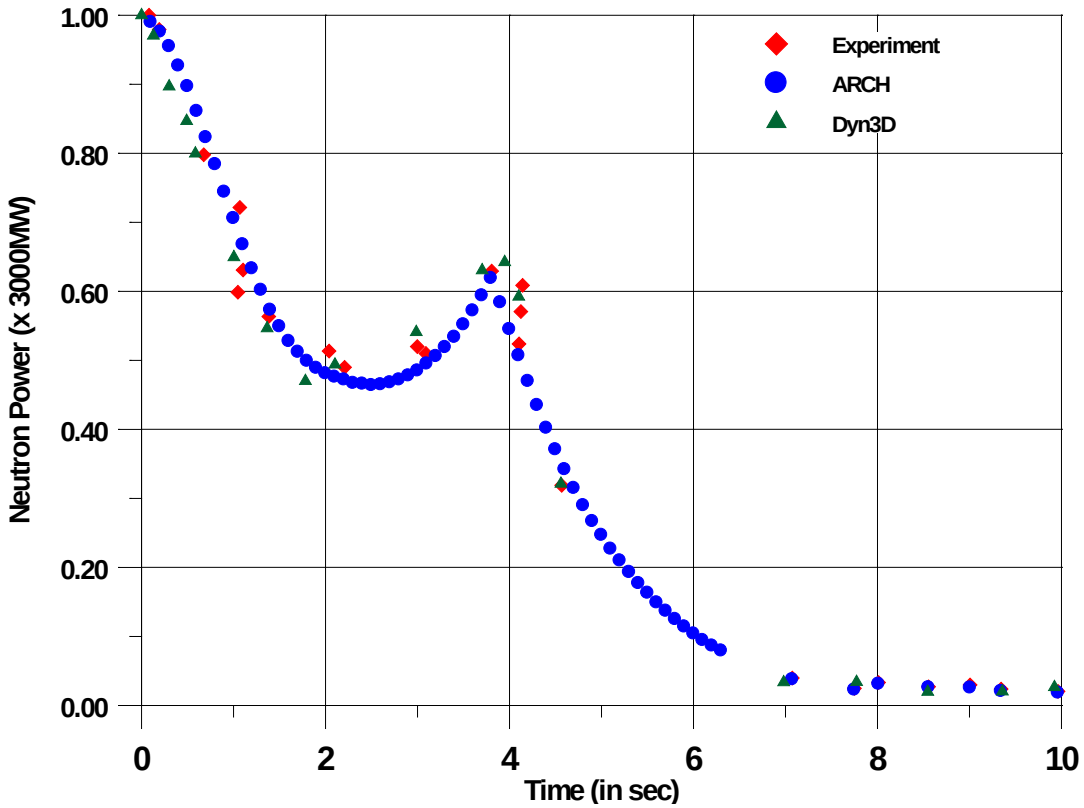


Figure 3 Reactor Power during transient "SCRAM due to reactor period T<10 s

METHODS & TECHNIQUES DEVELOPED IN CODE ARCH FOR 3D CORE TRANSIENTS OF PRESSURIZED HEAVY WATER REACTORS

Taresh Aggarwal*, D.K. Dwivedi, Anurag Gupta, Umasankari K
Bhabha Atomic Research Centre, Mumbai, India
e-mail:- taresh@barc.gov.in*

Abstract

A 3D space-time neutronics code ARCH based on multi-group neutron diffusion theory has been developed at RPDD, BARC. The numerical methods and techniques applied in the code have been successfully validated with several reactor benchmark problems. The qualified code has been extensively used for the design and safety analyses of the square and triangular-Z lattice-geometry based cores of Indian reactors for the last two decades. Recently, the modelling in the code has been suitably advanced to also consider the traverse movement of reactivity devices in the horizontal cores of Indian Pressurized Heavy Water Reactors (PHWRs) during the transients. The PHWRs are heavy water-moderated & cooled thermal reactor cores loaded with natural uranium fuel bundles at different burnup levels in equilibrium conditions. The core shutdown and regulation rods in PHWRs are inserted parallel to core radial direction in the inter-space moderator region of the fuel channels. The absorber rods reach the active core zone at different moments after the actuation of the shutdown system due to their traverse movement through the cylindrical surface. The paper briefly discussed the modeling and technique in the code for PHWRs and presents the results of a steady-state and transient case investigated with code ARCH using a representative data set of PHWR core.

Key words: 3D space-time code ARCH, nuclear core design and safety, PHWR, reactivity transients.

1. Introduction

The Indian PHWRs are designed and operated as natural uranium fuelled, heavy water moderated and cooled pressure tube type horizontal reactor cores. Currently, 16 units of PHWR-220MW are operating in various parts of the country and 2-units of PHWR-540MW at Tarapur, Maharashtra. The installation and operation of several 700 MWe PHWRs are planned in fleet mode. Recently India's first 700 MWe PHWR went critical at Kakrapar in Gujarat. PHWRs are designed to operate with natural uranium fuel, thus eliminating the requirement of fuel enrichment. Heavy water is used both as a moderator & coolant, which are separated physically as well as thermally from each other, unlike PWRs [1]. For the safe, economical & smooth operation, the dynamic behaviours of the cores are investigated and ensured at the design level. As safety is the highest priority right from the design stage to the commencement of long term commercial operations of these reactors, reactor physics plays a pivotal role in this regard.

The unintentional transients in PHWR cores could be initiated due to events like the positive reactivity insertion in the core due to accidental loss of regulation, voiding of coolant under any leak out from the heat transport system, darning of Liquid Zone Controls (LZCs) in 540 & 700 MWe PHWRs, pump failures etc. These events contribute directly or indirectly to the addition of positive reactivity in the core leading to a surge in power. There are designed control devices & safety systems to arrest the power surge and rise in peak temperature well below the safety limits. These devices get actuated timely after sensing such events. Detailed analysis of such transient scenarios

through computer simulations enables us to understand the consequences before happening, where the ability to mitigate and handle these scenarios is also tested. In this paper, the simulation results of code ARCH for a steady-state and transient case with a representative data set of PHWR core are discussed with a brief description of the technique in the code intended to PHWRs [2, 3].

2. 3D space-time code ARCH and simulation techniques for PHWRs

2.1. *Brief description of code ARCH*

ARCH (Analysis of Reactor transients in Cartesian and Hexagonal geometries) has been developed at Reactor Physics Design Division (RPDD), BARC as a comprehensive tool for various time-dependent neutronics analyses in both rectangular as well as triangular-Z lattice-geometry based designs. The code is based on diffusion theory and uses advanced sparse Krylov subspace solvers for the efficient solution. It is developed in F-90/95 with a modular structure and is user/developer-friendly. Recently ARCH has been integrated with RELAP5 for coupled Neutronics-TH analysis of AHWR. The code has options to perform simulations of operational and anticipated transients in addition to Core-follow-up & Refuelling; Xenon spatial transients; predication of multiple higher modes; Subcritical analysis with external neutron-source etc. [2]. 3D space-time code ARCH has neutronics capability for design and safety analyses of thermal-spectrum nuclear cores. The code has two modules for reactor transients: 1) Fully Implicit (FI) module based on direct integration of multigroup neutron flux using backward Euler and 2) computationally efficient Improved Quasi-Static (IQS) module [3]. Recently the code has been advanced to consider the traverse movement of reactivity devices for PHWR transients, a module added to compute the change in cross-section parameters in case of coolant voiding with a formulated function, model to consider the speeds of absorber rods through the lattice meshes of different burnup levels in the core [4]. These modelling and techniques in code ARCH for 3D space-time analyses of PHWRs are discussed in the next sub-section.

2.2. *Modelling of PHWR for the 3D core simulation*

The steady-state simulation of a 3D core is performed to calculate the parameters like power distribution, power peaking factor, peak channel power, reactivity coefficients and worth of reactivity devices. These parameters are essential to the safe and economical operations of nuclear reactors. The transients in an operating reactor core could be initiated via factors like the inadvertent movements of rods for reactivity regulation and control, or any imbalance in the rate of heat production to that of removal by the coolant etc. The positive reactivity in perturbations leads to reactor transient, consequently a surge in the core power. The coolant channel voiding in PHWRs results in the addition of positive reactivity. The coolant voiding phenomena are considered in simulation with the 3D neutronics codes like ARCH by changing and updating the macroscopic cross-section parameters at each calculation time step. As positive feedback of coolant voiding leads to a rise in core power, the transient need to be arrested by the shutdown system. However, an increase in power production raises the fuel temperature promptly, which would also introduce negative reactivity feedback because of Doppler's effect.

A steady-state of a PHWR core and the core transient initiated due to coolant voiding are investigated with in-house developed code ARCH. In the transient case, the power surge is assumed to be arrested by the actuation of the shutdown system without fuel temperature feedback. The actuation of the shutdown system comprising neutron absorber rods is considered with a time delay after the trip signal is generated at sensing the rise in the initial power level at a predefined value. As

PHWR cores are inclined horizontally, control and absorber rods move in the radial direction, i.e. perpendicular to the core axis, unlike the control devices in AHWR & conventional PWRs. The inception of rods through guide tubes located between the axial pressure tubes (with fuel bundles of different burnups) are realised at different moments in the active core due to their positions over cylindrical core surface. The movements of control rods are assumed by changing the macroscopic cross-sections of the meshes lying in the radial direction of the core map. As required input for the transient in code ARCH, the speeds of rods have been calculated from the rod drop characteristic (Table-1). Some results of code ARCH for the steady-state and transient are discussed in the next section. The transient is the case of coolant voiding in PHWR followed by activation of the shutdown system without fuel temperature feedback. The transient simulation with fuel temperature feedback is planned after suitable advancement in the multi-physics code system ARCH-RELAP5 [5] either using indigenous multi-physics code ARCH-TH under development at RPDD BARC [6].

Table-1: The calculated speed of shutoff rods insertion in the PHWR core for input in the code

Mesh no.	***Time (s)***	***% IN core***	***Speed (cm/s)***
0	0.000	0	0
1	0.252	4.3478	113.4
2	0.408	8.6957	200.2
3	0.566	13.043	176.6
4	0.688	17.391	328.9
5	0.782	21.739	274.1
6	0.886	26.087	
7	0.992	30.435	235.0
8	1.116	34.783	
9	1.199	39.130	411.0
10	1.316	43.478	329.0
11	1.377	47.826	376.0
12	1.480	52.174	
13	1.541	56.522	
14	1.609	60.870	
15	1.703	65.217	
16	1.760	69.565	
17	1.853	73.913	299.0
18	1.948	78.261	306.0
19	2.060	82.608	193.0
20	2.193	86.957	
23	4.497	100	60.0

Table-2: Normalized power distribution for 15th row at 12th axial plane in steady-state

Mesh #	***Power value ($\times 10^4$)***
4	1.0755
5	1.3420
6	1.5407
7	1.6229
8	1.5270
9	1.5243
10	1.5500
11	1.5690
12	1.5878
13	1.5811
14	1.5743
15	1.5743
16	1.5811
17	1.5878
18	1.5690
19	1.5500
20	1.5243
21	1.5270
22	1.6229
23	1.5407
24	1.3420
25	1.0755

3. Results and Discussion

The steady-state with a representative data set of PHWR core is performed with code ARCH to predict the parameters like power distribution (Table-2). The analyses of coolant voiding transient followed by scram in the core have been carried out with IQS and FI module of code ARCH and compared. The variation in normalized total core power during the transient is shown in Fig. 1. The net dynamic reactivity is also estimated with the code during the transient (Fig. 2). Initially, the core power increases because of positive reactivity feedback from coolant voiding. In the simulation, the trip set point is

chosen to be at 1.1 times the initial operating power. At 1.1 times the initial, the shutdown system is activated with a time delay of ~ 0.6 s. The transient power keeps rising during delay time while the peak value is observed at around ~1.4 s. The power reaches around ~3.25 times the initial level. With the insertion of shutoff rods, the negative reactivity introduced in the core leads to power setback and shutdown finally in 3.0 s of the transient. The results successfully demonstrate the simulation capability of 3D space-time code ARCH developed at RPDD, BARC.

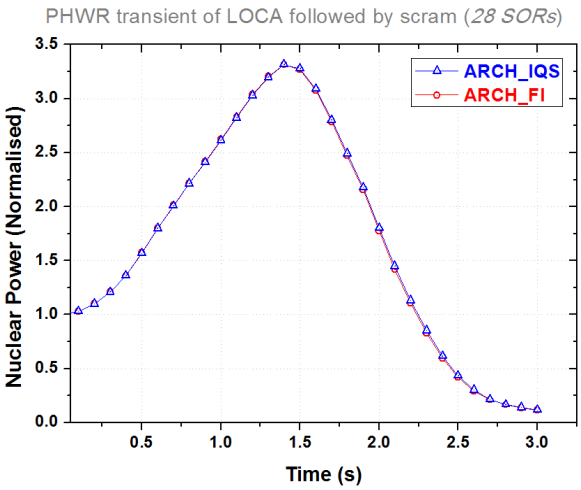


Fig. 1: Variation of normalized core power during transient of coolant voiding followed by scram

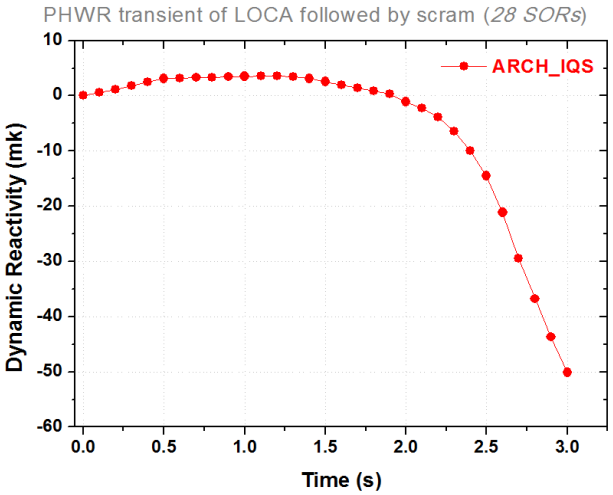


Fig. 2: Dynamic reactivity during the transient duration of coolant voiding followed by scram

4. Conclusion

The indigenously developed and benchmark validated neutronics code ARCH has been advanced for 3D space-time simulations of Indian Pressurized Heavy Water Reactors (PHWRs). The methods and techniques used in the code have been briefly discussed, especially in the case of a coolant voiding transient in a PHWR core. The considerations of control and shutoff rods movements in the case of PHWRs, which differ from the scenarios of AHWR & PWRs, have been highlighted. The simulation results of steady-state and a postulated case of coolant voiding transient followed by scram in PHWR core have been presented and analyzed. The results demonstrate the capability of in-house code ARCH for 3D neutronics simulations of PHWRs for reactor design and safety. The code capability could be enhanced next for PHWR transients with fuel temperature feedback.

References:

[1]. Physics of Nuclear Reactors, Edited by P. Mohanakrishnan, O.P. Singh, K. Umasankari, Academic Press, 2021.

[2]. Anurag Gupta. ARCH: a 3D space–time analysis code in cartesian and hexagonal geometries. In Proceedings of NSRP 19, Mamallapuram, TN, 12–14 Dec 2012.

[3]. Dwivedi el al. IQS module in code ARCH. Proceedings of ARP-2013, Mumbai, October 23–25.

[4]. Dwivedi et al., 2021. Report No.: RPDD / PHWR / 65 / November-2021

[5]. Aggarwal et al., "Simulation of Larger Duration Multiphysics Transients in AHWR with Coupled ARCH+RELAP5 Code System", Proceedings of ARP-2017, Mumbai, Dec. 6-9, 2017

[6]. Dwivedi et al., 2020. . Nuclear Engineering and Design, 370, 110881.

Estimate of spatial influence of neutron flux monitoring with SPNDs in AHWR

Anupreethi B.[2], Umasankari Kannan[1,2] and Anurag Gupta[1,2]
[1,] Reactor Physics Design Division, B.A.R.C., Mumbai, India
[2]Homi Bhabha National Institute, Mumbai, India
e-mail: - uma_k@barc.gov.in

Abstract

Spatial distribution of neutron flux is an important parameter which is required to be monitored for reactor control. The neutron flux is generally measured by a large set of distributed neutron monitors. Advanced Heavy Water Reactor (AHWR) is a boiling light water cooled thorium fuel based large sized reactor where heat removal is by natural circulation. The power distribution and control are very sensitive to the local perturbations and have to be effectively monitored. The core has been equipped as set of Self-Powered Neutron Detectors (SPNDs) for measuring the spatial distribution. AHWR core has been optimized with 28 locations provided for in-core detector housing (ICDH) unit, each proposed to be having six detectors distributed axially. The location of these ICDH units have been optimized using a clustering approach. The spatial influence of the SPND measurement has been determined in a detailed analysis by estimating the sensitivities when some SPNDs are missing. This paper will give an estimate of the spatial influence factor in the determination of neutron fluxes taking a few representative scenarios in AHWR.

1. Introduction

Large reactors if subjected to local perturbations, the neutron flux may lead to oscillatory behavior. These flux tilts have to be monitored and controlled. AHWR core has multiple burnup zones and also since boiling light water is used as coolant, there is strong coupling between neutronic power and heat removal aspects [1]. The flux variations are expected to be more as compared to pressurized water reactors. A typical flux distribution seen in AHWR is shown in Figure 1. SPNDs are the most appropriate neutron monitoring device that can be used inside the core. Flux mapping algorithms are used to reconstruct the flux shape in a reactor from the observed detector readings. The flux shape changes are manifested due to movement of control rods, changes in the coolant conditions, changes in local powers, refueling etc. A data driven approach has been used to optimize the location of in-core detector assemblies [2]. A correlation factor had been worked out and by clustering strongly correlated detectors, an optimized layout has been arrived at. A systematic simulation was done to optimise the ICDH locations from a possible 104 locations to 28 which can cater to the effective representation of operational and transient situations. Each of these 28 ICDH have six SPNDs distributed axially. The performance of detectors has been tested for a few operational scenarios such control rod movement, refueling and flux tilts due to

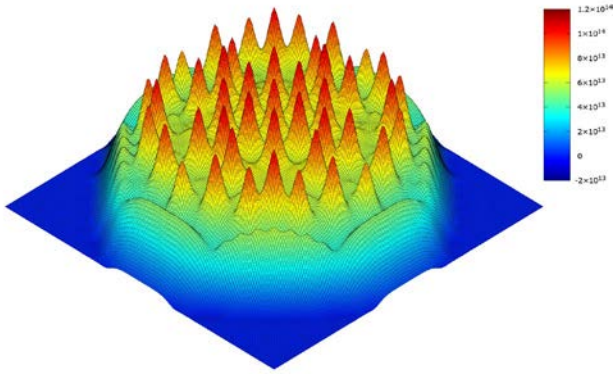


Figure 1. A typical steady state flux distribution in AHWR equilibrium core

xenon variations and the results were compared with a refence simulation [3]. In order to understand the influence that each in-core detector have spatially, few regions are chosen in the reactor core. Then the error in flux reconstruction is observed at these regions during absence of in-core detectors. This will help in understanding the influence each in-core detector have based on their geometrical placement.

2. Simulation methodology

For optimization of the number of ICDH units, a data-driven approach using the K-means clustering algorithm has been proposed [1]. The procedure involved the use of in-core detector measurements of few core flux shapes to group the in-core detectors based on relative correlation. The flux distribution and the detailed detector readings were calculated from a 3D diffusion theory code ARCH [4]. The in-core detectors within a cluster are strongly correlated and this property is used to arrive at the number and locations of in-core detectors. The flux reconstruction was performed using 35 eigen modes and the number of in-core detectors. [1]. Using the approach, the initial regularly spaced 104 ICDH units have been reduced to 28 ICDH units with 6 axially distributed SPNDs in each ICDH unit, giving a total of 168 SPNDs. The optimized layout of the 28 ICDH locations in AHWR is shown in Figure 2. The correlation factor matrix between the SPNDs threshold at midplane is shown in Figure 3.

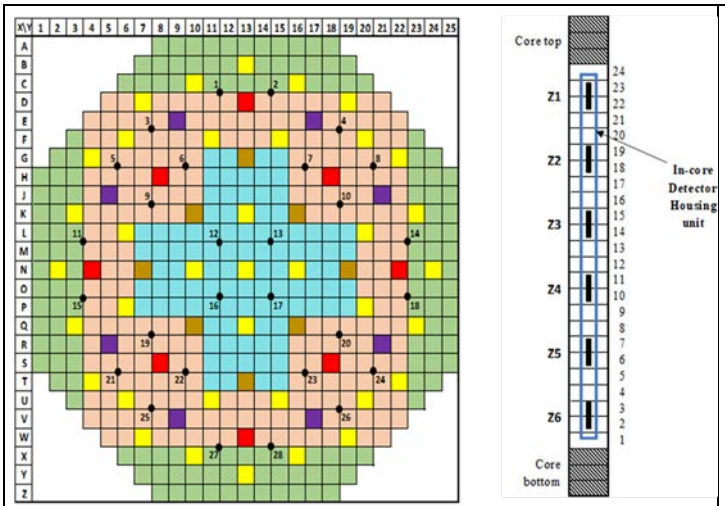


Fig 2. Layout of AHWR showing optimized location of ICDH and axial layout of SPNDs in an ICDH

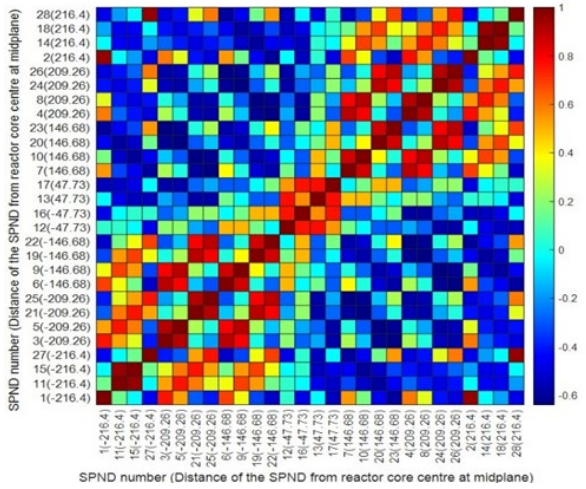


Fig 3. Correlation matrix between SPNDs in AHWR core (28 x 28)

As described earlier, in order to study the influence region of the SPNDs during normal operation, detailed simulation was done to estimate the error in mesh fluxes with respect to a reference simulation i.e.168 ICDHs were regularly placed. Three local regions designated as central zone CZ1, CZ2 and CZ3 were chosen in the core midplane as shown in Figure 4. The maximum error in the average neutron flux in the zone CZ2 when the individual SPNDs in that plane is missing has been estimated from first principles as deviation in the readings.

3. Results and discussion

The influence of each individual SPNDs on the reconstruction of neutron flux in any localised zone is derived from the detailed simulation by removing the corresponding readings from the ICDH. For

example, in order to estimate the influence of missing SPNDs in zone CZ2in the core midplane, 3D core simulation was performed with the missing SPND in that plane. This arises in 28 combinations. The spatial effect was then estimated by mapping the errors to the radial distance of the particular SPND to the zone of consideration i.e. CZ2. . Figures 5a through 5c gives the influence factor estimated from a sensitivity analysis due to the absence of SPND s in the core on each of the three zones considered namely CZ1, CZ2 and CZ3. It is seen that the SPNDs close to the region of consideration has maximum influence. The influence factor is found to be about 0.6 at distances of about ±87.5cm from the zone CZ2. This implies that the SPNDs a few pitches away from the local zone of consideration do not influence to a great extent in the reconstruction of the flux.

In order to cover the entire core simulations were done in several axial planes

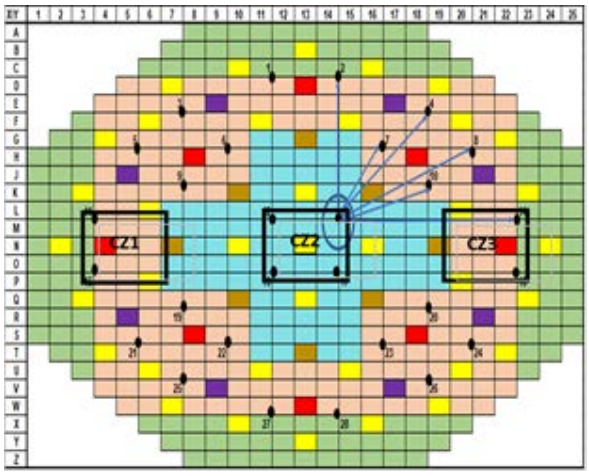


Fig. 4 Zones in AHWR layout for estimatation of influence factor of SPNDs

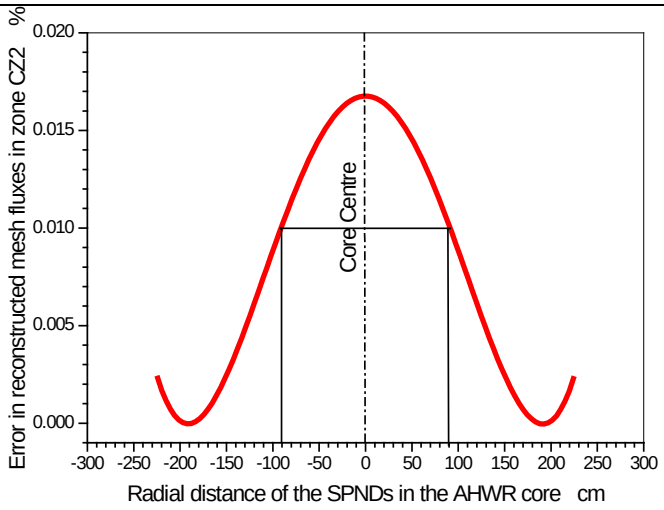
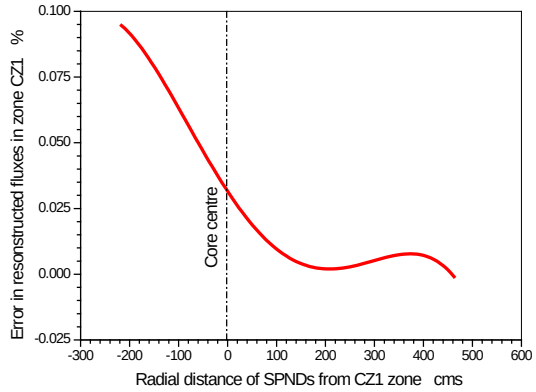
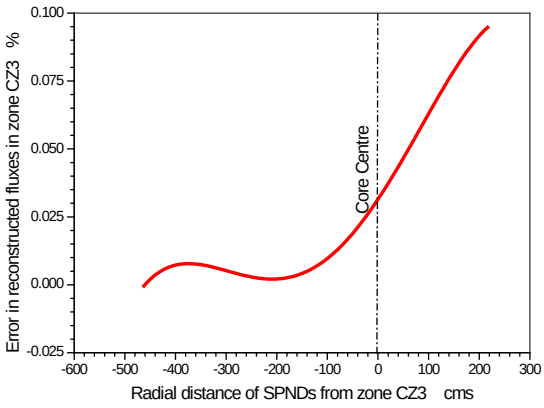


Fig. 5a Influence factor for flux reconstruction in CZ2 zone due missing SPNDs in central plane





AHWR core power distribution has the feature of being bottom peaked. To study this effect, two more planes one below the mid-plane (Z5) and one above was also considered (Z3) (see Fig.1). The result of the detailed sensitivity studies on the influence factor performed and translated to the radial distances from the regions of consideration is presented in Figure 6.

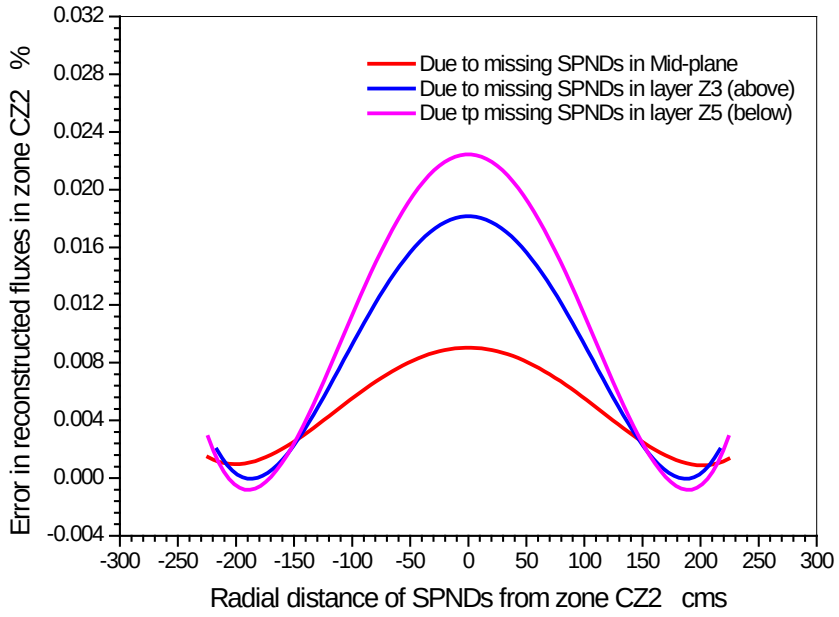


Fig. 6 Estimate of influence factor for flux reconstruction in the central CZ2 zone due missing SPNDs from Z3,Z4 and Z5 planes

4. Conclusion

The estimate of spatial region of influence of an SPND measurement is important for operational safety and has a bearing on the margins. The influence of detector readings on the flux reconstruction has been estimated in the equilibrium core of AHWR. This was estimated using a sensitivity approach where each SPND was excluded during the flux reconstructions. To simplify the study and to understand the region of influence, small specified regions were considered and the error in neutron fluxes in these regions was estimated with respect to a reference simulation where detailed set of 168 SPNDs were used. A spatial influence of greater that 60% for SPND measurement in AHWR core was found out to be ±87.5cm.

5. References

[1] Arindam Chakraborty et. al., "Safety Analysis Report (Preliminary) of AHWR," Doc. No. AHWR/SAR(P)/USI/01591, dated April 30, 2015.

[2] Anupreethi, B., Gupta, A., Kannan, U., Tiwari, A.P., 2020. Optimization of flux mapping in-core detector locations in AHWR using clustering approach. *Nucl. Eng. Des*. **366**, 110756.

[3] B. Anupreethi a, Vidya Sagar Yellapu, Anurag Gupta, Umasankari Kannan, Akhilanand Pati Tiwari, “Performance evaluation of AHWR flux mapping system during normal operational scenarios”, Nuclear Engineering and Design 390 (2022) 111686

[4] Gupta, A., 2012. ARCH-A 3D Space-Time Analysis Code in Cartesian and Hexagonal Geometries, in: National Symposium on Radiation Physics (NSRP-19). Mamallapuram, Tamilnadu.

A DESIGN STUDY FOR 500 MWe IPWR

Suhail Ahmad Khan and Umasankari Kannan
Bhabha Atomic Research Centre, Mumbai, India
email: - suhailak@barc.gov.in

Abstract

India is developing and designing domestic PWRs, called Indian PWR or IPWR, to augment the indigenous light water reactor program. To continue the design program, a 500 MWe IPWR is being designed. A preliminary design for equilibrium core of 500 MWe IPWR has been worked out. This design has 163 fuel assemblies. Each fuel assembly has 217 lattice locations. The design calculations have been performed using the indigenous VISWAM-TRIHEXFA code system. The present paper gives the details of the design and important core characteristics of the equilibrium core of 500 MWe IPWR.

1. Introduction.

India is developing and designing domestic PWRs, called Indian PWR or IPWR to have an indigenous capability for PWRs. A 2700MWTh/900 MWe IPWR has been designed earlier [1]. Currently, a 500 MWe IPWR is being designed. The designed operating power for this IPWR is taken as 1500 MWth. Enriched uranium oxide is used as fuel and batch refueling scheme is adopted for fuel cycle management. The fuel assembly (FA) of IPWR uses Gd as burnable absorber. The design calculations have been performed using the indigenous VISWAM-TRIHEXFA code system. The heterogeneous FA of IPWR is analyzed using the VISWAM [2, 3] to generate few group cross section library. The core calculation is performed using 3D diffusion theory code TRIHEXFA [4]. The brief description of IPWR lattice and core parameters are given in Section 2. Section 3 gives the brief description of the code systems used. Section 4 gives the result of the analysis followed by the conclusions in Section 5.

2. Description of 500 MWe IPWR

The previously designed 900 MWe IPWR FA has hexagonal FA having 331 lattice locations [1]. For 500 MWe IPWR, a newly designed FA having 217 lattice locations is considered as shown in Fig. 1. In this profiled FA, 204 lattice locations are used for fuel pins and 13 locations are to be used for control and instrumentation purpose. The 204 fuel pin locations are distributed into outer 48 pins with 2.6% enriched UO_2 fuel and inner 156 pins with 3% enriched UO_2 fuel. 15 fuel pins of inner fuel locations use 3% UO_2 with 3% Gd_2O_3 fuel as shown in Figure 1. The fuel pins of ID/OD 0.72/0.86 cm are arranged with pin pitch of 1.25cm. The clad material used is Zr alloy with 1% Nb. The ID/OD of guide tube is 1.05/1.20 cm.

The equilibrium core configuration for 500 MWe IPWR consists of 163 FAs arranged in a hexagonal lattice array of 18.8 cm assembly pitch shown in Figure 2. The core height is 285 cm. Soluble boron in moderator is used for burn up and xenon, Sm reactivity management. The cycle length is 480 effective full power days (EFPD). In the present study, the control and protection system is not considered. The control system will be designed and discussed in future calculations. A three batch mode of refueling scheme is used for fuel cycle management. The equilibrium core configuration is shown in Figure 2. The 163 FAs are distributed as 55/54/54 for three cycles as shown in Figure 2.

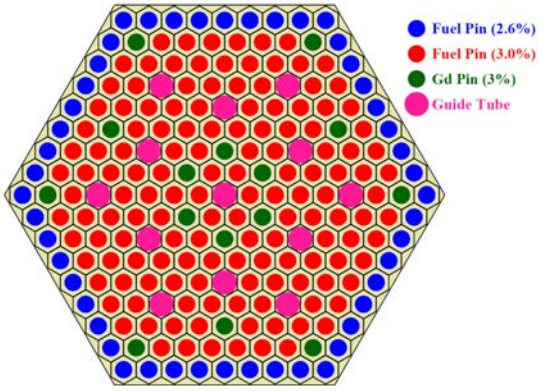


Figure 1 – Fuel Assembly Configuration

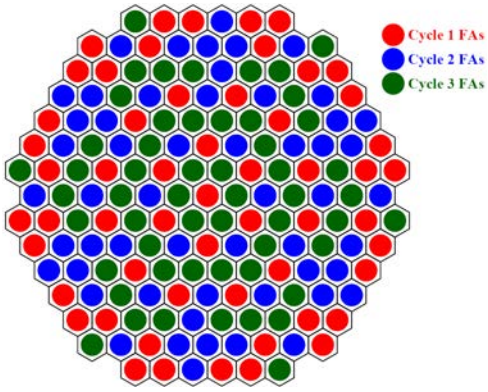


Figure 2 – Equilibrium Core Configuration

3. Nuclear Data and Calculation Tools

3.1 Nuclear Data Used

The present calculations have been performed using multigroup high temperature library 'HTEMPLIB' based on JEFF-3.1 nuclear data library [5]. This library has cross section data for 185 nuclides in 172 energy groups. The burnup chain in HTEMPLIB library is extended up to ^{252}Cf. The library has resonance tabulation for 48 nuclides. The resonance integral tables are available up to a temperature of 2500K.

3.2 Lattice Analysis code VISWAM

The lattice burnup code VISWAM has been indigenously developed to cater to the current and future requirements of reactor core design computations [2, 3]. There are two models available in VISWAM for FA burnup calculations.

One model is based on a combination of 1-D multi group transport and 2-D few group diffusion theory. A typical fuel assembly cell consists of fuel pins of different enrichments and various heterogeneous cells like control rod, water rod or burnable absorber rod (BAR) cells. In this model, the fuel pins are classified into various pin cell types based on the enrichment and Dancoff factors. The pin cells are treated using a series of 1-D transport calculations in multi-groups using the first flight collision probability method (P_{ij}). The square or hexagonal cell boundary is cylindricalised to allow 1-D treatment of the Wigner-Seitz cell. Heterogeneities present in the fuel assembly are treated using appropriate 1-D supercell simulations. The pincell homogenized cross sections are collapsed to few groups using appropriate supercell spectra. For non-fuel cells, the few group cross sections are obtained from the respective supercell calculation of a given heterogeneity. The fuel assembly cell is treated by 2-D few group diffusion theory using centre-mesh finite difference method.

The second model uses interface current method based on 2D collision probability. In this model, a lattice cell may be a fuel pincell, water rod cell or an absorber rod cell. The geometry of the cell is not changed, i.e., the outermost region of the cell is retained as the square or hexagonal shape without cylindricalisation. The collision probabilities are calculated for single lattice cell in 2D geometry. For fuel assembly (FA) calculation, the lattice cells are linked using interface currents by using the double P2 (DP2) expansion of angular flux at the pincell boundary. In this method, the neutron transport equation for group 'g' (the group index 'g' is omitted for

simplicity), when discretized over a region consisting of N_V zones and N_S surfaces reduces to linear flux and current equations (assuming flat flux approximation)

$$\Sigma_j V_j \phi_j = \sum_{\alpha=1}^{N_S} \sum_{\nu=0}^{N_\nu} P_{j\alpha}^{\nu} S_\alpha J_{-,\alpha}^{\nu} + \sum_{i=1}^{N_V} P_{ji}\, q_i. \quad (1)$$

$$S_\alpha J_{+,\alpha}^{\nu} = \sum_{\beta=1}^{N_S} \sum_{\mu=0}^{N_\mu} P_{\alpha\beta}^{\nu\mu}\, J_{-,\beta}^{\mu} S_\beta + \sum_{i=1}^{N_V} P_{\alpha i}^{\nu}\, q_i\,. \quad (2)$$

$$J_{-,\alpha}^{\nu} = \sum_{\beta=1}^{N_S} \sum_{\mu=0}^{N_\mu} A_{\alpha\beta}^{\nu\mu}\, J_{+,\beta}^{\mu}. \quad (3)$$

The summation over ν in above equations represents the order of expansion of angular flux at pincell boundary. Here $q_i = \Sigma_{si} V_i \phi_i + S_i V_i$ is the total source in region i, Σ_{si} is the self scattering cross section within the group and S_i is the fission and scattering source in a group given by

$$S_i = \left(\sum_{\substack{g'=1 \\ g' \neq g}}^{G} \Sigma_{si}^{g' \to g} \phi_i^{g'} + \frac{\chi_g}{k} \sum_{g'=1}^{G} \nu \Sigma_{fi}^{g'} \phi_i^{g'} \right). \quad (4)$$

Here, the symbols have their usual meanings. The results reported here have been obtained using the few group cross section lattice data generated using first model of 1D transport and 2D diffusion in VISWAM (PIJ=1) for obtaining quick results. A finally optimized design will be analyzed using PIJ=2 option.

3.3 Core Analysis Code TRIHEXFA

TRIHEXFA is a 3D diffusion theory code to perform the full 3D core calculation with burnup. It has been extensively validated against the many benchmarks and experimental data [4]. TRIHEXFA has been made compatible to the few group parametric database generated by lattice analysis code VISWAM. The simulation capabilities of TRIHEXFA have been improved by introducing new models like five group perturbation method and estimation of reactivity coefficients using first order perturbation theory.

4 Results and Discussion

The few group lattice parameters are generated for a set of boron values using VISWAM code. The details of lattice calculation are not reported in the present paper. The equilibrium core calculation is performed by using a pre decided loading pattern. The calculations, starting with Cycle 1, are repeated till a converged burnup profile of the core is obtained. Figure 3 shows the variation of critical soluble boron as a function of EFPD for equilibrium core. The critical boron is obtained with a target K_{eff} of 1.0. Figure 4 gives the variation of radial peaking factor with cycle burnup. The RPF values obtained from assembly homogenised calculation of TRIHEXFA are seen to be $\leq$ 1.45 throughout the equilibrium cycle. Figures 5 & 6 give the radial power distribution at BOC and EOC respectively. The power distributions are seen relatively uniform.

5 Conclusion

A design for equilibrium core of 500 MWe/1500MWTh IPWR has been worked out. This design has 163 profiled fuel assemblies. Each profiled fuel assembly has 217 lattice locations, with 204 fuel pin locations and 13 lattice locations for control and instrumentation purpose. The equilibrium core configuration for 500 MWe IPWR consists of 163 FAs arranged in a hexagonal lattice array of 18.8 cm assembly pitch. The core height is 285 cm. The design calculations have been performed using the indigenous VISWAM-TRIHEXFA code system. The cycle length for

the equilibrium core is estimated as 480 effective full power days (EFPD). The equilibrium core characteristics are encouraging and a more detailed study will be taken up in future.

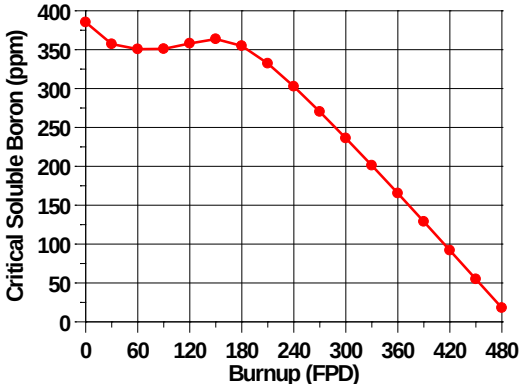


Figure 3 – Variation of Critical Soluble Boron with Cycle Burnup

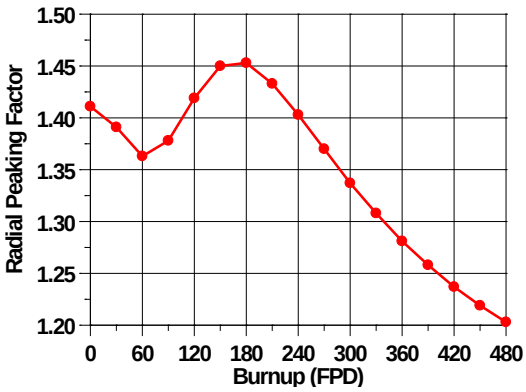


Figure 4 – Variation of RPF with Cycle Burnup

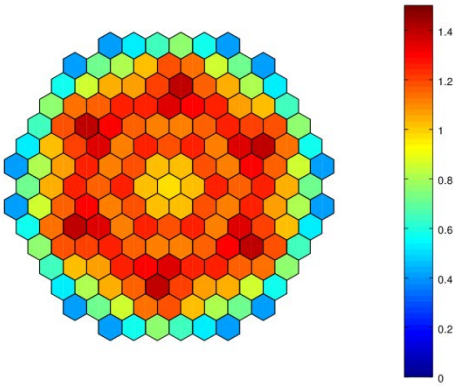


Figure 5 – Radial Power Distribution of Equilibrium Core at BOC

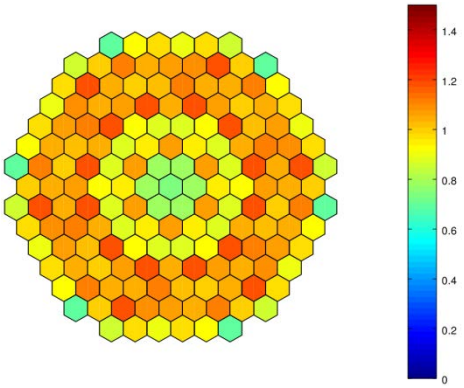


Figure 6 – Radial Power Distribution of Equilibrium Core at EOC

6 References

1. IPWR Design Report, Chapter 3 Reactor Physics Design
2. V. Jagannathan, Suhail Ahmad Khan and Arvind Mathur, "VISWAM–A Modular Code System for State of Art Analysis of Nuclear Reactors–Developmental Ideas and Current Status", *Proc. of ARP 2013–Advance in Reactor Physics: Simulation Techniques and Analysis Methodologies*, BARC Training School Hostel, Anushaktinagar, Mumbai, India, October 23–25, 2013 (2013)
3. Suhail Ahmad Khan, Arvind Mathur and V. Jagannathan, "Incorporation of Interface Current Method Based on 2D CP Approach in VISWAM Code System for Hexagonal Geometry", *Annals of Nuclear Energy* **92**,161 (2016)
4. V. Jagannathan, Suhail Ahmad Khan and Arvind Mathur, "Recent Advances in 3D Core Diffusion Code TRIHEX–FA", *Proc. of ARP 2013–Advance in Reactor Physics: Simulation Techniques and Analysis Methodologies*, BARC Training School Hostel, Anushaktinagar, Mumbai, India, October 23–25, 2013 (2013)
5. Suhail Ahmad Khan, V. Jagannathan, Usha Pal, R. Karthikeyan and A. Srivastava, "Need for High Temperature Nuclear Data Library for LWR Design Computations", *Journal of the Korean Physical Society*, Vol. **59**, No. 1, July 2011 (2011)

ANALYSIS OF VVER LATTICE BENCHMARK USING DP1 MODEL OF VISWAM

Suhail Ahmad Khan and Umasankari Kannan
Bhabha Atomic Research Centre, Mumbai, India
email: - suhailak@barc.gov.in

Abstract

The 19th AER symposium proposed a benchmark on core burnup calculations for VVER-1000 reactors for validation and verification of the reactor physics code systems. The benchmark included two stages: the first step comprised lattice calculation for all fuel assembly types and the second step consisted of the 3D core calculation. In the first step, different fuel assembly configurations were identified and their specifications were given. These assembly configurations specified in the benchmark problem have been analysed using the DP1 model available in lattice analysis code VISWAM. The present paper gives the burnup dependent k_∞ comparison for different assembly configurations with three evaluations and average results specified in the benchmark.

1. Introduction

In the 19th AER-Symposium, a paucity of well defined benchmarks for core burnup calculations for VVER-1000 reactors with modern fuel assembly (FA) design using Gd burnable absorber was noted [1]. There exist only a VVER-1000 OECD/NEA benchmark on FA burnup calculations with UO_2 and MOX fuel [2] and a benchmark investigating the physics of a whole VVER-1000 reactor core using two-thirds low-enriched uranium (LEU) and one-third MOX fuel [3]. Therefore, the development of a benchmark for VVER-1000 reactor core loadings with FA of modern design were proposed for validating and verifying the whole package of codes and data libraries for reactor physics calculations including FA modelling, FA data preparation and reactor core modelling. The benchmark was targeted to be completed in two stages. In the first stage, eight fuel assembly configurations were identified and their specifications were provided. These eight assembly configurations have been analysed using the DP1 model available in lattice analysis code VISWAM. In the present paper, the k_∞ obtained using VISWAM has been compared with other evaluations obtained using CASMO, HELOS, NESSEL and average results specified in the benchmark.

2. Description of Nuclear Data Library and VISWAM

The details of nuclear data library used in the present calculation and details of calculation models can be seen in another accompanying paper [4] in this conference.

3. Description of Benchmark

The first stage of benchmark exercise deals with the comparison of fuel assembly lattice calculation parameters. In this stage, eight fuel assembly configurations of TVSA design were identified and their specifications were provided. The design of the FAs of the TVSA type uses stiffening plates in the FA corners to improve geometric stability as shown in Figures 1 & 2. The eight types of TVSA FA differ in various enrichment values, number of fuel pins with different enrichment (radial profiling) as well as different pin umbers with burnable absorber and weight

percentage of the burnable absorber material Gd_2O_3 mixed with different enriched UO_2 fuel. The details of these assemblies are given in Table 1. Table 1 also provides the design data for the fuel pins with burnable absorber. The pin lattice layout of one profiled FA type is shown in the Figures 3. The detailed specification of other parameters for the benchmark problem can be found in [1].

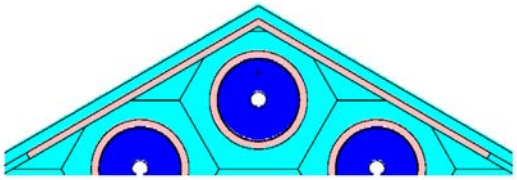


Figure 1 – TVSA Stiffening Angle Plate

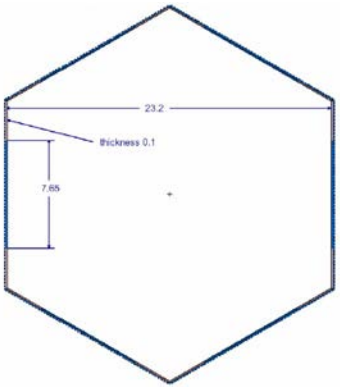


Figure 2 – Design of TVSA Stiffening Angle Plate

Table 1 – TVSA Fuel Assembly Types

FA Type	UO_2 Pins/ Enrichment (%)	No of Gd Pins (Gd_2O_3/^{235}U)
13AU	312/1.3	-
22AU	312/2.2	-
30AV5	303/3.0	9(5.0/2.4)
39AWU	243/4.0 60/3.6	9(5.0/3.3)
390GO	240/4.0 60/3.6	6(5.0/3.3)
398GO	306/4.4	6(5.0/3.3)
430GO	240/4.4 66/4.0	6(5.0/3.6)
439GT	306/4.4	6(5.0/3.6)

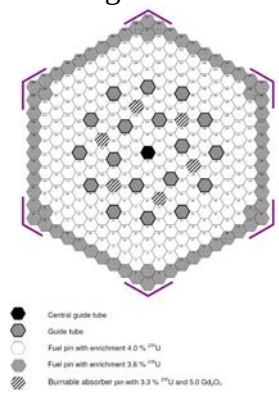


Figure 3 – Pin Configuration of FA Types 390GO

4. Results and Discussion

The burnup calculations for all the FA types were performed using the lattice analysis code VISWAM using nominal state parameter values specified in the benchmark. The DP1 model of VISWAM was used for these calculations. Since the TVSM assemblies use stiffening plate at the corners of the assemblies, VISWAM required some program modifications to model the stiffening plate. In VISWAM, the outermost layer had the provision to consider single material like water. To model the stiffening plate, provision was made to consider more than one material in the outermost layer. The material zone map to model stiffening plate in VISWAM is shown in Figure 4. In figure 4, material zones -1 & -2 have steel and zone -3 has water.

The k_∞ calculated by VISWAM as a function of burnup for all the FA types is compared with the benchmark results given in [1]. In the benchmark, evaluations obtained using CASMO, HELIOS and NESSEL code systems are provided. The benchmark also provides an average value of these

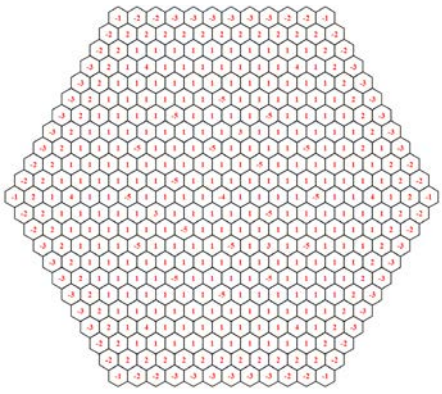


Figure 4 – Material Zone Map for modeling Stiffening Plate

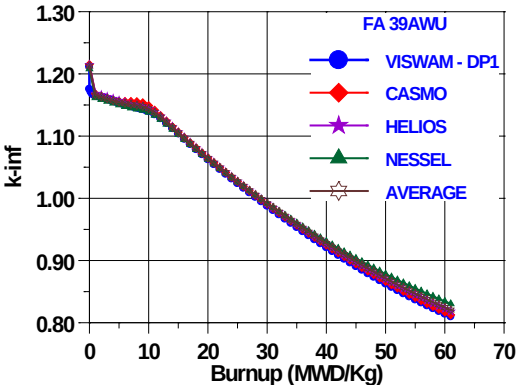


Figure 6 – Comparison of k_∞ for FA 39AWU

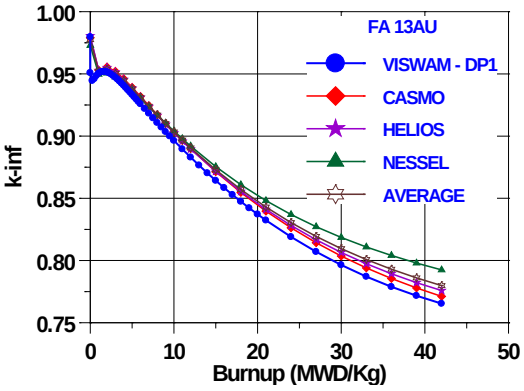


Figure 5 – Comparison of k_∞ for FA 13AU

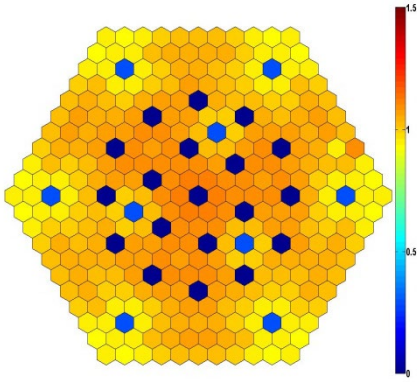


Figure 7 – Radial Power Distribution for 39AWU FA Type

evaluations. The comparison of k_∞ with benchmark evaluations at start and end of burnup points is given in Table 2. The variation of k_∞ with burnup is compared with other evaluations for FA 13AU (non Gd fuel) and FA 390AWU (having Gd) in Figures 5 & 6. Table 2 also gives the relative deviation of VISWAM k_∞ (in %) with other benchmark evaluations. The % deviation in k_∞ is calculated using following expression

$$\delta k_\infty(\%) = \frac{k_\infty^{benchmark} - k_\infty^{VISWAM}}{k_\infty^{benchmark}} X\ 100$$

It is seen that deviation in k_∞ is minimum for HELIOS evaluations at zero burnup for all FA types except 30AV5. For non-gadolinium fuel, maximum deviation in k_∞ is seen for NESSEL code at zero burnup. As a function of burnup, least deviation is seen w.r.t CASMO evaluations and maximum for NESSEL evaluations. For gadolinium fuel, the initial deviation in k_∞, in general, is of the order of ~ 0.2% for most of the FA types for all evaluations. As a function of burnup, generally, least deviation is observed for CASMO evaluations for all FA types. Here it should be noted the difference in k_∞ is due to factors such as different self shielding models, nuclear data sets and solution methods etc. However, the burnup slope of k_∞ obtained using VISWAM is similar to other evaluations for all FA types.

Figure 7 gives the radial power distribution at zero burnup for all FA 390AWU FA type having 9 Gd pins. The power distributions for other FA types are not given due to space limitations. This information is not available in benchmark for comparison purpose.

Table 2 – Comparison of VISWAM-DP1 k_∞ for different FA Types

Burnup (MWd/kg)	k_∞					Δk_∞ (in %) w.r.t.			
	CASMO	HELIOS	NESSEL	Average	VISWAM	CASMO	HELIOS	NESSEL	Average
FA 130AU									
0	0.97904	0.98058	0.97288	0.97750	0.97975	-0.073	0.085	-0.706	-0.230
42	0.77115	0.77584	0.79242	0.77980	0.76537	0.750	1.350	3.414	1.850
FA 30AV5									
0	1.13810	1.13816	1.13202	1.13609	1.13367	0.389	0.394	-0.146	0.213
61	0.77307	0.77978	0.79539	0.78275	0.77131	0.228	1.086	3.028	1.462
FA 39AWU									
0	1.21520	1.21464	1.20812	1.21265	1.21174	0.285	0.239	-0.299	0.075
61	0.81257	0.81812	0.83037	0.82035	0.80988	0.331	1.007	2.467	1.276
FA 390GO									
0	1.24590	1.24420	1.23894	1.24301	1.24240	0.281	0.145	-0.280	0.049
61	0.81275	0.81843	0.83023	0.82047	0.81002	0.336	1.028	2.434	1.274
FA 398GO									
0	1.25120	1.24935	1.24422	1.24826	1.24746	0.299	0.151	-0.260	0.064
61	0.81683	0.82240	0.83392	0.82438	0.81400	0.346	1.021	2.389	1.259
FA 430GO									
0	1.26990	1.26798	1.26274	1.26687	1.26670	0.252	0.101	-0.313	0.013
61	0.83759	0.83785	0.84840	0.84128	0.82983	0.926	0.957	2.189	1.361
FA 439GT									
0	1.27650	1.27507	1.26628	1.27262	1.27428	0.174	0.062	-0.632	-0.130
61	0.83712	0.84205	0.85229	0.84382	0.83404	0.368	0.951	2.141	1.159

5. Conclusion

The FA lattice level benchmark for VVER-1000 reactors proposed at the 19th AER symposium consisted of 8 TVSA FAs. These FAs have been analyzed using indigenous lattice physics code VISWAM. DP1 model of VISWAM was used to analyze all the fuel assembly types given in the benchmark. The resulting k_∞ with burnup has been compared with the evaluations obtained using CASMO, HELIOS and NESSEL code systems provided in benchmark. The results obtained using VISWAM show a similar trend as given in benchmark for FA types. In general, VISWAM k_∞ as a function of burnup showed least deviation w.r.t. CASMO evaluations.

6. References

1. T. Lotsch, V. Khalimonchuk, A. Kuchin. Correction and additions to the proposal of a benchmark for core burnup calculations for VVER-1000 Reactor
2. A VVER-1000 LEU and MOX Assembly Computational Benchmark, NEA/NSC/DOC(2002)10, (2002)
3. VVER-1000 MOX Core Computational Benchmark, NEA/NSC/DOC 17 (2005)
4. S. A. Khan and U. Kannan, "A Design Study for 500 MWe IPWR", paper submitted to *Advances in Reactor Physics (ARP-2022), Mumbai, India, May. 18-21, 2022*

ANALYSIS OF VVER-1000 PIN CELL BENCHMARKS USING ν-TRAC WITH ENDF/B-VIII.0 LIBRARY

Anmol Singh[*, 1], Usha Pal[*, 2], V. Harikrishnan[*, 3] and R. Karthikeyan[*,4]
[*]Reactor Physics Design Division, Bhabha Atomic Research Centre, Mumbai-400085, India
[1]anmol@barc.gov.in, [2]ushapal@barc.gov.in, [3]harikv@barc.gov.in, [4]rkarthi@barc.gov.in

Abstract

This paper presents VVER-1000 unit pin cell benchmarks analysis using ν-TRAC as well as validation of 172 multi-group nuclear data library based on evaluated nuclear data file ENDF/B-VIII.0 Historically, these pin cell benchmarks were studied as part of Fissile Materials Disposition Program (FMDP) of US DOE. It was jointly carried out by US and Russian agencies to explore the feasibility of using weapon grade plutonium in VVER-1000 and to validate their computational tools SCALE, HELIOS and MCU. In the present paper, lattice computation is carried out with ν-TRAC code based on method of characteristics (MOC). This code is being developed in BARC. The multi-group nuclear data library used in analysis, is generated using NJOY-2016 with ENDF/B-VIII.0. Here the results of ν-TRAC code using multi-group data library based on ENDF/B-VII.0 & ENDF/B-VIII.0 are compared with SCALE/SAS2H, HELIOS and MCU results and they are in very good agreement.

1 Introduction

Accuracy of lattice physics computation is highly dependent on modelling method as well as nuclear interaction data library. Neutron nuclear interaction data files are updated at regular time intervals with available improved mathematical models and cutting edge technology to perform measurement. Presently, a new version of evaluated nuclear data file ENDF/B-VIII.0 is released. A multi-group i.e. 172 groups, nuclear cross section library is generated based on ENDF/B-VIII.0 [1] using NJOY-2016 [2]. This study is performed to assess the validity and utility of ENDF/B-VIII.0 data file. In this paper two computational and experimental benchmarks are analysed. This study allows the comparison of computational codes, methods and nuclear data library. This study also validates the capabilities of ν-TRAC code as well as it validates the utility of ENDF/B-VIII.0 data file for practical problems and compare the results with well tested and accepted multi-group library based on ENDF/B-VII.0.

2 ENDF/B-VIII.0 Library Generation

The physics design of a nuclear reactor core requires a complete and thorough understanding of the interaction of the neutron with the constituent materials. This information is obtained from the nuclear data libraries. Owing to advances in experiments and modelling, the library is periodically updated. The evaluated nuclear data (ENDF/B) files are continuously updated and available from IAEA, but the files can't be used directly. ENDF/B VIII.0 (released in February 2, 2018) has been processed by NJOY-16 open source code [2] to generate WIMS 'XMAS' multigroup data library. The WIMS 'XMAS' library contains 172 group neutron cross sections tabulated at several temperatures given at some reference dilutions, average fission product yield, decay constant and the energy yield per fission. Flow of multi-group library generation is presented in **Figure 1**. The generated 'xsw' cross section files are processed by adapting the procedure outlined in WIMS Library Update Project (WLUP) [3], to Linux platform. The ENDFB8GX, thus generated library, is used in present analysis.

3 Brief Description of ν-TRAC

A code ν-TRAC to solve neutron transport equation (NTE) is being developed. It solves NTE with MOC technique [3] for 1-D slab and 2-D hexagon / Square geometries. Presently problem domain is discretised into Delaunay triangulation using Bowyer algorithm. Characteristic ray tracing through the problem domain are incorporated by means of intersection of them with the edges of meshes across the characteristic rays. To get precise results, a good number of characteristic rays needs to be considered

through the geometry. Afterwards, average angular flux values are evaluated and scalar flux in a mesh is calculated by combining angular flux values and weighting them with appropriate weighting factor. ν-TRAC is validated for numerous benchmarks [4, 5]. Results obtained are in good comparison with other published results. ν-TRAC is written in modular structure as presented in **Figure** 2. A detailed computational philosophy of ν-TRAC can be found in [5]. Visualization of the discretized geometry and raytracing through geometry is made possible through a visualization module incorporated into the code. ν-TRAC can perform transport calculation using region wise homogenised cross section in multi energy groups as well as standard multi group nuclear data library in WIMS format.

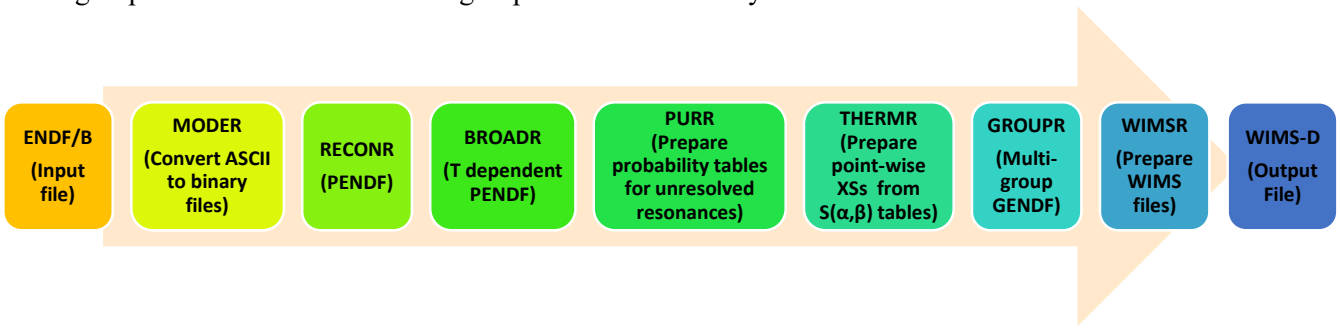


Figure 1: Schematic flow chart for generating multi-group nuclear data library using NJOY-2016

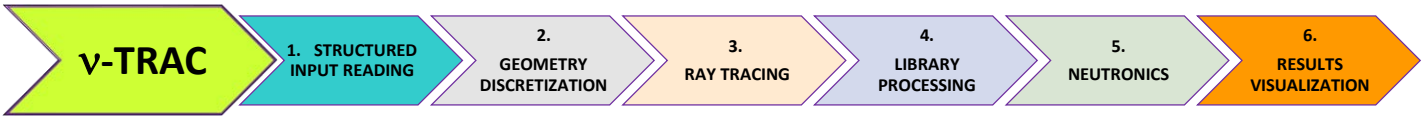


Figure 2: Modular Structure of ν-TRAC

4 VVER-1000 Pin cell benchmark Details

In present study,VVER-1000 pin cell benchmark have been analysed. The fuel pins are arranged on hexagonal pitch of 1.275 cm. Fuel pin diameter and clad outer diameter are given 0.772 cm and 0.9164 cm respectively. Specification of various fuel types are taken from [4, 5]. Two fuel variants V2 and V4 are included in the study. V2 is Weapon Grade Pu^{239} MOX (U^{235}, U^{238}, Pu^{239}, Pu^{240}, Pu^{241}, O^{16}). V4 is spent U with Fission products. The Isotope considered in V4 variants are U^{235}, U^{236}, U^{238}, Np^{237}, Pu^{238}, Np^{239}, Pu^{239}, Pu^{240}, Pu^{241}, Pu^{242}, Am^{241}, Am^{241m}, Am^{243}, Cm^{242}, O^{16}, Rh^{103}, Xe^{131}, Nd^{143}, Pm^{147}, Cs^{133}, Tc^{99}, Sm^{152}, Sm^{151}, Nd^{145}, Eu^{153}, Ag^{109}, Eu^{155}, Mo^{95}, Eu^{154}, Ru^{101}. These variants are studied for various state conditions (S1, S3-S6) as specified in [4, 5].

5 Results and discussion

Triangulated geometry and ray tracing through the geometry are presented in **Figure** 3 and **Figure** 4. A total of 150 rays are traced through geometry in 24 azimuthal directions and 6 polar directions are considered. 'ENDFB8GX.LIB' multi group library generated using NJOY-2016 based on ENDF/B-VIII.0 data file, is used for analysis. Computed k∞ values for V2 and V4 are shown in **Figure** 5 &**Figure** 6 respectively. **Table 1** shows the evaluated k∞ using different codes. Reactivity change between different states are in **Table 2.**

A general trend is observed in results of ν-TRAC code with ENDF/B-VII.0 and ENDF/B-VIII.0 library. The k_∞ values evaluated using ENDF/B-VIII.0 are lower than the values evaluated using ENDF/B-VII.0 except (V2,S6) variant. These observations will be further investigated for other lattices.

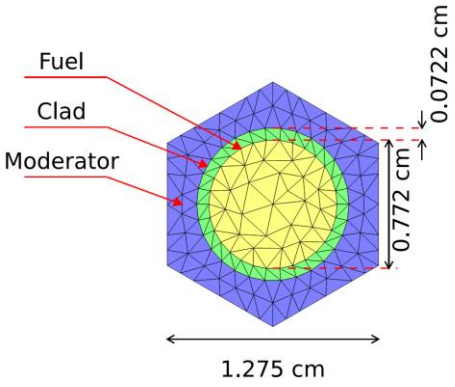


Figure 3: VVER-1000 pin cell geometry

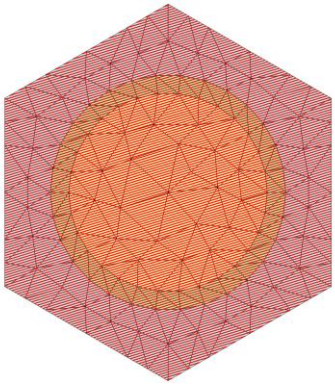


Figure 4: Raytracing through VVER pin

Table 1: Comparison of k_∞ values for different codes for VVER-1000 pin cell benchmark

Fuel Variants ↓	State →	S1 (T_f=1027, T_c=579 T_m=579, ^{eq}Xe, ^{eq}Sm, With B^{10})	S3 (T_f=1027, T_c=579 T_m=579, ^{eq}Xe, ^{eq}Sm, w/o B^{10})	S4 (T_f=1027, T_c=579 T_m=579, with B^{10})	S5 (T_f=579, T_c=579 T_m=579, with B^{10})	S6 (T_f=300, T_c=300, T_m=300, with B^{10})
V2	**ν-TRAC(ENDFB7)**	1.21600	1.24492	1.23614	1.25728	1.32951
	ν-TRAC(ENDFB8)	1.21476	1.24432	1.23507	1.25645	1.32992
	SAS2H	1.20540	1.23390	1.22500	1.24660	1.32480
	HELIOS	1.21880	1.24810	1.23830	1.25830	1.33090
	MCU	1.21350	1.26320[1]	1.23310	1.25140	1.32420
V4	**ν-TRAC(ENDFB7)**	1.02871	1.06956	1.06512	1.08280	1.12876
	ν-TRAC(ENDFB8)	1.02726	1.06852	1.06353	1.08131	1.12873
	SAS2H	1.01560	1.05560	1.05080	1.06860	1.11970
	HELIOS	1.02970	1.07070	1.06490	1.08210	1.12820
	MCU		1.12600[1]	1.08030	1.09560	1.13960

Table 2: Reactivity changes between different fuel variant and states for different codes

Fuel Variant	Codes	Reactivity Change %k_{inf}					
		(S1, S3)	(S4,S5)	(S5,S6)	(S4,S6)	(S1,S4)	(S1,S6)
V2	**ν-TRAC(ENDFB7)**	-1.910	-1.360	-4.598	-5.959	-1.340	-7.298
	ν-TRAC(ENDFB8)	-1.956	-1.377	-4.397	-5.775	-1.354	-7.129
	SAS2H	-1.916	-1.414	-4.735	-6.150	-1.327	-7.477
	HELIOS	-1.926	-1.284	-4.335	-5.619	-1.292	-6.911
	MCU	-1.932[2]	-1.186	-4.393	-5.579	-1.310	-6.889
V4	**ν-TRAC(ENDFB7)**	-3.713	-1.533	-4.090	-5.623	-3.323	-8.946
	ν-TRAC(ENDFB8)	-3.759	-1.546	-3.886	-5.432	-3.320	-8.752
	SAS2H	-3.731	-1.585	-4.271	-5.856	-3.298	-9.154
	HELIOS	-3.719	-1.493	-3.776	-5.269	-3.210	-8.479
	MCU		-1.293	-3.524	-4.817		

[1] This Variant were calculated with zero concentration of Xe^{135} and Sm^{149} [6]
[2] Corrected for various level of Xe^{135} and Sm^{149} [6]

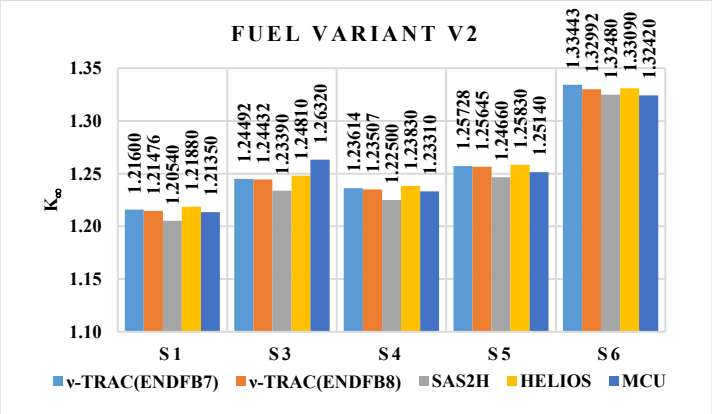


Figure 5: Comparison of k∞ for V2 fuel variant

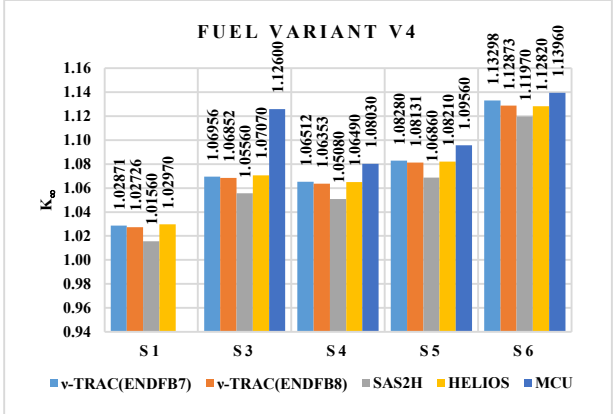


Figure 6: Comparison of k∞ for V4 fuel variant

6 Conclusion

This study shows a good agreement between the calculated Eigen values from ν-TRAC, SAS2H, HELIOS and with corrected Xe^{135} and Sm^{149} MCU. Results of ν-TRAC with multi-group nuclear data library based on ENDF/B-VII.0 as well as ENDF/B-VIII.0 are in excellent agreement among themselves as well as with other reference values. The results of the paper are part of extensive validation of ν-TRAC code and in-house generated multi-group nuclear cross section library based on ENDF-B-VIII.0 using NJOY-2016. A further validation of ν-TRAC code and nuclear data library is ensured by comparing the values of reactivity change between different states. It is observed that k_∞ values evaluated using ENDF/B-VIII.0 are lower than the values evaluated using ENDF/B-VII.0 except (V2,S6) variant. These observations will be further investigated and verified by evaluating integral parameters of different kind of lattices.

Acknowledgments

Sincere acknowledgements are due to Dr Argala Srivastava and Mr Krishna Kumar Yadav for several useful discussions and constant support during the development of ν-TRAC. Authors also acknowledge the contribution of Mr. Amod K. Mallick for his guidance in multi-group library processing. We also acknowledge Dr Umasankari Kannan for her constant encouragement.

References

[1] D. A. Brown and et al., "ENDF/B-VIII.0: The 8th Major Release of the Nuclear Reaction Data Library with CIELO-project Cross Sections, New Standards and Thermal Scattering Data," *Nuclear Data Sheets,* pp. 1-142, 2018.

[2] R. E. MacFarlane and et.al., "The NJOY Nuclear Data Processing System, Version 2016," LANL, 2016.

[3] J. Askew, "A characteristics formulation of the neutron transport equation in complicated geometries," 1972.

[4] A. Singh, U. Pal, R. Karthikeyan and A. K. Mallick, "Brief Description ofLattice code 'νTRAC' and its validation for Square and Hexagonal lattices," in *Advances in Reactor Physics (ARP-2022)*, Mumbai, 2022.

[5] A. Singh, U. Pal and A. K. Mallick, "ν-TRAC: A Neutron Transport Analysis Code based on MOC for 1-D Slab, 2-D Square and 2-D Hexagonal Geometries," *Annals of Nuclear Energy,* 2022 (Under Review).

[6] O. R. Vol.-3, "Neutronics Benchmarks for the Utilization of Mixed-Oxide Fuel: Joint U.S./Russian Progress Report of Fiscal Year 1997, Volume 3 – Calculation Performed in Russia," 1997.

A model for Quasi-Static Perturbation Analysis of 540MW (e) PHWR

A. Alok Jha[1], B. S.Samanta[1]
[1] *Tarapur Atomic Power Station, Palghar, India*
[1]*e-mail: - alokjha@npcil.co.in*

Abstract

With advancement in the computational methods and increase in the computation power, it is imperative that we develop an advanced state-of-the-art coupled CFD-reactor physics neutron code for detailed analysis of the fuel-coolant assembly to obtain better operating margin for fuel assembly peak power and fuel temperature. A detailed fuel-coolant temperature profile will allow us to study the radial and axial power peaking of the fuel assembly (column of bundles). We have developed a new coupled CFD- reactor physics neutron code using benchmark code TRIVENI and open-source industrial strength CFD code OpenFOAM. *A coupled CFD code for analysis of Indian PHWR fuel-coolant assembly has been developed for the first time*.

1. Introduction

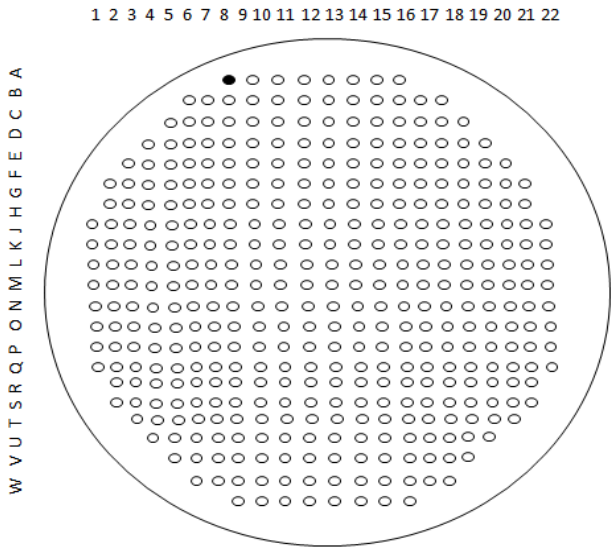


Figure 1. End face view of core showing fuel assmebly arrangement. The solid circle is fuel assembly A-8

540 MW(e) nuclear power plants are twin-unit CANDU design tube-type pressurized heavy water reactor (PHWR). The core consists of natural uranium fuel assembly housed in horizontal zirconium alloy tubes. These tubes are called as pressure tubes as high pressure (~15MPa) heavy water flows through it over the fuel assembly. Figure 1 shows the cross sectional view the core and fuel assemblies within. Each open circle represents one fuel assembly and there are 392 numbers of such assemblies in the core. Each fuel assembly is assigned an alpha-numeric tag, for example the fuel assembly shown as solid circle is fuel assembly A-8. Each fuel assembly consists of 13 number of CANDU design natural uranium oxide fuel bundles, each bundle is 49.5 cm in length. Each individual fuel bundle is made up of 37 elements and each element contains 35-37 sintered natural uranium oxide pellets encapsulated in zircalloy tubes [1].

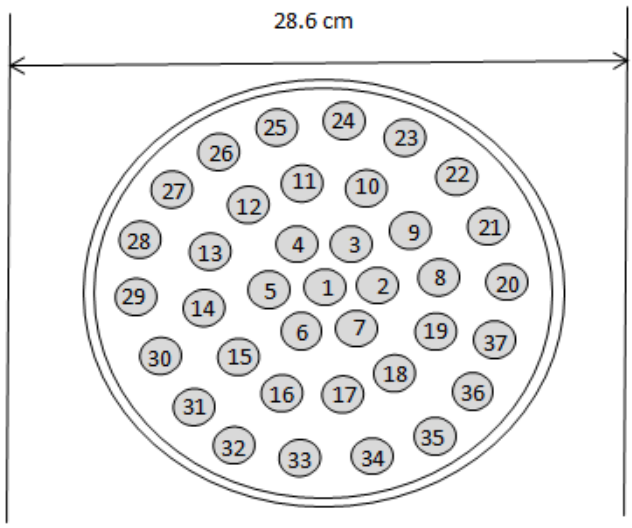


Figure 2.Cross sectional view of 37-element fuel natural uranium fuel

Cross sectional view of 37-element natural uranium fuel is shown in Figure 2. The fuel is housed in cylindrical zircalloy tubes and the coolant flows through the tubes to extract heat from the fuel. The corresponding increase in the coolant temperature leads to a redistribution of the fuel-coolant composite reactivity feedback which is important from reactor physics point of view. While developing the coupled code, we faced many challenges that we have successfully tackled as discussed here. The *first challenge* was the lack of reliable fuel heat transfer model. We developed a new mathematical model to evaluate the fission heat distribution inside the fuel. The *second challenge* was to develop a new model to compute coolant temperature in OpenFOAM [3,4]. We developed a new model that is capable of detailed coolant temperature calculations in OpenFOAM. The *third challenge* was to couple the codes TRIVENI [2] and OpenFOAM that are written in two different programming languages so that data exchange occurs between them in a synchronised manner. We achieved this feat by writing *controlling super-code in python programming language where we have leveraged the low-level operating system tools of python to handle and exchange data between the two codes*. We have provided option to write the intermediate simulation results in an external file so that the data can be plotted and analyzed using gnuplot, MATLAB etc. This new code is named *TRIVENI-OpenFOAM Coupled Code (TOCC)*. The code is used for the analysis of quasi-static perturbation arising from on-power refueling of the reactor. In on-power refueling eight out of the thirteen bundles of one fuel assembly are replaced with fresh natural uranium fuel and in a 24 hour period generally refueling of two channels are carried out. The new fuel bundles are inserted in the two assemblies from opposite ends of core and this method is known as bi-directional refueling. The bi-directional refueling scheme is shown in Figure 3.

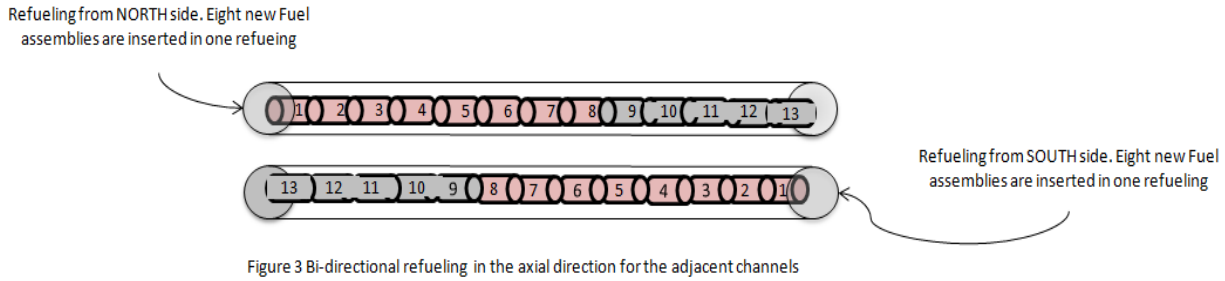


Figure 3 Bi-directional refueling in the axial direction for the adjacent channels

The refueling (fuel change inside core) process takes one hour and the reactor is maintained in nearly steady state power operation (by RRS or by operator intervention) throughout refueling. This duration is small for substantial Xenon and Iodine dynamics change of the core, but the local xenon and iodine concentration is changed due to replacement of the burnt fuel bundles by fresh fuel in the core. The reflection of local xenon and iodine perturbation appears in the full core after some time. In order to control and regulate reactor power locally, the core is divided in to seven radial zones shown in Figure 5. Reactivity control in these zones is achieved by regulating light water in the zone control compartments. A schematic showing the zone control compartments is shown in Figure 4. The main challenge during the refueling process are (i) *Control and regulation of core reactivity*, (ii) *xenon and iodine dynamics management*, (iii) *fuel bundle power management*, and (iv) *fuel temperature* management.

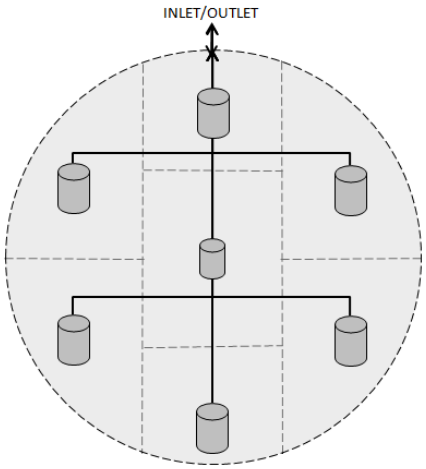


Figure 4. Light water filled zone control compartment for local flux/power control of the core. There is one zone control compartment in each zone of the reactor.

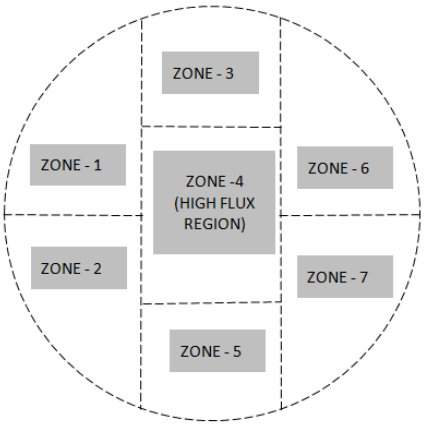


Figure 5 The seven radial zones of the the reactor

In order to operate the reactor within safe limits the reactor power is lowered for refuelling of certain channels in high flux region of the core. It leads to loss of electrical generation and hence loss of revenue for the power plant. However, experience shows that the estimates are overly restrictive and *reactor power can be manoeuvred with increased flexibility during the refueling and post refueling period thereby resulting in economic gain*. Due to lack of analysis tools, it was difficult to establish that better margins are available and that we can take advantage of this flexibility to operate the reactor at higher power. Keeping these targets in sight, we have analysed the on-power refueling using our code to obtain detailed fuel and coolant temperature profile of the fuel assembly undergoing refueling. The coolant feedback analysis using the newly developed code gives a better estimate of the fuel and coolant temperature that is also verified from the instrument measurement of resistance based detectors installed at each coolant outlet. Simulation results from the new code shows a close agreement with the detector measurements and hence *provides the quantitative values* that were lacking in the existing conservative analysis where predictions are based only on core neutron flux analysis. We present the simulation results for the refueling perturbation in this work to share the novel analysis method and the economic advantage from this advanced analysis methods using CFD over the existing conservative

estimates. The mesh for the geometrical discretization of the fuel-coolant assembly flow domain is shown in Figure 6.

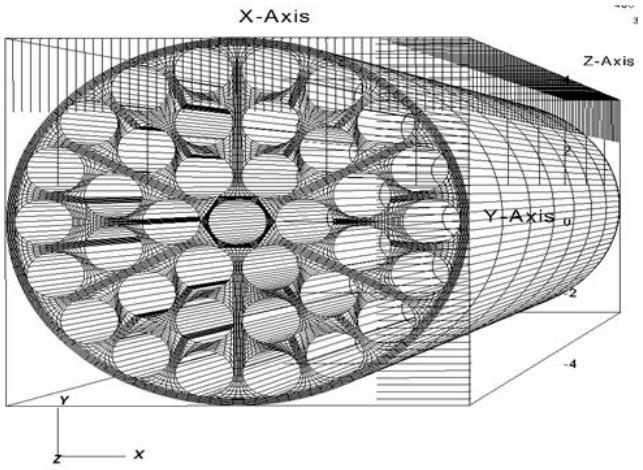


Figure 6 The geometrical discretization mesh of the fuel-coolant assembly

2. Results

We present detailed discussion of one fuel assembly J-05. Similar analysis methodology was applied for the other fuel assemblies. Fuel assembly J-05 is located in Zone-1 of the reactor core. A diagram showing the division of the reactor core in seven zones is shown in Figure 7. The fuel assembly J-05 is shown by a solid black circle. The shaded region is the zone-1 of the core. The other six zones are shown demarcated by solid lines. The dotted line shows the outline of the calandria. Each zone contains different number of fuel assemblies, and each zone produces different amount of power based on its average burnup. The total fission power contribution of the seven zones is 1830 MW thermal. The input conditions for the simulation are as follows. Coolant inlet temperature is 270^0C and fuel temperature is 317^0C for the reactor operating at 100% FP. The coolant outlet temperature change with respect for 0.02s, 4s, 7s and 10s after the refueling of one fuel-coolant assembly is shown in Figure 8. The colour grading is blue-yellow-red for low-to-high temperature. The blue colour at t=0 shows the coolant outlet temperature same as coolant inlet temperature of 270^0C at the start of the simulation. With increase in time the fuel heat extracted by the coolant causes an increase in the coolant outlet temperature shown in yellow for the intermediate time step of 4s. With time the coolant temperature further increases to the new equilibrium value of 306^0C after 10s. Since no new perturbation

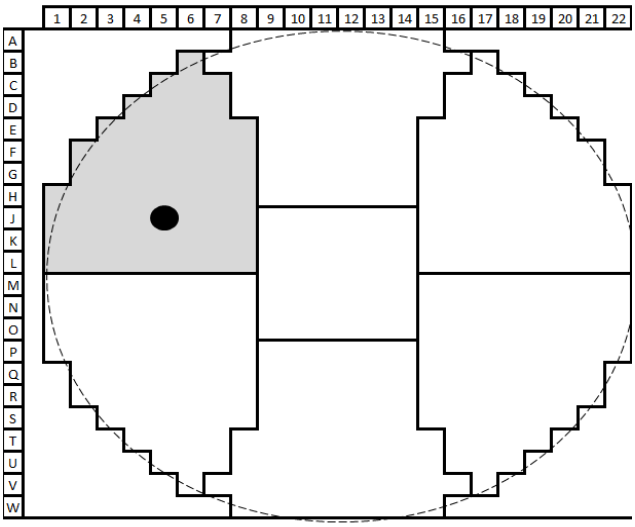


Figure 7 Location of fuel assembly inside the core. The solid black shows the location of fuel assmebly J-05. The shaded region is reactor core zone-1. The other zones are shown by solid line.

is being introduced we don't expect the coolant temperature to change afterwards. OpenFOAM iteration stops when the residue error for pressure and temperature is below $10e^{-5}$.

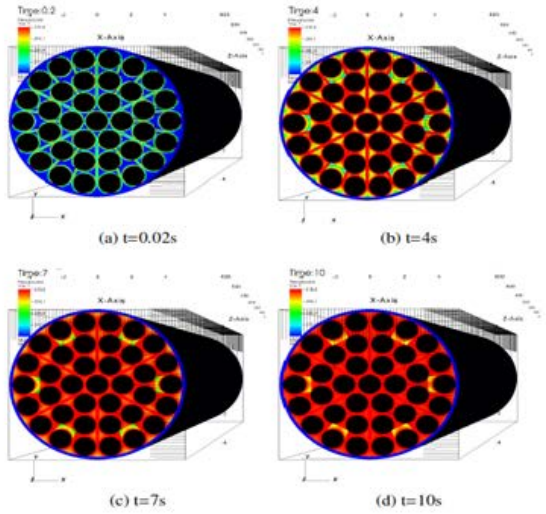


Figure 8 Simulated coolant outlet temperature after 0.02s, 4s, 7s and 10s. The coolant inlet temperature is 270^{0}C and fuel temperature is 317^{0}C corresponding to reactor operating at 100 % FP

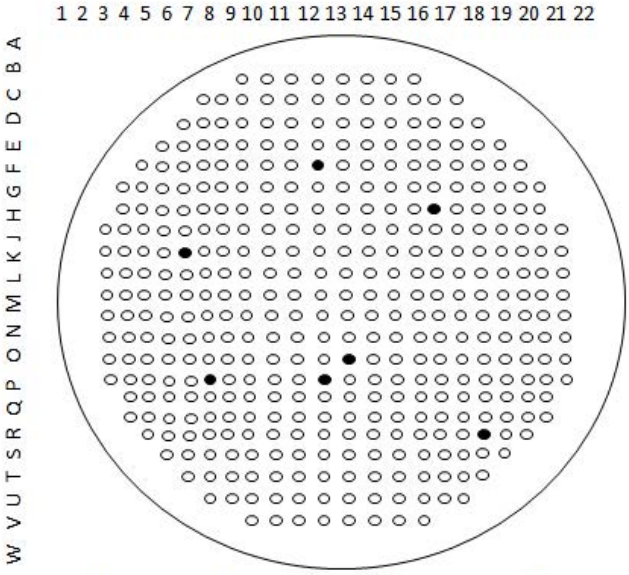


Figure 9 The location of Fuel assmeblies that were simulated for the comparison of coolant outlet temperature with detector measurement

We have simulated coolant outlet temperature of seven fuel assemblies for another refueling operation carried out on a different day. We have compared the coolant outlet temperature prediction from TRIVENI-OpenFOAM coupled code simulation with respect to the recorded detector measurements. Figure 9 shows the location of the fuel-coolant assembly inside the reactor core that were selected for simulation and comparison with detector readings. The selected channels are marked with solid circle. The coolant outlet temperature obtained from the simulation was compared with detector measurement of these fuel assemblies as shown in Table 1. We see there is very small relative error in the simulated and the measured value. The relative error is calculated from the expression shown below.

$$\text{Relative error} = \left[100 \times \frac{\text{Simulation Value} - \text{Detector Measurement}}{\text{Detector Measurement}}\right]$$

			Coolant Outlet Temperature (^{0}C)		
Reactor Zone	CH-ID	Zone power (% of Nominal power of the zone)	Simulation Result	Detector Reading	Relative error % (Simulation – Detector)/Detector
1	J-05	80.26	306	305.0	0.33
2	P-06	74.29	300	299.0	0.33
3	E-09	72.65	301	299.1	0.64
4	O-12	75.63	304	302.4	-0.53
5	P-11	71.13	301	301.5	-0.17
6	G-15	84.79	302	299.9	0.70

7	S-18	76.17	303	304	-0.33

Table 1 Comparison of detector measurements with the simulation results of TRIVENI-OpenFOAM coupled code.

3. Conclusion

A coupled CFD-reactor physics neutron code is developed for the first time for an Indian PHWR fuel-coolant assembly analysis. The code is reliable and used for better estimation of the fuel power, fuel and coolant temperature computation of the large core reactor. The simulation results help in greater confidence backed by quantitative data for reactor operation during and after on-power refueling operation and based on its predictions some relaxation is achieved in related operating margins of reactor. This is a major advantage as the increased power manoeuvrability allows for higher power generation of the reactor and it is directly translated into economic gains for a commercial nuclear power plant. The coupled code is valid for single phase coolant analysis for quasi-static perturbation and we are working to develop model to analyse space-time fuel- coolant dynamics of fast transients.

References

1. Design manual on 37-element fuel bundle, TAPP-3&4/DM/37000
2. Srinivasan K., Purandare H., Triveni 3-d fuel management code for PHWR CANDU, 1984
3. OpenFOAM-4.1 User manual, 2020
4. OpenFOAM-4.1 Programmer manual,2020

Neutronic Investigation of Burnable Poison Materials for Long Life Reactor Cores

Usha Pal[1], R. Karthikeyan[1] and Ravindra Babu[2]
[1]Reactor Physics Design Division, Bhabha Atomic Research Centre, Mumbai, India
[2]ALWR,Bhabha Atomic Research Centre, Vizag, India
e-mail:- ushapal@barc.gov.in

Abstract

The most common objective of in-core fuel management studies for a nuclear reactor is the maximization of the cycle energy production which is typically measured in effective full-power days. In a typical LWR, the reactor is shut down when its planned cycle length is reached. Advanced LWRs including SMRs has the design objective to achieve higher burnup level with longer operation cycle length and thereby less frequent refueling. This will necessitate the use of higher fissile loading in the core, which in turn results in large excess reactivity at the beginning of life. There will be a challenging requirement to operate the core with adequate shut down margin throughout the core life while maintaining the reactivity under control with acceptable thermal margins.In this paper the studies performed to achieve longer fuel cycle length by considering different burnable poison materials is presented.

1. Introduction

Light water reactors (LWR) provide nearly 90% of the world nuclear power generation. Of this, the PWR's share is ~75% and that of BWR's is ~15%. The LWRs employ refueling in batch mode. Owing to the use of slightly enriched Uranium, these reactors have substantial excess reactivity at the beginning of life that is needed to be suppressed during core power operation. Use of control rod for this purpose is not recommended since it leads to power peaking as fuel far from the control rod contribute to most of the power production and can potentially lead to unsafe situation such as in-core boiling and fuel rod failure. Current generation PWRs use soluble boron for reactivity suppression since it has the advantage of homogenous distribution throughout the core and does not lead to local power peaking. However, use of soluble boron in amounts required to suppress the entire reactivity at beginning of cycle (BOC) would compromise reactor safety as it would make the moderator temperature coefficient to be less negative. This puts an upper limit on the concentration of soluble boron that can be used in PWRs. An alternative method is to use a neutron absorbing element initially which would transmute to a non-absorbing element during the course of fuel depletion. Such elements are referred to as 'burnable poisons' and boron, gadolinium and erbium are among the three most widely used burnable poison materials.

Natural gadolinium has a large thermal cross section of 49,000 barns primarily due to the two isotopes ^{155}Gd and ^{157}Gd with isotopic abundance of 14.8% and 15.7% respectively. A graph of absorption cross section for the different isotopesof Gdis shown in Fig.1. Due to its high cross section, the depletion rate of Gd will be quite high and the design can be suitably optimised to minimise the burnup penalty.Erbium, in comparison to gadolinium has a low thermal cross section and primarily functions as an epithermal resonant absorber

Table-1Isotopic abundances and thermal capture cross sections at 0.0253 eV of Hf, Dy and boron

Element	σ_c(barns)	Nat.Abund (%)	Element	σ_c(barns)	Nat. Abund (%)
Hf^{174}		0.16	Dy^{156}	-	0.053
Hf^{176}		5.26	Dy^{158}	-	0.092
Hf^{177}	390.0	18.6	Dy^{160}	60.659	2.290
Hf^{178}	90.0	27.28	Dy^{161}	829.27	18.70
Hf^{179}	84.0	13.6	Dy^{162}	265.82	25.38
Hf^{180}	14.0	35.10	Dy^{163}	157.50	24.96

B^{10}	3840	19.80	Dy^{164}	2966.2	28.50

A graph of total cross section for these two isotopes is given in Fig.2.The two neutronically important isotopes of this element are ^{166}Er and ^{167}Er giving an elemental resonance integral of ~740 barns. Natural Hf has a thermal capture cross section of ~113barns with isotopes, $Hf^{174,176-180}$.Though, Hf^{177}has the highest neutron capture cross section (σ_c)in nat. Hf, its progressive capture products also have considerablecapture cross section , as shown in Fig.3.Similarly Dy with isotopes $Dy^{156,158,160-164}$, each of which has considerableσ_c,as shown in Fig.4,with isotopic abundances and thermal capture cross sections as shown in Table-1.

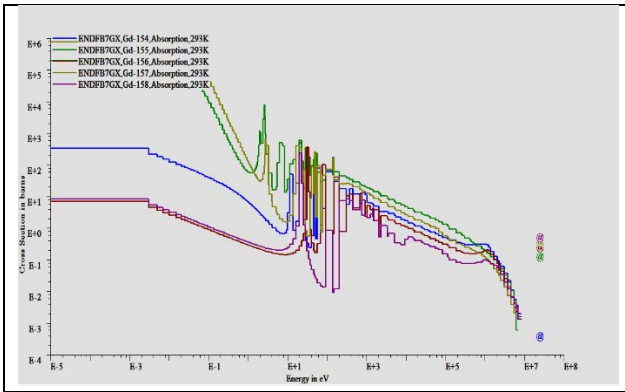


Fig.1 Absorption cross section for isotopes of Gd

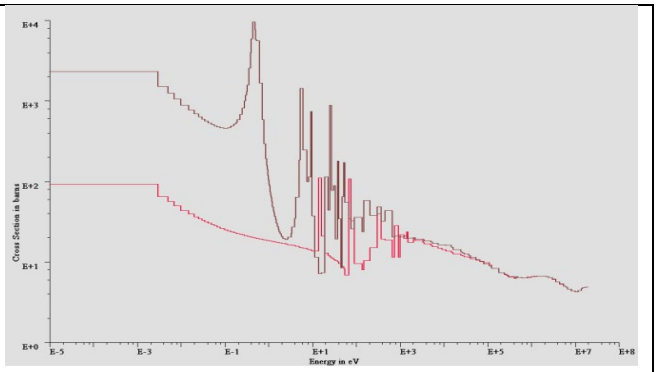


Fig.2Absorption cross section cross section for ^{166}Eand ^{167}Er

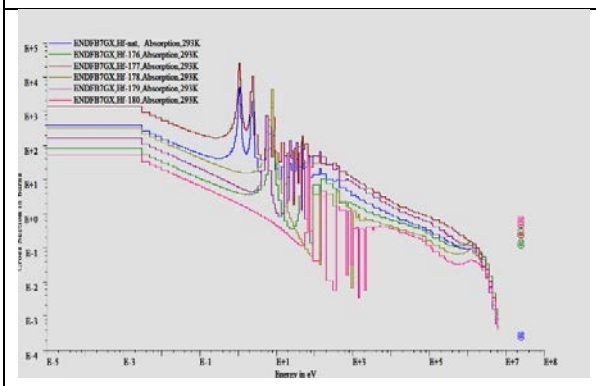


Fig.3 Absorption cross section for isotopes of Hf

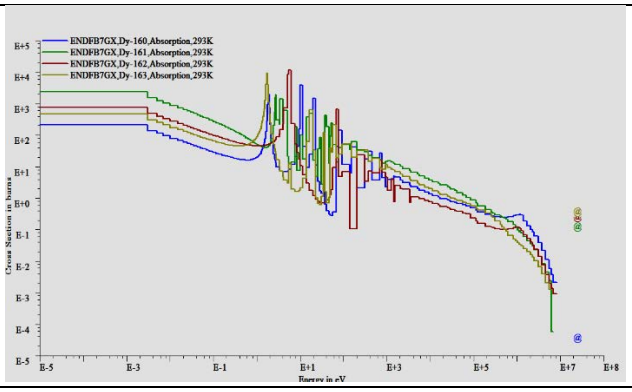


Fig.4 Absorption cross section for isotopes of Dy

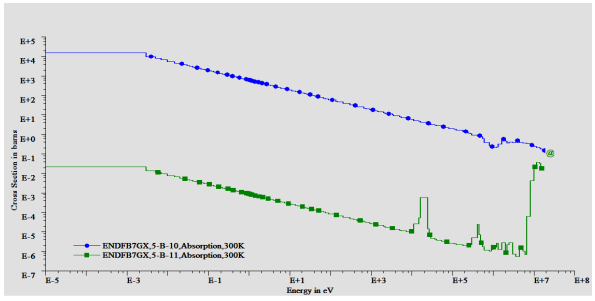


Fig.5 Absorption cross section for isotopes of boron

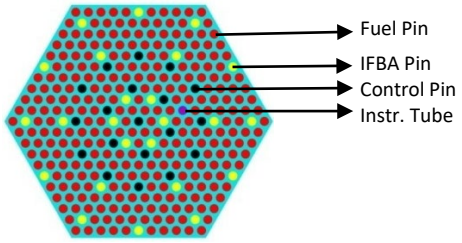


Fig.6FA with 24 absorber pins

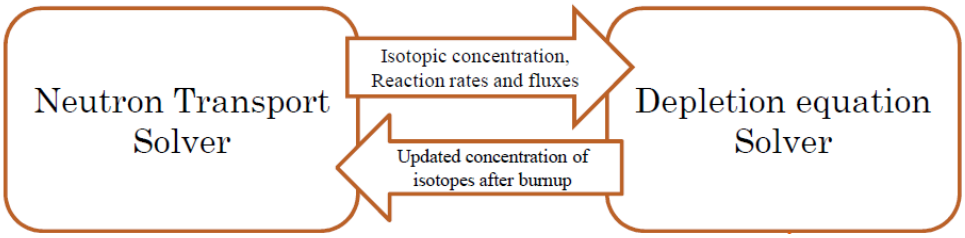
2. Geometry Description Use of BAs in LWR fuel / Fuel assembly (suggested section heading)

In the present study, the fuel assembly design similar to the one that was worked out as part of initial studies to arrive at an equilibrium core of IPWR [1] is considered. The FA has 331 locations, of which fuel pins occupy 311 locations, 18 locations are reserved for locating

control absorbers and one location for central tube. Clad ID/OD of fuel pinsis 7.87/9.4 mm,arranged in triangular pitch of 13.16 mm. Hexagonal FA pitch is 243 mm.U^{235} enrichment is considered to be 4.5%.Fig.6 shows the FA lattice with locations for 24 nos. of IFBA type burnable absorbers. To compare the burnup characteristics of different type of absorbers, calculations were carried out with natural Gd,natural Er,natural Dy, natural Hf and natural boron. The concentration of absorber was varied as 2wt%, 4wt% and 6wt% and 8wt% of heavy metal weight.

3. Calculation Methodology

Fuel assembly cell calculation was performed using Monte Carlo (MC) methods after dividing the fuel assembly into many active cells. From MC code K-infinity and different kinds of reaction rates like capture, fission rates are estimated for all the actinide and fission product isotopes at given burn-up step. Burnup calculation is performed using the code BURNCAL [2] that uses the reaction rates generated by the Monte Carlo code to solve the depletion equation for estimation of actinides and fission products concentrations at the next burnup step. The MC input is updated based on BURNCAL generated material composition and MC calculation is repeated. This is performed at each burnup step.



General expression for formation and loss of particular isotope by nuclear transmutation and radioactive decay can be written as

$$\frac{dN_i}{dt} = \sum_j \gamma_{j,i}\,\sigma_{f,j}N_j\,\emptyset + \sum_k \sigma_{c,k\to i}N_k\emptyset + \sum_l \lambda_{l\to i}\,N_l - (\sigma_{f,i}N_i\emptyset + \sigma_{c,i}N_i\emptyset + \lambda_i N_i) \quad \ldots\ldots \quad (1)$$

Where $\frac{dN_i}{dt}$ is the rate of change of concentration of i^{th} isotope, $\sum_j \gamma_{j,i}\,\sigma_{f,j}N_j\,\emptyset$ is production rate,$\sum_k \sigma_{c,k\to i}N_k\emptyset$ is production from neutron transmutation of all isotopes, $\sum_l \lambda_{l\to i}\,N_l$is the production due to decay of N_l, $\sigma_{f,i}N_i\emptyset$ is removal rate of isotope 'i' due to fission, $\sigma_{c,i}N_i\emptyset$ is removal rate perunit volume of isotope 'i' by neutron capture, $\lambda_i N_i$ is removal rate per unit volume of isotope 'i' by decay. The fuel depletion calculations are performed at a fixed specific power of 98.5W/cc up to a burnup of 60000MWd/t. Finer burnup steps were employed to improve the accuracy of results particularly till the burn out of gadolinium (Gd)/boron in IFBA.

4. Results and Discussion

K∞ vs burnup for the FA cell with 24 fuel pins mixed with 2wt% of absorber of typeGd/Dy/Er/B/Hfis presented in Figure-7. It can be seen that both Gd and boron are very good material to be used as burnable poison. Their concentration can be optimized so as to minimize the burnup penalty. Dy and Hf are good candidates as control material. It can be seen that boron is an excellent burnable poison for long life soluble boron free (or with minimum soluble boron) core with improved safety coefficients. However, since B^{10} undergoes (n,α) reaction, the pressure within the cladding/plenum increases and hence it would be better toconsider a combination of Gd or erbium along with boron based burnable poison to arrive at a design with minimum burnup penalty and lower reactivity swing.

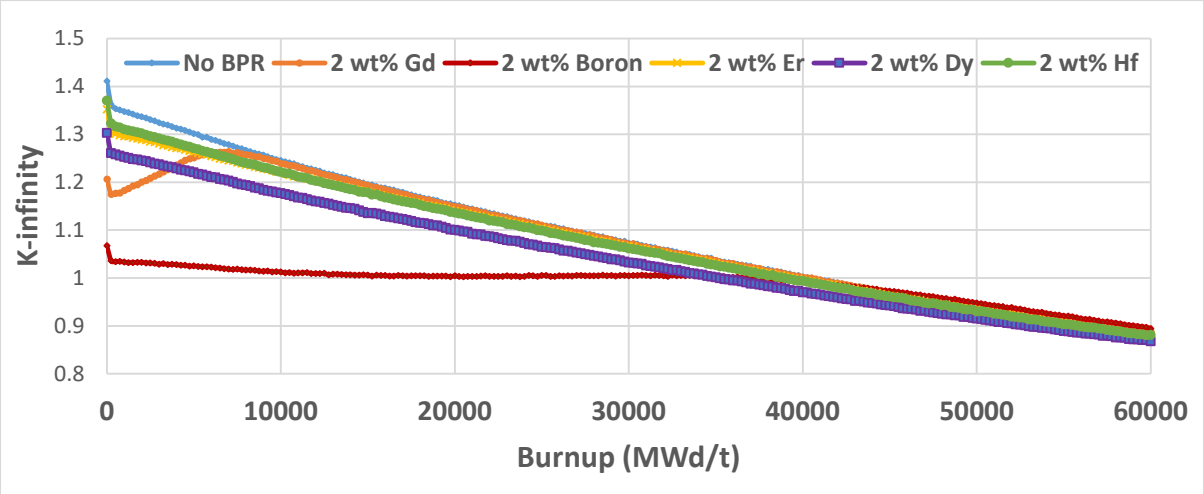


Fig.7 K_{∞}-infinity vs burnup for the FA cell with 24 IFBA pins of Gd/Dy/Er/B/Hf with 2wt% absorber

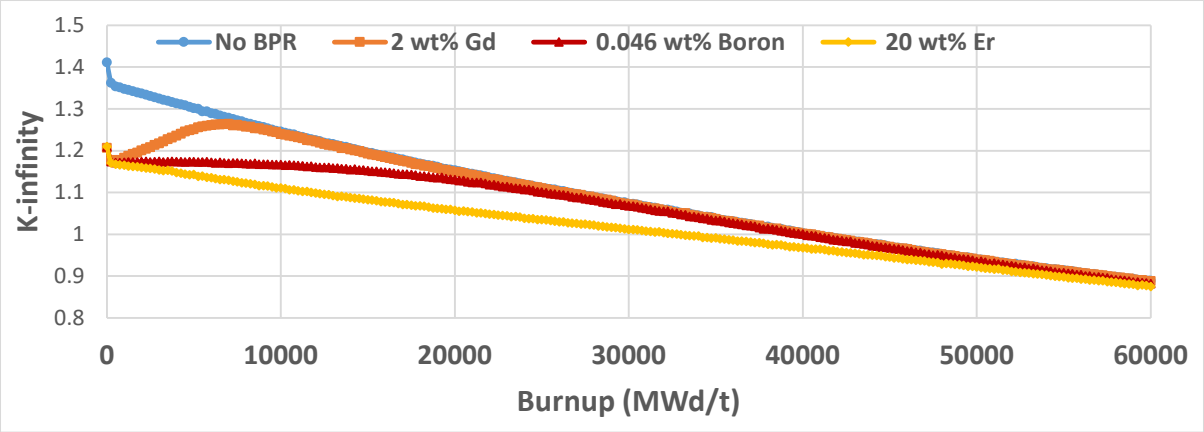


Fig.8 Burnup characteristics of Gd, boron and erbium

To compare the burnup characteristics of Gd with that of boron and Er, calculations were done with 2wt%Gd. Concentration of boron and Er that gives similar reactivity at zero burnup was iteratively obtained and burnup calculations were performed. It can be seen from Figure-8 that the reactivity suppressed by 20wt% of Er and 0.046wt% of boron are equivalent to that of 2 wt% Gd at zero burnup. It can be seen that boron suppresses the reactivity for a much longer nurnup.

5. Conclusions

Neutronic investigation of burnable poison materials for long life reactor cores is carried out using MCNP coupled with a burnup routine that makes use of the reaction rates generated by MCNP to solve the depletion equation for estimation of actinides and fission products as function of burnup. Burnupcharacteristics of different type of absorberswere compared for FA cell with 24 IFBA pins of Gd/Dy/Er/B/Hf with varying concentration. It was seen that 20 wt% of Er and 0.046 wt% of boron are equivalent to that of 2 wt% Gd at zero burnup. It was further seen that boron suppresses the reactivity for a much longer burnup as compared to similar weight fractions of Gdor erbium.

References:

[1] Usha Pal etal, ‘ Reactor Physics Design Studies for Equilibrium Core for Indian Pressurized Water Reactor, RPDD/LWRPS/IPWR/001/2013, April 9, 2013.

[2] Parma J. (Ed.), “BURNCAL: A nuclear Reactor Burnup code using MCNP Tallies”. Sandia National Laboratories, SAND2002-3868 (November 2002).

EFFECT OF TEMPERATURE ON NEUTRONIC BEHAVIOUR OF PHWR

Khaidem Charanjit Singh, Manisha Misra[1], Shailesh Mahawar and Rajib Maji[2]
Rajasthan Atomic Power Station-5&6, Rawatbhata Rajasthan Site, NPCIL, India
[1]*e-mail: - manishamisra@npcil.co.in*
[2]*e-mail: - rmaji@npcil.co.in*

Abstract

On several occasions, situation arises in an operating power plant which gives an opportunity for observing and validating design predictions of reactor core. Neutronic parameters in an operating power plant are kept in close surveillance for safe & smooth operation of the plant. It also helps in identifying situations which are suitable for verifying and validating design predictions and core behavior without affecting the normal power operation. The present paper is a basket of experiences of temperature effects on core neutronics in 220 MW PHWR.

1. Introduction

Effect of fuel, coolant and moderator temperature on core neutronic behaviour is, theoretically, well studied subject in the field of nuclear reactor. Verification of these theoretical studies has also been carried out in critical assemblies and research reactors. Verification of the same in power reactors is limited and done occasionally with carefully planned experiments. These experiments, however, require precious time which otherwise would have been utilized in power operation of the reactor. In RAPS-5&6 (220 MWe PHWR), several situations have been experienced in which these effects could be estimated and verified without affecting the reactor operation. The paper presents observed behaviour of feedback effects due to change in temperature of fuel, coolant & moderator.

2. Fuel Temperature/ Power coefficient of reactivity

Power coefficient of reactivity in a nuclear reactor refers to the effect on reactivity due to change in reactor power. The change in reactivity, basically, arises due to the change in neutron cross section with fuel temperature. At RAPS-5&6, there were several occasions where power got reduced in such a manner that the observed data during the power transient could be utilised for estimation of power coefficient with minimum effect of associated inherent difficulties [1]. The result of the estimation is presented in Table-1 and Fig-1 along with theoretically simulated behaviour using computer code REFGAIN [2].

Inherent difficulties associated with the power coefficient measurement are due to xenon feedback effect, adjuster rod position inaccuracies due to inherent delay by Reactor Regulating System response & correctness in power level indication during transient etc. To minimize these problems, data set were chosen such that i) reactor operated continuously at constant power prior to event, ii) reduced power level is preferably stable, iii) large reduction in power level within short duration, iv) time slot for calculation is as small as possible & v) there is no reactivity manoeuvring other than adjusters etc.

One of the important characteristics of power coefficient is that it reduces as in-core burnup increases [3]. The same cannot be directly inferred from our observed data because range of

power in the data set is not the same at different Full Power Days (FPDs). However, if mk/%FP is observed with respect to FPD for the different power range as depicted in Fig:1 then the same nature is revealed (even though mk/%FP has been estimated at different power bands). The observed variation in mk/%FP is in close agreement with the theoretically

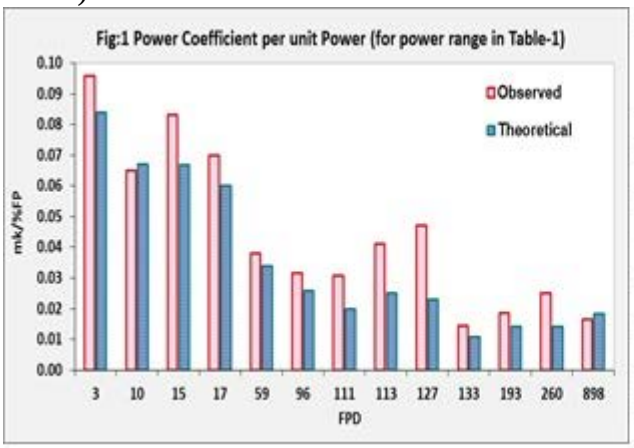


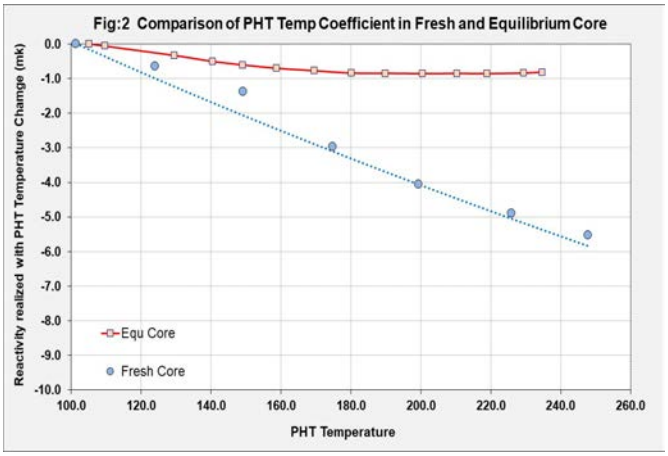
Table-1

FPD	(Power (%FP)	Observed Change in Reactivity due to Power Change (mk)	Power Coefficient (mk/%FP)	
			Observed	Theoretical
2.5	50-45	0.48	0.096	0.084
10.2	90-80	0.65	0.065	0.067
15.0	90-71	1.58	0.083	0.067
17.0	90-80	0.70	0.070	0.060
58.5	90-75	0.57	0.038	0.034
96.2	87-48	1.23	0.032	0.026
111.0	90-60	0.92	0.031	0.020
113.0	69-43	1.07	0.041	0.025
127.0	70-40	1.41	0.047	0.023
133.0	97-86	0.16	0.015	0.011
193.0	96-70	0.48	0.018	0.014
260.0	97-83	0.35	0.025	0.014
898.0	98-62	0.59	0.016	0.018

simulated behaviour [2,3]. However, it is noticeable that observed values are in general higher than the expected theoretical values. This nature gives an indication of systematic error which could not be minimized further. Error might have crept in because reactivity estimation is done from change in adjuster position and adjuster worth in the calculation is taken as per the calibration done in fresh core whereas theoretically there is a continuous change in worth of adjusters from fresh core to equilibrium core. This will overestimate the change in reactivity realization due to change in adjuster position. Moreover, all the data corresponds to power reduction cases and hence although small but there is always a reduction in PHT temperature also which might have introduced the error in one direction only.

3. Coolant Temperature

Theoretically, temperature coefficient of the coolant, fuel and moderator can be defined separately but practically when the coolant is heated or cooled, the temperature changes of coolant and fuel takes place together. Therefore “Channel (coolant channel) Temperature Coefficient” is defined as the result of both coolant and fuel temperature coefficient. The change in reactivity due to change in coolant temperature is basically attributed to spectral hardening, density change and doppler broadening due to change in fuel temperature [4].

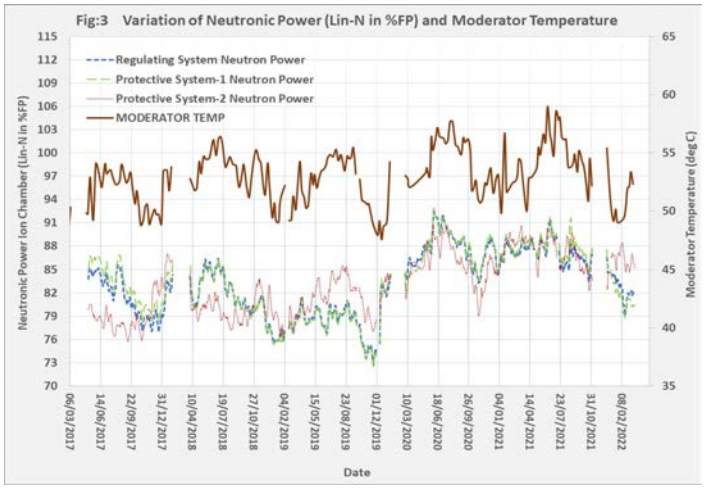


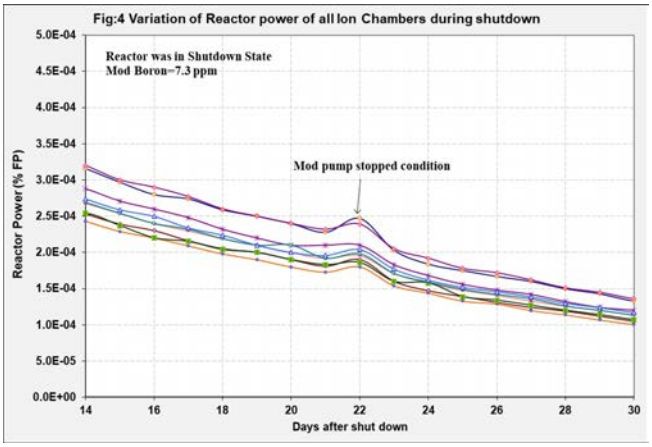
In fresh core during commissioning, coolant temperature coefficient was estimated when PHT (Primary Heat Transport) system was heated up with PCP heat only while reactor was critical. Regulating Rods moved out as PHT temperature was increased. Change in reactivity was observed to be ~9.6 mk for ~25°C to ~250°C in fresh core

conditions. In equilibrium core conditions, during one of the start-ups, PHT temperature was required to be reduced from 235°C to ~100°C keeping reactor in critical state due to some process requirement. This situation was utilized to estimate the PHT temperature coefficient in equilibrium core conditions. Regulating Rods moved from ~80 % IN to Fully IN position, indicating +ve reactivity addition. Results are given in Fig:2 along with fresh core data corresponding to the same temperature change. Assuming linearity, it can be predicted from the graph that the feedback reactivity coefficient is ~40 μK/°C in fresh core. In contrast to this, in equilibrium core conditions, it is only ~12 μK/°C upto ~180°C. This decrement of feedback reactivity coefficient in equilibrium core is in close agreement with design expectations [3].

4. Moderator Temperature

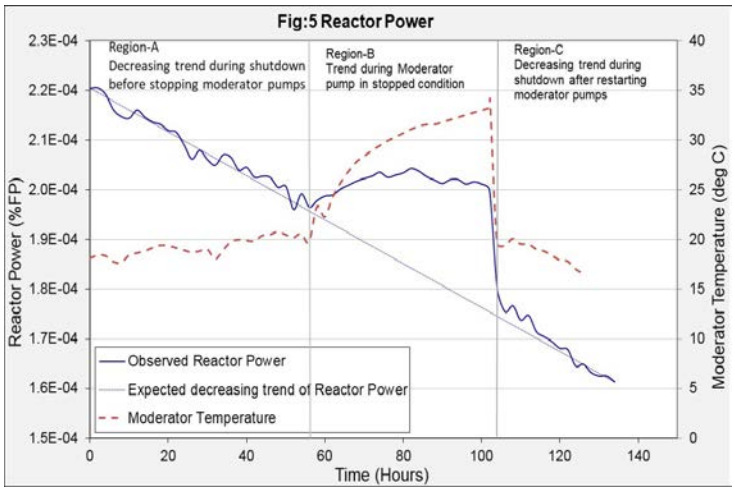
The change in reactivity due to change in moderator temperature is very small [3] and it is due to density change and spectral hardening due to change in neutron temperature. There were some plant process scenarios which were favorable to visualize the effect of moderator temperature on core neutronics. Variation of neutron signal of reactor (sensed by Ion chambers located outside the reactor core) along with the variation of moderator temperature (due to seasonal variation in ambient temperature and other operational factors) of ~5 years is displayed in Fig:3. It is clearly evident from the figure that neutron signal of all the ion chambers are showing similar trend which in turn mimics the variation of moderator temperature. Since the reactivity effect due to change in moderator temperature is known to be negligible (especially for ~10°C) and reactor was in auto regulation mode at same power level, therefore the cause of this variation of neutron signal due to feedback reactivity effect can be ruled out. The correlation between nature of variation of neutron signal and moderator temperature can only be attributed to the change in leakage neutron flux as seen by the ion chamber due to the change in moderator density. Small variations in neutron signal in the overall trend at many points are due to change in calibration range of ion chambers, change in core flux pattern or control rods position etc. The discontinuities in the curves are due to plant shutdown.





One specific situation was witnessed during shutdown state when increase in reactor power was observed instead of normal reducing trend as shown in Fig:4. It was observed that moderator circulation was stopped for planned maintenance activities during that particular time duration. Average neutron signal of all the ion chambers during the relevant time period is explicitly shown in Fig:5 along with moderator temperature.

Two major changes in moderator system parameters which affect core neutronic behavior were the change in moderator level and moderator temperature due to non-circulation of moderator water. From the observed change in moderator level and reactor power just before and after the moderator non- circulation condition, it was concluded that such variation cannot be explained with moderator level alone. In such a highly sub-critical state (in shutdown state), this change in power level corresponds to ~7 mk reactivity, if estimated using sub-critical formula [4]. As per the design data and operating experience, this amount of reactivity addition cannot be attributed to the feedback reactivity effects due to observed increase in level & temperature of moderator. Therefore, increase in moderator temperature affected the leakage neutron flux and it played a major role in increasing the reactor power. This effect became more pronounced due to presence of boron in moderator in shutdown state.



5. Summary

Process variations during reactor operation affect temperature of reactor components (fuel, coolant & moderator etc). These variations in temperature can be suitably used to witness the effect of temperature on core neutronics. In RAPS 5&6 220 MWe PHWR, some operational scenarios were utilized to establish an idea about the effect of temperature on fuel, primary coolant and moderator. The observed behavior of core neutronics is in accordance with the theoretical expectations. Even though the effect on reactivity due to change in moderator temperature is negligible but it appears that change in moderator temperature plays a major role on the leakage neutron flux and hence reactor power as sensed by the ion chamber.

6. References

[1] Rajib Maji, Shailesh Mahawar, Nirmal Vaishnav, "Estimation of Power Coefficient with observed power transient parameters in RAPS 5&6", *ARP-2013,* pp.425-429.
[2] RP&S, RSAD, NPCIL "Design Note on REFGAIN", Feb-2010.
[3] RP&S, RSAD, NPCIL "Design Manual on Physics-RAPP-5&6/DM/01100/1", Oct-2006.
[4] Samuel Glasstone & Alexander Sesonske, "Nuclear Reactor Engineering- Reactor Design Basics", Fourth Edition: Vol 1&2. 2003

A PARAMETRIC STUDY OF MULTIPLICATION FACTOR AND REACTIVITY COEFFICIENTS IN LIGHT WATER SPECTRUM

Suhail Ahmad Khan and Umasankari Kannan
Bhabha Atomic Research Centre, Mumbai, India
email: - suhailak@barc.gov.in

Abstract

In order to design LWR systems, we need to evaluate optimum physics design parameters. The neutron spectrum is primarily decided by moderator to fuel volume ratio (V_m/V_f) in thermal systems. Reactivity coefficients play an important role in defining the safety parameters of the reactor. It is important to evaluate the reactivity coefficients with improved accuracy. A parametric study has been performed to see the variation of infinite lattice k_∞ and reactivity coefficients of fuel assembly (FA) with fuel pin radius and lattice pin pitch. The present paper investigates the expected variation of reactivity coefficients with lattice design parameters.

1. Introduction

The neutron spectrum is primarily decided by moderator to fuel volume ratio (V_m/V_f) in thermal systems. In order to study design parameters for light water systems, a detailed study has been performed to study the spectrum of infinite cell lattice. In this study, the variation in infinite lattice k_∞ is studied by varying fuel pin radius and lattice pin pitch. By seeing the variation of k_∞ with moderator to fuel volume ratio (V_m/V_f), an optimum set of fuel pin radius and lattice cell pitch is obtained. Reactivity coefficients play an important role in defining the safety parameters of the reactor. It is important to know, for any given reactor design, the sign and magnitude of the various reactivity coefficients, as these coefficients determine the consequences of sudden changes in the operating parameters of the reactor. The lattice level behaviour of reactivity coefficients like fuel temperature coefficient (FTC) and coolant temperature coefficient (CTC) has been studied vis-à-vis basic design parameters.

2. Description of Nuclear Data Library and VISWAM

The details of nuclear data library used in the present calculation and details of calculation models can be seen in another accompanying paper [1] in this conference.

3. Results and Discussion

3.1 Parametric Study of Multiplication Factor (k_∞)

The parametric variation of multiplication factor (k_∞) is studied using the system of infinite lattice cell. The calculations are performed using infinite cell option available in VISWAM code system. In this option, a single lattice cell with its associated coolant is treated using 1D collision probability method in multigroup formalism. The external boundary of the lattice cell is cylindricalised and a white boundary reflective boundary condition is used.

In the first step, the variation of k_∞ with $\frac{V_m}{V_f}$ was studied for fuel of different enrichments. For calculating $\frac{V_m}{V_f}$, clad thickness was fixed and three sets of lattice pitch *viz*. 1.25cm, 1.30 and 1.35

cm were considered. The fuel radius was changed from 0.250 cm to 0.450 cm in steps of 0.025 cm. Three fuel enrichments *viz*. 3.0, 3.5 and 4.0% were studied for each lattice cell configuration. The k_∞ was calculated for each lattice cell configuration, thus, obtained. The variation of k_∞ with $\frac{V_m}{V_f}$ is plotted in Figure 1 for each pitch and three enrichments. The three figures show an expected shape. It is also seen that the optimum pitch is not a strong function of enrichment .i.e. the spectrum of the lattice is primarily decided by the fuel and coolant volumes which is an expected behaviour.

In the second step, fuel enrichment was not changed and of 3% enriched fuel was used. Four sets of lattice cell pitch *viz*. 1.25cm, 1.275cm, 1.30cm and 1.35 cm were considered. The fuel radius is varied from 0.25 cm to 0.45 cm. The fuel radius was changed using a fine step of 0.005 cm. Figure 2 gives the variation of k_∞ with $\frac{V_m}{V_f}$ for each lattice cell configuration. It is seen from Figure 2 that the peak k_∞ is 1.26186 ($\frac{V_m}{V_f}$=2.60), 1.26344 ($\frac{V_m}{V_f}$=2.65) 1.26431 ($\frac{V_m}{V_f}$=2.58) 1.26666 ($\frac{V_m}{V_f}$=2.55) for the four lattice cell pitches mentioned above.

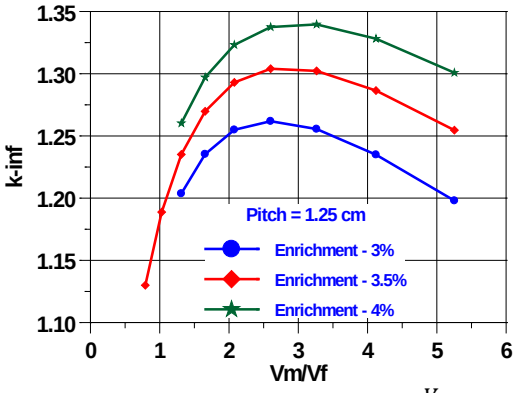


Figure 1a – Variation of k_∞ with $\frac{V_m}{V_f}$ for different enrichments

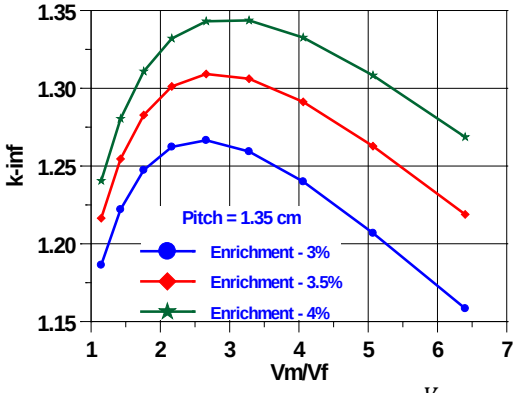


Figure 1c – Variation of k_∞ with $\frac{V_m}{V_f}$ for different enrichments

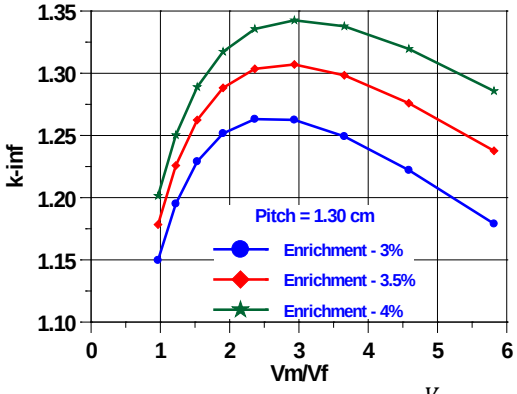


Figure 1b – Variation of k_∞ with $\frac{V_m}{V_f}$ for different enrichments

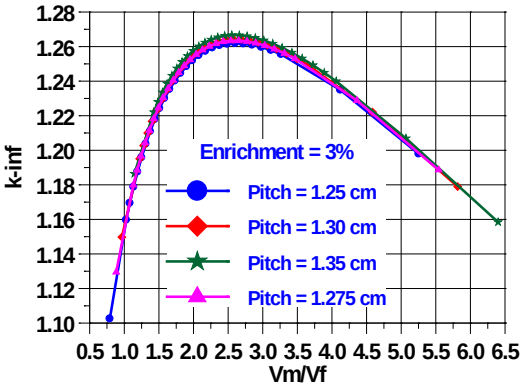


Fig. 2 – Variation of k_∞ with $\frac{V_m}{V_f}$ for 3% Enriched Fuel

3.2 Parametric Study of Reactivity Coefficients

The parametric study for reactivity coefficients has been performed using a fuel assembly (FA) problem. For performing the FA calculation, a profiled FA with 217 lattice locations was considered. In this profiled FA, 204 lattice locations are used for fuel pins and 13 locations are for guide tubes. The 204 fuel pin locations are distributed into outer 48 pins with 2.6% enriched UO_2 fuel and inner 156 pins with 3% enriched UO_2 fuel. 15 fuel pins of inner fuel locations use 3% UO_2 with 3% Gd_2O_3 fuel as shown in Figure 3.

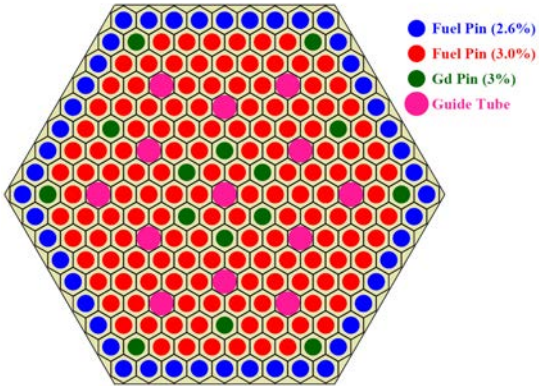


Figure 3 – Fuel Assembly Configuration

For performing parametric calculation, clad thickness of fuel pins, lattice cell pitch and FA pitch were fixed. The lattice pitch was taken as 1.25 cm and FA pitch as 18.8 cm. The fuel radius was varied from the optimum value of 0.325 cm (for pitch of 1.25 cm, refer to Figure 2) to 0.385 cm to see the effect of spectrum on lattice level reactivity coefficients. For calculating the reactivity coefficients FTC and CTC, the fuel temperature was changed by 50°C and coolant temperature was changed by 10°C w.r.t their nominal values respectively. The reactivity coefficients have been evaluated by the '2k method' using following expression

$$\frac{\partial \rho}{\partial T} = \left(\frac{1}{k_{\infty}^{ref}} - \frac{1}{k_{\infty}^{pert}} \right) / \Delta T$$

where k_{∞}^{ref} is the multiplication factor corresponding to nominal parameters and k_{∞}^{pert} is the multiplication factor obtained by changing fuel temperature (for FTC) or coolant temperature (for CTC) only and keeping other parameters same as of nominal state.

Figures 4 & 5 give the variation of FTC and CTC with $\frac{V_m}{V_f}$ at burnup levels of 0.0 and 30.0 MWD/KgHM. As seen from Figure 4, the FTC and CTC, both, are negative for all $\frac{V_m}{V_f}$ values at zero burnup. The coefficients are increasingly negative with reducing $\frac{V_m}{V_f}$ value i.e. as we move from optimal moderation or peak of Figure 2 towards the left side of curve or under moderated region. At 30 MWD/Kg, as seen from Figure 5, FTC shows the similar behaviour as for zero burnup. The CTC, however, is seen to be positive for optimum fuel radius of 0.325 cm. With reducing $\frac{V_m}{V_f}$ value i.e. as we move towards under moderated region, the CTC starts decreasing and eventually becomes negative for fuel radii of 0.335 cm and above. The positive value of CTC, thus, restricts the choice of fuel rod parameters in under moderated region i.e. the value

$\frac{V_m}{V_f} \leq 2.377$ should be taken for CTC to be negative. The actual value of CTC for a reactor design is estimated in full 3D core calculation. But, the present lattice level CTC estimation gives the expected behaviour for the core level CTC and helps in deciding the lattice parameters like fuel/clad radius and lattice pin pitch.

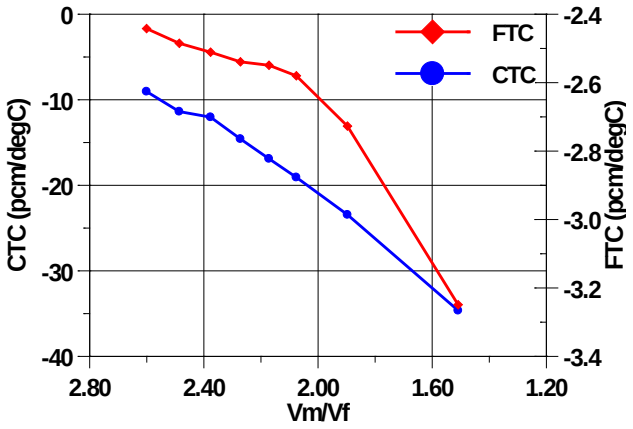


Figure 4 – Variation of FTC/CTC with $\frac{V_m}{V_f}$ at Burnup = 0.0 MWD/Kg

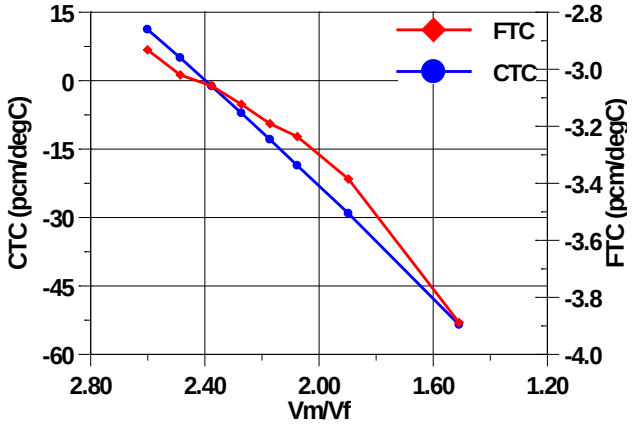


Figure 5 – Variation of FTC/CTC with $\frac{V_m}{V_f}$ at Burnup = 30.0 MWD/Kg

4. Conclusion

A parametric study on multiplication factor and reactivity coefficients in the light water spectrum has been performed. For k_∞, the study was performed in two steps. In the first step, the variation of k_∞ with $\frac{V_m}{V_f}$ was studied for fuel of different enrichments. It was seen that the optimum pitch is not a strong function of enrichment. In the second step, fuel enrichment was not changed and a 3% enriched fuel was used. Four sets of lattice cell pitch *viz*. 1.25cm, 1.275cm, 1.30cm and 1.35 cm were considered. The fuel radius is varied from 0.25 cm to 0.45 cm using a fine step of 0.005 cm. The optimum lattice configuration for each lattice pitch was obtained using VISWAM code system.

The parametric study for reactivity coefficients has been performed using a FA problem with 217 lattice locations. For performing parametric calculation, only fuel radius is varied to see the effect of spectrum on lattice level reactivity coefficients and other FA parameters were fixed. The reactivity coefficients FTC and CTC, thus, calculated are seen to be negative and becoming more negative with reducing moderation of the lattice at zero burnup. At 30 MWD/Kg, the CTC is seen to be positive for optimum lattice parameters and becomes negative when the moderation is reduced. The positive value of CTC, thus, restricts the $\frac{V_m}{V_f}$ value and $\frac{V_m}{V_f} \leq 2.377$ should be considered for negative CTC throughout the cycle life. The present lattice level FTC/CTC estimation gives the expected behaviour for the core level FTC/CTC and helps in deciding the lattice parameters like fuel/clad radius and lattice pin pitch.

5. References

1. Suhail Ahmad Khan and Umasankari Kannan, “A Design Study for 500 MWe IPWR”, paper submitted to *Advances in Reactor Physics (ARP-2022), Mumbai, India, May. 18-21, 2022*

RE-OPTIMIZATION OF WORTH OF RRS IN AHWR TO IMPROVE CORE POWER DISTRIBUTION

Vishal Bharti, Baltej Singh & Umasankari Kannan
Reactor Physics Design Division, BARC, Mumbai, India
e-mail: - vishalb@barc.gov.in

Abstract

AHWR core consists of 61 reactivity devices comprising of 37 shut off rods (SORs) as part of shut down system (SDS#1) and 24 rods as a part of Reactor Regulation System (RRS). The 24 rods are divided into three types of devices (8 Absorbers Rods (ARs), 8 Regulating Rods (RRs) and 8 Shim Rods (SRs)) to meet the reactor regulation requirements and they are uniformly distributed in the core (2 rods of each type of device per quadrant) to achieve the desired objectives of reactor regulation.

The reactivity worth of all the three devices is about 12 mk each. The movement of these devices during operation causes local flux peaking or local flux dip in the vicinity of devices. The local flux variations give power ramp to fuel located in the vicinity of these devices. Therefore, minimum required reactivity worth of these were assessed and the minimum required reactivity worth of ARs, RRs and SRs were worked out to be about 5.0 mk each. Therefore, the design of the reactivity devices was modified to achieve the desired reactivity worth and their effect on the core power distribution was also studied. This paper gives the details of the design modification of reactivity devices and its effect on the core power distribution as well as on core reactivity feedbacks.

1. Equilibrium core fuel cluster design and lattice calculations

AHWR equilibrium fuel cluster consist of 54 pins arranged in co-axial array of 12, 18 and 24 pins. The cluster has been designed to have axial as well as radial gradation for better thermal hydraulic compatibility. The cluster has been designed to contain (Th, Pu) MOX as fuel in the innermost ring and middle ring and (Th, ^{233}U) MOX as fuel in the outermost ring. The average Plutonium content in the innermost ring and middle ring is 4.74 % in (Th, Pu) MOX and average ^{233}U content in the outermost ring is 3.55% in (Th, ^{233}U) MOX to achieve the design discharge burn-up of ~40.0 GWd/Te. For the axial gradation, the cluster has been divided into two parts namely top half and bottom half, the ^{233}U content in the bottom half is higher than the top half. The two fuel pins of the innermost ring are doped with 2% Gd to facilitate on-power refuelling. The details of fissile content in different rings of the cluster are given in Table 1. The lattice calculations were carried out using neutron transport computer code ITRAN [1] using 69-group ENDF-B VI.8 nuclear data library.

Table1. Description of AHWR Equilibrium core cluster

Cluster Halves	Ring-wise Pu / ^{233}U content (%)			Nat. Gd in 2 pins of innermost ring
	Inner	Middle	Outer	
Top Half	6% Pu	3.9% Pu	3.3% U	2%
Bottom Half	6% Pu	3.9% Pu	3.8% U	2%

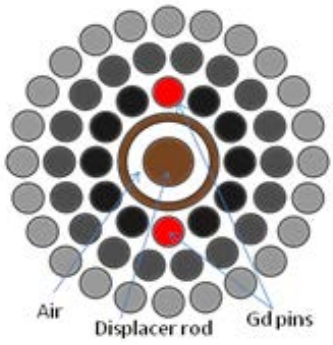
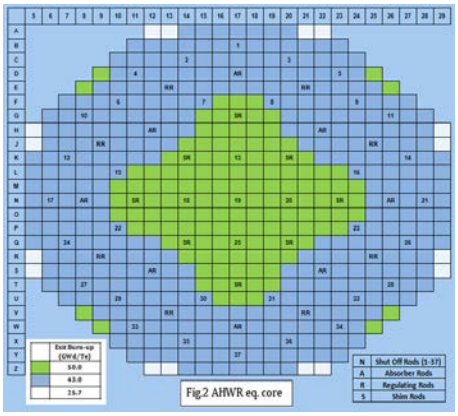


Fig.1 AHWR Eq. Core cluster

2. Equilibrium core

AHWR core consists of total 513 lattice locations, out of which 452 lattice locations are occupied by fuel channels and remaining 61 locations by reactivity devices. The core calculations were carried out using 3D diffusion theory code FEMINA [2]. The core has quarter core symmetry and all the reactivity devices have been distributed symmetrically in the core. The equilibrium core is designed to have three burn-up zones to achieve flat flux distribution. The schematic diagram of the AHWR equilibrium core with different discharge burn-up zones is shown in fig. 2.



3. Design modification to reduce reactivity worth of reactivity regulating devices

The present design configuration of Absorber Rod (AR) or Regulating Rod (RR) comprises of 40 B_4C pins encapsulated in the SS tube surrounded by heavy water moderator and distributed symmetrically at different lattice locations in the core. These B_4C pins are divided axially in compartments to avoid settling down of B_4C powder over a period of time. Similarly, each Shim Rod (SR) comprises of 80 B_4C pins encapsulated in the SS tube surrounded by heavy water moderator. The details of present design & modified design of ARs, RRs and SRs is given in the Fig 3a, Fig 3b & Fig.4 respectively.

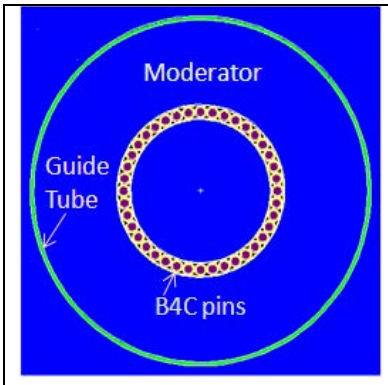


Fig. 3a: 40 pins B_4C AR / RR Rod

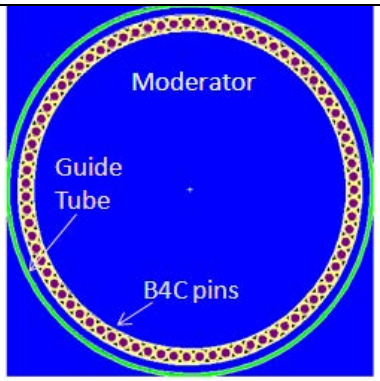


Fig. 3b: 80 pins B_4C SR Rod

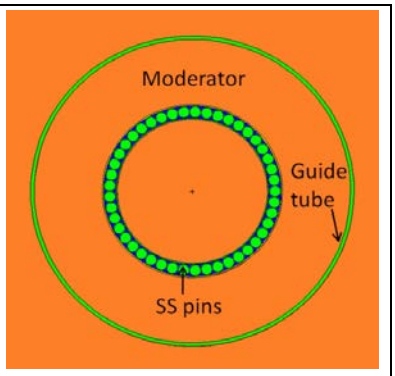


Fig. 4: 45 SS pins in AR, RR & SR Rod

The wall thickness of the B_4C filled SS Pins was increased to reduce the B_4C content in the SS Pins to achieve the desired worth of reactivity devices. The modified designs were simulated with lattice simulation code ITRAN and core calculation code FEMFOL [2] to estimate the reactivity worth of the regulating devices for their different geometries. In order to accommodate greater number of pins in the annulus space, the PCD of the ring of the SS pins was also increased from 6.0 to 6.8 cms. Therefore, the major changes in the configuration of RR, AR and SR for the desired reactivity worth is given below.

a) The 40 B_4C pins of AR / RR were replaced with 45 SS pins
b) The 80 B_4C pins of SRs have been reduced to 45 SS pins

The dimension's detail of the present design & modified design of reactivity devices (AR / RR / SR) are given in Table 2

Table 2. Comparison of present & modified design of ARs, RRs and SRs

	Existing Design		Modified Design
	AR & RR	**SR**	**AR, RR & SR**
No. of SS or B_4C filled SS pins	40	80	45
SS or B_4C filled SS Pin Diameter / WT, mm	4.7/0.63	4.7/0.63	4.7/2.35
PCD in mm	60.0	118.3	68
Inner SS carrier tube ID/OD, mm	54.3/55.3	112.6/113.6	62.3 / 63.3
Outer SS carrier tube ID/OD, mm	64.7/65.7	123/124	72.7 / 73.7
Inner/Outer SS carrier tube WT, mm	0.5/0.5	0.5/0.5	0.5 / 0.5
Density of B_4C powder in the pins, g/cc	1.764	1.764	N.A.

4. Estimation of core Power Distribution

The modified design of AR, RR & SR with their geometrical dimensions as given in the Table-2 was simulated using ITRAN to obtain two group cross-sections. The AHWR equilibrium core burn-up optimisation was also carried out and it was observed that discharge burn-up improves by about 3.6 GWd/Te due to reduction in the reactivity worth of reactivity devices. The core burn-up optimization showed that the reduction in the worth of reactivity devices make the power distribution more flat & as a result the maximum channel power reduced from 2.49 MW to 2.41 MW as shown in the Table 5 & Table 6 respectively. The worth of reactivity devices with modified design of RRS is given in Table 7. The change in power distribution may affect the core reactivity feedbacks, therefore the reactivity feedbacks for the core having reactivity devices with reduced reactivity worth was also estimated and the results have been compared in the Table 8.

Table: 5 Equilibrium core power distribution - Reference case

	13	12 14	11 15	10 16	9 17	8 18	7 19	6 20	5 21	4 22	3 23	2 24	1 25
A	1.84	1.71	1.65	1.63	1.63	1.66							
B	**SOR**	1.84	1.75	1.91	1.73	1.66	1.86						
C	1.84	1.78	2.05	**SOR**	2.07	1.90	2.04	2.09					
D	**AR**	1.78	1.98	2.16	2.05	2.16	**SOR**	2.15	2.01				
E	1.85	1.97	2.22	2.10	**RR**	2.09	2.31	2.30	2.01	2.01			
F	2.19	2.25	**SOR**	2.26	2.02	1.97	2.26	**SOR**	2.30	2.14	2.09		
G	**SR**	2.33	2.25	2.11	1.91	1.84	1.98	2.26	2.30	**SOR**	2.03	1.85	
H	2.34	2.15	2.06	2.08	1.89	**AR**	1.84	1.96	2.08	2.15	1.89	1.64	1.63
J	2.39	2.20	2.16	2.26	2.05	1.89	1.91	2.01	**RR**	2.03	2.05	1.72	1.61
K	**SOR**	2.42	2.38	**SR**	2.25	2.07	2.10	2.25	2.09	2.15	**SOR**	1.89	1.60
L	2.46	2.27	2.24	2.38	2.15	2.06	2.25	**SOR**	2.21	1.96	2.03	1.73	1.62
M	2.49	2.29	2.27	2.42	2.19	2.15	2.33	2.24	1.96	1.77	1.77	1.82	1.67
N	**SOR**	**2.49**	2.46	**SOR**	2.39	2.33	**SR**	2.18	1.84	**AR**	1.82	**SOR**	1.80

	Exit Burn-up (MWd/Te)
	48900
	37300
	29000

Table: 6 Equilibrium core power distribution with reduced worth of RRS

	13	12 14	11 15	10 16	9 17	8 18	7 19	6 20	5 21	4 22	3 23	2 24	1 25
A	1.82	1.69	1.77	1.73	1.62	1.58							
B	**SOR**	1.85	1.72	1.84	1.62	1.49	1.62						
C	2.10	1.89	2.03	**SOR**	1.95	1.72	1.78	1.79					
D	**AR**	2.04	2.01	2.19	2.10	2.06	**SOR**	1.86	1.75				
E	2.14	2.12	2.29	2.25	**RR**	2.13	2.13	2.04	1.73	1.75			
F	2.31	2.36	**SOR**	2.36	2.19	2.02	2.17	**SOR**	2.03	1.85	1.78		
G	**SR**	2.40	2.33	2.17	2.07	2.12	2.06	2.17	2.13	**SOR**	1.77	1.61	
H	2.36	2.18	2.10	2.12	2.18	**AR**	2.11	2.02	2.13	2.05	1.71	1.48	1.56
J	2.38	2.19	2.17	2.32	2.19	2.18	2.07	2.18	**RR**	2.09	1.94	1.60	1.59
K	**SOR**	2.39	2.38	**SR**	2.32	2.12	2.16	2.35	2.24	2.17	**SOR**	1.82	1.70
L	2.40	2.22	2.21	2.38	2.17	2.10	2.32	**SOR**	2.28	2.00	2.02	1.71	1.74
M	2.41	2.22	2.22	2.39	2.19	2.17	2.40	2.36	2.11	2.02	1.87	1.83	1.66
N	**SOR**	**2.41**	2.40	**SOR**	2.38	2.36	**SR**	2.30	2.13	**AR**	2.08	**SOR**	1.79

	Exit Burn-up (MWd/Te)
	50000
	43000
	25700

Table 7 Worth of reactivity devices

	Worth of reactivity devices mk			Avg. Discharge burn-up gain (GWd/Te)
	ARs	RRs	SRs	
Reference configuration	11.7	12.1	9.1	0
Modified Configuration				
45 SS pins (ARs/RRs/SRs)	5.0	5.0	4.7	3.6

Table 8 Core reactivity feedbacks

Safety parameters	**Reactivity mk**	
	(Ref case)	**RRS worth optimization**
Δρ (mk) (Moderator Temp)	+1.2	+1.4
Δρ (mk) (Channel Temp)	+5.1	+6.4
Δρ (mk) (fuel)	-3.4	-3.4
LOCA (mk)	-6.0	-4.1

5. Conclusion

The feedback due to Moderator temp & Channel temp is positive in the reference core due to plutonium resonance peak at 0.3 eV. The core calculations showed that the reduction in the reactivity worth of reactivity devices improved the discharge burn-up by 3.6 GWd/Te. The flattened power dist. results into less leakage of neutrons and the feedback due to coolant void turns to be less negative.

6. References

[1] P. D Krishnani, “Input preparation for computer code ITRAN”, Technical report No. BARC /RPDD /RP /011, June 23, 2010

[2] A. Kumar etc., “Nodal expansion method for reactor core cal.”, BARC-1249, 1984.

ANALYSIS OF FIRST APPROACH TO CRITICALITY (FAC) AND LOW POWER PHASE-B EXPERIMENTS OF KAPP-3 USING DRAGON AND DONJON CODE SYSTEM

L. Thilagam[1] and D. K. Mohapatra[1]

[1] Safety Research Institute, Atomic Energy Regulatory Board, Kalpakkam, India

[1]*e-mail: - thilagam@igcar.gov.in*

Abstract

First unit of Indian 700 MWe PHWR, Kakrapar Atomic Power Project - 3 (KAPP-3), attained criticality on 22nd July, 2020 in Kakrapar, Gujarat. During commissioning of KAPP-3, in order to support safety and licensing reviews, physics analysis capability has been developed at SRI/AERB using DRAGON-DONJON code system and extensive independent verification calculations were carried out. Further, the review calculations have been extended to analyze the first approach to criticality (FAC) and Phase – B low power physics experiments (LPPE) of KAPP-3. Comparison of the results of review calculations with the design calculations and the values observed during FAC and Phase-B LPPE of KAPP-3 are presented in this paper.

1. Introduction

More units of indigenously designed Pressurized Heavy Water Reactor (PHWRs) of higher power, 700MWe PHWRs are being commissioned to hasten nuclear power production in India. The concerned safety analyses reports were submitted to AERB for licensing reviews. In order to support the safety review of the associated design documents through independent verification calculations, physics analysis capability for 700MWe PHWR using DRAGON-DONJON code system [1] was developed at SRI, AERB. Subsequently, extensive independent verification calculations were carried out to support the safety review of design submissions on various stages. Salient lattice physics and core physics parameters were evaluated, compared with the design calculations and verified against the acceptance criteria. Furthermore, the review calculations have been extended to analyse the FAC and Phase – B LPPE of KAPP-3, the first 700MWe PHWR unit which attained criticality on 22nd July, 2020 in Kakrapar, Gujarat. Comparison of the results of review calculations with the design calculations and the values observed during FAC and Phase-B LPPE of KAPP-3 are presented in this paper.

2. Initial core loading pattern of 700MWe PHWR & Reactor state description

The initial core loading pattern optimized with 248 doubly depleted uranium (DDU: 0.28 w/wt% ^{235}U) bundles, which is reported in detail for results of designer's preliminary safety analysis [2] and in commissioning procedures/reports [3, 4] of first approach to criticality (FAC) and low power physics experiments (LPPE) of KAPP-3, is considered for the present study. In the initial fuel loading pattern, out of 248 DDU bundles, 72 DDU bundles only are loaded at neutronically important region (at 7th bundle position) and 176 DDU bundles are at 11th and 12th bundle positions in 88 intermediate fuel channels. Remaining 4456 fuel bundle locations occupied by natural uranium (NU) bundles.

In order to study the variation of effective neutron multiplication factor and reactivity due to draining of ZCCs, withdrawal of reactivity devices and boron removal during FAC and for analysis of Phase-B LPPE scenarios, the fresh core cold condition with the different configurations of reactivity devices and boron dilution as described in commissioning procedures/reports of KAPP-3 are considered.

3. Computational methodology

DRAGON-DONJON code system is an open-source advanced reactor physics code system developed and maintained by Ecole Polytechnique de Montréal, Canada [1]. DRAGON solves the multi-group neutron transport equation, and is used to simulate the two/three-dimensional (2-D/3-D) infinite lattice cell over a range of burnup. DONJON is a three dimensional (3-D) core physics analysis code designed around solution techniques of the neutron diffusion or simplified P_n equation.

In the present study, NU and DDU based 37 element fuel bundles of 700 MWe PHWR are simulated with and without reactivity devices using DRAGON employing the major evaluated file project, ENDF-B/VI.8 in 69 group WLUP library format. For solving the integral transport equation, the EXCELT option, which uses the full collision probability method for general 2D/3D geometries, is employed. The self-shielding calculations are performed by the SHI module by means of generalized Stammler method without Livolant and Jeanpierre (LJ) option and the burnup calculations are using the EVO module. The COMPO & CPO modules are utilized for production of equivalent fuel assembly parameters in consistent format that can be used in forgoing DONJON whole core calculations. The other modules like LIB, GEO, ASM, FLU, and EDI are also used. In all cases, the reflective boundary conditions are used.

In DONJON, 700 MWe PHWR core comprising of 392 fuel bundles is simulated in 3-D cartesian geometry (26 x 26 x 12 meshes with split option 2 in X & Y dimensions and split option 6 in Z dimension) employing MCFD 1 (mesh centered finite difference approximation) option in TRIVAT tracking module. The group constants of fuel bundles calculated by DRAGON are recovered using the CRE module and the FLUD module is to compute multiplication factor. The reactivity control devices are modelled using incremental cross-sections, calculated as the difference between a reference cross-section (e.g., withdrawn adjuster rod) and a perturbed cross-section (e.g., inserted adjuster rod).

4. Results and discussions

4.1 First approach to Criticality

The FAC of KAPP-3 was started with the initial conditions of all ZCCs fully filled, all reactivity devices (ARs, CRs and SRs) fully IN, SDS-1&2 poised and 28 ppm of boron in moderator. For approaching to criticality, the devices were removed one by one starting from draining of all ZCCs followed by withdrawal of all SR banks, CR banks and AR banks. The AR Bank-4 which was kept at 50% and the rest were taken fully OUT. Boron in moderator was diluted subsequently to attain criticality. The variation of effective neutron multiplication factor and reactivity due to draining of ZCCs, withdrawal of reactivity devices and boron removal during FAC, and critical boron were calculated and compared with the design calculations and observed values. DRAGON-DONJON review calculations predicted critical boron as 10.1 ppm against the design value of 10.47 ppm. The critical observed during FAC of KAPP-3 is 10.2 ppm which is in closer agreement with the theoretical predictions.

4.2 Phase-B LPPE

For analysis Phase-B LPPE conducted at 0.1% FP, the scenarios like calibration of average level (AVZL) of ZCCs against boron, measurement of worth of individual SRs, ARs and CRs, and calibration of banks of ARs, CRs, CR banks together, AR together with CR etc. were simulated using DRAGON-DONJON code and the results were compared with the design calculations and the values observed during measurements. Initial configuration for each of the scenarios are different

and are simulated as described in the commissioning procedures/reports of KAPP-3. As demonstration of the prediction capability of DRAGON-DONJON code during review, some of the results are presented as follows.

Reactivity change (mk) vs. AVZL (%FL) change observed during calibration of AVZL of ZCCs against boron is compared between the design and review calculations in Figure 1 which shows reasonably good agreement. The respective deviation of review from observed values plotted in Figure 1 shows reasonably good agreement of observed value with the theoretical review in the beginning, slightly larger before the end and again good at the end. Figure 2 displays worth of individual SRs which shows good agreement with review calculations within ±0.07 mk with the design and ±0.2 mk with observed values. The worth of individual CRs at different depth of insertion is given in Figure 3. The comparison of the integral worth as well as the S-curve shape seems to be fairly good for all CRs.

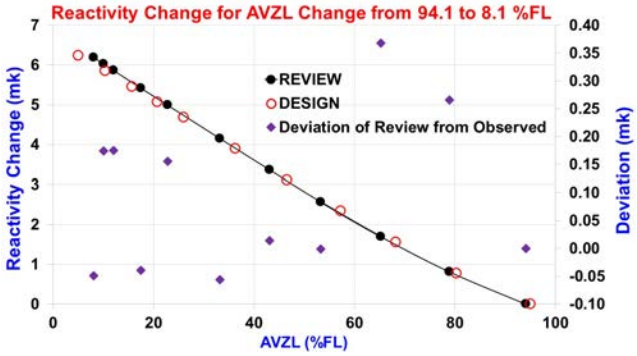


Figure 1 Calibration of AVZL of ZCC

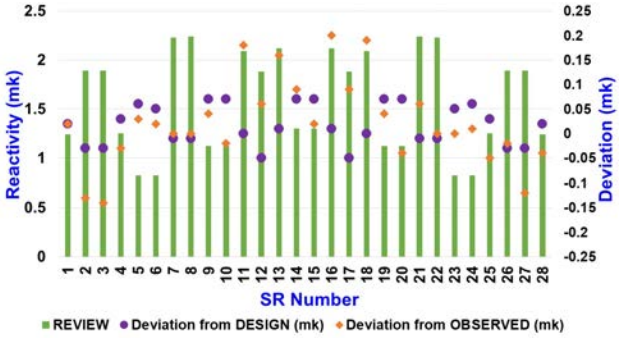


Figure 2 Worth of Individual SRs

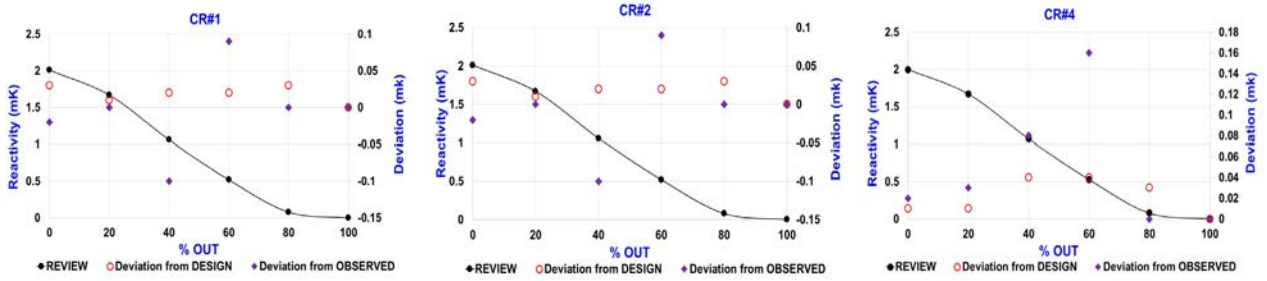


Figure 3 Worth of Individual CRs

Figure 4 shows the integral worth of individual ARs and Figure 5 shows the worth of AR bank #1 and the combined worth of the maximum worth AR banks (bank # 4 and 8) together as a function of insertion depths. Integral worth of individual AR shows good agreement with review calculations within ±0.02 mk with the design and ±0.06 mk with observed values. Integral worth of AR bank #1 calculated in review shows a maximum deviation of 0.06 mk with the observed value and for the combined worth of AR banks, slightly larger up to 0.24 mk. However, both the review and design calculations show good agreement among them.

The worth of the CR banks #1 & #2 and their combined worth as a function of different insertion depths are given in Figure 6. The integral worth agrees well with others. The S-curve is comparing reasonably well. The integral worth as calculated by review calculations are 5.17 mk, 7.30 mk and

13.06 mk for CR banks #1, #2 and combined worth, respectively against the observed values of 5.07 mk, 7.59 mk and 12.9 mk.

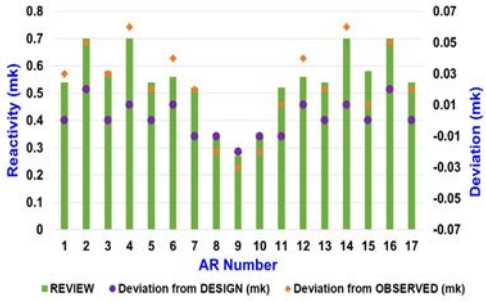


Figure 4 Worth of Individual ARs

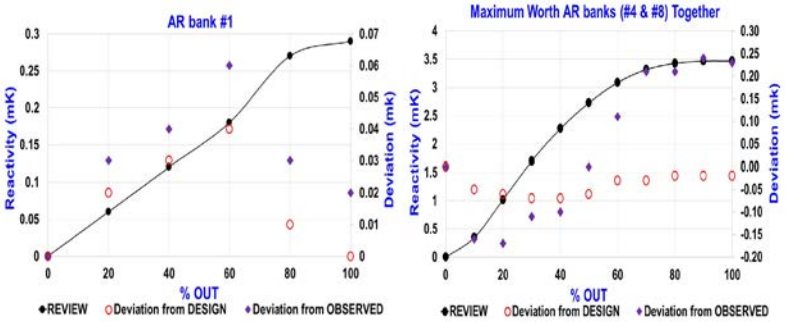


Figure 5 Calibration of AR banks

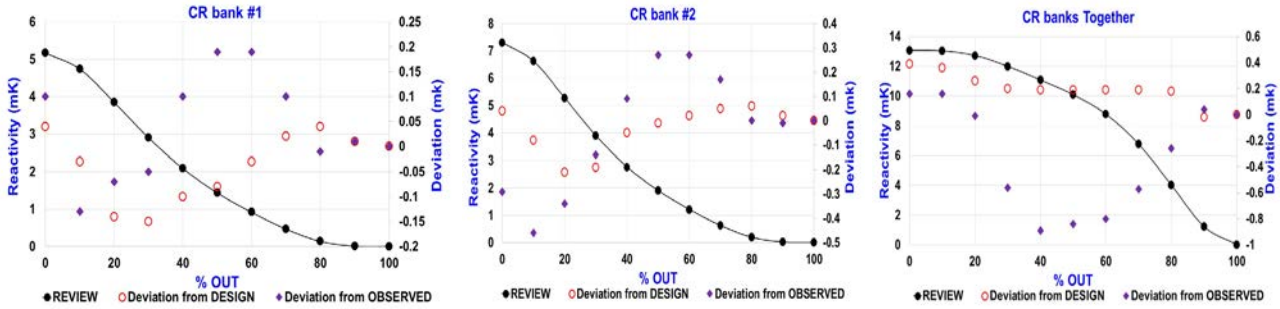


Figure 6 Calibration of CR banks

5. Conclusions

Theoretical simulations of FAC and experimental scenarios during Phase-B LPPE of KAPP-3 700MWe PHWR were carried out using DRAGON-DONJON code system as independent verification to support safety review of commissioning procedures/reports. The salient results viz., critical boron during FAC, calibration of average level (AVZL) of ZCCs against boron, worth of individual SRs, ARs and CRs, and individual worth of banks of ARs & CRs, AR banks together, CR banks together, AR together with CR bank etc. were calculated and compared with the design calculations and observed values. The comparisons in general show reasonably good agreement of the review calculations with the design as well as observed values.

6. References

[1] G. Marleau, A. Hebert and R. Roy, 2014, “A USER GUIDE FOR DRAGON VERSION 5”, *Technical report IGE-335*, Ecole Polytechnique, de Montreal, Canada, (2014)

[2] Preliminary Safety Analysis Report, Report No. KAPS – 3 & 4/PSAR – PART A/01590/Section 10.1/R-4, (2017)

[3] Commissioning Procedure for First Approach to Criticality (KAPP-3&4-01131-CP-01-Rev-3), (2019)

[4] Low Power Physics Experiments (Part-A) for Kakrapar Atomic Power Project - 3&4 (No. KAPP-3&4-01132-CR-0), (2020)

Estimation of Thermophysical Properties of Thorium Based MOX Fuel Using Classical Molecular Dynamics Simulation

Arindam Chakraborty[1*], Chandra Bhanu Basak[2] and Umasakari Kannan[1]

[1]Reactor Physics Design Division, Bhabha Atomic Research Centre, Trombay, Mumbai 400085
[2]Mechanical Metallurgy Division, Bhabha Atomic Research Centre, Trombay, Mumbai 400085
[*]e-mail: - arindamc@barc.gov.in

Abstract

Thorium based MOX fuels – (Th, U) MOX and (Th, Pu) MOX will be used in Advanced Heavy Water Reactor (AHWR) as fuel material. The thermo-physical properties like lattice parameter, thermal expansion co-efficient, enthalpy and specific heat at constant pressure are computed for temperature range 300K to 3200K using classical molecular dynamics simulation technique. The pure actinide oxide like UO_2, PuO_2 and ThO_2 were also simulated and the thermophysical properties are compared with experimental data to verify the simulation technique and the interatomic potential.

1. Introduction

The computational simulation of nuclear fuel materials is an important means of the development of advanced nuclear fuel. Different thermo-physical properties can be determined using classical molecular dynamics simulation. In the present study, different properties of nuclear fuels used in the Advanced Heavy Water Reactor (AHWR) [1] are estimated. The AHWR is being designed with (Th,U) MOX and (Th,Pu) MOX fuel.

In this study, classical molecular dynamics code LAMMPS [2] were used for simulation of nuclear fuels. The interatomic potentials developed by Cooper et al. [3,4] were utilized in these simulations.

2. AHWR

AHWR is being designed for large scale commercial utilization of thorium and technology demonstration of thorium fuel cycle. It is a vertical pressure tube type light water cooled and heavy water moderated thermal reactor. It contains 513 lattice location. Among these, 452 lattice locations are filled with fuel clusters and the rest 61 lattice locations are provided to host different reactivity devices. The composite fuel cluster of AHWR contains both (Th,U)MOX and (Th,Pu)MOX fuel pins in the equilibrium core cluster configuration. The objective of AHWR is to design an inherently safe reactor with maximum utilization of thorium. The fuel cycle of AHWR is self-sustain in ^{233}U.

3. Potentials

The interatomic potential plays a crucial role in the accurate simulation of the system with classical molecular dynamics. Different potential models [5,6,7] were used over the years for simulation of actinide oxides, which improved the estimate of the calculated properties. In this present study, a many-body potential model developed by Cooper et. al. [2,3] for different actinide oxide was utilized. The potential model is combined with pair potential and many-body EAM description of Daw and Baskes [8]. The potential function is shown in eq (1). This model is basically an empirical

fitting model where the fitting were done using different experimental data such as lattice parameter, bulk modulus and individual elastic tensor constants.

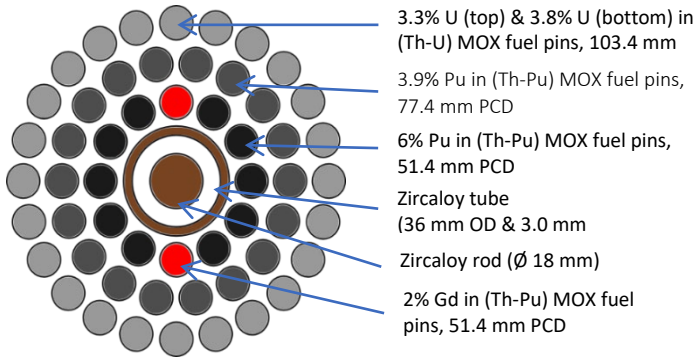


Figure 1: AHWR equilibrium core cluster cross section view

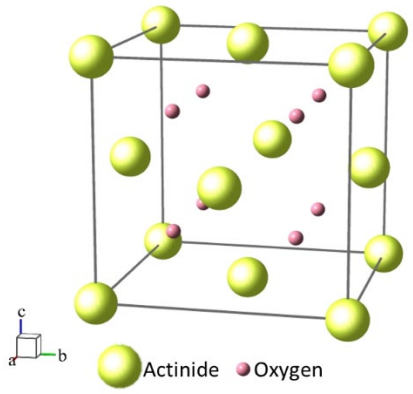


Figure 2: Fluorite structure of actinide oxides

$$E_i = \frac{1}{2}\sum_j \phi_{\alpha\beta}(r_{ij}) - G_\alpha \sqrt{\sum_j \sigma_\beta(r_{ij})} \tag{1}$$

The potential function consists of two major components – pair potential term (eq. 2) and many-body term. The pair wise interaction term consists of long-range Coulombic term (eq. 3) and short-range Morse (eq. 4) and Buckingham function (eq. 5).

$$\phi_{\alpha\beta}(r_{ij}) = \phi_C(r_{ij}) + \phi_B(r_{ij}) + \phi_M(r_{ij}) \tag{2}$$

$$\phi_C(r_{ij}) = \frac{q_\alpha q_\beta}{4\pi\epsilon_0 r_{ij}} \tag{3}$$

$$\phi_B(r_{ij}) = A_{\alpha\beta}\exp\left(\frac{-r_{ij}}{\rho_{\alpha\beta}}\right) - \frac{c_{\alpha\beta}}{r_{ij}^6} \tag{4}$$

$$\phi_M(r_{ij}) = D_{\alpha\beta}\left[\exp\{-2\gamma_{\alpha\beta}(r_{ij} - r_0)\} - 2\exp(-\gamma_{\alpha\beta}(r_{ij} - r_0)\}\right] \tag{5}$$

4. Results and discussions

Molecular dynamics simulation of actinide oxides and mixed oxides were carried out using LAMMPS. All actinide oxides have fluorite structure as shown in figure 2. The EAM potential was used for simulation with 10 × 10 × 10 supercell. The time step of 1 fs was taken for simulations. Calculations were carried out in the NPT ensemble with Nose–Hoover thermostat and barostat relaxation times of 0.1 ps and 0.5 ps respectively. Initially simulation was carried out for 10 ps to equilibrate the system.

The lattice parameters were calculated for all the lattice systems in the temperature range of 300 K to 3200 K. The variation of lattice parameter with temperature for UO_2, PuO_2 and ThO_2 are

shown in figure 3. It shows good agreement with experimental results obtained for UO_2 [9, 10], PuO_2 [11] and ThO_2 [12]. Thermal expansion coefficient for UO_2, PuO_2 and ThO_2 significantly increases above 2300 K.

Enthalpy for UO_2, PuO_2 and ThO_2 was calculated in the temperature range of 300 K to 3200 K with an interval of 100 K. The specific heat capacity at constant pressure (c_P) is estimated in this temperature range using eq. 6. The variation of c_P of UO_2, PuO_2 and ThO_2 with temperature is shown in figure 4.

$$c_p = \frac{1}{n}\left(\frac{\partial H}{\partial T}\right)_P \tag{6}$$

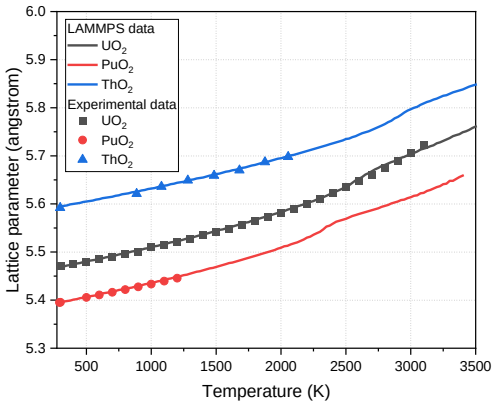


Figure 3: Variation of lattice parameters with temperature

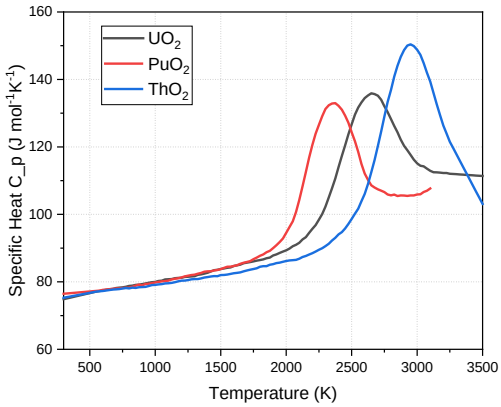


Figure 4: Variation of c_P with temperature

The properties of (Th, U) MOX and (Th, Pu) MOX are also estimated using molecular dynamics simulation. The variation of lattice pitches of MOX fuels with temperature are shown in figure 5. The variation of specific heat with temperature is shown in figure 6. It is observed that the variation of thermo-physical properties among these thorium based MOX fuels are small as the presence of other actinides are within 6%.

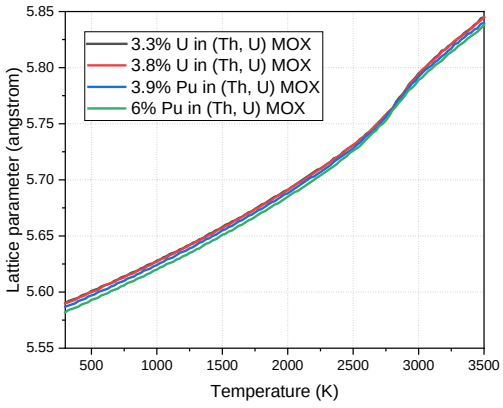


Figure 5: Variation of lattice parameters with temperature

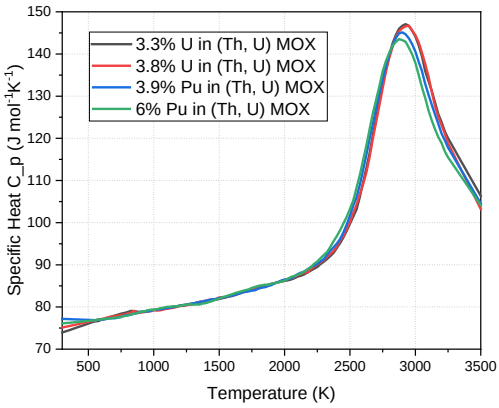


Figure 6: Variation of c_P with temperature

5. Conclusion

The lattice parameter for all the lattice shows an increasing trend with increase in temperature. The lattice parameter calculated for UO_2, PuO_2 and ThO_2 matches quite well with experimental data. The specific heat at constant pressure increases with temperature initially. The rate of increase is small up to ~ 2000K. After that, it starts to increase, attains a peak and then quickly falls to a lower value. The peak of specific heat of UO_2, PuO_2 and ThO_2 occur at different temperatures- peak specific heat for PuO_2, UO_2 and ThO_2 appears at 2375K, 2650K and 2950K respectively. The thermo-physical properties estimated for (Th, U) MOX and (Th, Pu) MOX fuel are very close to the properties of ThO_2. The variations are not significant. The lattice parameter of (Th, U) MOX fuel is slightly higher than (Th, Pu) MOX fuel. The peak value of specific heat of (Th, U) MOX fuel achieve little higher peak value and the peak attains at slightly higher temperature compared to (Th, Pu) MOX fuel. This study gives a general specification of the thorium based fuel at fresh condition. However, at higher fuel burn-up, other minor actinides will be present in the fuel. The effect of their presence in thermo-physical properties at high temperature will be studied in future.

References

1. Sinha, R. K., & Kakodkar, A. (2006). Design and development of the AHWR—the Indian thorium fuelled innovative nuclear reactor. *Nuclear Engineering and Design*, *236*(7–8), 683–700. https://doi.org/10.1016/J.NUCENGDES.2005.09.026
2. S. Plimpton, J. Comput. Phys. 117, 1-19 (1995).
3. Cooper, M. W. D., Rushton, M. J. D., & Grimes, R. W. (2014a). A many-body potential approach to modelling the thermomechanical properties of actinide oxides. *J. Phys.: Condens. Matter*, *26*, 105401. https://doi.org/10.1088/0953-8984/26/10/105401
4. Cooper, M. W. D., Rushton, M. J. D., & Grimes, R. W. (2014b). A many-body potential approach to modelling the thermomechanical properties of actinide oxides. *Journal of Physics: Condensed Matter*, *26*(10), 105401. https://doi.org/10.1088/0953-8984/26/10/105401
5. Walker, J. R., & Catlow, C. R. A. (1981). Structural and dynamic properties of UO2 at high temperatures. Journal of Physics C: Solid State Physics, 14(32), 979–983.
6. Basak, C. B., Sengupta, A. K., & Kamath, H. S. (2003). Classical molecular dynamics simulation of UO2 to predict thermophysical properties. *Journal of Alloys and Compounds*, *360*(1–2), 210–216. https://doi.org/10.1016/S0925-8388(03)00350-5
7. Arima, T., Yamasaki, S., Inagaki, Y., & Idemitsu, K. (2005). Evaluation of thermal properties of UO2 and PuO2 by equilibrium molecular dynamics simulations from 300 to 2000K. *Journal of Alloys and Compounds*, *400*(1–2), 43–50. https://doi.org/10.1016/j.jallcom.2005.04.003
8. Daw, M. S., & Baskes, M. I. (n.d.). Embedded-atom method: Derivation and application to impurities, surfaces, and other defects in metals. In *PHYSICAL REVIEW* (Vol. 8).
9. Kim Y-E, Park J-W and Cleveland J 2006 Thermophysical properties database of materials for light water reactors and heavy water reactors (Vienna: IAEA)
10. Fink J 2000 J. Nucl. Mater. 279 1–18
11. Yamashita T, Nitani N, Tsuji T and Inagaki H 1997 J. Nucl. Mater. 245 72–8
12. Hirata K, Moriya K and Waseda Y 1977 J. Mater. Sci. 12 838–9

STUDIES ON THE VARIATION OF REACTOR KINETIC PARAMETERS WITH LATEST ENDF-6 NUCLEAR DATA LIBRARIES

Arun Stanley[1], Puspendu Hazra[1], T. Sathiyasheela[1], K. Devan[1]
[1] Indira Gandhi Centre for Atomic Research, Kalpakkam, India
[1]*e-mail: - arunstanley@igcar.gov.in*

Abstract

Variation in the kinetic parameters like effective delayed neutron fraction (β_{eff}), precursor decay constants (λ) and neutron generation time (Λ) of a typical mixed oxide (MOX) fuelled Fast Breeder Reactor (FBR) is estimated using delayed neutron data from various ENDF-6 nuclear data libraries. Estimation of kinetic parameters was performed using an indigenous diffusion code in 2D cylindrical geometry. Variation in β_{eff} was also studied using FCA XIX and MASURCA R2 & ZONA2 benchmarks. Delayed neutron data from ENDF/B-VIII, JENDL3.3, JENDL4.0 and CENDL3.2 were used in the study. Spread in β_{eff} obtained is within ±2.5% of the mean value.

1. Introduction

Reactor kinetics parameters, which includes effective delayed neutron fraction (β_{eff}), precursor decay constants (λ) and neutron generation time (Λ), are major safety parameters for a reactor as they determine the reactor period for a given reactivity as well as the margin to prompt criticality. The key input to estimate these parameters is the delayed neutron data, i.e. the delayed neutron yield and spectrum of different fissionable nuclei in six precursor groups. This data is available in various nuclear data libraries published internationally.

In this study the variation in the kinetic parameters is estimated for a typical MOX fuelled, medium sized FBR, using delayed neutron data from ENDF/B-VIII, JENDL3.3, JENDL4.0 and CENDL3.2 nuclear data libraries. Neutron flux both direct and adjoint flux are needed for estimation of kinetic parameters, which is obtained from an indigenous multi-group diffusion code in 2D cylindrical geometry [1]. The same code can also estimate the kinetic parameters if the delayed neutron data is given as input. The MOX fuel considered for the FBR case study has an enrichment of 20.7% PuO_2 in core 1 and 27.7% PuO_2 in core 2 [2]. The reactor also consists of radial & axial blankets of 0.25% depleted UO_2. β_{eff} benchmark studies were performed using the FCA XIX cores and MASURCA R2 & ZONA2 cores [3] to verify the method of kinetic parameter estimation.

2. Reactor kinetics parameters

The reactor kinetics parameters are defined based on diffusion theory as follows [4]:

$$\beta_{i,eff} = \frac{\sum_{n=1}^{N} \int_V \sum_g \phi_g^* \chi_{g,n,i}^d \sum_{g'} \left(\nu_{d,i} \Sigma_f\right)_{ng'} \phi_{g'} dV}{f}, \qquad \beta_{eff} = \sum_{i=1}^{n_d} \beta_{i,eff} \tag{1}$$

$$\lambda_{i,eff} = \frac{\sum_n \lambda_{i,n} \beta_{i,n,eff}}{\beta_{i,eff}} \tag{2}$$

$$\Lambda = \frac{\int_V \sum_g \phi_g^* \phi_g / u_g dV}{f} \tag{3}$$

$$f = \sum_{n=1}^{N} \int_{V} \sum_{g} \phi_g^* \chi_g \sum_{g'} \left(\nu\Sigma_f\right)_{ng'} \phi_{g'} dV \tag{4}$$

where, ϕ and ϕ^* are the flux and adjoint flux, Σ_f is the fission cross section, χ is the fission spectrum, u_g is the group velocity, n_d is the number of precursor groups, N is the total number of nuclei and f is the adjoint weighted fission source. Delayed neutron yield, ν_d, and spectrum, χ^d, constitute the delayed neutron data. For flux and adjoint flux calculation ABBN 93 data library is used. ABBN 93 data is also used for Σ_f in Eq. (1) and $\nu\Sigma_f$ in Eq. (4). The delayed neutron data of all fissile and fertile nuclei is obtained from various ENDF-6 nuclear data libraries by using NJOY-2016 code.

3. β_{eff} benchmark studies

Experimentally determined values of β_{eff} of certain reactors are available in the literature. The β_{eff} benchmark problems FCA XIX (JAERI, Japan) and MASURCA R2 & ZONA2 (CEA, France) [3] are considered to verify the method of kinetics parameter estimation. FCA XIX-1 is a U based core, XIX-2 a Pu/Nat.U core and XIX-3 a Pu core, whereas MASURCA R2 is a U core and ZONA2 is a MOX core. These cores together consider different nuclide contribution from U-235, U-238 and Pu-239 to β_{eff}. The 2D cylindrical (r-z) geometry models of these cores from [3] are used to solve for the direct and adjoint flux. The number densities of each isotope in different regions of each core given in reference [3] are used to obtain the ABBN macroscopic cross section data in 26 energy groups for each individual volume of these cores in r-z geometry.

An indigenous diffusion code [1] is used to estimate the flux and adjoint flux of these cores. This code takes the r-z geometry model and the macroscopic cross section data of different regions as input. It uses a standard inner-outer iteration scheme [4] with Gauss-Seidel method for inner iterations and power method for outer iterations. The flux and adjoint flux thus obtained is used along with the delayed neutron data to estimate the kinetic parameters using Eqs. 1-4.

Effective delayed neutron fraction of FCA and MASURCA cores estimated using delayed neutron data from different data libraries is shown in Tables 1 and 2. Correction factors (heterogeneity, XYZ to RZ and transport corrections) from reference [3] were used for the FCA XIX cores.

Table 1. β_{eff} of FCA XIX cores (in pcm).

	XIX-1	**XIX-2**	**XIX-3**
ENDF/B-VIII	738	356	250
JENDL 3.3	734	361	246
JENDL 4.0	734	361	246
CENDL 3.2	758	368	245
Experimental [3]	742±24	364±9	251±4

Table 2. β_{eff} of MASURCA R2 & ZONA2 cores (in pcm).

	R2	**ZONA2**
ENDF/B-VIII	738	349
JENDL 3.3	738	356
JENDL 4.0	738	355
CENDL 3.2	759	363
Experimental [3]	721±11	349±6

For FCA XIX cores, we obtain β_{eff} within the experimental limits except for the Pu core XIX-3 where results are still very close to the limits. For MASURCA R2 core we get results higher than the experimental upper limit especially with the CENDL 3.2 library. As for the MOX core ZONA2 we get very good results except with CENDL 3.2 which slightly over predicts the value. All values are found to be within ±2.5% of the experimental mean value except for CENDL 3.2 for MASURCA cores which goes up to +5%.

4. FBR kinetics parameters

As mentioned earlier we use a typical 500 MWe MOX fuelled FBR for this study [2]. The flux and adjoint flux is calculated in 2D cylindrical geometry and kinetics parameters are estimated according to Eqs. 1-4. Results are shown in Table 3 and 4.

Table 3. β_{eff} in six precursor groups and total for the FBR core (in pcm).

	β_1	β_2	β_3	β_4	β_5	β_6	Total β_{eff}
ENDF/B-VIII	8	63	51	119	69	25	335
JENDL 3.3	8	75	60	121	54	20	338
JENDL 4.0	8	75	60	121	54	20	338
CENDL 3.2	8	73	57	123	60	25	346

Table 4. Precursor decay constants, λ (s^{-1}) in six groups and neutron generation time, Λ (s) for FBR.

	λ_1	λ_2	λ_3	λ_4	λ_5	λ_6	Λ
ENDF/B-VIII	0.013382	0.030867	0.11727	0.30797	0.88172	2.9410	4.1658e-7
JENDL 3.3	0.012904	0.030637	0.12874	0.34180	1.34220	3.4951	4.1658e-7
JENDL 4.0	0.012972	0.030648	0.12810	0.33690	1.24160	3.4363	4.1658e-7
CENDL 3.2	0.013003	0.031170	0.13367	0.34347	1.36720	3.7005	4.1658e-7

Effective delayed neutron fraction predicted by ENDF/B-VIII and JENDL 4.0 libraries are very close to each other while CENDL 3.2 predicts a slightly higher value similar to what was seen in the benchmark studies. All β_{eff} predictions are within ±2% of the mean value, 339 pcm. Whereas the precursor decay constants show variations up to ±7% excluding the large change exhibited by ENDF/B-VIII in groups 5&6. The neutron generation time does not change since it doesn't depend on the delayed neutron data.

5. Conclusion

Benchmark studies on effective delayed neutron fraction were successfully carried out using the FCA and MASURCA cores with ABBN 93 cross section data and latest delayed neutron data from ENDF-6 libraries. Variation in β_{eff} was found to be within ±2.5% of the experimental mean value for ENDF/B-VIII and JENDL 3.3 & 4.0 libraries while CENDL 3.2 library varied up to +5%. Variation in the reactor kinetic parameters of a typical MOX fuelled FBR core was also investigated. Changes in β_{eff} were found to be within ±2% of the mean value while the precursor decay constants vary up to ±7%. This variation in the prediction of kinetic parameters (β_{eff} and λ) should be taken in to account when estimating the margin to prompt criticality in nuclear reactors as well as any reactivity estimations using these parameters.

6. References

[1] Arun Stanley, "A multigroup 2-D diffusion code in rectangular and cylindrical geometries", *IGCAR/RDTG/NSDG/RND/SAS/296*, April 2020.

[2] Anuraj V. L, A. Riyas, G. S. Srinivasan, K. Devan and Abhitab Bachchan, "Stability characteristics of metal fueled fast reactor cores", *Nuclear Engineering and Design*, Vol. 340, 2018, pp 318-324.

[3] S. Okajima, T. Sakurai, J. F. Lebrat, V. Z. Averlant and M. Martini, "Summary on international benchmark experiments for effective delayed neutron fraction (β_{eff})", *Progress in Nuclear Energy*, Vol. 41, Iss. 1–4, 2002, pp. 285-301.

[4] Alan E. Waltar, Donald R. Todd and Pavel V. Tsvetkov, "Fast spectrum reactors", *Springer*, New York, 2012, ISBN: 978-1-4419-9571-1, pp. 49-135.

Advances in Reactor Physics (ARP-2022)
Mumbai, India, May. 18-21, 2022

DEVELOPMENT OF A NEW NEUTRON MULTI-GROUP CROSS SECTION SET IN ABBNFORMAT FROM THE LATEST ENDF-6 FILES FOR FAST REACTORS

Puspendu Hazra[1], A. Riyas[1], K. Devan[1]
[1]Indira Gandhi Centre for Atomic Research, Kalpakkam, India
[1]e-mail: - *hazra@igcar.gov.in*

Abstract

The neutron multi-group data plays a veryfundamental role in the reactor physics design analyses. For fast reactor applications, it is generally prepared by using the Bondarenko's self-shielding factor table method with Narrow Resonance approximation. The Russian adjusted ABBN-93 set, prepared based on FOND-2data libraryand pre-processing codes such as NJOY-91(American) and GRUCON (Russian), which was made available here based on an IPPE-IGCAR scientific collaboration, is being used for the neutronics analysis of fast reactorssince 1999. In recent years, the nuclear data has undergone several revisions which resulted the release of new ENDF-6 libraries such as ENDF/B-VIII, JENDL-4, JEFF-3.3, ROSFOND-2010, CENDL-3. The impact of these data on reactor core design can be assessed at IGCAR using deterministic code systems if multi-group database on the above libraries in ABBN format are available. It requires the in-house development of necessary tools and methodology. This paper discusses the development of a software package known as MDPC (Multigroup Data Preparation Code) for preparing a parallel ABBN set from the processed data of NJOY-16 and GRUCON codes. Multi-grouping method, energy group structure and data definitions of reference ABBN-93 are preserved in this code. For easy verification of the methodology being adopted in MDPC, a new multi-group set known as IGC-ABBN has been prepared from the same FOND-2 library for important fast reactor core materials. Preliminary validation exercise showed that the results from IGC-ABBN and the original ABBN-93 are very close to each other. Few more benchmark analyses are necessary to establish the correctness of the procedure and the methodology which is currently in progress.

1. Introduction

The Russian ABBN-93 [1] system was prepared by the Institute of Physics and Power Engineering (IPPE), Russia. Based on a collaborative agreement in 1999 between IGCAR and IPPE on fast reactors, a part of ABBN-93 system along with the processing code CONSYST-2 was made available at IGCAR for core neutronic analysis.ABBN-93 contains a large collection of data for various applications. The above data were prepared from FOND-2 library by using the processing codesNJOY-16 [2] and GRUCON [3] codes.

To prepare a parallel ABBN set, as a first step, it is necessary to perform pre-processing of ENDF-6 data using NJOY and GRUCON codes. Next, the processed output from the GENDF file has to be read as per the definition and format of each data. They are subsequently used for preparing the ABBN library. A tool known as MDPC (Multi-group Data Preparation Code)is developed for this purpose (Fig. 1). It is used for the preparation of anew multi-group library known as IGC-ABBN. FOND-2 library has been used to enable easy verification of processed data and methodology employed. Salient features of MDPC and IGC-ABBN are discussed in this paper.

2. Methodologies involved in MDPC

This section briefly describes the methodologies by which the following four types of multi-group data are prepared:

- Multi-group constants (data in 28 and 299 group structure for different reactions).
- Inelastic and elastic group to group transfer matrices.
- Self-shielding factors at 300K temperature.
- Doppler coefficients data for three temperatures, i.e. 300K, 900K and 2100K.

The group structure and weighting flux for multi-grouping are considered the same as in original ABBN set.

a. Multi-group constants

This data table contains all type of multi-grouped cross section like total, capture, inelastic, elastic, fission etc. Almost all the group cross sections are retrieved directly from the GENDF output of NJOY-2016. The average lethargy increment in elastic scattering (ξ_g) is calculated from the continuous lethargy increment $\xi(E)$ data generated by GRUCON as

$$\xi_g = \frac{\int_g^{g+1} \xi(E)\sigma_e(E)\phi(E)dE}{\int_g^{g+1} \sigma_e(E)\phi(E)dE};$$

where, the symbols have their usual meanings.

b. Elastic and inelastic group to group transfer matrices

For both elastic and inelastic reactions, the processing codes generate inter-group transfer cross sections ($\sigma_{e,l}^{g\to g+k}$). But the matrices given in the ABBN-93 set for elastic reaction are in probability structure.Hence, the probability of transfer is calculated in following method:

$$p_l^{g\to g+k} = \frac{\sigma_{e,l}^{g\to g+k}}{\sum_k \sigma_{e,0}^{g\to g+k}}, \qquad \sum_k p_0^{g\to g+k} = 1, \sum_k p_1^{g\to g+k} = \mu_e^g$$

Here, *'l'* signifies the moment of transfer and μ_e^g is the group averaged cosine of the elastic scattering angle.

For inelastic scattering, NJOY does not generate transfer matrices for "total"reaction rather it generates for all partial reactions like, all the excited states of (n,n') reactions, (n,2n), (n,3n) etc. Hence all the partial transfer cross sections has been summed up to get the probability of transfer as

$$\sigma_{in}^l(g \to k) = \sum_i \sigma_{in,i}^l(g \to k)$$

Here, *'I'* denotes the partial reactions.

c. Self-shielding factors and Doppler coefficients

The processing codes prepare cross sections $\sigma^g(\sigma_0, T)$ at three temperatures, i.e. 300K, 900K and 2100K. The self shielding factors are calculated for 16 different dilutions for the above three temperatures by the following relation;

$$f^g(\sigma_0, T) = \frac{\sigma^g(\sigma_0,T)}{\sigma^g(\infty,T)};$$

where, σ_0 is the dilution cross section and $\sigma^g(\infty, T)$ in the denominator denotes infinite dilution cross section. The Doppler increments are computed as:

$$\Delta_1(\sigma_0) = f(\sigma_0, T_2) - f(\sigma_0, T_1)$$
$$\Delta_2(\sigma_0) = f(\sigma_0, T_3) - f(\sigma_0, T_2)$$

3. Flowchart of preparation of IGC-ABBN

The flowchart belowin Fig.1describes various steps involved for the preparation of IGC-ABBN.There are four kinds of inputs in the input block. One of these is the ENDF-6 library (FOND-2) and other three inputs are in standard form for the pre-processing codes. Four modules have been used in NJOY to multi-group the data; RECONR, BROADR, UNRESR and GROUPR. The package MDPC controls all the processes involved in the flowchart. It helps to prepare the data for a single nuclide in a single run. The data has been prepared in both 28 and 299 group structures for U-235, U-238, Pu-239, Pu-240, Pu-241, Pu-242, C-12, O-16 and Sodium. And for other nuclides only 28 group data has been prepared, these are: Pu-238, Am-241, Fe, Cr, Ni, Si, Mn, Al, Cu and Molybdenum.

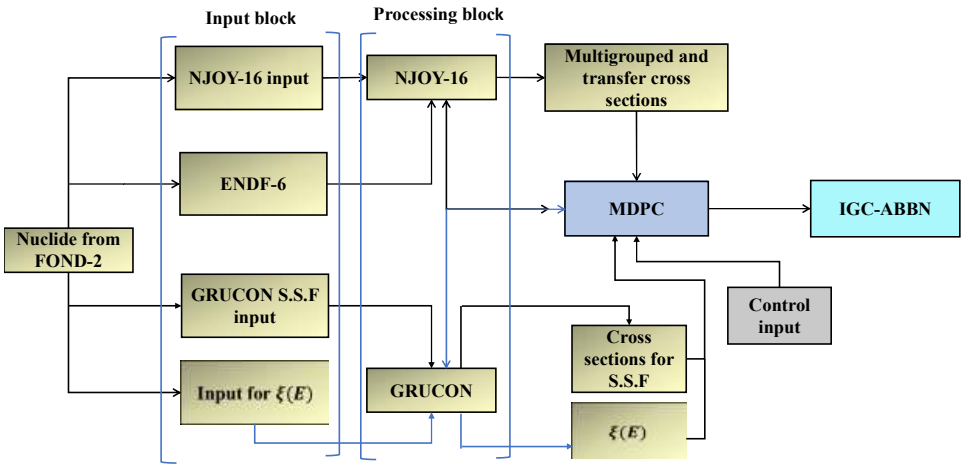


Fig. 1: Flowchart of IGC-ABBN preparation.

4. Benchmark studies

Two benchmarks are analysed as a part of validation of IGC-ABBN. They are: (a) ZPR-6-7 [4] and (b) 1200 MWe IAEA-ANL theoretical benchmark [5]. The 2-D neutron diffusiontheory code ALCIALMI is used to analyse these benchmarks. The self-shielded cross sections of nuclides present in the benchmark are prepared by using CONSYST-2 and EFCONSY codes. Six configurations are analysed for 1200 MWe benchmark. Results are given in Tables 1-3.

Table 1: Comparison of k-eff for ZPR-6-7: ABBN-93 (Ref.) vs. IGC-ABBN

Parameter	Experimental Value	Benchmark-model (expected)	With Reference old ABBN data	With newly prepared ABBN data
k_{eff}	1.00051 ±0.00087	0.9866 ± 0.0023	0.98333	0.98666

The benchmark model in table-1 above is the simplified R-Z model of the as-built experimental ZPR-6-7 core model. Hence, a difference in k_{eff} is there between the two models. In this study, only the benchmark model is analysed.

Table 2: Computed k-eff's for Different Configurations of 1200MWe Benchmark

Configuration	Description	k-eff	
		ABBN-93	IGC-ABBN
1	Reference benchmark with the average temperatures of all the nuclides as 1100K.	1.01148	1.01230
2	Sodium voided inner core with config.1.	1.03126	1.03149
3	Sodium voided inner core, outer core and axial blanket with config.1.	1.03028	1.03035
4	Reference with hot fuel nuclides (2200K) and other nuclides at 1100K.	1.00328	1.00372
5	Sodium voided inner core with config.4.	1.02515	1.02517
6	Sodium voided inner core, outer core and axial blanket with config.4.	1.02486	1.02477

Table 3: Sodium Void Worth and Doppler Worth

	ABBN-93 (Ref.)	IGC-ABBN
Sodium void worth (pcm)		
Inner core voided	1956	1896
Inner, outer core and axial blanket voided	1859.5	1783
Doppler worth (pcm)		
Sodiumin	-810	-847.5
Sodium out	-526.5	-541

5. Conclusions

A computer code MDPC has been developed for reading the GENDF formatted output files of NJOY and GRUCON codes and preparing ABBN formatted multi-group sets. Using it,a new set known as IGC-ABBN, based on FOND-2 library, has been prepared for important fast reactor core materials such as fuel, structural and sodium. Preliminary validation results of IGC-ABBN library against ZPR-6-7 and 1200 MWe IAEA/NEACRP theoretical benchmarks show a relative difference of minimum 0.1% to maximum 4.1% as compared to the original ABBN-93 set. This confirms the correctness of the methodology, format and the definitions of various data derived using MDPC. Processing of other data such as fission products (individual and lumped), delayed neutron data, subgroup parameters and gamma interaction data etc. is in progress. Future plan is to prepare ENDF/B-VIII and ROSFOND-2010 based ABBN libraries.

6. References

[1] (a) ABBN-93 Group Data Library-Part I: Nuclear Data for the Calculation of Neutron and Photon Radiation Functions, G. N. Manturov, INDC (CCP-409), IAEA, Vienna (1997).

(b) Description of Russian Multigroup Nuclear Data Library ABBN-93, ABBN Laboratory Report obtain from IPPE based on “Co-operation in Reactor Physics” between IPPE and IGCAR (1999).

(c) K. Devan, ‘Salient Features of ABBN-93 Constant System’, RPD/NDS/70 (1998).

[2] R. E. MacFarlane, ‘The NJOY nuclear data processing system, version 2016’, Theoretical DivisionLANL (2016).

[3]V. V. Sinitsa, ‘The GRUCON code package for evaluated nuclear data processing’, National Research centre, Kurchatov Institute (2017).

[4] L. G. Lesage, An Overview of the Argonne National Laboratory Fast Critical Experiments 1963-1990, Report ANL-NT-175, USA (2001).

[5] L. G. Lesage et al., Proceedings of NEACRP/IAEA Specialists Meeting on International Comparison Calculation of a Large Sodium Cooled Fast Breeder Reactors, held at ANL on Feb. 1978, Report-ANL-80-78 (1980).

QUANTIFICATION OF NUCLEAR DATA CONTRIBUTION TO UNCERTAINTY IN FUEL SA DECAY POWER

G. Pandikumar[1] and A. John Arul[1, 2]
[1]Indira Gandhi Centre for Atomic Research, Kalpakkam, Tamilnadu 603102, India
[2]Homi Bhabha National Institute, Training School Complex, Anushaktinagar, Mumbai-400094, India.

e-mail: - pkg@igcar.gov.in

Abstract

The uncertainty in decay power due to uncertainty in half-life and decay energy of radionuclide and Pu239 fission product yield has been carried out. Sensitivity method has been used to estimate the uncertainty. It is observed that the uncertainty in decay power due to decay energy, is dominant, and found to be about 5% at zero cooling period. The uncertainty in decay power due to half-life and due to FP yield are less than 1% respectively.

1.0 Introduction

The decay power is being estimated using the versatile point depletion code ORIGEN2.1 [1]. The code is associated with nuclear database suitable for various reactors. Accuracy of ORIGEN2.1 prediction depends on the accuracy of the nuclear data used for calculation. Consequent to uncertainty in nuclear data, uncertainty of 20% is added over the predicted decay power for all cooling periods. In the present work, uncertainty in decay power due to uncertainty in half-life and decay energy of radionuclides and Pu239 fission product yield has been carried out, using Jun-ichi Katakura [2] sensitive analysis methodology. Uncertainty in decay power due to uncertainty in neutron interaction cross section is not considered in the present study.

2.0 Summation calculation and sensitivity analyses

The code ORIGEN2.1 solves Bateman equation for finding the inventory of any nuclide at a time 't'. After estimating the number of atoms of all radionuclide, ORIGEN2 estimates the activity from individual radionuclide by multiplying N_i with decay constant, then the decay powers by multiplying the activity by decay energy. Individual radionuclide contributions are summed up to get total decay power. That is the decay power f(t) from fission products at a time t after an irradiation is calculated using

$$f(t) = \sum_{i=1}^{M} \lambda_i E_i N_i(t) \tag{2}$$

where M is the number of fission products, λ_i is the decay constant of nuclide 'i', E_i is the decay energy per decay of nuclide 'i', $N_i(t)$ is the number of nuclide 'i' at a time 't' after irradiation.

2.1 Sensitivity coefficients

The relative sensitive coefficient of the decay power f(t) to a variable P_k is given by

$$G(P_k, t) = \frac{\left(\frac{df}{dP_k}\right)}{\left(\frac{f(t)}{P_k}\right)} \tag{3}$$

In the present calculation, sensitivity coefficient with respect to decay constant, decay energy and fission product yield are calculated as

(i) Decay energy

$$G(E_i, t) = \frac{\lambda_i E_i N_i(t)}{f(t)} \tag{4}$$

(ii) Independent yield

$$G(Y_i, t) = \frac{Y_i \sum_{i=1}^{N_{max}} \lambda_i E_i N_i(t)}{f(t)} \tag{5}$$

Y_i is the independent fission product yield of nuclide 'i'. The summation extends to the maximum number N_{max} of the upstream side of the decay chain including the nuclide 'i'.

(iii) Decay constant

$$G(\lambda_i, t) = G(E_i, t) + \sum_{j=1}^{i} \sum_{k=j}^{N_{max}} Y_j \lambda_k E_k \lambda_i \left(\frac{dN_k^j}{d\lambda_k}\right) \Big/ f(t) \tag{6}$$

Most of the fission products are beta active. Successive beta decay of fission products form a mass chain (Since A remains same). The second summation represents sum over linearized mass chain. N_k^j represents the number of atoms in a linearized mass chain. The derivative is calculated using (dropping the super-script j as it indicates the mass chain)

$$\frac{dN_k}{d\lambda} = \frac{N_k(\lambda + \Delta\lambda) - N_k(\lambda)}{\Delta\lambda} \tag{7}$$

where $N_k(\lambda+\Delta\lambda)$ represents the concentration of a nuclide 'i' estimated using the half-life of nuclide 'i' including its uncertainty (i.e. using $t_{1/2} + \Delta t_{1/2}$) and similarly $N_k(\lambda)$ represents the concentration of a nuclide 'i' estimated using the half-life of nuclide 'i'. $\Delta\lambda$ is the uncertainty in decay constant.

2.2 Uncertainty in decay power

The uncertainties arising from individual components viz., decay energy, decay constant and fission product yield is calculated as follows

$$\left(\frac{\Delta f}{f}\right)_E = \left[\sum_i \left(G(E_i, t) \cdot \frac{\Delta E_i}{E_i}\right)^2\right]^{1/2} \tag{8}$$

$$\left(\frac{\Delta f}{f}\right)_\lambda = \left[\sum_i \left(G(\lambda_i, t) \cdot \frac{\Delta \lambda_i}{\lambda_i}\right)^2\right]^{1/2} \tag{9}$$

$$\left(\frac{\Delta f}{f}\right)_Y = \left[\sum_i \left(\frac{G(Y_i, t)}{Y_i}\right)^2 \mu_{ii} + \sum_i \sum_{j \neq i} \frac{G(Y_i, t) G(Y_j, t)}{Y_i Y_j} \mu_{ij}\right]^{1/2} \tag{10}$$

where μ_{ij} is the covariance matrix coefficient of the independent yields Y_i and Y_j. ΔE is the uncertainty in decay energy and.

$$\mu_{ii} = \sigma_i^2 \left(1 - \frac{\sigma_i^2}{\sigma^2 + \sum_{j=1}^{n} \sigma_j^2}\right) \tag{11}$$

$$\mu_{ij} = -\frac{\sigma_i^2 \sigma_j^2}{\sigma^2 + \sum_{j=1}^{n} \sigma_j^2} \tag{12}$$

where σ_i is the uncertainty of the independent yield Y_i, σ is the uncertainty of the mass yield, and n is the number of nuclides in the same mass chain.

The total uncertainty of the decay power is given by

$$\left(\frac{\Delta f(t)}{f(t)}\right) = \left[\left(\frac{\Delta f}{f}\right)_E^2 + \left(\frac{\Delta f}{f}\right)_\lambda^2 + \left(\frac{\Delta f}{f}\right)_Y^2\right]^{1/2} \tag{13}$$

3.0 Decay power uncertainty in PFBR Core1 SA

For PFBR [5] core1 fuel sub-assembly (SA), irradiated for a burnup of 100GWd/t, the decay power has been estimated for different cooling periods, using the code ORIGEN2.1. The concentrations of each fission products estimated using $t_{1/2}$ and $(t_{1/2} + \Delta t_{1/2})$ are retrieved from ORIGEN2.1 output.

The uncertainty in decay energy and half-life are retrieved from JENDL/DDF-2015 [3] and the fission product yield uncertainty is taken from JENDL/FPYD-2011 [4]. When uncertainty in decay energy is not given, that is, if $\Delta E=0.0$, the uncertainty is assumed 100% ($\Delta E=E$).

Table 1: PFBR Core1 fuel SA decay power and estimated uncertainty

Decay time	Uncertainty (%)			
	$\left(\frac{\Delta f}{f}\right)_E$	$\left(\frac{\Delta f}{f}\right)_\lambda$	$\left(\frac{\Delta f}{f}\right)_Y$	$\left(\frac{\Delta f}{f}\right)_{Total}$
1s	3.53	0.77	0.31	4.61
1m	2.21	0.23	0.31	2.75
10m	0.43	0.15	0.36	0.94
30m	0.44	0.12	0.40	0.96
1h	0.35	0.11	0.42	0.88
5h	0.39	0.14	0.37	0.90
10h	0.43	0.15	0.27	0.85
20h	0.46	0.15	0.14	0.75
2d	0.52	0.14	0.07	0.73
5d	0.38	0.13	0.07	0.58
10d	0.54	0.14	0.06	0.74
30d	0.29	0.22	0.03	0.54

Table 1 gives the uncertainty contributions from the components viz., decay energy, half-life and fission product yield (FPY). The uncertainty in decay power due to decay energy, is dominant, and found to be about 5% at zero cooling period. The uncertainty in decay power due to half-life and FPY are less than 1%. The uncertainty is more at shorter cooling period. This may be due to the difficulty in the measurements, particularly the decay energy of short lived fission products. Figure 1 gives the uncertainty (%) contribution from decay energy, half-life and fission product (FP) yield.

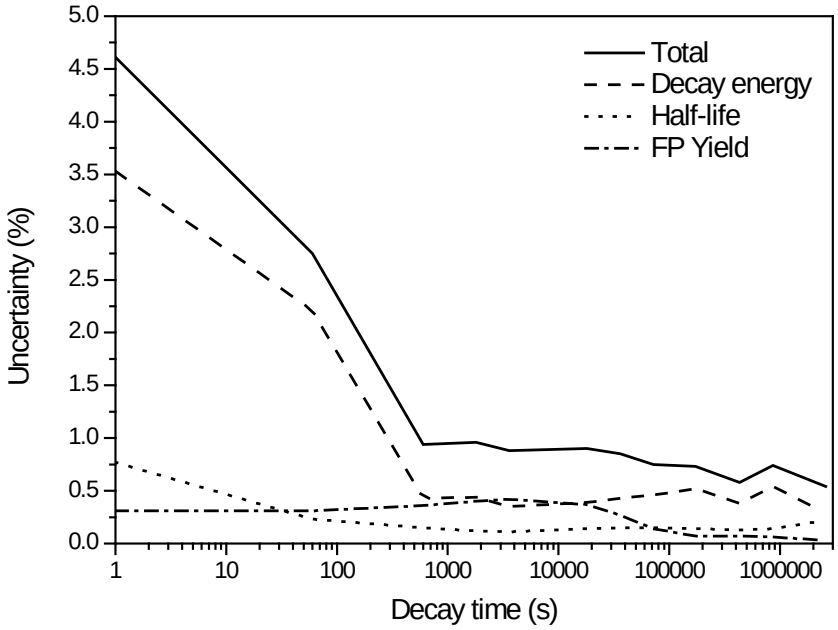


Fig. 1: Uncertainty (%) contribution from decay energy, half-life and FPY to PFBR fuel SA

4.0 Conclusion

Uncertainty in predicted decay power is estimated using sensitivity method. The uncertainty in decay power due to uncertainty in half-life and decay energy of radionuclide and Pu239 fission product yield has been carried out. It is observed that the uncertainty in decay power due to decay energy, is dominant, and found to be about 5% at zero cooling period. The uncertainty in decay power due to half-life and due to FP yield are less than 1% respectively. The uncertainty is more at shorter cooling period. This may be due to the difficulty in the measurements, particularly the decay energy of short lived fission products. Since, recent measurement in structural materials [6] indicates a C/E of ~10% in decay power, the major contribution is likely from neutron interaction cross section, which is being investigated.

References:

[1] G. Croff, "ORIGEN2: A Versatile Computer Code for Calculating the Nuclide Composition and Characteristics of Nuclear Materials", Nucl. Tech. 62 (1983).

[2] Jun-ichi Katakura, Uncertainty analyses of decay heat summation calculations using JENDL, JEFF, and ENDF files, Journal of Nuclear Science and Technology, Vol. 50, No. 8, 799–807, 2013. http://dx.doi.org/10.1080/00223131.2013.808004.

[3] J. Katakura and F. Minato "JENDL Decay Data File 2015, "*JAEA-Data/Code 2015-030* (Mar 2016).

[4] J. Katakura "JENDL FP Decay Data File 2011 and Fission Yields Data File 2011, "*JAEA-Data/Code 2011-025* (Mar 2012).

[5] Prototype fast breeder reactor, Preliminary Safety Analysis Report, Chapter 5.1, Reactor Physics, Indira Gandhi Centre for Atomic Research, Kalpakkam, May 2014.

[6] G. Pandikumar, D.V. Subramanian, Adish Haridas, Anupam Chakrabarthy, Decay power measurements from P91, SS316L, SS304L and D9 steels: Irradiation experiment in KAMINI, PFBR/01115/DN/1200/Rev-0, Dec 2019.

ESTIMATION OF UNCERTAINTY IN THE CONTROL ROD WORTH IN CANDU PHWR

M. Mohideen Abdul Razak

Bhabha Atomic Research Centre Facilities, Kalpakkam, 603127, India
e-mail: - mmar@igcar.gov.in

Abstract

It is important to predict the reactor core behaviour accurately for the safe operation of nuclear reactors under normal and hypothetical accidental scenarios. Under any abnormal situation arising during reactor operation, the reactor is brought to normalcy by adjusting the control rods. The worth of control rods is important in predicting the control rod position and to suppress the transient. The uncertainty in the worth of control rod, caused by a given level of uncertainty in the macroscopic thermal absorption cross section data is discussed. The uncertainty in the control rod worth in CANDU reactor (AECL-7236) is estimated for various levels of uncertainties in the thermal absorption cross section data. Here first order perturbation method is used to estimate the uncertainty. It is observed that for 1% uncertainty in the thermal absorption cross section, the uncertainty in the worth of control rod in the outer core is found to be 3.54%. The uncertainty in the worth of control rods in different region of the core is also discussed.

1. Introduction

The deterministic safety analysis as an essential for demonstrating the safety of nuclear power plants. Nuclear codes are used not only to estimate the behavior of nuclear reactor during off-normal conditions, but also for the evaluation of safety margins. Even though modern nuclear codes are based on the best available model, uncertainties are always present in the calculations. Uncertainties originate from different sources like for instance, a lack of knowledge in the physical interpretation and representation of the code models, as well as plant and fuel parameters that are fed as input data to the code. It is important to know the uncertainty in the neutron multiplication factor when the macroscopic cross section data are perturbed around the best estimate values. Uncertainties in neutron multiplication factor, worth of control rods, void coefficient have a high priority from the reactor safety point of view. On the other hand, the study of how the output parameter uncertainty (i.e. neutron multiplication factor, control rod worth etc.) can be apportioned to the different uncertainties in the input parameter (i.e. macroscopic cross section data) is known as the sensitivity analysis. The sensitivity analysis identifies the more influential input parameters which affect the output parameters. A high sensitivity coefficient implies that a particular input parameter is highly influential in affecting the reactor output parameter. In this paper we deal with the uncertainty in the control rod worth in CANDU PHWR (AECL-7236) [1].

2. Estimation of uncertainty in k_{eff}

The static uncertainty analysis is performed using first order perturbation theory [2]. Here the uncertainty in the neutron multiplication factor is directly obtained by solving the neutron diffusion equation along with the adjoint solution. Consider the static neutron diffusion equation (two-group, the constants carry usual meaning)

$$D_1\nabla^2\varphi_1 - \Sigma_{a1}\varphi_1 - \Sigma_{1\to2}\varphi_1 + \left(\frac{1}{k_0}\right)(\nu\Sigma_{f1}\varphi_1 + \nu\Sigma_{f2}\varphi_2) = 0 \quad (1)$$

$$D_2\nabla^2\varphi_2 - \Sigma_{a2}\varphi_2 + \Sigma_{1\to2}\varphi_1 = 0 \quad (2)$$

In matrix form, the neutron diffusion equation is written as

$$\hat{A}\varphi = \frac{1}{k_0}\hat{F}\varphi \quad (3)$$

$\hat{A}$ is the neutron destruction operator ($\widehat{A_1} = D_1\nabla^2 - \Sigma_{a1} - \Sigma_{1\to2}$), $\hat{F}$ is the neutron production operator ($\widehat{F} = \nu\Sigma_{f1} + \nu\Sigma_{f2}$) and k_0 is the eigen value. When the input parameter (absorption or fission cross section) is perturbed (i.e.$\Sigma'_{a1} = \Sigma_{a1} + \Delta\Sigma_{a1}$), the resulting perturbed neutron diffusion equation is given as

$$\widehat{A'}\varphi' = \frac{1}{k'_0}\widehat{F'}\varphi' \quad (4)$$

where $\widehat{A'}$ contains the perturbed input parameters (cross sections), ($\widehat{A'} = \hat{A} + \Delta A$) $\widehat{F'}$ contains the perturbed fission cross sections ($\widehat{F'} = \hat{F} + \Delta\hat{F}$) , φ' is the perturbed flux and k'_0 is the new eigen value ($k'_0 = k_0 + \Delta k$). The adjoint neutron diffusion equation, for the unperturbed system, is given as

$$\hat{A}\dagger\,\varphi\dagger = \frac{1}{k_0}\hat{F}\dagger\,\varphi\dagger \quad (5)$$

where $\hat{A}\dagger$ is the adjoint operator for $\hat{A}$ and $\varphi\dagger$ is the adjoint flux. Using the first order perturbation theory [4], the uncertainty in the multiplication factor is computed from Eqs. (3)-(5) and it is given as

$$\frac{\Delta k_0}{k_0} = \frac{-\langle\varphi,(\Delta\hat{A}\dagger)\varphi\dagger\rangle - \frac{1}{k_0}\langle\varphi,(\Delta\hat{F}\dagger)\varphi\dagger\rangle}{\frac{1}{k_0}\langle\varphi,(\hat{F}\dagger)\varphi\dagger\rangle} \quad (6)$$

Here the first order perturbation method is applied to estimate the uncertainty in the control rod worth of CANDU reactor.

3. CANDU PHWR Description

It is a realistic 3D PHWR benchmark kinetics problem [1] in Cartesian geometry. This is one of the widely studied benchmark problem. This core contains two radial fuel zones (inner core and outer core) surrounded by heavy water reflector. The axial length of the core in the horizontal Z direction is 600 cm. Along the horizontal direction (Z axis) the material distribution is uniform. The height and width of the core are 780 cm. The core is divided into a total of $18 \times 18 \times 10$ meshes. It has reflective symmetry in all XY, YZ and XZ planes passing through the centre of the reactor. The detailed description and core composition are given in [1].

4. Results and Discussion

The steady state of this benchmark reactor is well treated by [1], [3]. Under steady state condition, the k_{eff} is found to be 1.003555 [3]. The control rods are outside the core in steady state. The transient is created and the control rods fall to arrest the transient. The control rods fall in reflector, outer core and inner core. Out of four control rod banks only three fall. When the control rods are fully inserted the incremental rise in the cross section is taken as 6.15E-4. The control rod worth in three regions is calculated independently and they are given in Table 1. It is to be noted only those control rods, which fall during the transient, are considered for worth calculation.

Table 1. Worth of control rods in different regions.

S.N	Control rod presence	Worth (mk)
1	Reflector	1.43
2	Outer core	8.69
3	Inner core	13.52

The worth of control rod is calculated as $\rho = \left|\frac{1}{k_0} - \frac{1}{k_1}\right|$, k_0 and k_1 refer to the effective neutron multiplication factor before and after the insertion of control rod. Since the control rods absorb thermal neutron more effectively, it is important to evaluate the uncertainty in the control rod worth for a given perturbation in the thermal absorption cross section of control rod material. The uncertainty in the worth of control rod is given by

$$\Delta\rho = \left|\frac{\Delta k_0}{{k_0}^2} - \frac{\Delta k_1}{{k_1}^2}\right|$$

Since in the steady state, all the control rods are above the core, we assume that the initial uncertainty in the neutron multiplication factor is zero, i.e. $\Delta k_0 = 0$. Now the control rod (i.e. control bank) in reflector regions alone is considered (other control rods (i.e. banks) are parked above the reactor). The uncertainty in the thermal absorption cross section is varied between 0.1% - 1.0% and the uncertainty in the control rod worth is calculated. In a similar manner the uncertainties in the worth of control rods in outer core and inner core are calculated and the results are given in Table 2. While calculating the worth of any control bank, it is considered that all other control rod banks are above the core.

Table 2. Uncertainty in the worth of control rods in CANDU PHWR (AECL-7236)

S.N	Control rod presence	Uncertainty parameter, i.e. $\left(\frac{\Delta\Sigma_{a2}}{\Sigma_{a2}}\right)$	$\frac{\Delta k_1}{k_1}$ (%)	Worth of control rod	Uncertainty in the worth, i.e. $\left(\frac{\Delta\rho}{\rho}\right)$
1	Reflector	0.1% 0.5% 1.0%	1.022E-4 5.108E-4 1.022E-3	1.428 mk	0.007% 0.035% 0.071%
2	Outer core	0.1% 0.5% 1.0%	1.785E-3 8.929E-3 1.785E-2	8.694 mk	0.206% 1.03% 2.06%
3	Inner core	0.1% 0.5% 1.0%	3.00E-3 1.503E-2 3.00E-2	13.52 mk	0.22% 1.12% 2.24%

The first order perturbation method is used to estimate the uncertainty in the control rod worth. The uncertainty in the control rod worth in CANDU PHWR (AECL-7236) is estimated under steady state conditions. It is observed that an 1% uncertainty in the thermal absorption cross section gives an uncertainty in the worth of control rod (i.e. control bank) as 2.24% in the inner core.

5. References

[1] R.A. Judd, and B. Rouben, "Three dimensional kinetics benchmark problem in a heavy water reactor", *Report, AECL-7236*, 1981.

[2] Stacey, W.M., "*Nuclear Reactor Physics*", John Wiley & Sons, Inc., New York, 2001.

[3] M. Mohideen Abdul Razak, K. Devan, "The modified exponential time differencing method with IQS model for the neutronic analysis of PHWR transients", *Progress in Nuclear Energy*, vol 98, p 1-10, 2017.

DYNAMIC UNCERTAINTY ANALYSIS IN THE POWER TRANSIENT OF CANDU PHWR

M. Mohideen Abdul Razak
Bhabha Atomic Research Centre Facilities, Kalpakkam, 603127, India
e-mail: -mmar@igcar.gov.in

Abstract

The propagation of uncertainty in the macroscopic cross section with time and its effect on reactor power transient is discussed in this paper. Here the forward sensitivity analysis procedure with improved quasi static (IQS) method is used to estimate the uncertainty in the reactor transients. According to this method, the uncertainty in the input parameter (i.e. macroscopic cross section data or delayed neutron fraction) is directly incorporated in the time dependent neutron diffusion equation and the improved quasi static (IQS) method is applied to solve the equation to estimate the dynamic uncertainty in the flux (output parameter). In this paper, an 1% uncertainty in the first group of delayed neutron fraction (β_1) alone is considered and its impact on the uncertainty in the CANDU reactor power transient is discussed. This method can be also used to estimate the uncertainty in the CANDU reactor transient from simultaneous uncertainties in delayed neutron fractions.

1. Introduction

The study of behaviour of reactor core to various types of uncertainties in reactor physics parameters is important for the safe operation of nuclear reactors. A primary source of uncertainty in the reactor core behavior arises from the uncertainty in the nuclear cross section data. In any nuclear power plant (NPP), it is essential to know the reactor core behaviour when the reactor physics input parameters, i.e. macroscopic cross section data, are perturbed in the vicinity of their best estimate values. Some perturbed input parameters may be more influential in affecting the reactor output parameters, i.e. neutron multiplication factor, reactor power etc. and some parameters may be less influential in affecting them. Sometimes the uncertainty in the input parameter may be stationary or it may propagate with time. The propagation of uncertainty in the input parameter with time will affect the reactor core power, core temperature etc. during transient and in this case it is important to examine its effect on reactor core characteristics. The uncertainty and sensitivity analysis gives information about the identification of potentially important input parameters which are more influential in affecting the core behavior under normal and accidental conditions. Using the uncertainty and sensitivity analysis, the influential input parameters can be given more careful evaluation or measurement with least error. The sensitivity coefficient in defined as the ratio between the uncertainty in the output parameter (i.e. fractional change) and the uncertainty in the input parameter (i.e. fractional change). In this paper, the time evolution of uncertainty in reactor transient, caused by uncertainty in delayed neutron fraction is discussed. Here the Forward Sensitivity Analysis Procedure (FSAP) [1] with improved quasi static (IQS) method [2] is developed [3] to perform the dynamic uncertainty analysis in reactor transient. This method is applied to estimate the uncertainty in the CANDU reactor transient, caused by uncertainties in delayed neutron fractions.

2. Dynamic uncertainty estimation in reactor transient

The time dependent neutron diffusion equation (two energy-group, unperturbed system) can be written as

$$\frac{1}{v_1}\frac{\partial \varphi_1(\vec{r},t)}{\partial t} = -\widehat{A_1}\varphi_1 + \frac{(1-\beta)}{k_0}\left(\widehat{F_1}\varphi_1 + \widehat{F_2}\varphi_2\right) + \sum_i \lambda_i C_i \qquad (1)$$

$$\frac{1}{v_2}\frac{\partial \varphi_2(\vec{r},t)}{\partial t} = -\widehat{A_2}\varphi_2 + \widehat{G_1}\varphi_1 \quad (2)$$

where $\widehat{A_1} = D_1\nabla^2 - \Sigma_{a1} - \Sigma_{1\to2}$, $\widehat{F_1} = \nu\Sigma_{f1}$, $\widehat{F_2} = \nu\Sigma_{f2}$, $\widehat{A_2} = D_2\nabla^2 - \Sigma_{a2}$, $\widehat{G_1} = \Sigma_{1\to2}$

In the above Eqs. (1)-(2), the constants carry usual meaning. When the input parameters are perturbed by the uncertainties, $\delta D_1, \delta\Sigma_{a1}, \delta\Sigma_{a2}, \delta\beta, \delta\lambda_i$ etc., the time evolution of fast and thermal flux, with uncertainties $\delta\varphi_1$ and $\delta\varphi_2$, are written as

$$\frac{1}{v_1}\frac{\partial(\varphi_1+\delta\varphi_1)}{\partial t} = -\left(\widehat{A_1}+\delta\widehat{A_1}\right)(\varphi_1+\delta\varphi_1) + \left(\frac{1-(\beta+\delta\beta)}{k_0+\Delta k}\right)\left(\left(\widehat{F_1}+\delta\widehat{F_1}\right)(\varphi_1+\delta\varphi_1) + \left(\widehat{F_2}+\delta\widehat{F_2}\right)(\varphi_2+\delta\varphi_2)\right) + \left(\sum_i(\lambda_i+\delta\lambda_i)(C_i+\delta C_i)\right) \quad (3)$$

$$\frac{1}{v_2}\frac{\partial(\varphi_2+\delta\varphi_2)}{\partial t} = -\left(\widehat{A_2}+\delta\widehat{A_2}\right)(\varphi_2+\delta\varphi_2) + \left(\widehat{G_1}+\delta\widehat{G_1}\right)(\varphi_1+\delta\varphi_1) \quad (4)$$

$$\frac{\partial(C_i+\delta C_i)}{\partial t} = (\beta_i)\left(\left(\widehat{F_1}+\delta\widehat{F_1}\right)(\varphi_1+\delta\varphi_1) + \left(\widehat{F_2}+\delta\widehat{F_2}\right)(\varphi_2+\delta\varphi_2)\right) - (\lambda_i+\delta\lambda_i)(C_i+\delta C_i) \quad (5)$$

In Eqs. (3)-(5), $\delta\widehat{A_1} = (\delta D_1)\nabla^2 - \delta\Sigma_{a1} - \delta\Sigma_{1\to2}$, $\delta\widehat{A_2} = (\delta D_2)\nabla^2 - \delta\Sigma_{a2}$, $\delta\widehat{F_1} = \delta\nu\Sigma_{f1}$, $\delta\widehat{F_2} = \delta\nu\Sigma_{f2}$, $\delta\widehat{G_1} = \delta\Sigma_{1\to2}$.

From Eqs. (3)-(5), the time evolution of uncertainty in the fast flux ($\delta\varphi_1$) and thermal flux ($\delta\varphi_2$) are written as (keeping only first order terms)

$$\frac{1}{v_1}\frac{\partial(\delta\varphi_1)}{\partial t} = -\left(\widehat{A_1}\delta\varphi_1 + \delta\widehat{A_1}\varphi_1\right) + \left(\frac{1-\beta}{k_0+\Delta k}\right)\left(\widehat{F_1}\delta\varphi_1 + \delta\widehat{F_1}\varphi_1 + \widehat{F_2}\delta\varphi_2 + \delta\widehat{F_2}\varphi_2\right) + \left(\frac{-\Delta k}{k_0(k_0+\Delta k)}\right)(1-\beta)\left(\widehat{F_1}\varphi_1 + \widehat{F_2}\varphi_2\right) + \left(\frac{-\delta\beta}{k_0+\Delta k}\right)\left(\widehat{F_1}\varphi_1 + \widehat{F_2}\varphi_2 + \widehat{F_1}\delta\varphi_1 + \delta\widehat{F_1}\varphi_1 + \widehat{F_2}\delta\varphi_2 + \delta\widehat{F_2}\varphi_2\right) + \sum_i(\lambda_i\delta C_i + \delta\lambda_i C_i) \quad (6)$$

$$\frac{1}{v_2}\frac{\partial(\delta\varphi_2)}{\partial t} = -\left(\widehat{A_2}\delta\varphi_2 + \delta\widehat{A_2}\varphi_2\right) + \left(\widehat{G_1}\delta\varphi_1 + \delta\widehat{G_1}\varphi_1\right) \quad (7)$$

$$\frac{\partial(\delta C_i)}{\partial t} = \beta_i\left(\delta\widehat{F_1}\varphi_1 + \widehat{F_1}\delta\varphi_1 + \delta\widehat{F_2}\varphi_2 + \widehat{F_2}\delta\varphi_2\right) - \lambda_i\delta C_i - \delta\lambda_i C_i \quad (8)$$

Eqs. (6)-(8) are solved using improved quasi static method [3] and the uncertainty in the fast flux and thermal flux are obtained.

3. CANDU (AECL-7236) Benchmark description

It is a realistic 3D PHWR benchmark kinetics problem [4] in Cartesian geometry. This is one of the widely studied benchmark problem. The geometrical description of the core is as follows: This core contains two radial fuel zones (inner core and outer core) surrounded by heavy water reflector as shown in Fig. 1. The axial length of the core in the horizontal Z direction is 600 cm. Along the horizontal direction (Z axis) the material distribution is uniform. The height and width of the core are 780 cm. The core is divided into a total of $18 \times 18 \times 10$ meshes. It has reflective symmetry in all XY, YZ and XZ planes passing through the centre of the reactor. The core composition, delayed neutron fractions are given in [4]. The detailed description of this reactor can be found in [4].

4. Estimation of uncertainty in CANDU (AECL-7236) transient

Here the transient is created by decreasing the thermal absorption cross section in regions 5, 6, 10, 11, 17, 18, 22 and 23 [4]. The rate of decrease of thermal absorption cross section is given by [4]

$$\frac{\partial\Sigma_2}{\partial t} = \begin{cases} -1.0\times10^{-4}(cms)^{-1} & for\ t \le 0.4\ s \\ -8.88889\times10^{-6}(cms)^{-1} & for\ t > 0.4\ s \end{cases}$$

To arrest positive reactivity insertion, shut down devices are inserted asymmetrically and the insertion of shut down devices creates an incremental thermal absorption cross section [4]

$$\Delta\Sigma_2 = 6.15\times10^{-4}cm^{-1}$$

The incremental thermal absorption cross section is created in the regions 2, 4 7, 9, 12, 14, 16, 18, 19 and 21-24 [4]. The regions where absorbers are inserted are shown as shaded areas [4]. The absorber insertion starts at $0.6s$ with a constant velocity of $520\ cm/s$ in the Y direction. The moving absorber boundary is parallel to the XZ plane. The change in cross section is additive whenever the perturbations overlap. The transient lasts for $2.5\ s$. During the transient the power raises, reaches a maximum and then it starts decreasing. The power transient is given in Fig.2. Now a small uncertainty in the delayed neutron fraction (β_1) is assumed as $\frac{\Delta\beta_1}{\beta_1} = 1\%$. Under this condition the uncertainty in the power transient $\left(\frac{\Delta p}{p}\right)$ is estimated by solving Eqs. (6)-(8) and it is given in Fig. 3.

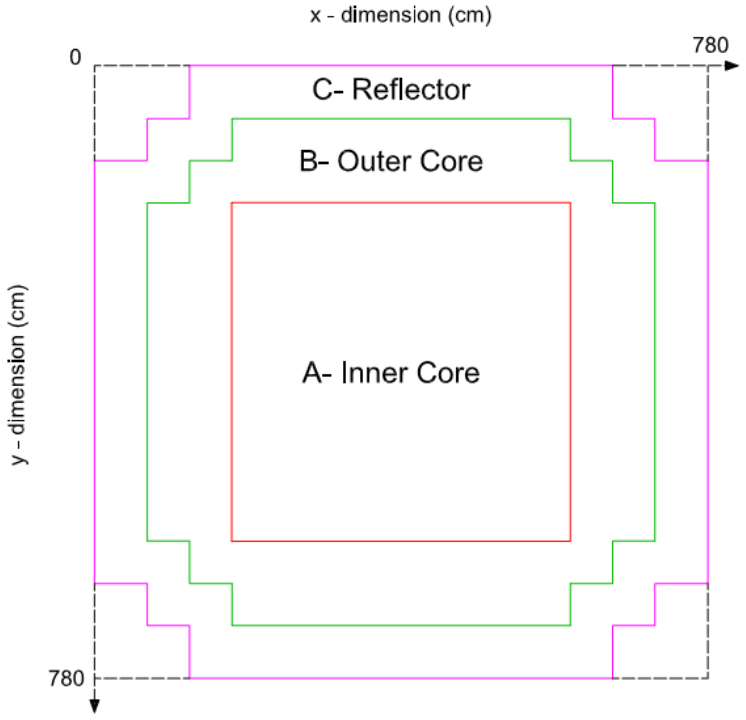


Fig. 1. Vertical cross section of CANDU 3D-PHWR.

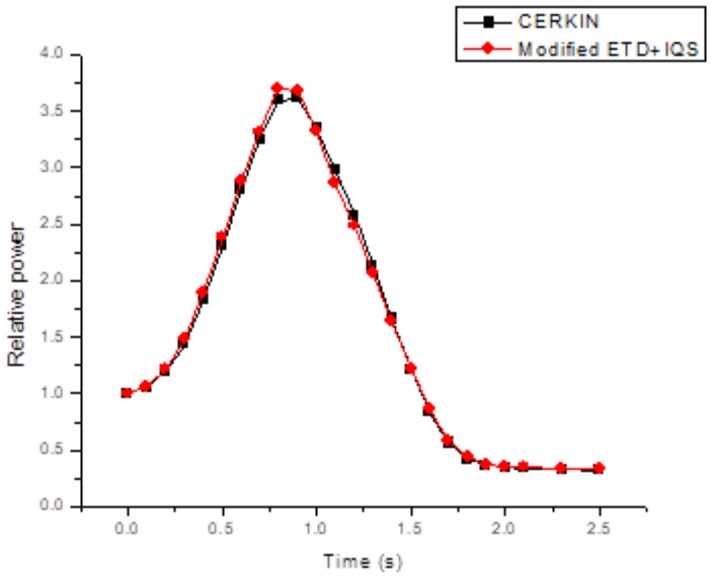


Fig. 2. The power transient in CANDU reactor. The power transient is obtained using modified exponential time differencing method [3] and CERKIN code [4]

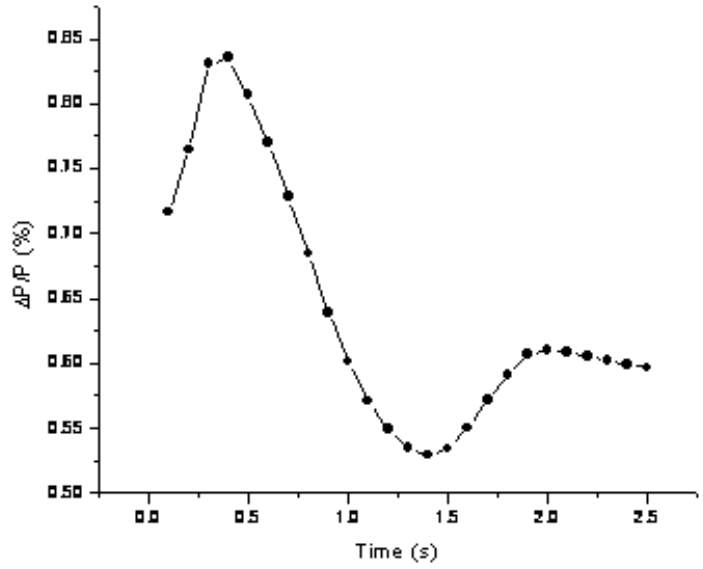


Fig. 3. The plot of uncertainty in power $\left(\frac{\Delta p}{p}\right)$ % with time for CANDU reactor.

5. Discussion and conclusions

The forward sensitivity analysis procedure is developed with improved quasi static (IQS) method for the estimation of dynamic uncertainty in reactor transients. Accordingly, the time evolution of the uncertainties in fast and thermal flux are developed. These equations are solved using IQS method. In IQS method, flux factorization technique is adopted. A new kind of point kinetics equations is developed and its solution with the shape function gives the uncertainty in fast and thermal flux. This computational method can be used to estimate the uncertainty in the core power,

core temperature caused by uncertainties in macroscopic cross sections and delayed neutron fractions. This method is applied to estimate the uncertainty in core power in CANDU benchmark reactor. In this benchmark the transient is created by decreasing the thermal absorption cross section and shut-down devices are inserted asymmetrically to arrest the transient. An uncertainty of 1% in the delayed neutron fraction is introduced, i.e. $\frac{\Delta\beta_1}{\beta_1} = 1\%$ and the resulting uncertainty in the power transient is estimated. It is observed that a maximum uncertainty of 0.835% is observed during the transient. The above computational method can be used to estimate the uncertainty in the transient with uncertainties in other macroscopic cross sections, i.e. absorption, scattering, fission etc. The above method can also be used to estimate the uncertainty in core power with multiple uncertainties simultaneously.

6. References

[1] Cacuci, G.D., "Sensitivity and Uncertainty Analysis, Theory, vol. 1", *CHAPMAN & HALL/CRC,* 2003.

[2] K.O. Ott, D.A. Meneley, "Accuracy of quasi-static treatment of spatial reactor Kinetics", *Nucl. Sci. Eng*. 36, 402, 1969.

[3] Razak, Mohideen Abdul, M.., 2019. "Studies on PHWR transients using modified exponential time differencing method with improved quasi model and associated dynamic sensitivity analysis", *Ph.D. Thesis– HomiBhabha National Institute (HBNI), Kalpakkam, Tamil Nadu, India*, 2019.

[4] R.A. Judd, and B. Rouben, "Three dimensional kinetics benchmark problem in a heavy water reactor", *Report, AECL-7236*, 1981.

LATTICE LEVEL SENSITIVITY ANALYSIS OF INDIAN PHWR

Ishi Jain, Manish Raj, Sherly Ray and M.P.S. Fernando
Nuclear Power Corporation of India Limited, Mumbai, India
e-mail: - ishi@npcil.co.in

Abstract

The reactor physics analysis is normally carried out in two steps, first at lattice level and then at core level. The lattice level analysis is performed generally in 2D, using the nuclear cross section data and computer codes that solve the transport equations by numerical methods. Nuclear cross section data is obtained from experiments and wherever experimental data is not available theoretical models are used to generate the data. Many such cross section data libraries are available online through IAEA and other international forums with their uncertainties in form of covariance matrices. Therefore, correctness/accuracy of the estimations depends on the accuracy of the cross section data, modelling, and the numerical methods used to solve the transport/diffusion equations. Since the cross sections are obtained from experiments and theoretical model, these data bound to have errors/uncertainty. This generates the necessity of sensitivity analysis in context of basic nuclear data, which is the first step for uncertainty analysis. In the present paper, the lattice level sensitivity analysis is performed for 19 and 37-element fuel cluster.

1. Introduction

In reactor design, the primary aim is to obtain the neutron flux distribution and the multiplication factor in the reactor. The reactor physics analysis is normally carried out in two steps, first at lattice level and then at core level. In first step, a representative region of the core called lattice cell, which is assumed to be repeating within the core, is modelled. Transport theory is applied to the lattice in fine energy groups and detailed spatial and spectral neutron flux distribution is obtained for the lattice. Mostly these calculations are performed in 2D. The properties of the heterogeneous lattice is homogenised and the fine group homogenised cross sections are condensed to few group cross sections using the detailed fine group flux distribution. These homogenised few group cross sections are used for 3D core calculation of second step wherein 3D neutron diffusion equations, which is an approximate form of transport equation, is solved in few groups to obtain the flux distribution and multiplication factor of the reactor. The flow of computational scheme is shown in figure-1. The correctness/accuracy of the estimations depends on the accuracy of the cross section data, modelling, and the numerical methods used to solve the transport/diffusion equations. Since the cross sections are obtained from experiments and theoretical model, these data bound to have errors/uncertainty. In the present work, the lattice level sensitivity analysis, which is a part of uncertainty analysis, is carried out for 19 and 37-element fuel cluster and the results are compared with the results available in literature [1].

2. Nuclear data and Uncertainty

Nuclear data is drawn either from experimental measurements or else predicted by some nuclear model calculations. The results are then combined carefully to produce a complete evaluated data file which is a large compilation consisting of highly-ordered data sets, grouped by materials and data types. Thus, the experimental uncertainties, uncertainties associated with the selection of physics model parameters and interpolation scheme are causing uncertainties on point wise data. The characterisation of these uncertainties is by the statistical measure of covariance, included in evaluated nuclear data files.

Detailed information contained in the evaluated data files exceeds the capacity of the calculation tools (i.e. computer programs) for practical neutron transport applications. The entire energy interval is

divided into a number of groups. Within a group, each energy-dependent parameter takes some average value. The accuracy of the calculation depends on the number of groups and the group averaging method. Usually a compromise must be made between the complexity in geometry and the number of groups. Since Lattice level calculations form the first calculation step at which problem dependent specifications are involved, uncertainties associated with the lattice calculations propagate through all subsequent calculations. Therefore, lattice level uncertainty analysis forms the foundation of reactor physics uncertainty analysis in general, as well as the capability to establish realistic and justifiable reactor safety margins that include the effects of fundamental nuclear data.

3. Direct Numerical Perturbation (DNP)

The approaches adopted in internationally available tools for performing lattice uncertainty estimation broadly fall into two categories, viz., Sensitivity-based approach and Statistical approach. The sensitivity-based approach can be further divided into two kinds, namely, Adjoint-based sensitivity & uncertainty analysis and direct numerical perturbation. In Direct Numerical Perturbation method, the partial derivatives of the output are estimated by making small changes to the input parameter of interest and evaluating the response with each change.

The implementation of the direct numerical perturbation method involves calculating partial derivatives of outputs with respect to each input of concern one at a time and uncertainty propagation is performed using the sandwich rule. The method produces the partial derivative and sensitivity coefficient of multiplication factor k, with respect to a particular cross-section in a particular energy group; for an isotope or nuclide. The dimensionless sensitivity coefficient is defined as:

$$S_{x_g} = \frac{\partial k(\sigma_g)/k(\sigma_g)}{\partial \sigma_g/\sigma_g} \quad \text{…Eq. (1)}$$

with σ_g being unperturbed g^{th}energy group cross-section of the nuclide and $k(\sigma_g)$ is multiplication factor when $\sigma_g$is used in calculations. A small perturbation on σ_g is made which will also result into perturbation in value of multiplication factor. The cross-sections of some energy groups have greater influence on *k* than others, thereby producing higher sensitivities, merely as a result of the relative widths of the groups in which they reside, and their occupying vastly different fractions of the available energy spectrum. Therefore, a modified sensitivity parameter, sensitivity per lethargy, S_{L,x_g} , which removes the biases in sensitivity coefficients and discontinuities in energy dependent sensitivity profiles that arise solely due to energy group widths, is defined as,

$$S_{L,x_g} = \frac{S_{x_g}}{\ln(E_{g+}/E_{g-})} \quad \text{…Eq. (2)}$$

Where E_{g+} and E_{g-} are upper and lower boundaries of g^{th}energy group. The sensitivity matrix thus obtained can be further used in estimation of uncertainty estimation using the Sandwich rule using the covariance matrix COV as follows:

$$\Delta^2 k = [S] \times [COV] \times [S^T] \quad \text{…Eq. (3)}$$

The study presented in this paper is up to estimation of sensitivity coefficients of the lattice.

4. Computer Codes used for analysis

Computer code CLUB [2] is used for solving the multi-group transport equation for the lattice. It takes the material properties, temperatures and geometry of the lattice as input and generates lattice parameters as a function of burn up, power distribution in each element/pin of the fuel bundle, neutron fluxes in different materials and regions of the lattice, few-group homogenised cross-sections etc. as output. A module SENCOF is developed to estimate the sensitivity coefficients in 69 groups using DNP method. The computer code READ-LIB [3] was developed to generate the input files required for transport theory based

code CLUB from the multi-group library in WIMS-D format. The code READ-LIB is called in module SENCOF along with code CLUB in sequential way for processing the multi-group (in the present paper 69 group) data and for using the perturbed data following consistency rules to estimate the sensitivity coefficients in 69 groups using DNP method. The flow chart is given in Figure-2.

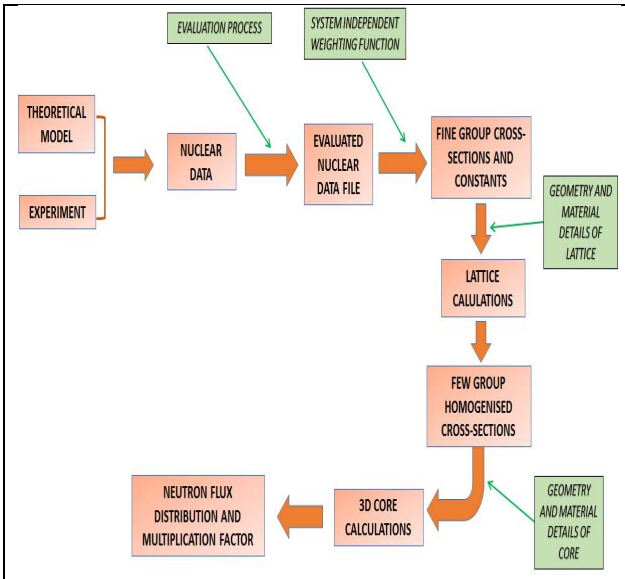


Figure-1 : Computational scheme

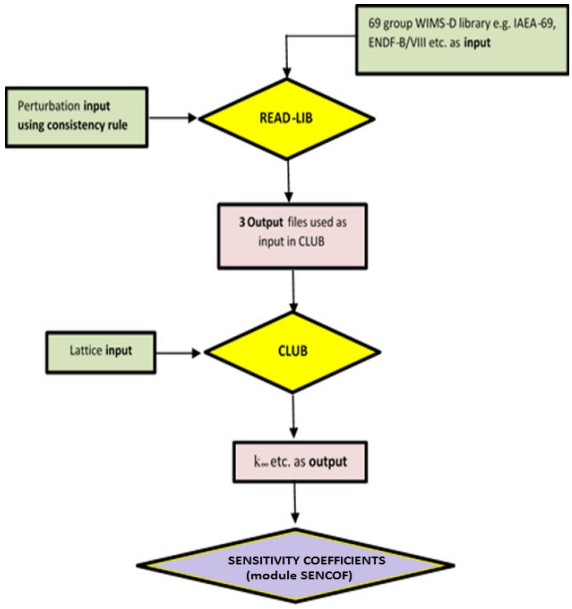


Figure-2: Flow chart of In-house developed code for sensitivity analysis

5. Analysis for IPHWR lattice with 19 and 37 element fuel clusters at 0 burnup

The sensitivity coefficients for U^{235}, U^{238}, H^1, H^2, O^{16} and Zr^{91} are estimated using the code SENCOF for 19 and 37 element lattices of IPHWR at 0 MWd/TeU burnup for different nuclear reactions. Figure-3 and 4 show the sensitivity profiles of major and minor contributors for 19 element IPHWR lattice at 0 MWd/TeU burnup. Figure-5 and 6 show the sensitivity profiles of major and minor contributors for 19 element IPHWR lattice at 0 MWd/TeU burnup.

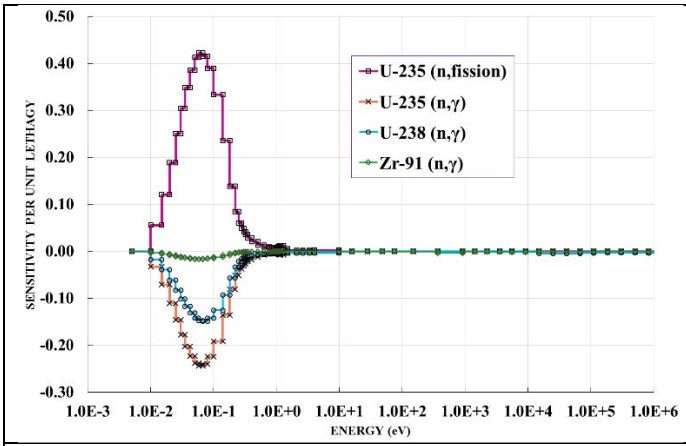


Figure-3 Sensitivity profile of major contributors for 19 element IPHWR at 0 Burnup.

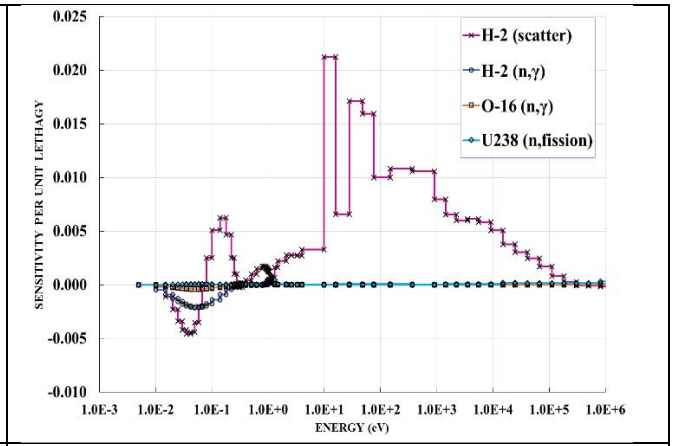


Figure-4 Sensitivity profile of minor contributors for 19 element IPHWR at 0 Burnup.

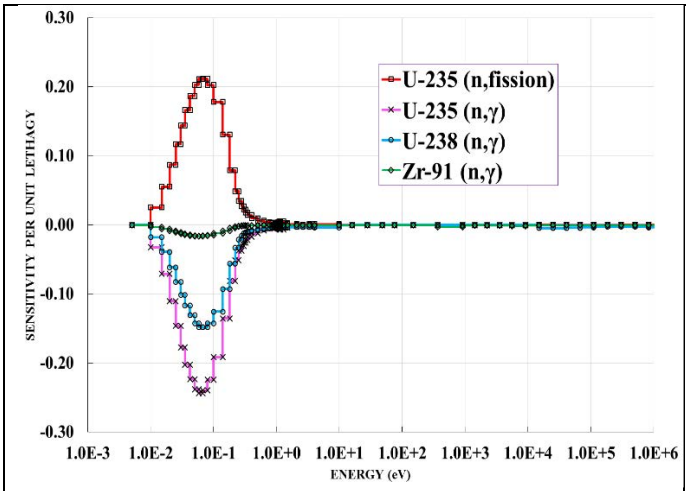


Figure-5 Sensitivity profile of major contributors for 37 element IPHWR at 0 Burnup.

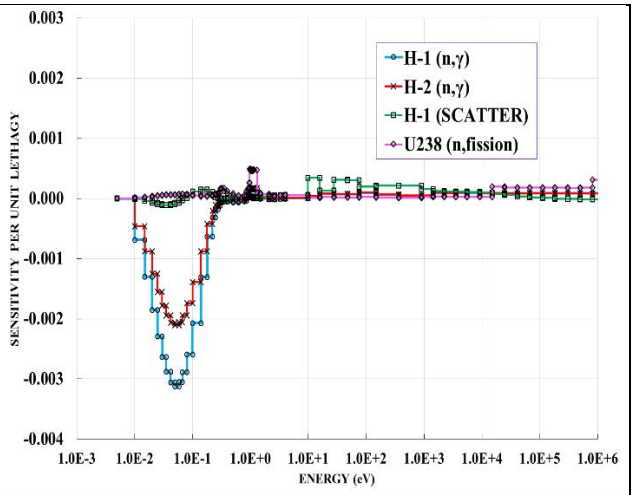


Figure-6 Sensitivity profile of minor contributors for 37 element IPHWR at 0 Burnup.

The negative sensitivity coefficient shows the negative impact on reactivity as cross-section increases. For example, k_∞sensitivity to H^2scattering cross-section is negative at very high energies as the coolant scatters the fission neutrons at the fuel/coolant interface and thereby reduces the fast fission probability. The sensitivity is positive at the intermediate energies due to the thermalizing of neutrons far from the fuel. At even lower energies, the sensitivity again becomes negative as a result of the up-scattering due to temperature difference between the coolant and moderator. The results of sensitivity analysis obtained with module SENCOF is found to be in good agreement with the results available in literature [1].

6. Conclusion

The objective of the work presented in the paper was to conduct lattice physics sensitivity analysis and lay a foundation for uncertainty analysis on IPHWR systems by developing and applying the method that comprehensively address all relevant sources of uncertainties. These uncertainties play a prominent role in steady-state reactor physics calculations such as those used for finalizing the maximum power license compliance, as well as for transients such as anticipated operational occurrences (AOO) and design basis accidents (DBA). To quantify the value of uncertainty the cross-sectional covariance for the relevant isotope and reaction (covariance matrix), in 69 x 69 structure, must be supplied from outside as 69 neutron energy group library is used in CLUB [2]. However, this desired group structure is not available on open IAEA platform online. Literature show that sophisticated and established tools like NJOY are capable of condensing the covariance matrix into desired group structure. The present lattice analysis codes cannot take the covariance matrix as calculated by NJOY directly.

7. References

[1] Ball, Matthew R., "Uncertainty Analysis in Lattice Reactor Physics Calculations", McMaster University, 2012.

[2] P. D. Krishnani, “CLUB-A Multi-group Integral Transport Theory Code for Lattice Calculations of PHWR Cells”, BARC/1992/E/017.

[3] Ishi Jain and Manish Raj, “Design note on preparation of IAEA supplied neutron cross-section data for computer code CLUB”, 700MWe/DN/01100/9019. NPCIL, 2015.

Nuclear data sensitivity of VVER-1000 pin-cell benchmark

V. Harikrishnan, Anek Kumar and Usha Pal
RPDD, BARC
e-mail: - harikv@barc.gov.in

Abstract

The VVER-1000 pin cell benchmark has been analyzed using Total Monte Carlo method. The uncertainty due to nuclear data has been estimated for important nuclides using Monte Carlo codes. The randomized nuclear data in ACE format from TENDL-2015 has been used as input for uncertainty propagation.

1. Introduction

Nuclear data evaluation is an evolving process due to the progress in experiments and theoretical modelling, there are several evaluated libraries such as the ENDF/B-VIII.0 [1], TENDL-2015 [2] etc. The evaluated nuclear data requires further processing using codes such as NJOY, PREPRO for use in reactor physics codes. The prepared libraries are adapted for use based on the performance by analyzing a series of benchmarks. The updated nuclear data is generated using advanced modeling tools and new experimental results. The newer evaluations of nuclear data provide an increasing emphasis on providing the uncertainties associated with nuclear data. With the availability of such data, there is ample scope to study effects of randomization and the propagation of uncertainties to reactor physics parameters. Analysis of reconstructed point-wise data revealed that 70 isotopes (including Zr, H^{1}, O^{16}, U^{235}, and U^{238} all have more than 1% deviation in total cross section w.r.t ENDF/B-VII.1) [3]. The first step in this process is to study the effect of changing cross sections on the k_{∞} (infinite neutron multiplication factor) which is the fundamental parameter in lattice analysis [4].

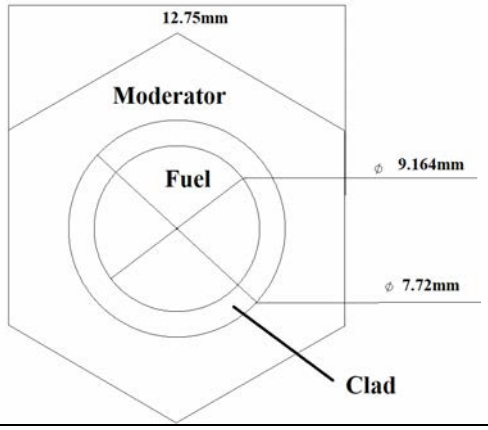
The TENDL library has been prepared using ENDF/B-VII.0 data and associated covariance, and the T6 code (TALYS, TASMAN, TAFIS, TANES, TARES and TEFAL codes) system. The open source code TALYS simulates neutron and gamma from thermal to 200MeV [5]. The T6 have been used to generate the TENDL library. The TENDL project has provided randomized cross sections using covariance data of important nuclides in ENDF as well as ACE format, required for uncertainty propagation that can be downloaded from its website [5]. The TENDL library has been used extensively to analyze benchmarks. The TMC (Total Monte Carlo) method has been evolved to understand the propagation of uncertainties, and determine the impact of nuclear data. The process of TMC is described below [6].

(i) A restricted number of isotopes for the criticality benchmark are considered.
(ii) For each isotope, a large number of ENDF/B files are created using random model and resonance parameters in the TALYS system.
(iii) ENDF/B files are processed with NJOY to generate ACE files for the Monte Carlo codes.
(iv) For the benchmark, several runs are performed using different set of ACE files for each isotope.

The TMC method has been used in several applications such as criticality-safety, shielding, pin cell/assembly burn-up, full core calculations of PWR, BWR, Gen IV systems etc. In this study the VVER-1000 pin cell benchmark is studied using the TMC approach with the M3C code.

2. Benchmark description

The VVER-1000 pin cell benchmark [9] describes a Uranium pin inside a hexagonal light water lattice. The fuel ID/OD is 7.72/9.164mm, and the lattice pitch is 12.75 mm. Unlike the real VVER pin, the benchmark doesn't consider the central hole. The moderator is light water at 293K with dissolved Boric acid. The benchmark in cold condition has been simulated using M3C Monte Carlo code using ACE files from the TENDL-2015 library. The geometry details and material compositions are given below

Geometry	Material Composition			
	U^{235}	8.7370E-04	O^{16} (in H_2O)	3.347E-02
	U^{238}	1.8744E-02	B^{10}	6.6262E-06
	$O^{16\,(fuel)}$	3.9235E-02	B^{11}	2.6839E-05
	H^1(in H_2O)	6.694E-02	Zr	4.23E-02

3. Code Description

M3C [7] is a multi-purpose three-dimensional continuous-energy Monte Carlo particle transport code, developed at BARC, India. The M3C code is specifically designed for reactor physics calculations, particularly at the fuel assembly level. M3C code has all the capabilities for use in practical reactor design. This code has been extensively validated for the calculation of effective and infinite multiplication factor (with reflective boundary condition) of fuel assembly in different nuclear reactors.

4. Results

The evaluated TENDL library yielded the k_∞ = 1.37086 with MCNP [8], and 1.370319 with M3C, close to reference [9], as seen from Table 1. The TMC calculations have been performed by individually varying H^1, O^{16}, U^{235}, and U^{238} nuclear data. Since the input is the same the only variation is in the nuclear data. The nuclear data has been randomized by varying the TALYS input parameters such as optical model, level density, photon strength and fission parameters. The random files are generated by running TALYS many times with input parameter vector sampled from a normal distribution with a specific width. The variation is best studied using a large number of nuclear data files. For this study 342 randomized ACE files of H^1, and O^{16}; and 100 randomized ACE files of U^{235} and U^{238} from TENDL-2015 have been used. The cross sections have been extracted and processed using Python, Fortran scripts. Fig. 1-4 show the total cross sections of H^1, O^{16}, U^{235} and U^{238}. The randomized cross sections w.r.t TENDL-2015 evaluated data are shown in Gray. The plots are generated with gnuplot. The k_∞ is expected to follow a normal distribution, as the input data parameters have also been accordingly varied. Hence the results have been fitted to a normal distribution and the average k_∞ and standard deviation have been obtained, as shown in Fig. 5-8. In this manner the uncertainties due to nuclear data can be identified. After performing the lattice analysis with a large number of ACE files, with randomized cross sections, for same input conditions. The estimated average k_∞ and standard deviation are given in Table 2. A possible reason for the mismatch of 0.5mk is due to limitations on the available Temperatures in the tsl (thermal scattering library) data, the bound cross sections of Hydrogen in water were generated at a slightly different temperature. While MCNP automatically Doppler broadens the input cross sections, M3C doesn't.

5. Conclusion

The VVER pin cell benchmark was analyzed using M3C code, supplied with ACE files from TENDL-2015 library, along with random ACE files supplied with TENDL-2015 library in the nuclear parameters. It is seen here that the uncertainty due to nuclear data is more due to H^1 as compared to O^{16}, as expected in such thermal Uranium lattices. The uncertainty due to nuclear data estimated is similar for M3C and MCNP codes.

6. Acknowledgements

The authors thank Dr. Umasankari Kannan, Head, RPDD, BARC, for her guidance and support. This work was possible due to the content available on the TALYS Evaluated Nuclear Data (TENDL) website. NJOY-2016 was obtained from http://www.njoy21.io. Ms Argala Srivastava, Krishna Kumar Yadav and Anmol Singh are specially thanked for their guidance and for support.

7. Bibliography

1. D.A.Brown. (2018). ENDF/B-VIII.0: The 8th Major Release of the Nuclear Reaction Data Library with CIELO-project Cross Sections, New Standards and Thermal Scattering Data. *Nuclear Data Sheets*, 148.
2. Koning. (2016). *TENDL library*. Retrieved from tendl.web.psi.ch/tendl_2015/tendl2015.html: tendl.web.psi.ch/tendl_2015/tendl2015.html
3. Cullen, D. (2018). *ENDF/B-VIII versus ENDF/B-VII: What's Different?* CA.
4. Kannan, U. (2010). *Development of new nuclear databases for advanced reactor sysems utilising Thorium.* Mumbai: University of Mumbai.
5. A.J. Koning, D. R. (2012). Modern Nuclear Data Evaluation with the TALYS code system. *Nuclear Data Sheets*, 2841-2934.
6. Koning, D. R. (2011). How to randomly evaluate Nuclear data. *NSE*, 68-80.
7. Kumar, A., Kannan, U., & Ganesan, S. (2019). Development of the Assembly-Level Monte Carlo Neutron Transport Code M3C for Reactor Physics Calculations. *Nuclear Science and Engineering*.
8. LANL, X.-5. (2003). *MCNP - A general Monte Carlo N-Particle Transport Code.* LANL.
9. A Nikalaichyk et al. Calculation of VVER MOX pin-cell benchmark with OpenMC code, ICNRP 2020

Table 1 k_{inf} using evaluated nuclear data

Monte Carlo Code (Nuclear Data)	k_{inf}
M3C (TENDL-2015)	1.370319 ± 0.000293
MCNP (TENDL-2015)	1.37086 ± 0.00035
OpenMC (ENDF/B-VII)	1.37972± 0.00023

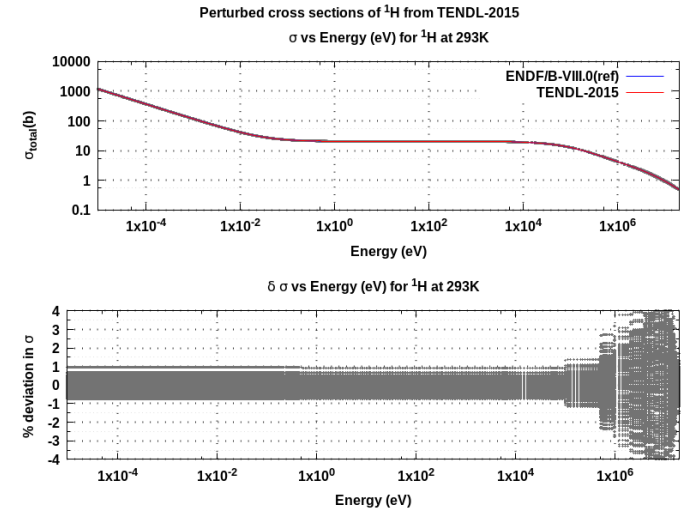


Fig. 1 Perturbed total cross sections of H^1

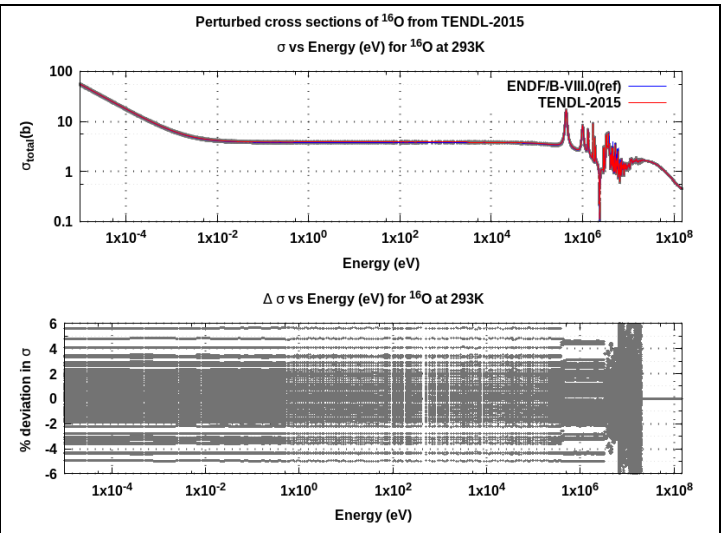


Fig. 2 Perturbed total cross sections of O^{16}

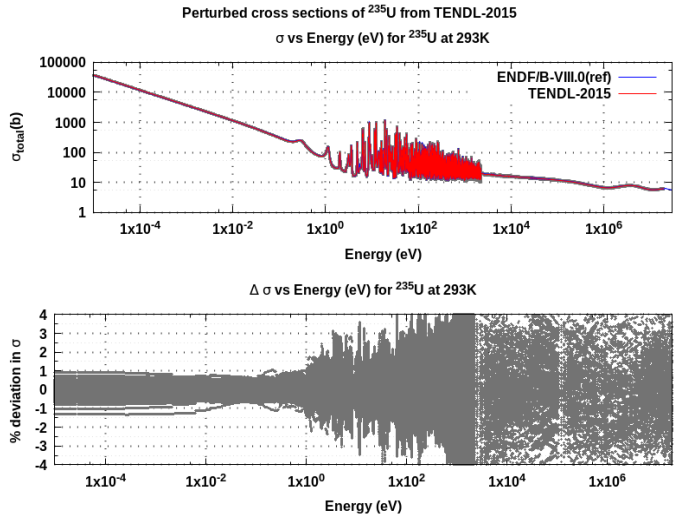


Fig. 3 Perturbed total cross sections of U^{235}

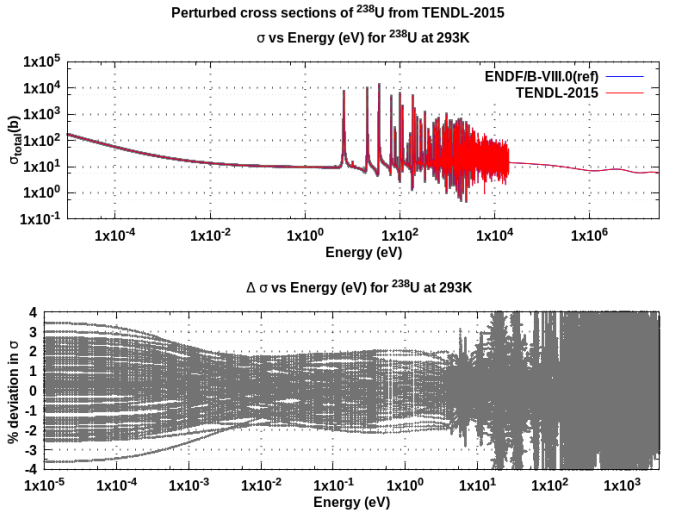


Fig. 4 Perturbed total cross sections of U^{238}

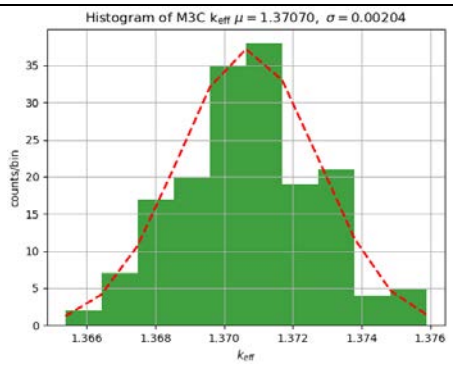


Fig. 5 k_{inf} distribution for H^1 perturbed samples

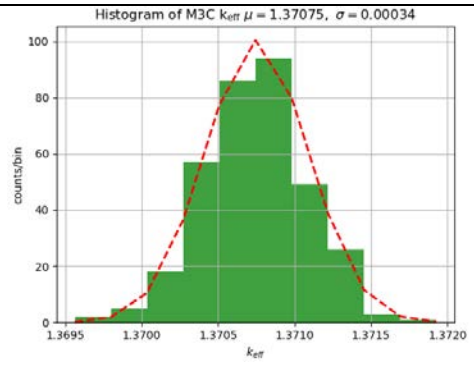


Fig. 6 k_{inf} distribution for O^{16} perturbed samples

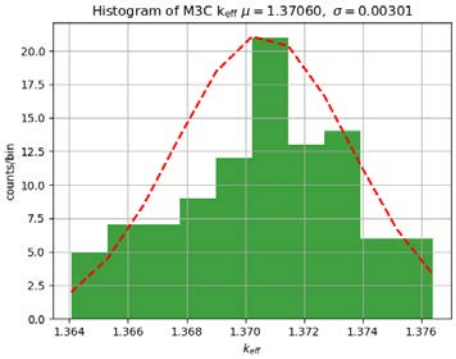


Fig. 7 k_{inf} distribution for U^{235} perturbed samples

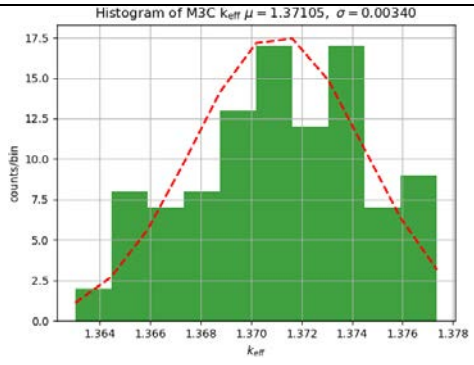


Fig. 8 k_{inf} distribution for U^{238} perturbed samples

Table 2 Results of TMC analysis of VVER-1000 pincell

Isotope varied	MCNP		M3C	
	k_∞	Std dev (pcm)	k_∞	Std dev (pcm)
H-1	1.37138	197	1.37070	204
O-16	1.37134	41	1.37075	34
U-235	1.37106	307	1.3706	301
U-238	1.37153	343	1.37105	340

Analysis of Doppler reactivity defect benchmarks using ENDFB8GX library

V. Harikrishnan, R. Karthikeyan and Usha Pal
LWRPS,RPDD,BARC
e-mail: -harikv@barc.gov.in

Abstract

A new 172 group WIMS formatted nuclear data library ENDFB8GX has been generated in-house from the latest ENDF/B-VIII.0 data using the open source data processing code NJOY-16. Extensive validation is required to incorporate the new library into physics design, analysis calculations. In this work, a set of computational benchmarks for the Doppler reactivity are simulated with the lattice cell code Dragon. The results are compared with existing older libraries, as well as published reference. The Doppler reactivity estimated with ENDFB8GX data compare closely with results from ENDFB7GX and ENDFB6GX as well as the reference for all the cases analyzed.

1. Introduction

The Doppler coefficient of reactivity is very important in the design and safe operation of nuclear reactors; it ensures safety during transients. The magnitude of Doppler reactivity is small, and it can't be directly measured. Therefore, uncertainties in Doppler coefficient up to 10% are traditionally accepted. Varying composition of Plutonium in fuel is an additional source of uncertainty. The Mosteller benchmarks [1] are a series of 16 computational pin-cell benchmarks with varying fuel composition, designed to retain the principal contributors to Doppler defect. The benchmarks have been analysed with the lattice cell code Dragon 3.06O [2]. The nuclear data inputs were 172 group WIMS formatted ENDFB8GX (generated in-house), ENDFB7GX, and ENDFB6GX (IAEA WLUP [3]).

2. ENDFB8GX

The latest ENDF-6 data - ENDF/B-VIII.0 [4] is the manifestation of progress in nuclear data experiments and modelling, and includes updated evaluations. This data available from BNL needs to be processed for use in reactor physics codes. The NJOY-16[5] is preferred due to its advanced features and is open source, hosted on git-hub. NJOY-16 runs on UNIX platform. The 172 groups WIMS formatted nuclear data is used by reactor analysis codes such as WIMS, Dragon etc. The library has 47 fast groups (20MeV-9.118keV), 45 resonance groups (9.118keV-4eV), and 80 thermal groups (below 4eV).Due to the finer group structure the important resonance effects are preserved while multi-grouping. The burnup chain has been extended up to ^{252}Cf. However, the processing in WIMS format has so far been on Windows platform [6] and the process has been adapted to Linux.

3. Dragon 3.06O

The benchmarks have been simulated with Dragon 3.06O lattice cell code, using the collision probability method. The self shielding calculations are performed with Livolant-Jeanpierre normalization which has shown improved accuracy for PWR lattices. The air gap between fuel and clad has been neglected. The modelling is similar to reference [7].

4. Mosteller Benchmark

These are a set of 16 computational benchmarks for studying the Doppler reactivity defect, proposed by R. Mosteller. These include an infinite array of identically fuelled pin cells with natural/ enriched UO_2, reactor-recycle mixed oxide (MOX) fuel, and Weapons grade MOX fuel. The fuel composition is given in Table 1. The clad is natural Zr. The Fuel Temperature rises from 600K at Hot Zero Power (HZP) to 900K at Hot Full Power (HFP). Xenon poisoning effects are not considered. The moderator is borated water with 1400ppm boron. The lattice description is given in Table 1.

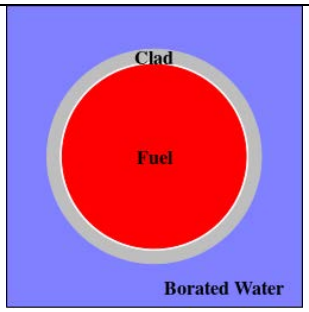


Figure 1 Benchmark description

Parameter	At 600K	At 900K
Fuel OD (cm)	0.78796	0.78866
Clad ID (cm)	0.80452	
Clad OD (cm)	0.91944	
Pitch (cm)	1.26678	

Table 1: Overview of Fuel Types in the Three Categories of Benchmark

UO_2 Lattices % of ^{235}U	Reactor Recycle Grade (RG) MOX	Weapons Grade (WG) MOX	Pu Composition (at.%)		
	% of PuO_2	% of PuO_2	Isotope	RG Pu	WG Pu
0.711	1.0	1.0	^{239}Pu	45.0	93.6
2.4	4.0	2.0	^{240}Pu	30.0	5.9
3.9	6.0	4.0	^{241}Pu	15.0	0.4
5.0	8.0	6.0	^{242}Pu	10.0	0.1

5. Results

All the 16 cases outlined in [1] have been analysed with ENDFB8GX, ENDFB7GX and ENDFB6GX. Processing with the new NJOY-16 also contributes to changes in cross sections. Fig. 1 shows the variation of Doppler coefficient over fuel content for UO_2, RG MOX, and WG MOX. Fig. 2 displays the deviation in the estimated Doppler Coefficient from reference values. The ENDFB8GX estimated Doppler coefficient deviates by 0.14 pcm/K (-2.73%) for natural Uranium from the reference. It is to be noted that this lattice is deeply subcritical, hence the deviation in reactivity is higher for a small change in k_{inf}. Due to the occurrence of absorption resonance near the thermal group boundary, high and low self-shielded ^{242}Pu cross sections are stored separately in the WIMS library with WIMS ID 242 (high self-shielded) and 1242 (low self-shielded). The effect of self-shielding on Doppler coefficient, and k_{inf} as a function of MOX content in fuel is seen in Fig. 3,4. Using low self-shielded ^{242}Pu, the k_{inf} decreases due to increase in absorption cross section. The k_{inf} and Doppler coefficients for some cases are listed in Tables 2-4, and compared with the results using Dragon code and ENDFB6GX library. The Doppler coefficients estimated with ENDFB8GX compare well with earlier libraries, as well as reference [7]. The Doppler coefficient is negative in all cases, ensuring negative feedback during transients.

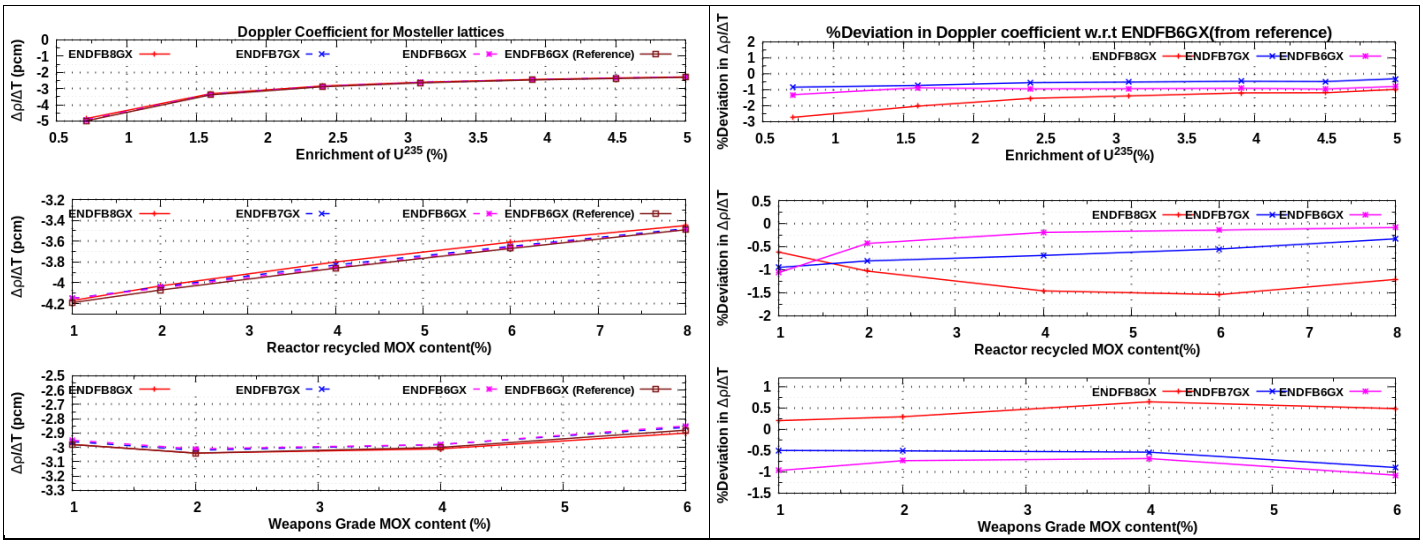


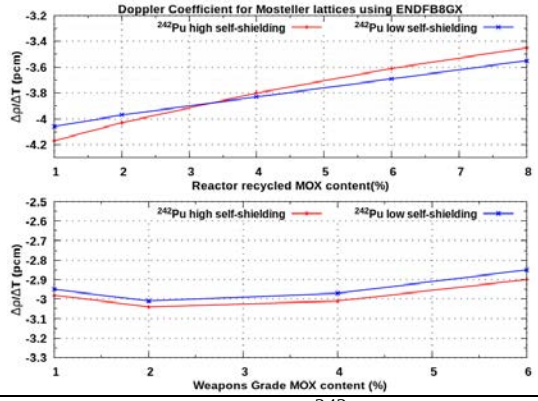
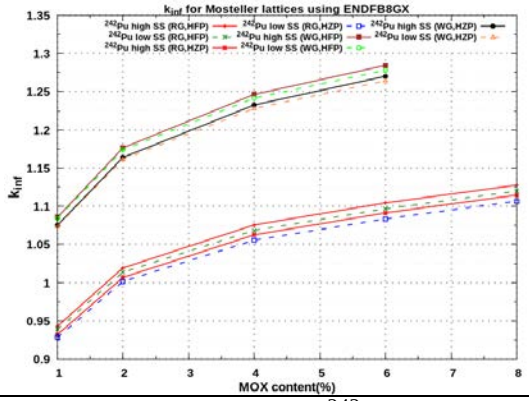
Fig.1 Doppler Coefficients estimated	Fig. 2 %Deviation from ENDFB6GX(Reference)
	
Fig.3 Using high and low ^{242}Pu self-shielding	Fig. 4 k_{inf} with high and low ^{242}Pu self-shielding

Table-2a UO_2 fuel using ENDFB8GX

^{235}U Enr(wt.%)	HZP k_{inf}	HFP k_{inf}	Doppler Defect (Δρ)(pcm)	Doppler Coefficient (Δρ/ΔT)(pcm)
0.711	0.66948	0.66301	-1456	-4.85
2.4	1.09917	1.08896	-853	-2.84
3.9	1.23722	1.22611	-732	-2.44
5.0	1.29562	1.28422	-685	-2.28

Table-2b UO_2 fuel using ENDFB7GX

^{235}U Enr(wt.%)	HZP k_{inf}	HFP k_{inf}	Doppler Defect (Δρ)(pcm)	Doppler Coefficient (Δρ/ΔT)(pcm)
0.711	0.66449	0.65800	-1485	-4.95
2.4	1.09710	1.08682	-862	-2.87
3.9	1.23760	1.22641	-737	-2.46
5.0	1.29735	1.28584	-690	-2.30

Table-2c UO_2 fuel using ENDFB6GX (Reference [7])

^{235}U Enr(wt.%)	HZP k_{inf}	HFP k_{inf}	Doppler Defect (Δρ)(pcm)	Doppler Coefficient (Δρ/ΔT)(pcm)
0.711	0.66364	0.65711	-1497	-4.99
2.4	1.09479	1.08450	-867	-2.89
3.9	1.23510	1.22390	-741	-2.47
5.0	1.29487	1.28337	-692	-2.31

Table-3a Reactor-Recycle MOX Fuel using ENDFB8GX

PuO_2 Enr. (wt.%)	HZP k_{inf}	HFP k_{inf}	Doppler Defect (Δρ)(pcm)	Doppler Coefficient (Δρ/ΔT)(pcm)
1	0.94293	0.93195	-1250	-4.17
4	1.07567	1.06264	-1140	-3.80
8	1.12768	1.11468	-1034	-3.45

Table-3b Reactor-Recycle MOX Fuel using ENDFB7GX

PuO_2 Enr. (wt.%)	HZP k_{inf}	HFP k_{inf}	Doppler Defect (Δρ)(pcm)	Doppler Coefficient (Δρ/ΔT)(pcm)
1	0.94090	0.93000	-1246	-4.15
4	1.07165	1.05861	-1149	-3.83
8	1.12289	1.10989	-1043	-3.48

Table-3c Reactor-Recycle MOX Fuel using ENDFB6GX (Reference[7])

PuO_2 Enr. (wt.%)	HZP k_{inf}	HFP k_{inf}	Doppler Defect (Δρ)(pcm)	Doppler Coefficient (Δρ/ΔT)(pcm)
1	0.94209	0.93106	-1257	-4.19

4	1.07193	1.05880	-1157	-3.86
8	1.12349	1.11043	-1047	-3.49

Table-4a Weapons-Grade MOX Fuel using ENDFB8GX

PuO_2 Enr. (wt.%)	HZP k_{inf}	HFP k_{inf}	Doppler Defect (Δρ)(pcm)	Doppler Coefficient (Δρ/ΔT)(pcm)
1	1.08552	1.07508	-895	-2.98
2	1.17654	1.16403	-913	-3.04
4	1.24645	1.23255	-904	-3.01
6	1.28445	1.27027	-869	-2.90

Table-4b Weapons-Grade MOX Fuel using ENDFB7GX

PuO_2 Enr. (wt.%)	HZP k_{inf}	HFP k_{inf}	Doppler Defect (Δρ)(pcm)	Doppler Coefficient (Δρ/ΔT)(pcm)
1	1.08639	1.07600	-889	-2.96
2	1.17671	1.16430	-906	-3.02
4	1.24487	1.23117	-894	-2.98
6	1.28127	1.26734	-857	-2.86

Table-4c Weapons-Grade MOX Fuel using ENDFB6GX (Reference[7])

PuO_2 Enr. (wt.%)	HZP k_{inf}	HFP k_{inf}	Doppler Defect (Δρ)(pcm)	Doppler Coefficient (Δρ/ΔT)(pcm)
1	1.08535	1.07493	-893	-2.98
2	1.17496	1.16252	-911	-3.04
4	1.24289	1.22916	-899	-3.00
6	1.27949	1.26548	-865	-2.88

6. Conclusion

The latest ENDFB8GX library developed in-house with open source NJOY-16 has been used to analyse Doppler reactivity computational benchmark lattices using Dragon code. The k_{inf} and Doppler reactivity are also computed for ENDFB7GX and ENDFB6GX. Reference[7] provides the results using Dragon code and ENDFB6GX library. The Doppler coefficients estimated with ENDFB8GX match closely with other results, especially with WG MOX fuel. The highest deviation in Doppler coefficient is -2.73% (pcm/K) for natural Uranium against reference value -4.99pcm/K. The Doppler coefficient estimated is negative in all cases. The Doppler coefficient becomes less negative on increasing the ^{235}U enrichment, or PuO_2 enrichment in fuel. The effect of high and low self-shielding in ^{242}Pu, with absorption resonance near thermal group boundary, is closely examined. By simulating variation in fuel temperature and composition, it is seen that the physical processes influencing the Doppler coefficient are reliably demonstrated with the new library ENDFB8GX.

7. References

[1] "Computational Benchmark to the Doppler Reactivity Defect", R. Mosteller, Report LA-UR-06-2968, Jun 15, 2006.

[2] "A User Guide for Dragon 3.06", G. Marleau, A. Hebert and R. Roy, Report IGE-174 Rev. 13, (2006).

[3] "WIMS-D library update: final report of a coordinated research project", ISBN 92–0–105006–2, 2007 (www.nds-iaea.org/wimsd/index.html).

[4] "ENDF/B-VIII.0: The 8th Major Release of the Nuclear Reaction Data Library with CIELO-project Cross Sections, New Standards and Thermal Scattering Data" by D.A.Brown et.al., Nucl. Data Sheets 148, Feb 2018.

[5] "The NJOY Nuclear Data Processing System, Version 2016"by R. E. MacFarlane et.al. LANL, Jul 3, 2018.

[6] "Generation of 172 Group WIMS Library 'LWRPS.LIB' for 185 Nuclides up to 252Cf", by S. A. Khan, Karthikeyan R. and Jagannathan V., RPDD/LWRPS/Note/006/2006, July 31, 2006.

[7] "Dragon evaluation of the benchmark for the Doppler reactivity defect" Joint International Topical Meeting on M &C + SNA 2007, Monterey, California, April 15-19, 2007

STOCHASTIC INTERPOLATION OF NUCLIDES TO REPRESENT DOPPLER BROADENED DATA IN REACTOR PHYSICS CALCULATION

Rashbihari Rudra[1], Rashmi Rai[1], K. P. Singh[1] and U. Kannan[1]
[1] Bhabha Atomic Research Centre, Mumbai, India
[1]*e-mail: - rrudra@barc.gov.in*

Abstract

Monte Carlo methods for neutron transport calculations are always considered for its high fidelity but often limited in use due to its intensive demand of computational resource. It is quite understandable that, to represent the continuous range of temperature in an operating reactor, hundreds of fuel and coolant temperatures are needed. Storing these many data is neither practical nor feasible. In the present work instead of storing a large number of pre-processed data, we have employed a method of approximating the cross section at various intermediate temperatures, given a set of cross-sections, Doppler broadened at a small number of reference temperatures.

1. Introduction

To perform the temperature dependent neutronic calculations in an exact way using Monte Carlo techniques require generation of a set of cross sections at the desired temperatures. This task is normally accomplished by the codes like NJOY, PREPRO. But in practice, NJOY calculation is not only time-consuming, the volume of data generated to represent exact temperatures, for representing a full core, needs a large memory resource. An additional complication in this approach is that we may not know the final temperature distribution in prior. Another way of generating the temperature dependent cross-sections is to utilize a scheme of interpolation among several cross-sections given at different temperatures. This alternative approach eases the data handling capability and reduces the computational cost significantly. In this paper, we tried out interpolation schemes, where the ACE formatted cross sections at different temperatures are interpolated to obtain the intermediate temperature cross sections. Using these interpolated cross sections k-calculations are performed. The accuracy of interpolation is dependent not only on the size of the temperature interval but also on the interpolation scheme used and the nature of cross-section.

.

2. Stochastic Mixing of Cross Section

Though any straight-forward simple interpolation scheme based upon physics nature of Doppler broadening is not possible, one is always free to try some purely numerical interpolation schemes. The stochastic interpolation scheme used to represent the cross section at intermediate temperature is based on the presumption that cross sections at some intermediate temperature T ($T_1 < T < T_2$) can be realised by stochastically adding cross section at temperature T_1 with probability p_1 with cross section at temperature T_2 with probability p_2.

$$\sigma(T) = \sigma(T_1) \times p_1 + \sigma(T_2) \times p_2.$$

The values of p_1 and p_2 depends upon T and the interpolation scheme used between T_1 and T_2.

For example, in case of Linear – Linear Interpolation the Doppler broadened cross section at some intermediate temperature T' can be written in terms of cross section at T_1 and T_2 as:

$$\sigma(E,T') = \sigma(E,T_1).\frac{T'-T_1}{T_2-T_1} + \sigma(E,T_2).\frac{T_2-T'}{T_2-T_1}$$

For Square root – Linear Interpolation:

$$\sigma(E,T') = \sigma(E,T_1).\frac{\sqrt{T'}-\sqrt{T_1}}{\sqrt{T_2}-\sqrt{T_1}} + \sigma(E,T_2).\frac{\sqrt{T_2}-\sqrt{T'}}{\sqrt{T_2}-\sqrt{T_1}}$$

For Log-Log Interpolation:

$$\log[\sigma(E,T')] = \log[\sigma(E,T_1)].\frac{\log[T']-\log[T_1]}{\log[T_2]-\log[T_1]} + \log[\sigma(E,T_2)].\frac{\log[T_2]-\log[T']}{\log[T_2]-\log[T_1]}$$

For Linear – Log Interpolation:

$$\log[\sigma(E,T')] = \log[\sigma(E,T_1)].\frac{T'-T_1}{T_2-T_1} + \log[\sigma(E,T_2)].\frac{T_2-T'}{T_2-T_1}$$

For Square root – Log Interpolation:

$$\log[\sigma(E,T')] = \log[\sigma(E,T_1)].\frac{\sqrt{T'}-\sqrt{T_1}}{\sqrt{T_2}-\sqrt{T_1}} + \log[\sigma(E,T_2)].\frac{\sqrt{T_2}-\sqrt{T'}}{\sqrt{T_2}-\sqrt{T_1}}$$

3. Result and Discussion

To study the interpolation scheme, we processed ENDF-VIII.0 library to obtain Doppler broadened ACE formatted cross section library at temperature 296, 600, 900 and 1200 K using code NJOY. The cross sections along with the energy grid are extracted from the ACE formatted file using the code CENT. A tolerance limit of 0.1% was used while running NJOY. Thus during the interpolation at a particular temperature, if the deviation of the interpolated data from the exact data at that temperature is below 0.1% then the interpolation scheme appears to be reliable and fruitful. The deviation is measured as:

$$\delta\sigma = \frac{|\sigma_{exact}(E,T) - \sigma_{int}(E,T)|}{\sigma_{exact}(E,T)}$$

Though a large number of nuclides have been studied, it is of worth to see how temperature interpolation works for U^{238} as a representative nuclide.

It is observed that exact representation of resonance cross section is difficult using interpolation schemes. The error introduced by different interpolation schemes in the thermal energy range (10^{-5} eV – 1 eV) are depicted in fig. 1. Here the minimal error is introduced by the square root – log interpolation scheme. Still the error produced by the square root interpolation is well within the tolerance (0.1%) limit. In fact, in thermal range all the four interpolation schemes except the linear-log produces error within tolerance limit. It is also observed that the error induced also reduces as the interpolating temperature interval reduces. The amount of error induced by interpolation scheme is lower in capture cross section compared to elastic scattering

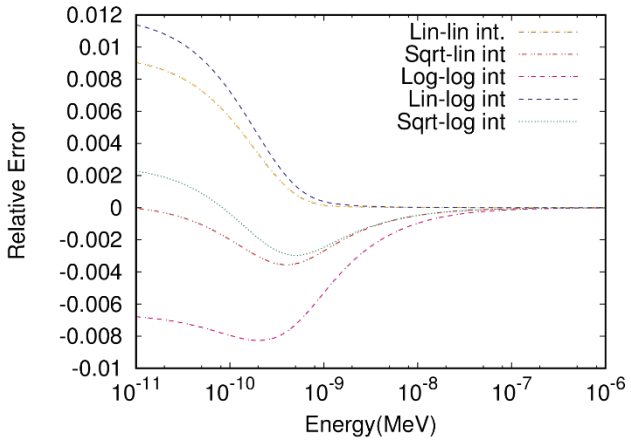


Fig. 1: Relative error introduced by interpolations in U^{238} total cross section in thermal range.

cross section. In the resonance region, the error

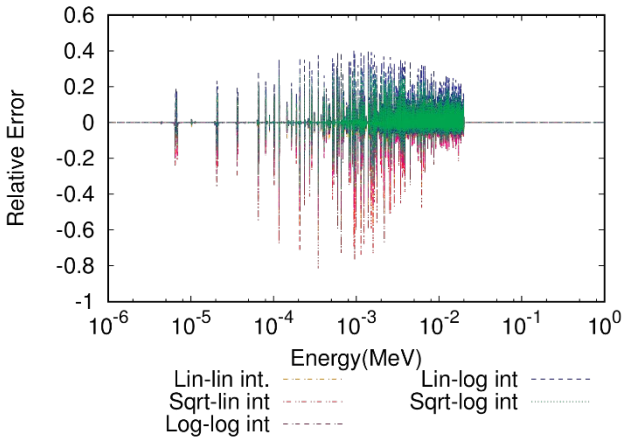


Fig. 2: Relative error induced by interpolation schemes in total cross section of U^{238}.

induced is much larger than the error in thermal region. The interpolation error in U^{238} in the entire energy range is shown in fig. 2. In the resonance region, the relative error increases with increase in resonance structures and the maximum error can be very high as large as 60% whereas the tolerance limit is 0.1%. No interpolation scheme is better in this region.

Though the interpolation scheme is not very promising in the resonance region, we tested the scheme for thermal reactor calculation. we took some well reported test problems to verify the validity of stochastic temperature interpolation scheme. The first problem taken is 19 pin PHWR cluster. The heavy water moderated standard 220 MW_e pressure tube type reactor uses natural uranium dioxide as fuel. Fuel pins of radius 0.7225 cm are arranged in an annular ring configuration. The effective fuel material density is 9.91 gm/cc and effective sheath material density 8.91 gm/cc. The clad outer radius is 0.7605 cm and the lattice pitch is 22.86 cm. K_{inf} was calculated for this standard configuration at different material temperatures. Fig. 3 shows a comparison of computed k_{inf} values using data file generated at problem temperature and stochastic linear interpolation mechanism. The word 'Exact' means that the data file is processed at that particular temperature using NJOY. Thus it is clear that k_{inf} values lie well within their tolerance limit indicating that the linear interpolation scheme is reliable. As the aim of this study is to check the validity of the data interpolation, no density effect was taken into account for both the fuel and moderator materials while increasing and decreasing temperature.

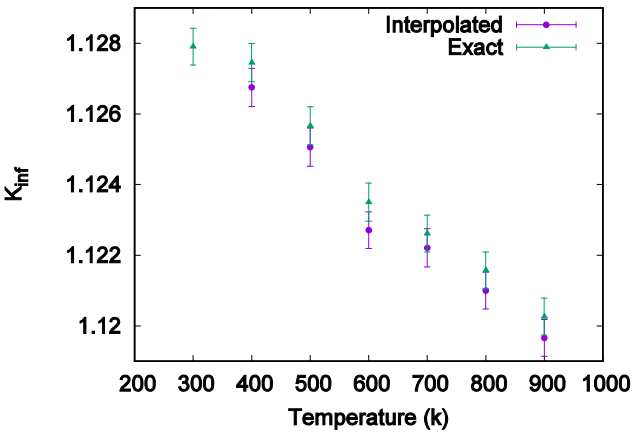


Fig. 3: Infinite multiplication factor of PHWR lattice computed using exact data and stochastically mixed data.

In fact, the large reactivity load induced by the density effect overrides the smaller reactivity change introduced by the temperature effect on nuclear data.

For a better grasp, we calculated the reactivity deviation in the stochastic interpolation method and the related uncertainties as a function of temperature. The reactivity is computed as

$$\delta\rho = \left[\frac{1}{K_{int}} - \frac{1}{K_{exact}}\right] \times 1000$$

Fig. 4 shows the reactivity deviation in mk versus temperature in the temperature range 300 to 900 K.

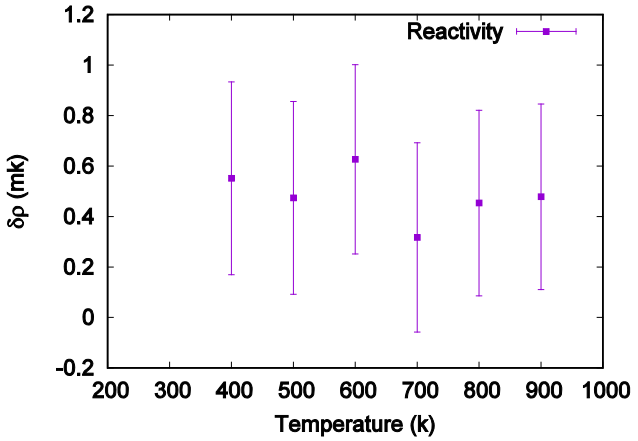
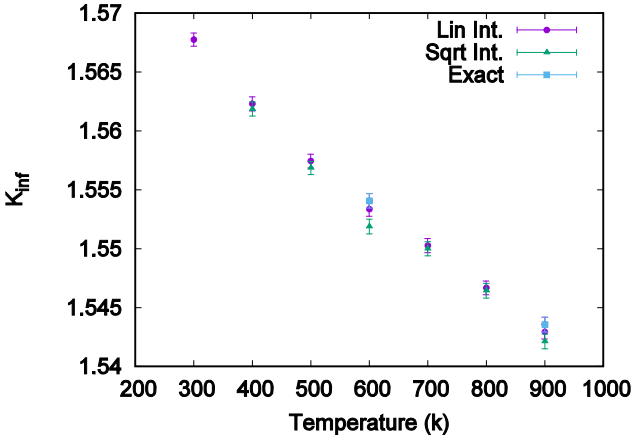


Fig. 4: Reactivity deviation introduced by temperature interpolation in 19 pin PHWR cluster.

In the second test problem we took the example of PWR pin cell. The fuel pallet radius is 0.4096 cm. Clad outer radius is 0.4750 cm and pin pitch is 1.26 cm. In this standard pin cell configuration, we tested both the linear and square root interpolation scheme. Fig. 5 shows the variation of Kinf with temperature. All kind of interpolations are done with the nearest NJOY processed data available.



For example, to interpolate at 400 and 500 K, Doppler broadened data at 300 and 600K are utilized. It is noticeable that both the square root and linear interpolation k-values lie within their standard deviation range, though the linear interpolation produces more accurate result throughout the entire temperature range. In case of 600K both the square root and linear interpolation were done using exact data files generated at 300k and 900K. Thus in this case the temperature difference between exact data is 600K whereas for other cases the interval difference is 300k. Thus if the temperature interval between the 'exact' data is more, then the linear interpolation technique produces comparatively more accurate result than the square root interpolation method. The same thing holds true for k-value at 900K. One more thing worth observing is that, as the operating temperature increases, the difference between the k-values obtained using linear and square root interpolations decreases steadily. One reason behind this might be the smoothening nature of Doppler broadened data.

4. Conclusion

Stochastic interpolation is a convenient and easy to implement method to handle temperature variation in reactor physics problems. For well thermalised systems, both the linear and square root interpolations produce reasonably accurate result though linear interpolation is slightly more accurate. In stochastic interpolation, smaller the interval between 'exact' data, more accurate is the predicted k-value. Thus an optimized value of temperature interval between exact data can be found out so that the inaccuracy is within tolerance limit yet data volume is not large.

5. References

[1] Cullen, D.E., 2010. Nuclear data preparation. In: Cacuci, D.G. (Ed.), *Handbook of Nuclear Engineering, Nuclear Engineering Fundamentals*, vol. 1. Springer, New York, pp. 319–325.

[2] R. Rudra, K. P. Singh and Degweker S. B., "Development of a general geometry continuous energy Monte Carlo code 'CENT' for reactor analysis", *ARP-2017,* Mumbai, India, 2017.

[3] MacFarlane, R.E., Muir, D.W., "The NJOY Nuclear Data Processing System, Version 91", *LA-12740-M*, Los Alamos National Laboratory, 1994.

[4] D. E. Cullen and C. R. Weisbin, "Exact Doppler Broadening of Tabulated Cross Sections," *Nucl. Sci. Eng.*, **60**, 199 (1976).

[5] S. Peng, A.B.S. Zhang, X. Jiang, "Investigations on the point-wise neutron cross-section temperature interpolation methods", *Ann. Nucl. Energy*, 45, (2012), 155–160.

[6] Rashbihari Rudra and Degwker, S. B., "CENT - A computer program for deciphering Ace files for continuous energy Monte Carlo and other applications", *BARC/ThPD/09/RR,* 2014.

UNCERTAINTY AND SENSITIVITY ANALYSI OF NEUTRON MULTIPLICATION FACTOR IN CANDU PHWR

M. Mohideen Abdul Razak[1], P. Ravindra Babu[2]

[1] Bhabha Atomic Research Centre Facilities, Kalpakkam, 603127, India

[2] Bhabha Atomic Research Centre Facilities, Vizag, India

[1]*e-mail: - mmar@igcar.gov.in*

Abstract

The uncertainty and sensitivity analysis of neutron multiplication factor in CANDU PHWR (AECL-7236) is presented in this paper. Errors and uncertainties are always present in the cross section data. From safety point of view, it is important to know the behavior of reactor output parameters, i.e. k_{eff}, when the input parameters, i.e. macroscopic cross section data are perturbed around their best estimate value. In this paper a parametric study is carried out to estimate the uncertainty in the k_{eff} caused by various uncertainties in the macroscopic cross section data of CANDU reactor. The first order perturbation method is applied to estimate the uncertainty in k_{eff}. It is observed that the thermal fission cross section is highly influential in affecting the k_{eff} as compared to other cross section data. A linear relationship between the sensitivity coefficient for k_{eff} is made and this relationship can be used to estimate the uncertainty in k_{eff} for a given uncertainty in the macroscopic cross section data.

1. Introduction

The study of behaviour of reactor core to various types of uncertainties in reactor physics parameters is important for the safe operation of nuclear reactors. A primary source of uncertainty in the reactor core behavior arises from the uncertainty in the nuclear cross section data. In any nuclear power plant (NPP), it is essential to know the reactor core behaviour when the reactor physics input parameters, i.e. macroscopic cross section data, are perturbed in the vicinity of their best estimate values. Some perturbed input parameters may be more influential in affecting the reactor output parameters, i.e. neutron multiplication factor, reactor power etc. and some parameters may be less influential in affecting them. Sometimes the uncertainty in the input parameter may be stationary or it may propagate with time. The propagation of uncertainty in the input parameter with time will affect the reactor core power, core temperature etc. during transient and in this case it is important to examine its effect on reactor core characteristics.

Uncertainty quantification (UQ) deals with the determination of uncertainty in the output parameter (neutron multiplication factor, flux, temperature etc.) based on the uncertainty in the input parameters [1], [2]. Sensitivity analysis (SA) gives information about the effect of contribution of specific input parameter uncertainty to the uncertainty in the output. The uncertainty and sensitivity analysis gives information about the identification of potentially important input parameters which are more influential in affecting the core behavior under normal and accidental conditions. Using the uncertainty and sensitivity analysis, the influential input parameters can be given more careful evaluation or measurement with least error.

2. CANDU PHWR (AECL-7236)

It is a realistic 3D PHWR benchmark kinetics problem [3] in Cartesian geometry. This is one of the widely studied benchmark problem. The vertical cross section view of the core is shown in Fig. 1. The geometrical description of the core is as follows: The core contains two radial fuel zones (inner core and outer core) surrounded by heavy water reflector. The axial length of the core in the horizontal

Z direction is 600 cm. Along the horizontal direction (Z axis), the material distribution is uniform. The height and width of the core are 780 cm. The core is divided into a total of $18 \times 18 \times 10$ meshes [3]. In the horizontal Z direction, a mesh spacing of 20 cm is used. The core composition and two group cross section data are given in Tables 1 and 2. Under normal operating conditions, the fissile component in the inner core is slightly less than that of the outer core.

3. Estimation of uncertainty in k_{eff}

The static uncertainty analysis is performed using first order perturbation theory [4] Here the uncertainty in the neutron multiplication factor is directly obtained by solving the neutron diffusion equation along with the adjoint solution. Consider the static neutron diffusion equation (two-group, the constants carry usual meaning)

$$D_1\nabla^2\varphi_1 - \Sigma_{a1}\varphi_1 - \Sigma_{1\to2}\varphi_1 + \left(\frac{1}{k_0}\right)(\nu\Sigma_{f1}\varphi_1 + \nu\Sigma_{f2}\varphi_2) = 0 \quad (1)$$

$$D_2\nabla^2\varphi_2 - \Sigma_{a2}\varphi_2 + \Sigma_{1\to2}\varphi_1 = 0 \quad (2)$$

In matrix form, the neutron diffusion equation is written as

$$\hat{A}\varphi = \frac{1}{k_0}\hat{F}\varphi \quad (3)$$

$\hat{A}$ is the neutron destruction operator ($\widehat{A_1} = D_1\nabla^2 - \Sigma_{a1} - \Sigma_{1\to2}$), $\hat{F}$ is the neutron production operator ($\widehat{F} = \nu\Sigma_{f1} + \nu\Sigma_{f2}$) and k_0 is the eigen value. When the input parameter (absorption or fission cross section) is perturbed (i.e.$\Sigma'_{a1} = \Sigma_{a1} + \Delta\Sigma_{a1}$), the resulting perturbed neutron diffusion equation is given as

$$\widehat{A'}\varphi' = \frac{1}{k'_0}\widehat{F'}\varphi' \quad (4)$$

where $\widehat{A'}$ contains the perturbed input parameters (cross sections), ($\widehat{A'} = \hat{A} + \Delta A$) $\widehat{F'}$ contains the perturbed fission cross sections ($\widehat{F'} = \hat{F} + \Delta\hat{F}$) , φ' is the perturbed flux and k'_0 is the new eigen value ($k'_0 = k_0 + \Delta k$). The adjoint neutron diffusion equation, for the unperturbed system, is given as

$$\hat{A}\dagger\,\varphi\dagger = \frac{1}{k_0}\hat{F}\dagger\,\varphi\dagger \quad (5)$$

where $\hat{A}\dagger$ is the adjoint operator for $\hat{A}$ and $\varphi\dagger$ is the adjoint flux. Using the first order perturbation theory [4], the uncertainty in the multiplication factor is computed from Eqs. (3)-(5) and it is given as

$$\frac{\Delta k_0}{k_0} = \frac{-\langle\varphi,(\Delta\hat{A}\dagger)\varphi\dagger\rangle - \frac{1}{k_0}\langle\varphi,(\Delta\hat{F}\dagger)\varphi\dagger\rangle}{\frac{1}{k_0}\langle\varphi,(\hat{F}\dagger)\varphi\dagger\rangle} \quad (6)$$

and the sensitivity coefficient of multiplication factor with respect to the input parameter Σ is computed as [1]

$$S(k_{eff},\Sigma) = \frac{\frac{\Delta k_0}{k_0}}{\frac{\Delta\Sigma}{\Sigma}} = -\Sigma\left(\frac{\langle\varphi,\left(\frac{\Delta\hat{A}\dagger}{\Delta\Sigma}\right)\varphi\dagger\rangle - \frac{1}{k_0}\langle\varphi,\left(\frac{\Delta\hat{F}\dagger}{\Delta\Sigma}\right)\varphi\dagger\rangle}{\frac{1}{k_0}\langle\varphi,(\hat{F}\dagger)\varphi\dagger\rangle}\right) \quad (7)$$

The uncertainties in the macroscopic cross sections are absorbed in the operators $\Delta\hat{A}$ and $\Delta\hat{F}$. Finite difference method is adopted to solve the forward and adjoint equations (Eqs.(3) & (4)) and the uncertainty in the k_{eff} and the sensitivity coefficient are estimated. A high sensitivity coefficient implies that the input parameter Σ is more influential in affecting the neutron multiplication factor. In general, the sensitivity coefficient is found to be higher for thermal fission cross section in water moderated reactors [5]. In CANDU PHWR (AECL-7236) the uncertainty is in k_{eff} is estimated for various uncertainties in the macroscopic cross section data. Here the uncertainty is applied in all regions of the reactor. The neutron multiplication factor k_{eff} may vary if the mesh size, in solving the neutron diffusion equation, is changed. But here the mesh size is kept constant while evaluating the neutron multiplication factor k_{eff} and its uncertainty $\frac{\Delta k_{eff}}{k_{eff}}$.

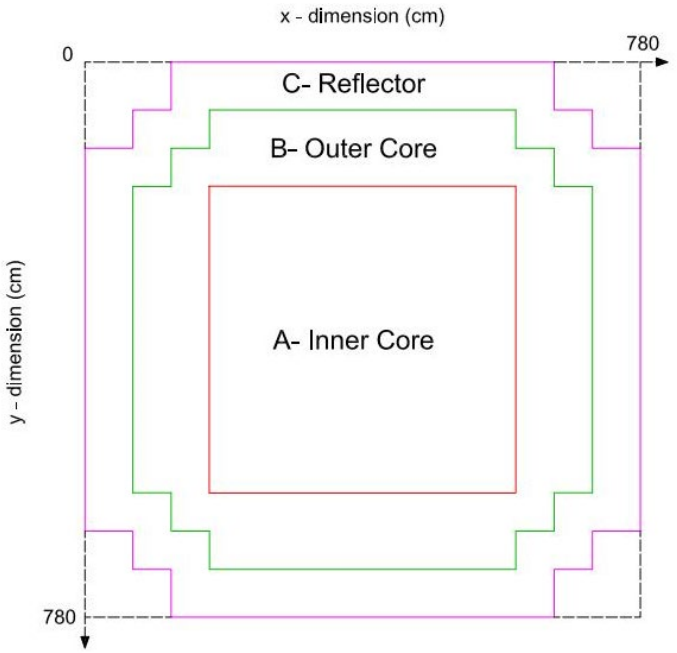


Fig.1 The vertical cross section view of CANDU PHWR. The three different regions of the core are shown.

Table 1. The uncertainty in the eigen value ($\Delta k / k$) caused by uncertainties in various macroscopic cross sections

S.N	Parameter	Uncertainty (%)	Δk/k (%)	Sensitivity coefficient
1	$\Delta\Sigma_{12}/\Sigma_{12}$	0.1	1.0738E-2	1.07E-01
2	$\Delta\Sigma_{12}/\Sigma_{12}$	0.5	5.3711E-2	1.07E-01
3	$\Delta\Sigma_{12}/\Sigma_{12}$	1.0	1.0748E-1	1.07E-01
4	$\boldsymbol{\Delta\Sigma_{a2}/\Sigma_{a2}}$	***0.1***	***9.8554E-2***	***9.86E-01***
5	$\boldsymbol{\Delta\Sigma_{a2}/\Sigma_{a2}}$	***0.5***	***4.9083E-1***	***9.82E-01***
6	$\boldsymbol{\Delta\Sigma_{a2}/\Sigma_{a2}}$	***1.0***	***9.7688E-1***	***9.77E-01***
7	$\Delta\Sigma_{a1}/\Sigma_{a1}$	0.1	9.4547E-3	9.45E-02
8	$\Delta\Sigma_{a1}/\Sigma_{a1}$	0.5	4.7256E-2	9.45E-02
9	$\Delta\Sigma_{a1}/\Sigma_{a1}$	1.0	9.4467E-2	9.45E-02
10	$\boldsymbol{\Delta\Sigma_{f2}/\Sigma_{f2}}$	**0.1**	**1.0045E-1**	**1.00E+00**
11	$\boldsymbol{\Delta\Sigma_{f2}/\Sigma_{f2}}$	**0.5**	**5.0430E-1**	**1.01E+00**
12	$\boldsymbol{\Delta\Sigma_{f2}/\Sigma_{f2}}$	**1.0**	**1.01372E-0**	**1.01E+00**

13	$\Delta D_1/D_1$	0.1	1.2810E-3	1.28E-02
14	$\Delta D_1/D_1$	0.5	6.4046E-3	1.28E-02
15	$\Delta D_1/D_1$	1.0	1.2808E-2	1.28E-02
16	$\Delta D_2/D_2$	0.1	1.7037E-3	1.70E-02
17	$\Delta D_2/D_2$	0.5	8.5181E-3	1.70E-02
18	$\Delta D_2/D_2$	1.0	1.7034E-2	1.70E-02

4. Discussion and Conclusion

The uncertainty and sensitivity analysis of neutron multiplication factor was performed for CANDU PHWR. The uncertainty and sensitivity analysis was carried out for various uncertainties in macroscopic cross section data. It was observed that the thermal fission cross section is more influential in affecting the k_{eff} and the second influential factor was found to be thermal absorption cross section data. The uncertainty in the macroscopic cross section data was varied between 0.01 (1%) and 0.05 (5%). It was observed that the variation of uncertainty in k_{eff} with the variation of uncertainty in thermal fission cross section was found to be follow a linear relation and the relation is given as

$$\frac{\Delta k}{k} = 1.075 * \frac{\Delta \Sigma_{f2}}{\Sigma_{f2}} - 3.25744 \times 10^{-4}$$

The above relation can be used to estimate the uncertainty in k_{eff} when the uncertainty in thermal fission cross section is known in the range 0.01-0.05.

CREDIT authorship contribution statement

M. Mohideen Abdul Razak: Conceptualization, Methodology, Formal analysis, Writing - original draft.
P. Ravindra Babu: Resources, Writing - review & editing.

Declaration of Competing Interest

The authors declare that they have no known competing financial interests or personal relationships that could have appeared to influence the work reported in this paper.

5. References

[1] Tae Young Han, Hyun Chul Lee, Jae Man Noh, "Development of a sensitivity and uncertainty analysis code for high temperature gas-cooled reactor physics based on the generalized perturbation theory", *Ann. Nucl. Energy*, vol. 85, p 501-511, 2015.
[2] Helton, J.C., Johnson, J.D., Sallaberry, C.J., Storlie, C.B., "Survey of sampling based methods for uncertainty and sensitivity analysis", *SANDIA report, SAND2006-2901*, 2006.
[3] Judd, R.A., Rouben, B., Three Dimensional Kinetics Benchmark Problem in a Heavy Water Reactor, *Report, AECL-7236*, 1981.
[4] Stacey, W.M., "*Nuclear Reactor Physics*", John Wiley & Sons, Inc., New York, 2001.
[5] Razak, Mohideen Abdul, M.., Studies on PHWR transients using modified exponential time differencing method with improved quasi model and associated dynamic sensitivity analysis – *Ph.D. Thesis – Homi Bhabha National Institute (HBNI)*, Kalpakkam, Tamil Nadu, India, 2019.

Physics Design Optimization of Liquid Hydrogen based Cold Neutron Source in HFRR

Dipankar Pal[1], Archana sharma[1] and Samiran Sengupta[1]
[1] Bhabha Atomic Research Centre, Mumbai, India
e-mail: - dipankar@barc.gov.in

Abstract

High Flux Research Reactor (HFRR) is an open tank in pool type reactor surrounded by heavy water reflector. A Cold Neutron Source Facility is planned in the proposed HFRR in the reflector region with Liquid Hydrogen (LH) at 20K used as a cold moderator. The shape and thickness optimization studies for moderator pot was carried out and cold flux was calculated for various moderator thickness and various pot shapes in different ortho Hydrogen concentration. Ellipsoidal shape moderator pot was found to deliver the maximum cold neutron flux. With 65% ortho-hydrogen concentration in LH (observed worldwide in LH based cold neutron source), it was observed that with 2 cm cold moderator thickness, maximum cold neutron flux is achieved. The paper describes the physics design optimization of CNS for HFRR.

1. Introduction

High Flux Research Reactor is a 40 MWt open tank in pool type reactor fueled with uranium silicide dispersed in aluminium matrix and cooled by upward flow [1] of demineralized light water. The reactor core is surrounded by heavy water reflector to provide a large irradiation volume. HFRR is going to provide extensive neutron beam tube research facility to the researchers in the basic sciences. There are six beam tubes in HFRR including a Cold Neutron Source Facility (CNS).

Neutrons from a reactor that are used for research application are those that have been slowed down from range of MeV (10^6 eV) to tens of meV (10^{-3} eV) by scattering in moderator and reflector. In a reactor, neutron energy spectrum is essentially Maxwellian with characteristic temperature somewhat higher than the actual temperature of moderator. For such spectrum, mean neutron wavelength and energy are 1.8 A^0 and 25 meV respectively and is well suited to the study of properties of condensed matter at atomic scale, where interatomic spacing is approximately 1 A^0 and characteristics vibrational energies are of order meV.

Nowadays, polymers which are being developed to replace traditional metal materials and Nano structures which are being developed with noble properties for processing drug delivery and biotechnological applications have characteristics dimensions best matched by neutrons of longer wavelength. However, fraction of neutrons with energies less than 5 meV (wavelength more than 4 A^0) in normal moderator spectrum is less than 2% of the total, which make their use inefficient in studies of polymer and nanomaterials and biomolecules. In order to address this problem cryogenically cooled moderators “Cold Neutron Sources” (CNS) are kept in reflector of neutron source. This cold source shifts the spectrum down in energy to a temperature somewhat above the cold moderator temperature, providing large gains in intensity for low energy neutrons [2]. A CNS facility has been proposed in HFRR with liquid hydrogen at 20K used as a cold moderator.

The CNS in HFRR will be placed at the position (420 mm, 500 mm) with respect to the center of core. A Plan view of CNS, HFRR core and Reflector is shown in Fig. 1a. The maximum unperturbed thermal neutron flux at the CNS thimble is 1.1×10^{14} n/cm^2/s and nuclear heat load in structural Aluminium and Liquid hydrogen are 0.52 W/g and 1.32 W/g respectively. This neutron flux will be feeding the cold

neutrons to the neutron guides through a 250 mm diameter beam hole that will guide the cold neutrons to the experimental facility installed in the GT Lab. This beam tube starts from window of the cold neutron source facility in the reflector vessel and run tangentially. Flux estimation has been carried out using Monte Carlo based computer code [3].

Cold neutron guide line in GT lab will have Small Angle Neutron Scattering (SANS) facility, triple axis spectrometer, quasi elastic neutron scattering spectrometer, neutron reflectometer, spin echo spectrometer, Ultra Small Angle Neutron Scattering (USANS) facility, prompt gamma Neuron Acivation analysis (NAA) and detector testing setup.

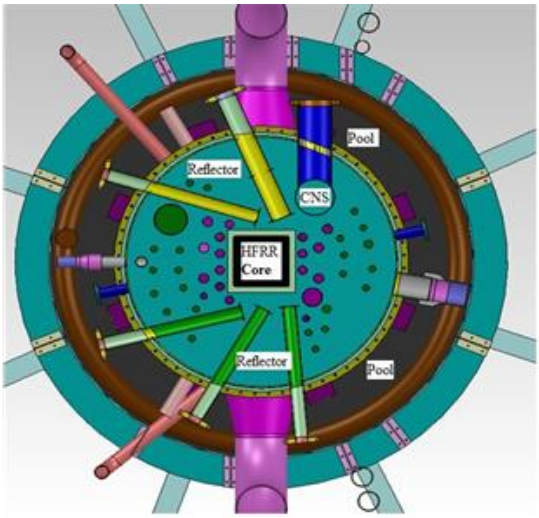


Fig. 1a: Plan view of CNS, HFRR core and Reflector

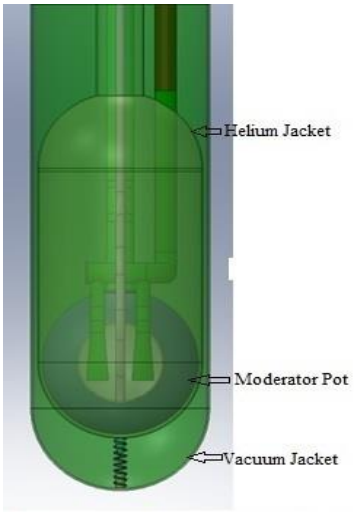


Fig. 1b: Three-dimensional view of CNS

2. Description of CNS

Structurally CNS consists of three main components as shown in Fig. 1b. The outermost component is vacuum jacket. The vacuum jacket accommodates all other components under a high vacuum environment and thus thermally isolates the components at cryogenic temperature from reactor environment. It is maintained at 10^{-6} mbar vacuum. This will protect the reactor in the worst case of safety failure. Inside vacuum jacket there is a helium jacket. The helium jacket surrounds the moderator cell and it is designed for 10 bar internal pressure. Helium at 16K will be passed through this jacket at a mass flow of 6g/s at 4bar (abs) pressure. The moderator cell inside helium chamber is the most important part of CNS. It is an ellipsoidal annulus containing 2.5 liters of liquid hydrogen. The pot has an exit hole towards CNS beam tube. All nuclear heat deposited in the moderator, the moderator pot and the helium jacket are transferred by helium to the helium chamber that is maintained at 16 K.

2.1 Design optimisation studies

A number of physics studies have been performed in arriving at the final design concept. A parametric study was first performed to determine the sensitivity of the cold source performance to the ortho/para hydrogen ratio, moderator thickness and pot shape.

In the liquid hydrogen, the spin states of the two H atoms may be aligned (as in para hydrogen) or not aligned (as in ortho hydrogen). Left undisturbed at cryogenic temperatures for many hours, the spin will tend to align, and para hydrogen will become predominate, although neutron irradiation can and does

cause hydrogen to transition back to the metastable ortho state. For energy of the neutron below 30 meV, the total neutron scattering cross sections for ortho hydrogen and para hydrogen are very different, with that for ortho-H being more than order of magnitude higher than that for para-H as shown in Fig. 2. This affects the slowing down probability and total number of collisions in finite sized cold moderator.

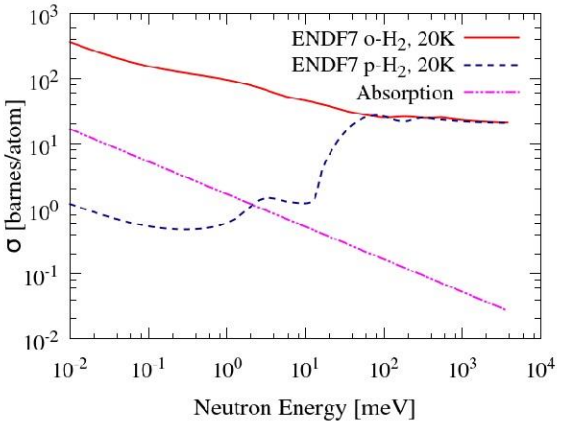


Fig 2: Scattering Cross Section for ortho and para hydrogen at 20 K [2]

An ellipsoidal annulus moderator pot with varying moderator pot thickness form 1 cm to 5 cm with outer ellipsoidal wall having major axis of 237 mm and minor axis of 219 mm have been studied. The study has been performed with different ortho hydrogen concentration in Liquid Hydrogen (LH).

Maximum cold neutron flux at the centre of moderator pot is observed at 4 cm cold moderator thickness in case of zero concentration of ortho hydrogen in LH as shown in Fig. 3. With different ortho-hydrogen concentration Moderator thickness are notably different for good physical reasons. Small amount of slowing down afforded by scattering in para-hydrogen resulted in insufficient opportunity for neutrons to scatter down to lower energies and eventually leading to high moderator thickness. With 65% ortho hydrogen as observed for LH based CNS facility in NIST [4] maximum cold flux was achieved with cold moderator thickness of 2 cm as shown in Fig 4.

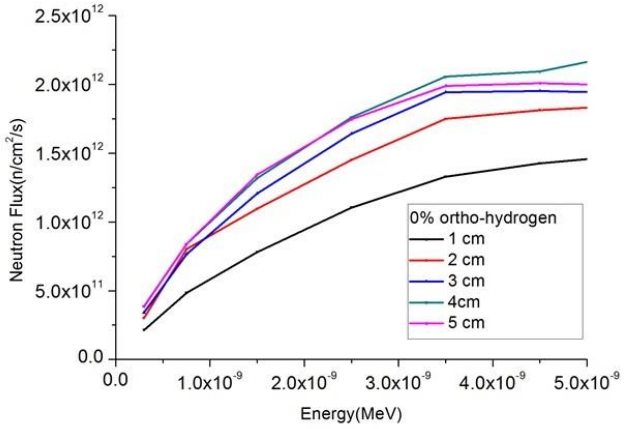


Fig 3: Cold neutron Spectrum for different moderator thickness with 0% ortho hydrogen

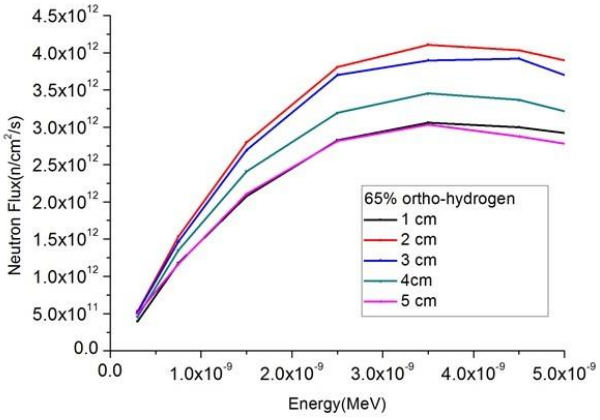


Fig 4 : Cold neutron spectrum for different moderator thickness with 65% ortho hydrogen

Considering the challenges of making ellipsoidal annulus moderator pot of aluminium, a study was carried out with simple cylindrical pot shape also. Fig. 5 shows neutron spectrum for both the shapes with moderator thickness of 2 cm and ortho-hydrogen concentration 65%. Neutron flux at 5 meV is doubled in case of ellipsoidal moderator pot because it offers more scattering probability, facilitates multiple scattering and intercepts neutrons from all directions. Thus, ellipsoidal pot shape was chosen.

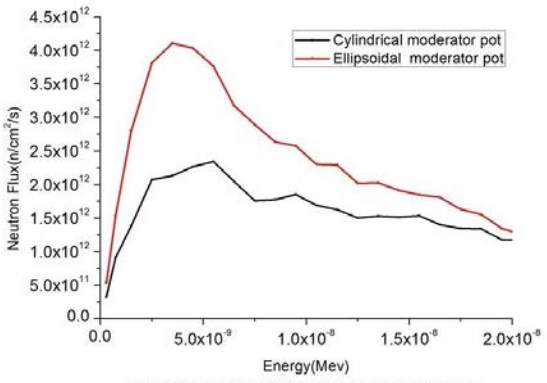


Fig 5: Comparison of different moderator pot shapes

2.2 Performance of cold neutron source

The performance of the cold neutron source has been evaluated by calculating gain factor and cold neutron spectrum. The gain factor is defined as the ratio of neutron flux with cold moderator and without cold moderator. In Fig. 6 it is shown that with the introduction of cold moderator neutron population has increased in low energy regime. Neutron population of wavelength more than 4 A^0 has increased more than 5 times and specifically population of neutron of wavelength 10 A^0 has increased 20 times as shown in Fig. 7. This gain factor is comparable and consistent with the existing cold source facilities worldwide.

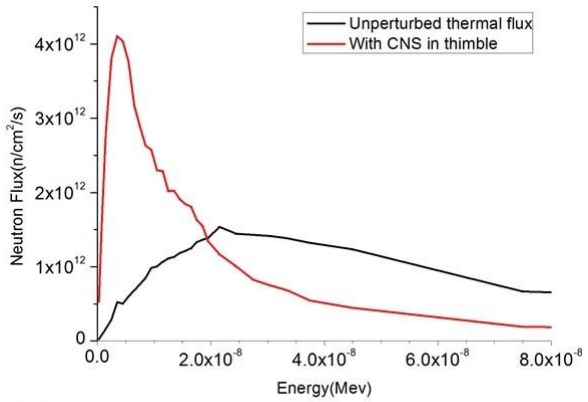


Fig 6 : Neutron Spectrum Shifting towards lower energy regime

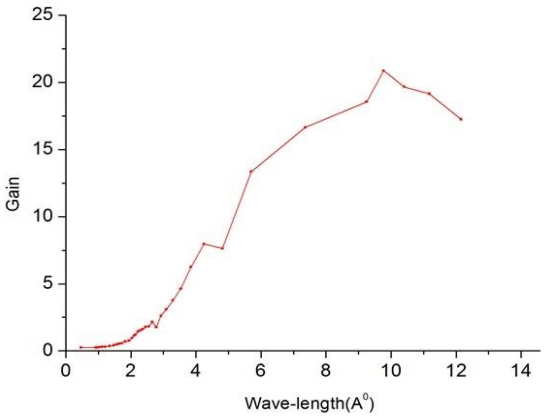


Fig 7 : Gain in Neutron Flux

3. Conclusion

Extensive physics evaluations have been performed in support of the design of Cold neutron source to be installed in proposed HFRR in Vizag. In the primary wavelength range of interest (> 4 A^0), the gain is found to be consistent with those seen for other cold source facilities worldwide. With 65% ortho-hydrogen in LH, optimum moderator thickness of 2 cm was finalized with ellipsoidal moderator pot. Position of CNS thimble in HFRR reflector was decided for maximum unperturbed thermal neutron flux and maximum heat load that can be extracted by cryogenic system. Unperturbed thermal neutron flux has been estimated to be about 1.1×10^{14} n/cm^2/s and cold flux i.e., neutron with energy less than 5 meV & wavelength more than 4A^0 after Liquid hydrogen moderator is about 3×10^{13} n/cm^2/s. Calculation shows that total cold flux at the beginning of the guide tube will be about 10^9 n/cm^2/s which will provide a good scope for the researchers.

4. References

[1] Primary coolant system PSAR part-A of HFRR, 2018

[2] James A Bucholz, “Physics analysis in the design of the HFIR cold neutron source”, XII International School on Nuclear Physics, Neutron Physics and Nuclear Energy, 1999, Varna, Bulgaria.

[3] MCNP: a General Monte Carlo Code for Neutron and Photon Transport, Dept. of Energy, Los Alamos Scientific Laboratory, 1979.

[4] P. Kopetka, R E Williams, J M Rowe, “NIST Liquid Hydrogen Cold Source”, NISTIR 7352.

Oxidation resistant Iron based alloy asClad Material in LWRs

Krishna Kumar Yadav, Usha Pal and R. Karthikeyan
Bhabha Atomic Research Centre, Mumbai, India
e-mail:- kkrishna@barc.gov.in

Abstract

The tragic Fukushima Daiichi Nuclear Plant accident has brought challenges to the nuclear industry and renewed attention to the pernicious interaction between zirconium alloys and hot steam during severe accidents. This brings a great effort to improve the safety in nuclear reactors by developing fuel or fuel clads with improved features in comparison to standard zirconium basedcladding commercial LWRs. Many studies have been initiated worldwide to find an advanced oxidation-resistantalternative cladding material to enhance fuel performance and safety, specifically under accident conditions. One of the candidate materials for fuel cladding in LWRs is oxidation-resistant iron alloys. Motivation behind this effort is due to specific limitation with zirconium alloys under design basis and beyond design basis nuclear reactor accident scenarios. Several new generations of increasingly higher performance steels are now commercially available that may offer significant performance improvements over the relatively simple austenitic steels that were utilized as cladding in some early commercial fission reactors. The stainless steel technology and the material science have been studied extensively and at present, understanding of the material is also superior. Use of stainless steel as cladding material has a potential advantage of reduced hydrogen generation in the event of severe accidents.

1. Introduction

The excellent behavior of zirconium alloy as well as significant advantage of neutron economy under normal operating state has resulted in the use of zirconium alloy as the cladding material. However, extensive metal-water reaction in the event of severe accidents and subsequent hydrogen generation can be considered to be a big disadvantage for zirconium alloy.

Changing zirconium alloy clad with iron alloy cladding would result in increased fissile inventory and subsequently increased enrichment in the core due to considerations of neutronics economy. However, the fuel cost has relatively less weightage towards the unit energy cost compared to operation and maintenance cost for the reactor [1]. The disadvantage in the fuel cost can be compensated, to some extent, by increasing the discharge burnup of the fuel resulting in better fuel utilization and possible increase in cycle length. This paper presents the results of a study that has been made to understand the reactor physics implications of using stainless steel as the cladding material.

In accidental scenarios, oxidation of alloy in steam environment is calculated using parabolic law. The rate constant in case of SS is very low compared to that with zirconium based alloy. Thus the rate of release of hydrogen into containment is expected to have less severity in place of Zr-alloy used clad [2,3]

2. Zirconium alloy cladding and its limitations under accident conditions

Over other cladding options, Zirconium alloy based claddings are used in nuclear reactors, since some decades due to its lower absorption cross section for thermal neutrons and successful manufacturing technology. In normal operation very well behaved zircoloy based clad shows limitations under design basis and beyond design basis accident conditions.

In case of Loss of coolant accident (LOCA), the current US regulatory limits peak clad temperature (PCT) to 1204 ℃ and equivalent cladding reacted(ECR) to 17% of initial cladding thickness. At temperature above 1200 ℃, the increased oxygen solubility in β-Zr phase causes reduction in ductility [4]. At higher burnups, zirconium alloy cladding experiences further

embrittlement due to hydrogen absorption as a result of waterside corrosion of the rod and hydride phase precipitation. Hydrogen present in the cladding lowers the creep resistance.

In case of reactivity induced accidents (RIAs), regulatory criteria set a maximum limit on energy deposition in the fuel during the transient. The fuel failure mechanism under RIA is dependent on burnups. At low burnups(<40 MWD/kgU), post-departure from nucleate boiling (DNB) is limiting, whereas at high burnups, pellet-clad mechanical interaction(PCMI) is dominant failure mechanism[5].

Beyond design basis accidents (BDBA) are accidents scenario not considered during design characteristics for nuclear plant as its occurrence probability is less than 10^{-4}per reactor year.Under BDBA scenario where clad temperature exceeds PCT limit of 1204 ℃, the zirconium alloy cladding system proves readily susceptible to severe degradation. The thermal hydraulic heat transfer coefficient from clad outer diameter to flowing water coolant decreases by four orders of magnitude under accident condition when fuel is exposed to slowly flowing or stagnant steam. Once temperature of fuel increases to very high value, zirconium undergoes rapid oxidation in high temperature steam environment. This results in rapid hydrogen production.

Zirconium alloys are protected against direct contact with water and water steam with surface layer of zirconium oxide (ZrO_2). At high temperature, the surface protective zirconium oxide layer is destroyed and removed resulting in formation of activated pure Zr which efficiently interact with steam. At temperature above 860 ℃, the zirconium-steam reaction proceeds with evolution of hydrogen and a large amount of heat Q =6.53MJ/kg is generated.

$Zr + 2H_2O(gas) = ZrO_2 + 2H_2 + Q$

3. Fuel Assembly Design considered in the analysis

The hexagonal lattice that has been considered in the analysis is shown in Fig.1. The fuel assembly has 311 locations occupied by fuel pins, 18 locations are available for control, one for instrumentation tube and one location acts as central spacer capture rod. An enrichment of 4.5% was considered in all the fuel pins. The outer diameter of fuel pellet is 7.87 mm, clad outer diameter is 9.4 mm and a pin pitch of 13.16 mm is considered. The fuel assembly pitch is 243 mm. This fuel assembly is part of a core design which is being evolved [6]. The core height is 3600 mm and core diameter is 3055 mm. The number of fuel assemblies is 151.

It is a well-known fact that burnable poisons either in form of stand-alone Burnable Poison Rods (BPRs) or Integrated Fuel Burnable Absorber (IFBA) are used to suppress initial excess reactivity. In these studies, IFBA has been considered, with Gd as part of fuel pin. After several iterative analyses, the Gd content has been considered to be 5 wt% and the choice of 24 Gd pin locations is as shown in Fig. 1

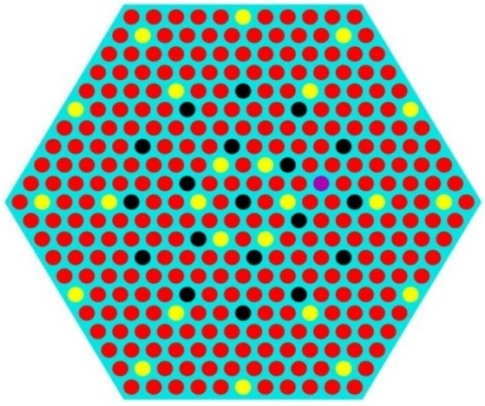


Fig.1 Fuel Assembly with 24 IFBA pins

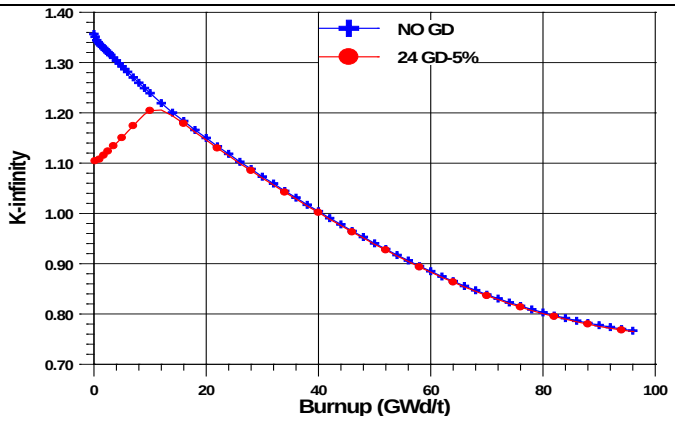


Fig.2 Lattice Characteristics of the Reference FA

4. Replacing clad material from Zr(1% Nb) to SS

It can be seen from Fig.2 that for an avg. enrichment of 4.5%, the k-infinity is ~1.36 in the absence of IFBA. For the purpose of direct comparison, calculations were carried out by changing the clad material from Zr (1% Nb) to SS maintaining the same clad thickness (0.76 mm). The fuel assembly characteristics were studied using code EXCEL [7], which employs a hybrid method of 1-D transport and 2-D diffusion. Nuclear data in 172 group WIMS format generated from point dataset of ENDF/B-VII.0 [8] was used in the analysis. Variation of K-infinity with burnup is shown in Fig.3.There is a near constant load of ~96 mk when stainless clad is used in place of Zr (1% Nb). It was found that with same clad thickness, U235 enrichment of 6.5% results in k_∞ at zero burnup, nearly similar to that of the reference case. However, beyond ~38,000 MWd/T, the reactivity is higher for the case with SS clad and is possible to get higher discharge burnup.

With reduced thickness of clad and varying enrichment calculations were performed. It can be seen from Fig.4 that with enrichment of 6.0 % and SS clad thickness of 0.6 mm assembly characteristics are similar to that of the reference. Using this modified FA, safety parameters were evaluated. It was found that the worth of 1200 ppm boron is ~73 mk/51 mk for 'reference'/'modified' FA respectively at zero burnup. No significant difference in Doppler load was found due to the modification in FA. As spectrum gets hardened in the 'modified' FA which resulted in lower boron worth for the modified FA.

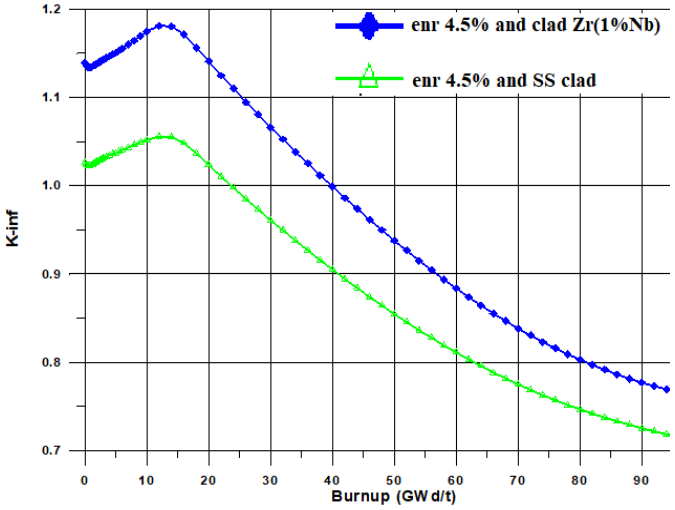


Fig.3Variation of K-inf with burnup with Zr 1%Nb and SS cladded FA

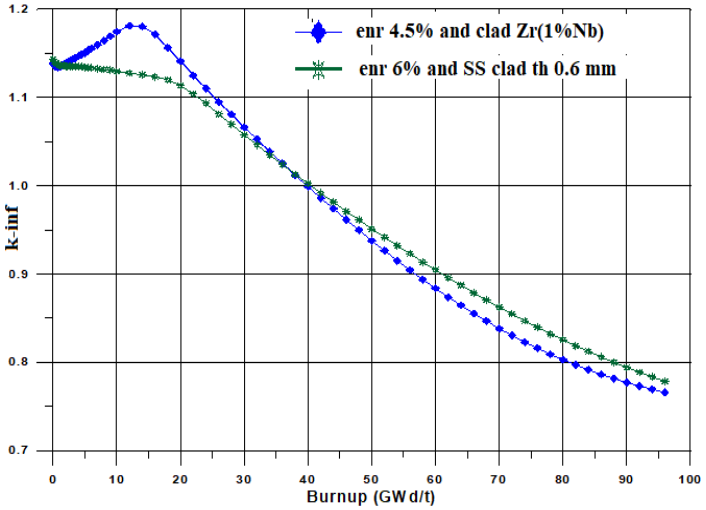


Fig.4Variation of K-inf with burnup for reference and modified FA

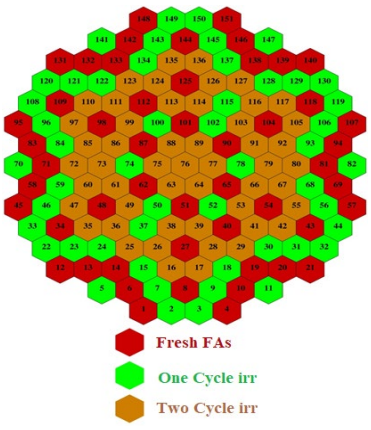


Fig.5 Core map with equilibrium shuffling scheme

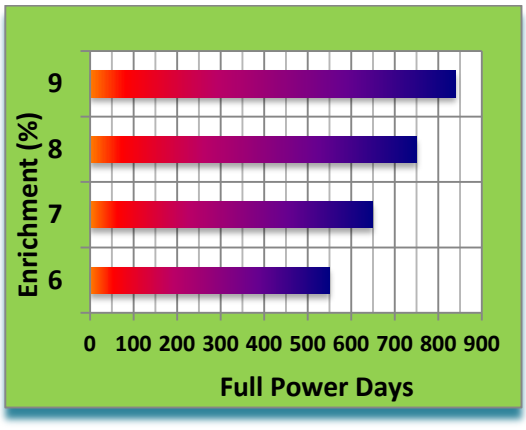


Fig.6 Comparison of Fuel cycle length for different enrichments

5. Core characteristics and safety analysis

For the current analysis, a typical LWR core design has been considered. The core map is shown in Fig.5. The core has 151 FAs arranged in a hexagonal lattice with a pitch of 243 mm. An

enrichment of 6.0% was considered in all the fuel pins. Since, stainless steel has better corrosion resistance, creepresistance and Young's modulus compared to Zr based cladding, it is possible to consider thinner cladding.A cladding thickness of 0.3mm is considered in this analysis.As shown in Fig.6, use of higher enrichments will result in longer fuel cycle length. However, this would result in higher soluble boron concentration at beginning of operation cycle.

Reactivity coefficients were evaluated at beginning of life of equilibrium core in the operating state. It can be found from Table-1 that for equilibrium core coolant temperature reactivity coefficient, fuel temperature reactivity coefficients, boron coefficient and power coefficients are negative with burnup. The critical boron concentration varies from 1825 ppm to 0 ppm after ~ 570 FPDs at 2700 MWt.

Table-1 Reactivity coefficients with burnup

FPD	*Coolant Density* (pcm/g/cc)	*Coolant Temperature* (pcm/°C)	*Fuel Temperature* (pcm/°C)	Boron coefficient pcm/(g/kg)	Power coefficient (pcm/MW)
0	12.41	-29.21	-1.745	-0.691	-0.451
30	13.23	-31.03	-1.760	-0.695	-0.463
150	16.75	-38.97	-1.781	-0.714	-0.513
300	21.43	-50.09	-1.914	-0.749	-0.597
450	26.16	-61.42	-2.045	-0.789	-0.680
540	29.00	-68.11	-2.108	-0.813	-0.726
570	29.93	-70.11	-2.127	-0.821	-0.738

6. Conclusions

Studies at lattice level and core level have been carried out on VVER like hexagonal LWR fuel assembly where the clad material has been changed from Zr-1% Nb to stainless steel. Salient observations are that there is reduced soluble boron worth, reduced xenon load and similar fuel temperature load. Requirement of increasedfuel inventory can be compensated, to some extent, by increasing the discharge burnup.

A core design was evolved considering athree-batch refueling scheme to minimize the radial power peaking factors with 50FAs per batch and considering a U^{235} enrichment of 6%. Average discharge burnup is ~53 GWd/tone. All the reactivity feedback coefficients are found to be negative.

References:

1. A Review of the Costs of Nuclear Power Generation', Michael T. Hogue, Bureau of Economic and Business Research, University of Utah, Salt Lake City, March, 2012
2. Hydrogen Generating Reactions in LWR Severe Accidents, L. Baker, Jr.
3. Oxidation of Alloys of in steam environment: A Review: Fry A, Osgerby S, Wright M, NPL Report MATC (A) 90, September 2002.
4. 10 Code of Federal Regulation 50.46.
5. J. Alvis,W. Liu, 'Fuel Reliability Program: Proposed Reactivity Insertion Accident (RIA) Acceptance Criteria, Revision1, 2015.
6. 'Reactor Physics Design Studies for Equilibrium Core for Indian Pressurized Water Reactor', Usha Pal, R. Karthikeyan, Argala Srivastava, Krishna Kumar Yadav and Anmol Singh, RPDD/LWRPS/IPWR/001/2013, April 9, 2013
7. 'EXCEL–A Combination of 1-D Transport and 2-D Diffusion Methods for Burnup Analysis of Hexagonal Lattice Assemblies', V. Jagannathan and R.P. Jain, 2009.
8. WIMS Library Update Project WLUP, 2001. <http://www.nds.iaea.org/wimsd/>.

PERFORMANCE ANALYSIS OF VARIOUS TRITIUM BREEDING SOLIDS IN FUSION REACTOR BLANKET

Aditi Ray[1,2]
[1] Theoretical Physics Section, Bhabha Atomic Research Centre, Mumbai, India
[2] Homi Bhabha National Institute, Anushaktinagar, Mumbai, India
e-mail: - aray@barc.gov.in

Abstract

One of the greatest challenges in successful deployment of fusion power plant is the design of tritium breeding blanket (TBB). Current paper investigates the performance of various lithium based solids as potential candidates for advanced helium cooled pebble bed (HCPB) TBB. Tritium breeding ratio (TBR) of two non-ceramic compounds, Li_3N and Li_2C_2, and six ceramic compounds, namely, Li_2O, Li_2TiO_3, $LiAlO_2$, Li_2ZrO_3, Li_4SiO_4, $Li_4Si_{0.9}Ti_{0.1}O_4$ are determined for a simplified (geometry) version of projected fusion reactor configuration. TBR for single tritium breeder module (TBM) is found to be increasing steadily with Li^6 enrichment, with the rate of increase being highest for Li_2O followed by Li_3N and Li_2C_2. Study reveals that breeding performances of all ternary compounds are comparable and much lower. Influence of Li^6 enrichment on neutron flux spectrum at external surfaces of both breeder and Be neutron multiplier are also analyzed. Role of multiple TBM is explained from the broadening of initial fast neutron spectrum by combined effect of thermalization and tritium production.

1. Introduction

Attractive features of fusion as a future source of energy are: abundance of fuel, high specific energy release per reaction and inherent safety of the process (in contrast to nuclear fission techniques) due to its thermonuclear nature. To achieve controlled nuclear fusion on earth various schemes have been put forward. Among them, as of today, the magnetic confinement fusion (MCF) in tokamak arrangement has been the most successful one. In 2021 Joint European Torus (JET) produced 59 MJ of energy with pulse duration of 5 seconds reaching Q (ratio of fusion power to plasma heating power) value of ~0.9, beating previous (1997, 2014) records. International Thermonuclear Experimental Reactor (ITER) [1] design envisages extended burn of Deuterium-Tritium (DT) plasma generating fusion power of 500 MW with a Q value of ten.

Deployment of fusion power plant [2] can be accelerated by innovative design concepts and development of appropriate material combinations for a number of components like, plasma first wall and divertor armor material, TBB [3] including coolants, etc. Extensive research on thermo-physical, structural and neutronic properties of plasma facing materials (tritium breeding module and divertor) are being carried out in different laboratories around the world. Typically tungsten is chosen for magnetic fusion reactor divertor and first wall plasma facing components. Other than Be, a number of different neutron multiplying materials have also been identified.

Design of TBB is one of the greatest challenges in MCF as both blanket and divertor have to fulfil several functions simultaneously at extreme conditions of thermal, mechanical, structural and neutron loads; at the same time would offer sufficiently long operation time. Li compounds like, liquid $Li_{17}Pb_{83}$, $LiBi_5Pb_4$, $LiF\text{-}BeF_2$, solid intermetallic alloy Li_7Pb_2 have already been identified as breeders. Advanced design concept like, HCPB blanket utilizes solid breeders as they are supposed to have better efficiency. Efficient tritium extraction, high temperature resistance and no magneto-hydrodynamic effect renders Li-based ceramics as promising tritium breeding materials [4]. Solid

compounds like Li_3N, Li_2O, $LiAlO_2$, Li_4SiO_4, Li_2ZrO_3, Li_2TiO_3 are relatively new entries in the long list. Each of these compounds has their merits and limitations due to varied reasons. For example, high reactivity with water and compatibility with steels reduced the attractiveness of high atomic density Li compound Li_2O. Resilience to mechanical loads puts restriction to the use of Li_4SiO_4. Efforts are made towards modifying the latter with addition of Li_2TiO_3 to serve the dual purpose - improve mechanical stability and enhance Li density. $Li_4Si_{1-x}Ti_xO_4$ ($x<0.2$) is an example of advanced ceramic breeder. Among the non-ceramic compounds, Li_3N has the highest Li atomic density and results in higher TBR. But relatively low melting temperature of Li_3N and its high reactivity with water hinders its practical use.

The present paper aims at making a comparative study on efficiency of various solid Li compounds as breeders and their effectiveness, along with neutron multipliers, in process of thermalization and breeding. We also introduce another non-ceramic solid, i.e., Li_2C_2 as efficient breeder.

2. Tritium breeding - theory and simulation

Operation of MCF is primarily based on the following fusion reaction:

$$D + T \rightarrow He^4\ (3.5\ MeV) + n\ (14.1\ MeV) \quad (1)$$

The isotopes of hydrogen atom are employed at a temperature of about 14-20 keV to achieve the highest reaction rate. The released energy is distributed between a neutron and an alpha particle. While the charged alpha particles are confined by the magnetic field, energetic neutrons escape from the plasma. Novelty of fusion power plant is that, it produces its own supplies of fuel (tritium) in a self-sustained manner. The neutrons produced by the fusion reactions are employed for producing tritium from the two naturally occurring Li isotopes according to the following reactions:

$$Li^6 + n \rightarrow He^4 + T + 4.8\ MeV, \quad (E_{th} = 2.47\ MeV) \quad (2)$$

$$Li^7 + n \rightarrow He^4 + T + n' - 2.5\ MeV \quad (3)$$

The reaction cross section of Li^6 increases with decreasing neutron energy and it reaches about 700 barns for thermal neutrons, while cross-sections of Li^7 are much lower (in mb). Therefore, Li^6 enrichment is a primary requirement. Tritium production is achieved by surrounding the plasma first wall with a so-called *blanket* containing tritium breeding material that absorbs the neutron energy. Blanket must contain coolant which extracts the heat and eventually converts into power. Produced tritium is finally injected into the plasma as new fuel.

Simulation system in the current work consists of DT plasma at the centre (radius 300 cm) surrounded by 1 cm thick W first wall followed by TBM as depicted in Fig. 1(a) by concentric spherical shell geometry. HCPB breeding blanket consists of a series of TBM in a multi-module arrangement. Each module has a sandwich-like configuration of solid breeder (1.6 cm), cooling channels (0.4 cm F82H steel), water (instead of liquid He) and Be neutron multiplier (6.6 cm). The module repeats (10-12 times) to fill a total thickness of about 60-70 cm so as to reach tritium breeding ratio more than 1 for the chosen breeder in projected design. However, the results presented here correspond to couple of modules. Current paper makes a comparative analysis of eight solid breeders as listed in Table-1. This has been realized by 3D Monte Carlo neutron transport calculation with ENDF/B cross section library. Calculation yields neutron flux distribution at different surfaces. Tritium production rate has been calculated by developing a program that calculates the total number of reactions, R and tritium production per reaction (TPR) as per the equations given below:

$$R = \int \sigma_{Li6(n,T)}(E)\,\phi(E)dE + \int \sigma_{Li7(n,n'T)}(E)\,\phi(E)dE\,, \quad (4)$$

$$TPR = \rho V N_A R\,(M_{Li6} + M_{Li7})/A \quad (5)$$

In the above $\sigma_{Li6(n,T)}(E)$ and $\sigma_{Li7(n,n',T)}(E)$ are the energy dependent cross-sections of Eqs. 2 and 3; $\phi(E)$ is the neutron flux, ρ is the density of breeder compound (Table-1); V is the volume of breeder shell; N_A is Avogadro number; M_{Li6} and M_{Li7} are masses of Li^6 and Li^7 in the breeder molecule of molar mass A. TBR is defined as the average number of tritium atoms produced in TBB for every fusion neutron generated in the plasma. Single module TBR (TBR-M1) is calculated by using neutron flux at external surface of W, $\phi(E)$ in Eq. 4. TBR due to two TBMs (TBR-M2) is obtained by calculating TPR with $\phi(E)$ corresponding to Be outer surface.

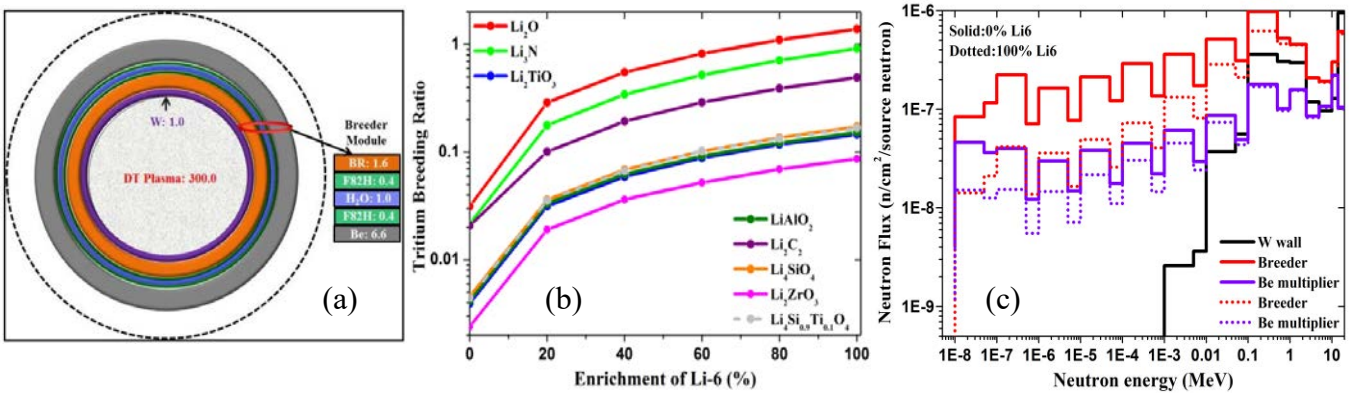


Figure 1*: (a) Simulation system showing DT plasma, W wall and single TBM (breeder, water enclosed in F82H steel channel and Be). (b) Variation of single module TBR with Li^6 enrichment for different breeders. (c) Neutron flux spectra at external surface of W wall, breeder and neutron multiplier. Solid and dashed lines refer to results for Li_2O with 100%Li^7 and 100%Li^6.*

Efficiency of tritium breeding is further increased by replenishing the neutrons absorbed in tritium by neutron multiplier and subsequent utilization of thermal neutrons in Li^6. Be experiences (n, 2n) multiplication reaction for neutrons having energy above the threshold of 1.86 MeV.

$$Be^9 + n \rightarrow Be^8 + 2n, \quad (E_{th}=1.86\ MeV) \quad (6)$$

Moreover, due to its very high moderating ratio (~134 at room temperature), it plays a significant role in thermalizing the neutrons before entering the second module.

2.1 Tritium breeding performance assessment

Single-module TBR of the selected solids is plotted as a function of Li^6 enrichment in Fig. 1(b). Observed one order increase in TBR from 100% Li^7 to 100% Li^6 indicates the necessity of enrichment. TBR-M1 corresponding to natural Li based solids is shown in Table-1. Interestingly, double-module TBR (TBR-M2 in Table-1) of ternary ceramics is enhanced to ten times their values obtained in single TBM (TBR-M1). This establishes the requirement of multiple layers of TBM. Roughly 10/12 modules need to be annexed to ensure minimum requirement of TBR>1, necessary for self-sustaining supply of fuel and hence operation of the reactor.

2.2 Influence of neutron distribution on TBR

Neutron flux spectrum at W surface shows minor modification of initial 14.1 MeV neutrons as shown in Fig. 1(c). However, significant level of thermalization is achieved with 100%Li^6 both at

breeder (Li_2O) and Be surface. Contribution of slow (0.01 eV<E<10 eV) and fast neutron fraction (E>1 MeV) for all eight breeders with 60% enrichment are presented in Table-1. Thermalization in water as well as Be has contributed in higher fraction of slow neutrons at Be outer surface. These neutrons are transported to the second TBM and eventually enhancing tritium production there as illustrated in Table-1 with natural Li based solids.

Table-1*: Parameters of solid breeders studied here. TBR of single and double modules for natural Li based solids. Contribution of slow and fast neutrons in flux spectrum obtained with different breeders containing 60%Li^6.*

Breeder	**Density (gm/cm^3)**	**Li atomic density (%)**	**TBR-M1 (Nat. Li)**	**TBR-M2 (Nat. Li)**	**Neutron flux (/sour. N) (Breeder surf.)**		**Neutron flux (/sour. N) (Multiplier surf.)**	
					Slow N frac.	**Fast N frac.**	**Slow N frac.**	**Fast N frac.**
Li_3N	1.27	75.0	0.0786	0.5082	4.20E-02	5.19E-01	6.79E-02	5.82E-01
Li_2C_2	1.30	50.0	0.0453	0.3205	4.57E-02	4.90E-01	7.58E-02	5.72E-01
Li_2O	2.01	66.6	0.1121	0.6989	4.07E-02	5.27E-01	6.66E-02	5.83E-01
Li_2TiO_3	3.43	33.3	0.0142	0.1015	4.83E-02	4.74E-01	7.95E-02	5.59E-01
$LiAlO_2$	2.62	25.0	0.0150	0.1114	5.02E-02	4.60E-01	8.52E-02	5.54E-01
Li_2ZrO_3	4.03	33.0	0.0086	0.0635	4.87E-02	4.72E-01	8.37E-02	5.51E-01
Li_4SiO_4	2.35	44.4	0.0164	0.1112	4.60E-02	4.90E-01	7.60E-02	5.67E-01
$Li_4Si_{0.9}Ti_{0.1}O_4$	2.37	44.4	0.0160	0.1087	4.56E-02	4.91E-01	7.55E-02	5.67E-01

3. Conclusion

High Li atomic density and hence high TBR is the most important factor for achieving efficient breeding. However, extreme environment of operating fusion power plant puts restrictions for using best breeding compound. In order to decide a trade-off, tritium breeding performance of eight different Li based solids has been studied for varying Li^6 enrichment. Study shows that Li_2C_2 can be a good alternative breeder material being third in TBR values. TBR of all ternary ceramics are found to be comparable and much lower than binary solids. The need for multiple TBMs is explained by comparing single *vs.* double-module TBRs and the slow and fast neutron contribution at breeder and multiplier surfaces.

4. References

[1] Y. Shimomura et al, "ITER: Opportunity of burning plasma studies", *Plasma Phys. Cont. Fusion,* **43,** 2001, A385.
[2] D. Maisonnier et al, "Power plant conceptual studies in Europe", *Nucl. Fusion,* **47,** 2007 1524.
[3] P. Pereslavtsev et al, "Neutronic analyses of design issues affecting the tritium breeding performance in different DEMO blanket concepts", *Fusion Engg. Design*, **109–111**, 2016, 1207-1211.
[4] C. E. Johnson et al, "Ceramic breeder materials: Status and needs", *J. Nucl. Mater.* **258–263**, 1998 140-148.

REACTION RATE SPECTRAL PROFILING OF PFBR BOL CORE CONFIGURATION WITH PIN LEVEL HETEROGENEITY EMPLOYING MESH TALLY

Bilal Hassan Khan[1]
[1] Indira Gandhi Centre for Atomic Research, Kalpakkam, India
[1]*e-mail: bhk780@igcar.gov.in*

Abstract

FMESH tally feature of MCNP was employed to score the neutron fluxes and reaction rates in 1 cm x 1 x 10 cm bins along different vertical zones. Since FMESH tally feature is defined as superimposed geometry outside the actual geometry it adds to the advantage that mesh structure is independent of actual cell configuration in MCNP input deck. A heterogenous pin wise modelling of PFBR BOL core was performed using updated number densities for different materials. A graphical description of spectral profile generated by plotting meshtal file in 2D,3D and 3D isometric views, helps in extracting useful insight from operational and analytical perspective.

1. Introduction

Spectral characterization measurements are one of the important phases that a reactor has to go through before making it operational at a desired power level. ICSA provides access near the core centre for a variety of instruments used in core monitoring and characterization. Neutron spectra for different energy ranges employs proton-recoil, carbon-recoil, proportional counters etc while fission chambers, foil activation analysis etc characterizes different reaction rates at specific locations. There is always a need for theoretical analysis to back up the results because the whole process from instrument calibration to actual characterization is highly involved. Theoretical values and practical measurements complement each other at different stages to streamline the process of reactor characterization. An exercise in the above context was taken up to evaluate the spectral profile for different reaction types at certain specific reactor locations and as a whole core also. The results obtained are per source particle but can be scaled to any operational power level or detector count response by multiplying with appropriate scaling factors. A superimposed mesh geometry defined outside the actual reactor geometry employing FMESH card tally is used to score flux and reaction rates in each bin.

2. Reactor modelling

The BOL core of PFBR (Figure 1) consists of 88 core-1 & 87 core-2 FSAs, 8 diluents, 1 ICSA, 3 Source SAs and 114 RB assemblies [1]. The reactor has been provided with 9 Control and Safety Rods (CSRs) distributed in 3rd and 6th ring of core, for start-up, power control, controlled shutdown and SCRAM of the reactor. There are 3 Diverse Safety Rods (DSR) in the 3rd ring only to SCRAM the reactor. For both the type of rods, B_4C is chosen as the absorber material. BOL core has been modelled with all CSR's docked at near critical position of 39 cm above core base plane with DSR's out. A detailed pin wise modelling of fuel SA's, RB's and CSR's have been carried out as displayed in (figure 2-3) respectively. The heterogenous material density data has been prepared using the reference data specification given in [1-2]. The core is assumed at 453 K and

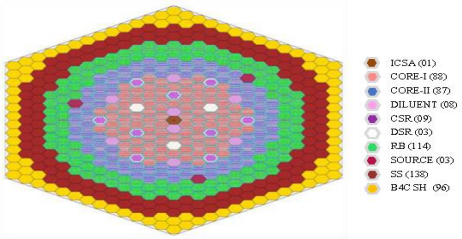


Figure 1. PFBR BOL Core layout

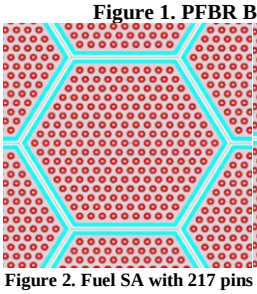


Figure 2. Fuel SA with 217 pins

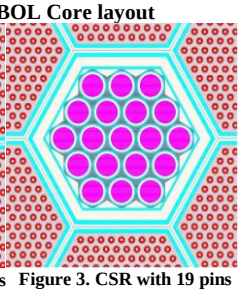


Figure 3. CSR with 19 pins

the corresponding cross section data from ENDF/B-VIII.0 library processed using NJOY21 have been used for carrying out the analysis.

3. Results

The results can be presented and analyzed in different ways but due to document size limitation we are only presenting the highlights of outcome while the inferences that can be made out will be detailed in internal report. Only sample output data is tabulated, as the meshtal text file containing all bin data amounts to 300 Mb electronic size. The superimposed mesh tally with 300x300 meshes of 1cm each along horizontal XY plane and 10 cm along vertical Z axis spanning 86 cm to 286 cm reactor height with z = 181 cm being the core mid plane has been defined in MCNP input deck FMESH tally card to obtain the flux and reaction rate profile.

3.1 299-Energy Group Spectral profile

299-energy group flux and reaction rate spectrum averaged over whole core was estimated and is given in (Figure 4-5). Many important features are prominent from the output data. The role of resonances e.g. Na-23, U-238, Pu-239, Pu-240, Pu-241 shows apparent dips and peaks in flux, capture and fission rates at specific peak energies. Flux shows few peaks between 100 keV to 1 MeV which can be further refined by evaluating localized spectra at some specific core locations.

Table 1. Sample values from normalised 299-energy group spectra.

E (eV)	Nubar	Inelastic	Elastic	Fission	Capture	Flux
4.32E+05	8.49E-03	2.69E-03	6.76E-03	9.60E-03	1.48E-07	8.47E-03
4.67E+05	1.00E-02	3.11E-03	7.99E-03	1.08E-02	6.62E-06	9.82E-03
5.04E+05	1.42E-02	4.32E-03	1.17E-02	1.06E-02	1.68E-05	1.43E-02
5.44E+05	1.51E-02	4.41E-03	1.29E-02	9.57E-03	2.45E-05	1.54E-02
5.88E+05	1.36E-02	4.08E-03	1.22E-02	8.71E-03	3.16E-05	1.40E-02
6.35E+05	1.30E-02	3.73E-03	1.22E-02	7.70E-03	4.33E-05	1.34E-02
6.86E+05	1.15E-02	3.21E-03	1.14E-02	7.36E-03	1.40E-04	1.20E-02
7.41E+05	1.03E-02	2.99E-03	1.07E-02	7.21E-03	4.35E-04	1.07E-02
8.00E+05	9.57E-03	2.66E-03	1.07E-02	6.60E-03	1.01E-03	1.01E-02
8.58E+05	8.90E-03	2.52E-03	1.03E-02	5.29E-03	1.62E-03	9.36E-03
9.20E+05	7.02E-03	1.97E-03	8.43E-03	4.14E-03	1.91E-03	7.32E-03

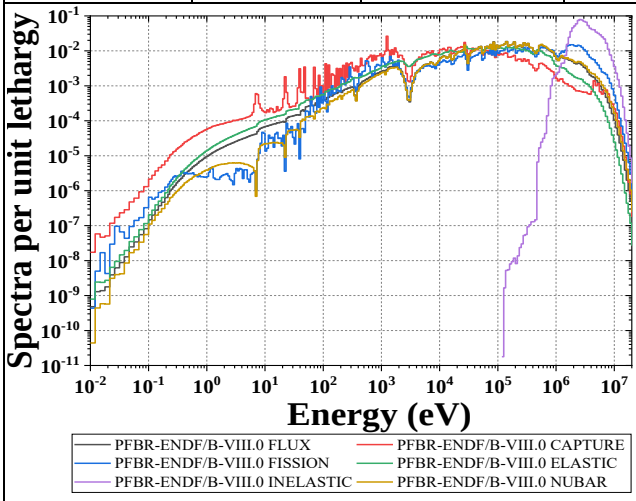


Fig 4. Unity normalised averaged PFBR spectra with Y-log

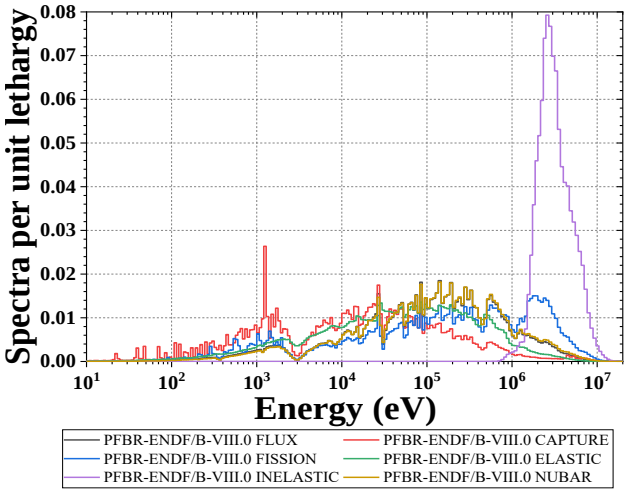


Fig 5. Unity normalised averaged PFBR spectra with Y-linear

3.2 Spectral distribution profile

The flux and reaction rates were scored in each bin (1cmx 1cm x10cm) and repeated for different zones. The tally values are stored in meshtal text file. A special JavaScript MeshTallyViewer.jar has been used to read the meshtal file to plot the flux and reaction rates with different colour scales for varying magnitudes (RAINBOW scale) wherein red implies highest and violet lowest magnitude. (Figure 6) displays the flux and reaction rate profile distribution in fast and epithermal energy ranges in three zones around core mid plane. It is worth to mention that the capture rates become prominent from 166-186 cm vertical zone and that too at CSR locations only since the control rods were docked at 39 cm from core base.

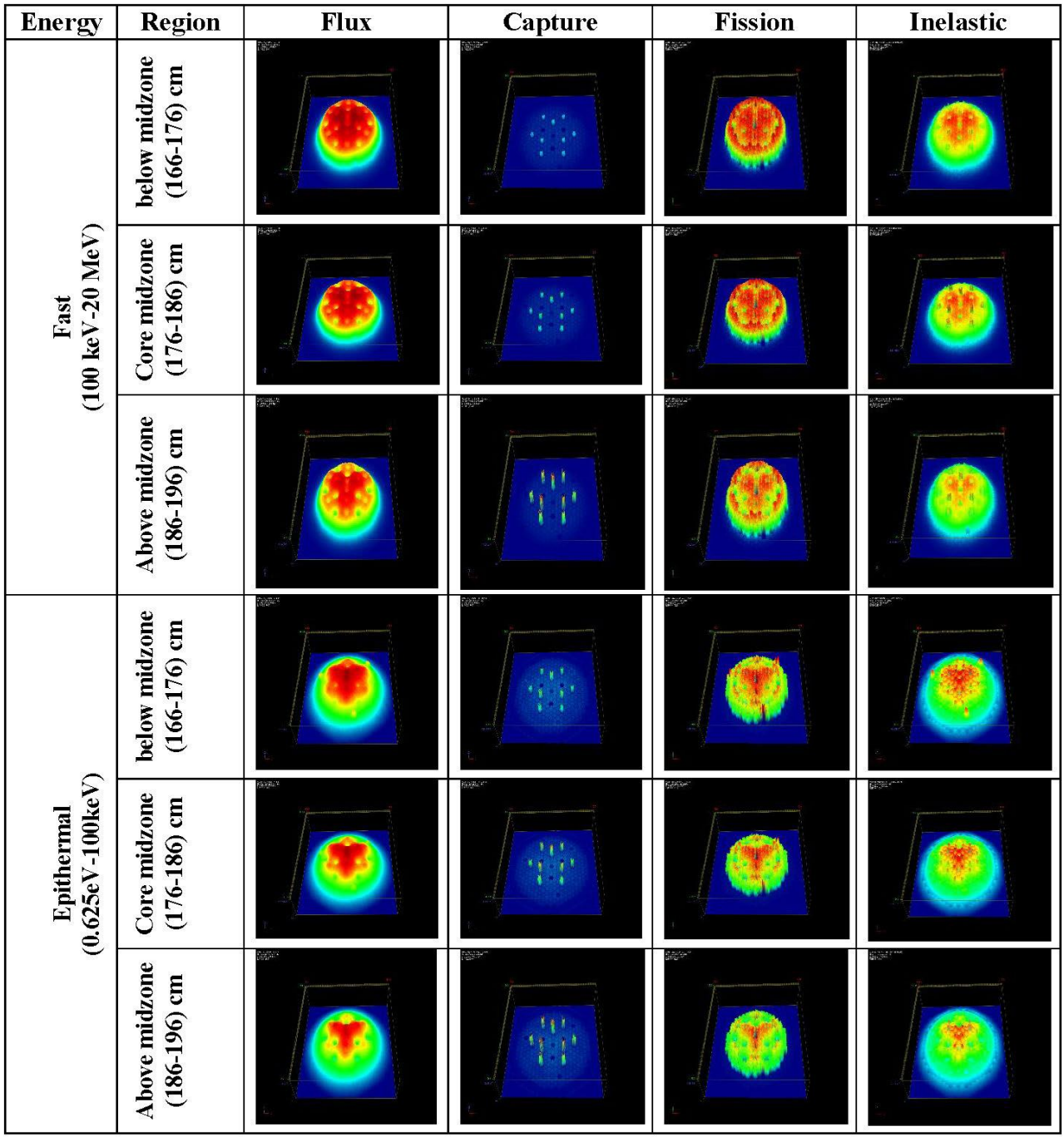


Figure 6. Reaction rate and Flux distribution for fast & epithermal E ranges in zones around core mid plane.

4. Conclusion

The superimposed mesh tally option in MCNP invoked through FMESH CARD has been applied to PFBR BOL core for obtaining the flux and reaction rate spectral profile and distribution. The flux and reaction rate profile are more reliable because of heterogenous 3-D modelling and Monte Carlo transport but comes at the cost of larger computation times. Latest ENDF/B-VIII.0 cross-section data library was adopted for evaluation. In future this approach can be used to get better insight into other significant parameters like power peaking factors, LHR distribution within individual fuel pins since even a mesh as small as 1mm x 1mm can be defined for carrying out analysis.

5. References

[1] PFBR/FSAR/R-1/MAR10 Chapter 5.1, Reactor Physics, (2016).

[2] Design specification for control & safety rod (CSR) subassembly, PFBR/31120/DN/1009/R-A, Aug (1996).

STUDIES ON CORE CHARECTERISTICS OF THE 40MWT FBTR CORE

Neethu Hanna Stephen[1*], Rajesh Chandrakanth[1], Raghu Kumar.G[1], Manimaran.N[1], Shanmugam.G[1] & Suresh Kumar. K.V[1]

[1] Indira Gandhi Centre for Atomic Reasearch Centre, Kalpakkam, Tamilandu, India

[1*]*e-mail: - neethu.stephen@gmail.com;neethu83@igcar.gov.in*

Abstract

Fast Breeder Test Reactor (FBTR) which is a loop type, sodium cooled fast reactor, is one of the high flux - high temperature reactor in India with design power of 40 MWt (13.2 MWe). To attain its design target power of 40 MWt, a core configuration has been proposed with 70 Mark I (MK I) fuel subassemblies. This study presents the neutronic data such as flux, neutron spectrum, danger coefficient of fissile, fertile and structural materials of the proposed core. LHR, power and (n, α) reaction rates of poison SA's are also computed. The peak flux in the core is 3.02×10^{15} n/cm^2/s. The peak LHR value of poison subassemblies is around 1.14kW/cm and the total power generated is 34.47 kW. Reaction rates corresponding to (n, α) interaction is 5.03E+22 /cm^3/year.^{241}Pu has the maximum danger coefficient ~716.5 pcm/kg. The residence time of poison SA from reactivity consideration is 969 FPD and 553 FPD from radiation damage considerations.

1. Introduction

Fast Breeder Test Reactor (FBTR) is a loop type, sodium cooled fast reactor, is the only high flux test facility available in India. Its design target power is 40 MWt (13.2 MWe) and is in operation since 1985 at various power levels up to 32 MWt. All the engineering systems in FBTR are designed for 40 MWt operations. It was planned to raise the power of FBTR to its design target power of 40 MWt by adding MK I (70%PuC+30%UC) fuel subassemblies with the peak power rated subassembly operating at 400 W/cm [1].

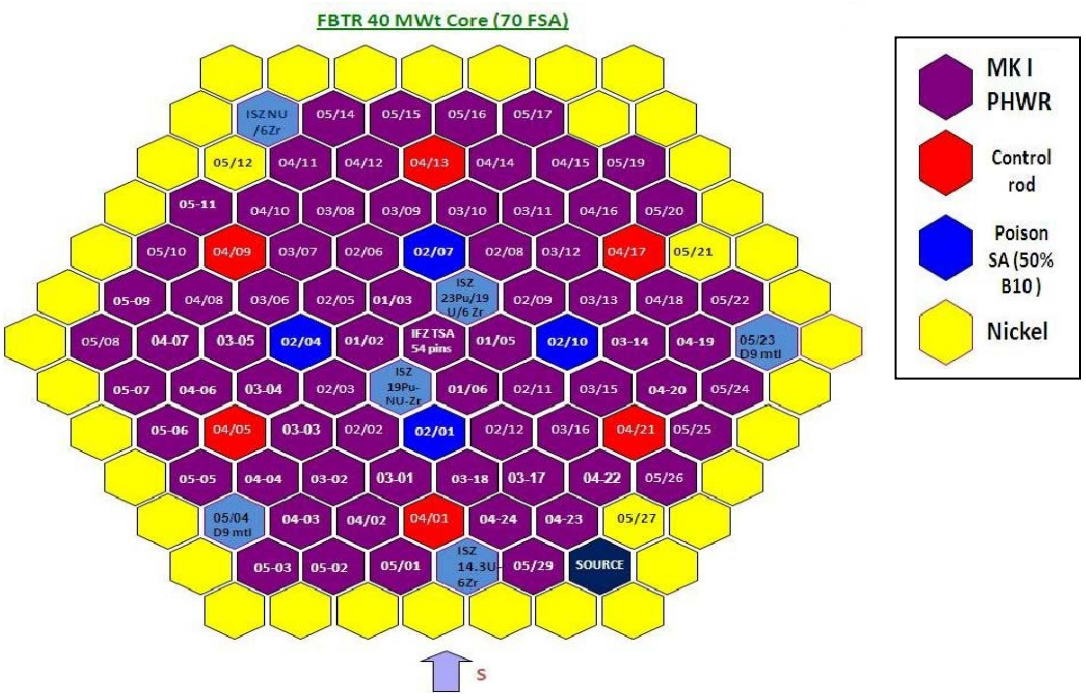
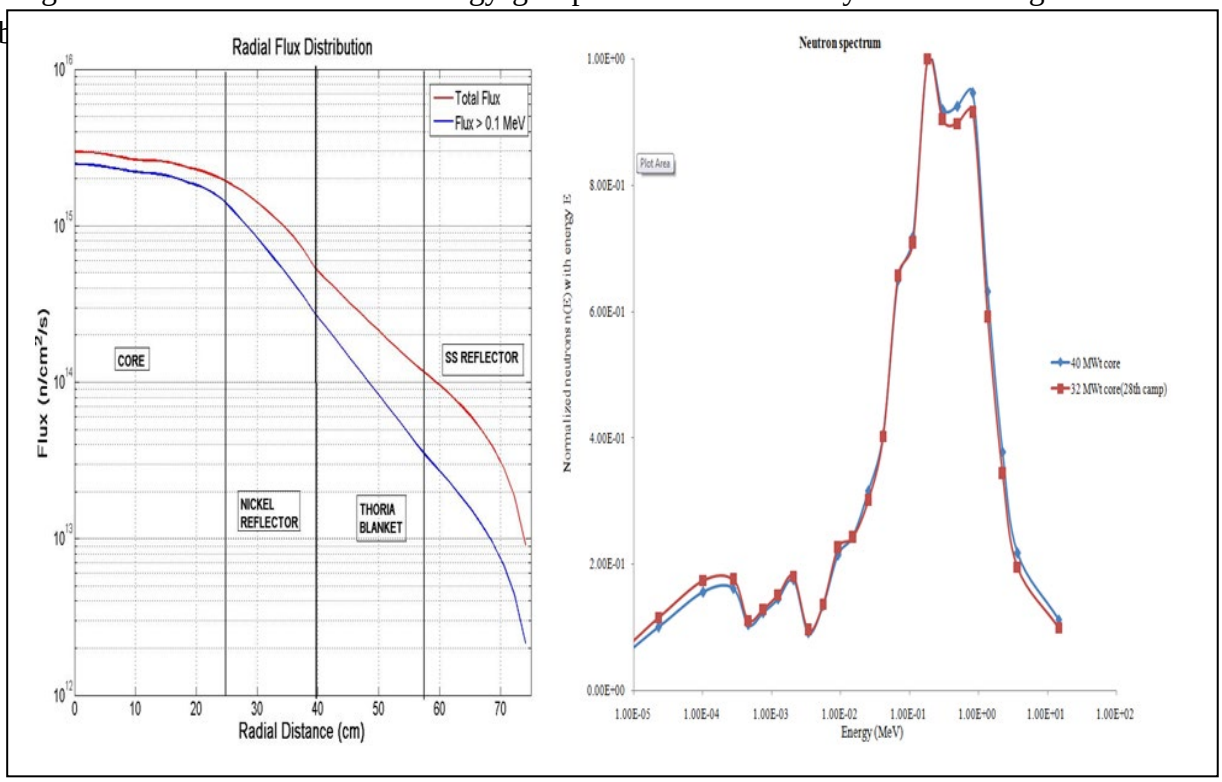


Figure 1. Proposed core configuration of FBTR 40 MWt core

To ensure a minimum shutdown margin of 4200 pcm, which is the technical specification requirement, it is proposed to add four poison (50% ^{10}B) subassemblies in the 2nd ring. Two locations in the first ring (01, 01) & (01, 04) are reserved for experimental subassemblies. The reactor attained its design target power 40MWt on 7th March 2022. The present paper discusses the neutronic parameters of the core with 70 MKI fuel Subassemblies.

1. Neutron flux distributions and one-group cross sections

The flux distribution has been computed using 2D-diffusion code ALCIALMI[2] and neutron spectrum with 3D transport code MCNP and is provided in Figure 2. The diffusion calculations were performed with 25 group cross-section CADRACHE version 2 CEV2M library and transport calculations with ENDF.B.VI.7 The peak flux in the core is 3.02x10^{15} n/cm^2/s. This corresponds to a peak linear power rating of 400 W/cm. The lower energy group fluxes are markedly lower in magnitude due to higher ab



The core averaged spectrum is very hard and close to the fission spectrum. Fast flux (> 0.1 MeV) constitute ~81% of the total flux in the core. The core averaged cross-sections for the fissile and fertile isotopes are generated using MCNP and is given in Table 1.

Table 1: Core averaged cross sections for fissile and fertile isotopes generated using MCNP

Cross Section (barn)	U 235	U 238	Pu 239	Pu 240	Pu 241	Pu 242
n,2n	3.46E-03	4.34E-03	1.85E-03	7.37E-04	6.22E-03	1.94E-03
Fission	1.39E+00	1.11E-01	1.68E+00	7.43E-01	1.86E+00	5.86E-01
Capture	2.56E-01	1.46E-01	1.70E-01	2.19E-01	2.11E-01	1.99E-01

2. Power & Residence time of poison subassembly

The minimum shut down margin (SDM) criteria of 4200 pcm is achieved by adding 4 poison B_4C subassemblies in the 2nd ring i.e. in (02, 01), (02, 04), (02, 07) & (02, 10) locations. Each poison sub assembly contains 50% enriched boron [1]. The total length of B_4C column is 37.5 cm. The top of the B_4C column aligns with the fuel pin top and the remaining 5.5 cm will be below the bottom of the fuel column. The poison subassemblies were modelled using MCNP and F4 &FS tally cards are used to compute flux and LHR. The results are given in Table 2.

Table 2: LHR, total power and (n,α) cross-section of poison SA

Poison SA location	Peak Flux ($n/cm^2/s$)	Peak LHR (W/cm)	Total power (kW)	n, α σ_a(barns)
(02,01)	2.63E+15	1134	34.47	1.15
(02,04)	2.67E+15	1123	34.31	1.13
(02,07)	2.62E+15	1122	34.21	1.14
(02,10)	2.68E+15	1140	34.76	1.14

The peak LHR value of poison subassemblies is around 1.14kW/cm and the total power generated is 34.47 kW. Reaction rates corresponding to (n, α) interaction is ~ 5.03E+22 /cm^3/year. Reactivity change or worth of the poison SA depends on the depletion rate of ^{10}B which is a function of the neutron flux and the enrichment of ^{10}B atoms. The number of ^{10}B atoms remaining in the poison SA after T full power days of operation is

$$N(t) = N_0 \exp(-\sigma_a * \varphi * t) \qquad (1)$$

Due to self shielding, the flux and absorption cross section in the three radial regions of B_4C pellets, in Figure 3, will be different and the depletion rate or the remaining ^{10}B atoms and computed using EQ (1). The variation of ^{10}B atoms as a function of fluence is given in Figure 3. The limiting factor on the residence time from reactivity consideration is computed by setting a change of about 10% on the total worth of the 4 poison SA. Accordingly, it is found that, with 969 FPD, overall worth of the poison SA is reduced by 10%.

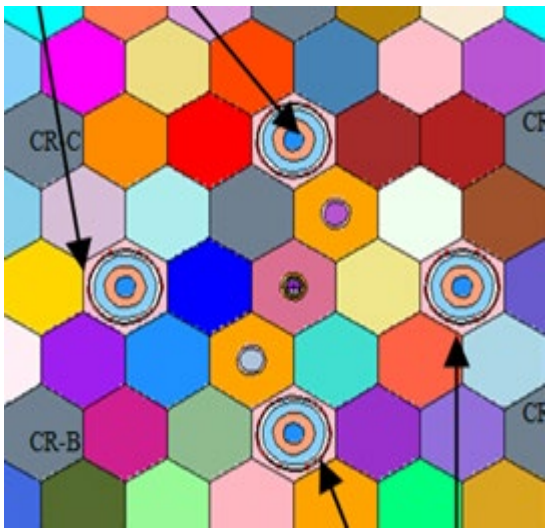


Figure 3: Radial regions of B4C to account self shielding effects

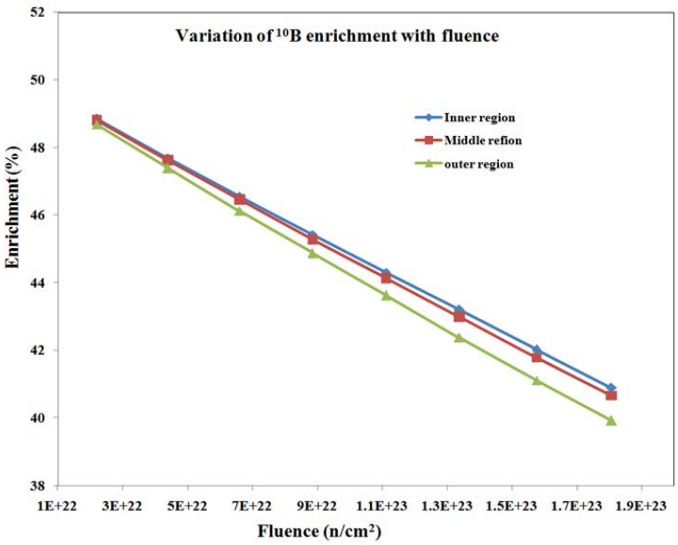


Figure 4: Variation of ^{10}B enrichment with fluence

Damage to materials due to neutron irradiation is quantified in terms of the displacement per atom (dpa). DPA is defined as the number of times an atom is displaced from its lattice position and total dpa (N_D) is computed as follows:

$$N_D = \sum_c T_c \sum_g \Phi_g \sigma_{dg}$$

Where Φ, σ, N and T refer to neutron flux (n/cm^2/s), microscopic dpa cross section (cm^2), number density (no of atoms/cm^3) of isotope and duration (sec) of campaign respectively. Since poison SA is in the inserted condition in the core, similar to a fuel SA, the wrapper and clad tube can withstand up to 83 & 81 dpa without losing its ductility and tensile strength. During 29th irradiation campaign, dpa per day in the (02, 10) location is around 0.15. With this rate, the poison SA can reside for 553 full power days or 1.52 full power years.

3. Core averaged danger coefficient

Danger Coefficient for a material is defined as the change in reactivity on introducing unit mass of the material in the reactor core. The calculations are carried out using the 2D code NEWPERT [3], which computes the effect of perturbation in terms of reactivity. The material is taken to be distributed uniformly in the core. The results of the calculation are given in Table 3. The code employs first order perturbation theory, and hence the reactivity change is linear in the amount of perturbing material

Table 3.Core averaged Danger Coefficients for fuel and structural Materials

Isotope	Danger Coefficient (pcm/Kg)	Ratio w.r.t. ^{239}Pu	Isotope	Danger Coefficient (pcm/Kg)	Ratio w.r.t. ^{239}Pu
^{232}Th	-28.9	-0.057	^{240}Pu	175.1	0.347
^{233}U	578.5	1.148	^{241}Pu	716.5	1.422
^{235}U	306.7	0.609	^{242}Pu	134.1	0.266
^{237}Np	31.4	0.062	Na	67.2	0.133
^{238}U	10.8	0.022	C	97.9	0.194
^{239}Pu	504	1	^{10}B	-5468.8	-10.851
Nat.B	-917.8	-1.821	Fe	20.6	0.041

The plutonium isotope ^{241}Pu has the maximum danger coefficient and the value is 716.5 pcm/kg. Among the isotopes ^{238}U and ^{232}Th, the former provides positive reactivity while the later provides negative reactivity.

4. Conclusion

The neutronic parameters of the proposed core of FBTR with 70 fuel subassemblies to reach its design target power of 40 MWt is generated using 2D codes ALCIALMI, NEWPERT and 3D transport code MCNP. The peak flux in the core is 3.02x10^{15} n/cm^2/s and the core averaged spectrum is very hard with fast flux (> 0.1 MeV) constitute ~81% of the total flux in the core. The peak LHR value of poison subassemblies is around 1.14kW/cm and the total power generated is 34.47 kW. Reaction rates

corresponding to (n, α) interaction is 5.03E+22 /cm^3/year.The plutonium isotope ^{241}Pu has the maximum danger coefficient and the value is 716.5 pcm/kg. The residence time of poison SA from reactivity consideration is 969 FPD and 553 FPD from radiation damage considerations.

References

[1] Sivakumar, S., & Raghukumar, G., Conceptual configuration of 40 MWt core for Fast Breeder Test Reactor, 2018. RFG/FBTR/S-RS-02/31400/TN-1045

[2] Narayanan, R., & John, T., M., 2000. ALCIALMI- The computer code for solving the neutron diffusion equation in two dimensional geometry, RG/RPD/CPS/14.

[3] John, T., M., 1984. Perturbation code for two dimensional diffusion equation , REDG/01150/RP-253.

Development of a Power and Flow Transient Model for Sodium Cooled Fast Reactor Core

Amandeep Singh[1], Obaidurrahman K.[2] and H. P. Gupta[3]

[1, 2] Atomic Energy Regulatory Board, Mumbai, India
[3]Ex BARC, Mumbai
[1]*e-mail: - aman@aerb.gov.in*

Abstract

Core disruptive accident may happen in fast reactor due to reactivity and flow transient. A thorough understanding of the progression of CDA and estimation of core energy released during the accident is necessary to design respective safety systems. An in-house model has been developed for pre-disassembly phase analysis in sodium cooled fast breeder reactors. The code includes the modelling of core neutronic, thermal hydrodynamic and elementary structural analysis. The capability of the model has been demonstrated by comparing the results with SAS-1A code for a test problems.

1. Introduction

Fast reactors could experience Core Disruptive Accident (CDA) if there is a mismatch between heat generation and heat removal from the core. This could be on account of Transient Over Power (TOP) event initiated by reactivity addition like uncontrolled withdrawal of Control and protection rods resulting in heat generation greater than heat removal or by deficient cooling transients initiated by Loss of Flow (LOF) or Loss of Heat Sink (LOHS) events resulting in lower heat removal rate than rate of heat generation. These accidents may lead to core melting and consequent core disruption. For fast reactor systems, understanding of the progression of CDA and estimation of core energy released during the accident is crucial for evaluating the actual damage caused to the main vessel and top shield, and the amount of sodium that can come out in the reactor containment building. The extreme complexity of modelling various underlying physical phenomena during CDA poses a challenge for safety analysis. The accident progression of Fast Reactor in CDA is required to be evaluated in three phases: Accident initiation (Pre-disassembly phase), Disassembly phase and Post Disassembly phase.

To develop independent analytical tool for the accident analysis in sodium cooled fast breeder reactors (FBRs) in AERB, an in-house computer model (TRAN-SCORE) has been developed for analysing flow and power transient for pre-disassembly phase in fast breeder reactors. On the initiation of accident, modelling of pre-disassembly phase includes; core neutronics with reactivity feedback, thermal hydraulics calculation for fuel, clad temperature, coolant dynamic, modelling of sodium boiling, clad deformation and dynamic behaviour of the molten fuel during slumping. The fuel, clad and coolant temperature feedbacks are calculated using the temperature obtained by solving heat transfer equation and two phase coolant dynamic equations. Fuel elastic deformation module has been incorporated in the code to find out the radial and axial stresses and strains for fuel and clad according to respective temperatures. Comparison of analysis in pre-disassembly phase using in-house developed code with SAS-1A results has been done for a test problem for single channel.

2. Salient feature of TRAN-SCORE Model

The basic calculation model used in TRAN-SCORE is designed to treat multichannel capability for large LMFBR reactor designs. Multichannel modelling is used to take account of spatial variation of radial power and burn-up distribution in the core. The analysis is based on the assumption that the behaviour of the entire core (before the disassembly phase) is represented by predefined multichannel

and their associated coolant which is intact throughout the transient. Reactor dynamic behaviour is calculated using a point kinetics model with the appropriate reactivity feedback. The core thermal hydraulics is modelled by an equivalent multichannel representation using heat transfer equations. The mass, momentum and energy conservation equations are solved for coolant dynamics. The main features of TRAN-SCORE is summarized as flows.

- Multichannel capability for radial distribution of power and kinetic parameters.
- One dimensional coolant dynamics module for coolant temperature, pressure and flow distribution with Euler method or Lagrangian method.
- An approximate slip flow model for sodium using with two phase mass, energy and continuity equation.
- A model for sodium slug expulsion when void fraction reaches its predefined maximum value.
- The fuel heat-transfer model can treat fuel pins which have a central void and thermal temperature dependent thermo-mechanical properties.
- Thermal expansion of fuel and clad has been taken with linear coefficient.
- Elastic deformation model for finding out fuel and clad stresses and strains which can also handle central cavity.
- Provision of real time reactivity feedbacks due to Doppler, coolant density and axial and radial core expansions.

3. Physical model and Governing equation

CDA modelling has been done through simulation of numerous physical phenomena like core neutronics with reactivity feedback, thermal hydraulics, coolant dynamic, modelling of sodium boiling using slip flow model and slug expulsion model and fuel elastic deformation model. Brief description of mathematical modelling of each phenomena is presented in the following subsections.

3.1 Fuel heat transfer model

This model is used to calculated temperature across fuel pin. Time dependent partial differential heat equation describing radial heat transfer in cylindrical geometry is solved. It is coupled with neutronic model for power density, coupled with fuel deformation model for mesh distribution and coupled with coolant dynamic model for boundary condition. Heat zero flux boundary condition is applied to the inner fuel surface node and heat flux at the outer fuel surface node through conduction will be equal to the sum of heat transfer through convection and radiation heat fluxes. Heat flux at the outer clad surface radial node through conduction will be equal to the sum of heat transfer through forced convection through coolant. The Heat transfer equation is discretised with the help of extrapolated Crank-Nicolson method and there will be N-coupled algebraic equations for N unknown radial node temperature that have to be solved simultaneously to obtain at each axial node. The algebraic equation are a tri-diagonal matrix and it is solved using Thomas algorithm.

3.2 Coolant dynamic model

Time dependent mass, momentum and energy equations are solved in 1D axial direction for multi-phase coolant. The modelling of single phase and two phase coolant are done differently. Coolant is assumed to be incompressible in single phase thus mass flux in axial direction remain constant at any time. The energy equation is discretised using an implicit Euler finite differencing scheme and solved to find temperature distribution along the coolant channel. Integral momentum conservation equation is solved to find out the pressure and flow distribution along the channel. The boundary conditions for coolant transport are known coolant inlet temperature and mass flux, exit pressure.

Two phase coolant dynamic equations are modelled using two different type of methods. First one is slip-flow model which is used till void fraction reaches a larger predefined value. When void fraction

reaches near to value 1.0 in coolant then slug expulsion model is used for the voiding calculation. In the slip flow model, it is assumed that vapor and liquid coolant moves with different velocity and vapor slips through the liquid. Vapor and liquid are in thermodynamic equilibrium phase. In the boiling regime, continuity equation and energy equation are solved to find out the flow distribution and void distribution with the assumption of constant density of vapor and liquid. The vapor quality of coolant is calculated using Lockhart-Martinelli two-phase flow parameter. An implicit characteristic method are used to find the numerical solution of two phase coolant dynamic equation. Iteration method is used for solving continuity and energy with the convergence criteria on vapor quality. The two phase momentum integral equation is solved to find out the pressure inside the channel.

Slug expulsion model is used to find out the voiding distribution due to high pressure inside the channel. The basic assumption for this method is that there will be differential pressure around the liquid slug (which has crossed 0.9 value of void fraction) which will move outside the channel and the vapor will axially expand inside the core. The momentum equation is solved using 4th order Runge-Kutta method and integral in the equation is solved using trapezoidal rule.

3.3 Point Kinetic model

To predict the neutron kinetics of the reactor, point kinetics model is used with the six delayed neutrons for reactor dynamic behaviour. The shape distribution inside the core is predefined shape function which is defined axial normalised factor for each channel with its respective channel power. The point reactor kinetic model is assumed to be adequate to calculate the neutronics because of tight neutron coupling of in compact fast reactor core. Point kinetic module calculate the initial conditions for point kinetic equations and solve the equation using MATLAB inbuilt subroutine (ode-23s) using the initially conditions and net reactivity. Reactivity feedbacks due to fuel heat up, fuel axial expansion, structural expansion and coolant density/voiding are calculated in real time.

3.4 Fuel deformation model

A fuel-deformation model computes the stresses and deformations occurring during transients, and treats elastic deformation of the cladding. The gap width is calculated as a function of time in the fuel deformation module. When estimate gaps thickness becomes zero where fuel and cladding come in direct contact, the thermal conductance of the gap is set equal to its maximum value. The stress equation of equilibrium for a thick hollow cylinder in the cylindrical coordinate with the assumption of axisymmetric problem are solved to find respective the stresses and strain for fuel and clad.

4. Results

Modelling of a fast reactor test problem for unprotected power transient has been done using in-house developed model for different UTOP and ULOF event and its results have been compared with SAS-1A results [1], [2]. SAS-1A computer code is a code designed for analysing both flow and power transients for large LMFBR core. Normalised power and feedback reactivity, fuel temperature radial distribution at different axial node at 0.4 sec have been compared with SAS-1A code results for 2.5$/sec reactivity insertion as shown in figure 1 and figure 2 respectively. It can be noted that estimated results are in good agreement with the SAS-1A results till the fuel temperature reaches its melting point. The deviation form SAS-1A code at the end of transient due to early initiation of boiling in the TRAN-SCORE code which is due to the absence of clad plastic and fuel dynamic model which are used after fuel melting.

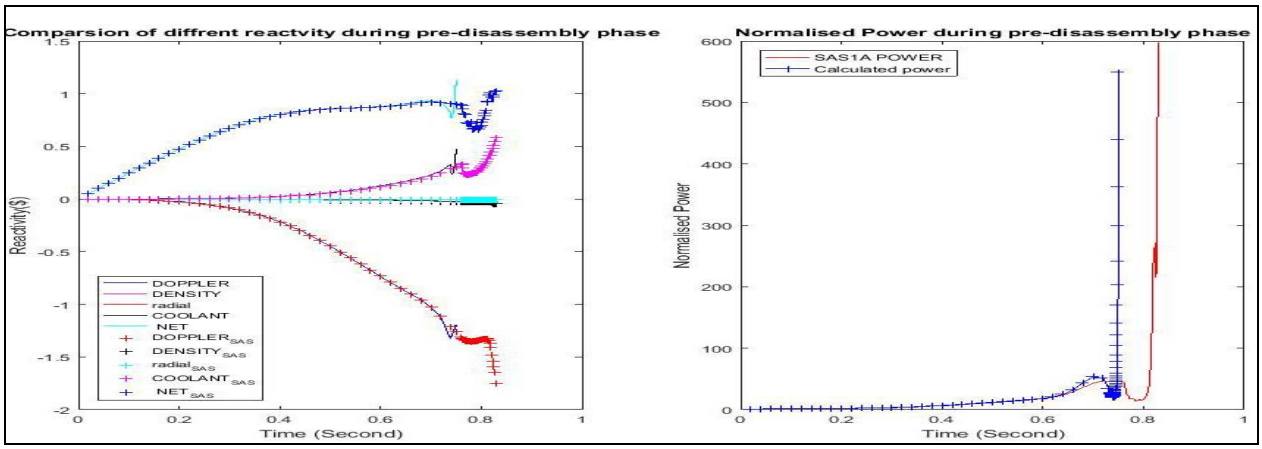


Figure 1: Comparison of Normalised power, reactivity feedback with SAS-1A code at 2.5$/sec reactivity insertion

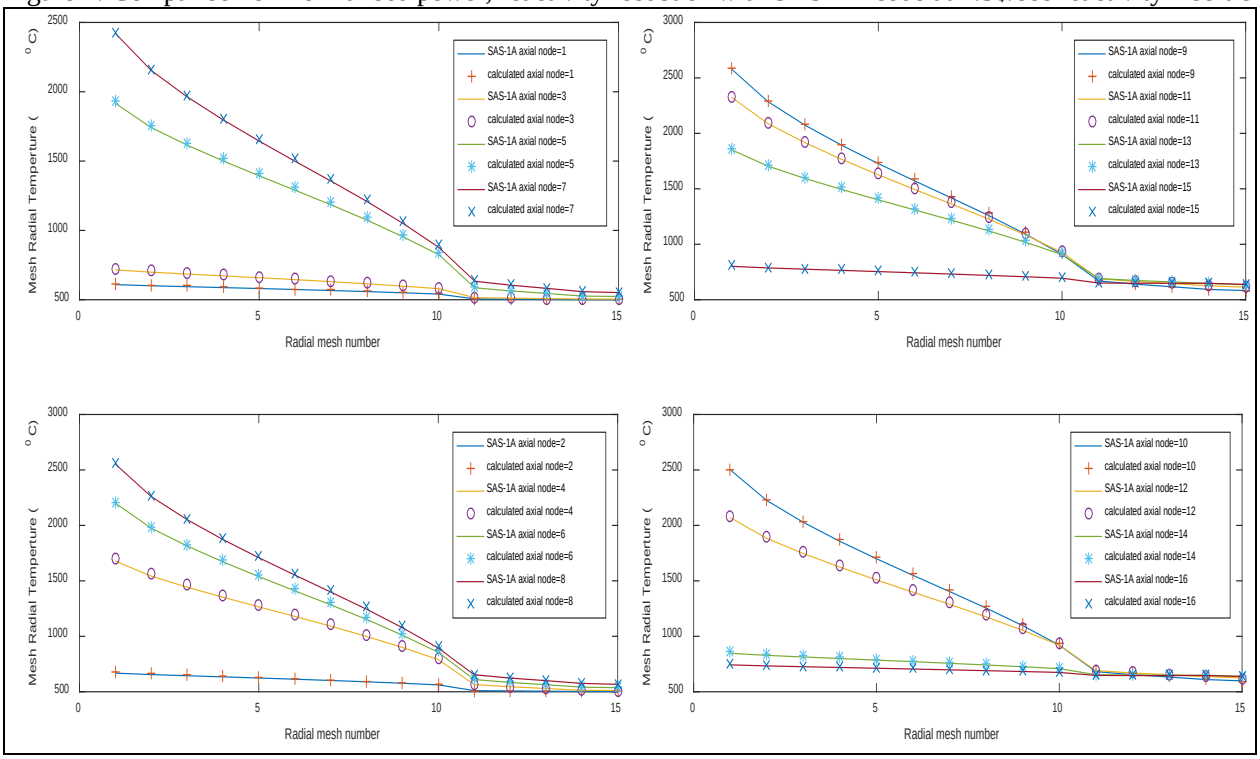


Figure 2: Comparison of fuel temperature radial distribution at different node with SAS-1A code

5. Conclusion

A reactor dynamic model, TRAN-SCORE, has been developed for pre-disassembly analysis in sodium cooled fast reactor. Core neutronics, thermal hydraulics and fuel thermo-mechanics have been modelled to capture integrated core behaviour during pre-disassembly phase of a CDA. Transient capability of TRAN-SCORE has been demonstrated by validating the code against SAS-1A code and it has been shown that the results obtained are in good agreement with SAS-1A code system. Post melting simulation of fuel behaviour and consequent core dynamic is in progress.

6. References

[1] *J. C. Carter, G. J. Fischer, T. J. Heames, D. R. MacFARLANE, N. A. McNeal, W. T. Sha, C. K. Santhanan and C. K. Youngdahl, "SAS1A, A computer code for the analysis of Fast Reactor power and flow transients," Argonne National Laboratory, 1970.*

[2] *A. Singh and H. P. Gupta, "Pre-disassembly phase analysis for Sodium cooled Fast breeder reactor," AERB/NSARG/TR/2019, Mumbai, June 2019.*

Development of a coolant dynamic model for Sodium Cooled Fast Reactor Core

Amandeep Singh[1], Obaidurrahman K [2] and H. P. Gupta[3]
[1, 2] Atomic Energy Regulatory Board, Mumbai, India
[3]Ex BARC, Mumbai
[1]*e-mail: - aman@aerb.gov.in*

Abstract

Coolant voiding may happen in fast reactor due to reactivity and flow transient. An analytical model for single and two-phase coolant dynamic model is necessary to find out the coolant behaviour inside the core to account feedback reactivity. An analytical model for coolant dynamic in TRAN-SCORE code is developed for predicting the coolant behaviour for single and two-phase coolant during the pre-disassembly phase analysis in sodium cooled fast breeder reactors. The model includes the modelling of continuity, momentum and energy equation for single and two-phase coolant. The capability of the model is demonstrated by comparing the results with SAS-1A code for a test problem. The developed model may be used to find out the coolant behaviour for sodium cooled fast reactor.

1. Introduction

Fast reactors are generally designed in such way that chances of sodium voiding in the core is very less but voiding can take place in the core in some of postulated initiated event. Feedback reactivity due to voiding is having crucial role in the accident analysis because of its positive nature in the large FBRs. For realistic assessment of the accident consequence, it is important to predict the core voiding and coolant temperature in order to estimate the core reactivity feedback. To model the coolant behaviour inside the channel, continuity, momentum and energy equations are solved for sodium. The modelling of single phase and two phase sodium coolant are done differently according to the phase of coolant.

Two phase coolant dynamic equations are modelled using two different type of methods. First one is slip-flow model which is used till void fraction reaches a larger predefined value. When void fraction reaches near to the predefined value in coolant then two phase slip model is not appropriate since a slug expulsion model is used for the voiding calculation for further calculation. Slug expulsion model is assumed that coolant is being expelled due to the vapor pressure. Governing equations for the coolant dynamic model for single and two phase coolant have been presented here and computational techniques to solve are also discussed. The comparison of the reactivity accident with SAS-1A has been presented and some of the analytical results are discussed.

2. Physical model

The heat produced in the fuel pin is removed through coolant circulation in the core. To provide a reasonable detailed profile of coolant thermal hydraulic properties, coolant dynamic phenomena is modelled. The boundary condition for outer clad temperature distribution in coolant dynamic model is provided through heat transfer model and initial condition for geometry and power distribution is provide through clad deformation model and point kinetic model respectively. When reactor is in steady state, steady state momentum and energy conservation equations are solved to find out temperature and pressure distribution inside the coolant channel. In transient state, continuity, momentum and energy conservation equations are solved according to the phase of sodium coolant. The details of module for coolant dynamics are as follows:

- One dimensional coolant dynamics module for coolant temperature, pressure and flow distribution with Euler or Lagrangian method.

- An approximate slip flow model for sodium using with two phase mass, energy and continuity equation.
- A two phase coolant model for sodium slug expulsion when void fraction reaches its predefined maximum value.

3. Governing equation

Time dependent mass, energy and momentum equations are solved in axial direction for multi-phase coolant for multi-channel. The modelling of single phase and two phase sodium coolant are done differently according to the phase of coolant and vapor is formed when coolant exceeds saturation temperature and superheat of coolant.

3.1. Single phase coolant dynamic

Coolant is assumed to be incompressible in single phase thus coolant dynamic equations become as

$$\frac{\partial G}{\partial z} = 0 \longrightarrow G(z) = \text{constant} \tag{1}$$

$$\frac{\partial G}{\partial t} + \frac{\partial}{\partial z}\left(\frac{G_l^2}{\rho_l}\right) + \frac{\partial p}{\partial z} + g\rho + \left(\frac{\partial p}{\partial z}\right)_{fr} = 0 \tag{2}$$

$$\rho C_l \frac{\partial T_l}{\partial t} + G C_l \frac{\partial T_l}{\partial z} = \gamma \phi(z,t) \tag{3}$$

The boundary conditions for the Eqns is coolant inlet temperature, exit pressure and coolant and clad temperature distribution at t=0 time which are calculated from the steady state calculation. The energy equation Eqn (3) are solved to find temperature distribution inside the coolant channel and the energy equation is discretised using an implicit Euler finite differencing scheme. Integral Momentum conservation equation (2) is solved to find out the pressure and flow distribution inside the channel.

3.2. Two phase coolant dynamic model

Two phase coolant dynamic equations are modelled using two different type of methods. First one is slip-flow model which is used till void fraction reaches a larger predefined value. When void fraction reaches near to value 1.0 in coolant then two phase slip model is not appropriate since a slug expulsion model is used for the voiding calculation for further calculation. In the slip flow model, it is assumed that vapor and liquid coolant moves with different velocity and vapor slips through the liquid. Vapor and liquid are assumed to be in thermodynamic equilibrium phase. In the boiling region, two phase continuity equation, energy and momentum are simplified as with the assumption of constant density of vapor and liquid.

$$(\rho_g - \rho_l)\frac{\partial \alpha}{\partial t} + \frac{\partial G}{\partial z} = 0 \tag{4}$$

$$(\rho_g + \rho_l x)\frac{\partial \alpha}{\partial t} + G\frac{\partial x}{\partial z} + \frac{G}{\lambda}\frac{\partial H_l}{\partial z} = \frac{\gamma \phi(z,t)}{\lambda} \tag{5}$$

$$\frac{\partial G}{\partial t} + \frac{\partial}{\partial z}\left(\frac{G^2}{\rho_l}\left[\frac{\beta x^2}{\alpha} + \frac{(1-x)^2}{1-\alpha}\right]\right) + \frac{\partial p}{\partial z} + g\rho_l\left(\frac{\alpha}{\beta} - \alpha + 1\right) + \frac{f_{sp}G^2}{2\rho_l D_h}(1-x)^{2-a}\phi_l^2 + \frac{\partial p}{\partial z} = 0 \qquad where\ \beta = \frac{\rho_l}{\rho_g} \tag{6}$$

Energy (Eqn6) and continuity equations (Eqn4) are solved to find out the flow distribution and void distribution inside the channel in the boiling region. The vapor quality of coolant is calculated using Lockhart-Martinelli two-phase flow parameter. The Energy equation (5) is discretized using an implicit characteristic method where space derivative and variables are averaged over time-step. To find the numerical solution of two phase coolant dynamic equation, the iteration method is used. The continuity and energy equation are solved together with the convergence criteria on vapor quality to

find out flow and void fraction distribution inside the boiling portion. The two phase momentum integral equation is solved to find out the pressure inside the channel. Modifications have been done in the model to solve two phase coolant dynamic equations for the stability of solution. To find out the stable solution during transition from single phase to two phases, a module has been developed to calculate time steps size. Time steps are calculated such that void will progress in next mesh of lower non-boiling leg at each fixed time which provides smother and stable solution of continuity, momentum and energy equation for two phase coolant dynamic model.

When core is partially voided in any accident and significant void is produced inside the channel. Slug expulsion model is used to find out the voiding distribution due to high pressure inside the channel due to vapor. The basic assumption for this method is that there will be differential pressure around the liquid slug (which has crossed 0.9 value of void fraction) which will move outside the channel and the vapor will axially expand inside the core. The driving pressure for the expansion of the vapor is coming from the coolant vapor pressure. The driving pressures are given by the difference between saturation pressure and pressure at the end of the channel. The momentum equation *(5)* is modified after neglecting gravitational force and spatial acceleration terms in the liquid slug and can be written as

$$\frac{\partial(\rho v)}{\partial t}+\frac{\partial p}{\partial z}+\left(\frac{\partial p}{\partial z}\right)_{fr}=0 \tag{7}$$

This equation is solved using 4th order Runge-Kutta method and integral in the equation is solved using trapezoidal rule. Boundary value of the problem has been calculated at the end of the slip flow model before entering into slug-expulsion model.

4. Results

Modelling of a fast reactor test problem for unprotected power transient has been done using in-house developed model and its results have been compared with SAS-1A results [1], [2] for different power and flow transients. Steady state and time dependent coolant temperature and pressure distribution along the axial height have been calculated using coolant dynamic module and results have been compared with SAS-1A results as shown in Figure 1. The difference of results with SAS-1A code results at time 0.5 sec are due to difference of predicted normalised power.

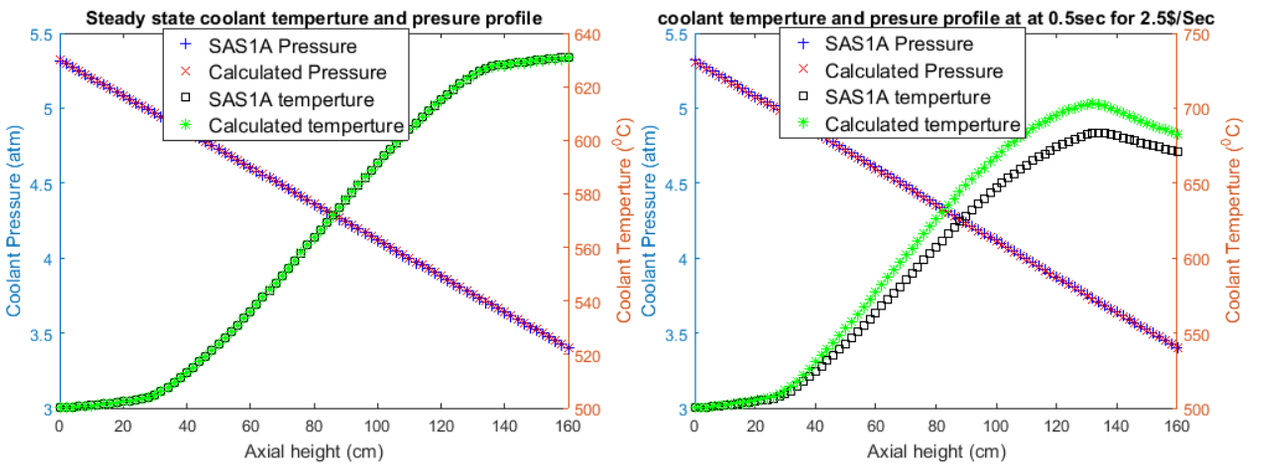


Figure 1: Comparison of coolant temperature and pressure profile at steady state and 0.5 sec

The calculated void fraction, mass flow rate, vapor quality and pressure distribution along the axial height are also presented in the Figure 2 for UTOPA transient (reactivity insertion rate 1.2$/sec). Comparison of void progression along the axial height with time has been also compared with SAS-1A results in figure 3. The predicted time when voiding start is different for both the codes due to the absence of the fuel dynamic model but estimated void progression profile along axial height with time matches very well with SAS-1A code. It can be concluded from the results that this module is working well for single and two phase coolant sodium.

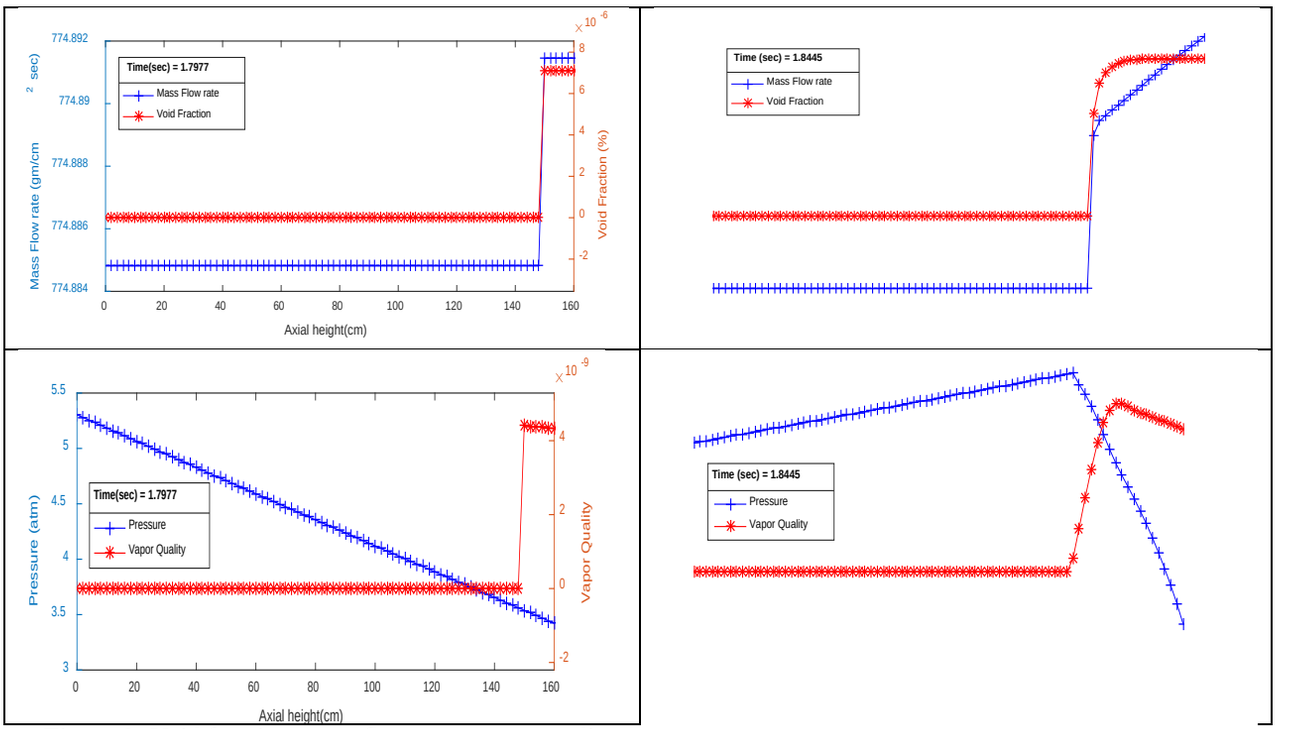


Figure 2: Void fraction, mass flow rate, vapor quality and pressure distribution along the axial height during the transient at different time.

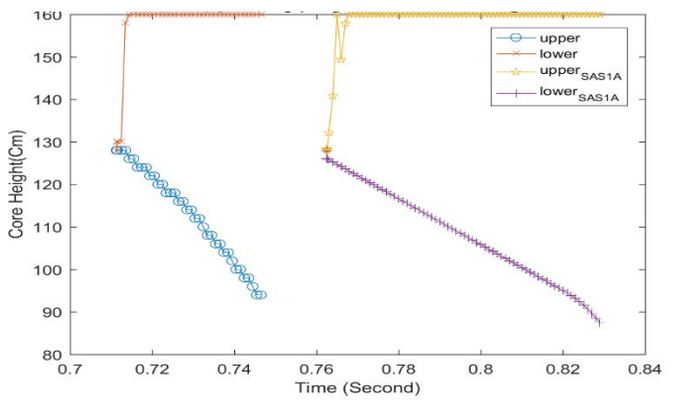


Figure 3: Comparison of void progression between developed code and SAS-1A code

5. Conclusion

A coolant dynamic model for new core dynamic code, TRAN-SCORE, has been developed for pre-disassembly analysis in sodium cooled fast reactor. The module has been demonstrated by validating the code against SAS-1A code and it has been shown that the obtained results are in good agreement with SAS-1A code system. The model has been found acceptable for single and two phase coolant dynamic equation for sodium cooled reactor. The results coolant temperature, pressure, vapor slug progression profile are matching well with SAS-1A results till fuel temperatures reach melting point. Void fraction, mass flow rate, vapor quality and pressure distribution are also calculated and results are as expected. This current module is having limitation of the flow regime for the stability of solution. Future work will be the detailed modelling of multiple-bubble slug-ejection model to calculate voiding due to boiling and this will be parallel to coolant dynamic model present in the SAS-2A code for better realistic solution.

6. References

[1] J. C. Carter, G. J. Fischer, T. J. Heames, D. R. MacFARLANE, N. A. McNeal, W. T. Sha, C. K. Santhanan and C. K. Youngdahl, SAS1A, A computer code for the analysis of Fast Reactor power and flow transients, 1970

[2] A. Singh and H. P. Gupta, "Pre-disassembly phase analysis for Sodium cooled Fast breeder reactor," AERB/NSARG/TR/2019, Mumbai, June 2019.

DEVELOPMENT OF MONTE CARLO MODEL OF TARAPUR BOILING WATER REACTOR TO ESTIMATE NUMBER OF SB-BE NEUTRON SOURCES

Indrajeet singh[1], Rashmi Rai[1], Pradeep Baraila[1], Arun Kumar Singh[1], Anurag Gupta[1], K.P. Singh[1] and Umashankari Kannan[1]
[1]Bhabha Atomic Research Centre Mumbai, India
[1]*e-mail: - jeet@barc.gov.in*

Abstract

Boiling Water Reactor (BWR) at Tarapur is shut down for a period of more than one and half years. It is planned to restart the reactor after the fuel shuffling of fresh and depleted fuel assemblies. During the criticality of reactor, the Source Range neutrons Monitors (SRMs) are used to get the reliable count rates and 3cps is the minimum count rate to guarantee the normal function of SRMs. In this context, external neutron sources, such as Sb-Be, can be used in the reactor core to achieve the minimum count rate criteria. This paper summarises development of three dimensional Monte Carlo model of BWR core to estimate the core multiplication factor (K-eff) and count rates at three SRM locations. In the developed model, five different burn-up zones are used to model the reload-2 pattern for the fuel shuffling of depleted and fresh fuel assemblies and about 210 isotopes are used to model actinides and fission products in exposed fuel assemblies of each of burn-up zone. After that neutron count rates at three SRM locations are estimated due to different combinations of five Sb-Be neutron source using Monte Carlo method.

1. Introduction

Estimation of the count rate in reactor with reload using this method is not straight forward as intensity and distribution of neutron source in irradiated core is quite complicated. As discussed in Ref. [1] that the external neutron source can be removed when core burn-up becomes more than 5GWd/T. Due to accumulation of heavy nuclei during reactor operation, spontaneous fissions would be sufficient to meet the requirement of minimum 3 counts per second (cps) in Source Range Monitors (SRM) in the cold shutdown condition with all control blades fully in. To start the reactor, no external neutron source is required within regular refueling outage. On the other hand, TAPS reactors are in shutdown state for prolonged period for major maintenance. It becomes important to compute the neutron source due to irradiated BWR fuel. Many transuranic isotopes such as Pu, Am and Cm are generated during irradiation of fuel bundle in reactor. In analysis carried out by M. Watanabe et. al., it is shown that there are three main contributors in neutron sources from irradiated fuel bundles, namely, ^{242}Cm and ^{244}Cm contribute through spontaneous fission, high energy γ emission from ^{140}La results in D (γ, n)H reaction and high energy α particles from heavy isotopes causes ^{18}O $(\alpha, n)^{21}$Ne reaction [2]. To estimate neutron strength due to these sources, knowledge of the accurate number density as function of time is crucial as decay constants of these three modes are very different. In the present analysis, only spontaneous fissions of heavy nuclei have been taken into account in the estimation of the source strength due to irradiated fuel. As sufficient time had been elapsed and half-life of ^{140}La is 40h for emission of γ and its precursors half-life is 12.8d [3], so the D (γ, n)H reaction can be neglected. ^{18}O$(\alpha, n)^{21}$Ne reaction can also ignored as source strength is very small in comparison to the spontaneous fission strength and due to the long shutdown period.

2. Analytical Estimation of Spontaneous Fissions in TAPS Reactor

To make an analytical estimate of spontaneous fission in TAPS reactor, lattice calculations are carried out using open source lattice code DRAGON and number densities of about 210 fission products and actinides are computed at burn-up of 8.75GWd/T, 10.0GWd/T, 15.0GWd/T, 17.5GWd/T and

18.25GWd/T [4]. Average burn-up of whole core in reload is about 12.5GWd/T. In actual condition, isotopic production is not uniform spatially among the fuel rods and within the fuel rods because of the differences in neutron flux, neutron energy spectrum and fuel compositions. However, number densities of ^{238}Pu, ^{239}Pu, ^{240}Pu, ^{242}Pu, ^{242}Cm and ^{244}Cm are taken corresponding to bundle average burn-up of 10.0GWd/T for spontaneous fission source strength calculation. It is important to note that reactor power is reduced from 210MWe to 160MWe. This results in lower density of ^{242}Cm which is one of the main contributor to the spontaneous fission neutrons.

2.1 Estimation of Neutron Flux Level

It can be seen from Table-1 that the spontaneous fission neutrons emission rates are calculated for each isotope of ^{238}Pu, ^{239}Pu, ^{240}Pu, ^{242}Pu, ^{242}Cm and ^{244}Cm assuming average burn-up of 10GWd/T.
Table 1 Spontaneous fission source calculation for average concentration at 10GWd/T

Isotopes	Atomic Weight	Number Density (atm/b-cc)	Weight (gm/cc)	$\frac{\text{neutrons}}{\text{gm/sec}}$	$\frac{\text{neutrons}}{\text{cc/sec}}$
^{235}U	235	3.09E-04	1.20E-01	8.00E-04	9.63E-05
^{238}U	238	2.13E-02	8.41E+00	1.60E-02	1.35E-01
^{238}Pu	238.049	2.31E-08	9.15E-06	2.50E+03	2.29E-02
^{239}Pu	239	6.94E-05	2.75E-02	3.00E-02	8.26E-04
^{240}Pu	240.054	1.66E-05	6.60E-03	9.05E+02	5.97E+00
^{242}Pu	242.059	9.03E-07	3.63E-04	1.68E+03	6.10E-01
^{242}Cm	242	7.50E-10	3.01E-07	2.13E+07	6.42E+00
^{244}Cm	244	7.85E-11	3.18E-08	1.10E+07	3.50E-01
Total Contribution					13.51

The spontaneous fission neutrons in fuel due to these six heavy isotopes is 13.51 n/cc-sec on average. Neutron source per unit volume of the reactor can be calculated by assuming that neutron source is uniform. Neutron source per unit volume of the reactor S =3.8 $\frac{\text{neutrons}}{\text{cc/sec}}$. Neutron flux due to this internal source in steady state subcritical condition is given by $\phi = \frac{Slv}{(1-K_{eff})} = \frac{S}{\Sigma_a(1-K_{eff})(1+M^2B^2)}$ Where, Σ_a= 0.028cm^{-1} effective one group absorption cross-section and $(1 + M^2B^2)$=1.02 [1]. For reload-2, BWR sub-critical multiplication factor (K-eff) is found to be 0.9268±0.00022 with all 69 control blades fully inserted [4]. The expected one group flux level in reactor core is found to be 1.80E+03 n/cm^2-sec (nv) using approximation of uniform source distribution.

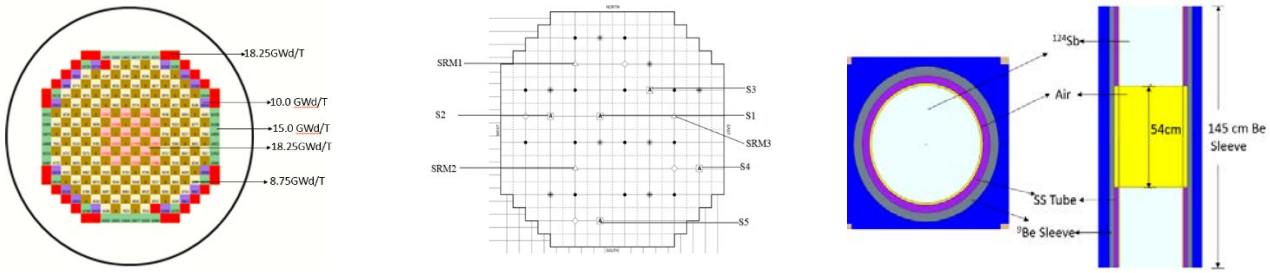
3. The External Photo-Neutron Source (Sb-Be)

Sb-Be neutron source is a typical external neutron source used in BWRs. In this type of neutron source, neutrons are produced in a (γ, n) reaction and therefore they are called photo-neutrons. Sb-Be source has two main components. The first component is ^{9}Be which has the lowest threshold of 1.666MeV for neutron ejection. Other component which serve as a source of high energy gamma rays. ^{124}Sb undergoes beta decay to form ^{124}Te and emits γ rays with half-life of 60.2 days. The γ ray emission in decay process of ^{124}Sb belongs to two energies groups 1.691MeV and 2.091MeV respectively [5-6].

3.1 Monte Carlo Model of BWR core and Sb-Be Source

3D Monte Carlo model of BWR reactor core is developed by including full geometrical details and five zone approximation for reload-2 pattern for fresh and exposed fuel assembly distribution (See Fig. 1a). The Monte Carlo result with detailed burn-up zones defined with fission products shows agreement with

3-D BWR simulator code COMETG within 0.1% [4, 7]. In Sb-Be neutron source, natural Antimony (consisting of 57.3% ^{121}Sb + 42.7% ^{123}Sb) in cylindrical geometry is used to irradiate in reactor to produce ^{124}Sb surrounded in Beryllium shell as target nuclei. Geometrical arrangement of Be and Sb to make a neutron source is shown in Fig 1c. Each Sb-Be neutron source consists of two Sb rods of length 45.72cm and radius 0.35052cm which are encased in stainless steel tube surrounded by a beryllium shell of length 145.415cm. The annular layer of Be outside the Sb does not have significant effect on the neutron flux required to activate the Sb, since the neutron absorption cross section for Be is very small. Inner and outer radius of Beryllium shell are 0.40894cm and 0.46482cm respectively [7].



(a) (b) (c)

Figure 1 Monte Carlo Model of BWR core (a) Locations of external neutrons sources (b) SB-Be neutrons source geometrical arrangement

4. Results and Discussions

In the present Monte Carlo simulation of BWR core, 6 million neutron histories are tracked from their birth to death (either by escape or absorption) to estimate minimum count rate of 3 cps at SRM (detector) locations in presence of different number of external Sb-Be sources. Each 3D BWR full core simulation with five burn-up zones requires about 3 hours of 6 nodes i.e.72cpus of AGRAA supercomputing facility. During the random walk in reactor core, all the physical events of each neutron are followed to estimate the neutron flux per history at detector locations. The neutron flux per neutron history are then normalised by neutron source strength. Once the absolute neutron flux is known, count rate is estimated using SRM sensitivity i.e.10^{-4} *cps/nv*.

4.1 Counts due to Spontaneous Fission Source in Fuel Assemblies and External Sb-Be Source

Although the analytical estimate indicates that the spontaneous fission source in fuel assembly is in sufficient to have minimum count rate at SRM locations, Monte Carlo simulations have been carried out to estimate contribution of fission source in absence of external Sb-Be sources to the neutron flux at detector locations. The neutron flux per history computed at SRM1, SRM2 and SRM3 locations are found to be 4.06E-05, 6.06E-05 and 6.31E-05, respectively. Main contribution to the spontaneous fission source is coming from 184 exposed fuel assemblies. Hence, total neutron source strength due to these assemblies is 3.69E+07 n/sec. Thus, the absolute flux at SRM location are 1.50E+03n/cm^2-s, 2.24E+03n/cm^2-s and 2.33E+03n/cm^2-s, respectively. These values of neutron fluxes are in line with that of the analytical estimate as discussed in Sec.2. Combined contributions of the spontaneous fission source and external Sb-Be neutron sources at SRM locations are presented in Table 2.

Table 2 SRM count rates due to different Sb-Be neutron sources and Spontaneous fission sources

Source	SRM-1	SRM-2	SRM-3
S1-S2	7.44	6.96	1.41
S1-S3	4.65	3.12	12.75
S1-S4	3.28	3.01	5.18

S1-S5	3.29	7.04	1.44
S2-S3	5.78	4.58	11.86
S2-S4	4.44	4.48	4.26
S4-S5	0.22	4.52	4.21
S1-S2-S3	8.89	7.25	12.89
S1-S3-S5	4.66	7.30	12.87
S2-S3-S5	5.77	8.73	11.98
S1-S2-S3-S4	8.89	7.40	16.80
S1-S2-S3-S4-S5	8.85	11.54	16.95

5. Conclusion

3D Monte Carlo model of TAPS reactor core is developed by including full geometrical details and five zone approximation for reload-2 pattern for fresh and exposed fuel assemblies. In computing the counts, each source pin is assumed to have minimum source strength of 3.1×10^8 neutrons/sec corresponding to 272 curies activity and SRM sensitivity is assumed to be 10^{-4} (*cps/nv*). The results of the analysis show that presence of three neutron sources in combination of S1-S2-S3, S1-S3-S5 or S2-S3-S5 results in each of the three SRMs reading above 4cps. Other than modelling approximations and nuclear data, Monte Carlo method have inherent uncertainty due to finite number of neutron histories. Therefore, the computed count rates also have ±2% average 3 sigma uncertainty. Thus, it can be concluded that three or more than three external sources will be enough to have reliable SRMs count rate (3cps) in BWR reactor core at the time of reactor start-up.

6. References

[1] P. Mohanakrishnan, "Estimation of neutron flux level produced by spontaneous fission in TAPS reactor" *Note No. TRPS-290, BARC*, 29 August 1980.

[2] Watanabe M, et. al., "Measuring the ratio of 242Cm in operating BWR cores using start-up range neutron monitors", *J Nucl. Sci. Technol*; 45:498– 509, 2008.

[3] Watanabe M, et. al., "Measuring the photo neutrons originating from D (γ, n) H reaction after the shutdown of an operational BWR", *J Nucl Sci Technol*.; 46:1099–1112, 2009.

[4] Indrajeet Singh, et. al., "Development of Monte Carlo Model of TARAPUR Boiling Water Reactor for K-eff Calculations," *Report No: RPDD/GE/48/Sep-2021*

[5] Avery M. Gag, "The Antimony-Beryllium Neutron Source for the LASL Water Boiler Reactor," LA-5571-MS, Informal Report UC-80 Reporting Date: March 1974 Issued: April 1974.

[6] Private communication with TAPS personals, "operational sources installed in the Tarapur Reactor"

[7] Amandeep Singh, et. al., "Analysis of TAPS BWR core using VISWAM code", *AERB/NSARG/TR/2019*

SHIELD OPTIMIZATION FOR OFFSET HANDLING MACHINE OF FUTURE FAST BREEDER REACTORS

Anupam Chakraborty[1], Anu Krishnan[2], D. Sunil Kumar[1], A. John Arul[1]
[1] Reactor Shielding and Data Division, IGCAR, India
[2] Component Handling and Mechanism Division, IGCAR, India
[1]*e-mail: - anupam93@igcar.gov.in*

Abstract

Offset Handling Machine is one of the major fuel handling machines for future fast breeder reactors. The outer tube of the machine which is going through the roof slab will act as a major radiation streaming source. To check that, shield plugs need to be introduced within the tube. As the outer tube along with shield plugs will move axially during handling operations, there are possibilities of increased radiation streaming at certain configurations. The present work is aimed at an optimization of the shield plug thickness and the gap between two plugs, so that the radiation dose rate limits at roof slab top are not exceeded. Deterministic neutron and gamma transport calculations have been carried out and an optimum configuration has been suggested.

1. Introduction

The experience gained in the design, manufacturing and testing of fuel handling machines for PFBR has given valuable feedback for future FBRs. Future FBRs envisage the use of a combination of Offset Handling Machine (OHM) within the main vessel and a simple shielded Subassembly Transfer Flask (STF) located outside the main vessel for ex-vessel handling of subassemblies (SA). The OHM (Figure 1) is used to transfer fresh and spent SA in sodium filled transfer pot (TP) from In-Vessel Transfer Position (IVTP) to Fuel Transfer Pot-1 and vice-versa. It provides a link between in-vessel transfer machine transfer arm and ex-vessel transfer machine STF. OHM consists of a long hollow cylindrical tube called outer tube with an offset arm welded to lower end for holding TP in vertical condition. Outer tube acts as a major radiation streaming source because it cannot be blocked totally by shield. Instead, shield plugs are introduced within the tube with some gap between any two. This arrangement reduces the hoisting load on the machine and serves the purpose of radiation shielding as well.

In the present study, the thickness and relative positions of the shield plugs have been optimized. Radiation transport calculations were carried out to estimate the neutron and gamma fluxes above roof slab for different shield configurations.

2. Dose rate limit criterion

All the shielding calculations have been carried out based on the condition that the total dose rate above the roof slab due to streaming radiation from OHM (both during reactor operation and fuel handling) should be less than 25 $\mu Sv\ h^{-1}$[1]. There are many sources of uncertainties like nuclear data (~20%), and flux uncertainties ($\propto$ shield thickness). It is found from experience that a safety factor of 2 covers these uncertainties sufficiently in general shielding problem. The same has been used here as well.

3. Source term

The optimization has to be carried out both for reactor operation and fuel handling campaign. For reactor operation, the only source term considered is the activated primary sodium pool. The saturated activity of primary sodium has been considered for this part. For fuel handling case, it is assumed that the reactor has been allowed to cool for 1 day. Consequently, the primary sodium activity was reduced. However, the major neutron and gamma source now is the spent fuel subassembly (FSA). For each axial region of the FSA, the steel activation gamma sources have been calculated. Also, the core decay gamma and neutron sources have been considered corresponding to 3 cycles (180 days irradiation + 60 days shutdown) of irradiation followed by 2 cycles of in-vessel cooling [2]. The total gamma and neutron flux distributions from spent FSA are shown in Figure 2.

4. Method of Calculation

The calculations have been carried out using the 2D discrete ordinates transport code DORT [3]. The 175-group neutron and 42-group gamma coupled microscopic cross section library, IGC-S3 [4] was used to prepare mixture cross sections for the problem. The problem geometry has been modelled in multiple stages using 2D R-Z cylindrical geometry.

There is an offset of about 130 cm between the OHM guide tube and the FSA pot for this mechanism. Therefore, in order to model in R-Z geometry, the calculation had to be carried out in two steps – (i) Symmetric about FSA axis, (ii) Symmetric about outer tube axis. In the first part, the full FSA and primary sodium sources had been modelled and gamma and neutron *angular fluxes* were estimated at a surface just above the FSA top. In the second part, the surface source obtained from the previous step has been used as boundary condition to model the outer tube penetration in the roof slab, along with the different shield plug configurations. Mesh sizes in both calculation steps have been taken to be 1 cm both radially and axially.

A large number of cases (~50) have been studied, with plug thicknesses and relative positions as variable parameters. Most of these steps have been automated using Python programming and its multithreading capabilities. All the pre- and post-processing works involving large data sets have been carried out using these auxiliary Python and Fortran programs to extract the desired quantities.

5. Results

All the cases and the maximum dose rates above roof slab in each case are given in Table 1. The highlighted case 14 refers to the position with maximum dose rate above roof slab. The total (neutron + gamma) dose rate for an optimum configuration has been shown in Figure 3 for reactor operation condition. Figure 4 shows two positions of the optimized shield plugs during fuel handling. In all the cases, it can be seen that the dose rate limit is not exceeded above roof slab.

6. Conclusion

Optimization for moving shield plugs have been carried out. A shield configuration of 40 cm SS304L shield plugs, separated by at most 120 cm has been suggested. The number of shield plugs required will be selected based on the extent of vertical movement to be allowed for the OHM. The automated procedure developed here has reduced computation time by a factor ~10.

7. References

[1] R. Indira, "Shield Design Criteria", *PFBR/01115/DN/1074, Rev. A-B*, Jan. 2001.

[2] Anupam Chakraborty, G. Pandikumar, Jose Varghese, D. Sunil Kumar, "Estimation of shield requirements for subassembly transfer flask", *FBR1&2/IGCAR/02110/DN/1000, Rev. 0*, November, 2018.

[3] W. A. Rhoads and R. L. Childs, "The DORT: Two-Dimensional Discrete Ordinates Transport Code", *Nucl. Sci. Engg.*, 99, 88, 1988.

[4] K. Devan, G. Pandikumar and V. Gopalakrishnan, "IGC-S3: A 217 Group (175n, 42γ) Coupled Cross Section Set from ENDF/B – VI", *RPD/NDS/99*, 2002.

Table 1 Maximum dose rates above roof slab for different cases studied.

Case	Shield Plug 1 Bottom (cm)	Maximum Dose Rate above Roof Slab (μSv h^{-1})	Case	Shield Plug 1 Bottom (cm)	Maximum Dose Rate above Roof Slab (μSv h^{-1})	Case	Shield Plug 1 Bottom (cm)	Maximum Dose Rate above Roof Slab (μSv h^{-1})
0	94.0 (Operation)	4.9	**7**	60	0.2	**14**	130	22.4
1	0.0 (Conc. start)	1.9	**8**	70	0.2	**15**	140	12.0
2	10	0.8	**9**	80	0.4	**16**	150	4.6
3	20	0.4	**10**	90	1.0	**17**	160	1.9
4	30	0.3	**11**	100	2.7			
5	40	0.2	**12**	110	6.9			
6	50	0.1	**13**	120	14.8			

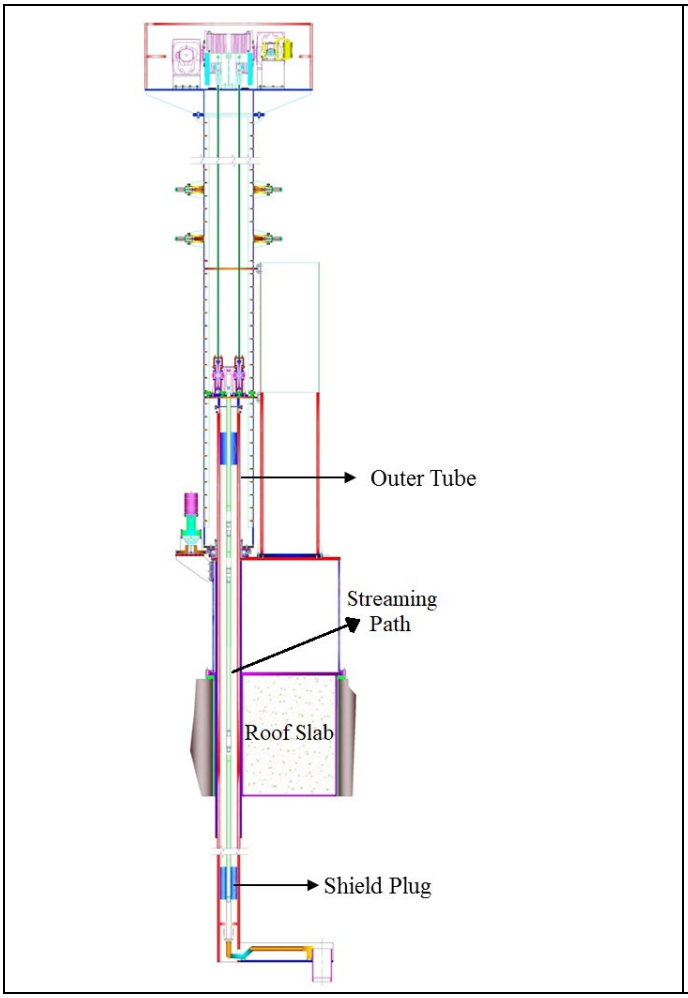


Figure 1 Offset Handling Machine.

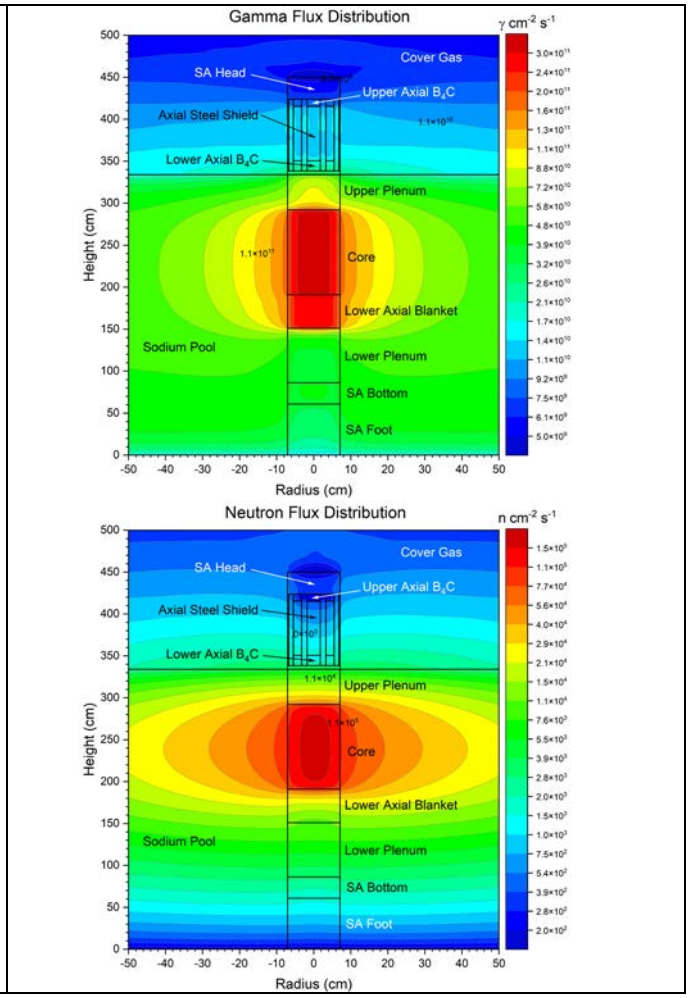


Figure 2 Source distributions for the spent FSA partially dipped in primary sodium pool.

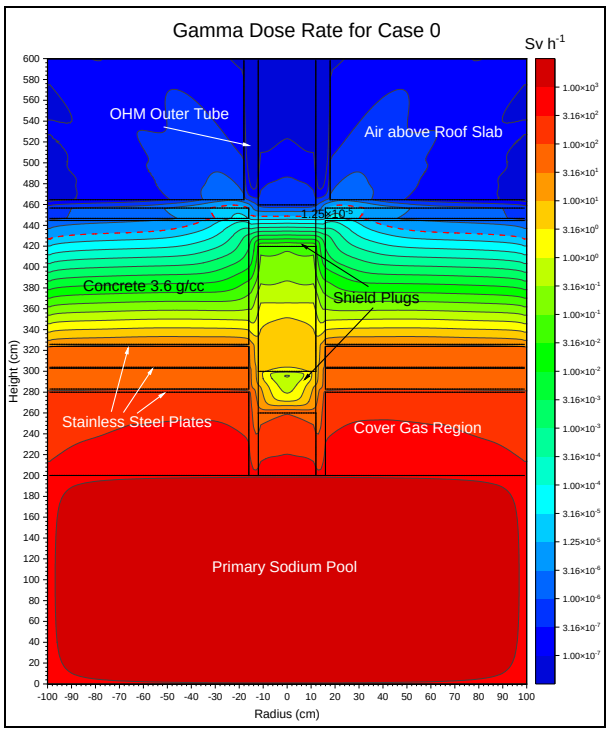


Figure 3 Total Dose Rate (Gamma) distribution for the case of Reactor Operation. The red-dashed contour indicates the dose rate limit above roof slab.

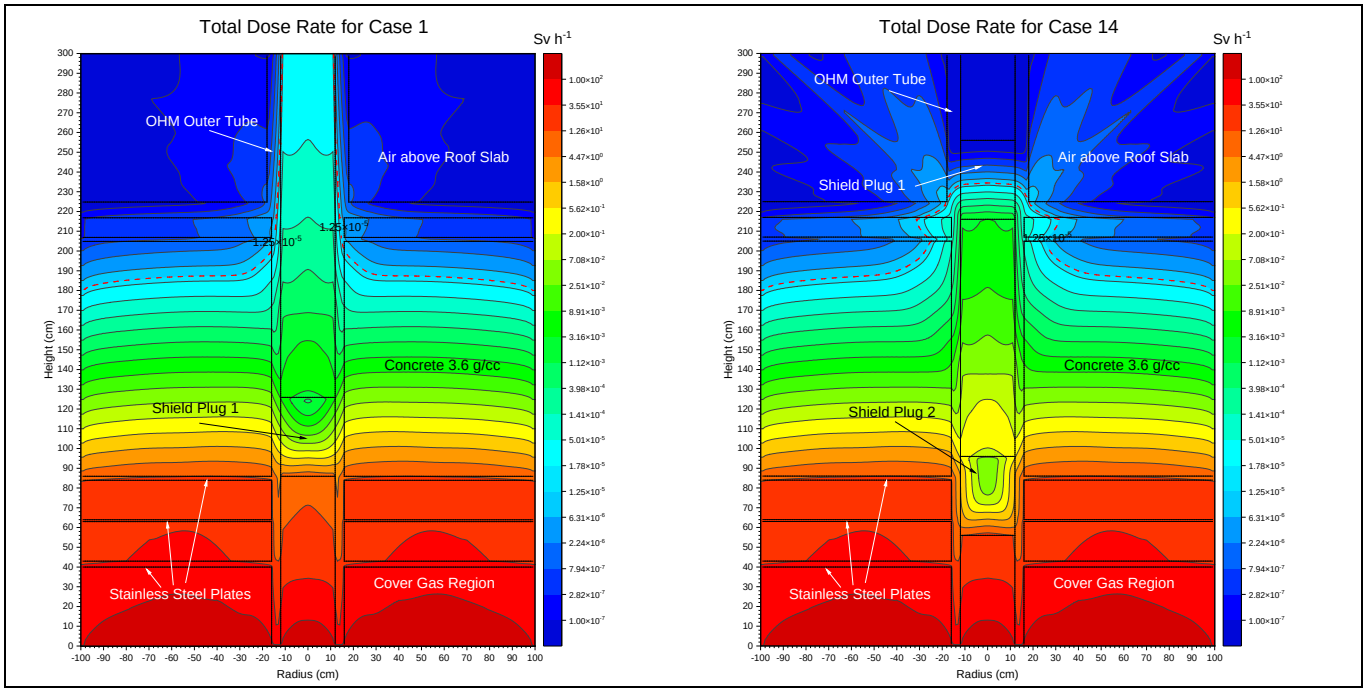


Figure 4 Total dose rate distribution for two extreme positions of a shield plug. Shield plugs are of thickness 40 cm and two such plugs are separated by 120 cm. Red-dashed contour indicates the dose rate limit above roof slab.

Machine learning assisted k-infinity prediction for analysis of Molten Salt Reactor

A. K. Srivastava, Anurag Gupta, Umasankari Kannan
Reactor Physics Design Division

Bhabha Atomic Research Centre, Mumbai 400085
e-mail: - ashishks@barc.gov.in

Abstract

Artificial neural networks (ANN) have attracted significant attention from researchers because many complex problems can be solved by training them. If enough data are provided during the training process, ANNs are capable of achieving good performance results. Present paper explores the possibility of uses of machine learning (ML) technique to assist a neutronics simulation of lattice used in molten salt reactor. An algorithm was developed to generate the problem dependent database of number density and k-infinity for a chosen fuel with specific lattice physics parameters (i.e temperature, geometry, library etc.) using open source lattice physics code DRAGON from SARRA code. The database was further divided for training and test datasets for training of keras based neural network model. The trained model was tested on test dataset for prediction of k-infinity based on number density in test data. The model succeeded in predicting k-infinity quite well on test data.

1. Introduction

A python based code package SARRA is being developed as a computational tool, which utilises lattice code DRAGON-5 [1] and in-house 3D time dependent diffusion code ARCH [2] for MSRs specific neutronics modelling like refueling. SARRA is incorporated with a sub-package for prediction of k-infinity based on ML technique to explore the suitability of ML technique for k-infinity prediction based on input of number density of 300 nuclides in the IMSR fuel with other lattice parameters i.e. temperature, geometry, library etc., being fixed. The sub-package provides a functionality to prepare the problem dependent database (currently, number density of 300 nuclides with associated k-infinity value prepared for an IMSR lattice problem using DRAGON), which further defines an ANN model using python package called keras [3] for training and testing on the generated data.

2. Lattice Description

A fuel lattice cell of IMSR (figure 1) is chosen for preparing number density- k-infinity database to be used for training and testing of ANN model. The fuel lattice was modelled using DRAGON code handling module from SARRA [4-6]. SARRA handles the initial fuel input data to prepare various DRAGON input of lattice shown in figure 1. The fuel input is subjected to various constraint on fuel isotopic composition which is defined judiciously and supplied as another input in SARRA in order to span over isotopic space of each nuclide in the current molten salt fuel. The constraint on fuel isotopic composition reduces the isotopic space domain substantially without loss of allowed isotopic fuel composition for a given problem. The judicious constraint on isotopic space not only save computational time due to reduction in number of cases for database creation but also reduces the size of database for training of ANN model.

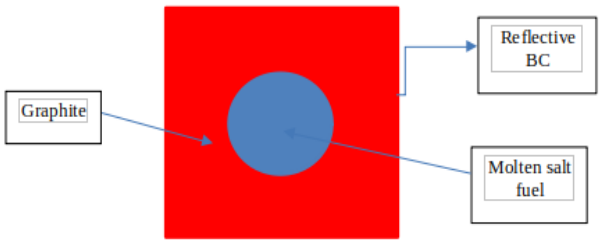


Figure 1: Modelled lattice cell containing molten salt fuel surrounded by graphite lattice

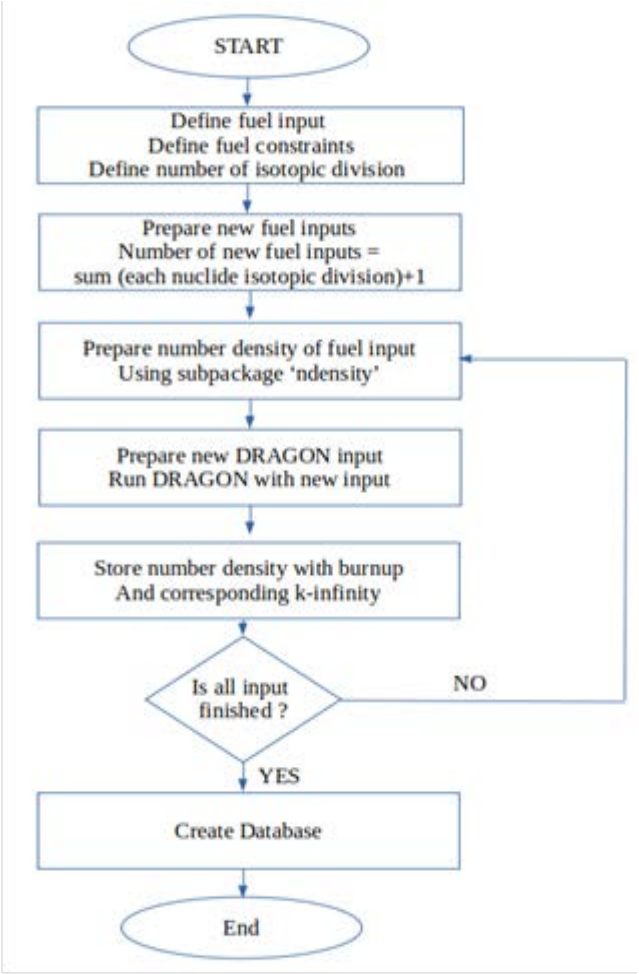


Figure 2: Flowchart for creation of database using DRAGON and SARRA

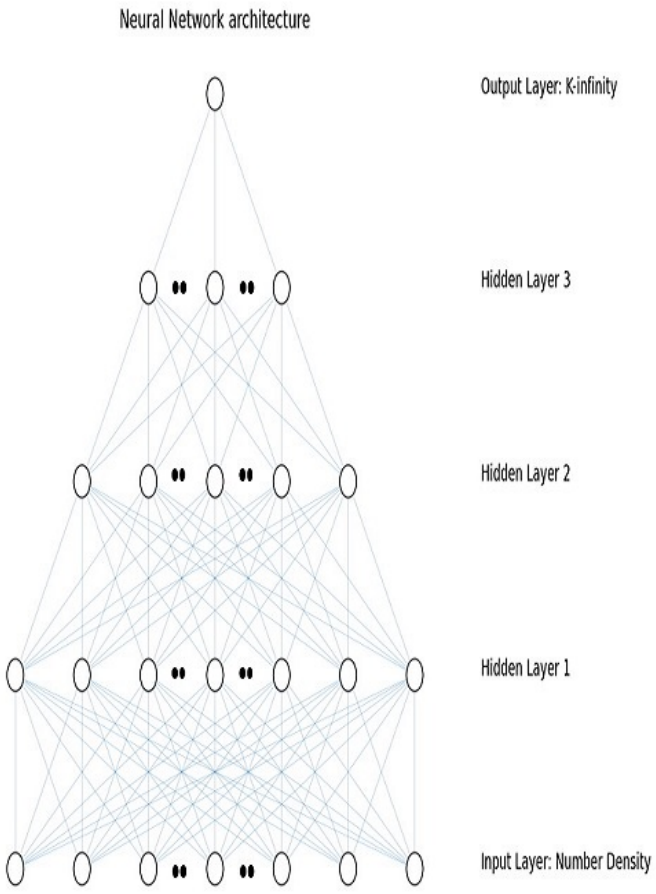


Figure 3: Schematic of neural network model used for training from training data

3. Methodology

The study in this paper can be divided in two main parts. Firstly, preparation of database of number density and k-infinity for current lattice dimensions and lattice parameters like temperature, fuel composition etc. Each database contains many datasets and each dataset is a vector of data of length of 301 numbers. First 300 numbers contains number density of fuel composition of various nuclides in specific order and last number is k-infinity for corresponding number density. An algorithm is developed

to prepare this database for a given lattice parameters and isotopic constraint. Secondly, the prepared database is divided in the two databases used for training and testing feed forward ANN model. The trained model is tested on test database for prediction of k-infinity corresponding to number density vector.

A flowchart for creation of number density – k-infinity database, which uses SARRA (and DRAGON) is shown in figure 2. It shows that, to create a database, SARRA must be provided with initial fuel input, fuel constraint and number of isotopic division of each nuclide. An algorithm called *Linearly Spaced Isotopic Composition (LSIC)* based on linear isotopic division of each nuclide is used to prepare fuel inputs uniformly in defined isotopic space. Total number of fuel inputs in the isotopic space of interest for creating a problem dependent database can be obtained by the following equation.

Total DRAGON lattice inputs for database creation = sum of each nuclide isotopic division + 1

Total datasets in database = Total DRAGON inputs * (number of burnup steps + 1)

Where, number of burnup steps is the total burnup level calculated in DRAGON excluding zero burnup data.

Isotope	Constraint on isotopic composition (IC)		Isotopic division in isotopic space
	Min. IC	Max. IC	
Li-6	0.0	1.0	30
Li-7	99.0	100.0	30
U-235	1.0	19.75	80
U-238	80.25	99.0	80

Table 1: Limits on isotopic constraint with isotopic divisions in each isotopic space

The database of 300 nuclides number density and respective k-infinity was prepared for a given IMSR LEU fuel parameters. The constraint on isotopic composition of Li and U is shown in table 1. In the current study, total DRAGON fuel inputs is 111 for isotopic constraints listed in table 1. These DRAGON inputs are run in loop to calculate k-infinity. Including the burnup calculation data, a final database is prepared for ML application. Once the database is prepared, the database was further divided into training and test dataset. A neural network model with architecture as (300, 300, 100, 10, 1) neurons in each layer (figure 3) was built using keras python package for training on training dataset and the model was tested on test dataset. In the ANN architecture first layer is input layer and last layer is k-infinity. For current study, using constraint data from table 1 and 20 burnup steps calculation total number of datasets in the database is estimated as following.

Total number of datasets in database = ((30+80) + 1) * (20 + 1) = 2331

4. Result

The prepared database for a specified lattice parameters of temperature, geometry and library was used to for training and testing of neural network model in ratio 80%-20% with a feed forward neural network model as shown in figure 3. The prediction of k-infinity for a given number density from test dataset from the trained model was performed. The results for prediction on test dataset were found to be quite good as shown in figure 4.

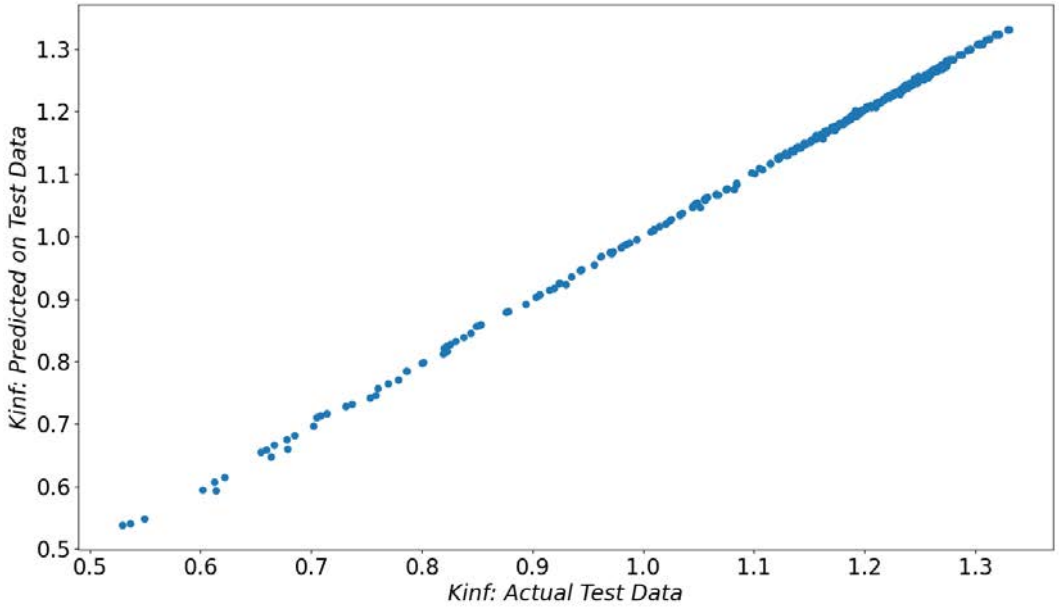


Figure 4: prediction of k-infinity with trained neural network model on test dataset

5. Conclusion

A machine learning approach to predict k-infinity for specified lattice parameters has been worked out. In the approach, an algorithm i.e. Linearly Spaced Isotopic Composition (LSIC) was developed to create a training and test database of number density and respective k-infinity for an initial fuel input of IMSR. For the study in the current report a database of 2331 data was prepared, out of which 80% of data was used for training the feed forward neural network model and 20% of data was used for testing the model. From the prediction of k-infinity on test data, it was found that trained model is able to predict k-infinity quite well.

6. References

1) Marleau, G., Hébert, A., 1993. DRAGON: A collision probability transport code for cell and supercell calculations. *Technical Report IGE-157. Ecole Ploytechnique de Montreal.*

2) Anurag, G., 2012. Arch: A 3d space-time analysis code in cartesian and hexagonal geometries. *In: Proceedings of 19th National Symposium on Radiation Physics (NSRP-19), Mamallapuram, India.*

3) https://keras.io

4) A.K.Srivastava, Anurag Gupta, Umasankari Kannan, Development of A Python Module "SARRA" For Refuelling Analysis Of MSR Using Lattice Physics Code DRAGON-5, *RPDD/MSR/33/APR-2019*

5) A. K. Srivastava, Anurag Gupta, Umasankari Kannan, "Development and implementation of reprocessing module in SARRA for analysis of MSR", RPDD /MSR/39/ FEB-2020

6) A. K. Srivastava, Anurag Gupta, Umasankari Kannan, "Development of module for implementation of feed fuel change in SARRA for MSR analysis", RPDD /MSR/41/ MAR-2020

Integration of DRAGON and ARCH with SARRA for analysing the neutronics aspect of refuelling and reprocessing in MSR

A. K. Srivastava, Anurag Gupta, Umasankari Kannan

Reactor Physics Design Division

Bhabha Atomic Research Centre, Mumbai 400085

Abstract

Molten Salt Reactors (MSRs) are being investigated worldwide due to it's unique characteristics of online refuelling and reprocessing of molten salt fuel. Thus, there is need of development of computational tools for analysis of online refuelling and reprocessing of circulating fuel systems like MSRs. A python based package called SARRA is being developed as a computational tool, which utilises lattice code DRAGON-5 and in-house 3D time dependent diffusion code ARCH for MSRs specific analysis like online refuelling and reprocessing. The present paper primarily discuss about the integration of DRAGON + ARCH code system within SARRA and it's ability to do refuelling and reprocessing analysis by one by one simulation of lattice and core. The impact of refuelling and reprocessing on k-effective in the analysed core is presented.

1. Introduction

The modelling of online refuelling and reprocessing of molten salt fuel in any circulating fuel reactors e.g. MSRs is a big computational challenge [1]. A python based SARRA [2-4] code is under-development to study the reactor physics aspect of refuelling and reprocessing of molten salt reactor. The present paper deals with integration of SARRA with the open source lattice code DRAGON [5], developed in Ecole Polytechnique de Montr´eal and in-house 3D time dependent neutron diffusion code ARCH [6]. In the present paper, lattice and core physics are modelled by DRAGON and ARCH. However, SARRA models the physics aspect of refuelling and reprocessing as well as handles DRAGON and ARCH input preparation and controls various operation related to refuelling and reprocessing. The 2 group cross-section required by ARCH in each refuelling cycle is also prepared by SARRA. Figure 1 shows the current features equipped in SARRA.

The core modelling capability for refuelling and reprocessing analysis by SARRA, at present is limited by the fact that it can model a core which contains only a single type of lattice for refuelling and reprocessing analysis. However, for analysis which does not require refuelling and reprocessing i.e. if the lattice and core analysis is to be performed for once, the 2 group cross-sections for multiple type of fuel and lattice can be generated by SARRA at once to be used in core analysis by ARCH. In this way SARRA also facilitates the 2 step neutronics modelling by explicitly handling various tasks like automatic preparation of 2 group cross-section, DRAGON generated cross-section into a format required by ARCH. SARRA is also equipped with various helper modules to check for various input error, input preparation module for DRAGON and ARCH, fuel number density preparation and handling etc.

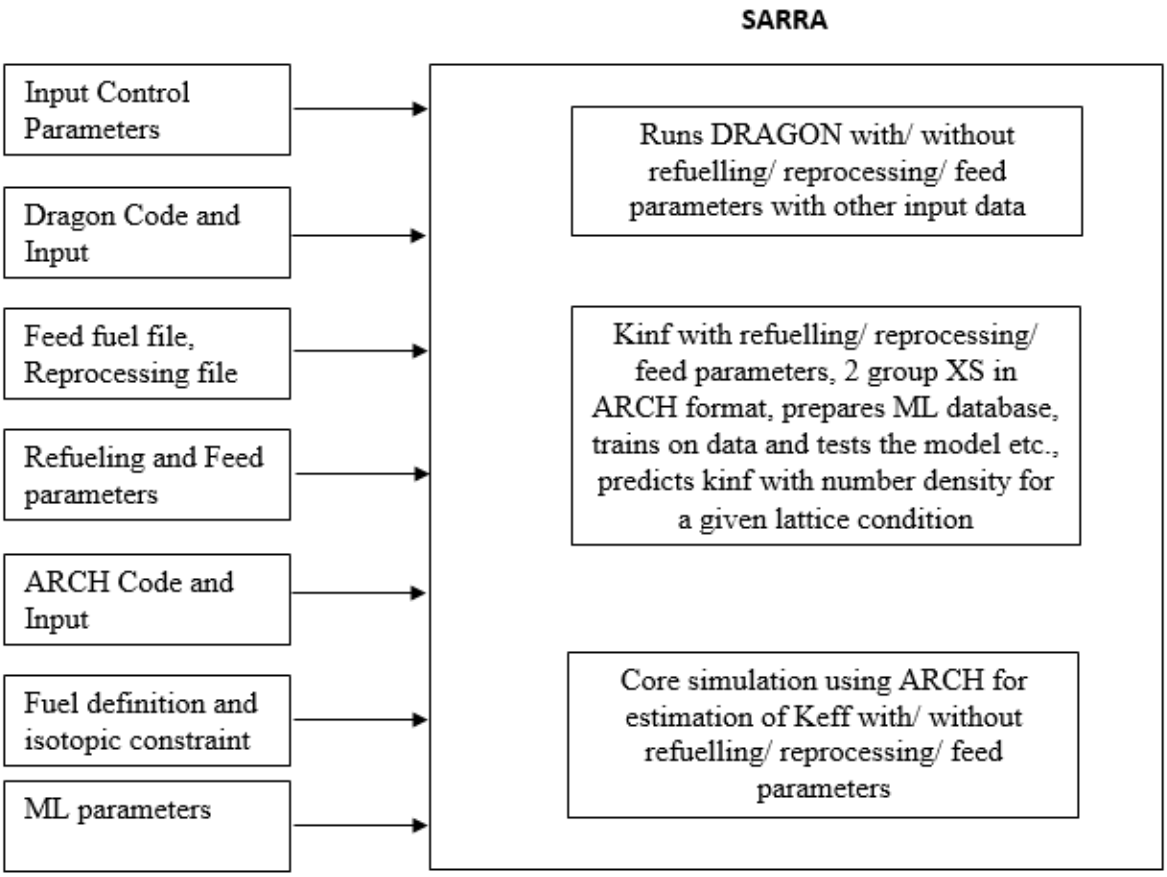


Figure 1: Current feature details in SARRA

2. Lattice and Core Description

A basic unit cell (fig.2) containing fuel-graphite system has been modelled with dimensions shown in table 1. Lattice analysis were subjected to uniform temperature of 922 K. The 2 group lattice parameters are generated (energy boundary at 0.414 eV) using Jeff 3.1.2 library in 172 energy groups in draglib format used by DRAGON code. The core analysed (fig.3) in the current paper is a single lattice type core, modelled by repeating arrangements of lattice. SARRA's feature of refuelling and reprocessing analysis with integrated lattice and core has been performed to demonstrate this capability.

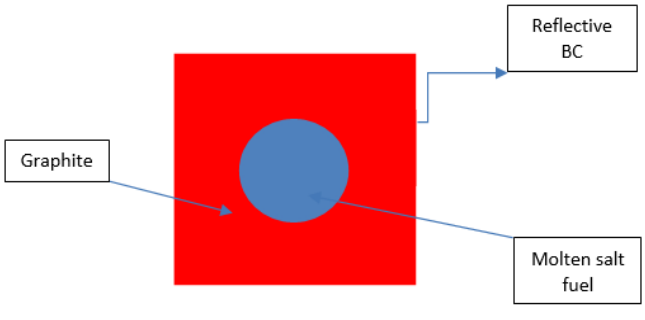


Figure 2: Modelled lattice cell containing molten salt fuel

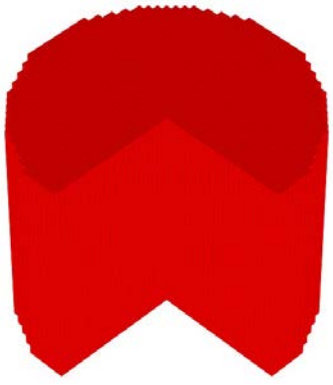


Figure 3: Cut view of modelled 3D core

For this, the details of refuelling and reprocessing parameters used for the analysis is listed in table 2. In the present analysis the core is being refuelled by 1% of volume of total fuel in each refuelling cycle, which has been set to 1 day. Also core is being reprocessed by fully removing Xe-135 at every 10th refuelling cycle.

Lattice parameters	
Type	*Cylindrical hole in Square graphite block*
Dimension (Radius, Side Length)	*0.8 cm, 3.5921 cm*
Fuel	*Fluoride based LEU fuel*
	U235 in U: 19.75 %
	Li7 in Li: 99.9%
	Density: 2.05724 g/cc
Graphite	*1.8 g/cc with 5 PPM Boron*
Core Parameters	
Type	*Single Lattice Core made of fuel lattice*
Dimension (Diameter, Height)	*176 cm, 190 cm*

Table 1: Lattice and core parameters used in current modelling

Refuelling Parameter	
Refuelling Rate	*0%, 1%, 10% of total fuel volume*
Duration of Refuelling	*1 Day*
Reprocessing Parameter	
Nuclides being reprocessed	*Xe-135*
Reprocessing efficiency	*100%*
Reprocessing duration	*Every 10 Day*

Table 2: Refuelling and reprocessing parameters used in current study

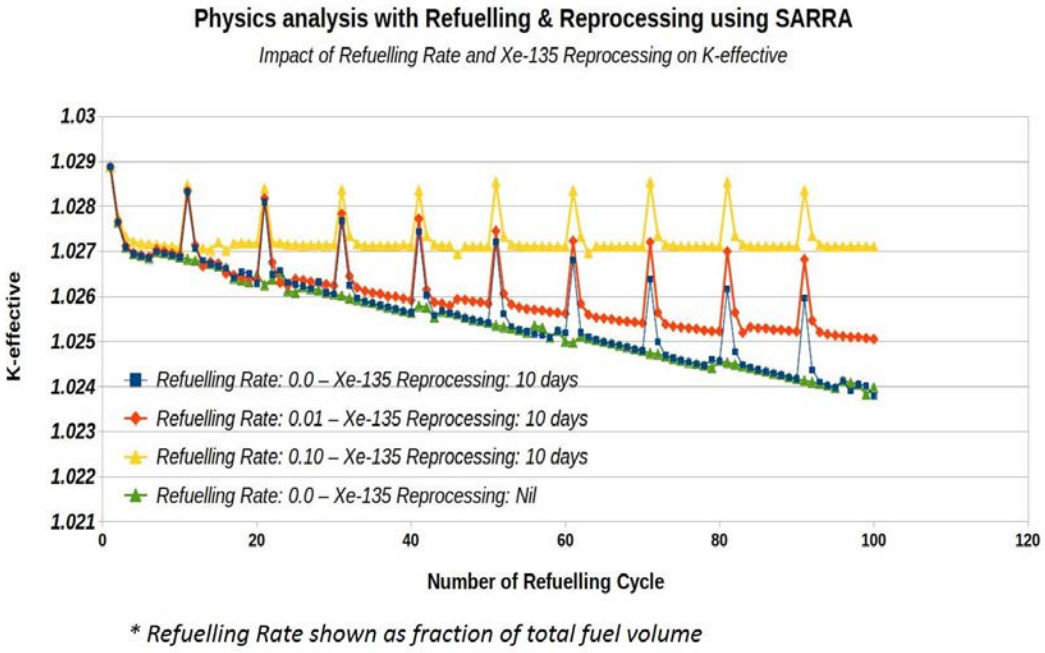


Figure 3: Impact of refuelling rate and Xe-135 reprocessing on k-effective on modelled core

3. Results

Schematic core is modelled in hot condition (922 K) with various reactor parameters as per description in table 1 and table 2. K-effective (at 0 burnup of core for each refuelling cycle) obtained at each refuelling/reprocessing interval is shown in figure 3 vs number of refuelling cycle. The effect of refuelling every day with various refuelling rate of 0%, 1% and 10% of total fuel volume is clearly observed by higher K-effective value for increases refuelling rate till the 100 refuelling cycle of the reactor. The effect of reprocessing of Xe-135 has been studied with 100% removal of Xe-135 at every 10^{th} day (or 10^{th} refuelling cycle). It is clearly observed that every instance of Xe-135 removal (at each 10^{th} cycle of refuelling) from the core results in increase in K-effective by ~2. The sudden spike in reactivity further falls down gradually to equilibrium Xe-135 level due to buildup of Xe-135 in nearly a couple of days.

4. Conclusion

The integration of DRAGON and ARCH with SARRA enables to model refuelling and reprocessing analysis of a single lattice type core at core level by using 2 group cross-section generated by lattice physics code DRAGON simultaneously. The study in current paper suggested that there is increase in K-eff (~ 2 mk) due to reprocessing of Xe-135 every 10^{th} day as compared to cases without reprocessing. Meanwhile, with sufficient refuelling it is possible to keep the reactivity stable at desired level and reactor operation can go on indefinitely without getting subcritical as far as refuelling perspective is considered. It can also be observed that after removal of Xe-135, it further starts building up for around 2 days till it gets saturated to the level of equilibrium xenon. At this point K-eff in case of reprocessed Xe-135 matches with the K-eff without reprocessing of Xe-135.

5. References

1) Andrei Rykhlevskii, Jin Whan Bae, Kathryn D. Huff, Modeling and simulation of online reprocessing in the thorium-fueled molten salt breeder reactor, *Annals of Nuclear Energy 128 (2019) 366–379*
2) "Development of a Python Module 'SARRA' for Refuelling Analysis of MSR Using DRAGON Code", A. K. Srivastava, Anurag Gupta, Umasankari Kannan, ICAER-2019, 10-12 December 2019, IIT Mumbai, Mumbai, India
3) "Development and implementation of reprocessing module in SARRA for analysis of MSR"; A. K. Srivastava, Anurag Gupta, Umasankari Kannan; RPDD /MSR/39/ FEB-2020
4) "Development of module for implementation of feed fuel change in SARRA for MSR analysis"; A. K. Srivastava, Anurag Gupta, Umasankari Kannan; RPDD /MSR/41/ MAR-2020
5) Marleau, G., Hébert, A., 1993. DRAGON: A collision probability transport code for cell and supercell calculations. *Technical Report IGE-157. Ecole Ploytechnique de Montreal*
6) Anurag, G., 2012. Arch: A 3d space-time analysis code in cartesian and hexagonal geometries. *In: Proceedings of 19th National Symposium on Radiation Physics (NSRP-19), Mamallapuram, India.*

RESPONSE MATRIX OF AN EXTENDED BONNER SPHERE SYSTEM USING MCNP5

Subhrojit Bagchi[1], A. John Arul[1]
[1]Indira Gandhi Centre for Atomic Research, Kalpakkam, India
[1]*e-mail: - bagchi@igcar.gov.in*

Abstract

A modified Bonner Sphere Spectrometer (BSS) is designed for measuring spectrum of high energy neutrons (>10MeV). The existing BSS, which has 7 polyethylene spherical shells, is modified with addition of several combination of lead. This spectrometer is modeled in MCNP5 and response function is generated for energy up to 1GeV neutron energy.

1. Introduction

Measurement of energy spectra of high energy neutrons, produced in an accelerator is a challenging job. The existing design of BSS, comprising of polyethylene moderators and a thermal neutron detector like He-3, has an intrinsic limitation in neutron spectrum measurements. BSS, even with a moderator diameter of 45.72 cm, can measure neutrons up to 10MeV [1]. The response function, which describes the number of (n, p) reactions in He-3 detector per unit flux, drops drastically beyond 10MeV. So detection of high energy neutrons (beyond 10MeV) becomes difficult. However, addition of polyethylene moderators makes the system heavy and bulky. Besides, it is also found that such addition does not improve the response function and also found overlapping of responses in higher energy region (>5MeV). In such a case, the unfolded neutron spectrum would be unreliable [2].

To overcome this problem, the BSS is modified by adding material other than polyethylene. Lead is chosen as adding material since it has a reasonably higher (n, xn) threshold reactions cross section. This threshold reaction drastically brings down the high energy neutrons below ~ 10MeV. Subsequently, the moderators enable the BSS system for high energy neutron spectrum measurements. In the present work, along with modular polyethylene, modular shells of lead radiator designs are explored for inclusion in BSS moderators. MCNP5 modelling is done for the design, and response functions are generated [3].

2. Effect of lead configuration

The following choices of lead radiator inclusion are considered. (a) thin layer of lead wrapping the outer surface of a polyethylene moderator, (b) lead (shell) layer implanted in-between two moderators, and (c) Lead core surrounding the ^{3}He detector (see Fig. 1). Let us assume that a parallel beam of high-energy neutrons is incident from the left side. Since the lead volume and neutron fluence are steady, each configuration will create similar number of optional neutrons from (n; xn) reactions. These secondary neutrons are also energetic and are directed forward. The probability of getting detected or escape of these neutrons will rely upon the thickness of polyethylene in their way. It is obvious that Case (a) scatters out several neutrons, and hence reduces the efficiency of the BSS system. In Case (c), the escape probability for scattered neutrons is negligible. The escape probability, in Case (b), depends on the polyethylene configuration nearby the detector that influences the moderation process. This has been verified theoretically by simulating the geometries in MCNP5.

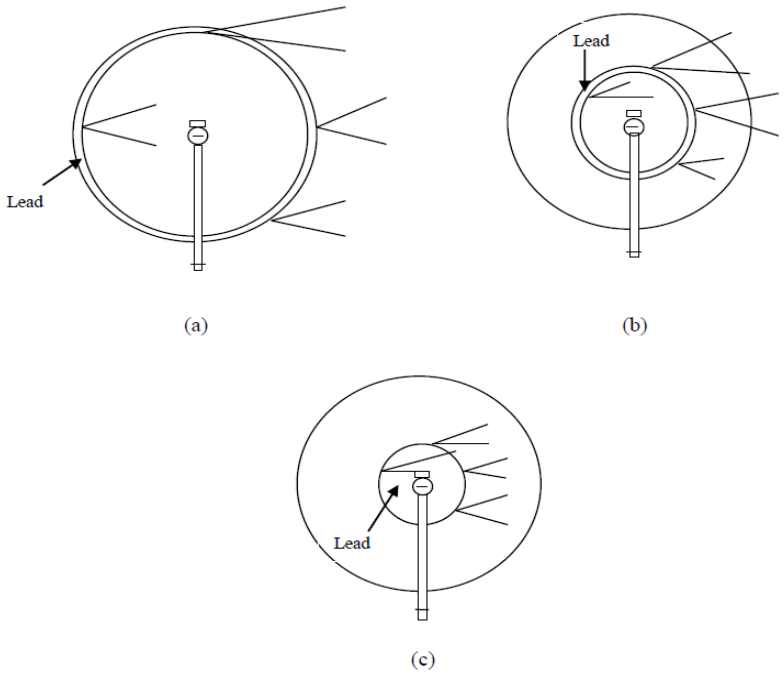


Fig. 1: (a) thin layer of lead wrapping the outer surface of a polyethylene moderator, (b) lead (shell) layer implanted in-between two moderators, and (c) Lead core surrounding the ^{3}He detector

3. Extended Bonner Sphere Spectrometer

It is observed from the different configuration of lead radiator that the Case (c), where lead core immediately surrounds the He-3 detector is most effective in neutron detection. An Extended BSS (EBSS) system is designed with a combination of lead core and five different sizes of polyethylene moderators. The diameter of the five moderators are 8.0, 14.2, 20.32, 25.40 and 30.48 cm. Table 1 gives the different configurations considered for the new BSS.

Table 1: Different configurations considered for the new BSS

Configuration	Combination
1	Bare He-3 detector
2	8 cm PE
3	14.2 cm PE (8cm Pb core)
4	14.2 cm PE (no Pb)
5	20.32 cm PE (8cm Pb core)
6	20.32 cm PE (no Pb)
7	25.40 cm PE (8cm Pb core)
8	25.40 cm PE (no Pb)
9	30.48 cm PE (8 cm Pb core)
10	30.48 cm PE (no Pb)

These 10 configurations gives a complete set of EBSS. A schematic drawing of the system is introduced in Fig. 2.

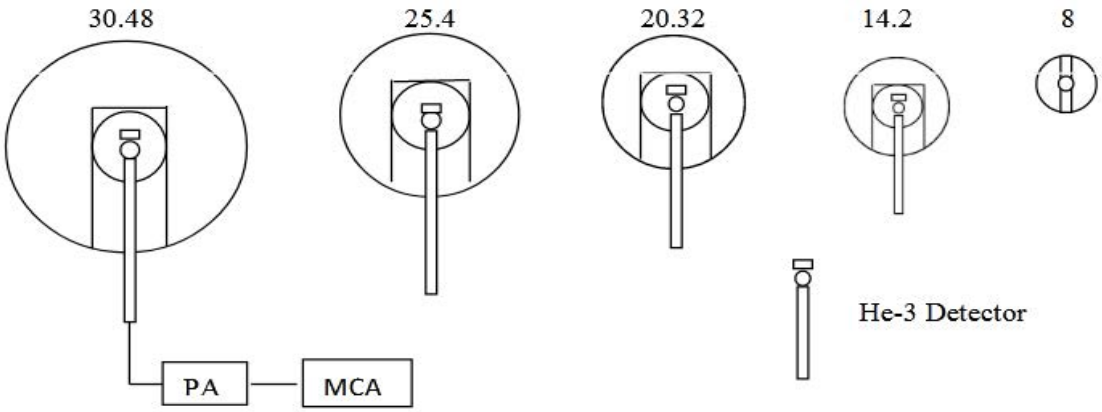


Fig2: Drawing of the extended Bonner sphere system

4. Calculation of the response matrix:

Response is defined as number of $^{3}He(n,p)^{3}H$ reactions taking place in the detector per unit flux [4]. The response matrix data should be measured using a series of mono-energetic neutron sources. However, due to lack of mono-energetic neutrons, the experimental measurement of the response matrix data is not possible. So, the response functions are generated by Monte Carlo simulation using MCNP code [3]. The source is randomly positioned at 1m away from EBSS and for bare and various moderator configurations, the rate of (n,p) reactions are tallied in MCNP. The thermal scattering law data S(α,β) has been used for hydrogen in Polyethylene to account for the molecular binding effects at low neutron energies [5]. Spectrum unfolding routine of EBSS uses response functions determined in 25 energy groups from thermal to 1 GeV. Response functions, as generated by the Monte Carlo N-Particle code, for the EBSS is shown in Fig. 3. The uncertainty of most calculated values is below 1% or 2%, but it reached up to 4% or 5% in a few cases.

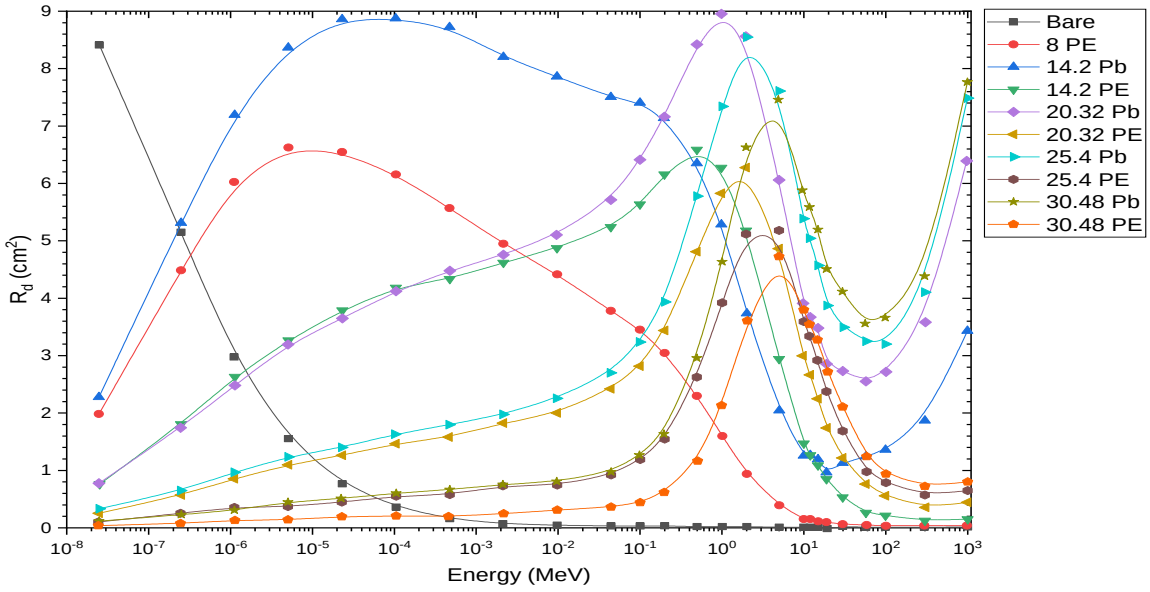


Fig3: Response Function curve for extended bonner sphere system.

5. Conclusion

A modified Bonner Sphere Spectrometer (BSS) is designed for measuring spectrum of high energy neutrons (>10MeV). The new system has a lower resolution at lower energy range basically due to fewer small spheres. Analysis of response function matrix of EBSS is similar like BSS, and hence more sensitive to lower energies. Compared to conventional BSS, the volume and the cross-section of the EBSS are more. In EBSS, the internal and external radii are adjusted to accommodate the lead embed. Due to its higher volume and surface area, the new system, EBSS, quantity of neutron incident is more and is added advantage. The difference in response function between spheres with and without lead is more striking for the smaller spheres, because fraction of the total moderator volume supplanted by lead is bigger. The response function of the configurations with Pb and PE in EBSS show increase in value beyond 100MeV. This suggests that the system can be used for high energy neutron spectrum measurements.

6. Acknowledgement

The authors would like to thank Shri Bilal Hassan Khan for kindly providing MCNP5 code, and advice on cross section installation. We also thank Dr. G. Pandikumar for useful discussions.

6. References

[1] C. Birattari, A. Ferrari, C. Nuccetelli, M. Pelliccioni, M.Silari, “Measurements and characterization of high-energy neutron fields “Nuclear Instr. and Meth. A 297 (1990) 250.

[2] J.B. McCaslin, in: H.W. Patterson, R.H. Thomas (Eds.), “Accelerator Health Physics”, Academic Press, New York,1981, pp. 621–626.

[3] Forrest Brown, "Monte Carlo Techniques for Nuclear Systems - Theory Lectures", LA-UR-16-29043, (2016)

[4] Robert Maglier et al, “Measuring neutron spectra in radiotherapy using the nested neutron spectrometer” Med. Phys. 42 (11), November 2015.

[5] Sujoy Sen, Subhrojit Bagchi, R.R. Prasad; “Determination of neutron energy spectrum at KAMINI shielding experiment location”.116, Applied Radiation and Isotopes, September, 2016.

TRITIUM PRODUCTION FROM LITHIUM UNDER IRRADIATION OF MOLTEN SALT FUEL IN A NUCLEAR REACTOR

Taresh Aggarwal*, Indrajeet Singh, Anurag Gupta, Umasankari K
Reactor Physics Design Division
Bhabha Atomic Research Centre, Mumbai, India
*taresh@barc.gov.in

Abstract

Tritium production & its permeation through structural materials is one of the challenges with molten salt based fuel cluster. Tritium is continuously generated due to neutron irradiation of salt as most of the salt configurations contain Lithium, Fluorine & Beryllium as one of their constituents. Most Tritium production occurs from ^{6}Li isotope of Lithium owing to its high neutron capture cross-section. In this paper, calculations for Tritium production from Lithium has been carried out for a given molten salt fuel configuration under neutron irradiation in a small research reactor.

Key words: Tritium production, Lithium, Molten salt reactors.

1. Introduction

Lithium is constituent of most of the salt configurations suggested for molten salt fuel based reactors owing to its ability to lower the melting points of these salts to a few hundred degrees Celsius. For operation of these reactors, it is desired to have low neutron absorption in Lithium to maintain neutron economy and minimizing Tritium production [1]. Lithium used in the salt must be enriched in ^{7}Li. ^{7}Li has a very small neutron absorption cross-section in comparison to ^{6}Li.^{6}Li thermal neutron absorption cross-section is around 940 barns. Lithium should be enriched beyond its natural 92.5% ^{7}Li level to minimise tritium production and to improve neutron economy.Various Tritium production pathways from molten salt fuel constituents [2]: In a molten salt based fuel configuration, containing Lithium as one of the constituent, primary Tritium producing reactions are: $^{6}Li\ (n,\ ^{3}H)\ ^{4}He$, having thermal microscopic cross-section of 940 b and $^{7}Li(n,\ n+^{3}H)^{4}He$, for which average microscopic cross-section is 20 mb. Other constituents such as ^{19}F & ternary events also contribute to Tritium production though have low relative production rates. Corresponding reaction for ^{19}F is $^{19}F(n,\ ^{3}H)^{17}O$. ^{6}Li, which is one of the major contributors for Tritium can be produced in situ from Beryllium [2] which is another common constituent with Lithium of most of the molten salt based fuel configurations. Corresponding reaction of ^{6}Li production from ^{9}Be is $^{9}Be(n,\ ^{3}H)^{7}Li$.However, salt used is not containing Beryllium so this reaction is not considered in present analysis.

Tritium formation can be alleviated by:

(a.) Removing some Tritium from salt by bubbling He gas through the salt (sparging)
(b.) Removing most of the Li6 from the Lithium (enrichment)

2. Reaction rate calculation using Monte Carlo simulations:

Monte Carlo is a stochastic method which is widely used in Reactor Physics for neutronics calculations. In this method probabilistic approach is used for sampling neutrons interacting in a medium. While simulating neutron histories tallies are accumulated for neutron flux, reaction rate etc. which are then averaged over all histories to obtain the required values of these quantities [3]. Reaction Rate corresponding to Tritium production per unit volume per unit time from Lithium isotope at operating power is defined as:

$$M \int \sigma(E)\phi(E)dE \tag{1}$$

where M is Lithium isotope number density & other symbols have their usual meanings.

To compute the total number of neutrons being produced per second, normalization factor has to be calculated at operating power. Representative value of operating power used for calculations corresponds to that of a small research reactor i.e. 100W.Since the Monte Carlo code results are normalized to one source neutron, the result has to be properly scaled in order to get absolute comparison to the measured quantities (flux, reaction rate, fission density, etc.). The neutron flux tally results can be scaled to a desired fission neutron source (power) level. The neutron birth rate in a fissile system can be calculated from the released energy per unit time i.e. the power of the system. The system producing power P needs $\frac{P}{w_f}$fission power per second, where $w_f$denotes effective energy released per fission event. Although the value of w_f will vary somewhat with the type of reactor and the detailed core composition, it is typically of the order of 200 MeV for steady state condition. This fission rate produces neutrons $\frac{P\nu}{w_f}$ per second, where ν denotes the average number of neutrons released per fission. Therefore, to normalize flux tally by the steady-state thermal power of a critical system, the following scaling factor in units of fission neutrons per unit time should be used [4].

$$C = \frac{P(w)\nu\left[\frac{\text{neutron}}{\text{fission}}\right]}{(1.6022E-13)\left(\frac{J}{Mev}\right)w_f(Mev/fission)} \tag{2}$$

The upper scaling factor is appropriate for critical i.e. steady-state power level systems only (k = 1). Tallies for subcritical and supercritical systems do not include any multiplication effects because fission is treated as absorption. Therefore, one must multiply the equation (2) by $\frac{1}{Keff}$on the right-hand side for subcritical and supercritical systems, respectively.

$$\phi\left[\frac{\text{neutron}}{cm2}.s\right] = C\text{x Flux Tally } [\frac{1}{cm2}] \tag{3}$$

where ϕ denotes the actual total neutron flux in the system.

2.1 Calculation of ^{6}Li &^{7}Li number densitiesin given molten salt based fuel:

Typical types of molten salts based fuels include Fluorides, Chlorides, mixtures/eutectic compositions. A molten salt mixture consists of different individual salt components mixed together into a multi-component system for e.g. LiF-NaF-KF (ternary mixture), LiF-BeF2(binary mixture) having different physical & chemical properties as compared with individual components. For example, melting points of each individual salt component are too high for coolant applications whereas mixing of several components into binary/ternary systems reduces the melting point of the resulting salt system to more practical levels [5].

Table 1: Weight fractions of different constituents of molten salt fuel

S No.	Salt constituent	Weight fraction
1.	^{7}Li	5.085E-02
2.	^{6}Li	5.137E-04
3.	^{19}F	3.352E-01
4.	^{235}U	4.294E-03
5.	^{238}U	6.091E-01

Different fissile & fertile isotopes of Uranium, Thorium in their fluoride form readily combines with these salt systems. The enrichment of Li in ^{7}Li is assumed to be 99% in the fuel salt under consideration with mole % of LiF is 74% and UF4 is 26%. Calculation have been carried out at room temperature i.e. 300K. The number densities of various elements in the salt is calculated and listed in Table-1. Fuel salt density is expected to change at different temperatures, so the number density change corresponding to the salt density variation is also given in Table-2.

Table 2: Calculated values of number densities of ^{6}Li &^{7}Li in molten salt fuel at a given salt density

S No.	Density of salt (g/cc)	Mass density (g/cc) (^{6}Li)	Number density (^{6}Li)	Mass density (g/cc) (^{7}Li)	Number density (^{7}Li)
1.	3.199	1.6437E-03	1.6326E20	1.6272E-01	1.3967E22
2.	2.814	1.4453E-03	1.4355E20	1.4309E-01	1.2282E22
3.	3.519	1.8080E-03	1.7958E20	1.7899E-01	1.5363E22

2.1 Calculation of Tritium production from ^{6}Li &^{7}Li:

To achieve statistically good results total 1050 batches of 10000 neutrons are used in the present Monte Carlo analysis. To allow uniform fission source distribution 50 batches with 10000 neutron histories discarded in each calculation. Statistical error in Tritium production calculation using Monte Carlo simulations for ^{6}Li case is in the range of ±0.25% & for ^{7}Li is in the range of ±2%.

Table 3: Calculated values of Tritium produced from ^{6}Li &^{7}Li at given salt density using Monte Carlo simulations.

S No.	Density of Salt (g/cc)	Reaction rate for Tritium production (per unit volume per second) (from ^{6}Li)	Weight of Tritium produced (g/cc/s) (from ^{6}Li)	Reaction rate for Tritium production (per unit volume per second) (from ^{7}Li)	Weight of Tritium produced (g/cc/s) (from ^{7}Li)
1.	3.19983	8.040E+06	4.026E-17	2.493E+03	1.248E-20
2.	2.81385	7.694 E+06	3.853E-17	2.563E+03	1.283E-20
3.	3.51981	8.336 E+06	4.175E-17	3.447E+03	1.726E-20

Reaction rates tabulated in Table 3 shows Tritium atom production rate of the order of 10^{3} from ^{7}Li though it is having very low neutron absorption cross-section (~20 mb) as compared with ^{6}Li which is having a much higher neutron absorption cross-section (~940 b) and have production rate of Tritium of the order of 10^{6} . This can be attributed to the fact that fuel salt used is 99% enriched in ^{7}Li isotope of Lithium leading to low number density of ^{6}Li as compared with ^{7}Li isotope of Lithium despite having large neutron absorption cross-section relative to ^{7}Li isotope.

3. Results &Discussion:

Calculated values of Tritium production rate per unit volume from irradiation of fuel salt are summarized in table 4. A 10 % decrease & increase is also considered in the density of fuel salt from the representative value of 3.19983 g/cc for calculation of Tritium production rate. Major contribution to Tritium production is from Li-6 isotope of Lithium. Total volume of Tritium produced will depend upon volume of salt being irradiated and time of irradiation. Tritium production rate for all three fuel salt densities is of the order of 10^{-17} g/cc/s. For a representative irradiation time of 24 hours or 1 day & fuel salt volume of 6000 cm^{3} total Tritium produced from Lithium is of the order of 10^{-8}g.

Table 4: Tritium produced rate from Lithium at given salt density

Lithium Isotope	Tritium production (Salt density = 3.19983 g/cc) (g/cc/s)	Tritium production (Salt density = 2.81385 g/cc) (g/cc/s)	Tritium production (Salt density = 3.51981 g/cc) (g/cc/s)
Li-6	4.0264E-17	3.8533E-17	4.1749E-17
Li-7	1.2485E-20	1.2835E-20	1.7261E-20
Total	**4.0276E-17**	**3.8545E-17**	**4.1766E-17**

Table 5: Tritium produced from Lithium at given salt density for a representative irradiation time & fuel salt volume

Tritium produced for a representative irradiation time & fuel salt volume (Irradiation time = 24 Hours = 1Day & Fuel Salt Volume = 6000 cm^3			
Lithium Isotope	**Tritium production (Salt density = 3.19983 g/cc) (g)**	**Tritium production (Salt density = 2.81385 g/cc) (g)**	**Tritium production (Salt density = 3.51981 g/cc) (g)**
Li-6	2.09E-08	2.00E-08	2.16E-08
Li-7	6.47E-12	6.65E-12	8.95E-12
Total	**2.09E-08**	**2.00E-08**	**2.17E-08**

4. Conclusion

Contribution of Tritium from Lithium isotopes ^{6}Li and ^{7}Li is calculated using Monte-Carlo simulations for a given molten salt configuration at different salt densities, irradiated under neutron flux of the order of a small research reactor.Results shows that the major contributor to the Tritium production is ^{6}Liisotope of Lithium due to high neutron capture cross-section. Tritium production rate & total Tritium produced for a representative irradiation time & fuel salt volume is found to be quite low.

5. References

[1] Charles W. Forsberg et al,"Tritium Control and Capture in Salt-cooled Fission and Fusion Reactors: Status, Challenges, and Path Forward", ANS-Nuclear Technology (Volume 197) Februrary-2017.

[2] Hans A. Schmutz, PiyushSabharwall, Carl Stoots, "Tritium Formation and Mitigation in High Temperature Reactors", Idaho National Laboratory, August 2012.

[3] P. Mohanakrishnan, Om Pal Singh, K. Umasankari "Physics of Nuclear Reactors", Academic Press, 2021.

[4] Luka Snoj, MatjažRavnik, "Calculation of Power Density with MCNP in TRIGA reactor",International Conference Nuclear Energy for New Europe 2006 Portorož, Slovenia, September 18-21, 2006.

[5] Mark Anderson et al, Heat Transfer Salts for Nuclear Reactor Systems - Chemistry Control, Corrosion Mitigation, and Modelling, Project report No. 10-905, NEUP, US DOE.

ISOTOPIC FISSION RATE AND POWER DISTRIBUTION FOR PFBR BOL CORE EMPLOYING MONTE CARLO TRANSPORT

Bilal Hassan Khan[1]
[1] Indira Gandhi Centre for Atomic Research, Kalpakkam, India
[1]*e-mail: bhk780@igcar.gov.in*

Abstract

Fission rate distribution is important for monitoring different aspects of reactor performance parameters. These can be used for power profiling, detector count rate mapping etc. A homogenized PFBR BOL core configuration has been modelled using 3D Monte Carlo transport with latest ENDF/B-VIII.0 cross section data to estimate isotopic reaction rates at different core locations. These fission rates were scaled with proper scaling factor to give the power distribution profile for 1250 MW thermal BOL core configuration.

1. Introduction

The multiplication factor is one of the most important properties of any fissile system. In the study of the steady-state solution of Boltzmann transport equation, K-eff is the multiplication factor which changes the relative level of the fission source in order to balance the neutron Boltzmann equation. MCNP employs the collision, track length, absorption estimators to estimate K-effective. These take advantage of the definition of neutron production rate $\nu\Sigma_f\phi$, in which all of the estimators are multiplied by the number of neutrons per fission ν and the fission cross section Σ_f. At the end of the problem, all three estimates are combined after which an overall combined cumulative estimate based on all the data is given. An attempt has been made to estimate the radial and isotopic fission rate distribution for PFBR BOL by tallying the $\Sigma_f\phi$ at different radial locations and for individual isotopes.

F4 and multiplier tally in MCNP [1] employs equation (1) to compute the reaction rates at different cell locations

$$F_R = C \int_{E_{min}}^{E_{max}} \Phi_{f4}(E)\,\sigma_r(E)\,dE \tag{1}$$

where the constant C is any arbitrary scalar quantity that can be used for normalization, Φ_{f4} is flux score in F4 tally, $\sigma_r(E)$ is microscopic cross section for reaction R taken from cross-section libraries and E_{min} and E_{max} denote minimum and maximum neutron energy in the system (usually 0 and 20 MeV, respectively). F_R is the reaction rate for reaction R.

Since the MCNP results are normalized to one source primary, the result needs to be properly scaled in order to get absolute comparison to the measured quantities (flux, reaction rate, fission density, etc.). The F4 tally results can be scaled to a desired fission neutron source (power) level. The scaling factor can be entered on the FM (tally multiplier) card or can be applied outside the code. The scaling factor S is computed for a desired power level as

$$S = \frac{P(W)}{1.6022 * 10^{-13}\,\frac{J}{MeV} * w_f\left(\frac{MeV}{fission}\right) * F_t\left(\frac{fissions}{sp * sec}\right)} \tag{2}$$

Where P(W) is the total thermal power to which one wishes to scale, w_f is the average energy released per fission and F_t is the total fission rate per primary given by f4 multiplier tally.

The option for calculation of power density is much simpler, but it has some limitations. This option is particularly useful when we want to calculate the power density in individual cells or fuel elements. First, we calculate fission density (normalized "per atom") i.e. calculate F_f in each cell containing fissile material and obtain

$$\left(F_f\right)_i = \left(C\int \Phi(E)\sigma_f(E)dE\right)_i \tag{3}$$

Where i denotes the cell index and C the atom density. Since the power produced in one cell is linearly proportional to the number of fissions in that cell, we can calculate the power produced in cell i, Pi, by multiplying the fissile system thermal power, P, by the relative number of fissions in cell i. As the relative number of fissions in cell i is proportional to the product of fission density in cell i and the volume of cell i, we obtain

$$P_i = \frac{\left(F_f\right)_i V_i}{\sum_i \left(F_f\right)_i V_i} P \tag{4}$$

2. Reactor modelling

PFBR core at its BOL state consists of 88 core-1 & 87 core-2 FSAs, 8 diluents, 1 ICSA at center, 3 Source SAs and 114 RB assemblies [2]. The reactor has been provided with 9 Control and Safety Rods (CSRs) distributed in 3rd and 6th ring of core, for startup, control of reactor power & controlled shutdown. 3 Diverse Safety Rods (DSR) in 3rd ring is only to SCRAM the reactor. For both the type of rods, B4C is chosen as the absorber material. BOL core has been modeled with all control and safety rods out. ICSA the central SA location is designated with ring location R0 and surrounding six SA's as R1 and so on. Homogenized material density data has been prepared using ATOMIX. ENDF/B-VIII.0 cross-section library data has been used to carry out the analysis. Fig 2 shows the ring location of different type of SA's with the quarter sectional view of PFBR BOL core while all other quarters being symmetric except the source SA which share 120-degree symmetric location.

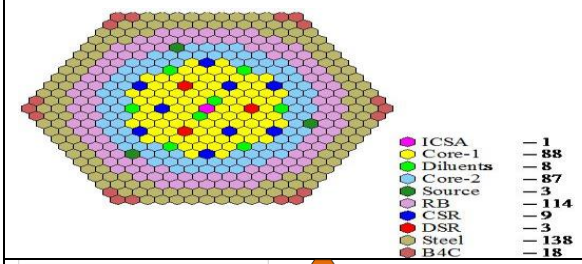


Figure 1 Core Configuration of PFBR BOL Core

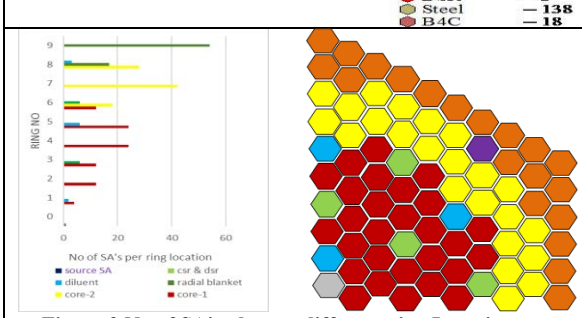


Figure 2 No of SA's along with quarter sectional view **different ring Locations**

3. Results

Using F4 tally and multiplier cards with isotopic number densities and fission cross section from ENDF/B-VIII.0 data library, isotopic fission rates per primary start particle at different locations have been estimated. The actual fission rates at a given power level are obtained by scaling with the scaling factor computed in equation (2) which are tabulated in table 1.0. Table 1.0 also displays Avg. υ for different isotopes and the percentage contribution to fission rate from different isotopes. It is evident that Pu-239, U-238 and Pu-241 along with Pu-240 are the major contributors to the total fission rate

with majority up to 73% coming from Pu-239,11% from U-238,7% from Pu-241 and 4% coming from Pu-240.

The power and fission rates from different SA's at different radial locations are given in table 2.0. and plotted in figure 3-4 respectively. The average isotopic fission rates and average power per SA shows a decreasing trend when going from core centre to core periphery. The results also highlight that the power of the order of 25 MWt comes from regions like RB, Diluents, LAB and UAB's which is contributed from the fissions taking place in uranium-based blanket.

Table 1.0 isotopic fission rate distributions in different regions.

Region	Fission rate							Power (MW)
	U-235	U-238	Pu-239	Pu-240	Pu-241	Pu-242	Total (Σi)	
Core-I	2.36E+17	2.01E+18	1.54E+19	1.12E+18	1.67E+18	4.35E+16	2.05E+19	6.50E+02
Core-II	1.35E+17	1.38E+18	1.32E+19	7.92E+17	1.41E+18	4.22E+16	1.73E+19	5.49E+02
ICSA	6.87E+14	3.84E+15	4.31E+16	2.47E+15	4.86E+15	4.31E+14	5.50E+16	1.74E+00
Source	7.99E+14	6.92E+15	7.62E+16	4.12E+15	8.32E+15	2.15E+14	9.79E+16	3.11E+00
Diluents	4.00E+16	2.04E+17					2.44E+17	7.74E+00
RB	2.40E+17	5.89E+17					8.29E+17	2.63E+01
LAB -UAB (C-I)	7.92E+16	1.69E+17					2.48E+17	7.87E+00
LAB -UAB (C-II)	4.94E+16	1.16E+17					1.66E+17	5.27E+00
Total (Σr)	7.81E+17	4.48E+18	2.88E+19	1.92E+18	3.10E+18	8.63E+16	3.94E+19	1.25E+03
Avg. υ	2.401	2.738	2.938	3.044	2.966	3.114	2.917	
Percentage %	1.98	11.37	73.01	4.87	7.86	0.22	100	

Table 2.0 Avg. Fission and power distribution of different SA types at different ring locations.

SA type	Avg. Fission rate (fissions/sec) /SA	Avg. power(MW)/SA	Ring Location
ICSA	5.50E+16	1.75E+00	R0
CORE-I	2.58E+17	8.17E+00	R1
	2.53E+17	8.02E+00	R2
	2.45E+17	7.78E+00	R3
	2.21E+17	7.00E+00	R4
	2.15E+17	6.81E+00	R5
	2.05E+17	6.50E+00	R6
CORE-II	2.26E+17	7.18E+00	R6
	1.60E+17	5.07E+00	R7
	1.51E+17	4.80E+00	R8
DILUENTS	2.57E+16	8.16E-01	R1
	2.39E+16	7.58E-01	R5
RADIAL BLANKET	8.57E+15	2.72E-01	R8
	2.74E+15	8.70E-02	R9
SOURCE	3.19E+16	1.01E+00	R8

650 MW is generated in Core I region with average of around 7 MW/SA and 549 MW is registered in Core II region with average around 5 MW/SA. Thermal power of 1.75 MW 3.11 MW is

registered in ICSA and Source SA's tallies. The power distribution can be further refined by employing mesh tally wherein even 1 m x 1mm x 1mm small bins can be defined and the tallies can be stored in these bins. This is important for detailed LHR, power peaking estimations for pin level reactor profiling.

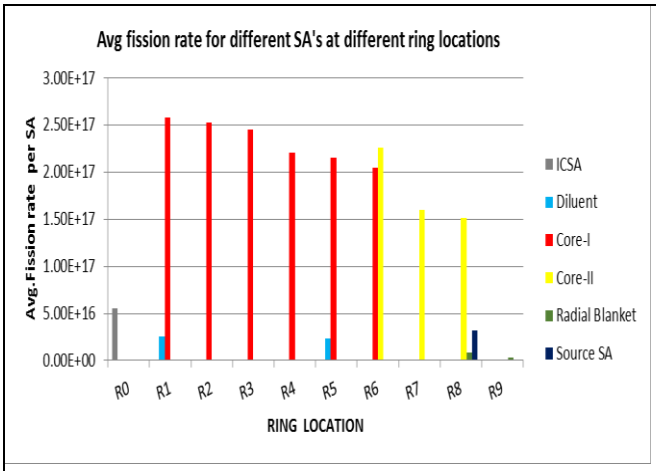


Figure 3

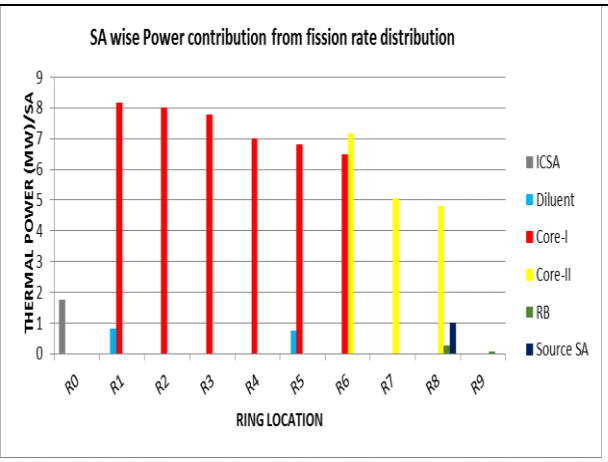


Figure 4

4. Conclusion

Above study establishes the fact that U-238 has a significant contribution of the order of 10% in the overall fission rate. The power contribution from radial blankets, Diluents, LAB & UAB mainly comes from U-238 fissions but the overall isotopic contribution to core reactivity can be established by individual isotopic reactivity worth's which account for other types of reactions also. Apart from this the study provides an insight into the power contribution by different types of SA's at different locations. This is significant in designing a suitable coolant flow profile at different power levels. When one gets familiarised with normalizing the results to a certain power level, Monte Carlo Transport becomes a versatile calculation tool for various reactor physics calculations.

5. References

[1] J.J. Briesmeister, "MCNP5- A General Monte Carlo N-Particle Transport Code, Version 5 Los Alamos National Laboratory", March, 2005.

[2] PFBR/FSAR/R-0/MAR10 Chapter 5.1, Reactor Physics, (2016).

ESTIMATION OF SHIELD REQUIREMENT FOR X-RAY RADIOGRAPHY FACILITY IN FRFCF

M. M. Shanthi, B. Sivakumar, D. Sunil Kumar,
A. John Arul, G. Sivasankaran and S. Raghupathy
Indira Gandhi Centre for Atomic Research, Kalpakkam, India
e-mail: - shanthi@igcar.gov.in

Abstract

Fuel fabrication plant of Fast Reactor Fuel Cycle Facility (FRFCF) is designed for the production of MOX fuel pin. As a part of quality control of PFBR fuel fabrication, these fuel pins are subjected to X-ray radiography to check the structural integrity of end plug weld. In this study neutron and gamma dose rate due to fuel pin and the X-ray source are estimated by simulating the geometric details of the X-ray radiography facility using 3D transport code MCNP[1]. The optimized shield thickness required for the facility is also estimated and discussed. To get reliable result importance sampling technique has been implemented.

1. Introduction

The X-ray radiography facility contains a fuel pin tray and an X-ray source (225 kV). The fuel pin tray is kept at an elevation of 80 cm from the floor level and the X-ray source is kept at an elevation of 130 cm. The position of the fuel pin tray is fixed. During scanning only the X- ray source will be moved along the length of the fuel pin. The stroke length of the X-ray source is 50 cm. So it can be moved up and down between the elevations 130 cm to 180 cm for better resolution. Movement of the X-ray source is taken care in the calculations for estimating the peak dose rate. Fuel pin tray contains 8 fuel pins, which are kept 1.8 cm apart. The dimension of the facility is 580 cm x 530 cm x 485 cm. The schematic of the facility is given in Figure 1. Annular MOX fuel pellets and solid blanket pellets (depleted UO_2) are stacked and loaded into the clad tubes made up of D9 steel. The length of the fuel pin is 258 cm. Radiograph of the fuel pin will be recorded either in an X-ray film or in a flat panel detector kept below the fuel pin.

2. Radiation sources

Fresh fuel pin contains both neutron and gamma ray sources. Neutron sources come from spontaneous fission and (α,n) reaction. Major sources of gamma radiations from the fuel pin are actinides and fission product impurities of the reprocessed mixed oxide fuel. Hence for dose estimation in addition to the X-ray source, neutron and gamma radiations from 8 fuel pins kept in the fuel pin tray are also considered. The neutron and gamma source strength per pin are 3.68E+4 n/s/pin [2] and 9.68E+10 γ/s/pin [3] respectively. X-ray photon source strength is estimated based on the X-ray photon intensity, leakage radiation and beam divergence given in the product specification [4]. Estimated X-ray photon source strength is 1.5448E+10 photons/s.

3. Design criteria [5, 6]

Shields are designed such that the dose rates in full occupancy area do not exceed 1μSv/h .

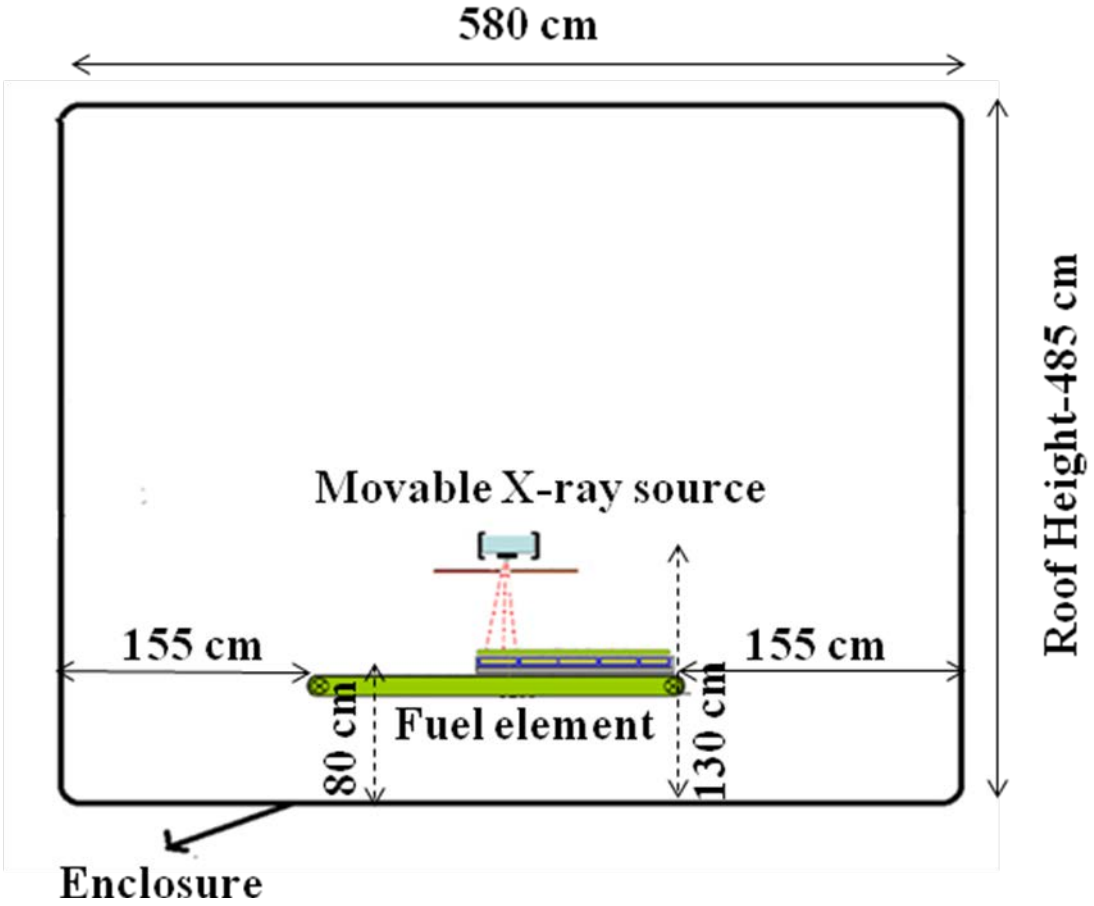


Figure 1 Schematic of the X-ray radiography facility (Sectional view)

4. Calculation Details

Detailed model of the helium bonded annular fuel pin is modeled using MCNP. Neutron and gamma transport calculations carried out separately to estimate the total dose rate. While scanning the fuel pin, X-ray source will be moved from one end of the fuel pin to other end. So dose due to X-ray source on all six sides are estimated separately by keeping the source above the bottom plug (left end) of the fuel pin, center of the fuel region and above the top plug (right end) of the fuel pin. The maximum dose rates on each side of the room are considered for shield design. For the purpose of dose estimation 10 cm^3 meshes are created virtually around the enclosure as shown in Figure 2 using lattice option of MCNP.

5. Results and Discussion

Dose rate due to neutron and gamma are estimated at all mesh points using F4 tally (calculates flux averaged over a cell). The total dose rate at each mesh point is calculated and the peak value of the total dose rate is given in Table 1. Without shield, the estimated peak total dose rates along

the length (front/back), breadth (left/right), bottom, and top side of the room are 24.6 μSv/h, 12.8 μSv/h, 2760 μSv/h, and 13.3 μSv/h respectively. Gamma rays from fuel pin mainly decide the dose rate on all sides except at the bottom. Dose rate at the bottom is dictated by X-ray photons. Dose due to neutron is less compared to other sources. Since Lead is a good gamma shield material, it is chosen for designing the shield.

Many neutron and gamma transport calculations have been carried out to optimize the shield thickness. To meet the design limit of 1 μSv/h, shield thicknesses required along the length and breadth side of the room are 38 cm Lead, and 36 cm Lead respectively. 17 cm Lead shield is required for the top side. Since the active fuel portion is very close to the floor, the neutron dose rates is more at the bottom compared to other sides. Hence, to attenuate both the neutron and gamma the bottom side requires 11.5 cm polyethylene followed by 8 cm Lead shield. The sectional view of the enclosure with shield is shown in Figure 3. The peak total dose rates and corresponding neutron and gamma dose rates on each side of the room with shield are given in Table 2.

Table 1: Estimated peak total dose rate without shield

Side	Neutron (μSv/h)	Gamma (μSv/h)	X ray (μSv/h)	Total (μSv/h)
Left (-X)	0.32	7.75	4.73	12.80
Right (X)	0.31	9.90	1.83	12.00
Front (-Y)	0.42	21.60	1.51	23.50
Back (Y)	0.43	22.60	1.54	24.60
Bottom (-Z)	1.82	72	2680	2760
Top (Z)	0.20	12.10	1.00	13.30

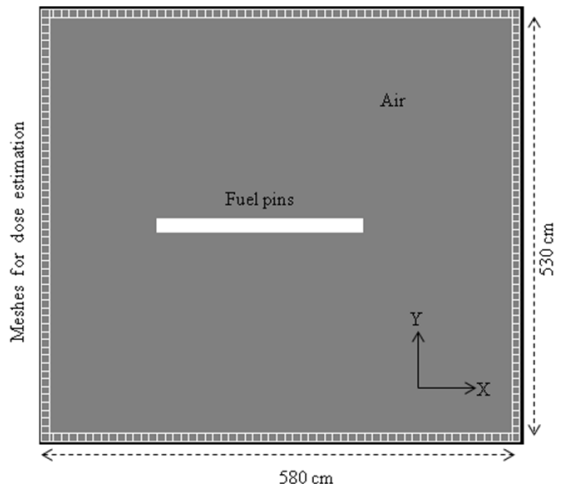


Figure 2 Plan view of the X-ray radiography facility without shield (simulated using MCNP)

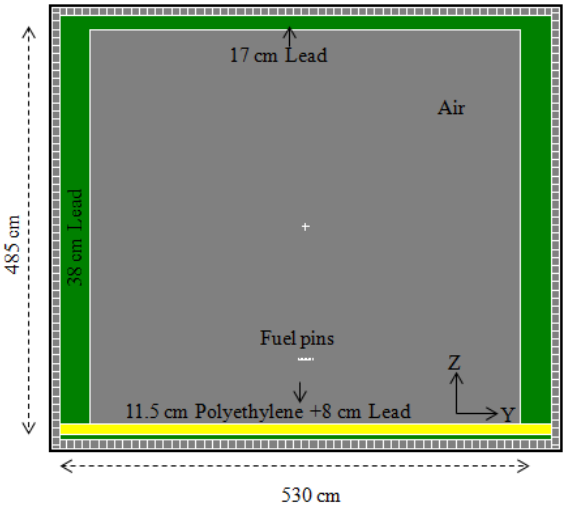


Figure 3 Sectional view of the X-ray radiography facility with shield (simulated using MCNP)

Table 2: Estimated peak total dose rate with shield

Side	Neutron (μSv/h)	Capture gamma (μSv/h)	Gamma (μSv/h)	X ray (μSv/h)	Total (μSv/h)
Left (-X)	1.38E-02	5.04E-04	3.14E-01	9.75E-03	3.38E-01
Right (X)	1.40E-02	5.10E-04	3.78E-01	3.40E-03	3.95E-01
Front (-Y)	1.21E-02	4.59E-04	3.85E-01	1.89E-03	4.00E-01
Back (Y)	1.43E-02	5.24E-04	2.99E-01	7.38E-04	3.14E-01
Bottom (-Z)	3.47E-01	8.33E-04	1.27E-01	0.00E+00	4.75E-01
Top (Z)	3.59E-01	8.29E-05	0.00E+00	0.00E+00	3.59E-01

6. Conclusion

Shield requirement for the X-ray radiography facility in FRFCF has been carried using 3D transport code MCNP. Calculations show that to meet the design limit of 1μSv/h, the shield thicknesses required along the length side, along the breadth side, and on the roof of the facility are 38 cm Lead, 36 cm Lead, and 17 cm Lead respectively. But for the floor 11.5 cm polyethylene followed by 8 cm Lead shield is required. Maximum dose rate estimated with this shield configuration is less than 0.5 μSv/h.

7. References

[1] Judith F. Briesmeister, (Editor) "MCNP – A general Monte Carlo N-Particle transport code", Version 4C, dated March 22, 2001.

[2] G. Pandikumar and V.Gopalakrishnan, "Nsource: Acode for calculating (α,n) and spontaneous fission neutron sources and spectra", RPD/NDS/139, April 2010.

[3] G.Radhakrishnan, "Shield design of core subassembly plant vault", FRFCF/60111/DN/1000/R-D, August 2011.

[4] Comet ,MXR-225HP/11, Product specification, version 7, 2018.

[5] R. Indira, "Shield design specifications", PFBR/01115/DN/1074, R-A, January 2001.

[6] Rajeev R.Prasad and Sujoy Sen, "Calculations and design of shield for 225 keV, 10 mAX-ray RABIT facility", RSDD/RSS/310, March 2013.

Advances in Reactor Physics (ARP-2022)
Mumbai, India, May. 18-21, 2022

DEVELOPMENT OF INVERSE KINETICS MODULE TO EVALUATE CONTROL ROD WORTHS AND SOURCE TERM ESTIMATION

Mainak Mallick[1], T. Sathiyasheela
Indira Gandhi Center for Atomic Research, Kalpakkam, India
e-mail: - *mainak@igcar.gov.in*

Abstract

This study has been initiated with a major focus to develop an in house code for carrying out inverse kinetics with high accuracy which can be used to predict control rod worth. This approach is also made to estimate the source term which is significantly important when the reactor is operating at low power. The code is validated against DSR drop and CSR rod balancing simulation experiment of PFBR.

1. Introduction

Control rods are playing an important role in controlling power and assuring safety of nuclear power plant. Control rod is withdrawn from or inserted into the reactor core in order to change the reactivity of the reactor and also to change the neutron flux. Determining worth of control rods is important during the reactor operation. Hence an inverse kinetics tool is developed to estimate the reactivity from the known power profile. It is based on point-reactor kinetics model where the variations in shape of the neutron flux across the reactor as a function of time is ignored. When the reactor is operating at steady state full power condition, source term is ignored during the simulation as its contribution is very small. However the contribution of source term is significant when the reactor is operating in the subcritical state and hence it must be taken into account for the simulations. In this present study an inverse kinetics module is developed and it is validated against DSR drop and CSR balancing experiment of PFBR. The source term contribution is also estimated and verified with the input data.

2. Methodologies involved in Inverse-Kinetics and source term estimation

The standard point-reactor kinetics model can be written in the following way [1]

$$\frac{dn(t)}{dt} = \frac{\rho(t)-\beta}{\Lambda} n(t) + \sum_{i=1}^{m} \lambda_i C_i(t) + S \qquad \text{..... 1}$$

$$\frac{dC_i(t)}{dt} = \frac{\beta_i}{\Lambda} n(t) - \lambda_i C_i(t) \qquad for\ i = 1,2,\dots,m \qquad \text{..... 2}$$

Where *n(t)* is the neutron density in the core, C_i is the precursor concentration of delayed neutrons of group *i*. *S* is the neutron source strength, Λ is the neutron generation time and ρ is the reactivity to be determined. *S* is assumed to be constant in time. β_i and λ_i are the fraction and decay constant of group *i*. By rearranging the equation (2)

$$C_i(t) = \frac{\beta_i}{\Lambda} \int_{-\infty}^{t} e^{-\lambda_i (t-t')} n(t') dt' \qquad \text{..... 3}$$

By substituting equation (3) in equation (1) it is possible to express $\rho(t)$ as a function of $n(t)$:

$$\rho(t) = \beta - \frac{1}{n(t)} \sum_i \beta_i \lambda_i \int_{-\infty}^{t} e^{-\lambda_i (t-t')} n(t') dt' - \frac{\Lambda S}{n(t)} + \frac{\Lambda}{n(t)} \frac{dn}{dt} \qquad \text{..... 4}$$

As the measured quantity in reactor is power P(t) and it is proportional to neutron density n(t), hence equation (4) can be written as

$$\rho(t) = \beta - \frac{1}{P(t)}\sum_i \beta_i\lambda_i \int_{-\infty}^{t} e^{-\lambda_i(t-t')}P(t')dt' - \frac{\Lambda S}{P(t)} + \frac{\Lambda}{P(t)}\frac{dP}{dt} \quad \text{..... 5}$$

The integral which is present in equation (5) is solved by using the following recursive relation [2]:

$$I_n = \int_{-\infty}^{t_n} e^{-\lambda_i(t_n-t')}P(t')dt'$$

$$= e^{-\lambda_i\Delta t}I_{n-1} + \int_{t_{n-1}}^{t_n}\left\{P_n - (t_n - t') \times \frac{P_n - P_{n-1}}{\Delta t}\right\} e^{-\lambda_i(t_n-t')}\, dt'$$

$$= e^{-\lambda_i\Delta t}I_{n-1} + \frac{P_n}{\lambda_i}\left(1 - \frac{1-e^{-\lambda_i\Delta t}}{\lambda_i\Delta t}\right) - \frac{P_{n-1}}{\lambda_i}\left(e^{-\lambda_i\Delta t} - \frac{1-e^{-\lambda_i\Delta t}}{\lambda_i\Delta t}\right) \quad \text{..... 6}$$

Equation (5) is re-arranged by introducing the following function g(t),

$$g(t) = \sum_i \beta_i\lambda_i \int_{-\infty}^{t} e^{-\lambda_i(t-t')}P(t')dt' \quad \text{..... 7}$$

$$or,\ \rho(t) = \beta - \frac{g(t)}{P(t)} - \frac{S_p}{P(t)}$$

$$or,\ g(t) = (\beta - \rho_2)P(t) - S_p \quad \text{..... 8}$$

g(t) and P(t) is fitted in a straight line to obtain the slope and intercept. The intercept represents the source term. The fitting has been done by using least square method.

3. Results

The power profile of DSR rod drop and CSR rod balance experiment of PFBR are simulated using transient analysis code PREDIS [3]. This power profile is validated against the inverse kinetics code. The experiment is assumed to be performed at such a power level so that the reactivity feedbacks are ignored and the source term contribution is neglected.

3.1. DSR rod drop experiment simulation:

In this simulation one DSR of PFBR is dropped first, then two DSR's are dropped together and then three DSR's are dropped together and the power profile is obtained. Motion of the rods is simulated using accelerated phase, terminal velocity phase and then decelerated phase [4]. The power profile is shown in Fig. 1. The integral worth of the rods is determined using inverse kinetics code, which is shown in Fig. 2. The comparison between input and output worth data is shown in Table-1.

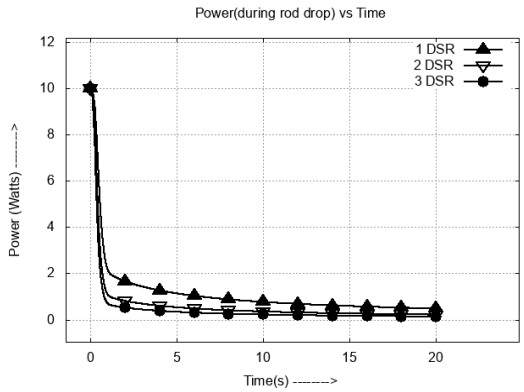


Fig 1: Power as a function of time when 1, 2 and 3 DSRs are dropped

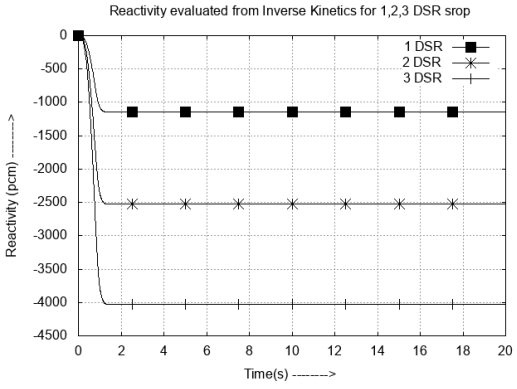


Fig 2: Reactivity as a function of time when 1, 2 and 3 DSRs are dropped

Table 1: Comparison of input and output results

Number of DSRs Dropped	Given Reactivity worth as input (pcm)	From inverse kinetics (pcm)
1 DSR	1144	1144
2 DSR	2522	2521.97
3 DSR	4022	4021.89

3.2. CSR rod balancing experiment simulation:

In this simulation a pair of diagonally opposite control rod of PFBR is chosen and one rod is inserted into the core where the other rod is withdrawn from the core. Initially the power is allowed to be stabilized at certain level by making the reactor critical and then movement of CSR is initialized. The CSR which is at the fully withdrawn position is marked as CSR 1 and the other one is marked as CSR 2. First CSR 1 is inserted, thus making the reactor subcritical hence the power decreases. A lower limit is set on the power level at which, the insertion of the CSR 1 is stopped. Withdrawal of CSR 2 starts and power level starts increasing, an upper limit is set on the power level, at which the rod withdrawal stops and rod insertion takes place. 50 pcm of positive and negative reactivity is added periodically in the reactor to simulate the experiment. This repetitive process goes on unless one rod is completely in and the other rod is completely out. The variation of input reactivity is shown in Fig. 3 and the power profile obtained from PREDIS is shown in Fig. 4. The integral worth calculated through inverse kinetics code is validated against the given input reactivity worth.

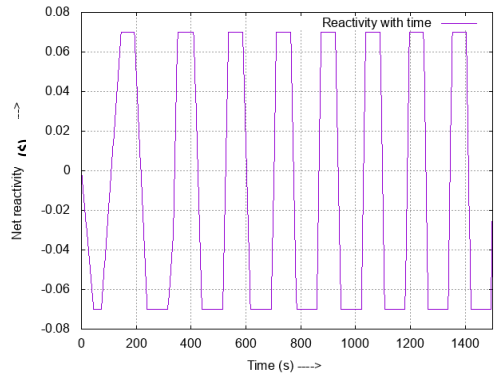


Fig 3: Variation of input reactivity with time in rod balance method

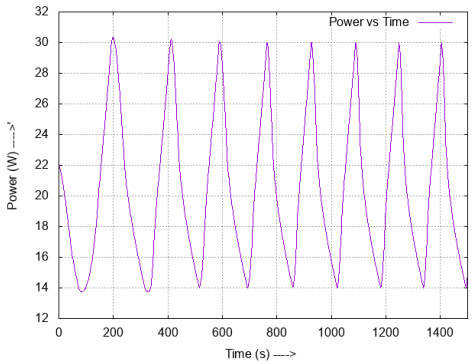


Fig 4: Variation of Power with time in rod balance method

Table 2 : Comaprison of input and output results for CSR rod balancing ion PFBR

	Input integral worth(pcm)	Integral worth calculated through inverse kinetics(pcm)	Error
CSR 1	1110	1106	0.36 %
CSR 2	1110	1104	0.18%

3.3 Results of source term estimation

It is assumed that the reactor is operating at sub critical steady state with $\rho = -500\ pcm$, P = 1.2427 W and S_p = 0.006215 W/s. Then, at time t = 10 second, the reactivity is changed to -200 pcm and a steady state is achieved with P = 3.106 W. The variation of power with time is obtained from transient code PREDIS which is shown in Fig. 5. Using the power profile a variation in $g(t)$ is obtained from equation (7). From the obtained $g(t)\ vs.P(t)$ data set

using least square fit method, the value of intercept obtained is: 0.0065959 W/s. This indicates the value of source term which is obtained as an output of the program. This is close to the input source term value 0.006215 W/s

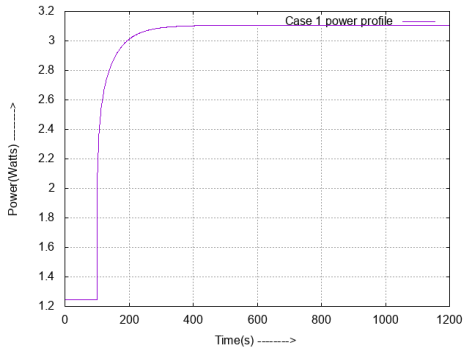


Fig 5: Time vs Power plot when the reactor is perturbed from -500 pcm to -200 pcm

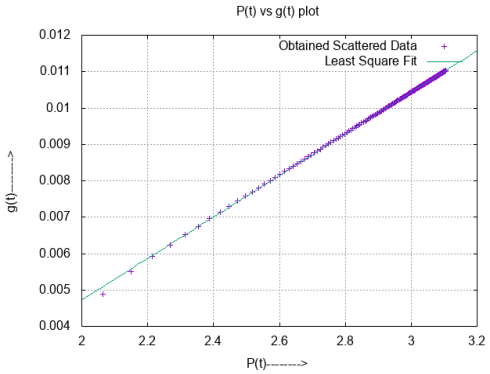


Fig 6: Least Square fit for the obtained between g(t) and P(t)

4. Conclusion :

An in house code is developed to carry out inverse kinetics analysis. The code is validated against the DSR drop and CSR rod balancing simulation experiments. It is also validated against the source term estimation. From the validation, it is understood that, the accuracy of the results obtained through this module is reliable and can be used for the determination of control rod worth in future.

5. References :

[1] Keepin G. R. (1965) *Physics of Nuclear Kinetics.* Addison-Wesley, New York

[2] J. E. Hoogenboom and A. R. Van Der Sluus, “Neutron Source Strength Determination for On-line Reactivity Measurements”, Delft University of Technology, Interfaculty Reactor Institute, The Netherlands, July 5, 1988

[3] R. Harish, et. al., KALDIS : “A Computer Code System for Core Disruptive Accident Analysis in Fast Reactors”, IGCAR Report, IGC – 208 (1999)

[4] Vaibhav Khulbey, Subhadip Kirtan, Nakul Choudhury, “Analysis of Error in Reactivity Worth of DSR in Rod Drop Mechanism for Various Methods in PFBR”, PFBR/TSG/RP/IR/11

INVESTIGATION OF HOMOGENEOUS VS. HETERGENOUS MODELIING EFFCETS FOR OECD/NEA MOX-3600 PIN CELL, FUEL ASSEMBLY AND CORE VARIANTS

L. Thilagam[1] and D. K. Mohapatra[1]
[1] Safety Research Institute, Atomic Energy Regulatory Board, Kalpakkam, India
[1]*e-mail: - thilagam@igcar.gov.in*

Abstract

Towards the development of inhouse physics analysis capability to support independent safety review of Fast Reactors in India, an OECD/NEA proposed large size SFR MOX-3600 core benchmark is analyzed using OpenMC code. Through the analysis, the effect of homogeneous vs. heterogeneous modeling is investigated for the benchmark variants comprising of various degree of calculational levels viz., a pin cell, a fuel sub-assembly and a whole core. The sodium void worth values at different fuel temperatures are calculated for the pin cell and fuel sub-assembly variants, whereas the core physics results include the sodium void worth, the doppler constant and the control rod worth. Comparison with the benchmark results in general show good agreement. The effect of homogenous modeling is observed to under-predict the neutron multiplication factors and over-predict the sodium void worth for all levels of calculational variants. The over-prediction of sodium void worth increases with increase in void percentage. The magnitude of the Doppler constant and control system worth are observed to be over-predicted in homogenous modeling.

1. Introduction

The benchmark exercise on neutronic analysis of Sodium-cooled Fast Reactor (SFR) cores with various fuel types and core sizes is provided by OECD/NEA to evaluate core performance characteristics of several Gen-IV SFR concepts and enable participants from various countries to compare their calculation results [1, 2]. Among several core concepts specified in this benchmark, the large size oxide core MOX-3600 is the most concerned one due to inconsistencies in the results submitted by the participants. The differences in the geometrical modelling of the core like heterogenous and homogenous, calculational methodologies and nuclear data with different neutron energy group structures led to wide range of results. In the present study, neutronic analysis of the same large size core MOX-3600 has been carried out using OpenMC code [3] to investigate the effect of homogeneous vs. heterogeneous modelling which is one of the main reasons for inconsistencies in the results.

2. MOX-3600 pin cell, fuel sub-assembly and core models

A brief description of the MOX-3600 SFR benchmark model is presented here. Detailed specification regarding the geometrical and material information are available in the literatures [1, 2]. The lay out of the large size 3600 MWth SFR MOX core is shown in Figure 1 along with the associated geometric models viz. pin cell, fuel sub-assembly, primary and secondary controls. As shown in the figure, the core consists of 453 fuel, 270 radial reflector and 27 control sub-assemblies. At the centre, there is a solid hexagonal block identical to the radial reflector assembly. The core is divided into inner and outer core zones with different fuel compositions, which are composed of 225 and 228 fuel sub-assemblies, respectively. The fuel pin consists of $(U,Pu)O_2$ pellets with Oxide Strengthened Steel (ODS) cladding. Axially, 1 metre active fuel is surrounded by two axial plenum regions and two axial reflectors. The fuel sub-assembly consists of a hexagonal wrapper tube that contains a triangular arrangement of helium bonded 271 fuel pins with helical wire wrap spacers. The hexagonal wrapper tube and the wire wrap spacers are made of EM10-like steel. The volume of

wire wrap spacers is included in the cladding volume by means of radius increase in order to simplify the pin description.

For control, two independent safety-grade reactivity control sub-systems are specified. The primary control system consists of 6 control subassemblies in the inner core and 12 control subassemblies at the interface between the inner and the outer zones. The secondary system contains 9 control subassemblies located in the 7th row.

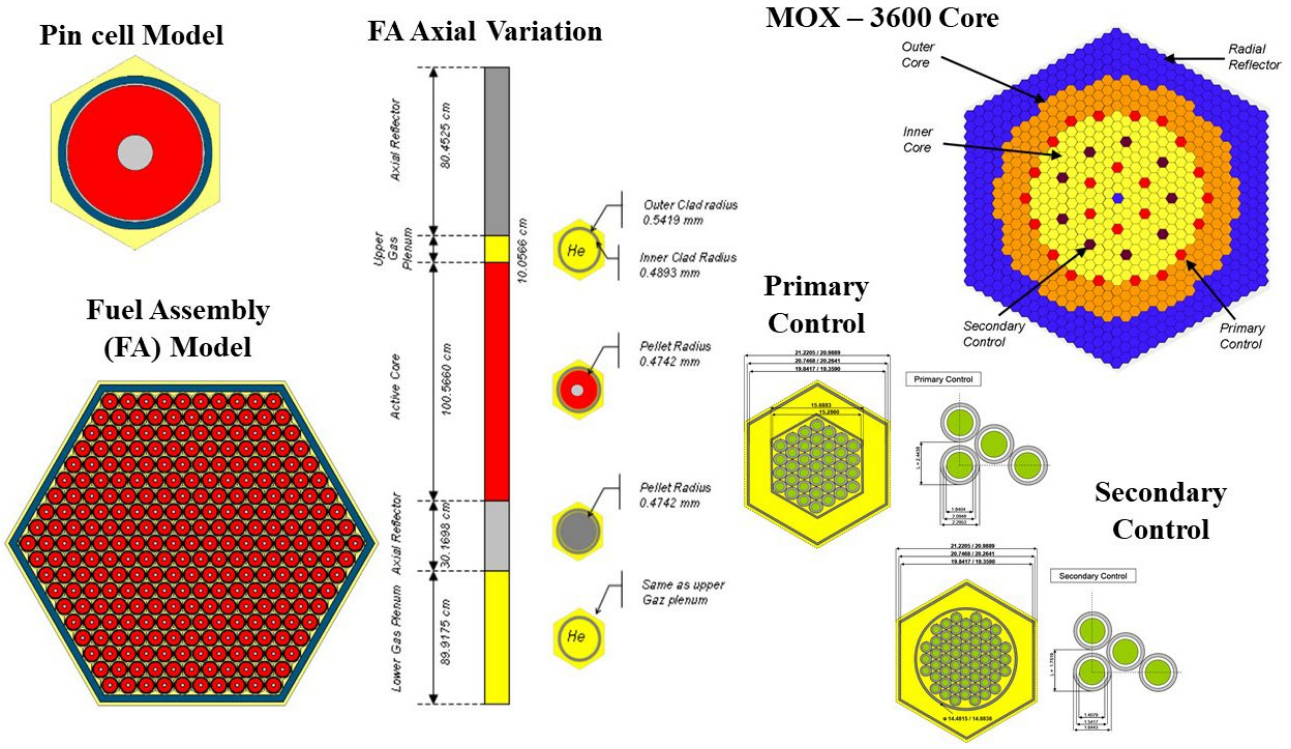


Figure 1 MOX-3600 Pin cell, Fuel Assembly, and Core Models.

3. Computational methodology

An open-source MC code OpenMC [3] is being developed by Computational Reactor Physics Group (CRPG) of Nuclear Science & Engineering (NSE) department at Massachusetts Institute of Technology (MIT). Similar to the state-of-art code like MCNP, it can model complex geometries in full 3D detail and it can use continuous energy cross section provided in ACE format. Input is provided in user friendly and easy to comprehend XML (eXtensible Markup Language) format and output is written in either binary or HDF5 format, a Hierarchical Data Format (HDF) designed to store and organize large amounts of data.

In OpenMC simulations, all pin cell, fuel sub-assembly, and core variants are modelled in a similar way as described in the benchmark reports [1, 2]. All simulations have been carried out using both the geometric models, homogeneous as well as heterogenous, employing the lib80x [4], LANL released ENDF/B-VIII.0 based ACE data files. The KCODE option is used employing 400 million neutron histories (2050 active cycles with 200,000 neutrons each, and 50 discarded cycles for converging the source distribution), leading to statistical uncertainties as low as 3.0×10^{-5} in the multiplication factors on the 1σ level.

4. Results and discussions

Results of the pin cell and fuel sub-assembly variants of the benchmark are presented in Table 1. As described in Table 1, the pin cell and fuel sub-assembly calculational level benchmark problems include nine variants each with various fuel temperatures and sodium void fractions. As mentioned earlier, both the homogeneous as well as heterogeneous models were simulated to estimate the effect on the calculational parameters.

Table 2 Results of MOX-3600 Pin cell and Fuel Assembly Variants.

Description, T_{fuel} (K), void %, $T_{non\text{-}fuel}$ (K)	k_∞		Homogeneous vs. Heterogeneous (pcm)		Void worth (pcm)	
	BM	OpenMC[#]/ΔK%	BM	OpenMC/Δ_{pcm}	BM	OpenMC/Δ_{pcm}
mox3600-pin-900, 0v, 740	1.20189	1.19996/-0.19				
mox3600-pin-900, 10v, 740	1.20495	1.20307/-0.19			211	215/4
mox3600-pin-900, 100v, 740	1.23750	1.23576/-0.17			2394	2414/20
mox3600-pin-1200, 0v, 740	1.19902	1.19708/-0.19				
mox3600-pin-1200, 10v, 740	1.20236	1.20046/-0.19			232	235/4
mox3600-pin-1200, 100v, 740	1.23530	1.23354/-0.18			2449	2469/20
mox3600-pin-1500, 0v, 740	1.19689	1.19558/-0.13				
mox3600-pin-1500, 10v, 740	1.20019	1.19894/-0.13			230	234/5
mox3600-pin-1500, 100v, 740	1.23374	1.23229/-0.14			2496	2492/-4
mox3600-pinhom-900, 0v, 740	1.20035	1.19835/-0.20	-107	-112/-5		
mox3600-pinhom -900, 10v, 740	1.20338	1.20153/-0.18	-108	-107/2	210	221/11
mox3600-pinhom -900, 100v, 740	1.23706	1.23509/-0.20	-29	-44/-15	2472	2482/10
mox3600-pinhom -1200, 0v, 740	1.19738	1.19555/-0.18	-114	-107/7		
mox3600-pinhom -1200, 10v, 740	1.20093	1.19884/-0.21	-99	-113/-14	247	230/-17
mox3600-pinhom -1200, 100v, 740	1.23445	1.23261/-0.18	-56	-61/-5	2508	2515/7
mox3600-pinhom -1500, 0v, 740	1.19531	1.19401/-0.13	-110	-110/0		
mox3600-pinhom -1500, 10v, 740	1.19886	1.19738/-0.15	-92	-109/-16	248	236/-12
mox3600-pinhom -1500, 100v, 740	1.23282	1.23161/-0.12	-60	-45/16	2545	2557/11
mox3600-fa-900, 0v, 740	1.15436	1.15252/-0.18				
mox3600-fa-900, 10v, 740	1.15808	1.15614/-0.19			278	272/-7
mox3600-fa-900, 100v, 740	1.19523	1.19342/-0.18			2962	2974/11
mox3600-fa-1200, 0v, 740	1.15133	1.14939/-0.19				
mox3600-fa-1200, 10v, 740	1.15506	1.15310/-0.20			280	280/-1
mox3600-fa-1200, 100v, 740	1.19283	1.19091/-0.19			3022	3033/11
mox3600-fa-1500, 0v, 740	1.14905	1.14771/-0.13				
mox3600-fa-1500, 10v, 740	1.15277	1.15139/-0.14			281	278/-2
mox3600-fa-1500, 100v, 740	1.19131	1.18951/-0.18			3087	3062/-25
mox3600-fahom-900, 0v, 740	1.14787	1.14565/-0.22	-490	-520/-31		
mox3600-fahom-900, 10v, 740	1.15143	1.14934/-0.21	-499	-512/-13	269	280/11
mox3600-fahom-900, 100v, 740	1.19033	1.18822/-0.21	-344	-367/-22	3108	3127/20
mox3600-fahom-1200, 0v, 740	1.14445	1.14259/-0.19	-522	-518/4		
mox3600-fahom-1200, 10v, 740	1.14826	1.14630/-0.20	-513	-514/-2	290	283/-7
mox3600-fahom-1200, 100v, 740	1.18782	1.18572/-0.21	-354	-368/-14	3190	3184/-7
mox3600-fahom-1500, 0v, 740	1.14236	1.14075/-0.16	-510	-532/-22		
mox3600-fahom-1500, 10v, 740	1.14632	1.14462/-0.17	-488	-514/-26	302	296/-6
mox3600-fahom-1500, 100v, 740	1.18592	1.18427/-0.17	-382	-372/10	3215	3221/6

[#] Std deviation on OpenMC k_∞ is ± 3.0 x 10^{-5} pcm & ΔK% = (OpenMC – BM) %, Δ_{pcm}= (OpenMC – BM) pcm

As reported in Table 1, the effect of homogenous modeling is to under-predict the infinite neutron multiplication factors (k_∞) up to ~113 pcm for fuel pin cell variants and up to ~532 pcm for fuel sub-assembly variants. With increase in void percentage, the under-prediction in k_∞ decreases mostly. The effect of homogenous modeling on sodium void worth is to over-predict it compared to heterogeneous modeling and the over-prediction of sodium void worth increases with increase in void percentage.

Results of core physics analysis viz., effective neutron multiplication factors (K_{eff}), sodium void worth, Doppler constant and control system worth are presented in Table 2 for homogenous and heterogeneous models. Similar to the results of fuel pin cell and sub-assembly variants, as compared to the heterogenous modelling the effect of homogeneous modelling is to under-predict the neutron multiplication factors (by ~ 603 pcm) and over-predict the sodium void worth ($\Delta\rho$(Na) = ~ 313 pcm). The magnitude of the Doppler constant and control system worth $\Delta\rho$ (CR) are observed to be over-predicted in homogenous modelling. Comparison with the benchmark mean results is found to be in good agreement with the results of the homogeneous modelling mostly as most of the participants of the benchmark employed homogeneous modeling.

Table 2 Results of MOX-3600 Core Variants.

Model	K_{eff}		Sodium void worth $\Delta\rho$(Na) pcm		$\Delta\rho$ (Doppler constant) pcm		Control worth $\Delta\rho$ (CR) pcm	
	BM Mean	OpenMC±1σ	BM Mean	OpenMC/ /Δ_{pcm}	BM Mean	OpenMC/ /Δ_{pcm}	BM Mean	OpenMC/ /Δ_{pcm}
Heterogeneous	1.0138	1.01244±0.00003	1937	1645/-292	-905	-898/7	6041	5738/-303
Homogeneous		1.00630±0.00003		1958/21		-924/-19		6499/458

5. Conclusion

An OECD/NEA proposed large size SFR MOX-3600 core benchmark has been analysed using a continuous energy OpenMC code. The effect of homogeneous vs. heterogeneous modeling on the calculational parameters has been investigated for the benchmark variants comprising of various degree of calculational levels viz., a pin cell, a fuel sub-assembly and a whole core. Results of the analysis indicate that the effect of homogenous modeling is to under-predict the neutron multiplication factors and over-predict the sodium void worth for all levels of calculational variants. The over-prediction of sodium void worth increases with increase in void percentage. The magnitude of the Doppler constant and control system worth are observed to be over-predicted in homogenous modeling of the whole core.

6. References

[1] OECD/NEA, "Benchmark for Neutronic Analysis of Sodium-cooled Fast Reactor Cores with Various Fuel Types and Core Sizes", *NEA/NSC/R (2015)9*, (2016).

[2] P Kang Seog Kim *et al.*, "Verification and Validation of the AMPX Multigroup Libraries for Advanced Reactor Analysis", *ORNL/SPR-2018/1014*, (2018).

[3] Paul K. Romano *et al.*, "OpenMC: A State-of-the-Art Monte Carlo Code for Research and Development," *Annals of Nuclear Energy*, 82, 90--97 (2015)

[4] Jeremy Lloyd Conlin *et al.*, "Release of ENDF/B-VIII.0-Based ACE Data Files", *LA-UR-18-24034*, (2018)

BENCHMARK ANALYSIS OF EBR-II SHUTDOWN HEAT REMOVAL TESTS

S.S. Singh[1], R. Karthik and D.K. Mohapatra
Safety Research Institute,
Atomic Energy Regulatory Board, Kalpakkam, India
[1]*email: - sudhansu@igcar.gov.in*

Abstract

An IAEA benchmark comprising the results of experiments conducted at EBR-II fast reactor is taken up for calculations using the in-house developed computational tool. The tests conducted in EBR-II fast reactor are representative of conditions during a station blackout. The computational tool that solves point kinetics equation with associated reactivity feedbacks, pressure and heat transfer equations in the primary, secondary and tertiary circuits are used to perform calculations using the benchmark data. The benchmark lists two Shutdown Heat Removal Tests (SHRT) namely SHRT-17 and SHRT-45R. While SHRT-17 is a protected loss of flow test, SHRT-45R is an unprotected loss of flow test. The results obtained from the calculations are compared with those of the benchmark for validation of the computational tool.

1. Introduction

Several experiments were conducted in the Experimental Breeder Reactor (EBR-II) operated by Argonne National Laboratory (ANL), USA to demonstrate passive safety in liquid metal cooled fast reactors. The results of two of the most important of such tests conducted at EBR-II are available from IAEA as a benchmark exercise. Calculations are performed using an in-house computational tool on the IAEA benchmark comprising the experimental results of the above two tests [1]. The computational tool solves the point kinetics equation through prompt jump approximation. Various reactivity feedbacks are also included in the model. Multichannel model is used for heat transfer in the primary circuit. The model was validated earlier using few postulated transients in CRBRP fast reactor [2].

2. EBR-II Reactor

The EBR-II reactor [3,4] had a thermal power of 62.5 MW and an electrical output of 20 MWe. It is a liquid sodium cooled fast reactor that uses metal fuel. At the time of shutdown heat removal tests, the reactor was operating with U-5Fs, a fissium fuel alloy (U-235 and fission products) specially fabricated for EBR-II. It is a pool type design with the major primary components of the reactor submerged in the primary tank. The EBR-II had 637 fuel subassemblies classified into three regions namely central core, inner blanket, or outer blanket. The central core consists of 61 subassemblies in five rows.

3. Brief Description of Shutdown Heat Removal Tests

The shutdown heat removal tests were conducted primarily to test the ability of reactor to withstand station black out conditions using passive reactivity feedback. Prior to the tests, the reactor was operated at full power so that the temperatures across the reactor are uniform. However, the full power operation time was limited so as to reduce the decay heat power. Both the tests simulate station blackout conditions. In one of the tests (SHRT-17), there were trips in the primary and secondary pumps and a scram at the same time. The power to the auxiliary pump present in the primary circuit was disabled even though it was usually available in station blackout conditions. In the second test (SHRT-45R), there were trips in the primary and secondary pumps but without scram. However, the power from the battery was available to the

auxiliary pump. One of the objectives of the tests was to study the effect of natural circulation in normalizing the fuel temperature.

4. Computational Methodology

In the in-house computational tool, the fuel section is divided into 11 regions for thermal modelling. The core is divided into three radial regions with three axial regions each. The control assemblies and blanket forms the other two radial regions with one axial region each. The mathematical model for the system analysis is in form of a coupled ordinary differential equation.

$$\frac{dx_i}{dt} = F_i(x_1, x_2, \cdots, x_n; t) \qquad (1)$$

i = 1, …, n
where
x_i = state variables,
F_i = differentiable functions, and
t = time, the independent variable.
The state variables are comprised of core neutronics, thermal-hydraulics of the primary, secondary and tertiary circuit. The equations are solved by a combination of Runge-Kutta and prompt jump approximation methods.

5. Results and Discussions

5.1 SHRT-17 Results

One of the important safety parameters, the power to flow ratio is shown in Fig. 1. As there is instantaneous scram, there is drop in power to flow ratio initially. Then there is an increase because of reduction in flow rate. It further decreases due to establishment of natural circulation. Fig. 2. shows the total power profile. As could be observed, there is a rapid fall in power immediately following the scram. Thereafter it levels off to fission product decay heat and begins to decrease at a very slow rate. The results of the variation in core outlet temperature are shown in Fig. 3. The trend is similar to that of power to flow ratio except for a small delay. Fig. 4.shows the variation of peak fuel, clad and sodium temperature with time. The results are also compared with that of the benchmark and found to be in good agreement. As power-to-flow ratio and peak fuel, clad and coolant temperatures are derived quantities, these are not provided in the original benchmark data. However, due to their safety significance these are shown here.

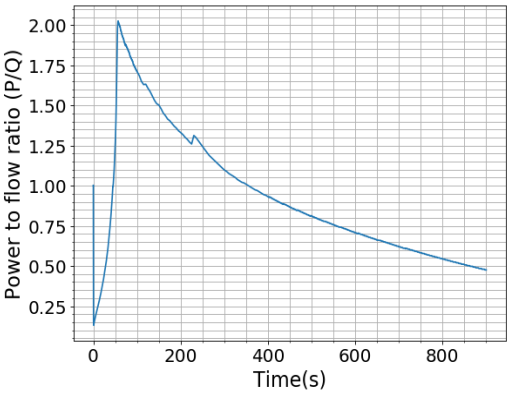


Fig. 1. Power to Flow ratio for SHRT-17 test

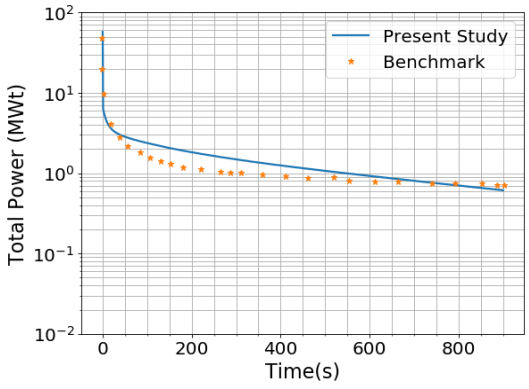


Fig. 2. Total Power for SHRT-17 test

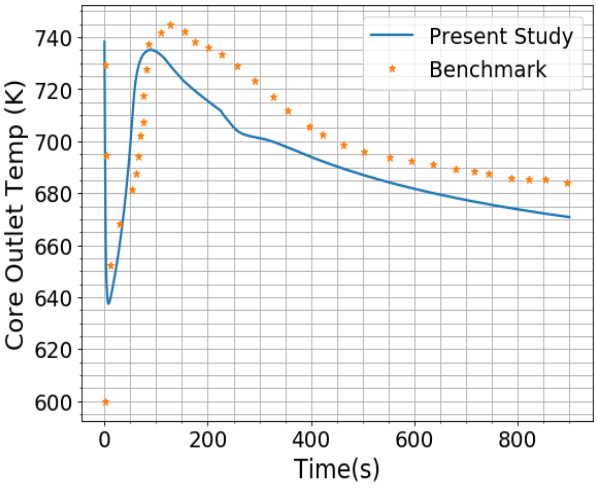


Fig.3. Core Outlet temperature for SHRT-17 test

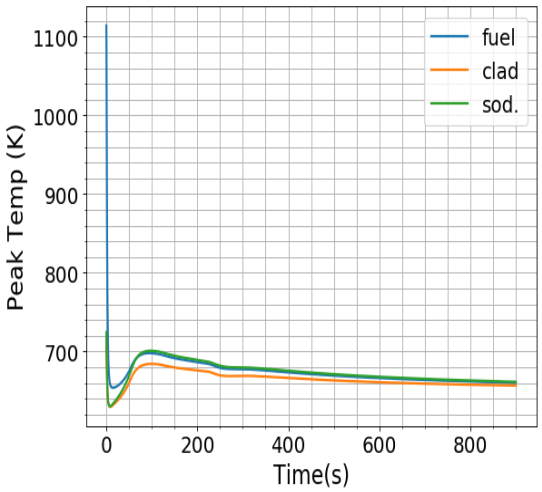


Fig.4.Variation of Peak fuel, clad, sodium temperature

5.2 SHRT- 45R Results

The evolution of net reactivity was estimated and is shown in Fig. 5. There is a fall in the net reactivity followed by an initial rise. The fall is attributed to the rise in temperature after which it rises again for stabilization. The evolution of mid-core temperature is shown in the Fig. 6. The variation in mid-core temperature essentially is similar to the variation in power to flow ratio. Fig. 7 shows the comparison of calculated power profile with the experimental values. The results of the evolution of peak fuel temperature are shown in Fig. 8. The estimation of peak fuel temperatures are well within the melting point of fuel. The results are again in good agreement with that of the benchmark. The differences between the calculated and benchmark could be attributed to approximations used in the modelling

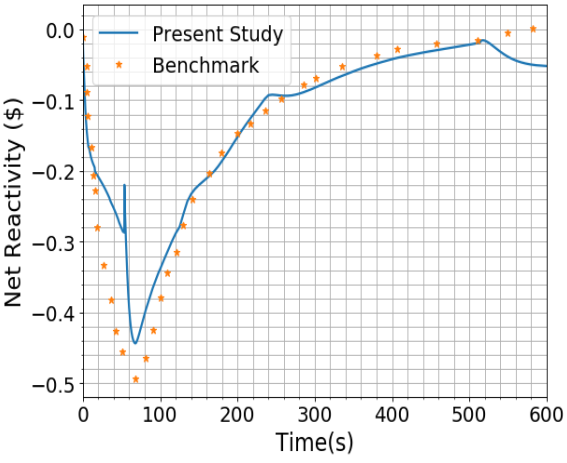


Fig.5. Net Reactivity for SHRT-45R test

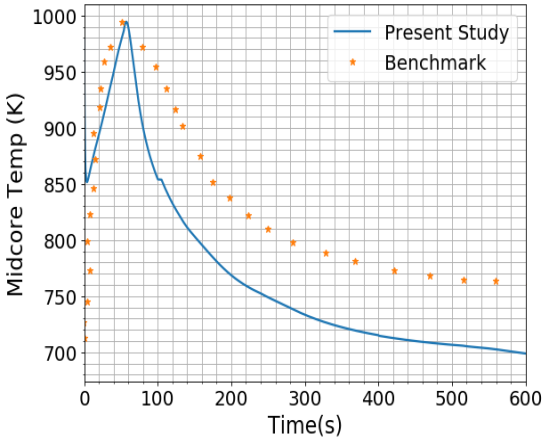


Fig. 6. Mid core temperature for SHRT-45R test

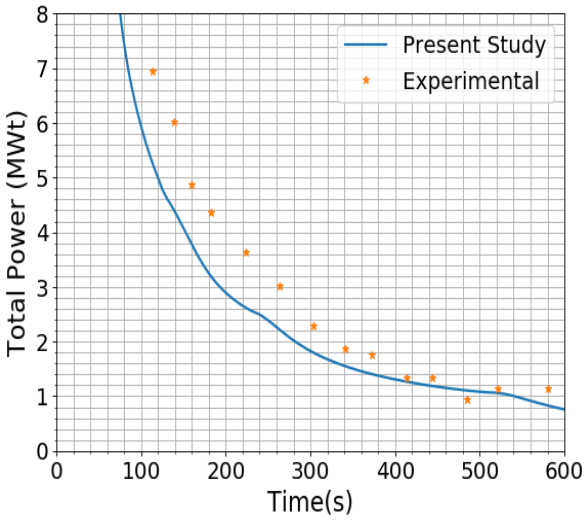


Fig.7. Total power for SHRT-45R test

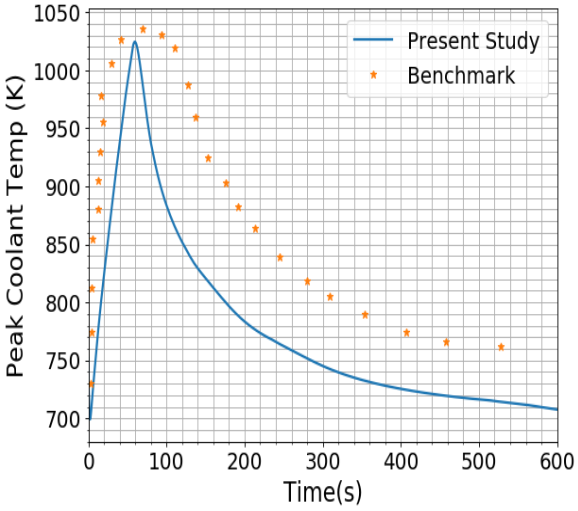


Fig. 8. Peak Fuel Temperature for SHRT-45R test

6. Conclusion

For independent safety evaluations of the fast reactor systems, continuous efforts are made for the development of in-house computational tools. In the present work, one such in-house developed computational tool was used to analyse two shutdown heat removal tests conducted at EBR-II fast reactor as a part of an IAEA benchmark exercise. Further, as a part of the validation of the in-house computational model and the tool, various parameters namely total power, net reactivity, power to flow ratio, mid core temperature, peak fuel temperature, peak clad temperature, peak sodium temperature, core outlet temperature, IHX outlet temperatures are calculated for both the tests. The results are in general found to be in good agreement with those of the benchmark. The discrepancies in power, temperatures, etc as observed in the present study are also found in other international evaluations. This could be because of the approximations used in the modelling. However, further modelling refinements are being undertaken to improve the results.

7. References

[1] "Benchmark analysis of EBR-II Shutdown Heat Removal tests", *IAEA-Tecdoc-1819*, August, 2017.

[2] Singh S.S., Karthik R., "Development of primary and secondary sodium circuit hydraulic model for fast reactors, *AERB/SRI/2021/3001*, March 2021.

[3] Sumner T., Wei T.Y.C., "Benchmark specifications and data requirements for EBR II Shutdown heat removal tests SHRT-17 and SHRT-45R", *ANL-ARC-226 Rev.1*, May 31, 2012

[4] Fei T., Mohamed A., Kim T.K., "Neutronics Benchmark specifications for EBR-II shutdown heat removal test SHRT-45R – Revision 1", *ANL-ARC-228 Rev.1*, January, 2013.

Development of initial core loading for 900 MW (e) IPWR

Devesh Raj, Umasankari Kannan
Bhabha Atomic Research Centre, Mumbai, India
[1]*e-mail: - draj@barc.gov.in*

Abstract

Indian Pressurised Water Reactor (IPWR) is a 2700 MWt (900 MWe) is a pressurized water reactor which has a cycle length 410 FPDs with three batch fuel management.. The design targets were kept in accordance with the design pursued all over the world with the modern features like the use of the burnable absorber to extend the cycle length along with other safety features. An initial core has been optimized using different fuel types and conforms to all the safety features as in the equilibrium cycle.. The lack of axial and radial burnup distribution in fresh fuel assemblies available for the initial core loading makes the core loading design challenging. This loading scheme uses eight distinct fuel assembly types which differ in enrichment and the Gd content in the IFBA pins. There is no axial profiling in fuel assemblies. A simple approach with the radial profiling of the fuel assembly where the fuel pins in the outer most ring have less enrichment than the inner pins is followed in the design of initial core. The current paper describes the development and estimated burnup characteristics of current IPWR initial cycle .

1. Introduction

The design of initial core loading pattern (and of subsequent transition core till the equilibrium cycle is attained) is done such that characteristics of resulting core falls within envelop of the equilibrium core. [1,2] This is required to ensure that all the associated system (operation, control and safety) with their stipulated operation range envisaged for the equilibrium core also works as expected for the initial and transition cores. The equilibrium core was designed and the detailed design report was submitted for the safety and regulatory assessment [1, 2]. The hexagonal lattice spectrum and burnup code EXCEL [3,4] and TRIHEX-FA [5] has been used for the lattice and the core calculation respectively.

2. Fuel assembly design

The fuel assembly design (FA) was developed from iterative lattice-core calculation for converged burnup profile. The initial fuel assembly design was chosen from the burnup and reactivity distribution of the equilibrium core during the burnup cycle. The broad characteristics based on which the fuel assembly types were chosen are as follows. The fuel assemblies together must facilitate loading of sufficient fuel to achieve a cycle length of 410 days. The characteristic of the equilibrium core designed earlier was the guiding factor. During the design of the equilibrium core it was observed that during the three batch fuelling scheme the core accumulates a burnup of 15,000 MWD/t over a burnup cycle. Therefore the initial core must have the distribution of fuel assemblies which can be discharged in one, two and three cycles respectively after (approximately) incurring a burnup of 15 MWD/Kg, 30 MWD/Kg and 45 MWD/Kg. The fuel assembly types that might be required were further diversified by using different Gd content to achieve the required reactivity and power distribution,.. The initial database for the fuel assembly cross sections for the 3D burnup dependent core calculation was made using coarse variation in dissolved boron content. Once the macro characteristics like cycle length, radial and axial power distributions were within the scope of achieving full cycle length, the choice of the fuel assembly was refined.

The much detailed burnup and dissolved boron dependent cross sections were calculated for about 20 fuel assembly types out of which a combination of 8 were used in the current design. The details of the fuel types is given in table 1. The average core enrichment is 2.64%. The judicious choice of the enrichment of fuel pins in the fuel assembly resulted in the low core enrichment which helped in keeping the power peaking factor within the limit. Due to low initial core enrichment the transition to second core will require more FA loading than 50 or 51. This is however a necessary trade-off in order to keep the power peaking factors/ core power distribution under the limit while keeping the fuel design simple. The reactivity characteristics is depicted in figure 1.

Table 1.0 Fuel types in the IPWR initial Core

Sl. No	Fuel type (#)	NFA	e% outer Pins	e% Inner Pins	No of IFBA	% Gd2O3 content in IFBA
1	1600	20	1.6	1.6	-	-
2	2000	67	2.0	2.0	-	-
3	3000	12	3.0	3.0	-	-
4	3020	04	3.0	3.0	24	2.0
5	3025	04	3.0	3.0	24	2.5
6	3530	14	3.5	3.5	24	3.0
7	4200	26	3.9	4.3	-	-
8	4225	04	3.9	4.3	24	2.50

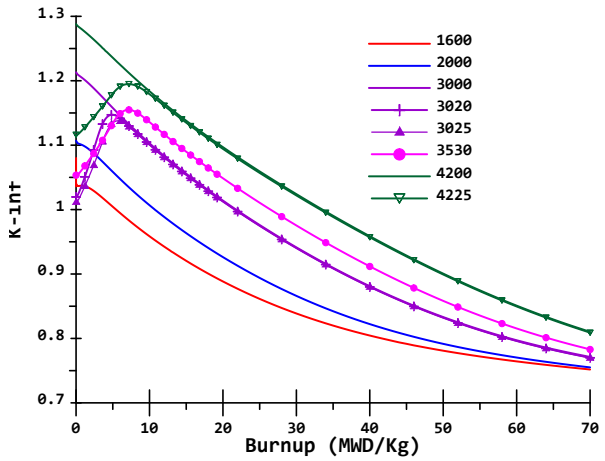


Figure 1 The burnup dependent reactivity of fuel types

3. Core loading scheme and the burnup characteristics

The core follow-up calculation has been done by using Fine Mesh Finite Difference code TRIHEX-FA which solves the neutron diffusion equation in hexagonal geometry [5]. The code subdivides the hexagonal mesh in triangles and solves the hexagonal problem using triangular finite difference. Each hexagonal mesh of pitch 24.3 cm. encompassing 331 triangular lattice locations (311 fuel pins) is further subdivided in to 24 triangular meshes. The entire active core consisting of 151 fuel assembly is represented by 3624 triangular meshes in radial direction. The active core region has been modelled to have 72 meshes for a height of 360 cm. Thus the complete active core is represented by 260928

(=151x24x72) right triangular prismatic meshes. The model also considers axial reflector regions and radial reflector regions consisting of core baffle, core barrel, biological shield and reactor pressure vessel. The core follow up calculation is done in 82 steps with a uniform burnup step of 5 FPD. After each burnup step the mesh burnup is updated. The appropriate cross sections for the mesh depending upon the fuel type in the mesh is obtained by the interpolation from the data generated at the stage of assembly level calculation. The fuel assembly cross section data generated for the core calculation is given in table 2. (The corresponding data for the two types of control section, B4C and DyO2TiO3, was also generated for the control worth calculation).

Table 2 The matrix for the fuel assembly cross section database

Parameter	Range of Values	The current set of values
Brunup	0.0-70 MWD/Kg	in 150 steps
Dissolved Boron	0.0 to 1400 (8)	0.0, 200.0, 400.0, 600.0, 800.0, 1000.0, 1200.0, 1400.0 ppm of Natural Boron
Coolant Temperature	286.83 to 328.16 (9)	286.83, 292.00, 297.16, 302.33, 307.5, 312.66, 317.83, 323.0, 328.16 (°C)
Coolant Density*	0.7520 to 0.6583 (9)	0.7520, 0.74240, 0.7329, 0.7227, 0.7110, 0.6999. 0.6859, 0.6727, 0.6583 (g/cc)
Fuel Temperature	250.0 to 2000.0 (6)	250.0, 400.0, 625.0, 1000.0, 1500.0, 2000.0 °C
Dissolved Boron for temperature Variation	0.0 -1000.0 (6)	0.0, 200.0, 400.0, 600.0, 800.0, 1000.0, ppm of Natural Boron for each value of coolant and fuel temperature.

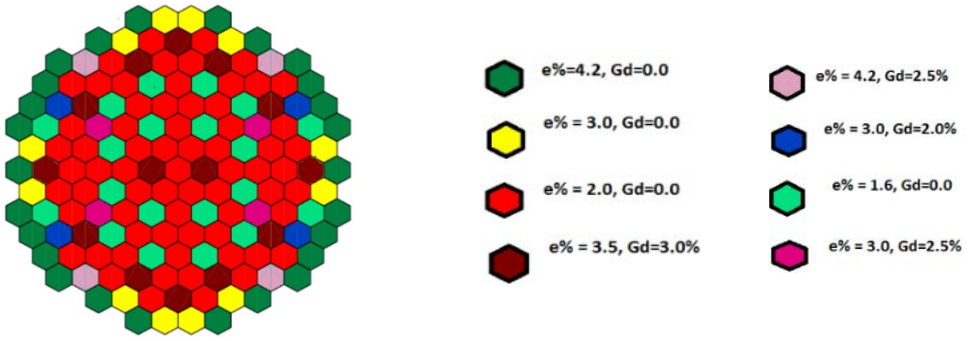


Figure 2 IPWR Initial core loading

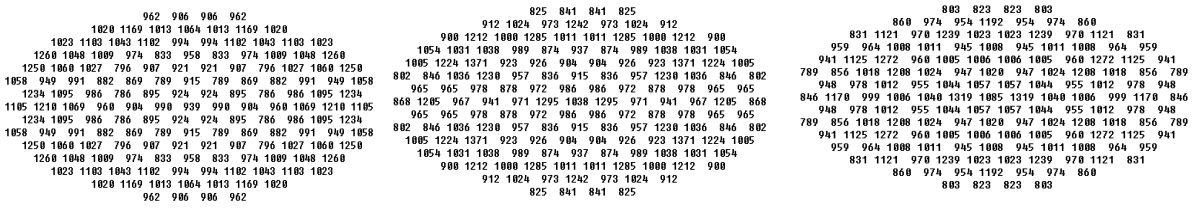
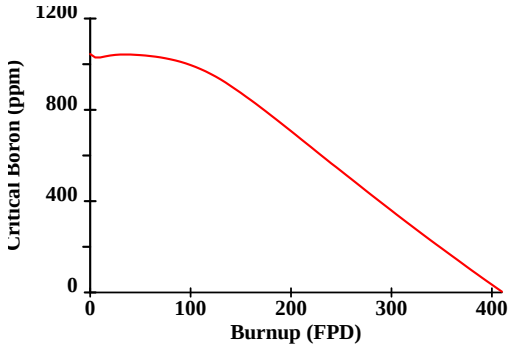


Figure 3 Fuel assembly power distribution at BOC, MOC and EOC

The range of parameters is chosen such that all the core states can be represented for the given scope of the calculation. The parametric variation given in the table 2 corresponds to the requirement in 3D

hot core follow up calculation with mesh wise variation of coolant and fuel temperature. The matrix for all the variable parameters given in table 2 is only a subset of the cross section set used for the follow up of the initial core loading with full power operation with equilibrium xenon and samarium. The fuel assembly power distribution at BOC, MOC and the EOC is given in figure 3. The core loading scheme is depicted in figure 2 and the critical boron over the cycle is given in figure 4. The end of cycle burnup distribution is given in figure-5.



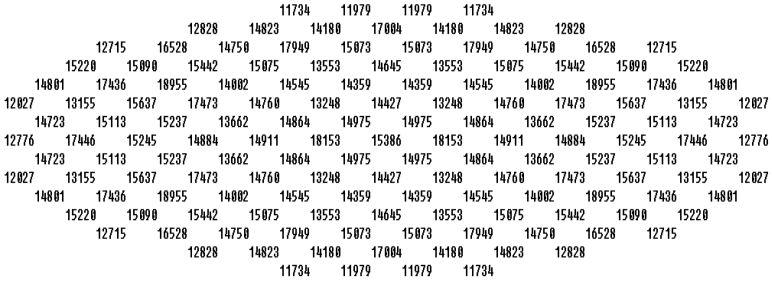


Figure 4 Variation of critical soluble boron Figure 5 Burnup distribution at EOC

The loading scheme for the first reload after initial core or second core has also been designed. The transition cores beyond second core loading is under development. The equilibrium core loading pattern is expected to be achieved in about five cycles while equilibrium power distribution will be attained in about eight fuel cycles.

4. Conclusion

Initial core loading for the IPWR has been performed. Judicious use of burnable absorber Gd and optimised fuel enrichment are important aspect of this core loading so that the initial reactivity has been kept low. This results in low initial critical boron (<1200 ppm) which ensures negative coolant reactivity coefficient for all operational regimes.

5. References

[1] Devesh Raj, Umasankari Kannan, “Design of IPWR Initial core with low Excess Reactivity and Estimation of Cycle Characteristics: Fuel Assembly Design”, RPDD/IPWR/75 A, April 20, 2019.

[2] Devesh Raj, Umasankari Kannan, “Design of IPWR Initial core with low Excess Reactivity and Estimation of Cycle Characteristics: Core Burnup Characteristics”, RPDD/IPWR/75 B, April 20, 2019.

[3] Jagannathan, V., Jain, R.P., 2008. EXCEL – A Combination of 1-D Transport and 2-D Diffusion Methods for Burnup Analysis of Hexagonal Lattice Assemblies, B.A.R.C. Report under preparation, 2008.

. [4] L. Thilagam, C. Sunil Sunny, V. Jagannathan, K.V. Subbaiah, A VVER-1000 LEU and MOX assembly computational benchmark analysis using the lattice burnup code EXCEL, Annals of Nuclear Energy 36 (2009) 505–519.

[5] L. Thilagam, C. Sunil Sunny, V. Jagannathan, K.V. Subbaiah, VVER-1000 MOX Core Computational Benchmark analysis using indigenous codes EXCEL, TRIHEX-FA and HEXPIN, Annals of Nuclear Energy 36 (2009) 1502–1515.

Optimization study of AHWR Equilibrium Core after prolonged EMCCR

Sandeep Singh[1], Arindam Chakraborty[1], Amit Thakur[1] and Umasankari Kannan[1]
[1] Reactor Physics Design Division, B.A.R.C., Mumbai, India
[1]*e-mail: -* *sandeepss@barc.gov.in*

Abstract

A study has been carried out to accurately estimate the various core parameters and reactivity requirements, when fuel will be reloaded into the reactor after 3 years of cooling due to complete *en-masse* coolant channel replacement (EMCCR) in AHWR. Equilibrium core has been simulated for three burn-up zones in normal operating condition and after 3 years of cooling, using transport theory-based lattice code DRAGON5 coupling with multigroup neutron cross section library. Core parameters such as core reactivity, neutron flux distribution and power distribution have been estimated using nodal expansion method based computer code FEMINA. A loss of ~ 4 mk has been observed in the excess reactivity of the core. The power distribution does not change significantly after reloading the core.

1. Introduction

Advance Heavy Water Reactor (AHWR) is a 920 MW_{th} vertical pressure tube type reactor cooled by light water and moderated by heavy water. The operating life of coolant channel in AHWR is assumed to be ~20-30 years and the core will undergo a complete *en-masse* coolant channel replacement (EMCCR). The fuel from the core needs to be stored in Spent Fuel Storage Bay (SFSB) for about 3 years. In this work, A study has been carried out to estimate the various core parameters and reactivity requirements, when the fuel will be reloaded into the reactor after 3 years of cooling. As a part of this study, A code validation exercise was carried out in which isotopic composition at 40 GWd/Te was estimated and compared for equilibrium core cluster using different lattice codes namely DRAGON5, ITRAN, WIMS and ORIGEN [1]. To simulate the equilibrium core of AHWR three burn-up zones have been calculated and lattice calculations have been carried out for equilibrium core using DRAGON5 code. DRAGON5 [2] is an open-source lattice code which is used to perform transport calculations inside cells and assemblies for multi-dimensional reactor geometry with various methods. It is designed around a scripting language, known as CLE-2000. It is divided into many calculation modules linked together using the GANLIB kernel driver. It can directly access standard microscopic cross-section libraries in various formats including WIMS libraries. Homogenized cross-sections have been generated for the three burn-up zones in normal operating condition and after 3 years of cooling period. Core calculation has been carried out before and after the cooling at an average in core burn-up of ~20 GWd/Te with FEMINA [3] code which solves diffusion equation by Nodal Expansion Method. It uses few groups homogenized cross-sections generated by lattice code and provides the information about the core parameters like neutron flux distribution, power distribution, change in core excess reactivity, maximum channel power (MCP), maximum mesh power (MMP), peak node location etc.

The fuel cluster of equilibrium core consists of 54 pins arranged in three concentric rings containing 12, 18 and 24 pins respectively. The 12 pins of the innermost ring contain 6% Pu in (Th, Pu) MOX and the 18 pins of the middle contain 3.9% Pu in (Th, Pu) MOX. The 24 pins of the outer ring contain average 3.55% of Uranium in (Th, U) MOX (the bottom half of the active fuel contain 3.8 % U and the top half contain 3.3 % U). The U^{233} content in the Uranium has been assumed to be about 78%. The core excess reactivity of the cluster is suppressed by adding 2% Gadolinium (burnable

poison) in two fuel pins of the inner ring. The cross section view of the equilibrium core fuel cluster is shown in Figure 1.

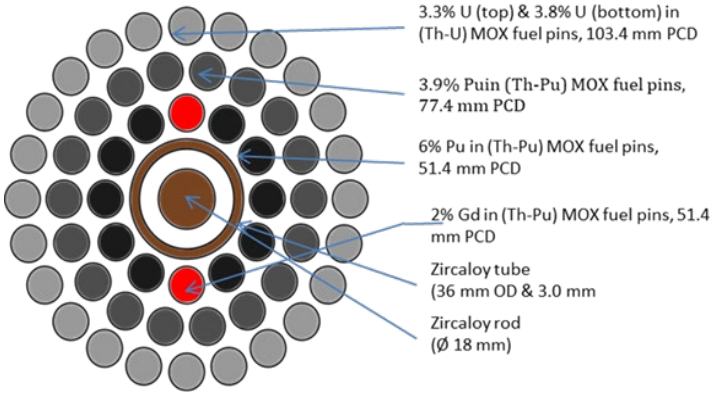


Figure 1: Cross section view of the AHWR Eq. Core fuel cluster

2. Lattice simulations

To simulate the equilibrium core of AHWR three burn-up zones i.e., 23, 19 and 14.5 GWd/Te having ~20 GWd/Te average core burn-up have been calculated. Figure 2 shows the burn-up distribution having three burn-up zones inside the core. Lattice simulations have been carried out for both top and bottom equilibrium core clusters with DRAGON5 code using 69 energy groups ENDFB-VI.8 nuclear data library having 92 depleting isotopes.

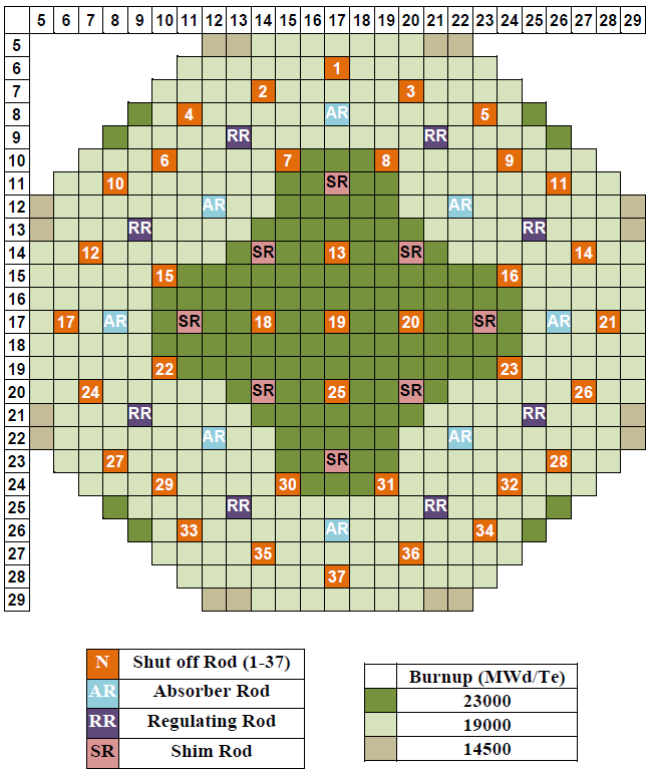


Figure 2: Burn-up distribution inside the core

The EXCELT module is used to perform full cell collision probability tracking and SHI module is used for self-shielding calculations. The reactivity variation with time during full power and zero power operation for cooling is shown in Figure 3.

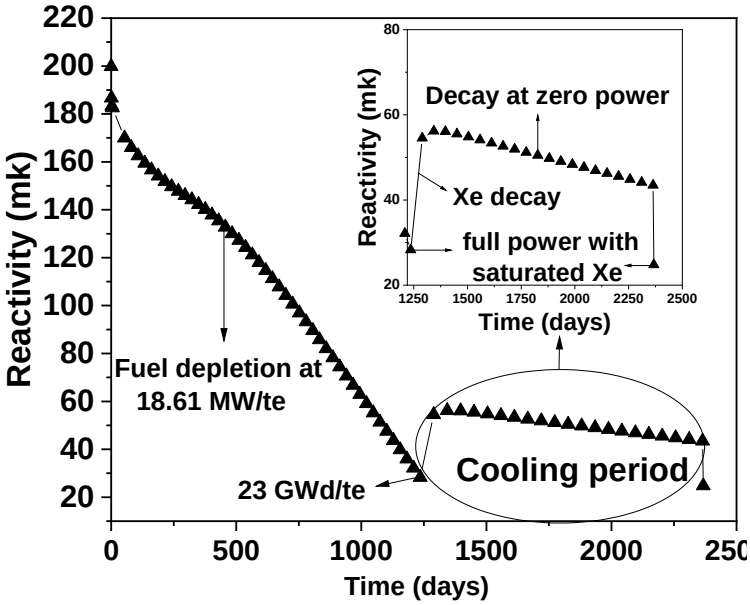


Figure 3: Reactivity variation with time during full power operation and zero power operation for cooling

Initially fuel depletion calculations were carried out with average specific power of 18.61 MW/Te using EVO module of the code to achieve the required burn-up. Further, to simulate the cooling, fuel depletion calculations were carried out at zero power for 3 years in small time steps. It can be observed from Figure 3 that initially in normal operating condition reactivity decreases due to the fuel depletion at full power, when cooling starts the reactivity slightly increases due the decay of saturated ^{135}Xe. Then reactivity decreases due to the natural radioactive decay of fissile isotopes. For each burn-up zone two energy group homogenized cross sections have been generated before and after 3 years of cooling period for core calculations.

3. Core calculation

The computer code FEMINA has been used to carry out the core simulations at an average core burn-up of ~20 GWd/Te. The core excess reactivity is estimated to be ~ 20.1 mk at the instant the fuel was removed and 16.4 mk when the fuel was reloaded into the core after the cooling period. The power distribution does not change significantly after reloading the core. Figure 4 shows the quarter core channel power distribution after reloading the core. The maximum channel power is estimated to be 2.46 MW.

4. Conclusion

To study the effect of prolonged EMCCR in AHWR, equilibrium core clusters have been simulated for three burn-up zones in normal operating condition and after 3 years of cooling using lattice code DRAGON5. The computer code FEMINA has been used to estimate the core excess reactivity and power distribution. It is observed that if fuel will be reloaded into the reactor after 3 years of cooling

there will be a loss of **3.7 mk**. This loss can be compensated using normal refuelling scheme of AHWR.

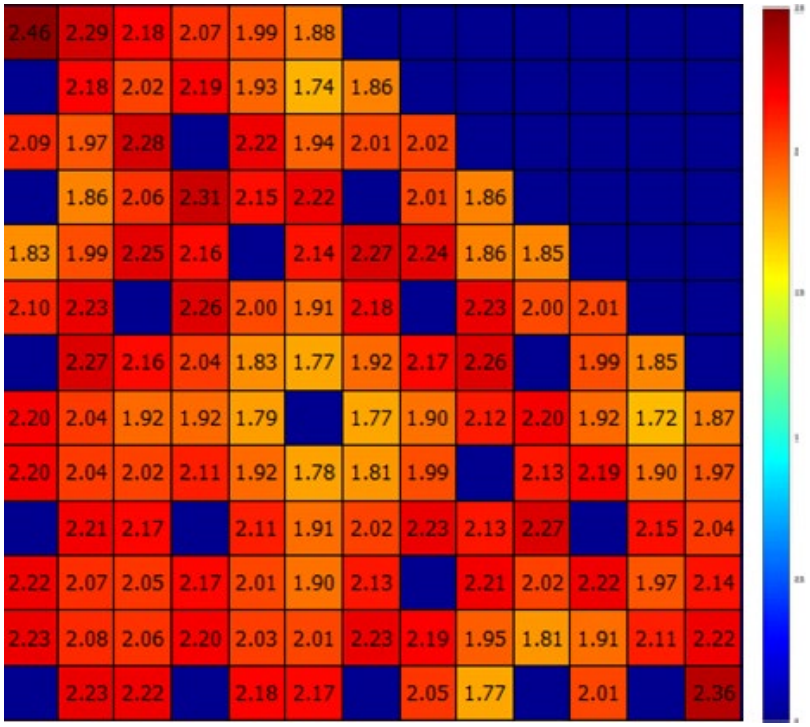


Figure 4: Channel power distribution (MW) after reloading the core

5. References

[1] Singh, S., et al., Comparison of isotopic compositions of discharged fuel with different codes after prolonged cooling for efficient recycle in AHWR. *Technical Report No. RPDD/AHWR/464 Dated: May 10, 2021*.

[2] Hébert, A., DRAGON5: Designing Computational Schemes Dedicated to Fission Nuclear Reactors for Space. *Proceedings of Nuclear and Emerging Technologies for Space, 2013*.

[3] Kumar, A. and R. Srivenkatesan, Nodal expansion method for reactor core calculation. 1984 (*Technical report No. BARC-1249*).

[4] Marleau, G., A. Hebert, and R. Roy, A USER GUIDE FOR DRAGON VERSION5. *TECHNICAL REPORT IGE–335, Ecole Polytechnique de Montreal, 2022*.

Optimization of Local Shield for IHX of FBR 1 & 2

Rajeev Ranjan Prasad[1], D Sunil Kumar[1] and A John Arul[1]

[1] Reactor Shielding and Data Division, IGCAR Kalpakkam, India.

e-mail: - rajeevphy@igcar.gov.in

Abstract

Optimization of the local shield for IHX of FBR 1 & 2 has been carried out, using deterministic particle transport coupled with stochastic Monte Carlo method. The local shield has been optimized using borated steel with suitable combination of axial and radial core bulk shielding configurations. This paper describes the details of the calculation and design of the local shield for IHX of the FBR 1 & 2.

1. Introduction

FBR 1 & 2 is a pool type homogeneous fast reactor of power 600 MWe. In pool type fast reactor, intermediate heat exchanger (IHX) is immerged in primary sodium pool. The secondary sodium flowing through it gets activated. This activated secondary sodium results radiation doses at steam generator building. Compare to Prototype Fast Breeder Reactor (PFBR) in FBR 1 & 2, leakage in the top axial direction has increased due to removal of top axial blanket to minimize sodium void coefficient [1]. The radial extent of the FBR 1 & 2 grid plate for loading of subassemblies is limited to 331.5 cm as shown in Fig.1. The design of core bulk shield(around the active core) has been carried out with a combination of boron carbide (powder) and stainless steel in the axial direction and a ferro-boron (pellet/powder) in the radial direction using particle transport code DORT [2]. Since the core bulk shield has been optimized for sufficient counts for the neutron detectors mounted at lattice plate (above the core) for monitoring of the reactor core hence it is not sufficient to bring down the secondary sodium activity in the IHX to the allowed limit. In this work the design and optimization of the local shield of the IHX and estimation of secondary sodium activity and its dose rate in steam generator building has been carried out.

2. Methods of Calculation

Since the geometry and positioning of the IHX is asymmetric with respect to the core center hence using 2D code DORT it is not possible to calculate secondary sodium activation accurately. Also attenuations of neutron flux is more than 10^{10} order makes it difficult for Monte Carlo method to calculate the same. Hence calculation has been done in the hybrid mode viz. angular flux has been estimated at the boundary of the IHX using deterministic particle transport code DORT and then modeling of the IHX has been done in Monte Carlo Code for further estimation of the secondary sodium activity and corresponding dose rate in the steam generator building.

The optimization of the core bulk shield has been performed for various suitable combinations of top axial and radial shield configurations. A combination of 10 cm boron carbide (powder), 65 cm stainless steel and 10 cm boron carbide (powder)above the fuel and radial blanket subassembly and 8 rows (equivalent to 99.13 cm) of ferro-boron subassemblies in the radial directionhas been arrived as the core bulk shield configurations [2].

The spatial and angular distribution of the incident neutron source for Monte Carlo simulation of IHX were generated from the angular flux distribution obtained using DORT at a radius corresponding to primary sodium beginning. Boundary flux has been obtained using S_8P_3 approximation for quadrature and anisotropy in 175 energy group structure. FBR 1 & 2 has four IHX located symmetrically in four quadrants hence using symmetry only one IHX is simulated.The volume averaged secondary sodium activity (SSA) in IHX is calculated by segmenting the IHX in various zones as shown in the Fig. 2. The secondary sodium activity (SSA) has been estimated using the following equation

$$\boldsymbol{SSA} = \frac{\sum_i \boldsymbol{R_i V_i f}}{\sum_i \boldsymbol{V_i V_{fi}}}$$

where$\boldsymbol{R_i}$ is secondary activation rate in the i^{th} region,$\boldsymbol{V_i}$ is the volume of the i^{th} region,$\boldsymbol{V_{fi}}$ is the volume fraction of secondary sodium in the i^{th} region.The secondary sodium activation rate in i^{th} region is given by

$$\boldsymbol{R_i = N_i V_{fi} \int \varphi_i(E)\sigma(E)dE}$$

where N_i is number density of secondary sodium (number of atoms /cc) in the i^{th} region.

3. Dilution of the Activity

Since secondary sodium flows through IHX, it is only exposed to neutron flux for a short time (7.22 sec) periodically with a circulation period of 68.5 sec. Due to this the saturation activity has to be reduced by a factor to get the equilibrium activity. The calculated SSA has been diluted over the entire sodium volume in the loop by multiplying with a factor ' f ' called dilution factor defined as

$$f = 2\frac{V_{IHX}}{V_{loop}} \cong \frac{e^{-\lambda t_c}\left(1 - e^{-\lambda t_i}\right)}{(1 - e^{-\lambda \tau})} \cong \frac{t_i}{\tau}$$

where λ is decay constant of radioactive sodium (Na24), t_i is activation time, t_c is cooling time and τ is circulation time, V_{IHX} is the volume of the secondary sodium in the IHX up to the primary sodium level (12.7 m^3). V_{loop} is the volume of the secondary sodium in the entire loop (244.05 m^3). The volume of the secondary sodium in the loop and in the IHX is taken as in PFBR. The factor 2 appears for number of IHX in a loop. The value of the f = 10 %.

The experience of worldwide laboratories employing hybrid calculation indicated that there is under prediction of the secondary sodium activation. Thus the result has been reported with a suitable bias factor validated with experimental bench mark based on APSARA experiments [4] a bias factor of 3.64 was obtained for secondary sodium activation estimated with MCNP. Applying same bias factor calculation the secondary sodium activity has been optimized using borated steel with 1.2 % natural boron and normal stainless steel as local neutron shield of IHX to bring down the secondary sodium activity within 92 Bq/cc.

4. Results and Discussion

Secondary sodium activity in IHX has been estimated for FBR 1 & 2 using two dimensional transport calculations coupled with

Monte Carlo simulation. The maximum secondary sodium activity without local shield for FBR 1 & 2 is 141Bq/cc and corresponding dose rate at 1m from the pipe surface in the steam generator building is 38.5 μSv/h. To bring down this dose rate within the design limit of 25 μSv/h, a local shield in semicircular form in the side of the IHX facing the core as well as on the bottom dished head of the IHX is recommended. To achieve the required thickness of the local shield around the IHX several Monte Carlo neutron transport calculation has been carried out with varying thickness of stainless steel and 1.2 % natural borated steel.

- At IHX radial core facing side - Semicircular shell shield of 0.5 cm borated steel with 1.2 % natural boron.
- At the bottom dished head of IHX 0.5 cm borated steel with 1.2 % natural boron.

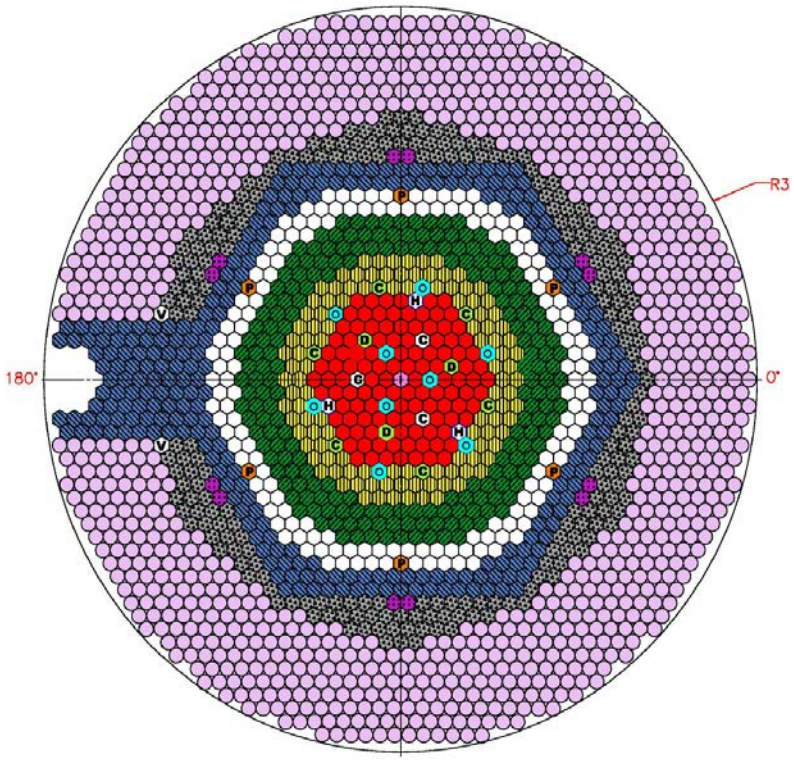
5. References

[1] A. Bachchan, D. Paul and K. Devan, ‘‘Conceptual Design of 600 MWe Oxide Fuelled SFR’’, CFBR/01113/DN/1001(Rev. B), September 2014.

[2] W.A. Rhoads and R.L. Childs, "The DORT: Two Dimensional Discrete Ordinates Transport Code’’, Nucl. Sci. Engg., 99, 88, 1988.

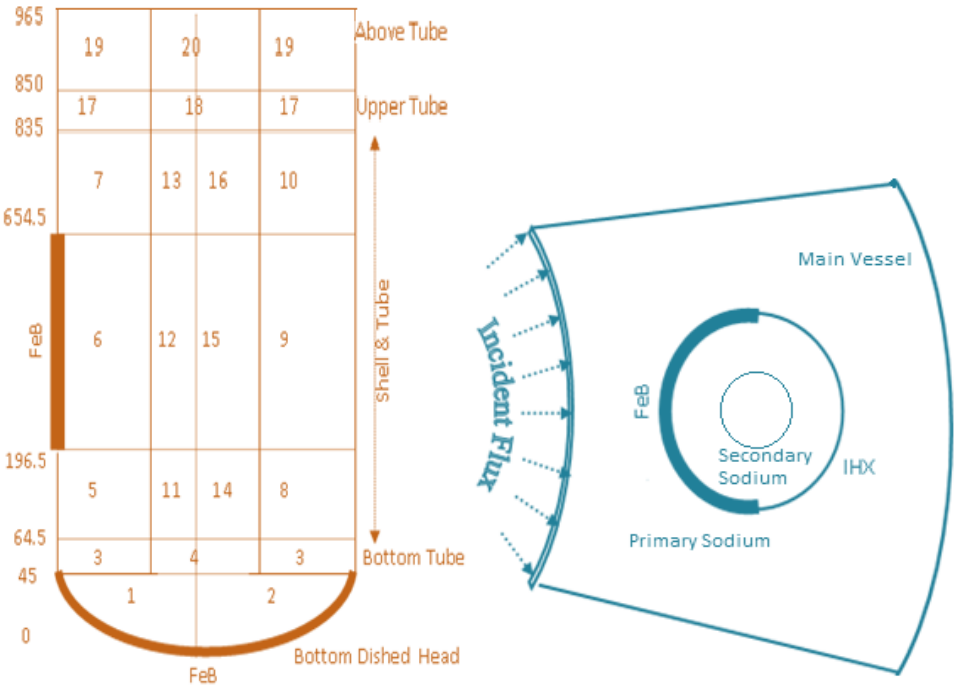
[3] G Radhakrishnan, "Permissible Secondary Sodium Activity Based on Detailed Piping Layout in Steam Generator Building", PFBR/01115/DN/1084, Rev-B, Feb-2006.

[4] R. Indira, "Feedback from APSARA Bulk Shielding Experiments on Bias Factors to be used in In-vessel Shield Design", Letter No. RSS/RPD/REG/177, Dated 01/02/2004.



SYMBOL	TYPE OF SUBASSEMBLY	No.
	FUEL – I	114
	FUEL – II	114
I	ICSA	1
	RADIAL BLANKET	198
C	CONTROL AND SAFETY ROD	9
D	DIVERSE SAFETY ROD	3
	DILUENTS	9
H	HSAR	3
	STEEL REFLECTOR	156
P	PURGER	6
	B_4C SHIELDING (INNER)	266
	STORAGE LOCATION	221
	STORAGE LOCATION (SPECIAL HANDLING)	12
	OUTER SHIELDING	977
	TOTAL SUBASSEMBLIES	2089
V	VACANT LOCATION	2
	TOTAL LOCATIONS	2091

Fig.1 Cross-sectional view of FBR 1 & 2



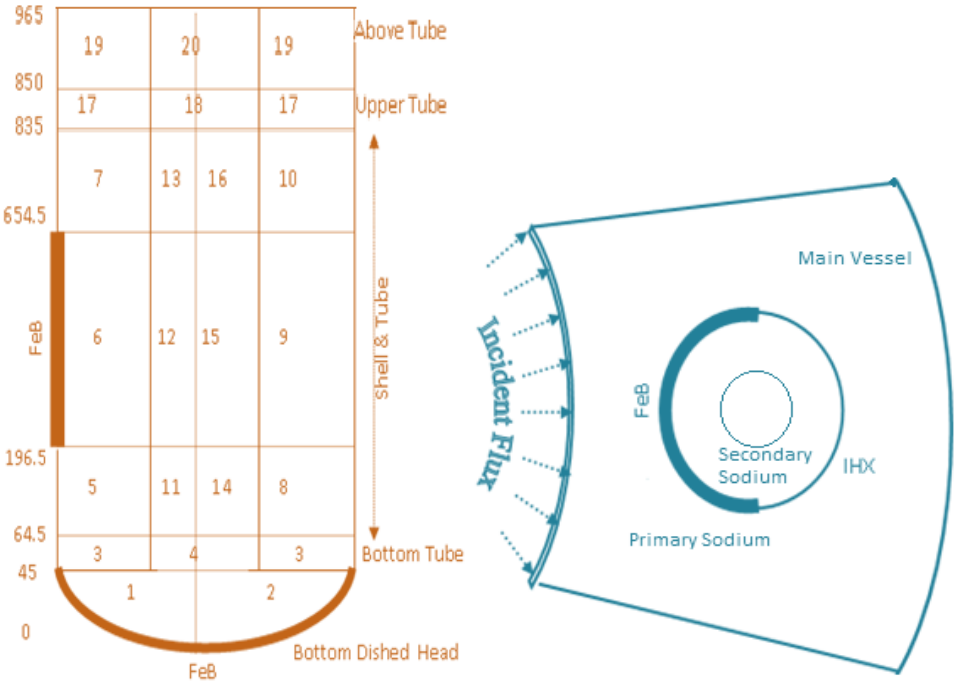


Fig. 2 Schematic diagram of the shielded IHX of the FBR 1 & 2 lateral and top view.

CONCEPT OF TRANSITION FROM 32 MWt CORE TO 40 MWt CORE

G. Raghu Kumar[1] and E. Radha,
[1] Indira Gandhi Centre for Atomic Research, Kalpakkam, India
[1]*e-mail: - grk@igcar.gov.in*

Abstract

Fast Breeder Test Reactor (FBTR) is sodium cooled, mixed carbide fuelled loop type fast reactor. FBTR is mainly used to get experience in the operation of sodium cooled fast reactor and to serve as an irradiation facility for the development of FBR fuels and structural materials. FBTR which is operated in campaigns and Upto 29th campaign FBTR produced 32 MWt power and it was proposed [1] to take this power to its design power of 40 MWt. This document provides the details about the changes that were carried out in the core to get 40 MWt power.

1. Introduction

FBTR is originally designed to operate at 40 MWt using MOX fuel with 30% PuO_2 and 70%UO_2 with 85% enriched U. However, due to the non-availability of enriched uranium, an alternate Pu-rich fuel, namely carbide fuel was decided for the initial core with 70% Pu -30% UC. Due to this high Pu content, the core has become compact and total requirement for Pu has come down. FBTR was made critical in 1985 with 22+1 Mark-I sub-assemblies (SA). The target power for the initial core was 10.6 MWt. The core was expanded progressively by adding FSA at peripheral location and carbide fuel of Mark-II composition (55% PuC + 45% UC) was introduced to increase the reactor power. Based on the encouraging out-of pile tests and stage wise PIE , LHR of Mark –I fuel was progressively raised from 250 W/cm to 400 W/cm. Eight high Pu MOX SA (44 % PiO2 + 56 % UO2) was introduced in the core in 200. Different types of fuel used in FBTR are listed in Table 1.

Type	Fuel composition	Pu composition
Mark I (HG)	70% PuC + 30% UC; U is natural uranium	^{239}Pu 92.13%, ^{240}Pu 7.63%, ^{241}Pu 0.196%, ^{242}Pu 0.039%
Mark I (PHWR)	70% PuC +30% UC; U is natural uranium	^{239}Pu 68.79%, ^{240}Pu 24.6%, ^{241}Pu 5.26%, ^{242}Pu 1.35%
Mark II	55% PuC + 45% UC; U is natural uranium	^{239}Pu 68.79%, ^{240}Pu 24.6%, ^{241}Pu 5.26%, ^{242}Pu 1.35%
MOX	44% PuO_2 +56% UO_2; U is natural uranium	^{239}Pu 68.79%, ^{240}Pu 24.6%, ^{241}Pu 5.26%, ^{242}Pu 1.35%

Table1 Types of fuel in FBTR

All the engineering systems in FBTR are designed for 40 MWt operations. The only design objective not realized, so far, was attaining 40 MWt power. The constraint in raising reactor power to 40 MWt by adding more Mark-I SAs was due to shutdown margin. Hence, the feasibility of raising the reactor power using alternate methods has been studied. Theoretical studies have indicated that the maximum power attainable is limited to 32 MWt with 56 mark I subassemblies after replacing all the existing Mark II and MOX subassemblies. Any further increase in the number of subassemblies reduces the shutdown margin below the Tech spec limit of 4200 pcm. In this note, a possible Mark I core configuration for realizing 40 MWt for FBTR is presented. Study was carried out with different core configuration using B_4C poison subassemblies at center, first ring & second ring and with different B_4C enrichment. Based on this, an optimum configuration was chosen.

2. Core configuration for the proposed 40 MWt

In the 27th irradiation campaign reactor power level was 32 MWt which is maximum attainable with 56 Mark I fuel SAs. Having reached the maximum power level possible with Mark I subassemblies, subsequent power campaigns will involve fuel subassembly replacements and no further increase in the number of subassemblies. Anticipating that the transition to 40 MWt core will be taken up during the 31st campaign, the Mark I fuel subassemblies replacing the existing MOX and Mark II in the present core are assumed have attained a burn up of 10 GWd/t in the calculations. Burn up distribution among the remaining fuel subassemblies has been taken to be that of the 26th campaign. Any additional subassembly added to reach 40 MWt configuration is taken to be fresh. With the addition of fuel subassemblies, shutdown margin decreases. To overcome this, ***it is proposed to introduce B_4C SAs similar to control rod at specific locations in the core***. Several core configurations and effects of various B-10 enrichments have been studied for their suitability in meeting the requirements. Among these, the configuration whose reactor physics parameters are commensurate with the Tech Spec requirements is given in Fig. 1. It was proposed that two locations in the first ring are reserved for testing advanced fuel types.

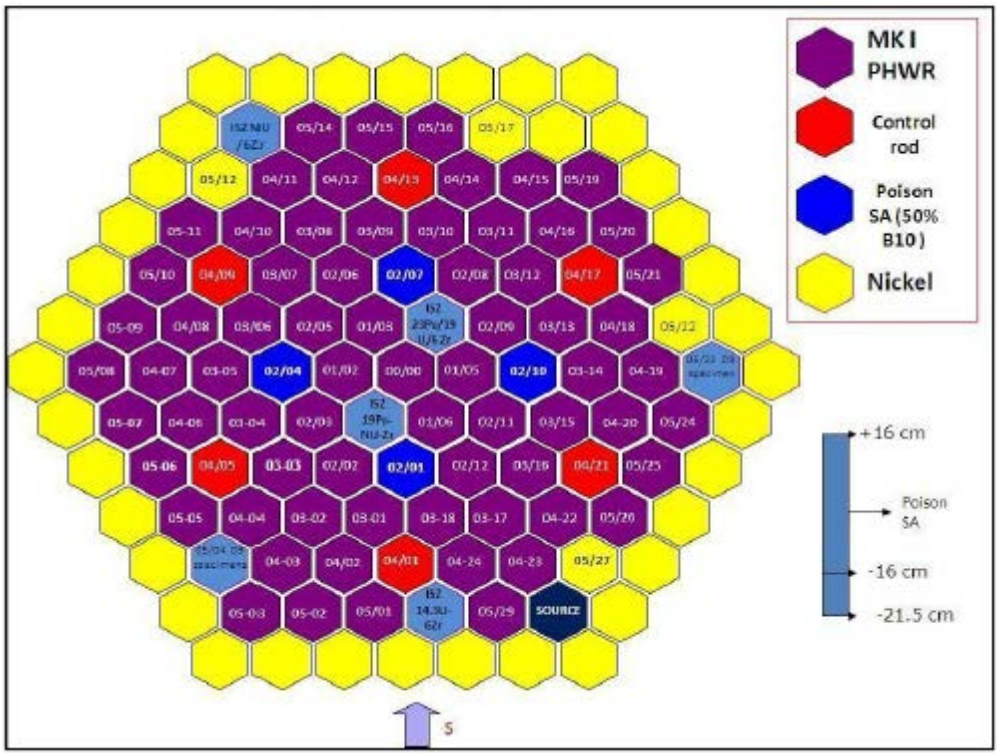


Figure 1 Core configuration for 40 MWt

2.1 Poison SA

Four equi-angular locations (02-01, 02-04, 02-07 and 02-10) in the second ring have been chosen to load the B4C (enriched to 50% in B-10) subassemblies based on the results obtained for various locations and enrichments. The arrangement of B4C column in these subassemblies is very similar to that in the control rods. The diameter of the B4C column is 38 mm, same as that in the control rod. The required column height of B4C is 375 mm. The top of the B4C column is aligned with the top of the fuel column whose length is 320 mm. The remaining 55 mm of B4C column will be below bottom elevation of the fuel column. This additional length serves two purposes. It increases

the magnitude of the negative reactivity introduced by these B4C subassemblies, thereby increasing the shutdown margin. The design of B4C poison SAs are like any other SAs and are supported on the grid plate. However, for study purpose, a hypothetical event of ejection of a B4C subassembly from its location was considered. Due to availability of 55 mm of B4C column below the core, the reactivity change to the core is minimized, essentially by ensuring that the fuel column is covered even in the ejected condition It may be noted that due to physical location of CCPM at 70 mm above the top of SAs, the maximum lift possible is only 70 mm. Based on the calculations, the reactivity addition due to ejection of one B4C subassembly, with CCPM in position, is 30 pcm.

2.2 Operational parameters

The estimated total worth of the control rods for the proposed core configuration was 10660 pcm. The shutdown margin at the beginning of the campaign is 4790 pcm, which has sufficient margin above the Tech. Spec limit of 4200 pcm. The available excess reactivity is 5870 pcm. Considering the maximum allowed withdrawal of control rods to 405 mm, the length of a campaign is estimated to be 95 days, assuming the burn up loss of reactivity is -1 pcm/MWd.

Even though it was anticipated that the transition to 40 MWt may take place in the 31^{st} irradiation campaign, but it was later decided to have the transition to 40 MWt in the 30^{th} campaign itself[2]. Due to this, there is change in the burn up of the subassemblies and hence SDM of the proposed core, while rest of the features of the core remain the same as that of the proposed 40 MWt core.

The core configuration at the end of 29^{th} irradiation campaign after the failed fuel identification consists of 45 MK-I fuel subassemblies (FSA) and 8 MOX. To achieve 40 MWt core, 8 MOX fuel need to be discharged and 27 fresh FSA to be loaded along with 4 poison SA. Totally core will have 69 Mark –I FSAs. Since it involved lot of transfer operation, the fuel handling was split in such a way that each step has a core change of ~ 2000 pcm.

3. Conclusion

The power generation in FBTR can be raised to 40 MWt, by expanding the core with 70 Mark I fuel SAs, the minimum shutdown margin criteria of 4200 pcm is ensured by adding four poison B_4C SAs with 50% B^{10} enrichment in the specific locations of 2^{nd} ring. It is suggested to load these absorber subassemblies in the locations 02-01, 02-04, 02-07 and 02-10. With this arrangement, the maximum power attainable is 41.3 MWt when the peak LHR in the core is 400 W/cm. However the operating power will be limited to 40 MWt by setting LCO & LSSS parameters.

4. References

[1] S. Sivakumar and G. Raghu Kumar, "Conceptual configuration of 40 MWt core for Fast Breeder Test Reactor", RFG/FBTR/S-RS-02/31400/TN-1405, 2018.

[2] Neethu Hanna Stephen and E. Radha, "Transition from 53 SA Core to 69 Mark I SA Core for 40 MWt Operation ", RFG/O&MG/TSD/RPS/S-RS-02/31400/TN – 1106 Rev-01, 2021.

BIFURCATION ANALYSIS OF LARGE PRESSURIZED HEAVY WATER REACTORS

Abhishek Chakraborty[1] and M. P. S. Fernando
Nuclear Power Corporation of India Limited, Mumbai, India
[1]*e-mail: abhishekc@npcil.co.in*

Abstract

Stability analysis can be performed by transient analysis using different system codes which model the phenomena in detail. These system codes can capture the intrinsic nonlinearities in the system but the simulations have to be performed for different values of parameters and initial perturbations. This becomes a computationally intensive work and the estimation of the stability characteristics for the entire domain is difficult using this method. Linear Stability Analysis is valid for small perturbations, and the system behavior for “large” perturbations cannot be predicted by the linear stability analysis i.e., the system might exhibit “unstable” periodic solutions on the stable side and “stable” periodic solutions on the unstable side of the stability boundary. Hence, a detailed bifurcation analysis is required to estimate the "global" stability characteristics of the system. In this study, the bifurcation characteristics of 700MWe PHWR considering reactivity feedbacks due to Xenon, fuel temperature and coolant temperature has been investigated using reduced order models.

1. Introduction

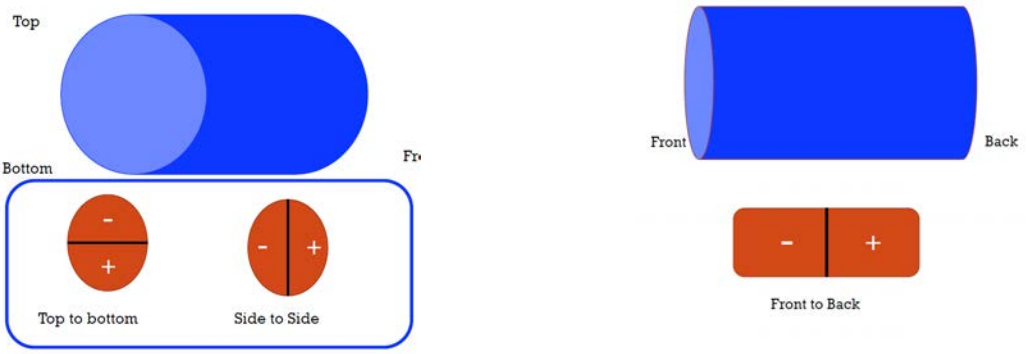
The effects of Xenon are a potential source of instability in PHWRs which operate in thermal spectrum. The production rate of Xe-135 depends upon the I-135 concentration, and, hence upon the neutron flux history. On the other hand, the removal of Xe-135 depends on the instantaneous flux through the neutron absorption process and also through the Xe-135 decay process. Xenon oscillations are produced due to the mismatch between Xenon removal and Xenon build up from Iodine decay. This mismatch can establish an oscillatory regime in reactor power which can cause the power to exceed the allowable limits.

Reduced Order Models (ROM) are very widely used for analysing stability characteristics of highly nonlinear systems like Boiling Water Reactors. These are simplified models derived from the system equations by certain approximations such that the phenomena is well captured. These models generally reduce the partial differential equations describing the system dynamics by to a system of Ordinary Differential Equations (ODEs). The main advantage of ROM is that they can be used for both linear and nonlinear stability analysis. The stability maps are constructed based on these models for identifying the stable and unstable regimes in different parameter spaces. Then, numerical simulation using system codes are carried only for certain regions of interest are thereby saving a lot of computational time and effort for estimating the stability characteristics. In addition, the stability maps give an overall picture of the stable and unstable parameter space and it’s very convenient to estimate the instability threshold.

2. Stability Analysis

Xenon induced spatial oscillations can be studied by means of modal expansion technique. In this technique, the space-time dependent neutron flux can be described as a Superposition of the fundamental mode and higher harmonics. The fundamental mode and the higher harmonics are the solutions of the neutron diffusion eigenvalue equation. The fundamental mode has the lowest eigenvalue or the highest multiplication factor. A sub-critical reactivity is associated with each of the higher order modes and is used to assess its importance from a spatial control point of view. This modal reactivity is a measure of the susceptibility of the reactor to flux shape disturbance due to the

particular mode. For a large PHWR, it is found that the sub-criticality associated with the first azimuthal mode is the least. The top to bottom and the side to side modes are degenerate modes with identical subcriticality and are most susceptible to Xenon induced spatial oscillations. In addition to the azimuthal modes, the axial mode can also be excited in certain situations. Hence, the reactor core is divided diametrically into two equal halves (azimuthally and axially) for the analysis using multipoint kinetics and is shown in Figure 1.



(a) Azimuthal modes (b) Axial modes

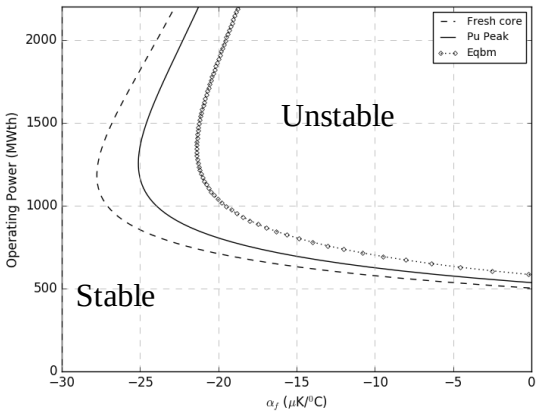
Figure 1 A PHWR divided into two regions (azimuthally and axially)

2.1 Stability maps

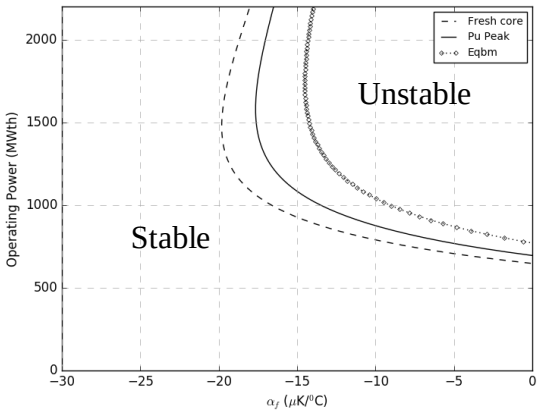
In this study, nonlinear analysis has been carried out using the code BIFOR. BIFOR (Bifurcation Formulae for Ordinary-differential system) is a semi analytical bifurcation code developed by Hassard [1] which calculates the bifurcation parameters like the critical value of the parameter, type of bifurcation, frequency of oscillation, etc. The code is based on the Semi Analytical Bifurcation Method. The code assumes that a pair of eigenvalues are purely imaginary (with the rest of the eigenvalues being negative) and reduces the system to 2×2 by center manifold theorem. The system is reduced to the Poincare normal form which for a Hopf Bifurcation is a 2-dimensional autonomous system and the bifurcation parameters like β_2 are estimated. The value of β_2 indicates the stability of the periodic solutions. $\beta_2 > 0$ indicates subcritical Hopf Bifurcation, $\beta_2 < 0$ indicates supercritical Hopf Bifurcation and $\beta_2 = 0$ denotes a Generalized Hopf Point.

The stability analysis was carried out separately for two modes of oscillations for 700 MWe PHWR i.e., Side to Side/Top to bottom and front to back (axial) modes for three core burnup states, namely, the fresh core, Plutonium Peak and Equilibrium Core. The Fresh core of 700 MWe PHWR consists of 248 Deeply Depleted Uranium (DDU) bundles and 4456 Natural Uranium (NU) bundles[2]. The reactor is designed to operate in the equilibrium core condition for most of its life.

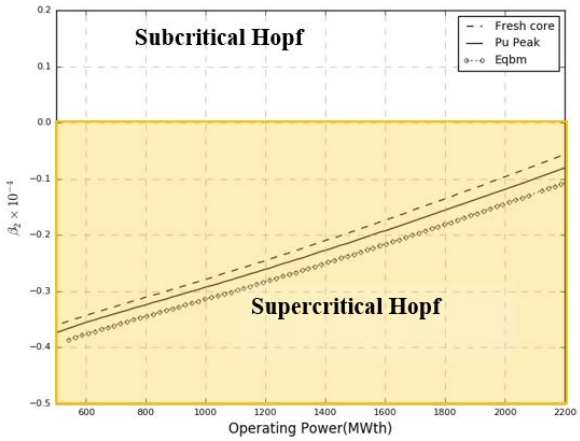
Stability maps were generated in the Operating power Vs fuel temperature coefficient (α_f) for a constant value of coolant temperature coefficient (α_c) for different core burnup conditions viz., fresh core, Plutonium peak and Equilibrium Core. The value of coolant temperature coefficient (α_c) considered for generation of the stability map 1 are 6 $\mu K/^0C$, 10 $\mu K/^0C$ and 10 $\mu K/^0C$ for fresh core, Plutonium peak and equilibrium core respectively. The stability map for azimuthal and axial mode of oscillation are given in Figure 2.



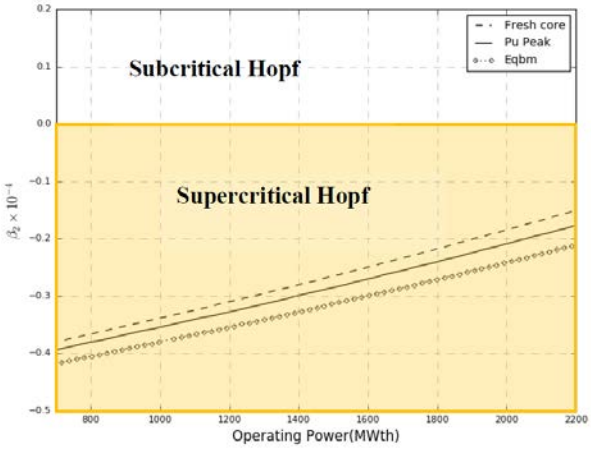
(a) Stability map for Azimuthal mode



(b) Stability map for Axial mode



(c) β_2 variation for Azimuthal mode

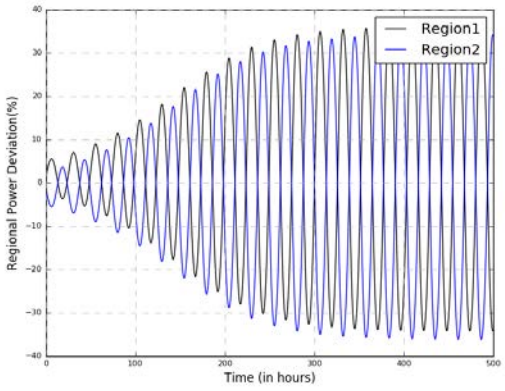


(d) β_2 variation for Axial mode

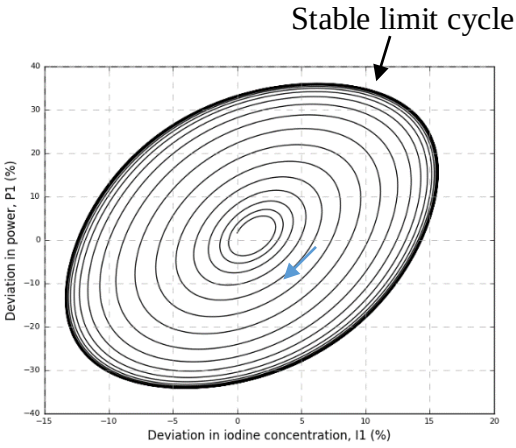
Figure 2: Stability maps and Floquet exponents

2.2 Verification using numerical simulations of trajectories

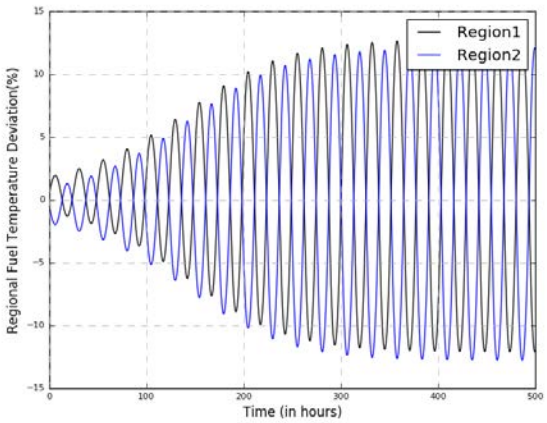
In order to verify the stability boundary and the nature of Hopf bifurcation, numerical simulations were performed at different points in the stability map in the α_f vs. f plane and the results are given in Figure 3.



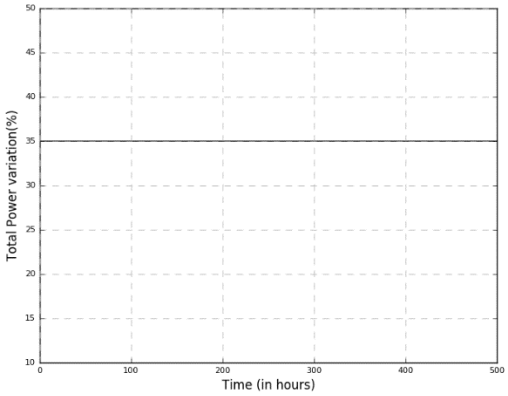
a) Time series representation



b) State space representation



c) Regional fuel temperatures



d) Variation of total power with time

Figure 3 Supercritical Hopf nature of oscillations

Since the parameter values corresponding to this point are on the unstable side of the stability boundary, the growing oscillations are expected. Since, the point lies on the Supercritical Hopf bifurcation region, the trajectory settles on a stable limit cycle as shown in Figure 3. Stable focus was observed on the stable side, constant amplitude oscillations were observed on the stability boundary and stable limit cycle was observed on the unstable side. Hence, it can be confirmed by numerical simulations that the system exhibits Supercritical Hopf Bifurcation in this region which is consistent with the results of the bifurcation code, BIFOR.

3.0 Conclusion

In this work, a methodology for carrying out stability analysis of 700MWe PHWR considering Xenon induced spatial oscillations is developed using reduced order models. These models are capable to capture the phenomena of interest very well with simplified equations. Reduced order models are very widely used for analyzing stability characteristics of highly nonlinear systems. These models are used for both linear and nonlinear stability analysis. The stability maps are constructed based on these reduced order models to identify the stable and unstable regimes and then analysis for certain regions of interest are carried out using system codes. Thus a lot of computational time and effort for estimating the stability characteristics is reduced. For estimating the nonlinear stability characteristics for 700MWe PHWR, the code, BIFOR (based on Semi Analytical Bifurcation Method) was used to find out the existence of Hopf Bifurcation in different parameter spaces. The existence of Supercritical Hopf bifurcation was found based on the sign of the Floquet exponent estimated by BIFOR. Supercritical Hopf bifurcation is a soft bifurcation and has stable limit cycles on the unstable side of the stability boundary. The transition point from Supercritical Hopf to Subcritical Hopf bifurcation was also found but it was beyond 110%FP in which the set of equations modelling the coolant condition changes. Hence, no “hard” or Subcritical Bifurcation existence was found in the operating regime for 700 MWe PHWR.

4.0 References

[1] B. Hassard, “Theory and Applications of Hopf Bifurcation.”, Cambridge University Press, 1981.

[2] Preliminary Safety Analysis Report for 700 MWe PHWR.

NONLINEAR STABILITY ANALYSIS OF BOILING WATER REACTOR BY LYAPUNOV EXPONENTS

S. S. Singh
Safety Research Institute, Atomic Energy Regulatory Board, Kalpakkam, India
email: sudhansu@igcar.gov.in

Abstract

Boiling water reactors (BWRs) are susceptible to reactivity instabilities when operated at low flow conditions. Studies on nonlinear dynamics and stability analysis of BWR was carried out earlier by March-Leuba et. al. In this study, amathematical model for analysing nonlinear instability in BWRs wasproposed and qualitative behaviour in nonlinear regime was studied by deterministic and stochastic methods.In the present study, the mathematical model of Leubahas been suitably modified by including normalized form of neutron point kinetics equation. Further, computational tools have been developed to study formation of attractors during different type of transients and to calculate largest Lyapunov exponents. Nonlinear stability analysis for BWRs has been carried out by parametrically varying the feedback gain which correlates fuel temperature and void formation. Stability boundary has also been evaluated. When the feedback gain is increased beyond the stability limit, period doubling and bifurcation in the amplitude of neutron density are observed.

1. Introduction

The BWRs have been experimentally found to behave as linear systems under normal operating conditions. However, stability tests have shown that this type of reactor is susceptible to reactivity instabilities when operated at low flow conditions.Qualitative studies on nonlinear dynamics and stability analysis of BWR was initially carried out by March-Leuba et al.[1]. In this study it was established that when such instabilities occur, limit cycles are observed where the neutron density shows oscillatory behaviour. Subsequently, a phenomenological model was originally developed for analysing the nonlinear instability in BWRs [1]. In the present study, the mathematical model proposed by March-Leuba et al. has been suitably modified to include normalized point kinetics equation. Computational tools were developed to construct attractors and to calculate largest Lyapunov exponent. Nonlinear stability analysis is carried out alternatively by calculating the largest Lyapunov exponent for different values of the feedback gain.

2. Modified Model of BWR Dynamics

A phenomenological model for studying nonlinear BWR dynamics must contain the essential processes that control the dynamics behaviour of a BWR, yet it should be simple enough to allow numerical simulation of a wide range of reactor operating conditions. A simplified model has been proposed for the nonlinear study of a BWR dynamics which contains one-point representation of reactor kinetics, a one-node representation of the heat transfer process in the fuel, and a two-node representation of the channel thermal-hydraulics to account for the void reactivity feedback [1]. In the present study, the set of equations has been modified by including normalized form of neutron point kinetics equation. Mathematically the model is represented by the following system of ordinary differential equation:

$$\frac{dn(t)}{dt} = \frac{\rho(t)-\beta}{\Lambda} n(t) + \frac{\beta}{\Lambda} c(t) + \frac{\rho(t)}{\Lambda} \quad (1)$$

$$\frac{dc(t)}{dt} = \lambda n(t) - \lambda c(t) \quad (2)$$

$$\frac{dT(t)}{dt} = a_1 n(t) - a_2 T(t) \quad (3)$$

$$\frac{d^2\rho_\alpha(t)}{dt^2} + a_3 \frac{d\rho_\alpha}{dt} + a_4 \rho_\alpha = k * k_0 T(t) \quad (4)$$

and

$$\rho(t) = \rho_\alpha(t) + DT(t)$$

where

n(t) = excess neutron density normalized to the steady state neutron density

c(t) = excess delayed neutron precursors concentration normalized to steady state precursor concentration

T(t) = excess average fuel temperature

$\rho_\alpha(t)$ = excess void reactivity feedback

The specific numerical values for the resulting model parameters are taken from thestability testsconducted at the Vermont Yankee reactor [1]. The parameter ***k***, which is proportional to the void reactivity coefficient and the fuel heat transfer coefficient, controls gain of feedback and thus defines stability of the reactor model. By artificially increasing the value of *k* above 1,the model can be made unstable and can be used to study BWR dynamic behaviour in the nonlinear regime.

2.1 Definition of Attractors

An attractor is an attracting set that contains a dense orbit in the phase space [2]. In the present study the phase space is constructed from n(t) and dn(t)/dt.In literature, there are three known type of non-strange attractors: the fixed point attractor, the limit cycle attractor and the torus attractor. These are nonfractal attractors, the behaviour of which can be accurately predicted. The fixed point is associated with attractors whose orbits approach an equilibrium state; the limit cycle corresponds to a periodic motion; and the torus corresponds to quasiperiodic motion.

2.2 Computing Lyapunov Exponents

If the displacement between the i-th point and a neighbouring point at time $t_i$is d_i, and the initial displacement between the two points is d_{0i} at t_{0i}, then the Lyapunov exponent is defined as

$$\lambda = \lim_{n\to\infty} \frac{1}{n} \sum_{i=1}^{n} \frac{1}{(t_i - t_{0i})} \ln \left| \frac{d_i}{d_{0i}} \right| \quad (5)$$

Following algorithm is used to compute Lyapunov exponent of an attractor:

- Pick a random point
- Select a nearby point
- Advance both orbits a small amount and calculate the new separation d_1
- Calculate the local Lyapunov exponent, $\frac{1}{t_{step}} \ln \left| \frac{d_1}{d_0} \right|$
- Readjust the second orbit. This should be done so that its displacement from the reference orbit is again d_0, but in the same direction as d_1.
- Repeat n times to produce an average Lyapunov exponent.

$$\lambda = \frac{1}{n(t_{step})} \sum_{i=1}^{n} \ln \left| \frac{d_i}{d_0} \right| \quad (6)$$

3. Results and Discussions

A computer program has been developed to study the nonlinear behaviour of a BWR. The coupled set of ordinary differential equation of the model has been solved by backward difference formula algorithm. The largest Lyapunov exponent of the system is evaluated by orbit separation method. The Lyapunov spectrum is calculated by Gram-Schimdt orthonormalization method. The methodology and the programs were validated for several test problems.

For the deterministic numerical analysis, a 10% step-type perturbation was introduced in the neutron population. The solution was then allowed to converge freely to its final state. Evolution of normalized neutron density and phase space representation of n and dn/dt are shown in Fig. 1 for three different values of feedback gain: (a) k= 1.0, (b) k = 1.4, and (c) k = 2.0. The concern in nonlinear regime is the stability of oscillation. It is observed that there are clear differences in the way limit cycle is reached in the three cases. In case (a), the normalized neutron density oscillates at an amplitude 1.5 which results in a limit cycle in phase space. As the k value is increased in case (b), it is observed that the amplitude never converges to a final value. The limit cycle becomes unstable and is following a new limit cycle of its own with twice the original period. This process is called a period-doubling pitch-fork bifurcation. In case (c), the amplitude of oscillation is quite irregular.

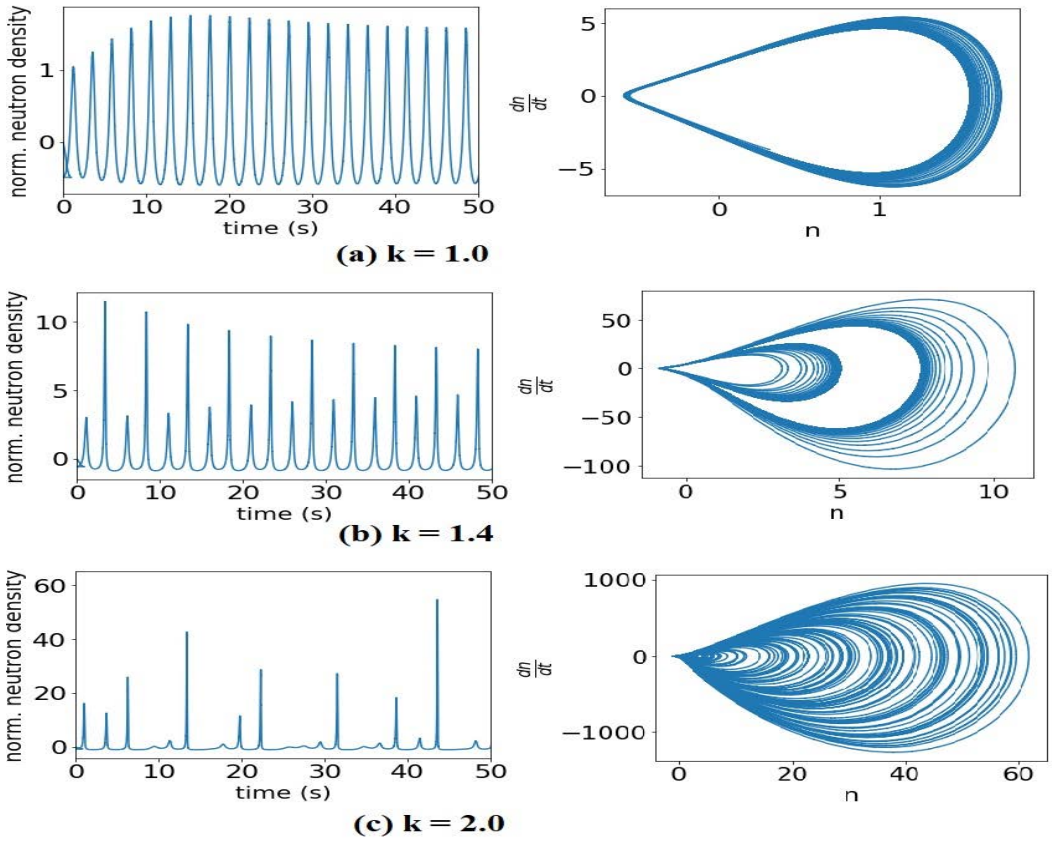


Fig.1. Variation of normalized neutron density and phase space representation.

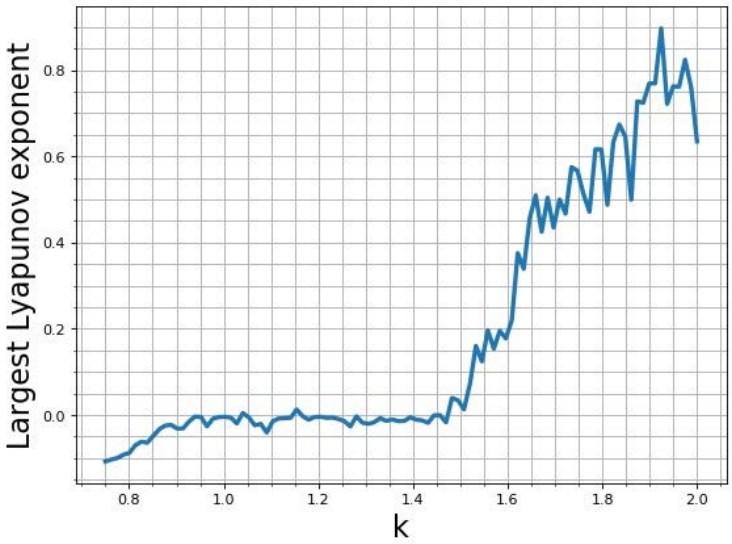


Fig. 2. Variation of largest Lyapunov exponent with change in feedback gain

A novel approach has been adapted to characterize stability boundary of the system. By definition, if the largest Lyapunov exponent (LLE) is negative then the system is stable. If it is positive the system is unstable. If LLE is zero the system will give rise to limit cycle orbit. LLE of the model has been calculated for k = 0.75 – 2.0. 100 points are taken for the analysis. The LLE versus k is plotted in Fig. 2. It is seen that for k value 0.9 – 1.4 the LLE is equal to zero. This will result in formation of limit cycle attractor. Beyond k = 1.4, the LLE is positive which will make the system unstable.

4. Conclusion

A modified mathematical model has been developed to characterize nonlinear instability in a BWR. Computational tools were developed to get the phase space representation and to calculate Lyapunov exponent. Nonlinear stability analysis was carried out by varying the feedback gain. Bifurcation phenomena has been observed during construction of attractors. Stability boundary has been evaluated by plotting Lyapunov exponent versus feedback gain. It has been concluded that the BWR system is unstable in low-flow conditions. In future the study will be extended by calculating fractal dimensions from Lyapunov spectrum.

References

[1] J. March-Leuba, D. G. Cacuci, and R. B. Perez, “Nonlinear Dynamics and Stability of Boiling Water Reactors: Part 1- Qualitative Analysis,” *Nuclear Science and Engineering* , Vol. 93, Issue. 1986, pp. 111-123.

[2] R. L. V. Taylor and J. David, “Attractors: Nonstrange to Chaotic,” SIAM, Issue. 2011, pp.72-80.

INSIGHTS FROM REACTOR PHYSICS DESIGN REVIEW OF IPHWR-700

Susheel Kumar[1], Amandeep Singh, Soumen Koner, Obaidurrahman K. and Utkarsh S.C.
Atomic Energy Regulatory Board, Mumbai, India
[1]*e-mail: - skumar@aerb.gov.in*

Abstract

The review of the reactor physics aspects of PHWR-700 MWe design has been carried out by the reactor physics group and respective committee of AERB to support the multi-tier regulatory review and consenting process. The review was carried out in line with design/ safety requirements brought out in various regulatory documents and utilizing the experience of previous safety reviews. The review of PHWR-700 focused on the First of a Kind (FOAK) systems and features. Specific design features, associated safety issues of 700 MWe PHWR core and key aspects of relevant regulatory assessment at AERB have been presented in this article.

1. Introduction

Capacity of Indian PHWRs has been enhanced from 220 MWe to 540 MWe and subsequently 700 MWe. Core design of 700 MWe PHWR is based on 540MWe reactors operating at Tarapur, with a notable difference of partial coolant boiling near channel exit. There are 392 fuel channels, each having 12 fuel bundles (37 fuel element cluster). As the core is physically identical to the 540 MWe core, additional 25 % fission power generation in the core is achieved through flux flattening (giving additional ~ 7% fission power) and increasing average linear heat rating of the fuel elements (giving additional ~ 18% fission power). This has resulted in overall increased time average coolant channel power, bundle power and fuel linear heat rating. The primary heat transport (PHT) system of 700 MWe PHWR consists of 392 horizontal coolant channels arranged in two independent coolant loops (with an interleaving configuration unlike 540 MWe) which contain heavy water as coolant at high pressure and high temperature. Boiling to the extent of about 2 to 3 % at channel exit in conjunction with slightly increased coolant flow has been incorporated to enhance removal of the additional core heat. Up-to 85 % full power, the coolant is predicted to be in single phase and beyond 85 % FP, boiling may start towards the end of 10^{th} bundle position in the channel. Increased power generation from the similar core has in-principle reduced the thermal margins in 700 MWe core therefore a few additional design systems have been installed in 700 MWe PHWR to augment the core safety. The First of A Kind (FOAK) systems/ features of the 700 MWe with respect to Indian PHWRs include partial boiling of coolant at the channel exit (above about 85%FP), Regional Overpower Protection System (ROPS), interleaving of feeders to bring down the void reactivity in case of Large Loss of Coolant Accident (LBLOCA), Passive Decay Heat Removal System (PDHRS), Containment Spray System (CSS) and steel lined Primary Containment [9, 10, 11].

2. Insights from physics design review of various systems and design provisions

The salient aspects of the review carried of various systems and design provisions related to core neutronic design are brought out in the following subsections:

2.1 Reactivity feedbacks and effect of partial coolant boiling

Extremely soft neutron spectrum and separate coolant moderator circuit lead to weak reactivity feedbacks in PHWRs. This feature of weak power reactivity coefficient (PCR) is well known in PHWR type design and is catered through RRS [4]. In-principle, a design with mild negative PCR

value, would still require a reactor control system (Reactor Regulating System- RRS) for stable reactor operation e.g. design of 220 MWe incorporates RRS for stability and control even though negative magnitude (though very small) of PCR has been maintained in the entire power operating regime in line with AERB guidance [3]. In 700 MWe PHWR core design due to positive contribution from allowed partial coolant voiding near channel exit, PCR has worsened further and has been a significant concern for the reviewers regarding the core stability and reactor safety.
The AERB safety review focussed on the core stability analysis carried out to assess the effectiveness of RRS to provide for stable operation of the reactor and acknowledged that the core neutronic behaviour is stable with RRS. Additionally, the operating and regulatory experience of other countries wherein similar PHWR design based reactors have been operating for quite some time was also utilized during the review. The position of Canadian regulator (CNSC) on the issue is that the power coefficient of reactivity of CANDU reactors does not pose a significant risk and that a reactor design that has a positive power coefficient of reactivity is quite acceptable provided that the reactor is stable against power fluctuations, and that the probability and consequences of any potential accidents that would be aggravated by a positive reactivity feedback are maintained within prescribed limits [5]. IAEA Safety Standards also require that design provides for the control of plant behaviour by means of inherent and engineered features [12].

2.2 Regional overpower Protection System (ROPS)

ROPS enables reactor trip on local overpower to avoid the on-set of fuel sheath dry out or fuel centre line melting. ROPS senses excess power in any local region of the core by means of two sets of arrays of detectors with each set (ROPS-1 and ROPS-2) causing the actuation of respective shutdown system at the predefined trip set-point [6]. The design basis of ROPS is a slow loss of reactivity control wherein malfunction of certain reactivity devices or RRS leads to slow insertion of positive reactivity and consequent slow increase in reactor power and degradation of MCHFR (minimum critical heat flux ratio). The design of ROPS is based on estimation of Critical Channel Power (CCP, defined as the channel power at which the fuel sheath dry-out or fuel melting occurs) for various possible flux shapes, and determining the trip set-points in such a manner that reactor trips before any fuel channel in the core reaches its CCP [1]. ROPS has been incorporated in the PHWR -700 MWe design as the values of minimum Critical Channel Power Ratio (min CCPR; the ratio of channel power where the fuel sheath dropout occurs to the instantaneous channel power) has reduced significantly than in 540 MWe design and Channel Outlet Temperature (COT) based power setbacks are not possible. The refuelling ripples are catered through calibration of ROPS detectors by multiplying it with channel power peaking factor (i.e. CPPF defined as maximum of ratio of instantaneous channel power to time averaged channel power) when the reactor is in steady state. Lower CPPF value provide more operating margin from ROP trip.

The review focussed on various design aspects and on the rationale to arrive at trip set points of ROPS-1 and ROPS-2 including the adequacy of the number of flux shapes considered in designing ROPS, appropriateness of and comparison between steady-state calculations and transient analyses, identification and demonstration of most enveloping flux shape for carrying out transient analysis, slowest possible insertion of positive reactivity, initial values for bundle and channel powers and utilization of operating and regulatory experience of other countries operating similar designs. Steady state calculations appear to be more conservative for estimation of CCPs based on the assumption following which neutronic and thermal power lag is neglected. Few advantage of carrying out the steady state analysis are that the validity of the analysis is explicitly ascertained for all the considered neutron flux shapes as well as for various possible initial channel powers. In

absence of the steady state analysis these concerns have to be separately addressed. The regulatory decision making on the aspect relied on the comprehensiveness of the steady-state estimations until more experience on the associated design and operational aspects is generated.

2.3 Design changes in Flux Mapping System

As large PHWR cores are neutronically loosely coupled and, therefore, prone to spatial instabilities, in-core detectors and liquid zone compartments (LZCs) are provided for detecting and suppressing these local oscillations in addition to global power control. Flux Mapping System (FMS) is present in large PHWRs to correct the zonal detector readings. This system uses flux synthesis method to reconstruct the flux shape in the reactor with the help of several Vanadium self-powered neutron detectors (SPNDs). As the coolant is not in sub-cooled condition at the channel exit, COT based power set-backs are not available in 700 MWe PHWRs. In 700 MWe design FMS computed bundle powers, channel powers and zonal powers fed to RRS to trim down the reactor power at the specified rate of 0.1%FP/sec as per the RRS logic to ensure the reactor operation adhere with the Technical Specifications [8].

The review focussed on the accuracy and validation of FMS estimations for steady-state reactor operation as well as dynamic situations e.g. for catering Xenon oscillations, unavailability of certain number of FMS SPNDs and its effect on FMS accuracy, addressing the unavailability of FMS itself. There are certain changes in design of FMS of 700 MWe with respect to that of 540 MWe including use of more number of higher harmonics and perturbation modes, daily updation of fundamental mode in FMS, follow-up of sensitivity of each SPND. While reviewing these aspects, it was acknowledged that incorporation of these modifications has resulted in better accuracy of FMS estimations.

2.4 Interleaving of feeders to reduce the void reactivity

Both 540 MWe and 700 MWe PHWRs, primary heat transport system has two independent and identical loops of figure of eight. While in 540 MWe PHWR, coolant channels in each vertical half of the reactor are served by one loop, 700 MWe has these loops feeding alternate channels (Figure-1) [9]. This is done by adopting interleaving of feeders, as against distribution in two vertical halves.

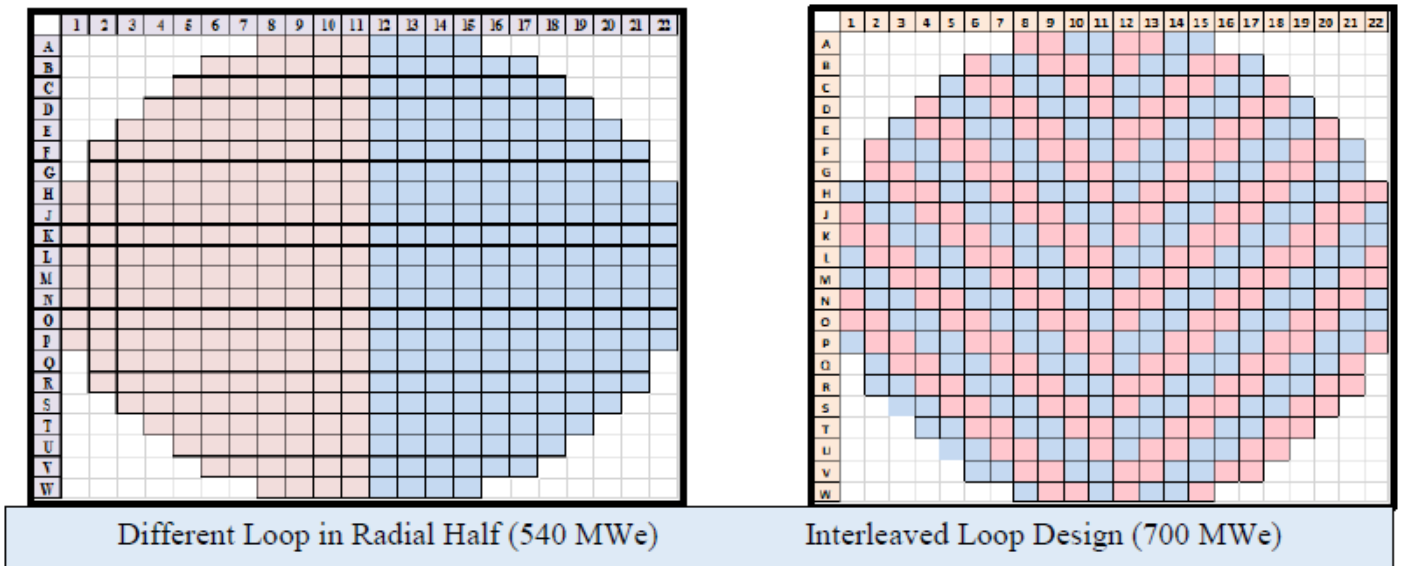


Fig-1: Two loops of primary heat transport system (540 MWe and 700 MWe)

This arrangement, which is introduced for the first time in any PHWR in the world, minimises positive void reactivity by uniformly distributing voids in the event of loss of coolant. Interleaving has made feeder layout even more complex and increased feeder lengths. The results of LOCA analysis (using ATMIKA and 3-D neutron kinetics code IQS-3D) considering interleaving of feeders configuration were reviewed. It was acknowledged that the LBLOCA study demonstrates that interleaved configuration has higher safety margins in terms of peak power, margin to prompt-criticality, adiabatic heat deposition, sheath temperature excursion and clad oxidation [10].

3. Summary

The salient aspects of safety review of physics design of PHWR-700 MWe has been brought out. The incorporation of design changes e.g. partial coolant boiling at the channel exit, enhanced flux flattening through different burn-up zones and interleaving of feeders have been explained. The review of changes of core neutronic and reactivity feedback characteristics and design bases of FOAK systems / features has been presented. The extraction of higher power from 37 fuel pin bundle is addressed through incorporation of a number of new systems/ features. Safety review at AERB has been carried out based on review experience of earlier PHWRs, compliance to required safety goals and relevant practices elsewhere in PHWR operating countries. Wherever necessary, independent verification analysis has also been done at AERB to support the review process.

4. References

[1] Atomic Energy Regulatory Board, “Annual Report, 2020 of Atomic Energy Regulatory Board”, Published by Head, R&DD, AERB.

[2] S. Banerjee and H. P. Gupta, “Development of Technologies and Safety Systems for Pressurised Heavy Water Reactors (PHWRs) in India”, *ASME Journal of Nuclear* Engineering and Radiation Science. Apr 2017, 3(2): 020902, Paper no: NERS-16-1072

[3] AERB Safety Guide on Core Reactivity Control in PHWRs (AERB/SG/D-7)

[4] Nik K. Popov and Victor G. Snell, “Safety and Licensing Aspects of Power Reactor Reactivity Coefficients”, Proceedings of the 20th International Conference on Nuclear Engineering collocated with ASME Power Conference ICONE20-POWER 2012, California, USA

[5] ‘Mythbusters – Myth: CANDU reactors are dangerous due to their power coefficient of reactivity’, CNSC website: http://nuclearsafety.gc.ca/eng/resources/mythbusters/index.cfm

[6] Surendra Mishra, “Optimization Studies For Physics Problems in Indian PHWRs”, Ph.D. Thesis submitted to Homi Bhabha National Institute, April 2012

[7] Nuclear Power Corporation of India Limited (NPCIL), “Status report 105 - Indian 700 MWe PHWR (IPHWR-700)” (available at IPHWR-700.pdf (iaea.org))

[8] Abhishek Chakraborty, M. P. S. Fernando & A. S. Pradhan, “Performance of Flux Mapping System During Spatial Xenon Induced Oscillations in PHWRs”, In: Bose, M., Modi, A. (eds) Proceedings of the 7th International Conference on Advances in Energy Research

[9] “700 MWe Indian Pressurized Heavy Water Reactor”, INS News Letter, Vol 20 Issue 03, Nov 2020

[10] Kumar, Nrependra et. al.,“Safety margin improvement by adopting the feature of interleaving in 700 MWe PHWR”, Proceedings of the international workshops on NPPs-safety and sustainability and new horizons in nuclear reactor thermal-hydraulics and safety

[11] Yadav, S.K. et. al., “Assessment of decay heat removal capability of passive decay heat removal system (PDHRS) of 700 MWe Indian PHWRs”, Proceedings of the international workshops on NPPs-safety and sustainability and new horizons in nuclear reactor thermal-hydraulics and safety.

[12] “Safety of Nuclear Power Plants: Design”, IAEA/SSR-2/1 (Rev-1), 2016

LOSS OF REGULATION SCENARIO IN AHWR ORIFICED CORE

A. Srivastava[1], A. D. Contractor and Rajesh Kumar
Reactor Safety Division, RD & DG
Bhabha Atomic Research Centre, Mumbai, India
[1]*e-mail: - abhisri@barc.gov.in*

Abstract

A vertical pressure tube type boiling light water cooled and heavy water moderated reactor has been designed with various advanced safety features. One of the important passive design features of this reactor is that the heat removal is achieved through natural circulation of primary coolant at all power level with no primary coolant pumps. Design has been improved by orificing the inlet feeder to enhance the stability of the reactor. To check the adequacy of core heat removal capability during increase in reactor power following the uncontrolled withdrawal of bank with maximum worth control rods, a Loss Of Regulation Accident (LORA) scenario has been analyzed for the orifice core. The paper highlights the detailed case studies of LORA transient and its effect on important reactor parameters like pressure, clad temperature along with other parameters.

1. Introduction

Recent inclination in nuclear industry is towards providing as many passive features as possible, including those during operating conditions. These enhance safety substantially. One of such conceptual design is natural circulation pressure tube boiling water reactor. The proposed Advanced Heavy Water Reactor (AHWR) is a 920 MW_{th} vertical pressure tube type boiling light water cooled and heavy water moderated reactor [1].

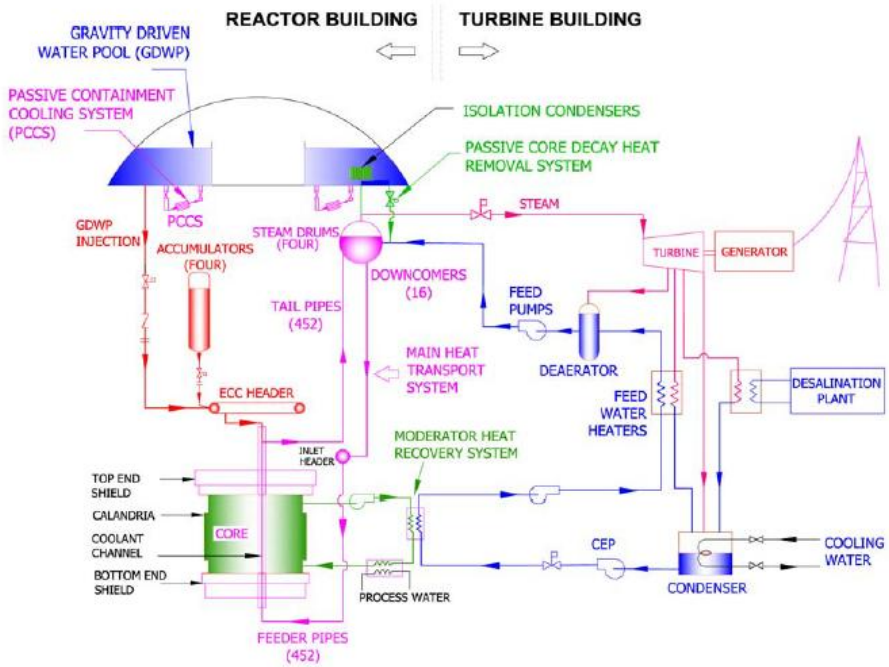


Figure 1 Schematic of AHWR

The Main Heat Transport System of the AHWR consists of reactor core, core inlet, core outlet, bottom extensions, inlet feeders, tailpipes, steam drums, downcomer and inlet header as shown in Fig. 1.

LORA i.e. positive reactivity addition scenario due to uncontrolled withdrawal of control rod results in increase in reactor power. This leads to increase in system pressure and temperature. The core flow should be adequate enough to keep the fuel temperature within limit. It is desirable to study the design capabilities to limit the consequences of this scenario for the present AHWR orifice core.

2. Problem Description

For LORA transient insertion of 12.1 mk reactivity in 867 sec with availability of all shutdown system has been considered. During postulated Loss Of Regulation Accident (LORA), Reactor protection on high power trip has been ignored in the present analysis. The reactor power as well as system pressure continue to rise. The 2nd trip signal is generated based on high system pressure i.e. 7.6 MPa which leads to reactor scram.

3. Modelling of Reactor in RELAP5

RELAP5 code [2] has been used to simulate this LORA transient. Reactor system such as Main Heat Transport (MHT) system, Isolation Condenser (IC) are modelled [3] in RELAP5. The physics parameters used in the analysis are listed in Table 1.

Table 1 Reactor kinetics Parameters

Fuel Temperature Coefficient	-20.6 μk/°C (285 to 450°C)
Channel Temperature Coefficient	+22.9 μk/°C (62.5 to 285°C)
Coolant Void Coefficient	-70.0 μk/% void (0.74 to 0.45 g/cc)
	-100.0 μk/% void (0.45 g/cc to 0 g/cc)
	-88.0 μk/% void (0.74 g/cc to 0 g/cc)
Moderator temperature	+33.8 μk/°C (27 to 62.5°C)
Delayed Neutron Fraction	0.0034
Neutron Generation time	0.19 ms
SDS#1 Worth (35 SORs, 2 maximum worth SORs missing)	51.3 mk
High neutron flux	> 110 % Of Normal Value
High neutron log rate or period	> 10 %/s or <10 s
Total length of travel	390 cm

4. Results and Discussion

The sequence of event following LORA for orifice core is given in Table 1.

Table 1 Sequence of Event

POSTULATED	OBSERVED
Positive reactivity addition starts	t=0 s
CSDV opens	t = 244 s
Reactor Scram ignored on 110% power signal (1st Signal)	t=258.76 s

MSIV closure on high steam flow (140%)	t=348.65 s
Reactor Scram on high pressure signal at 7.6 MPa (2nd Signal)	t=355.74 s
Turbine trips on Reactor Scram Signal	t=355.94 s
IC opening signal (7.65 MPa)	t=356.7 s
End of transient	t=1100 s

Positive reactivity insertion as shown in Fig. 3 results in slow increase in the power. Power increase leads to increase in steam flow as more steam is produced. The feed also increases. The reactor power as depicted in Fig. 4 crosses 110% FP set point for reactor trip but this signal is ignored.

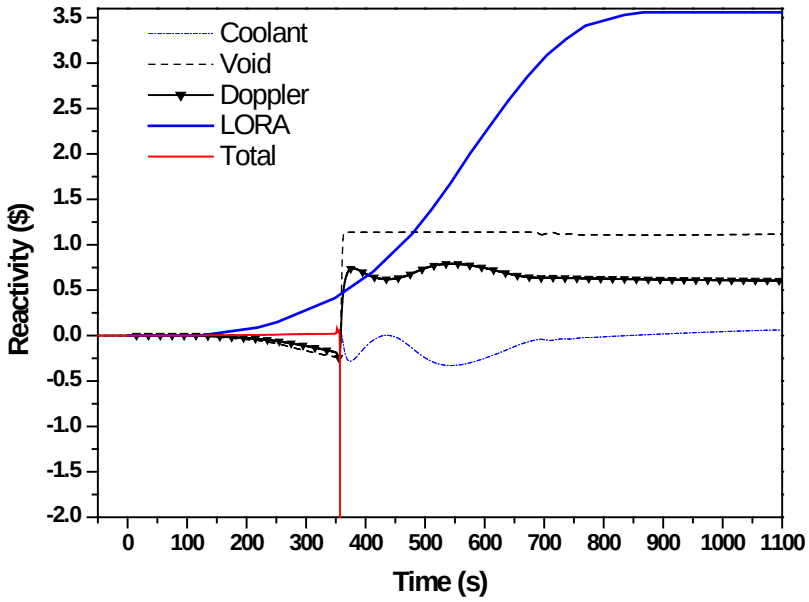


Figure 3 Reactivity transients during LORA

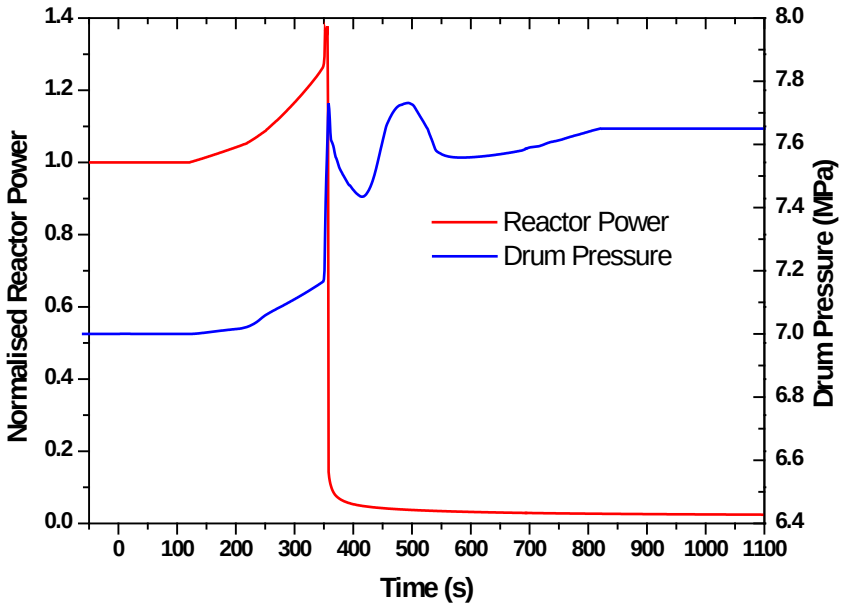


Figure 4 Reactor and Drum Pressure transients during LORA

Further power increase leads to increase in steam flow. The steam flow is unable to limit the pressure rise thus pressure slowly builds up as shown in Fig. 4. Once steam flow crosses 140% limit MSIV closes leading to bottling of the MHT. This results in sudden increase in pressure and collapse of void. Reactor power rises rapidly owing to positive reactivity feedback. Pressure crosses 7.6 MPa resulting in reactor trip. Reactor trips leads to decrease in power and also IC opening at 7.65 MPa removes the heat from MHT. This combined action arrests the pressure rise and pressure stabilises around 76.5 bar and IC keeps on removing the decay heat. The clad temperature increases during the transient, as shown in Fig. 5, is not much as increase in reactor power leads to increase in the steam flow thus heat removal is maintained.

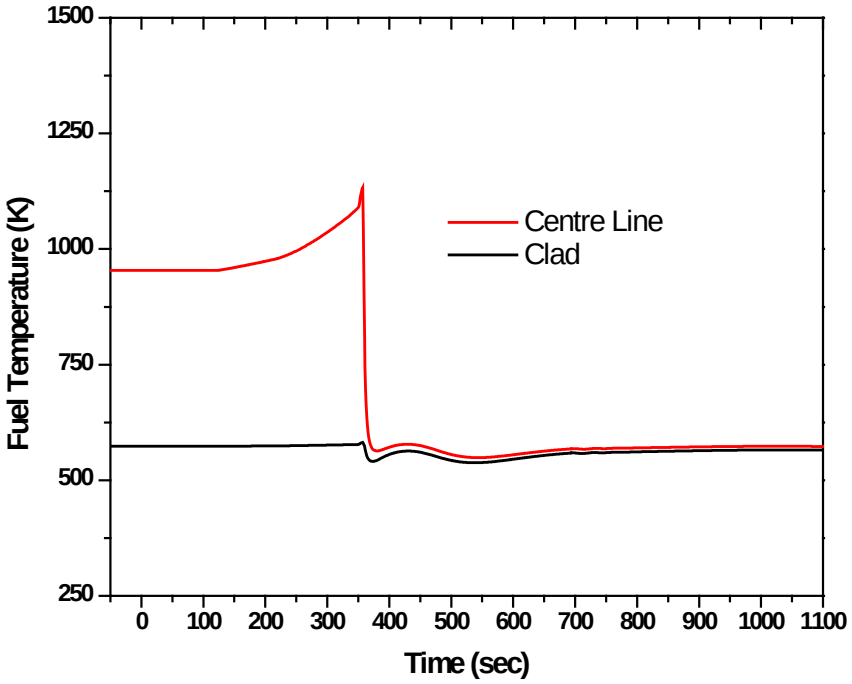


Figure 5 Fuel Temperature transients during LORA

5. Conclusion

LORA for orifice core has been analysed. Analysis shows that reactivity feedbacks and consequent reactor trip are sufficient to contain the power. Further decay heat removal through IC keeps the fuel temperature well within limits.

6. References

[1] Sinha R. K. and Kakodkar A., “Design and development of the AHWR—the Indian thorium fuelled innovative nuclear reactor”, Nuclear Engineering and Design, 236, pp. 683-700, 2006.

[2] Fletcher, G. D., Schultz, R. R., 1995. “RELAP5/MOD3.2 Code Manual”, Idaho National Engineering Laboratory, Idaho.

[3] A. Srivastava, H.G. Lele, A.K. Ghosh and H.S. Kushwaha, “Uncertainty analysis of LBLOCA for Advanced Heavy Water Reactor”, Annals of Nuclear Energy, Vol. 35, Issue 2, 323-334(2008).

LORA ANALYSIS OF AHWR EQUILIBRIUM CORE USING MODAL KINETICS METHOD

Arindam Chakraborty[1*], Debasmit Sarkar[1], Baltej Singh[2] and Umasankari Kannan[1]
[1]*Reactor Physics Design Division, Bhabha Atomic Research Centre, Trombay, Mumbai 400085*
[2]*Ex-employee, Department of Atomic Energy, Mumbai-400001*
[*]*e-mail:arindamc@barc.gov.in*

Abstract

The space-time neutronic behaviour of AHWR plays very crucial role in design and operation of the reactor. A methodology based on modal kinetics was implemented in the neutron diffusion code NDIFF3D for space-time neutronic analysis of AHWR. This method is computationally inexpensive compared to direct solution approach with relatively accurate result. The loss of regulation accident (LORA) in initial, intermediate and equilibrium core of AHWR was simulated. The results are compared with the data calculated with 3DFAST.

1. Introduction

The space-time neutronic behaviour of AHWR [1,2] is very important for analysis of reactor safety study.The loss of regulation (LOR) analysis was carried out for initial, intermediate and equilibrium cores of AHWR with space-time kinetics code NDIFF3D [3] using modal kinetics method [4,5]. The modal kineticsmethod implemented in NDIFF3D is validated against AECL 3D benchmark problem [6].The LOR is reactivity induced transient due to the multiple failures in Regulation Rods (RRs). There could be uncontrolled withdrawal of reactivity devices at their maximum rated speed during LOR. In AHWR 8 RRs are grouped into two banks bases on symmetry. In the present analysis, uncontrolled withdrawal of one bank of regulating rods (RRs) of maximum reactivity worth at speed 0.45 cm/s from the core is considered. The LOR analysis of all three core of AHWR are compared with 3DFAST [7] which solves space-time kinetics equation with improved quasistatic (IQS) method [8]. In section 2, a brief description of AHWR core is given. In section 3, the details of LOR transients in three different cores are described. The results are described in section 4. Section 5 presents the conclusions.

2. AHWR Core

The AHWR is designed as a 920 MWth (980MW fission power) vertical pressure tube type thorium based reactor cooled by boiling light water and moderated by heavy water. Based on the reactor physics and U-233 inventory requirements, the timeline of the core is broadly categorized into three time zones: initial, intermediate and equilibrium core. Different fuel clusters are used in these three time zones. The design calculations for AHWR lattice for all these clusters have been carried out using transport theory code ITRAN [9]. ITRAN simulates lattice cell to compute few group homogenized cross-sections. ENDFB VI.8 nuclear data library in 69 group WIMS format has been used for lattice calculations. Furthermore, the core calculations are performed using diffusion theory code FEMINA (based on nodal expansion method) [10]. Since the NDIFF3D code solves neutron diffusion equation using finite difference method, the mesh sizestaken in FEMINA are subdivided into 4 equal meshes in XY plane to obtain results similar to FEMINA.

2.1.Reactivity devices of AHWR:

The AHWR core has 24 control devices and 37 primary shut down devices. The control devices are divided into 3 categories:

a) 8 ARs, which are fully inside the core in nominal core configuration.
b) 8 RRs, which are 67% inside the core in nominal core configuration.
c) 8 SRs which are fully outside the core in nominal core configuration.

All the control devices (as well as primary shut down devices) are inserted from the top of the core through Zircaloy guide tubes. 8 ARs are divided into two banks, each consisting of 4 ARs. During operations of the reactor, rods corresponding to the same bank will be moving together. Similarly, the SRs and RRs are also divided into banks. The core-map showing the positions of the different reactivity devices with corresponding bank numbers are shown in Figure-1.

2.2. Initial core of AHWR:

AHWR initial core is designed to have two differently reactive clusters. The core has 108 low reactive clusters (Fuel type-1) each containing (Th, Pu) MOX with 2.1% Pu and 344 high reactive clusters (Fuel type-2) each containing (DU, Pu) MOX with 1.5% Pu as fuel. The initial core excess reactivity is suppressed by adding 50 ppm of boron in the moderator.

2.3. Intermediate core of AHWR:

To build-up U-233 inventory required for equilibrium core cluster, an intermediate core cluster [2] is designed for in-situ production of U-233. The intermediate core fuel cluster has design exit burnup of about 40GWd/Te. Each intermediate cluster needs about 6.2 kg of Pu. The intermediate core has been designed to have three burnup zones for flux flattening.

2.4. Equilibrium core of AHWR:

The AHWR equilibrium core is optimised with three different burnup zones. The inner and middle ring of fuel cluster contains 6% Pu in (Th, Pu) MOX and 3.9% Pu in (Th, Pu) MOX respectively. the 24 fuel pins of the outermost ring are designed to have axially graded fuel. Bottom half of the 24 fuel pins of the outermost ring contain 3.8% U in (Th, U) MOX and remaining top half contain 3.3% uranium in (Th, U) MOX. The fissile uranium isotope content in the uranium has been assumed to be about 81% (78% ^{233}U and 3% ^{235}U). To make the cluster suitable for on-power refuelling, excess reactivity of the cluster has been suppressed by adding 2% Gadolinium (burnable poison) in two diagonally opposite fuel pins of the innermost ring.

3. LORA analysis of AHWR

In LOR analysis of AHWR, bank#1 of regulating rods (RRs), consisting of 4 symmetric rods are assumed to be continuously moving out of the core at a design speed of 0.45 cm/s while the other bank has been assumed to be stationary at 67% IN position. Due to the movement of bank#1, positive reactivity is introduced in the core and continuous power rise is observed until the total power reaches to the trip set point of 110% Full power (FP) to trip the reactor. A delay of 1.15 sec (signal sensing and processing delay) has been assumed before the actuation of shut down system-1 (SDS-1). The SDS-1 is assumed to be consisting of 37 shut off rods (SORs) falling under gravity. The LOR transient without considering the effects of any reactivity feedbacks is simulated for all three AHWR core using modal expansion method module of NDIFF3D. Earlier the LOR analysis in AHWR equilibrium core [11] was performed using 3DFAST. For comparison purpose, the same problem in initial and intermediate cores were also simulated using 3DFAST.

4. Results

For LOR analysis, first a set of 30 eigen-modes of steady state neutron diffusion equation is obtained for AHWR using steady state module of NDIFF3D. Subsequently these steady states were used to simulate the time dependent LOR incident using modal kinetics module of NDIFF3D.

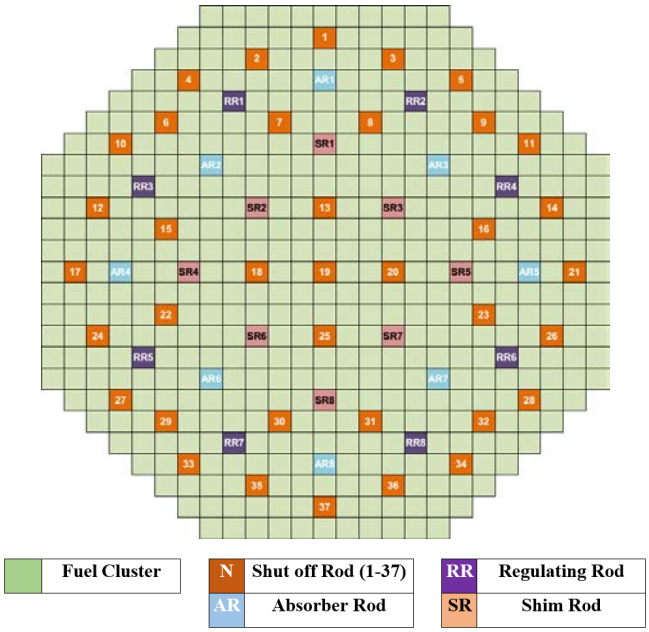


Figure-1: Core map showing locations of different clusters in AHWR

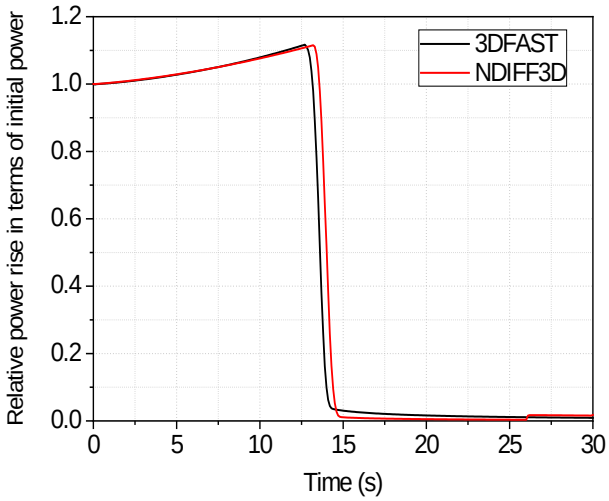


Figure-2: Change in power in LOR transient for equilibrium core of AHWR

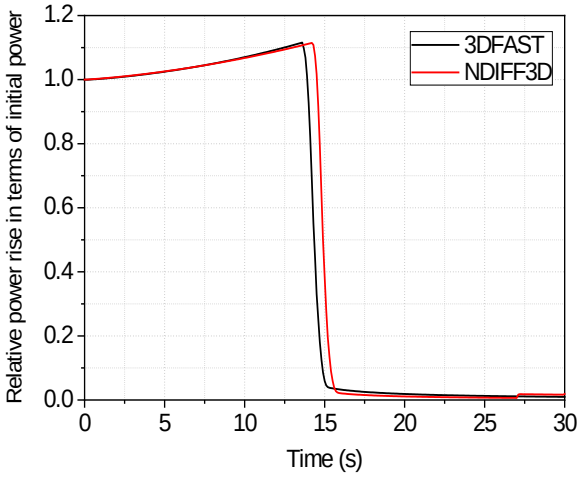


Figure-3: Change in power in LOR transient for initial core of AHWR

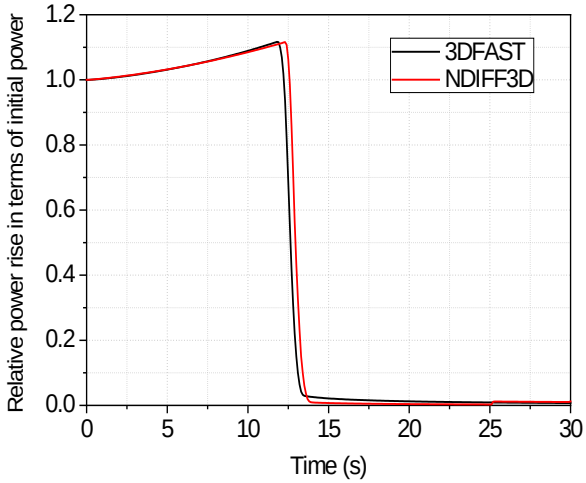


Figure-4: Change in power in LOR transient for intermediate core of AHWR

The variation of relative power with time for the LOR analysis of AHWR equilibrium core is shown in Figure – 2. The trip-set power level of 110% FP after initiation of LOR is coming after about 11.7 seconds for NDIFF3D and 11 seconds in 3DFAST.

The variation of relative power with time for the LOR analysis of AHWR initial core is shown in Figure – 3. The trip-set power level of 110% FP after initiation of LOR is coming after about

13.1 seconds for NDIFF3D and 12.3 seconds in 3DFAST. Steady state excess reactivity at this moment predicted by 3DFAST and NDIFF3D are 7.87 mk and 7.89 mk respectively.

The variation of relative power with time for the LOR analysis of AHWR intermediate core is shown in Figure – 4. In this case, the trip set power level of 110% FP after initiation of LOR is coming after about 11.2 seconds in NDIFF3D and 10.6 seconds in 3DFAST. Steady state excess reactivity at this moment predicted by 3DFAST is 8.3 mk and by NDIFF3D is 8.7 mk.

5. Conclusion

LOR analysis of initial, intermediate and equilibrium core of AHWR was simulatedusing modal expansion method. Number of modes used in the calculation is 30. The results were compared with the results obtained from 3DFAST. It is observed that rate of rise in power due to withdrawal of one bank of RR is slower in modal expansion compared to IQS method for both the cores. Due to this, the trip set power level of 110% FP after initiation of LOR is attained earlier in IQS method as compared to modal expansion method. In this study, no thermal hydraulic feedbacks were considered.

Reference

[1] R. K. Sinha and A. Kakodkar, “Design and development of the AHWR—the Indian thorium fuelled innovative nuclear reactor,” Nucl. Eng. Des., vol. 236, no. 7–8, pp. 683–700, Apr. 2006.

[2] A. Chakraborty et. al. “Safety Analysis Report (Preliminary) of AHWR”, AHWR/SAR(P)/USI/01591, April 30, 2015.

[3] Arindam Chakraborty, Debasmit Sarkar and Baltej Singh, “Development of computer code for modal kinetics analysis of AHWR”, Technical report no. RPDD/AHWR/415 Dated June14, 2018

[4] J. C. Luxat and G. M. Frescura, “Space-Time Neutronic Analysis of Postulated Loss-of-Coolant Accidents in CANDU Reactors,” Nucl. Technol., vol. 46, no. 3, pp. 507–516, 1979.

[5] Arindam Chakraborty, Debasmit Sarkar and Baltej Singh, “Analysis of AHWR by modal techniques”, Advances in Reactor Physics 2017, Mumbai, December 6-9, 2017

[6] R. A. Judd and B. Rouben, “Three-dimensional kinetics benchmark problem in a heavy water reactor.” 1981.

[7] H P Gupta, “Analysis of super delayed-critical transients in Thermal reactors using 2-D and 3-D adiabatic and improved quasistatic models”, Ann.nucl.Energy,Vol.13,No.3, pp.115-124,1986.

[8] Ott, K., Meneley, D.; Accuracy of the quasistatic treatment of spatial reactor kinetics; Nucl. Sci. Eng. 36, 381–419, 1969

[9] P. D. Krishanani, “Input Preparation of the Computer Code ITRAN”, Note No. RPDD/RP/11/2006

[10] Arvind Kumar and R. Srivenkatesan, “FEMINA- Nodal Expansion Method for Reactor Calculations”, Report No. BARC-1249 (1984).

[11] Amit Thakur, Baltej Singh and H P Gupta, “LORA analysis for AHWR Classical core”, Technical Report RPDD/AHWR/333, dated March 14, 2016

Linear Stability Analysis of IPWR (900 MWe) Equilibrium Core

Gopal Mapdar[1], Umasankari Kannan[1]
[1] Bhabha Atomic Research Centre, Mumbai, India
e-mail: - gmapdar@barc.gov.in

Abstract

Indian Pressurized Water Reactor (IPWR) is being designed with the aim of obtaining better fuel utilisation with enriched uranium. Stability Analysis is one of the main important aspects of safety studies. A preliminary linear stability analysis has been performed for IPWR equilibrium core using point reactor and lumped fuel and coolant temperature feedback model. The stability region for IPWR with respect to fuel and coolant temperature feedback has also been found.

1. Introduction

Stability analysis is an important aspect in the safety studies. A stable neutronics power response to a reactivity perturbation is required from safety point of view. During Reactor operation, many intentional or unintentional reactivity perturbations like movement of control rod, change in boron concentration in coolant, fluctuation in coolant flow, variation in power demand etc. will come in to play. Stable reactor comes back to a normal steady state after the reactivity perturbation but unstable reactor goes away from its steady state after introduction of reactivity perturbation leading to an accidental power rise. Therefore the stability analysis is a necessity in order to assess the safe operating regimes of a reactor.

2. Reactor Neutronics Modelling

A simple methodology based on reactor point kinetic model with fuel and coolant temperature feedback has been used for the stability analysis of IPWR equilibrium core[2]. The lump feedback model is considered in this case. The point kinetic equations considering six group delayed neutrons is shown below.

$$\frac{dP(t)}{dt} = \left(\frac{\rho(t)-\beta}{\Lambda}\right)P(t) + \sum_{j=1}^{6}\lambda_j C_j(t) \text{----------(1)}$$

$$\frac{dC_j(t)}{dt} = \frac{\beta_j}{\Lambda}P(t) - \lambda_j C_j(t)\,;\; j = 1,2,3,4,5,6. \text{----------(2)}$$

where P(t) - reactor power , C(t) - delayed neutron precursor concentration, ρ(t) - reactivity, at time t. Λ - neutron generation time, β_j and λj - and Precursor Decay Constant for j^{th} group. $\beta=\sum_{j=1}^{6}\beta_j$ - Effective Delayed Neutron fraction.

Now instantaneous reactivity ρ(t) could be written as sum of external reactivity $\rho_{ext}(t)$ (due to change in control rod position, change in boron in coolant) and feedback reactivity $\rho_{fb}(t)$ (due to resulting fuel and coolant temperature change).

$$\rho(t) = \rho_{ext}(t) + \rho_{fb}(t) \text{---------- (3)}$$

In steady state operating condition at t=0, ρ(0) is zero and state operating power P_0 and precursor concentration C_{j0} can be obtained from eqs.(1) &(2) equating to zero.

Now a small reactivity perturbation δρ(t) around the steady state is considered.

$$\delta\rho(t) = \rho(t) - \rho(0) = \delta\rho_{ext}(t) + \delta\rho_{fb}(t) \text{--------- (4)}$$

Due to this perturbation in reactivity the change in the reactor power and precursor concentration are taken as $\delta P(t)$ and $\delta C_j(t)$.

$$P(t) = P_0 + \delta P(t) \quad \text{and} \quad C_j(t) = C_{j0} + \delta C_j(t) \text{---------- (5)}$$

Putting eqs. (4) & (5) in eqs. (1) & (2), the following eqs. are obtained, (after little simplification and only the liner terms are considered)

$$\frac{d\delta P(t)}{dt} = \frac{\delta\rho(t)P_0}{\Lambda} - \frac{\beta\delta P(t)}{\Lambda} + \sum_{j=1}^{6}\lambda_j\delta C_j(t) \text{--------- (6)}$$

$$\frac{d\delta C_j(t)}{dt} = \frac{\beta_j \delta P(t)}{\Lambda} - \lambda_j \delta C_j(t)\ ;\ j = 1,2,\dots 6 \text{----------(7)}$$

Taking the Laplace transforms of eqs. (6) & (7). {The Laplace transforms of functions are denoted by the same functional notation e.g. L[X(t)] = X(s)}.Now after simplifying, the Reactor Transfer Function G(s) can be obtained as

$$G(s) = \frac{\delta P(s)}{\delta \rho(s)} = \frac{P_0}{s\left[\Lambda + \sum_{j=1}^{6} \frac{\beta_j}{s+\lambda_j}\right]} \text{----------(8)}$$

For one group delayed neutron Reactor Transfer Function G(s) can be express as

$$G(s) = \frac{\delta P(s)}{\delta \rho(s)} = \frac{P_0(s+\lambda)}{s\Lambda(s+\lambda+\frac{\beta}{\Lambda})} \text{----------(9)}$$

3. Reactor Feedback Modeling

The effect of reactivity perturbation will create reactor power change that leads to change in fuel (T_f) and coolant (T_c) temperature. These changes in T_f and T_c introduce reactivity change which is known as reactivity feedback (ρ_{fb}). The reactivity feedback due to fuel and coolant temperature effect could be written as

$$\delta\rho_{fb} = \alpha_f \delta T_f + \alpha_c \delta T_c \text{---------- (10)}$$

where the fuel and coolant temperature reactivity feedback coefficient are defined by

$$\alpha_f = \frac{\partial \rho_{fb}}{\partial T_f}, \quad \alpha_c = \frac{\partial \rho_{fb}}{\partial T_c} \text{----------(11)}$$

In the lump model time dependent fuel and coolant temperature in a reactor coolant segment can be derived from heat energy balance between fuel pin and energy transferred to the flowing coolant ,

$$\frac{dT_f}{dt} = a_1 P - a_2(T_f - T_c) \text{----------(12)}$$

$$\frac{dT_c}{dt} = a_3(T_f - T_c) - a_4(T_f - T_{c_{in}}) \text{----------(13)}$$

Where T_f ,T_c and T_{cin} are the average fuel ,coolant and coolant inlet temperature of the reactor and the constants a_1, a_2, a_3, a_4 are defined as

$$a_1 = \frac{1}{m_f C_f},\ a_2 = \frac{h_{eq} A_{eq}}{m_f C_f},\ a_3 = \frac{h_{eq} A_{eq}}{m_c C_c},\ a_4 = \frac{2m_{flow}}{m_c} \text{--(14)}$$

Where m_f , m_c , C_f , C_c , m_{flow} , h_{eq} , A_{eq} are fuel mass, coolant mass, fuel heat capacity, coolant heat capacity, coolant mass flow rate, the equivalent heat transfer coefficient between fuel and coolant, the corresponding equivalent area of heat transfer fuel to coolant respectively.

Due to the change in reactor power the change happened in T_{f0} and T_{c0} by δT_f and δT_c respectively,

$$T_f(t) = T_{f0} + \delta T_f(t) \quad \text{and} \quad T_c(t) = T_{c0} + \delta T_c(t) \text{----------(15)}$$

Now putting eqs. (15) in eqs. (12) & (13), the following eqs. are obtained, (after little simplification)

$$\frac{d\delta T_f(t)}{dt} = a_1 \delta P(t) - a_2(\delta T_f(t) - \delta T_c(t)) \text{----------(16)}$$

$$\frac{d\delta T_c(t)}{dt} = a_3(\delta T_f(t) - \delta T_c(t)) - a_4 \delta T_f(t) \text{----------(17)}$$

Taking the Laplace transforms of eqs. (16) & (17) and after simplification

$$\frac{\delta T_f(s)}{\delta P(s)} = \frac{a_1(s+a_3+a_4)}{s^2+s(a_2+a_3+a_4)+a_2a_4} \text{----------(18) and } \frac{\delta T_c(s)}{\delta P(s)} = \frac{a_1 a_3}{s^2+s(a_2+a_3+a_4)+a_2a_4} \text{----------(19)}$$

The feedback transfer function H(s) can be written as

$$H(s) = \frac{\delta\rho_{fb}(s)}{\delta P(s)} = \alpha_f \frac{\delta T_f(s)}{\delta P(s)} + \alpha_c \frac{\delta T_c(s)}{\delta P(s)} \text{---------- (20)}$$

$$\mathbf{H(s)} = \frac{\delta\rho_{fb}(s)}{\delta P(s)} = \frac{\alpha_f a_1 s + \alpha_f(a_1a_3+a_1a_4)+a_1a_3\alpha_c}{s^2+s(a_2+a_3+a_4)+a_2a_4} \text{----------(21)}$$

4. Block Diagram

The closed loop block diagram for the reactor system is shown in Fig:1. G(s) and H(s) are forward transfer function and feedback transfer function respectively. The overall transfer function Tr(s) of the system can be written as

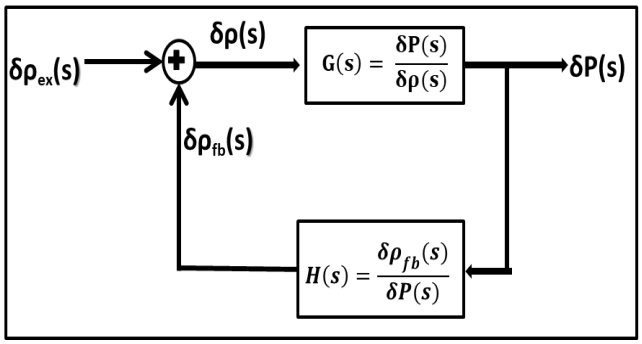


Fig:1 Closed loop block diagram of the reactor system with feedback

$$Tr(s) = \frac{\delta P(s)}{\delta \rho_{ex}(s)} = \frac{G(s)}{1-G(s)H(s)} \text{------(22)}$$

The condition for stability of the closed loop reactor system is that the poles of the overall transfer function Tr(s) must be in the negative (left) side of the complex plane. Then when we invert the Laplace transform, the transient response P(t) is a linear combination of terms **exp(s_jt)**. If one or more of the sj has a positive real part the response to perturbation will grow indefinitely and the linear system is unstable. If all the s_j have negative real parts, then the response to a perturbation will ultimately decay to zero as t → ∞.

The characteristic equation (polynomial of complex variable **s**) is form by setting the denominator of the Tr(s) equal to zero.

$$1 - G(s)H(s) = p_n s^n + p_{n-1}s^{n-1} \ldots + p_1 s^1 + p_0 s^0 = 0 \text{ ----------(23)}$$

The roots of this characteristic polynomial equation are the poles of transfer function Tr(s). So the roots must have negative real parts for stability of the reactor system. The stability of the system can be determined by stability analysis technique such as Nyquist Plot, Bode plot, Routh-Hurwitz criteria etc.

Table:1 (Point kinetics and Thermal Hydraulics data for IPWR)

Reactor state	Λ x10^{-6} Sec^{-1}	α_f pcm/^oC	α_c pcm/^oC	a_1 CJ^{-1}	a_2 Sec^{-1}	a_3 Sec^{-1}	a_4 Sec^{-1}
BOC	18.7	-2.46	-21.20	4.015 x 10^{-8}	0.7069	0.3874	2.8333
EOC	20.1	-3.43	-23.30				
	β_1 x10^{-3}	β_2 x10^{-3}	β_3 x10^{-3}	β_4 x10^{-3}	β_5 x10^{-3}	β_6 x10^{-3}	β x10^{-3}
BOC	0.21	1.20	1.02	2.20	1.16	0.54	6.33
EOC	0.17	1.10	0.91	1.98	1.05	0.46	5.67
	λ_1 x10^{-2}	λ_2 x10^{-2}	λ_3 x10^{-}	λ_4 x10^{-}	λ_5 x10^{-}	λ_6 x10^{-}	λ x10^{-}
BOC	1.33	3.17	11.90	31.10	94.10	287.00	8.97
EOC	1.34	3.12	11.80	30.80	91.40	283.00	8.93

5. Stability Analysis of IPWR

IPWR is a typical PWR type reactor with slight enriched uranium fuel and water as coolant and moderator. The point kinetic parameters and thermal hydraulics constants for lumped fuel and coolant model of IPWR at Beginning of Cycle (BOC) and End of Cycle (EOC) core condition are listed in Table-1.

The open loop transfer function (G(s)H(s)) for IPWR are determined at BOC & EOC with one & six group delayed neutron and given in eqs. (24) to (27) respectively.

$$G(s)H(s) = \frac{142.598s^2 + 48084.449s + 4312.028}{s^4 + 342.520s^3 + 1331.875s^2 + 678.141s} \quad --(24)$$

$$G(s)H(s) = \frac{184.978s^2 + 49296.205s + 4400.676}{s^4 + 286.107s^3 + 1110.303s^2 + 565.155s} \quad --(25)$$

$$G(s)H(s) = \frac{142.60s^7 + 48683.01s^6 + 206690.02s^5 + 219791.10s^4 + 72181.21s^3 + 7711.41s^2 + 242.61s + 2.03}{s^9 + 346.61s^8 + 2616.31s^7 + 6721.25s^6 + 6900.94s^5 + 3007.63s^4 + 504.71s^3 + 27.64s^2 + 0.32s} \quad ---(26)$$

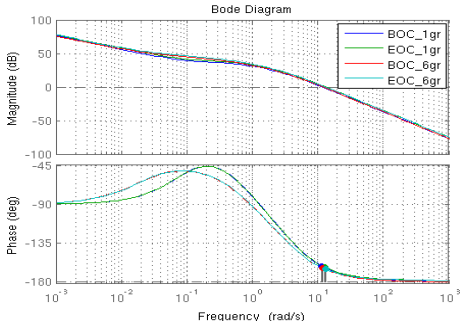
$$G(s)H(s) = \frac{132.67s^7 + 45283.03s^6 + 189080.12s^5 + 197160.25s^4 + 63878.26s^3 + 6753.24s^2 + 210.67s + 1.76}{s^9 + 290.33s^8 + 2170.21s^7 + 5519.74s^6 + 5601.32s^5 + 2414.41s^4 + 401.10s^3 + 21.79s^2 + 0.25s} \quad ---(27)$$

Table:2 (The poles of Transfer Function)

BOC	**1gr**	**-338.590**	**-1.920**	**-1.920**	**-0.088**					
	6gr	**-338.946**	**-1.688**	**-1.688**	**-2.872**	**-0.942**	**-0.310**	**-0.119**	**-0.032**	**-0.013**
EOC	**1gr**	**-282.141**	**-1.938**	**-1.938**	**-0.088**					
	6gr	**-282.815**	**-1.650**	**-1.650**	**-2.832**	**-0.915**	**-0.307**	**-0.118**	**-0.031**	**-0.013**

The poles of the Transfer function have been calculated and given in Table: 2 for IPWR. All the poles are negative real part.

The Bode and Nyquist plot are done for Open loop transfer function (GH) and given in Fig:2. In all the cases the system has no phase crossover frequency in Bode plot. In Nyquist plot the system is far from the critical point (-1,0). All these plots imply that the IPWR equilibrium core is stable against the small reactivity perturbation. The stability region of the IPWR with respect to the reactivity coefficients αf and αc is determined and shown in Fig: 3. The shaded portion in Fig: 3 indicates the region of stability[1].



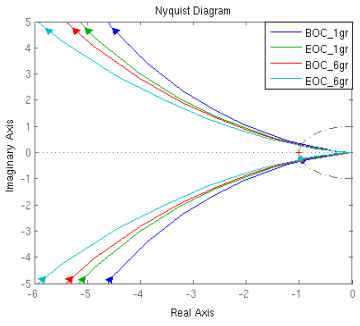


Fig:2 (Bode and Nyquist plot for open loop transfer function G(s)H(s))

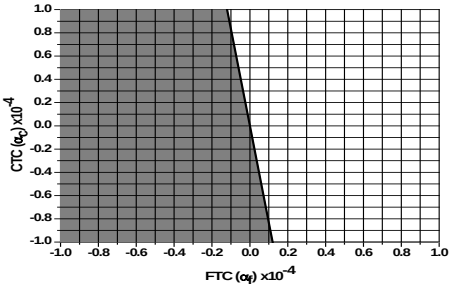


Fig:3 (Stability Region for IPWR)

6. Conclusion

The Linear Stability analysis of IPWR has been carried out using the point kinetics and lumped Fuel and Coolant Temperature feedback reactor model with transfer function approach. The small perturbations of the variables around their steady state value are considered to avoid the non-liner terms. Six group Delay neutron fraction (β) and precursors decay constant (λ) are used in the calculation. The stability region against α_f and α_c has been studies. The liner stability of IPWR has been studies with different stability analysis technique to explore IPWR stability against small reactivity perturbation.

7. References

(1) Kale, et al, 'Liner stability analysis of a nuclear reactor using the lumped model': NT&RP, 31, 2016

(2) 'Design note on Physics design of Indian Pressurized Water Reactor (IPWR)' :RPDD / IPWR / 019 / 6th April 2015

(3) D.K.Dwivedi, et,al, 'Liner stability analysis of a CHTR with lumped fuel and coolant feedback model': ARP-2017

Preliminary LORA Analysis for IPWR Equilibrium Core

Gopal Mapdar[1], D K Dwivedi[1], U Kannan[1]
[1] Bhabha Atomic Research Centre, Mumbai, India
[1]*e-mail: - gmapdar@barc.gov.in*

Abstract

Indian Pressurised Water Reactor (IPWR) is being designed for a cycle length of 410 full power days with enriched uranium in a three batch refuelling cycle. The core has 103 control rods groups in 10 groups. Reactor control is achieved by the tenth group consisting of six control rods During normal operation (NOC), control group rod ejection from the core is the most credible accident from positive reactivity addition point of view. This kind of scenario known as Loss of Regulation accident (LORA). An attempt is made to study the transient response of IPWR equilibrium core during a LORA situation.

1. Introduction

Indian Pressurized Water Reactor (IPWR) is a 2700MWth/ 900MWe indigenous pressurized water reactor under design [1]. The core has 151 fuel assemblies (FA) arranged in a hexagonal pitch of 243mm. Each fuel assembly has 331 fuel locations with pin pitch of 13.16 mm, out of which 18 are identified for control rod guide tubes, one for in-core instrumentation, central one for water rod and the rest 311 for fuel pins. Integral fuel burnable absorbers (IFBA), have been used to suppress the initial reactivity. The fuel composition and the neutronics parameter of the core affect the transient behavior in response to postulated initiating events(PIEs). It is necessary to demonstrate through safety analysis that during the transients, this core configuration meets all the safety requirements. The preliminary LORA analysis of IPWR equilibrium core has been done by PATH(pointkinetic-thermalhydrolic code)[2] at BOC and EOC. The initial positive reactivity is introduced by withdrawing the working Control group rods at the start of the transient at HFP.

2. Brief introduction of code PATH

The LORA has been analyzed by using in-house computer code PATH [2]. Its solves point kinetics equation with forth order Runge-Kutta as well as Implicit Euler method. Several model for TH feedbacks during transient such as adiabatic lumped fuel, lumped fuel & coolant and 1D-radial heat conduction base thermal hydraulics are developed in code PATH. The point kinetics and thermal-hydraulics are internally coupling in this code. The capabilities in the code have been validated with benchmark problems [2]. In the present analysis, 1D-radial heat conduction base TH model have been used for feedbacks in the core.

3. Modeling of IPWR FA Channel

Each hexagonal lattice cell pin is constituted with fuel pellet, gas gap, clad and coolant. 14 coaxial cylindrical meshes are considered along the radial direction from fuel pellet central line to coolant boundary of another hex cell. The coolant boundary radius is determined by converting the hexagonal cell in to circular one where the area is conserved. Among 14 meshes, 10 are there in fuel pellet itself as the temperature variation is much more in fuel pellet than in clad or coolant. 80 meshes are taken for axial direction. The inlet temperature and flow rate of coolant is taken as 292^{o}C and 0.308kg/sec. The other neutronics parameter like Fuel Temp Coefficient (**FTC**), Coolant Temp Coefficient (**CTC**), Prompt neutron life time($\boldsymbol{\iota}$), and six group delay neutron fraction ($\boldsymbol{\beta_i}$) and decay constant($\boldsymbol{\lambda_i}$) for BOC and EOC is given in Table-1. The initial axial profiles of average fuel and coolant temperatures of average powered pins in average and peak power producing channels at hot operating condition are

predicted and shown in Fig. 1. The average radial temperature profile in an averaged powered fuel pin in the core from fuel center to coolant is computed for initial operating condition and given in Fig. 2.

Table : 1. Core neutronics parameter at BOC and EOC

	FTC (/°C)	CTC (/°C)	l μS	λ_1 (S^{-1})	λ_2(S^{-1})	λ_3(S^{-1})	λ_4(S^{-1})	λ_5(S^{-1})	λ_6(S^{-1})
BOC	-2.46E-5	-0.35E-3	18.7	1.33E-2	3.17E-2	1.19E-1	3.11E-1	9.41E-1	2.87E+0
EOC	-3.43E-5	-0.56E-3	20.1	1.34E-2	3.12E-2	1.18E-1	3.08E-1	9.14E-1	2.83E+0
				β_1	β_2	β_3	β_4	β_5	β_6
BOC				2.08E-4	1.20E-3	1.02E-3	2.20E-3	1.16E-3	5.40E-4
EOC				1.72E-4	1.10E-3	9.07E-4	1.98E-3	1.05E-3	4.63E-4

Fig. 1. Axial profile of average fuel and coolant temperatures in average and peak powered channels in the core

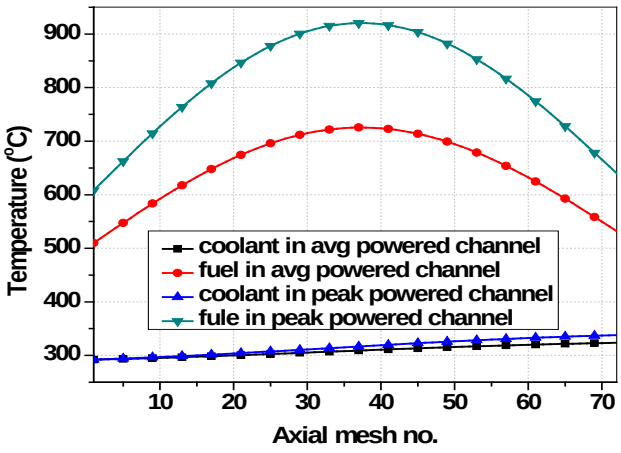
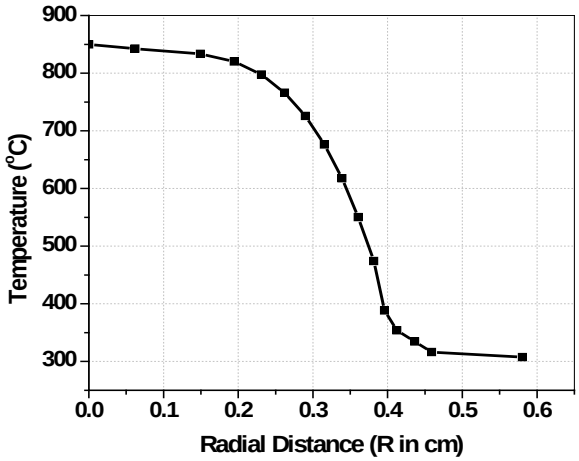


Fig. 2. Radial shape of average temperature in average powered pin in the core



4. Analysis of LORA in IPWR

The LORA analysis has been carried out at BOC and EOC. In this analysis, shutdown by the control rod cum shut-off rods has been demonstrated. The transient has been simulated at 100% full operating condition. The transient has been initiated by ejecting the working Control (6 rods of 10th bank)group rods, where 1.05 mk amount of total positive reactivity has been introduced in the core. The rate of ramp reactivity addition by this CR ejection process is dependent on the CR ejection time. Three different cases of CR rod ejection with three different time (0.1, 0.5 and 1.0 sec) has been consider for the transient. First trip (Lin-N trip) at 110% power is ignored and total delay of 1.0 Sec is considered between trip initiation and the start of introduction of negative reactivity. After trip initiation the shut off rods enter into the core and introduced negative reactivity of amount 160 mk in two seconds . The rate of negative reactivity addition by shutoff rods is taken from S-curve corresponding to the insertion of all banks for IPWR. The results for simulation are shown in Table:1 and Table:2 for BOC and EOC respectively. The time evolution of power and fuel central line temperature (peak temp) during LORA at BOC and EOC is given in Fig:2 and Fig:3 .

Table : 2. RR ejection and trip by CR at BOC							
Ejection time (sec)	LIN-N trip		Trip Time (sec)	Peak Power		Fuel Temperature	
	Power (%)	Time (sec)		Value (%)	Time (sec)	Average (^{o}C)	Peak (^{o}C)
0.1	110	0.06	1.06	1.199	0.12	596.65	861.10
0.5	110	0.28	1.28	1.192	0.51	596.63	861.11
1.0	110	0.57	1.57	1.173	1.01	596.65	861.12

Table : 3. RR ejection and trip by CR at EOC							
Ejection time (sec)	LIN-N trip		Trip Time (sec)	Peak Power		Fuel Temperature	
	Power (%)	Time (sec)		Value (%)	Time (sec)	Average (^{o}C)	Peak (^{o}C)
0.1	110	0.05	1.05	1.223	0.13	594.72	858.10
0.5	110	0.26	1.26	1.197	0.51	594.62	857.70
1.0	110	0.56	1.56	1.159	1.00	594.49	857.64

Fig : 2. Variation of power and fuel peak temp during LORA at BOC

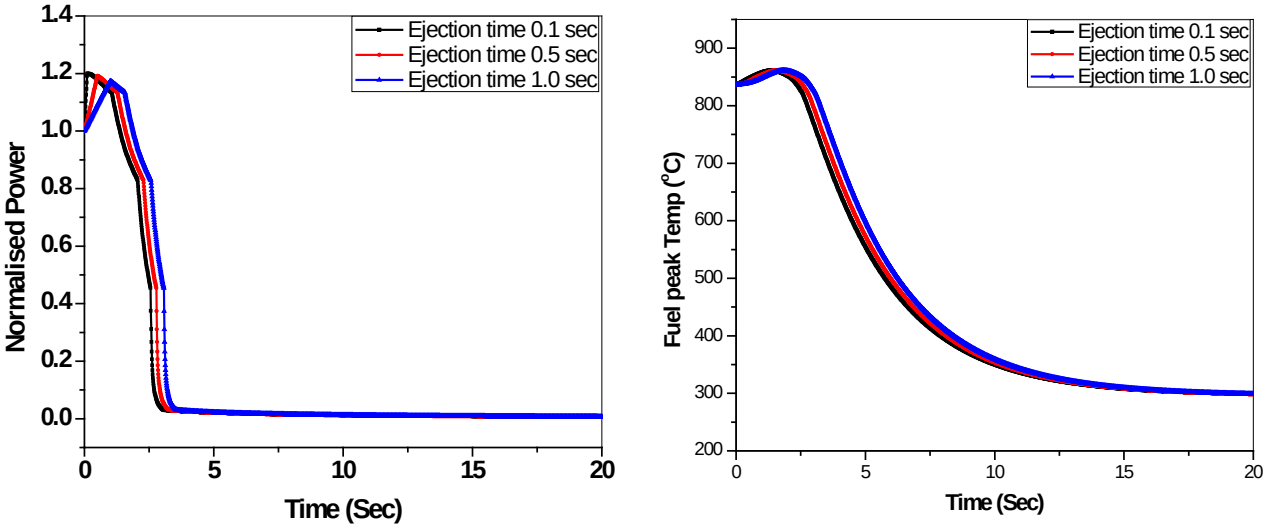
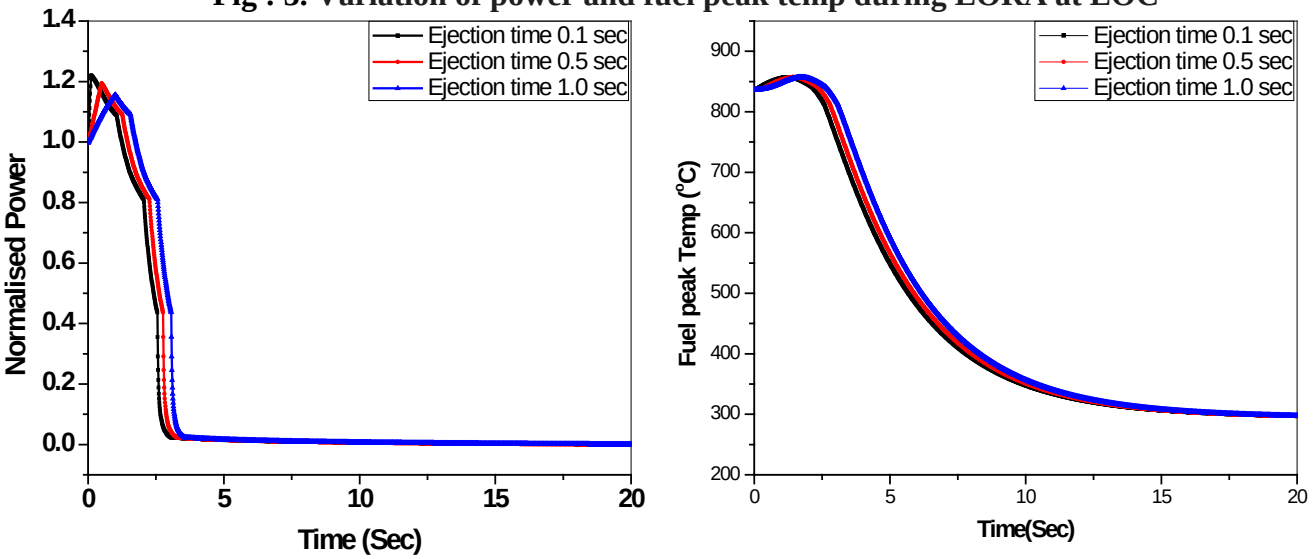


Fig : 3. Variation of power and fuel peak temp during LORA at EOC



5. Conclusion

Core transient response during a case of LORA has been analyzed for IPWR equilibrium core. The inlet and outlet average coolant temp is 292.15^{o}C and 323.62^{o}C at normal operating condition. During the LORA transient the power rise is more prominent at EOC hence the fuel peak temperature rise is more in EOC compare to BOC. The rate of power rise is sharper with less ejection time of Control group rod. This core configuration meets all the safety requirements. However, 3D space time simulation coupled with thermal hydraulics are required for details LORA analysis of this IPWR Core.

References

[1] "Conceptual Design of IPWR : Reactor Physics Design", IPWR/RPDD/005/ 19th April 2013.

[2] DK Dwivedi, A Gupta, U Kannan,"Development and validation of code 'PATH' for Pointkinetics Analysis with Thermal Hydraulics feedback" , RK08.023/ARP-2017, Dec6-9,2017, Mumbai

[3] VA Kale, SK Dubay, Obaidurrahman k, A J Gaikwad," Transient response of alternate configuration PHWR core", RK06.015/ARP-2017, Dec6-9,2017, Mumbai

SIGNIFICANCE OF LOW POWER REACTIVITY INDUCED EVENTS FOR VVER-1000 SAFETY ANALYSIS

S. K. Shukla[1], Sanuj Chaudhary[2] and P. Krishna Kumar[3]
[1, 2 & 3] Nuclear Power Corporation of India Ltd, Mumbai, India
[1]*e-mail: - sshukla@npcil.co.in*

Abstract

In a VVER-1000 regulation of reactor power and control of the fission chain reaction is carried out by movement of Control Rods and varying concentration of boric acid in the coolant. Control rods provide faster reactivity changes. Present study emphasis on significant reactivity excursion events at Hot Zero Power (HZP) such as control rod group withdrawal and control rod sudden ejection. At low power worth of the control rod is more comparted to its worth at full power, which leads to large relative increase in reactor power during withdrawal or ejection of the rod. This event results in large relative increase of fuel pellet temperature and enthalpy. VVER safety systems are designed to prevent any fuel damage in such reactivity initiated accidents.

The objective of this study is to observe the extent of reactivity excursion and temperature and enthalpy increase of fuel during the transient and establish compliance to acceptance criteria parameters.

1. Introduction

In KKNPP-3&4, absorber rods can be inserted into the core through the guide tubes provided in the top of the core. One control protection system absorber rod (CPSAR) is a cluster of 18 absorbing elements. One CPSAR can be inserted in one fuel assembly. These control rods are subdivided into 10 groups. Reactivity regulation is based on changing the position of control rods of one of the group in the core. This group is called as working group (Group-10). Other group's rods are generally out and they fall down into the core only when a large reduction in reactor power is required at a fast rate or when reactor is to be shutdown.

In uncontrolled withdrawal of Control Rods group, the working group moves upward, without monitored signal for its movement. This leads to insertion of positive reactivity in the core leading to increase of neutron power and reactor pressure and temperature. In case of ejection, sudden fast motion of rod from the initial position to the extreme upper position occurs in a fraction of second due to the coolant pressure. Such event can take place as a result of rupture of CPS drive housing. Control rod ejection event can occur with or without break. Preliminary analysis has shown that ejection without break leads to more severe consequences therefore results for the case of rod ejection without break are presented in this paper.

The maximal rate of reactivity insertion during normal operation and anticipated operational occurrences, caused by CPS ARs withdrawing and boron dilution, shall not exceed 0.07 β_{eff}/s. Reactivity addition associated with an accidental withdrawal of a control group (or groups) is also limited by the maximum rod speed (or convening speed) and by the efficiency of the group. Limitations for a single CPS AR efficiency for the states at HZP and rated power are specified in the Core Design for keeping of fuel damage established limits. The given constraints are checked by calculation and shall be followed at any moment of cycle.

2. Calculation Methodology & Modelling

The neutron kinetics and thermal-hydraulic behaviour during the event of withdrawal of control rod group and ejection of control rod was analyzed using thermal hydraulic computer code RELAP-5/MOD 3.2 [1]. This model provides continuity, momentum, and energy equations for both the liquid and the vapour phases within a control volume. The energy equation contains source terms which couple the hydrodynamic model to the heat structure conduction model by a convective heat transfer formulation. The code contains special process models for critical flow, abrupt area changes, branching, cross flow junctions, pumps, accumulators, valves, core Neutronic, and control systems. A counter current flow limitation model can also be applied at vertical junctions.

The feedbacks due to fuel temperature and coolant temperature are simulated using control parameters coupled with Neutronic point kinetics model. Decay heat data is used from the 1979 standard data (American National Standard for Decay Heat Power in Light Water Reactors) for U-235 in light water reactors. The events are analysed using the developed RELAP model for VVER-1000.

2.1 Nodalization of Primary and Secondary Circuit

Core is modelled using 3 channels which include one most powered channel, one channel with average power and one bypass channel. Nodalization of primary circuit involves reactor, four circulation loops and pressurizer. To describe the reactor, four elements are considered: reactor core, down comer, lower plenum and upper plenum. Reactor core is represented by a maximum power channel, average power channel and bypass path.

Nodalization of secondary circuit involves four steam generators; steam lines from each SG to main steam header (MSH) on which main steam isolation valves (MSIV's) are located. All four steam lines from SGs join MSH followed by turbine stop valve, governor valve and finally connecting to turbine. The relief devices like atmospheric steam discharge valves (BRU-A) and Steam generator relief valves (SG-PSD) are also modelled. The steam generator blowdown and emergency cool down (SGECD) safety system is also modelled.

3. Results and Discussion

Initially plant is considered at 1.04 % of nominal power with only two reactor coolant pumps (RCP) operating. At low power worth of the control rod is more comparted to its worth at full power, which leads to large relative increase in reactor power during withdrawal or ejection of the rod at MCL as compared to full power (Figures 1 to 4). The sequence of events for control rod withdrawal and ejection events at MCL is presented in Table 1. Figures 5 & 6 represent fuel temperature increase during withdrawal and ejection of control rod.

Table 1: Sequence of Events

Control Group Withdrawal		Control Rod ejection	
Time, s	**Event**	**Time, s**	**Event**
0.0	Beginning of withdrawal of control rod working group	0.0	Ejection of control rod with maximum worth
58.1	Generation of the first signal for reactor scram (due to increase in	16.5	Generation of the first signal for scram (due to increase in primary circuit pressure)

	primary circuit pressure)		
62.0	Atmospheric steam discharge valve operation (Pressure reaches set point for BRU-A opening)	20.5	Atmospheric steam discharge valve operation (Pressure reaches set point for BRU-A opening)
69.5	Pressurizer relief valve operation (Pressure reaches set point for PRZ PSD opening)	27.5	Pressurizer relief valve operation (Pressure reaches set point for PRZ PSD opening)
91.4	The end of control rods drop, reactor is in subcritical state	53.05	End of drop of control rods, reactor is in sub critical condition
1800.0	The end of calculation	2800.0	End of calculation

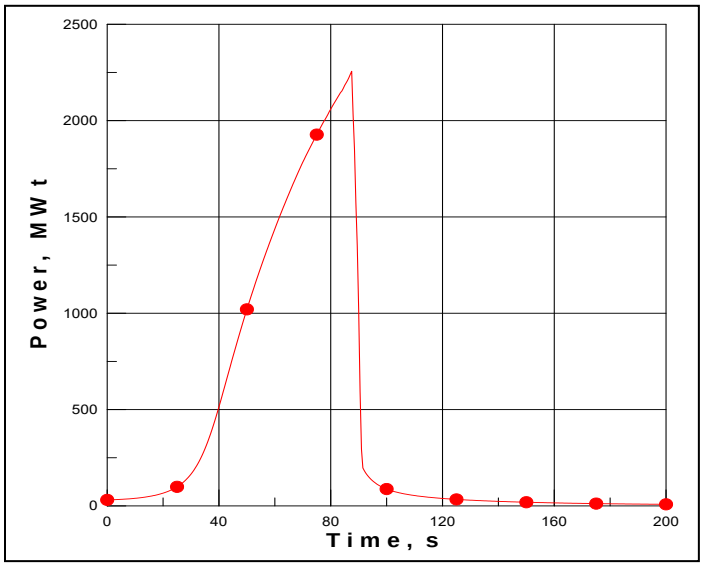


Figure 1: Control Group Withdrawal at MCL

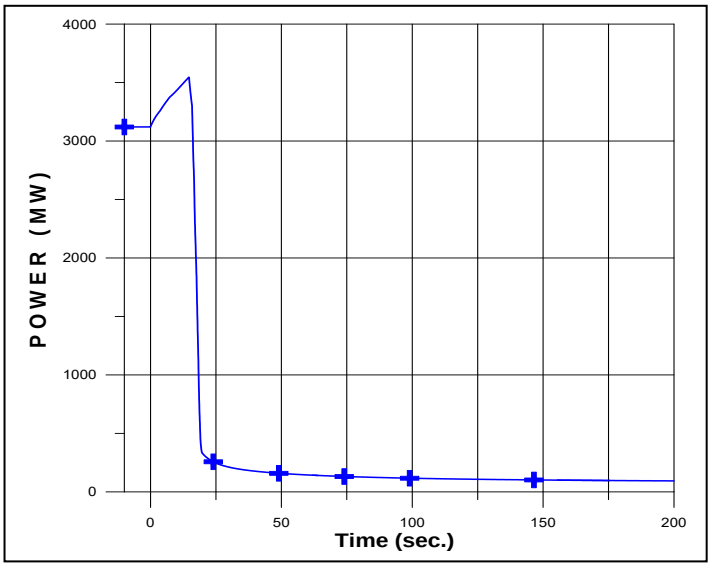


Figure 2: Control Group Withdrawal at Full Power

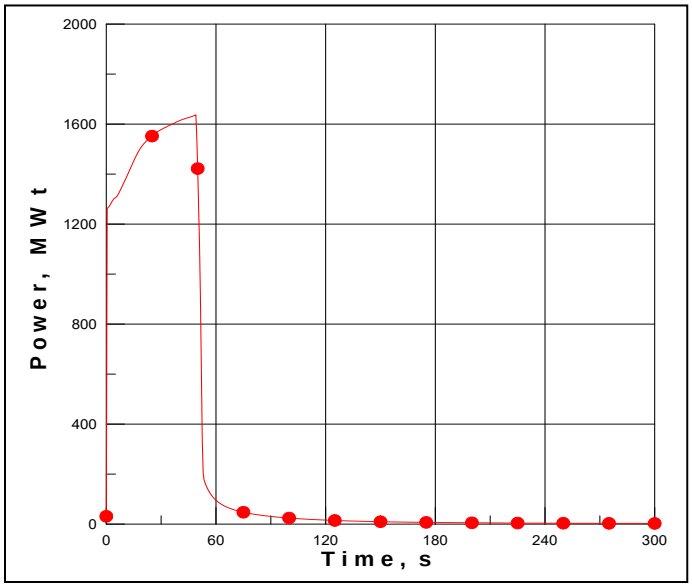


Figure 3: Control rod ejection at MCL

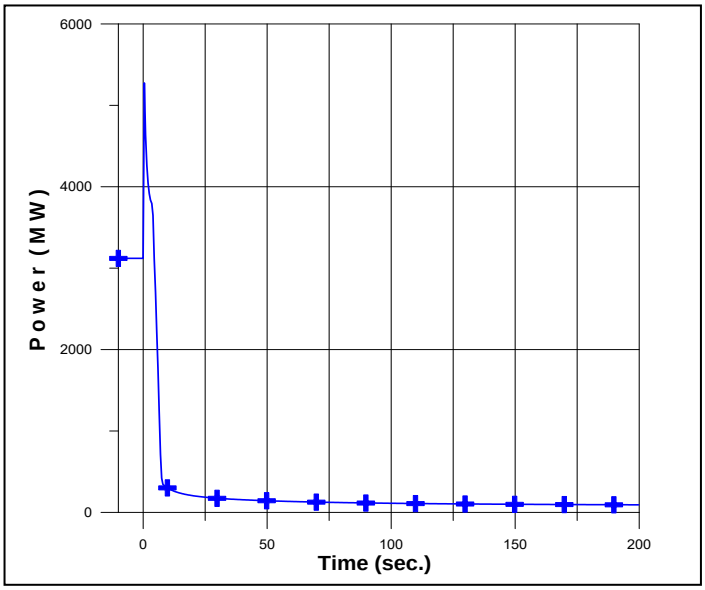


Figure 4: Control rod ejection at Full Power

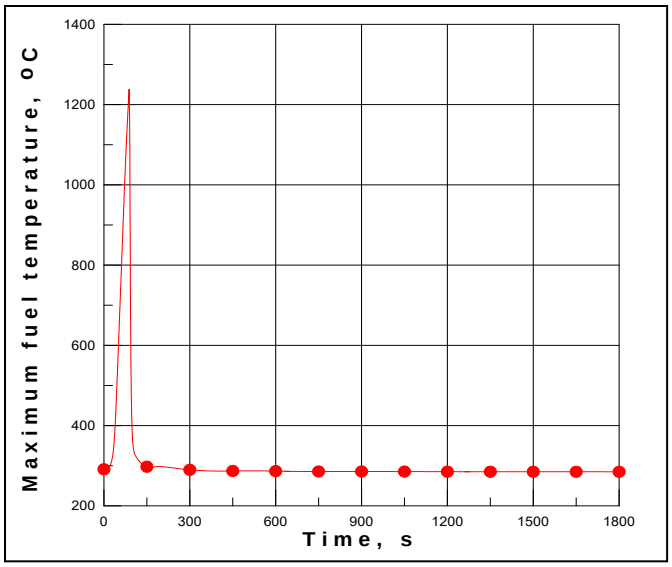


Figure 5- Control Group Withdrawal

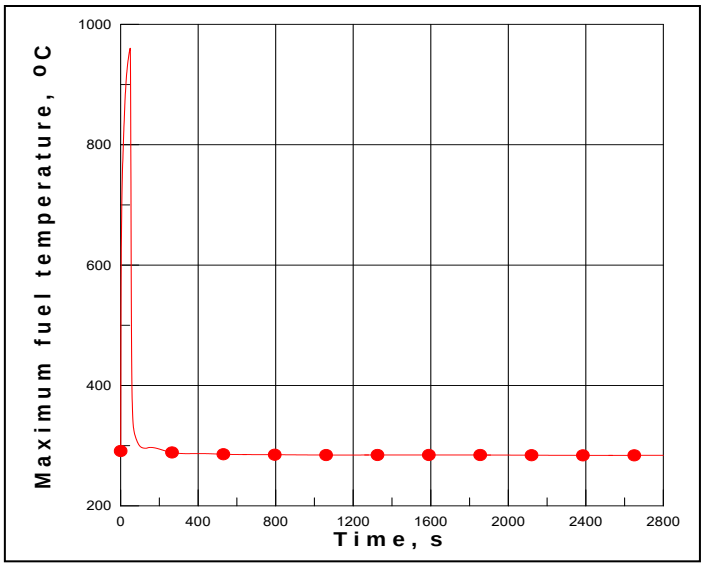


Figure 6: Control Rod Ejection

Most conservative (+ve) value of coolant temperature coefficient is used in the analysis. Max value (minimum negative) of fuel temperature coefficient is used. For control group withdrawal max power observed during the transient was 72 times of initial value at MCL and 1.13 times of initial value at full power. Similarly for control rod ejection, max power observed during the transient was 52.5 times of initial value at MCL and 1.67 times of initial value at full power. Max value of primary pressure is reached during control group withdrawal at MCL and amounts to 18.9 Mpa. Max value of coolant temperature at core outlet is reached during control group withdrawal at MCL and amounts to 338 ^{o}C.

4. Conclusion

Reactivity Initiated Accidents at MCL power such as those presented in this paper are part of reactor design basis. The MCL power events are significant due to its characteristics in VVER. These events are analyzed in the present paper and compliance with relevant acceptance criterion is established. It is demonstrated that safety systems can prevent deformation and melting of fuel with a considerable margin even during MCL power events.

5. References

[1] V. H. Ransom et al., RELAP5/MOD2 Code Manual, Volume 1: Code Structure, System Models, and Solution Methods, NUREG/CR-4312, EGG-2396, August 1985. , F: Article title. Journal 2(5), 99–110 (2016).

LINEAR STABILITY ANALYSIS OF A LARGE PHWR

Rakesh Kumar [1], Obaidurrahman K.[2] , Suneet Singh[3]
[1,2] Atomic Energy Regulatory Board, Mumbai, India
[3] Indian Institute of Technology, Mumbai, India
Email:- [1] rakeshsingh@aerb.gov.in

Abstract

Linear stability analysis of Pressurized Heavy Water reactor (PHWR) has been carried out using equations governing the neutron kinetics and core thermal hydraulics along with poison feedback. A theoretical model to study the neutronic stability of the PHWR has been developed and a closed-loop system of PHWR has been established, which involves the neutronics and reactivity feedbacks. The eigenvalue analysis approach has been used to assess the stability of the reactor. The stability map thus obtained clearly demarcates the stable and unstable regimes in terms of reactivity coefficients.

1. Introduction

PHWRs of different capacities are the mainstay of Indian nuclear power programme. Core design of power reactors demands in-depth assessment of stability, through which reliable operation of nuclear reactor within the desired regime can be assured. Core stability is governed by neutron kinetics parameters and nature and magnitude of anticipated perturbations. This paper aims to bring out neutronic stability aspects of a PHWR.

An operating condition can be considered stable if in response to external perturbations, system returns to the initial steady state. An unstable system tends to amplify external perturbations, diverging from the initial state. The dynamic behaviour of nuclear reactors in general, can be assumed to be linear for small deviations around steady operating condition. This makes it possible to study stability of PHWRs using locally linearized equations. Linear stability analysis can quantify the stability margin at operating conditions under small perturbations. In the present work, stability studies have been performed using point model of the reactor where reactor kinetics is modelled using point kinetics equations and fuel-coolant dynamics along with poison feedback is modelled through ODEs. Reactivity feedbacks have been accounted through different coefficients of reactivity.

2. Mathematical Modelling

Lumped model representing the transient evolution of the reactor has been used in the present study i.e., the equations governing the neutron kinetics, poison dynamics and reactor thermal-hydraulics are independent of space. This approximation simplifies the calculations while incorporating all the necessary physical aspects of reactor dynamics. Although it does not address the spatial effects, it is useful for the quick assessment of global stability of nuclear reactors.

2.1 Reactor Kinetics Model

The reactor has been modelled through point kinetics equations with delayed neutron precursors as follows [2] –

$$\frac{dP}{dt} = \left(\frac{\rho - \beta}{\Lambda}\right) P + \lambda C \tag{1}$$

$$\frac{dC}{dt} = \frac{\beta}{\Lambda} P - \lambda C \tag{2}$$

2.2 Thermal Hydraulics Model

The equations governing temporal variation of fuel and coolant temperature in an average reactor coolant channel can be obtained from energy balance between the fuel pin and the coolant flowing outside.

$$\frac{dT_f}{dt} = a_1 P - a_2\left(T_f - T_c\right) \tag{3}$$

$$\frac{dT_c}{dt} = a_3\left(T_f - T_c\right) - a_4\left(T_c - T_{c_{in}}\right) \tag{4}$$

T_f and T_c are the core averaged fuel and coolant temperatures respectively. $T_{c_{in}}$ is the coolant temperature at the inlet of the reactor core. $a_1, a_2, a_3$and a_4 are constants at a given steady operating state and are defined below

$$a_1 = \frac{1}{m_f C_f}, \quad a_2 = \frac{h_{eq} A_{eq}}{m_f C_f}, \quad a_3 = \frac{h_{eq} A_{eq}}{m_c C_c} \;\&\; a_4 = \frac{2\dot{m}_{flow}}{m_c} \tag{5}$$

h_{eq} is the equivalent heat transfer coefficient between the fuel and coolant corresponding to area A_{eq}.

2.3 Reactivity Feedback

Changes in reactor power due to external perturbations lead to changes in fuel and coolant temperature. So feedback reactivity can be represented as

$$\rho_{fb} = f_n(T_f, T_c) \tag{6}$$

Thus, differential change in feedback reactivity can be expressed as

$$\delta\rho_{fb} = \alpha_f \delta T_f + \alpha_c \delta T_c \tag{7}$$

where, reactivity coefficients α_f and α_c are fuel and coolant temperature coefficient of reactivity

2.4 Xenon Feedback

Xenon-135 (Xe^{135}) is a fission product which has very high capture affinity and acts as a neutron poison due to its large neutron absorption cross section and it can have significant influence on slow power transients in thermal reactors as it introduces reactivity changes due to changes in its concentration in the core. The modes of production and removal of Xe^{135} are schematically shown in Fig. 1.

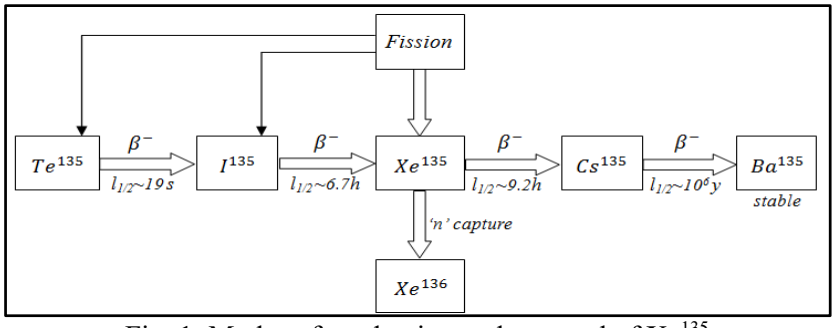


Fig. 1. Modes of production and removal of Xe^{135}

Half life of Tellurium is very small (~ 19 seconds); therefore it can be assumed that Iodine is produced directly from fission. The equation depicting overall production and loss mechanism of Xenon and Iodine inside reactor is shown below:

$$\frac{dI}{dt} = \gamma_I \Sigma_f P - \lambda_I I \tag{8}$$

$$\frac{dXe}{dt} = \lambda_I I + \gamma_{Xe} \Sigma_f P - \lambda_{Xe} Xe - \overline{\sigma_{Xe}} XeP \tag{9}$$

The feedback reactivity due to Xenon is given by

$$\rho_{fb,Xe} = \frac{\overline{\sigma_{Xe}}}{\nu \Sigma_f} \left(Xe(t) - Xe(0) \right) \tag{10}$$

where,
I is Iodine concentration
Xe is Xenon concentration
$Xe(0)$ is Xenon concentration at equilibrium point
γ_I is fission yield of Iodine
γ_X is fission yield of Xenon
λ_I is decay constant of Iodine
λ_X is decay constant of Xenon
$\overline{\sigma_{Xe}} = \frac{\sigma_{ax}}{E_{eff} \Sigma_f V}$ is power normalised microscopic absorption cross-section
σ_{ax} is microscopic absorption cross-section of Xenon
Σ_f is one group condensed macroscopic fission cross-section of i[th] region

3. Modelling & Simulation

The reactor is essentially a non-linear system, so these equations are linearised by expanding each function in Taylor series and neglecting higher order terms. Finally a system matrix A is obtained by computing Jacobian at steady state values. Thus state evolution equation obtained in terms of deviation from steady state can be written as:

$$\dot{x} = Ax \tag{11}$$

where,

$$x = [\, P \; C \; T_f \; T_c \; I \; Xe]$$

$$\underline{A} = \begin{bmatrix} \frac{-\beta_{eff}}{\Lambda} & \lambda_{eff} & \frac{\alpha_f T_{f0}}{\Lambda} & \frac{\alpha_c T_{c0}}{\Lambda} & 0 & -\frac{\overline{\sigma_{Xe}}}{\nu \Lambda \Sigma_f} P_0 \\ \frac{\beta_{eff}}{\Lambda} & -\lambda_{eff} & 0 & 0 & 0 & 0 \\ a_1 & 0 & -a_2 & a_2 & 0 & 0 \\ 0 & 0 & a_3 & -(a_3 + a_4) & 0 & 0 \\ \gamma_I \Sigma_f & 0 & 0 & 0 & -\lambda_I & 0 \\ \gamma_{Xe} \Sigma_f - \overline{\sigma_{Xe}} Xe_0 & 0 & 0 & 0 & \lambda_I & -(\lambda_{Xe} + \overline{\sigma_{Xe}} P_0) \end{bmatrix} \tag{12}$$

The equilibrium point can be obtained by equating R.H.S of eqn (1-4,8-9) to zero. Thus, for given values of reactivity coefficients α_f and α_c, stability of the reactor system can be assessed by using eigenvalues of the system [1].
All the symbols used in the mathematical model carry their usual meaning in reactor analysis.

4. Results

The methodology discussed above has been used for linear stability analysis of 500 MWe PHWR. The point kinetics parameters corresponding [2]are listed in Table 1. Thermal hydraulic constants (in Eq. (3) and (4)) for lumped fuel and coolant model are given in Table 2. These coefficients have been worked out based on core geometry and thermo physical data. Using these values, and stability region for the reactor is plotted. For assessing intrinsic stability eigenvalue crossover condition has been applied, which require that there should be no eigenvalues with positive real part. This criterion gives inequalities with $\alpha_f$and α_c as parameters/unknowns. The plots of inequalities thus obtained give the stability map. The stability map is so obtained is shown in Fig.1 & 2. The region to the left of stability boundary is stable. It was observed that stability region shrinks when effect of Xenon is accounted into system. Slope of the stability boundary indicates that stability is largely influenced by changes in the fuel temperature coefficient and to a less extent by changes in coolant temperature coefficient. This is consistent with the fact that fuel temperature reactivity effect is a prompt effect whereas coolant reactivity feedback is a delayed effect. Reactor stability is assessed at typical operating point ($\alpha_{f,op}$,$\alpha_{c,op}$) and it can be noted that at this operating point, the reactor is unstable without a dedicated control system.

Table 1 Parameters of PHWR

Thermal Power (P_0), W	1800×10^{6}
One group delayed neutron fraction (β)	0.0075
One group decay constant (λ), s^{-1}	0.0910
Neutron generation time (Λ), s	7.9×10^{-4}
Iodine decay constant (λ_I), s^{-1}	2.94×10^{-5}
Xenon decay constant (λ_{Xe}), s^{-1}	2.1×10^{-5}
Iodine yield from fission	0.0618
Xenon yield from fission	0.006

Table 2 Thermal-Hydraulic Constants

a_1, $^oC/J$	7.5×10^{-8}
a_2, s^{-1}	0.2110
a_3, s^{-1}	0.1400
a_4, s^{-1}	2.0300

5. Conclusion

Linear stability analysis of PHWR has been carried out using lumped reactor transient model with feedback effects from fuel, coolant and poison dynamics. Governing equations have been linearised and eigenvalues of the system has been used to assess system stability. On imposing the Schurr's criterion, inequalities are obtained in terms of fuel and coolant reactivity coefficients which are used to generate stability maps. At its typical operating point ($\alpha_{f,op}$,$\alpha_{b,op}$), the reactor is found to be inherently unstable, necessitating a reliable regulation for stable operation. Although in this paper we have only addressed global stability but spatial instability is also prominent issue for large reactor. But this analysis technique can easily be extended to more sophisticated multipoint kinetics technique along with spatial distribution of reactivity devices.

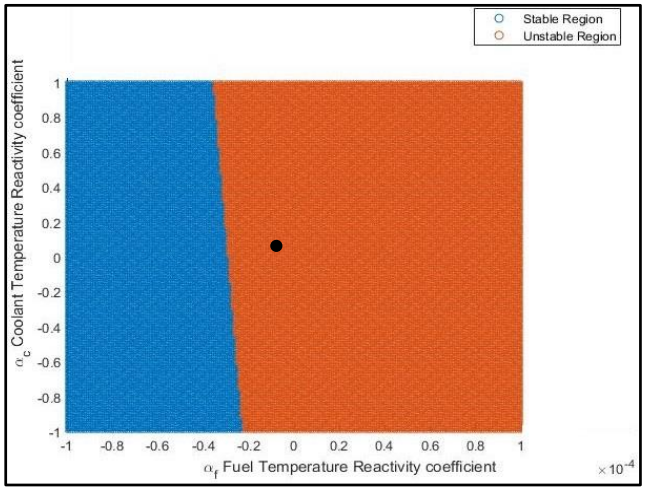


Fig 1 Stability map with Xenon effects

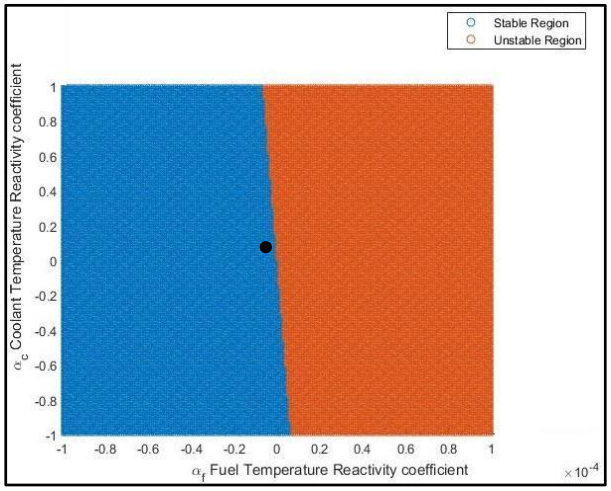


Fig 2 Stability map without Xenon effects

References

[1] V. A. Kale, R. Kumar, K. Obaidurrahman and A. J. Gaikwad, "Linear Stability Analysis of a Nuclear Reactor using the Lumped Model," Nuclear Technology & Radiation Protection, vol. 31, no. 3, pp. 218-227, 2016.

[2] A. P. Tiwari, "Modeling and Control of a Large Pressurised Heavy Water Reactor," PhD Thesis, Indian Institute of Technology, Bombay, 1999.

WORTH COMPUTATION OF GEM ASSEMBLIES IN FFTF CORE

Abhitab Bachchan[#], Puspendu Hazra, A. Riyas and K. Devan
Indira Gandhi Centre for Atomic Research, Kalpakkam, India
[#]*e-mail: - abslindia@igcar.gov.in*

Abstract

In the 400-MWt fast-flux test facility (FFTF), the gas expansion module (GEM) was tested in July 1986. Incorporation of GEM into the liquid-metal reactor designs is intended to enhance the inherent safety of the core by allowing the reactor to passively shut down even in the hypothetical event of an unprotected (no scram) loss-of-flow accident. The loss of flow test (no. 13) without SCRAM (LOFWOS) is analysed at IGCAR as a part of an IAEA collaborative research project (CRP). The paper describes the GEM assembly design and its worth estimation using deterministic and stochastic codes.

1. Introduction

The Fast Flux Test Facility (FFTF) was a 400 MWt, oxide fuelled, liquid sodium-cooled fast neutron flux test reactor operated in US. This reactor was built to assist in developing and testing advanced fuels and materials for fast breeder reactors. In July 1986, a series of unprotected transients (with the plant protection system intentionally disabled) were performed in the FFTF as a part of passive safety demonstration program [1]. The 'loss of flow without scram (LOFWOS) test #13' was one of them. This test was conducted to verify the safety performance of the core during a loss of flow accident. In 2018, under the direction and support of the International Atomic Energy Agency (IAEA), Argonne National Laboratory (ANL) has proposed the FFTF LOFWOS Test #13 as a coordinated research project (CRP) for the validation of simulation tools in the domain of sodium-cooled fast reactor (SFR) safety. This benchmark includes analyses of neutronics, thermal-hydraulics and transient properties.

As a part of neutronics analysis, together with various safety coefficients, the worth of GEM is estimated. Estimating GEM worth is challenging mainly because of its position in the core and its design. Its reactivity worth is estimated using 2k method and also by using 1st order perturbation theory in 2D and 3D geometries. A brief introduction of the FFTF core and details of LOFWOS Test No. 13 are given in Sections 2 and 3, respectively. The calculation method is briefly discussed in Section 4, followed by results and discussions in Section 5.

2. GEM design and LOFWOS Test #13

Figure 1 gives the radial core configuration of FFTF-8C containing 199 hexagonal assemblies [1]. Ninety-eight reflector assemblies follow the active fuel region with 80 Driver Fuel Assemblies (DFA). Six control rods (CRs) in the 4th ring and three safety sods (SRs) in the 2nd ring were provided to control neutron population in the core. Nine GEM assemblies were placed at the active fuel and reflector region interface in the 6th ring to enhance passive reactor control. By design, GEMs were hollow tubes (3.658 m long pipe) sealed at the top and open at the bottom with argon cover gas trapped inside (Figure 2).

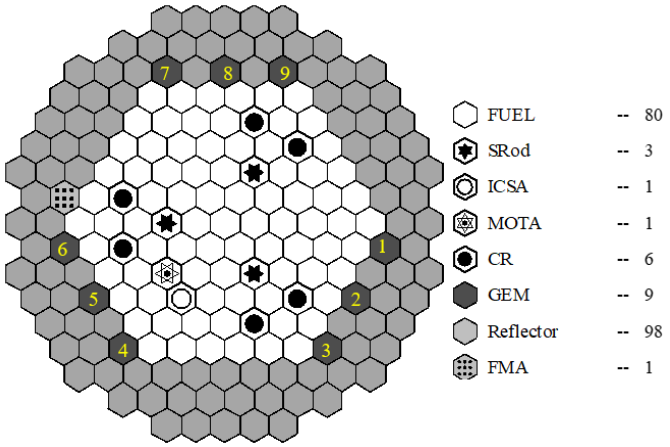


Figure 1 Radial Configuration of FFTF Core

The GEMs are designed such that when primary pumps are operating at full flow, the pressure head of the primary pumps causes sodium levels to rise in the GEM assembly and compresses the gas to a level above the top of the fuel column. Following a pump trip, a corresponding decrease in the sodium pressure, the trapped gas would expand and displace sodium. The GEM assemblies are placed at the core -radial reflector interface. The drop in sodium level increases core neutron leakage and hence inserts negative reactivity as feedback.

The LOFWOS Test #13 was initiated at 50% power & 100% flow, and the three primary sodium pumps were simultaneously tripped [1]. The plant protection system was modified to allow the test to run without the control rods being inserted prematurely. Several trip-set points were either disabled or bypassed, and various additional trip functions were installed to compensate for bypassing the trips for low flow rate and decreased power rate.

It is to be noted that no instrument was installed to measure the GEM sodium levels during the experiment. So, an empirical correlation (Equation 1) was derived for the sodium level in GEM with the core flow rate for the specified power and temperatures of neighbouring assemblies as

$$L(cm) = 265 - \frac{539504}{244.013 + F^2} \qquad (1)$$

where L is the sodium level in GEM above the top of the inlet flow holes, and F is the primary system flow rate in percentage. The GEM sodium level was calculated using the derived correlation (Equation 1) and illustrated in Figure 2. It is to be noted that this correlation was derived using the ideal gas law starting from an initial gas pressure equal to the static pressure with the pumps off plus the dynamic pressure resulting from the primary pumps.

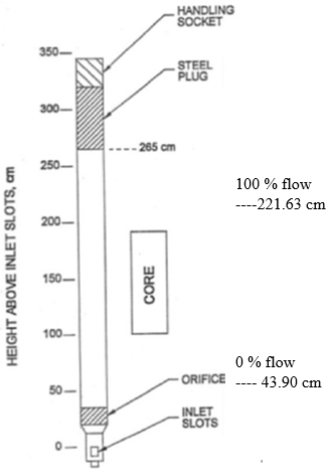


Figure 2 GEM Sodium Level

3. Computational method

The nuclear data, computer codes and method of neutronics analysis/computation of reactivity worth of GEM assemblies are given in Table 1. In deterministic method, the homogenous model is used, which is prepared by conserving the volume of each material in a hexagonal structure for all regions. The temperature-dependent self-shielded cross-sections of all the specified homogeneous mixtures are prepared by using the code CONSYST-2 [2]. The adjusted Russian multigroup library ABBN-93 [3] in the 26-groups is used in all deterministic calculations. For better criticality prediction, spatial heterogeneity effects for fuel and absorber rods are also taken into account while preparing their self-shielded cross-sections. Transport theory correction is also added to the predicted 3-D diffusion theory-based k-eff. The ACE data file prepared from ENDF/B-VII.0 using NJOY21 is used in the calculation using the stochastic method. For most of the assemblies, the axial regions are chosen to be homogeneous, whereas heterogeneous description is used for the fuel region fuel assembly, absorber region of control and safety rods and gas and sodium-filled regions of GEM assembly (Figure 3).

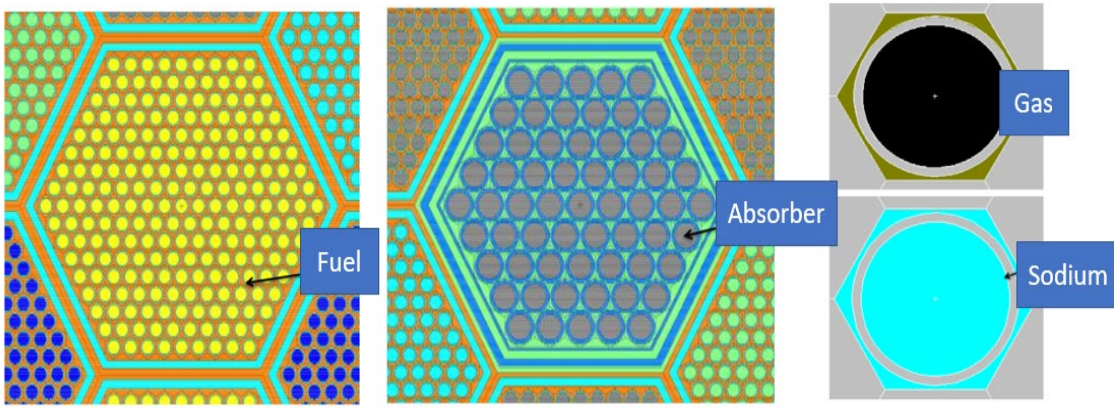


Figure 3 Heterogeneous model of fuel, absorber and gas & sodium-filled regions

For the GEM reactivity worth estimation, two methods, viz. 2k and 1st order perturbation methods are used. The 2k method (Equation 2) is used for worth estimation using 3D diffusion theory-based code FARCOB [4] and Monte Carlo (MC) code [5]. Using perturbation theory, the GEM worth is estimated using diffusion theory-based code PERT3D [6] in 3D & PERTNEW in 2D [7]. The 1st order perturbation theory method (1-D and 3-D) used (Eq. 3).

$$\Delta\rho = \left(1-\frac{1}{k_1}\right)-\left(1-\frac{1}{k_2}\right) \tag{2}$$

$$\Delta\rho = \left(1-\frac{1}{k}\right)-\left(1-\frac{1}{k'}\right) = \frac{\left\langle \Phi^{+}(\lambda'\Delta P-\Delta L)\Phi' \right\rangle}{\left\langle \Phi^{+} P \Phi' \right\rangle} \tag{3}$$

where k_1 is the reference neutron multiplication factor, k_2 is the neutron multiplication factor after the change of sodium level. The Φ^{+} is the adjoint flux of the unperturbed core, k and k' are the neutron multiplication factors of unperturbed and perturbed systems and ΔP & ΔL are changes in production and loss operators. In the first-order approximation, both the perturbed and unperturbed fluxes are assumed to be the same. i.e. Φ' is equal to Φ.

4. Results and discussion

FFTF-8C core is simulated by using the specified temperature and material data of IAEA CRP. The estimated k-eff in the critical configuration using FARCOB code is 0.99939 and it is 1.00359 ± 0.00003 using Monte Carlo code. In GEM assemblies, the total expansion of gas/reduction in the sodium level from 100 % flow to 0 % flow is 177.73 cm. It is to be noted that the total active length of the core is 90 cm and at 227°C, the total measured worth for the pumps-on to the pumps-off condition of nine GEMs was -1.31$ (~435 pcm) [8].

The estimated total reactivity addition by the expansion of gas in GEM using both methods is given in Table 1. The estimated worth using 2k method with FARCOB (3D diffusion, homogeneous) code is -531 pcm, which is ~22 % higher than the measured worth. The estimated reactivity worth using the 1st order perturbation method in 3D is about -536 pcm, which is close to the 3D value using the 2k method and at the same time ~23 % higher than the measured value. The estimated reactivity in 2D is - 498 pcm, which is 14 % higher than the measured value and less by -6.1 % in comparison to the 3D value. The 9 GEMs assembly worth (-447 pcm) estimated using MC code by considering the heterogeneous model is just 3 % higher than the measured one. This indicates that prediction by the stochastic method with the heterogeneous model is closer to the measured value.

The estimated individual GEM assembly worth using the 3D perturbation method is in the range of - 43.9 pcm to -73.6 pcm (Table 2). This shows the absence of both axial and radial symmetry in 3D modeling of GEM assemblies with respect to the core centre. The reactivity addition

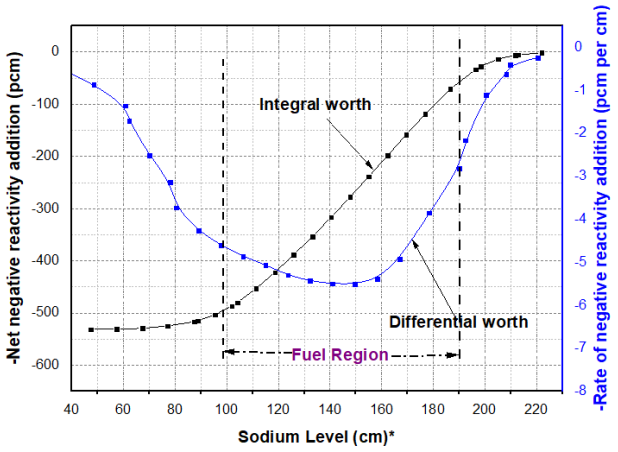
rate with change in sodium level using FARCOB and MC code is shown in Figure 4. The observed maximum rate of reactivity addition is – 5.5 pcm/ cm using FARCOB code, whereas it is 6.1 pcm/cm using the MC code. The estimated negative reactivity feedback with the level of sodium is shown in Figure 4.

Table 1 Reactivity worth of 9 GEM assemblies

Method/Code	Model	Value, pcm	C/E
2k			
FARCOB	3D/homo	-531	+1.22
MC Code	3D/hetero	-447	+1.03
1st Order Perturbation/Homogeneous			
PERT3D	3D-HEXZ	- 536	+ 1.23
NEWPERT	2D-RZ	- 498	+1.14

Table 2 Individual GEM assembly worth

SA Index	Worth (pcm)
1	-67.2
2	-73.6
3	-51.5
4	-45.3
5	-54.4
6	-43.9
7	-65.9
8	-76.8
9	-57.6



* *With respect to the top of inlet flow holes*

Figure 4 Reactivity feedback of GEM assembly

5. Conclusions

The GEM reactivity feedback worth is estimated as a part of the benchmark analysis of FFTF LOFWOS Test #13 under an IAEA-CRP. The 2k and 1st order perturbation methods are used. A significant difference is seen in the simulated value using diffusion theory with respect to the measured worth. Both 2k and perturbation methods predict worth very closely. The stochastic method using heterogenous model predicts very close to the measured value.

6. References

[1] T. Sumner et al., "Benchmark Specification for FFTF LOFWOS Test #13", *ANL-ART-102 (Rev 2)*, Nuclear Engineering Division, Argonne National Laboratory, USA, December 22 (2017).

[2] G. N. Manturov and Mark N. Nikolaev and A. M. Tsiboulya, "*Description of the CONSYST2 Code System for Applying the ABBN-93 Nuclear Data Set to Different Applications*", Report IGCAR-IPPE (1998).

[3] Manturov, G. N., 1997, ABBN-93 group data library part-I: nuclear data for the calculations of neutron and photon radiation functions. In: INDC (CCP)-409/L, IAEA,Vienna.

[4] P. Mohanakrishnan, "Development and validation of a fast reactor core burnup code–FARCOB", Annals of Nuclear Energy, 35 (2), pp. 158-166 (2008).

[5] J. F. Briesmeister, "*MCNP - A General Monte Carlo N-Particle Transport Code"*, Version 4C, Los Alamos, New Mexico (2000).

[6] A. Riyas, "*Three-dimensional perturbation analysis of a fast reactor core"*, Nuclear Engineering and Design, Volume-337, pages 74–83 (2018).

[7] T. M. John, "*NEWPERT- Perturbation Code for Two-Dimensional Diffusion Equation"*, REDG/01150/RP-253 (1984).

[8] D. M. Lucoff, "*Passive Safety Testing at the Fast Flux Test Facility", Westinghouse Hanford Company, WHC-SA—0046/DE89 010116 9(1987).*

CLAD RELOCATION DYNAMICS FOR LMFBR ULOFA ANALYSIS

Anuraj V L[1], T. Sathiyasheela[2] and K. Devan[3]
[1,2,3] Indira Gandhi Centre for Atomic Research, Kalpakkam, India
[1]*e-mail: - anuraj@igcar.gov.in*

Abstract

A single channel model for clad relocation based on Ishii's model is developed and integrated with the in house developed safety analysis code PREDIS. Reactivity feedback due to the relocation of molten clad is estimated. ULOFA analysis is carried out using the modified code for PFBR core and the mechanical energy release is estimated.

1. Introduction

In case of Prototype Fast Breeder Reactor (PFBR), ULOFA (Unprotected Loss of Flow Accident) leads to Core Disruptive Accident (CDA). The accident is initiated when power supply to coolant circulating pump fails, results in flow coast down and overheating of fuel. This leads to increase in coolant temperature, coolant voiding and positive reactivity addition. Clad melting will be initiated soon after the sodium voiding. Reactivity changes due to coolant voiding, relocation of molten steel and fuel are significantly high and it drastically changes the course of transient. In the present study a single channel model for clad relocation based on Ishii's model [1, 2] is developed and integrated with the existing transient analysis code PREDIS [3]. The modified code is then used for ULOFA analysis of PFBR.

2. Clad Motion

During the initiation phase of loss of flow accidents, the vapor phase of coolant is assumed to be incompressible, and the molten clad is assumed to be moving as a film under the influence of gravity, the channel pressure gradient, the frictional drag due to streaming sodium vapor and friction between moving cladding and the fuel pin. Because of the high upward sodium vapor flow there will be an initial upward motion of molten clad and it is possible that the molten steel reaches the blanket region and freezes. This frozen layer of steel can block the vapor flow completely or even flow reversal.

3. Ishii's model of molten clad motion for fast reactor loss of flow accidents

Ishii's model is based on a single channel film flow model in which molten clad is considered moving as a film rather than as entrained droplets. In this model it was assumed that the coolant channel was voided prior to the initiation of the molten clad motion, which is case for ULOFA. The one-dimensional equation of motion for the sodium vapor and the molten clad are given by [1, 2]

$$\frac{\partial}{\partial t}(\alpha_g v_g) + \frac{\partial}{\partial Z}(\alpha_g v_g^2) = -\frac{\alpha_g}{\rho_g}\frac{\partial p}{\partial Z} - \alpha_g g - \frac{\tau_g P_g}{\rho_g (A_g + A_{cm})} \tag{1}$$

$$\frac{\partial}{\partial t}[(1-\alpha_g) v_c] + \frac{\partial}{\partial Z}[(1-\alpha_g) v_c^2] = -\frac{(1-\alpha_g)}{\rho_c}\frac{\partial p}{\partial Z} - (1-\alpha_g) g + \frac{\tau_g P_g + \tau_c P_c}{\rho_g (A_g + A_{cm})} \tag{2}$$

The one-dimensional vapor continuity equation

$$\frac{\partial}{\partial t}(\alpha_g \rho_g) + \frac{\partial}{\partial Z}(\alpha_g \rho_g v_g) = \Gamma_g - (\alpha_g \rho_g v_g)\frac{\partial}{\partial Z}[ln(A_g + A_{cm})] \quad (3)$$

Here α is the void fraction *v* the velocity, *ρ* density, *P* pressure and *A* the flow area per channel. The suffix *g* denotes sodium vapor and *c* denotes clad. More details on the theory part of the model can be found in Ref [1]. The extent of clad melting is calculated from clad temperature and heat balance calculations. The momentum and continuity equations are solved by simple Euler method to get the clad film velocity. The net displacement of molten clad and the associated reactivity changes are estimated. A typical coolant channel in the present analysis is shown in Figure 1. The length of the heat generating section is denoted by l_F, whereas the upper and lower ends of the melted cladding section are Z_2 and Z_1, respectively. The total length of the molten clad film is denoted by λ_m and the thickness of the film by δ, whereas the initial solid cladding thickness is δ_c.

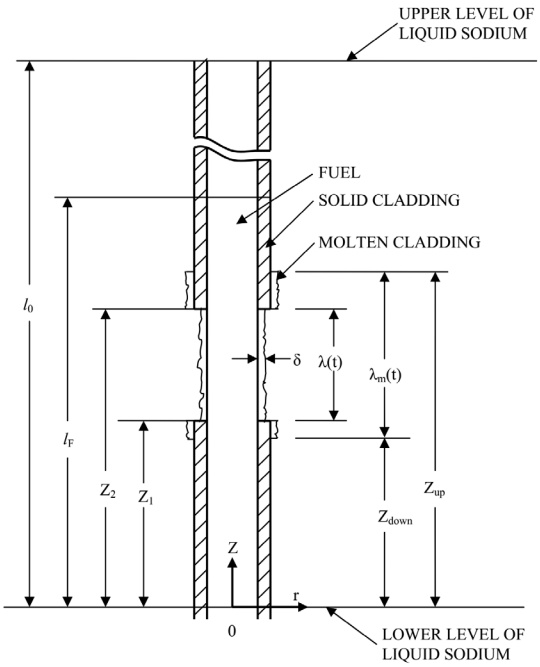


Figure 1 Schematic of the clad motion model

When the molten clad film reaches the axial blanket region by the upward motion induced by the sodium vapor drag, liquid starts to freeze upon contact with the cold cladding surfaces. By knowing the initial molten clad temperature and the upper blanket clad temperature, the one-dimensional solidification problem can be formulated as discussed below.

$$\rho_c C_c \frac{\partial T}{\partial t} = k_c \frac{\partial^2 T}{\partial x^2} \quad (4)$$

Where *x* is the coordinate perpendicular to the surface of the cladding, with its origin at the outer surface. T the temperature, C_c and k_c are specific heat and thermal conductivity of clad.

3.1 Computation scheme

Ishii's model uses a simple heat transfer model for temperature calculations which assumes a fuel pin with no division into axial meshes. The model has been modified to suit the mesh wise calculations in PREDIS. The height of one mesh considered in the PREDIS model is 10 cm for fuel region and 15 cm

for the blanket region. Such large meshes are not suitable for simulation of clad relocation using the said model and therefore finer meshes are to be used. For clad melting and relocation simulation a mesh size of 1 cm is used. Clad removal worth in the core region for PFBR is positive, while it is negative for the blanket region. Therefore, clad relocated from core and freezing in the upper axial blanket will add a considerable amount of positive reactivity into the system. The net positive reactivity added to the system due to clad relocation is calculated for the accurate prediction of the transient propagation in such an accident case.

4. Results and discussion

A new subroutine RELOCS is developed and integrated with the PREDIS code for the simulation of molten clad motion and freezing. Under ULOFA the reduction in heat removal leads to coolant boiling followed by melting of clad and fuel. Once the fuel melts the slumping of molten fuel causes large reactivity addition resulting surge in power. Pre-disassembly phase is terminated when the fuel temperature in the highest rated mesh crosses the boiling point. The pressure due to fuel vapor expansion disassemble the core and make it sub-critical terminating the accident. The disassembly phase calculations are done using VENUS code.

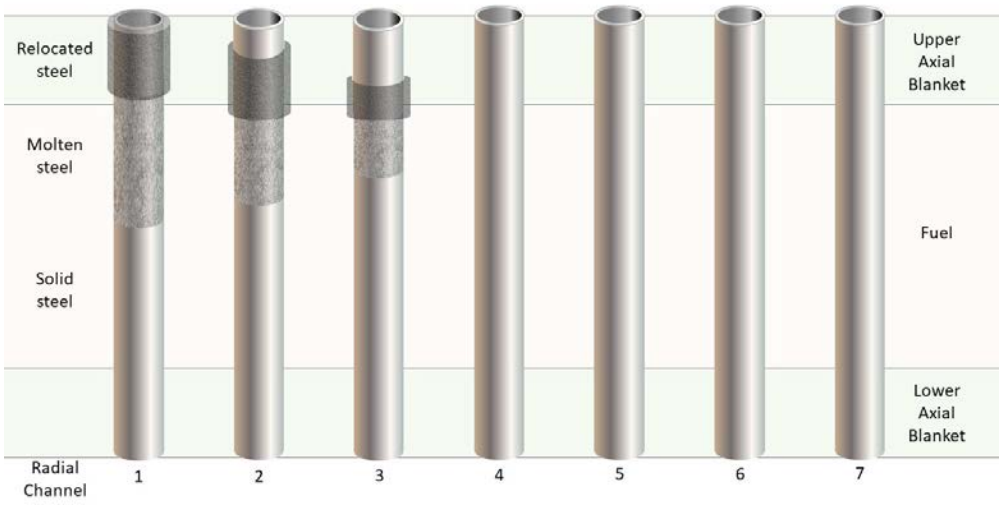


Figure 2 Status of clad relocation at the end of pre-disassembly phase.

The condition of clad melting and relocation at the end of pre-disassembly phase is depicted in Figure 2. Each of the 7 radial channels is represented by a pin. The time evolution of reactor power and net reactivity during the pre-disassembly are shown in Figures 3 and 4.

The reactivity addition rate due to fuel slumping and clad motion makes the net reactivity close to 1$. The large power and lower heat removal cause initiation of fuel boiling and the fuel vapor thus produced causes disassembly of the core. During the disassembly phase no heat transfer is assumed from fuel to coolant. The positive reactivity addition due to fuel slumping and clad motion results in power rise leading to further fuel boiling. The negative feedbacks from Doppler and fuel displacement bring the net reactivity below zero and the power drops rapidly. The whole duration of this disassembly phase is few tens of millisecond. The ULOFA analysis is carried out with and without the clad relocation model, the duration of the disassembly phase and fuel melt and vapor fractions are close to each other.

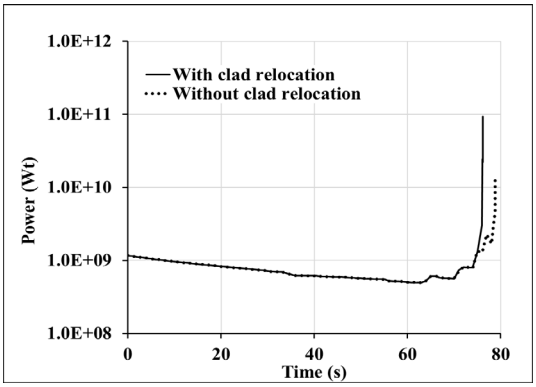


Figure 3 Reactor power evolution with and without clad relocation feedback

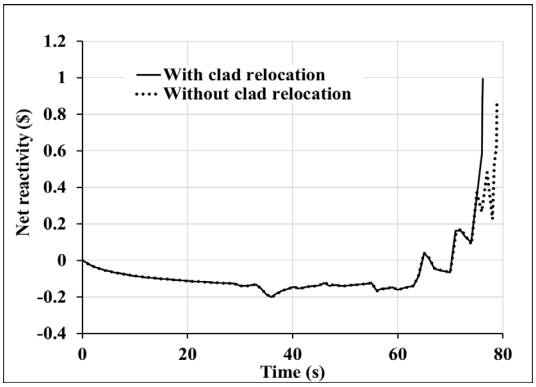


Figure 4 Net reactivity evolution with and without clad relocation feedback

The positive reactivity addition due to clad motion is found to be 1.46 $ at the end of pre-disassembly phase. The reactivity addition rate due to clad relocation is 16 $/*s*. Clad motion and fuel slumping together makes the net reactivity addition rate 21 $/*s* at the end of pre-disassembly phase. The mechanical energy release corresponding to the calculated reactivity addition rate of 21$/*s* is 2.1*MJ* which is more than the value obtained without clad relocation model. For a conservative reactivity addition rate of 65$/*s* the mechanical energy release is 103 *MJ* close to the design value of 100 *MJ*.

5. Conclusion

Clad relocation dynamics is included in the safety analysis code PREDIS. ULOFA analysis of PFBR is carried out with the modified code and it is compared against the reference case without clad relocation model. The reactivity addition rate due to clad relocation is found to be more than that from fuel slumping, and mechanical energy release is found to be close to the reference value of 100 *MJ* estimated without the clad relocation feedback. The model has not yet benchmarked against experimental results and the results discussed here are of preliminary nature. Accurate models for sodium vapor flow and molten fuel motion model under development are to be coupled with the clad motion model to have a more realistic simulation of the transient.

6. References

[1] M. Ishii, W. L. Chen, and M. A. Grolmes, “Molten Clad Motion for Fast Reactor Loss-of Flow Accidents”, *Nuclear Science and Engineering*, Vol. 60, Iss.4, 1976, pp.435-451.

[2] M. Ishii, W. L. Chen, and M. A. Grolmes, “Multichannel Model for Relocation of Molten Fuel Cladding in Unprotected Loss-of-Flow Accidents in Liquid-Metal Fast Breader Reactors”, *Nuclear Science and Engineering*, Vol. 69, Iss.2, 1979, pp.297-318.

[3] R. Harish, T. Sathiyasheela, G.S. Srinivasan and Om Pal Singh, “KALDIS: A Computer Code System for Core Disruptive Accident Analysis in Fast Reactors”, *IGCAR Report, IGC-208, 1999.*

Stability analysis of AHWR

Amit Thakur[1] and Umasankari Kannan
Bhabha Atomic Research centre, Mumbai, India
[1]*email:- thakur@barc.gov.in*

Abstract

The stability analysis for Advanced Heavy Water Reactor (AHWR) has been carried out through development of reduced order model and considering fuel temperature and void feedbacks through thermal hydraulics equations (lumped). The feedback effect of Xe-I equations has also been studied in this paper. The stability curve has been plotted and it was observed that AHWR operates in stable region and there is insignificant change in stability boundary with or without Xe-I equations. A numerical model has also been devloped for simulations of this reduced oreder model to actually observe the bahavior of reactor during small perturbations

1. Introduction

Stability analysis in linear and non-linear domain is an important part of reactor dynamics study. A reduced order model comprising of a point kinetics model for neutronics and a one node lumped parameter model for fuel and coolant thermal hydraulics has been developed for Advanced Heavy Water Reactor (AHWR) [1-3]. This dynamical system has intrinsic non-linearity. The instabilities arising due to Xe-I equations are also included in this study. The equilibrium points and the region of stable operation of reactor have been studied.

2. Mathematical model AHWR

Considering only 1 group of delayed neutrons, we get

$$\frac{dN}{d\tau} = \left(\frac{\rho(t)-\beta}{l}\right)\cdot N + \lambda C \quad (1)$$

$$\frac{dC}{d\tau} = \frac{\beta}{l}\cdot N - \lambda C \quad (2)$$

The feedback loop can be written as:-

$$C_f \frac{dT_f(\tau)}{d\tau} = P(\tau) - U(T_f(\tau) - T_{sat}) \quad (3)$$

$$\frac{h_{fg}}{v_g}\frac{dV(\tau)}{d\tau} = U\left(T_f(\tau) - T_{sat}\right) - P_0 \quad (4)$$

Here, the terms have their usual meanings. The non-linearity arising due to boiling of coolant has not been considered.The Xe-I equations can be written as:-

$$\frac{dI}{d\tau} = \gamma_I \Sigma_F \phi - \lambda_I I \quad (5)$$

$$\frac{dX}{d\tau} = \gamma_X \Sigma_F \phi + \lambda_I I - \lambda_X X - \phi\sigma_X X \quad (6)$$

Multiply both sides by $\frac{\sigma_X}{F\Sigma_a}$ and defining 'ρ_I 'as I$\cdot \frac{\sigma_X}{F\Sigma_a}$ and 'ρ_X 'as X$\cdot \frac{\sigma_X}{F\Sigma_a}$then

$$\frac{d\rho_I}{d\tau} = (\gamma_I \Sigma_F \phi)\cdot\left(\frac{\sigma_X}{F\Sigma_a}\right) - \lambda_I \rho_I$$

$$\frac{d\rho_I}{d\tau} = \phi \cdot \left(\frac{\gamma_I \Sigma_F \sigma_X}{F\Sigma_a}\right) - \lambda_I \rho_I \quad (7)$$

$$\frac{d\rho_X}{d\tau} = \phi \cdot \left(\frac{\gamma_X \Sigma_F \sigma_X}{F\Sigma_a}\right) + \lambda_I \rho_I - (\lambda_X + \phi\sigma_X)\rho_X \quad (8)$$

The expression for reactivity can be written as

$$\rho(\tau) = \rho_0 + \alpha_f\left(T_f(\tau) - T_{f0}\right) + \alpha_v \frac{(V(\tau)-V_0)}{V_0} + (\rho_X - \rho_{X0}) \quad (9)$$

Here, 'ρ_0' is small input perturbation reactivity.

To estimate the equilibrium points, first we introduce new dimensionless variables by following way: -

$x_1 = \frac{N-N_0}{N_0} = \frac{P-P_0}{P_0}$…(10a); $x_2 = \frac{C-C_0}{C_0}$…(10b); $x_3 = \frac{T_f - T_{f0}}{T_{f0}-T_{sat}}$…(10c);

$x_4 = \frac{V-V_0}{V_0}$…(10d); $t = \frac{\beta\tau}{l}$…(10e); $\rho_i = \frac{\rho_I - \rho_{I0}}{\rho_{I0}}$…(10f); $\rho_x = \frac{\rho_X - \rho_{X0}}{\rho_{X0}}$ …(10g)

For steady state operation, using equation 2 & 4 we have

$$C_0 = \frac{\beta}{l\lambda} N_0 \quad \ldots(11a); \quad T_{f0} = T_{sat} + \frac{P_0}{U} \quad \ldots(11b)$$

Further,

$$dt = \frac{\beta}{l} d\tau \qquad \phi(0) N_0 \cdot \gamma_I \cdot y = \lambda_I \rho_{I0} \quad (12)$$

In matrix form the equations can be jointly written as after neglecting small non-linear terms

$$\frac{dx}{dt} = [A]x \quad (13)$$

$$\dot{X} = f(X, u)$$

Where $x = [x_1, x_2, x_3, x_4, \rho_i, \rho_x]^T$ are the small variationsnear the equilibrium point. And the matrix A is

$$A = \begin{bmatrix} -1 & 1 & \frac{\alpha_f(T_{f0}-T_{sat})}{\boldsymbol{\beta}} & \frac{\alpha_v}{\boldsymbol{\beta}} & 0 & \frac{\rho_{X0}}{\boldsymbol{\beta}} \\ \frac{\beta}{l\lambda} & -\frac{\beta}{l\lambda} & 0 & 0 & 0 & 0 \\ \frac{P_0 \cdot l}{\beta \cdot C_f \cdot (T_{f0}-T_{sat})} & 0 & -\frac{P_0 \cdot l}{\beta \cdot C_f \cdot (T_{f0}-T_{sat})} & 0 & 0 & 0 \\ 0 & 0 & \frac{P_0 \cdot l \cdot \nu_g}{h_{fg} \cdot \beta \cdot V_0} & 0 & 0 & 0 \\ \frac{1}{\beta} \cdot \lambda_I & 0 & 0 & 0 & -\frac{1}{\beta} \cdot \lambda_I & 0 \\ X1 & 0 & 0 & 0 & X5 & X6 \end{bmatrix}$$

Where,

$$\frac{C_0}{N_0} = \frac{\beta}{l\lambda}; \frac{U \cdot l}{\beta \cdot C_f} = \frac{P_0 \cdot l}{\beta \cdot C_f \cdot (T_{f0}-T_{sat})}, \quad X1 = \frac{l}{\beta} \cdot (\lambda_X - \gamma(\lambda_X + \phi(0) N_0 \sigma_X),$$

$$X5 = \frac{l}{\beta} \cdot \gamma \cdot (\lambda_X + \phi(0) N_0 \sigma_X), X6 = -\frac{l}{\beta} \cdot (\lambda_X + \phi(0) N_0 \sigma_X)$$

The analysis around the stability boundary has been carried. The perturbation around chosen equilibrium point has been considered for stability analysis. If x_{eq} is the equilibrium point and $x_d$is small perturbation around it, thenthe eigen values of matrix A will describe the stability behavior of AHWR.

3. Stability Analysis for AHWR

The various values of parameters considered for AHWR are given below in table-1.

Table-1:- AHWR parameters considered for stability analysis			
Parameter	**Value**	**Parameter**	**Value**
λ (1g, s^{-1})	0.079	**β**	0.00343
l(ms)	0.19	**P_0 (MW)**	920.0
T_{f0}(K)	723.0	**T_{sat} (for coolant, K)**	560.0
Vo (m^3)	4.32564	**C_f (fuel, J/K)**	19196440.0
h_{fg} (m^3/Kg)	1500000.0	**Vg (J/Kg)**	0.027
γ_I	0.06445	**γ_X**	0.005912
λ_I	0.10552 hr^{-1}	**λ_X**	0.07585 hr^{-1}
Σ_F	2.3585E-3 cm^{-1}	**Σ_{ath}**	4.8649E-3 cm^{-1}
σ_X	1.41E-18 cm^2	**$\phi(0)$**	4.62E+13cm^{-2} s^{-1}
$\gamma = \gamma_I/(\gamma_X + \gamma_I)$			0.915977374

A computer program in python has been developed to determine the regions of stable operation for AHWR. During the stability studies, the α_f and α_v have ben varied to examine the regions for stable operation. The stability curve generated by this code has been given in fig 1.It is observed that AHWR is stable due to negative void co-efficient and FTC. It has also been observed that there is insignificant effect on stability boundary when Xe-I equations have been considered.

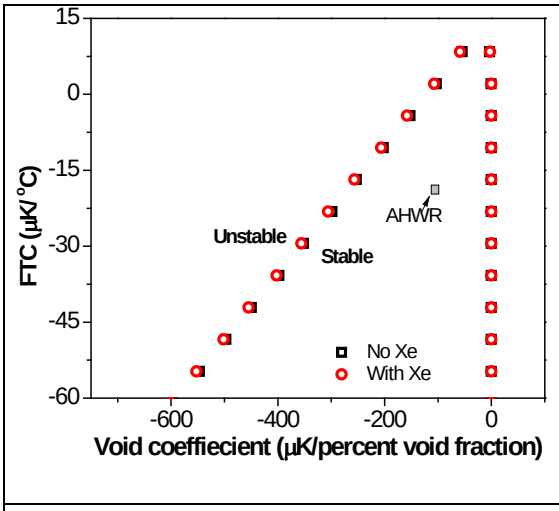


Figure 1. Stability curve for AHWR

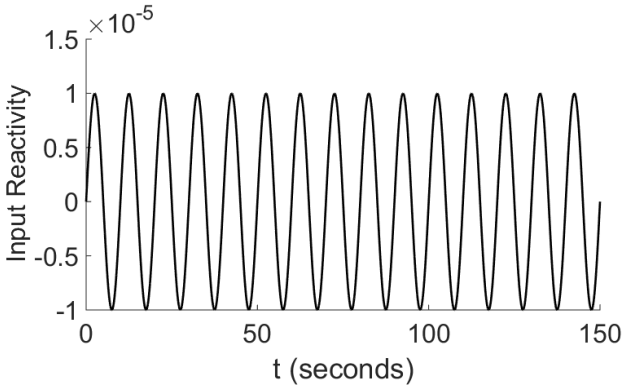


Figure 2: Input Reactivity Vs Tme

4. Numerical Simulations

The lumped paramteric kinetic feedback model given by equations 1-6 is develeped and programmed in python. Both stable and unstable regions of the stability curve have been analysed by simulation of reactor behaviour through input sinusoidal reactivity.Table 2 gives the values of FTC and void coeefficients considered for this analysis. The input reactivity of ~0.01mk has been given sinusoidal form of perturbation. Figure 2 shows the input sinusoidal reactivity considered for this analysis.

Table 2: Different values of FTC and void reactivity coefficient for this analysis				
Case-No.	**Region**	**FTC (α_F)**	**Void (α_V)**	**Remark**

1	Stable	-30E-6	-100E-6	Operating Region
2	Stable	+2E-6	-20E-6	Stable with +ve FTC and negative void
3	Unstable	+2E-6	-200E-6	+ve FTC but large –ve void
4	Unstable	-15E-6	-300E-6	Left side of slanted boundary line

5. Conclusions

The results for these numerical simulations have been consitant with the stability map plotted earlier. It is observed that for fig 3 is for operating region of AHWR and it shows that behanior is stable. For unstable regions the oscillations grow with time as shown in fig 5 & 6. An intereting case with positive FTC is also shown in fig 4. It falls in stable region of stability zone and stable behavior of reactor is observed when subjected to sinusoidal reactivity perturbations.

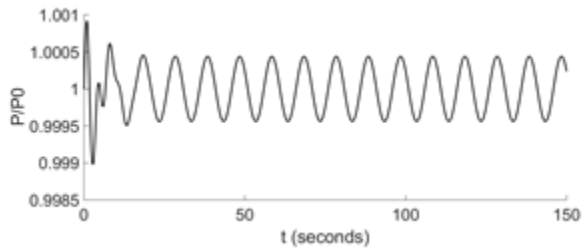


Fig 3: Stable operating region (α_F = -30E-6 and α_V = -100E-6)

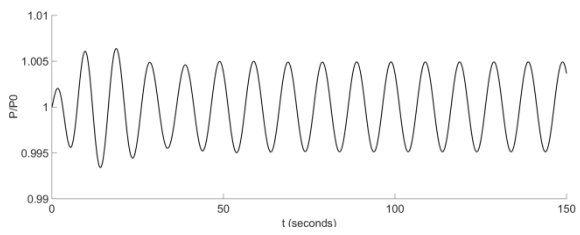


Figure 4: Stable region (α_F = +2E-6 and α_V = -20E-6)

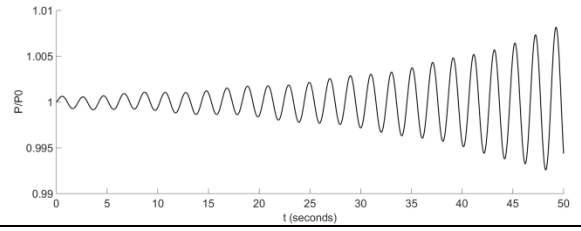


Fig 5: Unstable operating region (α_F = -15E-6 and α_V = -300E-6)

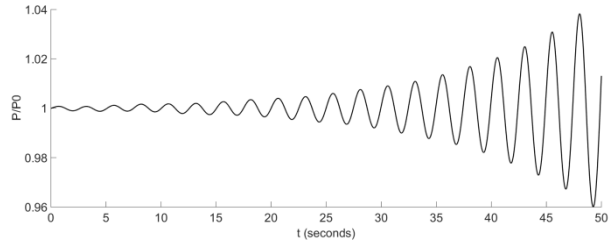


Figure 6: Unstable region (α_F = +2E-6 and α_V = -200E-6) for sinusoidal reactivity

6. Referances

[1] A Thakur and U Kannan, “Stability analysis of AHWR considering Xe-I feedback and point model equations” Technical Report No. RPDD/AHWR/466/ June, 2021

[2] A Thakur and U Kannan, “A reduced order model considering point kinetics and thermal hydraulics for analysis of stability regions of AHWR” Technical Report No. RPDD/AHWR/442/ June, 2021

[3] P Wahi and V Kumawat, “Nonlinear stability anlysis of a reduced order model of nuclear reactors: A parameteric study relevant to AHWR”, Nuclear Engineering And Design 241 (2011) 134-143

STUDY OF ATWS SCENARIO WITH PASSIVE SYSTEMS FOR VVER-1000 REACTORS

Anirban Biswangri[1], Manish Mehta[2], P Krishna Kumar[3] and Y K Pandey[4]
[1,2,3,4] Engineering LWR Directorate
Nuclear Power Corporation of India Limited, Mumbai, India
[1]*e-mail: -anirbanbiswangri@npcil.co.in*

Abstract

ATWS (Anticipated Transient without SCRAM) refers to a condition in which transient occurs followed by the failure of control rod insertion. The transient considered for this study is uncontrolled withdrawal of CPS-AR (Control and Protection System Absorber Rods) group at power. This condition falls under the plant state category of Design Extension Condition without core melt (DEC-A). Due to the postulated initiative event there is an insertion of positive reactivity causing the neutron power to increase. The consequences of the power rise result in increase of primary pressure and temperature. Consideration of failure of reactor SCRAM results in the actuation of passive safety system which arrest the rise in the neutronic power and makes the reactor subcritical. The analysis is carried out using RELAP-5/MOD 3.2 computer code. In this analysis individual feedbacks such as coolant temperature, fuel temperature and boron reactivity are evaluated and the combine effect of these feedbacks during the events is also studied. This paper also emphasis on the fact that in VVERs the failure of reactor SCRAM can be mitigated using passive systems such as Quick Boron Injection System (QBIS).

1. Introduction

VVER-1000 is pressurized water reactor (PWR) consisting of two independent and diversified means for making the reactor subcritical, one is by insertion of control rods and other by boron injection system. ATWS refers to a scenario in which an abnormal condition in plant which require the reactor protection system (RPS) to initiate SCRAM (rapid insertion of control rods) to shut down the reactor but due to malfunctions the insertion of control rods does not takes place. The transient considered for this study is uncontrolled withdrawal of CPS-AR group at full power resulting in the insertion of positive reactivity. The positive reactivity insertion causes the reactor power to rise and resulting in the generation of Emergency Protection (EP) signal but due to the failure of SCRAM, control rod insertion into the core does not occur. ATWS signal is generated resulting in the actuation of safety system to mitigate the consequence. In VVER two safety system are designed to mitigate the consequences of ATWS type of scenarios out of which one is a passive system and other is an active system. In this study the handling of ATWS scenario with passive system is emphasized. The analysis is carried out using RELAP-5/MOD3.2 incorporating different reactivity feedbacks such as coolant temperature, fuel temperature and boron reactivity

2. Calculation methodology and Modelling

RELAP-5/MOD 3.2[1] computer code was used to analyse the thermal-hydraulic behaviour of the ATWS type of events postulated in VVER type of reactors. To analyse the system thermal hydraulic behaviour Reactor Core, Primary Circuit and Secondary Circuit modelling is done. The Core consists of a Hot Fuel Assembly (FA), Average Power FA and By-pass. The primary circuit is modelled using four loops and each loop consists of one horizontal Steam generator (SG) and Reactor Coolant Pump (RCP). In VVER, two safety systems are designed to mitigate the consequences of ATWS one is Quick Boron injection system (QBIS) and another one is Emergency boron injection system (EBIS). These system supply boron solution into core and make the core

sub-critical when the ATWS signal is generated. The QBIS system consists of four tank each connected across the RCP and EBIS system supply boron solution into the main coolant pipelines. QBIS and EBIS were also modelled and the rate of boron addition by these systems in the core during such events was also verified. In the calculation methodology, single failure criteria (SFC) is also assumed in which failure of one train of safety system is also assumed. Point kinetics has been incorporating coolant density, boron concentration and fuel temperature feedbacks effects are also taken into account. In this present study the mitigation of the ATWS scenario with the help of passive system (QBIS) is presented. QBIS system is designed to inject sufficient amount of concentrated boron solution into the primary circuit to make the reactor sub-critical during the coast down time in case of SCRAM failure. QBIS system consists of a tank which is connected across RCPs by quick acting valves, these valves remains closed in the normal operating conditions and open only when the ATWS signal is actuated. The schematic diagram of single channel QBIS system is shown in Figure-1.

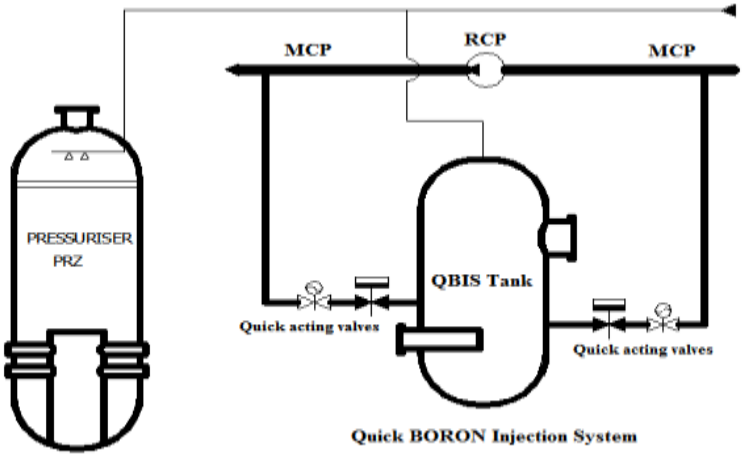


Figure-1: Schematic Diagram of QBIS

2.1 Input condition

The input condition considered during this analysis are conservative in nature. Fuel temperature coefficient is taken as maximum negative and the coolant density coefficient is considered as minimum negative, the most conservative combination of coefficients are chosen for the fuel temperature and coolant density. Boric acid coefficient is taken as minimum negative. The list of parameters are given in Table-1

Parameter	Values
Reactor Power	3120MWth (104%)
Fuel temperature Coefficient	Maximum negative
Coolant Density Coefficient	Minimum negative
Boric acid Coefficient of reactivity	Minimum negative
Primary Pressure	15.7 MPa
Coolant temperature at core inlet.	292.1 ^{o}C

Table-1 Input Conditions

3. Results and discussion

3.1 Event Progression:

The event scenario considered in this study is uncontrolled withdrawal of control rods from initial position. Withdrawal of working group with its maximum velocity is considered as postulated initiating event. Due to the insertion of positive reactivity the power increase is observed and reaches emergency protection settings. Once the EP signal is generated, and the neutron flux does not decrease as shown in Figure-2, ATWS signal gets actuated and QBIS is actuated. QBIS supplies boron solution at a temperature of 55^{o}C into the three loops of the primary circuit. For conservative analysis the loss of offsite power is assumed prior to the EP signal actuation is assumed and the RCP sets trips due to this assumption. During the coastdown of the RCPs, the boron solution from the QBIS tank is supplied into the primary circuit making the reactor sub-critical. After the termination of RCP coastdown the natural circulation is established in the reactor coolant system. The reactor power is reduced by the actuation of QBIS and residual heat can be removed by SG-ECD. The reactivity feedbacks during the postulated initiated event is shown in Figure-3 which demonstrates that the total reactivity in the core is always negative. The negative reactivity is attributed due to the addition of boron solution into the core, as the power decreases the fuel temperature feedback becomes positive but the overall reactivity is negative which makes the reactor sub-critical. In this study only the passive system are taken into consideration for making the reactor sub-critical. However an active system, EBIS also actuates when the ATWS signal is generates and it helps in maintaining long term sub-criticality margin. Table-2 shows the chronological sequence of the event.

Time, s	Event
0.0	Beginning of withdrawal of control rod
5.3	Trip of all RCP sets due to the assumption of loss of offsite power supply
6.2	Beginning of generation of EP signal by the increase in neutron flux to 107%
11.5	Generation of ATWS signal, and start-up of QBIS system
12.9	Start-up of decay heat removal system.
16.5	Complete opening of QBIS valves
17-42	Periodic operation of SG- Pulse Safety Device as its setpoint of opening is reached.
200	End of Calculation

Table-2 Event Sequence

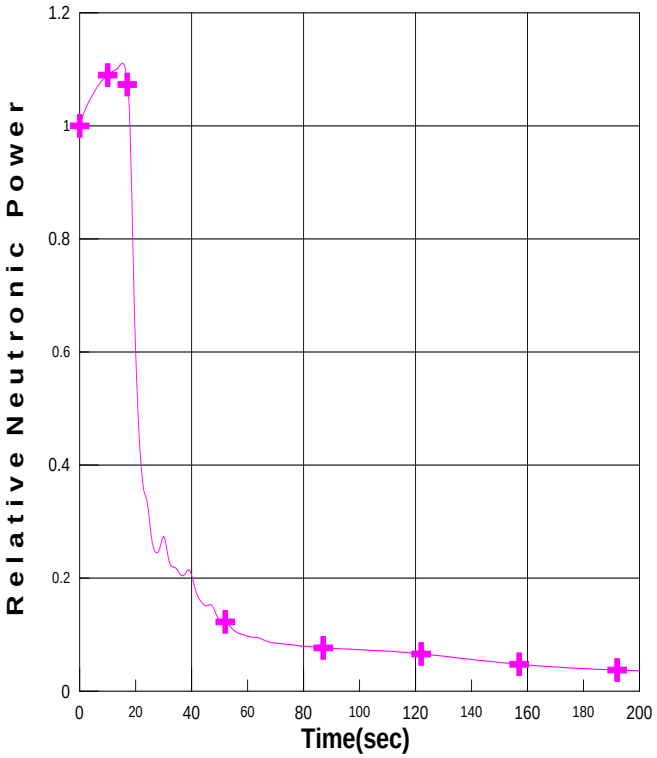


Figure-2 Relative Neutronic Power

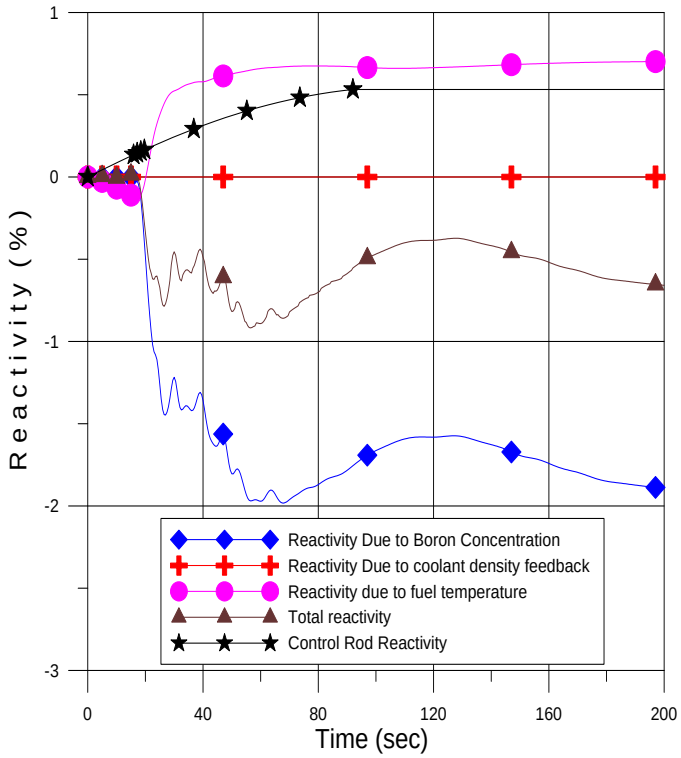


Figure-3 Reactivity Feedbacks

4. Conclusion

In this study, it is demonstrated that in reactivity insertion type events followed by ATWS the actuation of QBIS which is a passive system is sufficient to bring the reactor to sub-critical stage. The boron solution is supplied into the reactor coolant system by taking credit of the RCP coastdown. The decay heat is removed by natural circulation and further removed by decay heat removal system. ATWS scenario falls under the category of DEC-A, and from this study it is evident that in VVER with the help of passive system the initial consequences of ATWS type of events can be mitigated. However, for maintaining long term sub-criticality an active system such as EBIS is used which supplies borated water into the reactor coolant system.

5. References

[1] V. H. Ransom et al., RELAP5/MOD2 Code Manual, Volume 1: Code Structure, System Models, and Solution Methods, NUREG/CR-4312, EGG-2396, August 1985.

Estimation of Critical Channel Powers in 700 MWe IPHWR for Independent Assessment of ROPS Design

Vivek A. Kale[1] and Obaidurrahman K.[2]
[1&2] Atomic Energy RegulatoryBoard, Mumbai, India
[1]*e-mail: -vakale@aerb.gov.in*

Abstract

This article presents the methodology for the calculation of critical channel power (CCP) in 700 MWe IPHWR core with few examples. CCP is the power at which fuel dryout (or melting) occurs anywhere in the core. Calculation of CCP for different reactivity device configurations is an important step in the design of regional overpower protection system of the PHWRs. The calculation involves determination of critical heat flux and peak fuel temperatures for all the coolant channels. The minimum of these CCPs among all the channels is used as an input for the determination of trip setpoints of the ROPS. The present exercise provides an independent verification of CCPs for selected core configurations. For most of the selected configurations, estimated CCP values are close to the design values. The present study also indicates that the variations in the thermal hydraulic boundary conditions, solution methodology and correlations could have significant influence on the CCP values and hence on trip set points of the ROPS. The influence of these uncertainties need to be accounted in the design. The framework developed under the present work has provided a basis to undertake the independent verification of the ROPS design in IPHWR-700.

1. Introduction

The Regional Overpower Protection System (ROPS) of the 700 MWe PHWRs is first of a kind in Indian PHWRs. It consists of two independent protection systems [1] with associated self-powered neutron detectors (SPNDs) placed strategically in the core and segregated among 6 protection channels (3 for each protection system). The trip set points (TSPs) of the detectors are decided so as to prevent occurrence of critical heat flux (CHF) or fuel melting. For any reactivity device (RD) configuration, the reactor power at which this (CHF or fuel melting) occurs in any coolant channel is called the critical channel power (CCP). This calculation involves determination of CHFRs and fuel temperatures for all the coolant channels by solving fuel and coolant heat transport equations using in-house computer code REDAC [2]. This is done for a range of RD configurations/power distributions (the 'design basis set' for ROPS) [3]. These configurations include the RD positions with which the reactor is likely to operate most of the time (the 'nominal configuration') and several other off-nominal configurations. This paper presents the methodology and examples of the independent verification calculations for selected configurations.

The steady state approach has been adopted, where the total reactor power is increased in steps preserving the specified power distribution for a given configuration until the CCP is reached. For a given configuration, every channel has its own CCP value. Minimum of all these CCPs is referred to as the mCCP for that configuration. mCCP value is one of the inputs in determining detector TSPs for that configuration. TSP for the protection system is chosen as the minimum among all the configurations. This ensures reactor trip prior to dryout.

2. Mathematical Model and Computational Setup

Coolant channel thermal hydraulics is represented by 1-D steady state coolant transport equations for each coolant channel separately. The coolant transport equations (continuity, momentum and energy) are coupled with the 1-D heat conduction equation for the fuel pin. The source term of the conduction equation is dependent on the power distribution in the core, which is used as an input for the configuration under consideration. The coolant transport equations together with the equation of state (and appropriate closure relationship for the pressure loss coefficient) are solved numerically to obtain coolant state at each node along the coolant channel. The heat transfer coefficient between the fuel surface and the coolant is calculated using Dittus-Boelter correlation for single phase flow and using modified Chen's correlation [4] for subcooled and saturated flow boiling. The pellet-clad gap heat transfer coefficient is assumed to be constant. In single phase, the pressure loss coefficient is calculated using the correlation proposed by Venkat Raj [5]. For two phase flow, two phase multiplier approach is used which is obtained using Friedel correlation [5]. The coolant transport equations are solved using Chatoorgoon's [6] algorithm. This algorithm employs implicit finite difference formulation where the coolant transport equations are integrated from one computational node to the next and convergence on density is obtained at each node. Fixed core inlet and outlet coolant pressures (values at steady state 100 % FP for each channel) are used as the boundary conditions. Initially, the pressure loss coefficients need to be adjusted slightly for each channel to obtain the design coolant mass flow rate at 100%FP (full power). The coolant inlet temperature is assumed to be constant for all the channels.

The CHF is calculated using the Groeneveld Look-up table [7] with correction factors to account for the PHWR bundle geometry. These correction factors take into account the effects of spacers, non-uniform heat flux distribution among different pins, fuel pin diameter correction etc. [5]. In each channel, peak fuel temperature is calculated separately for the hottest pin with highest heat generation rate among the 37 pins. CHFR calculations are based on the average fuel pin for each channel. Light water thermodynamic properties have been used in the present analysis. Given power distribution at 100% FP is the starting point for the calculation. Subsequently, the total reactor power is increased in steps (each step is a steady state) retaining the power distribution, until either of the CCP criteria is reached (CHFR<1.1 or fuel melting). Size of power steps is reduced as the CCP is approached. Near CCP, power step size of 0.01%FP is used.

3. Results and Discussion

Fig. 1 shows the estimated CCP values for all the channels for nominal power distribution. It is observed that for this configuration, the CCP for all the channels appears due to coolant dryout/CHF ('D' after each CCP value indicates dryout). CCP values for the peripheral channels are considerably higher than the central channels. The minimum CCP (mCCP) obtained for this configuration is 129.95% (Channel L-15) which is very close to the design value. This value can be used as the basis for the respective trip set point.

During the design process, mCCP value is calculated for all the possible configurations under consideration ('design basis set' of configurations for ROPS). As an example, for the configuration with ARs 100%IN, ZCCs = 70%FL except ZCC-5,12 drained, CRs OUT; the CCP is found to be 104.5%. It is observed that for some configurations where the power distribution is highly distorted (w.r.t. nominal), the CCP is below 100% FP i.e. for these configurations, some channels approach CHF even when the total/global power is below 100% FP. The reactor cannot be allowed to operate at full power in such configurations (e.g. CCP = 91.8% for configuration with ARs 100%IN, ZCCs = 44%FL, CR-1,3,4 IN and CR-2 OUT). For the selected configurations, the difference between the calculated values and the design values were found in the range of 0.1% to 4%. The configurations where the product of normalized

CCP and detector readings is the lowest can be considered the limiting cases for determining the trip set points of ROPS detectors. The uncertainties in the CCP values for such configurations also need to be accounted in the design. For example, it was found that the changes in thermal hydraulic boundary conditions (inlet temperature, boundary pressures) by about 1% would lead to changes of similar magnitude in the CCP.

4. Conclusion

The present article provides an independent verification of CCPs for a few core configurations. CCPs are important to safety as they form the basis for ROPS TSPs. Results show that for most of the configurations, the predictions are close to the design estimated values. The present study also indicates that the variations in the thermal hydraulic boundary conditions, solution methodology and correlations could have significant influence on the CCP values and hence on TSPs. The influence of these uncertainties need to be accounted in the design**.** The framework developed under the present work has provided a basis to undertake the independent verification of the ROPS design in 700 MWe IPHWR.

5. References

[1] S. A. Bhardwaj, "The future 700 MWe pressurized heavy water reactor," *Nuclear Engineering and Design,* vol. 236, no. 7-8, pp. 861-871, 2006.

[2] V. A. Kale and K. Obaidurrahman, "Simulation of IAEA Reactivity Initiated Transient Benchmarks Using Reactor Dynamics Code 'REDAC'," *Journal of Nuclear Engineering and Radiation Science,* vol. DOI: 10.1115/1.4045394, 2019.

[3] V. A. Kale and K. Obaidurrahman , "Assessment of Proposed ROPS Trip Setpoints for IPHWR-700 and CANDU ROPS Design Perspectives," NSARG, AERB, Mumbai, 2021.

[4] N. Todreas and M. Kazimi, Nuclear Systems I - Thermal Hydraulic Fundamentals, Taylor and Francis, 1993.

[5] IAEA TECDOC 1203, "Thermohydraulic relationships for advanced water cooled reactors," IAEA, Vienna, Austria, 2001.

[6] V. Chatoorgoon, "SPORTS – A Simple Non-Linear Thermalhydraulic Stability Code," *Nuclear Engineering and Design,* vol. 93, pp. 51-57, 1986.

[7] D. Groeneveld, J. Shan, A. Vasić, L. Leung, A. Durmayaz, J. Yang, S. Cheng and A. Tanase, "The 2006 CHF look-up table," *Nuclear Engineering and Design,* vol. 237, pp. 1909-1922, 2007.

	1	2	3	4	5	6	7	8	9	10	11	12	13	14	15	16	17	18	19	20	21	22
A								167.84D	158.64D	155.00D	154.71D	155.21D	154.56D	159.40D	167.38D							
B						164.55D	152.82D	144.40D	139.76D	137.81D	138.04D	137.74D	138.20D	139.41D	144.95D	152.30D	165.29D					
C					158.64D	145.95D	137.80D	137.04D	134.70D	133.53D	135.11D	135.69D	133.00D	135.41D	136.52D	138.17D	145.46D	159.45D				
D				157.93D	143.92D	138.23D	133.80D	133.89D	132.26D	131.90D	132.45D	132.31D	131.86D	132.27D	134.00D	133.00D	138.81D	143.46D	158.55D			
E			160.42D	144.79D	136.28D	135.45D	133.00D	132.48D	133.29D	133.40D	134.60D	134.35D	133.22D	133.57D	132.51D	133.07D	134.77D	136.51D	144.28D	161.37D		
F		167.36D	147.72D	137.95D	136.67D	134.38D	133.27D	132.85D	133.91D	134.02D	135.12D	135.56D	134.20D	133.69D	132.90D	133.25D	135.16D	136.14D	138.44D	147.21D	168.13D	
G		154.23D	139.63D	137.44D	136.70D	135.00D	133.95D	133.57D	132.86D	133.65D	133.74D	133.29D	133.48D	133.10D	133.53D	133.93D	135.21D	136.20D	137.01D	140.37D	153.49D	
H	165.70D	143.41D	137.53D	134.03D	134.44D	134.87D	134.36D	133.14D	133.13D	132.33D	132.79D	133.00D	132.81D	132.60D	133.40D	134.26D	134.60D	134.83D	134.37D	137.21D	143.93D	165.15D
J	156.50D	141.54D	134.16D	133.18D	134.64D	134.40D	133.27D	134.27D	132.53D	131.15D	132.33D	132.53D	130.60D	133.26D	133.73D	133.33D	134.86D	133.94D	132.76D	134.68D	141.02D	157.20D
K	152.31D	138.10D	133.54D	132.72D	133.00D	133.28D	132.26D	130.10D	134.27D	133.87D	133.82D	133.76D	134.36D	133.57D	130.60D	132.24D	133.05D	133.18D	132.88D	132.76D	138.47D	151.95D
L	149.61D	137.10D	131.80D	130.73D	130.84D	131.54D	130.53D	130.60D	131.23D	133.36D	134.48D	133.91D	133.00D	131.91D	129.95D	130.75D	131.49D	130.97D	130.75D	132.08D	136.56D	150.16D
M	151.11D	135.67D	131.80D	130.53D	131.84D	132.58D	132.60D	130.70D	132.49D	131.40D	133.66D	134.25D	131.65D	131.87D	131.49D	131.84D	133.00D	131.71D	130.47D	131.53D	136.21D	150.53D
N	152.09D	137.50D	131.40D	132.27D	131.38D	130.60D	132.60D	133.58D	133.64D	134.36D	134.12D	133.52D	134.20D	134.16D	133.00D	133.40D	130.27D	131.58D	132.29D	131.64D	137.04D	152.57D
O	157.11D	141.71D	133.15D	131.26D	132.60D	131.05D	133.41D	132.20D	133.16D	133.20D	131.86D	131.95D	133.62D	132.60D	133.00D	132.72D	131.40D	132.39D	131.26D	132.37D	142.01D	156.39D
P	165.43D	143.84D	134.11D	133.47D	132.44D	133.40D	132.43D	134.28D	132.22D	133.40D	132.60D	133.00D	132.78D	133.00D	133.47D	132.78D	133.25D	132.48D	133.07D	134.53D	143.31D	166.08D
Q		152.45D	141.55D	134.45D	136.13D	134.29D	134.20D	134.62D	133.58D	132.87D	134.38D	133.91D	133.57D	133.00D	135.02D	134.22D	134.16D	136.49D	134.81D	141.00D	153.12D	
R		168.37D	148.95D	140.38D	138.27D	134.90D	132.79D	133.86D	133.65D	135.00D	134.27D	134.47D	134.47D	133.95D	133.80D	132.82D	135.08D	138.74D	139.83D	149.43D	167.60D	
S			162.86D	146.71D	141.56D	137.80D	134.73D	133.41D	133.80D	134.03D	135.11D	135.41D	134.20D	133.51D	133.47D	134.28D	138.22D	141.18D	146.95D	162.08D		
T				161.22D	146.04D	140.45D	135.54D	134.07D	133.53D	131.37D	135.59D	135.43D	131.36D	133.58D	133.80D	136.01D	140.20D	146.27D	160.28D			
U					162.17D	146.66D	141.97D	138.47D	134.75D	132.82D	137.21D	137.09D	133.41D	134.20D	138.99D	141.66D	147.08D	161.28D				
V						169.69D	153.80D	146.05D	139.13D	141.65D	139.94D	140.11D	141.31D	139.18D	145.57D	153.99D	169.05D					
W								171.36D	160.34D	154.20D	152.66D	152.48D	154.39D	159.87D	171.71D							

Fig. 1 CCP values for all the coolant channels at nominal power distribution (‘D’ indicates dryout)

Incorporation of kinetic module in WIMS

Anindita Sarkar[1], Umasankari Kannan
Reactor Physics Design Division, Bhabha Atomic Research Centre
[1]*e-mail: - anindita@barc.gov.in*

Abstract

A module for estimation of kinetic parameters has been integrated with the lattice code WIMS for estimation of burnup dependent kinetic parameters. This module has been used to estimate kinetic parameters of AHWR, PHWR and IPWR. The results have been found to be at par with the existing values. The variation of the kinetic parameters with the inclusion higher actinides for PHWR and IPWR has also been studied.

Introduction

A new module has been developed for estimation of kinetic parameters of the fuel assemblies using WIMSD[1]. Neutron transport equation is solved for the fuel assembly. The lattice constants generated are used to solve the adjoint diffusion equation to compute the adjoint flux. These multigroup adjoint fluxes and the direct fluxes along with the basic nuclear data are used to estimate the kinetic parameters namely delayed neutron fraction, neutron generation time and neutron lifetime. This methodology has been introduced in the WIMS code. This new module has been tested for PHWR[2], AHWR-Ref[3] and AHWR-LEU[4]. The kinetic parameters of IPWR[5] have been estimated using this module.

Description of the auxiliary programs of the module

ADJOINT.FOR: Adjoint flux is estimated by solving the adjoint equation[6].

$$M^{+}\,\Phi^{+} = \tfrac{1}{K} F^{+}\,\Phi^{+}$$

Writing in the matrix element form

$$\begin{pmatrix} D_1B^2+\Sigma_{R1} & -\Sigma_{s12} & -\Sigma_{s13} & ----- & -\Sigma_{s1G} \\ -\Sigma_{s21} & D_2B^2+\Sigma_{R2} & -\Sigma_{s23} & ----- & -\Sigma_{s2G} \\ -\Sigma_{s31} & -\Sigma_{s32} & D_3B^2+\Sigma_{R3} & ----- & -\Sigma_{s3G} \\ --- & --- & ----- & ------ & ----- \\ -\Sigma_{sG1} & -\Sigma_{sG2} & -\Sigma_{sG3} & --- & D_GB^2+\Sigma_{RG} \end{pmatrix} \begin{pmatrix} \Phi_1^{+} \\ \Phi_2^{+} \\ \Phi_3^{+} \\ -- \\ \Phi_G^{+} \end{pmatrix} =$$

$$\tfrac{1}{K} \begin{pmatrix} \chi_1\upsilon_1\Sigma_{f1} & \chi_2\upsilon_1\Sigma_{f1} & \chi_3\upsilon_1\Sigma_{f1} & ---- & \chi_G\upsilon_1\Sigma_{f1} \\ \chi_1\upsilon_2\Sigma_{f2} & \chi_2\upsilon_2\Sigma_{f2} & \chi_3\upsilon_2\Sigma_{f2} & ---- & \chi_G\upsilon_2\Sigma_{f2} \\ \chi_1\upsilon_3\Sigma_{f3} & \chi_2\upsilon_3\Sigma_{f3} & \chi_3\upsilon_3\Sigma_{f3} & ---- & \chi_G\upsilon_3\Sigma_{f3} \\ ---- & ----- & ----- & ---- & ---- \\ \chi_1\upsilon_G\Sigma_{fG} & \chi_2\upsilon_G\,\Sigma_{fG} & \chi_3\upsilon_G\Sigma_{fG} & ---- & \chi_G\upsilon_G\Sigma_{fG} \end{pmatrix} \begin{pmatrix} \Phi_1^{+} \\ \Phi_2^{+} \\ \Phi_3^{+} \\ -- \\ \Phi_G^{+} \end{pmatrix}$$

.....(1)

Here Φ_g^+ represents the 'g' th group adjoint flux.

This program takes the lattice parameters from the WIMS code and estimates the groupwise adjoint flux.

KINCAL.FOR: This module is used for estimation of kinetic parameters of FA. This module utilises, adjoint fluxes from the adjoint module, nufission reaction rates from WIMS and six group delayed neutron data and delayed neutron spectrum to estimate the delayed neutron fraction using equation 2. These are summed up for all the fine groups and then for all the isotopes to estimate the beta effective .

$$\beta_j = \frac{\sum_i \left[\sum_g \left(\chi_{dj} \right)_g \Phi_g^+ \beta_j \sum_{g'} \left(\upsilon \Sigma_f \right)_{g'} \Phi_{g'} \right]}{\sum_i \left[\sum_g \chi_g \Phi_g^+ \sum_{g'} \left(\upsilon \Sigma_f \right)_{g'} \Phi_{g'} \right]} \qquad \text{.....(2)}$$

$$\beta_{eff} = \sum_j \beta_j \qquad \text{.....(3)}$$

where,
g ang g′ are energy groups which runs from 1 to 69 , 'i' represents for isotopes.
The neutron generation time is estimated using equation 4.

$$\langle \Lambda \rangle = \frac{\sum_g \Phi_g \Phi_g^+ / v_g}{\sum_g \left(\chi_g \Phi_g^+ \right) \sum_{g'=1} \left(\upsilon \Sigma_f \right)_{g'} \Phi_{g'}} \qquad \text{.....(4)}$$

$$\langle l \rangle = \frac{\sum_g \Phi_g \Phi_g^+ / v_g}{\sum_g \sum_{ag} \Phi_g \Phi_g^+} \qquad \text{.....(5)}$$

Here 'v_g' is the average velocity of neutron in group 'g'. The group velocity is estimated in the 69 WIMS energy group structure. The mean neutron lifetime is estimated using equation 5.

Results

All the kinetic modules have been integrated with WIMS code in Chain 14 and Chian 15. WIMS-Beta has been used to estimate the kinetic parameters of PHWR, AHWR-Ref and AHWR-LEU. For PHWR U^{235} , U^{238} and Pu^{239} have been considered. For AHWR Th^{232}, U^{233}, U^{235} and U^{238} has been considered. The results are given in Table 1and Table 2 respectively.

It is evident from the tables that the results estimated using new methodology are in agreement with the established values. WIMS-Beta has been used to estimate the kinetic parameters of IPWR fuel assembly. The adjoint flux of IPWR estimated with Adjoint.for, has been plot in Fig. 1. The results are given in Table 3. Design calculation for IPWR has been

TABLE:1 Kinetic Parameters of PHWR estimated using WIMS-beta

PHWR BU (MWD/t)	Effective beta (mk)		Mean neutron lifetime (X1E-4 s)	
	WIMS-Beta	Lit[4]	WIMS-Beta	Lit
0.0	7.3738	6.90	6.2820	6.46
3500	5.2455	4.955	5.4651	6.02

TABLE:2 Kinetic Parameters of AHWR estimated using WIMS-beta

Reactor	Effective beta (mk)		Mean Neutron lifetime	
	WIMS-Beta (mk)	ITRAN (mk)	WIMS-Beta (μs)	ITRAN (μs)
AHWR-Ref(Bottom)	2.632	3.300	0.128	0.159
AHWR-Ref(Top)	2.629	3.215	0.147	0.165
AHWR-LEU(Bottom)	7.189	7.839	0.153	0.179
AHWR-LEU (Top)	7.185	7.768	0.162	0.191

TABLE: 3 Kinetic Parameters of IPWR estimated using WIMS-beta

IPWR	Delayed Neutron Fraction		Mean Neutron lifetime	
(Burnup MWD/t)	WIMS-Beta (mk)	EXCEL(mk)	WIMS-Beta (X 1E-5 s)	EXCEL (X 1E-5 s)
0	7.4504	7.79	1.421	1.800
15000	6.071	6.32	1.490	2.070
30000	5.461	5.67	1.500	2.150
45000	5.053	5.22	1.551	2.290

performed with EXCEL code also. The kinetic parameters for IPWR has been compared with the values calculated using EXCEL code. The results obtained using WIMS-Beta are found to be in agreement with the values obtained using EXCEL.

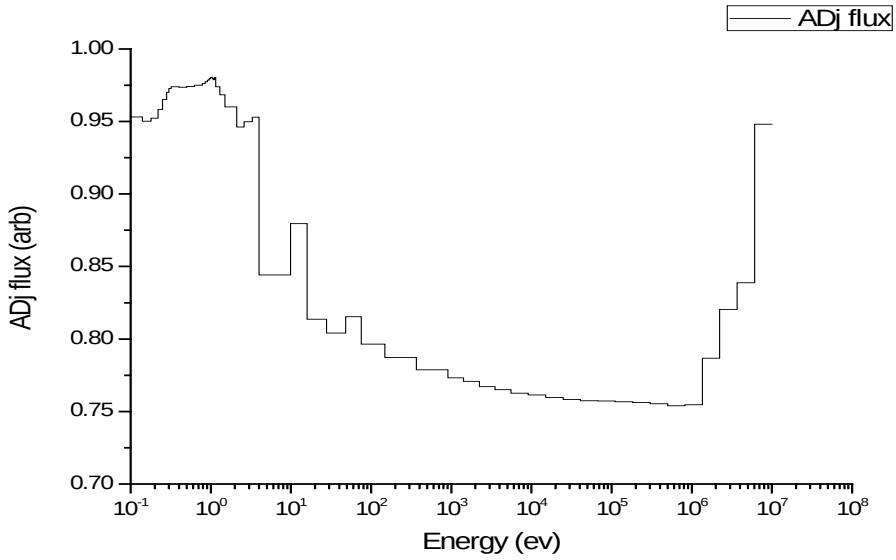


Fig 1. Adjoint Flux of IPWR at equilibrium burnup

Another study has been performed to study the effect of inclusion of higher actinides on the kinetic parameters of PHWR and IPWR. The effect of including Pu ^{241} , Pu ^{242} , Am ^{241}, Am ^{243}and Cm ^{242} on the kinetic parameters of PHWR has been studied. It has been observed that the kinetic parameters of PHWR does not change with the inclusion of higher actinides. Similar study for IPWR have also been performed. It is observed that as higher actinides are included delayed neutron fraction decreases. This is due to the fact that as the mass of fissioning actinide increases there is a shift in the mass of fission products and hence the production of bromine is reduced. Since bromine family is the major contributor of delayed neutron and since its proprotion is reduced there is reduction in delayed neutron fraction. However mean generation time and mean lifetime is not affected by inclusion of higher actinides.

Conclusion

A new module has been integrated in WIMS for estimation of bunrunup dependent kinetic parameters. This new module has been validated for PHWR, AHWR and IPWR.

References

1. Askew, J.R, Fayers, F.J., and Kemshell, P., 1966. A general description of the lattice code WIMS. British Nuclear Energy Society, p. 564, Oct 1966.
2. Design Manual of Kaiga Atomic Power Plant- 3&4, NPCIL, October 2020.
3. Arvind Kumar, “A new cluster design for the reduction of void reactivity in AHWR”, proceedings of the annual conference of Indian Nuclear Society on power from thorium, status, strategies and directions, Mumbai, India (2000).
4. AHWR-LEU SARP, Arindam Chakraborty et. al., BARC, March 2013
5. Conceptual Design of IPWR : Reactor Physics Design IPWR/RPDD/005/ 19th April 2013.
6. G.M.Behera and A.Kumar, BARC/RPDD/AHWR/04, Evaluation of kinetic parametrs using WIMS code.
7. J.J. Duderstadt and L.J. Hamilton, “Nuclear Reactor Analysis”.

ANALYSIS OF UNPROTECTED TRANSIENTS OF INTERRUPTIONS IN HEAT REMOVAL IN IMSR-5MW WITH CODE PATH

D.K. Dwivedi*, Anurag Gupta and Umasankari K.
Reactor Physics Design Division, Bhabha Atomic Research Centre, Mumbai, India
*e-mail: - ddwivedi@barc.gov.in

Abstract

Indian Molten Salt Reactor, IMSR-5MWt, is being designed as an experimental core to demonstrate the indigenous technology of circulating fuel reactors. The reactor type is recognized as the potential design for the third stage of the Indian nuclear power programme. The thermal spectrum core has been envisaged with molten fuel salt LiF-CaF_2-ThF_4-UF_4 flowing in moderator tubes of graphite under forced circulation. The circulating fuel reactors have several advantages regarding core safety and higher fuel utilization. But the fuel salt circulation out to the core results in the loss of delayed fission neutrons, whereas the high melting points of these salts raise concerns of accidental loss of heat removal due to loss of flow in the primary circuit or failure of the heat sink. Therefore, in scenarios of loss of fuel salt flow and a failure of the heat sink, the passive safety characteristics of IMSR-5MWt core have been investigated assuming unprotected circumstances, i.e. without activation of the scram during the transients. In this context, the unprotected transients of loss of fuel salt flow and loss of heat sink have been simulated with code PATH. The point kinetics code PATH can consider the drift loss of the delayed neutron precursors and has 1D-radial heat conduction based thermal-hydraulics to evaluate the temperatures in the average channel of the core. The results and findings of the analysis are described in this paper.

1. Introduction

The circulating fuel-salt type MSRs are suitable to be designed as breeders, particularly for thorium utilization in the third stage of the Indian nuclear power programme [1]. In this context, the design of an Indian Molten Salt Reactor, IMSR-5MWt, is being worked out to serve as an experimental core to demonstrate the indigenous technology of circulating fuel reactors [2]. The thermal spectrum core consists of molten fuel salt LiF-CaF_2-ThF_4-UF_4 flowing in moderator tubes of graphite under forced circulation during normal operations. The design and safety of circulating fuel reactors have several advantageous features like highly negative temperature coefficients and online refuelling & reprocessing consequence in better core safety, stability during operation and higher fuel utilization. Also, the high boiling temperature point of fuel salt facilitates the low-pressure operation of the primary circuit. Despite these, the circulating fuel salts with high melting points in the MSRs impose several technological challenges, e.g. circulation of fission occurring salt leading to loss of delayed neutrons from the critical core, modelling of multi-physics phenomena, compatibility of structural material etc. Also, the fuel salt in the primary circuit is susceptible to solidifying under an inadvertent scenario of overcooling, which would result in loss of flow.

The circulating fuel salts in MSRs simultaneously act as the coolant to transport nuclear heat from the primary to the secondary side. The loss of flow of fuel salt because of solidification or loss of pumped circulation (e.g. pump coast-down) leads to the interruption in the core heat removal and the addition of positive reactivity of fuel salt flow subsequently. In almost similar consequences, any failure of the heat sink, i.e. interruption in heat transfer to the secondary side, could immediately result in a rise of core inlet temperature and subsequent loss of heat removal from the primary circuit and an increase in core temperature. Therefore, in the unforeseen scenarios of loss of heat removal due to loss of fuel salt flow

or failure of the heat sink, the passive safety characteristics of the core have been investigated assuming unprotected circumstances, i.e. without activation of scram during the transients. In this regard, the unprotected transients of loss of fuel salt flow and loss of heat sink have been simulated with code PATH. The indigenously developed and validated point kinetics code PATH [3] can also consider the drift loss of the delayed neutron precursors as a phenomenon in circulating fuel reactors. The code has 1D-radial heat conduction based TH capability to predict the time-dependent temperature profile in the average powered channel of the core [3 & 4]. The results are discussed and reported in subsequent sections after a short description of the code used.

2. The methods and models in code PATH for circulating fuel reactors

The in-house developed code PATH solves point kinetics equations with decay rates of multi-group of delayed neutron precursors using a higher-order Padé approximant based solver in option to RK4 and Implicit Euler methods [3, 4]. The integrated thermal-hydraulics (TH) capability in the code is based on 1D-radial heat conduction in the average powered channel of the core as well as lumped fuel and coolant optionally. The neutronics and TH capabilities of the code are extensively validated with several benchmark problems available in the literature [3, 5]. The capability of the code has also been suitably advanced for point dynamics of circulating fuel type MSRs [6], which is briefly mentioned in the following discussion. The point kinetics equations for circulation fuel reactors are as follow:

$$\frac{dP(t)}{dt} = \frac{\rho(t)-\beta}{\Lambda} P(t) + \sum_{d=1}^{D} \lambda_d C_d(t) \qquad \text{---- (1)}$$

$$\frac{dC(t)}{dt} = \frac{\beta_d}{\Lambda} P(t) - \lambda_d C_d(t) - \frac{C_d(t)}{\tau_c} + \left[\frac{C_d(t-\tau_l) e^{-\lambda_d \tau_l}}{\tau_c} \right] \qquad \text{---- (2)}$$

Here the symbols have their usual meanings. The parameter τ_c is the fuel transit time in the core (i.e. total fuel in the core/ mass flow rate) and τ_l is the fuel transit time in the external loop (i.e. total fuel mass in the external loop/ mass flow rate). In the 1D model of precursors drift, the third term in the right-hand side (RHS) of equation (2) is defined rate of removal of precursors from the core due to fuel flow (i.e. $C_d(t)/\tau_c = v_c \, \partial C_d/\partial z$ and $\tau_c = \Delta z / v_c$, where Δz is the axial length and v_c is the drift speed of the molten fuel salt in the axial direction of the core). The last term at RHS in equation (2) accounts for the fraction of delayed-neutron precursors that did not decay in the external loop and are reintroduced in the core after a delay of τ_l . Here $\rho(t)$ is net reactivity at a time 't' in the core, which is as follows:

$$\rho(t) = \rho_0 + \rho_{rd}(t) + \rho_{fd}(t) \qquad \text{---- (3)}$$

Here, ρ_0 = initial core reactivity at t = 0, $\rho_{rd}(t)$ = external reactivity duel absorber rod movements and $\rho_{fd}(t)$ = feedback reactivity due to change in temperature and power.

The third and fourth terms at RHS in equation (2) are included to account for the loss and gain of delayed neutron precursors due to fuel-salt flow. From the steady-state condition, the initial reactivity due to the fuel-salt flow resulting in delayed neutron lost in transit is given as follows:

$$\rho_0 = \beta - \sum_{d=1}^{D} \frac{\beta_d}{\left(1 + \frac{1}{\lambda_d \tau_c} \left[1 - e^{-\lambda_d \tau_l} \right] \right)} \qquad \text{----- (4)}$$

Where the ρ_0 arises as negative reactivity due to loss of delayed neutrons because of fuel-salt flow and need to be compensated by control rod action for critical core operation. The effective fraction of delayed neutrons in steady flow condition in circulating fuel reactor can be represented as follow:

$$\beta_{eff} = \beta - \rho_0 = \sum_{d=1}^{D} \frac{\beta_d}{\left(1 + \frac{1}{\lambda_d \tau_c}\left[1 - e^{-\lambda_d \tau_l}\right]\right)} \qquad \text{----- (5)}$$

In equation (3), the feedback $\rho_{fd}(t)$ can be estimated as follow:

$$\rho_{fd}(t) = \alpha_{fs}\left[T_{fs}(t) - T_{fs}(0)\right] + \alpha_{gr}\left[T_{gr}(t) - T_{gr}(0)\right] \qquad \text{------ (6)}$$

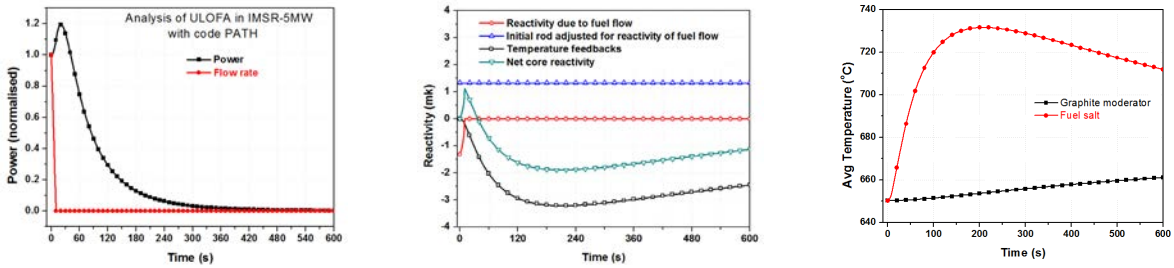
Here, α_{fs} and α_{gr} are the feedback coefficients of reactivity due to change in temperature of fuel-salt and graphite moderator. $T_{fs}(t)$ and $T_{gr}(t)$ are the temperature of fuel-salt and graphite moderator during transient with their initial (at t=0) values as $T_{fs}(0)$ and $T_{gr}(0)$ respectively.

In the case of circulating fuel type MSRs, most of the fission energy is retained in the molten fuel salt, which is also acting as the coolant, which is carrying out heat from the core. However, inside the graphite moderator, only around 2-3% of fission energy is deposited directly by the moderation of fast neutrons in addition to heat convection from the flowing fuel salt in the channels. The change in mass flow during transient for loss of mass flow rate is assumed as a given input. The close loop model of TH is considered for loss of heat sink simulation with the code. Therefore, TH of the code has been modified accordingly to consider these peculiar features of circulating fuel reactors [6].

3. Results and analysis of IMSR-5MWt transients

In the conceptual design of IMSR-5MW, the core consists of graphite as moderator channels where LEU based molten fuel salt LiF-CaF_2-ThF_4-UF_4 flows with inlet and average outlet temperatures at 635 ^oC and 665^oC under the forced circulation at full power. The average mass flow rate in the core is about 66.7 kg/s. The neutronics parameters in the operating condition like Λ, β, α_{fs} and α_{gr} are 3.6576×10^{-5} s, 6.7 mk, -3.94×10^{-5}k/^oC and -2.41×10^{-6} k/^oC respectively. The fuel residing time in the core and ex-core circuit are 16.5 and 8.5 s. The reactivity loss due to fuel salt flow and the effective fraction of delayed neutrons in the core are calculated to be 1.32 mk and 5.38 mk respectively with code PATH. The unprotected transients of interruptions in heat removal in IMSR-5MWt are investigated for cases- (i) loss of flow of fuel salt in the core and (ii) loss of heat sink, which are discussed ahead.

In case of unprotected loss of flow accident (ULOFA), the mass flow rate is assumed to be decreasing to 0.5% of the nominal value within 10 s (Fig.-1 (a)). The shutdown and control systems are not activated during the transient. The core reactivity is changing due to a decrease in the mass flow rate of fuel salt as well as changes in the temperatures of fuel salt and graphite moderator.

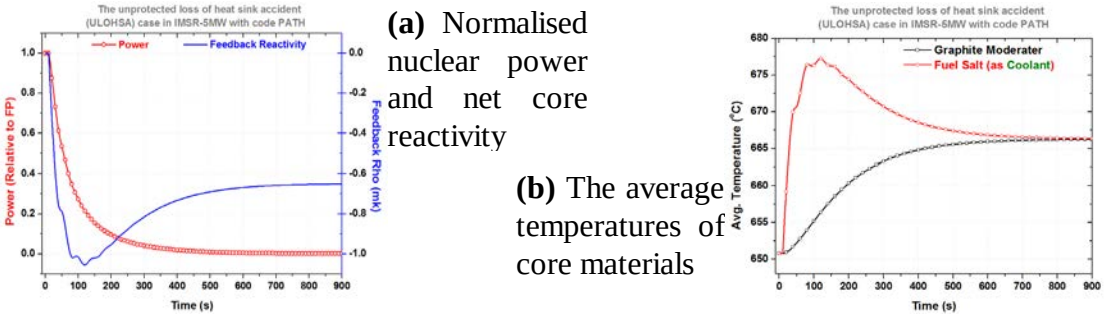


(a) Normalised core power **(b)** Reactivity in the core **(c)** Core average temperatures

Fig.-1: Prediction of IMSR-5MWt during a case of ULOFA with code PATH

The predicted core power during the transient is shown in Fig. 1(a). The reactivities due to various causes in the core are given in Fig. 1(b). The variations in average temperatures of fuel salt and graphite moderator are estimated and given in Fig. 1(c). The core power is observed to be increasing initially.

Then, the power set-back leads to a passive shut down of the core. It shows that the core design is inherently safe. The average temperatures of the fuel salt and the graphite are also computed. It is found to be rising initially and would be stabilizing much after 10 min of the initiating moment.



(a) Normalised nuclear power and net core reactivity

(b) The average temperatures of core materials

Fig.-2: Prediction of IMSR-5MWt during a case of ULOHSA with code PATH

In case of unprotected loss of heat sink accident (ULOHSA) in the operating core at full power, the scram is assumed to fail to act. The circulating fuel salt from the core outlet returns to the inlet with a time delay (τ_l). There is no loss in fuel salt enthalpy due to interruption occur in the heat transfer from the primary to the secondary side. However, the mass flow rate is assumed to be invariable during the transient in forced circulation cooled core. The core heating with higher inlet temperature during ULOHSA leads to a rise in fuel-salt temperature initially, which leads to the passive insertion of negative reactivity as feedback. The negative reactivity feedback in the core results in power setback and passive shutdown of the reactor finally (Fig.-2(a)). The temperatures of the core materials are estimated and reported in Fig.-2(b). It has been observed that the temperatures of the core materials stay within the safety limits. The analysis demonstrates the passive safety feature of the designed core.

4. Conclusion

An experimental core of the Indian Molten Salt Reactor, IMSR-5MWt, is being designed to demonstrate the indigenous technology of circulating fuel reactors. The conceptual core design has been investigated for the unprotected loss of heat removal transients- (i) loss of fuel salt flow and (ii) loss of heat sink accident in full-power configuration. The safety transients of IMSR-5MWt have been simulated with in-house developed and validated code PATH. The neutronics and thermal-hydraulics capability in the code are advanced for circulating fuel reactor analysis. The results and predictions show that the core passively shuts down during these transients, whereas materials' temperatures stay within the safety limits. The study numerically demonstrates the passive safety features of the designed reactor core.

Acknowledgement

The first author is thankful to Shri A.K. Srivastava, RPDD, BARC, for providing the core kinetics parameters of IMSR-5MWt for the point kinetics simulations of the reactor transients.

References

[1]. Krishnani, P. D. , 2015. Proceedings of ThEC15 conference held at Mumbai, October, 2015.
[2]. Srivastava et al., 2019. RPDD/MSR/31-A/Feb.-2019.
[3]. Dwivedi et al., 2017.Proceedings of DAE-BRNS symposium ARP-2017, RK08-023, Dec-2017.
[4]. Dwivedi et al., 2020. Development of module SHAKTI. RPDD/HTR/104/June-2020
[5]. Dwivedi et al., 2020. Nuclear Engineering and Design, 370, 110881.
[6]. Dwivedi et al., Report no. RPDD/MSR/35, 45, 51 & 61 published during year 2019 to 2021.

SPACE TIME MONTE CARLO CODE KINMC FOR SIMULATING REACTOR TRANSIENTS

Argala Srivastava and K. P. Singh
Bhabha Atomic Research Centre, Mumbai, India
e-mail: - argala@barc.gov.in

Abstract

In Nuclear Reactor Physics, deterministic and hybrid calculation methods dominate the field of transient analysis. This implies that important safety assessments are subject to many approximations which are needed by these methods. This paper proposes, a more accurate method based on transport Monte Carlo for space time simulations. This method is developed by the numerical recipes proposed earlier by us for full space time simulations by Monte Carlo. Having verified the recipes on simpler models i.e. on Point Kinetics and Diffusion theory MC models, they are finally implemented in the Space Time Kinetics Code KINMC. KINMC Code uses the Delta Neutron Tracking Method for neutron transport. The code explicitly treats the six groups of precursors and used population and weight control of precursors and neutrons as well as the concept of mean number of secondaries in a collision for variance reduction. The efficacy of this code is tested by comparison with the results of realistic space time kinetic benchmarks involving multi region reactors and energy dependence. 1D Benchmark and TWIGL 2D Benchmark are analyzed by KINMC. Results are in good agreement within the standard deviation.

1. Introduction

An understanding of the time dependent behavior of the neutron population in a nuclear reactor is of utmost importance for safe and reliable operation of nuclear reactors. For the simulation of the dynamic behavior of a nuclear system, a number of deterministic codes exist and are in current use [1, 2]. As opposed to the deterministic methods, the Monte Carlo method is a stochastic method that has been in use for a long time, but was used rather restrictively due to its large computing requirements. The radical increase in the availability of computing power in recent times permits the use of Monte Carlo (MC) methods more routinely for solving reactor physics problems. In this paper a time dependent neutron transport code (KINMC) has been developed on Transport MC Method for use in time dependent situations such as pulsed neutron experiments and nuclear reactor transient analysis. Several new schemes had been proposed earlier by us and developed to manage variance and computing time issues associated with MC based kinetics [3]. These include measures for neutron and precursor population and weight control, forced decay of precursors without combining them together and the use of mean number of secondaries per collision.

The proposed new techniques are first applied to and tested in simpler models such as the Point Kinetics MC Model and the few group diffusion theory MC models, as it is easier to test new techniques in these simpler models. In this paper, we have applied these developed schemes to the transport based Monte Carlo method and it has led to the development of the transport based space time kinetics code KINMC. KINMC is validated with transient problems benchmarked with time dependent transport code. Section 2 describes the methodology used for the simulation. In Section 3, we discuss the validation of the code with space time simulations done with transport based codes. Section 4 presents the conclusions.

2. Methodology

Initially a steady state simulation is performed at t=0 sec for a given test problem. Total number of thermal neutron at the steady state is estimated by dividing the number of fission events with the product of the fission cross section and the velocity of the neutron in that group. Similarly, total number of fast neutrons at the steady state is estimated by dividing the number of slowing down events with the product of the slowing down cross section and the velocity of the neutron in that group. This way we can obtain the ratio of thermal to fast neutrons in the system at t=0 sec. 10^5 thermal neutrons are considered and fast neutrons are considered in ratio of thermal to fast neutrons. 10^5 fission sites are randomly selected form the stored fission sites which are the sites for the thermal neutrons at t=0 sec. In the problem domain having multiple regions denoted by x, having different fission cross sections, $\Sigma_f(x)$, in each region the number of fission sites $n_2(x)$ are counted. Then the number of precursors in the steady state is given by,

$$C_{i0x} = \sum_x (\beta_i \nu \Sigma_f(x) V / \lambda_i) n_2(x) \quad (1)$$

Where, summation is over total number of regions in the problem domain. β_i is the delayed neutron precursor of the i[th] group, ν is the number neutrons produced per fission, Σ_f is the fission cross section, λ_i is the decay constant of the each precursor group, $n_2(x)$ is the thermal neutrons in the region x and V is the neutron velocity. Thus, for a population of 10^5 neutrons, there will be 10^9 precursors. This poses the first challenge population of 10^5 neutrons is probably the minimum that would be required to get any statistically meaningful results whereas modeling more than 10^9 precursors explicitly is virtually impossible on current desktops [4]. Hence, we lump these precursors into a more manageable number say 10^5 and assign a weight

$$W_p = \sum_i \sum_x C_{iox} / 10^5 \quad (2)$$

and the sites of these precursors are randomly selected from the fission sites. Now, all 10^5 precursors are allowed to decay in each time bin. Weights of the decayed and undecayed precursor are $W_p(1-e^{-\lambda \Delta t})$ and $W_p e^{-\lambda \Delta t}$ respectively .At the end of each time bin, average weight of the precursors is calculated which is

$$W_{avg} = [(N_{pf} W(1-e^{-\lambda \Delta t})) + (N_{pi} W(e^{-\lambda \Delta t}))] / N_{pi} \quad (3)$$

Where, N_{pi} and N_{pf} is the number of initial precursors and final precursors produced in the bin.

The neutrons are tracked one by one. In the case of space dependent transport MC simulations the next event is a collision event, for which the coordinates of the collision point are also sampled in addition to the time and a check is made whether the particle has leaked out of the system, in which case the history is terminated. Time of the event of the neutron is estimated by

$$t = -t_i + \frac{s}{v} \quad (4)$$

$$s = -\frac{1}{\Sigma_m} \ln \xi \quad (5)$$

Where, t_i is the initial time, s is the distance travelled to the collision, v is the velocity of the neutron, Σ_m is the maximum total cross section of all materials of the medium and ξ is a random number The new (pseudo) collision point is obtained from the direction and the above sampled distance. The collision point is accepted as a real collision with a probability Σ_t / Σ_m. Else the point is rejected and treated as a pseudo collision. If the neutron lies within the time boundary and if the particle has suffered

a pseudo collision then it is tracked in the same direction. If the event is recorded as a real collision, it is checked if the neutron has suffered scattering/ fission taking it into the same group or out of the group.

3. Test Problem and Results

We have tested capability of the KINMC Code firstly on 1D transient benchmark [5] and then on 2D Space time transient of TWIGL [6] Reactor. The standard problem described by Sjenitzer and Hoogenboom, 2013 was analyzed to test the transport MC technique discussed in Section 2. The problem consists of a cuboid of dimension 10 x 12 x 24 cm placed in a vacuum and is near critical. After 10 seconds, the density of the Uranium is increased making the system super critical. The transient is followed for 30 sec and at t=40 sec, system is bought back to critical state. The steady state K_{eff} at t=0 sec estimated by MC is 0.9999 ± 0.0004. The variation of neutron power with time obtained by simulation using transport MC is compared with the results of Hoogenboom et. al. as shown in Fig. 1. The estimated absolute standard deviation in the power is about 0.05. The TWIGL reactor (Hoffman, 2013) is a 2D seed-and-blanket geometry 1.6 m along each side [Figure 2]. It is surrounded by a vacuum and typically modeled with one-quarter or one-eighth core symmetry. The problem specifies one delayed neutron group and cross sections for two energy groups within three different material regions: Regions 1 and 2 are seed regions while Region 3 is the blanket region. The transient was driven by varying the thermal absorption cross section in Region 1. Figure 3 gives the relative power estimated by KINMC. The absolute standard deviation estimated is ~ 0.01.

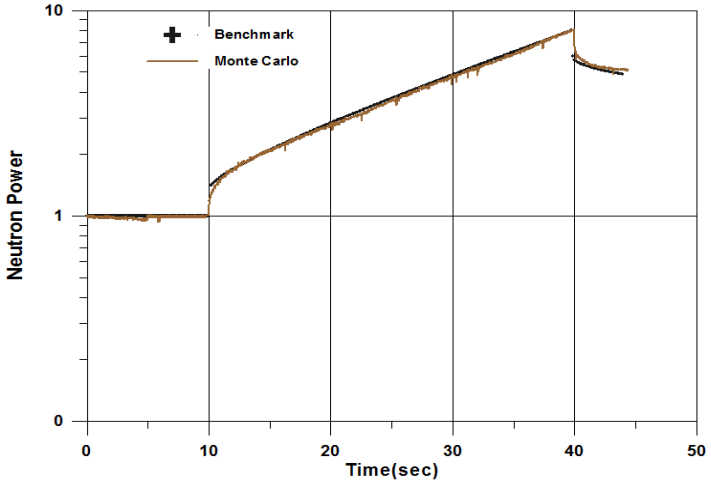


Figure 1 Neutron power estimated by KINMC for a transient in a cuboid of U-235

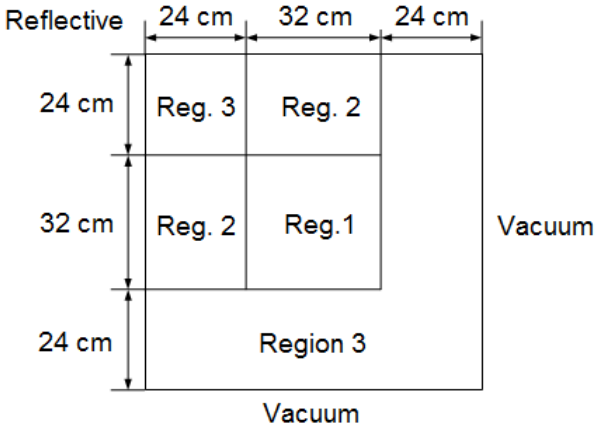


Figure 2 Geometry for the south-east quadrant of TWIGL

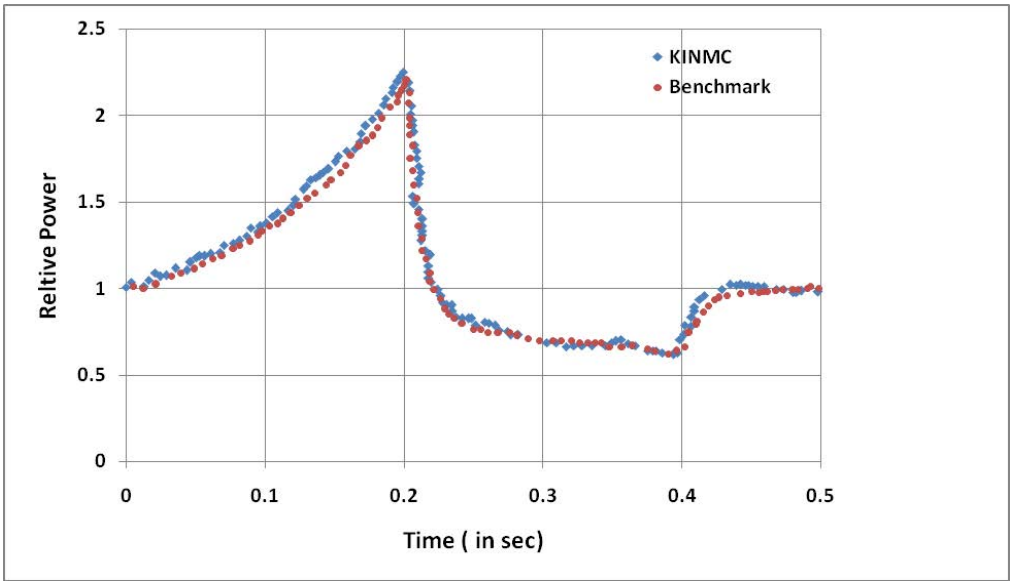


Figure 3 Variation of relative neutron power with time estimated by KINMC

4. Conclusions

In this paper, development of a multi-region multi-group Transport based MC kinetics code KINMC is discussed. KINMC is based on Transport MC Method and has the capability of solving multi group space time transients. It explicitly treats the six groups of precursors and uses the concept of mean number of secondaries in a collision for variance reduction. The efficacy of this method is tested by comparison with results of realistic space-time kinetics benchmarks based on Transport theory methods involving multi-region reactors and energy dependence. Comparison of our results with these benchmarks show satisfactory agreement and thus provides a more complete validation of our methods. The capability of KINMC code will be extended to perform continuous energy space time simulations based on transport MC methods in future.

5. References

1.Askew, J. R. et al. (1966), "A general description of the lattice cell code WIMS", Journal of the British Nuclear Energy Society, 5.
2.Marleau G., Hébert A., Roy R. (2011), "A User Guide for DRAGON Version 4", Institut de génie nucléaire, Département de génie mécanique, École Polytechnique de Montréal.
3.Srivastava Argala, Singh K. P. and Degweker S. B. (2018), "Monte Carlo Methods for Reactor Kinetic Simulations", Nuclear Science and Engineering, 189, 152-170.
4. Argala Srivastava, K. P. Singh and S. B. Degweker, Nuclear Science and Engineering, "Monte Carlo Methods for Reactor Kinetic Simulations", 2018, 189, 152-170.
5.Sjenitzer B. L. and Hoogenboom J. E. (2013), "Dynamic Monte Carlo Method for Nuclear Reactor Kinetic Calculations", Nuclear Science and Engineering 175(1), 94-107.
6.Ang Zhu, Yunlin Xu et. al., Transient Method for pin resolved whole core transport using the 2D-1D Methodology in MPACT, ANS, MC2015, Nashville, April 19-23, 2015.

Implementing Weighted Delta Tracking Method in Dynamic Monte Carlo Code KINMC

Argala Srivastava, K. P. Singh and Umasankari Kannan
Bhabha Atomic Research Centre, Mumbai, India
e-mail: - argala@barc.gov.in

Abstract

This paper presents the implementation of the weighted Delta Tracking Method in KINMC Code for the simulation of the Reactor Transients. KINMC is developed on the numerical recipes proposed earlier by us for full space time simulations by Monte Carlo Method. It explicitly treats the six groups of precursors and uses population weight control of precursors and neutron as well as the concept of mean secondaries in a collision. It has capability of solving multi group transient by both Diffusion based MC and by Transport based Delta Tracking method. In this paper, we have attempted to increase the performance of Transport based Delta Tracking method routine in KINMC by implementing weighted Delta Tracking Method proposed by Morgan and Kotlyar. Weighted tracking method uses statistical weight scheme instead of rejection scheme to treat the pseudo collision of neutrons in the scattering medium. We have analyzed 1D Benchmark and TWIGL 2D transient benchmark by the weighted delta tracking method and have found that this method is computationally efficient and more accurate than the Delta tracking method.

1. Introduction

Monte Carlo is a valuable tool to provide a reference for deterministic methods in steady state calculation. In the recent years, intensive research efforts have focused on MC method in transient analysis. For transient analysis, which is crucial for safety calculations it is desirable to have a higher fidelity method and thus Monte Carlo is an interesting option to perform reliable and accurate transient calculations. Sjentizer and Hoogenboom [1] developed a Dynamic MC Method for transient analysis and it was later implemented in TRIPOLI and SERPENT code system [2 & 3]. Later, several Monte Carlo Codes viz. G4-STORK, MCATK, TART, GUARDYAN, McCard, Nauchi's modification to MCNP-5 have included time dependent capability in the existing codes [3-5]. We have also developed Space Time Monte Carlo Code KINMC based on the numerical schemes proposed earlier by us [6]. KINMC Code simulates neutron transport either by Diffusion based MC or by Transport based Delta Tracking method. In an attempt to increase the computational efficiency of the KINMC code, we have incorporated the weighted delta tracking method proposed by Morgan and Kotlyar [7] in the code. Weighted delta tracking method is an improvement to the delta tracking method. Delta tracking is essentially based on a rejection sampling technique. The principle in the Delta Tracking Method is to homogenize the material total cross sections in such a way that sampled path lengths are valid over the entire geometry. The Delta tracking method was proposed as an alternative method to the well established surface tracking method used in the most of the Monte Carlo based codes for complex geometries. But, Delta tracking method's efficiency is highly reduced in the presence of high absorbing medium since it follows rejection method. In 2015, Morgan et. al. [7] proposed the improvement over the Delta algorithm by moving from rejection techniques to a weighting method. Thus, instead of rejecting a virtual collision with a probability p, the particle and its daughters should be given the weight, based on p. Kotlyar et. al. has examined the efficiency of this method on a simple 1D geometry and have found it to be computationally efficient [8]. In this paper, we have further analyzed the efficacy of the weighted delta algorithm on the transient calculations with KINMC. We have analyzed the 1D

transient benchmark and 2D TWIGL Benchmark with this method and have compared the results with those obtained by using Delta tracking method.

2. Modifications in the Methodology

The steady state simulation routine based on Delta Tracking Method in KINMC is modified to include weighted delta tracking method. In delta tracking method, firstly the maximum total macroscopic cross-section of all materials in the geometry at the particle energy is found. If this is called as Σ_m, then the distance to the next collision (irrespective of the cross section of the medium in which the particle is located) is sampled using

$$s = -\frac{1}{\Sigma_m} \ln \xi$$

ξ is the random number. If Σ_t is the actual cross section at the point of collision, the point is accepted as a collision site with a probability Σ_t / Σ_m and rejected with a probability 1-Σ_t / Σ_m and this collision is considered as virtual collision. In case of rejection, the neutron flight is continued from this point with the same direction and energy. The method requires the program to only determine the medium at any given point which is much simpler than ray tracing. In the weighted delta tracking method, instead of rejecting the virtual collision, the particle is given a weight equal to Σ_t / Σ_m and it is considered as a collision point. Thus, all the particles survive all the collisions. The weighted delta tracking method results in producing particles of lower weights. Therefore, Russian roulette method is implemented to reduce the variance in the tallied values. The modified algorithm for steady state simulation in KINMC is given below:

- ***Initially all the particles are assigned weight w=1.0. Particles are tracked one by one.***
- ***Maximum value of the total cross section of the regions in the problem domain is stored as*** Σ_m
- ***Direction cosines and mean free path of the particle is sampled. If the particle is leaked out of the geometry, tracking is stopped. For the particles inside the geometry domain, total macro scopic cross section of the region where the particle is, is stored.***
- ***Probability of virtual collision is checked. If it is a virtual collision, particle weight is reduced by the factor*** Σ_t / Σ_m ***i.e.*** $w_i = w_{i-1} . \Sigma_t / \Sigma_m$ ***and the probability of absorption or scattering event is checked. If it is a real collision, particle weight is maintained as its initial weight before collision probability of absorption or scattering event is checked.***
- ***If scattering event is probable, then particle is scattered to the respective energy group depending on the probability of scattering cross section for different energy groups. Particle is further tracked with new direction cosines. For absorption event, neutron is forced to undergo fission and mean number of neutrons of weight*** $w_i = w_{i-1} \nu\Sigma_f / \Sigma_a$ ***are produced in the event.***
- ***Weights of all the neutrons in one cycle are added and stored. Above process is repeated for*** 10^5 ***particles for 1000 cycles. First 100 cycles are passives cycles and are neglected. Ratio of total weights of the neutrons in the consecutive cycles gives the estimate of the K-eff of the geometry modeled.***

3. Test Problem and Results

We have tested capability of the modified algorithm of KINMC Code firstly on 1D transient benchmark and then on 2D Space time transient of TWIGL Reactor. The standard problem described by

Sjenitzer and Hoogenboom, 2013 [1] was analyzed to test the modified transport MC technique discussed in Section 2. The problem consists of a cuboid of dimension 10 x 12 x 24 cm placed in a vacuum and is near critical. After 10 seconds, the density of the Uranium is increased making the system super critical. The transient is followed for 30 sec and at t=40 sec, system is bought back to critical state. Simulation was performed with Delta algorithm method and with weighted Delta algorithm method. Steady state Keff estimated by the two methods are 1.0000±0.0004, and 0.9999±0.0002 respectively. Table 1 gives the comparison of the mean variance, run time value and Figure of Merit (FOM) value for the two methods for the transient simulation up to 50 sec.

$$FOM = (1/((variance)^2 X computational\ time)$$

It is observed that the mean variance estimated by the two methods is not much different but there is a reduction in computational time by ~ 2 times and significant gain in (Figure of merit (FOM) by 3 times. The TWIGL reactor [9] is a 2D seed-and-blanket geometry 1.6 m along each side. It is surrounded by a vacuum and typically modeled with one-quarter or one-eighth core symmetry. The transient was driven by varying the thermal absorption cross section in Region 1. In this transient, the thermal absorption cross section in Region-1 [9] is linearly decreased from 0.15 cm^{-1} to 0.1465 cm^{-1} over a 0.2 sec period. Steady state Keff values obtained by Delta tracking and by weighted Delta tracking method is 0.9164 ± 0.0008 and 0.9166 ± 0.0007. Reference solution obtained by Time dependent MOC (Hoffman, 2013) is 0.9167. It is found that the estimated K_{eff} values are comparable with the deterministic values within the standard deviation. Fig. 1 gives the relative power estimated by KINMC with weighted delta tracking method. The reference solution (Time dependent MOC) is also shown for the purpose of comparison and comparison is found to be good. Table 2 gives the comparison of the mean variance, run time value and Figure of Merit (FOM) value for the two methods for the transient simulation up to 0.5 sec. It is observed that the mean variance estimated by the weighted delta tracking is lesser than the delta tracking method. There is a gain in computational time by ~ 2 times and FOM for weighted delta tracking is 3.4 times more than the delta tracking method.

4. Conclusions

An attempt to increase the performance of Transport based space time simulation routine in KINMC code is done by implementing weighted Delta Tracking Method proposed by Morgan and Kotlyar. Weighted tracking method uses statistical weight scheme instead of rejection scheme to treat the pseudo collision of neutrons in the scattering medium. We have analyzed 1D Benchmark and TWIGL 2D transient Benchmark by the weighted delta tracking method and have found that this method is computationally faster and more accurate than the standard ray tracing method or Delta tracking method. The computational time for the transient calculation reduces by ~ 2 times and FOM increases by ~ 3 times with delta tracking method and thus makes it significantly efficient. In future, we plan to apply weighted delta tracking method for transient problems involving strong absorbing medium.

5. References

1. Sjenitzer B. L. and Hoogenboom J. E. (2013), "Dynamic Monte Carlo Method for Nuclear Reactor Kinetic Calculations", *Nuclear Science and Engineering 175(1), 94-107.*
2. Margaux Faucher et.al. 'New Kinetic Simulation capabilities for TRIPOLI 4: Methods and applications', Annals of Nuclear Energy 120 (2018) 74-88.

3. Jakko Leppanen, Maria Pusa, Tuomas Vitanen et.al., ' The Serpent Monte Carlo Code : Status, development and applications in 2013', Annals of Nuclear Energy, Vol. 82, August 2015, page 142-150.
4. Liam Rusell, Adriaan Buijs and Guy Jonkmans, 'G4 – STORK: A GEANT 4 – based Monte Carlo reactor kinetics simulation code', Annals of Nuclear Energy 71 (2014) 451-461.
5. Terry Adams et. al., 'Monte Carlo Application Toolkit (MCATK)', Annals of Nuclear Energy 82(2015) 41-47.
6. Srivastava Argala, Singh K. P. and Degweker S. B. (2018), "Monte Carlo Methods for Reactor Kinetic Simulations", *Nuclear Science and Engineering, 189, 152-170.*
7. L. W. G. Morgan and D. Kotlyar, 'Weighted Delta Tracking for Monte Carlo Particle Transport', ANE, Vol. 85, Nov. 2015, Pages. 1184-1188.
8. J. Leppanen, Performance of Woodcock delta tracking in lattice physics applications using the Serpent Monte Carlo reactor physics burn up calculation code, Annals of Nuclear Energy 37 (5) (2010) 715-722.
9. Hoffman A. J., 'A time dependent Method of Characteristics Formulation with Time Derivative Propagation", dissertation submitted to Nuclear Engineering and Radiological Sciences, University of Michigan', 2013.

Table 1 Comparative result for the different tracking methods for 1D Transient Benchmark

Method	Mean Variance	Runtime	FOM
Standard Delta Method	0.00000625	150 CPU hrs	1066.67
Weighted Delta Method	0.00000400	80 CPU hrs	3125.00

Table 2 Comparative results for the different tracking methods for TWIGL Benchmark

Method	Variance	Runtime	FOM
Standard Delta Method	0.00000064	13 CPU hrs	1953
Weighted Delta Method	0.00000049	5 CPU hrs	6802

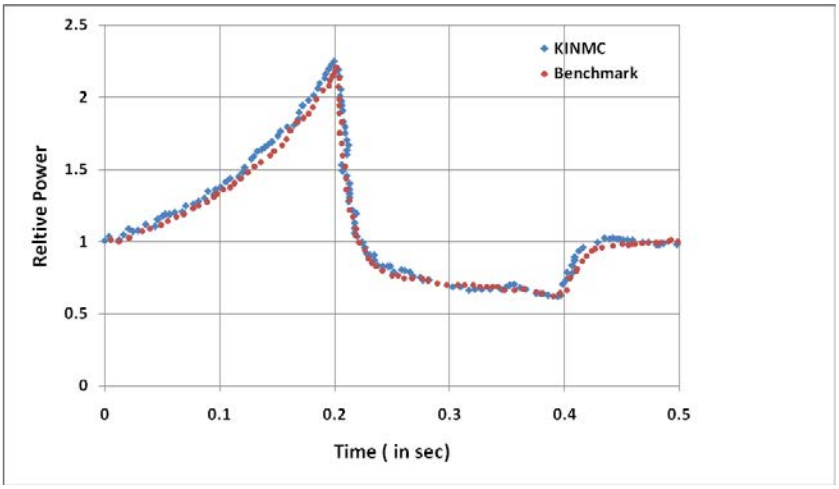


Fig. 1 Variation of relative neutron power with time estimated by KINMC

3D MULTI-PHYSICS ANALYSIS OF HOT STARTUP TRANSIENTS OF NATURAL CIRCULATION COOLED CHTR

D.K. Dwivedi*, Anurag Gupta and Umasankari K.
Reactor Physics Design Division, Bhabha Atomic Research Centre, Mumbai, India
*e-mail: - ddwivedi@barc.gov.in

Abstract

The 100 kWt Compact High Temperature Reactor (CHTR) is being designed as a technology demonstrator for the Indian HTR programme for hydrogen production by an efficient thermo-chemical splitting of water. CHTR is a thorium-based TRISO fuelled, BeO moderated, LBE cooled prismatic vertical core to achieve 1000ºC outlet temperature at full power. The core heat is designed to be taken out passively through the natural circulation of LBE coolant in the central channels of 19 fuel assemblies. Natural circulation cooled CHTR will be started from a low power level with stagnant coolant condition to full power. Therefore, the startup procedure of the core has to be established to raise the core power level safely and avoid chance of flow instability. In this regard, the hot startup of CHTR, from critical core configuration at 1 Wt power, has been investigated with indigenously developed and benchmark validated 3D multi-physics code ARCH-TH. The multi-physics simulation of the power rise in the range 1 W to 10 kW indicates that the low powered channels are susceptible to flow reversal. Further investigation suggests that predicted flow reversal could be mitigated by slightly increasing the cooling in PHX/ heat pipes, i.e. reducing the outlet temperature of PHX for an initial time interval. The results of the study are discussed and analyzed in this paper.

1. Introduction

The 100 kWt CHTR is being designed as a technology demonstrator for the Indian comprehensive programme for hydrogen production through the efficient S-I cycle [1]. CHTR is a ^{233}U-Th carbide-based TRISO fuelled, beryllium oxide moderated, lead-bismuth eutectic (LBE) cooled reactor core to achieve 1000ºC outlet with coolant inlet temperature at 900ºC at full power [2]. In normal operating conditions, the core heat is to be removed passively under the natural circulation of LBE as the primary coolant. The coolant flows through the central channels of 19 fuel assemblies from bottom to top of the core and returns through 18 downcomers. All the 19 channels and 18 downcomers core are coupled through the common upper and lower plenums (Fig.1.a and 1.b). High-temperature sodium heat pipes inserted in the downcomers near the upper plenum serve as a primary heat exchanger and transfer heat from the primary to the secondary side. The coolant inlet enthalpy is at 900ºC in normal hot operating conditions. However, the core inlet temperature is assumed to be controllable, i.e. decreased or increased depending on the cooling on the secondary side. The core has 12 control rods (CRs) of tungsten and tantalum alloy partially inserted in the outer coolant channels from the top reflector side for power control and regulation [2].

The hot startup of CHTR during the initial life-cycle, from critical core configuration at 1 Wt power, has been investigated with indigenously developed and benchmark validated 3D multi-physics code ARCH-TH. The neutronics capability in the code is based on multi-group neutron diffusion theory using FDM for space discretization and Implicit Euler and an efficient IQS method for transients [3,4]. The TH module in the code has been developed for 1D-radial heat conduction and 1D-axial flow of coolant in the channels, which can simulate natural circulation in a coupled multi-channel system [4]. The neutronics and thermal-hydraulics capability in the code have been suitably validated with reactor benchmark problems and experimental data of an LBE natural circulation loop operated at BARC [5].

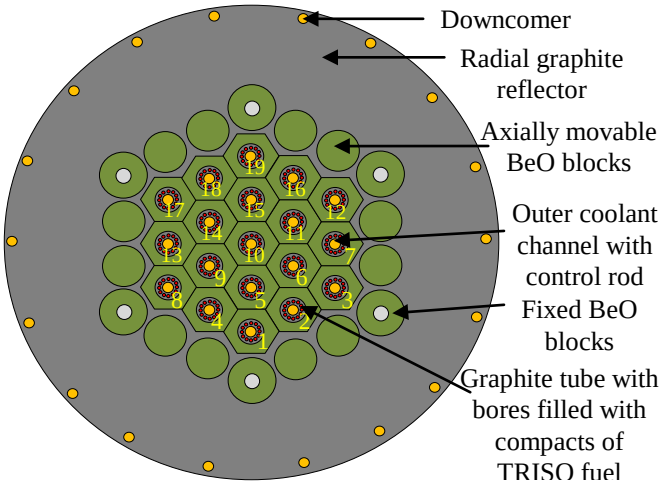


Fig. 1.a: Cross-sectional schematic of CHTR core depicting position of the channels

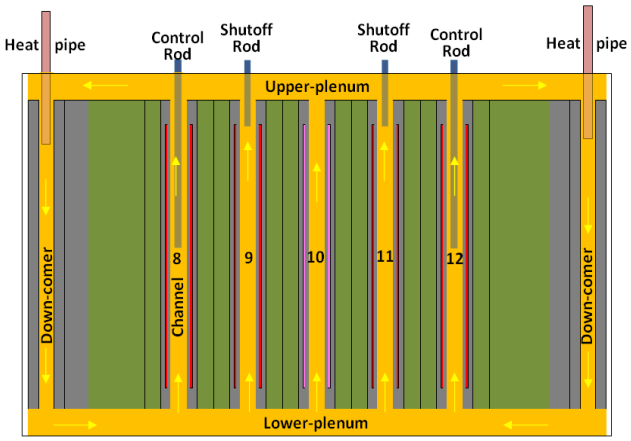


Fig. 1.b: Axial schematic of CHTR core with channels connected at lower and upper plenum

The natural circulation systems with coupled multi-channel are susceptible to reverse flow and instability during startup [5-8]. The flow reversal in the system can degrade equipment performance and cause a significant hammer effect resulting in damage if the reverse flow rate is significantly high []9, 10]. Therefore, the hot startup of the CHTR at low power has been investigated with coupled neutronics- thermal hydraulics phenomena in the high-temperature core. The simulation indicates the probability of flow reversal in low-powered channels during power rise from 1 W to 10 kW. The startup of CHTR has been investigated subsequently to assess the possible measure to mitigate the flow reversal. The results of the multi-physics simulations of the CHTR startup and findings are discussed in the next section.

Table-1: Reactivity addition due to partial withdrawal of control rods (CRs) in the different channels for power rise from 1W to ~50kWt during hot startup of CHTR

Step	CR in the channel	Instant of time (s)	Reactivity added in the core (mk)
1	2	5 to 7	+0.17
2	16	3000 to 3002	+0.17
3	13	3900 to 3902	+0.18
4	7	4200 to 4202	+0.18
5	18	4500 to 4502	+0.18
6	4	4800 to 4802	+0.18
7	3	5100 to 5102	+0.13
8	19	5400 to 5402	+0.13
9	8	5700 to 5702	+0.13
10	12	6000 to 6002	+0.13
11	17	6300 to 6302	+0.12
12	1	6600 to 6602	+0.07

The power rise in the hot critical core of CHTR (from10^{-5} times to 50% of full power) is achieved by taking the control rods partially out in steps (Table-1). In this case, the reactivity addition rates are considered to be less than or equal to the 3.0 cent/ s (as β=~4.5 mk = 100 cent for CHTR).

2. Analysis and results of multi-physics simulations of CHTR hot start-up

The withdrawals of 12 CRs in CHTR introduce positive reactivity in small steps for the core criticality and power rise and regulation. In the analysis, these CRs are partially taken out in small steps one by one from their initial critical positions in the core operating at 1W power. The partial withdrawals of these rods introduce positive reactivity given in Table-1. At such a low power level, the LBE coolant in the reactor core is almost in stagnant condition. The coolant temperature at the core inlet is considered at 900ºC, which is assumed to be almost constant during normal operations. However, to mitigate the flow reversal during the low power range of core startup, the inlet core temperature is assumed to be cooled by ~2°C for an initial interval in the next simulation. The results like core power, reactivity, channel outlet temperatures and coolant mass flow rates are predicted for both scenarios as follows:

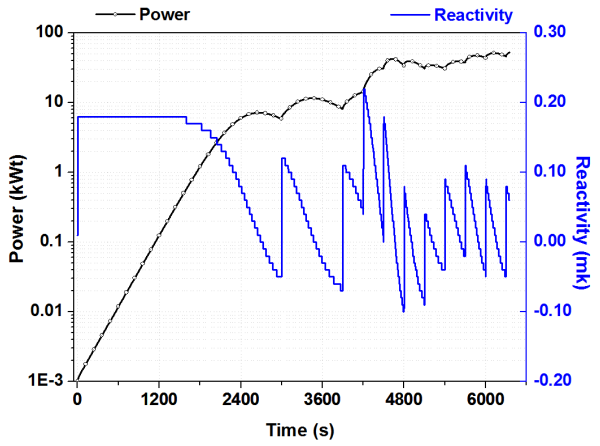


Fig.-2.a: Power and reactivity during hot start-up of CHTR under natural circulation of LBE coolant at 900º at core inlet

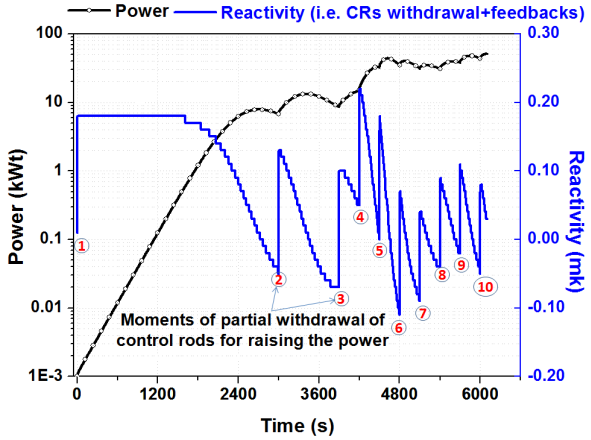


Fig.-3.a: Power and reactivity during hot start-up with reduced inlet coolant temperature for initial intervals

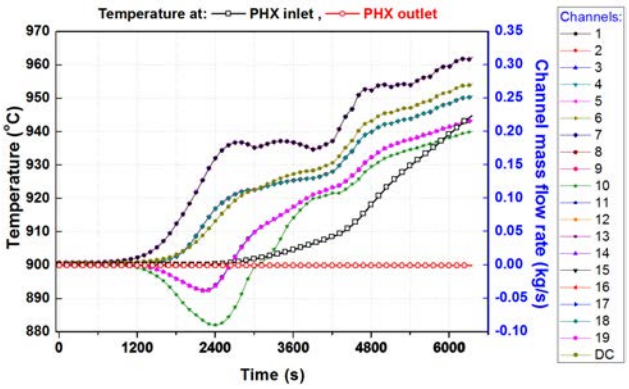


Fig.-2.b: The coolant temperature at core inlet & outlet and PHX, and mass flow rates in the channels during hot startup

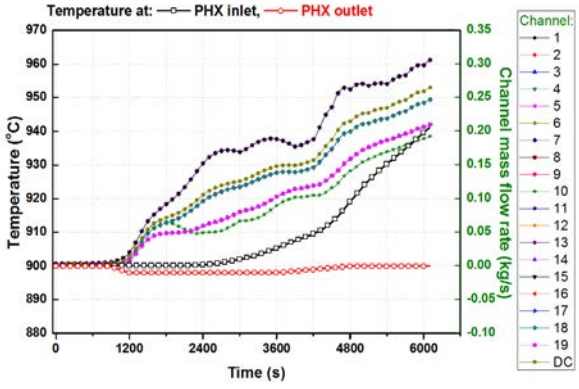


Fig.-3.b: Temperature of coolant and mass flow rates in the channel after reduced PHX outlet temperature for a small intervals

In the first case, the inlet temperature of the coolant is considered to be at 900ºC, which is unchanged during the transient (Fig.-2.a & b). In the second case of the start-up, the core inlet temperature has been varied as follows (Fig.-3.a and b):

T_{in} = 900°C during $0\ \text{s} > t \leq 900\text{s}$

T_{in} = 900°C to 898°C cooling linearly, $900\ \text{s} > t \leq 1200\ \text{s}$

T_{in} = 898°C $1200\ \text{s} > t \leq 3600\ \text{s}$

T_{in} = 898°C to 900°C heating linearly, 3600 s>t ≤ 4800 s

T_{in} = 900°C t > 4800 s

The predicted variations of neutronics and thermal hydraulics parameters in CHTR with code ARCH-TH have been compared for both the scenarios (Fig. 2. a & b and Fig. 3. a & b). In the first case (Fig. 2. a & b), flow reversal in low powered channels has been observed (i.e. channel no. 1, 3, 8, 10, 12, 17 and 19) are susceptible to reverse flow during power rise from 1 W to ~ 10 kW. It could be expected as all the fuel channels and downcomers are coupled with asymmetrical heating and different flow resistance conditions in all the coolant channels.

Therefore, to avoid the flow reversal in the low powered channels, the cooling of LBE coolant flowing to the core inlet has been initially controlled under almost stagnant flow conditions. The conductivity of liquid metal coolant LBE is considerably high, so better cooling of the coolant in the downcomers can be achieved even under stagnant flow by reducing inlet temperature or increasing the mass flow rate of the secondary side. The inlet cooling from 900°C to 898°C could subsequently result in a higher mass density of LBE coolant in the downcomers, which would increase the driving force of natural circulation in the primary circuit. This phenomenon would increase the mass flow rates in the channels upward initially (Fig.-3.b). Therefore if the core power increases in this condition from 1W to ~10W, no flow reversals in the low-powered assemblies are observed. However, in the present core design of CHTR, in the higher power range, such occurrences of flow reversal are not found. Therefore, when the core power in CHTR is raised sufficiently high, i.e. ~10 kW, the coolant to the core inlet could be resumed at 900°C in hot operating configuration. Thus, cooling the inlet core temperature during the low-power start-up in CHTR could be one of the possible measures to mitigate the flow reversal.

3. Conclusion

The 100 kWt CHTR has been designed with the natural circulation of LBE coolant for enhanced safety features with passive core heat removal. However, during hot start-up of the core, critical at 1 W, the low powered channels are predicted to be susceptible to flow reversal. Thus, to mitigate this phenomenon of flow instability in CHTR during the start-up, further investigation is carried out with in-house developed and validated 3D multi-physics code ARCH-TH. It has been found that the reverse flow in the channels could be mitigated after increased cooling of coolant flows to the core inlet during initial intervals of the start-up as one of the possible measures. However, the other measures in this aspect, like adjusting the flow resistance in the channels and flattening the radial power profile, could also be explored in the future.

References

[1]. Sinha et al., 2016. Woodhead Publishing Series in Energy, pp. 413-452.
[2]. Dwivedi et al., 2017. Annals of Nuclear Energy, 110, 306–316 (2017).
[3]. Dwivedi et al., 2018. https://newprairiepress.org/asemot/2018/
[4]. Dwivedi et al., 2019. Thorium—Energy for the Future, Select Papers from ThEC15, pp. 381-389. https://doi.org/10.1007/978-981-13-2658-5_31
[5]. Dwivedi et al., 2020. Nuclear Engg. and Design, 370, 110881 (2020).
[6]. Linzer and Walter, 2003. Appl. Thermal Eng. 23, 2363–2372.
[7]. Gros, 2012,' Liquid-Salt-Cooled Reactor start-up with natural circulation under Loss-Of-Offsite-Power (LOOP) conditions', Georgia Institute of Technology.
[8]. Gros and Grgic, Journal of Energy, vol. 61 (2013) Special Issue, p. 113–130
[9]. Czyszczewskic, POWER, June-2017
[10]. Radaideh et al., (2019), Nuclear Engineering and Technology, 51, 1532-1539

EXPONENTIAL–TIME DIFFERENCING METHOD FOR SOLVING REACTOR POINT KINETICS EQUATIONS WITH TEMPERATURE AND POWER FEEDBACK AND IT'S VALIDATION BY ANALYSING THERMAL REACTOR BENCHMARKS

P. Ravindra Babu[1], Usha Pal[2], R.N. Sen[1], R. Karthikeyan[2] and M.M.A.Razak[3]

[1] Bhabha Atomic Research Centre, Visakhapatnam, India

[2] Bhabha Atomic Research Centre, Mumbai, India

[3] Bhabha Atomic Research Centre, Kalpakkam, India

[1]*e-mail: - ravindrab@barc.gov.in*

Abstract

Exponential Time Differencing method with Taylor Series Expansion (ETD-TS) is used for solving nonlinear systems of point kinetics equations (PKEs). Integral forms of PKE are expanded using Taylor Series Expansion method. Thermal Reactors benchmark with step, compensated ramp reactivity insertions are considered for estimation of power transients with temperature feedback. Comparison of results with other numerical methods i.e. SCS (Shifted Chebyshev Series), ITS2 (Integral Taylor Series 2), confirms the validity and accuracy of this method. Time step of 10^{-2} – 10^{-5} sec is considered for estimation of power transients.

1. Introduction

For reactor safety, it is important to estimate the power values at different time intervals by solving point kinetics equations. These equations provide useful information on the dynamics of the reactor core during start up (or) shutdown condition and considerable power change in the plant. Temperature feedback effect is considered in PKEs for improving accuracy of results. Currently, different numerical methods like ITS2 [1] and SCS [2] are available to solve PKEs with temperature feedback. Exponential time differencing method is used earlier in the field of computational electro dynamics, where the problem of electric and magnetic fields in a box with absorbing boundaries are stiff in nature. However Exponential Time differencing method can be applied to PKEs for estimation of power transients.

In this paper, new advanced method ETD-TS is used to solve PKEs with temperature feedback. PKEs are integrated using exponential factor. The integral form of PKEs is solved using Taylor series expansion method. Smaller time step ~ 10^{-2} sec is sufficient for estimation of power transients with step reactivity insertion. But, for transients with compensated ramp reactivity insertion, time step size ~10^{-5} sec can be used in ETD-TS method to estimate the power transients and computational time is less, when compared with ITS-2 method and SCS methods. However, in terms of accuracy, it is at par with other methods.

2. Point kinetics equations and ETD-TS method

Point kinetics equations are coupled equations and has to be solved simultaneously. ETD – TS method has four different steps:

1. Multiplying the PKE's with exponential Integrating factor
2. Integrating the PKE's within the time limits 't_n' to 't_{n+1}'
3. Expanding the neutron density and precursor concentrations using the Taylor series expansion
4. Estimation of Right hand side of the integral values to calculate the neutron density and precursor concentrations at n+1th time step.

$$\frac{dP(t)}{dt} = \frac{(\rho(t)-\beta)}{\Lambda}P(t) + \sum_{i=1}^{6}\lambda_i * C_i(t) \quad \ldots\ldots(1)$$

$$\frac{dC_i(t)}{dt} = \frac{\beta_i}{\Lambda}P(t) - \lambda_i * C_i(t) \quad (2)$$

P(t) = power in watts; $C_i(t)$ = i^{th} group precursors concentration (atoms/cm3) ;
β= effective value of beta;Λ = mean neutron generation time;
λi = decay constant of i^{th} group precursor; βi = i^{th} group precursor beta value;

From Eq.(1) and Eq.(2) we can write PKE with feedback in the matrix form as shown below:

$$\begin{pmatrix} dP(t)/dt \\ dC1(t)/dt \\ dC2(t)/dt \\ dC3(t)/dt \\ dC4(t)/dt \\ dC5(t)/dt \\ dC6(t)/dt \\ dTemp(t)/dt \end{pmatrix} = \begin{pmatrix} \frac{(\rho(t)-\beta)}{\Lambda} & \lambda1 & \lambda2 & \lambda3 & \lambda4 & \lambda5 & \lambda6 & 0.0 \\ \beta_1/\lambda1 & -\lambda1 & 0.0 & 0.0 & 0.0 & 0.0 & 0.0 & 0.0 \\ \beta_2/\lambda2 & 0.0 & -\lambda2 & 0.0 & 0.0 & 0.0 & 0.0 & 0.0 \\ \beta_3/\lambda3 & 0.0 & 0.0 & -\lambda3 & 0.0 & 0.0 & 0.0 & 0.0 \\ \beta_4/\lambda4 & 0.0 & 0.0 & 0.0 & -\lambda4 & 0.0 & 0.0 & 0.0 \\ \beta_5/\lambda5 & 0.0 & 0.0 & 0.0 & 0.0 & -\lambda5 & 0.0 & 0.0 \\ \beta_6/\lambda6 & 0.0 & 0.0 & 0.0 & 0.0 & 0.0 & -\lambda6 & 0.0 \\ U(t) & 0.0 & 0.0 & 0.0 & 0.0 & 0.0 & 0.0 & 0.0 \end{pmatrix} \begin{pmatrix} P(t) \\ C1(t) \\ C2(t) \\ C3(t) \\ C4(t) \\ C5(t) \\ C6(t) \\ Temp(t) \end{pmatrix}$$

Right hand side of above 8×8 square matrix is the coefficient matrix 'A(t)'.

The general form of first order stiff ODE [3] is written as:

$$\frac{du}{dt} = cu + F(u,t) \quad (3)$$

Here 'c' is stiffness coefficient. The value of $u(t_{n+1})$ can be written as follows after applying the procedure of exponential differencing method [3]:

$$u(t_{n+1}) = u(t_n)e^{ch} + e^{ch}\int_0^h e^{-c\tau}F(u(tn+\tau), tn+\tau)d\tau \quad (4)$$

Eq.(5) and (6) can be achieved after integration of (1) and (2) and multiplying both sides of equation (1) and (2) with integrating factor $e^{t/\Lambda}$ and applying the similar procedure in [3]:

$$P(tn+1) = P(tn)e^{\frac{-h}{\Lambda}} + \frac{1.0}{\Lambda}\int_0^h P(tn+\tau)e^{\frac{\tau-h}{\Lambda}}\left(1.0-\beta+\rho(tn+\tau)\right)d\tau$$

$$+\int_0^h e^{\frac{\tau-h}{\Lambda}}\sum_{i=1}^{6}\lambda_i C_i(tn+\tau)\,d\tau \quad (5)$$

$$C_i(tn+1) = C_i(tn)e^{\frac{-h}{\Lambda}} + \left(\frac{\beta_i}{\Lambda}\right)\int_0^h e^{\frac{\tau-h}{\Lambda}}P(tn+\tau)d\tau + \left(\frac{1.0}{\Lambda}-\lambda_i\right)\int e^{\frac{\tau-h}{\Lambda}}C_i(tn+\tau)d\tau \quad (6)$$

With Taylor series expansion power at time $t_n+\tau$ can be written as shown below:

$$P(t_n+\tau) = \sum_{i=0}^{n}\frac{\partial^i P(t_n)}{\partial\tau^i}\frac{\tau^i}{i!} \quad (7)$$

2.1 Temperature Feedback and it's Numerical Solution

Fuel Temperature feedback equation and its solution algorithm using ETD-TS method is as shown below [2]:

$$\frac{dTemp(t)}{dt} = K_c P(t)$$

$\rho(t_n) = \rho_0 + \alpha*(Temp(t) - Temp(0))$; here '$\rho_0$' is constant, in case of step reactivity.

In the case of compensated ramp reactivity, $\rho(t) = a(t-t_0)$-b$\int_{t_0}^{t} n(t')dt'$.

Temperature at time t_{n+1} sec is estimated after applying the procedure in [3] and finally we obtained the below Eq:

$$\text{Temp}(t_{n+1}) = \text{Temp}(t_n) \times e^{-\frac{h}{\Lambda}} + e^{\frac{h}{\Lambda}} \times \left[\int_0^h U(t_n+\tau)e^{\frac{\tau}{\Lambda}}d\tau + \frac{1.0}{\Lambda}\int_0^h Temp\,(t_n+\tau)\,d\tau\right]$$

Here K_c is heat constant of reactor. 'α ' is fuel temperature coefficient of reactivity. Temp(t) is fuel temperature at time 't' seconds. 'ρ(t)' is core reactivity at time 't'.

2.2 Power Transients of thermal reactor caused by step reactivity with Temperature Feedback

In this case, ETD-TS method has been applied to solve the point kinetics equations for thermal reactors, in presence of Newtonian temperature feedback. Six groups of delayed neutrons are considered in this problem. Step reactivity of 1.0 $ is applied and power transients are analysed. The decay constants of neutron precursors and delayed neutron fractions for thermal reactor are taken as $\lambda_1 = 0.0124s^{-1}$, $\lambda_2 = 0.0305s^{-1}$, $\lambda_3 = 0.111\ sec^{-1}$, $\lambda_4 = 0.301\ sec^{-1}$, $\lambda_5 = 1.13\ sec^{-1}$,. $\lambda_6 = 3.00\ sec^{-1}$, $\beta_1 = 0.00021$, $\beta_2 = 0.00141$, $\beta_3 = 0.00127$, $\beta_4 = 0.00255$, $\beta_5 = 0.00074$, $\beta_6 = 0.00027$. Table-1 shows the transient power results with different values of 'h' values. Transient results are compared with SCS method and ITS2 method values.

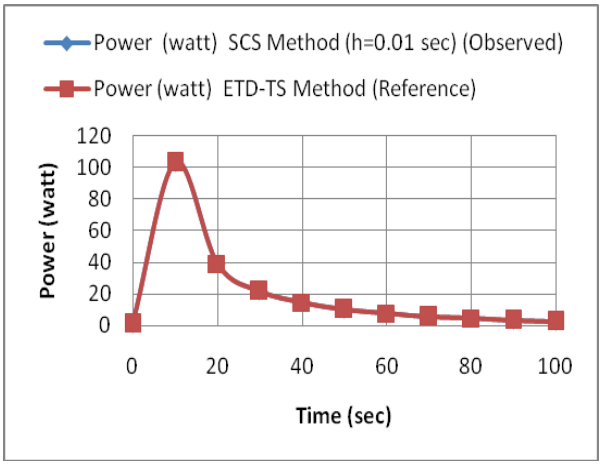
Table 1 Comparison of transient values of power and reactivity values initiated due to step reactivity (2.0 $)

Time (sec)	Power (Watt) ETD-TS Method (Observed) (h=0.1 sec) n=5	Power (Watt) ETD-TS Method (Observed) (h=0.05 sec) n=5	Power (Watt) ETD-TS Method (Observed) (h=0.01 sec) n=5	Power (Watt) SCS – method (Reference) (h=0.01 sec)	Reactivity ρ(t) $ ETD-TS Method (Observed) (h=0.01 sec)	Reactivity ρ(t) $ ITS2 Method (Reference) n=5	Temperature (^{0}K) ETD-TS Method (Observed) (For 2$ case) (h=0.01 sec)
0.0	1.0000	1.0000	1.0000	1.0000	2.0000	2.0000	293.0000
20.0	38.8049	39.0941	39.1389	39.1389	-1.6133	-1.6133	759.1225
50.0	10.2598	10.3090	10.3186	10.3186	-1.8430	-1.8430	788.7475
80.0	4.4771	4.4951	4.4994	4.4994	-1.9233	-1.9233	799.1112
100.0	2.7415	2.7524	2.7551	2.7551	-1.9508	-1.9508	802.6584

Table 2 Comparison of ETD – TS power values with different numerical methods (with step reactivity of 2.0 $)

Time (sec)	Power (Watt) NAM Method (Reference) h=0.001 sec	Power (Watt) PCA Method (Reference) h=0.001 sec	Power (Watt) SCS – method (Reference) (h=0.01 sec)	Power (Watt) ETD-TS Method (Observed) (h=0.01 sec) n=5
0.0	1.0000	1.0000	1.0000	1.0000
20.0	39.1793	39.0022	39.1389	39.1389
50.0	10.3277	10.2872	10.3186	10.3186
80.0	4.4855	4.4994	4.4994	4.4994
100.0	2.7575	2.7463	2.7551	2.7551

β_{eff} = 0.00645, Λ = 0.00005 (sec), α = 0.00005 (K^{-1}) , K_c = 0.05 (K/MWs)**.** Transient power estimated up to 100.0 sec with ETD-TS method. Results are in excellent agreement with reference values. Computational time is 26.0 sec for these transient calculations. Fig.1-2 shows P, ρ vs time plots. Similarly, Table 2 shows the comparison of ETD-TS results with NAM (New Analytical Method) [6] , PCA (piecewise continuous approximation method) [5] and SCS methods. Comparison shows that Transient power values Estimated with ETD-TS method is more accurate when compared with NAM and PCA method values. Also,ETD-TS method uses the time step size of (h=0.01 sec), which is much larger than the time steps used in NAM and PCA methods (h=0.001 sec). This indicates that present method is more efficient and accurate than NAM and PCA methods. ETD-TS method values are in good agreement with most accurate SCS method values.



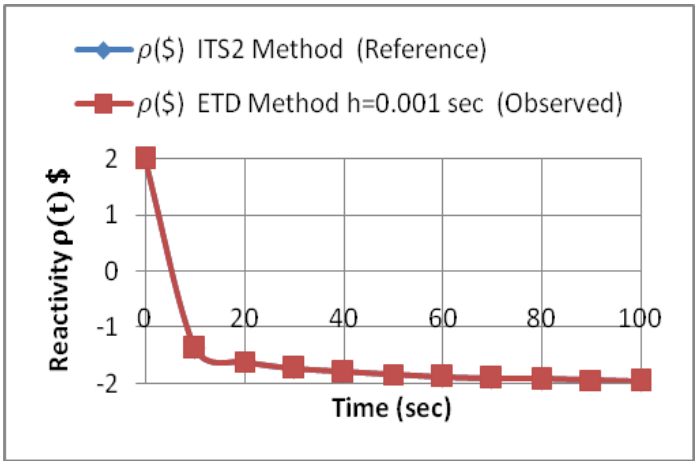


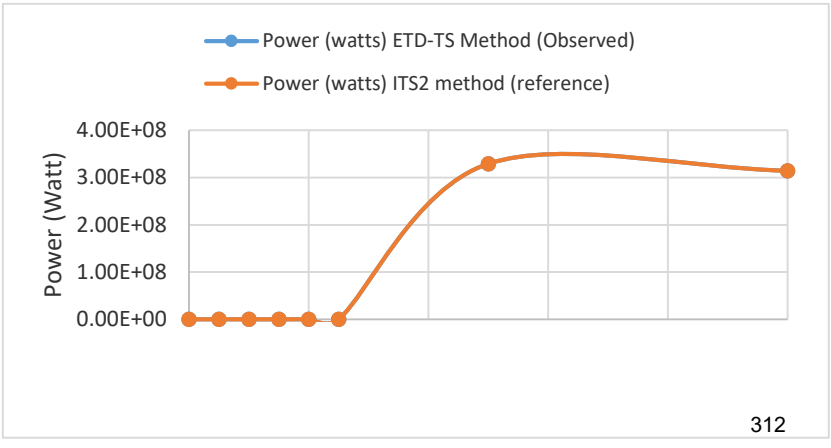
Fig.1 Comparison of Transient Power (Watt) Fig.2 Comparison of Transient Reactivity ($)

2.3 Power Transients of thermal reactor caused by compensated ramp reactivity with Power Feedback

The power transients caused by step reactivity of 0.043 $ with compensated ramp reactivity is considered. Six group kinetic parameters are λ_1 = 0.0124sec^{-1}, λ_2 = 0.0305sec^{-1}, λ_3 = 0.111 sec^{-1}, λ_4 = 0.301 sec^{-1}, λ_5 = 1.13 sec^{-1},. λ_6 = 3.00 sec^{-1}, β_1 = 0.00021, β_2 = 0.00141, β_3 = 0.00127, β_4 = 0.00255, β_5 = 0.00074, β_6 = 0.00027. β_{eff} = 0.0065, Λ = 0.00005 (sec). Here, time step chosen for all the calculations using ETD-TS method is h = 0.000025 sec. Power values are estimated up to 10.0 seconds. Transient power values are in excellent agreement with ITS2 method values at all the time steps and results are shown in Table 3.

Table 3 Comparison of Power transients due ramp reactivity with a=0.003 s^{-1} and b=10^{-11} cm^3/sec

Time (sec)	Power (watts) ETD-TS (observed) (h = 0.000025 sec) n=3	Power (watts) ITS2 method (reference)
0.00	1.0000	1.000E+00



0.50	1.324E+00	1.324E+00
1.00	2.053E+00	2.053E+00
1.50	4.347E+00	4.347E+00
2.00	2.392E+01	2.392E+01
2.50	1.438E+04	1.438E+04
5.00	3.293E+08	3.293E+08
10.00	3.145E+08	3.145E+08

Fig.3 Comparison of Power Transients Initiated due to compensated ramp reactivity with temperature feedback.

3. Conclusion

ETD-TS method is used for solving point kinetics equations with multi group of delayed neutrons in the presence of temperature feedback. Thermal reactor benchmark problems with step (2.0 $) and compensated ramp reactivity insertions are considered for validation of this method. Results are compared with values obtained from SCS and ITS2 methods. It is observed that ETD-TS method estimates the power transients for longer duration of time with more accuracy. Relative errors are observed i.e., 0.00 for all the cases. Computational time (26.0, 36.0 sec) is lesser than SCS (1.2, 1.5 hrs) and ITS2 (52.0, 56.0 sec) methods for step and compensated ramp reactivity benchmark case. ETD-TS method is more accurate compared to PCA and NAM methods and uses larger time steps when compared with these methods. Above benchmarks are calculated with time step size of the order of 10^{-2} to 10^{-5} sec. This method can be further used for estimation of power transients in 3D space-time calculations.

4. References

1. Serigo Q. et al, “Solution of the point reactor kinetics equations with temperature feedback by the ITS2 method”, *Progress in Nuclear Energy*, Vol (91), pages 240-249,2016.
2. Y.M. Hamada, “A New Accurate Numerical Method Based on Shifted Chebyshev Series for Nuclear Reactor Dynamical Systems”, *Science and Technology of Nuclear Installations*, Hindawi, Article ID 7105245, pages 1-15, 2018.
3. S.M.cox et al, “Exponential time differencing method for stiff systems”, *School of Mathematical Sciences, University of Nottingham*, UK, Dec 2000.
4. M.M.A.Razak et al, “The modified exponential time differencing (ETD) method for solving reactor point kinetic equations”, *Annals of nuclear energy*, vol.76, pages 193-199, 2015.
5. Kinard.M, Allen. E.J., “Efficient Numerical Solution of Point Kinetics Equations in Nuclear Reactor Dynamics”, *Annals of nuclear energy*, vol. 31, page 1039,2004.
6. Nahla.A.A., “An efficient technique for point reactor kinetics equations with Newtonian temperature feedback effects”, *Annals of nuclear energy*, vol.38,2810,2011.

EXTENDING THE CAPABILITY OF THE CODE "KINFIN" FOR SIMULATING HEXAGONAL CORES

Debasmit Sarkar[1], Argala Srivastava and K .P. Singh

Reactor Physics Design Division,
Bhabha Atomic Research Centre, Trombay, Mumbai 400085
[1]e-mail: - debasmit@barc.gov.in

Abstract

KINFIN is a three dimensional space time kinetics code originally written to solve neutron diffusion equation for rectangular meshes. Recently, the code is updated by incorporating provision of solving neutron diffusion equation in triangular meshes. Along with this, different features are implemented in the code for improved efficiency. The aim of this paper is to assess the prediction capability of KINFIN code for hexagonal core simulations in comparison with available international benchmark problems. The validation of the updated code has been carried out by comparison of the K-eff and power distribution with AER FCM 101 Benchmark results. Deviation in K-eff from the reference value is 0.004%.

1. Introduction

KINFIN is a three dimensional space time kinetics code which solves multi-energy group neutron diffusion equation using finite difference method. Both steady state and transient behavior of the reactor core can be estimated by KINFIN. The neutron kinetics is calculated by using direct method for rectangular geometry. The code has capability to estimate higher eigen modes and alpha modes. In the present work, we have extended the capability of the KINFIN Code for simulating steady state and transient states of hexagonal cores. We have tested this code with AER FCM 101 benchmark and compared the results with those recommended by 2^{nd} order solution of CEA reactor code CRONOS. In Section 2, the methodology used in the code for introducing hexagonal simulation is briefly described. In Section 3, AER FCM 101 benchmark specifications are given which are used for the calculations and results thereof. Section 4 presents the conclusions.

2. Methodology: Simulation of the hexagonal geometry

For simulating the hexagonal core, the first step is to generate the hexagonal grid. For the generation of the hexagonal grid, first the hexagons are labeled based on an intermediate coordinate (i, j) from the ring number and location of hexagon in the ring. The central hexagon is considered to be in ring-1, n^{th} ring will have $6 \times (n-1)$ hexagons in it. As an example, in Figure 1, the hexagon count (Hex id) in two rings and their corresponding intermediate coordinates are given.

Next step is to find the fine grid X and Y range. The input geometry can be defined in different axial levels. In each axial level, either number of hexagonal rings, or radius of XY map or both can be given. The program scans all the defined levels in the input and determines the fine grid extent (NOXM and NOYM) based on the maximum of no of rings and maximum radius. As an example, in Figure-2, three levels are defined, bottom most level has n_1 number of hexagonal

rings and outer radius is R_1 and so on. NOXM and NOYM will be determined based on the divisions according to n_2 and R_2.

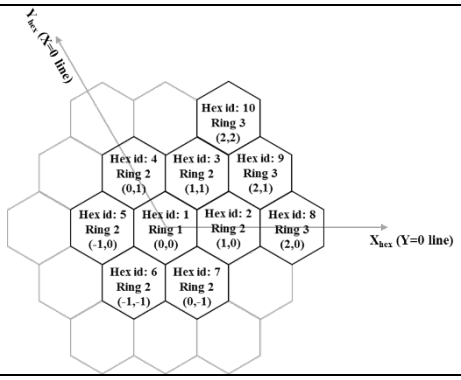


Figure 1 Structure of the hexagonal grid

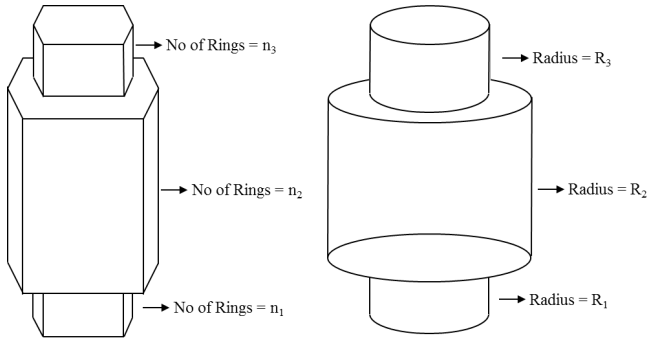


Figure 2 Definition of Rings at different axial level of the core

Last step for triangular grid generation is to find the position of triangular meshes in final fine grid corresponding to a given hexagon. To identify all the triangles in final triangular grid that belong to a hexagon at (i, j) in X_{hex}-Y_{hex} coordinate, first a key-triangle close to the centre of the hexagon is determined. All other triangles in the hexagon are found relative to that key-triangle using a stencil. The stencil is a function of the number of triangles in which a hexagon is divided. In figure 3, this process is illustrated. Here the key-triangle is identified to have coordinate (itri, jtri) about the fine grid XY.

For simulating hexagonal core, the problem domain is divided into a number of mutually exclusive and exhaustive set of uniform triangular prism meshes. The neutron diffusion equation over a mesh then becomes,

$$\vec{\nabla} \cdot \vec{J} + \Sigma_r \Phi = S$$

The multi-group neutron diffusion equation in terms of the coupling coefficient can be written as,

$$\sum_{n \in surfaces} \mathbf{XDIJ_{g,n}}\left(< \Phi_{\mathrm{g}} > - < \Phi_{\mathrm{g,n}} >\right) + \Sigma_{r,g} V < \phi_g > = \frac{\chi_g V}{k_{eff}} \sum_{g'} \left(\nu \Sigma_f\right)_{g'} < \Phi_{\mathrm{g'}} > + V \sum_{g' \neq g} \Sigma_s (g' \to g) < \Phi_{\mathrm{g'}} > + Q_g V$$

For uniform triangular prism meshes, the coupling coefficients of triangular meshes is modified as

$$\mathbf{XDIJ} = \frac{s_i}{\frac{h}{D} + \frac{h_n}{D_n}} = \frac{s_i}{\frac{2V}{3Ds_i} + \frac{2V}{3D_n s_i}} = \frac{s_i}{\frac{2}{3dx1} + \frac{2}{3dx2}} = 1.5 \times s_i \times \frac{dx1 \times dx2}{dx1 + dx2}$$

Where $dx1 = D \times \frac{s_i}{V} \& dx2 = D_n \times \frac{s_i}{V_n}$

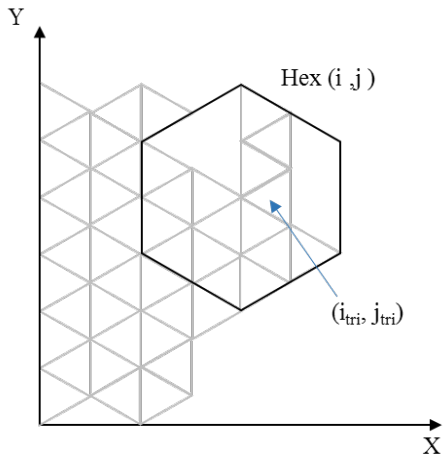


Figure 3 Triangular Grid

Some new features are added in the code to make it computationally efficient and user friendly:

- **Auto-determination** of input type – input for rectangular geometry or hexagonal geometry. Complete care is taken to provide **backward compatibility**, *all existing KINFIN inputs will run without any modifications.*
- Triangular input is **key-value** pair based input, with self-explanatory keys. Majority of these keys are optional and they have **default values**, if a user doesn't use the key in making his input, the default value will be used.
- Complete **generalized efficient triangular mesh generation**. Each hexagon can be divided into $6 \times \text{nDiv}^2$ small equilateral triangles, input key `nDiv:`can be any integer.

3. Results and Discussion

We have analyzed AER-FCM-101 benchmark [2] with the updated KINFIN code for testing the hexagonal module. AER-FCM-101 is a 3D benchmark of Schulz which models a VVER-1000 core in steady state. The assemblies are homogeneous, represented by given two-group diffusion theory parameters. There are seven material compositions including four enrichments, burnable absorber, control rods and reflector. A finger-tip control rod is half-inserted. The central assembly contains axially eccentric burnable absorber of Eu_2O_3. The core height is 355 cm, covered with axial and radial reflectors. The nodes are large, with assembly lattice pitch of 24.1 cm. We have tested the accuracy of the eigenvalue k_{eff} of our code with the benchmark results. Convergence criteria $\varepsilon_f = 10^{-4}$ for the flux and $\varepsilon_l = 10^{-6}$ for the eigenvalue are used as iteration limits. Each hexagon is divided into 216 equal triangles. Axially the meshes are also divided in fine meshes, each of size ~ 2 cm. The k-eff estimated by KINFIN is 1.049483 and that estimated provided by CRONOS 2-nd order recommended solution is 1.049526. The normalized power distribution in 30 degree core sector is also compared as shown in Figure 4. It is observed that there is a maximum deviation of ~0.6% with the reference value for fuel assembly number 16 which is at core fuel-reflector interface.

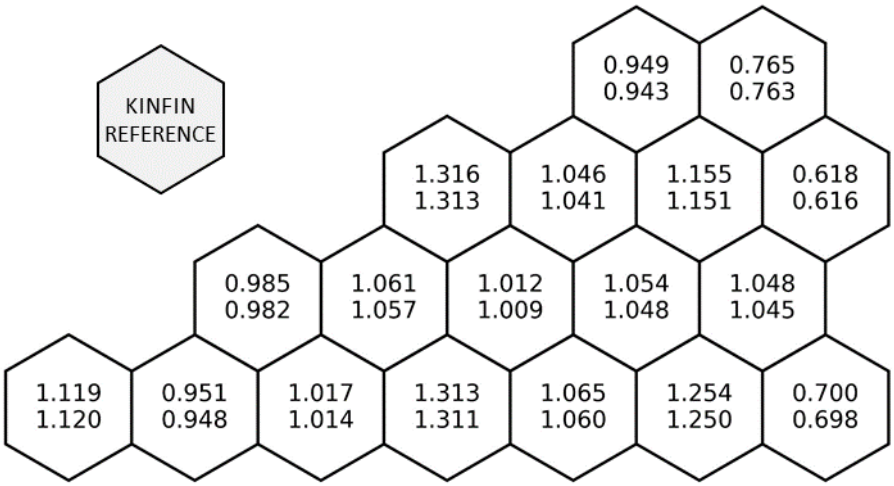


Figure 4 Comparison of the power distribution for 30 degree core sector

4. Conclusions

In this paper we have extended the capability of KINFIN code for simulating hexagonal cores. In the earlier version of the code, only rectangular meshes could be used. The validation of the updated code has been carried out by comparison of the results with AER FCM 101 Benchmark and comparison is within 0.004% deviation in K-eff and <1% deviation in estimated power. It is planned to validate the code with varieties of other hexagonal steady state and kinetic benchmarks.

5. References

1 Singh K. P., Modak R. S., Degweker S. B and Singh Kanchi (2009), " Iterative schemes for obtaining dominant alpha modes of the neutron diffusion equation", *Annals of Nuclear Energy, 36, Pages 1086.*

1. N. P. Kolev, R. Lenain, C. Fedon Magnaud, " AER FCM 101 Benchmark Specification Sheet, AER Benchmark Book, ARKI-KFKI (Hungary)

STOCHASTIC FORMULATION OF REACTOR KINETICS-A BRIEF SURVEY

Amritha Krishnan S[1], Anurag Gupta[2] and Rajarshi Das[1]
[1]Kakrapar Atomic Power Project, Gujarat
[2] Bhabha Atomic Research Centre, Mumbai, India
[1]*e-mail: - amrithakrishnans@npcil.co.in*

Abstract

Reactor kinetics studies are generally carried out through point reactor kinetics equations or space time kinetics if required. These are deterministic equations which predict the time evolution of mean neutron population and precursor densities. However, in a low neutron population scenario such as reactor start-up, statistical fluctuations are significant which need careful consideration in the estimation of sub-critical reactivity. Stochastic formulation of zero power kinetics is presented along with a brief survey of existing solution methods. In this paper, solutions of stochastic point kinetics equations based on piecewise constant approximation have been compared against the Monte-Carlo simulations results available in literature.

1. Introduction

A nuclear reactor system is characterized by many dynamic variables viz. neutron flux level, fuel temperature, coolant flow, etc. These dynamic variables fluctuate statistically around a mean value i.e. we can associate a probability that they will assume a certain value. The deterministic equations like point kinetics equations necessarily predict mean neutron population and precursor densities.

Fluctuations in the neutron population of core appear as random variations of the detector counts at low power, or as fluctuations of the detector current at high power, representing two classes of neutron fluctuations [1]. The former class is known as **zero power noise** and the latter one as **power reactor noise**. Both the classes differ in their physical origin, field of utilization and mathematical description [1]. At low power levels, the statistical fluctuations associated with the fundamental nuclear processes dominate. The main concern in zero power noise theory is the determination of statistics of neutron population in a multiplying system along with statistics of detector counts in a time interval. The major applications of the theory are measurement of sub-critical reactivity of the core, the detection and quantification of nuclear fissile material in SafeGuards. At high power levels, the reactor noise is predominantly due to non-nuclear processes like turbulence in coolant flow, vibrations in mechanical constructions, etc. Here, the effect on statistics of neutron population because of branching processes is suppressed.

2. Stochastic Formulation

The following noise sources are mainly responsible for fluctuations in zero-power systems[2]:

a) Fluctuations in the number of neutrons per fission, i.e. there is a probability distribution p(ν) that ν neutrons will be emitted per fission. In conventional reactor theory we are only concerned with the average value $\bar{\nu} = \sum_{\nu} \nu p(\nu)$. Momentary local increases in ν can lead to corresponding local increases in the multiplication factor and hence the neutron flux

b) Fluctuations in the time between nuclear events. There is a probability law describing the time spent between collisions, viz. $P(\tau)d\tau = e^{-\tau/\bar{\tau}}\, d\tau/\bar{\tau}$ where $\bar{\tau}$ is mean lifetime between collisions, P(τ)dτ is the probability that a particular event will occur in the time interval (τ, τ+dτ) after the previous event of that type.

c) The probability that a particular event will be a fission, a scattering or an absorption. (arising out of cross sections).

In majority of the work till now, the zero power noise has been modeled using Fokker-Planck equations (FPE) for probability generating functions. Recently, a new approach has been followed using Stochastic Differential Equations (SDE). The advantage is that SDE describes the neutron population directly whereas FPE describes its probability density function. Moreover, SDE approach offers the ability to couple the neutron population with additional random variables such as detector count rates and non-linear effects corresponding to Reactor Regulating System (RRS).

2.1 Stochastic Differential Equations

The method by which evolution dynamics are approximated by SDE is referred to in the literature as diffusion approximation. A SDE equation is of the form,

$$dX_t = b(t, X_t)dt + \sigma(t, X_t)dW_t \qquad (1)$$

where X_t is a stochastic process, $b(t, X_t)$ is slowly varying called drift and $\sigma(t, X_t)$ is rapidly varying called diffusion, W is a Brownian motion (white noise) or standard Wiener process. A process *X* is regarded as a solution to if it satisfies for every t,

$$X_t = x + \int_0^t b(X_s)\, ds + \int_0^t \sigma(X_s)\, dW_s \qquad (2)$$

where the last term in the integral is known as *Ito's* integral. The special where σ=0 is an ordinary differential equation. Diffusion approximation refers to the identification of Central Limit Theorem-scale limits describing the neutron dynamics over time (as well as other stochastic processes), not to be confused with spatial diffusion approximation, associated with Fick's law[3].

The most efficient and widely applicable approach to solving SDEs seems to be the simulation of sample paths of time discrete approximations [4]. This is based on a finite discretization of the time interval [0, T] under consideration and generates approximate values of the sample paths step by step at the discretization times. Figure-1 gives one simulated sample path of wiener process which is used to represent any stochastic variable under consideration.

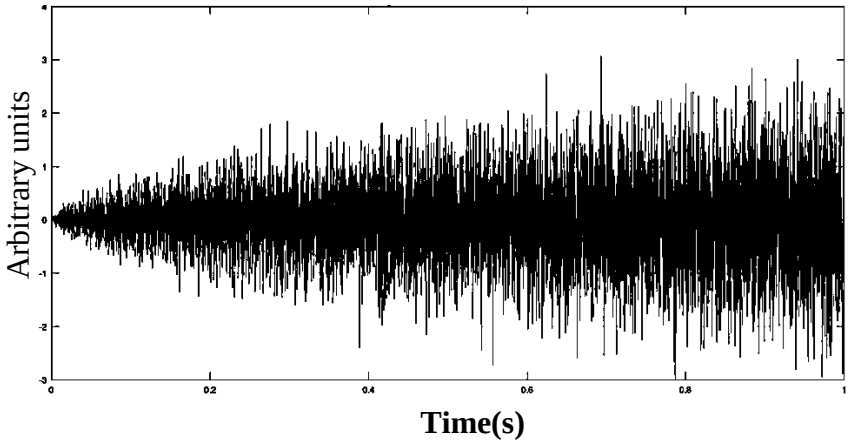


Figure 1: Sample Path of Wiener Process

2.2 Stochastic Point Kinetics Equations

Starting from time dependent neutron diffusion equation and separating the birth, death processes into different terms we arrive at Stochastic Point Kinetics Equations (SPKE)[5]:

$$\frac{d\hat{P}(t)}{dt} = A\hat{P}(t) + \hat{Q}(t) + B^{1/2}\frac{d\hat{W}}{dt} \qquad (3)$$

where $\hat{P}(t)$ is vector of neutron population and precursor densities, A is the coefficient matrix of deterministic Point Kinetic Equations of (m+1)×(m+1) dimensions, $\hat{Q}(t)$ is a vector of extraneous neutron sources, B is the cross-covariance matrix of neutron population and precursor densities, $\hat{W}$ is a vector of Standard Gaussian random variables which are independent.

$$\hat{P}(t) = \begin{pmatrix} N(t) \\ c_1(t) \\ . \\ . \\ C_m(t) \end{pmatrix}, \quad \hat{Q}(t) = \begin{pmatrix} q(t) \\ 0 \\ . \\ . \\ 0 \end{pmatrix}, \hat{W}(t) = \begin{pmatrix} W_1(t) \\ W_2(t) \\ . \\ . \\ W_{m+1}(t) \end{pmatrix}, \quad A = \begin{bmatrix} \frac{\rho(t)-\beta}{\Lambda} & \lambda_1 & \lambda_2 & \cdots & \lambda_m \\ \frac{\beta_1}{\Lambda} & -\lambda_1 & 0 & \cdots & 0 \\ \frac{\beta_2}{\Lambda} & 0 & -\lambda_2 & \cdots & 0 \\ \vdots & \vdots & \vdots & \ddots & \vdots \\ \frac{\beta_m}{\Lambda} & 0 & \cdots & 0 & -\lambda_m \end{bmatrix}$$

$$B = \begin{bmatrix} \xi & a_1 & a_2 & \cdots & a_m \\ a_1 & b_{1,1} & b_{1,2} & \cdots & b_{1,m} \\ a_2 & b_{2,1} & b_{2,2} & \cdots & b_{2,m} \\ \vdots & \vdots & \vdots & \ddots & \vdots \\ a_m & b_{m,1} & \cdots & \cdots & b_{m,m} \end{bmatrix} \text{ where } \xi = \left(\frac{-1-\rho(t)+2\sum_{i=1}^{m}\beta_i+(1-\sum_{i=1}^{m}\beta_i)^2\nu}{\Lambda}\right)n(t) + \sum_{i=1}^{m}\lambda_i C_i(t) + q(t)$$

$$a_i = \frac{\beta_i}{\Lambda}[(1-\sum_{i=1}^{m}\beta_i)\nu - 1]n(t) - \lambda_i C_i(t) \; ; \; b_{i,j} = \frac{\beta_i\beta_j}{\Lambda}n(t) + \delta_{i,j}\lambda_i C_i(t)$$

The notations used above have their usual meaning. There are several numerical solution methods existing for (3) and are summarized in Table-1 below:

Table-1: Existing Solution Methods for solving SPKE

Sr. No.	Method	Description
1.	Piece-wise Constant Approximation	The reactivity and source functions are considered piecewise constant. Eigen values and Eigen vectors are computed at each time step.
2.	The Euler–Maruyama Method	The Euler–Maruyama approximation is the simplest time discrete approximations of an Itô-process. It is equivalent to Euler methods of ODE.
3.	Taylor 1.5 Approximation	The order 1.5 strong Taylor scheme can be obtained by adding more terms from Itô-Taylor Expansion
4.	Implicit Euler Mauryama Method	This is similar to Predictor Corrector method with the predictor y_{n+1} inserted into the corrector equation to give the next iterate y_{n+1}.

A FORTRAN module has been developed to numerically solve (3) based on Piece-wise Constant Approximation in which reactivity and source functions are considered piecewise constant in a given time step. Following benchmark problem [5] was selected for the study:

$\Lambda = 0.00002$,$\beta = 0.007, \beta_i = [0.000266, 0.001491, 0.001316, 0.002849, 0.000896, 0.000182]$

ν=2.5, $q(t) = 0.0$, $\lambda_i = [0.0127, 0.0317, 0.115, 0.311, 1.4, 3.87]$, $\hat{P}(0) = 100\left[1, \frac{\beta_1}{\lambda_1\Lambda}, \ldots., \frac{\beta_6}{\lambda_6\Lambda}\right]$.

Following solutions were obtained and compared against Monte-Carlo Simulations available in literature (Table-2):

Table-2: Comparison of Mean neutron population and Standard Deviation with Monte Carlo simulation results and Stochastic PCA:

Case	Reactivity	Parameter	Monte Carlo	Stochastic PCA
1	Step reactivity ρ=0.003 at t=0.1s	Mean	183.04	186.17
		Standard Dev.	168.79	164.56
2	Step reactivity ρ=0.007 at t=0.001s	Mean	135.67	135.89
		Standard Dev.	93.38	92.96

In estimating the mean and standard deviation about 5000 runs were carried out. Some of the sample runs carried out for case-1 are shown below in Figure-2. The neutron population at $N(t=0)$=100.

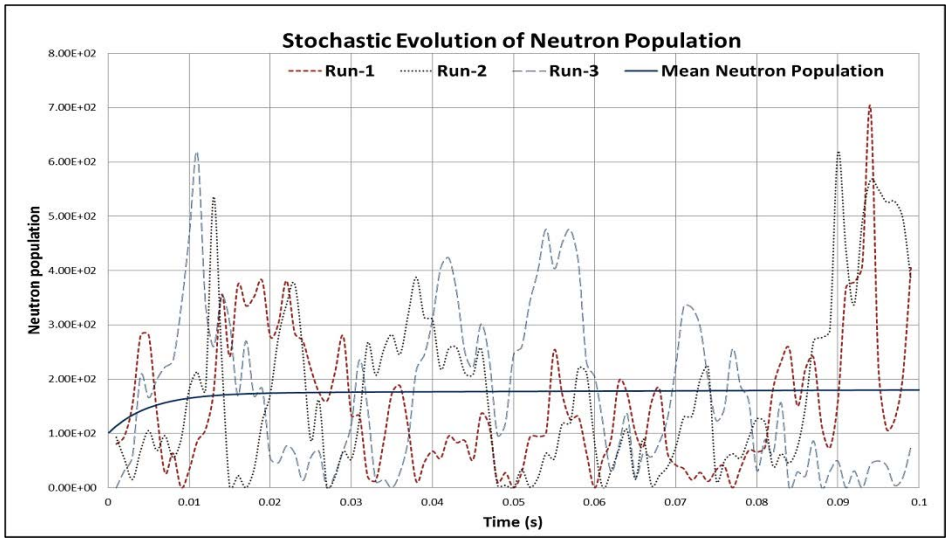


Figure-2: Sample paths of wiener process used for solving SPKE in case-1

3. Conclusion

A brief survey of existing numerical methods for solving Stochastic Point Kinetics Equation has been carried out. Specifically, Stochastic PCA method has been showing good agreement with Monte-Carlo Simulation results available in literature.

4. References

[1] Handbook of Nuclear Engineering (Volume -1) Dan Gabriel Cacuci, August 2010.

[2] Random Processes in Nuclear Reactors, M.M.R.Williams, Pergamon Press,1974

[3] Modeling Zero Power Reactor Noise and Neutron Count Distribution: A Stochastic Differential Equations Approach, by C. Dubi, R. Nuclear Science & Engineering, Jeju, Korea, April 16-20, 2017

[4] Kloeden, P.E., Platen, E., 1992. Numerical Solution of Stochastic Differential Equations through computer Experiments. Springer-Verlag, New York.

[5] Hayes, J.G., Allen, E.J., 2005. Stochastic point kinetic equations in nuclear reactordynamics. Ann. Nucl. Energy 32, 572.

PHYSICS & THERMAL-HYDRAULIC CALCULATIONS FOR CORE POWER & CRITICAL POWER RATIO ESTIMATION FOR ORIFICED AHWR INITIAL CORE

Vishal Bharti[1], D.K. Chandraker[2], Amit Thakur[1] & Mukesh Kumar[2]
[1] Reactor Physics Design Division, BARC, Mumbai, India
[2] Reactor Engineering Division, BARC, Mumbai, India
e-mail: - vishalb@barc.gov.in

Abstract

In AHWR core, the outer low power channels are orificed to achieve uniform steam quality w.r.t. the un-orificed channels in the core to ensure adequate thermal margins. However, during experiments, it was observed that there was flow instability during the power raising transients at low power which gets dissipated after ~13% FP and the flow remains stable up to 100% FP. It was also observed that the large scale flow oscillations at low channel power get disappeared if all the channels in the core are orificed ensuring stable operation during the entire power transient. Therefore, Physics and Thermal-Hydraulic coupled calculations were performed to study the effect of full core orificing of initial core on power distribution and Critical Power Ratio (CPR). This paper gives the details of change in core power distribution & CPR for fully orificed initial core compared to partial orificed initial core.

1. Description of computer codes used for coupled calculations

The 3D diffusion code FEMFOL [1] has been used for Physics calculations and the Thermal-Hydraulic calculations have been carried out by ARTHA [2] code. The brief description of the codes is given below.

1.1 Physics calculations

The lattice calculations for the 54 pins AHWR initial core fuel clusters were performed by using a neutron Transport Theory code ITRAN / CLUB [3] using 69 energy groups nuclear data library based on ENDF/B-VI.8. The lattice calculation provides the cell averaged cross sections in two energy groups for their direct use in the diffusion theory code FEMFOL to simulate the actual core geometry.

1.2 Thermal-Hydraulic calculations

ARTHA (AHWR Thermal Hydraulic Analysis) was developed by Reactor Engineering Division for the thermal hydraulic analysis of AHWR and is capable of analysing full core (452 fuel channels). The code evaluates the CPR in the channels and minimum CPR in the core.

2. External coupling of FEMFOL and ARTHA

The externally coupled Physics and Thermal-Hydraulic calculations were carried out by external coupling of FEMFOL and ARTHA code. The codes were run in tandem. The coupled calculations have been carried out for both initial core with 50 ppm boron in the moderator as well as at onset of refuelling without boron in the moderator as follows.

1. For the partial orificed initial core (as shown in Fig. 1) at average core coolant density of 0.45 g/cc.
2. For fully orificed initial core at average core coolant density of 0.4257 g/cc.

The core power distribution of FEMFOL is used as input to ARTHA and it generates the core coolant density distribution corresponding to the core power distribution. The coolant density profile generated by ARTHA is used as input to the FEMFOL for generating the new core power distribution. This iterative process was repeated till the core coolant density distribution converges. The convergence of coolant density distribution results into convergence of core power distribution.

3. Core Power Distribution

The Physics & Thermal Hydraulic calculations were carried out for both partial orificed and fully orificed initial core. The calculations have been carried out at 20 FPDs with boron as well as at onset of refuelling i.e. 304 FPDs of reactor operation. The quarter core power distribution after Physics & Thermal-Hydraulic calculations at 20 FPDs of reactor operation with 50 ppm of boron in the moderator for both partial and fully orificed initial core is shown in Table 1 & Table 2 respectively.

Similarly, the quarter core power distribution after Physics & Thermal-Hydraulic calculations at onset of refuelling for both partial and fully orificed initial core is shown in Table 3 & Table 4 respectively.

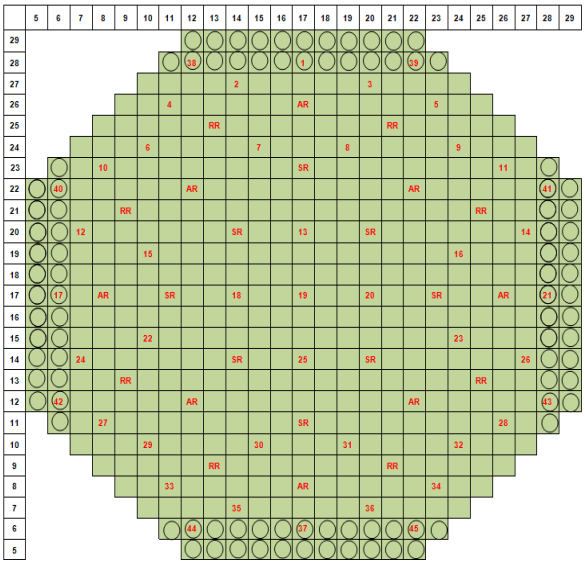


Fig. 1 AHWR Initial Core (with peripheral orificed channels as indicated by circles)

	13	12 14	11 15	10 16	9 17	8 18	7 19	6 20	5 21	4 22	3 23	2 24	1 25
A	1.71	1.61	1.57	1.52	1.43	1.33							
B	**SOR**	1.94	1.84	2.00	1.80	1.61	1.54						
C	2.06	1.98	2.27	**SOR**	2.24	1.99	1.96	1.75					
D	**AR**	2.00	2.16	2.40	2.28	2.35	**SOR**	2.01	1.73				
E	1.99	2.10	2.15	2.26	**RR**	2.37	**2.46**	2.36	1.92	1.72			
F	2.26	2.19	**SOR**	2.22	2.28	2.25	2.46	**SOR**	2.30	1.97	1.72		
G	**SR**	2.22	2.20	2.29	2.19	2.16	2.25	2.20	2.25	**SOR**	1.93	1.53	
H	2.15	2.21	2.20	2.21	2.15	**AR**	2.13	2.18	2.29	2.31	1.97	1.60	1.32
J	2.10	2.00	2.04	2.19	2.19	2.15	2.17	2.25	**RR**	2.26	2.22	1.79	1.42
K	**SOR**	2.08	2.08	**SR**	2.19	2.21	2.28	2.21	2.25	2.39	**SOR**	2.00	1.51
L	2.08	2.12	1.98	2.08	2.04	2.20	2.20	**SOR**	2.15	2.16	2.27	1.85	1.56
M	2.04	1.96	2.13	2.09	2.01	2.22	2.23	2.20	2.11	2.01	1.99	1.94	1.60
N	**SOR**	2.05	2.09	**SOR**	2.11	2.16	**SR**	2.27	2.00	**AR**	2.07	**SOR**	1.70

Table 1: Quarter core power distribution for partial orificed initial core after coupled calculations at 20 FPDs

	13	12 14	11 15	10 16	9 17	8 18	7 19	6 20	5 21	4 22	3 23	2 24	1 25
A	1.76	1.65	1.61	1.56	1.47	1.37							
B	**SOR**	1.98	1.88	2.04	1.83	1.64	1.57						
C	2.08	1.99	2.28	**SOR**	2.25	1.98	1.96	1.57					
D	**AR**	2.00	2.15	2.40	2.28	2.35	**SOR**	1.96	1.73				
E	1.99	2.10	2.14	2.26	**RR**	2.36	**2.46**	**SOR**	1.90	1.71			
F	2.26	2.19	**SOR**	2.21	2.26	2.23	2.44	**2.46**	2.29	1.96	1.72		
G	**SR**	2.22	2.19	2.27	2.16	2.14	2.23	2.44	2.25	**SOR**	1.92	1.55	
H	2.14	2.20	2.18	2.18	2.13	**AR**	2.11	2.23	2.28	2.30	1.95	1.62	1.34
J	2.09	1.98	2.01	2.17	2.16	2.12	2.13	2.11	**RR**	2.25	2.22	1.81	1.45
K	**SOR**	2.07	2.06	**SR**	2.17	2.17	2.25	2.13	2.23	2.38	**SOR**	2.02	1.54
L	2.07	2.10	1.95	2.06	2.01	2.17	2.18	2.25	2.12	2.14	2.26	1.87	1.59
M	2.03	1.94	2.11	2.07	1.98	2.19	2.21	2.18	2.08	1.99	1.98	1.96	1.63
N	**SOR**	2.03	2.07	**SOR**	2.09	2.14	**SR**	2.21	1.98	**AR**	2.07	**SOR**	1.74

Table 2: Quarter core power distribution for fully orificed initial core after coupled calculations at 20 FPDs

	13	12 14	11 15	10 16	9 17	8 18	7 19	6 20	5 21	4 22	3 23	2 24	1 25
A	**SOR**	2.21	2.09	**SOR**	2.01	2.11	**SR**	2.07	2.42	**AR**	2.14	**SOR**	2.11
B	2.22	1.99	2.13	2.26	1.92	2.05	2.02	1.98	1.92	1.90	2.01	2.16	2.15
C	2.08	2.10	1.94	2.05	2.05	1.99	1.93	**SOR**	1.91	2.03	2.28	2.05	2.13
D	**SOR**	2.02	2.13	**SR**	2.04	1.96	1.99	1.87	1.92	2.21	**SOR**	2.24	2.10
E	2.00	1.86	1.91	2.23	2.02	1.90	1.85	1.85	**RR**	2.05	2.26	2.05	2.01
F	2.10	2.03	1.98	2.00	1.93	**AR**	2.45	1.86	2.01	2.05	2.02	1.91	2.62
G	**SR**	2.01	1.95	2.03	1.92	1.91	1.95	1.94	2.16	**SOR**	2.14	2.13	
H	2.05	1.98	**SOR**	1.96	**2.69**	1.96	2.16	**SOR**	2.06	2.07	2.22		
J	2.40	1.92	1.95	2.05	**RR**	2.11	2.26	2.23	1.90	2.07			
K	**AR**	1.89	2.05	2.28	2.12	2.11	**SOR**	2.09	1.88				
L	2.11	2.00	2.29	**SOR**	2.28	2.05	2.16	2.20					
M	**SOR**	2.14	2.04	2.25	2.06	1.92	2.13						
N	2.07	2.12	2.10	2.08	2.00	2.61							

Table 3: Quarter core power distribution for partial orificed initial core after coupled calculations at 304 FPDs

	13	12 14	11 15	10 16	9 17	8 18	7 19	6 20	5 21	4 22	3 23	2 24	1 25
A	**SOR**	2.20	2.07	**SOR**	1.99	2.10	**SR**	2.05	2.38	**AR**	2.12	**SOR**	2.11
B	2.21	1.97	2.11	2.25	1.90	2.03	2.00	1.96	1.90	1.87	1.99	2.15	2.14
C	2.07	2.08	1.92	2.03	2.02	1.95	1.91	**SOR**	1.89	2.00	2.27	2.04	2.12
D	**SOR**	2.00	2.12	**SR**	2.02	1.92	1.96	1.86	1.91	2.20	**SOR**	2.24	2.10
E	1.98	1.84	1.89	2.21	1.99	1.87	1.82	1.84	**RR**	2.04	2.24	2.05	2.01
F	2.09	2.01	1.95	1.97	1.91	**AR**	2.42	1.84	2.01	2.04	2.01	1.91	2.63
G	**SR**	2.00	1.94	2.00	1.89	1.88	1.93	1.93	2.16	**SOR**	2.14	2.13	
H	2.04	1.97	**SOR**	1.95	**2.66**	1.94	2.15	**SOR**	2.05	2.07	2.23		
J	2.37	1.90	1.94	2.04	**RR**	2.11	2.26	2.23	1.90	2.09			
K	**AR**	1.87	2.02	2.27	2.11	2.10	**SOR**	2.10	1.90				
L	2.10	1.99	2.28	**SOR**	2.27	2.04	2.16	2.22					
M	**SOR**	2.14	2.04	2.25	2.06	1.92	2.14						
N	2.07	2.12	2.11	2.09	2.00	2.62							

Table 4: Quarter core power distribution for fully orificed initial core after coupled calculations at 304 FPDs

Table 1 & Table 2 showed that the maximum channel power remains ~ 2.46 MW for both partial orificed as well as for fully orificed initial core. Similarly, Table 3 & Table 4 showed that that the maximum channel power was comparable for both partial orificed & fully orificed initial core. The maximum change in the core channel power distribution between partial and fully orificed initial core was ~ 2.0 to 3.0 percent.

4. Conclusion

Physics-Thermal Hydraulic coupled calculations carried out for initial core at 20 FPDs and at 304 FPDs of reactor operation showed that the change in maximum channel power after full core orificing is insignificant as compared to partial orificed initial core. The full core orificing of initial core led to reduction in the average coolant density from 0.45 g/cc to 0.4257 g/cc. The maximum change in the channel power in the fully orificed initial core was ~ 3 percent as compared to the partial orificed core.
The full core orificing led to reduction in the core flow by 18% and the core exit quality increased to ~24%. The In-house developed correlation for the Critical Power Ratio (CPR) estimation showed that adequate the minimum CPR is above the limiting value of 1.2 and reduction in the coolant flow due to full core orificing does not have significant effect on the thermal margin.

5. References

[1] Arvind Kumar and R. Srivenkatesan, “Nodal expansion method for reactor core calculation”, BARC-1249, 1984.

[2] D. K. Chandraker, N. K. Maheshwari, D. Saha and R. K. Sinha, A Computer code for the Thermal Hydraulic Analysis of A Natural Circulation Reactor, 16th National Heat and Mass Transfer Conference and 5th ISHMT-ASME Heat and Mass Transfer Conference, Deptt. of Mechanical Engg. Jadhavpur University, Calcutta, India, Jan. 3-5, 2002.

[3] P. D Krishnani, “Input preparation for computer code ITRAN”, Technical report No. BARC /RPDD /RP /011, June 23, 2010

APPROACH FOR COUPLING OF KKNPP SYSTEM THERMAL HYDRAULICS COMPUTER CODE ATMIKA-LWR WITH 3D KINETICS CODE

Vivek Singla[1], Paresh Patra[1], Sanjay Singh[1], Hemant Kalra[1] and Y.K. Pandey[1]
[1]Nuclear Power Corporation of India Limited, Mumbai, India
[1]*e-mail: - vsingla@npcil.co.in*

Abstract

Modern safety standards for nuclear power plants (NPP) require the modelling of complex transients where there is a strong interaction between the thermal-hydraulic system behaviour and the space-dependent neutron kinetics. The objective of the present study is to establish the methodology to couple the KKNPP System Thermal-Hydraulic computer code ATMIKA-LWR with the space dependent neutronic code DRAGON-DONJON, thereby allowing the simulation of coupled thermal hydraulic neutronic transients. The simulation of transients/accidents using space dependent neutronics code is very useful in scenarios where a tight coupling of thermalhydraulics of the plant and neutronic behavior of the reactor core is very critical. The steady state as well as transient neutronic calculations has been performed using DRAGON-DONJON code. An approach has been finalized to couple the system thermal-hydraulic computer code ATMIKA-LWR and neutronic code DRAGON-DONJON using an external script.

1. Introduction

KKNPP VVER 1000 MWe reactors belong to the family of Pressurized Water Reactors (PWRs) which are the predominant type in operation, world over. This type of reactor uses light water as coolant and moderator and enriched uranium as fuel. To perform the thermal hydraulic safety analysis of KKNPP VVER 1000 MWe reactors, the computer Code "ATMIKA-LWR" is developed by the NPCIL. The code is used to carry out safety analysis of KKNPP reactors to verify and understand the basis for the design of control and safety systems, evaluation of operator guidelines, analyses for change in system configuration during lifetime of reactor, simulation of plant events and licensing analysis. The code has the capability to simulate the overall thermal hydraulics of the plant, reactor kinetics and various control systems viz. Primary pressure control, SG pressure and level control, Power control system along with Emergency protection, Preventive Protection, Emergency core cooling safety injection systems and various automatic actuation logics. Presently the ATMIKA-LWR code uses Point Kinetics model to obtain reactivity feedbacks during the transient analysis. The need of space dependent neutronics code arises during simulation of transients/accidents where a tight coupling of thermalhydraulics of the plant and neutronic behaviour of the reactor core is very critical. Such kind of transients and accidents are overcooling transients caused by leakage in steam system (MSLB), boron dilution, control rod ejection, partial loss of forced reactor coolant flow (RCP trip) etc. Therefore, the present work is carried out to initiate the coupling of computer code ATMIKA-LWR with neutron physics code DRAGON-DONJON, thereby allowing the simulation of coupled thermal hydraulic neutronic transients.

2. Modelling methodology and validation of codes

2.1 KKNPP System Thermal Hydraulics Computer Code: ATMIKA-LWR

The computer Code "ATMIKA-LWR" is developed with the objective to perform thermal hydraulics safety analysis of KKNPP reactors indigenously. To estimate reactor power, Neutron Point Kinetics model is presently used and the 3-D reactor kinetics model work is in the scope of present work. The integrated coupled modelling of plant control systems, neutron physics and thermal-hydraulics is carried out in computer code for analyzing dynamic behavior of plant during plant transient conditions.

KKNPP-1&2 1000 MWe reactor are having 4 loops with 4 horizontal steam generators. The entire Thermal-hydraulics of the KKNPP systems is simulated by dividing the entire system into a number of lumped control volumes (C.V.) called nodes. The nodalization for KKNPP reactor [1,2] is carried out by making control volumes for Primary and secondary circuit system, SG feed water line from Deaerator to SG inlet, SG steam lines up to Governor Valve and Primary Make up and Blow down System. The primary circuit nodalization is shown in Figure 1.

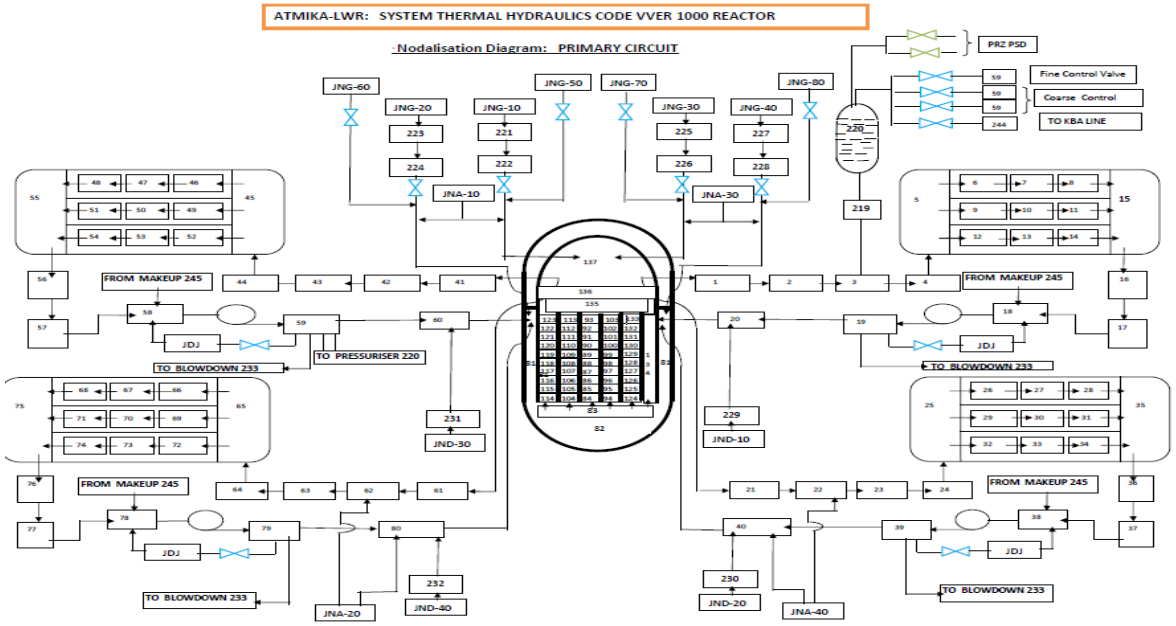


Figure 1 Nodalization diagram of Primary circuit.

Computer code ATMIKA-LWR is assessed and benchmarked with various commissioning test [4] for KKNPP-1&2 such as Turbine trip, load rejection, Manual EP, RCP trip test etc. & simulation of unplanned plant transient events [2]. In addition, ATMIKA-LWR code results are also benchmarked with results of KKNPP safety analysis reports [3].

2.2 Core neutronics: DRAGON/DONJON

DRAGON-DONJON is an open-source code developed at École Polytechnique de Montréal. The DRAGON code is capable of solving multigroup neutron transport equation in two and three dimensions. In the present work, a series of lattice calculations are done to generate input data for

DONJON. The DONJON code has the capability of solving neutron diffusion and spatial kinetics equations in three dimensions. In the present work, this code is used to compute the steady state and transient power distribution in KKNPP core.
Initially, to gain the confidence in DRAGON-DONJON code, literature study has been carried out [5]. This literature study involves the validation of IAEA benchmark calculations for "In-core fuel management code package validation for WWERs" [6]. In continuation, the study of KKNPP reactor core is done in DRAGON-DONJON code to perform the steady state and transient neutronic calculations which is briefly described in the following subsections.

2.2.1 DRAGON lattice cell calculations

Analysis of the KKNPP fuel assembly is done in DRAGON code. Four different types of fuel assemblies are there in KKNPP reactor core depending on their enrichments, which are modelled in DRAGON for lattice cell calculations (including control rods, guide tubes etc.).
A multi-component database is created with fuel burnup, coolant density, boron concentration in the coolant, and fuel temperature as interpolation parameters. At each parameter point, calculations are done by the DRAGON code and cross-sections are saved in multi-parameter database. For the purpose of validation, the results of the DRAGON lattice cell calculations for KKNPP fuel assemblies are compared with the respective results of the validated codes CASMO, HELIOS and NESSEL. The results of the code DRAGON are in good agreement with the codes CASMO, HELIOS and NESSEL.

2.2.2 DONJON calculations

The KKNPP full core calculations are carried out using DONJON computer code. The code interpolates the cross-section database generated by DRAGON to perform core calculations. The code perform the steady state core calculations with diffusion theory, two energy groups and a finite element solver (TRIVAC: module of DONJON) and provide the power distribution within the core for specified control rod positions & core power level. Figure 2 shows the modules used by DONJON to perform core calculations to obtain steady state power distribution. The geometric details of the core are the input to GEO module. NCR module interpolates the cross-section database generated by DRAGON for specified state of the core. The FLUD/DELTA module performs the core calculations to give steady state power distribution.

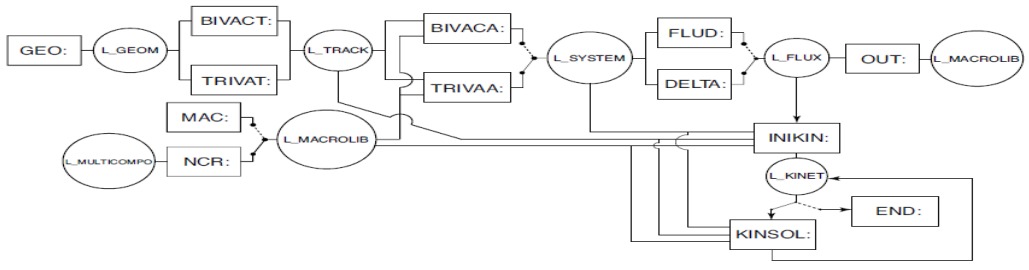


Figure 2 DONJON approach to simulate steady state and spatial kinetics [7]

In continuation further, the transient calculations are performed with DONJON for KKNPP core. The kinetic parameters required to perform the transient calculations are obtained from the steady state solution calculated by DONJON for the state of the core just before the initiation of transient.

This is done by the INIKIN module used by DONJON as can be seen in Figure 2 (INIKIN module post processes the solution of FLUD module). The input for the KINSOL to perform transient calculation, are the initialized kinetic parameters and the perturbation in reactor core state as compared to just previous state of core which can be change in control rod, temperature of fuel/coolant, coolant density etc. The sample case studies for steady state as well as spatial kinetics simulations are carried out.

3. Approach for coupling of ATMIKA-LWR with DONJON code

A method for transient coupling of these two independent codes ATMIKA-LWR and DONJON is developed to perform neutronic-thermalhydraulics transients. The key facilitator of transferring the data between codes is DONJON's FUELMAP data structure. The results of the simulations in DONJON code gets stored in FUELMAP data structure. FUELMAP contains burnup, thermal hydraulic data and power data for each node in DONJON which gets updated at every time step. An external script has to be developed to transfer the information between the two codes.

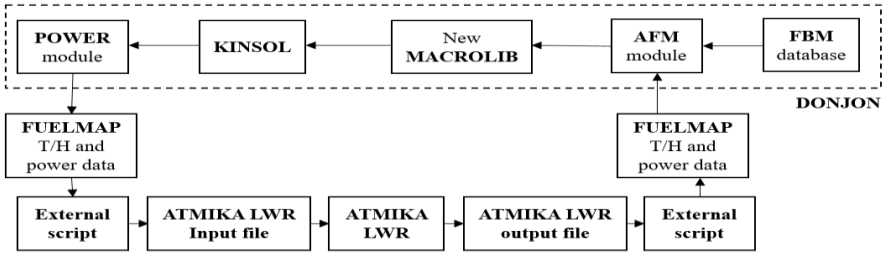


Figure 3 ATMIKA-LWR and DONJON coupling procedure

The initial conditions for the transient simulations will be created by coupling the initial steady state DONJON and ATMIKA-LWR models, thereby ensuring self-consistent distributions of thermal hydraulic and power parameters. DONJON will solve the spatial kinetic equations and will update the power values of each node in FUELMAP which will be transferred to ATMIKA-LWR input file using external script. Further, ATMIKA-LWR will perform the thermal hydraulic calculations and will transfer the required plant parameters such as control rod positions, density and temperature of fuel and coolant etc. of each node to the DONJON FUELMAP for the next time step using external script. This transfer of information is represented in Figure 3. In the next iteration (time step), the DONJON will read the FUELMAP and new macroscopic cross-sections will be created based on updated thermalhydraulic conditions and again solve the spatial kinetic equations and so-on. In this way, the neutronic code DONJON will provide the reactivity feedback to thermalhydraulic code ATMIKA-LWR to perform coupled thermal hydraulic neutronic transients.

4. Conclusion

Following are the conclusions of the present work:

- The System Thermal-Hydraulics computer code ATMIKA-LWR has been developed to carry out the thermal hydraulic safety analysis of KKNPP. The code is benchmarked with KKNPP plant commissioning test data, unplanned plant transient events and Safety Analysis Reports.
- For 3 D Kinetics calculations, the International Open Source computer code DRAGON-DONJON is used.

- Study is carried out to validate the results of Lattice cell calculations for KKNPP fuel assemblies using DRAGON code. The results (k-infinity values) are in good agreements with the results of CASMO, HELIOS and NESSEL. In continuation further, the cross-section database for KKNPP fuel assemblies (all 4 types) have been generated which are used to perform core calculations in DONJON.
- The flux distribution calculations are performed using DONJON code. The sample case studies for steady state as well as spatial kinetics simulations are carried out.
- The approach for coupling of ATMIKA-LWR with International Open Source computer code DRAGON-DONJON using External script is finalised.

5. References

[1] Kalra H. et.al, "Development of Plant system Thermal Hydraulics Neutronics computer code ATMIKA LWR for Kudankulam VVER 1000MWe reactor", Oct 14-18, 2019; 29th Symposium of AER on VVER Reactor Physics and Reactor Safety, Slovakia.

[2] Test case study for verification and benchmarking of computer code 'ATMIKA-LWR', Document no.: I02.KK16.0.0.TM.TR.PR001 (R0).

[3] Final Safety Analysis Report of KKNPP unit 1&2.

[4] KKNPP 1& 2 Commissioning Test Reports.

[5] W.F.G. van Rooijen, Md. J.H. khan, A. Hebert, V. Salino, "Analysis of a VVER-1000 in-core fuel management benchmark with DRAGON and DONJON", Journal of Nuclear Science and Technology, Vol. 11, No. 4, 2017.

[6] IAEA "In-core fuel management code package validation for WWERs", International Atomic Energy Agency, November, 1995.

[7] Alain Hébert et al., "A user guide for TRIVAC VERSION 5", Ecole Polytechnique de Montréal, 2021.

Acknowledgement

The authors would like to thank Shri H. P Rammohan, Former Executive Director NPCIL, NPCIL Engg-LWR group, PHWR Physics group and RPDD division of BARC for their support.

A CONDENSED OVERVIEW OF AERB BENCHMAR ON COUPLED CODE SYSTEMS (ABCS)

Obaidurrahman K., Santosh Kumar Pradhan
Atomic Energy Regulatory Board, Mumbai, India
e-mail: - obaid@aerb.gov.in

Abstract

Coupled core neutron kinetics and system thermal hydraulics modelling of NPPs has become a necessity in the present era of best estimate analysis. Coupled code systems need a thorough validation to ensure that complex coupled computing is reliable for safety analysis. A number of international benchmarks have been taken up to evolve required validation matrix for these elaborate codes, however access to these reference benchmark problems is limited. There has been a strong necessity to establish the credibility of coupled code systems, developed within DAE through validation against reference problems. Consistent with this necessity, AERB has proposed a detailed benchmark exercise. This article presents a brief overview of this benchmark problem.

1. Introduction

Transient response evaluation of NPPs has been one of the important dimension of nuclear reactor safety. As a conventional practice, until recent years most of the safety analyses have been successfully performed using thermal-hydraulics system codes with simplified core neutronics (0-D or 1-D). However, these codes cannot afford situations where complex feedback exists between core neutron kinetics and thermal-hydraulics or when core and/or system asymmetric phenomena are involved. Availability of advanced computing resources has rendered the flexibility to use the complex coupled computer codes simulating multi-disciplinary phenomenon. This has made direct modelling of the interaction between the 3D neutron kinetics and the thermal-hydraulics phenomena feasible. This approach consists of incorporating three-dimensional kinetic modelling of reactor core into thermal-hydraulic system codes. One of the important benefits of such analysis approach is relaxation of safety margins without compromising the NPP safety, allowing higher operating power and extended fuel cycles. Many initiatives have been taken up worldwide to couple core 3D kinetics codes with system codes. These complex code systems require intensive validation exercises to establish their credibility as best estimate analysis tool. Traditionally, the validations of coupled codes are carried out based on comparison between codes. It is desirable that the coupled codes need to be validated against plant data, though it is recognized that available plant transient data will represent only mild transient that will not cover the ranges of application in accident analysis. Numerous international benchmark exercises have been taken up under the ambit of OECD-NEA, however access to detailed data of these benchmark exercise is restricted.

A few initiatives have been taken up during the last decade towards coupling of core 3D neutron kinetics with system thermal hydraulics codes at BARC, NPCIL and AERB to pursue analysis and independent verification objectives. It is necessary to establish the adequacy of these code systems through validation against some reference problems. Due to limited access to the international benchmark problems, AERB has proposed a benchmark for the coupled code systems. The proposed ABCS benchmark problem is integrated core and system dynamic analysis of one loop loss of coolant accident (LOCA) in a 540 MWe PHWR. Objective of the present benchmark is to provide a basis to assess the modelling capabilities of the coupled codes in estimating the key safety parameters,

necessitated during safety analysis, through inter code comparison. Two phases of the benchmark exercise include steady state and transient core neutronics (Phase 1A), steady state and transient system thermal hydraulics (Phase 1B and Phase 1C) as first phase and coupled spatial core neutronics and thermal hydraulics as second phase (Phase 2).

2. Phase 1

First phase of benchmark deals with individual core neutronics and thermal hydraulics modelling to provide required confidence in these single physics modules. This will ensure that complete coupled neutronics- system thermal hydraulics modelling will have a self-consistent steady state core and system characteristics. Following successful validation of individual physics modules in Phase-1, second phase of exercise will provide a basis to assess integrated modelling capabilities of coupled codes. First phase of the benchmark is comprised of three exercises described in the following.

2.1 Phase 1A: Steady State and Transient Core Neutronics

Exercise Phase-1A provides a basis for assessment of 3D core neutronics modelling capabilities of codes through inter code comparison. Indian 540 MWe PHWR [1, 2] has been chosen as reference core (Figure 1). Core geometrical details and region wise state dependent two group lattice constants have been specified. In addition, details of reactivity devices and their incremental cross sections have also been specified.

	1	2	3	4	5	6	7	8	9	10	11	12	13	14	15	16	17	18	19	20	21	22	23	24	25	26	27	28
1	0	0	0	0	0	0	0	0	0	0	0	0	1	1	1	1	0	0	0	0	0	0	0	0	0	0	0	0
2	0	0	0	0	0	0	0	0	0	1	1	1	1	1	1	1	1	1	1	0	0	0	0	0	0	0	0	0
3	0	0	0	0	0	0	0	1	1	1	1	1	1	1	1	1	1	1	1	1	1	0	0	0	0	0	0	0
4	0	0	0	0	0	1	1	1	1	1	2	2	2	2	2	2	2	2	1	1	1	1	1	0	0	0	0	0
5	0	0	0	0	1	1	1	1	2	2	2	2	2	2	2	2	2	2	2	2	1	1	1	1	0	0	0	0
6	0	0	0	1	1	1	1	2	2	2	2	2	2	2	2	2	2	2	2	2	2	1	1	1	1	0	0	0
7	0	0	0	1	1	1	2	2	2	2	2	2	2	2	2	2	2	2	2	2	2	2	1	1	1	0	0	0
8	0	0	1	1	1	2	2	2	2	2	2	2	2	2	2	2	2	2	2	2	2	2	2	1	1	1	0	0
9	0	0	1	1	2	2	2	2	2	2	2	2	2	2	2	2	2	2	2	2	2	2	2	2	1	1	0	0
10	0	1	1	1	2	2	2	2	2	2	3	3	3	3	3	3	3	3	2	2	2	2	2	2	1	1	1	0
11	0	1	1	2	2	2	2	2	2	3	3	3	3	3	3	3	3	3	3	2	2	2	2	2	2	1	1	0
12	0	1	1	2	2	2	2	3	3	3	3	4	4	4	4	4	4	3	3	3	3	2	2	2	2	1	1	0
13	1	1	1	2	2	2	2	3	3	3	3	4	4	4	4	4	4	3	3	3	3	2	2	2	2	1	1	1
14	1	1	1	2	2	2	2	3	3	3	3	4	4	4	4	4	4	3	3	3	3	2	2	2	2	1	1	1
15	1	1	1	2	2	2	2	3	3	3	3	4	4	4	4	4	4	3	3	3	3	2	2	2	2	1	1	1
16	1	1	1	2	2	2	2	3	3	3	3	4	4	4	4	4	4	3	3	3	3	2	2	2	2	1	1	1
17	0	1	1	2	2	2	2	3	3	3	3	4	4	4	4	4	4	3	3	3	3	2	2	2	2	1	1	0
18	0	1	1	2	2	2	2	2	2	3	3	3	3	3	3	3	3	3	3	2	2	2	2	2	2	1	1	0
19	0	1	1	1	2	2	2	2	2	2	3	3	3	3	3	3	3	3	2	2	2	2	2	2	1	1	1	0
20	0	0	1	1	2	2	2	2	2	2	2	2	2	2	2	2	2	2	2	2	2	2	2	2	1	1	0	0
21	0	0	1	1	1	2	2	2	2	2	2	2	2	2	2	2	2	2	2	2	2	2	2	1	1	1	0	0
22	0	0	0	1	1	1	2	2	2	2	2	2	2	2	2	2	2	2	2	2	2	2	1	1	1	0	0	0
23	0	0	0	1	1	1	1	2	2	2	2	2	2	2	2	2	2	2	2	2	2	1	1	1	1	0	0	0
24	0	0	0	0	1	1	1	1	2	2	2	2	2	2	2	2	2	2	2	2	1	1	1	1	0	0	0	0
25	0	0	0	0	0	1	1	1	1	1	2	2	2	2	2	2	2	2	1	1	1	1	1	0	0	0	0	0
26	0	0	0	0	0	0	0	1	1	1	1	1	1	1	1	1	1	1	1	1	1	0	0	0	0	0	0	0
27	0	0	0	0	0	0	0	0	0	1	1	1	1	1	1	1	1	1	1	0	0	0	0	0	0	0	0	0
28	0	0	0	0	0	0	0	0	0	0	0	0	1	1	1	1	0	0	0	0	0	0	0	0	0	0	0	0

Figure 1: Radial core map of 540 MWe PHWR (Four regions)

Exercise 1A consists of two steps; viz. steady state and transient. Steady state exercise aims to evaluate core physics models through the estimation of multiplication factor, shut-off rod worth, channel and bundle powers as well as fuel and coolant state dependent reactivity effects based on specified lattice constants. Transient exercise aims to evaluate space-time

kinetics capabilities of the models through analysis of a reactivity perturbation introduced through a virtual density reduction in one half of the core, simulating one loop LOCA condition. Power excursion following LOCA is arrested through SCRAM with and without availability of two most effective shot of rods. Transient results in the form of normalized core power, intact and broken loop power, evolving 2D and 3D peaking factors etc. are required to be reported by participants. Desired output format tables have been specified. Assessment of results would be through inter code comparison.

2.2 Phase 1B: Steady State System Thermal Hydraulics

Exercise Phase-1B provides a basis for assessment of steady state system thermal hydraulic modelling of primary and secondary heat transport system of the plant. The data required for analysis was obtained from the plant drawings, preliminary safety analysis reports, design basis reports, results of Phase 1A etc. and specified along with the initial and boundary conditions. A schematic of the PHT system is provided in Figure 2.

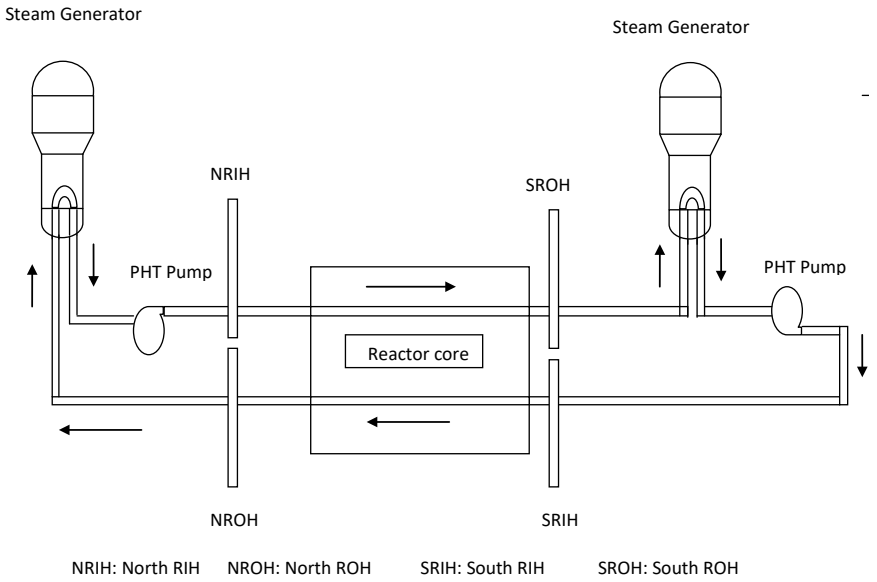


Figure 2: Schematic of Primary Heat Transport System

The axial power profile of channel M09 is assumed to be the one for for all the channels. Four quadrant homologous curves for head and torque are provided for PCPs. The two phase head multiplier as a function of void fraction are also specified. The thermal-hydraulic details of pressuriser and feed bleed system were specified along with the associated primary pressure and inventory control logics. The details of secondary side of SGs with steam lines up to MSIVs are provided. ECCS geometric details, thermal hydraulics parameters and associated logics are specified. The thermo-physical data such as thermal conductivity and volumetric heat capacity as a function of temperature for different core and structural materials are provided.

The steady state level qualification is specified. This includes comparison of geometrical parameters from nodalisation with plant data, boundary conditions of nodalisation with plant specifications and important thermal hydraulic parameters for steady state (which are derived from code output) with plant nominal data. A list of the geometrical values and of the thermal-hydraulic parameters to be checked is given together with acceptable errors. The parameters to be reported for comparison with plant nominal values are also specified.

2.3 Phase 1C: Transient system thermal hydraulics with point kinetic approximation

This phase establishes interaction between system thermal hydraulics and core neutronics with core modelled using point kinetics. The established TH model of Phase 1B are used to simulate two transients; the first one being a reactivity driven transient (1C1) and the second one being a system driven transient (1C2). The methodology for comparison of steady state as well as time dependent parameters are also provided. Core average kinetics parameters as estimated in Phase 1A have to be used for reactor kinetics. The objective of Phase 1C1 (reactivity initiated transient- ramp reactivity case) is to study the evolution of reactor power and effect of feedback (Doppler and void) for a reactivity driven transient with detailed system TH model and point kinetics based core neutronics model. The objective of Phase 1C2 is to study the evolution of reactor power and effect of feedback (Doppler and void) for a system driven transient (coolant void induced i.e. LOCA) with detailed system TH model and point kinetics based core neutronics model. The finalized specification along with required results have been disseminated among the participants of the benchmark.

3. Phase 2

With individual modules validated from Phase-1, second phase of the exercise is expected to provide a basis to assess the credibility of 'coupling' of the codes, through inter code comparison. This phase involves detailed analysis of one loop LOCA in the core with detailed neutronic treatment of the core to emphasize the finer spatial resolution of core neutronic behaviour. The reactor is at steady state with 100% FP at the beginning of the transient. The transient is initiated with a break in one of the RIH in loop-1. A couple of break sizes (22.5 % and 100% DEGB) have been specified. The duration of the transient is 600 seconds. Reactor trip parameters should be applied as specified and decay heat following trip should be modelled as specified table. State dependent lattice constants should be used to account reactivity feedback. For coarse mesh models, appropriate node average properties is proposed to be used. All 28 SORs are dropped inside the core as per drop characteristics. Integrated core and system transient response in the form of core power, power distribution, peaking factor, average and peak temperatures at specified locations and other hydrodynamic details of cooling circuits to be reported as specified in results tables.

4. Summary

AERB coupled benchmark provides a reference problem to assess the complex coupled code systems employed for best estimate analysis of large power reactors. Detailed specifications and transient problem definition has been finalized after extensive scoping calculations and feedback from the participants. Authors may be approached for benchmark specifications.

5. Acknowledgements

Authors are grateful to NPCIL for providing detailed data for drafting benchmark specifications. Contributions from benchmark participants have been immensely useful in fine tuning the specifications. Support and guidance received from DAE steering committee on safety research is gratefully acknowledged.

6. References

[1] S.S. Bajaj, A.R. Gore, The Indian PHWR, Nuclear Engineering and Design 701–722, 236 (2006)

[2] Official communications with NPCIL

DEVELOPMENT AND VALIDATION OF MULTI-PHYSICS CAPABILITY IN CODE ARCH-TH FOR 3D CORE TRANSIENTS OF WATER COOLED REACTORS

D.K. Dwivedi*, Anurag Gupta and Umasankari K.
Reactor Physics Design Division, Bhabha Atomic Research Centre, Mumbai, India
e-mail: - ddwivedi@barc.gov.in

Abstract

3D multi-physics code ARCH-TH has been indigenously developed for coupled neutronics - thermal-hydraulics (N-TH) analyses of reactor core transients. The neutronics and fuel temperature feedback module in the code are successfully validated with dynamics benchmarks of VVER-440. The code has been recently enhanced for thermal-hydraulics (TH) feedbacks of water-cooled reactors (WCRs). The homogeneous equilibrium model (HEM) is developed in the code for mass, energy and momentum conservations in WCRs during operation and transients. The code has been subsequently validated with the AER-Dyn003 dynamic benchmark of VVER-440 to check its viability. The benchmark simulation of a control rod ejection accident in VVER-440 core requires 3D neutronics thermal-hydraulics capability for two-phase flow during the transient. The power excursion in the benchmark is supposed to be passively controlled by the reactivity feedback due to changes in fuel temperature and moderator density. A hot channel calculation is optionally included in the benchmark. The predictions of code ARCH-TH have been compared with other coupled N-TH code systems. The benchmark results are of the code is found to be in good agreement with others. The code is being extensively utilized for the design and safety analyses of IPWR.

1. Introduction

The advanced design of nuclear reactors necessitates multi-physics tools for accurate and efficient predictions of complex phenomena of coupled neutronics- thermal-hydraulics during core transients. In this perspective, a 3D multi-physics code ARCH-TH has been developed for design and safety analyses of indigenous design of reactors like HTRs, IPWR and AHWR [1]. The code has been extensively validated with AER-Dyn001 and AER-Dyn002 dynamic benchmarks of VVER-440 and results are subsequently reported in literature [2]. The reactors like IPWR and AHWR are the modern concept of light water cooled reactors, which are being designed at BARC. The TH module in code ARCH is being further developed with special focus to enhance the in-house multi-physics capability for WCRs. For the simulation of two-phase flow based thermal-hydraulics phenomena in the channels of water cooled reactors like VVER-440, the homogeneous equilibrium model (HEM) is developed in the code ARCH-TH. The theory and developed TH model have been briefly described in the next section.

2. Theory and Model of developed TH capability in ARCH-TH

The TH module of code ARCH-TH has been further developed with the homogeneous equilibrium model (HEM). The model assumes that there is no relative velocity between two-phases (i.e. homogeneous flow with slip ratio, S =1.0) and the vapour and liquid phases are in thermodynamic equilibrium. For 1D flow of the fluid, the mass conservation equation can be written as follows [3]:

$$\frac{\partial}{\partial t}\{\rho_v \alpha + \rho_l(1-\alpha)\}A_z + \frac{\partial}{\partial z}\{\rho_v \alpha v_{vz} + \rho_l(1-\alpha)v_{lz}\}A_z = 0 \quad \text{..... (1)}$$

Here, the symbols α, A_z, ρ_v and ρ_l are the void fraction, flow area, mass density of vapour and liquid phases of the fluid at time t and position z. The parameters v_{vz} and v_{lz} are the vapour and liquid

velocities respectively in the axial direction. In HEM model, $v_{vz} = v_{lz} = v_{mz}$ is assumed, where v_{mz} is the average axial velocity of homogeneous mixture with mass density ρ_m (i.e. $\rho_m = \rho_v \alpha + \rho_l(1-\alpha)$). Thus the above equation can be written as follows,

$$\frac{\partial}{\partial t}(\rho_m A_z) + \frac{\partial}{\partial z}(\rho_m v_{mz} A_z) = 0 \ldots\ldots\ldots \quad (2)$$

The equation (1) for vapour and liquid phases can be written separately as follows:

$$\frac{\partial}{\partial t}\{\rho_v \alpha\} + \frac{\partial}{\partial z}\{\rho_v \alpha v_{vz}\} = \Gamma_v \text{: for vapour, ...(3)}$$

$$\frac{\partial}{\partial t}\{\rho_l(1-\alpha)\} + \frac{\partial}{\partial z}\{\rho_l(1-\alpha)v_{lz}\} = \Gamma_l = -\Gamma_v \text{: for liquid .....(4)}$$

Here, jump condition is considered as : $\Gamma_v + \Gamma_l = 0$.

For 1D flow, the momentum conservation of coolant can be written as follows:

$$\frac{\partial}{\partial t}\{\rho_v \alpha v_{vz} + \rho_l(1-\alpha)v_{lz}\}A_z + \frac{\partial}{\partial z}\{\rho_v \alpha v_{vz}^2 + \rho_l(1-\alpha)v_{lz}^2\}A_z$$
$$= -\left(\frac{\partial p A_z}{\partial z}\right) + p\frac{\partial A_z}{\partial z} - \int_{P_z} \tau_w \, dP_z - \{\rho_v \alpha + \rho_l(1-\alpha)\} g \cos\theta \, A_z$$

Here, τ_w is the shear stress at the walls due to friction. In HEM, the above equation will be as follows:

$$\frac{\partial}{\partial t}(\rho_m v_{mz} A_z) + \frac{\partial}{\partial z}(\rho_m v_{mz}^2 A_z) = -\left(\frac{\partial p A_z}{\partial z}\right) + p\frac{\partial A_z}{\partial z} - \int_{P_z} \tau_w \, dP_z - \rho_m g \cos\theta \, A_z \quad \ldots\ldots \quad (5)$$

Similarly, for energy balance, we can write equation as follows:

$$\frac{\partial}{\partial t}\{\rho_v \alpha h_v + \rho_l(1-\alpha)h_l\}A_z + \frac{\partial}{\partial z}\{\rho_v \alpha h_v v_{vz} + \rho_l(1-\alpha)h_l v_{lz}\}A_z = \left(\frac{\partial p}{\partial z}\right)A_z + q' + Q' \quad \ldots\ldots \quad (6)$$

Here, q' and Q' are the linear heat addition rate from the walls and heat generation rate in the coolant respectively. The symbols h_v and h_l are the enthalpy of vapour and liquid phases of the coolant fluid. In HEM, the equation for energy conservation can be written as follows:

$$\frac{\partial}{\partial t}(\rho_m h_m A_z) + \frac{\partial}{\partial z}(\rho_m v_{mz} h_m A_z) = \left(\frac{\partial p}{\partial z}\right)A_z + q' + q_c' \qquad \ldots\ldots\ldots \quad (7)$$

Here, h_m is the static mixture enthalpy averaged over area A and defined as follows:

$$h_m = \frac{1}{\rho_m}\{\rho_v \alpha h_v + \rho_l(1-\alpha)h_l\} \ldots\ldots\ldots\ldots \quad (8)$$

In Equation (1) to (8), the symbols have their usual meanings if not explicitly mentioned. In saturated conditions, Equation (1) to (8) in ρ_m, $\rho_m v_{mz}$ ($=G_m$), h_m and pressure p can be solved if state equation for the fluid and q', q_c' and τ_w are specified in the relation to other variables. The mass, momentum and energy conservation equations given by Equation (2), (5) and (7) can be extended to single phase coolant, saturated mixture and single-phase vapour flow sections of the fuel channels. In the code, for thermo-physical properties of light-water coolant, the water-steam table is considered as given in Todreas and Kazimi (2012) [3].

In the code ARCH-TH, the convection heat transfer from cladding to water coolant is calculated with Dittus-Boelter correlation (i.e. $h_z = \frac{Nu.k}{D}$) as follows:

$$Nu_{DB} = 0.023 \, Re^{0.8} Pr^{0.4} \quad \ldots\ldots\ldots(9)$$

The Equation (9) is applicable for coolant heating for the range: 0.7 <Pr< 100, Re> 10000, and channel length to hydraulic diameter ratio (L/D) is more than 60. [3]. The parameter Re and Pr are the Reynolds number and Prandtl number are evaluated at local average temperature of the coolant.

During subcooled boiling, the heat transfer is computed with Thom correlation [3] as follows:

$$q''(= h_z(T_w - T_c)) = \frac{\exp\left(\frac{2p}{8.7}\right)}{(22.7)^2}(T_w - T_{sat})^2 \quad \ldots\ldots\ldots \quad (10)$$

Here, q'' and p are the heat flux in MW/m^2 and local pressure in MPa. The parameters T_w, T_c and T_{sat} are the temperatures of the wall, average coolant and saturated coolant in ^oC.

The coolant inlet temperature in the channels and pressure at the channel-outlets are considered as the given boundary conditions. The TH model computes 1D-radial heat conduction in all axial meshes of average powered rod/ pin in every channel/ assembly with given inlet mass flow rate and temperature [2]. It is used for solving energy conservation equation in the channels as an open loop of coolant with possible two phase flow during transient. An option for the hot channel is also incorporated in the code. The temperature dependent thermo-physical properties of the fuel, clad and gas-gap such as thermal capacities and conductivities are considered as per given correlations in the benchmark AER-Dyn003 [4]. The developed TH model in code ARCH-TH is validated with dynamic benchmark results of VVER-440 and discussed in the subsequent section.

3. Results and Discussions

The AER-Dyn003 benchmark in hexagonal core geometry concerns a control rod ejection accident case of light water reactor VVER-440 [4]. In the stationary state the core thermal power is 1.375 kW. In the benchmark problem, all fission power in the core is considered to be prompt, i.e. there is no delayed energy release (decay heat). The energy released is taken as 200 MeV/fission. About 97.5% of total fission power (into fuel) is released uniformly in fuel pellet and rest of 2.5% is assumed to be deposited as heat directly into the coolant (which also acts as neutron moderator) of the respective fuel assembly. The transient is assumed to be started at low power and end-of-cycle conditions. The transient is

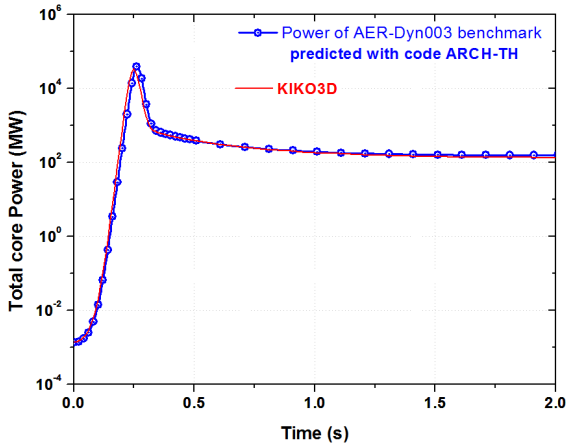


Fig.-1 :Total core power versus time

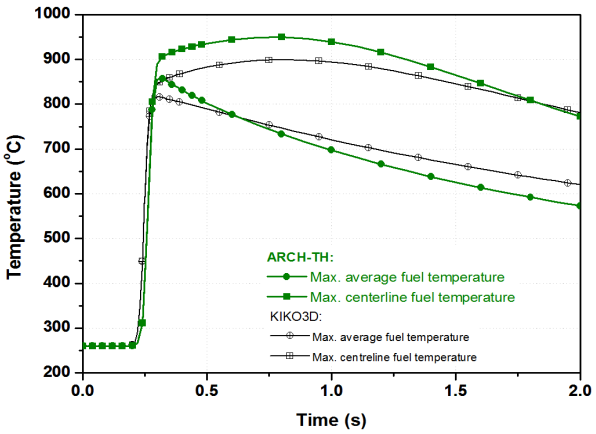


Fig.-2 : The peak centreline and average fuel temperatures versus time

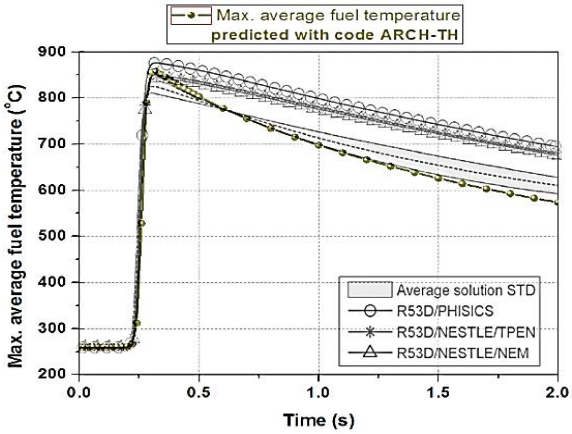


Fig.-3: The peak of average fuel temperature compared with RELAP5-3D/PHISICS

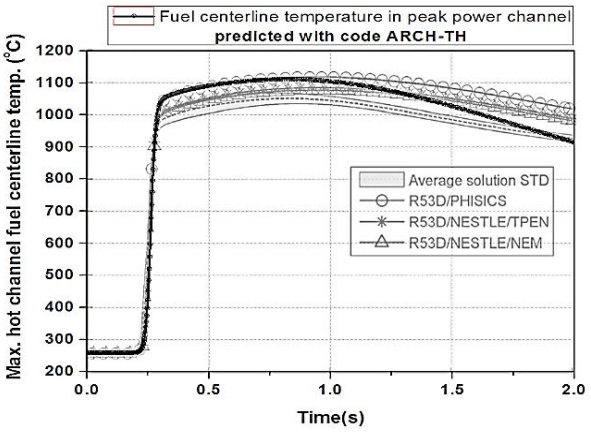


Fig.-4: The peak fuel centreline temperature in the hot channel versus time.

simulated without reactor scram and after a power excursion the reactor stabilizes at a power level determined by the feedbacks from change in fuel temperature and moderator density. The reactivity feedbacks of fuel temperature and coolant density are modelled as given in the benchmark.
In the benchmark of VVER-440 transient, all the channels are considered thermal-hydraulically identical, with the same mass flow rates, pressure drops, number of pins, etc. In steady-state as well as during the transient the mass flow distribution between the assemblies is to be determined on the basis of the pressure balance over the core. The reactor outlet pressure and inlet temperature are given as about 12.1 MPa and 260^{o}C respectively. The pressure difference over the core and the coolant inlet temperature are assumed to be invariable during the transient. The total inlet mass flow is 3400 kg/s for the entire core in stationary state.

The transient is supposed to be initiated due to an eccentric rod ejected at t = 0s with a constant speed of 12.5 m/s during 0.16s. Other rods of the bank remain at 200 cm inserted in the core and no reactor trip is assumed in the calculation. The transient has been simulated for the duration of 5 s. For the optional hot channel calculation in the transient benchmark, the excess power factor (i.e. peaking) of 1.25 times of the power of the hottest assembly has been considered [4].

The reactivity worth of ejected control rod in the benchmark is estimated as 1.9020 $ with code ARCH-TH. The variation of power with code ARCH-TH has been estimated and shown in Fig.-1. It is found that the results of the code are matching very well with other code [5] (Fig.-1).The variation of maximum average and centreline temperatures of the fuel in the core have been estimated with code ARCH-TH and are shown in Fig.-2 to Fig.-4. It is found that the results are matching very well with KIKO3D (Fig.-2). The variation of fuel temperatures during transient have also been compared with RELAP5-3D/PHISICS code system [6] and the results are found in good agreement (Fig.-3 and Fig.-4).

4. Conclusion

The TH module of 3D multi-physics code ARCH-TH has been advanced to simulate two-phase flow during transient in light water cooled reactor cores like VVER. At present, homogeneous equilibrium model (HEM) for two-phase TH is developed. The code solves 1D-radial heat conduction in average powered pin/ rod of each channel with given inlet mass flow rate, temperature of coolant and outlet pressure in the core. The capability in code has been validated with AER-Dyn003 benchmark problem of VVER-440 control rod ejection transient. The results of ARCH-TH have been compared with KIKO3D and RELAP5-3D/ PHISICS code system and the results are found in good agreement. The non-equilibrium based hydraulic model in the code can be developed in future for more accurate predictions of related TH phenomena. The code is being utilized for design and safety studies of IPWR.

References

[1]. Dwivedi et al.,. Nuclear Engineering and Design, 2020, 370, 110881.

[2]. Dwivedi et al., Annals of Nuclear Energy, 110, 2017, pp. 306-316

[3]. Todreas and Kazimi, vol-1, *CRC Press, Taylor & Francis Group, ISBN:978-1-4398-0887-0.*

[4]. R. Kyrki-Rajama¨ KI, AER Benchmark Book, Hungary (Dec. 29, 1999).

[5]. M. Telbisz, 2000, *http://aerbench.kfki.hu/aerbench/dyn003_solaeki.txt*

[6]. Balestra et al. 2018, *Nuclear Technology · volume 193 · 175–182 · January 2016.*

BRIEF DESCRIPTION OF LATTICE CODE 'ν-TRAC' AND ITS VALIDATION FOR SQUARE AND HEXAGONAL LATTICES

Anmol Singh[*, 1], Usha Pal[*, 2], R. Karthikeyan[*, 3] and Amod Kishore Mallick[*, 4]
[*]Reactor Physics Design Division, Bhabha Atomic Research Centre, Mumbai-400085, India
[1]anmol@barc.gov.in, [2]ushapal@barc.gov.in, [3]rkarthi@barc.gov.in, [4]amod@barc.gov.in

Abstract

A Neutron Transport Analysis Code (ν-TRAC) is being developed in BARC. ν-TRAC solves the characteristic form of Maxwell Boltzmann neutron transport equation using the Method of characteristics (MOC). A module to read multi group library is coupled with ν-TRAC to perform cell calculation in multi groups. Dancoff factor for the fuel lump are evaluated using neutron current method and Carlvik`s algorithm. Equivalence principle is used to evaluate self-shielded cross section in resonance energy groups. The results of ν-TRAC have been compared with benchmark problems in few energy groups as well as with multi group nuclear data library in WIMS format. The code has been extensively validated by analysing numerous benchmarks for 1-D slab and 2-D hexagon / Square geometries. The results are in very good agreement with the benchmark results.

1. Introduction

A code ν-TRAC to solve neutron transport equation (NTE) has been developed. It solves NTE with MOC technique for 1-D slab and 2-D hexagon / Square geometries. Problem domain is discretised into Delaunay triangulation using Bowyer & Watson algorithm. This algorithm is based on *circumcircle property* which grantees that no other point lies within the circumcircle of triangle. Characteristic ray tracing through the problem domain are incorporated by means of intersection of them with the edges of meshes across the characteristic rays. To get precise results, a good number of characteristic rays needs to be considered through the geometry. Library processing module is incorporated to deal with multi group nuclear data library. Subsequently, average angular flux values are evaluated and scalar flux in a mesh is calculated by combining angular flux values and weighting them with appropriate weighting factor. A brief flow of calculation in ν-TRAC is discussed in later sections of the paper.

2. Theory and Geometrical Interpretation of MOC

In MOC first order partial differential equations (PDE) is solved as initial value problem. Let us consider the general quasilinear PDE of first order as neutron transport equation is a PDE of first order. For simplicity, consider only two independent variables.

$$a(x,y,u)\frac{\partial u(x,y)}{\partial x} + b(x,y,u)\frac{\partial u(x,y)}{\partial y} = c(x,y,u) \qquad (1)$$

Solution of the above equation $u(x,y)$ and $f\big(x,y,u(x,y)\big) = 0$ represents a surface $S \equiv x,y,u(x,y)$ embedded in $\boldsymbol{R}^3$. Normal to the level surface is given by the gradient of scalar function $f\big(x,y,u(x,y)\big)$. $\vec{\nabla} f$ is the normal vector at any point on the solution surface. Eq. (1) can be written in following form $\vec{A}.\vec{\nabla} f = 0$. As $\vec{\nabla}$f is the normal vector to the solution surface, $\vec{A}$ is always tangential to the solution surface at all points in space (x,y,u(x,y)).

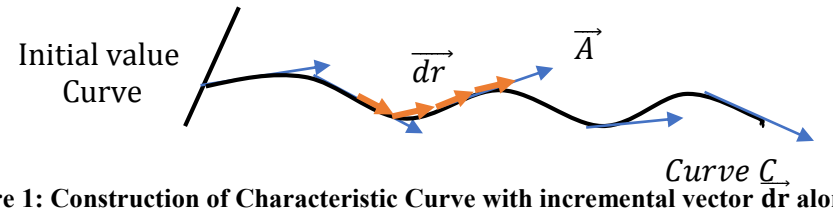


Figure 1: Construction of Characteristic Curve with incremental vector $\overrightarrow{dr}$ along $\vec{A}$

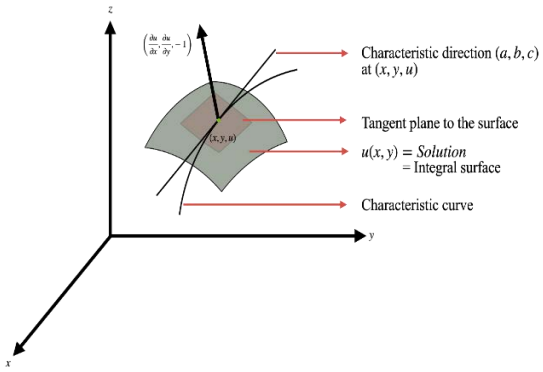


Figure 2: Geometrical interpretation of MOC.

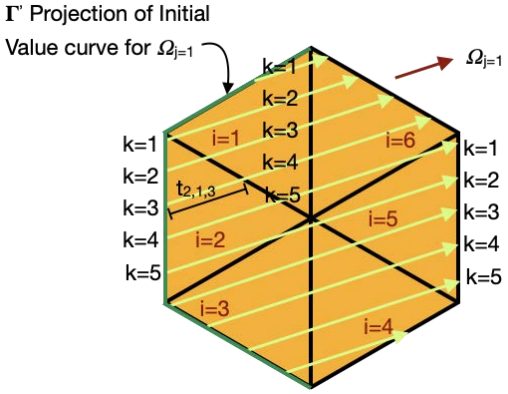


Figure 3: MOC formalism across hexagonal geometry

Now, to find the solution of the differential equation, we need to construct a solution surface 'S', such that at every point (x,y,u(x,y)) on surface 'S', $\vec{A}$ is in tangential plane. Next challenge is to construct such surface. We start by looking for a curve C which lies in S. A small incremental movement on the solution surface in the direction of $\vec{A}$ i.e. $\overrightarrow{dr}$ satisfies a condition $\vec{A} \times \overrightarrow{dr} = 0$. A curve $'C'$ can be constructed on solution surface $'S'$ by integration of such small increments as shown in **Figure 1**. This curve is called integral curve or characteristic curve for vector field defined by (a, b, c). Once all characteristic curves are found, the solution surface can be constructed by the union of all these characteristic curves. This is the basic necessary geometrical interpretation of method of characteristics. Its interpretation is given in **Figure 2** and **Figure 2**.

The Boltzmann equation is obtained as the particle balance relation for the neutral particles located in a volume element. This equation is also applicable for neutron in the volume of interest. The steady state form of the neutron transport equation is as follows:

$$\hat{\Omega}.\nabla\Psi(\vec{r},E,\hat{\Omega}) + \Sigma_t(\vec{r},E)\Psi(\vec{r},E,\hat{\Omega}) = Q(\vec{r},E,\hat{\Omega}) \qquad (2)$$

neutron transport equation is converted into following characteristic form

$$\frac{d\Psi(\vec{r}+s\hat{\Omega},E,\hat{\Omega})}{ds} + \Sigma_t(\vec{r}+s\hat{\Omega},E)\Psi(\vec{r}+s\hat{\Omega},E,\hat{\Omega}) = Q(\vec{r}+s\hat{\Omega},E,\hat{\Omega}) \qquad (3)$$

This equation will be solved along the characteristic curves i.e. direction of neutron movement across the problem geometry. Modular structure of ν-TRAC is presented in **Figure 4**.

3. Results and Discussion

ν-TRAC has been validated extensively by analysing numerous lattice benchmarks in 1-D slab, 2-D square and hexagonal geometries with provision to ***use homogenised cross section as well as standard multi group nuclear data library*** [1]. Here, few Results of ν-TRAC are presented in **Table *3-1*** for 1-D benchmarks, 2-D benchmark with homogenised set of cross section data and 2-

D pin cell benchmark using 172 group multi group nuclear data library as illustrated in **Figure *5***.

Table 3-1: Results of *ν*-TRAC

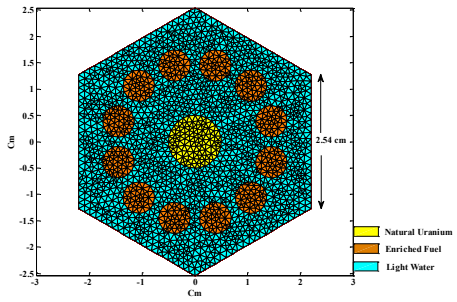
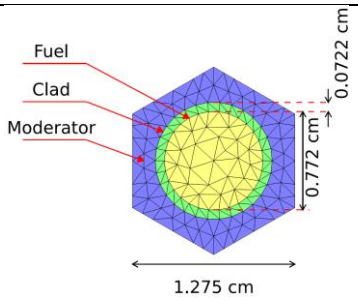
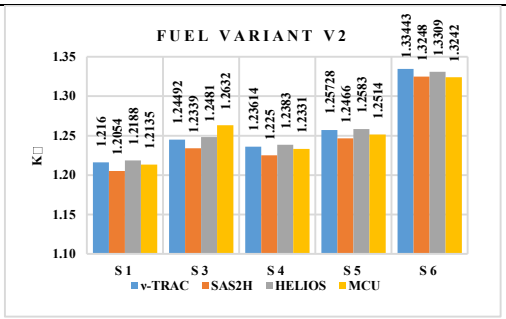
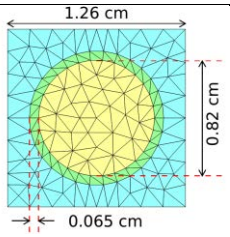
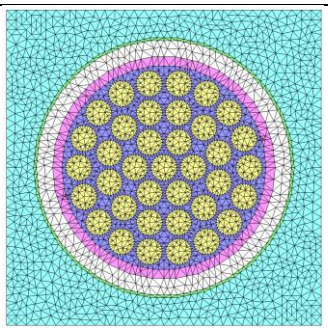
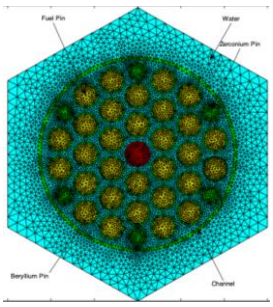
Benchmark	*ν*-TRAC Results	
	Geometry	**Eigen Value**
One group -one medium-slab (1-D)	PUa-l-0-SL, 1-D slab [2]	0.9999787
Hexagonal cell with central breeding pin(2-D, Homogenized XS) [1][3]		**1.0879 (*ν*-TRAC)** 1.090803 (MG-MCNP3B) 1.086598 (TEPFEM) 1.085775 (TPTRI)
VVER-1000 Pin cell (2-D, ENDFB7GX.LIB) [1][4]		
Rowland Pin Cell (2-D, MOX, CaseA, ENDFB7GX.Lib)[5]		**1.22416 (*ν*-TRAC)** 1.22647 (±0.0006) (MCNP) 1.22513 (±0.00016) (TRIPOLI) 1.2237 (±0.0008)(MORSE-K)

Table 3-2: Cluster modelling in *ν*-TRAC

PHWR Cell Geometry Modelling	Hezagonal FA Modelling in *ν*-TRAC	
		**1.5925(*ν*-TRAC)** 1.5898 (EXCEL)

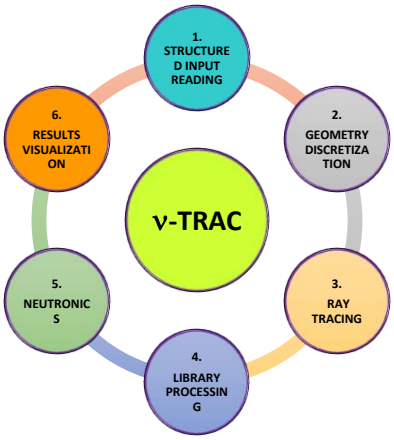


Figure 4: Modular Structure of ν-TRAC

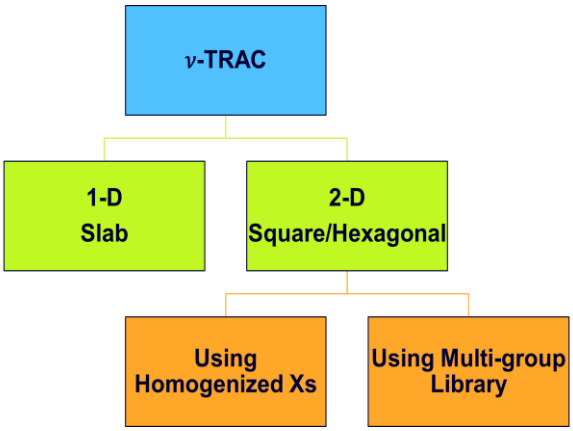


Figure 5: Classification of results of ν-TRAC

4. Conclusion

A computer code ν-TRAC is being developed for neutronic analysis of complex heterogeneous geometry of a nuclear reactor. ν-TRAC solves the neutron transport equation using the method of characteristics. The heterogeneous problem domain is discretised using Delaunay triangulation. Visualization of the discretized geometry and raytracing through geometry is made possible through a visualization module incorporated into the code. ν-TRAC can handle 1-D slab, 2-D hexagonal and 2-D square geometries. ν-TRAC can perform transport calculation using region wise homogenised cross section in multi energy groups as well as standard multi group nuclear data library in WIMS format. As a part of extensive validation of ν-TRAC, results from this code for a variety of benchmark problems have been compared with those obtained from other codes and are found to be in excellent agreement.

5. Acknowledgement

Sincere acknowledgements are due to Dr Argala Srivastava, Mr Krishna Kumar Yadav and Mr. V. Harikrishnan for several useful discussions and constant support during the development of ν-TRAC. We also acknowledge Dr Umasankari Kannan for her constant encouragement.

References

[1] Anmol Singh, Usha Pal and A. K. Mallick, "νTRAC: A Neutron Transport Analysis Code based on MOC for 1-D Slab, 2-D Square and 2-D Hexagonal Geometries," *Annals of Nuclear Energy,* 2022. (under review)

[2] A. Sood, R. Arthur and D. K. Parsons, "Analytical Benchmark Test Set for Criticality Code Verification," *Progress in Nuclear Energy,* vol. 42, no. 1, pp. 55-106, 2003.

[3] M. W. J. Wood, "Recent progress in the application of the finite element method to the neutron transport equation," *Progress in Nuclear Energy,* vol. 14, no. 1, pp. 21-40, 1984.

[4] O. R. Vol.-3, "Neutronics Benchmarks for the Utilization of Mixed-Oxide Fuel: Joint U.S./Russian Progress Report of Fiscal Year 1997, Volume 3 – Calculation Performed in Russia," 1997.

[5] J. Rowlands, "LWR PIN CELL BENCHMARK INTERCOMPARISONS," JEFF Report 15, September 1999.

DEVELOPMENT OF MONTE CARLO -REACTION RATES (TALLY) BASED BURNUP CODE AND ITS VALIDATION THROUGH LWR BENCHMARK EXERCISES

P RavindraBabu[1], Usha Pal[2], and R N Sen[1] and R. Karthikeyan[2]
[1] Bhabha Atomic Research Centre, Vizag, India
[2] Bhabha Atomic Research Centre, Mumbai, India
[1]*e-mail: - ravindrab@barc.gov.in*

Abstract

A burnup code, TALBURN is developed using tally information generated using Monte Carlo code MCNP. The code uses Euler method with Backward Difference Formulae (BDF) as the integration method to estimate fuel and fission product composition as a function of burnup. Validation of the code is done by analyzing benchmarks and comparing the results of isotopic composition and Eigen values predicted by TALBURN with that obtained using deterministic codes like WIMS8A, HELIOS, TVS-M and MULTICELL and with Monte Carlo codes like MCU.

1. Introduction

In many nuclear reactor applications such as fuel management and reactor core design, burn up calculations are essential. Monte Carlo method is very useful in simulating complicated reactor geometry when compared with conventional deterministic codes. MCNP is the most widely used code among existing standard multipurpose continuous energy Monte Carlo codes. MCNP can be used for calculations of multiplication factor, reaction rates, neutron fluxes, spectra etc.

In the past few decades, a number of Monte Carlo burn-up calculation code systems like MCB [1], and BURNCAL[2] have been developed. A new burn-up code 'TALBURN' that uses the reaction rates generated by the Monte Carlo code to solve the depletion equation for estimation of actinides and fission products concentrations is presented in this paper. Validation of the methodology used in TALBURN is performed by analysing the VVER-1000 LEU and MOX assembly computational benchmark [3].

2. Benchmark specification

The benchmark model consists of two different hexagonal Fuel Assemblies (FAs): a uniform LEU fuel assembly and a profiled MOX assembly which are schematically shown in Figures 1&2. Each of the

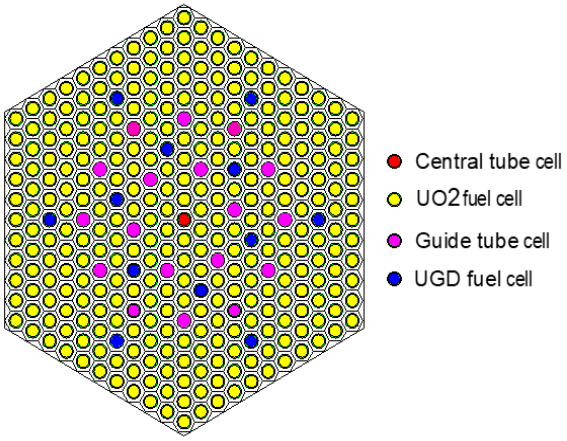


Fig.1 Schematic view of LEU FA

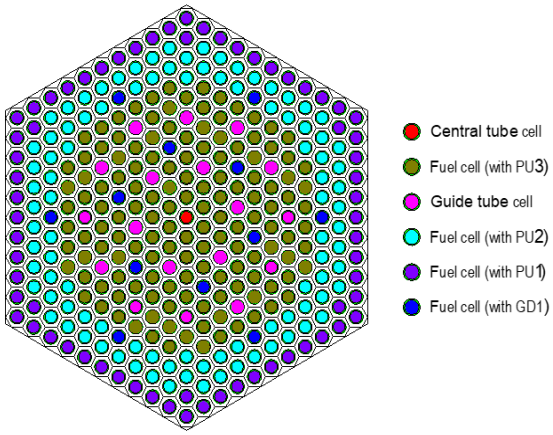


Fig.2 Schematic view of MOX FA

FAs consists of total 331 cell locations at a regular pin pitch of 12.75mm. LEU FA considers two types of fuel pins which include 300 fuel pins of 3.7wt% ^{235}U and 12 uranium-gadolinium pins with 3.6 wt% of ^{235}U and 4 wt% Gd_2O_3. The FA also has one central water filled instrumentation tube and 18 water filled control guide tubes of ID/OD 10.9/12.646mm.

The MOX FA consists of four types of fuel pins. 138 fuel pins with 4.2 wt% fissile Pu occupies the central region of the FA, surrounded by 96 fuel pins with 3.0 wt% of fissile Pu. 66 fuel pins with 2.0 wt% fissile Pu are present at the outermost region of the FA. The 12 uranium-gadolinium pins with 3.6 wt% ^{235}U and 4.0 wt% Gd_2O_3 are distributed inside the assembly as shown in Figure-2. The FA also has one central water filled instrumentation tube and 18 water filled control guide tubes of ID/OD 10.9/12.646mm. These assemblies are advanced designs, which are under active development in Russia for VVER-1000 reactors. These assembly designs use Gd_2O_3 mixed with UO_2 as burnable absorbers to control core reactivity at beginning of core life (BOC). The geometry data for LEU and MOX FAs and number densities of fuel and non- fuel isotopes are used as prescribed in the benchmark report [3]. Temperature of fuel and coolant is considered as 1027^0K and 575^0K respectively.

2.1 Burn up calculation method

TALBURN code uses BDF method for solving the depletion equation for better accuracy. General expression for formation and loss of particular isotope by nuclear transmutation and radioactive decay can be written as follows:

$$\frac{dN_i}{dt} = \sum_j \gamma_{j,i}\sigma_{f,j}N_j\emptyset + \sum_k \sigma_{c,k\to i}N_k\emptyset + \sum_l \lambda_{l\to i}N_l - (\sigma_{f,i}N_i\emptyset + \sigma_{c,i}N_i\emptyset + \lambda_i N_i) \quad \ldots\ldots \quad (1)$$

Where $\frac{dN_i}{dt}$ is the rate of change of concentration of i^{th} isotope, $\sum_j \gamma_{j,i}\sigma_{f,j}N_j\emptyset$ is production rate, $\sum_k \sigma_{c,k\to i}N_k\emptyset$ is production from neutron transmutation of all isotopes, $\sum_l \lambda_{l\to i}N_l$ is the production, $\sigma_{f,i}N_i\emptyset$ is removal rate of isotope 'i' due to fission, $\sigma_{c,i}N_i\emptyset$ is removal rate per unit volume of isotope 'i' by neutron capture, $\lambda_i N_i$ is removal rate per unit volume of isotope 'i' by decay.

2.2 Solution Technique

Total 33 actinides and 75 fission products are taken into account for solving above burnup equation (1). Separate fission yields are used for each actinide and fuel isotope.MC code is coupled with TALBURN code to perform lattice level and core level burn-up calculations. In MC-TALBURN, Adam Moulton second order implicit scheme (BDF) [4] is used, which can do the burn-up calculations with enough accuracy. Nuclide concentrations at k^{th} burnup step are estimated as function of the reaction rates at $(k-1)^{th}$ burnup step and k^{th} burnup step. Reaction rates corresponding to particular power value is estimated using conversion factor. Nuclide concentrations (N_i) are defined by following differential equations in matrix form as

$$\frac{dN_i}{dt} = f(i,k) \ (i=1,3) \ldots\ldots\ldots\

(where 'ϑ_{avg}' is Average number of neutrons generated from fission event)
'Q' is average energy recoverable from fission event (J/fission)

2.4 Steps Involved in the MC-TALBURN code

I. Read reaction rates from MC code k^{th} burnup step.

II. Estimate depleted number densities of F.P and Actinides of different fuel and burnable poison cells by solving Eq.(1)&(2) with BDF method and Cramer's rule.

III. Update the number densities in the MC code and estimate Eigen value and reaction rates at $(k+1)^{th}$ burn-up step.

IV. Repeat the steps I-III until the end of last burn-up step.

2.5 Results and Discussion

To assess the validity and applicability of MC-TALBURN code system, A VVER-1000 LEU & MOX computational benchmark has been analysed by applying reflective boundary conditions on each surface of the hexagon. Burnup calculations were performed with the power density of 108 W/cm^3 at operating conditions, up to the burn up of 40.0 MWd/Kg. k_∞ values are compared with benchmark mean values and was found to be in good agreement. Benchmark mean values was assessed using results from codes like WIMS8A, HELIOS, TVS-M, MULTICELL and MCU.

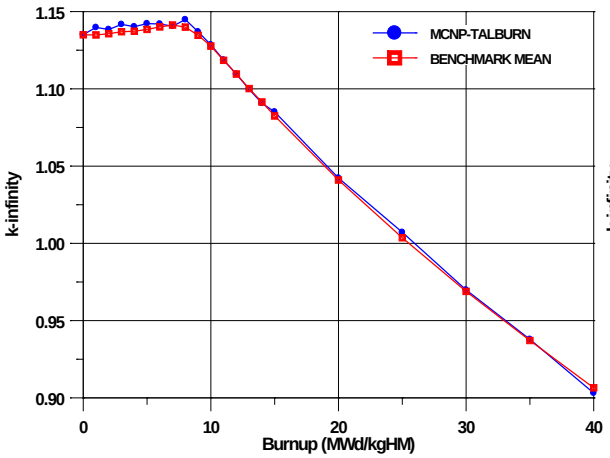


Fig.3: K-inf (vs) Burnup plot of LEU FA

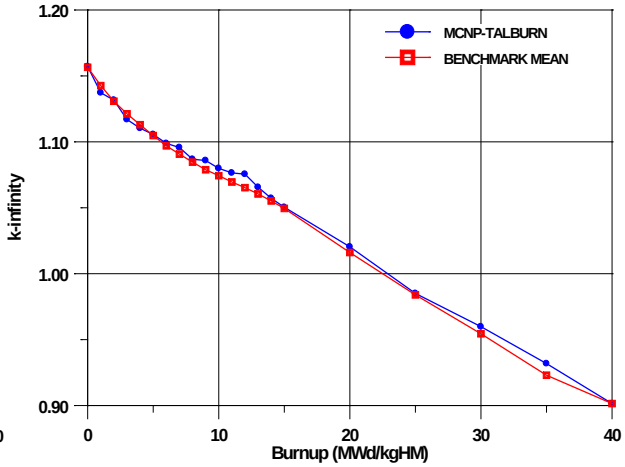


Fig4: K-inf (vs) Burnup plot of MOX FA

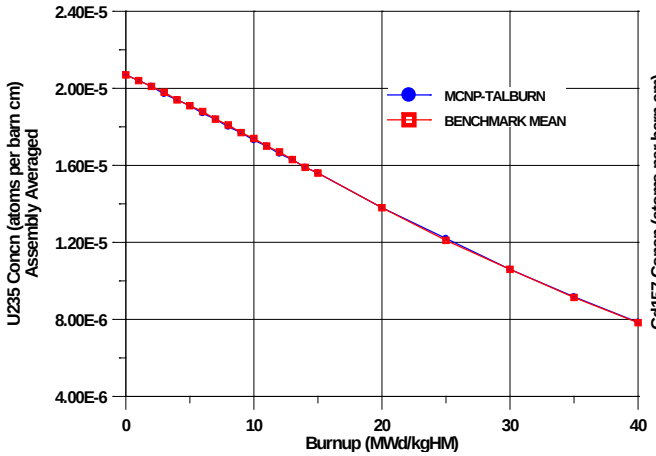


Fig.5. U-235 Ass. avg. Concentration vs Burnup of MOX FA

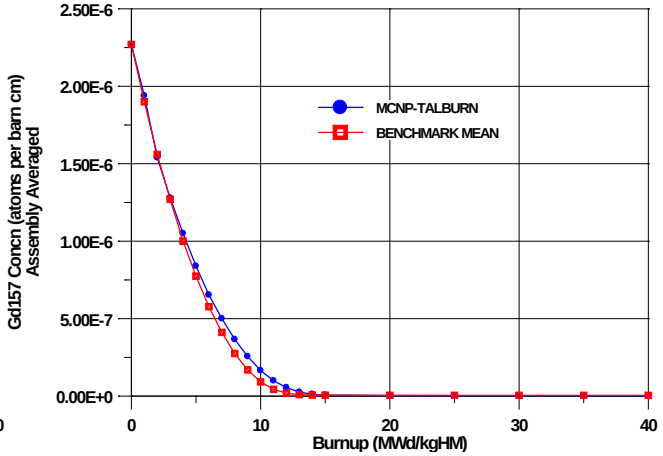


Fig.6. Gd -157 Ass. avg. Concentration vs Burnup of MOX FA

Table 1: k_∞ vs. Burn up data comparison of LEU FA & MOX FA (std deviation ±1.5 mk)

Burnup (MWd/kg)	LEU FA			MOX FA		
	k_∞*	$k_{\infty\,\#}$	Devn. (mk)	k_∞*	$k_{\infty\,\#}$	Devn. (mk)
0.0	1.13513	1.1350	0.10	1.15711	1.1566	0.38
10.0	1.12851	1.1277	0.64	1.07995	1.0744	4.78
20.0	1.04233	1.0410	1.23	1.02038	1.0160	4.22
30.0	0.96985	0.9689	1.01	0.95983	0.9544	5.93
40.0	0.90312	0.9065	-4.13	0.90146	0.9015	-0.05

*(MC- TALBURN) #Reference

Assembly averaged concentrations of few actinides and fission products are estimated up to 40.0 MWd/kg. Results are compared with benchmark mean concentrations and the maximum deviation is below 5.0% for all the nuclides.

3. Conclusions

Development and validation of a burn-up calculation code system MC-TALBURN is presented. The code processes and uses the reaction rate information from the output files of the Monte Carlo code and performs burnup calculation. TALBURN uses BDF based approach, which permits to increase time step size without loss of accuracy. Total 75 fission products and 33 actinides are considered for burnup calculation, which improves the accuracy of results. MC-TALBURN approach was validated by analysis of VVER-1000 LEU and MOX FA computational benchmark. For both LEU and MOX assemblies, the absolute error from the BM values for k_∞ is found to be within 6.0 mk (0.6 %) and relative deviation from the BM values for isotopic composition of considered isotopes is within 5% at the end of burn-up. In general MC-TALBURN code results show a good agreement with the reported results.

4. References

[1] Cetnar, J. et al., "User Manual for Monte-Carlo Continuous Energy Burnup (MCB) Code Version 1C"., *Royal Institute of Technology*, 2002, Stockholm, Sweden.

[2] Parma J. (Ed.), "BURNCAL: A nuclear Reactor Burnup code using MCNP Tallies". *Sandia National Laboratories*, SAND2002-3868 (November 2002).

[3] "A VVER-1000 LEU and MOX assembly computational benchmark", *Nuclear Science* (NEA/NSC/DOC (2002)10.

[4] S.P.Venkateshan, "Computational methods in Engineering" , *IIT Madras*,2014.

USE OF BOND ENERGY CLUSTERING ALGORITHM FOR OPTIMIZATION OF IN-CORE DETECTOR LOCATIONS IN AHWR

B. Anupreethi[1], Anurag Gupta[1,2], Umasankari Kannan[1,2] and Akhilanand Pati Tiwari[1,2]
[1] Homi Bhabha National Institute, Mumbai, India
[2] Bhabha Atomic Research Centre, Mumbai, India
[1]*e-mail: - anupreethi@barc.gov.in/preethianu90@gmail.com*

Abstract

Measurements from in-core detectors serve as input to the neutron flux monitoring system. In large reactors such as Advanced Heavy Water Reactor (AHWR), for effective neutron flux reconstruction, the in-core detectors are required to be placed at optimum locations as placement at all locations in the reactor core is not practically feasible. This paper is an attempt to solve the optimization problem of in-core detector placement in AHWR using a clustering technique, particularly, the Bond Energy Clustering Algorithm (BEA). BEA has been applied to the in-core detector measurements and the in-core detectors are grouped as clusters based on the correlation. One or few detectors from each cluster can be chosen as optimal locations after inspection. It has been inferred that the higher the uncorrelation among detectors, the higher the number of optimal detectors. The final placement is dependent on the initial choice of detector arrangement and the correlation threshold applied. Finally, these in-core detector locations have been validated using the flux synthesis method for a few reactor operational scenarios.

1. Introduction

The large neutronic dimensions in AHWR results in neutronic decoupling between regions in the core, requiring continuous monitoring. The objective of the paper is to optimize the in-core detector locations in the AHWR core which is one of the inputs to the neutron flux monitoring system. The Self-Powered Neutron Detectors (SPNDs) are distributed axially in In-Core Detector Housing (ICDH) units. Several evolutionary algorithms are available in the literature to address the optimization problem but they are dependent on the proper definition of the objective function. A data-driven approach, i.e., K-means clustering algorithm was applied to the in-core detector measurements of AHWR and it resulted in 168 SPNDs distributed in 28 ICDH units [1]. Literature also suggested the use of bond energy algorithm (BEA), another clustering technique used in LING AO reactor for the optimization of in-core detectors and other areas such as structural health monitoring, product design, development, etc [2]. An attempt has been made to solve the optimization problem using BEA in this paper. Similar to K-means clustering algorithm, BEA also works on the in-core detector measurements. This data-driven technique uses correlation as a parameter and computes bond energy among in-core detectors for grouping them as blocks of sub-matrices or clusters. The in-core detectors in each sub-matrix are strongly correlated and optimal in-core detector locations can be determined from the sub-matrices directly after inspection. The higher correlation value indicates greater redundancy, therefore, the selection of in-core detectors with minimal mutual information provides independent information.

2. Bond Energy Clustering

2.1 Algorithm

BEA clustering technique generally identifies the natural clusters present in the data and groups them based on the correlation. Fig. 1 provides the schematic representation of the process involved in the optimization. Initially, a Pearson correlation matrix is formed based on the in-core detector measurements. The values of the correlation matrix range from -1(no correlation) to +1(strong

correlation). A threshold is applied to filter the highly correlated in-core detectors. Now, the matrix element (d) with a value '1' indicates a strong correlation between the in-core detectors and a value '0' indicates the less or no correlation depending on the chosen threshold as shown in (1). This is the input to the clustering algorithm [3].

$$\begin{bmatrix} x_{1,1} & x_{1,2} \dots & x_{1,N_d} \\ x_{2,1} & x_{2,2} \dots & x_{2,N_d} \\ \vdots & \vdots & \vdots \\ x_{N_s,1} & x_{N_s,2} \dots & x_{N_s,N_d} \end{bmatrix} \rightarrow \begin{bmatrix} c_{1,1} & c_{1,2} & \dots & c_{1,N_d} \\ c_{2,1} & c_{2,2} & \dots & c_{2,N_d} \\ \vdots & \vdots & \dots & \vdots \\ c_{N_d,1} & c_{N,2} & \dots & c_{N_d,N_d} \end{bmatrix} \rightarrow \begin{bmatrix} d_{1,1} & d_{1,2} \dots & d_{1,N_d} \\ d_{2,1} & d_{2,2} \dots & d_{2,N_d} \\ \vdots & \vdots & \vdots \\ d_{N_d,1} & d_{N_d,2} \dots & d_{N_d,N_d} \end{bmatrix} \quad (1)$$

In-core detector measurements (x) — # flux shapes N_s × # Detectors N_d

Correlation matrix (c) — Pearson correlation

After application of a threshold — $d_{ij} = 1$ if $|c_{ij}| \geq \delta$; 0 otherwise

The procedure of the clustering algorithm is as follows: A row 'h' is chosen at first and the bond energy (E) between that row and the remaining rows is computed using (2).

$$E_{h,h+i}^{(r)} = \sum_{k=1}^{N_d} d_{h,k}.d_{h+i,k} \quad (2)$$

The row which has the highest bond energy with the row 'h' is moved to the position next to row 'h' and the same procedure is repeated for the remaining rows. Post this, column rearrangement is performed in the same way, however, it is not required if the matrix with 'd's is symmetric. The final transformed matrix contains several diagonal sub-matrices, from which the optimized locations are chosen. Fig. 1 shows an example of the correlation matrix, clustered SPND matrix with rearranged rows and columns after application of BEA, and the next step, i.e., the selection of in-core detector locations from these clusters. Finally, the chosen locations are validated by performing flux reconstruction for a few reactor operational scenarios.

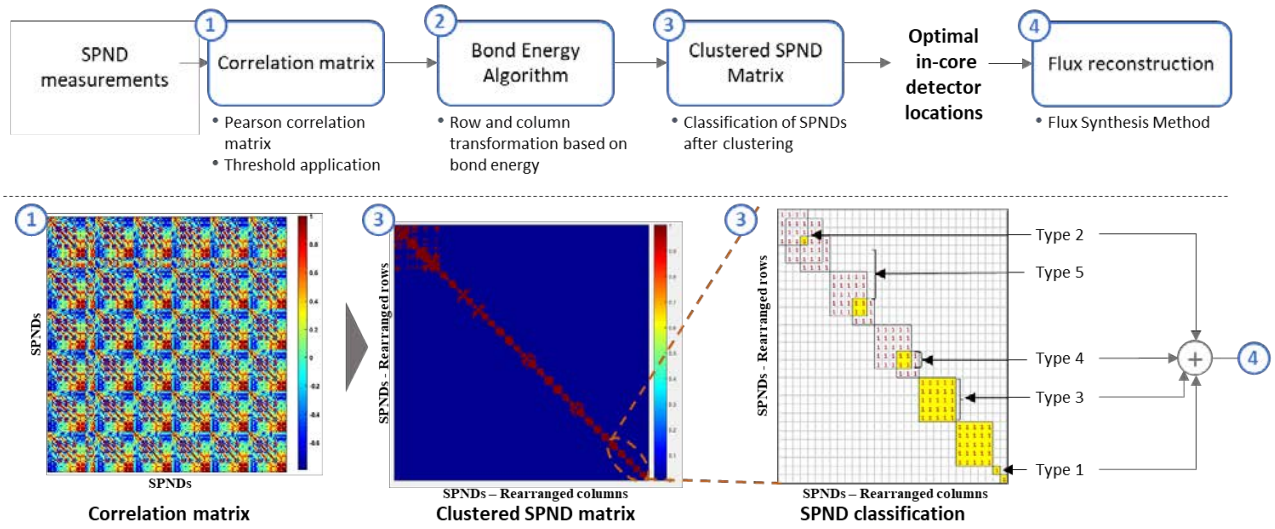


Figure 1 Schematic representation of the flow of BEA

Generally, the detectors are classified into five types as shown in Fig. 1. If there is only one element in the sub-matrix, it is classified as a type 1 detector. If there is only one element overlapping two or more sub-matrices, they are classified as type 2 detectors. If there are more than one element in the sub-matrix and no elements of this sub-matrix belong to others, then they are type 3 detectors. If more elements are overlapping two or more sub-matrices, the intersection elements are classified as type 4 detectors. The elements that do not belong to any of these four types are termed type 5 detectors. Type

1 and type 2 detectors directly qualify as the optimal locations whereas a combination of type 3 and type 4 detectors are chosen based on the average correlation degree for all potential combinations as given in [2-3]. Since type 5 detectors are correlated either with type 3 or 4, they can be neglected. Finally, the locations are further verified whether they are a subset of the other chosen locations, and such locations are not included in the final placement.

2.2 Application of BEA to AHWR

As a preliminary study, this BEA technique has been applied to the already existing 200 SPNDs distributed in 32 ICDH units in AHWR and the optimization of in-core detectors has been attempted. It was found that with a correlation threshold of 0.975, the number of SPNDs was reduced to 59 from 200 [4]. In this placement of 59 SPNDs, some of the ICDH units had only 1 or 2 SPNDs. This has not served our purpose of minimizing ICDH units. Therefore, a systematic procedure for the placement of in-core detector locations in AHWR using BEA has been attempted. Few design considerations such as the initial placement of 104 ICDH units with 6 SPNDs in each unit (Fig. 2(a) and (b)), multi-plane optimization, superimposing the locations from multiple axial planes for final selection, and application of geometrical limitations are the same as the procedure described in [1] for *K*-means clustering algorithm. These two algorithms differ in the way that the correlation parameter and the procedure to select the optimal locations are handled.

BEA algorithm was applied to the in-core detector measurements of 104 in-core detectors placed in each of the six axial layers separately, i.e., multi-plane optimization. A series of thresholds (δ) ranging from 0.5 to 0.975 has been applied to separate the strongly correlated SPNDs. For this paper, a threshold that is in the strong correlation category, i.e., 0.8 is chosen. BEA is applied and the optimal locations in each axial plane are identified based on types as shown in Fig. 1. The final optimal layout after superimposing the locations from six axial planes consists of 44 ICDH units with 6 SPNDs in each ICDH unit (Fig. 2(c)), giving a total of 264 SPNDs as against 168 SPNDs obtained from *K*-means clustering algorithm.

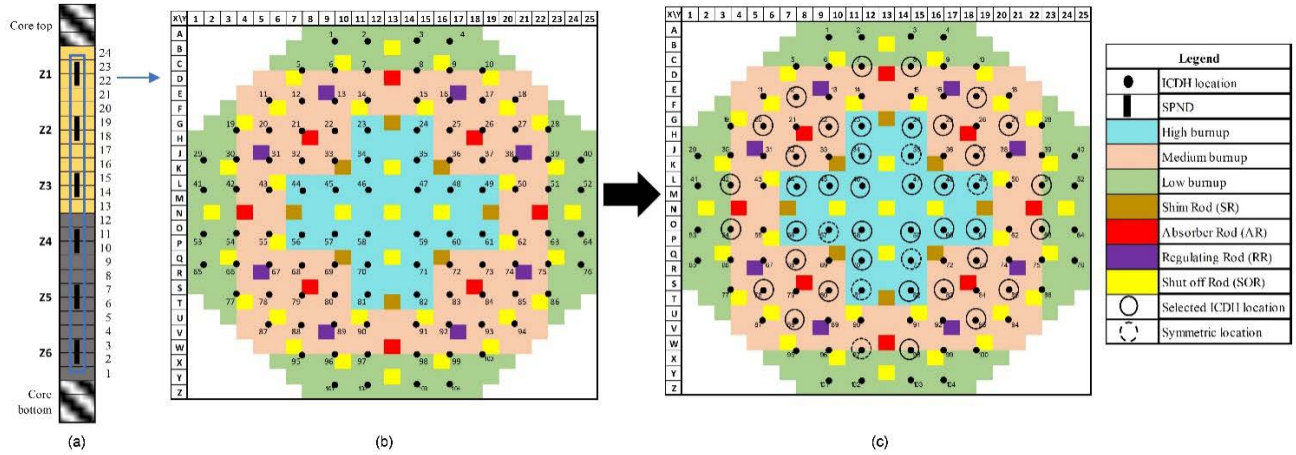


Figure 2 AHWR core layout – (a) axial distribution of SPNDs (b) cross-sectional view of an axial layer considered for multi-plane optimization (c) Optimized in-core detector housing units layout – after superimposing the locations from all 6 axial layers and applying limitations

2.3 Validation of the optimal in-core detector locations using flux reconstruction

The optimal locations need to be validated for their use in monitoring. This is done by studying their performance in flux reconstruction for a few steady-state reactor operational scenarios such as refuelling of a coolant channel H-15 and movement of 4 regulating rods at 100% out position. The flux

reconstruction has been carried out using the flux synthesis method which uses eigenmodes of the reactor reference configuration and the in-core detector measurements [5]. Root-mean-square (RMS) error in mesh flux has been used as the performance measure. Flux reconstruction results of the initial 624 SPNDs, i.e., before optimization have been chosen as the reference for comparison. Fig. 3 shows the performance of 624, 264, and 168 SPNDs for the two scenarios considered. Overall, the RMS error is less than 10% and the error decreases with an increase in the addition of eigenmodes for flux reconstruction that saturates at around 35 eigenmodes. It can be inferred that the performance of 264 SPNDs obtained using BEA is similar to that of 168 SPNDs obtained from *K*-means clustering algorithm. As the optimization aims to have a minimum number of ICDH units for installations, the bond energy algorithm and technique to choose the optimal locations could be further improved.

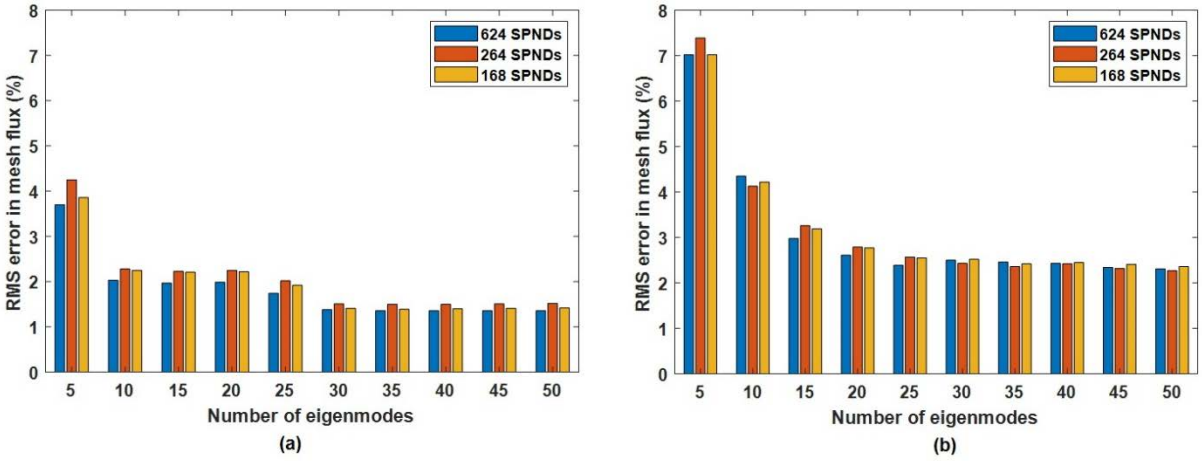


Figure 3 Flux reconstruction using flux synthesis method – (a) refuelling of a coolant channel (b) Movement of 4 RRs (2, 4, 6, and 8) 100% out

3. Conclusion

Using BEA, the initial 104 ICDH units have been reduced to 44 ICDH units for the correlation threshold of 0.8. Optimization using BEA mainly depends on the choice of the initial set of SPND locations and the correlation threshold. The BEA technique presented in the paper was helpful in the identification of clustering methodology suited for optimization of in-core detector locations in AHWR. Performance analysis of the AHWR flux mapping system with these 44 ICDH units for transient reactor conditions can be carried out and the improvement of the procedure of the BEA could be explored. Further studies on the identification of redundant detector locations will be helpful.

4. References

[1] B. Anupreethi, A. Gupta, U. Kannan, and A. P. Tiwari, “Optimization of flux mapping in-core detector locations in AHWR using clustering approach,” Nucl. Eng. Des., vol. 366, no. 110756, 2020.

[2] W. Li et al., “Comparison of three methodologies for optimization of the layout of in-core detectors with a specific number of detectors,” Ann. Nucl. Energy, vol. 126, pp. 359–366, 2019.

[3] W. Lu, R. Wen, J. Teng, X. Li, and C. Li, “Data correlation analysis for optimal sensor placement using a bond energy algorithm,” Meas. J. Int. Meas. Confed., vol. 91, pp. 509–518, 2016.

[4] B. Anupreethi, A. Gupta, U. Kannan, and A. P. Tiwari, “Optimization of In-Core Detector Locations in AHWR Using Bond Energy Algorithm,” in Proceedings of the 2020 International Conference on Nuclear Engineering collocated with the ASME 2020 Power Conference, Virtual, Online: ASME, 2020.

[5] B. Anupreethi, A. Gupta, U. Kannan, and A. P. Tiwari, “Computation of Higher Eigenmodes Using Subspace Iteration Scheme and Its Application to Flux Mapping System of AHWR,” in Proceedings of the 7th International Conference on Advances in Energy Research. Springer Proceedings in Energy, M. Bose and A. Modi, Eds. Singapore: Springer Singapore, 2021, pp. 349–357.

A FINITE VOLUME METHOD BASED MULTI-GROUP NEUTRON DIFFUSION MODEL FOR CRITICALITY PROBLEMS IN 2D R-Z GEOMETRY

R. Kondala Rao1[1], P. Mangarjuna Rao 2[2], K. Natesan 3[2] and S. Raghupathy 4[2]

[1] Indira Gandhi Centre for Atomic Research, A CI of Homi Bhabha National Institute, Kalpakkam 603102, Tamilnadu, India

[2] Reactor Design and Technology Group, Indira Gandhi Centre for Atomic Research, Kalpakkam 603102, Tamilnadu, India

[1]*e-mail: - rkrao@igcar.gov.in*

Abstract

A multi-group neutron diffusion model based on finite volume method has been developed for solving the steady state neutron diffusion equation in cylindrical axi-symmetric geometry. A computer code named MANDIR-CRZ has been developed and employed to evaluate multiplication factor (k_{eff}) and neutron flux distributions for two benchmark problems. The details of the numerical model and the code results for benchmark problems are presented.

1. Introduction

Numerical solutions of the multi-group neutron diffusion equations in cylindrical geometry are essential for the safety analysis of core disruptive accident in a fast breeder reactor (FBR) [1]. A multi-group neutron diffusion model has been developed for solving the steady state neutron diffusion equation in cylindrical axi-symmetric geometry. Finite volume method is used for the spatial discretization. Both up-scattering and down-scattering of neutrons is considered in multi-group energy formulation. Gauss-Seidel iterative method is employed for solving the resultant algebraic equations. A computer code named MANDIR-CRZ (Multigroup Analysis of Neutron DIffusion in Reactor for Cylindrical R-Z geometry) has been developed and is employed to reconstruct the neutron flux and k_{eff} results for two benchmark problems. The details of numerical model and results for benchmark problems are discussed in the following sections.

2. Description of the model

The steady state multi-group neutron diffusion equations for 2D axi-symmetric geometry is

$$\nabla.\left[D_g(r,z)\nabla\Phi_g(r,z)\right]+Q_g(r,z)=0 \quad (1)$$

where all the symbols have their usual meaning [2] and

$$Q_g=-\Sigma_{a,g}(\vec{r},z)\Phi_g(r,z)-\sum_{g'=1}^{G}\Sigma_{s,g,g'}(r,z)\Phi_g(r,z)+\sum_{g'=1}^{G}\Sigma_{s,g',g}(r,z)\Phi_{g'}(r,z)+\frac{\chi_g(r,z)}{k_{eff}}\sum_{g'=1}^{G}\nu\Sigma_{f,g'}(r,z)\Phi_{g'}(r,z) \quad (2)$$

The actual 3D cylindrical problem is reduced to 2D axisymmetric (r-z) problem if the geometry and boundary conditions follow azimuthal symmetry as shown in Figure 1. The integration of eq. (1) over control volume gives

$$\int_V \nabla.\left[D_g(r,z)\nabla\Phi_g(r,z)\right]dV+\int_V Q_g(r,z)dV=0 \quad (3)$$

The differential volume of each CV is $dV = 2\pi r.dr.dz$.

Applying Gauss-Divergence theorem to the diffusion term in eq. (3) and approximating the surface integral as the product of face center value and surface area of face [3], we get

$$\int_V \nabla.\left[D_g(r,z)\nabla\Phi_g(r,z)\right]dV=\int_S D_g(r,z)\nabla\Phi_g(r,z).\hat{n}dS=\sum_{f=1}^{N_f}\left(D_g(r,z)\right)_f\left(\nabla\Phi_g(r,z)\right)_f.\hat{n}_f\Delta A_f \quad (4)$$

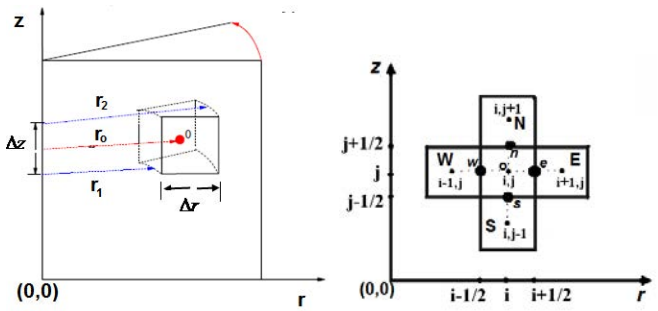


Figure 1 Depiction of control volume for cylindrical r-z geometry

where N_f is total number of faces of the CV and $\hat{n}_f$ is unit normal vector at face centre. The index *f* represents the face number. The gradient of flux in cylindrical *r-z* system is

$$\nabla\Phi_g(r,z)=\frac{\partial\Phi_g}{\partial r}\hat{r}+\frac{\partial\Phi_g}{\partial z}\hat{z} \tag{5}$$

For orthogonal mesh, the product of unit normal vectors with unit vectors of coordinates and surface areas of each face are as follows.

$$\left.\begin{array}{l}\text{For east face } \hat{r}_e.\hat{n}_f=1,\ \hat{z}_e.\hat{n}_f=0 \text{ and } \Delta A_e=2\pi r_e.\Delta z\\ \text{For west face } \hat{r}_w.\hat{n}_f=-1,\ \hat{z}_w.\hat{n}_f=0 \text{ and } \Delta A_w=2\pi r_w.\Delta z\\ \text{For north face } \hat{r}_n.\hat{n}_f=0,\ \hat{z}_n.\hat{n}_f=1 \text{ and } \Delta A_n=\pi\left(r_e^2-r_w^2\right)\\ \text{For south face } \hat{r}_s.\hat{n}_f=0,\ \hat{z}_s.\hat{n}_f=-1 \text{ and } \Delta A_s=\pi\left(r_e^2-r_w^2\right)\end{array}\right\} \tag{6}$$

The volume integral of source term is approximated as follows.

$$\int_V Q_g(r,z).dV=\int_r\int_z Q_g(r,z).2\pi r.dr.dz=2\pi Q_o\int_r r dr\int_z dz=\pi Q_o.\left(r_e^2-r_w^2\right).\Delta z \tag{7}$$

Where Δz is the width of the CV in *z*-direction. Q_o is the average value of source term in the CV. Substitute eqs. (4) – (7) in eq. (3) to derive the expression

$$\left[\left(rD_g\frac{\partial\Phi_g}{\partial r}\right)_e-\left(rD_g\frac{\partial\Phi_g}{\partial r}\right)_w\right].\Delta z+\left[\left(D_g\frac{\partial\Phi_g}{\partial z}\right)_n-\left(D_g\frac{\partial\Phi_g}{\partial z}\right)_s.\frac{\left(r_e^2-r_w^2\right)}{2}\right]+Q_o.\frac{\left(r_e^2-r_w^2\right)\Delta z}{2}=0 \tag{8}$$

For internal CVs, the effective diffusion coefficient values at face centres are approximated using **inverse distance-weighted harmonic mean** [3] of the two neighbouring cell-centre values. The flux gradients at the face centre are approximated using **central differencing scheme** [3]. For boundary cells, the expressions for flux gradients and effective diffusion coefficient are derived in terms of neighbouring cell centre values close to the boundary face using **Taylor's series approximation** [3]. The expressions derived for the effective diffusion coefficients and flux gradients at boundary faces are given below.

$$\left.\begin{array}{l}\text{At } r=0,\ \left(D_g\right)_w=\dfrac{3D_{g,1,j}-.D_{g,2,j}}{2},\ \left(\dfrac{\partial\Phi_g}{\partial r}\right)_w=\dfrac{\left(9\Phi_{g,1,j}-\Phi_{g,2,j}-8\Phi_{g,r=o,j}\right)}{3\left(\Delta r_{1,j}\right)}\\ \text{At } r=R,\ \left(D_g\right)_e=\dfrac{3D_{g,M,j}-.D_{g,M-1,j}}{2},\ \left(\dfrac{\partial\Phi_g}{\partial r}\right)_e=\dfrac{\left(-9\Phi_{g,M,j}+\Phi_{g,M-1,j}+8\Phi_{g,r=R,j}\right)}{3\left(\Delta r_{M,j}\right)}\\ \text{t } z=0,\ \left(D_g\right)_s=\dfrac{3D_{g,i,1}-.D_{g,i,2}}{2},\ \left(\dfrac{\partial\Phi_g}{\partial r}\right)_s=\dfrac{\left(9\Phi_{g,i,1}-\Phi_{g,i,2}-8\Phi_{g,i,z=o}\right)}{3\left(\Delta z_{i,1}\right)}\\ \text{At } z=H,\ \left(D_g\right)_n=\dfrac{3D_{g,i,N}-.D_{g,i,N-1}}{2},\ \left(\dfrac{\partial\Phi_g}{\partial r}\right)_n=\dfrac{\left(-9\Phi_{g,i,N}+\Phi_{g,i,N-1}+8\Phi_{g,i,z=H}\right)}{3\left(\Delta z_{i,N}\right)}\end{array}\right\} \tag{9}$$

The code employs the power iteration method [4] for outer iteration and the Gauss Seidel [3] iteration method for inner iteration.

3. Results and discussion

3.1 FBR 2-group problem

The benchmark problem represents the simplified form of the SNR-300 fast reactor [5]. The k_{eff} value predicted by the code approaches the reference value as the mesh number increases as shown in Table 1. The neutron fluxes at z=88.25 cm along the radial direction are compared with the reference [5] values in Figures 3a and 3b respectively. The code predicted neutron flux distributions are in good agreement with the reference results.

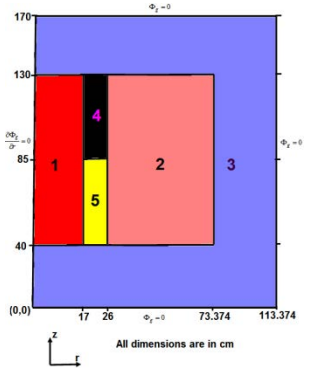
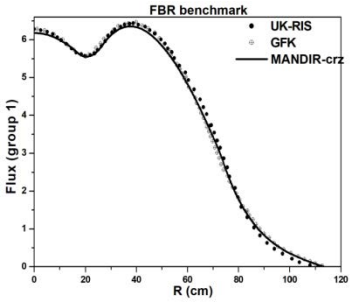


Figure 2 FBR benchmark problem

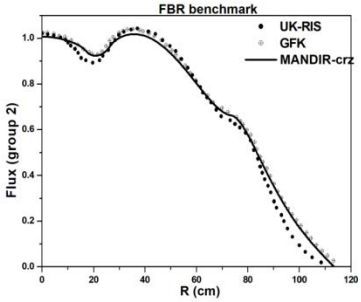
Table 1 k_{eff} values for the FBR benchmark

S.No.	Number of meshes	k_{eff}
1	100 x 100	0.99833
2	200 x 200	0.99869
3	400 x 400	0.99954

*Reference [5] k_{eff} value: 1.00000



(a) Group 1



(b) Group 2

Figure 3 Comparison of neutron fluxes at z=88.25 cm for FBR 2-group benchmark problem

3.2. Dodd's benchmark problem

The Dodds' problem is a simplified R-Z geometry two-group model of a plutonium/tritium production reactor [6]. This model consists of seven fuel materials and two axial reflector regions as shown in Figure 4. The k_{eff} values calculated by the code approaches the reference [6] value (0.867053) with the increase in number of meshes as shown in Table 2. The neutron fluxes at core mid plane along the radial direction are compared with the reference [6] values in Figures 5a and 5b respectively. The code predicted neutron flux distributions are in reasonable agreement with the reference results.

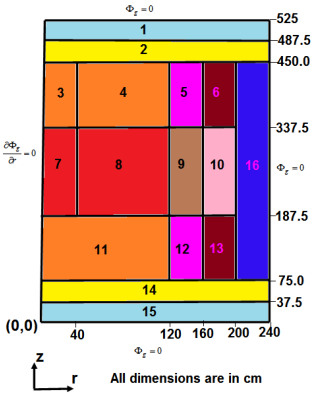
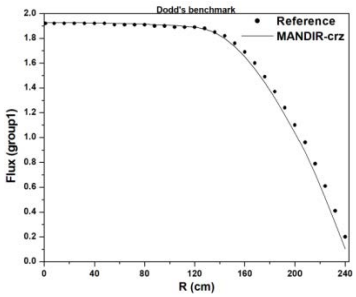


Figure 4 Dodd's benchmark problem

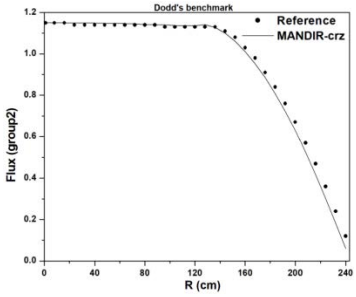
Table 2 k_{eff} values for the Dodd's benchmark

S.No.	Number of meshes	k_{eff}
1	24 x 42	0.867472
2	48 x 84	0.867249
3	120 x 210	0.867182
4	240 x 420	0.867153
5	480 x 700	0.867086

*Reference [6] k_{eff} value: 0.867053



5(a) Group 1



5(b) Group 2

Figure 5 Comparison of neutron fluxes at z=262.5 cm for Dodd's benchmark problem

4. Conclusion

A computer code named MANDIR-CRZ has been developed for solving multi-group neutron diffusion equation in cylindrical axi-symmetric geometry. The code has been validated using the FBR 2-group and Dodd's benchmark problem results.

5. References

[1] A.E. Waltar and A.B. Reynolds, " Fast Breeder Reactors", Pergamon press, 1981.

[2] J.J. Duderstadt and L.J. Hamilton, "Nuclear Reactor Analysis", *John Wiley and Sons*, 1976**.**

[3] S. Mazumdar, "Numerical Methods for Partial Differential Equations Finite Difference and Finite Volume Methods", *Elsevier*, 2016**.**

[4] E.E. Lewis and W. F.Miller, "Computational Methods of Neutron Transport", *John Wiley & Sons*, 1984.

[5] A. Buffoni, J.K. Fletcher, A. Galati, F.N. McDonnell, A. Musco and L. Vath, "Survey of the results of a two-dimensional kinetic benchmark problem typical for a Fast Reactor", P*roceedings of the joint NEACRP/CSNI specialists meeting on new developments in three-dimensional neutron kinetics and review of kinetics benchmark calculation*, Garching,1975 Jan. 22-24.

[6] ANL-7416, Supplement 2, "Argonne Code Center: Benchmark Problem Book, Benchmark Problem ID.7-A2", *Argonne National Laboratory*, 1977.

Stability Analysis for Multi-group *k*-eigenvalue Iterations with Linear Prolongation CMFD Acceleration

Lakshay Jain[1,2], P. Mohanakrishnan[3], R. Karthikeyan[2] and Umasankari Kannan[1,2]

[1] Homi Bhabha National Institute, Mumbai, India

[2] Bhabha Atomic Research Centre, Mumbai, India

[3] Atomic Energy Regulatory Board, Mumbai, India

[1]*e-mail: - lakshay.jain@gmail.com*

Abstract

Fourier analysis has been used in this paper to investigate the convergence stability of linear prolongation coarse mesh finite difference (lpCMFD) accelerated multi-group *k*-eigenvalue calculations (hereafter referred to as *k*-lpCMFD). Being inherently non-linear, the iterative system is first linearized around the exact solution for a simplified infinite 1D homogeneous problem. The error iteration matrix subsequently obtained via multi-group Fourier analysis is then used to determine the theoretical spectral radius of the problem. The numerical spectral radius is found to be in excellent agreement with the theoretical predictions. The results complement existing one-group studies and provide improved understanding of the convergence behavior of *k*-lpCMFD.

1. Introduction

The linear prolongation coarse mesh finite difference (lpCMFD) method was recently proposed by Wang and Xiao for stabilization of conventional CMFD acceleration technique [1]. lpCMFD has been adopted in several neutron transport codes for acceleration of multi-group *k*-eigenvalue transport calculations (hereafter referred to as *k*-lpCMFD). However, the convergence behavior of *k*-lpCMFD has only been investigated for one-group problems [1, 2] despite its popular use in the multi-group form. Thus, the stability analysis of *k*-lpCMFD has been presented in this paper using multi-group Fourier analysis.

2. Theory and Formulation

2.1 Multi-group *k*-eigenvalue Iterations with lpCMFD Acceleration

The iterative discrete ordinates (S_N) form of the 1D multi-group *k*-eigenvalue transport equation, along the spatial discretization given in Figure 1, is shown in Eq. (1).

$$\frac{\mu_n}{h_j}\left(\psi_{n,j+\frac{1}{2}}^{(l+1/2,\varsigma)} - \psi_{n,j-\frac{1}{2}}^{(l+1/2,\varsigma)}\right) + \Sigma_{t,j}\Psi_{n,j}^{(l+1/2,\varsigma)} = \frac{1}{2}\left(\Sigma_{s,j}\phi_j^{(l+1/2,\varsigma-1)} + \lambda^{(l)}F_j\phi_j^{(l)}\right), \quad 0 < \varsigma \le \sigma \tag{1a}$$

$$\Psi_{n,j}^{(l+1/2,\varsigma)} = \frac{1}{2}(I+\alpha_{n,j})\psi_{n,j+\frac{1}{2}}^{(l+1/2,\varsigma)} + \frac{1}{2}(I-\alpha_{n,j})\psi_{n,j-\frac{1}{2}}^{(l+1/2,\varsigma)} \tag{1b}$$

$$\phi_j^{(l+1/2,\varsigma)} = \sum_{n=1}^{N} w_n \Psi_{n,j}^{(l+1/2,\varsigma)}, \quad \phi_j^{(l+1/2,0)} = \phi_j^{(l)} \tag{1c}$$

where μ_n, w_n, h_j and $\lambda\left(=1/k_{eff}\right)$ denote the directional cosine and weight, fine mesh width, and multiplication factor inverse, respectively. n, j, l, ς, N and σ represent the direction, fine mesh, outer and inner iteration indices, the number of directions and inner (scattering) sweeps per outer iteration, respectively. $\psi_{n,j\pm\frac{1}{2}}$, $\Psi_{n,j}$ and ϕ_j are $G \times 1$ sized vectors representing fine mesh boundary angular flux, centered angular flux and scalar flux, respectively. $\Sigma_{t,j}$, $\Sigma_{s,j}$ and F_j are $G \times G$ sized matrices representing total and scattering cross-sections, and fission operator, respectively. I and $\alpha_{n,j}$ are the identity and diagonal finite difference coefficient matrix of size $G \times G$, where the diagonal elements of latter are given by Eq. (2).

$$\alpha_{n,j,g} = \begin{cases} \coth\left(\frac{\Sigma_{t,j,g}h_j}{2\mu_n}\right) - \frac{2\mu_n}{\Sigma_{t,j,g}h_j}, & \text{Step characteristics (SC)} \\ 0, & \text{Diamond differencing (DD)} \end{cases} \tag{2}$$

where g is the energy group index. Similarly, the multi-group coarse mesh finite difference (CMFD) neutron balance equation can be expressed in matrix-vector notation shown in Eq. (3).

$$\frac{1}{h_k}\left(J_{k+\frac{1}{2}}^{(l+1,M)} - J_{k-\frac{1}{2}}^{(l+1,M)}\right) + \left(\Sigma_{t,k} - \Sigma_{s,k}\right)\Phi_k^{(l+1,M)} = \lambda^{(l+1,M-1)}F_k\phi_k^{(l+1,M-1)}, \ \lambda^{(l+1,0)} = \lambda^{(l)}, \ M > 0 \tag{3a}$$

$$J_{k\pm\frac{1}{2}}^{(l+1,M)} = \mp\bar{D}_{k\pm\frac{1}{2}}^{(l+1/2)}\left(\Phi_{k\pm1}^{(l+1,M)} - \Phi_{k}^{(l+1,M)}\right) + \hat{D}_{k\pm\frac{1}{2}}^{(l+1/2)}\left(\Phi_{k\pm1}^{(l+1,M)} + \Phi_{k}^{(l+1,M)}\right),\ M > 0 \tag{3b}$$

where h_k and k represent the coarse mesh width and index, respectively while M is the CMFD inner iteration index. $J_{k\pm\frac{1}{2}}$ and Φ_k denote the homogenized coarse mesh boundary current and scalar flux vectors, respectively. $\Sigma_{t,k}$, $\Sigma_{s,k}$ and F_k represent the homogenized coarse mesh total and scattering cross-section, and fission operator, respectively. $\bar{D}_{k+\frac{1}{2}}$ and $\hat{D}_{k+\frac{1}{2}}$ are diagonal operators (given by Eqs. (4) and (5)) representing the coarse mesh boundary diffusion coefficient and drift-diffusion coefficient, respectively.

$$\bar{D}_{k+\frac{1}{2}} = 2(h_{k+1}D_k + h_k D_{k+1})^{-1} D_{k+1} D_k\ , \qquad D_k = \frac{1}{3}{\Sigma_{t,k}}^{-1} \tag{4}$$

$$\hat{D}_{k+\frac{1}{2},g}^{(l+1/2)} = \frac{J_{k+\frac{1}{2},g}^{(l+1/2)} + \bar{D}_{k+\frac{1}{2},g}^{(l+1/2)}\left(\Phi_{k+1,g}^{(l+1/2)} - \Phi_{k,g}^{(l+1/2)}\right)}{\Phi_{k+1,g}^{(l+1/2)} + \Phi_{k,g}^{(l+1/2)}},\quad J_{k+\frac{1}{2}}^{(l+1/2)} = J_{k+\frac{1}{2}}^{(l+1/2,\sigma)},\ \Phi_{k+1}^{(l+1/2)} = \Phi_{k+1}^{(l+1/2,\sigma)} \tag{5}$$

lpCMFD is different from CMFD only *w.r.t.* the flux update. While a flat ratio based fine mesh flux update (given by Eq. (6)) is used in CMFD, lpCMFD uses the flux update shown in Eq. (7).

$$\phi_{j,g}^{(l+1)} = \frac{\Phi_{k,g}^{(l+1)}}{\Phi_{k,g}^{(l+1/2)}}\phi_{j,g}^{(l+1/2)},\ \ j \in k \tag{6}$$

$$\begin{aligned}
\phi_{j,g}^{(l+1)} &= \phi_{j,g}^{(l+1/2)} + \delta\phi_{j,g}^{(l+1)} \\
\delta\phi_{j,g}^{(l+1)} &= \delta\Phi_{k-\frac{1}{2},g}^{(l+1)} + \frac{x_j - x_{k-\frac{1}{2}}}{h_k}\left(\delta\Phi_{k+\frac{1}{2},g}^{(l+1)} - \delta\Phi_{k-\frac{1}{2},g}^{(l+1)}\right) \qquad , \qquad j \in k \\
\delta\Phi_{k\pm\frac{1}{2},g}^{(l+1)} &= \frac{1}{2}\left[\left(\Phi_{k\pm1,g}^{(l+1)} - \Phi_{k\pm1,g}^{(l+1/2)}\right) + \left(\Phi_{k,g}^{(l+1)} - \Phi_{k,g}^{(l+1/2)}\right)\right]
\end{aligned} \tag{7}$$

2.2 Linearization

As mentioned earlier, the *k*-lpCMFD is inherently non-linear and must be linearized prior to carrying out its Fourier analysis. This is done by expanding the iterative terms around the exact solution considering only the zeroth $\left(O(\phi_0)\right)$, first $\left(O(\varepsilon)\right)$ and higher order $\left(O(\varepsilon^2)\right)$ error terms. An infinite homogeneous medium problem discretized into J uniform fine and K uniform coarse meshes (with size h and H, respectively) is considered to simplify the subsequent linearization and Fourier analysis. Each coarse mesh consists of p uniform fine cells and periodic boundary conditions are applied on both edges. The model problem has a group-wise flat flux solution. Let the solution after l iterations, expressed as a function of error around the true solution, be given by Eq. (8) where the iteration index has been omitted for brevity.

$$\phi_j = \phi_0 + \varepsilon\tilde{\phi}_j + O(\varepsilon^2) \tag{8a}$$

$$\psi_{n,j\pm\frac{1}{2}} = \frac{1}{2}\phi_0 + \varepsilon\tilde{\psi}_{n,j\pm\frac{1}{2}} + O(\varepsilon^2) \tag{8b}$$

$$\Psi_{n,j} = \frac{1}{2}\phi_0 + \varepsilon\tilde{\Psi}_{n,j} + O(\varepsilon^2) \tag{8c}$$

$$\lambda = \lambda_0 + \varepsilon\tilde{\lambda} + O(\varepsilon^2),\ \lambda_0 = \frac{\underline{\mathbf{1}}^T(\Sigma_t - \Sigma_s)\phi_0}{(\upsilon\Sigma_f)\phi_0} \tag{8d}$$

$$J_{k\pm\frac{1}{2}} = \underline{\mathbf{0}} + \varepsilon\tilde{J}_{k\pm\frac{1}{2}} + O(\varepsilon^2) \tag{8e}$$

$$\Phi_k = \phi_0 + \varepsilon\tilde{\Phi}_k + O(\varepsilon^2) \tag{8f}$$

$$\hat{D}_{k\pm\frac{1}{2}} = \underline{\underline{\mathbf{0}}} + \varepsilon\tilde{D}_{k\pm\frac{1}{2}} + O(\varepsilon^2) \tag{8g}$$

$$\delta\phi_j = \underline{\mathbf{0}} + \varepsilon\delta\tilde{\phi}_j + O(\varepsilon^2),\quad \delta\Phi_{k\pm\frac{1}{2}} = \underline{\mathbf{0}} + \varepsilon\delta\tilde{\Phi}_{k\pm\frac{1}{2}} + O(\varepsilon^2) \tag{8h}$$

where the error quantities corresponding to the first order error are denoted by tilde $\left(\tilde{\ }\right)$ notation. $\underline{\mathbf{1}}$, $\underline{\mathbf{0}}$ and $\underline{\underline{\mathbf{0}}}$ denote the unit and null vectors (size $G \times 1$), and the null matrix (size $G \times G$), respectively, and $\varepsilon \ll 1$. Substituting Eq. (8) in Eqs. (1), (3), (5) and (7), the $O(\phi_0)$ terms cancel out. Neglecting the $O(\varepsilon^2)$ terms yields the linearized form of *k*-lpCMFD containing only the $O(\varepsilon)$ terms, as

shown in Eqs. (9) to (12). It can be shown that the error in eigenvalue (but not the eigenfunction) reduces to zero after a single *k*-lpCMFD iteration, *i.e.*, $\tilde{\lambda}^{(l)} = 0$.

$$\frac{\mu_n}{h}\left(\tilde{\psi}^{(l+1/2,\varsigma)}_{n,j+\frac{1}{2}} - \tilde{\psi}^{(l+1/2,\varsigma)}_{n,j-\frac{1}{2}}\right) + \Sigma_t \widetilde{\Psi}^{(l+1/2,\varsigma)}_{n,j} = \frac{1}{2}\Sigma_s \tilde{\phi}^{(l+1/2,\varsigma-1)}_j + \frac{\lambda_0}{2} F\tilde{\phi}^{(l)}_j + \frac{\tilde{\lambda}^{(l)}}{2} F\phi_0,\ 0 < \varsigma \le \sigma \tag{9a}$$

$$\widetilde{\Psi}^{(l+1/2,\varsigma)}_{n,j} = \frac{1}{2}(I+\alpha_n)\tilde{\psi}^{(l+1/2,\varsigma)}_{n,j+\frac{1}{2}} + \frac{1}{2}(I-\alpha_n)\tilde{\psi}^{(l+1/2,\varsigma)}_{n,j-\frac{1}{2}} \tag{9b}$$

$$\tilde{\phi}^{(l+1/2,\varsigma)}_j = \sum_{n=1}^{N} w_n\, \widetilde{\Psi}^{(l+1/2,\varsigma)}_{n,j},\ \tilde{\phi}^{(l+1/2,0)}_j = \tilde{\phi}^{(l)}_j \tag{9c}$$

$$\widetilde{D}^{(l+1/2)}_{k\pm\frac{1}{2}}\phi_0 = \frac{1}{2}\left[\tilde{J}^{(l+1/2)}_{k\pm\frac{1}{2}} \pm \bar{D}\left(\widetilde{\Phi}^{(l+1/2)}_{k\pm1} - \widetilde{\Phi}^{(l+1/2)}_{k}\right)\right],\quad D = \frac{1}{3H}{\Sigma_t}^{-1} \tag{10}$$

$$\tilde{J}^{(l+1)}_{k\pm\frac{1}{2}} - \tilde{J}^{(l+1/2)}_{k\pm\frac{1}{2}} = \mp\bar{D}\left[\left(\widetilde{\Phi}^{(l+1)}_{k\pm1} - \widetilde{\Phi}^{(l+1/2)}_{k\pm1}\right) - \left(\widetilde{\Phi}^{(l+1)}_{k} - \widetilde{\Phi}^{(l+1/2)}_{k}\right)\right] \tag{11}$$

$$\tilde{\phi}^{(l+1)}_j = \tilde{\phi}^{(l+1/2)}_j + \delta\tilde{\phi}^{(l+1)}_j,\ \delta\tilde{\phi}^{(l+1)}_j = \delta\widetilde{\Phi}^{(l+1)}_{k-\frac{1}{2}} + \frac{x_j - x_{k-\frac{1}{2}}}{h_k}\left(\delta\widetilde{\Phi}^{(l+1)}_{k+\frac{1}{2},g} - \delta\widetilde{\Phi}^{(l+1)}_{k-\frac{1}{2},g}\right),\ j \in k \tag{12}$$

2.3 Fourier Analysis

The $O(\varepsilon)$ terms are expressed using the Fourier ansatz defined in Eq. (13), which are a function of the error mode frequency (θ). Only errors with frequency $\theta_m = \frac{2\pi m}{ph\Sigma_{t,g}K}, (m = 1,2,\dots,K-1)$ can exist within the system due to the presence of periodic boundary conditions.

$$\tilde{\phi}^{(l+1/2,0)}_j = \tilde{\phi}^{(l,0)}_j = \tilde{\phi}^{(l)}_j = \omega^l e^{i\theta x_k \Sigma_t} r_j \tag{13a}$$

$$\tilde{\psi}^{(l+1/2,\varsigma)}_{n,j-\frac{1}{2}} = \omega^l e^{i\theta x_k \Sigma_t} a_{n,j} \tag{13b}$$

$$\widetilde{\Psi}^{(l+1/2,\varsigma)}_{n,j} = \omega^l e^{i\theta x_k \Sigma_t} b_{n,j} \tag{13c}$$

$$\widetilde{\Phi}^{(l+1/2)}_{k} = \omega^l e^{i\theta x_k \Sigma_t} R \tag{13d}$$

$$\widetilde{\Phi}^{(l+1)}_{k} - \widetilde{\Phi}^{(l+1/2)}_{k} = \omega^l e^{i\theta x_k \Sigma_t} Y \tag{13e}$$

where, $a_{n,j}$, $b_{n,j}$, r_j, R and Y are vectors of size $G \times 1$ whose elements are arbitrary constants and ω represents the error decay/growth factor. The outer (eigenvalue) iteration consisting of ς inner (scattering) sweeps can be obtained by substituting Eq. (13) in Eq. (9), as given in Eq. (14).

$$\tilde{\phi}^{(l+1/2,\varsigma)} = \widetilde{\boldsymbol{H}}^{(\varsigma)}\tilde{\phi}^{(l)},\quad \widetilde{\boldsymbol{H}}^{(\varsigma)} = \boldsymbol{U}^{\varsigma} + (\boldsymbol{U}-I)^{-1}(\boldsymbol{U}^{\varsigma}-I)\boldsymbol{U}\boldsymbol{S}^{-1}(\boldsymbol{T}-\boldsymbol{S}) \tag{14}$$

where $\boldsymbol{U} = \frac{1}{2}\sum_{n=1}^{N} w_n \boldsymbol{A}_n \boldsymbol{B}_n^{-1}\boldsymbol{T}^{-1}\boldsymbol{S}$, $\boldsymbol{A}_n = \begin{bmatrix} \frac{1}{2}(I-\alpha_n) & \frac{1}{2}(I+\alpha_n) & \cdots & 0 \\ 0 & \frac{1}{2}(I-\alpha_n) & \ddots & \vdots \\ \vdots & \ddots & \ddots & \frac{1}{2}(I+\alpha_n) \\ \frac{1}{2}(I+\alpha_n)e^{i\theta ph\Sigma_t} & \cdots & 0 & \frac{1}{2}(I-\alpha_n) \end{bmatrix}$, $\boldsymbol{B}_n = \boldsymbol{A}_n + \frac{\mu_n}{h}\boldsymbol{T}^{-1}\begin{bmatrix} -I & I & \cdots & 0 \\ 0 & -I & \ddots & \vdots \\ \vdots & \ddots & \ddots & I \\ e^{i\theta ph\Sigma_t} & \cdots & 0 & -I \end{bmatrix}$, $\boldsymbol{T} = \begin{bmatrix} \Sigma_{t,1} & 0 & \cdots & 0 \\ 0 & \Sigma_{t,2} & \cdots & 0 \\ \vdots & \vdots & \ddots & \vdots \\ 0 & 0 & \cdots & \Sigma_{t,p} \end{bmatrix}$ and $\boldsymbol{S} = \begin{bmatrix} \Sigma_{s,1} & 0 & \cdots & 0 \\ 0 & \Sigma_{s,2} & \cdots & 0 \\ \vdots & \vdots & \ddots & \vdots \\ 0 & 0 & \cdots & \Sigma_{s,p} \end{bmatrix}$.

Substituting the Fourier ansatz given in Eq. (13) in Eqs. (11) and (12) and performing algebraic rearrangement, the fine mesh flux error update can be derived as given in Eq. (15).

$$\tilde{\phi}^{(l+1)} = \boldsymbol{M}\tilde{\phi}^{(l)},\quad \boldsymbol{M} = \widetilde{\boldsymbol{H}}^{(\sigma)}\tilde{\phi}^{(l)} + [\gamma_1\ \gamma_2\ \cdots\ \gamma_p]^T\left[2\bar{D}[I-\cos(\theta ph\Sigma_t)]\right]^{-1}\left(I - e^{i\theta ph\Sigma_t}\right)\widetilde{\boldsymbol{C}}^{(\sigma)} \tag{15}$$

where, $\widetilde{\boldsymbol{C}}^{(\sigma)} = \frac{1}{2}[I \quad 0 \quad \cdots \quad 0]_{1\times p} \sum_{n=1}^{N} \mu_n w_n \boldsymbol{B}_n^{-1} \widetilde{\boldsymbol{H}}^{(\sigma-1)}$ and $\gamma_j = \frac{2p-2j+1}{4p} e^{-i\theta ph\Sigma_t} + \frac{2j-1}{4p} e^{i\theta ph\Sigma_t} + \frac{1}{2} I \;\; \forall \;\; 1 \le j \le p$. The largest absolute eigenvalue of the error iteration matrix $(\boldsymbol{M})$, given by Eqs. (16), represents the spectral radius (ρ) of *k*-lpCMFD.

$$\rho = \max_{1\le g\le G} \; \max_{\theta_{g,m}=\frac{2\pi m}{K\Sigma_{t,g}H}} \; \max_{1\le j\le p} |eig(\boldsymbol{M})|, \; m = 1, 2, \ldots, K-1 \tag{16}$$

3. Results

A 2-group, 1D problem consisting of 10 fuel pins with a uniform pitch has been used to compare the numerically estimated spectral radius (using S_8 quadrature and step-characteristics discretization) with theoretical predictions based on the Fourier analysis presented in Sec. 2. Each pin contains a central fuel region (F) of size 1 unit surrounded by moderator (M) of 2 units thickness on both sides, as shown in Figure 2. Reflective and vacuum boundary conditions have been applied on the left and right edges of the problem, respectively. The two-group cross-sections can be found in Ref. [3]. It can be seen from Figure 3 that the numerical estimates compare favorably with the theoretical predictions. This verifies the multi-group Fourier analysis of *k*-lpCMFD.

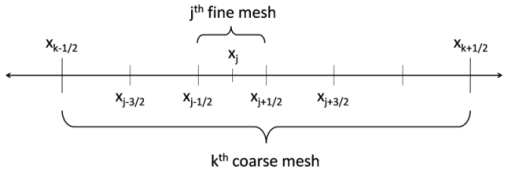


Figure 1 – Spatial discretization

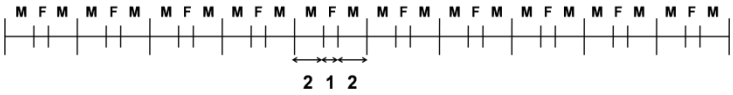


Figure 2 – 1D model problem

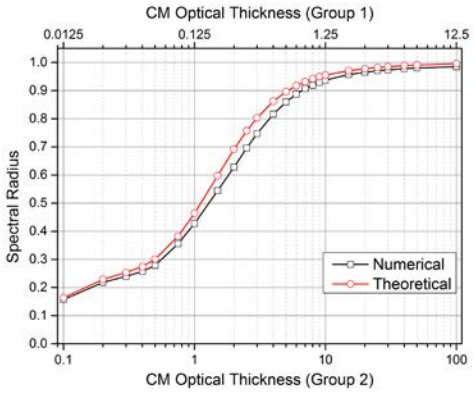


Figure 3 – Numerical vs theoretical spectral radius for k-lpCMFD

4. Conclusion

In this paper, the convergence performance of *k*-lpCMFD has been studied for multiple energy groups using Fourier analysis. Such a multi-group analysis, which has been performed for the first time for lpCMFD, complements existing results in the 1D and 2D mono-energetic domains. The theoretical predictions for spectral radius have been found to be in excellent agreement with the numerical estimates. This study provides deeper insight into the convergence behavior of lpCMFD accelerated *k*-eigenvalue calculations into the more commonly used multi-group form.

5. References

[1] Wang, D., Xiao, S. (2018). "A Linear Prolongation Approach to Stabilizing CMFD", Nuclear Science and Engineering 190 (2), 45–55.

[2] Chan, Y., Xiao, S. (2019). "Convergence Study of CMFD and lpCMFD Acceleration Schemes for k-eigenvalue Neutron Transport Problems in 2D Cartesian Geometry with Fourier Analysis", Annals of Nuclear Energy 133, 327–337.

[3] Jain, L., Mohanakrishnan, P., Karthikeyan, R., Kannan, U. (2021). "Convergence Study of CMFD based Acceleration Schemes for Multi-group Transport Calculations with Fission Source using Fourier Analysis", Annals of Nuclear Energy 160, 108314.

Introduction of Hexagonal Lattice Core Analysis in NDIFF3D

Arindam Chakraborty[1], Debasmit Sarkar, K P Singh and Umasankari Kannan
Reactor Physics Design Division,
Bhabha Atomic Research Centre, Trombay, Mumbai 400085
[1]e-mail: - arindamc@barc.gov.in

Abstract

The space-time diffusion code NDIFF3D was developed for Cartesian geometry. It solves multi energy group neutron diffusion equation in three-dimension geometry using centre-mesh finite difference method. The hexagonal lattice core simulation capability was added to NDIFF3D by incorporating triangular mesh handling capability. For the calculation with smaller mesh sizes, each hexagon can be subdivided into uniform triangles. Few benchmark problems were solved to validate the code. The k_{eff} and power distribution agree well with reference results.

1. Introduction

The hexagonal lattice arrangement is preferred in fast reactor core and pressurised water reactor core like VVER. The space-time neutron diffusion code NDIFF3D [1], based on centre-mesh finite difference method was originally developed for Cartesian geometry. The provision of triangular-Z mesh option is introduced in the computer code NDIFF3D to simulate the reactor cores designed with hexagonal assembly. The provision for auto-triangularisation is provided to tackle the problem where smaller mesh size is required. A Python API is also developed for ease of input description and post-processing of output data. The Python API can directly interact with the dynamically linked library generated from FORTRAN code. User can define the input in Python script and directly call FORTRAN subroutines to solve the problem from script. The *Matplotlib* [2] library was used for plotting and visualizing data.

2. Theory and Methodology

The steady state multi-group neutron diffusion equation [3, 4] that describes energy dependent angle integrated neutron flux φ_g of a reactor is written as,

$$-\nabla.D_g\nabla\varphi_g + \Sigma_g^r\varphi_g - \sum_{\substack{g'=1 \\ g'\neq g}}^{G}\Sigma_{g'\to g}^s\varphi_{g'} = \frac{1}{k_{eff}}\chi_g\sum_{g'=1}^{G}\nu\Sigma_{g'}^f\varphi_{g'};\ \ g = 1,..,G \qquad (1)$$

Here $D_g, \Sigma_g^r, \nu\Sigma_g^f$ and $\Sigma_{g'\to g}^s$ are diffusion coefficient, total removal cross-section, ν-times fission cross-section in energy group g and scattering cross-section from energy group g' to g respectively. χ_g is fission spectrum in energy group g & k_{eff} is the eigenvalue.

Neutron flux and current are generally accepted to be continuous within solution domain [4]. On the boundary, the following equation is considered as the boundary condition:

$$D_g\frac{\partial\varphi_g}{\partial\hat{n}} + \Gamma_g\varphi_g = 0 \qquad (2)$$

Where $\hat{n}$ is the outward normal to the boundary surface and Γ_g is albedo factor-neutron current to flux ratio on the boundary, whose value dependents on the boundary condition.

A core represented by regular hexagonal geometry in XY plane can be decomposed into six equilateral triangles [5]. Along with z-direction, a three-dimensional mesh in the core is represented by a triangular prism. Each of these mesh is denoted by (i, j, k) where i and j are coordinates in XY plane and k represents mesh number in Z-direction, as illustrated in figure 1. The spatial difference equations are obtained by integrating the neutron diffusion equation (1) over each triangular prism region, which gives $N \times G$ spatially discretized equations-

$$\sum_{k=1}^{5} \overline{D_g^{ok}}(\phi_g^k - \phi_g^o)A_{ok} + \sum_{g=1}^{G} \Sigma_g^{ro}\phi_g^o - \sum_{\substack{g'=1 \\ g' \neq g}}^{G} \Sigma_{g' \to g}^{so}\,\phi_{g'}^o = \frac{1}{k_{eff}}\chi_g \sum_{g'=1}^{G} \nu\Sigma_{g'}^{fo}\phi_{g'}^o \qquad (3)$$

$$o = 1, \dots, N; g = 1, \dots, G$$

These set of equations can be represented in matrix form as:

$$A\phi = \frac{1}{k_{eff}}F\phi \qquad (4)$$

It is a generalized eigenvalue equation. It can be solved using several methods like power iteration, Arnoldi etc.

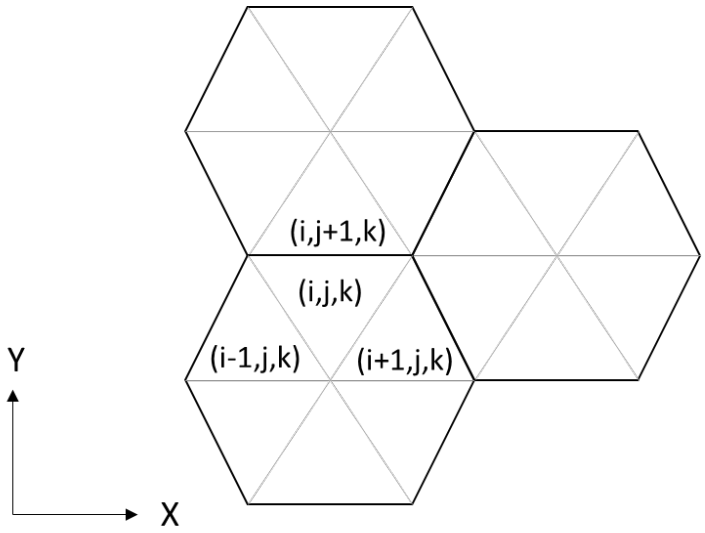


Figure-1: Rectangular grid of triangles in XY plane

3. Results and Discussions

Two hexagonal benchmark problems were selected to validate the code NDIFF3D. The first problem is two dimensional modified IAEA PWR problem and second problem is VVER-1000 core based AER benchmark.

3.1. Two-Dimensional Modified IAEA PWR Problem with Reflector:

The two-dimensional Modified IAEA PWR problem [6] was solved using NDIFF3D for validation of the two-dimensional hexagonal core calculation capability. In this benchmark problem, the square geometry of 2D IAEA PWR assemblies are converted to hexagonal assemblies by Y. A. Chao & Y. A. Shatilla [6]. The steady state diffusion equation is solved for estimation of k_{eff} and flux distribution. The core contains 127 fuel assemblies, out of which 13 are rodded. The assemblies are homogeneous, represented by given two-group diffusion theory parameters. There are two different type of fuel assemblies. The assembly lattice pitch is 20 cm. Core is surrounded by one layer of water reflector. The albedo factor of 0.5 is assumed in this problem. The power iteration method was used for calculation of k_{eff}. The convergence criteria of 10^{-5} was taken for flux and 10^{-6} was taken for k_{eff}. For this calculation, each hexagonal assembly is divided into 864 triangles. The k_{eff} estimated by NDIFF3D is 1.005416 and the same estimated by DIF3D-FD is 1.005507. The difference is about 9 pcm. The channel power distribution is shown figure 2. The maximum difference in channel power distribution compared to reference value is about 1%.

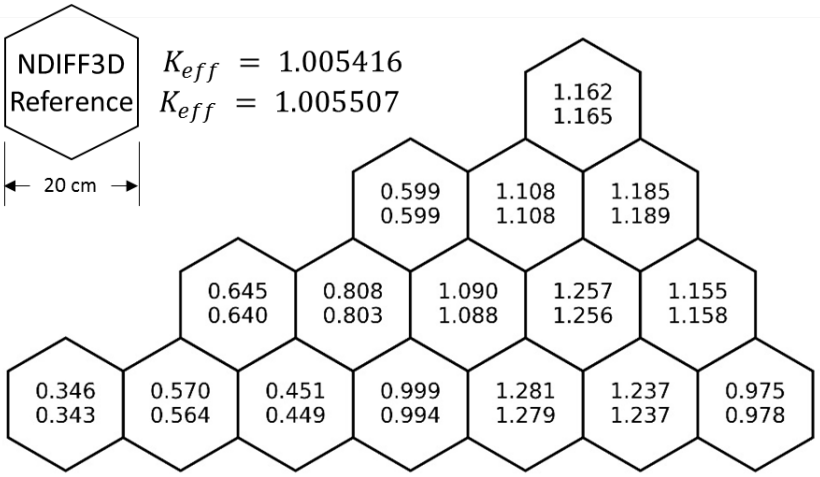


Figure 2: Channel power of IAEA 2D hexagonal benchmark problem with reflector

3.2.AER Benchmark:

The AER-FCM-101 benchmark [7] was solved using NDIFF3D for validation of the three-dimensional hexagonal core calculation capability. The benchmark problem models VVER-1000 core in 3D hexagonal geometry. The steady state diffusion equation is solved for estimation of k_{eff} and flux distribution. The core contains 151 fuel assemblies. The assemblies are homogeneous, represented by given two-group diffusion theory parameters. Seven different fuel assemblies are used in the problem. The assembly lattice pitch is 24.1 cm and the active core height is 355 cm. There are radial as well as axial reflective region present in the core. The power iteration method was used for calculation of k_{eff}. The convergence criteria of 10^{-5} was taken for flux and 10^{-6} was taken for k_{eff}. For this calculation, each hexagonal assembly is divided into 216 triangles and axial mesh length was taken ~2 cm. The k_{eff} estimated by NDIFF3D is 1.04951 and

the same estimated by CRONOS2 is 1.04953. The difference is about 2 pcm. The channel power distribution is shown in figure 4. It is observed that the maximum deviation in channel power is less than 0.4% with the reference value.

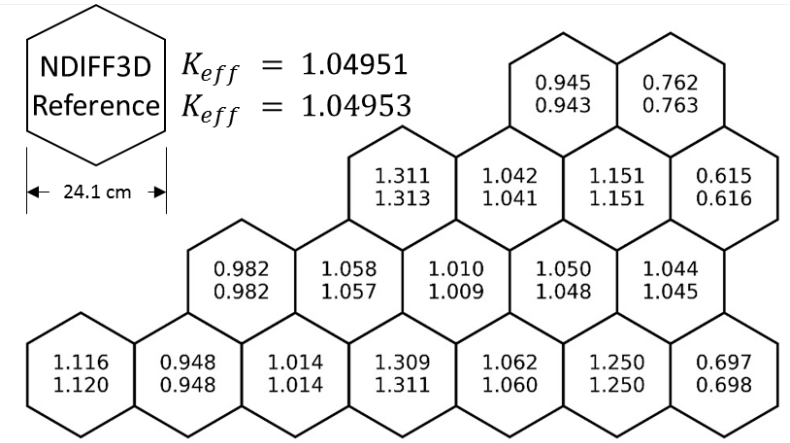


Figure 3: Channel power of 3D AER benchmark problem with reflector

4. Conclusion

The capability of neutron diffusion code NDIFF3D was extended by incorporation of the triangular-Z geometry. It is validated by solving two different benchmark problems. The deviation in k_{eff} calculated for 2D modified IAEA PWR benchmark problem and 3D AER benchmark problem is less than 10 pcm from reference value. The channel power distribution deviates within 1%. The kinetic benchmark problems will be solved in the future.

References

1. Arindam Chakraborty et.al. “Development of computer code for modal kinetics analysis of AHWR”, Report no. RPDD/AHWR/415, June 14, 2018.
2. J. D. Hunter, “Matplotlib: A 2D Graphics Environment”, Computing in Science & Engineering, vol. 9, no. 3, pp. 90-95, 2007
3. V. Jagannathan and R P Jain, “THIHEX-3D – a multigroup diffusion theory code for hexagonal lattice core analyses with auto-triangularisation”, Thechnical report , BARC-1515, August 1990.
4. Tej Singh, Use of higher nodal methods for effecient solution of three dimensional space time diffusion equations in nuclear reactor cores with hexagonal geometry; PhD thesis, Nov, 2017
5. R W Hardie and W W Little Jr., “3DB, A three-dimensional diffusion theory burnup code”, BNWl-1264, UC-32, Mathematics and Computers, March 1970
6. Y. A. Chao & Y. A. Shatilla (1995) Conformal Mapping and Hexagonal Nodal Methods —II: Implementation in the ANC-H Code, Nuclear Science and Engineering, 121:2, 210-225, DOI: 10.13182/NSE95-A28559
7. N. P. Kolev, R. Lenain, C. Fedon Magnaud, “AER FCM 101 Benchmark Specification Sheet, AER Benchmark Book, ARKI-KFKI (Hungary)

Advances in Reactor Physics (ARP-2022)
Mumbai, India, May. 18-21, 2022

STEMPWR - A NEUTRON TRANSPORT THEORY CODE FOR PWR TYPE GEOMETRIES

Kapil Deo
Reactor Physics Design Division, Bhabha Atomic Research Centre, Mumbai, India
e-mail: - kapil@barc.gov.in

Abstract

A neutron transport theory code (STEMPWR) based on method of characteristics have been developed. For validation of the code, a 3 by 3 PWR and a 4 by 4 BWR benchmark problem was simulated. The paper gives an overview of the results obtained for this validation exercise. STEMPWR results were found to be in very good agreement with the reference values.

1. Introduction

In view of various advantages of Method of Characteristics in the field of Neutron transport theory, a series of neutron transport code has been developed at RPDD. Initially, a 1D neutron transport theory code, INMOCS1[1] was developed to simulate neutron transport equation in 1D slab, cylinder and spherical geometries. For further extension of MOC simulation to higher dimensions, the code STEMPC was developed to carry out MOC based neutron transport simulation in pin cell geometries [2]. A separate program for ray tracing in cluster geometry (CLTRACK) has also been developed [3]. As a next step towards the development of assembly level MOC program, a code STEMR (Solution of Transport Equation by MOC in 2D Rectangular geometry) was developed [4].

In continuation of these developments, **STEMPWR (Solution of Transport Equation by MOC in PWR type assemblies)** was developed. For development of STEMPWR, the ray tracking and the track normalization functions of STEMPC and STEMR were integrated such that the tracking can now be carried over the entire PWR type assemblies. Section 2 of this paper gives a brief overview of STEMPWR. In section 3, the description of the benchmark problems for validating the code STEMPWR, is described. The results of benchmarking of the code are compiled in section 4.

2. Brief Overview of STEMPWR

Basic structure of STEMPWR is similar to the structure of STEMPC/STEMR. New functions were developed as needed. The main program acts as an I/O interface between user and the modules of the code. These modules can be broadly classified into two groups - Ray Tracing Group and Neutronics Group. Former group contains modules for plotting and ray tracing over the problem geometry. There are provisions for plotting the basic problem geometry, mesh structure and track rays. The ray tracing modules generates segment length of a ray, in each of the intercepted mesh in a successive order. This information for all the rays is stored in a single 1D track array 'TRK'. Modules of Neutronics group use this array to carry out MOC simulations. The problem geometry remains abstract to neutronic modules and the only link between them is the array 'TRK'.

The neutronic modules solves the neutron transport equation using the Method of characteristics [5]. The theoretical aspect of this method has been separately dealt with, in an earlier work [1]. The implementation strategy of this method for 2D problems has been described in [4].

3. Description of the benchmarks for validation of STEMPWR

For validation of STEMPWR a number of benchmarks having PWR type geometries has been simulated. Here, the results obtained for two popular benchmark problems are described.

A. CEA-1 PWR benchmark [6]

This problem has been analysed by different international groups. This benchmark problem has been designed to test the accuracy of the transport codes for the calculation of a PWR like assembly. The Assembly consists of 9 cells (Fig. 1). The eight outer rods are fuel and the central rod is a burnable poison. A source of unit strength is placed in the moderator region. Macroscopic cross-sections for different region is provided. The region averaged flux at different location (regions marked with nos. 1-6 in Fig. 1) have to be estimated.

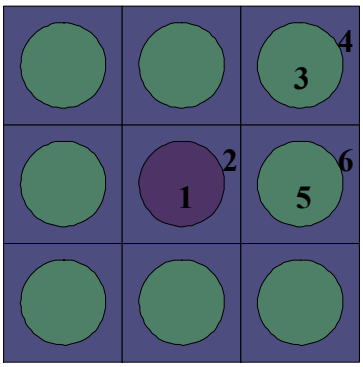


Figure 1

B. 4 by 4 BWR Lattice

This benchmark was originally proposed by Hong and Cho [7]. It contains theBWR cells in a 4 by 4 arrangement, with two Gadolinium pins. The fuel rods consist of 3 wt.% UO2. The poisoned rods contain 3wt.% UO2 and 3 wt. % Gd_2O_3. The fuel is wrapped by Zircaloy-2 clad and moderated by water. The two group macroscopic cross-sections for different materials has been taken from [8]. Reflective B.C. is specified on all the four sides.

4. Results

A. Results for STEMPWR simulations of PWR benchmark

In this problem, the central rod is a burnable absorber, hence more number of meshes has to be used in this cell, in comparison to other cells. Fig. 2 shows a sample meshing pattern where two rings each is used in both the moderator and fuel regions. The poison cell is having four rings in moderator and fuel region. All the cells are divided into eight regions in azimuthal direction. The lines shown in the figures are sample ray trace data corresponding to a large value of ray separation (10 cm). It can be noted that the meshing patterns and the ray trace data are all plotted in-situ by the code STEMPWR. The region averaged fluxes corresponding to different locations is given in Table 1.

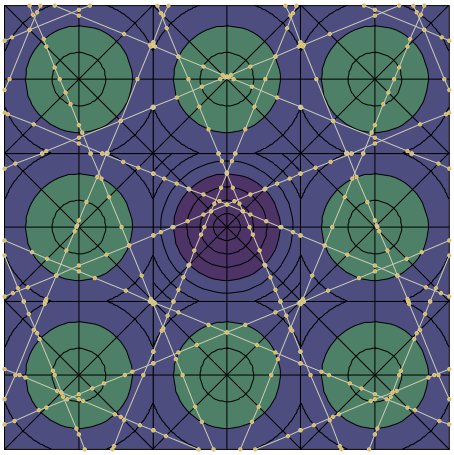


Figure 2

Table 1: Average region fluxes for different regions for PWR benchmark

Region No. (See Fig. 1)	1	2	3	4	5	5
Ref. Monte Carlo Values	0.3204	3.210	3.942	4.400	3.637	4.110
STEMPWR Values	0.3168	3.0355	3.9903	4.0432	3.7845	3.8392

The average region fluxes obtained with STEMPWR are compared with the reference monte carlo values given in [6]. Reflective B.C. were used on all the four sides. The reflective B.C. implementation in STEMPWR is the one suggested by Hong and Cho [7]. For this, each boundary is divided into different cells. All the neutron current ending in the respective cells are collected and they are equally divided among the reflected rays. Fig. 3 gives the plot of average leakage fluxes per ray, for the two polar angles used for the simulation.

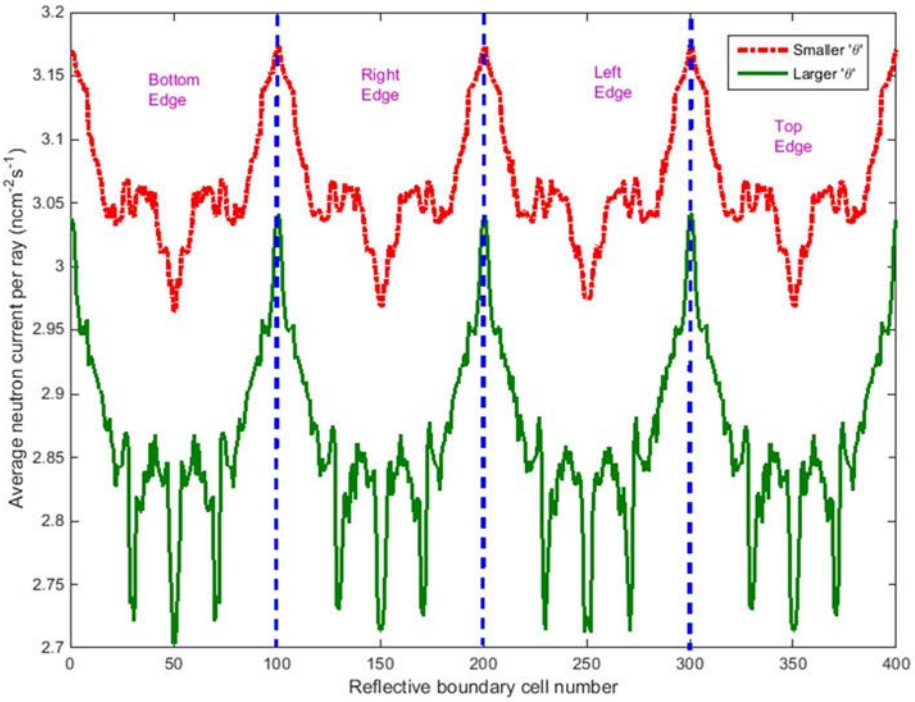


Fig. 3: Average reflected neutron current for different boundary cells of PWR benchmark

B. Results for STEMPWR simulations of 4 by 4 BWR lattice

The results obtained using the code STEMPWR, for this benchmark problem, is given in Table 2. These results have been obtained for eight divisions in azimuthal direction. In the radial direction, 2 rings in fuel, 1 ring in clad and 2 ring in moderator has been used for regular fuel cell. For the poison fuel cell, 4rings in fuel, 1 in clad and 4 rings in moderator region was used. The reference K-eff values correspond to the MOCUM code and is taken from [8]. Additionally, the K-eff values calculated from DRAGON [9] code (also taken from [8]) are also given for reference. Although the ray tracing methodology of STEMR and MOCUM are different, the simulation parameters like ray separation, azimuthal quadrature, polar quadrature etc. were kept to be similar to minimise the respective errors. The variations of average leakage current per ray, for the two polar angles used for the simulation, are given in Fig. 4.

Table 2: Results for STEMPWR analysis of 4 by4 BWR benchmark

	DRAGON	MOCUM	MOCUM err (%)	STEMPWR	STEMPWR err (%)
K-eff	0.986561	0.987785	0.12	0.987316	0.08
Normalized Pin Power					
Pin 1	6.9391E-2	6.9476E-2	0.10	6.9378E-2	-0.02
Pin 2	6.6246E-2	6.6268E-2	-0.04	6.6147E-2	-0.15
Pin 3	6.9398E-2	6.9441E-2	0.05	6.9424E-2	0.04
Pin 4	7.2549E-2	7.2626E-2	0.09	7.2762E-2	0.29
Pin 5	6.2429E-2	6.2322E-2	0.15	6.2467E-2	0.06
Pin 6	2.4344E-2	2.4265E-2	-0.33	2.4252E-2	-0.38

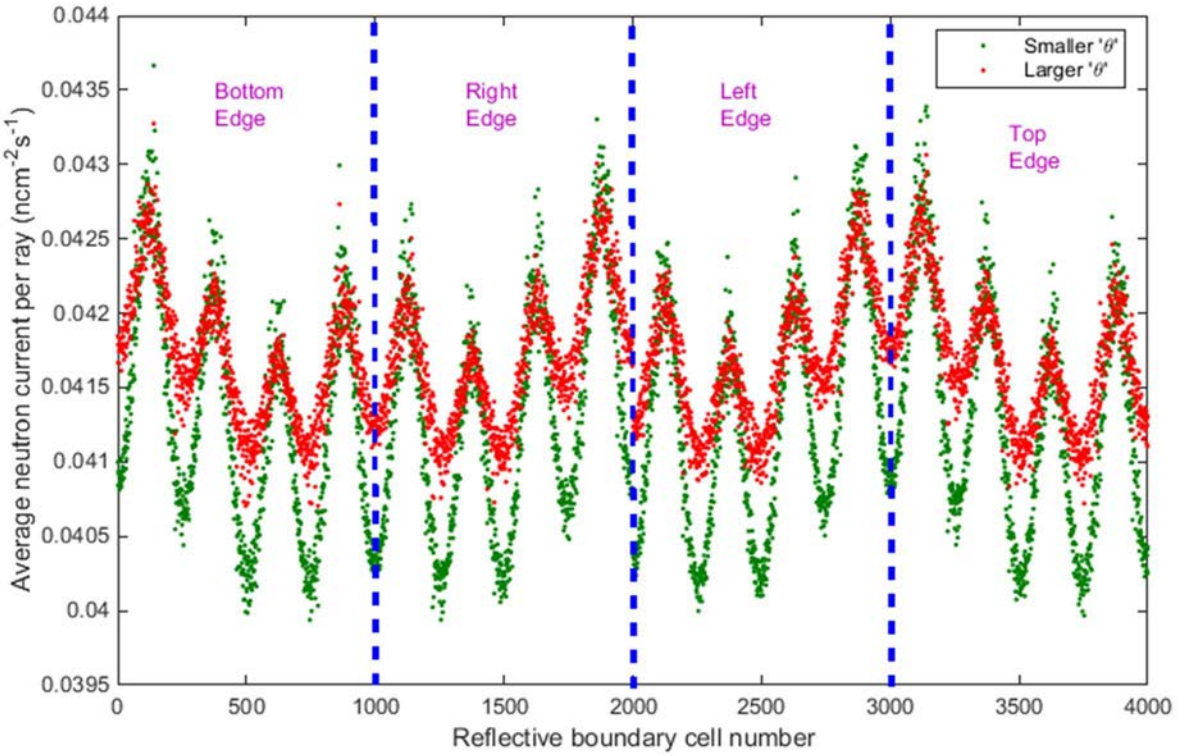


Fig. 4: Average reflected neutron current for different boundary cells of BWR benchmark

5. Conclusion

A 2D MOC code for simulation of PWR type assemblies, STEMPWR, has been developed. The code STEMPWR is another addition to the STEM series of code. The code was used to simulate two well-known benchmark problems, viz. 3 by 3 PWR benchmark and 4 by 4 BWR benchmark. The results obtained for both the benchmarks were in very good agreement with the reference values.

6. References

1. Kapil Deo, P.D. Krishnani and R.S. Modak, BARC Tech. Rep., BARC/2014/E/015, Dec., 2014
2. Kapil Deo, Divisional Report - RPDD/EP/91, 15th May, 2014
3. Kapil Deo, Divisional Report - RPDD/EP/94, June 05th, 2014
4. Kapil Deo, Divisional Report - RPDD/EP/108, 20th March, 2015
5. J. R. Askew, F. J. Fayers and P. B. Kemshell, Journ. of Brit. Nucl. Energy Soc., 5, No. 4, 564, 1966
6. Kavenoky et. al., IAEA-TECDOC-254, Vienna, 1981.
7. S.G. Hong and N. Z. Cho, Ann. Nucl. Energy 25 (8), 1998, 547–565.
8. Xue Yang and Nader Satvat, Annals of Nuclear Energy 46 (2012) 20-28.
9. G. Marleau, A. Hébert and R. Roy, Rep. IGE- 174 Rev. 7, 2008, Inst. de génie nucl, École Polytechnique de Montréal, Montréal, Québec.

Solving Neutron Diffusion Equation using Machine Learning

Saivirinchi P[1], Lakshay Jain[2]andKondayya Gundra[3]
[1]Indian Institute of Science, Bangalore, India
HomiBhabha National Institute[2]
[3]Bhabha Atomic Research Centre, Mumbai, India
[3]*e-mail:-naiduk@barc.gov.in*

Abstract

In this work, the use of physics informed neural networks to solve the neutron diffusion equation has been presented. The robust and powerful nature of neural networks has been leveraged to solve multi-group neutron diffusion equations at random points in 1D and 2D geometries quickly and efficiently.

1. Introduction

Neutron diffusion equation is commonly used in reactor core calculations for nuclear reactor design and analysis. However, thesolution accuracy depends on the discretization scheme used along with complexity of the mesh structure which isproblem dependent. Instead, this problem has been solved in this paper in a novel manner using machine learning and artificial neural networks.

2. Neural Networks

Artificial neural networks (see Figure 1)have found widespread application in many fieldsdue to its powerful ability to discover complex patterns in large data setscoupled withminimal human intervention. It hasalso attracted attention for solving varied engineering problems in recent years. In addition they also produced outstanding results in various disciplines including language processing, object recognition, finance, and market analysis, etc.Neural networks (NN) are comprised of multiple layers of artificial neurons or nodes,containing an input layer, one or more hidden layers, and an output layer. Each node connects to another and has an associated weight and threshold. If the output of any individual node is above the specified threshold value, that node is activated, sending data to the next layer of the network. Otherwise, no data is passed along to the next layer of the network.Traditionally, NNis given input in the first layer and its output is compared with the expected output.The weights and biasesfor each node are adjusted accordingly, using a suitable regression model. This process is repeated for a number of iterations until error between the expected output and output from the NNreduces to the desired level.

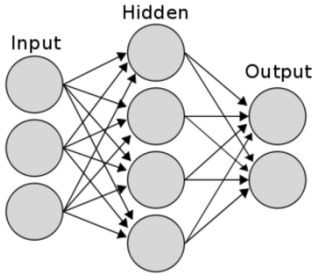


Figure 1 – Conventional neural network

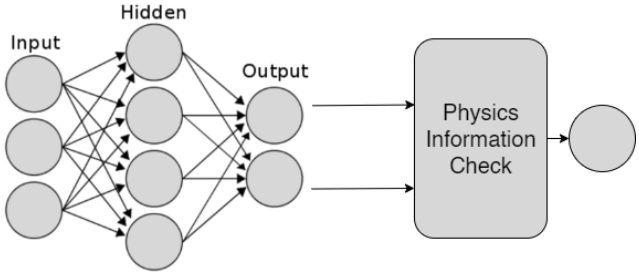


Figure 2 – Physics informed neural network

There is one caveat in using NN,i.e., it requires large amounts of input and output data to train the system and obtain the results. However, such data is not available while solving the neutron diffusion equation for obvious reasons. But, physics informed neural networks (PINN) [1] can be used to overcome this lack of data for an unsolved system. PINNis designed to use the physics information like partial differentials, boundary conditions, etc., to obtain the optimal solution. PINN can be obtained from conventional NN by adding anadditional layer after the output layerto check whether the system

satisfies the underlying physics-based conditions (see Figure 2). The neutron diffusion equation is solved using this ideology.

3. Solution of 1-D Neutron Diffusion Equation

The mono-energetic1D neutron diffusion equation is shown in Eq. (1).

$$-D\frac{d^2\phi}{dx^2} + \Sigma_a\phi = \frac{\nu\Sigma_f}{k}\phi \tag{1}$$

where standard notation has been used.For a homogeneous problem with $\frac{-a}{2} \leq x \leq \frac{a}{2}$and zero flux boundary conditions,the analytical solution can be obtained as given in Eq. (2).

$$\phi(x) = F\cos\frac{\pi x}{a}, \quad k = \frac{\nu\Sigma_f}{\Sigma_a + D\left(\frac{\pi}{a}\right)^2} \tag{2}$$

where F is an arbitrary free parameter[1]. Eq. (1) can be re-written as Eq. (3), which is used by the PINN for calculating errors, i.e., deviation of the solution from the underlying physics.

$$D\frac{d^2\phi}{dx^2} - \Sigma_a\phi + \frac{\nu\Sigma_f}{k}\phi = 0 \tag{3}$$

To solve the 1D neutron diffusion equation, anNNis designed with one input x, and one output $\phi(x)$. $\phi(x)$is then passed through Eq. (3) to obtain *error from function*$\left(MSE_f\right)$. Similarly, the boundary conditions passed through the NN,are also comparedwith expected value (zero in this case) to determine*error from B.C*(MSE_{bc}).For the free parameter(F), we fit the NN at known random point with its corresponding flux density to compute $error_0(MSE_0)$.

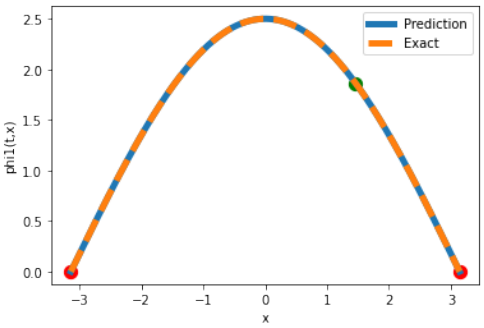


Figure 3 – Mono-energetic flux profile for 1-D slab (random point used is depicted as green dot, while red dots represnts boundary values)

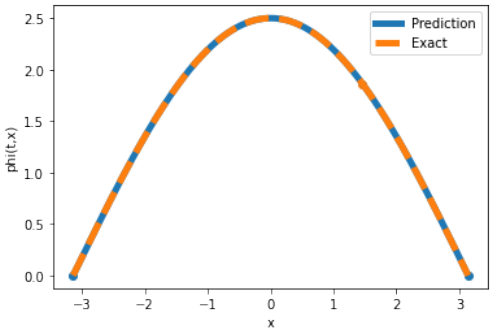


Figure 4 – Flux profile for 1-D slab in group 1

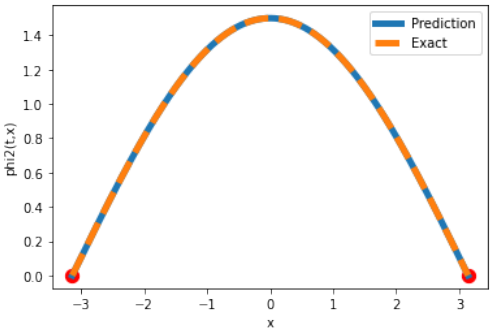


Figure 5 – Flux profile for 1-D slab in group 2

With the three errors defined, the loss function is computed as the summation of mean squares of these errors and is obtained using Eq. (4).

[1]Scalar flux value at one random point (or equivalently normalized flux distribution) must be known to determine F.

$$Loss = MSE_0 + MSE_{bc} + MSE_f \quad (4)$$

The NN is run with Adam and L-BFGS-B optimizers for 1000 iterations and its output is compared with the analytical solution as shown in Figure 3 to verify the solution. It may be noted that $a = \pi$ for the results plotted in Figure 3. It can be observed that the flux distribution obtained from the PINN is in excellent agreement with the analytical solution for this problem.

The 1D 2-group neutron diffusion equation, given in Eq. (5),can be similarly solved using PINN with two outputs,$\phi_1$andϕ_2, instead.The scalar flux profilefor a homogeneous 1-D slab problem with$\frac{-\pi}{2} \leq x \leq \frac{\pi}{2}$and zero flux boundary condition, obtained by solving of Eq. (5) using PINN technique has been plottedin Figure 4 and Figure 5. It can be seen that the results in good agreement with the analytical solution, verifying the application of PINN for solving the neutron diffusion equation.

$$-D_1 \frac{d^2\phi_1}{dx^2} + \Sigma_{a,1}\phi_1 = \frac{\chi_1}{k}\sum_{g=1}^{2} \nu\Sigma_{f,g}\phi_g + \Sigma_{s,2\to1}\phi_2 \quad (5a)$$

$$-D_2 \frac{d^2\phi_2}{dx^2} + \Sigma_{a,2}\phi_2 = \frac{\chi_2}{k}\sum_{g=1}^{2} \nu\Sigma_{f,g}\phi_g + \Sigma_{s,1\to2}\phi_1 \quad (5b)$$

4. Solution of2-D Neutron Diffusion Equation with 2 groups

Let us now consider the 2-D neutron diffusion eigenvalue equation with 2 energy groups, which is given in Eq. (6).

$$-D_1\nabla^2\phi_1 + \Sigma_{a,1}\phi_1 = \frac{\chi_1}{k}\sum_{g=1}^{2} \nu\Sigma_{f,g}\phi_g + \Sigma_{s,2\to1}\phi_2 \quad (6a)$$

$$-D_2\nabla^2\phi_2 + \Sigma_{a,2}\phi_2 = \frac{\chi_2}{k}\sum_{g=1}^{2} \nu\Sigma_{f,g}\phi_g + \Sigma_{s,1\to2}\phi_1 \quad (6b)$$

In orderto solve Eq. (6) using PINN, a similarNN as applied in the previous cases isused, except that the PINN hastwo inputs x and y, and two outputs$\phi_1$andϕ_2.Also, thephysics loss function used in the PINN is defined by replacing Eq. (1) by Eq. (6).

The PINN technique is used to solve Eq. (6) for a 2-D homogeneous slab problem with$\frac{-\pi}{2} \leq x \leq \frac{\pi}{2}and\frac{-\pi}{2} \leq y \leq \frac{\pi}{2}$.Using 20,000 random pairs of x and y as input, the loss from the NNcalculated using Eq. (4) is used to determine the optimizedsolution. After running the PINN for about 1000 iterations, the error reduces significantly and scalar flux solution is obtained. Themean square errors in flux densities in group 1 and group 2 are7.16×10^{-4}and6.96×10^{-4}, respectively. The scalar flux distributions for the two groups are shown in Figure 6 and Figure 7.

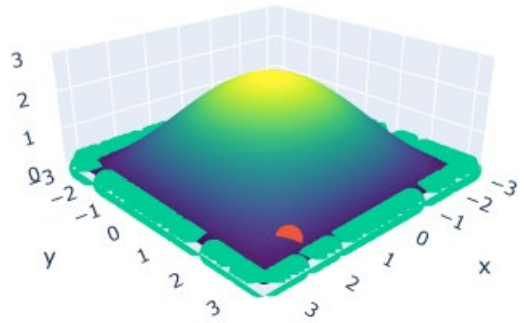


Figure 6 – Flux profile for 2-D slab in group 1 (random point used shown in red)

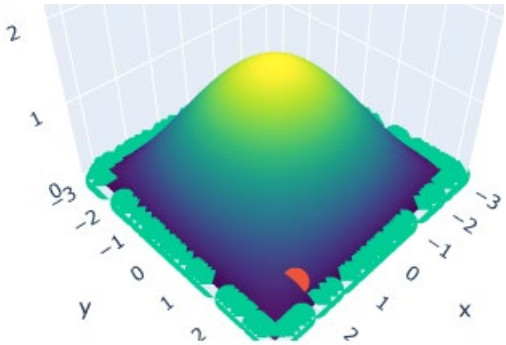


Figure 7 – Flux profile for 2-D slab in group 2

5. Conclusion

The application of physics informed neural networks (PINN) to solve the neutron diffusion eigenvalue equation has been presented in this paper. PINN leverages the underlying mathematical model

(differential equations) to overcome the lack of huge amounts of data for solving various engineering and physics problems. Scalar flux distributions obtained by PINN method for different cases have been found to be in good agreement with corresponding analytical results. This verifies the use of this novel scheme for modeling neutron diffusion. In future, the use of PINN will be extended to more generic neutron diffusion problems and possibly to other problems of interest in reactor physics.

6. References

[1] Raissi, M., Perdikaris, P., Karniadakis, G.E.(2019). “Physics-informed Neural Networks – A Deep Learning Framework for Solving Forward and Inverse Problems involving Nonlinear Partial Differential Equations”, Journal of Computational Physics378, 686–707.

IMPLEMENTATION OF A MODEL FOR ESTIMATING GASEOUS FISSION PRODUCT RELEASE FROM FUEL

G. Pandikumar[1] and A. John Arul[1, 2]
[1]Indira Gandhi Centre for Atomic Research, Kalpakkam, Tamilnadu 603102, India
[2]Homi Bhabha National Institute, Training School Complex, Anushaktinagar, Mumbai-400094, India.

[1]*email: pkg@igcar.gov.in*

Abstract

Accurate modelling of fission gas release and transport has many applications such as cover gas activity estimation and gas leaker localization. A FORTRAN code 'FISGASR' has been developed for the estimation of release of gaseous fission product in fuel pellet-clad gap. Release of gaseous fission products from pellet through recoil and knock-on from open surfaces such as cracks and diffusion from fuel grain. The code estimates a quantity called as release rate to birth rate (R/B). FISGASR has been validated against theoretical and experimental benchmarks from literature.

1. Introduction

Accurate modelling of fission gas release and transport has many applications such as cover gas activity estimation and gas leaker localization. Based on the literature survey, the works of R. J. White and M.O. Tucker [1] and Yang-Hyun Koo, et al [2] give very detailed explanation on fission gas release mechanism. By implementing the model, a FORTRAN code 'FISGASR' has been developed for the estimation of gaseous fission product inventory in fuel-clad. This analytical method predicts equilibrium inventory of stable and unstable gaseous fission products present in the fuel-clad gap of fuel pin during steady state operation. The theory as well as the parameters developed in are most appropriate for thermal reactor UO_2 fuel type. The sensitive parameters which could largely affect estimations for FBRs are pellet temperature, grain radius, fission rate and fuel type (MOX). With appropriate input parameters of FBRs, it is assumed that the FISGASR estimation also holds for FBRs. FISGASR has been validated against theoretical and experimental benchmarks.

2. Fission Gas Release Mechanism

Release of gaseous fission products from pellet can occur through two paths viz. (i) recoil and knock-on from open surfaces such as cracks (ii) diffusion from fuel grain. A quantity called as release rate to birth rate (R/B) is estimated, for the two paths, to find the amount of unstable gas release as follows:

$$\left(\frac{R}{B}\right)_{gap} = \left(\frac{R}{B}\right)_{c} + \left(\frac{R}{B}\right)_{gb}$$

where

$$\left(\frac{R}{B}\right)_{c} = \left(\frac{S}{V}\right)_{c} * \sqrt{\frac{D}{\lambda}} \qquad \left(\frac{R}{B}\right)_{gb} = \left(\frac{S}{V}\right)_{gb} * \sqrt{\frac{D}{\lambda}}$$

$(R/B)_{gap}$ is the ratio of release rate of unstable fission gas from pellet to gap to their birth rate, $(R/B)_{c}$ is the ratio of release rate of unstable fission gas from pellet to gap through crack to their birth rate, $(R/B)_{gb}$

is the ratio of release rate from the pellet to the gap through grain boundary tunnel networks to birth rate in the pellet, D is the diffusion co-efficient of fission gas atom (m^2/s), $(S/V)_c$ is the surface to volume ratio for a cracked body (m^{-1}), $(S/V)_{gb}$ is the ratio of the surface area covered by grain corner bubbles to grain volume (m^{-1}) and B is the birth rate density (atoms/m^3/s) which is the product of yield of i^{th} fission product and FR (is the fission rate density fissions/m^3/s). The following sections explain the method used for finding $(S/V)_c$ and $(S/V)_{gb}$ which are essential for the estimation of R/B value.

2.1 Diffusion Co-efficient

The release processes of both stable and unstable fission products are assumed to be primarily controlled by atomic diffusion through the fuel matrix. The diffusion process is found to dependent on temperature. Irradiation-induced migration dominates the diffusion process at temperatures below 1000 ^oC and is temperature independent. For temperatures between 1000 and 1400 ^oC, vacancies necessary for the gas atom diffusion are assumed to be created both thermally and by the damage cascades related to fission fragments. Above 1400 ^oC, a purely thermally activated diffusion coefficient is applied, that is, thermally created vacancies for diffusion are predominant. These three temperature regimes are reflected in the three components of the single gas atom diffusion coefficient (m^2/s) often applied in the fuel performance codes [2].

Diffusion coefficient $D = D_1 + D_2 + D_3$ (m^2/s)

$D_1 = 7.6 \times 10^{-10} e^{(-3.03/8.617E-05*T)}$ *Temperature > 1400 ^oC*

$D_2 = s^2 j_v V$ *(1000 ^oC < T < 1400 ^oC)*

$D_3 = 2.0 \times 10^{-40}$ FR *T < 1000 ^oC*

$V = \frac{\alpha_s s^2}{2Z}\left\{\left[1.0 + \frac{4KZ}{j_v \alpha_s s^2}\right]^{1/2} - 1.0\right\}$ is the irradiation induced vacancy concentration, α_s is fixed sink strength (~ 10^{15} m^{-2}), s is atomic jump distance (~3×10^{-10} m), Z is number of sites around a point from which recombination is inevitable (~ 100), j_v is vacancy jump rate = 10^{13} * exp (-5.42×10^4/RT) (1/s), K is defect production rate per atom (~ 2.0×10^{-4} /s atom), T = Temperature (K). The diffusion coefficient is also modified for taking into account of the trapping of gas atoms in the fuel matrix into the bubbles at a rate 'g' and resolution of gas atoms from the bubbles into the fuel matrix at a rate ' b' '. The corrected diffusion coefficient is

$$D' = \frac{Db'}{b' + g}$$

where $b' = 3.03 * FR * \pi * l_f(\bar{R} + Z_0)^2$,

$g = 4\pi \bar{R} C_B^{tot} D$,

$\bar{R} = 5.0 \times 10^{-10}\left\{1.0 + 106\, e^{-0.75/kT}\right\}$,

$C_B^{tot} = \frac{1.52 \times 10^{27}}{T} - 3.3 \times 10^{23}$

Z_0 is the range of fission fragment influence ~10^{-9} (where single graze or collision destroys the gas bubbles in the fuel matrix), l_f is the flight distance of the fission fragment 6.0× 10^{-06} m.

2.2 Recoil and Knock-on

Fission energy deposited cause increase in fuel pellet temperature. Consequent to heat flow and thermal conductivity, the temperature across a pellet varies as follows: (a) higher value at fuel pellet centreline and (b) gradually decreasing temperature profile both along radial and axial directions. Such temperature gradient in a fuel pellet results in developing cracks along radially as well as axially. The open surface area caused by such cracks is estimated for each cracked segment. The total area thus obtained is divided by the pellet volume to get $(S/V)_c$.

2.3 Gas atom diffusion from fuel grain

Uranium oxide (and Plutonium oxide) exists in the form of small grain of size (radius) 5 to 25 micron. In FISGASR, the model given in [1] is considered for the release of fission gas atoms from fuel grain which assumes the following sequence of operations.

After a short irradiation period, a fine intra-granular bubbles nucleate by collecting some of the produced gaseous fission products. The formation of intra-granular fission gas bubble as well as its growth stabilizes in such a way that the size and concentration of bubbles remains constant for further irradiation. While some gases leads to the formation of bubbles, others diffuse to grain boundary.

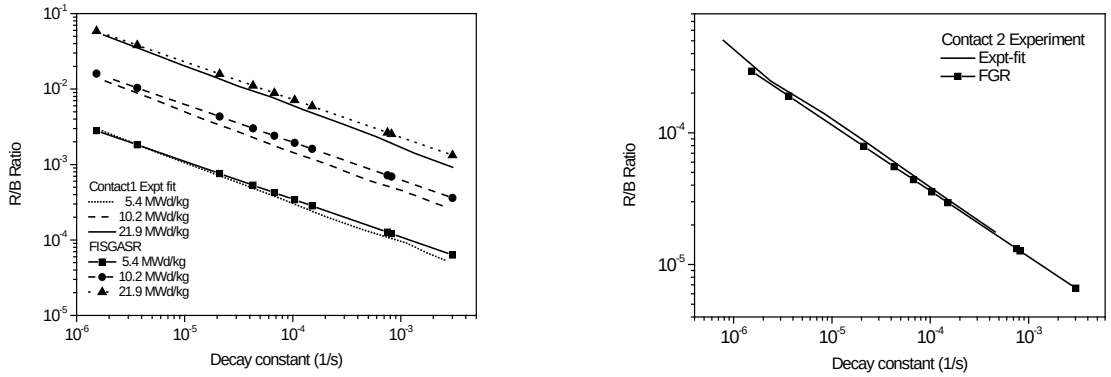
The fission gas atoms in the grain boundary does not directly release to the exterior of the fuel pellet. Rather, first it leads to the formation of lenticular shaped grain face bubbles and are allowed to grow to a saturation level according to the arrival rate of gas atoms to the grain face. The time taken for the grain face bubble saturation is estimated. Some of the unstable fission gas atom are likely to remain trapped indefinitely in the grain face bubble. This delays the release of unstable fission gas atoms to the exterior of fuel pellet. The average delay time at the grain face is then calculated. Beyond the grain face saturation and delay, further production of gas atoms are assumed to be released to grain edge and then to grain corner.

Instead of spherical fuel grain, a more realistic grain shape is considered to get accurate treatment of grain edge and grain corner swelling. The grains of UO_2 (or PuO_2) is approximated to be a tetrakaidecahedron (TKD). When packed together an array of TKD can fill all available space in a solid and thus represents an ideal basic building block. The meeting point of each face is shared by two grains, of each grain edge by three grains and of each grain corners by a four grains.

The grain edge bubble formed at the junction of three grains, has a shape of triangulated bubble, and receives fission gas atoms from three grains. Continued inflation of the bubble leads to pinch-off and coalescence of neighbouring grain edge bubbles, leading to a formation of tunnel. The sequence of pinch-off and coalescence continues until the pinch-off occurs in the middle of the grain edge. From then on, the grain edge bubbles are confined to grain corners. The grain corner bubbles grow according to the arrival rate of gas atoms. The increase in radius of the grain corner bubble, r_c, which depends on temperature and irradiation time, is calculated and is used in deriving $(S/V)_{gb}$ values. The growth of grain corner bubbles proceeds until the fractional grain corner swelling ($\Delta V/V$) is greater than 8.7% (where experimental values match the predictions according to [1]). Beyond this point, r_c is assumed to take a constant value of 0.88a ('a' being spherical grain radius). Appendix 1 gives the flowchart of R/B calculation.

3. Validation of FISGASR

FISGASR is validated against several unstable fission gas release experiments. However, the results corresponding to CONTACT experiment which was carried out jointly by CEA and FRAMATOME for the study of fuel-cladding gap evolution and fission gas release is given. Two special fuel rods (named as CONTACT1 and CONTACT2), having UO_2 fuel, designed for the purpose, is loaded in SILOE (17X17) PWR reactor. The diameter and height of the fuel pellet are 8.19mm and 14mm. The fuel pin length is 70mm. The CONTACT1 and CONTACT2 fuel center line temperatures are 1500K and 965K. In CONTAC1 experiments, R/B values are estimated for three burnup values viz. 5.4, 10.2 and 21.9 MWd/kg. Similarly, in CONTACT2 experiment also, R/B values are estimated for three burnups viz. 0.44, 7.11 and 11.78 MWd/kg. As given in [2], for both cases, $(S/V)_c$ is taken as 50 cm^{-1}. Since the fuel centre line temperature is low (965 ^oC) in CONTACT2 case, fission gas release through crack route is apparent. Using FISGASR (R/B) values are estimated for these benchmarks and compared. Figures 3 gives the comparison of FISGASR estimated R/B values with Yang-Hyun Koo model [2] predictions. It is observed that the R/B values estimated using FISGASR closely matches with that of Koo fit.



(a) CONTACT1 (b) CONTACT 2

Figure 3: Comparison of FISGASR predicted R/B values with reported

4. Conclusion

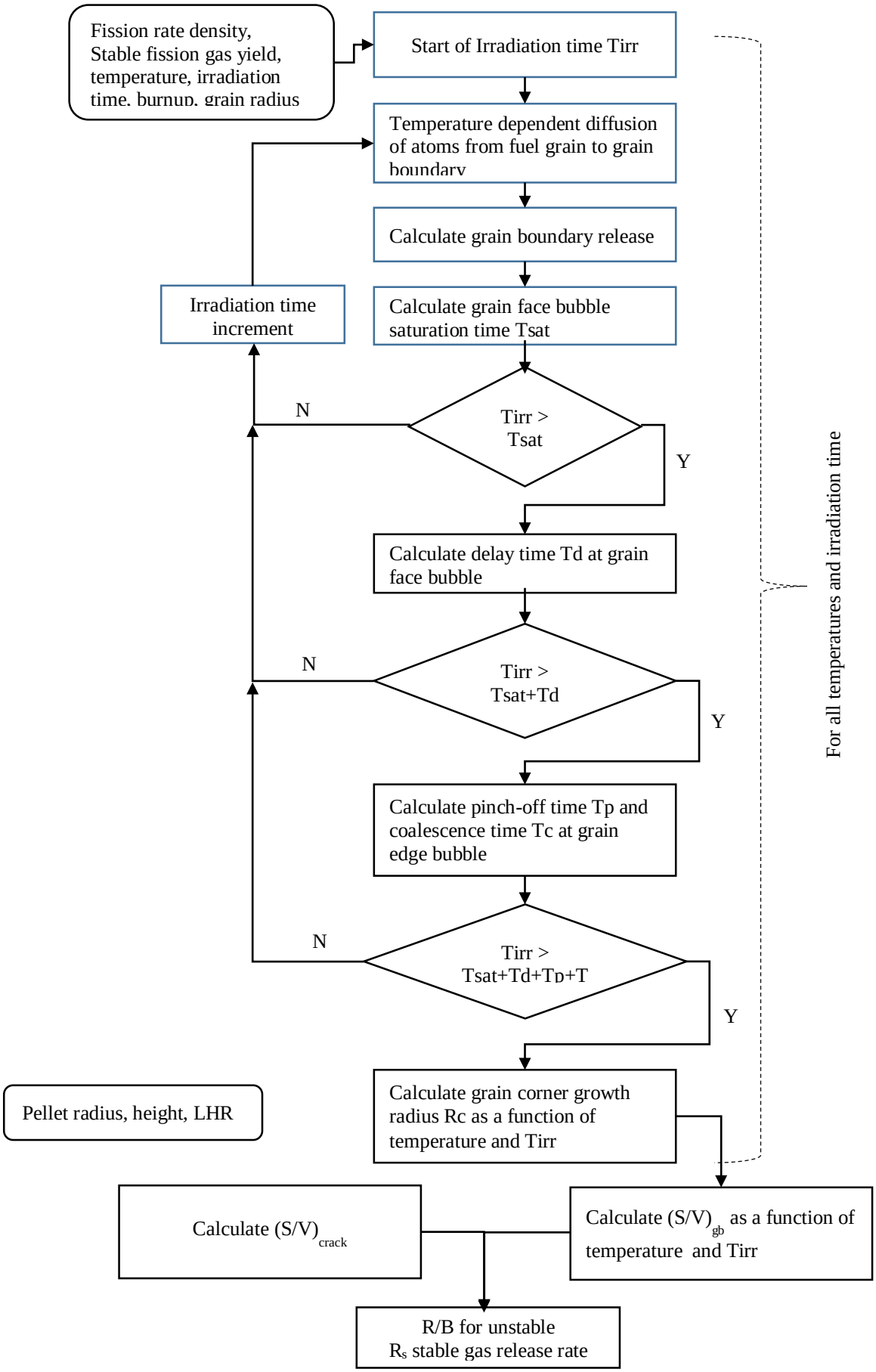
A FORTRAN code 'FISGASR' has been developed for the estimation of release of stable gaseous fission product from pellet and release-to-birth ratio for unstable gaseous fission products in fuel-clad gap. The FISGASR has been developed based on a model most appropriate for thermal reactor UO_2 fuel type. The sensitive parameters which could largely affect estimations for FBRs are pellet temperature, grain radius, fission rate and fuel type (MOX). With appropriate input parameters of FBRs, it is assumed that the FISGASR estimation also applicable for FBRs. FISGASR has been validated against theoretical and experimental benchmarks from literature. Based on the results and comparison study, FISGASR is recommended for unstable fission gas release estimation.

References

[1] R. J. White and M.O. Tucker, A new fission gas release model, J. Nuc. Mat 118 (1983) 1-38.

[2] Yang-Hyun Koo, et al. 'An analysis method for the fuel rod gap inventory of unstable fission products during steady state operation', J. Nuc. Mat. 209 (1994) 62 – 78.

Appendix 1: Flowchart of R/B calculation



New empirical formula for evaluating gamma build-up factor in double-layer shield and its validation with FLUKA code

Avijit Das*[1,2], Aditi Ray[1,2], Tej Singh[1]
[1]Bhabha Atomic Research Centre, Mumbai-400085, India
[2] Homi Bhabha National Institute, Mumbai-400094, India
[*]*e-mail: -avijit@barc.gov.in*

Abstract

Designing shield for coupled neutron and gamma radiation field is a complex problem as it involves combination of High-Z as well as Low-Z materials in composite or laminar form with optimized thicknesses. Suitable empirical formulae for double-layer exposure build-up factor (DEBF), the essential building block of multi-layer gamma build-up factor, makes radiation shield designing much efficient over detailed transport calculations. A new empirical formula has been constructed to predict DEBF for any arbitrary combination of layer materials, applicable over wide range of layer thicknesses and gamma energies. The proposed formula is shown to predict DEBF in *Iron/Water*, *Iron/PMMA*(poly-methyl methacrylate) and *Iron/HDPE* (high density polyethylene) shields with good accuracy compared to the results obtained using*open-source* Monte Carlo code, FLUKA, thereby ascertaining the robustness of the formula.

1. Introduction

Radiation shielding is essential in various nuclear installations like nuclear reactors, fuel re-processing plant, isotope handling facilities, etc. Combinations of High-Z (Iron, Tungsten, Lead, etc.)and Low-Z (Water, HDPE, Graphite, Concrete,Aluminium, etc.) materials in the form of multi-layer/stratified shield are known to be more effective for both neutronand gammaradiations. Attenuation of gammais generally estimated from its flux, determined either by detailed particle transport methods or simple point-kernel techniques, that relies on accurate gamma build-up factors (BF).Evaluating gammaBF for multi-layer shields from detailed transport calculations is a formidable task and computationally intensive. So, suitable empirical formulaeare constructed to describe BF for stratified shield as a function of DEBF. Thus, DEBF is the main building block of all empirical formulae.

There are two different approaches for constructing empirical formulae for DEBF, namely, formulae combining sum and differences of single-layer BFs [1] and those that combine products and quotients of individual BFs [2]. The first approach has been validated using Monte Carlo method-based codes EGS4 [1],MCNP [3] and MCBLD [4] while the second approach has been validated using deterministic method based discrete ordinate transport code, SN1D [2]. Nevertheless, these formulae have the limitations that they cannot be extended to arbitrary layer thicknesses and gamma energy. Moreover, the coefficients of the existing analytical functions are not always simple functions of physical parameters. Thus, there is a genuine need to develop a robust analytical function that can be applied for any material combinations and valid over wide range of gamma energies.

Recently, a new empirical formulafor double-layer shieldhas beenconstructed [5] on the basis of product of single-layer BF generated by FLUKA[6]. Coefficients of the new analytical functionare expressed in terms of gamma energy, layer thickness (in mean free path unit), mass attenuation coefficient and BF of individual components.The proposed formula has been validated by estimating DEBF in Iron/water and Iron/PMMA shield. Good agreement has been observed with the DEBF obtained from FLUKA code.

In this paper, we extend the study by estimating DEBF of Iron/HDPE shield, widely used material for reactor applications. The performance of above three double-layer combinations has been compared in terms of their gamma attenuation at 1 and 10 MeV.

2. New empirical formula and the associated parameters

Empirical formulae for DEBF are built on some suitable function of BF of individual layers determined by any of the transport method, largely Monte-Carlo method. DEBF combines infinite homogeneous BFs of individual layers as [2]:

$$B(X_1, X_2) = \frac{B_1(X_1)}{B_2(X_1)} B_2(X_1 + X_2)\,\mathrm{F}(X_1, X_2) \tag{1}$$

$$\mathrm{F}(X_1, X_2) = \frac{B(X_1, X_2) B_2(X_1)}{B_1(X_1) B_2(X_1 + X_2)} \tag{2}$$

In Eq. 1, $B_1(X)$ and $B_2(X)$ are BF of layer materials 1 and 2 respectively for thickness X in mean free path unit (*mfp*); $X_1$and X_2 are the thicknesses (*mfp*) of first and second layer.In this work we have proposed a new empirical function for the correlation function $F(X_1, X_2)$ as given below:

$$F(X_1, X_2) = \left[a \tanh\left\{ \frac{(X_2 + 0.5)}{t} \right\} + cX_2^{\,b} \right]^{\alpha} \tag{3}$$

First term describes the asymptotic rise of $F(X_1, X_2)$ with X_2 whereas second term expresses power law dependence of X_2.The parameter α is +1 if $B_2(X) \geq B_1(X)$ and -1 if $B_2(X) < B_1(X)$, for any X.Therefore, if the coefficients a, t, b and c can be related to physical parameters of the individual layer materials, then expression of F (Eq. 3) will be very effective in predicting BF and hence gamma attenuation for a given double-layer shield within 10% error limit.

As shown in Ref. 5, parameters '*b*' and '*c*' of Eq. 3are functions of energy dependent cross-sections of the two materials through the following relations:

$$b = \left[1 - \frac{(\mu_c/\rho)_2}{(\mu_c/\rho)_1} \right]; c = 3 \times \left| \left(1 - \frac{(\mu_t/\rho)_2}{(\mu_t/\rho)_1} \right) \right| \tag{4}$$

In the above $\frac{(\mu_c/\rho)_2}{(\mu_c/\rho)_1}$ and $\frac{(\mu_t/\rho)_2}{(\mu_t/\rho)_1}$ are the ratios of mass attenuation coefficient for incoherent scattering and total mass attenuation coefficient of the second material to that of first material. The parameter '*a*' and '*t*',are expressedby two different functions of X_1in two different energy regimes as:

$$a = \begin{cases} \dfrac{B_2(X_1)+1}{B_1(X_1)+1} \times \left(1 - e^{-X_1}\right) & ; \ \mathrm{E} \leq 3 \text{ MeV} \\ \dfrac{B_1(X_1)+1}{B_2(X_1)+1} \times \dfrac{\left(1 - e^{-X_1}\right)}{\left[\dfrac{(\mu_t/\rho)_1}{(\mu_t/\rho)_2}\right]} & ; \ \mathrm{E} > 3 \text{ MeV} \end{cases} \text{ and } t = \begin{cases} X_1 \log\left[\dfrac{B_2(X_1)}{B_1(X_1)}\right] + \dfrac{1.6}{E}\left[\dfrac{(\mu_t/\rho)_2}{(\mu_t/\rho)_1}\right] & ; \ \mathrm{E} \leq 3 \text{ MeV} \\ \left[\dfrac{B_1(X_1)}{B_2(X_1)}\right] + 1.6\left[\dfrac{(\mu_t/\rho)_1}{(\mu_t/\rho)_2}\right] & ; \ \mathrm{E} > 3 \text{ MeV} \end{cases} \tag{5}$$

3. Results and discussion

At first we estimate the single layer BF of Iron, water, PMMA, HDPE using FLUKA. The coefficients of the empirical formula namely, *a,b,c,t* have been calculated using XCOM database and FLUKA resultsusingEqs. 4 and 5. Subsequently the DEBF of *Iron/Water*, *Iron/PMMA* and *Iron/HDPE*due to point isotropic mono-energetic gamma sourcehave been calculated using *FLUKA.* Schematic diagram as well as representative FLUKA simulation geometry are shown in Fig. 1.In Table-1 we have compared few representative cases of DEBF generated by FLUKAand those by Eq. 1, along with Eq. 2 - Eq. 5 for a representative iron thickness (X_1) of 5 *mfp*. The quantitative accuracy with which the proposed empirical function is able to predict DEBF,is measured bypercentage relative deviation

defined as $\Delta = \left[\left(B_{\text{FLUKA}} - B_{\text{Formula}} \right) / B_{\text{FLUKA}} \right] \times 100$. It can be observed that, for 1 MeV point isotropic gamma,Δ is less than 5% for all three double-layer combinations.

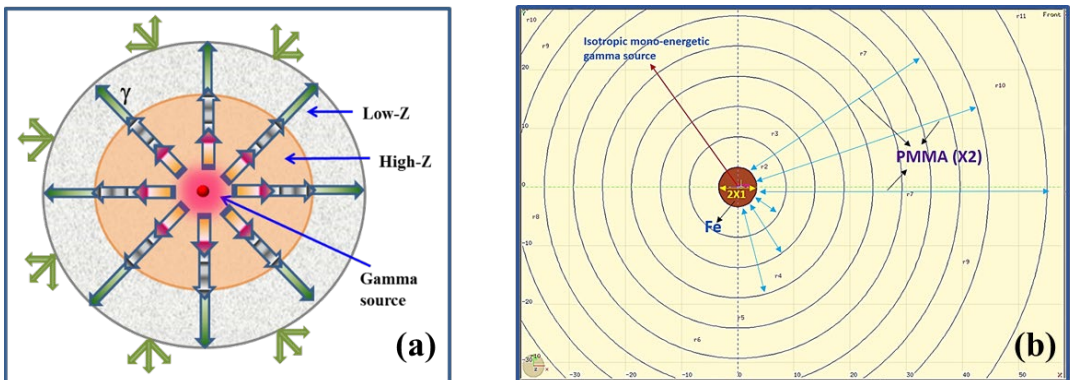


***Fig 1**: a)Schematic diagram; b) FLUKA (FLAIR) simulation geometry for the DEBF calculation*

***Table 1:**Comparison of DEBF obtained by FLUKA code with empirical formula for 1 MeV* gamma

X_2 (mfp)	FLUKA	Eq. 1	Δ (%)	FLUKA	Eq.1	Δ (%)	FLUKA	Eq. 1	Δ (%)
	Iron/Water			*Iron/PMMA*			*Iron/HDPE*		
2	16.4	16.8	*-2.0*	16.7	16.7	*0.0*	17.3	17.7	*-2.0*
3	21.5	22.0	*-2.3*	22.0	22.1	*-0.5*	23.6	23.2	*1.7*
4	26.5	26.1	*1.5*	27.3	27.4	*-0.4*	29.6	28.7	*3.2*
5	31.4	30.7	*2.0*	32.4	32.6	*-0.6*	35.6	33.9	*4.7*
6	36.2	35.4	*2.3*	37.6	37.8	*-0.5*	41.2	39.3	*4.6*
7	41.2	40.2	*2.5*	42.8	43.0	*-0.5*	47.0	44.7	*5.0*
8	46.3	45.1	*2.4*	48.2	48.5	*-0.6*	52.6	50.3	*4.3*
10	56.7	55.6	*1.9*	59.2	59.5	*-0.5*	64.6	62.2	*3.7*

For better understanding, the role of three hydrogenous materials namely, Water, PMMA and HDPE in gamma build-up, we have graphically represented few random cases of DEBF in Fig. 2. Panels (a), (b) and (c) of Fig. 2 correspond to Iron/Water, Iron/PMMA and Iron/HDPEsystem respectively for three representative iron thicknesses namely, 2, 5 and 10 mfp.Dotted lines and scattered data refer to Eq.1and FLUKA generated results.

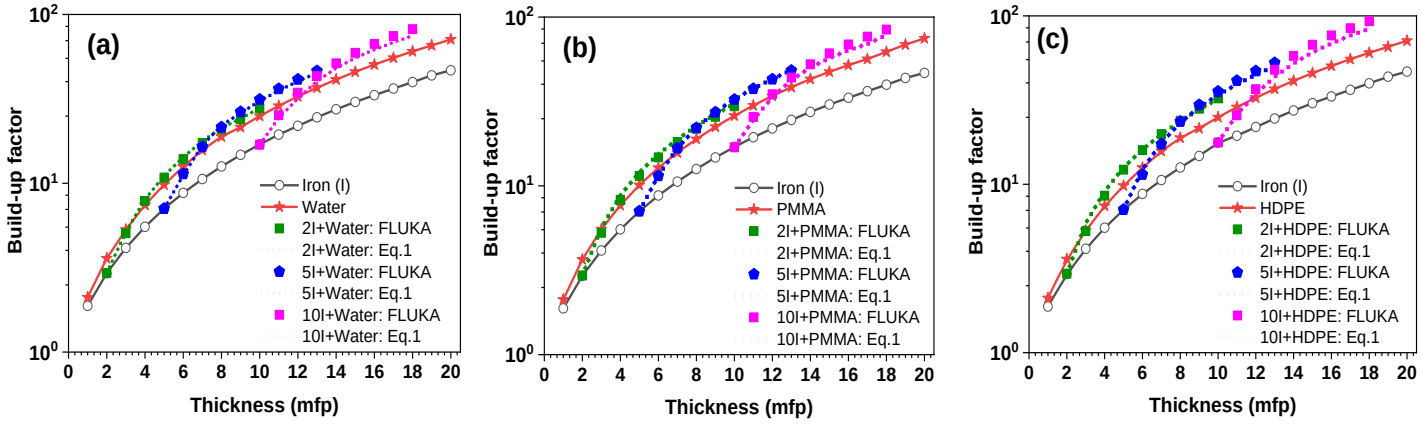


***Fig 2:** Thickness variation of single-layer BFas well as DEBFin (a) Iron/Water, (b)Iron/PMMAand (c) Iron/HDPE for 1 MeV gamma. Here xI refers to iron thickness of x mfp, with x=2, 5 and 10.*

Similar analysis has also been carried out to evaluate DEBF for higher energy (10 MeV) gamma as shown in Fig. 3. It has been found that Δ in this case is less than 10 % for all the cases.

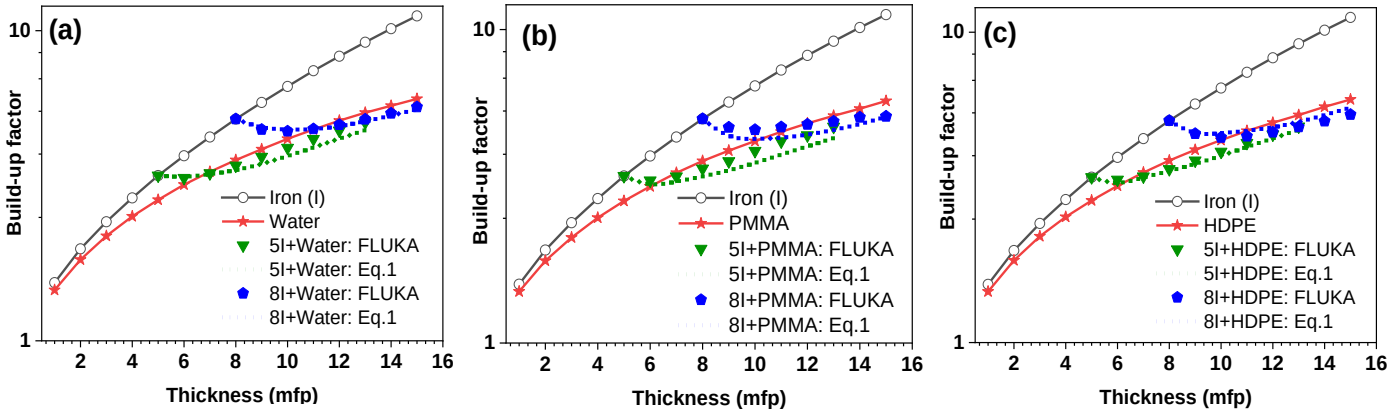


Fig 3:*Same as Fig.2 but for 10 MeV gamma source and iron thicknesses of 5 (5I) and 8 (8I) mfp.*

To provide a general comparison for the performances of Water, PMMA and HDPE as a double layer shield along with Iron, we consider a double-layer combination with 10.6 cm of iron followed by 98.6 cm of Water/PMMA/HDPE. With the help of mass attenuation data and DEBF for 1 MeV gamma, it is found that, the attenuation in Iron/PMMA is about 56% and 70 % more than Iron/Water and Iron/HDPE systems respectively.The difference in attenuation for 10 MeV is of the same order.

4. Conclusion

In this paper we have constructed a new empirical formula for determining DEBF of any arbitrary layer combination of double layer shield.Validity and robustness of the formula is demonstratedby comparing DEBF of Iron/water, Iron/PMMA and Iron/HDPE shield for 1 MeV and 10 MeV gammawith those obtained by FLUKA. Study revealed thatPMMA serves the best purpose for attenuatinggamma radiation.

5. Acknowledgement

Authors express their sincere gratitude to Shri C.G. Karhadkar, Director, Reactor Group, BARC,Shri H.G. Gujar, Head, RRSD for their support to carry out this work.

6. References

[1] U.T. Lin and S.H. Jiang, “A dedicated empirical formula for γ-ray build-up factors for a point isotropic source in stratified shields”, *Radiation Physics and Chemistry*, 48(4), 1996, pp.389-401.

[2]Assad et al., “A new approximating formula for calculating gamma-ray build-up factors in multilayer shields”, *Nuclear science and engineering*, 132(2), 1999, pp.203-216.

[3] Basu et al., “An improvement to the Kalos’ formula for double layer gamma ray exposure build-up factors for shielding materials of nuclear and radiological facilities”, *Annals of Nuclear Energy*, 151, 2021, p.107944.

[4] A. Das and T. Singh, "Development of a new Monte Carlo based transport code to calculate photon exposure build-up factors in various shielding arrangements.", *Radiation Physics and Chemistry* 194, 2022, p.110028.

[5] Das et al., “Determination of double-layer gamma build-up factor using Monte Carlo code, FLUKA: Development of new empirical formula”, *Radiation Physics and Chemistry* 196, 2022, p.110122

[6] Ferrari et al., “FLUKA: a multi-particle transport code”, CERN-2005-10, 2005, INFN/TC05/11, SLAC-R-733.

Extension of Pomraning'ssimplified spherical harmonics model to general *N* and finite medium

Abhishek Mishra[1,3], Aditi Ray[2,3] and Tej Singh[1]

[1]Research Reactor Services Division, Bhabha Atomic Research Centre, Mumbai, India

[2]Theoretical Physics Section, Bhabha Atomic Research Centre, Mumbai, India

[3]Homi Bhabha National Institute, Anushaktinagar, Mumbai, India

[1]*e-mail: -abhiknm@barc.gov.in*

Abstract

We present mathematically consistent derivation of SP_N equations in second-order differential form. Derivation led to N^{th} order SP_Nequations consisting of $(N+1)/2$ equations in terms of even-order scalar functions.This has been achieved by employing variational method for solution of neutron transport equation with a trial function originally proposed by Pomraning. The present derivation can be applied to any arbitrary order SP_N equations. We also present the derivation of new Marshak-like boundary conditions for even-parity angular flux.

1. Introduction

Simplified Spherical Harmonics (SP_N) methodwas proposed by Gelbard as an alternative to P_N method to reduce the computational burden encountered in solving three-dimensional (3D) neutron transport problem[1]. Though Gelbard derived SP_N equations heuristically,but the model showed improvement over diffusion approximation (P_1solutions) in many general geometry reactor problems [2]. The first mathematical foundation of SP_N equations was built as late as 1993 through asymptotic approach [3,4] as well as variational analysis [4].Since then there has been constant interest in developing alternative derivations of SP_N equations and applying them to different systems [2].Recently,Chao has proposed generalized (G)SP_N making it fully equivalent to $P_N$form and devised numerical methods to solve them for reactor problems [5]. In a recent work, we have shown the equivalence of GSP_N and SP_N equations [6].

Pomraning obtained SP_N equationsusing certain trial function in the self-adjoint variational characterization of even-parity transport equation [4]. This resulted in second-order differential form of SP_1 and SP_3 equations for even-parity angular flux. However, extending it to higher order N would require cumbersome algebraic manipulations.

Pomraning proposed an *alternative* trial function which was never utilized for the present purpose. Current paper presents the mathematical formulations for deriving SP_N equations from this alternative trial function. To the best of our knowledge,this is the first successful attempt towards this. Additionally, in contrast to Pomraning's derivation, we have extended the variational framework to finite medium. This is fulfilled by deriving, perhaps for the first time, mathematically consistent Marshak-like boundary conditions for even-parity angular flux.

2. Neutron transport equation for even-parity angular flux

The one-energy-group, time-independent neutron transport equation for isotropic scattering and isotropic sources (fission as well as external) can be written as,

$$\hat{\Omega}\cdot\vec{\nabla}\psi\left(\vec{r},\hat{\Omega}\right)+\sigma\psi\left(\vec{r},\hat{\Omega}\right)=\frac{1}{4\pi}\left\{\sigma_s\phi\left(\vec{r}\right)+\nu\sigma_f\phi\left(\vec{r}\right)+S_0\left(\vec{r}\right)\right\}, \tag{1.1}$$

where we have used, $S\left(\vec{r},\hat{\Omega}\right)=\frac{1}{4\pi}S_0\left(\vec{r}\right)$, $\int_{4\pi}\sigma_s\left(\hat{\Omega}'\to\hat{\Omega}\right)\psi\left(\vec{r},\hat{\Omega}'\right)d\hat{\Omega}'=\frac{1}{4\pi}\sigma_s\phi\left(\vec{r}\right)$ and $\phi\left(\vec{r}\right)=\int_{4\pi}\psi\left(\vec{r},\hat{\Omega}'\right)d\hat{\Omega}'$ is the scalar neutron flux. Remaining symbols have their usual meanings.

Dividing eq.(2.1) by σ and expressing the distance in units of mean free path, we can write,

$$\hat{\Omega}\cdot\vec{\nabla}\psi\left(\vec{r},\hat{\Omega}\right)+\psi\left(\vec{r},\hat{\Omega}\right)=\frac{Q\left(\vec{r}\right)}{4\pi}, \tag{1.2}$$

Where we have assumed $1/\sigma = 1$ mfp and $c=\sigma_s+\nu\sigma_f$,

$$Q\left(\vec{r}\right)=c\phi\left(\vec{r}\right)+S_0\left(\vec{r}\right), \tag{1.3}$$

Writing Eq.(2.2) for $-\hat{\Omega}$,

$$-\hat{\Omega}\cdot\vec{\nabla}\psi\left(\vec{r},-\hat{\Omega}\right)+\psi\left(\vec{r},-\hat{\Omega}\right)=\frac{Q\left(\vec{r}\right)}{4\pi} \tag{1.4}$$

Next, we decompose the angular flux appearing in above equations into even (ψ_e) and odd (ψ_o) parity components. We eliminate the odd components from Eqs. (2.2) and (2.4) to get the following second-order form of transport equation.

$$-\left(\hat{\Omega}\cdot\vec{\nabla}\right)^2\psi_e\left(\vec{r},\hat{\Omega}\right)+\psi_e\left(\vec{r},\hat{\Omega}\right)=\frac{Q\left(\vec{r}\right)}{4\pi} \tag{1.5}$$

2.1 Derivation of SP_N equations by variational method

The *alternative*trial function proposed by Pomraning is [4],

$$\psi_e\left(\vec{r},\hat{\Omega}\right)=\sum_{n=0}^{(N-1)/2}\left(\frac{4n+1}{4\pi}\right)\left\{L_{2n}\left(\hat{\Omega}\cdot\vec{\nabla}\right)\right\}\left(\nabla^2\right)^{-n}\psi_{2n}\left(\vec{r}\right), \tag{1.6}$$

where *N* is an odd integer and the operator L_{2n} is defined as

$$L_{2n}\left(\hat{\Omega}\cdot\vec{\nabla}\right)=a_{n0}\nabla^{2n}+a_{n1}\nabla^{2(n-1)}\left(\hat{\Omega}\cdot\vec{\nabla}\right)^2+a_{n2}\nabla^{2(n-2)}\left(\hat{\Omega}\cdot\vec{\nabla}\right)^4+\ldots+a_{nn}\left(\hat{\Omega}\cdot\vec{\nabla}\right)^{2n}. \tag{1.7}$$

The coefficients a_{ni} in Eq. (2.7)are same as appear in even order Legendre polynomial P_{2n}.
We first use the form of ψ_e, given by Eq.(2.6), into Eq. (2.5)and apply the resulting equation by operator w_{2m} definedas $w_{2m}\left(\hat{\Omega},\vec{r}\right)=\left(\hat{\Omega}\cdot\vec{\nabla}\right)^{2m}$.Then, we integrate the whole expression over entire angular domain. In order to integrate, we use following identity.

$$\int_{4\pi}d\hat{\Omega}w_{2m}F\left(\vec{r}\right)=\frac{4\pi}{2m+1}\nabla^{2m}F\left(\vec{r}\right)\qquad m\geq 0. \tag{1.8}$$

This results into following equation.

$$\begin{aligned}&\sum_{n=0}^{(N-1)/2}\left[\left(4n+1\right)\left\{\begin{aligned}&a_{n0}\frac{1}{2m+1}\nabla^{2m}+a_{n1}\frac{1}{2\left(m+1\right)+1}\nabla^{2m}\\&+a_{n2}\frac{1}{2\left(m+2\right)+1}\nabla^{2m}+\ldots+a_{nn}\frac{1}{2\left(m+n\right)+1}\nabla^{2m}\end{aligned}\right\}\right]\psi_{2n}\left(\vec{r}\right)\\&-\sum_{n=0}^{(N-1)/2}\left[\left(4n+1\right)\left\{\begin{aligned}&a_{n0}\frac{1}{2\left(m+1\right)+1}\nabla^{2(m+1)}+a_{n1}\frac{1}{2\left(m+2\right)+1}\nabla^{2(m+1)}\\&+a_{n2}\frac{1}{2\left(m+3\right)+1}\nabla^{2(m+1)}+\ldots+a_{nn}\frac{1}{2\left(m+n+1\right)+1}\nabla^{2(m+1)}\end{aligned}\right\}\right]\psi_{2n}\left(\vec{r}\right)\\&=\frac{1}{2m+1}\nabla^{2m}Q\left(\vec{r}\right).\end{aligned} \tag{1.9}$$

This is the general form of SP_N equation for any arbitrary N. It should be noted that in Eq. 2.9, *N* is odd and $0\leq n, m\leq (N-1)/2$. For a given *N*, the number of different valuesthat *m*can assume is the number of equations under SP_N approximation.
For illustration, here we present the explicit SP_N equations for *N* = 1 and 3.

SP₁ equation: $$-\frac{1}{3}\nabla^2\psi_0(\vec{r})+(1-c)\psi_0(\vec{r})=S_0(\vec{r}) \tag{1.10}$$

SP₃ equations: $$-\frac{2}{3}\nabla^2\psi_2(\vec{r})-\frac{1}{3}\nabla^2\psi_0(\vec{r})+(1-c)\psi_0(\vec{r})=S_0(\vec{r}) \tag{1.11}$$

$$-\frac{2}{15}\nabla^2\psi_0(\vec{r})-\frac{11}{21}\nabla^2\psi_2(\vec{r})+\psi_2(\vec{r})=0 \tag{1.12}$$

In the above equations, we have used Eq. (2.3)and the fact that for any *N*, the leading space-dependent scalar function $\psi_0(\vec{r})$ in the trial function expansion is always equal to the scalar flux $\phi(\vec{r})$. This is not the case with the trial function originally utilized by Pomraning where scalar flux becomes combination of higher order space-dependent scalar functions too for $N>1$.

3. Derivation of boundary conditions

To apply the above form of SP_N equation to finite media, appropriate boundary conditions are required. In traditional SP_N theory, planar boundary conditions are usedthat assumes locally one-dimensional (1D) behaviour of angular flux nearboundary. In order to derive appropriate boundary conditions,we have relaxed this assumption. Our approach is similar to that of Marshak boundary conditions for P_N equations.The true boundary condition for an angular flux equation is that the incident angular flux at boundaries is known [7]. The procedure adopted here is described below.

In terms of even-parity angular flux, the boundary conditions of known incident flux are written as [7]:

$$\hat{\Omega}\cdot\vec{\nabla}\psi_e(\vec{r}_s,\hat{\Omega})-\psi_e(\vec{r}_s,\hat{\Omega})=-\psi_{in}(\vec{r}_s,\hat{\Omega}) \quad \text{for} \quad \hat{\Omega}\cdot\hat{n}_s<0, \tag{2.1}$$

$$\hat{\Omega}\cdot\vec{\nabla}\psi_e(\vec{r}_s,\hat{\Omega})+\psi_e(\vec{r}_s,\hat{\Omega})=\psi_{in}(\vec{r}_s,-\hat{\Omega}) \quad \text{for} \quad \hat{\Omega}\cdot\hat{n}_s>0, \tag{2.2}$$

where, $\hat{n}_s$ is the outward normal at boundary point $\vec{r}_s$ and $\psi_{in}(\vec{r}_s,\pm\hat{\Omega})$ are known.

These boundary conditions are true for exact even-parity angular flux and thus cannot be satisfied by even-parity angular flux approximated to a series of finite terms. The obvious way to develop boundary conditions that are consistent with our flux approximation is to use this flux expansion in Eqs. (3.1) and (3.2). Using Eq. (2.6)in Eq. (3.1), operating the resulting equation by the operator $w_{2m+1}=\left(\hat{\Omega}\cdot\nabla\right)^{2m+1}$ and integrating final equation over $\hat{\Omega}$ in the regime $\hat{\Omega}\cdot\hat{n}_s<0$, we get

$$\int_{\hat{\Omega}\cdot\hat{n}_s<0} d\hat{\Omega}\sum_{n=0}^{(N-1)/2}\left(\frac{4n+1}{4\pi}\right)\left[\begin{Bmatrix}a_{n0}w_{2m+2}+a_{n1}\nabla^{-2}w_{2m+4}\\+a_{n2}\nabla^{-4}w_{2m+6}+\ldots+a_{nn}\nabla^{-2n}w_{2(m+n)+2}\end{Bmatrix}-\begin{Bmatrix}a_{n0}w_{2m+1}+a_{n1}\nabla^{-2}w_{2m+3}\\+a_{n2}\nabla^{-4}w_{2m+5}+\ldots+a_{nn}\nabla^{-2n}w_{2(m+n)+1}\end{Bmatrix}\right]\psi_{2n}(\vec{r}_s)$$
$$=-\int_{\hat{\Omega}\cdot\hat{n}_s<0} d\hat{\Omega}w_{2m+1}\psi_{in}(\vec{r}_s,\hat{\Omega}). \tag{2.3}$$

Similarly, using Eq. (2.6)in Eq. (3.2) and following the same procedure except for integration domain being $\hat{\Omega}\cdot\hat{n}_s>0$,we get,

$$\int_{\hat{\Omega}\cdot\hat{n}_s>0} d\hat{\Omega} \sum_{n=0}^{(N-1)/2} \left(\frac{4n+1}{4\pi}\right) \left[\begin{Bmatrix} a_{n0}w_{2m+2} + a_{n1}\nabla^{-2}w_{2m+4} \\ +a_{n2}\nabla^{-4}w_{2m+6} + \ldots + a_{nn}\nabla^{-2n}w_{2(m+n)+2} \end{Bmatrix} + \begin{Bmatrix} a_{n0}w_{2m+1} + a_{n1}\nabla^{-2}w_{2m+3} \\ +a_{n2}\nabla^{-4}w_{2m+5} + \ldots + a_{nn}\nabla^{-2n}w_{2(m+n)+1} \end{Bmatrix} \right] \psi_{2n}\left(\vec{r}_s\right) \tag{2.4}$$

$$= \int_{\hat{\Omega}\cdot\hat{n}_s>0} d\hat{\Omega} w_{2m+1} \psi_{in}\left(\vec{r}_s, -\hat{\Omega}\right).$$

Eqs. (3.3) and (3.4) constitute the general Marshak-like boundary conditions for SP_N equation (Eq. 2.9).

4. Conclusion

We have derived SP_N equations in a mathematically consistent way of variational method using an *alternate trial function*suggested by Pomraning for derivation of higher order SP_N equations. To the best of our knowledge, this is the first such attempt in this regards. Further, we have supplemented our SP_N equations with new boundary conditions.

Acknowledgement
Authors would like to thank Shri C. G. Karhadkar, Director, Reactor Group and Shri H. G. Gujar, Head, Research Reactor Services Division for their support in pursuing the work.

References

[1] E. M. Gelbard, "Simplified Spherical Harmonics equation and their use in shieldingproblems", *Technical Report*, WAPD-T-1182 (Rev.1), Bettis Atomic Power Laboratory,1961.

[2] R. G. McClarren, "Theoretical aspects of the simplified P_N equations", *Transp. Theory Stat. Phys.* 39, 2010, 73–109.

[3] E. W. Larsen, J. E.Morel and J. M. McGhee, "Asymptotic derivation of the simplified P_N equations", *Mathematical Methods and Supercomputing in Nuclear ApplicationsProceedings*,**1**, 1993, 878.

[4] G. C. Pomraning, "Asymptotic and variational derivations of the simplified PNequations", *Ann. Nucl. Energy***20**, 1993, 623–637.

[5] Y. A. Chao, "A new and rigorous SP_N theory – Part IV: Numerical qualification of $GSP_3^{(0)}$ and the generalized transverse integration nodal method", *Ann. Nucl. Energy***149**, 2020, 107768 and references therein.

[6] A. Mishra, A. Ray and T. Singh, "On Simplified Spherical Harmonics (SP_N) and Generalized SP_N (GSP_N) formulations", *Ann. Nucl. Energy***173**, 2022, 109071

[7] W. M. Stacey, "Nuclear Reactor Physics", *Wiley*, 2007.

ANALYSIS OF KUCA-A TYPE CORE USING DETERMINISTIC CODE

K.P.Singh [1] and A.K. Singh [2]
[1] Bhabha Atomic Research Centre, Mumbai, India
[2] Bhabha Atomic Research Centre, Mumbai, India
[1]*e-mail: - kpsingh@barc.gov.in*

Abstract

This paper discusses the analysis of KUCA type-A core using a deterministic code 'KINFIN'. Objective of the analysis is to investigate the validity of multigroup deterministic code 'KINFIN' to analyze static and kinetic experiments in the determination of sub-criticality. Using static and kinetic deterministic codes, evaluation of fundamental K and fundamental prompt alpha eigenvalue has been done for the core configurations of KUCA –Type-A core. It has been found that the diffusion based deterministic codes in sub-critical reactor analysis have limitations due to high heterogeneity and presence of large void to accommodate external neutron source. However, for quicker analysis, the deterministic codes are still useful.

1. Introduction

Several ADS experiments were carried out at Kyoto University Research Reactor Institute (KURRI) with primary focus towards establishing suitable measurement techniques for the measurement of sub-critical reactor neutronics parameters and benchmarking the computational tools used for the design and analysis of Accelerator Driven Subcritical Reactor. The KUCA type-A[1]core is constituted with fuel assemblies which in turn are constituted by stacking highly enriched (93%) uranium-aluminium (U-Al) alloy plates with polyethylene plates. The core is reflected by polyethylene. The sub-criticality in the core is achieved by the insertion of control rods or safety rods, or both. Using the code KINFIN[2], evaluation of prompt fundamental alpha eigenvalue and K eigenvalue has been done. This paper presents the results for sub-criticality determination of KUCA-A core using static and kinetic deterministic codes.

2. Description of KUCA A-type core

KUCA is a multi-core type critical assembly having three independent cores, namely, two solid-moderated cores (A, B cores) and one light water-moderated core (C core). The core has a provision to couple with external neutron sources. A variant of the A-core (A1/8"P60EUEU(3)) having five different core configuration was used for measuring the neutronics parameters of the core. The reactor cores are constructed with a combination of 25 fuel assemblies (Figure-1). There are three control and three safety rods (C1, C2, C3, S1, S2, S3) in KUCA core. Different sub-criticality levels are achieved using different number of fuel assemblies and different control/safety rods insertions.

The lattice assemblies are in the form of 2" sq rectangular parallelepiped. The upper and lower parts of the fuel region were polyethylene reflector layers of more than 50 cm long. The fuel rod, a highly-enriched uranium-aluminium (U-Al) alloy, consisted of 60 cells of polyethylene plate 1/8" thick, and a U-Al plate 1/16" thick and 2" sq.

3. Description of the code KINFIN

Computer code 'KINFIN' is a three dimensional space time kinetics code which solves the few group time dependent diffusion equation with delayed neutrons. This code, solves multi-group neutron

diffusion equation by finite difference methods in Cartesian geometry, calculates core reactivity, core fission power distribution and multi-group fluxes in and around the core region. It has several modules for different evaluations. 'KINFIN' can calculate the prompt and delayed α-modes, the λ-modes, as well as fixed source and time dependent problems.

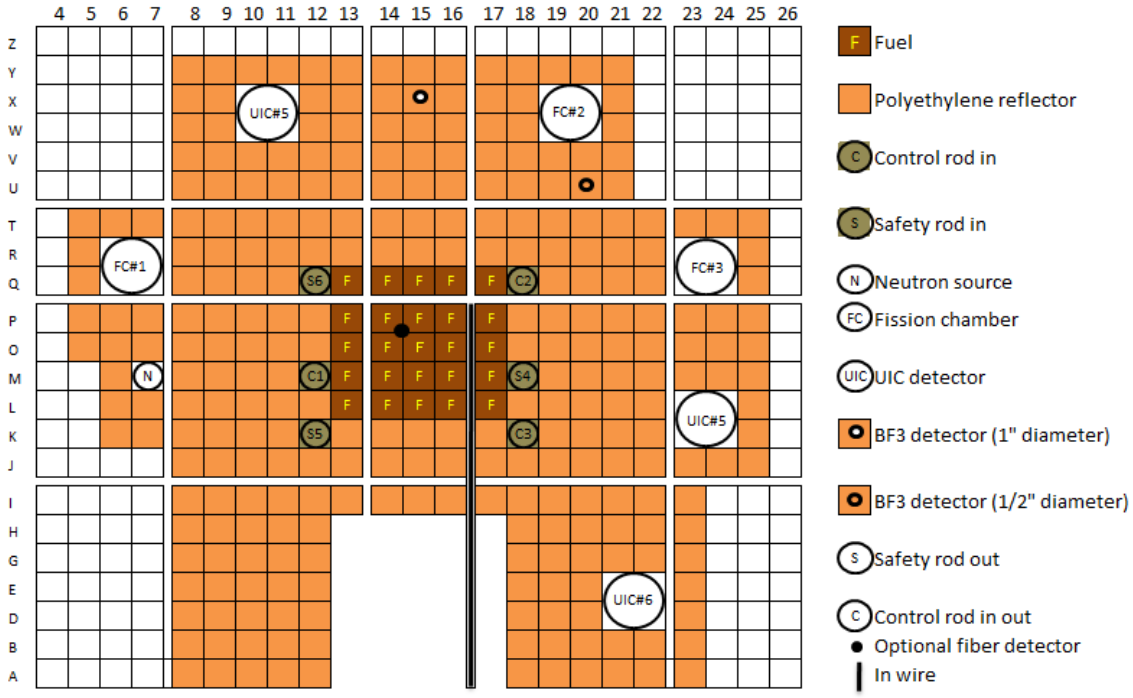


Figure 1 KUCA-A core configuration.

4. Modelling of the core

The KUCA core configurations were modelled and analysed using one dimensional transport theory lattice code WIMSD4[3], two dimensional transport theory lattice code TWOTRAN[4] and three dimensional multi-group diffusion theory code KINFIN. Three dimensional core calculations were done using neutron cross-section in three energy groups. WIMSD-4 code and 69 neutron energy group ENDF/B-VI cross section data library is used to generate three group cross sections (macroscopic) of all core materials at lattice level, which are subsequently used as input to TWOTRAN and KINFIN for assembly and core level calculations respectively.

5. Results

The effective multiplication factor for the core A-I4[1] has been obtained with WIMS-TWOTRAN-KINFIN combination and compared with MCNPX[1]. As seen in the Table-1, there is a difference of ~10 mk between our result and MCNPX. This can be attributed to effect of homogenization, diffusion approximation in core calculation and use of only 3 energy groups in core calculations. In future, we are likely to increase number of representative energy groups and use full transport method for the analysis.

Table-1: Keff value comparison

KINFIN	Reference
0.9645	0.9731

We have evaluated fundamental prompt α/K eigen value/mode and prompt neutron generation time (Table-2, Figure-2&3) for the core. A full 3D, time-dependent analysis was also performed with the KINFIN code for a pulsed neutron experiment with a single pulse width of 100 ns. In Figure-4 is given the time-dependent neutron flux in group 3 (thermal flux), roughly in the center of the core. After the source pulse, many α-modes are excited, but ultimately only the fundamental prompt α-mode remains, once the higher modes have died away. Using slope fit method (Figure-5), the evaluation of fundamental alpha has been carried out.

Table-2: Prompt neutron generation time and fundamental prompt alpha eigenvalue

Prompt neutron generation time	26 micro-second	
Fundamental prompt alpha eigenvalue	KINFIN 1262 sec^{-1} (power iteration) 1270 sec^{-1} (slope fit)	Experiment (1083 to 1205) sec^{-1}

.

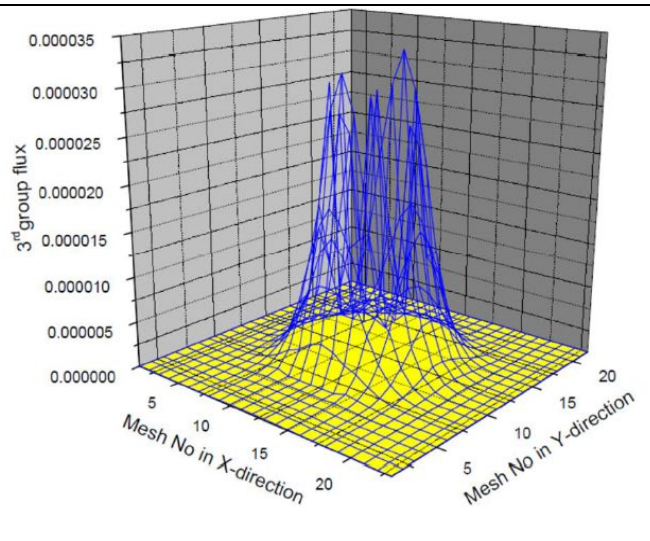


Figure-2: Fundamental alpha mode

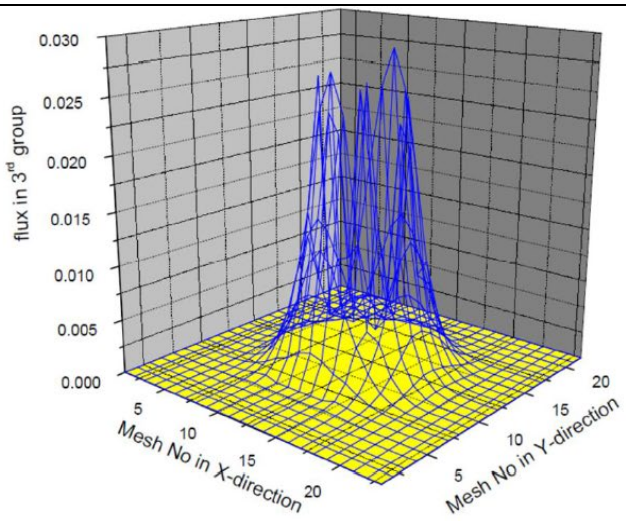


Figure-3: Fundamental K mode

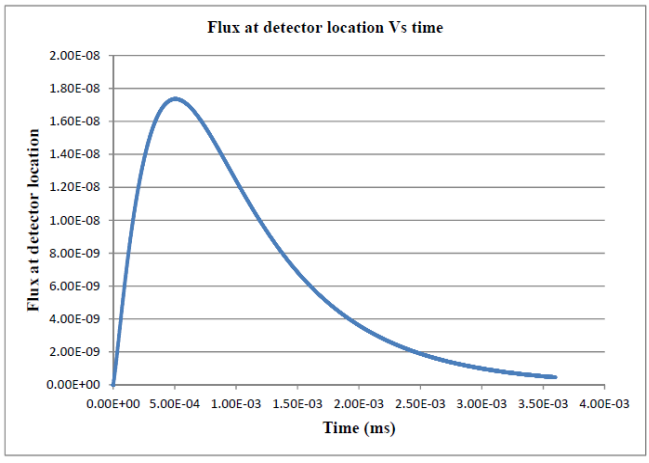


Figure-4: Neutron flux behaviour with time due to pulse neutron source

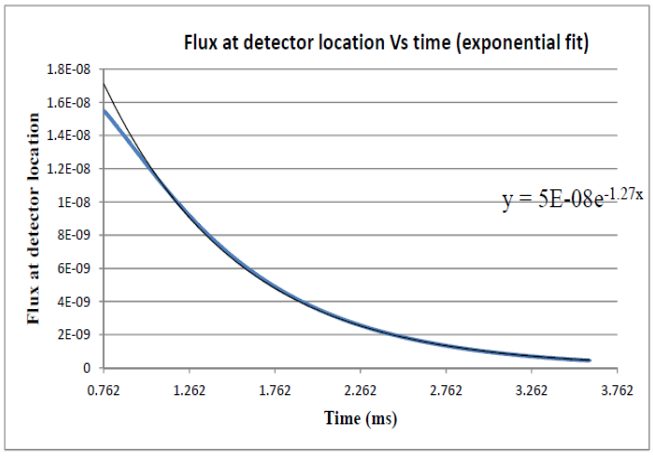


Figure-5: Exponential fitting for obtaining fundamental α (Detector placed at 15X [figure-])

6. Conclusion

The validity of the calculation tool adopted and the data library used for the calculation of sub-criticality are tested through this benchmark. Fundamental α and K-mode has been estimated using code combination KINFIN-WIMSD4-TWOTRAN. It has been found that the use of diffusion based deterministic codes for sub-critical reactor analysis has limitations due to presence of high heterogeneity and large void for accommodating external neutron source. However, for quicker analysis, the deterministic codes are still useful. In future we are likely to do core calculation using deterministic neutron transport code in more number of energy groups as compared with three groups used in the present analysis. In KUCA-A core, nature of alpha and K-mode are found to be similar. This is due to the lesser sub-criticality (high Keff, 0.97) level of the core.

7. References

[1] Cheolho Pyeon ,"Experimental Benchmarks of Neutronics on Solid Pb-Bi in Accelerator-Driven System with 100 MeV protons at Kyoto University Critical Assembly".

[2] K. P. Singh, R. S. Modak, S.B.Degweker and Kanchi Singh, "Iterative Schemes for obtaining dominant alpha-modes of the neutron diffusion equation", *Annals of Nuclear Energy*, 36(2009) 1086-1092.

[3] Askew, J.R., Fayer, F.J. and Kemshell, P.B., "A Genral Description of Lattice Code WIMSD", *Journal of the British Nuclear Energy Society* 5 (4), 564. 1966.

[4] Lathrop, K.D. and Brinkley, F.W, "Theory and use of the general geometry TWOTRAN Program", *Los Alamos Scientific Laboratory*, LA-4432 1970.

DEVELOPMENT OF MONTE CARLO CODE FOR THE ASSESMENT OF CRITICALITY OF FISSILE SYSTEMS

Sachin Shet[1*] and K.V. Subbaiah[1]
[1]*Manipal Centre for Natural Sciences, Centre of excellence,*
Manipal Academy of Higher Education (MAHE), Manipal, Karnataka-576104.
[*]shet.sachin@manipal.edu

Abstract

An Indigenous Monte Carlo code, MCkeff, for solving the steady-state neutron transport equation is currently under development at the Manipal Centre for Natural Sciences to estimate the neutron multiplication factor (k_{eff}) of systems containing fissile materials such as U-235 and Pu-239. Any arbitrary configuration of materials contained in cells can be described by its bounding signed analytical linear or quadratic surfaces (half-spaces) combined with Boolean operators of intersection and union. In the present code, the events simulated are elastic scattering, fission, inelastic scattering, (n, xn) and several other absorption reactions (n, c) given in any particular ENDF evaluation. For reactions which results with one or more secondary neutrons, energy and angles are sampled as per the laws prescribed in the ENDF 6 file. Special treatment is employed in the code for thermal neutrons (<4eV) using S (α, β) cross-sections (for light nuclides) and for intermediate energy neutrons (few keV to tens of keV) in heavy elements to account for self-shielding effects on cross-sections using probability tables of cross-sections. At the end of the simulation, the neutron multiplication factor (k_{eff}) of a system is estimated.

1. Introduction

Safety in the Nuclear industry is of utmost importance as it involves handling large quantities of fissile isotopes of uranium and plutonium. Some places where a large amount of fissile material is involved are fuel storage, fuel reprocessing, fuel fabrication, etc. The crucial parameter in handling fissile materials is the neutron multiplication factor (k_{eff}) of the system. A precise estimate of this parameter is essential to avoid criticality accidents [1]. Monte Carlo Codes are preferred due to flexibility in handling complicated geometrical arrangements of materials, ease of incorporating detailed physical processes, and simplicity in estimating errors associated with the results. The theory behind this method is described in detail in the references [2-4]. Several Monte Carlo codes [5-8] exists to estimate the k_{eff} of a system. An overview of general-purpose Monte Carlo radiation transport codes existing in the ORNL/RSICC library is published by Kirk [9]. It is known that the Monte Carlo methods consume a lot of computer resources and computation (CPU) time to get the result of a problem with a desirable precision. This prohibits the usage of few of the previously available codes for computation as they are obsolete due to sea changes in the hardware and software of the computer industry besides the development of new algorithms. A new Monte Carlo code MCkeff has been written from scratch, keeping in mind the advances made over time.

2. Method of solution

For criticality problems, a steady-state neutron transport equation, which is in the Eigen value-form, is solved [10-11]. The eigenvalue equation(ref [12] eq. 1) is:

$$[\Omega \cdot \nabla + \Sigma_t(\vec{r}, E)]\, \Psi(\vec{r}, E, \Omega) = \iint \Psi(\vec{r}, E', \Omega')\, \Sigma_s(\vec{r}, E' \rightarrow E, \Omega \cdot \Omega')\, d\Omega'\, dE'$$

$$+ \frac{1}{k_{eff}} \frac{\chi(E)}{4\pi} \iint \nu \ \Sigma_f(\vec{r}, E') \ \Psi(\vec{r}, \mathrm{E}', \Omega') \ dE' \ d\Omega'$$

Where,

$\Psi(\vec{r}, E, \Omega)$	- neutron angular flux
$\Sigma_t(\vec{r}, E)$	- total cross section
$\Sigma_f(\vec{r}, E')$	- fission cross-section
ν	- the average number of neutrons emitted per fission
(r, E′ → E, Ω′ → Ω)	- the probability of transfer from (E′, Ω′) to (E, Ω)
k_{eff}	- is the neutron multiplication of the system.

The left-hand terms represent the neutron leakage and absorption and the first term on the right-hand side is the scattering term, and the second term describes the neutron production term due to fission. The constant k_{eff} is an eigenvalue included in the above equation to match both sides of the equation. The Monte Carlo method proceeds for the solution by the methods of successive generations or power iteration method [13] to estimate the largest eigenvalue of the system. This calculation scheme is employed in MCkeff. The definition of k_{eff} is given as

$$\mathrm{k_{eff}} = \frac{\text{fission neutrons produced in the current generation}}{\text{fission neutrons started in the previous generation}}.$$

In Monte Carlo simulations, generation means tracking neutron events from the birth of a neutron (site of fission) to its death (parasitic absorption or escape from the system) over a batch of neutrons. Any individual history (sequence of recorded events) from the batch may not have any physical meaning. However, an average of histories over a large number contains the physical characteristics of the medium. The required parameter can be deduced from the histories. At the end of tracking neutrons, the predetermined number of neutrons, k_{eff} is estimated, and fission sites are stored for subsequent iterations. The iterations are stopped when the value of k_{eff} of a system converges. At the end of the simulation, the code estimates from the recorded histories the neutron multiplication factor (k_{eff}) of a system

The salient features of the MCkeff code are:

- Written from scratch incorporating FORTRAN 2008 features for Windows and Linux Operating systems.
- The input file is a filed free text file. The structure and format followed are the same as that of other Monte Carlo codes.
- Input checking is done extensively to detect all possible errors, and messages of fatal errors and warnings are displayed on the screen.
- It allows building a complex configuration of materials in geometric regions (cells) bounded by linear and/or quadratic surfaces combined with Boolean operators of intersection and union. Besides, it allows urinary complement operator of a cell.
- It has provision for specifying universes and lattices, enabling built of complex repeated structures with ease
- Interactive debug features of 2D geometry plotting. Attempts are being made to run on Parallel computers.

3. Results

The newly developed code testing and validation of the results are carried out by the Validation of full core problem and other criticality benchmark problems.

Validation of full core problem and other criticality benchmark problems

Hoogenboom et al. [16] had proposed a criticality Benchmark problem of a typical reactor core to test the efficacy of newly developed Monte Carlo codes. Fig. 1 shows the layout of the (A) ¼th of the core, (B) fuel assembly within a core, including guide tubes and (C) the fuel pin. MCkeff and OpenMC were run with 100,000 particles per cycle, 150 inactive batches, and 4000 active batches. These two codes do not use any biasing techniques or convergence acceleration techniques, using the same ENDF/B-VII.1 libraries. Table 1 shows the k_{eff} results with their standard deviations.

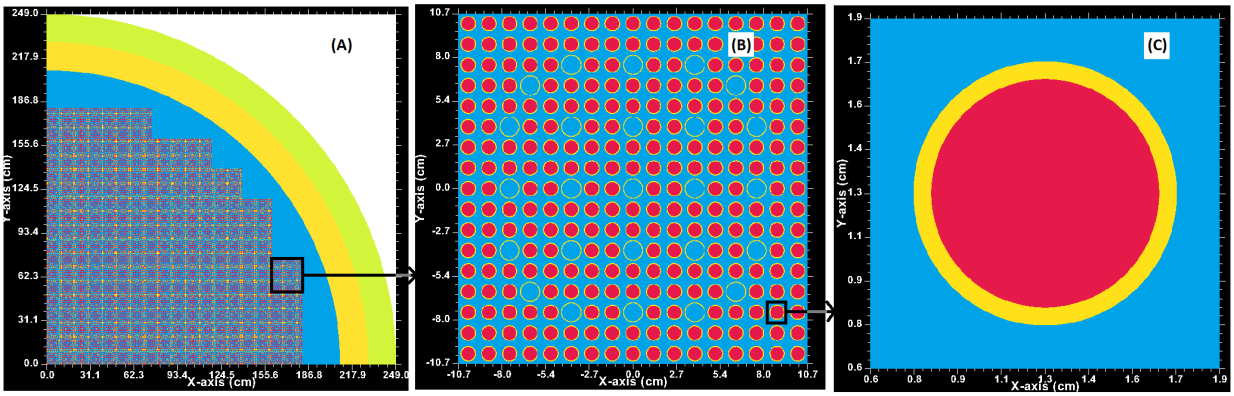


Fig. 1. shows the layout of (A) the ¼ th core, (B) fuel assembly within a core including guide tubes and (C) the fuel pin.

Table 1. Comparison of k_{eff} values for performance Benchmark problem with 2 different codes

Performance benchmark	$k_{eff} \pm 1\sigma$
MCkeff	1.00088 ± 0.00004
OpenMC	1.00105 ± 0.00004

From the above table, it is clear that the k_{eff} value of MCkeff is in good agreement with OpenMC with a minimal difference of less than 100 pcm in reactivity.

Conclusions

A new Monte Carlo neutron transport code, called MCkeff, has been developed to estimate the neutron multiplication factor of fissile systems. The code is developed in Fortran language using GNU compiler and is compatible with both Windows and Linux based operating systems. A point-wise, continuous energy ACE format cross-section was used to treat neutron-nuclei collision physics accurately (without approximations). For constructing geometrical shapes containing homogenous material regions, first and second degree signed surfaces along with intersection and union operators are permitted. Since MCkeff is developed from scratch, it will be rather easy to incorporate advances happening in the computer industry as well as in the physics models.

Acknowledgements

This work was performed under the Department of Atomic Energy – Board of Research in Nuclear Sciences (DAE-BRNS) project No.36(4)/14/40/2015. The authors are thankful to DAE-BRNS for the sanctioning of the project. The authors are grateful to Manipal Centre for Natural Sciences, Centre of excellence, MAHE for allowing to use the facilities. Authors are thankful to Jayant Krishan Kapil deo Singh, S Anand, P S Sharma of HPD, BARC and Shri. Narsiah, of RSSD, BARC for evaluating the code and for providing useful suggestions.

References

[1] Knief, R. A., Society, A. N., & Commission, U. S. N. R. (1985). Nuclear Criticality Safety: Theory and Practice. The Society.
[2] Carter, L. L., & Cashwell, E. D. (1975). Particle-transport simulation with the Monte Carlo method.
[3] Hammersley, J. M., & Handscomb, D. C. (1964). Monte Carlo methods. Methuen; Wiley.
[4] Lux, I., & Koblinger, L. (1991). Monte Carlo particle transport methods: Neutron and photon calculations. Boca Raton: CRC Press.
[5] Cramer, S. N. (1984). KENO-V code. https://inis.iaea.org/search/search.aspx?orig_q=RN:16061204
[6] X-5 Monte Carlo Team, 2008a. MCNP - A General Monte Carlo N-Particle Transport Code, Version 5. LA-UR-03-1987, Los Alamos National Laboratory
[7] Romano, P. K., & Forget, B. (2013). The OpenMC Monte Carlo particle transport code. Annals of Nuclear Energy, 51.
[8] Leppänen, J. (2013). Serpent–a continuous-energy Monte Carlo reactor physics burnup calculation code. VTT Technical Research Centre of Finland, 4.
[9] Kirk, B. L. (2010). Overview of Monte Carlo radiation transport codes. Radiation Measurements, 45(10), 1318–1322.
[10] Fynn Scheben, (2010). Iterative Methods for Criticality Computations in Neutron Transport Theory, PhD Thesis, University of Bath, Bath.
[11] Lieberoth, J. (1968). A Monte Carlo technique to solve the static eigenvalue problem of the Boltzmann transport equation. Nukleonik, 11(5).
[12] Forrest B. Brown (2009), A Review of Monte Carlo Criticality Calculations - Convergence, Bias, Statistics, LA-UR-08-06558, American Nuclear Society – LANL
[13] Lieberoth, J. (1968). A Monte Carlo technique to solve the static eigenvalue problem of the Boltzmann transport equation. Nukleonik, 11(5).
[14] X-5 Monte Carlo Team, "MCNP - A General Monte Carlo N-Particle Transport Code, Version 5, Volume III: Developer's Guide," LA-CP-03-0284, Los Alamos National Laboratory (2008).
[15] OpenMC documentation, Users guide, Page 430 chapter 5. Releases · openmc-dev/openmc (github.com)
[16] Hoogenboom, J. E., Martin, W. R., & Petrovic, B. (2011, July). The Monte Carlo performance benchmark test-aims, specifications and first results. In International Conference on Mathematics and Computational Methods Applied to (Vol. 2, p. 15).

A MULTIGROUP SPACE TIME KINETICS CODE IN 2D RECTANGULAR AND CYLINDRICAL GEOMETRIES WITH DOPPLER FEEDBACK

Arun Stanley[1], T. Sathiyasheela[1]
[1] Indira Gandhi Centre for Atomic Research, Kalpakkam, India
[1]*e-mail: - arunstanley@igcar.gov.in*

Abstract

A multi-group space time kinetics code is developed in FORTRAN and benchmarked. Direct method is used for solving the space time kinetics equations. Finite difference method is used for spatial discretization and backward Euler method for temporal discretization. TWIGL and Dodd's benchmark problems for rectangular and cylindrical geometries were considered. The LRA-BWR benchmark problem was also solved with Doppler feedback. All benchmark results agreed satisfactorily with the reference results.

1. Introduction

Space time kinetics (STK) model is used to study the space dependent changes in the neutron flux of a reactor with time especially in cases where large spatial decoupling is present or where core geometry itself changes (Eg. Transients in large thermal reactors or hypothetical core disruptive accidents (HCDA) in Liquid-Metal Fast Breeder Reactors (LMFBR)). In this study space time kinetics equations are solved directly using a simple finite differencing model and backward Euler method. The code is developed in FORTRAN 95 language. It is capable of handling any number of energy groups and precursor groups and both rectangular (x-y) and cylindrical geometries (r-z) in 2 dimensions. Two numerical benchmark problems are considered without feedback: TWIGL [1,2] and Dodd's [3]. In the third benchmark problem, known as LRA-BWR [4], a Doppler feedback model is also used along with an adiabatic fuel heat-up thermal model.

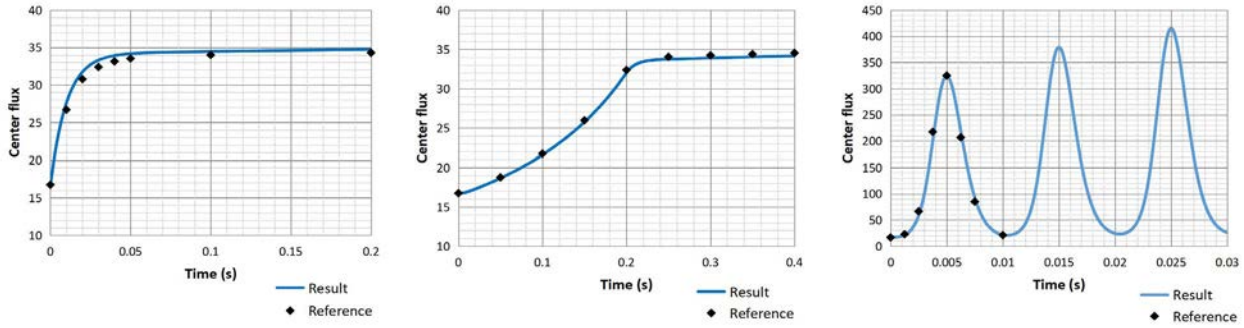
2. Numerical modelling and benchmarking

The complete space time kinetics equations in multigroup and their matrix form can be found in references [1,2]. A standard five point finite difference formula for spatial discretization of the leakage term is used in both 2D rectangular and cylindrical geometries while temporal discretization is done using the standard backward Euler method. Gauss Seidel iteration is carried out to solve the resulting matrix equation at every time step and sparse matrix techniques are employed since the elements of the coefficient matrix are mostly zero. The boundary condition used is such that the flux and precursor densities are zero at the boundaries. The initial flux shape is found by solving the time independent diffusion equation using inner-outer iteration scheme [5]. The flux thus obtained is normalised for the initial power. The kinetics calculation is assumed to start from steady state so as to get the initial precursor density in terms of the initial flux. An adaptive time step scheme is employed in which the time-step, Δt, is modified according to the backward Euler local error estimate at every time step.

2.1 TWIGL benchmark

TWIGL [1,2] is a 2D rectangular heterogeneous problem with two energy groups and one precursor group. It has 160cm x 160cm geometry with 20 x 20 mesh size. It is a critical assembly (k = 1). k obtained from the diffusion code is 0.99999. **(i) Step reactivity change:** The thermal absorption cross section in the driver region (refer [1] for details) was reduced by 0.0035 cm^{-1} to get a step reactivity change of 51 cents. The thermal flux value at the center of the reactor was used for

comparison and is given in Figure 1(a). Maximum deviation from reference is about 4%. **(ii) Ramp reactivity change:** A ramp reactivity change of about 2.5 $/s was introduced by reducing the thermal absorption cross section in the driver region linearly up to 0.2s with a rate of 0.0175 cm^{-1}/s. The comparison of thermal flux at the center of the reactor is given in Figure 1(b). Maximum deviation from reference is about 1%. **(iii) Sinusoidal reactivity change:** The thermal absorption cross section of driver region is perturbed sinusoidally with a period T = 0.01s. The comparison of thermal flux at the center of the reactor is given in Figure 1(c). Maximum deviation from reference is about 1%.

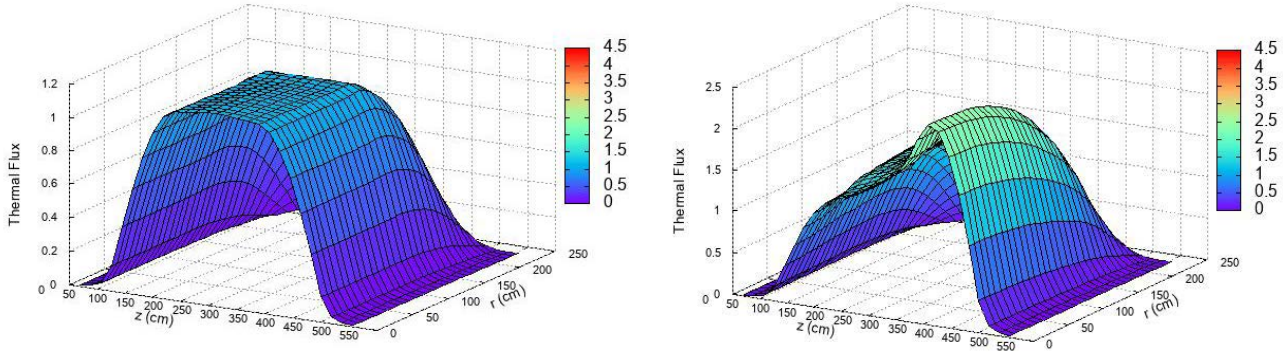


(a) (b) (c)

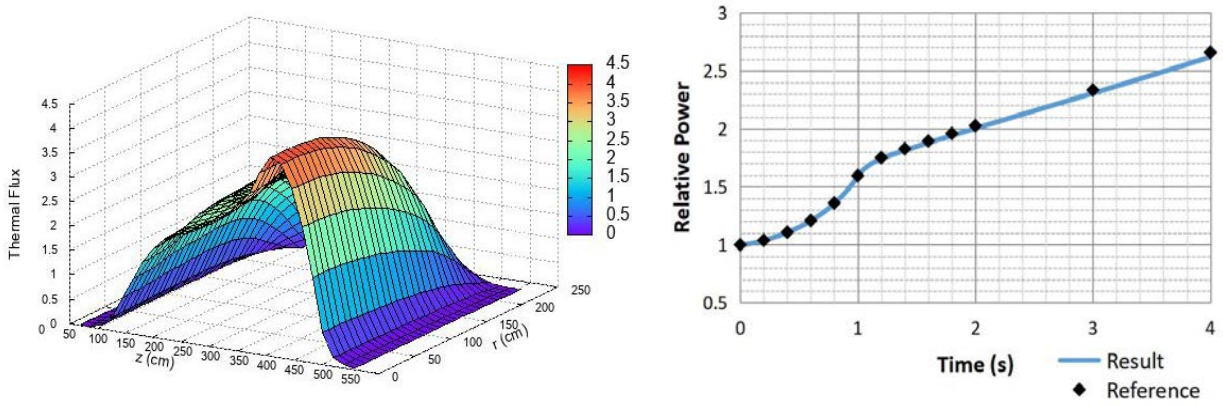
Figure 1. TWIGL benchmark results: center thermal flux value with time for (a) step, (b) ramp and (c) sinusoidal reactivity changes. Reference values are only available up to 0.01s in the sinusoidal case.

2.2 Dodd's benchmark

Dodd's benchmark [3] is a 2D cylindrical heterogeneous problem with two energy groups and six precursor groups. The core has a radius of 240cm and height of 525cm (12 x 28 mesh size). Reactor is subcritical with multiplication factor k = 0.86705. The diffusion code calculates k as 0.86714. A transient is introduced by increasing the thermal absorption cross section in the top region and reducing it in the bottom region linearly at a rate of 3% change per second up to 1s. The thermal flux at t = 0s, t = 1s & t = 4s is shown in Figure 2(a)-(c). A tilt in the flux shape is observed due to the asymmetrical perturbation in the absorption cross sections. The relative power of the reactor is compared in Figure 2(d). Maximum deviation from reference in relative power is 1.4%.



(a) (b)



(c) (d)

Figure 2. Dodd's benchmark results: thermal flux at (a) t = 0s, (b) t = 1s and (c) t = 4s shows the tilting of the flux. (d) Relative power with time.

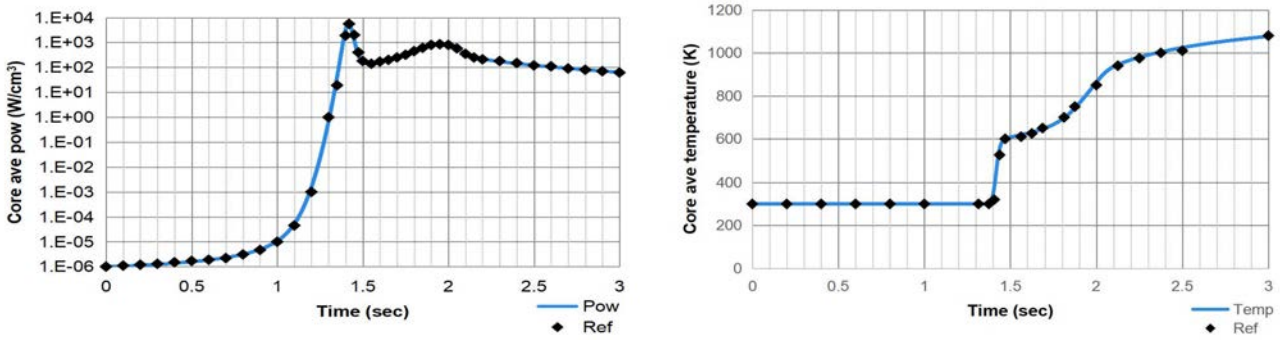
2.3 LRA-BWR benchmark problem

LRA-BWR is a 2D rectangular (x-y) BWR model problem with two energy groups and two precursor groups. It is of 330cm x 330cm size which is modeled using 132 x 132 meshes. The original problem used coarse mesh methods with 11 x 11 mesh [4]. The multiplication factor obtained from the diffusion code using 132 x 132 mesh size is k = 0.99669 compared to the reference value of 0.99633. Further refinement of mesh did not yield considerable improvement and only served to increase computational load. In this problem a Doppler feedback model is also incorporated along with an adiabatic fuel heat up thermal model as below:

$$\Sigma_{a1}(r,t) = \Sigma_{a1}(r,0)\left[1+\gamma\left(\sqrt{T(r,t)}-\sqrt{T(r,0)}\right)\right] \quad (1)$$

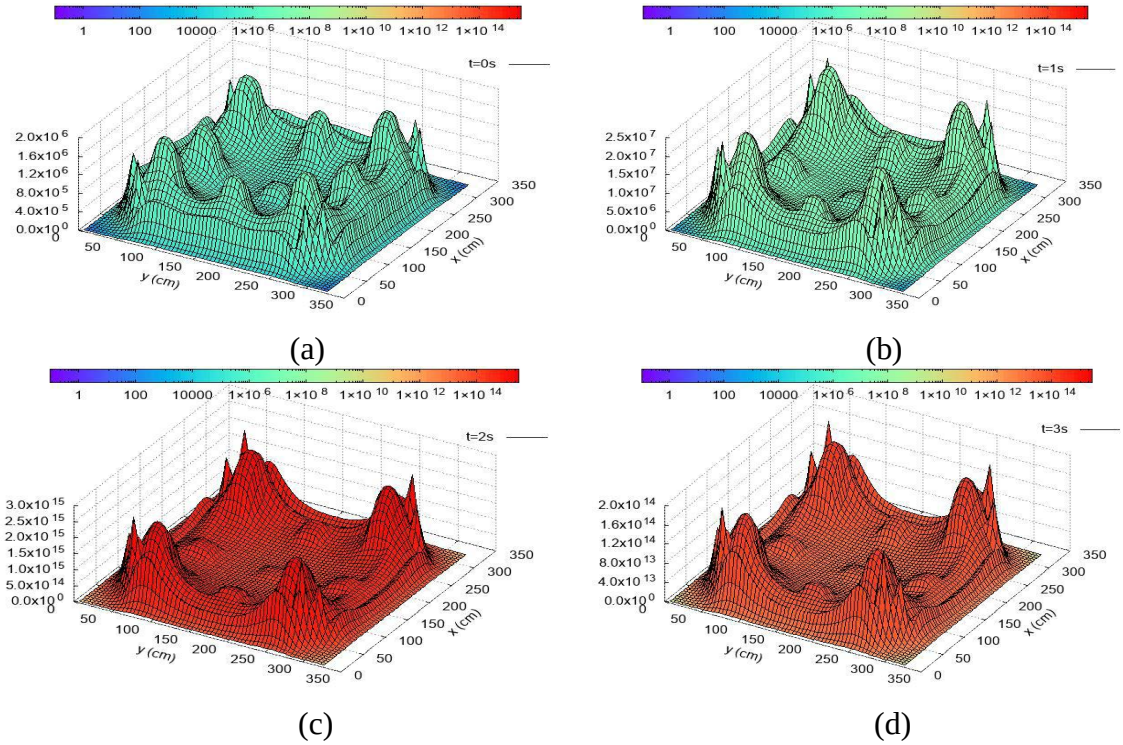
$$\frac{\partial}{\partial t}T(r,t) = \alpha\sum_{g}\Sigma_{fg}(r,t)\phi_g(r,t) \quad (2)$$

Where, Σ_{a1} is the fast absorption cross section, Σ_f is the fission cross section, T is the temperature, ϕ is the neutron flux, γ is the feedback constant and α is the conversion factor. The transient is a simulation of control rod withdrawal at the four corners of the reactor by reducing the thermal absorption cross section at a rate of 6% change per second up to 2s. The average power density and temperature of the core is plotted in Figure 3. The maximum deviation from reference is about 2%. The thermal flux at times t = 0s, 1s, 2s & 3s are shown in Figure 4. Considerable peaking of the flux is observed at the four corners of the reactor where the control rod is being withdrawn. This indicates the spatial decoupling present in the core.



(a) (b)

Figure 3. LRA-BWR core average (a) power density and (b) temperature with time



(a) (b)

(c) (d)

Figure 4. LRA-BWR thermal flux at (a) t = 0s, (b) t = 1s, (c) t = 2s and (d) t = 3s

3. Conclusion

A multigroup space time kinetics code is developed using simple finite difference methods and a backward Euler method and benchmarked in 2D rectangular and cylindrical geometries. Two numerical benchmark problems without feedback and one with Doppler feedback were analysed and results showed satisfactory agreement with the reference values. The computational time required for the first two problems were less than two minutes. The third problem took 4 hrs to complete. This problem involves a larger mesh size (132x132) compared to the first and second problems (20x20 and 12x28) resulting in a larger matrix equation to be solved each time step. It also involves a super prompt critical transient with steep variations in flux requiring smaller time steps.

4. References

[1] A. E. Aboanber and A. A. Nahla, "Solution of two-dimensional space–time multigroup reactor kinetics equations by generalized Padé and cut-product approximations", *Annals of Nuclear Energy,* Vol. 33, Iss. 3, 2006, pp. 209-222.

[2] A. E. Aboanber and A. A. Nahla, "Adaptive matrix formation (AMF) method of space–time multigroup reactor kinetics equations in multidimensional model", *Annals of Nuclear Energy*, Vol. 34, Iss. 1, 2007, 103-119.

[3] Argonne National Laboratory, "Argonne code centre: Benchmark problem book", ANL-7416, Suppl. 2, 1977, pp. 182-200.

[4] Argonne National Laboratory, "Argonne code centre: Benchmark problem book", ANL-7416, Suppl. 2, 1977, pp. 552-576.

[5] J. J. Duderstadt and L. J. Hamilton, "Nuclear reactor analysis", *Wiley,* 1991.

NODAL INTEGRAL METHOD FOR SOLUTION OF TIME DEPENDENT NEUTRON DIFFUSION EQUATION

Manish Raj[1], Sherly Ray[1], M.P.S. Fernando[1] and Suneet Singh[2]
[1] Nuclear Power Corporation of India Limited, Mumbai-94, India
[2] Indian Institute of Technology Bombay, Mumbai-76, India
e-mail: rmanish@npcil.co.in

Abstract

Nodal Methods (NM) are the backbone used as early as 1976 for reactor design/analysis because of their accuracy, even with coarse mesh structures, compared to the most of the other methods such as finite difference (FD), finite element method (FEM), flux synthesis method (FSM) etc. used in solving the neutron diffusion equation. The accuracy, even with coarse mesh, has led the development of nodal methods not only in the field of reactor physics but also in several other fields of physics such as fluid flow, heat and mass transfer. The methodology of Nodal Integral Method (NIM) is similar to analytical nodal method with transverse integration process except the scheme is developed in terms of surface fluxes instead of node average flux. The comparison of eigenvalues as well as the dynamic power profile obtained with present methodology, with that of the AECL-7236 benchmark show that the method is capable of accurately predicting the eigenvalues and other parameters for the reactor core.

1. Introduction

There are two class of methods used for determining the fundamental quantities such as effective multiplication factor and flux inside the core; required for any nuclear reactor design. Out of these two class of methods, one class of methods are based on transport theory which takes larger time and, therefore, are less suitable for many practical scenarios and are usually used for computation of a few group constants. The methods of other class are based on diffusion theory and take less time and, hence, are widely used for core simulation. However, because of the approximation assumed in second class of methods (based on diffusion theory), they are less accurate compared to the methods based on transport theory. Many methods for solving the steady state and/or the time dependent neutron diffusion equation are presently available in literature. The various methods such as finite difference method (FDM) [1], finite element method (FEM), flux synthesis method (FSM) and Nodal methods (NM) are used to solve the steady state and/or the time dependent neutron diffusion equation.
The methodology of NIM is similar to analytical nodal method with transverse integration process except the scheme is developed in terms of surface fluxes instead of node average flux. The comparison of eigenvalues as well as the dynamic power profile obtained with present methodology, with that of the AECL-7236 benchmark [2] considering 3-D diffusion equation in 2 energy groups with 6 groups of delayed neutrons, show that the method is capable of accurately predicting the eigenvalues and other parameters for the reactor core.

2. Nodal Integral Method (NIM)

The time dependent neutron diffusion equation is parabolic equation similar to the heat equation. The solution of which can be easily obtained numerically with NIM approach. For simplicity, the solution methodology for one group, one dimensional time dependent neutron diffusion equation using NIM is described. The extension to multi-group and multi-dimension would be straight forward, however, not trivial. Furthermore the delayed neutron term is not included explicitly as it will only change the source term. The precursor equation is first order ODE and hence can be solved by any available method in literature. Therefore only the solution methodology of time dependent neutron diffusion with source is

presented here. The source, in general, is the sum of fission source, precursor contribution and external source.

One dimensional, one group time dependent neutron diffusion equation with source is given as,

$$\frac{1}{Dv}\frac{\partial\varphi}{\partial t} = \frac{\partial^2\varphi}{\partial x^2} + \frac{\mathrm{S(x,t)}}{D} \quad (1)$$

Now the whole domain is divided into small nodes both in space as well as in time. The node width in space is '2a' (shown in figure-1) and the interval in time is assumed to be '2τ'.

----------|------- (i-1)th mesh --|---------(ith mesh)-----|--------(i+1)th mesh------|----------|

Figure-1 Mesh structure in 1-D (mesh width is '2a')

Averaging both sides of equation (1) over time gives, for a node

$$\int_0^{2\tau}\frac{1}{Dv}\frac{\partial\varphi}{\partial t}\frac{dt}{2\tau} = \int_0^{2\tau}\frac{\partial^2\varphi}{\partial x^2}\frac{dt}{2\tau} + \int_0^{2\tau}\frac{\mathrm{S}}{D}\frac{dt}{2\tau} \quad (2)$$

$$\int_0^{2\tau}\frac{\partial^2\varphi}{\partial x^2}\frac{dt}{2\tau} = \frac{d^2}{dx^2}\overline{\varphi}^{\tau}(x) = \int_0^{2\tau}\frac{1}{Dv}\frac{\partial\varphi}{\partial t}\frac{dt}{2\tau} - \int_0^{2\tau}\frac{\mathrm{S}}{D}\frac{dt}{2\tau} \quad (3)$$

The right hand side of the above equation (3) is in general would be function of 'x' and is called the pseudo source. In the subsequent derivation it is assumed to be constant. Where $\overline{\varphi}^{\tau}(x)$ and $\overline{\varphi}^{x}(t)$ are mesh flux averaged over time and mesh flux averaged over space respectively.

In other words,

$$\int_{t1=0}^{\mathrm{t2}=2\tau}\frac{1}{Dv}\frac{\partial\varphi}{\partial t}\frac{dt}{2\tau} - \int_0^{2\tau}\frac{\mathrm{S}}{D}\frac{dt}{2\tau} = \overline{S}^{\tau}(x) \approx \overline{S_0}^{\tau} \quad (4)$$

The solution of the equation (2) with constant pseudo source $\overline{S_0}^{\tau}$ would be,

$$\overline{\varphi}^{\tau}(x) = \overline{S_0}^{\tau}\frac{x^2}{2} + Ax + B \quad (5)$$

The constants A and B are determined from boundary conditions:

$$\overline{\varphi}^{\tau}(x = +a) = \overline{\varphi_i}^{\tau} \quad (6a)$$

$$\overline{\varphi}^{\tau}(x = -a) = \overline{\varphi_{i-1}}^{\tau} \quad (6b)$$

and are given as,

$$A = \frac{\left(\overline{\varphi_i}^{\tau} - \overline{\varphi_{i-1}}^{\tau}\right)}{2a} \text{ and } B = \frac{\left(\overline{\varphi_i}^{\tau} + \overline{\varphi_{i-1}}^{\tau} - \overline{S_0}^{\tau}a^2\right)}{2} \quad (7)$$

Similarly averaging both sides of equation (1) over space, for a node,

$$\int_{-a}^{+\mathrm{a}}\frac{1}{Dv}\frac{\partial\varphi}{\partial t}\frac{dx}{2\mathrm{a}} = \int_{-a}^{+\mathrm{a}}\frac{\partial^2\varphi}{\partial x^2}\frac{dx}{2\mathrm{a}} + \int_{-a}^{+\mathrm{a}}\frac{\mathrm{S}}{D}\frac{dx}{2\mathrm{a}} \quad (8)$$

Finally we have,

$$\frac{1}{Dv}\frac{d\overline{\varphi}^{x}(t)}{dt} = \int_{-a}^{+\mathrm{a}}\frac{\partial^2\varphi}{\partial x^2}\frac{dx}{2\mathrm{a}} + \int_{-a}^{+\mathrm{a}}\frac{\mathrm{S}}{D}\frac{dx}{2\mathrm{a}} = \overline{S}^{\mathrm{x}}(t) \quad (9)$$

Assuming, $\overline{S}^{\mathrm{x}}(t) \approx \overline{S_0}^{\mathrm{x}}$ i.e. constant pseudo source.

The solution of the above equation (9) is straight forward and is given as,

$$\overline{\varphi}^{x}(t) = (t - t_1)Dv\overline{S_0}^{\mathrm{x}} + \overline{\varphi}^{x}(t_1) \quad (10)$$

The unknowns in the equations (5) and (10) i.e. pseudo source $\overline{S_0}^{\mathrm{x}}$ and $\overline{S_0}^{\tau}$ are obtained by solving the constraint equations as follows:

Constraint-1

The average over time and space (for a node) is given as [using equation (1)],

$$\int_{t_1}^{t_2}\int_{-a}^{+a}\left(\frac{1}{Dv}\frac{\partial\varphi}{\partial t}\right)\frac{dx}{2a}\frac{dt}{2\tau}=\int_{t_1}^{t_2}\int_{-a}^{+a}\left(\frac{\partial^2\varphi}{\partial x^2}\right)\frac{dx}{2a}\frac{dt}{2\tau}+\int_{t_1}^{t_2}\int_{-a}^{+a}\left(\frac{S(x,t)}{D}\right)\frac{dx}{2a}\frac{dt}{2\tau} \quad (11)$$

The term on LHS of equation (14) can be written as,

$$\int_{t_1}^{t_2}\int_{-a}^{+a}\left(\frac{1}{Dv}\frac{\partial\varphi}{\partial t}\right)\frac{dx}{2a}\frac{dt}{2\tau}=\int_{t_1}^{t_2}\left(\frac{1}{Dv}\frac{d\overline{\varphi}^{x}(t)}{dt}\right)\frac{dt}{2\tau}=\overline{S_0}^{x} \quad (12)$$

Similarly the first term on RHS of equation (11) is written as,

$$\int_{t_1}^{t_2}\int_{-a}^{+a}\left(\frac{\partial^2\varphi}{\partial x^2}\right)\frac{dx}{2a}\frac{dt}{2\tau}=\int_{-a}^{+a}\left(\frac{d^2\overline{\varphi}^{\tau}(x)}{d^2x}\right)\frac{dx}{2a}=\overline{S_0}^{\tau} \quad (13)$$

Hence we have,

$$\overline{S_0}^{x}=\overline{S_0}^{\tau}+\frac{\overline{S}^{x\tau}}{D} \quad (14)$$

Constraint-2

The average over a node can also be obtained using either of equations (5) or (10) as follows:

$$\int_{t_1}^{t_2}\overline{\varphi}^{x}(t)\frac{dt}{2\tau}=\int_{t_1}^{t_2}(t-t_1)Dv\overline{S_0}^{x}\frac{dt}{2\tau}+\overline{\varphi}^{x}(t_1) \qquad \text{[Using equation (10)]} \quad (15)$$

$$\overline{\varphi}^{x\tau}=\frac{(t_2-t_1)^2Dv\overline{S_0}^{x}}{4\tau}+\overline{\varphi}^{x}(t_1) \quad (16)$$

Similarly using equation (5),

$$\int_{-a}^{+a}\overline{\varphi}^{\tau}(x)\frac{dx}{2a}=\int_{-a}^{+a}\overline{S_0}^{\tau}\frac{x^2}{2}\frac{dx}{2a}+\int_{-a}^{+a}\frac{\left(\overline{\varphi_i}^{\tau}-\overline{\varphi_{i-1}}^{\tau}\right)}{2a}x\frac{dx}{2a}+\frac{\left(\overline{\varphi_i}^{\tau}+\overline{\varphi_{i-1}}^{\tau}-\overline{S_0}^{\tau}a^2\right)}{2} \quad (17)$$

$$\overline{\varphi}^{\tau x}=\frac{\left(\overline{\varphi_i}^{\tau}+\overline{\varphi_{i-1}}^{\tau}\right)}{2}-\frac{\overline{S_0}^{\tau}a^2}{3} \quad (18)$$

From equations (16) and (17) we have a relation between the pseudo sources as,

$$\frac{(t_2-t_1)^2Dv\overline{S_0}^{x}}{4\tau}+\overline{\varphi}^{x}(t_1)=\frac{\left(\overline{\varphi_i}^{\tau}+\overline{\varphi_{i-1}}^{\tau}\right)}{2}-\frac{\overline{S_0}^{\tau}a^2}{3} \quad (19)$$

Solving equation (14) and equation (19) we have the expressions for pseudo sources as,

$$\overline{S_0}^{\tau}=\frac{\frac{\left(\overline{\varphi_i}^{\tau}+\overline{\varphi_{i-1}}^{\tau}\right)}{2}-\frac{\overline{S}^{x\tau}}{4\tau}(t_2-t_1)^2v-\overline{\varphi}^{x}(t_1)}{\frac{D}{4\tau}(t_2-t_1)^2v+\frac{a^2}{3}} \quad (20)$$

$$\overline{S_0}^{x}=\frac{\frac{\left(\overline{\varphi_i}^{\tau}+\overline{\varphi_{i-1}}^{\tau}\right)}{2}-\frac{\overline{S}^{x\tau}}{4\tau}(t_2-t_1)^2v-\overline{\varphi}^{x}(t_1)}{\frac{D}{4\tau}(t_2-t_1)^2v+\frac{a^2}{3}}+\frac{\overline{S}^{x\tau}}{D} \quad (21)$$

Once the pseudo sources are obtained the time dependent solution can be easily found either from equations (20) or (21) for node average flux $\overline{\varphi}^{x\tau}$ variation with time. However it is to be noted that these sources for each nodes are required to be estimated at each time steps.

3. Results and discussion

The methodology developed here is verified against AECL-7236 benchmark. The AECL-7236 benchmark is a well-established three dimensional kinetics benchmark problem for a heavy water reactor. It was published in February 1981. The solution of the benchmark were generated using the quasi-static code, CERKIN. The benchmark is designed to provide a test of the capabilities of multi-

group multi-dimension kinetic codes in Cartesian geometry. The results for steady state case of AECL-7236 benchmark have been discussed in reference [3]. The time dependent part of AECL benchmark is given in figure-1. The results are found to be in good agreement with that given in AECL-7236 benchmark.

In another case, the fluxes at ion-chamber locations are estimated in time dependent neutron diffusion theory based computer code NIM. It is well known that diffusion theory based codes are valid only up to the core boundary and these Ion-chambers are placed out of the core. Therefore, the absolute fluxes at their locations cannot be compared directly with the estimated fluxes. However, the time profile of power drop or rise can be compared provided the estimated values are near these location (within the core). The estimated power profile near I/C locations are compared with that observed during trip test and are shown in figure-2. The RRS and RPS-1 ion-chambers are placed on the east side of the core whereas RPS-2 ion-chamber is placed on the west side of the core. It is clear from these curves that RRS and RPS-1 power profiles are almost same as expected because they are on the same side of the core. While on the other hand the power drop is different for RPS-2 as it is located on the other side and at different position w.r.t. the central mid plane of the core. Similar type of variation is also obtained in the estimated powers at these locations. Furthermore, the estimated variation of power with time at I/C locations is in good agreement with the observed power vs. time profile.

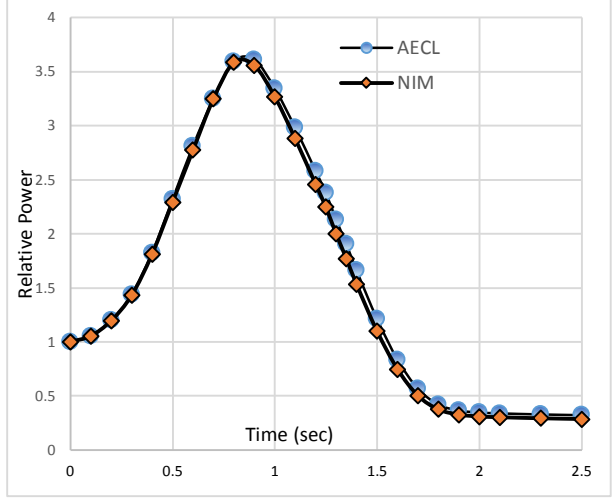


Figure-1 Relative power variation with time (AECL-7236 Benchmark)

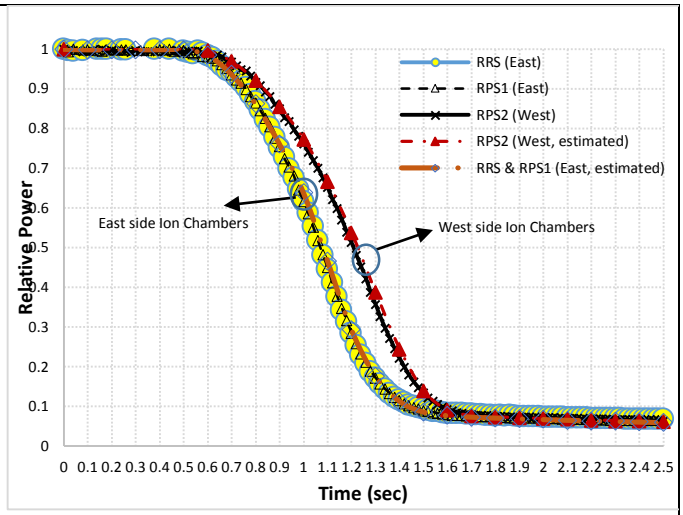


Figure-2 Comparison of Power profile at I/C locations
(Using observed SDS-1 (28 SR) position vs. time profile during Phase-B experiment at KAPP-3)

4. Conclusion

The results obtained by the developed computer code, based on NIM, to solve the time dependent neutron diffusion equation is validated against the AECL-7236 benchmark as well as the observed Phase-B data at KAPP-3. The steady state k-eff value with NIM approach in the present mesh structure of 18*18*10 is 1.003169 and FDM approach with 52*52*40 mesh structure gives the k-eff value 1.003161 as reported in reference [5]. This shows that the NIM approach is about 25 to 30 times accurate with FD approach. The code is also validated against the ABCS benchmark [4] and the results are found to be in good agreement.

5. References

[1] G. G. Botte, J. A. Ritter, R. E. White, 'Comparison of finite difference and control volume methods for solving differential equations', Computers and Chemical Engineering , 24 , 2633–2654, 2000.

[2] R.A. Judd and B. Rouben, "Three Dimensional Kinetics Benchmark problem in a Heavy Water Reactor", AECl-7236, February 1981.

[3] Manish Raj et. al., "Solution of Steady State neutron diffusion equation using Nodal Integral Method", Proceedings of the Advances in Reactor Physics, Mumbai, India, 2017 Dec. 06-09.

[4] Obaidurrahman K. and Santosh Pradhan, "AERB benchmark for coupled code system (ABCS)", AERB/NSARG/TR/2020/01, Atomic Energy Regulatory Board, Mumbai, India.

[5] R.S.Modak, Anurag Gupta, "New application of Orthomin (1) algorithm for k-eigenvalue problem in Reactor Physics", Annals of Nuclear Energy 33 (2006) 538-543.

Development of Lattice and Core Models for PHWR in VISWAM Code System

V. Jagannathan[1], S.Koner[2] and Obaidurrahman K.[2]

[1] Consultant, Atomic Energy Regulatory Board, Mumbai, India
[2] Atomic Energy Regulatory Board, Mumbai, India

[1]*e-mail: - v_jagan1952@rediffmail.com*

Abstract

The ring cluster lattice geometry in VISWAM code has been customized to analyse the PHWR fuel cluster [1]. The ring cluster model has been validated against DRAGON and CLUB codes for advanced fuel cluster of ATBR [2]. Simulation of reactivity devices (RDs) entering in perpendicular direction to the fuel channels of PHWR required 3D supercell model to be incorporated in VISWAM. The centre mesh finite difference of the core diffusion module is customized for PHWR simulation. Auto prescription of the 'ΔΣ' values in meshes in core regions influenced by RDs for a variety of device configurations has been implemented. The lattice and core models are used to analyse FAC and Phase-B experiments of KAPP-3 core.

1. Introduction

Independent verification at AERB necessitate the capability of analyzing the neutron physical characteristics of the 700 MWe PHWR core. Consistent with this objective, the lattice module of VISWAM code system was further developed to include the ring cluster geometry of PHWRs. The simulation of reactivity devices that enter in vertical direction in the horizontal reactor of PHWR required the incorporation of 3D supercell model at lattice level. A diffusion iterative model was used to obtain the equivalent diffusion parameters of the strong absorbing devices of ARs, CRs, SRs and the ZCCs considered in PHWRs.

2. Model for PHWR fuel cluster

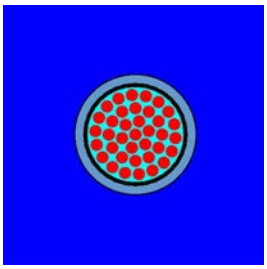


Fig.1 PHWR 37 Rod Cluster

The ring geometry of PHWR fuel cluster is circular. The one-dimensional supercell approach developed earlier for square or hexagonal fuel assemblies was adopted for the ring geometry as well. The calculations are done with the 172 energy group "HTEMPLIB" library in WIMS/D format based on JEFF 3.1 point nuclear data library. The 37 rod fuel cluster of both natural UO_2 and depleted UO_2 types have identical geometrical design as indicated in Fig.1. There are 1, 6, 12, 18 fuel pins in the four fuel rings. The Zr alloy clad allows a thin air gap, which is explicitly considered in VISWAM. The fuel pellet is divided into three rings of equal volume. By distributing the coolant volume in the coolant pressure tube equally to all fuel pins, we get an effective radius for the coolant and the equivalent hexagonal lattice pitch is used in Dancoff factor calculation using the hexagonal option in Carlvick's routine. The Dancoff factor for each ring is further modified using empirical formulae to account for the (PT+ Air gap + CT) and D_2O regions surrounding the fuel cluster. The resonance integral interpolations are done for the fuel temperature and the background cross sections derived from equivalence relations. Mutual shielding of resonance capture of various nuclides in fuel is accounted. After four fuel pincell

calculations are done in 172 groups by P_{ij} method, the fuel pincell consisting of pellet, air gap, clad and coolant regions are homogenized to get the multigroup cross sections of the fuel paste rings.

A 1D cylindrical supercell calculation is performed with the four fuel paste rings surrounded by four rings of pressure tube (PT), air gap, calandria tube (CT) and cylindricalized D_2O moderator regions. The supercell ring spectra are used to collapse the cross sections to few energy groups for performing diffusion calculation for the fuel cluster cell in (r,θ) geometry. A diffusion iterative technique (DIT) is an intermediate step to obtain transport-diffusion correction factors for the strong absorbing fuel cluster regions. In this step only three regions are considered, viz., i) central fuel cluster homogenized in all the four rings, ii) (PT + Air gap + CT), iii) D_2O moderator. Few group cross sections (5 energy groups, with energy boundaries at 19.64 MeV, 9.118keV, 4eV, 0.625eV, 0.14eV and 10^{-5}eV) are obtained by collapsing the multigroup homogenized cross sections with respective supercell region spectra. The fuel cluster material cross sections are multiplied by the transport-diffusion correction factors in respective energy groups.

For the few group diffusion calculation in (r,θ) geometry, 6 macro ring regions are considered radially corresponding to four fuel rings, (PT + air gap + CT) and D_2O moderator regions. The number of angular directions are decided such that in each ring each fuel pin is fully contained in a set of adjoining arc segments. This is important to obtain pin wise power distribution and verify that they are identical for each pin of a fuel ring, confirming azymuthal symmetry. 25 distinct angles were required. Radially 30 fine regions were considered. For a good convergence of flux in minimum number of outer iterations, the diffusion calculation required acceleration techniques like a) coarse mesh rebalancing with each ring treated as a coarse mesh, b) line inversion along radial lines. The fuel cluster homogenized cross section in five & two energy groups are obtained. The kinetics parameters β_{eff}, ℓ are obtained by perturbation theory expressions using direct and adjoint flux weighting. The depletion equations are solved in three fuel rings for each pin of the four pincell/burnup type of the fuel cluster. Fourth order Runge Kutta method is used. 69 fission products inclusive of one pseudo fission product and 35 actinides from ^{232}Th to ^{252}Cf are considered. ^{105}Rh and ^{135}Xe are considered as saturated fission products corresponding to the absolute flux level in each fuel ring zone.

The uncontrolled fuel cluster is simulated first with the nominal values of several reactor state parameters like soluble boron, fuel temperature, coolant void fraction, coolant temperature, moderator temperature, coolant purity, moderator purity, average linear heat generation rating. Subsequently each of the above parameters is varied one at a time and a full-fledged lattice database is generated in cold and hot states.

2.4 Reactivity Device Simulations

A schematic diagram illustrating the 3D supercell model used for simulating the RD along with the fuel cluster, (PT+ air gap +CT) and D_2O moderator regions is shown in Fig.2. A number of steps are to be followed prior to the above 3D supercell simulation by few group diffusion theory. They are discussed below under various bullets.

- Obtain few group cross sections of the homogenized fuel cluster region with the DIT correction, (PT + air gap+ CT) region and D_2O moderator region.
- Simulate the RD by a one-d multigroup transport theory model. For this purpose, the annular ring regions consisting of the RD materials are surrounded by D_2O up to GT, a fuel paste of the uncontrolled fuel cluster material with outer radius of $\sqrt{(2PL/\pi)}$. All cross sections are obtained by collapsing with supercell spectra of the one-d supercell transport calculation for RD.

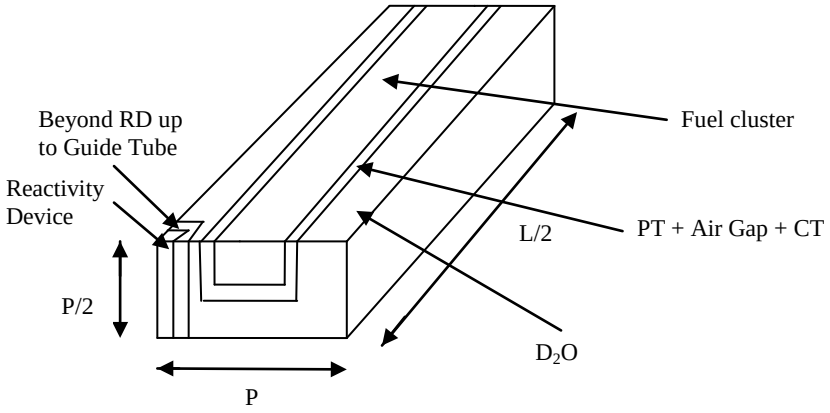


Fig. 2 A schematic Diagram for 3D Supercell Simulation in Cartesian Geometry

- An α type (current to flux ratio) boundary condition is considered on the surface of RD. From the 1-D RD supercell simulation, the net few group leakage into the RD is determined.

$$L_g^{tr} = \Sigma_{rg}\,\Phi_g - \sum_{g'} \Sigma_{sg'\rightarrow g}\,\Phi_{g'}$$

  The symbols have their usual meaning.

  A guess value of α_g is obtained as: $\alpha_g = L_g^{tr} / (2\pi r_{RD}\Phi_g)$, r_{RD} is radius of the RD outer surface.

- A diffusion calculation is then performed in 1-D cylindrical geometry with the RD region treated by α type boundary condition. A centre mesh FD code was developed for the internal boundary condition treatment. With the converged flux, the diffusion leakage is determined as:

$$L_g^{diff} = \alpha_g\,\Phi_{gi}\,2\pi r_{RD} / (1+ \alpha_g\, h_i/2D_i)$$

Φ_{gi} is the flux at the neighbouring mesh 'i' of the RD and h_i is the mesh width. The boundary condition α_g is modified such that the transport leakage shall be reproduced and the diffusion calculation is repeated. The next step is to perform the diffusion calculation in equivalent Cartesian geometry. The RD, GT and the fuel paste regions are converted into equivalent square regions. The RD square width 'a' is calculated as: $a = \sqrt{\pi} \times r_{RD.}$ Since the surface area of square is larger, the boundary condition α_g is modified as: $\alpha_g^{sq} = \alpha_g^{circ} \times \sqrt{\pi}/2$. Diffusion iterations are done as above and revised α_g^{sq} is obtained such that the transport leakage is reproduced. With the modified fuel cluster cross sections and the α_g^{sq} of the final 2D calculations, it is possible to perform the 3D supercell simulation of the problem depicted in Fig.2.

2. PHWR core modeling - Special features

The initial core of 700 MWe core considers depleted uranium bundles in some channels for initial power flattening. Axially there is no space for D_2O reflector. Extrapolation distance is used as boundary condition in all directions. The core is symmetric with ± 11 fuel cluster pitches in both x- and y-directions. Radial zones with reflector are modelled as extending to a maximum of ±14 pitches. The calandria tank radius is 392 cm in the central region. Reduced radius of 330 cm is considered in the axial subshell regions on either side. The model converts this circular boundary to equivalent zig-zag boundary core for Cartesian square mesh simulation. The top most mesh in y-direction may be curtailed depending on the moderator fill level resulting in smaller thickness of less than a pitch for the top layer of the radial reflector. Axially each fuel bundle length is divided in to two equal meshes.

The most distinguishing feature of PHWR core simulation is the modeling of reactivity devices (RDs). This is because the RDs do not have a specific lattice pitch and are of multiple varieties. As per the 3-D supercell simulation of the RD at lattice level, a single RD is assumed to influence the cross section of two lattice pitches in the x-direction, full length of insertion in y-direction and a length of ±L/2 in z-direction. As mentioned above, in axial direction uniform mesh size of L/2 is considered. Since the Z-coordinate of RD can be anywhere within an axial mesh, the zone of influence is considered to be extending up to ±L/2 distance. This length is mostly spread in three axial meshes, except for devices located at core midplane. The control perturbation of a RD is weighted with length fraction in the y-direction. In z-direction a recipe of using a tent-like weighting function is suggested to concentrate the perturbation in the vicinity of the device. This shape has been considered as the ratio of epithermal to thermal flux from the surface of the RD to the edge of the 3D supercell in z-direction. These shapes are calculated at the lattice level and are made available as fifth order polynomial function for treatment at core level. It is an arduous task to identify all RDs and their extent of influence for each mesh even for a single reactivity device configuration. In VISWAM, this information is generated by the code itself. The user needs to provide only the number and types of RDs and the fraction of their insertion depth for a given device configuration. The code generates the information of the types of RD or their guide tube and the weighting fraction fy, fz in y-, z- directions for each mesh influenced by one or more devices. The ’ΔΣ’ perturbation due to each type of RD is summed up to provide the change in few group cross sections of a mesh. Another parameter influencing the few group cross section is the variation in purity values of coolant and moderator. In VISWAM, a special database is generated for both these types of purity changes. The cross sections are perturbed suitably for the actual purity values that may be different from their nominal values.

3. Summary

VISWAM code has been employed for independent verification analysis at AERB. The developmental efforts in VISWAM code system to implement PHWR lattice and core models have been described here. VISWAM PHWR models have been validated against a few reference problems and in addition the code has also been used for the analysis of FAC and Phase-B experiments.

References

[1] V. Jagannathan, Suhail Ahmad Khan, and L. Thilagam, ‘Incorporation of Ring Cluster Geometry in VISWAM Code System’, *Advances in Reactor Physics (ARP-2017), Mumbai, India, Dec. 06-09, 2017.*

[2] V. Jagannathan, ‘Thorium breeder reactors as a power source for 21st century and beyond, Int. J Energy Res. 2018; 42:117–133. wileyonlinelibrary.com/journal/er Copyright © 2017 John Wiley & Sons, Ltd. pp 117-133. DOI: 10.1002/er.3951.

[3] S. Koner, V. Jagannathan and Obaidurrahman K., ‘Analysis of First approach to Criticality (FAC) and Phase-B experiments of KAPP-3 using VISWAM code’, *Advances in Reactor Physics (ARP-2022), Mumbai, India, May. 18-21, 2022.*

Development of Spiral Pin by Pin Finite Difference Model for Hexagonal Lattice Core

V. Jagannathan
Consultant, Atomic Energy Regulatory Board, Mumbai, India

[1]*e-mail: - v_jagan1952@rediffmail.com*

Abstract

VISWAM code lattice model for hexagonal fuel assemblies considers irregular mesh finite differencing with the actual dimensions of the thin water gaps surrounding the regular hexagonal lattice structure. The pin-by-pin 3D core diffusion code HEXPIN developed for the few group database of EXCEL lattice code considers uniform hexagonal meshes radially with the half integral meshes of adjacent fuel assembly cells coalescing into integral hexagonal cells. In order to use the VISWAM few group cross section database, a new code HEXPINSP has been developed. In this code each cell of every fuel assembly cell is spirally numbered with the same material description as at the lattice level. The assembly cells and the outer reflector layers are also spirally numbered. Diffusion kernels are evaluated by the same irregular mesh finite differencing. The (SS: H_2O) ratios in reflector cells are evaluated internally by the code. The Choleski decomposition method is employed for pincell layers within each assembly cell and continued for assembly layers of active core and reflector zones. It is possible to analyze full core as well as 60° symmetric core. Validation of the code is in progress and no results are presented.

1. Introduction

The generic VISWAM lattice burnup code has been provided to AERB for analysing square, hexagonal and ring cluster geometric cores. Review requirements at AERB had necessitated the capability of analyzing hexagonal lattice cores at a pin level. The pin-by-pin 3D core diffusion code HEXPIN developed for the few group database of EXCEL lattice code considers uniform hexagonal meshes radially with the half-integral cells of adjacent fuel assembly cells or one third meshes of corner cells coalescing into integral hexagonal cells. There is also a problem due to the fact that assembly pitch does not normally fit integral number of pincells with the lattice pin pitch. HEXPIN used an effective pin pitch and needed to modify the few group cross sections to conserve the volume.

2. HEXPINSP Code Development

VISWAM code lattice model for hexagonal fuel assemblies considers irregular mesh finite differencing with the actual dimensions of the thin water gaps surrounding the regular hexagonal lattice structure. In order to use the VISWAM few group cross section database, a new code HEXPINSP has been developed. In this code each assembly cell adopts the same material and geometric description that are considered at the lattice level. Hence it allows the cross sections to be used as such with no modification. The cells of each assembly are spirally numbered from centre to last layer of thin water gaps. The same irregular mesh finite differencing is used. Fig.1 shows the typical cell description of an assembly cell. The colour scheme of the pincells refer to their burnup types for which the few group cross sections are differentiated and are provided in the VISWAM few group lattice database. There are also nonfuel cells such as water rod cell or control rod cells and the edge water cells. These cells belong exclusive to each fuel assembly type. This is an important improvement over the earlier HEXPIN code

where there was ambiguity in ascribing the cross sections of border cells shared by adjacent multiple fuel assemblies.

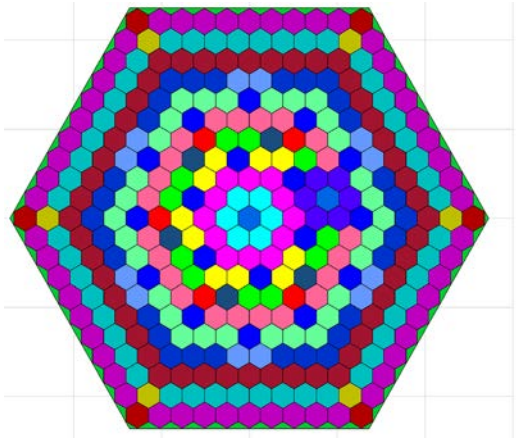


Fig.1 A Schematic Description of Cells within an Assembly Cell

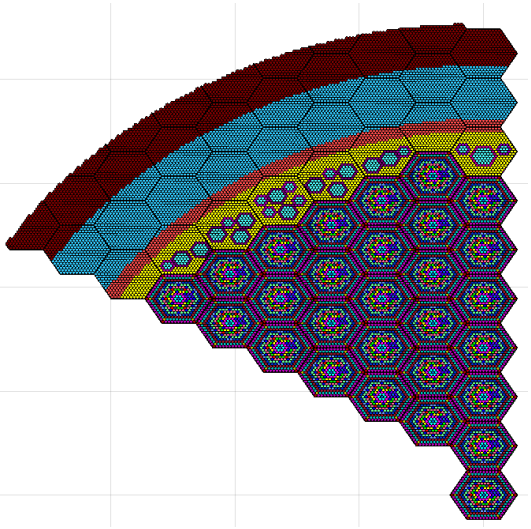


Fig.2 60° Symmetric core

The core description is enabled by stacking each assembly cell lay out with respect to its assembly cell centre coordinates. Fig.2 shows the layout of 60° symmetric core along with the reflector zones. The reflector layers beyond the active core consist of core baffle with surveillance thimbles of water, core barrel, downcomer water and reactor pressure vessel. The circular thimbles of different radii are approximated by hexagonal cells up to the required area. The inner hexagonal cells are pure water regions (blue) while their boundary cells (maroon colour) are (steel: water) mixture, preserving the area of water and steel. The zig-zag boundaries of core barrel and pressure vessel radii approximate the actual circular boundaries. There was a considerable caution and effort needed to appropriately orient them in the six 60° sectors, since their coordinates were provided only in the first sector of positive sign while the others were obtained by rotational symmetry. For this purpose, the (x, y) coordinates of the corners of each hexagonal cell or pentagonal cells in the core were generated and were used for the 2D plot of the whole active core along with reflector zones. The MATLAB support software provided by SRI, AERB was very useful to produce this plot [2]. It also helped in confirming the correct orientation the reflector assembly cells, surveillance thimbles and other regions. The correctness of the full 360° (core + reflector) zones description can be seen in Fig.3.

VISWAM lattice code provides a material description file as '.mbz' file for each fuel type. At core level it is necessary to provide only the fuel assembly types in the core in a map form. The code automatically superimposes the two data to generate the detailed material description in the whole active core, either full core or 60° symmetric core. In HEXPIN the pin locations were numbered continuously from bottom to top boundaries and from left to right, with all positive coordinates with left bottom corner as origin. This scheme is found to be unsuitable to treat the 60° symmetric core where the assembly cells appear in a zig-zag manner on the symmetric boundaries. The reflector description was also provided by external processing while it is done internally HEXPINSP code. In HEXPINSP code the origin is at core centra and the coordinate spread in minus and positive directions. The HEXPINSP code will be economical and useful for the scoping multi-fuel cycle analysis of the VVER-KK type cores with the 60° symmetry option.

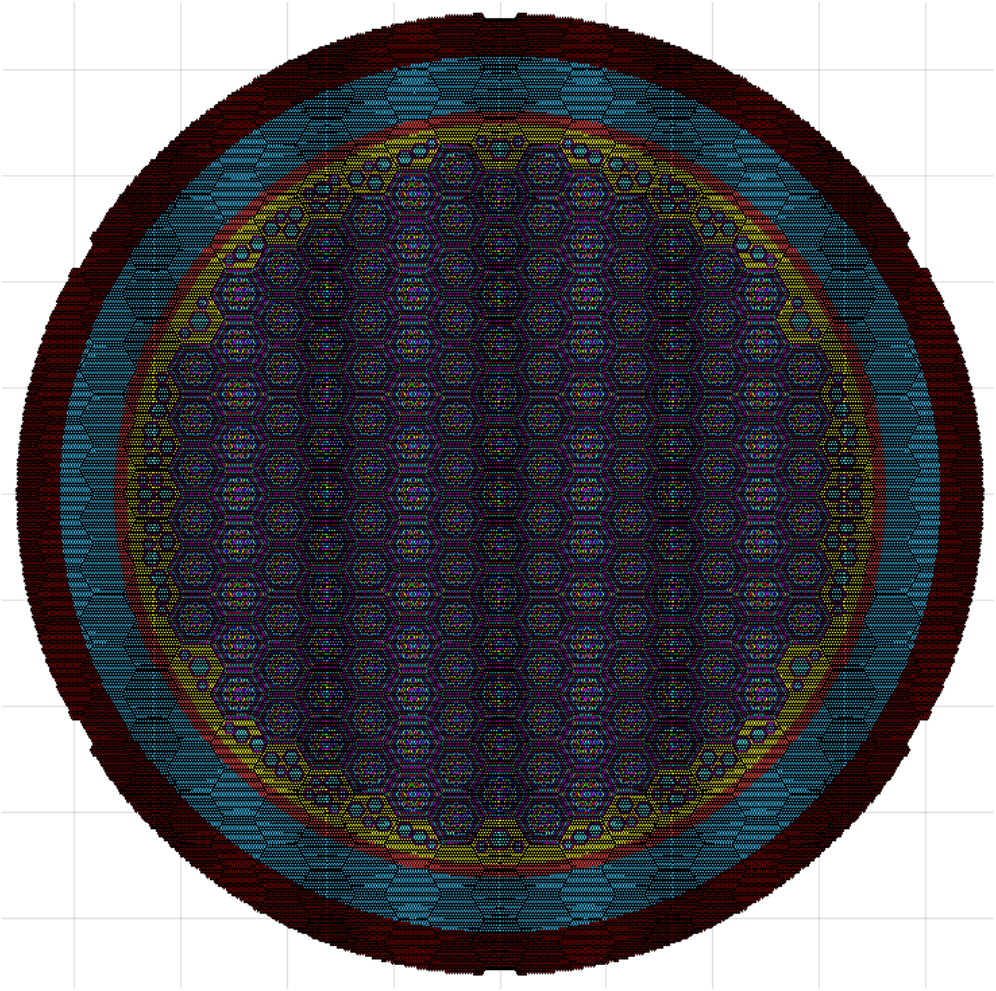


Fig.3 Full Core + Reclector Zone Description in a Pin by Pin Model

3. Solution Model

The finite difference diffusion kernel needs the coupling of meshes of different shapes and sizes and material types. Within an assembly cell regular-regular hexagonal cells are linked. For the last fuel pincell layer, regular cell with thin side pentagonal mesh or with a corner pentagonal mesh are connected. For the boundary layer there is coupling of thin pentagonal mesh with another pentagonal mesh of the same assembly cell or the same shape of a neighbouring assembly cell. The corner pentagonal cell is linked to a pentagonal mesh of the same assembly cell or the corner cell of a neighbouring assembly cell. The code addresses each such coupling explicitly and generates the coupling kernel with actual dimensions. The detailed description of these coupling kernel evaluation can be found in Ref.1.

The flux distribution solution is by Choleski decomposition method. The solution starts from the central fuel assembly of the core and proceeds spirally to the core boundary and up to peripheral reflector layers. The size of the vector for solution is the number of cells within one assembly cell and is identical in all assembly cells except the boundary ones at RPV which are partial ones depending on the circular shape of the RPV boundary. To enable the partial solution in any assembly cell, the leakage source from the neighbouring assembly cells is taken to r.h.s. or added to the fission and scattering source vector. The solution for integral assembly cells is similar to what is already implemented at VISWAM lattice level code. However, the solution for the partially cut assembly cells on RPV layer

where several cells are absent in a random manner is a new challenge. This kind of spirally outward progressing wavefront of solution method is expected to improve the convergence rate since the error propagates from high to low flux regions. At present the layer by layer circular Choleski decomposition method is working for each pincell layer of each fuel assembly from core center to reflector layer of assembly cells. The preliminary results are being scrutinized for correctness of the obtained results. Some validation results may possibly be included at the time of the conference.

4. Summary

With the experience of the erstwhile HEXPIN code, a new the pin-by-pin model code for the hexagonal lattice core has been incorporated in the new HEXPINSP code after eschewing the deficiencies noted in the earlier version of HEXPIN code. This code is capable of providing economical analysis of 60° symmetric core for the fuel cycle studies of VVER-KK core. Validation of the model against a few benchmark references is in progress.

5. References

1. V. Jagannathan, 'Detailed Description of the HEXPINSP Pin by Pin code Development and the User's Manual', AERB Report under preparation, 2022.

2. 'MATLAB Software for viewing VVER hexagonal pin by pin modelling'. Private Communications from Dr. L Thilagam, SRI, AERB, October, 2020.

Monte Carlo Scheme for Computation of Dancoff Factor

Amod Kishore Mallick[1,2], Argala Srivastava[1] and Umasankari Kannan[1,2]
[1] Bhabha Atomic Research Centre, Mumbai, India
[2] Homi Bhabha National Institute, Mumbai, India
[1]*e-mail: - amod@barc.gov.in*

Abstract

Lattice cell transport simulation generally makes use of multi-group nuclear data library. WIMS-D multi-group nuclear data libraries are very popular and widely used in such transport simulations. To obtain cross-section data required for neutron transport simulation, the library needs to be processed especially the resonance self-shielding corrections. This processing is based on equivalence theorem and requires computation of Dancoff factor for each fuel element present in the lattice cell. An accurate estimation of Dancoff factor is thus essential to arrive at correct self-shielded resonance cross-sections. Monte Carlo methods can be used to compute Dancoff factors with great accuracy. This paper describes the Monte Carlo scheme for Dancoff factor computation. The scheme has been incorporated in Monte Carlo code PATMOC and numerical results from this code are presented to verify the accuracy of this scheme.

1. Introduction

Lattice calculations using deterministic transport methods require multi-group cross-section data. WIMSD nuclear data libraries [1] are very popular and widely used for lattice calculations. The library lists cross section data for each relevant nuclide in various energy groups in fast, resonance and thermal regions. For resonant nuclides, it also lists resonance integral data which are required to be processed to obtain resonance energy region absorption (and nu-fission) cross sections for the resonant nuclides. The processing of library tabulated resonance integral data using equivalence theorem requires, among other things, Dancoff factor [2] for each fuel pin containing resonant nuclide, and it depends on the geometrical arrangement of these pins in the lattice cell. Depending on the geometrical arrangement, different pins can have different Dancoff factors.

A code using such library, therefore, needs to compute Dancoff factor for each fuel pin or it should be supplied by the user through the input. It is generally seen that legacy lattice transport codes generally use Carlvik's routine [3] for computing Dancoff factor, which is meant for a single pincell lattice, and then use appropriate approximations based on the location and surrounding neighbour pins to estimate Dancoff factor for different pins. This results in approximations in resonance self-shielding treatment. The approximation involved in computation of Dancoff factor may be computed very accurately (barring statistical uncertainty) by using Monte Carlo methods as full geometrical details of the lattice can me modelled with this. The computed Dancoff factor may be fed in the code through input file. In this paper, we give the brief description of Monte Carlo scheme for Dancoff factor computation. The scheme was also included in indigenous Monte Carlo code PATMOC [4, 5] for practical use. The results of this code also validates the scheme and are presented here.

2. Monte Carlo Scheme for Dancoff Factor Computation

2.1 Dancoff Factor

The probability of neutron escaping a fuel pin to collide in non-fuel region before it makes any collision in any fuel region is called escape probability. The escape probability reduces if the fuel pin under consideration is surrounded by another fuel pins as compared to the case if there are no other fuel pins. The factor by which the escape probability reduces is termed as Dancoff factor named after Dancoff who proposed a method to compute this reduction factor. The resonance absorption in one fuel pin therefore gets affected due to the presence of other fuel pins nearby and is dictated by the Dancoff factor. There are more than one ways to define it. The definition that we have used in our computation scheme is this: the probability of neutrons coming out of the surface of fuel rod (with white distribution) to collide in the non-fuel region before it strikes any fuel rod is called Dancoff factor. Dancoff correction, on the other hand, is the probability of neutrons emitting from fuel rod (with white distribution) to strike another fuel rod without colliding in any non-fuel material and this is simply one minus Dancoff factor.

2.2 Algorithm for Dancoff Factor Computation

Using the above definition of Dancoff factor, its computation using Monte Carlo involves execution of following simple steps:

i. Sampling starting position of a neutron uniformly from surface of fuel pin under consideration.
ii. The direction of emission from the surface is sampled from white distribution.
iii. Neutron is transported in that direction till it hits a region with fuel material or its weight becomes low (smaller than the pre-defined value) or it escapes from the system. Weight deposited in the non-fissile material during the transport is accumulated to estimate of Dancoff factor.
iv. Execute above steps for a number of histories (say, N).
v. Final result is then obtained as the mean of individual history estimates. The error on the final result is obtained using Central Limit Theorem (CLT).

The implementation of the above steps is described below briefly for a 2D lattice cell consisting of cylindrical fuel pins. one by one. To illustrate the algorithm, we assume here that the Dancoff factor for the infinite cylindrical fuel pin parallel to z-axis (with (A, B, 0) being the center of the cylinder) defined by following equation

$$(x - A)^2 + (y - B)^2 - R^2 = 0 \quad ----(1)$$

is to be computed. The details of geometry around these fuel pins may be arbitrary. As geometrical arrangement is assumed to be infinite in one direction (2D structure), staring position of neutrons is sampled from only one plan perpendicular to this infinite direction. For the above defined cylinder, the neutrons may be sampled from the surface of cylinder at z = 0 only. Due to this, only x and y coordinate needed to be sampled which is sampled uniformly as follows:

i. Get a random number uniformly between 0 and 1, say, r
ii. x = A + R * cos(2πr) and y = B + R * sin(2πr)

Once position is sampled, the direction of motion (emission) is sampled as follows. The outward normal to the surface at the neutron's starting position on the surface is obtained. For Infinite Cylinder Parallel to Z-axis in our case, normal to equation turns out to be,

$$\boldsymbol{n} = \frac{x - A}{R}\boldsymbol{i} + \frac{y - B}{R}\boldsymbol{j} \qquad (2)$$

Once the normal to surface is obtained, direction is sampled from white distribution. The white distribution is given by,

$$f(\mu, \varphi) = \frac{\mu}{\pi} \, d\mu \, d\varphi \qquad (3)$$

Where, $\mu = \cos(\theta), 0 \leq \mu \leq 1;\ 0 \leq \varphi < 2\pi$, and θ is the angle from normal to surface and φ is the azimuthal angle. As μ and φ are independent, they can be sampled independently. μ can be sampled easily using inversion method by using a random number r as,

$$\mu = \sqrt{r} \qquad (4)$$

And, similarly φ can be sampled using inversion method using another random number r as,

$$\varphi = 2\pi r \qquad (5)$$

Knowing the normal vector and, μ and φ by which the neutron direction is rotated with respect to the normal, the direction cosines of neutron direction can be obtained with some algebra [5].

After sampling position and direction, neutron is transported in this direction till it encounters another region with fuel or it escapes from the system. Neutron with weight one and a score with value zero is started from the region of sampled position in the sampled direction. As it passes through one region, the score and weight of the neutron is updated as follows.

$$score = score + \ weight * \ \left(1.0 \ - e^{-sigma*d}\right) \qquad (6)$$

where, 'sigma' is the cross-section of the material of the region of neutron's flight path (d). Weight of neutron is reduced corresponding to the length of flight path as,

$$weight = weight * \ e^{-sigma*d} \qquad (7)$$

A number of histories are simulated to get samples of Dancoff factor for each history. The final result is obtained by averaging the sample estimates and error on the result is obtained using CLT as follows. Let $\{x_i, i = 1, N\}$ are history estimates of Dancoff factor for N histories. Sample mean and sample variance are then computed as,

$$sample\ mean, \bar{x} = \sum_{i}^{N} x_i \qquad (8)$$

$$sample\ variance, s^2 = \sum_{i}^{N} (x_i - \bar{x})^2 \qquad (9)$$

Final estimate of Dancoff factor and the associated error is given as:

$$\text{dancoff factor: } \ \bar{x} \ +/- \ \frac{s}{\sqrt{N}} \qquad (10)$$

3. Numerical Results

The numerical scheme discussed in this paper has been employed in a general-geometry multi-group Monte Carlo code PATMOC [6, 7]. The results of this scheme, as computed using PATMOC, is presented here to show its accuracy and validity. The lattice cell we have considered is a 19-Pin hexagonal bundle in infinite moderator (with cross-section 2.0 cm^{-1}) as shown in Figure 1. The four pins (A, B, C, D) as shown in the figure are selected for Dancoff computation. They represent pins of all rings and are symmetrically different. In the outer ring pin C and D represent two different neighboring environments and hence Dancoff corrections are also different for them. Table 1 compares the computed results with the reference [2] values and we can see that our results agree very well with the reference results.

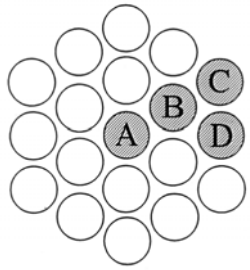


Fig-1: 19-Pin hexagonal fuel bundle.

Table 1- Dancoff Corrections for different fuel pins in hexagonal cluster

SN	Pin	Our value	Reference Value (DANCOFF-MC)
1	A	0.14865 +/- 0.00011	0.1489 +/- 0.0004
2	B	0.14862 +/- 0.00011	0.1486 +/- 0.0004
3	C	0.07420 +/- 0.00011	0.0740 +/- 0.0003
4	D	0.09911 +/- 0.00012	0.0989 +/- 0.0004

4. Conclusion

A numerical scheme to compute Dancoff factor using Monte Carlo method is discussed. The suggested scheme has been incorporated in an indigenous Monte Carlo code PATMOC. The results presented show the accuracy and effectiveness of the scheme. Being a general geometry code, PATMOC after incorporation of this scheme can now also be used to compute Dancoff factors of any arbitrary lattice cell. The computed values can be fed in deterministic transport codes for faithful processing of nuclear data library of complex lattice cell.

5. References

[1] Leszczynski, F., Aldama, D.L., Trkov, A., 2007. WIMS-D library update. Technical report, International Atomic Energy Agency.

[2] S Feher et. al, "Monte Carlo Calculation of Dancoff Factors in Irregular Geometries", *Nuclear Science and Engineering, 117, 227-238* (1994)

[3] I Carlvik, "The Dancoff Correction in Square and Hexagonal Lattices", *NSE*, **29**, 325-336, (1967)

[4] Amod Kishore Mallick and Umasankari Kannan, "PATMOC: A Multi-group Monte Carlo code for Neutron Transport Simulation", RPDD/EP/164 (2018)

[5] Amod Kishore Mallick and Anurag Gupta, "Sub-Space Iteration Based Monte Carlo Scheme for Simultaneous Computation of Multiple Dominant k-eigenmodes and Acceleration of Fission Source Iterations", Annals of Nuclear Energy, 166 (2022).

[6] Amod Kishore Mallick and P D Krishnani, "Extension of Monte Carlo code PATMOC for Dancoff Factor calculation in arbitrary 2D arrangement of cylindrical fuel pins", RPDD/EP/112 (2015).

[7] Amod Kishore Mallick, Argala Srivastava, Umasankari Kannan and P D Krishnani, "Monte Carlo Computation of Dancoff Factors for 2D Reactor Lattice Cell", NSRP-21, March 5-7, 2018, Indore, India.

Development of PATMOC – An Indigenous General-geometry Multi-group Monte Carlo Code for Full Core Neutron Transport Simulations

Amod Kishore Mallick[1,2], Anurag Gupta[1,2], Indrajeet Singh[1] and Umasankari Kannan[1,2]
[1] Bhabha Atomic Research Centre, Mumbai, India
[2] Homi Bhabha National Institute, Mumbai, India
[1]*e-mail: - amod@barc.gov.in*

Abstract

An indigenous Monte Carlo code named PATMOC has been developed for reactor physics applications. The code uses Constructive Solid Geometry techniques for geometry representation and can model arbitrary complex geometry such as full reactor core. It is based on multi-group formalism and uses WIMS-D nuclear data libraries for practical simulations. It is meant for criticality and source mode simulations to compute k-eff and various tallies such as flux, reaction rates, power distribution, etc. It has been tested for its algorithmic accuracy against numerous benchmarks such as Takeda LWR and C5G7 full core problems. The code has further been successfully validated by simulating practical systems such as AHWR-CF, Apsara-U, and BRAHMMA, and now has become a useful tool for reactor physics simulations.

1. Introduction

PATMOC (**PA**rticle **T**ransport with **MO**nte **C**arlo) [1, 2] is an indigenous multi-group Monte Carlo code for neutron transport simulations recently developed at Reactor Physics Design Division of BARC. In its current state of development, this code can be used to perform Eigen (criticality) mode and Source mode simulations used in day to day reactor physics studies. In this paper, we discuss briefly the features and capabilities of the code, results of its benchmarking against numerical benchmarks, and results of its application on practical reactor systems.

2. Features and Capabilities of PATMOC

2.1 Geometry

The code uses Constructive Solid Geometry (CSG) technique for geometry modeling. In CSG, geometry is defined as collection of homogeneous regions with each region defined by the surfaces (and boundary conditions, if any) enclosing it. All surfaces of 1st (planes) and 2nd (sphere, cylinder, ellipse, parabola, hyperbola, etc) degree and all major boundary conditions, namely Vacuum, Reflective, White, and Periodic are supported by the code. It also has 'Universe' and 'Lattice' (both rectangular and hexagonal) features for efficient and easy modeling of lattice kind arrangement of clusters/assemblies inside reactor core. With these features, a wide variety of geometrical configurations such as full reactor core relevant to reactor physics studies can be modelled and simulated.

2.2 Simulation Methods

The code supports both analog and non-analog methods of Monte Carlo simulation and can be chosen by the user. It can be used for Criticality simulations as well as for Source mode simulation for sub-critical system with external source. Point sources and volume sources of various shapes such as box, cylinder and sphere are currently supported by the code for Source mode simulation. Other than this, there is mode for Dancoff factor computation. Arbitrary complex lattice cell can be modelled explicitly to compute Dancoff factors of each fuel pin very accurately using Monte Carlo transport. The computed Dancoff factors can be fed in deterministic lattice transport codes which generally use various approximation in computing Dancoff factors. There is another mode for generation of resonance self-shielded cross-section data set from WIMS-D nuclear data library [3]. Given lattice cell description and library, the code when run in this mode computes Dancoff factor for each pin and processes the library to do resonance and other treatments to arrive at the final cross-section data of each material in the lattice to be used in neutron transport simulations.

2.3 Tally

In criticality simulation, code, by default, computes k-eff/k-inf. Similarly, in source mode simulation, k-source is computed by default for sub-critical system with external source. For these tallies, it uses all three basic estimators, namely Absorption, Collision, and Track length, and final results with minimum variance obtained by combining these estimates are provided. Other than this, various kinds of tallies such as volume flux, surface flux, different reaction rates, leakage from system, etc. are also supported by the code. A scheme of 'Scores' and 'Filters' for defining tallies has been adopted in the code. Using this, a tally in specified region of phase space such as flux in a particular cell and in some particular energy group can be computed.

2.4 Nuclear Data Library

The code is based on multi-group formalism and uses WIMS-D format nuclear data library for practical simulations. Both 69- and 172-group libraries are supported. The processing of WIMS-D library to obtain resonance self-shielded cross section data for simulation requires Dancoff factors. These Dancoff factors are computed very accurately within the code again using Monte Carlo methods. It also uses anisotropic scattering data (up to P1) supplied in the WIMS-D library for simulation.

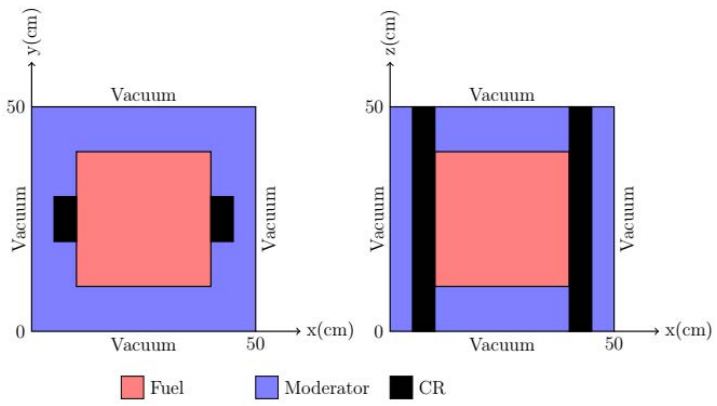
2.5 Input Preparation

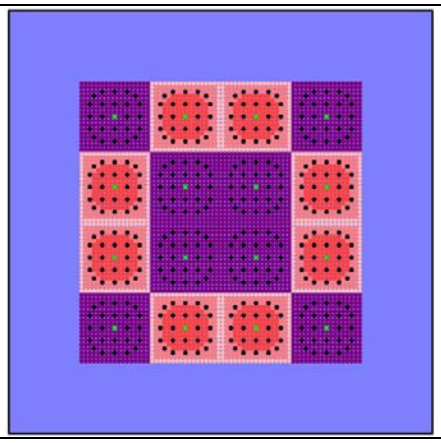
Keyword based input preparation scheme has been adopted to have a simple, logical, and consistent methodology to model a problem. In this scheme, input consists of sets of data with one set of data being called a 'card'. Each card begins with an identifier keyword followed by data. Identifier keyword fixes the type and number of data appearing on the card. A set of keywords have been devised for different information required by the code. This has also improved the readability of the input and made the editing of existing inputs easier and faster.

3. Benchmarking of PATMOC

The code has been verified for its algorithmic accuracy against numerous analytical/numerical benchmarks. We present here results of two of OECD/NEA benchmarks: Takeda modeled BWR core

and C5G7 PWR core. Figure-1a and 1b give the geometrical representation of these cores. Table 1 gives the PATMOC results of Takeda problem for CR In and Out cases, and compares it with the reference values. We can see that the results are in good agreement. Table 2 gives the PATMOC results of C5G7 problem for 2D and 3D version of the benchmark, and compares it with the reference values. Here also we can see that the results are in good agreement.





(a) Horizontal and vertical cross section of Takeda core | (b) Horizontal cross section of C5G7 core

Figure-1: Core geometry of OECD/NEA Takeda BWR and C5G7 benchmarks

Table-1: k-eff results for Takeda 3D BWR benchmarks

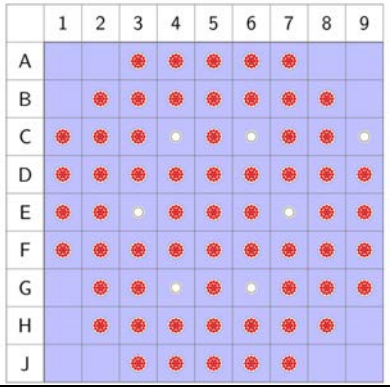
S.N	Benchmark Problem	PATMOC	Benchmark reference	Diff (mk)
1.	CR Out	0.97722 ± 0.00034	0.97763	-0.41
2.	CR In	0.96224 ± 0.00034	0.96221	0.03

Table-2: k-eff results for C5G7 benchmarks

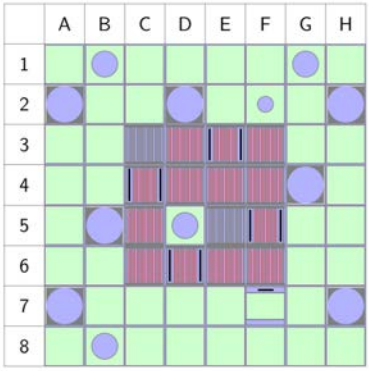
S.N	Benchmark Problem	PATMOC	Benchmark reference	Diff (mk)
1.	2D Geometry	1.18660 ± 0.00006	1.18655	0.05
2.	3D Geometry	1.18390 ± 0.00006	1.18381	0.09

4. Usages of PATMOC

With current features and capabilities, PATMOC is well suited for use in simulation of practical reactor systems. We have used it extensively for analyzing various reactor physics experiments carried out in AHWR-CF and Apsara-U reactors. Figures 2a and 2b show the core configuration of AHWR-CF and Apsara-U respectively. A few of the results estimated using PATMOC and its comparison with experimentally measured values are presented here to demonstrate its working as well as the accuracy. Table-3 compares the k-eff estimated by PATMOC for the observed critical core configuration for two cases: reference core and reference core with a 6-pin (Th-Pu) MOX experimental cluster at E5 location in core. We see that the results are around within 1mk which is very good agreement with the measured results. Similarly, Table-4 compares the k-eff estimated by PATMOC for the observed critical core configuration of Apsara-U with the designer's estimate and the observed value. Here, we see that the PATMOC estimate is closer to the designer's estimate and both of them differ from the measured values by around 7 mk.



(a) Horizontal cross section of AHWR-CF core



(b) Horizontal cross section of Apsara-U core

Figure-2: Core configuration of AHWR-CF and Apsara-U reactors

Table-3: Estimated k-eff for AHWR-CF critical core configuration

S.N	Core	Observed critical height (cm)	PATMOC k-eff	Observed k-eff	Diff (mk)
1.	Reference core	226.7	1.00074 ± 0.00015	1.0	0.7
2.	Core with Experimental cluster at E5 location	233.3	1.00107 ± 0.00015	1.0	1.1

Table-4: Estimated k-eff for observed critical core configuration of Apsara-U

PATMOC k-eff	Designer's estimate of k-eff	Observed k-eff
1.00653 ± 0.00025	1.00714	1.0

5. Conclusion

An indigenous general-geometry multi-group Monte Carlo code named PATMOC has been developed for reactor physics applications on full core reactor system. The code has been extensively benchmarked, is being used in regular reactor physics simulations of reactors/facilities such as AHWR-CF and Apsara-U reactors, and now has become a useful tool for reactor physics studies.

6. References

[1] Amod Kishore Mallick and Umasankari Kannan, "PATMOC : A Multi-group Monte Carlo code for Neutron Transport Simulation", RPDD/EP/164 (2018)

[2] Amod Kishore Mallick and Anurag Gupta, "Sub-Space Iteration Based Monte Carlo Scheme for Simultaneous Computation of Multiple Dominant k-eigenmodes and Acceleration of Fission Source Iterations", Annals of Nuclear Energy, 166 (2022).

[3] Leszczynski, F., Aldama, D.L., Trkov, A., 2007. WIMS-D library update. Technical report, International Atomic Energy Agency.

Acknowledgements: First author sincerely thanks Dr. Rajeev Kumar, Dr. P D Krishnani (Former Head, RPDD), Dr. K P Singh and other members of RPDD for their kind help, support and encouragement in this work.

Treatment of Convergence Instability in MOC Iterations with Large Negative Self-Scattering Cross Sections in DIAMOND

Lakshay Jain[1,2], R. Karthikeyan[2] and Umasankari Kannan[1,2]
[1] Homi Bhabha National Institute, Mumbai, India
[2] Bhabha Atomic Research Centre, Mumbai, India
[1]*e-mail:- lakshay.jain@gmail.com*

Abstract

Transport correction is widely used to account for anisotropic scattering effects in neutron transport calculations due to its efficient treatment of scattering anisotropy through isotropic scattering approximation. However, transport correction may lead to negative self-scattering cross-sections (XS) which can degrade the stability of method of characteristics (MOC) transport iterations. In this paper, the treatment of convergence instability in MOC iterations implemented in the code DIAMOND, arising due to large negative self-scattering XS has been presented.

1. Introduction

Accuracy of nuclear reactor simulations relies on the detailed heterogeneous modeling with minimum simplifications and/or assumptions. Inclusion of anisotropic scattering effects is of primary importance to the overall accuracy of the neutron flux distribution obtained using high fidelity neutron transport modeling. Transport correction of the cross-sections (XS) [1] is a frequently used method in neutron transport codes, like DIAMOND [2], for efficiently capturing the effects of anisotropic scattering through isotropic scattering source approximation. Although different forms of the transport correction have been developed, most use a lower in magnitude transport XS $\left(\Sigma_{tr,g}\right)$ to replace the total XS $\left(\Sigma_{t,g}\right)$. The same transport correction $\left(\Delta\Sigma_{tr,g}\right)$ is also applied to the self-scattering XS $\left(\Sigma_{s,g\to g}\right)$ in order to preserve the XS balance, as shown in Eq. (1). The smaller magnitude of $\Sigma_{tr,g}$ accounts for the increased propagation of the neutrons in the forward direction.

$$\begin{aligned}\Sigma_{tr,g} &= \Sigma_{t,g} - \Delta\Sigma_{tr,g} \\ \Sigma'_{s,g\to g} &= \Sigma_{s,g\to g} - \Delta\Sigma_{tr,g}\end{aligned} \tag{1}$$

where $\Sigma'_{s,g\to g}$ represents the transport corrected self-scattering XS. However, the magnitude of $\Delta\Sigma_{tr,g}$ may be large when using a fine energy grid, particularly for strongly scattering materials like light and heavy water. If $\Delta\Sigma_{tr,g} > \Sigma_{s,g\to g}$, this can lead to large negative transport corrected self-scattering XS. Although the method of characteristics (MOC) formulation guarantees a positive solution of the neutron transport equation, $\Sigma'_{s,g\to g} < 0$ can eventually lead to unphysical and negative neutron fluxes in some regions. This can adversely affect the stability of MOC iterations giving rise to oscillations and negative multiplication factor, ultimately leading to divergence [3]. Theoretical analysis of the convergence behavior of MOC iterations with negative self-scattering XS has been presented in Tabuchi *et al*. [4]. The stabilization of MOC iteration scheme implemented in the code DIAMOND in the presence of large negative self-scattering XS has been discussed in this paper.

2. Stabilization of MOC Iterations

The multi-group neutron transport equation with isotropic scattering approximation can be expressed using the matrix-vector notation shown in Eq. (2), where k denotes the effective multiplication factor (or dominant eigenvalue), ϕ represents the scalar flux vector, T is the transport sweep operator, and F and S are the fission and scattering operators, which can be defined using Eq. (3).

$$\phi = T^{-1}\left(\frac{1}{k}F + S\right)\phi \tag{2}$$

$$F_{(i,g),(i,g')} = \frac{1}{4\pi}\chi_{i,g}\nu\Sigma_{f,i,g'} \quad , \quad S_{(i,g),(i,g')} = \frac{1}{4\pi}\Sigma'_{s,i,g'\to g} \tag{3}$$

where $\chi_{i,g}$ represents the neutron fission spectrum and $\nu\Sigma_{f,i,g}$ is the production XS. The row and column index are represented using (i,g) where i and g denote the region and energy group, respectively. The row/column indices can be determined as $i \times G + g$, G being the total number of energy groups. Eq. (2) is usually solved iteratively since direct inversion of the matrix T is computationally very expensive for most realistic problems. Two popularly used iterative techniques used to solve Eq. (2) are:

i. The inner-outer iteration scheme in which the fission source $\left(\frac{1}{k}F\phi\right)$ is held constant during the inner (scattering) sweeps and only the scattering source $(S\phi)$ is iterated. $\frac{1}{k}F\phi$ is then updated in the outer (k-eigenvalue) iterations.
ii. The source iteration scheme without explicit inner sweeps in which the complete neutron source term on the right-hand side of Eq. (2) $\left(\left[\frac{1}{k}F + S\right]\phi\right)$ is updated after every iteration.

However, the convergence of these iterative systems is not guaranteed in the presence of large negative self-scattering XS (diagonal elements of S). The forthcoming discussion on stabilization of the MOC iterations in the code DIAMOND has been presented and implemented *w.r.t.* source iterations without inner sweeps.

The stabilization scheme is based on a mathematically equivalent and valid form of Eq. (2), given in Eq. (4), where A is any arbitrary matrix such that $I + A$ can be inverted.

$$\phi = (I + A)^{-1}\left[T^{-1}\left(\frac{1}{k}F + S\right) + A\right]\phi \tag{4}$$

The same iterative scheme used to solve Eq. (2) can be employed for solving Eq. (4). Ideally, inversion of the matrix $I + A$ should be very simple so as to minimize any additional computational burden in the iterative process. Thus, A is chosen to be a diagonal matrix whose elements can be computed using Eq. (5).

$$A_{(i,g),(i,g)} = \begin{cases} \frac{-\gamma\Sigma'_{s,i,g\to g}}{\Sigma_{tr,i,g}} & , \quad \text{for} \quad \Sigma'_{s,i,g\to g} < 0 \\ 0 & , \quad \text{otherwise} \end{cases} \tag{5}$$

Here, γ represents the damping coefficient with $\gamma \in [0,1]$. For $\gamma = 1$, no negative diagonal elements are present in the iteration matrix, while $\gamma = 0$ represents the unaltered iterative system represented by Eq. (2). The diagonal stabilization scheme used in DIAMOND has been adapted from Ref. [5]. Some important implementation details may also be mentioned here.

i. Negative sources are reset to zero during the initial 5 MOC transport iterations.
ii. Negative scalar fluxes, if any, are always reset to zero.
iii. An additional scalar flux vector ϕ is used with no other significant changes required.
iv. Warning message is displayed whenever negative source/scalar flux fix-up is used.

3. Results

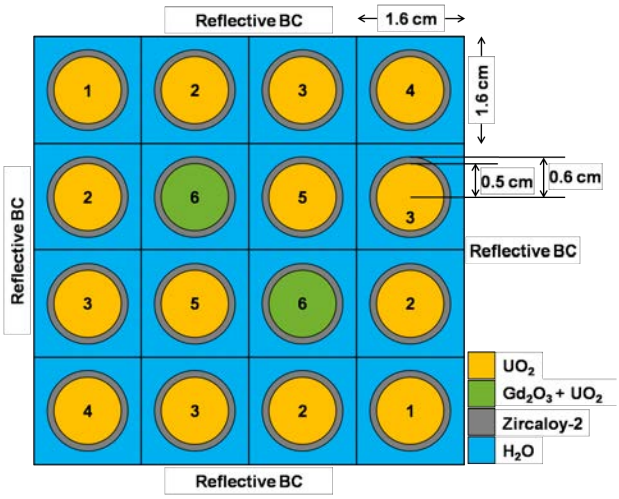


Figure 1 – Maeder-Wydler benchmark problem

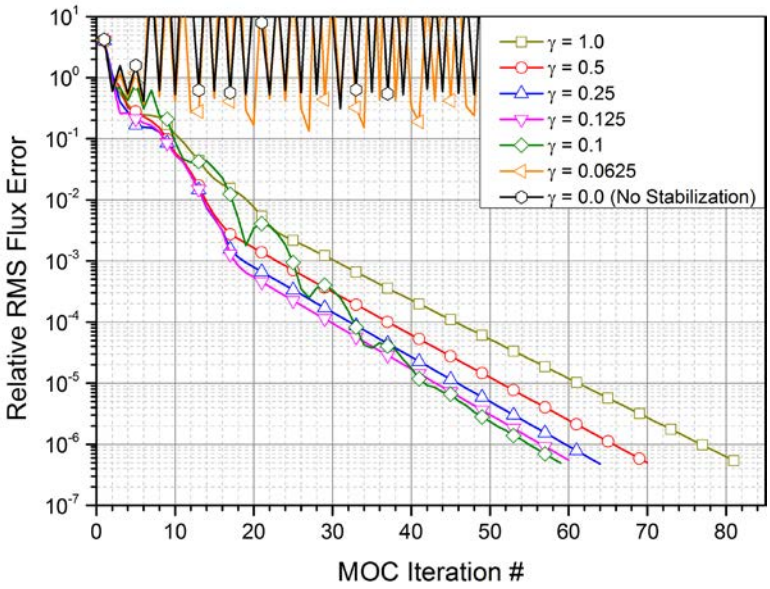


Figure 2 – Convergence behavior for Maeder-Wydler benchmark problem

The Maeder-Wydler BWR benchmark problem, shown in Figure 1, has been modeled with 172-group transport corrected macroscopic XS obtained using DRAGON. The problem consists of 14 UO_2 and 2 UO_2 + Gd_2O_3 fuel pins with a square pitch of 1.6 cm arranged in a 4×4 lattice configuration. The convergence behavior of MOC iterations with different damping coefficients for negative self-scattering XS (γ) has been plotted in Figure 2. It can be seen that the conventional MOC iterations with no stabilization ($\gamma = 0$) or very small damping coefficient ($\gamma = 0.0625$) show instability and are unable to converge. However, the MOC iterations are observed to be stable for all other cases with a non-zero damping coefficient ($\gamma \geq 0.1$). The system converges in lesser number of iterations with a

smaller damping coefficient before the improvement in performance saturates for $\gamma \simeq 0.125$. Use of a smaller damping coefficient than the optimum value is unable to overcome the convergence instability caused by the presence of large negative self-scattering XS. This is because the damping coefficient stabilizes the iterative system in a manner similar to the under-relaxation scheme. Thus, the MOC iterations are insufficiently under-relaxed and fail to converge with very small damping coefficients. On the contrary, very large damping coefficients stabilize the system but at the cost of loss of convergence speed. Thus, the damping coefficient should be chosen so as to not be too small or large.

Conclusion

Transport correction is popularly used for modeling of anisotropic scattering in neutron transport calculations. However, the transport correction XS may often be larger in magnitude than the self-scattering XS. In such a case, application of the transport correction to macroscopic XS may lead to large negative self-scattering XS which destabilize the transport calculations. The stabilization scheme implemented in the code DIAMOND, to treat the convergence instability of MOC iterations in the presence of large negative self-scattering XS has been presented in this paper. The scheme has been used for the treatment of the Maeder-Wydler benchmark problem with 172-group macroscopic XS. The results show that this scheme improves the convergence performance of transport iterations and removes the instability arising due to negative self-scattering XS.

4. References

[1] Bell, G., Hansen, G., Sandmeier, H. (1967). “Multitable Treatments of Anisotropic Scattering in S N Multigroup Transport Calculations”, Nuclear Science and Engineering 28 (3), 376–383.

[2] Jain, L., Karthikeyan, R., Kannan, U. (2020). “DIAMOND – A Method of Characteristics Neutron Transport Code using Unstructured Meshing”, Annals of Nuclear Energy 137, 107086.

[3] Jain, L. (2022). “Study of Neutron Transport in Heterogeneous Assemblies using Method of Characteristics Coupled with Delaunay Triangulation”, PhD Thesis, Homi Bhabha National Institute.

[4] Tabuchi, M., Yamamoto, A., Endo, T., Sugimura, N. (2013). “Convergence Analysis of MOC Inner Iterations with Large Negative Self-scattering Cross-section”, Nuclear Science and Engineering 50 (5), 493–502.

[5] Gunow, G., Forget, B., Smith, K. (2019). “Stabilization of Multi-group Neutron Transport with Transport-corrected Cross-sections”, Annals of Nuclear Energy 126, 211–219.

A MULTIGROUP NEUTRON DIFFUSION MODEL FOR SPACE-TIME REACTOR KINETICS PROBLEMS IN 2D CARTESIAN GEOMETRY

R. Kondala Rao 1[1], P. Mangarjuna Rao 2[2], K. Natesan 3[2] and S. Raghupathy 4[2]

[1] Indira Gandhi Centre for Atomic Research, A CI of Homi Bhabha National Institute, Kalpakkam 603102, Tamilnadu, India

[2] Reactor Design and Technology Group, Indira Gandhi Centre for Atomic Research, Kalpakkam 603102, Tamilnadu, India

[1]*e-mail: - rkrao@igcar.gov.in*

Abstract

A direct space-time nuclear reactor kinetics model has been developed for solving time dependent multi-group neutron diffusion equations along with the time dependent delayed neutron precursor equations. A computer code named MANDIR-2DC has been developed and employed to reconstruct the results of 2D TWIGL and 2D LRA BWR benchmark problems.

1. Introduction

Accurate prediction of the spatial and temporal behavior of neutron flux and power distribution is essential for competent design and reliable safety analysis of a nuclear reactor core [1]. A space-time nuclear reactor kinetics model has been developed which can **directly** solve the space and time dependent multi-group neutron diffusion equations along with the time dependent delayed neutron precursor concentration equations. The numerical model employs an orthogonal mesh based finite volume method for spatial discretization and implicit method for time discretization. A computer code named MANDIR-2DC (Multigroup Analysis of Neutron DIffusion in Reactor for 2D Cartesian geometry) has been developed and is employed to study space-time reactor kinetics benchmark problems.

2. Description of the numerical model

The time dependent neutron flux of energy group *g* at a point in the reactor core is given by

$$\frac{1}{v_g}\frac{\partial \phi_g(\vec{r},t)}{\partial t} = \nabla.\left[D_g(\vec{r})\nabla\Phi_g(\vec{r},t)\right] - \Sigma_{a,g}(\vec{r},t)\Phi_g(\vec{r},t) - \sum_{g'=1}^{G}\Sigma_{s,gg'}(\vec{r},t)\Phi_g(\vec{r},t) + \sum_{g'=1}^{G}\Sigma_{s,g'g}(\vec{r},t)\Phi_{g'}(\vec{r},t)$$
$$+ (1-\beta).\frac{\chi_g^p}{k_{eff}}\sum_{g'=1}^{G}\nu_g(\vec{r},t)\Sigma_{f,g'}\Phi_{g'}(\vec{r},t) + \sum_{d=1}^{N_d}\lambda_d(\vec{r},t)\chi_g^d C_d(\vec{r},t) \quad (1)$$

The concentrations of delayed neutron precursors are described by the set of equations

$$\frac{\partial C_d(\vec{r},t)}{\partial t} = -\lambda_d(\vec{r},t)C_d(\vec{r},t) + \beta_d\sum_{g'=1}^{G}\frac{\nu\Sigma_{f,g'}}{k_{eff}}\Phi_{g'}(\vec{r},t) \quad (2)$$

where all the symbols have their usual meaning [2]. Eq. (1) can be reduced to the form

$$\frac{1}{v_g}\frac{\partial \phi_g(\vec{r},t)}{\partial t} = A\Phi_g \quad (3)$$

where *A* is an operator representing sum of losses and gains. Applying the backward Euler scheme to eq. (3),

$$\frac{1}{v_g}\frac{\left(\Phi_{g,i,j,k}^{n+1} - \Phi_{g,i,j,k}^{n}\right)}{\Delta t} = A^{n+1}\Phi_{g,i,j,k}^{n+1} \quad (4)$$

The present model employs the cell centered finite volume method.

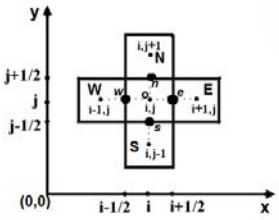


Figure 1 Control volume representation for 2D Cartesian geometry

Integrating the eq. (4) over control volume,

$$\int_V \frac{1}{v_g}\frac{\left(\Phi^{n+1}_{g,i,j,k}-\Phi^{n}_{g,i,j,k}\right)}{\Delta t}.dV=\int_V A^{n+1}\Phi^{n+1}_{g,i,j,k}.dV \tag{5}$$

Applying Gauss-Divergence theorem to the diffusion term in eq. (4) [3], we get

$$\int_V \nabla.\left[D_g(x,y)\nabla\Phi_g(x,y)\right].dV=\int_S D_g(x,y)\nabla\Phi_g(x,y).\hat{n}dS=\sum_{f=1}^{N_f}\left(D_g(x,y)\right)_f\left(\nabla\Phi_g(x,y)\right)_f.\hat{n}_f\Delta A_f \tag{6}$$

where N_f is total number of faces of the CV and $\hat{n}_f$ is unit normal vector at face centre. The index f represents the face number. The gradient of flux in 2D Cartesian system is

$$\nabla\Phi_g(x,y)=\frac{\partial\Phi_g}{\partial x}\hat{x}+\frac{\partial\Phi_g}{\partial y}\hat{y} \tag{7}$$

For orthogonal mesh,

$$\left.\begin{array}{l}\text{For east face, } \hat{x}.\hat{n}_f=1,\ \hat{y}.\hat{n}_f=0 \text{ and } \Delta A_e=\Delta y=y_{j+1/2}-y_{j-1/2}\\ \text{For west face, } \hat{x}.\hat{n}_f=-1,\ \hat{y}.\hat{n}_f=0 \text{ and } \Delta A_w=\Delta y=y_{j+1/2}-y_{j-1/2}\\ \text{For north face, } \hat{x}.\hat{n}_f=0,\ \hat{y}.\hat{n}_f=1 \text{ and } \Delta A_n=\Delta x=x_{i+1/2}-x_{i-1/2}\\ \text{For south face, } \hat{x}.\hat{n}_f=0,\ \hat{y}.\hat{n}_f=-1 \text{ and } \Delta A_s=\Delta x=x_{i+1/2}-x_{i-1/2}\end{array}\right\} \tag{8}$$

Substitute eqs. (7) – (8) in eq. (5) to derive the expression for the diffusion term

$$\int_V \nabla.\left[D_g(x,y)\nabla\Phi_g(x,y)\right].dV=\left[\left(D_g\frac{\partial\Phi_g}{\partial x}\right)_e-\left(D_g\frac{\partial\Phi_g}{\partial x}\right)_w\right].\Delta y+\left[\left(D_g\frac{\partial\Phi_g}{\partial y}\right)_n-\left(D_g\frac{\partial\Phi_g}{\partial y}\right)_s\right]\Delta x \tag{9}$$

The volume integral of source/loss term is approximated as follows.

$$\int_V Q_g(x,y).dV=\int_x\int_y Q_g(x,y).dx.dy=Q_{go}.\Delta x.\Delta y \tag{10}$$

where Q_{go} is the average value of the variable in CV. For internal CVs, the effective diffusion coefficient values at face centres are approximated using **inverse distance-weighted harmonic mean** and flux gradients are approximated using **central differencing scheme** [3]. For boundary cells, the expressions are derived in terms of neighbouring cell centre values using Taylor's series approximation and are given below [3] .

$$\left.\begin{array}{l}\text{At } x=0,\ \left(D_g\right)_w=\dfrac{3D_{g,1,j}-.D_{g,2,j}}{2},\ \left(\dfrac{\partial\Phi_g}{\partial x}\right)_w=\dfrac{\left(9\Phi_{g,1,j}-\Phi_{g,2,j}-8\Phi_{g,x=o,j}\right)}{3\left(\Delta x_{1,j}\right)}\\ \text{At } x=X,\ \left(D_g\right)_e=\dfrac{3D_{g,M,j}-.D_{g,M-1,j}}{2},\ \left(\dfrac{\partial\Phi_g}{\partial x}\right)_e=\dfrac{\left(-9\Phi_{g,M,j}+\Phi_{g,M-1,j}+8\Phi_{g,x=X,j}\right)}{3\left(\Delta x_{M,j}\right)}\\ \text{At } x=0,\ \left(D_g\right)_s=\dfrac{3D_{g,i,1}-.D_{g,i,2}}{2},\ \left(\dfrac{\partial\Phi_g}{\partial y}\right)_s=\dfrac{\left(9\Phi_{g,i,1}-\Phi_{g,i,2}-8\Phi_{g,i,y=o}\right)}{3\left(\Delta y_{i,1}\right)}\\ \text{At } y=Y,\ \left(D_g\right)_n=\dfrac{3D_{g,i,N}-.D_{g,i,N-1}}{2},\ \left(\dfrac{\partial\Phi_g}{\partial y}\right)_n=\dfrac{\left(-9\Phi_{g,i,N}+\Phi_{g,i,N-1}+8\Phi_{g,i,y=Y}\right)}{3\left(\Delta y_{i,N}\right)}\end{array}\right\} \tag{11}$$

Eqs (9)-(11) are substituted in the eq. (5) to get the final algebraic form of the equations for each CV. Implicitly discretized equation for delayed neutron precursor density is

$$C_{d,i,j}^{n+1} = \frac{1}{\left(1+\Delta t.\lambda_{d,i,j}^{n+1}\right)}.C_{d,i,j}^{n} + \frac{\Delta t.\beta_{d,i,j}^{n+1}}{\left(1+\Delta t.\lambda_{d,i,j}^{n+1}\right)}.\sum_{g'=1}^{G}\frac{\nu\Sigma_{f,g',i,j}^{n+1}}{k_{eff}}.\Phi_{g',i,j}^{n+1} \quad (12)$$

3. Results

3.1 2D TWIGL benchmark problem

This problem represents a two dimensional neutron kinetic model of square unreflected seed-blanket reactor core (Figure 2) with two neutron energy groups and one delayed neutron precursor family [4]. The code predicted k_{eff} value approaches the reference [4] value 0.913214 as the mesh number of increases as shown in Table 1. The temporal variations of the core relative powers for ramp and step perturbation cases are shown in Figures 3 and 4 respectively. The code predicted power results are in good agreement with the reference values.

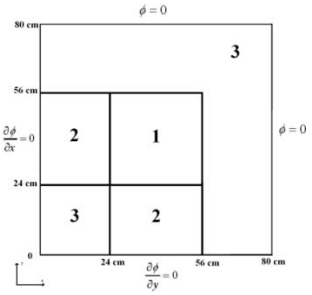


Figure 2 Geometry of 2D TWIGL benchmark problem

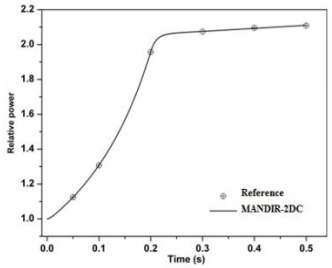


Figure 3 Core relative powers during ramp perturbation transient

Table 1 k_{eff} values for the 2D TWIGL benchmark

S.No.	Number of meshes	k_{eff}
1	80 x 80	0.9131005
2	160 x 160	0.9131761
3	320 x 320	0.9132008

*Reference [4] k_{eff} value: 0.913214

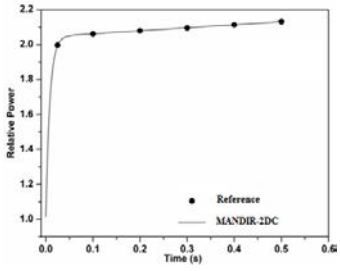


Figure 4 Core relative powers during step perturbation transient

3.2 2D LRA BWR transient benchmark problem

The 2D LRA BWR benchmark problem is a simplified boiling water reactor neutron kinetics problem with two neutron energy groups and two delayed neutron precursor families [5]. The values of k_{eff} calculated approaches the reference value 0.996368 as the mesh number increases as shown in Table 2. A super-prompt critical transient is induced to the initial steady state by a rapid withdrawal a control rod represented by a region P shown in Figure 5. A simple thermal feedback is introduced using an adiabatic heat up model with a space dependent Doppler feedback. The progression of the

core average power density and the average fuel temperature with time are shown in Figures 6 and 7 respectively. The code predictions for power and temperature are in line with reference results with almost same magnitude and trends except some small time delay. The results are in good agreement with the reference results.

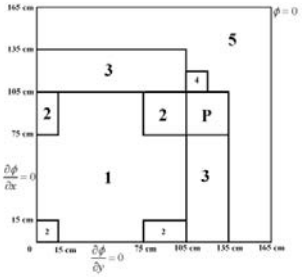


Figure 5 Geometry of 2D LRA BWR benchmark problem

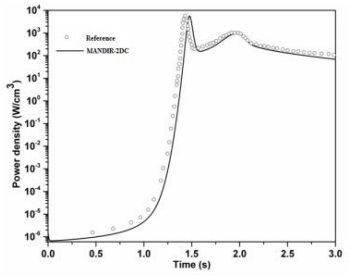


Figure 6 Temporal variation of core average power density

Table 2 k_{eff} values for the 2D LRA BWR benchmark

S.No.	Number of meshes	k_{eff}
1	33 x 33	0.996452
2	66 x 66	0.996207
3	165 x 165	0.996325

*Reference [5] k_{eff} value: 0.996368

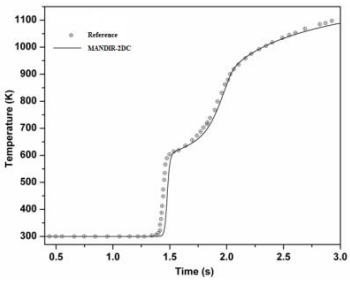


Figure 7 Temporal variation of core average fuel temperature

4. Conclusion

A computer code named MANDIR-2DC has been developed for solving nuclear reactor space-time kinetics problems in 2D Cartesian geometry. The code has been validated using the 2D TWIGL and 2D LRA BWR transient benchmark problem results. The present model will be upgraded to 3D and will be used for the analysis of criticality and space-time reactor kinetics problems of FBR during different phases of core disruptive accident.

5. References

[1] J.B Yasinsky and A.F.Henery, Some numerical experiments concerning space–time reactor kinetics behavior. *Nucl. Sci. Eng*. 22, 1965, 171–181.

[2] J.J. Duderstadt and L.J. Hamilton, "Nuclear Reactor Analysis", *John Wiley and Sons,* 1976**.**

[3] S. Mazumdar, "Numerical Methods for Partial Differential Equations Finite Difference and Finite Volume Methods", *Elsevier,* 2016**.**

[4] L.A. Hageman and J.B. Yasinsky, Comparison of alternating-direction time-differencing methods with other implicit methods for the solution of the neutron group-diffusion equations. *Nucl. Sci. Eng.* 38, , 1969, 8–32.

[5] ANL-7416, Supplement 2, "Argonne Code Center: Benchmark Problem Book, Benchmark Problem", *Argonne National Laboratory,* 1977.

DEVELOPMENT OF A CORE MODEL FOR REAL TIME FLUX DISTRIBUTION MONITORING IN PWR

Mihir Naskar[1], Gopal Mapdar[2], S. K. Sen[1], Anurag Gupta[2], Umashankari Kannan[2]

[1]Reactor Control Division
[2]Reactor Physics Development Division

Bhabha Atomic Research Centre
Trombay, Mumbai - 400085, India

e-mail: mnaskar@barc.gov.in

Abstract

A comprehensive core model based on steady state two group diffusion theory is developed for a PWR. Finite difference approximation in three dimensions is used to solve the model with square lattice configuration. A code in 'C' programing language is developed to implement this model with emphasis on real time application. To validate the code, IAEA 3D PWR benchmark problem and Indian PWR core are considered. The modelling approach and a comparative study of computational results are presented in the paper.

1. Introduction

Commercial power reactors are equipped with in–core neutron detectors for flux measurements at different locations inside reactor core. These measurements along with suitable software routines are used for estimation of 3*D* flux distribution or flux map inside the reactor core in real time at required intervals. Most power reactors employ In-core Instrumentation System (ICIS) for different core calculations for safe operation of the reactors as well as monitoring the shape of core flux distribution. A suitable core model with reasonable computational accuracy with faster speed of computation is highly recommended for use in real time core monitoring system.

In this work, approach has been made to develop a comprehensive reactor model based on steady state two group diffusion theory to be used in a real-time system. Finite difference approximation in three dimensions is used to model a generic reactor core, such as a PWR core, with square lattice configuration. A 'C' code is developed to implement this model with emphasis on real time application. To validate the model, IAEA 3D PWR benchmark problem is solved and results are compared. Also, IPWR core calculations using a square geometry configuration are carried out using this model. A comparative study on performance of the code is presented in this paper.

2. Diffusion Theory Model of Reactor Core

A suitable mathematical model that represents the reactor core with reasonable accuracy with a speed of real time computation is required for development of ICIS. The real-time core scenario can be estimated by using this core model along with a set of in-core self-powered neutron detectors (SPND) readings. Diffusion theory approximation for reactor core with a set of in-core detector equations can be utilized for real-time flux distribution calculations.

Though the neutron flux inside a reactor is spread over a wide range of energy spectrum, a two-energy group approximation provides a fairly accurate model for core computations. The neutron flux density can be approximated using two group diffusion equations, where the energy groups can be expressed as fast group and a thermal group. The steady state form of the equations is given in the following [1].

$$D_1\nabla^2\phi_1 - \sum_{a1}\phi_1 - \sum_{12}\phi_1 + \sum_{21}\phi_2 + \left(\frac{1}{k}\right)\nu\left(\sum_{f1}\phi_1 + \sum_{f2}\phi_2\right) = 0; \quad (1)$$

$$D_2\nabla^2\phi_2 - \sum_{a2}\phi_2 + \sum_{12}\phi_1 - \sum_{21}\phi_2 = 0; \quad (2)$$

where ϕ_1 and ϕ_2 denote the fast and thermal group neutron fluxes, D_1 and D_2 represents the diffusion coefficients, $\sum_{a1}$ and $\sum_{a2}$ are the neutron absorption cross– sections and $\sum_{f1}$ and $\sum_{f2}$ represent the fission cross–sections for fast and thermal groups respectively. $\sum_{12}$ and $\sum_{21}$ denote scattering cross–sections between fast and thermal group. ν represents average number of the neutrons produced in a fission event and k is the effective multiplication factor.
These equations represent a set of partial differential equations and can be solved by using finite difference methods by discretizing the spatial variables in the equations. Using matrix notations, the above equations can also be written as:

$$M_{11}\Phi_1 = \left(\frac{1}{k}\right)(F_{11}\Phi_1 + F_{12}\Phi_2); \quad (3)$$

$$M_{22}\Phi_2 = F_{21}\Phi_1; \quad (4)$$

where, Φ_1 and Φ_2 are column vectors of respectively the fast and thermal fluxes in the finite difference meshes. The elements of the matrices M_{11} and M_{22} are composed of leakage and absorbtion terms of the corresponding energy groups, i.e, fast and thermal neutrons. F_{11} represents the fission terms for the fast group, F_{12} represents the production of fast neutron due to up–scattering and F_{21} represents the terms corresponding to the down–scattering.
The equations for fast group and thermal group can be assembled into square matrices with dimension '$N \times N$'. Each of this square matrix is highly sparse with only seven diagonals for 3D approximation. Matrix for each group is symmetric and positive definite. Thus, the two group diffusion equations in eq. (3) and eq. (4) can be reduced into standard minimization problem and can be solved using iterative methods, such as pre-conditioned conjugate gradient method [2], etc. In the present work, pre-conditioned conjugate gradient method with ILU (0) preconditioner is used for solving the matrix equations.

3. Testing and Validation

A 'C' code based on finite difference approximation of two group diffusion equations is developed in Reactor Control Division (RCnD), BARC, for simulation of IAEA 3D benchmark. The code uses a square lattice configuration for the finite difference grid of the reactor core with zero flux boundary condition. Steady state form of the diffusion equation is used for obtaining the two group flux distribution. The output of the code is compared with the benchmark results for estimation of error characteristics and validation.
This code is also used for simulation of Indian PWR. The hexagonal mesh in IPWR is replaced with equivalent square mesh with same mesh volume. Steady state solution of diffusion equation is obtained with the equilibrium core of IPWR. The results are compared with HEX3D code developed by RPDD, BARC with satisfactory accuracy. In the following detailed description of the simulation is presented.

3.1 IAEA 3D PWR Benchmark

The International Atomic Energy Agency (IAEA) has published a typical three-dimensional PWR benchmark problem which is widely used in verification of neutron diffusion calculation codes. This PWR is taken as a benchmark for validation of the present code. There are 177 Fuel Assemblies (FAs) arranged in the reactor core, and 13 groups of these FAs are having inserted control rods. There are 9 fully rodded fuel assemblies and 4 partially rodded fuel assemblies in the core, with 15 fuel assemblies across the core major axis.

The partially controlled region covers top 80 cm of the active core height. The core contains 64 reflector assemblies surrounding it. The fuel assembly pitch is 20 cm, the active height of the fuel

assembly is 340 cm and there is a 20 cm axial reflector region at the bottom and top of the core. The core arrangement is symmetric.

Distribution of fast flux and thermal flux is computed along with multiplication factor k_{eff}. Distribution of channel power is also computed using the code. Reference values for comparison are taken from NESTLE code [3], that used standard finite difference method (FDM). The error in computing channel power distribution is found to be within the range of 2 – 10% for different channels. The distribution of channel power is illustrated in fig. 1. The value of k_{eff} is given in Table-1. The error in calculating $\mathbf{k_{eff}}$ is found to be 0.5 mk.

Table 1: 3D PWR Multiplication factor

Multiplication Factor, k_{eff}	
NESTLE code (reference), 5 cms × 5 cms × 10 cms (mesh size)	**1.02864**
Computed, 10 cms × 10 cms × 20 cms (mesh size)	**1.02916**

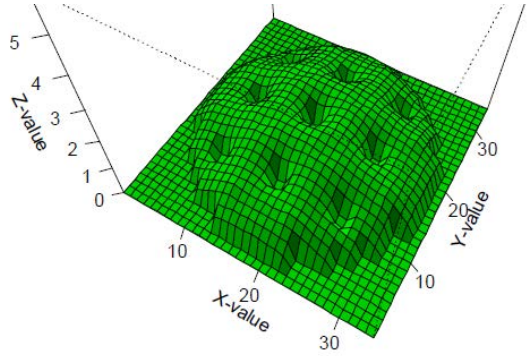


Figure 1: Channel Power Distribution of IAEA 3D PWR

3.2 The Indian PWR core

The Indian PWR core has 151 fuel assemblies arranged in a hexagonal pitch of 243 mm. The core is designed for a rated power of 2700 MWth (900 MWe) [4]. The hexagonal lattice of the core is converted into a square lattice for ease of implementation and simplicity. Also, square lattice is preferred for use in PHWR, AHWR type reactors. Further, for ease of computation, hexagonal geometry of Indian PWR core can be approximated with a square lattice with equal mesh volume. Each hexagonal fuel assembly can be considered as a square assembly having equal volume with similar neutronic properties. The equilibrium core of IPWR is shown in fig. 2. The equivalent core configuration with square lattice is shown in fig. 3. Each mesh has a dimension of 11.2 cms × 11.2 cms × 20 cms. For discretization of 2 group diffusion equation, the IPWR core can be further subdivide into finer grid as shown in fig. 3. Here, each fuel assembly is subdivided into four meshes. Total area of these four meshes is equal to the area of the corresponding hexagonal mesh. With this approximation, finite difference technique can be applied to solve the diffusion equation for IPWR core.

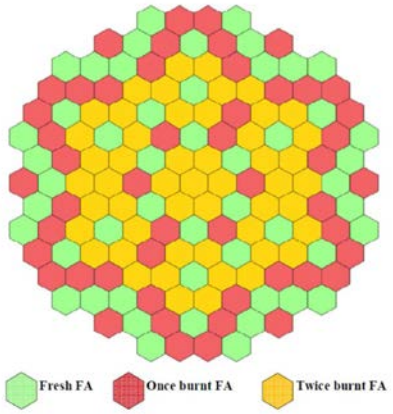


Figure 2: Indian PWR Core

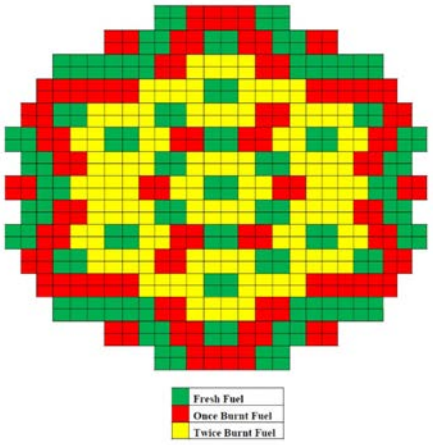


Figure 3: Indian PWR Core Configuration with Four Square Mesh per Fuel Assembly

Computations were carried out using the "C' code developed in RCnD, BARC. Distribution of fast flux and thermal flux are computed along with multiplication factor k_{eff}. Power in each fuel assembly is also computed using the code. Reference values of all the quantities are taken from HEX3D code from RPDD, BARC. The value of k_{eff} is given in Table-2. The error in square lattice modelling is 4.37 mk. The distribution of fuel assembly power is illustrated in fig. 4. All fuel assembly powers are normalized to 1.0.

Table 2: IPWR Multiplication factor

Multiplication Factor, k_{eff}	
Hexagonal Lattice Modelling	**1.08160**
Equivalent Square Lattice Modelling	**1.07723**

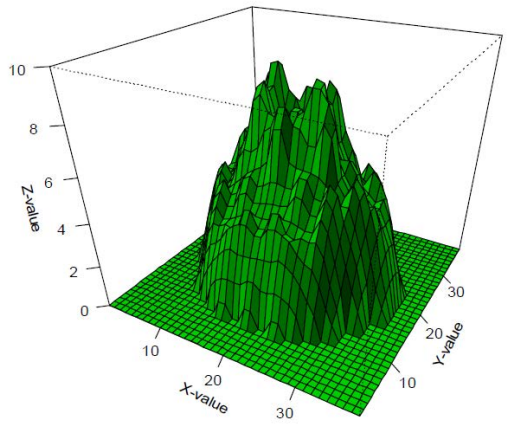


Figure 4: Distribution Fuel Assembly Power for Indian PWR

4. Conclusion

A comprehensive code has been developed for calculation of core power distribution in a PWR. The code uses a reactor model with square lattice and solved using finite difference method. IAEA 3D PWR and Indian PWR, are simulated using the code. Since the Indian PWR has a hexagonal geometry, each of its hexagonal mesh is modelled with equivalent square for use in the code. Results are compared with reference solutions and found to be satisfactory.

5. Reference

[1] Mihir Naskar, A. P. Tiwari, S. V. G. Menon and Vinod Kumar, "Finite Difference Approximation for Computation of Neutron Flux Distribution in a Large PHWR", International Conference on Quality, Reliability and Control (ICQRC) 2001, Mumbai, India.

[2] Yousef Saad, "Iterative Methods for Sparse Linear Systems". PWS Publishing Company.

[3] "Static Benchmarking of the NESTLE Advanced Nodal Code". Russell D. Mosteller, Los Alamos National Laboratory.

[4] Conceptual Design Report of Indian Pressurized Water Reactor (IPWR), BARC/IPWR/RPG/09/2013, Sept-2013, Rev.0.

Acknowledgements

The authors wish to express their gratitude to Shri U. W. Vaidya, Head, RCnD, BARC for encouragement and support during the course of the work.

Development of MLIB - A 'Plug n Play' Module for Processing of WIMS-D Nuclear Data Library for Reactor Physics Simulations

Amod Kishore Mallick[1,2], Lakshay Jain[2], Umasankari Kannan[1,2] and R. Karthikeyan[1]
[1] Bhabha Atomic Research Centre, Mumbai, India
[2] Homi Bhabha National Institute, Mumbai, India
[1]*e-mail: - amod@barc.gov.in*

Abstract

WIMS-D libraries are very popular and are widely used in reactor physics simulations. A number of new lattice transport codes are being developed using new methods of calculations. A code developer who aspires to use these libraries needs to write his or her own library reading and processing modules. The lack of single authentic and complete reference which gives exact details of the structure and processing of this library for its use in neutron transport codes makes this task very time consuming, if not difficult. In this regard, we have developed a stand-alone, independent, and complete module, named MLIB, for the library processing. The module can be plugged very easily in any multi-group neutron transport code to do the library processing job. MLIB has been tested against benchmark problems and practical lattices, and has so far been incorporated in two lattice transport codes being developed, namely PebMC and NuTRAC.

1. Introduction

Updated WIMS-D multi-group nuclear data libraries from IAEA WLUP [1] project are very popular and are being used widely in various reactor physics codes for lattice cell simulation. A code developer who aspires to use these libraries need to write his or her own library reading and processing modules to make its use in the code. There is, however, a lack of single authentic and complete reference which gives exact details of structure of this library and its processing for its use in neutron transport codes. The details about these are found in bits and pieces, and are scattered in literature. Because of this, the task of using WIMS-D library in a code becomes time consuming, if not difficult.

In view of this, we have developed an independent, stand-alone, 'plug-n-play' module, named MLIB (Multi-group LIBrary processor) [2], which takes care of reading and processing of the library and gives out final cross-section data sets required for neutron transport simulation. The algorithms and methodologies used in this module for library processing have been tested successfully against benchmark problems and practical lattices. With this, the module is now ready to be plugged in a transport code for the library processing job. This will be especially useful for new transport codes under development as the developer can now focus on its core job of programming neutron transport phenomena. Production level transport codes already in use for practical simulations can also make use of this as an optional method for library processing. This paper discusses about the module MLIB, its internal structure, how it works, its basic features, benchmarking, how to use in a transport code and future scope of development.

2. Structure of MLIB and How to use it in transport code

MLIB is basically a package for library processing. A host transport code makes use of this package by calling some of its routines with proper inputs. Inputs include material description and name of WIMS nuclear data library file for processing cross section data. The description contains material

composition and its temperature for different materials contained in lattice. Nuclides present in the materials are identified by their WIMS-IDs. In case of resonant fuel materials, additional information like Dancoff factor, Bell factor and Escape cross section of the region containing this material are also required as input. Carlvik's routine to compute Dancoff factor for Pin Cell is contained in the MLIB and can be used by the host code.

When invoked from the host code with proper input arguments, MLIB reads the WIMS library to fetch nuclear data for the required nuclides and does resonance self-shielding treatment, suitable interpolation over temperature, etc. This resonance treatment is based on the equivalence principle using one term rational approximation. For materials containing multiple resonant nuclides, a recipe for interference correction is also used to take into account the effect of resonance absorption of one nuclide on other to obtained interference corrected resonance cross sections. The final multi-group cross-section data set (total/transport, capture, fission, full scattering matrix, fission spectrum, etc.) required for transport simulations are given in the output arguments. Additionally, final cross section data is also saved in a text file (default file name - 'mlibxs.txt').

MLIB consists of 10 files containing a total of 10 modules with each module dedicated for a unique purpose. The modules define data structures, parameters, variables, and various routines used for library processing. Module 'mlib' contained in the 'mlib.F90' file is the controlling module which uses all other modules to read and process WIMS library and gives back the final cross section data set. MLIB has numerous functions and subroutines but only five of them are public and using these five routines whole work of library processing is carried out. The names of these routines are listed below in Table-1. The arguments of these routines can be found in reference [2].

Table-1: Routines in MLIB used for library processing

S.N.	Routine
1	init_mlib
2	get_danc_xs
3	get_pin_cell_dancoff
4	get_xs
5	finalize_mlib

The host program calls 'init_mlib' when using the MLIB before calling other routines and it ends with 'finalize_mlib'. The processed cross-section data are obtained by calling 'get_xs' routine required for neutron transport simulation. Routines 'get_danc_xs' and 'get_pin_cell_dancoff' are called to compute Dancoff factor required for resonance treatment.

MLIB package can easily be used in a transport code by following these steps:

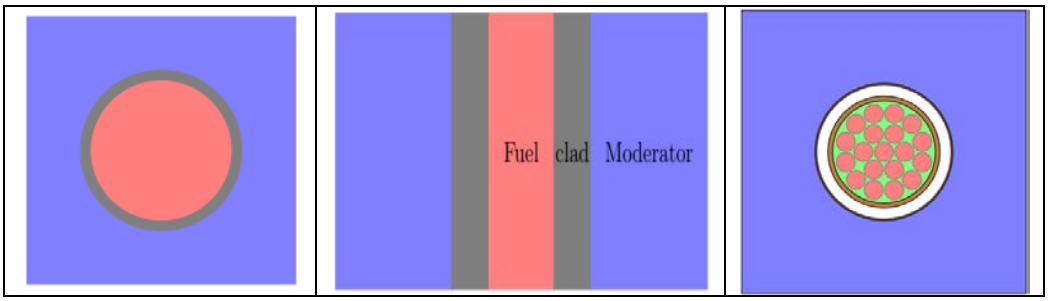
i. Include all the 10 source files of the MLIB module with the source files of transport code (called host) during program compilation.
ii. Make use of the 'use mlib' statement at the beginning of host program where the routines of MLIB would be called.
iii. Define the following variables as allocatable arrays in the host program which contains the 'use mlib' statement. The data structure of these variables can be found in reference [2].

```
type(material info), allocatable, dimension(:) :: mat_data
type(xs), allocatable, dimension(:) :: mat_xs
```

iv. Allocate these arrays to a suitable size depending on the number of distinct materials used in the problem to be simulated.
v. Define various materials in the 'mat_data' variable by giving its constituents, temperature and other values. Remember that for resonant materials (like fuel materials), the 'mat_data' also requires entry for Dancoff factor, Bell factor, and escape cross section.
vi. Start library processing by calling 'init_mlib'.
vii. Call the 'get_danc_xs' routine to compute the potential scattering cross-section of each material required for Dancoff calculation for each fuel pin type
viii. Get the Dancoff factor for each fuel region using this cross section. This is required to be done by the host transport code. Alternatively, MLIB supports computation of Dancoff factor for square and hexagonal pin cell. It can be done by calling 'get_pin_cell_dancoff'.
ix. Update 'mat_data' for each fuel pin after computing the Dancoff factors. Corresponding Bell factor and escape cross section also should be input. The widely used values of Bell factor and escape cross-section for typical fuel pin types can be found in reference [2].
x. Call 'get_xs' routine to obtain processed cross-section data. The 'mat_xs' argument returns this processed cross-section data. It contains the macroscopic cross-section of each material for all reaction types. As an example 'mat_xs(1) % sum % sigma_abs(:)' gives the array of macroscopic absorption cross section of material 1 in all energy groups.
xi. Store the processed cross section saved in 'mat_xs' in appropriate internal data structure of the host transport code for further transport calculations.
xii. End library processing by calling 'finalize_mlib'.
xiii. Deallocate 'mat_data' and 'mat_xs'.

3. Testing MLIB

To test the working of MLIB and its accuracy in library processing, we have simulated many lattice cells. We have used MLIB generated cross section data in DIAMOND [3], a deterministic neutron transport code under development, for the simulations and compared the results with reference values obtained from other codes such as WIMSD-4, DRAGON, and Monte Carlo code PATMOC [4] using the same library (WIMSD format 69-group ENDF-B/VII.1 library). The results of few such simulations are presented here. This includes the Rowland's Pin-cell benchmark [5] which is a square pin cell with light water coolant with 4 different cases corresponding to different temperature and density of materials. APSARA-U Pin-cell is a slab type pin cell geometry and corresponds to the unit cell of recently commissioned APSARA-U reactor. PHWR lattice corresponds to the lattice cell of 220 MW PHWR lattice cell containing 19-pin cluster. Figure 1 gives the geometry of these lattice cells and Tables 2, 3, and 4 lists the results using MLIB and its comparison with the reference values.



(a) Rowland pin cell	(b) APSARA slab pin cell	(c) PHWR lattice cell
Fig.-1: Different kinds of lattice cells simulated to test MLIB		

Table-2: Results for Rowland pin cell benchmark problems			
Case	DIAMOND with MLIB	Reference	
		WIMSD-5A (Trkov)	PATMOC
1	1.38400	1.38411	1.38425 ± 0.00014
2	1.33286	1.33166	1.33294 ± 0.00015
3	1.29953	1.29828	1.30013 ± 0.00015
4	1.31492	1.31362	1.31495 ± 0.00015

Table-3: Results for APSARA-U Slab Pin Cell		
DIAMOND with MLIB	Reference	
	WIMSD-4	PATMOC
1.657393	1.65699	1.65779 ± 0.00015

Table-4: Results for PHWR lattice			
DIAMOND with MLIB	Reference		
	DRAGON	WIMSD-4	PATMOC
1.11826	1.11783	1.11583	1.11896 ± 0.00011

4. Conclusion

We have developed an independent, stand-alone library processing package, named MLIB, for use in neutron transport codes. MLIB supports both 69- and 172-group library processing and has been tested on various lattice cell problems. It has been incorporated in two lattice transport codes, and currently is in the process of being plugged in one more code. Being a ‘plug-n-play’ kind, MLIB can be helpful to new neutron transport code developers who can use this for library processing in their code so that they can focus on their major task of high fidelity modelling of neutron transport phenomena.

5. References

[1] Leszczynski, F., Aldama, D.L., Trkov, A., 2007. WIMS-D library update. Technical report, International Atomic Energy Agency.

[2] Amod Kishore Mallick, Lakshay Jain, Umasankari Kannan and Ramamoorthy Karthikeyan, “MLIB (Multigroup LIBrary processor): A ‘Plug n Play’ Module for Processing of WIMS-D Nuclear Data Library for Reactor Physics Simulations’’, RPDD/EP/160 (2018).

[3] Lakshay Jain, R. Ramamoorthy and U. Kannan, “DIAMOND – A Method of Characteristics neutron transport code using unstructured meshing”, ANE, 137 (2020) 107086

[4] Amod Kishore Mallick and Anurag Gupta, “Sub-Space Iteration Based Monte Carlo Scheme for Simultaneous Computation of Multiple Dominant k-eigenmodes and Acceleration of Fission Source Iterations”, Annals of Nuclear Energy, 166 (2022) 108783

[5] J. L. Rowlands et. al., LWR Pin Cell Benchmark ", JEFF Report-15 (1999)

Production of Ru-105 and Rh-105 through proton induced reaction on natural Uranium

Najumunnisa T[1], M. M. Musthafa,[2] C. V. Midhun[3], Alok Saxena[4] P. Surendran[5], J. P. Nair[6] and Anil Shanbhag[7]

[1] AKNM Government Polytechnic College, Tirurangadi, Kerala, India

[2,3] Department of Physics, University of Calicut, Kerala, India

[4]Nuclear Physics Division, BARC, Mumbai, India

[5,6,7]BARC-TIFR Pelletron Group, BARC, Mumbai, India

[1]*e-mail: - tnajumunnisa@gmail.com*

Abstract

The cross-section for the formation of Ru-105 and Rh-105 are measured through the proton induced reaction on natural Uranium for three proton energies 12.12 MeV, 17.24 MeV and 21.44 MeV. The theoretical formulation has been performed using the code TALYS 1.95.

1. Introduction

Nuclear data are required as a function of energy for the structural integrity of nuclear reactors. In the Gen IV reactors and fusion reactors, a strong secondary proton spectrum is formed as a result of neutron impact on fuel, fragments as well as the structural components [1,2]. This proton spectrum energy ranges upto 20 MeV [3]. These secondary protons can also induce fission on U-238, and a different mass distribution of fission fragments will be formed. These newly formed fragments also be responsible for altering the neutron flux. Again the neutrons so produced will interact with fission fragments and the structural materials. Hence it is necessary to analyze the fission product formed in proton induced fission of U-238 over energy interval of 0 – 20 MeV. In this perspective we have experimentally measured the cross-section for the time dependent formation of the fission fragments Ru-105 and Rh-105 after the proton irradiation on U-238. Production of such isotopes will affect the structural stability and core criticality of a reactor as it initiates secondary reactions from primary neutrons and charged particles [4]. Further, Rh-105 is a medically important isotope.

2. Experimental Analysis

The experiment has been carried out at Tata Institute of Fundamental Research (TIFR), Mumbai, India. Stacked foil activation technique has been employed. The natural Uranium samples of thickness 8.6 mg/cm^2 were prepared by the rolling method in the size of 1cm x 1cm. A stack of three Uranium samples with energy degraders were irradiated using a proton beam of 22 MeV energy and 23 nA average current for 88 minutes. The energy degradation was calculated using the simulation code SRIM [5]. The mean energies falling on each sample accounting for the mean energy loss over the samples and are considered as the incident energies. Mean incident energies on the three uranium samples are 21.44 MeV, 17.24 MeV and 12.12 MeV respectively. The beam current was monitored continuously by current integrator connected to the Faraday cup kept behind the target stack. The activity induced in this samples were followed using 100cc HPGe detector with a low background setup, coupled to the PC based multichannel analyzer.

The irradiated samples are kept for some times for cooling due to strong activity and after some hours, each samples are taken one by one for counting. Thus obtained spectrum shows the peaks corresponding to the characteristic gamma rays of Ru-105 viz. 724.3 keV (47.3 %), 469.37 keV (17.5

%) and 676.36 keV (15.7 %). Since the half life of Ru-105 is 4.44 h and is 100% β- emitter, producing Rh-105. So in order to get high population of Rh-105, we have waited for one day and the counting is repeated again. The second counting of each samples are carried out separately and the characteristic gamma rays of Rh-105 viz. 318.9 keV (19.1 %) and 306.1 keV (5.1 %) are identified clearly. The characteristic gamma rays of Rh-105 were very feeble in the first counted spectrum and are well evolved in the second counting. This shows that the Rh-105 are not formed directly during irradiation and is formed by the decay of Ru-105.

From the observed intensities of characteristic gamma rays, the cross-sections for the formation of fission product Ru-105 was calculated using eqn. (1) [6], as if the entire Ru-105 is produced during the irradiation itself. This is justified as the precursors of Ru-105 *viz.* Nb-105, Mo-105 and Tc-105 are extremely short lived, decaying completely to Ru-105 as shown in Fig. 1. In the case of Rh-105, the cross-section is calculated by accounting the decay of Ru-105 and generation of Rh-105 using the eqn. (2) [7]. Measurements were done for incident proton energies 12.12 MeV, 17.24 MeV and 21.44 MeV, and are plotted in Fig. 2. as a function of incident proton energy. The expression for the production cross-section of a particular isotope from the observed intensities of characteristic gamma rays is given below

$$\sigma = \frac{A\lambda \exp(\lambda t_2)}{(N_0 \phi G_E \theta k (1-\exp(-\lambda t_1))(1-\exp(-\lambda t_3)))} \quad (1)$$

where A represents the total number of activities counted under the corresponding gamma peak, λ is the decay constant of the particular residual nucleus, φ is the incident proton flux, N_0 is the number of the target nuclear isotope per unit area of the irradiated sample, G_E is the geometry dependent efficiency of the detector for the given gamma ray energy, θ is branching ratio of the particular gamma ray, K is the self-absorption correction factor for the gamma ray in the sample and t_1 , t_2 , t_3 are respectively the irradiation time, the cooling time and the counting time of the sample. The activity of Rh-105 is calculated is calculated using the equation given below

$$A_d(t) = A_p(t)\frac{\lambda_d}{(\lambda_d - \lambda_p)}(1-\exp(-(\lambda_d - \lambda_p)t)) \quad (2)$$

where $A_d(t)$ is the activity of the daughter nucleus and $A_p(t)$ is the activity of the parent nucleus at time t and λ_d and λ_p are the decay constants of daughter and the parent.

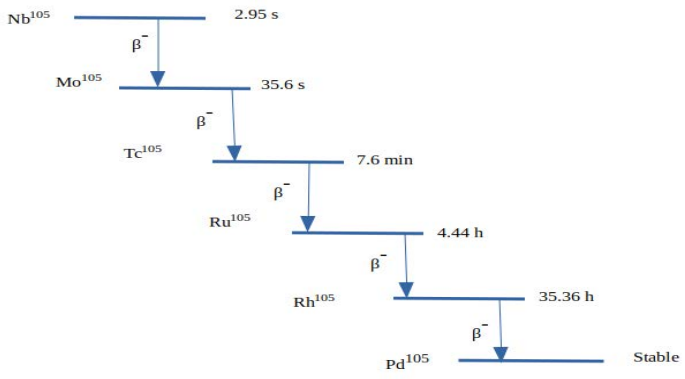


Fig.1. Fig. 2. Decay chain of Nb-105

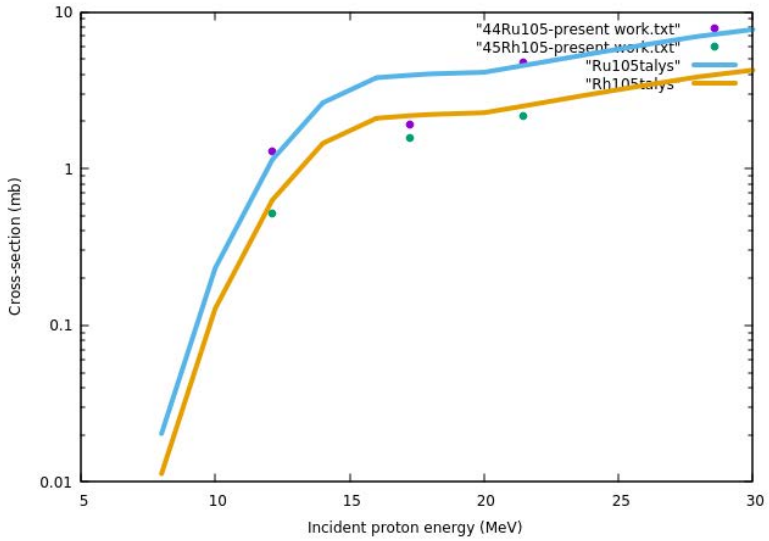


Fig. 2. Excitation function for the formation of Ru-105 and Rh-105

3. Theoretical Analysis

The theoretical analysis has been done using nuclear reaction code TALYS 1.95 [8]. In Talys, the fission fragment calculation has been done using GEF model [9] and Temperature-dependent Brosa model [10]. The fission fragment mass distribution is determined with a revised version of the multi-modal random neck-rupture model (MM-RNRM) [11]. Calculations of proton induced fission of U-238 in TALYS 1.95 predict the formation of the fission fragments Nb-105, Mo-105 and Tc-105 and does not predict the formation of Ru-105 or Rh-105. Thus the cross-section fo the formation of these nuclei are calculated from the fission product yield of their precursors Nb-105 → Mo-105→ Tc-105→Ru-105→Rh-105. The results of the TALYS calculation are also plotted in Fig. 2. From this figure, it can be seen that TALYS 1.95 code reproduces the measured cross-section data over the measured energy ranges on accounting the non- equilibrium of the precursors. This indicates that the produced nuclei Ru-105 and Rh-105 are coming after successive beta decays of Nb-105, Mo-105 and Tc-105 and not through direct formation.

4. Conclusion

The time dependent production of Ru-105 and Rh-105 from proton induced fission of natural Uranium was measured for incident proton energies 12.12 MeV, 17.24 MeV and 21.44 MeV. Production of such delayed isotopes are important in structural analysis as well as criticality of the reactor calculations.

5. References

[1] Report summary of European facility for innovative reactor and transmutation neutron data, project report on 2013, Belgium, id:211499, https://cordis.europa.eu/project/rcn/ 88553/ reporting/en.

[2] ITER Physics Basis Editors, ITER Physics Expert Group Chairs and Co-chairs and ITER Joint Central Team and Physics Integration Unit, Nucl. Fusion, 39, 2137 (1999).

[3] Jyoti Pandey, *et al*, "Determination of 59 Ni(n, x p) reaction cross sections using surrogate reactions", PHYSICAL REVIEW C 99, 014611 (2019).

[4] S. Ganeshan, P RAMANA journal of physics, Vol. 68, No. 2, February 2007, pp. 257–268

[15] J. F. Ziegler, The Stopping and Range of Ions in Matter, vol. 2–6 (Pergamon Press) (1977–1985)

[6] M.M. Musthafa, Manoj Kumar Sharma, B.P. Singh, R. Prasad, Appl. Radiat. Isot. 62 (3) (2005) 419–428.

[7] Levin, Craig (2004). *Emission Tomography Volume 816 || Basic Physics of Radionuclide Imaging. , (2004), 53–88.*

[8] A.J. Koning, S. Hilaire and M.C. Duijvestijn, "TALYS-1.0", Proceedings of the International Conference on Nuclear Data for Science and Technology, April 22-27, 2007, Nice, France, editors O.Bersillon, F.Gunsing, E.Bauge, R.Jacqmin, and S.Leray, EDP Sciences, 2008, p. 211-214.

[9] K.-H. Schmidt and B. Jurado, Phys. Rev. C 82 (2011) 014607.

[10] M.C. Duijvestijn, A.J. Koning, and F.-J. Hambsch, Phys. Rev. C 64, 014607 (2001).

[11] U. Brosa, S. Großmann and Müller, Phys. Rep. 197, 167 (1990).

Analysis of First approach to Criticality (FAC) and Phase-B experiments of KAPP-3 using VISWAM code

S.Koner[1], V. Jagannathan[2] and Obaidurrahman K.[1]
[1] Atomic Energy Regulatory Board, Mumbai, India
[2] Consultant, Atomic Energy Regulatory Board, Mumbai, India

[1]*e-mail: - skoner@aerb.gov.in*

Abstract

The ring cluster lattice geometry is incorporated in VISWAM code to analyse PHWR fuel clusters. The lattice and core physics analysis of KAPP-3 was performed with VISWAM code using the core design data of KAPP-3. In this paper, the results of analysis of First Approach to Criticality (FAC) and Phase-B experiments carried out in KAPP-3 are presented. The calculated k_{eff} values during the approach to first criticality were compared with design and observed values. Also, the calculated results of Phase-B low power physics commissioning experiments were compared with the design and observed values. The VISWAM calculated core physics characteristics matches well with the observed data during the experiments.

1. Introduction

VISWAM code has been employed for lattice and core physics analysis of 700 MWe PHWR at AERB for independent verification analysis. The code is structured in modular form for lattice and core calculation of different type of reactor cores with square, hexagonal or ring cluster geometry [1]. Lattice module of VISWAM considers a combination of 1-D multi-group transport and 2-D few group diffusion method for lattice burnup analysis. An advanced 2-D Collision Probability (CP) method based on interface current approach has also been developed for hexagonal and square lattice fuel assemblies. The ring cluster module based on 1-D supercell approach has been validated against the DRAGON and CLUB codes [2]. Core module of VISWAM is 3D core diffusion model, based on centre-mesh finite difference method. In the present exercise, VISWAM code system has been deployed for the analysis of FAC and phase-B experiments of KAPP-3.

2. Calculation Model

In the lattice model, each fuel ring is considered as one fuel pincell type. Since there is azimuthal symmetry, one burnup type is adequate in each fuel ring. After the four fuel-pincell calculations are done using HTEMPLIB cross section library in WIMS/D format in 172 groups by Pij method, the fuel pincell consisting of pellet, air gap, clad and coolant regions are homogenized to get the multigroup cross sections of the fuel paste rings. A cylindrical supercell calculation is performed with the four fuel paste rings surrounded by four concentric rings of pressure tube (PT), air gap, calandria tube (CT) and cylindricalized D_2O moderator regions. The supercell ring spectra are used to collapse the cross sections to few energy groups for performing diffusion calculation for the fuel cluster cell in (r,θ) geometry. Fuel cluster cell is homogenized using the few group flux distribution of diffusion simulation. For obtaining the perturbation of cross sections due to any type of reactivity device (RD) like AR, ZCC or SR, 3-D supercell model is used. RD region is simulated by internal boundary condition obtained through a 1-d transport simulation with the RD regions surrounded by a cylindricalized fuel paste region. A diffusion iterative technique (DIT) is an intermediate step to

obtain transport-diffusion correction factors for the strong absorbing fuel cluster and RD regions. The kinetics parameters β_{eff}, ℓ are obtained by perturbation theory expressions using direct and adjoint flux weighting. The depletion equations are solved in four fuel rings of the fuel cluster using fourth order Runge Kutta method.

The five group homogenised cross-section database is used for core calculation. The active core region is discretised with P x P x L/2 uniform meshes where P is fuel cluster pitch, L is fuel bundle length. Radial D_2O reflector is accounted with 3 pitches in main shell and one pitch in subshell. No axial reflector is considered. Extrapolation distance of 6.6 cm is used in all boundaries. The presence of RDs in various device configuration is processed by the code to prescribe the $\Delta\Sigma$ values for the meshes influenced by each RD and their overlapping, if any. The core analysis can be carried out as a function of burn-up and other reactor state variables like boron, temperatures of fuel and coolant, xenon and Samarium. Cold database is used for FAC and Phase-B experimental analysis.

3. Results and discussions

The lattice database was generated using the data of KAPP-3. As a part of validation of core physics models, analysis of FAC and the Phase-B low power physics experiments of KAPP-3 was carried out using VISWAM.

3.1 First Approach to Criticality

The first approach to criticality was simulated by VISWAM code using initial conditions of the core and k_{eff} was calculated for each step of criticality process for FAC. The calculated value of critical boron was 10.58 ppm using VISWAM code whereas the design calculation and observed results were 10.47 ppm and 10.2 ppm respectively. The FAC calculation was done considering AR bank#4 was kept 50% IN and other AR banks are kept fully out. The calculated k_{eff} for the observed critical boron was found to be 1.004 by VISWAM code.

3.2 Phase-B experiments simulation

The configurations of different Phase-B experiments such as calibration of ZCCs, Individual SR, CR calibration, Individual AR/AR banks calibration etc. were simulated using VISWAM code. For brevity selected results are presented. Fig.1 to Fig.8 present the results of Phase-B low power physics commissioning experiments by VISWAM code. The power during these experiments is 0.1% F.P. The initial state of each experiment is different with respect to soluble boron and reactivity device configuration. Initially, ZCCs were calibrated against boron. During the calibration of reactivity devices, the reactivity is compensated by ZCC level and when this level reaches extreme limits, the soluble boron is adjusted to bring the level back to working range.

Fig.1 gives the reactivity change during the calibration of ZCCs. It is observed that VISWAM code under predicts the reactivity change at the start of draining but predicts fairly well at middle levels and over predicts slightly at final drained level. Fig.2 gives the comparison of integral worth of individual SRs. The comparison of VISWAM calculated values with design and observed values is fairly good. Comparison of calculated S-curve for the worth of individual CR was carried out with the design and observed values. Fig.3a and Fig.3b show the comparison of the worth of individual CR rods (1, 4) at different insertion depths. The comparison of the S-curve shape is fairly good for the CRs. Fig.4 gives the comparison of the integral worth of individual ARs as obtained by VISWAM with design and observed values. The comparison is reasonably good. The worth of the long length ARs at locations (8,

9, 10) which are at core mid plane is the least due to proximity of Dep-U fuel. VISWAM values are under predicted for these ARs by about 10%.

Comparison of worth of different AR banks was carried out between VISWAM-calculated value and observed values. Fig.5a & Fig.5b show the comparison of the worth of AR banks# 4 and 8 respectively at different insertion depths. The comparison of AR banks worth is fairly good. The worth of the highest worth bank #4 is predicted as 1.93 mk by VISWAM code, which is closer to the observed value of 1.87mk. The worth of AR banks 7 and 8 are calculated by VISWAM code as 1.26mk and 1.29 mk which are close to the observed values of 1.31mk and 1.33mk. Fig.6 gives the comparison of the combined worth of the maximum worth AR banks (bank # 4 and 8) together as a function of insertion depths. The S-curve as well as the integral worth compares well with observed values with a slight underprediction by 4.6%. Fig.7 shows the comparison of the CR Bank#1 worth as a function of different insertion depths. VISWAM calculated values are lower than observed value by -11% at 10% OUT condition but is closer to the observed value in the end. Fig.8 gives the worth of the two CR banks together. The CR banks were withdrawn in steps of 10%. 0.4 ppm of boron was added at 20%, 30% and 60% positions of CR. VISWAM code simulated these conditions. Variation in ZCC AVZL was not considered. Reactivity change was cumulatively added. The integral worth calculated by VISWAM is close to design and observed values.

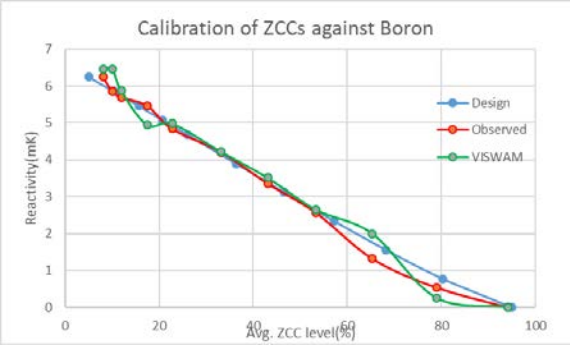


Fig. 1: Calibration of ZCC at KAPP-3

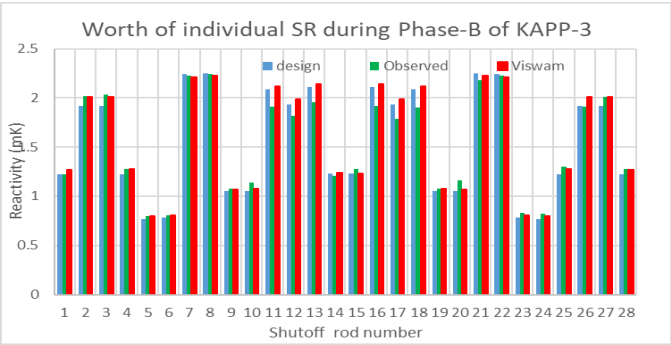


Fig. 2: Worth of individual SRs at KAPP-3

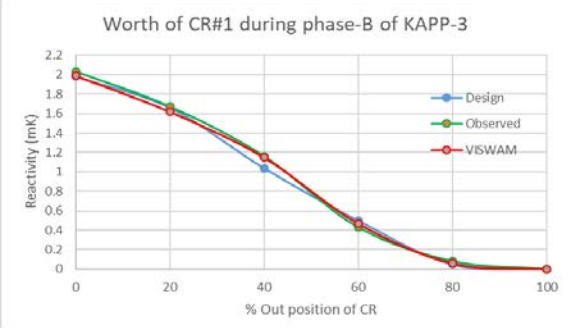


Fig. 3a: Worth of CR#1 at KAPP-3

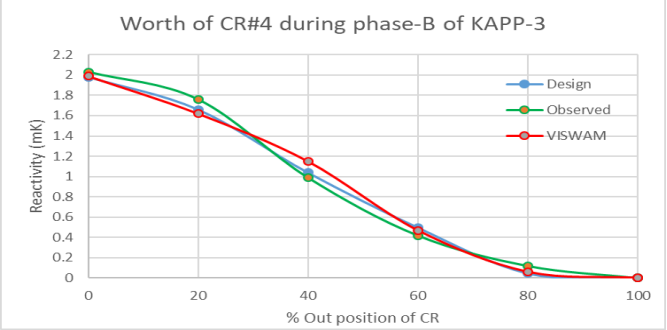


Fig. 3b: Worth of CR#4 at KAPP-3

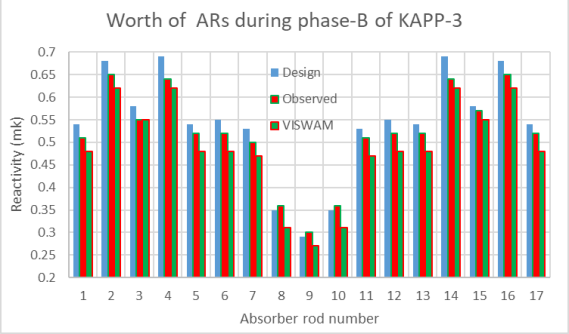


Fig. 4: Worth of ARs at KAPP-3

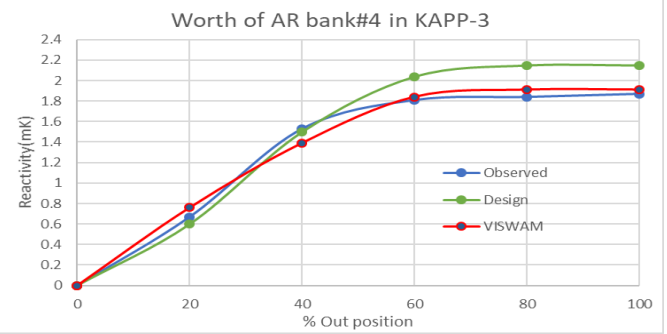


Fig. 5a: Worth of AR bank#4 at KAPP-3

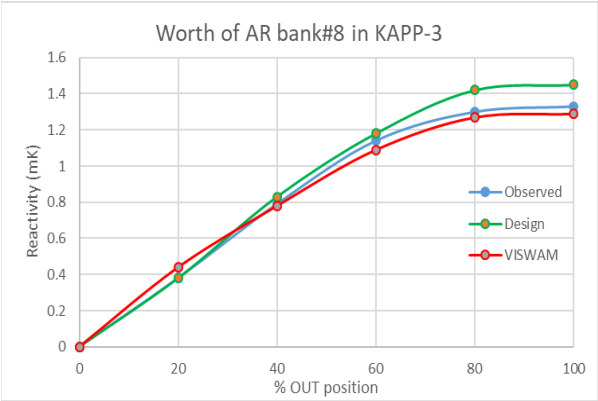


Fig. 5b: Worth of AR bank#8 at KAPP-3

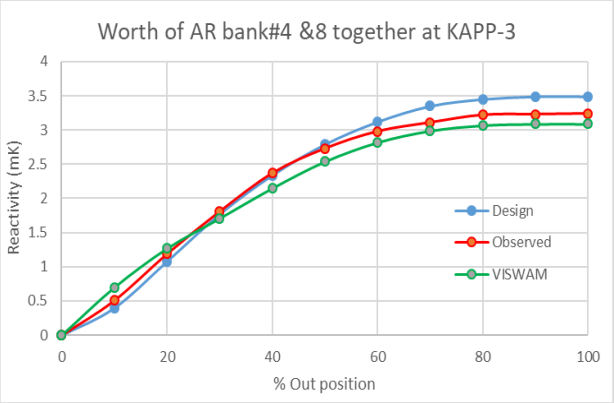


Fig. 6: Worth of AR bank 4 &8 together at KAPP-3

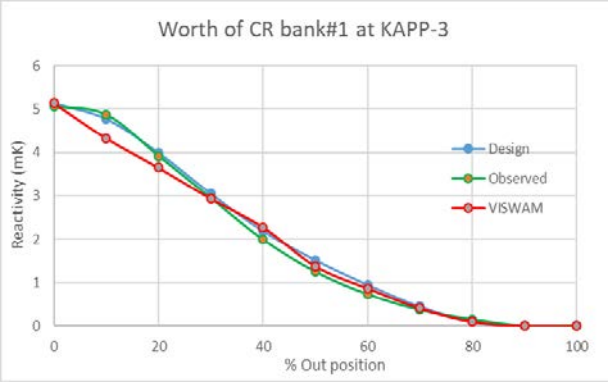


Fig. 7: Worth of CR bank#1 at KAPP-3

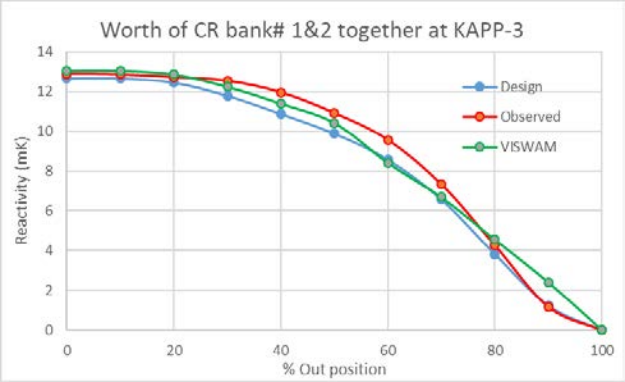


Fig. 8: Worth of CR banks # 1&2 together at KAPP-3

4. Conclusion

VISWAM code lattice and core diffusion model for analysing the 700 MWe PHWR core in cold state has been developed. The VISWAM code was used to analyse the first approach to criticality and some important Phase-B low power physics experimental scenarios. It is observed that VISWAM code predicts the critical boron within 0.38 ppm. The calculated Individual and integral worth of all RDs are matching well with design and the observed values.

The usage of VISWAM code for enabling the simulation of a variety of reactivity device configurations is rendered easy by auto-identification of meshes influenced by a cluster of RDs normally present in the PHWR core. It has been established as a useful tool for independent verification analysis of the physical characteristics of the PHWR core.

5. References

[1] V. Jagannathan, Suhail Ahmad Khan, and L. Thilagam, 'Incorporation of Ring Cluster Geometry in VISWAM Code System', Advances in Reactor Physics (ARP-2017), Mumbai, India, Dec. 06-09, 2017.

[2] V. Jagannathan, 'Thorium breeder reactors as a power source for 21st century and beyond, Int. J Energy Res. 2018; 42:117–133. wileyonlinelibrary.com/journal/er Copyright © 2017 John Wiley & Sons, Ltd. pp 117-133. DOI: 10.1002/er.3951.

NOISE EXPERIMENT IN BRAHMMA SUBCRITICAL SYSTEM USING ACCELERATOR BASED NEUTRON SOURCE

N K Ray[1*], T Patel[1], R Kumar[2], T Roy[1] and P S Sarkar[1]

[1]Technical Physics Division, Bhabha Atomic Research Centre, Mumbai 400085, India

[2]Reactor Physics Design Division, Bhabha Atomic Research Centre, Mumbai 400085, India

[*]*e-mail: - nirmal@barc.gov.in*

Abstract

Degweker and Rana [1] had postulated a noise theory based on exponentially correlated Gaussian source characteristics for subcritical system. First ever experimental validation of this noise theory for different beam pulse shape has been carried out using D-T neutron generator. During validation experiments, source characterization has been carried out to determine the distribution function, source correlation factor and D^+ beam pulse shape. It has been observed that the D-T neutron source follows Gaussian distribution function, source neutrons are correlated along with correlation factor is very large compared to the prompt neutron decay constant of subcritical system and the pulsed D^+ beam is rectangular in shape. In noise experiments, time stamped data has been analyzed using various noise methods. The measured prompt neutron decay constant is in good agreement with theoretical estimate ($2.310\pm0.058\,ms^{-1}$) using deterministic method [2].

1. Introduction

Accelerator Driven Subcritical system (ADS) can be used for incineration of long lived minor actinides along with thorium utilisation for power production. However, power produced in ADS is inversely proportional to subcriticality of the core and can be increased by reducing it. Therefore, the reactivity needs to be monitored for safety of ADS in addition to energy gain. Thus, it is essential to develop a suitable and robust reactivity measurement method for ADS.

Previous experimental research on noise based reactivity measurement in subcritical system using accelerator based neutron source had been carried out under assumption of Poisson source characteristics [3]. However, the inherent fluctuations in the beam current and accelerating voltage makes the accelerator based neutron source non-Poisson in nature. In this context, Degweker and Rana [1] had derived the noise descriptors for accelerator based neutron source under consideration of exponentially correlated Gaussian character. The Gaussian character refers to the fact that the neutron population follows Gaussian statistics rather than Poisson statistics and exponential correlation refers to the fact that neutrons are correlated exponentially from one pulse to the next. The decay time of the correlated neutrons is termed as source correlation factor.

Further, the proposed neutron source in future ADS will be accelerator based spallation source. In case of spallation neutron source, which is periodic and the cascade event will emit 20-30 neutrons per incident proton at 1GeV energy. These neutrons are also correlated because of the cascade chain reaction. Thus, it is essential to consider the non-Poisson character of accelerator based neutron source during noise based reactivity measurement methods.

The paper discusses the first ever experimental validation of the noise theory [1] for different pulse shape using D-T neutron generator and BRAHMMA subcritical system.

2. Theoretical review

In case, the accelerator beam pulse width is small compared to the prompt neutron decay time of the subcritical system and assuming the neutron pulses as a sum of Dirac-delta function, the theoretical

formulae for variance to mean ratio minus one (*V/M-1)* and Auto-Covariance function (*ACV)* are discussed by Degweker and Rana [1]. Authors have mentioned the decay constant of the correlated source neutrons as source correlation factor (β). In case, $\beta >> f$ and $f >> \alpha$, the *V/M* -1 is given by:

$$\frac{V}{M}-1=\frac{\lambda_d\left\{m_2-m_1^{\,2}+2m_1Y_1\right\}}{m_1\alpha}*\left(1-\frac{1-e^{(-\alpha T)}}{\alpha T}\right) \tag{1}$$

The Auto-Covariance function (*ACV*) is given by:

$$ACV=\frac{f^2\lambda_d^2m_1^2}{\alpha^2}+\frac{f\lambda_d^2}{2\alpha}\left(m_2-m_1^2+2m_1Y_1\right)e^{-\alpha T} \tag{2}$$

where, λ_d is the probability of detection second, m_1 and m_2 are the first and second moment of source multiplicity distribution, α is the prompt neutron decay constant, β is the source correlation factor, f is the frequency of the external neutron source, T is the gate width and Y_1 a constant given by:

$$Y_1=\frac{\lambda_f\left\langle\nu(\nu-1)\right\rangle}{2\alpha} \tag{3}$$

where, λ_f is the probability of fission per second and ν is the number of neutron per fission.

On the other hand, there could be such a situation when the pulse width is comparable to the prompt neutron decay time ($1/\alpha$). According to authors [1], for a periodic pulse train of finite width and rectangular shape, the *V/M* -1 and two time probability function (*ACV*) are given by:

$$\frac{V}{M}-1=\underbrace{\left(\frac{\lambda_d\lambda_f\left\langle\nu(\nu-1)\right\rangle}{\alpha^2}+\frac{\lambda_d\left\langle\nu_{sp}(\nu_{sp}-1)\right\rangle}{\alpha\bar{\nu}_{sp}}\right)}_{1st-Term}\left(1-\frac{1-e^{-\alpha T}}{\alpha T}\right)+\underbrace{\frac{4m_1\lambda_d\alpha}{\sigma^2Tf}\left[\sum_{n=1}^{\infty}\frac{(1-\cos(\omega_n\sigma))\sin^2(\omega_nT/2)}{n^2\pi^2\omega_n^2(\omega_n^2+\alpha^2)}\right]}_{2nd-Term} \tag{4}$$

$$ACV=\frac{m_1\lambda_d^2f}{2\alpha}\underbrace{\left[\frac{\left\langle\nu(\nu-1)\right\rangle\lambda_f}{\alpha}+\frac{\left\langle\nu_{sp}(\nu_{sp}-1)\right\rangle}{\bar{\nu}_{sp}}\right]}_{1st-Term}e^{-\alpha T}+\frac{m_1^2\lambda_d^2f^2}{\alpha^2}\underbrace{\left[\sum_{n=1}^{\infty}\frac{4\alpha^2(1-\cos(\omega_n\sigma))\cos(\omega_nT)}{\sigma^2\omega_n^2(\omega_n^2+\alpha^2)}\right]}_{2nd-Term} \tag{5}$$

The above formulae (equations 4 and 5) have two terms. The first term represents the correlated part, and the second term represents the uncorrelated oscillatory part. The least square fitting of the above formulae will give the prompt neutron decay constant of the subcritical system. The prompt neutron decay constant (α) is related to the reactivity (ρ), delayed neutron fraction (β_{eff}) and neutron generation time (Λ) as:

$$\alpha=\frac{\beta_{eff}-\rho}{\Lambda} \tag{6}$$

3. Experimental setup

The experimental setup consists of Purnima Neutron Generator (PNG) (Figure 1 (a)), BRAHMMA subcritical system (Figure 1(b)), ^{3}He detectors and time stamp data acquisition system.

The BRAHMMA subcritical system (k_{eff}=0.89) [4], which has been used for noise studies, consists of metallic natural Uranium (3.2 tons) as fuel in 13X13 square lattices. The system has used High Density Polyethylene (HDPe) and Beryllium Oxide (BeO) as moderator and reflector respectively. The front half of the central 3X3 lattice serves as cavity for external neutron source, and the rear half is filled with Lead and BeO as shown in Figure 1(c).

4. Experimental Results

Initial characterization of PNG have been carried out to measure the source correlation factor, pulse shape and pulse width. The pulse shape and the width have been measured by introducing an ACCT in the beam path of PNG (Figure 1(d)). During noise experiments with PNG, accelerator frequency 10 kHz has been used for Dirac-Delta pulse (pulse width: 10 µs), and 1 kHz has been used for finite pulse width (100 µs). The measured pulse shape at 10 kHz using ACCT (Figure 1(e)) is rectangular (Figure 1(f)). Finally, after source characterization, PNG has been coupled with BRAHMMA subcritical system, as shown in Figure 1(d)) for further noise experiments.

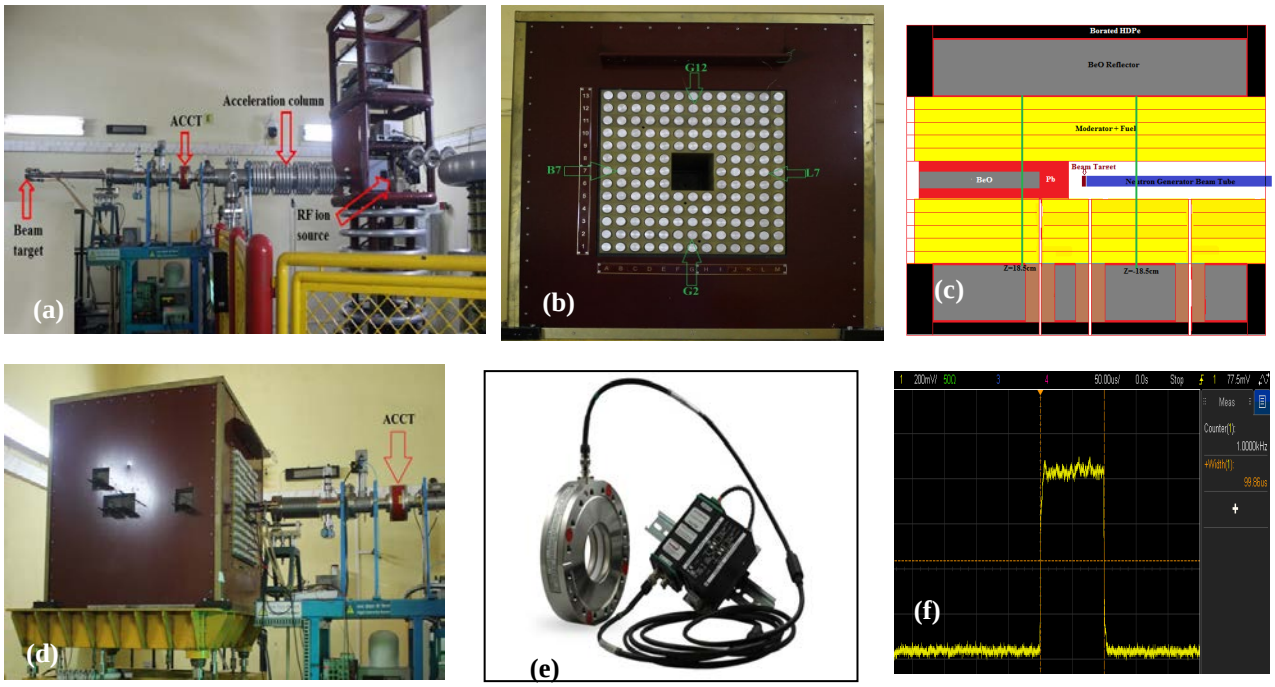


Figure 1 (a) Purnima Neutron Generator (PNG), (b) BRAHMMA subcritical system and detector location in radial direction (B7, L7, G2 and G12), (c) schematic of detector locations in axial direction (Z=±18.5 cm), (d) BRAHMMA coupled with PNG, (e) The ACCT (Bergoz Instrumentation) and (f) measured pulse shape and at accelerator frequency 1 kHz.

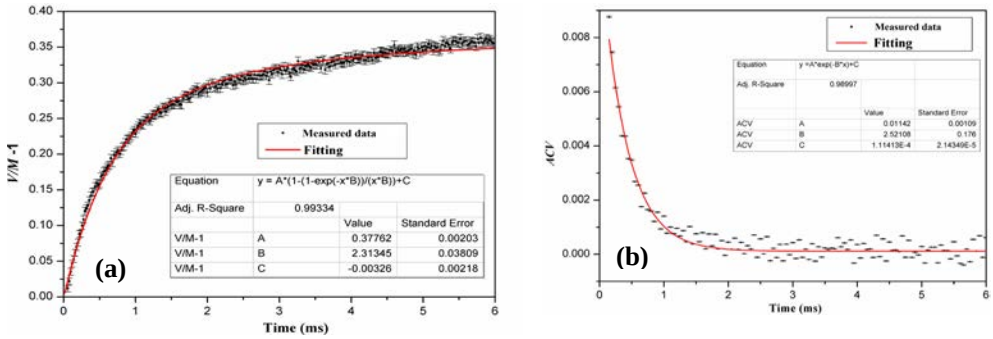


Figure 2 Experimental data fitted with analytical equations, (a) *V/M*-1 and (b) *ACV* at accelerator frequency 10 kHz [3].

In case of accelerator frequency 10 kHz, the pulse width (10 µs) is very small compared to the prompt neutron decay time ($1/\alpha$~433 µs) of BRAHMMA, and the measured source correlation factor (β=50.44 ms^{-1}) is very large compared to α (2.310±0.058 ms^{-1}). Also, the accelerator frequency 10 kHz

is large compared to α. Therefore at 10 kHz, equations 1 and 2 have been used to calculate the prompt neutron decay constant in *V/M-1* and *ACV* method respectively. On the other hand, the measured pulse width using ACCT (Figure 1 (e)) at 1 kHz has finite width (99.86 μs) as shown in Figure 1 (f) and comparable to the prompt neutron decay time ($1/\alpha$~433μs) of BRAHMMA. Thus, for accelerator frequency 1 kHz, equations 4 and 5 have been used to calculate α using the measured data in *V/M*-1and *ACV* method respectively. The measured *V/M-1* and *ACV* at accelerator frequencies 10 and 1 kHz have been shown in Figure 2 and 3 respectively. In case of 10 kHz, measured α by fitting of experimental data with analytical equations in *V/M-1* and *ACV* are 2.313±0.038 ms^{-1} and 2.521±0.176 ms^{-1} respectively, whereas, in case of 1 kHz the values are 2.284±0.042 ms^{-1} and 2.360±0.023 ms^{-1} respectively. It has been observed that the measured α at 1 kHz using *V/M-1* and *ACV* is close to the theoretical estimate (2.310±0.058 ms^{-1}) [2], whereas, at 10 kHz measured α using *ACV* is higher compared to the theoretical estimate. This can be attributed towards the scattered data point due to the periodic oscillation in measured *ACV* after 0.5 ms which has been observed by further reducing the gate width (*T*~1μs).

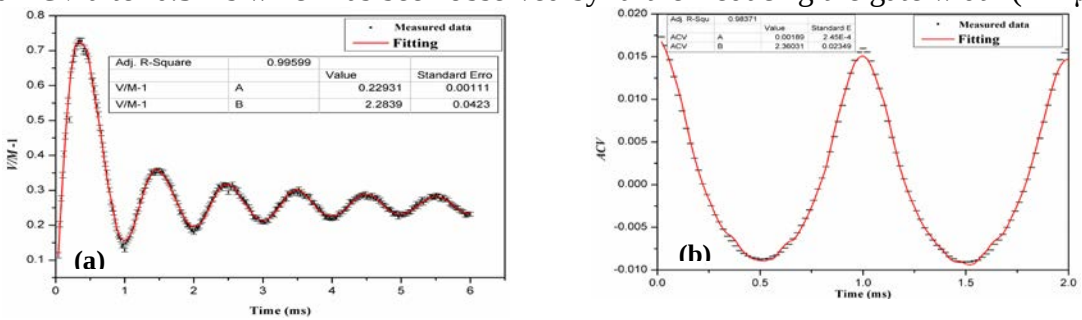


Figure 3 Experimental data fitted with analytical equations, (a) *V/M*-1 and (b) *ACV* at accelerator frequency 1 kHz [5].

5. Conclusion

Fast ever experimental validation of the noise theory developed under consideration of non-Poisson source characteristics has been discussed in this paper. The theoretical postulate for Dirac-delta pulse and finite width of rectangular pulse have been used at accelerator frequencies 10 kHz and 1 kHz respectively. In case of 10 kHz, the noise descriptors are similar to the isotopic Poisson source [2], whereas, in case of 1 kHz, periodic oscillation arises because of uncorrelated oscillation of neutron population in subcritical system. Finally, the prompt neutron decay constant of BRAHMMA subcritical system measured using the postulate is in good agreement with the theoretical estimate.

6. Acknowledgement

Authors are thankful to Dr. S. B. Degweker, Dr. Y. S. Rana, Dr. Amar Sinha, Dr. L. M. Pant and Dr. S. C. Gadkari for their suggestions during experiments.

7. References

[1] Degweker, S. B., and Rana, Y. S., *Annals of Nuclear Energy*, 34(6), 2007, 463-482.

[2] Kumar, R., Degweker, S. B., Roy, T., Singh, K. P., Samanta, S., Bajpai, S., ... and Sinha, A., *Annals of Nuclear Energy*, 103, 2017, 315-325.

[3] Ray, N. K., Pant, L. M., Patel, Tarun, Kumar, Rajeev, Roy, Tushar, Sarkar, P. S., Sinha, Amar, Gadkari, S. C., *Progress in Nuclear Energy*, 117, 2019,103087.

[4] Sinha, A., Roy, T., Kashyap, Y., Ray, N., Shukla, M., Patel, T., et al., *Ann. Nucl. Energy*, 75, 2015, 590–94.

[5] Ray, N. K., Patel, T., Kumar, R., Sarkar, P. S., & Pant, L. M., *Progress in Nuclear Energy*,120, 2020, 103191.

XENON SPATIAL OSCILLATION EXPERIMENTS IN KAKRAPAR ATOMIC POWER PROJECT-3

Amritha Krishnan S[1], Abhishek Chakraborthy[2], Rajarshi Das[1], Shankar Venkatramani[1], M.P.S Fernando[2]

[1] Kakrapar Atomic Power Project-3&4, Gujarat, India

[2] Nuclear Power Corporation of India, Mumbai, India

[1]*e-mail: - amrithakrishnans@npcil.co.in*

Abstract

Large power reactors such as KAPS-3&4 have small neutron migration area compared to the core dimensions due to which reactivity perturbations are confined locally and don't propagate throughout the core. Therefore, these reactors are termed as loosely coupled neutronically and are unstable against xenon induced spatial power oscillations at high powers. Spatial power monitoring systems such as Flux Mapping System (FMS) are employed for early detection and control of xenon oscillations in these reactors. During Phase-C experiments of KAPS-3, actual xenon spatial oscillations experiments were carried out by deliberately inducing azimuthal and axial excitation modes at different powers of 28%FP and 40%FP. This paper presents the observations during xenon oscillations experiments carried out in KAPP-3.

1. Introduction

Pressurized Heavy Water Reactors (PHWRs) are nuclear fission based nuclear reactors which use Natural Uranium (NU) as fuel and heavy water as moderator and coolant. India presently has 17 PHWRs in operation. Out of these 17 PHWRs, 15 are 220MWe PHWRs and the rest are 540MWe PHWRs. Fourteen more PHWRs of 700MWe capacity each are planned to be installed out of which one unit, KAPP#3, has achieved criticality in July 2020 and the other three units are in the advanced stage of commissioning.

With the same core configuration of 540MWe reactor, the reactor power output has been increased to 700MWe (25% increase) by increasing linear heat rating (18%) of the bundles and more flattening of flux distribution (7%). This extra generation of power is extracted by allowing coolant boiling at the exit of the channel to the tune 2 to 3 % quality [1]. Due to higher operating power in 700MWe PHWR with 37-element bundle design, operating bundle powers are closer to the bundle power envelope. Due to reduced operating margin, bundle power limit is enforced online in 700MWe using FMS.

On account of more flux flattening compared to 540MWe, the 700MWe reactors are more prone to xenon induced spatial oscillations. Moreover, boiling at the coolant exit makes the temperature based setbacks ineffective as temperature remains constant even during a power excursion. Therefore, spatial power monitoring systems such as Flux Mapping System (FMS) which are based on direct measurement of neutron flux are all the more significant in 700MWe PHWRs. The accuracy in prediction of zone power distribution by FMS is tested against the benchmarked codes such as IQS-3D during Phase-C experiments in 700MWe. This was done by deliberately inducing xenon tilts without spatial power control systems in place and allowing the zone powers to oscillate for about 100hours at 28%FP and 40%FP. These two power levels were chosen so that converging and diverging types of spatial oscillations can be studied.

2. Xenon Spatial Oscillations in 700MWe PHWR

Xenon-135 is a fission product with significant thermal absorption cross-section of 2.6×10^6 barns. Local changes in Xenon concentration due to global/local changes in power distribution can lead to slow power oscillations. An increase in local reactivity leads to an increase in neutron flux, leading to lower Xenon concentration [5]. This gives a positive reactivity feedback leading to higher neutron flux in that region. Eventually, the increased neutron flux level will lead to a higher I-135 concentration, which will then result in an increase in Xe-135 concentration. This reduces the neutron flux level in the region below its average value, assuming the total reactor power output is constant. In this way, the neutron flux can oscillate in different regions of the core, with a period of oscillation ranging from 15 to 30 hours [2].

The Flux Mapping System (FMS) for 700MWe PHWR consists of the physical system of multiple vanadium SPNDs as input sensors and the flux mapping software. 106 Vanadium SPNDs are placed in 26 Vertical Flux Units (VFUs) across the core to provide accurate measure of neutron flux. The dominant process of generation of current in Vanadium SPNDs is beta decay of Vanadium-52.

The space-time dependent distributions of neutron flux, can be expanded as a weighted series of fixed number of λ modes which are linearly independent, with a set of time-dependent weighting amplitudes as given below in (1):

$$\emptyset_g(\vec{r}, t) = \sum_{m=1}^{M} a_m(t)\psi_{mg}(\vec{r}) \qquad (1)$$

where $a_m(t)$ is the combining coefficient corresponding to mode 'm' and likewise ψ_{mg} is the flux value of m^{th} mode at point 'r' corresponding to energy group 'g'. Lambda (λ) modes used as the expansion functions in (1) are solutions of time-independent diffusion equation

$$-\nabla . D_g^0 \nabla \psi_{mg} + \Sigma_g^{r0}\psi_{mg} - \sum_{g \neq g'} \Sigma_{g \to g'}^0 \psi_{mg'} = \lambda_m \chi_g \sum_{g'} \nu \Sigma_g^{f0} \psi_{mg'} \quad (2)$$

For each eigenfunction ψ_{mg} of the above equation, there is an associated eigenvalue λ_m. With each eigenvalue, there is an associated multiplication factor $k_m = 1/\lambda_m$. The flux shape or eigenfunction corresponding to the lowest eigenvalue or highest multiplication factor is known as fundamental mode. The remaining higher eigenfunctions or modes are called harmonics [2,6].

Spatial perturbations, transients and oscillations of the neutron flux can be described as a superposition of the fundamental mode and higher harmonics .A sub-critical reactivity is associated with each of the higher order modes and is used to assess its importance from a spatial control point of view. This modal reactivity can be thought of as a measure of the susceptibility of the reactor to flux shape disturbance due to the particular mode. If eigenvalue separation of any mode is less than the equilibrium Xenon reactivity load, then the reactor is unstable against Xenon induced oscillations [2,6].The contribution of a higher mode depends on the location of the perturbation and on the value of a parameter called eigenvalue separation. For 700MWe reactor, the important higher modes are the first azimuthal (1) (-13.5mk), first azimuthal (2) (-14.6mk) and first axial (-25.5mk) modes.

2.1 Experiment

The 700MWe PHWR is divided into 14 zones in which the individual zone levels vary together for bulk power control and differentially for individual zone power control. Figure-1 gives the schematic of individual Zone Control Compartments of 700MWe PHWR. Accurate zone powers are

computed real time by FMS based on vanadium SPND readings and communicated to RRS in every execution cycle. Based on the zone powers computed by FMS, RRS differentially manoeuvre zone levels to maintain the desired flux shape.

FMS communicates the accurate zone powers to RRS in fractional units of nominal individual zone powers which are already available within FMA. In order to create the required tilt fraction (~10%) for the excitation mode under study, the nominal individual zone powers were varied. Based on the new nominal powers, individual zone levels readjusted so as to make actual zone powers close to new nominal powers. The reactor was allowed to operate in this configuration for 60 hours so that xenon load distribution corresponds to altered zone power distribution. Specific adjuster rods were also manoeuvred in addition to changing nominal zone powers to maintain the required tilt fraction throughout the period of 60 hours.

After a period of 60 hours, the nominal zone powers were reverted back to original design values. Again, individual zone levels adjusted so as to bring actual zone powers close to nominal powers. By reverting back to original design values of nominal zone powers, effectively a perturbation has been initiated within the reactor. This is because the xenon load distribution corresponded to tilted configuration. In order to allow the xenon spatial oscillations without any interference from regulating system, spatial power control was made ineffective by setting flux tilt control gain value to zero. Reactor was allowed to operate for about 100 hours without any spatial control. Depending on the operating power and the mode of excitation, the xenon oscillations were either converging or diverging. After 100 hours of operation in this fashion, spatial power control was made available by setting the flux tilt control gain to the original value.

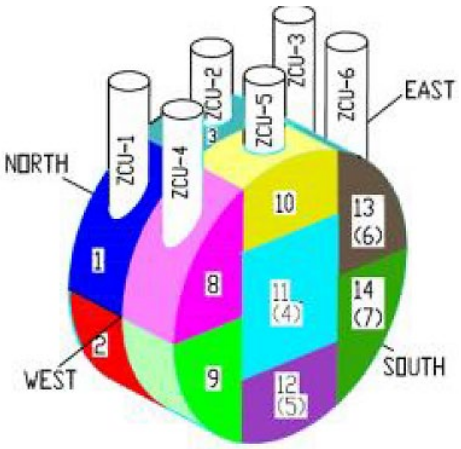


Figure 1 Zone Control Compartment design in 700MWe PHWR

3. Results and Discussion

Xenon Oscillations experiments were carried out at two different powers, 28%FP and 40%FP. Since eigenvalue separation of first azimuthal (1) is the lowest (- 13.5mk), this is the most probable mode of excitation. If first azimuthal (1) is shown to converge, then other higher modes of excitation are definitely of converging nature at that power. The 1st azimuthal (1) was of converging nature at 28%FP. Figure-2 shows the zone power variations for 100 hours period of oscillations. Therefore, 1st azimuthal (2) and 1st axial modes also would be of converging nature.

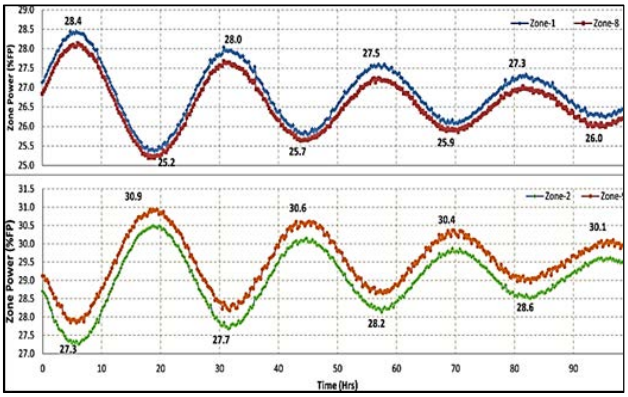


Figure 2 Zone Power variations at 28%FP [3]

At 40%FP, all the three possible modes of excitations were studied and shown in terms of power tilt fraction. Power tilt (in %) is the ratio of difference in powers (in MWs) of zones across the stability line to the total power.

For 1st Azimuthal (1) at 40%FP, it is clearly evident from Figure-3 that the oscillations were diverging. Therefore, reactor is unstable against 1st Azimuthal (1) at this power. Tilt fraction indicated is purely top to bottom as the other types of tilts were absent during the excitation of 1st Azimuthal (1).

For 1st Azimuthal (2) at 40%FP, the oscillations were converging. However, inherent top to bottom tilt of about (-3%) due to Adjusters not fully inserted started dominating after few cycles.

For 1st Axial at 40%FP, the axial oscillations converge (Figure-4) and inherent top to bottom tilt dominated as the experiment proceeded further similar to 1st Azimuthal (2).

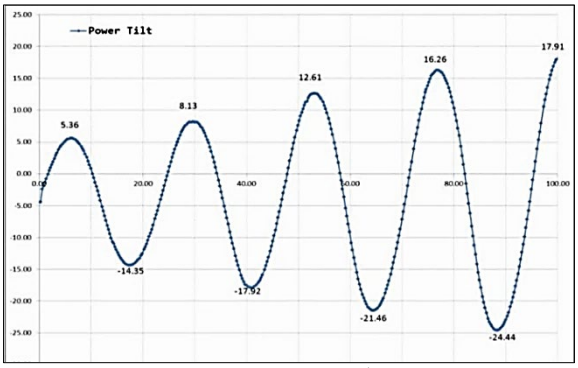


Figure 3 Percentage tilt for 1st Azimuthal (1) at 40%FP [3]

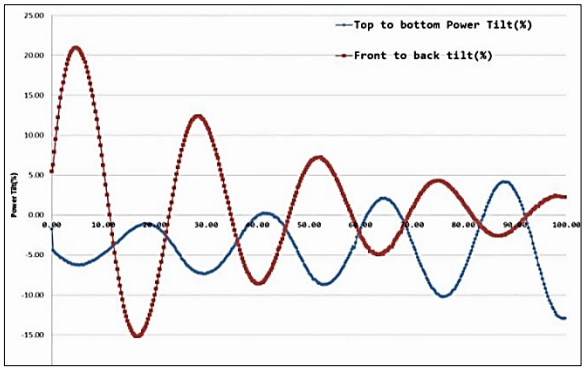


Figure 4 Percentage tilt for 1st Axial at 40%FP [3]

4. Conclusion

Xenon spatial oscillations were experimentally carried out during Phase-C experiments of KAPP-3. Based on the sub-criticality values associated with different λ modes, 1st azimuthal (1), 1st azimuthal (2) and 1st Axial modes are more prone to get excited. The 1st azimuthal (1) excitation mode was observed to be of converging nature at 28%FP. However, at 40%FP, 1st azimuthal (1) was of diverging nature and other two modes were observed to converge. Inherent tilts in the reactor core can interfere with other λ modes of excitations. Since experiments were conducted for fresh core, the transition from converging nature of oscillations to diverging nature could happen at lower powers due to smaller feedback coefficients in equilibrium core.

5. References

[1] Reactor Physics Design Manual, KAPP-3&4/DM/01100/00001/R0,2017

[2] Study of Xenon dynamics using Modal Expansion Method for 700MWe PHWR, 700MWe/DN/01100/9013,2012

[3] Commissioning Report on Xenon oscillation studies, KAPP-3&4/01133/RP/Phase-C /04

[4] J.B. Yasinsky and A.F. Henry, "Some numerical experiments concerning space-time reactor kinetics behavior", Nuclear Science and Engineering, Volume 22, pages 171-181, 1965.

[5] Nuclear Reactor Analysis by W.M.Stacey

[6] PhD Thesis on Development of Space-Time Kinetics Technique to Analyze Localized Perturbations in Pressurized Heavy Water Reactor, by Dr. M.P.S. Fernando, IIT Bombay, 1998.

Measurement of Critical Height with (Th-Pu)MOX Experimental cluster of different Enrichments in AHWR-CF Extended Core

Sudipta Samanta[1*], Amod Kishor Mallick[1], Deep Bhandari[1], Kapil Deo[1], Rajeev Kumar[1,2], Neelima Prasad[1] and Umasankari Kannan[1,2]

[1] Bhabha Atomic Research Centre, Mumbai, India

[2] Homi Bhabha National Institute, Mumbai, India

[*]*e-mail: - sudiptas@barc.gov.in*

Abstract

AHWR Critical Facility (AHWR-CF) is primarily meant for conducting reactor physics experiments to validate the computational tools used in AHWR design [1]. The modeling of AHWR type of advanced fuel cluster having (Th-Pu)MOX fuel is very crucial to the design and errors in modeling techniques are required to be established by performing experiments. For this purpose, two special experimental clusters with (Th-1%Pu)MOX and (Th-8%Pu)MOX were manufactured by RED, BARC. Various integral and differential experiments were performed with these experimental cluster at different lattice locations of AHWR-CF. Comparing these measured and estimated values of reactor physics parameters with AHWR design codes will help in validation of computer codes and suitability of using nuclear data libraries used in the design.

1. Introduction

The Advanced Heavy Water Reactor (AHWR) is an innovative reactor being designed at BARC for large scale utilization of Thorium. This reactor has many inherent safety features. AHWR is governed by the use of thorium in a closed fuel cycle. The AHWR design envisages using MOX clusters with different combination of (Th,^{233}U)MOX and (Th, Pu)MOX at different stages of its operation. The simulation of this cluster with all its heterogeneities is quite complex. Simulations of such advanced fuels is very important to the design calculations and errors in modeling techniques are required to be verified by performing experiments. Apart from the errors due to the approximations in the modeling technique, the basic nuclear cross-section set also has a considerable contribution to the errors in various design parameters. Thus validation of the design parameters and the calculation models are required.Two different types of experimental clusters having fuel as (Th-Pu)MOX with different Pu enrichments (1% and 8%) were manufactured. The experimental clusters are consist of 19 pins having same geometrical dimension as AHWR fuel pins. Different integral and differential experiments were performed at AHWR-Critical Facility at cold clean state which aid in validation of the AHWR design tools [2,3].

2. AHWR Critical Facility

The AHWR-CF is a heavy water moderated, air cooled, natural uranium fueled vertical reactor. The current core configuration of CF consists of 61 fuel clusters, 6 Shut off Rods (SORs) and one Absorber Rod (AR). Each cluster consists of 19 fuel pins of natural uranium arranged in 3 rings of 1, 6 and 12 pins respectively. The clusters are arranged in the core in a square pitch of 24.5 cm. The core is placed inside the cylindrical tank of radius 165 cm. The radius of effective active core in this tank is around 110 cm. The active fuel starts from 30 cm above the tank bottom and extends up to 250 cm.

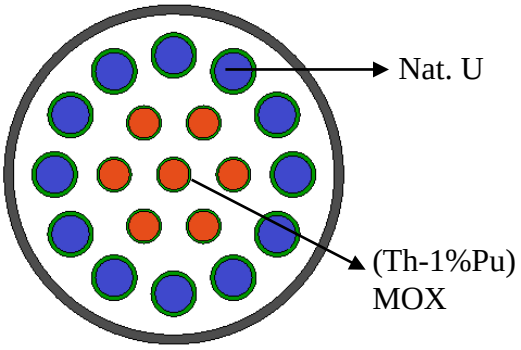
2.1 Details of experimental clusters

The experimental clusters were made up of 19 pins, similar to natural Uranium cluster, arranged in three rings of 1, 6 and 12. Inner seven pins (1+6) are identical and composed of (Th-Pu) MOX enrichment. The geometrical dimensions of these pins are same as that of AHWR fuel pins. Outer twelve pins, all of which are also identical, are axially graded and composed of 60 cm of ThO_2 sandwiched between 80 cm of natural Uranium on either side. Geometrically, these twelve pins are similar to the fuel pins of natural Uranium clusters. Two different types of [Th-Pu]MOX clusters were used for integral experiments-

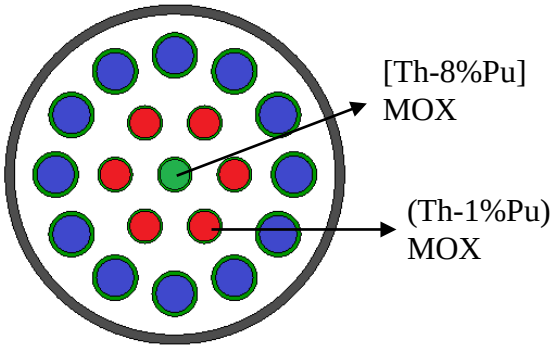
A. {(Th, 1%Pu)MOX, NU-ThO_2-NU} where all inner 7 pins are made of [Th-1%Pu]MOX as fuel.
B. {(Th, 8%Pu)MOX, NU-ThO_2-NU} where central pin is [Th-8%Pu]MOX fuel pin and middle 6 pins are made of [Th-1%Pu]MOX.

The schematic diagram of horizontal cross section of the experimental clusters with their axial grading of fuel in pins of the outer most ring and CF reference cluster is given in figure-1.

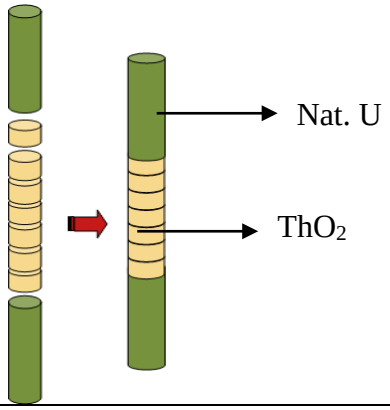
Fig -1: Schematic of cross section of experimental clusters and reference cluster



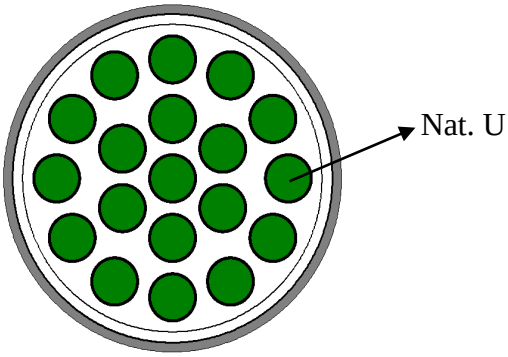
[Th-1%Pu]MOX experimental cluster



[Th-8%Pu]MOX experimental cluster



Axial grading of Outermost ring pins



Nat. Uranium reference cluster

3. Pre-experimental analysis

Detailed simulations were carried out to estimate core characteristics like K-effective, core reactivity, power level and counts in the start-up detectors for various states during approach to criticality while performing these experiments. These, along with Critical Height and worth of 6-SORs (for critical core configuration), were estimated for various experimental core configurations. Deterministic codes WIMSD and FEMPAR were used for these calculations. WIMSD code is a transport theory code for

lattice simulations and was used to obtain lattice homogenized and condensed cross sections for different kinds of lattices. ENDF-B/VI.8 nuclear data library was used for the lattice simulations. The diffusion theory core level code FEMPAR was used to calculate the K-effective and core reactivity at different moderator levels.

4. Experimental details

The criticality experiments were performed in modified core configurations by replacing one Nat-U Cluster of the extended core with the experimental clusters. This was done for 6 different core configurations corresponding to the 6 different locations of experimental clusters. These 6 locations are shown in different colors inside the extended core map in Fig-2. These positions correspond to E5, F4, F3, F2, B3 and F1 lattice locations. The experiments consisted of measurement of Critical Height and worth of 6-SORs in Extended Core with an experimental cluster. Criticality was approached by following the established procedure of controlled increase of moderator height from the dump level (125 cm) in steps, and monitoring the count rates in two pulse channel counters (PC-1 & PC-2) located in the graphite reflector below Reactor Tank. At each step, 'Inverse of Count Rate' versus moderator level was plotted to find the extrapolated expected Critical Height as shown in Fig.-3. The moderator level was increased in steps as per the approved procedure. Criticality was achieved by manually controlling the moderator level. After making the reactor critical, the power was stabilized at 10 mW for few minutes. The reactor was then shutdown by tripping it manually. The data of count rates as function of time was obtained for estimation of combined worth of 6-SORs.

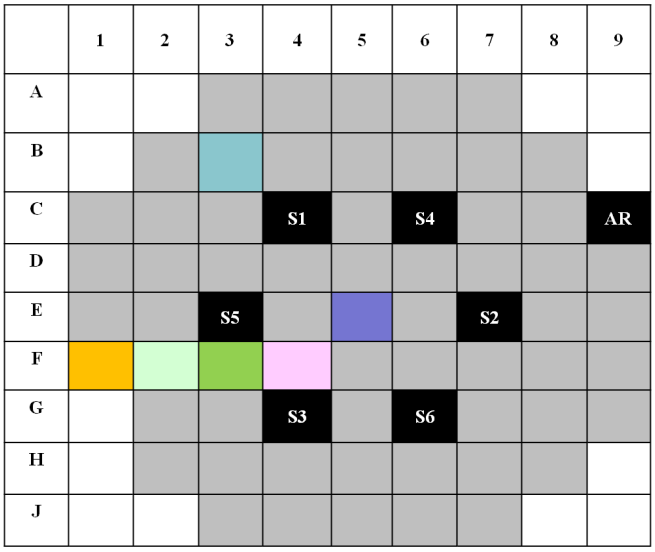


Fig -2: Six different core configurations (shown in color) with experimental cluster

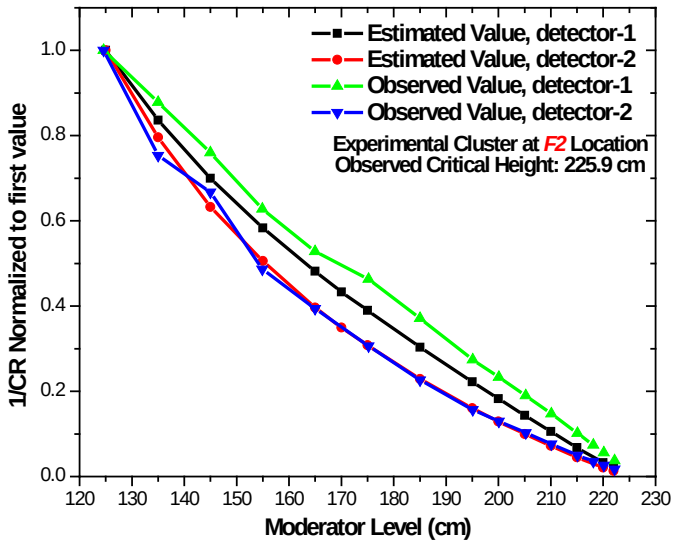


Fig -3: Inverse of count rate vs. mod height for [Th-8%Pu]MOX cluster at F2 location

5. Results

The observed results of these experiments are presented below. Table-1 lists measured critical heights along with its comparison with the theoretically estimated values. The experimentally measured combined worth of all 6 SORs for all the six core configurations vary from 102.6 mk to 104.4 mk. The observed load of the experimental cluster was less towards the core periphery than

the central locations. The difference in measured and estimated critical heights were more in the central locations of the core i.e. maximum flux locations.

Table –1 : Comparison of critical height of AHWR-CF with one experimental cluster

Location of experimental cluster	**{(Th, 1%Pu)MOX, NU-ThO_2-NU}**		**{(Th, 8%Pu)MOX, NU-ThO_2-NU}**	
	Measured critical height (cm) (±0.1 cm)	Estimated critical height (cm)	Measured critical height (cm) (±0.1 cm)	Estimated critical height (cm)
E5	233.8	235.2	230.5	232.3
F4	232.8	233.9	229.8	231.4
F3	230.3	231.4	228.2	229.4
F2	227.2	227.9	225.9	226.7
F1	224.9	225.4	223.9	224.7
B3	226.1	226.6	225.0	225.8

6. Conclusion

The experimental results are in good agreement with the estimated values. The differences between measured and estimated values may largely be attributed to heterogeneity of experimental cluster, uncertainty in its composition, modeling approximations and uncertainty in nuclear data library. The results of these experiments would further improve confidence in our design tools and choice of nuclear data library used for AHWR design.

7. References

[1] N. Prasad, U. Kannan, B. Chakraborty, R. Kumar, B. K. Mohan, and R. Srivenkatesan, “Physics design of critical facility for AHWR and MWe PHWR (revision-1)," RPDD/AHWR/96, (2008).

[2] Neelima Prasad, Amod Kishore Mallick, Sudipta Samanta et.al.; “Post Analysis of Integral Experiments with one {(Th,Pu)MOX, NU-ThO2-NU} Cluster in Extended Core of Critical Facility at E-5, F-4, F-3, F-2, B-3 and F-1 Locations”, RPDD/CF/404/ June 30, 2017.

[3] Amod Kishore Mallick, Neelima Prasad, Sudipta Samanta et.al.;“Analysis of Integral Experiments with one {(Th,Pu)MOX, NU-ThO2-NU} Cluster in Extended Core of Critical Facility”, RPDD/EP/154/ March 8, 2018.

IRRADIATION STUDY OF THORIUM IN PHWR SPECTRUM USING IN-HOUSE CODE ADWITA

Devesh Raj, Umasankari Kannan
Bhabha Atomic Research Centre, Mumbai, India
[1]*e-mail: -draj@barc.gov.in*

Abstract

. .A few thoria bundles were used in PHWRs for initial flux flattening. They were irradiated to a maximum of 13000 MWd/te and discharged. For the back-end process of this fuel, it is important to assess the activity in the spent thoria fuel. In this paper we present some results obtained on decay of reprocessed uranium, generated from thorium bundles irradiated in Indian PHWRs. The presence hard gamma emitters, which are progeny of ^{232}U in the discharged fuel and in reprocessed uranium, complicate reprocessing and fuel fabrication. Therefore it is necessary to quantify the buildup of isotopes that are generated in irradiation and the decay after end of irradiation and also after reprocessing. In this work we havefollowed the irradiation of thorium in PHWR and have analysed buildup of ^{232}U together with other uranium isotopes and the decay characteristics of reprocessed uranium. These inputs are required for deciding when to fabricate new fuel assemblies from the reprocessed uranium. We conclude that best time to attempt fabrication of fuel out of reprocessed uranium isotopes is just after reprocessing

1. Introduction

. In irradiation of thorium, during irradiation the reactor can burn ^{233}U build in situ and the discharged fuel can be reprocessed to utilise the bred ^{233}U. The presence of hard gamma emitters in the decay chain of ^{232}U, ^{208}Tl, pose difficulty in fabrication of fuel from the reprocessed uranium.It is important to estimate build-up of ^{232}U during the irradiation and its decay progeny along with ^{233}U to provide knowledge required to make decision about the reprocessing. Since thorium has been irradiated in 220 MWe PHWRS and theoretical studies have been made, we have taken the irradiation of thorium in 220 MWe PHWRS as the representative case [1,2] for the thorium utilization. The code ADWITA [3] and the cross-section library developed for the 220 MWe PHWRS [4] has been used for the irradiation of the thorium and the decay of the reprocessed uranium.

2. Irradiation of thorium in 220 MWe PHWRS reactor

Irradiation of thorium was done for 1000 days at a flux of 2.1e+14 n/cm2-s using ADWITA. The irradiation of thorium for 1000 days results in a burnup of 34GWd/t or fluence of about 18 n/kb.The accumulation of uranium isotopes and ^{208}Tl given in table 1 is depicted in figure-1 and accumulation of ^{232}U in total uranium is depicted in figure-2.

Table 1 Mass of some isotopes after irradiation for 1000 days (g/tHM) in thoria bundle

Isotope	0 Days	50 Days	100 Days	500 Days	1000 Days
208Tl	0.0000E+00	2.0863E-11	1.6212E-10	1.2165E-08	5.2078E-08
232U	0.0000E+00	4.8573E-02	1.8949E-01	3.0885E+00	7.4597E+00
233U	0.0000E+00	1.3127E+03	3.5878E+03	1.5052E+04	1.8355E+04

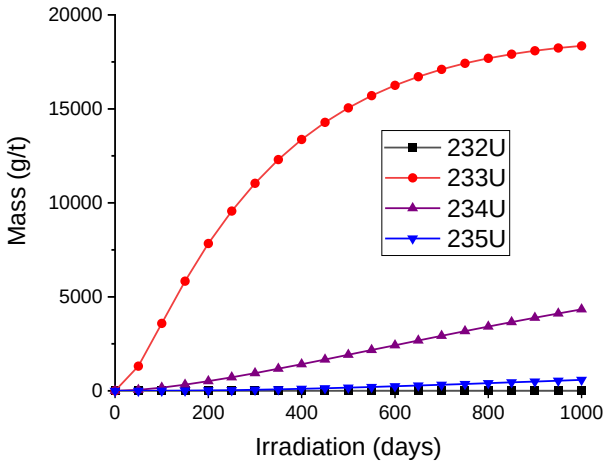


Figure 1 Accumulation of U isotopes

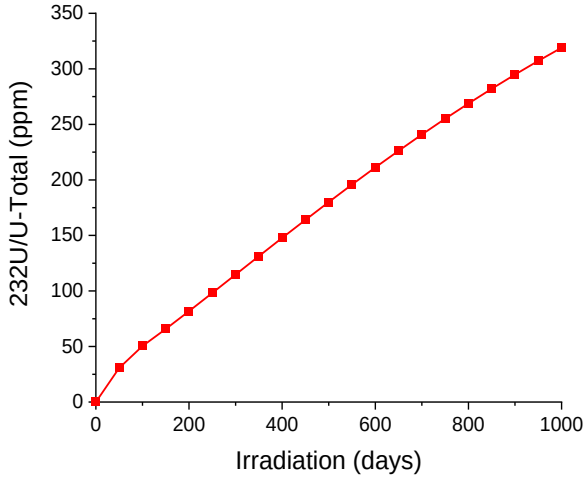


Figure 2 Accumulation ^{232}U in total U

During the irradiation for 1000 days accumulated ^{233}U is about 18.4 g/kg while ^{232}U is 0.00746 g/kg. From these estimations ^{232}U in total uranium in the irradiated thoria bundle is about 320 ppm.

3. Decay of the reprocessed uranium isotopes

The decay of one ton inventory of reprocessed uranium (containing only uranium isotopes) was followed for ten thousand days to estimate accumulation of decay products and variation of activity with time. The average composition of discharged uranium obtained from burnup simulations was assumed for these simulations.

The total activity during the cooling up to 10,000 days from 1tonne of reprocessed uranium is given in figure 3.

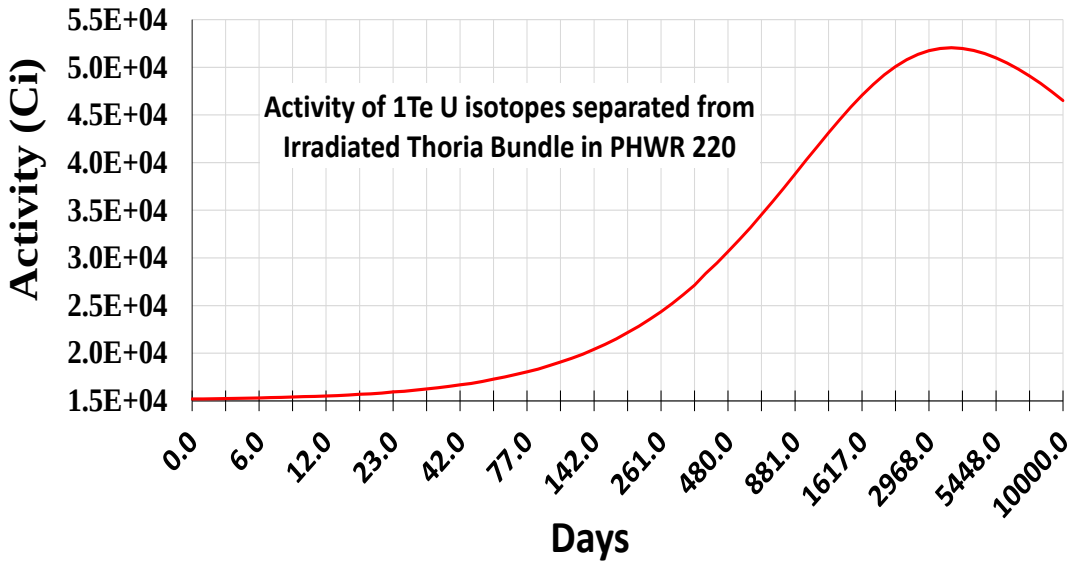


Figure 3 Activity of U isotopes and its decay progeny after reprocessing

^{208}Tl being hard gamma emitter (2.6 MeV) is identified as the most important isotope contributing to the dose rate. The estimated mass and the activity due to ^{208}Tl and total activity is given in table 2.

Table 2 Activity of reprocessed U fuel

Cooling Time	Mass of ^{208}Tl (g/Te)	Activity due to ^{208}Tl (Ci/Te)	Total Activity (Ci/Te)
1 day	2.350E-10	6.92E-02	1.521+04
10 day	3.591E-08	1.058E+01	1.543E+04
30 day	1.760E-07	5.186E+01	1.624E+04
1 year	2.084E-06	6.139E+02	2.713E+04
5 years	6.203 E-06	1.726E+03	4.856E+04
10 years	6.507E-06	1.920 E+03	5.210E+04
15 years	6.364E-06	1.875 E+03	5.100E+04

The other major contributors to the activity (α, β, and γ) was identified and their contribution to the total activity estimated.Up to 10,000 days the major contributors to the activity are ^{233}U, ^{232}U, ^{212}Pb, ^{212}Bi, ^{216}Po, ^{220}Rn, ^{224}Ra, ^{228}Th, ^{212}Po, ^{208}Tl, ^{234}U. There are 11 isotopes including the initial U isotopes and their progeny which have activity greater than 0.1 Ci/kg at the end of 10,000 days are Tl^{208}, Pb^{209}, Pb^{212}, Bi^{212}, Bi^{213}, Po^{212}, Po^{216}, At^{217}, Rn^{220}, Fr^{221}, Ra^{224}, Ra^{225}, Ac^{225}, Th^{228}, Th^{229}, U^{232}, U^{233}, and U^{234}. The main contribution to activity comes from decay of U^{233} owing to its large atom fraction (about 91.355 %). The U^{232} contributes about half the activity due to U^{233} despite small atom fraction (about 0.0275%) owing to its small half-life (68.9 Years vs.0.16 MY). While U^{233} and U^{232} remains more active than any of the decay products till the end of cooling time (here 10,000 days). The U ^{234} remains so till about 100 days. Beyond 100 days activity of U^{234} is less than several decay products, namely, ^{228}Th, Pb^{212}, Bi^{212}, Po^{216}, Rn^{220} and Ra^{224}.

The time dependence of activity of isotopes are plotted in figure-4a and 4b. The time scale on X-axis is logarithmic interpolate between day 0 and 10,000. Such time step is advisable to capture, if any, rapid variation in activity at the beginning due to short lived nuclides The α decay products of U^{233} and U^{232}, Th^{229} and Th^{228} feeds the other short-lived nuclides of the chain. The decay progeny of these two thorium isotopes attain radioactive equilibrium in about 100 days and 50 days respectively. However the activity of the chain fed by U^{233} (Th^{229} etc.) is about 2 orders of magnitude less than the chain fed by U^{232} (Th^{228} etc.).

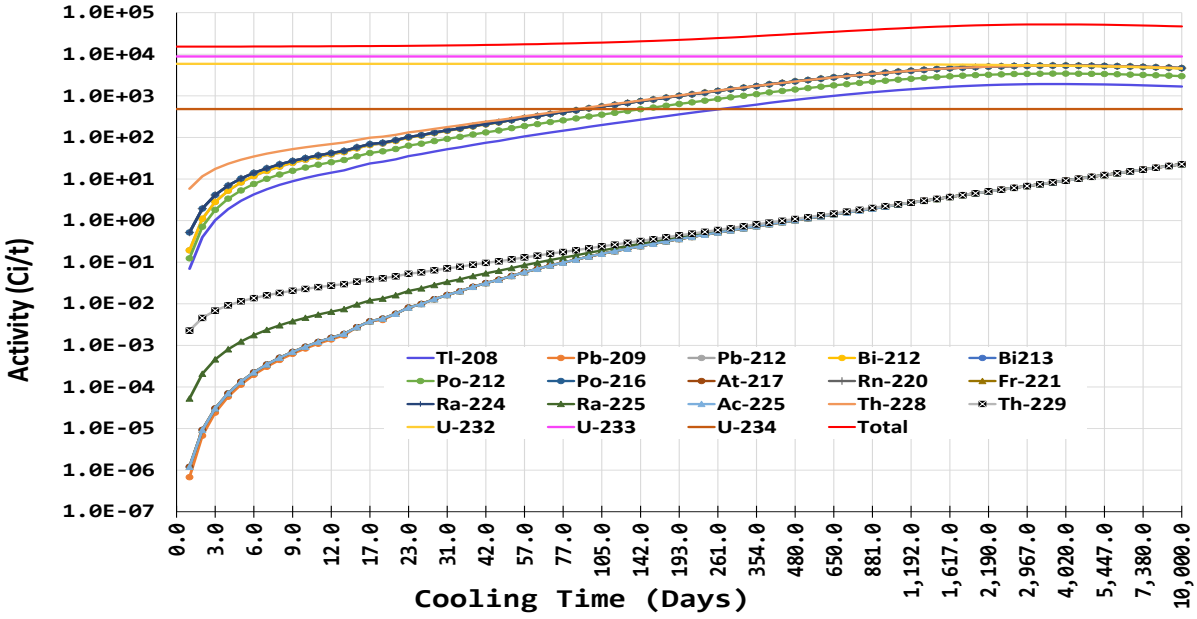


Figure 4aActivity of U isotopes and its decay progeny after reprocessing (y-axis log scale)

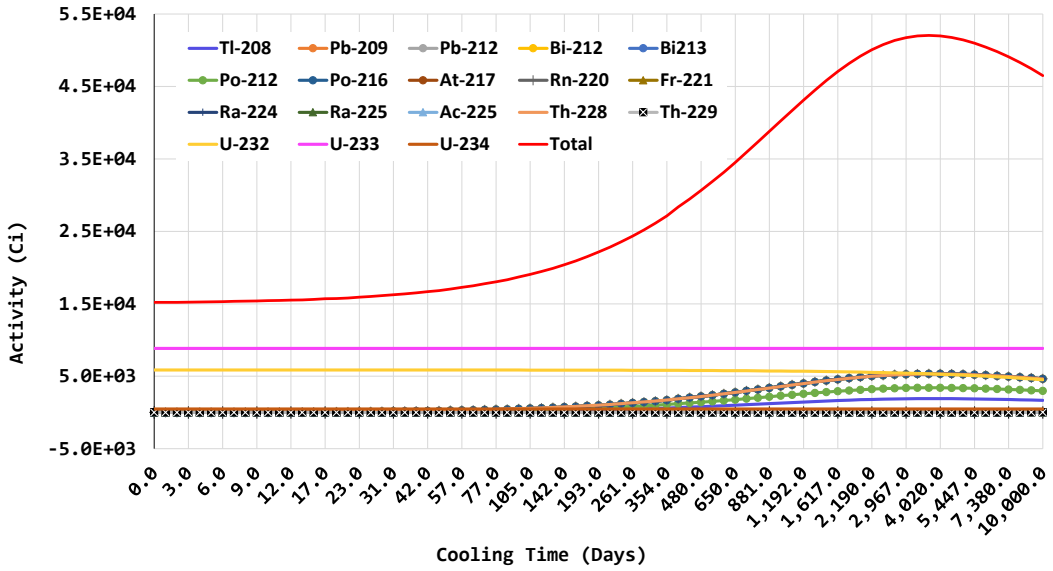


Figure 4b Activity of U isotopes and its decay progeny after reprocessing (y-axis linear scale)

The total activity starting from 1.5e04 Ci/t reaches its maximum 4.8e04 Ci/t in about 3500 days. It further decreases and comes down to 4.5e04 Ci/t at 10000 day, about 3 times higher than the initial value.

4. Conclusion

The lowest activity of U isotopes occurs just after separation of U isotopes from the irradiated thoria bundle. The activity of the aggregate increase thereafter and reaches about twice its initial value of 15000 Ci/t in about 480 days. The trend proceeds reaching maximum 4.8e04 Ci/t in about 3500 days. It further proceed to decrease and comes down to 4.5e04 Ci/t at 10000 day, about 3 times higher than the initial value. Therefore best time to attempt fabrication of fuel out of reprocessed uranium is just after reprocessing.

5. References

[1] Balakrishnan, K. (1996). Thorium Utilisation in Thermal Reactors. PhD Thesis. University of Mumbai, Mumbai, India

[2] P.D. Krishnani, Baltej Singh, Umasankari Kannan and R. Srivenkatesan, “Thorium utilization in AHWRs and Indian PHWRs”, Paper presented in the International Conference on Nuclear Science and Engineering, ICANSE2007, 13-14, Nov 2007, Bandung, Indonesia.

[3] Devesh Raj, Umasankari Kannan, “Development of Computer Code ADWITA and Data Library for the Solution of Transmutation Chain Equations and Application to the Analysis of Nuclear Fuel Cycles”, Annals of Nuclear Energy, 164 (2021), 108619.

[4] Devesh Raj, P.D.Krishnani, Umasankari Kannan, “CROSS SECTION DATA FOR POINT REACTOR FUEL CYCLE CODE”, *Proceedings of the Advances in Reactor Physics*, Mumbai, India, 2013 Oct. 23-25.

CRITICAL CALIBRATION OF REACTIVITY DEVICES IN KAPP-3

Rimpi[1], Himanshu Mishra[1], Satyendra Kr. Gautam[2] and Rajarshi Das[1]
[1] Kakrapar Atomic Power Project-3&4, Gujarat, India
[2] Rajasthan Atomic Power Project 7&8, Rawatbhata, India
[1]*e-mail: - rimpi@npcil.co.in*

Abstract

KAPP#3 reactor is the first among the proposed fleet of indigenous 700MWe PHWRs. In order to generate benchmarking data, various set of tests were carried at low power. Critical calibration of reactivity devices was one such important activity. The reactivity devices were calibrated individually and in different combinations so as to simulate regular reactor operation and postulated Loss of Regulation Accident scenarios.

1. Introduction

The spatial power profile and power level is controlled by a set of reactivity devices whereas another set of reactivity device take the reactor promptly to safe shutdown state. The first set of reactivity devices viz. Zonal Control Compartments (ZCCs), Adjuster rods (ARs) and Control Rods (CRs) are under controlled by the Reactor Regulation System (RRS). Shutoff rods (SRs) come under the control of Shutdown system 1 (SDS # 1) and the system of rapid injection of Gadolinium poison directly into the moderator through six poison injection tubes comes under the control of Shutdown system 2 (SDS # 2). The reactivity devices are described in brief in the next section.

The critical calibration is carried out at low power so that temperature feedback and fission product buildup do not interfere with the measurements; at the same time the reactor should be on 'auto' control so that RRS is able to maintain the reactor critical during the measurements.

2. Reactivity devices

The design characteristics of the reactivity devices used in KAPP-3&4 reactor is shown in the table-1.

Table-1: Reactivity device data

Sr.#	Reactivity device	Number of devices	Absorbing material
1.	Zone Control Compartments	14	H_2O
2.	Adjuster Rods (AR)	17 (8 banks)	stainless steel
3.	Control Rods (CR)	4 (2 banks)	SS/Cd/SS
4.	Shut-off Rods of SDS-1 (SR)	28 (2 banks)	SS/ Cd/ SS
5.	Poison Injection Units of SDS-2	6	$Gd(NO_3)_3.6H_2O$

The functions of different reactivity devices are:

a) ZCCs provide short term reactivity control and maintain reactor power at demanded level, correct any distortion or oscillation of power caused by reactivity perturbation.
b) ARs provide flattening of neutron flux distribution and reactivity for xenon override capability during reactor start-up. ARs act as a reactivity 'bank' during refuelling outages.

c) CRs provide rapid power reduction and compensate the reactivity increase following power reduction.

d) The shutdown systems SDS-1 and SDS-2 trip the reactor by fast insertion of a large amount of negative reactivity into the core when certain plant parameters exceed operating limits and conditions. SDS-1 actuates by dropping the shut-off rods (SRs) into the core while SDS-2 actuates by addition of liquid poison in the form of gadolinium nitrate $Gd(NO_3)_3.6H2O$ directly into the moderator.

ZCCs are the primary reactivity device elements used for power control. The average water level of the ZCCs (AVZL) is maintained within upper and lower bounds. The ARs, CRs either move IN or move OUT if the AVZL touches these bounds. The nominal configuration of reactivity devices is such that AVZL is maintained between 40 to 60% FL with all ARs kept fully IN, all CRs and SRs kept fully OUT.

The top view of core showing location of various reactivity devices is shown in Figure-1.

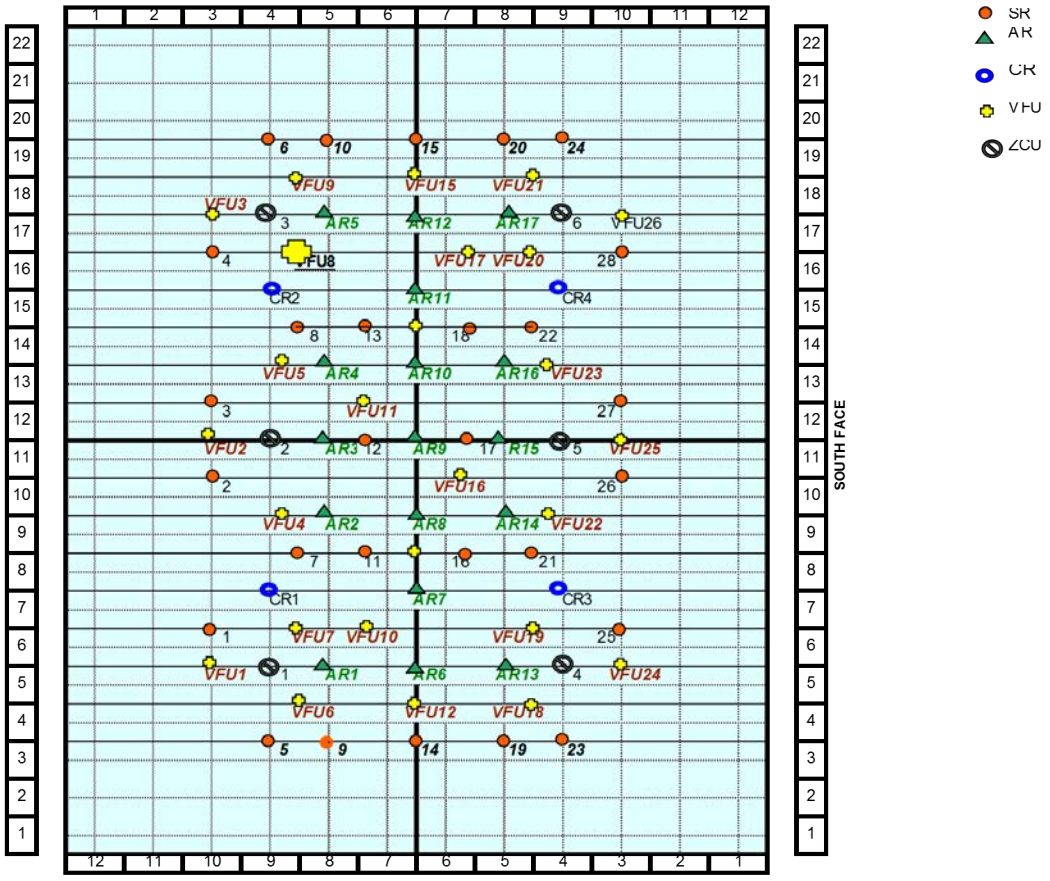


Figure-1: Location of reactivity devices

3. Procedure followed for worth measurement

Since ZCCs are the primary device for controlling reactivity, the AVZL was first calibrated against boron by adding boron solution of known concentration (reactivity coefficient of boron ~7.8 mk/ppm) in the moderator. This addition of negative reactivity was compensated by a corresponding drop of AVZL. This process was continued till AVZL was brought down to 5%

from its initial value of 95% FL. The worth of ZCC corresponding to a change from 95 to 5% FL was thus determined.

Subsequently, the reactivity worth of individual SRs, CRs and ARs were determined by noting the change of AVZL after rod insertion and withdrawal. Calibration of AR banks was done by noting the change of AVZL during withdrawal of AR banks in small steps. The AR banks were moved out in sequential order (i.e. withdrawal of bank #2 after bank #1 was withdrawn, the process was continued till the last bank, i.e. bank # 8 was withdrawn). Since the worth of ZCC is not large enough to handle the positive worth progressively introduced by AR bank withdrawal, known concentration of boron was added to the moderator from time to time, in order to keep AVZL within operating range during bank calibration. Similarly, when CR banks were calibrated by insertion of the bank, boron was removed from the moderator to prevent reduction of AVZL below normal operating level.

The combined reactivity worth of AR banks 4 and 8 together, CR banks 1 and 2 together and AR bank 4 with CR bank 1 were also measured since withdrawal of two sets of banks together is considered under different LORA scenarios. However static worth measurement of SR banks was not done since it was considered inappropriate to maintain the reactor critical with shutdown system inside the core. The reactivity realized during SDS # 1 and SDS # 2 actuation was measured by performing dynamic tests.

4. Results of calibration:

Since the accurate calibration of ZCCs was the requirement for subsequent calibration of other reactivity devices, calibration of ZCCs was repeated to minimize the possibility of error. The observed slope for the AVZL change was 0.00861 ppm/AVZL (%FL) against the estimated slope of 0.00889 ppm/AVZL (%FL). The calibration curve of AVZL vs boron concentration in moderator is shown in Figure-2.

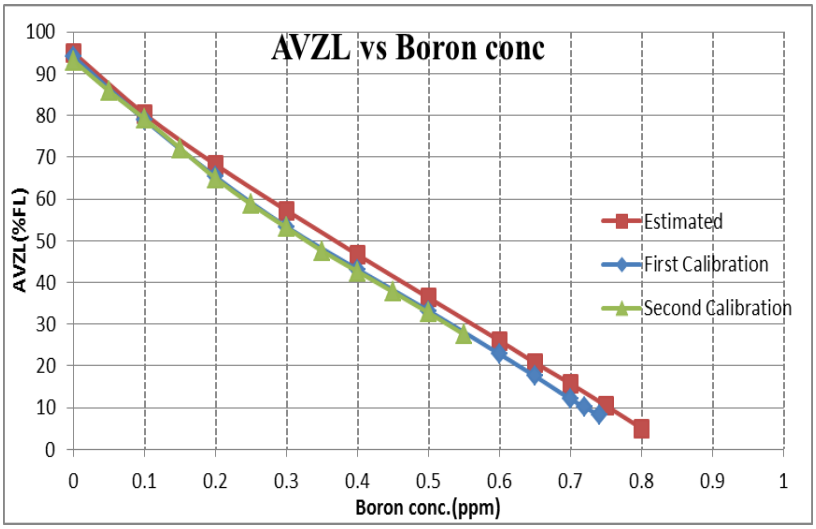


Figure 2: AVZL vs Boron conc. of KAPP-3

The total observed worth of ZCCs (0 to 100 %FL) is 0.861 ppm (6.71 mk) against estimated worth of 0.889 ppm (6.93 mk)

The comparison of estimated and measured worth for the other reactivity devices is shown in the table-2.

Table-2: Results of reactivity device worth measurement in mk

Reactivity Device	Estimated Worth	Measured Worth	Percent deviation $\left(100 \times \frac{(\text{Est}-\text{Obs})}{\text{Est}}\right)$
Individual SRs	0.77-2.25	0.80-2.23	-10.5 to + 9.1
Individual CRs	1.98-1.99	1.98-2.03	-2.5 to +0.5
Individual ARs	0.29-0.69	0.30-0.65	-3.4 to 7.2
AR Bank-1	0.29	0.29	0.0
AR Bank-2	1.03	0.93	+ 9.7
AR Bank-3	0.75	0.69	+ 8.0
AR Bank-4	2.15	1.87	+ 13.0
AR Bank-5	1.07	1.06	+ 0.9
AR Bank-6	1.27	1.12	+11.8
AR Bank-7	1.42	1.31	+ 7.7
AR Bank-8	1.45	1.33	+ 8.3
CR Bank-1	5.13	5.07	+1.2
CR Bank-2	7.26	7.59	-4.5
AR Bank(4&8)	3.49	3.24	+7.2
CR Bank# 1& AR Bank#4	7.18	6.87	+4.3
CR Banks 1&2	12.67	12.9	-1.8

5. Conclusion:

The experimental results for all the tests were found to be in good agreement with theoretical predictions.

6. References

[1] Reactor Physics Design Manual, KAPP-3&4/DM/01100/00001/R0, 2017

[2] Commissioning Report on Low Power Physics experiments (LPPE) Part-A, KAPP3&4/01132/RP/Phase-B /01

Simulation of the Integral Experiments of AHWR Critical Facility with Diffusion based Monte Carlo Method

Argala Srivastava, Deep Bhandari, K. P. Singh and Umasankari Kannan
Bhabha Atomic Research Centre, Mumbai, India
e-mail: - argala@barc.gov.in

Abstract

In the present paper, we discuss the Simulation of Integral Experiment of the AHWR Critical Facility with Diffusion based Monte Carlo method (MC). Diffusion based MC Method is recently developed and is used for the space time simulations in neutron multiplication assemblies. Kinetics simulations are best solved using transport MC route, but this requires long computational time. Diffusion based MC method provides a faster solution in such space-time simulations. As a step towards more detailed benchmarking, the ability and accuracy of this method was tested on recent experiment done in Critical Facility for Advanced Heavy Water Reactor. The integral experiments with one Thoria based MOX experimental cluster in core of AHWR Critical Facility were analyzed with this method and were compared with the observed experimental values. The experiments consisted of measurement of Critical Height and worth of shut off rods with experimental cluster placed at different lattice locations. Neutron count rates as function of time after reactor trip for estimation of worth of shut off rods was also simulated by the time dependent MC algorithm developed recently by us. The estimated values are in good agreement with the experimental results.

1. Introduction

Monte Carlo (MC) calculations are mostly performed by the non analog technique for the purpose of computational efficiency. However, for simulation of noise experiments for measurement of reactor kinetics parameters, the analog MC is more appropriate. Since analog MC is highly computationally time consuming, the concept of the diffusion theory based analog MC technique to reduce the computing time was proposed by Rana and Degweker, 2013 [1]. Rana and Degweker, developed the analytical Green's function approach as well as the finite difference based numerical approach for diffusion theory Monte Carlo. Application of Diffusion based MC has been extended for transient analysis [2] and for the estimation of higher Eigen modes [3]. Besides providing a simple model for testing these ideas regarding Monte Carlo Space Time Kinetics, the diffusion theory MC model permits an exact comparison of the results of MC simulation with the large number of kinetics benchmarks that have been solved using deterministic diffusion theory methods. The aim of this paper is to validate the kinetic MC methods with results from experiments performed in a research facility.

2. Diffusion based MC Method : Methodology

In this method, the finite difference form of the diffusion equation is used to estimate the probabilities of absorption, slowing down or migration to a neighboring mesh. The problem geometry is discretised in rectangular meshes and the neutron history is followed as per the diffusion process across various meshes. Starting from an initial spatial distribution across meshes corresponding to a critical state, the

neutrons are tracked one by one. The diffusion kernel is converted into probabilities per unit time. The probability per unit time for diffusion of the neutrons to the neighboring meshes is given by,

$$P_u = [D_{i,j,k} D_{i,j+1,k} V_g] / [h_j (D_{i,j+1,k} h_i + D_{i,j,k} h_{i+1})], \quad P_d = [D_{i,j,k} D_{i,j-1,k} V_g] / [h_j (D_{i,j-1,k} h_i + D_{i,j,k} h_{i-1})]$$

$$P_r = [D_{i,j,k} D_{i+1,j,k} V_g] / [h_j (D_{i+1,j,k} h_i + D_{i,j,k} h_{i+1})], \quad P_l = [D_{i,j,k} D_{i-1,j,k} V_g] / [h_j (D_{i-1,j,k} h_i + D_{i,j,k} h_{i-1})]$$

$$P_f = [D_{i,j,k} D_{i,j,k+1} V_g] / [h_j (D_{i,j,k+1} h_i + D_{i,j,k} h_{i+1})], \quad P_b = [D_{i,j,k} D_{i,j,k-1} V_g] / [h_j (D_{i,j,k-1} h_i + D_{i,j,k} h_{i-1})]$$

$$P_t = P_u + P_d + P_l + P_r + P_f + P_b + P_a$$

Where, h_i are the mesh widths in the of the i^{th} mesh. V_g is the velocity of the group g. P_u is the probability (per unit time) of the diffusion of the particle in the upper mesh. Similarly, P_d, P_r, P_l, P_f, P_b is the the probability (per unit time) of the diffusion of the particle in the down, right, left, front and back mesh respectively. P_a is the probability (per unit time) of the absorption (more generally removal) of a neutron in the existing mesh and P_t is the total probability per unit time. A neutron for example will undergo absorption in the mesh with probability P_a / P_t. It leaks out if it crosses the geometry domain. The algorithm for the tracking of the neutron in the problem geometry using Finite Diffusion Kernel is: *Divide the problem domain in (i,j,k) meshes. Randomly select the meshes and start tracking the particle with its initial position in the selected mesh. Check for the probability of the particle leaking in the left, right, top, bottom, back, front meshes. If the particle has leaked in any one of the specified meshes move the particle in that mesh and continue the particle tracking. If the specified mesh has vacuum boundary, particle is killed and its tracking is stopped. If the specified mesh has reflective boundary then particle remain in the original mesh and is not leaked. Continue the particle tracking. If the particle has not leaked in any one of the specified meshes, then check for the probability of fission or capture or slowing down of the particle. If the particle is captured, particle is killed and its tracking is stopped. If sampled collision is fission, number of neutrons emitted in this fission is stored in a tally to be used for estimating Keff after all neutron histories are generated .Tracking of neutron is continued in this manner till it gets escaped, captured or undergoes fission.*The algorithm time dependent MC simulation is discussed in detail in Reference [2].

3. AHWR CF : Integral Experiments

AHWR Critical facility (CF) is a heavy water moderated, air cooled, natural uranium fueled vertical reactor. Fuel is in the form of clusters and is arranged in the core in square lattice pattern with lattice pitch of 24.5 cm [4]. The integral experiments at CF were performed by replacing one Nat-U Cluster of the core with the Thoria based MOX experimental cluster. This was done for 6 different core configurations corresponding to the 6 different locations of experimental cluster. These positions correspond to E5, F4, F3, F2, B3 and F1 lattice locations as shown in Figure 1. [4]. The integral experiment consisted of measurement of critical height and worth of 6 SORs for the core with, Thoria based MOX experimental cluster. At first, the experimental cluster was placed at E5 location and critical height measurement experiment was performed. Criticality is achieved by controlling moderator height. The reactor was then shutdown by tripping it manually. The data of count rates as function of time was obtained for estimation of combined worth of 6-SORs. Then the experimental cluster was shifted to other locations (C-4, C-6, E-3, E-7, G-4 and G-6) and critical height was measured.

4. Results and Discussion

10^7 neutrons and 500 neutron histories were considered in the simulation of the Integral experiments of CF. The two group lattice parameters needed for the simulation were generated by using WIMS code. In Table 1, the observed critical heights have been tabulated for the seven different core configurations and are compared with the estimated values by diffusion MC method. These values are also compared with those estimated by 3D space time kinetics Code KINFIN [5]. The critical heights observed experimentally for all the seven configurations are in good agreement with the theoretically estimated values by diffusion MC. The maximum difference is 0.5 cm for the core configuration having experimental cluster at E5 which corresponds to 0.08 mk with the standard deviation of ± 0.0002. Figure 2 gives the comparison of the normalized thermal flux estimated by diffusion based MC and with KINFIN for the experimental cluster placed at E5, locations. The neutron counts with respect to moderator level during approach to criticality for the experimental cluster placed at E5 location was also estimated and was compared with the experimental values. The K-eff values as a function of the moderator height is estimated and is converted into counts by considering the same experimental count at the initial moderator level Figure. 3 shows the variation of the N0/Ni (N0 is the initial count at t=0 sec and Ni is the count varying with time) with moderator level during approach to criticality with experimental cluster placed at E5 location. The trend of observed N0/Ni ratio versus moderator level during approach to criticality, for all the six core configurations, was similar to the estimated trend. Neutron count rates as function of time after reactor trip for estimation of worth of shut off rods was also simulated by applying the time dependent MC algorithm developed recently by us [2]. Figure 4 show the comparison of the change in power with time recorded by the detectors with the estimated values. It is seen that comparison are in good agreement within the standard deviation of ± 0.005.

5. Conclusions

Diffusion based MC Method is a new and unique dynamic Monte Carlo Method which has been developed recently which enables to analyze the static and transient behavior of a nuclear reactor without any approximation to the geometry or any discretisation. To test the ability and accuracy of this method on the practical reactor system, it is applied to the experimental results of Critical Facility for Advanced Heavy Water Reactor. The integral experiments with one Thoria based MOX experimental cluster in the core of AHWR Critical Facility were analyzed with diffusion based Monte Carlo Method and were compared with the observed experimental values. Neutron power as function of time after reactor trip for estimation of worth of shut off rods was also simulated by the time dependent MC algorithm developed recently by us. The observed values and is in good agreement within the standard deviation with the experimental results.

References

1. Y.S.Rana, Arun Singh and S. B. Degweker, 'Diffusion Theory Based Analogue Monte Carlo for Simulating Noise Experiments in Sub-critical Systems', Nuclear Science and Engg., 174, 245 – 263 (2013)
2. Argala Srivastava, K. P. Singh and S. B. Degweker, Nuclear Science and Engineering, "Monte Carlo Methods for Reactor Kinetic Simulations", 2018, *189*, 152-170.
3. Argala Srivastava, Amod Kishore Mallick, K. P. Singh, S. B. Degweker and Umasankari Kannan ,"A Diffusion Monte Carlo Based Algorithm for Estimation of Higher Modes of a Reactor", Nuclear Science and Engineering, 2019, 193, 1044-1053.

4. Deep Bhandari, Rajeev Kumar, Amod Kishore Mallick, Sudipto Samanta and Umasankari Kannan, ' Analysis of the extended core of AHWR-CF and estimation of moderator level coefficient and worth of shut off rod by WIMS-ARCH code', RPDD/EP/181/2019; June 2019.
5. Singh K. P., Modak R. S., Degweker S. B and Singh Kanchi (2009), " Iterative schemes for obtaining dominant alpha modes of the neutron diffusion equation", *Annals of Nuclear Energy*, 36, pg. 1086 (2009).

Table 1 Comparison of the Critical Height of core and SOR worth with Experimental Cluster at different lattice locations

S.No.	Location of the cluster	Calculated Critical Height (cm)		Observed Critical Height (cm)	Calculated SOR Worth (mk)	Observed SOR Worth (mk)
		Diffusion MC	KINFIN		Diffusion MC	
1	E5	234.3	232.8	233.8	108.1	108.3
2	F4	232.9	232.4	232.8	108.2	108.8
3	F3	230.7	230.5	230.3	109.0	109.7
4	F2	227.4	227.4	227.2	112.0	112.2
5	B3	225.0	224.2	224.9	110.0	110.3
6	F1	226.5	226.1	226.1	112.0	111.9

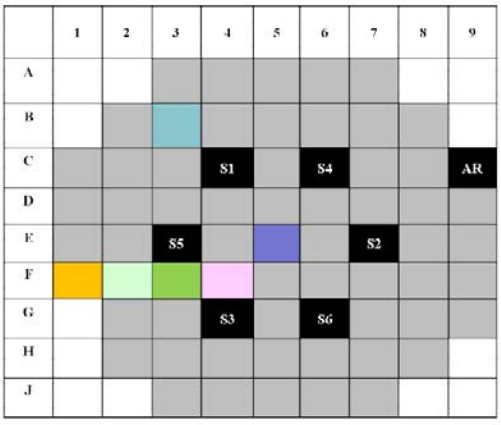


Figure 1 Core Configuration of the Critical Facility core for performing experiments. S1 - S6 are the locations of the shut off rods, AR – Adjuster Rod Colored boxes refer to the locations where the experimental cluster is placed

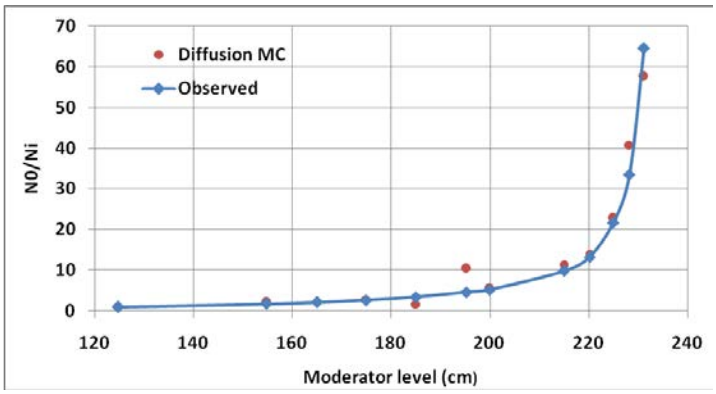


Figure 3 N0/Ni versus Moderator Level

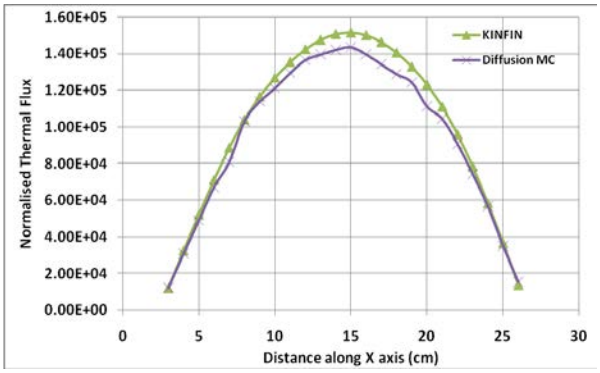


Figure 2 The variation of the normalized thermal flux (n/cm^2/sec). Comparison between values estimated by KINFIN and Diffusion MC

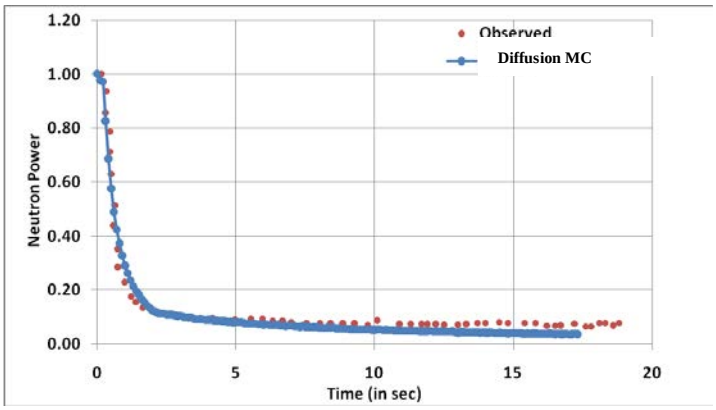


Figure 4 Variation of neutron power with time during reactor trip by SORs

STUDY OF VARIANCE IN THE COUNTING STATISTICS OF RADIATION DETECTORS

D. V. Subramanian, A. John Arul and Adish Haridas
Indira Gandhi Centre for Atomic Research, Kalpakkam, India
[1]*e-mail: - dvs@igcar.gov.in*

Abstract

It is well known that nuclear decay events follow the Poisson process. When radiation detectors are used to record the number of decay events in a given interval of time, the recorded counts usually follow the Poisson distribution. The inherent fluctuations represent an unavoidable source of uncertainty in all nuclear measurements and often can be the predominant source of error. Sometimes, the detectors and associated electronics may introduce additional errors which may lead to deviation from the expected Poisson behavior. This study presents the statistical characterization of counts recorded using HPGE, BGO and CdZnTe detectors with standard gamma reference sources. It is observed that the fractional error (σ / Mean) decreases, as the average counts increase in HPGe and BGO detectors, as expected. In the case of CdZnTe, the observed fractional error is more than that of the other two detectors.

1. Introduction

Radiation refers to the whole electromagnetic spectrum as well as to all atomic and subatomic particles that are emitted during a radioactive decay process. Radiation emission process is statistical in nature. For measuring gamma activity and radiation dose, different types of γ – ray detectors are used. High Purity Germanium (HPGE), Sodium Iodide (NaI), Bismuth Germanate (BGO), LanthanamBromde (LaBr) and Cadmium Zinc Telluride (CdZnTe) are some of the most frequently used γ – ray detectors. During measurements the radiation energy is deposited in a detector and gives rise to an electrical pulse which in turn measured as counts.

Due to the statistical nature of incident radiation, there exist fluctuations in the measured counts. A study is performed with radiation detectors to characterize the fluctuations in the measured counts and hence the variance in the counting statistics of the detectors. For this study, three detectors viz., HPGE, BGO and CdZnTe are considered. Among these HPGE and CdZnTe are semiconductor detectors and BGO is a scintillator [1]. Standard gamma reference sources are used to measure counts for a specified time. Experimental data is acquired, for different the counting times and for different the source positions with respect to each detector. After collecting the data, the experimental mean and the sample variance are computed. The values are compared among three detectors to find how the detectors vary in the above mentioned properties.

2. Counting statistics

When radiation detectors are used for radiation measurement they are subject to some degree of statistical fluctuations because radioactive decay is a random process [2]. When the term counting statistics is considered, it includes the framework of statistical analysis required to process the results of nuclear counting experiments and to make predictions about the expected precision of quantities derived from these measurements.

The value of counting statistics is used in one way to check on the normal functioning of radiation counting equipment. In another way it deals with the situation in which we have only one measurement. After collecting experimental data by using the detectors, any set of data can be completely described by its frequency distribution function F(x). Two properties of this frequency distribution function are of particular interest are the experimental mean and the sample variance.

The experimental mean is given by equation 1

$$\bar{x}_e \equiv \frac{1}{N}\sum_i x_i \tag{1}$$

Where, N is the number of observations. The experimental mean is the value about which the distribution is centered.

The sample variance is provided by equation 2

$$s^2 = \frac{1}{N-1}\sum_{i=1}^{N}(x_i - \overline{x_e})^2 \tag{2}$$

Where N is the number of observations, $x_i$is each data point and $\bar{x}_e$is the experimental mean. The sample variance is a measure of the width of the distribution or the amount of internal fluctuation in the data. For a Poisson process, the variance must be equal to the mean. In this study the ratio of the sample variance to mean (sample fractional error) is compared to the theoretically expected fractional error.

3. Detector specifications and details of measurements

The following Table 1 provides the specifications of 3 different detectors used for acquiring the gamma spectrum of standard sources.

Table 1: Detector specifications

Parameters	HPGE	BGO	CdZnTe (newly developed)	CdZnTe (commercially available)
Type	P-type Coaxial	Scintillation	Planar	Quasi hemisphere
Band gap (eV)	0.67 (at 77 K)	10	1.57	1.57
Ion-pair creation energy (eV)	2.96	> 60	4.64	4.64
Resolution (%)	0.7% at 122 keV	11% at 662 keV	6-8%	2%
Bias (V)	+2000	+790	+350	+1000
Energy range (keV)	40-3000	40-3000	<100	40-3000
Size (mm)	Dia-56, Ht-55.9	Dia-120, Ht-100	7x 5 x 0.25	10x10x5

HPGE detector used is a 30% (relative efficient) detector. It is DSG make detector used for gamma spectrum acquisition in the Health Physics lab. BGO is a large volume detector (size 120mm x 100mm) used for simultaneous acquisition of betas and gammas in decay heat measurements. It is a SCIONIX make detector in the Activation Analysis lab of KAMINI reactor. CdZnTe is newly grown semiconductor detector of Material Science Group. At present it is in development stage and used for measuring gamma energies less than 100 keV. Apart from that one set of readings are obtained from commercially available CdZnTe detector used for measuring Pu gamma energies of PFBR core Sub Assemblies.

During measurements Cs-137 gamma source is used with BGO detector and spectrum is acquired for two times. During the first occasion the source is placed close to the detector (~ 1 mm) and spectrum is acquired for different timings. For each time ten spectrums are collected. In the second occasion, the source is kept at different distances from detector surface. For each distance ten spectrums are collected. The same measurement procedure is followed with HPGE detector also. The only difference is the use of Co-60 gamma source for spectrum acquisition for different timings. With CdZnTe one set of measurements are taken for different distances with Am-241 source. All the detectors are used on different dates for measurements. The gross counts in the source peak of interest for ten times, their Mean, Poisson 1σ, 1σ / Mean, Standard Deviation (SD) and SD / Mean are computed.

4. Discussions

In case of both BGO and HPGE, the measurements are carried out with respect to various timings and various distances. But in case of CdZnTe the measurements are performed with respect to distance only. The values, 1σ / Mean known as T-FE (Theoretical Fractional Error) & Standard Deviation / Mean known as S-FE (Sample Fractional Error) are plotted against average counts for different counting times and different distances for BGO are shown in figures 1A and 1B. Similar plots are made for HPGE and CdZnTe. They are show in figures 2A & 2B and 3A & 3B. For each plot maximum ratio of S-FE to T-FE are also found.

BGO graphs

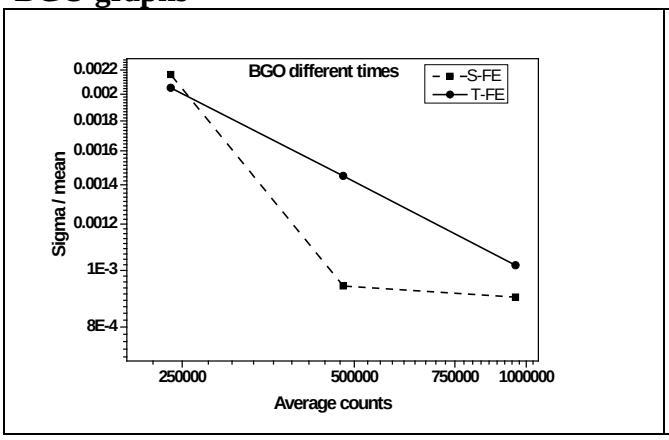


Figure 1A: In BGO at different counting times

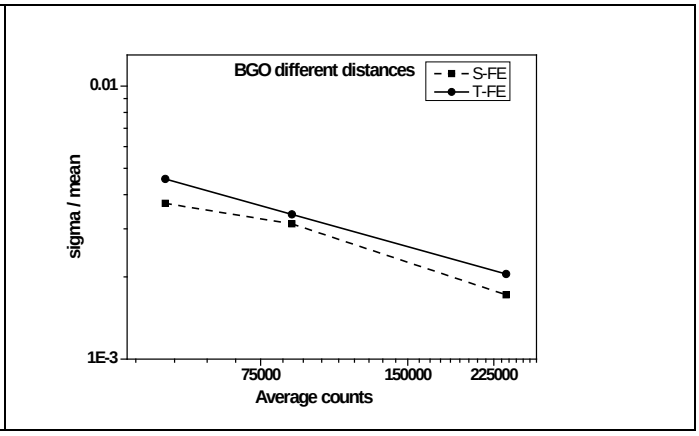


Figure 1B: In BGO at different distances

HPGE graphs

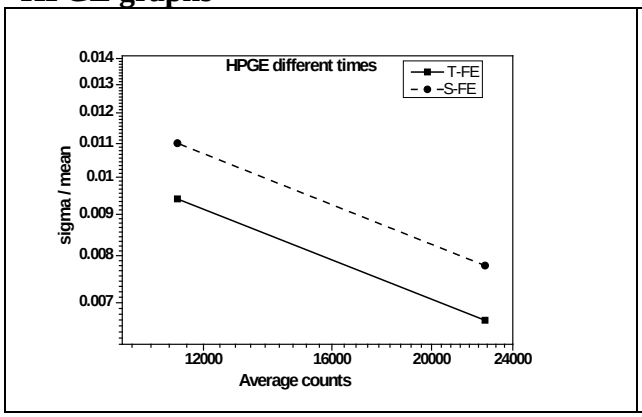


Figure 2A: In HPGE at different counting times

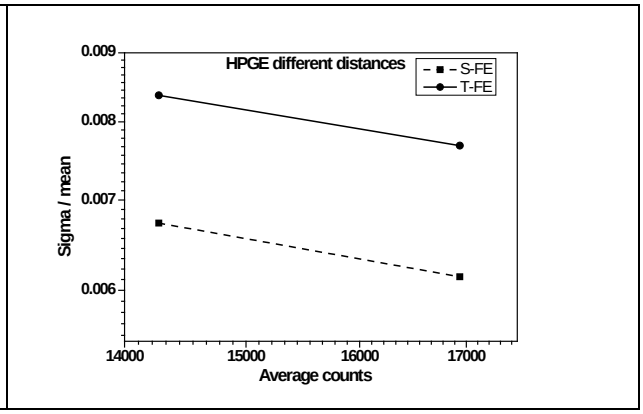


Figure 2B: In HPGE at different distances

CdZnTe graphs

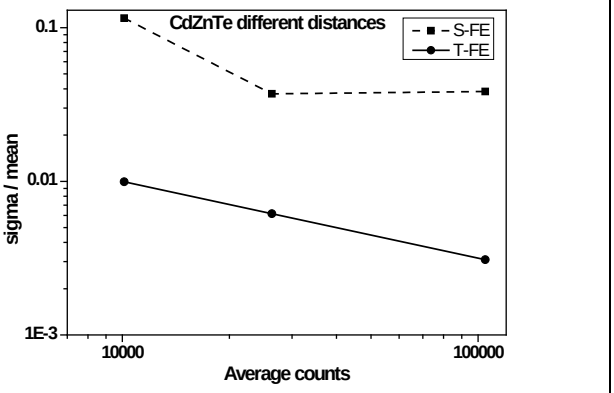


Figure 3A: In CdZnTe at different distances with single source (Am-241)

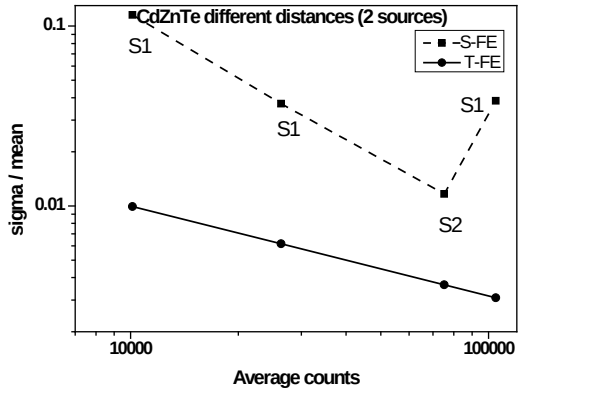


Figure 3B: In CdZnTe at different distances with 2 sources (Am-241 & Pu isotopes)

With BGO, only Cs-137 source of strength 26.7 kBq is used. Two different sources of different strengths are used while measuring with HPGE and CdZnTe. While with HPGE Co-60 source of strength 5.8 kBq as well as Cs-137 are used. Am-241 and PFBR core Sub Assembly are used as sources while using CdZnTe. It is observed that the values T-FE decreases as the average counts increases. It is seen in all detectors. But the values S-FE don't follow the same trend. It depends on the fluctuations in the observed gross counts of the detectors. Electronic noise and lower readings may also be reasons. For CdZnTe the values of standard deviation (S.D) are generally much higher than other two detectors. The maximum ratio of S-FE to T-FE in case of BGO is found to be 0.648 and in case of HPGE, it is found to be 0.799. It is found to be 12.42 in case of CdZnTe.

5. Conclusion

The objective of the study is to characterize the fluctuations in the observed counts of CdZnTe by comparing it with other 2 types of radiation detectors such as BGO and HPGE. It is observed that for CdZnTe, the Standard Deviation is generally more than other two detectors. CdZnTe is observed to give maximum ratio for S-FE to T-FE. The cause for the higher ratio in case of CdZnTe is being studied.

6. References

[1] Gordon Gilmore, "Practical Gamma-ray Spectrometry", 2nd ed., John Wiley & Sons Ltd, 2008.

[2] Glenn F.Knoll,"Radiation detection and measurement", 4th ed., John Wiley & Sons Ltd, 2010.

PERFORMANCE TESTING OF NEW MODIFIED CRITICALITY ACCIDENT DOSIMETER BADGE USING AHWR CRITICAL FACILITY

Deepa Sathian[1,3], A.K. Bakshi[1,3], Umasankari Kannan[2,3], B.K. Sapra[1,3]

[1]Radiological Physics and Advisory Division, [2]Reactor Physics and Design Division,
[3]Homi Bhabha National Institute, Anushaktinagar, Mumbai-94, India
Bhabha Atomic Research Centre, Mumbai, 400094,
e-mail: - deeps@barc.gov.in

Abstract

A new modified criticality accident dosimeter (CAD) badge has been developed for more accurate neutron and gamma dose measurements. Study has been carried out for testing this badge at the neutron spectrum of advanced heavy water reactor (AHWR) critical facility, BARC. The induced activities were measured with calibrated n-type HPGe gamma spectrometer. The spacial distribution of total thermal neutron fluence rates were measured with bare gold, copper, indium foils of CAD badge at 100 W reactor power at the D-9 location. The maximum thermal neutron equivalent fluence rate was found to be (1.92±0.004) x 10^8 n cm^{-2} s^{-1} and corresponding dose rate as 144 mGy h^{-1} respectively. Fast neutron fluence rates were found to be below detectable limit at this location.

1. Introduction

A criticality accident is an unplanned or uncontrolled nuclear excursion resulting from the inadvertent assembly of a quantity of fissile material in a physical geometry such that the configuration is capable of supporting a nuclear chain reaction [1]. This excursion could involve fissile material only or it could include the fissile material in close proximity to hydrogenous material. Where the fissile materials are being processed in quantities exceeding the minimum critical amounts, an extremely high radiation risk to workers can arise from the possibility of a criticality excursion. Such possibilities could exist in nuclear fuel processing plants, fuel storage facilities, critical experimental facilities or experimental research reactors and power reactors. A new modified criticality accident dosimeter has been developed with various activation foils and TLDs for more reliable measurements of neutron and gamma dose. The Criticality Accident Dosimeter (CAD) badge is worn at the chest level by personnel working in nuclear fuel reprocessing plants, fuel storage facilities, experimental nuclear reactors and other areas where there are possibilities of accidental criticality. These badges can be used during special operations such as fuel handling at power reactors. They may also be used as “area monitors” by mounting them at strategic locations in the vicinity of interest. However, they have been designed specifically to act as accidental dosimeters and are not practical for estimating personnel doses incurred during normal operations. The initial testing of this newly developed CAD badge has been carried out in the thermal neutron spectrum at D-9 location of AHWR critical facility, BARC.

2. Materials and Methods

2.1 The Dosimetry System

The new modified criticality accident dosimetry system consists of activation foils of gold, copper, indium, rhodium, iron, sulphur, nickel, magnesium and aluminium for neutron dose estimation and ^{7}LiF:Mg:Ti (TLD-700) ^{6}LiF:Mg:Ti (TLD-600) discs for gamma-neutron dose measurements. Bare and Cd covered gold, copper and indium foils are used for thermal and intermediate energy neutrons. Indium is used as exposure indicator, and along with rhodium, iron, sulphur, nickel, magnesium and aluminium is used for fast neutron measurements. The characteristics of these detectors are given in Table-1. The foils are permanently sealed in a plastic badge holder of dimensions 8 cm (L) x 5 cm (W) x 0.8 cm (thickness). Each dosimeter badge has a permanent identification number printed on it. The modified CAD badge along with the arrangement of the detectors and TLD discs is shown in Fig.1 and Fig. 2

Table-1 Characteristics of Activation Detectors used in the Criticality Accident Dosimeter (CAD) Badge

Activation Foils	Nuclear Reaction	Cross-section	Half-life	Neutron Energy Interval
Gold	^{197}Au (n,γ)^{198} Au	98.6 b	2.7 d	Thermal neutrons (<0.4 eV)
Copper	^{63}Cu (n,γ)^{64}Cu	4.5 b	12.7 h	
Indium	^{115}In(n,γ)^{116}In	166 b	54 min	
Gold (Cd)	^{197}Au (n,γ)^{198} Au	1560 b (RI)	2.7 d	Epi-thermal & Intermediate neutrons (0.4 eV – 100 keV)
Copper (Cd)	^{63}Cu (n,γ)^{64}Cu	5.6 b (RI)	12.7 h	
Indium (Cd)	^{115}In(n,γ)^{116}In	3243 b (RI)	54 min	
Rhodium	^{103}Rh (n, n')^{103}Rh^{m}	733 mb	57 min	Fast neutrons >0.75 MeV
Indium	^{115}In(n,n')^{115m}In	188 mb	4.5 h	Fast neutrons >1.2 MeV
Sulphur	^{32}S(n,p)^{32}P	65 mb	14.3 d	Fast neutrons >2.9 MeV
Iron	^{54}Fe(n,p)^{54}Mn.	78 mb	312.13 d	Fast neutrons >3.1 MeV
Nickel	^{58}Ni(n,p)^{58m}Co	113 mb	72 d	Fast neutrons >3.8 MeV
Iron	^{56}Fe(n,p)^{56}Mn.	1.05 mb	2.57 h	Fast neutrons >6.0 MeV
Magnesium	^{24}Mg(n,p)^{24}Na	1.52 mb	15 h	Fast neutrons >6.8 MeV
Aluminium	^{27}Al(n,α)^{24}Na	0.693 mb	15 h	Fast neutrons >7.2 MeV
Copper	^{63}Cu (n,2n)^{62}Cu	0.092 mb	9.78 min	Fast neutrons >12.4 MeV



Figure 1 Modified CAD Badge- Front & Back side

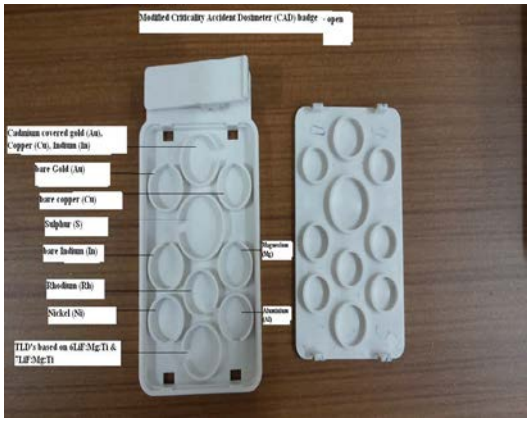


Figure 2 Modified CAD Badge open

2.2 The Method of Neutron Flux and Dose calculation

The activation method for measuring thermal and fast neutron distributions is convenient when a sensitive, compact detector is required. Activation detectors are widely used for flux and spectrum measurements in intense neutron fields. The activation method of neutron detection is based on the fact that many elements become radioactive when exposed to a neutron flux. The build-up to saturation activity and the decay to zero activity follow an exponential law. The procedure involves exposing the sample serving as neutron detector to the neutron flux for a measured length of time 't' and then removing it to a counting position and counting its induced radioactivity beginning at a time 't_1' and ending at time 't_2' measured from the end of the exposure. The total no. of counts during the interval from 't_1' to 't_2' is first corrected for background. The net number of counts, C, is then reduced to the counting rate which would have been obtained right at the end of exposure, if exposure had been carried to saturation. This particular counting rate will be called $C_{0\ sat}$, the initial saturation counting rate [2]. Then

$$C_{0\ sat} = \frac{C}{\tau\,(e^{-t1/\tau} - e^{-t2/\tau})\,(1 - e^{-t/\tau})} \qquad \text{---------- (1)}$$

where ' τ' is the mean life time of the activity and is equal to T/0.693, is the natural logarithm of 2. From the activity, the neutron fluence rate is measured using the formula

$$\phi = \frac{A\ (Bq/gm)}{N\sigma\,(1-e^{-\lambda ti})} \qquad \text{---------- (2)}$$

[3] Where, ϕ = Neutron fluence rate in n cm^{-2} s^{-1}, A =Removal Specific activity of the foil in Bq g^{-1}, σ = Reaction cross-section in cm^2, t_i = Time of irradiation, N= No. of atoms/g. From the fluence rate, the dose rate is calculated using appropriate fluence to absorbed dose equivalent conversion factor [1].

3. Experiment

A study has been carried out for testing the new modified criticality accident dosimeter (CAD) badge at advanced heavy water reactor (AHWR) critical facility, BARC. For this purpose, two modified CAD badges were irradiated for 2 h in the D-9 location of the critical facility at a reactor power of 100 W. The badges were processed after 1 h cooling time and foils of the badges were counted on a calibrated HPGe gamma ray spectrometer. It was observed that, out of the various activation foils [Au, Cu, In, Rh, Fe, Ni, Mg, Al, S] in the CAD badge, only gold, copper and indium were activated due to the thermalization of fission neutrons of the reactor core initially with D_2O moderator and further with graphite blocks present at the D-9 location. The nuclear reactions involved in the measurements were: $^{197}Au(n,\gamma)^{198}Au$, $^{63}Cu(n,\gamma)^{64}Cu$ and $^{115}In(n,\gamma)^{116m}In$. Induced activity and neutron fluence rates were calculated using the efficiency of the gamma peak, isotopic abundance of the foil, gamma radiation abundance, cross section of the foil element, weight of the foil, irradiation time and decay time. The thermal neutron dose-rates were calculated using the corresponding absorbed dose conversion factor.

4. Results and Discussion

Table-2 presents the thermal equivalent fluence rate and dose rate measured by bare Au, Cu and In foils at D-9 position of AHWR at 100 W reactor power. The variation in fluence-rate with respect to these foils is attributed to the spacial distribution of foils in the badge and difference in cross-section variation of foils for the thermal neutron spectrum at D-9. The fluence-rate variation with respect to the badges may be due to the change in the position of two badges during their simultaneous irradiation.

Table-2: Results of thermal neutron fluence-rate and dose-rate at the D-9 location of AHWR critical facility at 100 W reactor power using criticality accident dosimeter (CAD) badge

Location in the Reactor	Criticality Badge Name	Sample Name	Total Thermal Neutron Fluence-rate (Westcott) n cm^{-2} s^{-1}	Total Thermal Neutron Dose-rate mGy h^{-1}
D-9	CAD Badge-1	Au (bare)-1	(1.77±0.01) x 10^8	132.5
		Cu (bare)-1	(1.36±0.01) x 10^8	102.0
		In (bare)-1	(0.98±0.01) x 10^8	73.5
	CAD Badge-2	Au (bare)-2	(1.92±0.004) x 10^8	144.0
		Cu (bare)-2	(1.39±0.02) x 10^8	104.0
		In (bare)-2	(1.16±0.006) x 10^8	87.0

4. Conclusion

The spacial distribution of total thermal neutron fluence rate equivalent at D-9 location of AHWR critical facility at 100 W reactor power was evaluated from CAD Badge-1 and CAD Badge-2 using Au, Cu, In bare foils. The maximum thermal neutron dose-rate was evaluated as 144 mGy h^{-1} with bare gold foil of CAD badge.

5. References

[1] TRS-211, *"Dosimetry for Criticality Accidents"*, IAEA, Vienna, (1982), p177-178.

[2] Beckurts K. H. and Wirtz K., *Neutron Physics*, (1964), p.298-301.

[3] Deepa Sathian et.al, "Streaming Neutron Measurements in Indian Research Reactors using Activation Detectors", *Radiation Protection and Environment*, Vol.33, No. 1-2, (2010), p44-47.

A study of alpha-induced pre-equilibrium neutron emission in natural Titanium

Gokul Das H[1*], M M Musthafa[1], Midhun C V[1] , Swapna B[1], Vafiya T[1], Najmunnisa T[1], F S Shana[2], Rijin N T[3], S Dasgupta[4], J Datta[4], S Ganesan[5], S V Suryanarayana[6,7]

[1] Department of Physics , University of Calicut, Calicut University P O , 673635

[2]Govt. Arts and Science College, Meenchanda, Kozhikode ,

[3]Department of Physics , Jain University, Banglore , 560069,

[4] Analytical Chemistry Division, BARC, VECC Kolkata, 700064

[5]Formerly Raja Ramanna Fellow of DAE, BARC, Mumbai, 400085

[6]Nuclear Physics Division, BARC, Mumbai, 40085

[7]Manipal Centre for Natural Sciences, MAHE,Manipal 576104

(corresponding author e-mail: - gokulphysikss@gmail.com)*

Abstract

Alpha particles are formed inside the reactor environment through the neutron induced fission, spontaneous decay of heavy elements or neutron-induced reactions on structural materials. These alpha particles can further produce neutrons through (a,xn) reactions on structural materials inside the reactor, leading to the excess yield of neutrons. Hence the study of (a,xn) reaction cross sections on reactor structural materials is important to account for these secondary neutrons produced. In this work ^{nat}Ti(a,x)^{51}Cr reactions have been subjected to study.

1. Introduction

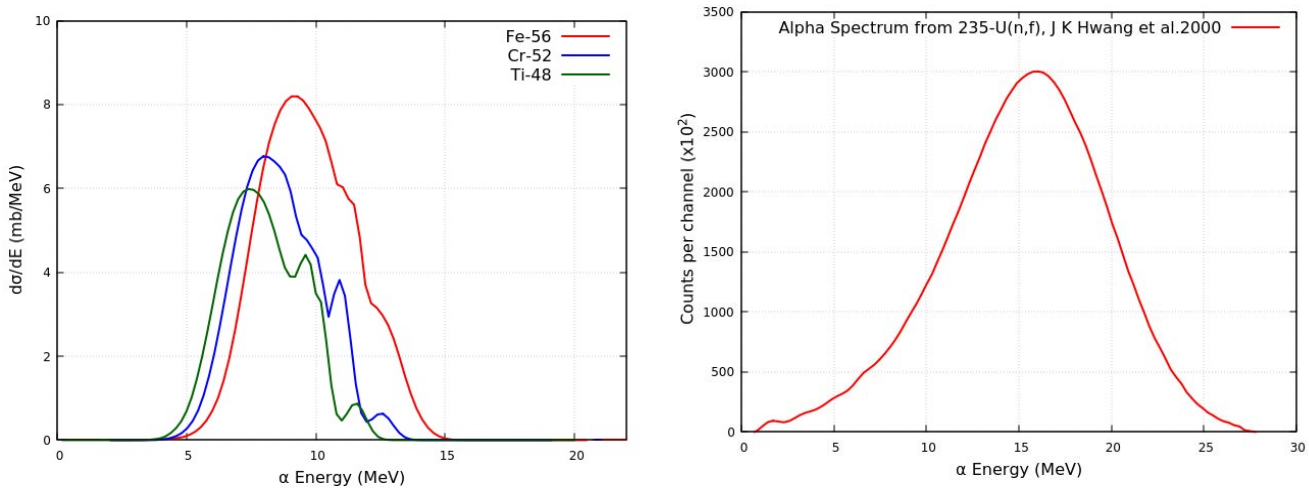
There are different pathways for the formation of alpha particles inside the reactor. Alphas produced directly out of ternary fission can have energies up to ~30-35 MeV [7] and can lead to a significant amount of secondary reaction channels. Another mode of formation of alpha particles inside the reactor is through (n,a) reactions from structural materials of the reactor. The reactor structural materials, under the constant exposure to the high energy, high intensity neutron flux yield alpha particles. Alpha particles, thus formed, can have energies as high as 15 MeV or more depending upon the incident neutron energy. These alpha particles usually get trapped inside the structural materials as Helium bubbles and cause serious structural damages to the reactor. Further, some short-lived isotopes of polonium and astatine formed from the decay chains of Uranium, Plutonium, Actinium etc., can yield alpha particles with energies up to 9 MeV[1]. These excess alphas may generate excess neutrons following various pathways. These excess neutrons produced by alpha induced reactions from all materials in a reactor may be important when considered for neutron balance equations. Hence the study of high energy alpha-induced reactions and corresponding neutron yields are of importance in fission and fusion reactor designs. Titanium is one of the major neutron facing structural material in fission and fusion reactors. In this work, ^{nat}Ti(a,x)^{51}Cr reactions are focused with a special interest.

2. High energy alpha production inside the reactors

High energy alpha particles are produced as the result of ternary fission inside the reactor environment. The alpha energy through this mode can go as high as ~30-35 MeV[7]. High energy alpha particles are produced, through the (n,xa) channels also, in the structural materials of the reactor. In nuclear fusion reactors, D-T fusion yields neutrons [2] around 14.1 MeV energy. In fission reactors, the energies of prompt fission neutron are represented by various distributions which approximately follow a Maxwell-Boltzmann distribution from 0-20 MeV with the most probable distribution around 2-3 MeV energy range[3][4]. Charged particles such as alphas and protons will be created by these fast neutrons.

Also, these charged particles can cause further neutron yielding reactions on their interactions with reactor structural materials. Thus produced neutron spectrum will be different from the

fission neutron spectrum. In order to account for this additional neutron flux contribution in Monte Carlo transport calculations, the reaction cross sections for these (a,xn) channels has to be calculated accurately. Neutron-induced alpha spectrum for some of the important structural materials at 14 MeV neutron energy is calculated with the help of TALYS 1.95 [5]code (figure-1) and it shows that the alpha energy can vary up to 15 MeV and in some cases, can go upto ~20 MeV. Hence the study of (a,n) excitation functions at high alpha incident energies is important. In order to account for the neutrons arising from the alpha induced reactions precisely, the alpha spectrum in the reactor environment has to be obtained accurately.



(a) (b)

Figure1:(a) Alpha spectrum with incident neutron energy 14 MeV calculated using TALYS 1.95 (b) Alpha spectrum from 235-U(n,f) from J.K Hwang et al.[7]

3. Experimental Details and Data Analysis

The raw experimental cross-section data available for ^{48}Ti(a,n) in the IAEA-EXFOR [8] library is compared with the cross-sections available in basic evaluated nuclear data library TENDL-2019 [9] (figure-2). It is clear that, the evaluated data is in good agreement with the experimental data at lower alpha incident energies (below 14 MeV), but under predicts the experimental data when the alpha incident energy gets higher(above 14 MeV). We are therefore motivated to study ^{nat}Ti(a,x)^{51}Cr residual cross section in which ^{48}Ti(a,n) is the prominent channel (figure 3). The experiment was performed at K-130 Cyclotron facility at VECC Kolkata employing stacked foil activation technique. The stacks were irradiated, for ~ 5 hours, by alpha beams of energies 21.3 and 28.6 MeV at ~130 pnA alpha beam current. The thickness of the natural titanium foil was ~ 10 micrometers. The energy reductions of the projectile on different foils were calculated with the help of SRIM[10] code. ^{nat}Ti(a,xn) yields ^{51}Cr residue having a half-life of 27.7025(24) days.
The characteristic gammas from the residue ^{51}Cr in the irradiated foils were measured using the HPGE detector (CANBERRA) and the spectrum was analysed using CANDLE[11] software. The cross-section was calculated using the basic activation equation,

$$\sigma = \frac{C\,\lambda}{\varepsilon\, I\, N\, \varphi \left(1 - e^{-\lambda t_{irrad}}\right)\left(1 - e^{-\lambda t_{count}}\right) e^{-\lambda t_{cool}}}$$

where C is the count, $\lambda$is the decay constant, I is the branching ratio of the particular gamma ray, $\varepsilon$is the full photo-peak efficiency, N the number of target atoms, φ is the incident flux, t_{irr}, t_{count} , t_{cool} are the irradiation, counting and cooling time respectively[6].

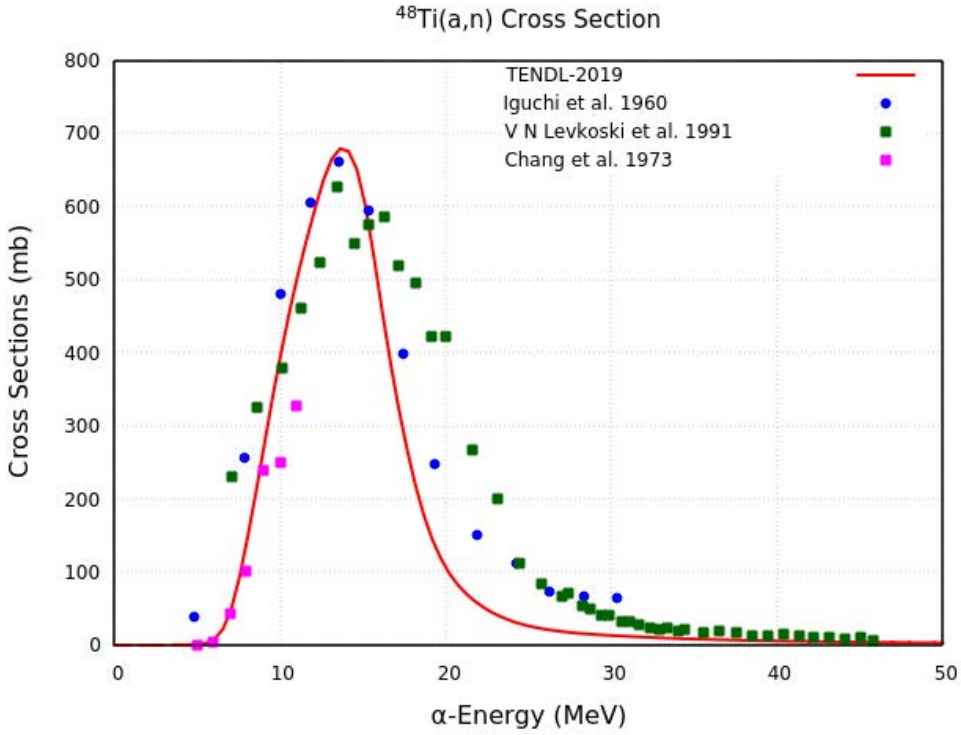


Figure 2 : Comparison of the available EXFOR data for $^{48}Ti(a,n)$ with the basic evaluated nuclear data library TENDL 2019

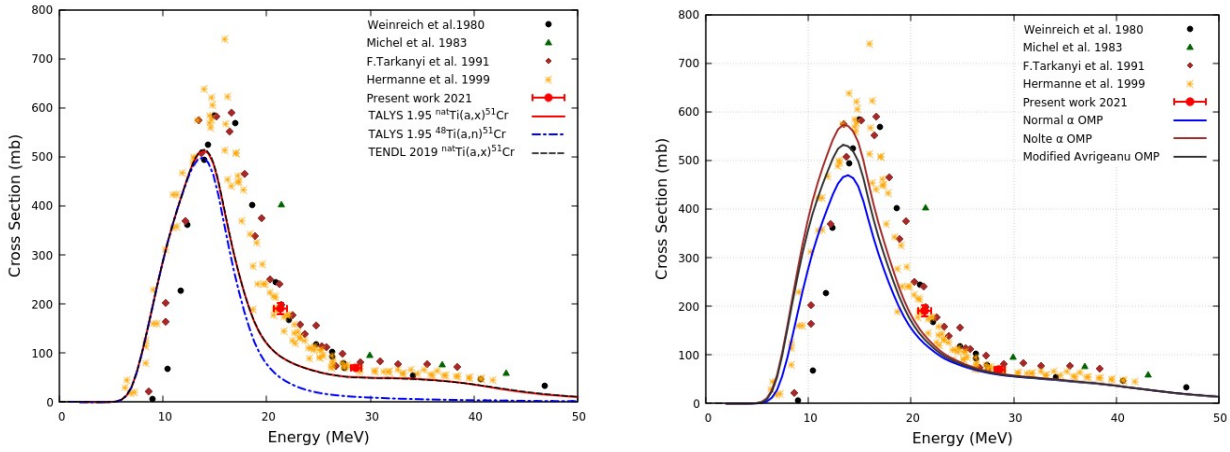


Figure 3: (a) Excitation function of $^{nat}Ti(a,x)^{51}Cr$ obtained experimentally with contribution from $^{48}Ti(a,n)$, $^{49}Ti(a,2n)$ and $^{50}Ti(a,3n)$ channels calculated using TALYS 1.95. (b) $^{nat}Ti(a,x)$ ^{51}Cr experimental data with different alpha Optical Potentials

Different alpha optical model potentials hardwired in TALYS 1.95 code were used in the attempt to optimise the experimental data obtained (figure 3 (b)).

3. Result and Discussion

The experimentally obtained ^{nat}Ti(a,x) ^{51}Cr cross-section shows a good agreement with the previous experimental data available in IAEA EXFOR. Theoretical calculations, carried out using TALYS-1.95 code show good agreement with the experimental data at lower-alpha incident energies but under predict the cross-section at higher alpha energies. Different alpha optical models hardwired in TALYS 1.95 code was used to optimise the data and the discrepancy was solved up to some

extent, but not satisfactorily. This indicates a higher per-equilibrium component in the neutron emission and has to be properly accounted for in the model calculations.

4.Conclusion

In the reactor environment, high energy, high-intensity neutron flux can generate alpha particles of energy up to ~ 35 MeV. These alpha particles can generate secondary neutrons inside the reactor through the (a,xn) channels. The cross-section data of the nuclear reaction $^{nat}Ti(a,x)^{51}Cr$ are experimentally measured using the stack foil activation method and are compared with the theoretical simulations from TALYS 1.95. The presently measured experimental data are in general agreement with the previously reported experimental data available in the IAEA EXFOR library. At the pre-equilibrium region(~15 MeV to above) the excitation function continues to exhibit a discrepancy between the theoretical calculation and experimental measurement, where the former under predicts the latter. Hence, there is a need to revisit the pre-equilibrium component in the model calculations.

6. Acknowledgment

Authors acknowledge the financial support provided by DAE-BRNS under research project, Sanction Order 36(6)/14/30/2017-BRNS/36204. We are thankful to Dr. Chandana Bhattacharya, Experimental Nuclear Physics Division , VECC and A A Mallick ACD, BARC, VECC, Kolkata and all K-130 Cyclotron facility staff for their huge support.

7. Reference

[1] S.P Simakov and Q.Y van den Berg, “Update of the a-n Yields for Reactor Fuel Materials for the Interest of Nuclear Safeguards,” *Nuclear Data Sheets 139*, (2017), Page 190

[2] R. A. FORREST, “Data Requirements for Neutron Activation Part I : Cross-Sections,” *Fusion Eng. Des.*, 81, (2006), Page 2143

[3] Catherine Romano and David Brown et al., “The (a,n) nuclear data scoping study,” *Oak Ridge University Public Release*, 2020 Sep. 5

[4] Trkov, Andre, and Brown, David A, “*ENDF-6 Formats Manual: Data Formats and Procedures for the Evaluated Nuclear Data Files”*, United States: N. p., 2018. Web. doi:10.2172/1425114.

[5] Koning A, S. Hilaire, and S. Goriely, "*User Manual of Talys-1.95, 20121*," 2021 Dec. 30

[6] Gordon Gilmore, “Practical Gamma Ray Spectrometry- 2nd Edition,” J*ohn Wiley & Son’s Limited*, ISBN: 978-0-470-86196-7, 2008

[7] J K Hwang and A V Ramayya, “He^5 Ternary fission yields of ^{252}Cf and $^{235}U(n,f)$,” *Physical Review C, Volume 61, 047601*, 2000 March 15

[8] N Otuka and E Dupont et al., “Towards a More Complete and Accurate Experimental Nuclear Reaction Data Library (EXFOR): International Collaboration Between Nuclear Reaction Data Centres (NRDC),” *Nuclear Data Sheets, Volume 120*, 2014 June, Page 272

[9] A.J. Koning and D.Rochman, "TENDL: Complete Nuclear Data Library for Innovative Nuclear Science and Technology," *Nuclear Data Sheets Volume 155*, 2019, Page 1

[10] Ziegler, James F., Matthias D. Ziegler, and Jochen P. Biersack, "SRIM–The stopping and range of ions in matter (2010)," *Nuclear Instruments and Methods in Physics Research Section B: Beam Interactions with Materials and Atoms 268.11-12* (2010): Page 1818

[11] Ajith Kumar B P and E T Subramaniam et al., “High Speed Distributed Data Acquisition System,” *DAE Proceedings Vol.44B*, 2001, Page 390

DESIGN OF A SHORT BEAM TUBE FOR NEUTRON TOF FACILITY BASED ON 30MEV ELECTRON ACCELERATOR

Kapil Deo and Umasankari Kannan
Reactor Physics Design Division, Bhabha Atomic Research Centre, Mumbai, India
e-mail: - kapil@barc.gov.in

Abstract

The measurements in neutron Time-of-Facilities (n-TOF) have been instrumental in having a better understanding of nuclear data important to various field of sciences. Using n-TOF neutron induced cross-sections can be measured for a large range of energies in a single experiment. A neutron time of flight (n-TOF) facility based on 30 MeV electron LINAC has been proposed by BARC. Design of a short beam tube for the same is presented in this paper. The neutron transport through the beam tube was simulated using the monte carlo code, Fluka.

1. Introduction

The neutron Time-of-flight (n-TOF) facility has unique significance in field of nuclear physics, astrophysics and reactor physics. In a n-TOF, neutron pulse is allowed to travel down a beam tube. As they travel down the tube, the neutrons get separated in time. The arrival time of neutrons in the experimental area is related to its initial speed. The nTOF facility can provide neutron energies from a few meV to several MeV to study neutron-nucleus cross-section relevant for both basic and applied sciences. The nTOF facility is very much required for frontier research in nuclear physics, astrophysics and also for the measurement of the precision cross section relevant to applied sciences such as reactor physics and medical isotope production. This is a powerful tool for transmission experiments, capture reaction, fission, elastic and inelastic cross-sections.

A neutron time of flight (n-TOF) facility based on 30 MeV electron LINAC has been proposed. The neutrons are to be produced through (γ, n) reaction using Ta or other heavy targets. Assuming a thick Ta target, it is expected to have ~5E+11 neutrons/kW/s at the production target. The neutron beam from the production target will be collimated to three beam lines. Each beam line is proposed to have a dedicated experimental area.

In the present work, a preliminary design of the shortest beam tube (length ~ 10 m) has been worked out. Section 2 of the paper describes the design of the beam tube. Section 3 describes the neutron transport simulations across the beam tube. The monte carlo code, Fluka, has been used for the simulations.

2. Description of beam tube design

A. Beam tube layout

As mentioned in the previous section, the neutrons are produced by interaction of accelerated electrons with thick Ta target. The beam tubes carrying the neutron current to the experimental area passes through a thick Pb shielding. A suitable layout for beam exit through the shield wall thickness was to be arrived at from the proposed design of the target hall [2]. The beam-tube layout discussed in this report is based on the following dimensions:

1. Distance of nTOF target from shield wall – 1500 mm
2. Thickness of shield wall – 3200 mm
3. Angle between the beam tubes 20^{o}.
4. Inner Width of the plug in shielding wall (through which beam tubes will emerge) = 1893 mm

5. Outer Width of the plug in shielding wall (through which beam tubes will emerge) = 3421 mm

Based on these dimensions, a layout of beam tubes from target hall to experimental area was worked out. The objective in planning the layout was to maximize the beam tube diameter in the available space. The maximum diameter of the beam tube, that could be achieved, is 20 cm. Fig. 1 gives an overview of the beam tube layout.

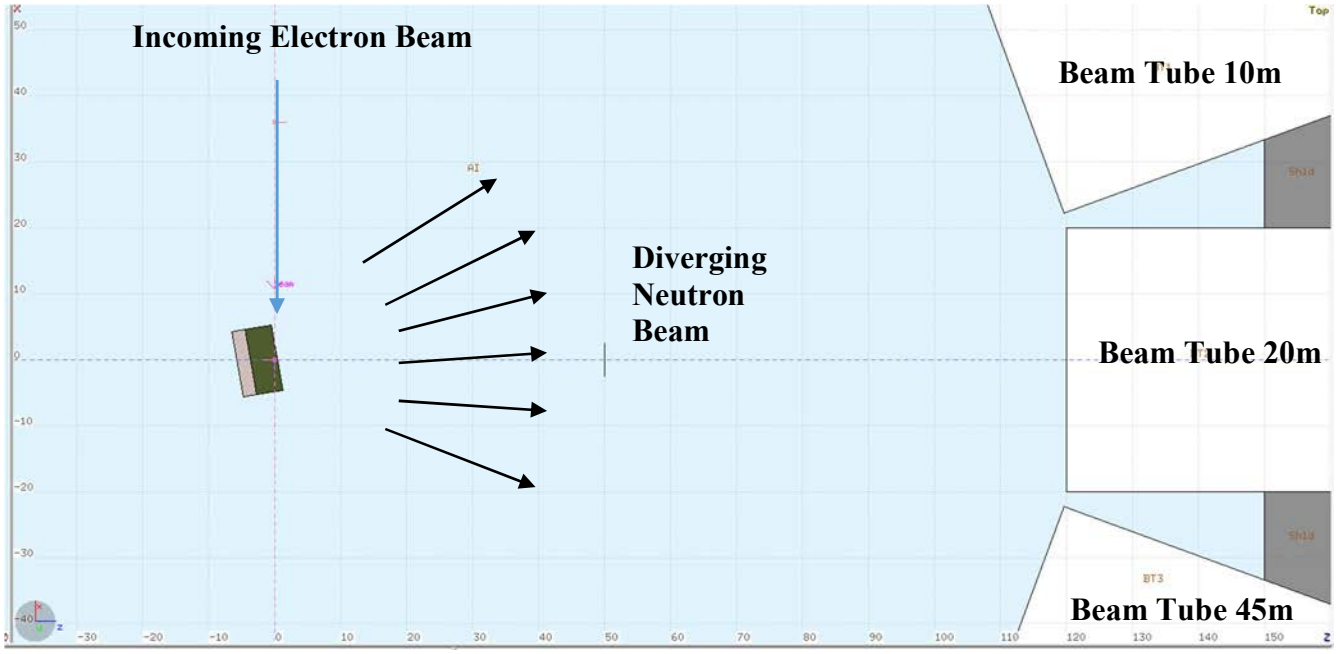


Fig. 1 Overview of the beam tubes layout in the proposed n-TOF

B. Components of 10 m Beam Tube

The proposed neutron time-of-flight facility will have three beam tubes of varying beam tube lengths. Basic objective in a beam tube design for neutron cross section should be to maximize neutron flux and minimize gamma flux in the experimental area. Based on the beam tube design of CERN nTOF EAR 2 [3], a preliminary beam tube design for 10 m flight path has been arrived at. The major beam tube components can be broadly outlined as follows:

1. Shielding near the source end – This is meant for minimising the gamma rays inside the beam tube and also to minimise the neutron and gamma field outside the beam tube.
2. Filter Station - A provision has to be made to install a filter material of choice in the beamline.
3. Collimators - The main purpose of a collimator is to achieve a parallel beam of neutrons. One collimator is placed near the source end of the tube and another is placed near the target end.
4. Beam Dump - This lies beyond the experimental area and serves as final point of dissipation of beam energy. This also ensures that there is minimum scattering back of neutrons in experimental area.

The beam dump design and source shielding design are external to beam tube and they are not discussed here. The source end collimator consists of a cylindrical tube of Fe having 45 cm radius and 100 cm length. The collimator at the detector end is more complex. It is divided in two portions. The first portion has three pieces of Fe tube (60 cm, 70 cm and 70 cm) having radii 35

cm, 32 cm and 28 cm. The second portion consists of 6 pieces of polyethylene tube (total length 1 m) having inner radius such that the final beam tube radius is 10 cm. The last four polyethylene pieces further has B_4C core (of funnel shape). At the end of second collimator a 20 cm thick lead shield (having a 10 cm opening) is placed. For the present calculation, Outer Beam tube shielding is assumed to be of concrete. Both the collimators are contained inside the 10 m length beam tube which is itself made up of stainless steel. An outline of the beam tube is shown in Fig. 2.

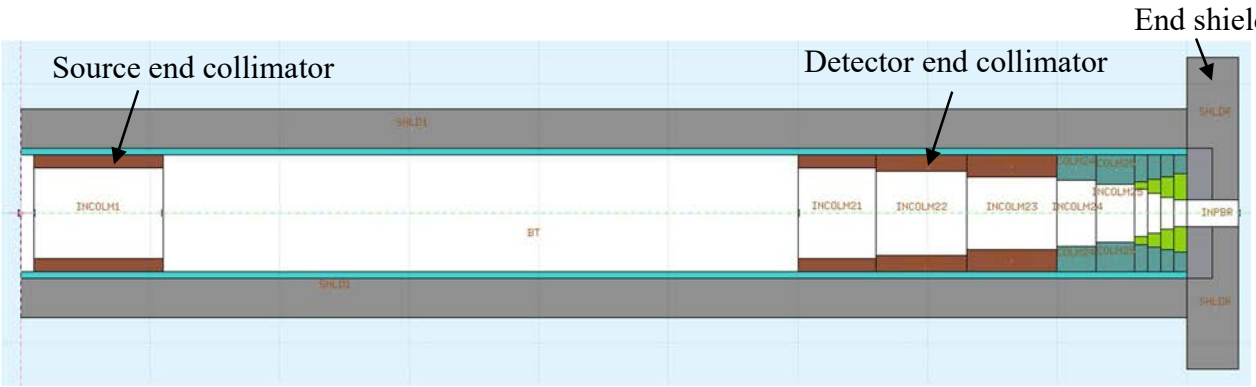


Fig. 2: Components of 10 m beam tube (Unmoderated case)

3. Results and Discussions

For simulation of the neutron transport inside the beam tube 30 MeV electron striking a Ta target was taken as the source of neutrons. The neutron transport simulation of the source neutrons across the beam tube layout was carried out using the monte carlo code Fluka [4]. The beam tubes are simply assumed to be consisting of vacuum and there is no collimator/support for the tubes, in these simulations. For neutron production, a cylindrical target of length 10 cm and dia 4 cm was placed near origin, such that the axis of the cylinder makes an angle of 10° with the direction of incoming electron beam. A 2 cm dia Be tube (acting as reflector of neutrons) is placed on the rear side of the target. Fig. 3 shows the neutron spectrum obtained at 50 cm away from the target. A flux level of the order of 1.0E-8 per electron at the exit end of 10 m flight path was obtained.

Further, separate Fluka simulations were carried out for studying collimation properties of the 10 m beam tube design. The simulation was carried for both cases of unmoderated and moderated source neutrons. For the moderated case, a 3 cm layer of light water was placed before the beam tube entrance. The total source neutron fluence in unmoderated case was 4.21E-05 ($n/cm^2/e^-$) and for the moderated case it was 4.82E-6 ($n/cm^2/e^-$). The emergent neutron fluence in the unmoderated case was 9.06E-10 ($n/cm^2/e^-$) and in the moderated case it was 9.82E-10 ($n/cm^2/e^-$). However, it may be noted that sufficient statistics could not be achieved in many of the neutron groups at emergent side. The design will be further optimised for choice of materials and dimensions of different components.

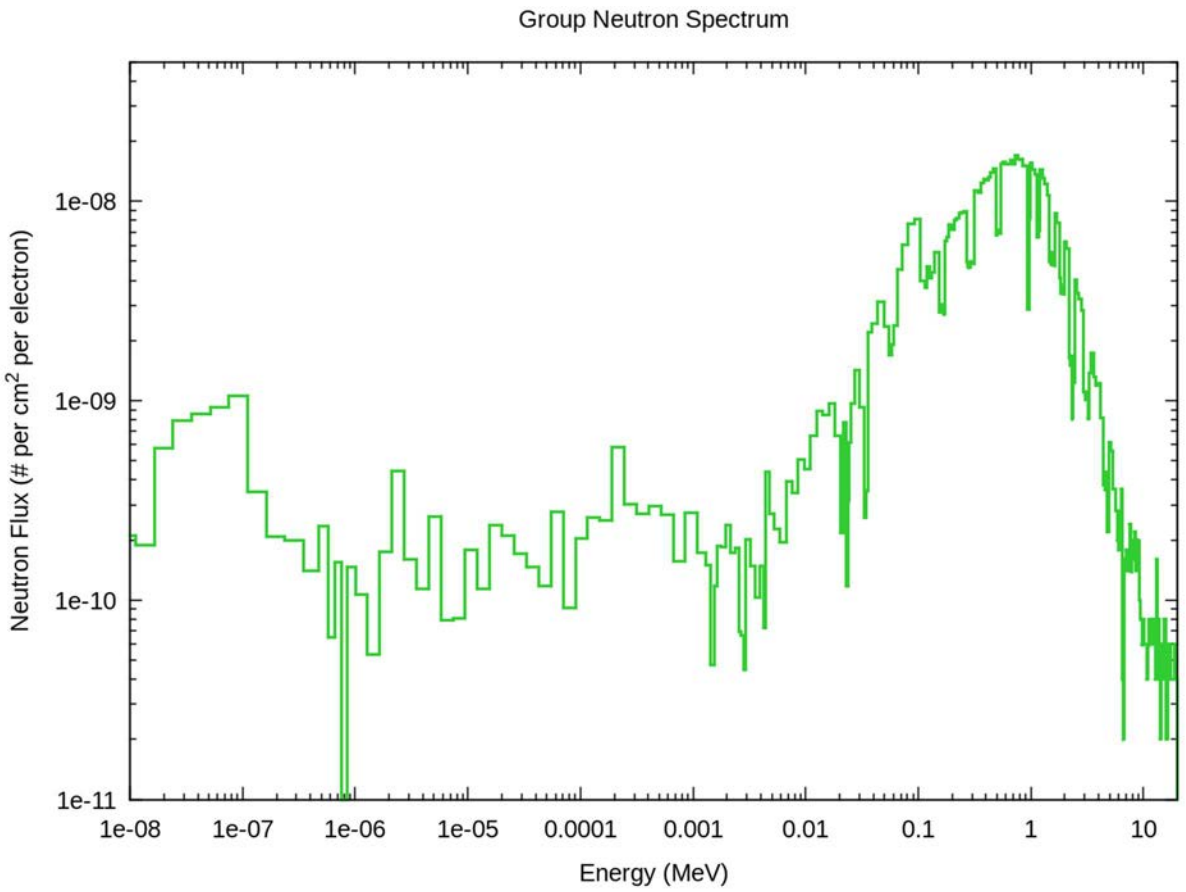


Fig. 3 Group neutron spectrum at 50 cm from the Ta target

4. Conclusion

For a proposed n-TOF facility, a layout for three beam tubes was worked out. For the shortest of the three beam tube (10 m length), the collimating units were also designed. Neutron transport through the overall beam tube layout and the 10 m beam tube, was separately studied. The montecarlo particle transport code Fluka was used for these studies. The emergent neutron flux in the experimental area seems to be sufficient for carrying out different experiments.

5. References

1. Private commncation, Dr. Asavari. Proposed nTOF target hall layout
3. C. Weiss et. al., "The new vertical neutron beam line at the CERN n_TOF facility design and outlook on the performance", The new vertical neutron beam line at the CERN n_TOF facility design and outlook on the performance, *NIMA 799 (2015) 90–98*
4. T.T. Bohlen, F. Cerutti, M.P.W. Chin, A. Fasso`, A. Ferrari, P.G. Ortega, A. Mairani, P.R. Sala, G. Smirnov, and V. Vlachoudis, "The FLUKA Code: Developments and Challenges for High Energy and Medical Applications", *Nuclear Data Sheets 120, 211-214 (2014)*

Monte Carlo Characterization of Neutron Spectrum at Irradiation Locations of APSARA-U Reactor

Amod Kishore Mallick[1,2], Rajeev Kumar[1,2] and Umasankari Kannan[1,2]
[1] Bhabha Atomic Research Centre, Mumbai, India
[2] Homi Bhabha National Institute, Mumbai, India
[1]*e-mail: - amod@barc.gov.in*

Abstract

A new indigenous research reactor named APSARA-U has recently been commissioned for isotope production and for many other R&D activities using neutron source. D5, G4, and H7 are three major (lattice) locations of core, meant for irradiation. The knowledge of characteristic of the neutron spectrum at these locations is therefore very important. We have simulated full APSARA-U reactor core using indigenous Monte Carlo code PATMOC to characterize neutron spectrum at these irradiation locations. Additionally, the neutron flux in different energy regions and neutron spectrum shaping factor (α) have also been computed. This paper presents results of this study, which may help in better planning of the irradiation experiments, carried out at these locations.

1. Introduction

A new research reactor, named APSARA-U [1], has recently been commissioned in Bhabha Atomic Research Centre. This reactor is meant for isotope production and scientific research using its neutron beam lines. A new experimental research reactor needs to be characterized experimentally to validate its suitability for different kinds of applications, it has been designed for. Experiments have been done for this characterization, and more are being planned. In this regard, it is being proposed to characterize neutron spectrum experimentally at various locations in the core.

Ideally speaking, in thermal nuclear reactor, neutron spectrum has Maxwellian type distribution in the thermal energy region, Watt type spectrum in the fast region, and the neutron flux vary as inversely proportional to neutron energy in the in-between energy region. The fraction of neutrons in these energy regions vary from one reactor type to another, and for one location to other in the same reactor. Thermal-to-epithermal flux ratio (f) is one such characterizing parameter of a spectrum which signifies the ratio of fraction of neutrons in the thermal region to that in the rest of energy region. The other important parameter is α and is described below.

The notion that neutron flux is inversely proportional to the neutron energy, that is $\varphi(E) / 1=E$, in the energy region between thermal and fast is based on various theoretical considerations. In practical situations, theoretical considerations used are almost never satisfied. Accordingly, the deviation from the $1/E$ distribution is expected. The actual spectrum is of the form $1/E^{(1+\alpha)}$, with α being 0 for the ideal case. The different locations of a reactor may have different neutron spectrum with different value of α. α thus gives the quantitative information about the extent of neutron thermalization. A negative value indicates under-thermalization and positive value over-thermlaization, with more the positive value more is the thermalization. The value of α is necessary input in activation analysis and measurement of resonance integral of the nuclides.

D5, G4, and H7 are the three major irradiation locations inside APSARA-U core. For these

locations, we have done Monte Carlo study of the neutron spectrum characteristics. We have used our own indigenous Monte Carlo code PATMOC [2, 3] to simulate Apsara-U full reactor. The estimates of f and α were derived from the computed neutron spectrum. The neutron flux in different energy regions have also been obtained from the spectrum. This paper gives the details of these simulations and the results obtained.

2. APSARA-U Reactor

APSARA-U is a pool type reactor with core made up of an array of 8 x 8 square lattices having 7.97 cm pitch. The central 4 x 4 lattice locations contain the active reactor core. All other lattice locations are occupied by solid BeO reflector blocks, special BeO blocks with provision for isotope irradiation, fission counter, thermocouple, and a Fine Control Rod. Out of these 16 active core lattice locations, 15 are meant for loading fuel assemblies, and the remaining one is occupied by Hollow Beryllium Plug (HBP) and act as an irradiation facility. There are two different kinds of fuel assemblies, namely Standard Fuel Assembly (SFA) and Control Fuel Assembly (CFA). Out of the 15 lattice locations for fuel assemblies, 11 are meant for SFAs and 4 for CFAs. If any of the fuel lattice location is not occupied by fuel assembly, then it is occupied with dummy fuel assembly made up of aluminum. The schematic layout of the current core configuration is given in Figure 1.

The fuel assembly is made up of fuel plates containing uranium silicide dispersed in aluminum matrix (U_3Si_2 - Al_x). The uranium used is LEU with 17% (w/w) U-235 enrichment. SFA is made up of 17 such fuel plates, whereas CFA is made up of 12 fuel plates. The fuel plates of SFA and CFA are identical in all respect. CFA also contains Hafnium based control/shutoff plates other than fuel. CFAs at lattice locations at C-4 and F-5 are meant to act as Shutoff devices, while two other at lattice locations D-6 and E-3 are meant to act as control-cum-shutoff devices.

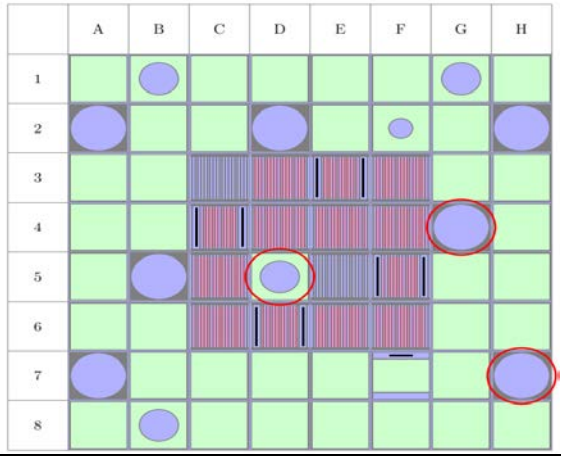


Figure-2: APSARA-U reactor core with lattice locations highlighted where neutron spectrum characteristics are investigated

3. Details of Monte Carlo Simulation

Some information regarding the Monte Carlo code and the model and parameters used in these simulations may be desired here. About PATMOC, this is an indigenous multi-group Monte Carlo code

for neutron transport simulations. Code supports both eigen (criticality) and source mode simulations, and can be used to compute k-eff and various tallies like flux and different reaction rates. It uses Constructive Solid Geometry (CSG) techniques and can model complex geometry such as full reactor core. It uses WIMSD format multi-group nuclear data library [4] for the practical simulation. The code has been verified and validated against numerous benchmarks including OECD/NEA benchmarks like VVER, C5G7, and existing reactor such as AHWR-CF. With these features, the code is now being used regularly for various reactor physics studies

The Apsara-U reactor was modelled in full detail for this simulations taking into consideration of all geometrical details of core. The core configuration used for the current simulation is shown in the Figure 1. The simulations were carried out to compute the neutron spectrum at axially middle at the three lattice locations, namely D5, G4, and H7. We have used surface flux tallies at these locations to compute neutron spectrum. We have numerically estimated the value of α from the computed spectrum. The resonance energy region of the computed neutron spectrum was fitted with the expected form i.e. $\varphi(E) = 1/E^{(1+\alpha)}$ to obtain the value of α. The ENDF-B/VII.1 69-group WIMSD library was used for these simulations for which the resonance energy region falls between 4.0 eV to 9.118 KeV.

4. Results

The results of Monte Carlo simulation are presented here. Table 1 gives total flux, f ($\varphi_{th}/\varphi_{epi}$), the thermal to epithermal flux ratio and Cadmium ratio of Au at the three irradiation locations. The flux value given here is the normalized value per neutron simulated. Total fission reaction rate of the core for the same (i.e per simulated neutron) is 0.416/s. Using this as the scaling factor, we can compute the flux at appropriate power (number of fission/s in the core) of reactor. Table 2 gives the comparison of fraction of flux in different energy regions. We can clearly see that H7 has more thermal neutrons than that at G4 which has more than that at D5. This is as per the expectation since D5 is inside the active core, G4 is just outside the active core, and H7 is the farthest from the active core among these. We have also estimated the alpha value by appropriate curve fitting of the computed 69 group neutron spectrum. The neutron spectrum and curve fitting is shown in Figure 2 and the obtained alpha values are listed in Table 3.

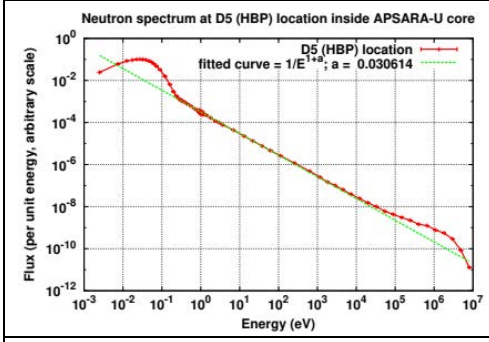
Table-1: **Estimated values of total flux, f ($\varphi_{th}/\varphi_{epi}$, 0.5 eV thermal cut-off) and Cadmium ratio for various locations**

Location	Flux*	f ($\varphi_{th}/\varphi_{epi}$)	Cadmium ratio
D5	9.446e-04 ± 0.3%	1.2403 ± 0.0063	2.4668 ± 0.0396
G4	6.527e-04 ± 0.3%	1.6130 ± 0.0098	2.8847 ± 0.0574
H7	1.398e-04 ± 0.6%	4.3661 ± 0.0730	4.6536 ± 0.2605

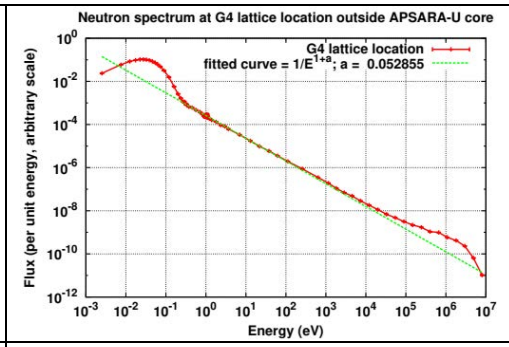
*: This corresponds to flux per neutron simulated for which there are 0.416 fission reactions in the core per second.

Table-2: Estimated fraction (%) of neutron flux in different energy regions for various locations (Maximum uncertainty is < 1%)

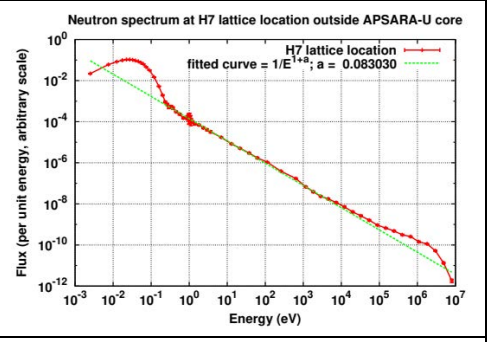
Energy region	D5	G4	H7
10 MeV < E ≤ 0.821 MeV	11.0	9.6	3.1
0.821 MeV < E ≤ 0.50 eV	33.6	28.7	15.5
0.50 eV < E ≤ 0 eV	55.4	61.7	81.4
All energy (0 - 10 MeV)	100.0	100.0	100.0



(a) D5



(b) G4



(c) H7

Figure-2: Neutron spectrum and curve fitting to obtain the estimate of alpha for different locations

Table-3: Estimated values of alpha for various locations	
Location	**alpha**
D5	0.0306142 ± 0.00503 (16.4%)
G4	0.0528553 ± 0.00893 (16.9%)
H7	0.0830295 ± 0.02034 (24.5%)

5. Conclusion

An indigenous multi-group Monte Carlo code PATMOC was used to study the characteristics of neutron spectrum at three major irradiation locations (D5, G4, and H7) of Apsara-U reactor. The full energy range neutron spectrum was estimated and parameters such f (thermal to epithermal flux ratio), Cadmium ratio, spectrum shaping factor (alpha), were derived from it. We can see that the estimated value of alpha increases as we move away from the core center, and this is as per the expectation. The Monte Carlo results presented in this paper would be of great help in planning the experiments at these locations.

6. References

[1] T. Singh, P. Pandey, T. Mazumdar, K. Singh, and V. Raina, “Physics design of 2MW upgraded Apsara research reactor”, *Annals of Nuclear Energy*, vol. 60, (2013).

[2] Amod Kishore Mallick and Umasankari Kannan, “PATMOC: A Multi-group Monte Carlo code for Neutron Transport Simulation”, RPDD/EP/164 (2018).

[3] Amod Kishore Mallick and Anurag Gupta, “Sub-Space Iteration Based Monte Carlo Scheme for Simultaneous Computation of Multiple Dominant k-eigenmodes and Acceleration of Fission Source Iterations”, Annals of Nuclear Energy, 166 (2022).

[4] Leszczynski, F., Aldama, D.L., Trkov, A., “WIMS-D library update”. Technical report, International Atomic Energy Agency, (2007).

Measurement of Neutron Flux Profile at Apsara-U for the Study of Neutron Transmutation Doping in Silicon

Amod Kishore Mallick[1,2], Rajeev Kumar[1,2], Sudipta Samanta[1], Deep Bhandari[1], Kapil Deo[1], Umasankari Kannan[1,2], Tej Sigh[1], Sajin Prasad S.[1] and Ranjit Sharma[1]

[1] Bhabha Atomic Research Centre, Mumbai, India
[2] Homi Bhabha National Institute, Mumbai, India
[1]*e-mail: - amod@barc.gov.in*

Abstract

There is a plan to have a Neutron Transmutation Doping (NTD) facility in Apsara-U reactor. As part of the feasibility study, a Silicon ingot was placed at the periphery of the core for measurement of uniformity and other characteristics of neutron flux over its surface. Large number of activation monitors was used on the surface of Si ingot to measure the thermal flux profile along the surface and other neutron spectrum characteristics. This paper discusses the measurement of neutron flux and its results.

1. Introduction

Semiconductor doping is required for manufacturing of electronics devices. Neutron Transmutation Doping (NTD) is a doping technique which uses thermal neutron flux and is in use for doping in Silicon. When Silicon is irradiated in thermal neutron flux, Si-30, which is around 3% in the natural Silicon, absorbs neutron and forms Si-31 which is radioactive. It decays by beta emission forming P-31 atom acting as dope in Silicon. Doping using NTD is especially useful when precise and high uniformity in doping is required.

It is being planned to have a Neutron Transmutation Doping (NTD) facility in Apsara-U reactor for doping in Silicon. The uniformity in doping is very much depended on the uniformity of thermal neutron flux on the surface of ingot being doped. As part of the feasibility study, a Silicon ingot was placed at the required location in the periphery of the core for measurement of uniformity and other characteristics of flux over its surface. The activation monitors were used for these measurements. This paper gives the details of experimental arrangements and the results of measurement.

2. APSARA-U Reactor and Experimental Arrangement

APSARA-U [1] is a pool type reactor with core made up of an array of 8 x 8 square lattices having 7.97 cm pitch. The central 4 x 4 lattice locations contain the active reactor core. All other lattice locations are occupied by solid BeO reflector blocks, special BeO blocks with provision for isotope irradiation, fission counter, thermocouple, and a Fine Control Rod. Out of these 16 active core lattice locations, 15 are meant for loading fuel assemblies, and the remaining one is occupied by Hollow Beryllium Plug (HBP) and act as an irradiation facility. There are two different kinds of fuel assemblies, namely Standard Fuel Assembly (SFA) and Control Fuel Assembly (CFA). Out of the 15 lattice locations for fuel assemblies, 11 are meant for SFAs and 4 for CFAs. SFA is made up of 17 such fuel plates, whereas CFA is made up of 12 fuel plates. The fuel plates of SFA and CFA are identical in all respect. CFA also contains Hafnium based control/shutoff plates other than fuel. CFAs at lattice locations at C-

4 and F-5 are meant to act as Shutoff devices, while two other at lattice locations D-6 and E-3 are meant to act as control-cum-shutoff devices. The schematic layout of the core configuration is given in Figure 1.

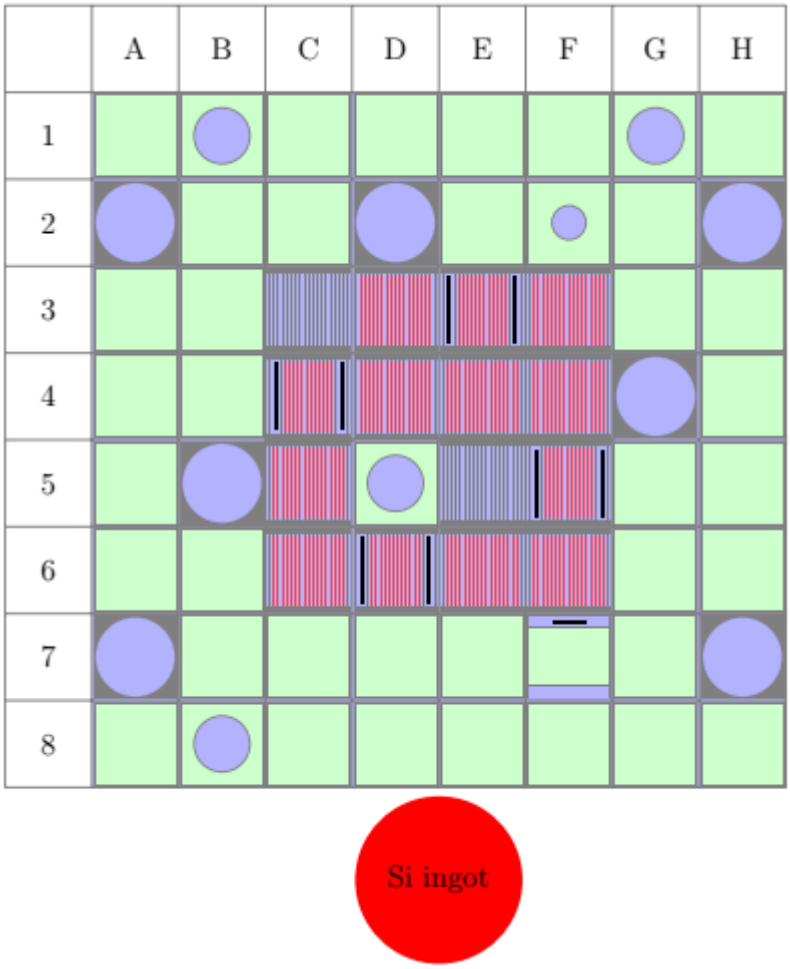


Figure-1: APSARA-U reactor core with location of Silicon Ingot on which flux profile measurement was carried out

A Silicon ingot is in the shape of a cylinder of diameter of 15 cm and length of about 28 cm was placed just outside the core in axially middle of the core as shown in Figure 1. The experimental measurement was required to know the flux variation on the surface of this ingot. To estimate the neutron flux profile on the surface of Silicon ingot, 32 Gold (Au) foils were used. The bare Au foils with no 1 to 11 were placed axially on the front-side (facing the reactor core) of the ingot, and foil no 12-22 were placed corresponding locations on diametrically opposite (facing away from the core) side of the ingot. Foils from 1 to 11 (and correspondingly 12 to 24) were placed from top to bottom on the ingot. Taking distance from the top of ingot, foils 1 to 11 were placed at these distances respectively: 0, 2, 4, 6, 10, 14, 18, 22, 24, 26, and 28 cm.

Three bare foils (Nos. 25-27) were placed on the top surface and three more (Nos. 28-30) on bottom surface at the corresponding locations. These foils were placed on the diameter joining the position of foils placed on front and back side of Si ingot. Foil 26 (and correspondingly 29) was placed at the center of top (bottom) surface with 25 and 27 (28 and 30) at equal distance of 3.75 cm in opposite

directions. Foil 25 (28) is nearer to front side and 27 (30) nearer to back side. Additionally, two pair of foils, with each pair containing a bare and a cadmium-covered gold flux monitor were kept for measuring absolute thermal flux value. One pair was kept on the front side and another on back side near the top elevation of Si ingot. To reduce interference from Cadmium, the bare and cadmium covered foils (of a pair) was put on symmetrically sideways. The bare foil was put 4 cm away (sideway) in one direction and Cadmium covered foil at 4 cm away in opposite direction.

The silicon ingot along with the flux monitors were irradiated at 600 KW reactor power for 30 minutes. The flux monitors were retrieved after sufficient cooling. The induced gamma activity in gold foils was counted using High Purity Germanium (HPGe) gamma detector [2]. Gamma counts of 411 KeV energy form active gold samples were taken for data analysis. The reaction rates per atom obtained from the measured activity were used to get the flux profile variation along the surface of Si ingot [3].

3. Results

We present here the measured profile of Au-197(n,γ) reaction rates along the surface of Si ingot. Table-1 shows the axial variation of Au reaction rate on the Si ingot, in both the front and back side. We can see that the reaction rate does not vary much axially implying uniformity of flux. Axially along the surface, the ratio of maximum to minimum of the reaction is 1.23 and 1.29 on front and back sides respectively. Also, the reaction rates at the back side are almost half of that at the corresponding location on front side showing the attenuation of flux. Table-2 gives the variation of Au reaction rates along the diameter of the Si ingot on top and bottom surface. Table-3 gives the thermal flux and the Cadmium ratio on the front and back side of the Silicon Ingot. It is clear from this table the high level of thermalization as Cadmium ration is very high, 11 and 32 on front and back side. The value of thermal flux is of the order of 10^{11} n/cm2/sec at the ingot location for the 600KW power of the reactor.

Table-1: Axial variation of measured Au(n,γ) reaction rate

Distance from the top elevation (cm)	Reaction rate (< ±5%) (per sec per atom)	
	Front	**Back**
0	7.05E-11	3.21E-11
2	6.67E-11	3.39E-11
4	6.76E-11	3.68E-11
6	6.60E-11	3.78E-11
10	6.85E-11	4.02E-11
14	6.89E-11	4.07E-11
18	7.06E-11	4.15E-11
22	7.15E-11	4.00E-11
24	7.30E-11	3.85E-11
26	7.41E-11	3.72E-11
28	8.13E-11	3.37E-11

Table-2: Measured Au-197(n,γ) **Reaction rate on top and bottom**				
S.N.	Top surface		Bottom surface	
	Gold foil id	Reaction rate **(< ±5%)** (per sec per atom)	Gold foil id	Reaction rate **(< ±5%)** (per sec per atom)
1	25 (front)	4.71E-11	28 (front)	5.90E-11
2	26 (middle)	4.04E-11	29 (middle)	4.26E-11
3	27 (back)	3.54E-11	30 (back)	4.08E-11

Table-3: Measured Cadmium ratio		
Position	Cadmium ratio	Thermal flux **(< ±5%)** (E < 0.5 eV)
Front	11.0	5.48E+11
Back	32.2	3.37E+11

4. Conclusion

Experimental measurements have been done to assess the neutron flux uniformity on the cylindrical Si ingot surface placed just outside the core of the Apsara-U reactor as part of NTD feasibility study. It was observed that axially along the surface, the ratio of maximum to minimum of the reaction is 1.23 and 1.29 on front and back sides of the ingot respectively. From the measured Cadmium ratio, it is apparent that there is high level of thermalization. The measured value of thermal flux is of the order of 10^{11} n/cm^2-sec at the ingot location for the 600 KW power of the reactor.

5. References

[1] T. Singh, P. Pandey, T. Mazumdar, K. Singh, and V. Raina, "Physics design of 2MW upgraded Apsara research reactor", *Annals of Nuclear Energy*, vol. 60, (2013).

[2] A. Edward Profio (1976), Experimental Reactor Physics, John Wiley & Sons, New York.

[3] Rajeev Kumar, Amod Kishore Mallick, Sudipta Samanta, Deep Bhandari, Kapil Deo, Umasankari Kannan, Sajin Prasad S. and Ranjit Sharma, "Measurement of neutron flux profile on Silicon ingot irradiated in Apsara-U", *RPDD/EP/205/Rev_0*, [2020]

Monte Carlo Characterization of Neutron Spectrum at Ion-chamber Irradiation Locations of AHWR Critical Facility

Amod Kishore Mallick[1,2], Sudipta Samanta[1], Rajeev Kumar[1,2] and Umasankari Kannan[1,2]
[1] Bhabha Atomic Research Centre, Mumbai, India
[2] Homi Bhabha National Institute, Mumbai, India
[1]*e-mail: - amod@barc.gov.in*

Abstract

AHWR Critical Facility has two out-core ion-chamber cavities below the reactor tank which acts as thermal flux irradiation locations for many experiments, neutron detector testing being an obvious example. These cavities, named as D-9 and D-10 are around 40cm away from the active reactor core, with 30cm heavy water in-between them. The knowledge about the neutron spectrum, the absolute value of flux and its variation along the length of the cavity is essential for knowing the suitability and for proper planning of an experiment. With the availability of general-geometry Monte Carlo code, it is now feasible to model and simulate the full system very accurately to study the neutron flux characteristics in any region. In this work, we have done a Monte Carlo study using our indigenous code PATMOC to characterize the neutron flux environment in these ion-chamber cavities. The estimated results are also compared with the available measured data. The Monte Carlo results of this study supplement the measured results, giving further insights into the flux profile and its characteristics which will be very helpful in better planning the experiments in these cavities.

1. Introduction

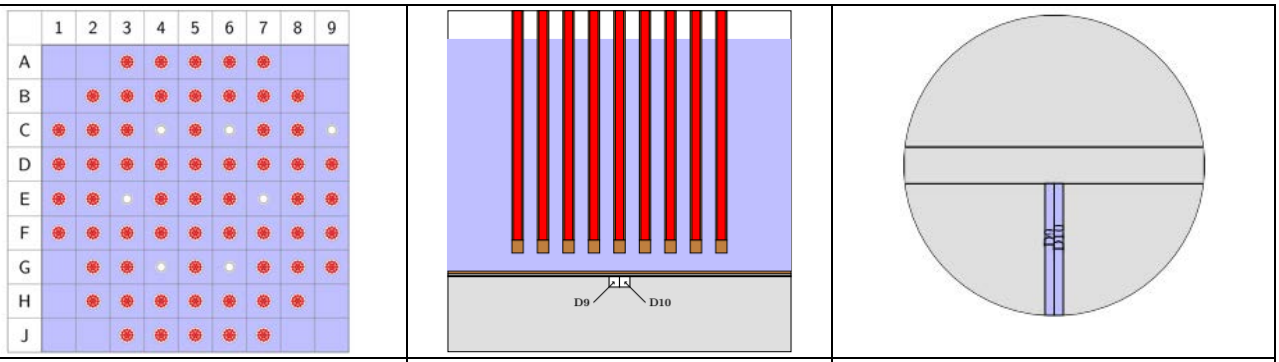
AHWR Critical Facility (AHWR-CF) [1] is primarily meant for conducting experiments to validate the computational tools used in AHWR design calculations. This facility, however, also provides out-core locations where the neutrons leaking from the core can be used for other general purpose experiments. Two such locations, namely D-9 and D-10 ion-chamber cavities located in the bottom graphite reflector are specially designed for this purpose. These locations are used for detector testing and other such uses. The knowledge about the neutron spectrum and the absolute value of flux and its profile along the length of the cavity is essential for proper planning of any such testing. It is, therefore, desirable to know the flux profile along the length of these cavities and the spectrum of the neutron flux.

A few experiments to characterize these cavities have been done earlier to estimate flux at one location and relative variation along the length. The detailed neutron spectrum measurements, however, were not done. With the availability of general-geometry Monte Carlo code, it is feasible now to model and simulate the full system very accurately to study the neutron flux characteristics in any region. In this work, we have done Monte Carlo study to characterize the neutron flux environment in these cavities. We have used indigenous Monte Carlo code PATMOC [2, 3] for this study. The Monte Carlo results are also compared with the available measured results. The results of this study give further insight into the flux profile and its characteristics, which will be very helpful in better planning the experimental measurements at these cavities.

2. AHWR Critical Facility

AHWR-CF is a heavy water moderated, air cooled, natural uranium fueled vertical reactor. The current core configuration of CF consists of 61 fuel clusters, 6 Shut off Rods (SORs) and one Absorber Rod (AR). Each cluster consists of 19 fuel pins of natural uranium arranged in 3 rings of 1, 6 and 12 pins respectively. The clusters are arranged in the core in a square pitch of 24.5 cm. The core is placed inside the cylindrical tank of radius 165 cm. The radius of effective active core in this tank is around 110 cm. The schematic diagram of horizontal and vertical cross section of the core is given in Figure 1. The active fuel starts from 30 cm above the tank bottom and extends up to 250 cm. Below the tank bottom, there is a 1 cm air gap, followed by 1.7 cm thick aluminum plate which is then followed by 72 cm graphite block acting as bottom reflector. Out of the 72 cm graphite block, upper 10 cm is equipped with empty channels to place neutron monitors and experimental devices. Two of these channels are D-9 and D-10 for neutron flux experiments.

The D9 and D10 ion-chamber cavities are located just below the aluminum plate on which the reactor tank rests. The cavities are symmetrically placed and are like a square-shaped horizontal cylindrical tube with around 150 cm length. The inner most location of cavity is around 20 cm away from the core center. The schematic diagram of the position and extent of cavities are given in Figure 1.



(a) Core horizontal cross section | (b) Core vertical cross section | (c) Horizontal cross section at ion-chamber location

Figure-2: Core configuration and Ion-chamber locations of AHWR Critical Facility

3. Details of Monte Carlo Simulation

Some information regarding the Monte Carlo code and the model and parameters used in these simulations may be desired here. About PATMOC, this is an indigenous multi-group Monte Carlo code for neutron transport simulations. Code supports both eigen (criticality) and source mode simulations, and can be used to compute k-eff and various tallies like flux and different reaction rates. It uses Constructive Solid Geometry (CSG) techniques and can model complex geometry such as full reactor core. It uses WIMSD format multi-group nuclear data library [4] for the practical simulation. The code has been verified and validated against numerous benchmarks including OECD/NEA benchmarks like VVER, C5G7, and existing reactor such as AHWR-CF, Apsara-U, and BRAHMMA. With these features, the code is now being used regularly for various reactor physics studies

The CF reactor was modelled with full geometrical details for the simulation. The model included the reactor core and different regions below the reactor tank including the D9 and D10 ion-chamber cavities. The cavities are square shaped cylinder, but for simplicity of modelling we have assumed it be

a circular cylinder having equal cross-section area. Most of the experiments are carried in the innermost regions of cavity. For computing the spectrum parameters, we have used tally averaged over the 40 cm length at the innermost region. To obtain the variation of flux along the length, the cylindrical cavity was subdivided into smaller cells each with 10 cm length. The tallies were used to compute the flux and other quantities up to 13 cells from the inner most region. ENDF-B/VII.1 69-group WIMS nuclear data library [4] was used for these simulations.

4. Results

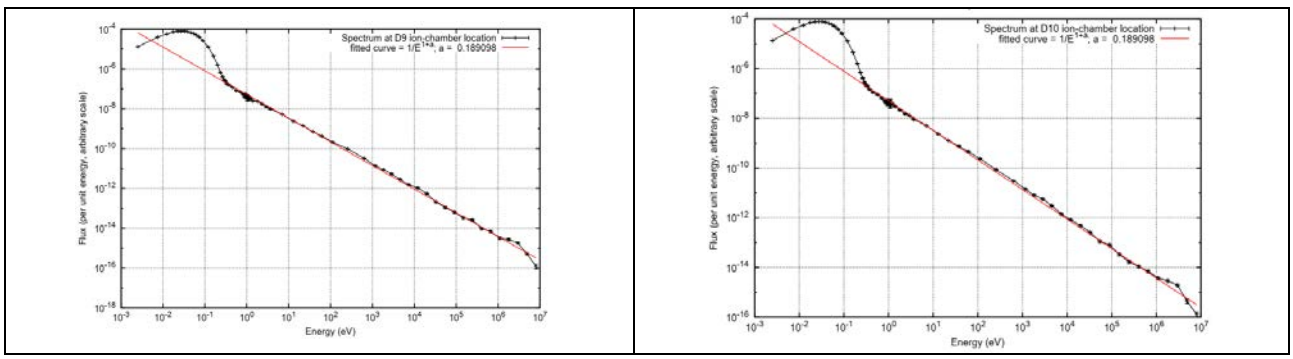
The results of Monte Carlo simulation are presented here. Table 1 gives total flux, f ($\varphi_{th}/\varphi_{epi}$), the thermal to epithermal flux ratio, and Cadmium ratio of Au at inner position of the ion-chamber cavities. The flux value corresponds to value per simulated neutron for which the total fission reaction rate of the core is 0.405/s. Using this as scaling factor, we can compute the flux at any power of reactor. Table 2 gives the comparison of fraction of flux in different energy regions. We can clearly see that the flux has around 95% thermal component which is not surprising as it is out-core location with 30cm heavy water reflector between this and the active core. We have also estimated the value of neutron spectrum shaping factor (alpha) by appropriate curve fitting of the computed 69 group neutron spectrum. The neutron spectrum and curve fitting is shown in Figure 2 and the obtained alpha values are listed in Table 3. Activation foil (Au) along the length of the cavity was irradiated to measure the neutron flux variation along the length. Figure 3 gives the comparison of estimated Au(n,g) reaction rate with corresponding measured values, and it shows a very good agreement. The figure also shows the estimated value of neutron spectrum averaged over the length of the cavity.

Table-1: Estimated values of total flux, f ($\varphi_{th}/\varphi_{epi}$, 0.5 eV thermal cut-off) and Cadmium ratio for various locations

Location	Flux*	f ($\varphi_{th}/\varphi_{epi}$)	Cadmium ratio
D-9	6.214e-06 ± 0.23%	19.87 ± 1.24%	10.10 ± 3.12%
D-10	6.203e-06 ± 0.23%	19.94 ± 1.23%	10.40 ± 3.20%
*: for total fission reaction rate of the core equal to 0.405/s. This corresponds to flux per unit neutron simulated.			

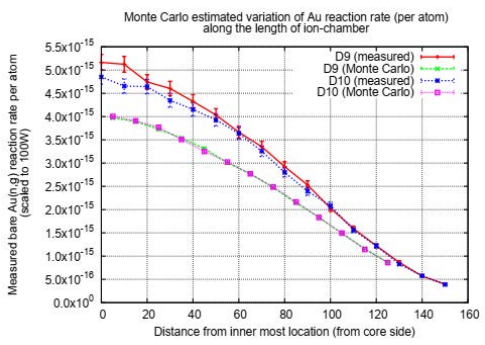
Table-2: Estimated fraction (%) of neutron flux (max error: 1.2%) in different energy regions for various locations

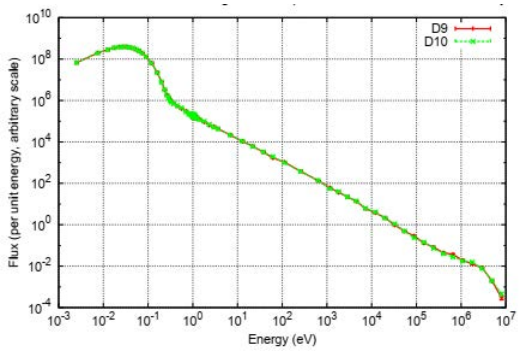
Energy region	D-9	D-10
10 MeV < E ≤ 0.5 eV	4.8	4.8
0.50 eV < E ≤ 0 eV	95.2	95.2
All energy (0 - 10 MeV)	100.0	100.0



(a) D-9	(b) D-10
Figure-2: Neutron spectrum and curve fitting to obtain the estimate of alpha for different locations	

Table-3: Estimated values of alpha for various locations	
Location	**alpha**
D-9	0.18910 ± 9.6%
D-10	0.18910 ± 8.9%





(a)	(b)
Figure-3: (a) Comparison of estimated and measured Au-197 (n,γ) reaction rate along the length of the cavity, and (b) estimated neutron spectrum averaged over the length of the cavity	

5. Conclusion

An indigenous multi-group Monte Carlo code PATMOC was used to to characterize the D-9 and D-10 out-core ion-chamber cavities located in the bottom graphite reflector of AHWR-CF. In this we have estimated neutron spectrum, f (the thermal to epithermal flux ratio), Cadmium ratio of Au, and neutron spectrum shaping factor. The profile of flux along the length of cavity was also estimated in terms of the Au-197(n,γ) reaction rate and the same was compared with the measured values, and it shows a very good agreement further validating the code for its ability, accuracy, and usefulness. The Monte Carlo results provide detailed insight into the flux characteristics of the ion-chamber cavities and would be very useful for better planning of the future experiments in these cavities.

6. References

[1] N. Prasad, U. Kannan, B. Chakraborty, R. Kumar, B. K. Mohan, and R. Srivenkatesan, “Physics design of critical facility for AHWR and MWe PHWR (revision-1),” RPDD/AHWR/96, (2008).

[2] Amod Kishore Mallick and Umasankari Kannan, “PATMOC: A Multi-group Monte Carlo code for Neutron Transport Simulation”, RPDD/EP/164 (2018).

[3] Amod Kishore Mallick and Anurag Gupta, “Sub-Space Iteration Based Monte Carlo Scheme for Simultaneous Computation of Multiple Dominant k-eigenmodes and Acceleration of Fission Source Iterations”, Annals of Nuclear Energy, 166 (2022).

[4] Leszczynski, F., Aldama, D.L., Trkov, A., “WIMS-D library update”. Technical report, International Atomic Energy Agency, (2007).

Analysis of the extended core of AHWR-CF with one Experimental Cluster by WIMS-ARCH code

Deep Bhandari, Amod Kishore Mallick, Sudipta Samanta, Rajeev kumar and Umasankari Kannan

Bhabha Atomic Research Centre, Mumbai, India

e-mail: - dbhan@barc.gov.in

Abstract

Critical Facility is low power research reactor which consists of a simple and precise geometry to study the physics design of AHWR. Theoretical models are developed to simulate the physical processes and the geometrical details of a reactor, including all the reactivity devices. Theoretical analysis of the extended core of the AHWR-CF with experimental cluster is performed by lattice level calculation and core level calculation with WIMSD code ARCH [3] code respectively. Critical height of CF reactor core with the experimental cluster at different locations of the core, moderator level coefficient, worth of SOR etc. were estimated and were compared with experimentally observed values.

1. Introduction:

To simulate physical processes and the geometrical details of a reactor, different theoretical models are developed. The analytical calculations of the reactor core are performed in two stages i.e. lattice level calculation and Core level calculation. In this paper, lattice level calculation and core level calculation has been performed with WIMS-D and ARCH code respectively. WIMS-D is a Transport theory code for lattice simulations and has been used to obtain four group homogenized and condensed cross sections and lattice parameters using 69 group ENDFB-VIII library. ARCH is a 3D space-time core neutronics analysis Code. Four group homogenized lattice parameters, derived from lattice level calculation, have been used in core calculation. This report summarizes the description of experimental cluster, estimation and comparison of critical height of CF core with experimental cluster at various locations with those of the measured values, moderator level coefficient near critical height moderator level coefficient near critical height and the worth of SOR's with experimental cluster at E5 location, axial flux profile at E5 location and power profile at an elevation of 130 cm from reactor tank bottom.

2. Experimental cluster:

The experimental cluster [1] is made up of 19 pins, like natural Uranium cluster, arranged in three rings of 1, 6 and 12 pins. Inner seven pins (1+6) are identical and are composed of (Th-Pu) MOX with 1% Pu enrichment. Outer twelve pins, all of which are also identical, are axially graded and composed of 60 cm of ThO_2 sandwiched between 80 cm of natural Uranium on either side. The details of this cluster are summarized in Table-2.1. and schematic diagram [2] is given in Fig 2.1.

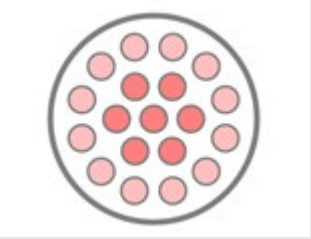


Figure-2.1: Schematic diagram of arrangement of fuel pins in experimental cluster

Table-2.1: Description of {(Th-1%Pu) MOX, NU-ThO_2-NU} Experimental Cluster	
Fuel Pins	
Ring 1 and Ring 2	
Fuel Type	(Th, Pu) MOX, 1% Pu (w/w)
Density	9.3 g/cc
Pu Vector - Pu-239/240/241/242	68.79/24.60/5.26/1.35
Pin Radii (mm)/ material	4.875, 5.0, 5.6/Fuel, Air, Clad
Clad Material / Density (g/cc)	Zr/6.655
Clad thickness (mm)	0.6
Ring 3	
Fuel	Axially graded
Fuel Type / Length axially	NU-ThO2-NU / 80-60-80 cm
Density	18.5-9.3-18.5 g/cc
Pin Radii (mm)/ material	6.0, 7.35 / Fuel, Clad
Clad Material / Density (g/cc)	Al / 2.699
Clad thickness (mm)	1.35
Flow Tube	
IR/OR (mm)	51.7/ 54.7
Material / Density (g/cc)	Al / 2.699
Coolant	
Material	Air

3. Estimation of critical height with experimental cluster:

The normalized value of k-eff in extended core has been determined as 1.00449 with the corresponding critical height of the moderator (IP= 99.88) 222.2 cm. Critical height has been estimated with the experimental cluster in six locations i.e., E5, F1, F2, F3, F4, B5 and estimated values were compared with the experimentally measured values [1]. Table 3.1 shows the estimated and measured values of k-eff at various location.

Table 3.1: Estimated and measured values of k-eff at various locations.						
	Locations of experimental cluster					
Critical height (cm)	E5	F1	F2	F3	F4	B3
Estimated	233.85	225.0	227.35	230.45	232.7	226.25
Measured	233.8	224.9	227.2	230.3	232.8	226.1

From the table it is observed that theoretical values are in good agreement with the experimental values for all locations.

4. Estimation of moderator level coefficient with experimental cluster at E5 location near critical height:

Moderator level coefficient has been estimated around critical height with experimental cluster at E5 location. Height of moderator was increased by 1 cm and the change of the reactivity was calculated from its previous value. Near the critical height moderator level was increased by 0.5 cm and corresponding change of reactivity was calculated. Estimated moderator level coefficient is about **0.055 mk/mm.**

5. Worth of SOR's in extended core with experimental cluster in E5 location:

Worth of six SOR's located at C4, C6, E3, E7, G4, G6 has been estimated by estimating change in reactivity when SOR is 100% out from core and 100% inside the core within the Guide tubes at respective locations. The difference of these two reactivity gives the worth of SOR. All the estimations of worth have been calculated at the critical height of moderator 233.85 cm. Estimated worth of six SOR is **108.1 mk,** which is in good agreement with Experimentally measured worth 103.1 mk [1] with C/E value 1.06.

6. Axial flux distribution along experimental cluster at different lattice location and core power profile with experimental cluster at E5 at a height of 130 cm from reactor tank bottom:

Figure 6.1 Axial variation of neutron flux at various locations

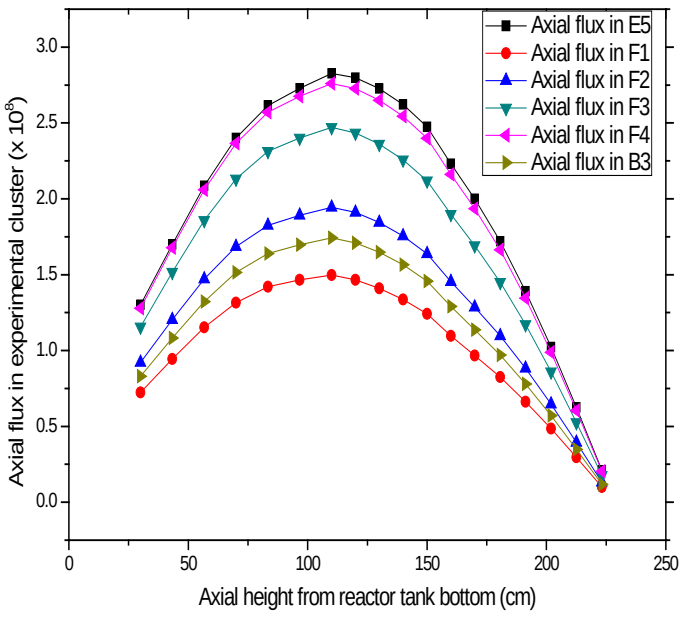


Fig 6.2 Distribution of power at a height of 130 cm from reactor tank bottom.

	1	2	3	4	5	6	7	8	9
A			1.15	1.26	1.31	1.25	1.13		
B		1.29	1.52	1.75	1.76	1.74	1.49	1.27	
C	1.15	1.5	1.89	0	2.22	0	1.86	1.51	0
D	1.26	1.68	2.1	2.26	2.23	2.25	2.08	1.67	1.28
E	1.3	1.81	0	2.29	1.44	2.28	0	1.8	1.3
F	1.29	1.68	2.09	2.26	2.23	2.26	2.09	1.68	1.25
G		1.53	1.87	0	2.22	0	1.88	1.49	1.15
H		1.27	1.5	1.74	1.76	1.75	1.51	1.29	
J			1.14	1.26	1.31	1.26	1.15		

SOR position
Absorber rod position
Natural Uranium with 100 ppm copper
Natural Uranium with 1000 ppm copper

The axial variation of neutron flux has been estimated by ARCH code in core level calculation. The fuel region was divided by 18 meshes axially and corresponding to this each meshes neutron flux was estimated with experimental cluster placed at six locations i.e. E5, F1, F2, F3, F4, and B3. Fig 6.1 shows the variation of axial flux at various locations. Fig 6.2 shows distribution of power profile at a height of 130 cm from reactor tank bottom with experimental cluster at E5 location.

Axial flux in the experimental cluster follows the cosine pattern and magnitude of flux is maximum when experimental cluster is placed at E5 location and it is minimum when it is placed in F1 location. It is observed from the power distribution that power produced by experimental cluster (E5 location) is less compared to NU cluster and power production is more near central region of the core and less in peripheral region of the core.

7. Discussion and concluding remarks:

The estimated critical heights are in good agreement with the experimentally observed values with the experimental cluster in different lattice location. The estimated maximum difference in critical height is 0.15 cm having experimental cluster in F2, F3, and B3 location and minimum difference is 0.05 cm having experimental cluster in E5 location. This difference is quite small indicating that theoretical calculations are supported with the experimental ones. The differences arise due to the approximations made during the core modeling, nuclear data library, uncertainty of the fuel composition etc. Reactor core simulation consists of two parts namely lattice level calculation and core level calculation. In lattice level calculation it is assumed that lattice is infinitely extended in axial direction and repeated in radial direction, whereas only one experimental cluster of finite length was placed in the central lattice of core surrounded by the natural uranium cluster. This assumption contributes errors to the lattice calculation. Moreover, uncertainty in density and the composition, nuclear data library, approximation in core modeling are also the sources of errors. Considering these factors, the experimental results are in very good agreement with the theoretical estimated values.

8. Acknowledgement:

Author is grateful to all the members of ERPS section in RPDD for their kind help and cooperation in all possible ways for providing me all the necessary documents and relevant information about AHWR-CF, WIMS input etc. which are helpful for the analysis.

9. References:

[1] Amod Kishore Mallick, Neelima Prasad, Sudipta Samanta, Kapil Deo, Rajeev Kumar and Umasankari Kannan," Analysis of Integral Experiments with one {(Th-1%Pu) MOX, NU-ThO2-NU} Experimental Cluster in Extended Core of AHWR Critical Facility", RPDD/EP/154, March 08, 2018

[2] Amod Kishore Mallick, Deep Bhandari, Sudipta Samanta, Kapil Deo, Rajeev Kumar and Umasankari Kannan, Y.K.Upreti, V. Shivakumar and V. Joemon, Sajin Prasad S. and Ranjit Sharma, S. K. Verma and S. K. De,"Measurement of Radial and Axial Flux Profile in (Th-1%Pu) MOX Experimental Cluster in AHWR-CF", RPDD/EP/168/ March 13th, 2019

Validation of Multi-group Diffusion Code NEM3D

Sandeep Singh[1], Arindam Chakraborty[1], Amit Thakur[1] and Umasankari Kannan[1]
[1] Reactor Physics Design Division, B.A.R.C., Mumbai, India
[1]*e-mail: - sandeepss@barc.gov.in*

Abstract

Validation of the computer codes is an important exercise for design and safety of the reactors. This paper presents a verification and validation of the Nodal Expansion Method (NEM) based code NEM3D for AHWR-CF. For validation core simulations of AHWR-CF were carried out using NEM3D. The critical height of the moderator was estimated and compared with the experimentally observed value. The worth of reactivity devices, neutron flux distribution and the channel power distribution were also estimated and compared with the same generated with the reference code FEMINA. The results obtained using NEM3D show a good agreement with the reference data.

1. Introduction

AHWR Critical Facility (AHWR-CF) is a low power research reactor with a nominal power of 100 W. This facility is used for understanding and validation of the physics design parameters and theoretical models used for AHWR and PHWR. The computer codes used for the theoretical calculations are validated by comparing the results with experiments performed in Critical Facility. NEM3D is a three-dimensional, multi-group, neutron diffusion theory-based computer code [1]. It has been developed to solve reactor core problems in rectangular geometry. The code is based on Nodal Expansion Method (NEM) [2]. In this method, three-dimensional diffusion equation is converted into a set of three one dimensional equations by integrating the diffusion equation over two transverse directions. Further, one dimensional nodal flux is approximated using a fourth order polynomial expansion. The code can be used for the calculation of effective multiplication factor, neutron flux and power distribution in a steady state condition. Core simulation of AHWR-CF was carried out using NEM3D in order to validate the code. The required critical height of the moderator was estimated and compared with the experimentally observed value. The worth of reactivity devices, neutron flux distribution and the channel power distribution was also estimated in the core using NEM3D and compared with the same obtained with the reference code FEMINA [3].

2. Extended core of AHWR-CF

The extended core of CF consists of 68 lattice locations in a lattice pitch of 245 mm [4]. Out of 68 locations 61 locations are loaded with 19 pin natural uranium metal fuel clusters, 6 locations are used for shut-off rods and one lattice location in the reflector region is used for absorber rod. The active fuel length is 220 cm. Heavy water with a purity of 99.88% is used as moderator and reflector in the core. The radial reflector thickness is 54.75 cm. A schematic layout of the extended core of CF is given in Figure 1.

3. Calculation

Core calculation require homogenised macroscopic cross-sections for different type of materials present in the core. Four energy group homogenised cross-sections were taken from earlier calculations carried out using lattice code ITRAN [4][5]. The energy group limits are 10 MeV, 0.821 MeV, 5.53 KeV and 0.625 eV. The neutron fission spectrum used in core calculation is 0.7664062, 0.2334129, 0.00018092 and 0. A fuel mesh size of 12.25 cm i.e. (half of the lattice pitch) was taken in core calculation.

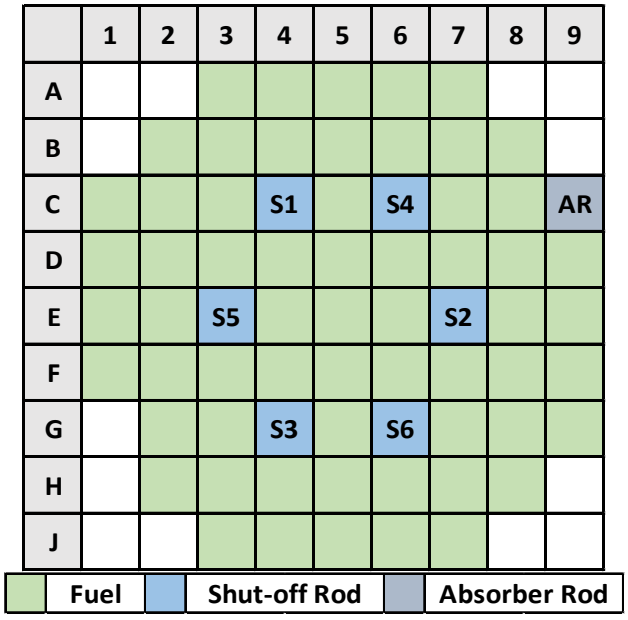


Figure 1: CF extended core layout

A relatively tight eigenvalue and mesh-wise flux convergence criteria of 10^{-6} was used with boundary condition of no incoming current at the outer boundary of the core. Iteration technique based on the standard nested combination of outer and inner iterations was used to solve steady-state neutron diffusion equation.

3.1 Estimation of critical height and worth of reactivity devices

A series of full core calculations were carried out to find out the critical height of the moderator by increasing the moderator height in the core. The critical height of the moderator was estimated to be 222.3 cm which is very close to the experimental value of 222.6 cm [6]. The worth of 6 SOR's and one AR in the reflector region was also estimated. Table 1 gives the comparison of critical height and worth of reactivity devices with the reference value. It is observed that maximum deviation in the worth of reactivity devices is less than 1 mk.

Table 1: Comparison of critical height and worth of reactivity devices

Core parameters	**NEM3D**	**Reference**
Critical height of moderator	222.3 cm	222.6 cm
Worth of 6 SOR's	111.2 mk	111.8 mk
Worth of AR	3.65 mk	3.61 mk
Worth of 6 SOR's + AR	116.6 mk	117.3 mk

3.2 Neutron flux distribution

The average neutron flux in four energy groups was estimated at each mesh location and normalized to the total power of the core i.e.,100 W. NEM3D has a plotting module for data visualization which uses portable GNUPLOT graphics library for generating plots of material map, power distribution and flux distribution inside the core. The average neutron flux distribution at 102 cm height of active fuel region in four energy groups is shown in Figure 2. It is evident from the figure that thermal flux (< 0.625 eV) is peaking at the shut off rod locations due to the presence of heavy water moderator. The average thermal neutron flux is of the order of 10^8 n/cm^2/sec. The estimated neutron flux distribution has very good agreement with the reference code [4].

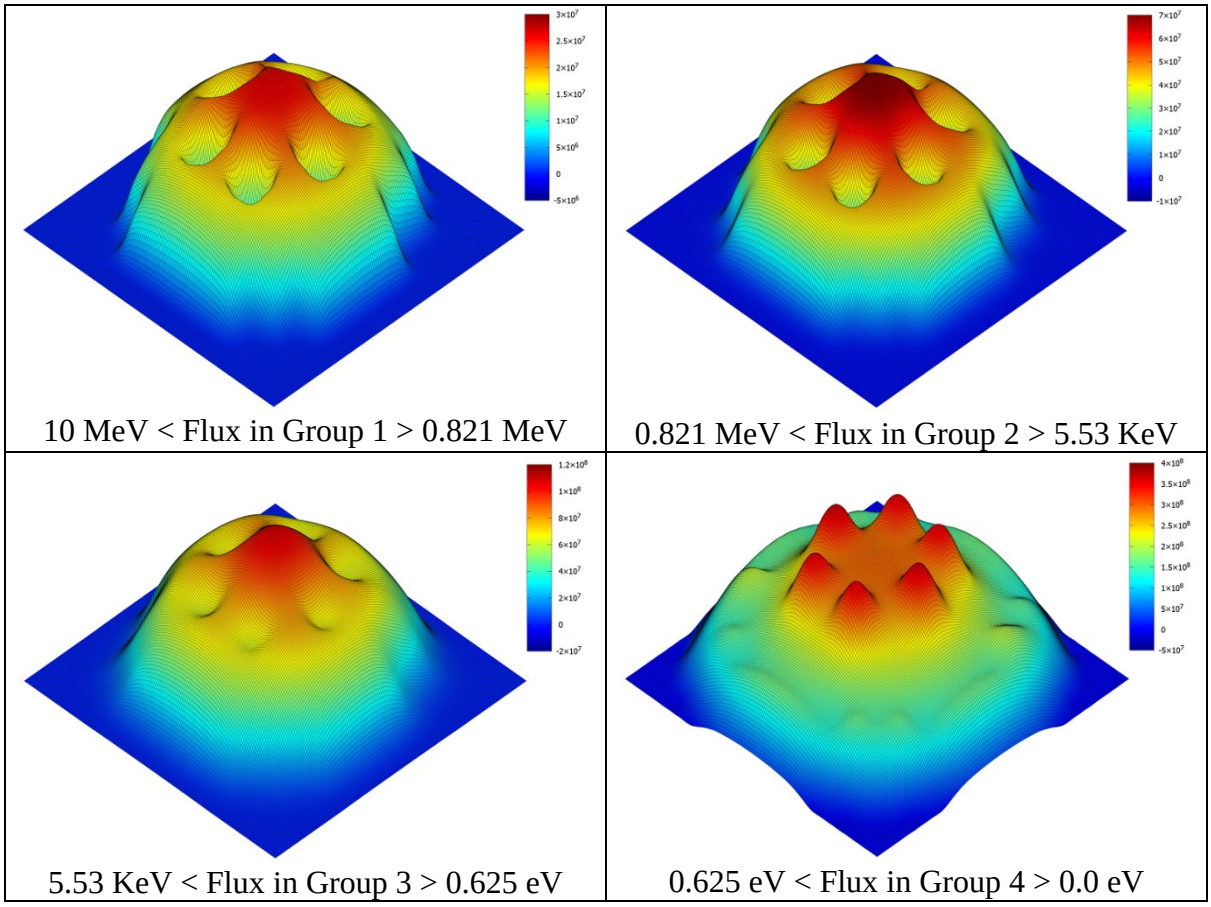


Figure 2: Four group average neutron flux at 102 cm height of active fuel region

3.3 Channel power distribution

The channel power distribution was estimated and compared with the reference code FEMINA in Table 2. First bold face values in the square box represents the channel power obtained with NEM3D and second value represents the percentage deviation from FEMINA code. The maximum channel power estimated using NEM3D was 2.35 W at E4 location which is very close to the reference value of 2.36 W. A maximum deviation of 1.7% was observed in the channel power distribution.

Table 2: Channel power distribution obtained using NEM3D

	1	2	3	4	5	6	7	8	9
A			**1.13** 0.46	**1.26** 0.54	**1.32** 0.67	**1.26** 0.97	**1.12** 1.16		
B		**1.23** 0.06	**1.46** 0.60	**1.71** 0.37	**1.73** 0.26	**1.70** 0.02	**1.45** 0.43	**1.22** 1.04	
C	**1.12** 0.10	**1.44** 0.42	**1.84** 0.45	**S1**	**2.22** 0.27	**S4**	**1.83** 0.26	**1.48** 1.06	**AR**
D	**1.25** 0.00	**1.64** 0.69	**2.07** 0.75	**2.30** 0.50	**2.30** 0.43	**2.30** 0.20	**2.07** 0.00	**1.64** 0.42	**1.29** 1.67
E	**1.31** 0.01	**1.76** 0.86	**S5**	**2.35** 0.45	**2.33** 0.32	**2.35** 0.19	**S2**	**1.77** 0.23	**1.32** 1.30
F	**1.28** 0.66	**1.63** 1.07	**2.06** 0.90	**2.30** 0.28	**2.30** 0.55	**2.30** 0.36	**2.08** 0.23	**1.64** 0.03	**1.26** 0.97
G		**1.46** 0.93	**1.82** 0.81	**S3**	**2.21** 0.51	**S6**	**1.84** 0.17	**1.44** 0.15	**1.13** 0.81
H		**1.21** 0.69	**1.44** 1.01	**1.70** 0.56	**1.73** 0.55	**1.71** 0.27	**1.47** 0.00	**1.23** 0.36	
J			**1.11** 0.03	**1.26** 0.34	**1.32** 0.40	**1.26** 0.56	**1.13** 0.67		

NEM3D
Deviation (%)

4. Conclusion

The core of AHWR-CF was simulated to validate the code NEM3D. The critical height of the moderator was estimated to be 222.3 cm which is in good agreement with the experimental value of 222.6 cm. The maximum deviation in the worth of reactivity devices is less than 1 mk. The channel power distribution shows a maximum deviation of 1.7%. The neutron flux distribution also shows a good agreement with the reference.

5. References

[1] Singh, S., et al., NEM3D: A three dimensional multi group diffusion theory code based on nodal expansion method for rectangular geometry. *Technical Report No. RPDD/AHWR/423 Dated: Jan 29, 2019.*

[2] Singh, T., et al., NEMSQR: A 3-D Multi Group Diffusion Theory Code Based on Nodal Expansion Method for Square Geometry. *Annals of Nuclear Energy, 2014. 64: p.230-243*

[3] Kumar, A. and R. Srivenkatesan, Nodal expansion method for reactor core calculation. 1984. *Technical report No. BARC-1249.*

[4] Prasad, N., A.K. Mallick, and P.D. Krishnani, Design of extended core of Critical Facility by loading 61 clusters of 19 pin metallic natural uranium-Rev 3. 2013. *Technical Report No. RPDD/CF/223*.

[5] Krishnani, P.D., ITRAN-A multigroup integral transport theory code for analysis of cluster lattice. 2006.

[6] Prasad, N, S. Samanta, K. Deo and P.D. Krishnani, Approach to Criticality - Extended core of Critical Facility, *Technical Report No. RPDD/ AHWR-CF /233 /April 15, 2013*

CONCEPTUAL DESIGN OF DELAYED NEUTRON PRECURSORS (DNP) FLOW EXPERIMENT IN APSARA-U FOR MSR PROGRAM

Indrajeet Singh[1], Amod Kishore Mallick[1,2], Anurag Gupta[1,2] and Umasankari Kannan[1,2]
[1] Bhabha Atomic Research Centre, Mumbai, India
[2] Homi Bhabha National Institute, Mumbai, India
[1]*e-mail: - jeet@barc.gov.in*

Abstract

Molten Salt reactors are characterized by circulating molten fuel salt which also acts as coolant. To perform neutronics experimental studies similar to that in circulating fuel reactors, a loop containing fissionable material dissolved in solvent can be specially designed by replacing one of the fuel assembly in traditional research reactors such as in Apsara-U or AHWR-CF loaded with the solid fuel assemblies and facilitate the fuel flow. In this work, Apsara-U reactor core is simulated using 3D space time kinetics code ARCH. The ARCH model is used to estimate the loss of delayed neutrons fraction from the reactor core due to fuel flow allowed in the one fuel assembly location (E4) of the Apsara-U core. This paper summarises the experimental feasibility study to calculate Delayed Neutron Precursors (DNPs) loss as a result of fuel flow in proposed loop configuration using modified ARCH code for Molten Salt Reactor applications.

1. Introduction

BARC is working on design and development of Indian Molten Salt Breeder Reactor (IMSBR) for ensuring long term self-sustaining nuclear energy security. As compared to the traditional solid fuel reactors, MSRs are very different nuclear system having fuel in liquid state circulating throughout the primary circuit to remove heat produced via fission in the core. Consequence of heat transfer by fuel salt itself is that the dynamics of MSRs becomes complex and highly non-linear in nature [1]. The DNPs drift along the primary circuit diminishes the total delayed neutrons fractions (β) and their distribution in the core. This is because DNPs half-lives are such that there is finite probability to decay out of the core and few DNPs re-enter the core without emitting neutrons. 3D space time kinetics code ARCH is augmented with several new modules in order to predict the accurate neutronics behaviour of MSRs by accounting the effect of fuel flow [2]. The modified ARCH solves 1D six-group delayed neutron precursors (DNP) equations in each neutronics mesh. Calculations show that the DNP circulation in primary circuit results in loss of delayed neutron fractions (β_{eff}). The loss of delayed neutrons calculated using ARCH code are compared with that of the values obtained from the Molten salt reactor experiment (MSRE) and recent publications [2]. Results show good agreement with published results. However, experimental result for U-235 fuel is found to be lower by about 20% than the ARCH computed value. On the other hand, ARCH computed result for the U-233 based fuel salt shows very good agreement with that of the MSRE experimental values.

These observations indicate that new development requires validation studies against an experimental result. Therefore, it is proposed to carry out a series of experiments in research reactors. Apsara-U reactor is chosen in order to design DNP circulation experiment [3]. The study includes development of ARCH model of Apsara-U reactor and calculation of the loss of delayed neutrons fraction from the reactor core due to fuel flow allowed in the E4 lattice locations. Fuel flow is not possible in this reactor as all the fuel assemblies are in solid form. Therefore, a loop containing fissionable material dissolved in solvent need to be specially designed to replace one of

the Standard Fuel Assembly (SFA) and facilitate the fuel flow in Apsara-U research reactor. This paper summarises the experimental feasibility study to calculate the DNP loss as a result of fuel flow in proposed loop configuration using modified ARCH code for MSR applications.

2. Results and Discussions

2.1 Simulations of Critical Core Configuration of Apsara-U

The criticality of Apsara-U reactor is achieved with 9 SFAs and 4 CFAs with two remaining fuel lattice locations, namely D3 and E6 filled with dummy fuel assembly. In this critical core configuration, the average CSRs positions was 63.35% UP, and FCR position was 45.3% UP [4-5] This critical core configuration was analysed using ARCH code. Various neutronics parameters, such as k-effective, worth of various combinations of the reactivity devices, and worth of BeO reactor have been computed and the obtained results are compared against two references, namely the experimentally observed values and the estimated values from Monte Carlo simulation. The ARCH estimated k-eff of the observed critical core, and this core with various combinations of reactivity devices in down condition are listed in Table 1.

Table-1 Comparison of ARCH result with that of the PATMOC

Case	Core configuration	PATMOC	ARCH
1	OBSERVED critical core	1.00653	1.01626
2	Case 1 with SOR-1 DN	0.96883	0.97775
3	Case 1 with SOR-2 DN	0.9638	0.97239
4	Case 1with SOR-1 & SOR-2 DN	0.91435	0.91988
5	Case 1 with CSR-1 UP	1.01648	1.02794

Table-2 Worth of various reactivity devices

Reactivity Devices	PATMOC	ARCH	Measured
SOR-1	38.7	38.76	41.8
SOR-2	44.0	44.39	37.2
SOR-1 & SOR-2	100.2	103.11	134
CSR-1	35.4	36.71	32.4

It can be seen from Table 1 that computed values of k-eff using ARCH code for Apsara reactor simulations in different core configurations show a bias of about 10mk against results obtained from multi-group Monte Carlo code PATMOC [5]. This needs to be addressed in subsequent study by generating the lattice parameters for ARCH code. However, the calculations of differential worth of different reactivity devices using ARCH code as listed in Table 2 show good agreement with PATMOC result and experimental measurement. With this bias in ARCH model of Apsara-U reactor, analyses have been done to estimate the effect of fuel flow on DNPs distribution and on loss of reactivity.

2.2 Effect of Fuel Flow on DNP Distribution

At first, DNP distribution in critical core configuration of Apsara-U core with 9SFA is computed when fuel in all assemblies is stationary. The core map of Apsara-U is shown in Figure-1. It is found

that they follow the distribution of neutron flux i.e. cosine with reflector and control effect. Then the effect of fuel flow on DNP distribution is computed by allowing fuel flow in one of the fuel assembly. In the present work, E4 location in reactor is chosen to have flowing fuel (composition of fuel is unchanged). It is assumed that fuel is flowing with speed of 10cm/s and it takes about 19 seconds to return into the reactor core after traversing through the external loop. Drifting of DNPs along with fuel flow in external loop results in reduction of DNPs concentration and change in distribution. To see the effect explicitly, DNPs distribution at E4 location is compared for flowing and stationary fuel. It can be seen from Figure-1 that the DNP distribution is having centered peak when fuel remains stationary. In case of flowing fuel assumption, DNP distribution shows peak towards top of the reactor. In Figure-2, the DNPs magnitude in case of stationary fuel is found to be higher as compared to that in case of moving fuel in same assembly E4. This clearly indicates that effective decay of DNP in the core must be less when fuel is assumed to be moving (β_{eff} for stationary fuel in Apsara-U is 0.0071). Thus drifting of DNPs from the core to the external loop along the fuel flow result in loss of delayed neutron fraction.



Figure 2: Schematic of APSARA-U core [2]

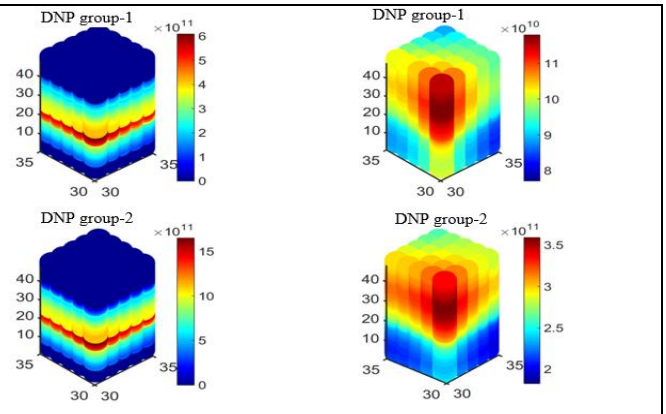


Figure 1: Comparison of DNP distribution for stationary fuel (left) and flowing fuel (right) in E4 assembly. Other fuel assemblies are unchanged i.e. fuel remains stationary.

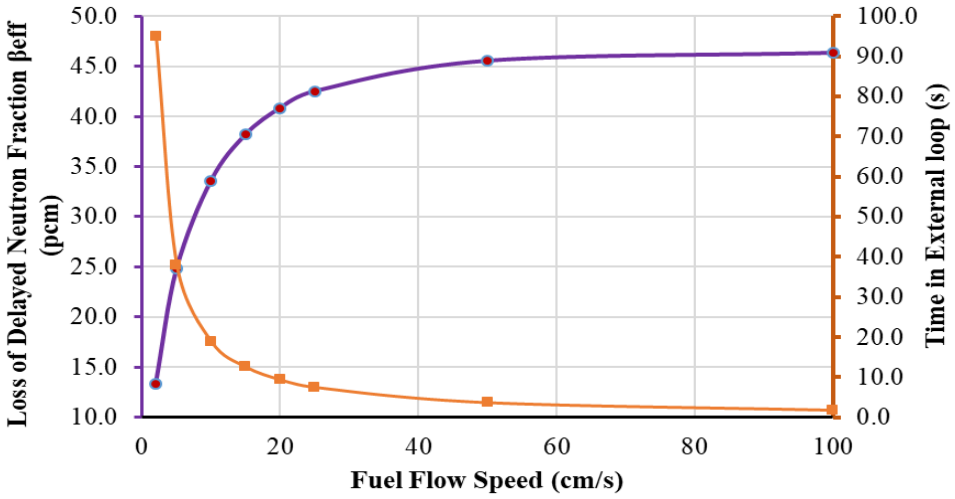


Figure 3 Variation of reactivity loss in Apsara-U core with speed of fuel in E4 assembly

2.3 Loss of Reactivity Due to DNP Drift in E4 SFA

To estimate the loss of reactivity, Apsara-U core is simulated using ARCH code and computed k-eff for all assemblies with stationary fuel except fuel at E4 location. The calculations are repeated for several velocity of fuel in loop from 2cm/s to speed of 100cm/s. It is assumed that the length of external loop is two times the reactor core height. Thus fuel takes almost twice the time it takes in reactor core. It can be seen form Figure-3 that the loss of reactivity due to decay of DNP out of the core increases with fuel speed. It reaches to maximum value and after that it stabilized. It is because as speed of fuel increases DNP spend less time in external loop and they return to reactor core before they decay delayed neutron.

3. Conclusion

In the present work, analysis of Apsara-U reactor has been carried out using 3D-space time kinetics code ARCH for conceptual design of DNP circulation experiment for MSR application. This includes development of ARCH model of critical core configuration of Apsara-U followed by computation of worth of various reactivity devices such as CFA, SOR and FCR. Then, the calculation of DNPs distribution when fuel in all assemblies is stationary and compared it with that when the fuel in E4 assembly is assumed to be circulating with some speed. It is found that the DNP distribution was top peaked in direction of fuel flow and this results in loss of delayed neutron fraction. The loss of delayed neutrons for different fuel flow speed have been estimated and found that it increases with flow speed and reaches to a maximum value. This maximum value becomes independent of fuel speed. The loss of reactivity due to fuel flow is significant from experimental view point. The present analysis suggests that the experiment is feasible even with single assembly fuel flow with speed of 20cm/s or so.

Acknowledgement: Authors are thankful to Dr. Tanay Mazumdar, RPNES, BARC and Dr. Tej Singh, head, RPNES, BARC for providing the kinetic parameters of Apsara-U research reactor.

4. References

[1] S. J, Ball, T.W. Kerlin, “Stability Analysis of the Molten-Salt Reactor Experiment”, Technical *Report, ORNL-TM-1070*, December-1965.

[2] Indrajeet Singh, Anurag Gupta and Umasankari Kannan, “Incorporation of Solution Scheme of 1D Space and Time Dependent Precursor Equation in 3D ARCH Code to Study the Kinetics of Molten Salt Reactor,” *Report No: RPDD /MSR*/18/26-March/2017.

[3] Tej Singh et al., “Physics design of 2 MW upgraded Apsara research reactor” *Annals of Nuclear Energy* 60 (2013) 141–156

[4] Umasankari Kannan et. al. “Independent Design Evaluation of 2MW Modified APSARA”, *RPDD*/Gen/4 (2014).

[5] Amod Kishore Mallick, Rajeev Kumar and Umasankari Kannan, “Analysis of Plate-type Geometry Reactor Systems using Multi-group Monte Carlo Code PATMOC”, *Report No: RPDD/EP/191*, June 30, 2020.

Theoretical Calculation of Excitation Function of Proton Induced Reaction and Evaluation of Recommended data by TALYS – 1.95 and Empire – 3.2.2 Code

Sourav Mondal[1] and Rebecca Pachuau[1]
[1]Department of Physics, Banaras Hindu University, Varanasi 221005, India

Abstract

Radio-isotopes produced via proton induces reaction holds special significance regarding Nuclear Medicine, astrophysical p-process, theragnostic and diagnostic processes. ^{76}Br is positron emitter and it is useful in the functional studies via Positron Emission Tomography (PET). On the other hand, ^{77}Br bears the potential for the application in single photon emission computed tomography (SPECT) which involves electron capture process. Positron Emission Tomography and SPECT have been in high application in case medical physics, diagnostics, therapy and nuclear medicine. ^{61}Cu is a radioisotope used in Positron Emission Tomography. It is especially inexpensive for production of stuffs in medical cyclotrons which makes it an attractive radionuclide of copper. In this work theoretical calculation is done using two Nuclear-Code simulation software and from measured by calculated data important conclusion has been carried out for Recommended data evaluation via common 3-Sigma range of theoretical codes.

1. Introduction

The evaluation of charged particle reaction cross section data was initiated a few years ago under a Co-ordinated Research Program (CRP) of the IAEA [1]. For the time being we know; nuclear model calculations are an integral part of recent nuclear data evaluation procedures. The radionuclides can be produced through different nuclear reactions with different projectile combinations. However, the proton induced reactions appear to be very important and promising [2]. Radio bromides holds significant place in medical applications, as for theragnostic and diagnostics purposes. In particular, Positron Emission Tomography (PET) is an advanced imaging system, with its high ability in the diagnosis of oncological (study of cancer), neurological and cardiological diseases [3]. This decade has seen importance of PET scan in nuclear medicine and it has generated a particular interest in developing new radionuclides to be used in Molecular imaging of Cancer. PET is being used in Cardiovascular Molecular Imaging, study of Psychiatric disorder and in study of Thyroid Cancer. For internal radionuclide which is involved therapeutic treatment, a precise dose of radiation is required to be placed in the seditious cells to attain the expected healing. PET is consistent in the detection of Aphasia, Alzheimer's disease [4], Parkinson's disease [5], Huntington's disease and epilepsy. SPECT has witnessed revolutionary success rate in imaging. The field of PET imaging has changed considerably in recent years, shifting toward production and use of metal radionuclides. For this broad range of application in various fields the three radioisotopes ^{76}Br, ^{77}Br and ^{61}Cu are widely used.

2. Methodology

2.1. Code Description of TALYS – 1.95 Code and EMPIRE – 3.2.2 Code

TALYS – 1.95 is a nuclear reaction model code which is used for analysis and prediction of nuclear reaction yields. In TALYS – 1.95, one can simulate the nuclear reactions that involves particles as projectiles in the wide energy range from 1 MeV to 200 MeV. Those things are taken care of, in a single reaction model code.

Consisting 6 different Nuclear Level Density Models and each model having 8 photon strength functions, provides a wide range of opportunity for simulating nuclear reaction curves.

The basic objective behind its construction is the simulation of nuclear reactions that involve neutrons, photons, protons, deuterons, tritons, ^{3}He and alpha-particles, in the 1 keV - 200 MeV energy range and for target nuclides of mass 12 and heavier. [6]

EMPIRE – 3.2.2 code is adaptable and can perform whole nuclear reaction cross section calculation covering a vast energy ranges up to several MeV. For Optical model and direct reaction ECIS-06 code has been implemented here. Here 4 level density model is available.

2.2. Measured by Calculated (M/C) Data and calculated data for Se(p, n) reactions by using TALYS-1.95 and Empire – 3.2.2 Code.

The present computations have been performed to predict the measured by calculated cross-sectional data for the radionuclides produced by proton irradiation of Se and Cu targets. The calculations are performed using TALYS-1.95 default parameters at first and then varying the level density models to study how the choice of different level density model can affect the results and also default Empire – 3.2.2 Code prediction. For these three reactions we plot the measured by calculated data along with the energy to see the fluctuations of experimental data with theoretical data. The goodness of the fit test is given by two the parameters: a) Chi Squaredvalue, b) R squared value.

For fit the more R squared value go towards 1, better the fit is. We witness the experimental data is scattered which is available in the EXFOR data base whereas theoretical simulated data curves are smooth in nature. The ratio points lysing outside the 3-Sigma limits are generally thrown away to give recommended data. The problem is TALYS-1.95 best-y cannot produce good data sets as TALYS-1.95 best produces lower cross section as the energy gets high in value. So (M/C) points lie outside good data range. So, it is good to go for each level density model and see for which model TALYS-1.95 recommended data and EMPIRE – 3.2.2 recommended data range matches. We see for these three reactions LDMODEL 3 (for ^{76}Se(p,n)^{76}Br), LDMODEL 3 (for ^{77}Se(p,n)^{77}Br) and LDMODEL 4 (for ^{61}Ni(p,n)^{61}Cu) matches with EMPIRE – 3.2.2 calculations. Within 3-Sigma 99.9996 % of data falls within so we generally exclude very few data and none for some cases focusing on the suitable energy range.

3. Results and Discussion

As it is completely theoretical work cross section for level density models have been calculated thoroughly and then from the measured by calculated data the required recommended data has been produced.

3.1. ^{76}Se(p,n)^{76}Br, ^{77}Se(p,n)^{77}Br and ^{61}Ni(p,n)^{61}Cu reactions

After the evaluation of 3-Sigma range for each reaction we come to the conclusion that for the first reaction **^{76}Se(p,n)^{76}Br;** range is **0 – 2.12 [Figure 2]** unit for EMPIRE – 3.2.2 whereas TALYS-1.95 is giving **0 – 2.04** unit range **[Figure 1**]. For the second reaction**^{77}Se(p,n)^{77}Br** it is coming out to be **0 – 1.91** unit for EMPIRE – 3.2.2 **[Figure 4]** and for TALYS-1.95 it is **0 – 2.5** unit **[Figure 5]** and lastly for third reaction **^{61}Ni(p,n)^{61}Cu** it is **0 – 1.78** for EMPIRE – 3.2.2 **[Figure 7]** and **2.01** for TALYS-1.95 [Figure 8]. So, all the Experimental data can be considered as good data points and can be used to predict recommended data. For each reaction, only the newly measured data are considered for the present study. Hence, for the first reaction we used data of V.N. Levkovski only, for second reaction we also used data of V.N. Levkovski and for third, of B.P. Singh and F. Szelecsenyi. In the following images the results are depicted. Recommended data plots are given in **Figure 3, Figure 6** and **Figure 9** respectively for ^{76} Br, ^{77} Br and ^{61} Cu production.

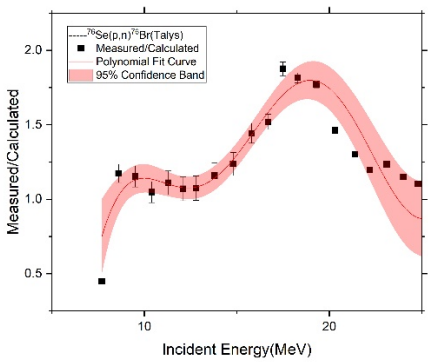


Figure 1

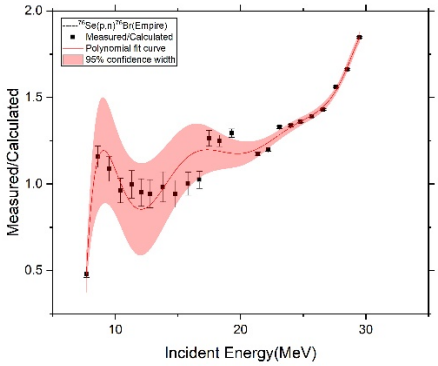


Figure 2

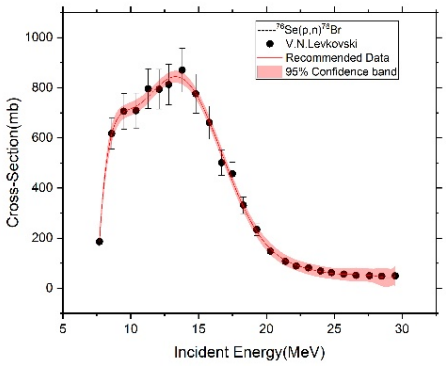


Figure 3

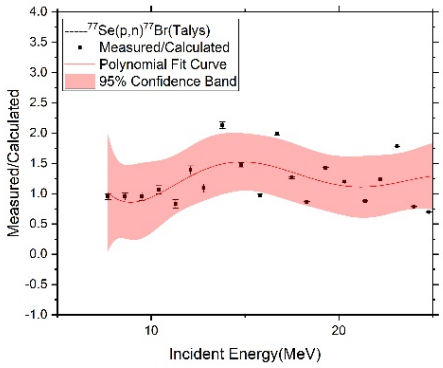


Figure 4

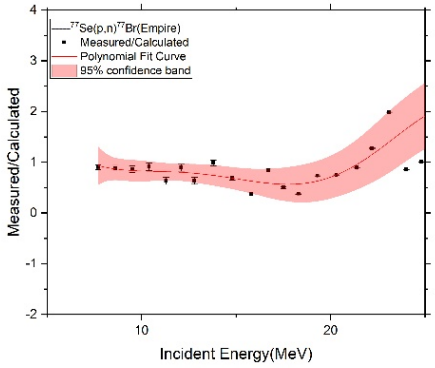


Figure 5

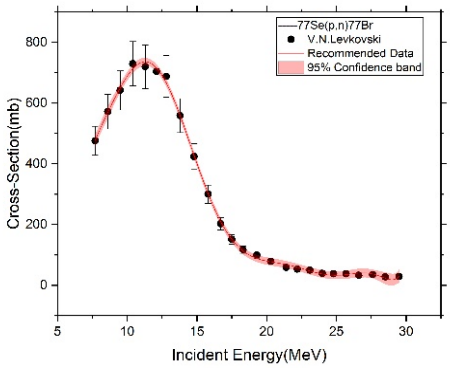


Figure 6

Conclusion

The theoretical calculations of the excitation functions for the proton induced reactions on ^{76}Se, ^{77}Se and ^{61}Ni isotopes have been studied using the TALYS – 1.95 and EMPIRE – 3.2.2 nuclear reaction model codes. Using these two codes, we have evaluated the measured by calculated data and recommended data by statistical analysis. As shown in the figures, theoretical prediction is consistent for predicting the recommended energy level but some data points for m/c lie outside the 95 % confidence width. This analysis will be qualitatively helpful for the production of radio- isotopes used in various purposes such as nuclear medicine and other medical applications. However,there is no report on the detail uncertainty propagation and correlation coefficients between the

different energies. Hence, there is still a need of new precise measured data along with detail analysis.

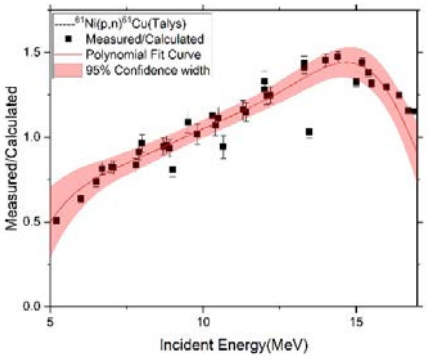


Figure 7

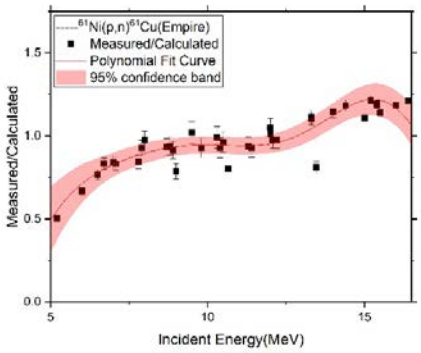


Figure 8

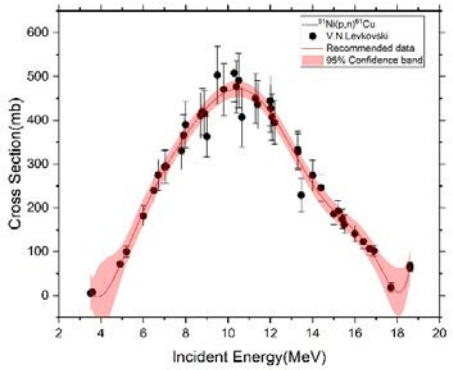


Figure 9

REFERENCES:

[1] www.iaea.org/resources/databases/charged -particle-cross-section-database.

[2] Andrew S. Voyles, Amanda M. Lewis, Jonathan T. Morrell, M. Shamsuzzoha Basunia, Lee A. Bernstein, Jonathan W. Engle, Stephen A. Graves, Eric F. Matthews, Proton-induced reactions on Fe, Cu, and Ti from threshold to 55 MeV, Eur. Phys. J. A (2021) 57:94 https://doi.org/10.1140/epja/s10050-021- 00401-2.

[3] Use of PET/CT scanning in cancer patients: technical and practical considerations, doi: 10.1080/08998280.2005.11928089.

[4] de Leon, M.J.; Li, Y.; Okamura, N.; Tsui, W.H.; Saint-Louis, Les A.; Glodzik, L.; Osorio, R.S.; Fortea, J.; Butler, T.; Pirraglia, E.; Fossati, S.; Kim, HeeJin; Carare, R.O.; Nedergaard, M.; Benveniste, H.; Rusinek, H. Cerebrospinal Fluid Clearance in Alzheimer Disease Measured with Dynamic PET. J. Nucl. Med. 2017, 58 (9), 1471–1476. doi:10.2967/jnumed.116.187211.

[5] Kang, Y.; Henchcliffe, C.; Verma, A.; Vallabhajosula, S.; He, B.; Kothari, P.J.; Pryor, K.O.; Mozley, P.D. 18F-FPEB PET/CT Shows mGluR5 Upregulation in Parkinson's Disease. J. Neuroimaging 2019, 29 (1), 97–103. doi:10.1111/jon.1.

[6] A.J. Koning, J.P. Delaroche b, Local and global nucleon optical models from 1 keV to 200 MeV, Nuclear Physics A 713 (2003) 231–3

NEUTRON MONITORING OF KAKRAPAR ATOMIC POWER PROJECT-3 CORE DURING EXTENDED SHUTDOWN

Himanshu Mishra[1], Gaurav Agrawal[2] and R. Das[1]
[1]Kakrapar Atomic Power Project-3&4, Gujarat, India
[2] Nuclear Power Corporation of India Ltd., Mumbai, India
[1]*e-mail: - hmishra@npcil.co.in*

Abstract

In nuclear reactors, core power monitoring is carried out by different types of neutron detection instrumentation. Ion chambers are used in the operating power range (10^{-7}% FP to 150%FP), in-core SPNDs in the range of 5%FP to 150%FP and the source range detectors are used when power falls below the measurement range of ion chambers. Sufficient degree of overlap is provided between the different types of detectors. Boron coated detectors or fission chambers are mainly used for neutron power monitoring at very low power levels e.g. during first approach to criticality or long shutdowns. In this paper, analysis of neutron monitoring of KAPP-3 core during long shutdown has been presented. Comparison also has been made with observations.

1. Introduction

After achieving first criticality of KAPP-3, India's first indigenous 700MWe reactor, many physics experiments were carried out successfully to establish the neutronic characteristics of reactor core at low power. Subsequently, reactor power was raised and the satisfactory performance of Flux Mapping System, Reactor protection and regulation systems were demonstrated. However, KAPP-3 had to be taken for shutdown, after short operation of few FPDs, for carrying out maintenance works. Even after shutdown, sufficient photo neutron source strength enables monitoring of neutron power by ex-core or in-core neutron detectors.

After shutdown, initially neutron power monitoring is done through ex-core ion chambers. However, as shutdown is extended and neutron power falls below the range of ion chambers, ex-core boron coated detectors are used for power monitoring. As PHWRs are heavy water moderated and cooled, photo-neutrons are produced in the core due to interaction of core gammas (>2.2 MeV) with deuterium atom [1]. These photo-neutrons are monitored by ex-core/in-core detectors. Here, we have presented the analysis for estimation of variation of neutron counts at ex-core detector locations. Also, further analysis is carried out to estimate the rate of power drop under different subcritical conditions.

2. Analysis

When reactor is shutdown, hard gamma rays emitted during fission-product decay can produce photo neutrons in pressurized heavy water reactors (PHWR). In order to assess the adequacy of the various neutron power monitoring systems during long shutdown an accurate estimation of photo-neutron source strength is an important operational requirement. Hence analysis is carried out to estimate the source strength responsible for photo-neutron production. Further analysis is also carried out to find the neutron flux at ex-core detector location.

2.1 Gamma Strength Estimation

Gamma source strength responsible for photo-neutron production is estimated using ORIGEN-2 computer code which is an isotope generation and depletion computer code for use in simulating nuclear

fuel cycles and calculating the nuclide compositions and characteristics of materials contained therein. It employs a point isotope generation and depletion model to compute time dependent concentrations and source term (heat, radiation). The principal use of ORIGEN-2 is to calculate the radionuclide composition and other related properties of nuclear materials [2].

To assess the expected change in neutron power/count-rate at ex-core location during reactor shutdown, variation of gamma (E_Υ>2.2 MeV) strength, responsible for photo-neutron production, was estimated using ORIGEN-2 considering reactor operating history. Photo-nuclear cross-section for deuterium has been shown in figure-1 [1].

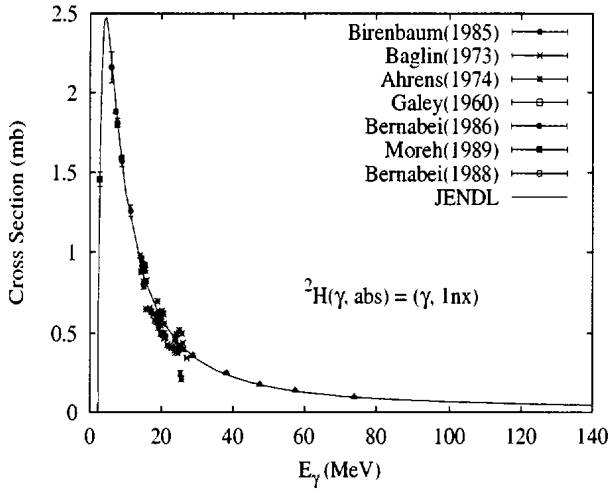


Figure-1: Cross sections for photo-neutron production

2.2 Comparison with observation

First requirement of installation of ex-core start-up detectors, after low power physics experiments, was during reactor shut down from 28th April 2021. After 35 days of shut down ex-core boron coated detectors were installed for core monitoring. Up-to 97 days of shutdown, core monitoring was carried out by ex-core detectors. Variation of counts with time is also estimated based on the variation of gamma (E_Υ>2.2 MeV) source strength. Variation of observed neutron counts with shut-down time, at all three ex-core detectors is given in figure-2. Variation of estimated neutron counts is also given in figure-2.

From figure-2 it can be seen that results obtained from the estimations are in good agreement with the observed count rates from the boron coated start-up detectors housed in the calandria vault location.

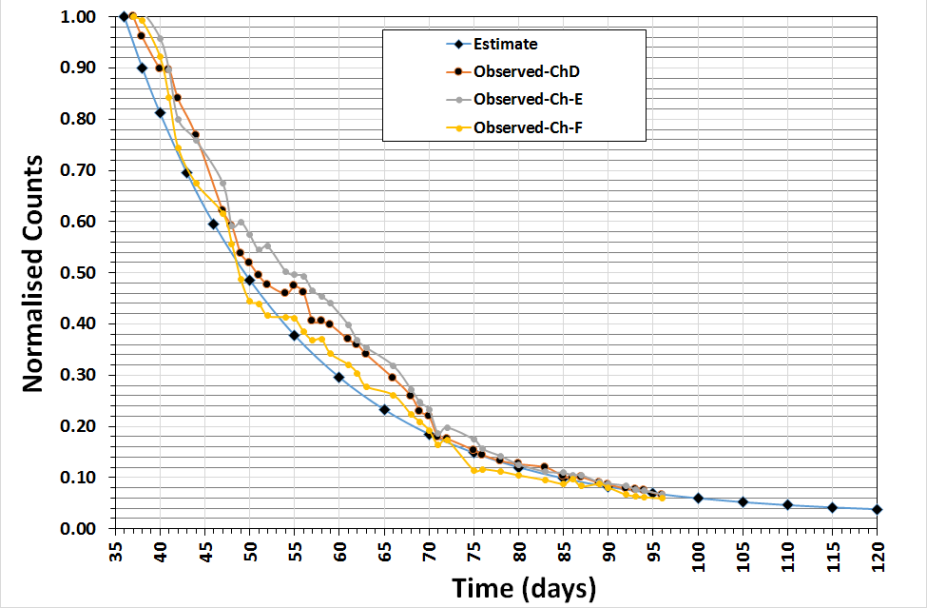


Figure 2: Neutron counts behaviour with time for initial 120 days shut-down

2.3 Variation of count for different subcritical state

The sensitive obtained during calibration of Boron Lined proportional counter (ex-core detectors) are in range of ~ 4 cps/nv. Considering margin, counts above 10 cps are considered reliable for core monitoring. Hence, effective core monitoring through ex-core detector can be done till counts at detector are above 10 cps. In case of extended shutdown, for core monitoring installation of in-core detector (fission detector) is required. Installation of in-core detector is a tedious exercise and involves radiation dose consumption. In place of this core monitoring through ex-core detectors can be extended by changing the sub-criticality of the reactor, without compromising safety. As core sub-criticality changes neutron multiplications changes, neutron reaching to the ex-core detectors changes. As ex-core detectors are placed in ion-chamber housings which are outside the core, simulation is carried out to estimate the neutron flux at this location. For this, gamma spectrum (E_γ>2.2 MeV) is used as input and full core simulation is carried out using Monte-Carlo methods in coupled gamma neutron mode. Gamma spectrum is estimated for core averaged bundle power with core operating history. This spectrum is considered to be same at all bundle location in the core. However, actual bundle power distribution is used as input so that gamma can be emitted from each bundle as per its power. Neutron counts at ex-core detectors is estimated for different sub-critical state of the reactor and variation of neutron counts with time is also estimated for these states and given in figure-3 [3].

Case-1*: Reactor sub-critical by 80mk (SRs + CRs fully IN and all other devices as per pre trip condition)

Case-2: Reactor sub-critical by 20mk (3.3ppm boron in moderator, SDS-1 poised and all other devices as per pre trip condition)

Case-3: Case-2 + SDS-1

Case-4: Case-2 + SDS-2 actuated with 15ppm Gd

* Reference state

Case-1 is standard shutdown configuration of reactor. Case-2 is considered because it has less sub-criticality but meets the sub-criticality of more than 10mk.

Case-3 and case-4 are considered because of any SID-1 and SDS-2 may actuate due to spurious trip.

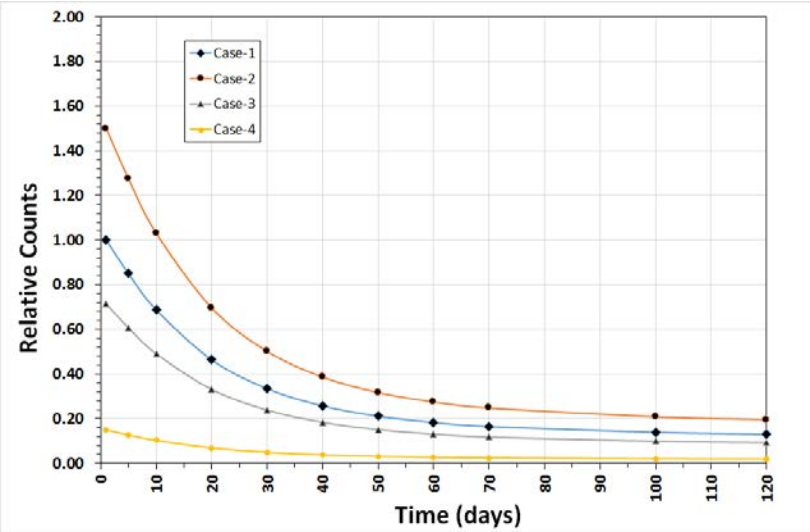


Figure 3: Relative counts variation after shutdown

Time period of effective core monitoring through the ex-core detector can be obtained from figure-3 for any sub-critical state if initial counts at ex-core detectors are known.

3. Conclusion

After reactor shut-down, neutron core monitoring through ion-chamber or ex-core detector can be done effectively as source of photo-neutron production is generated sufficiently. The source i.e. gamma spectrum (E_Υ >2.2 MeV), needs to be estimated correctly. The gamma spectrum is estimated by ORIGEN-2 code by giving reactor actual power history and is used in the core simulation to obtain the neutron counts at ex-core detector location. Variation of neutron counts for different sub-critical condition gives the time period of effective neutron power monitoring through ex-core detector. As sub-criticality decreases neutron counts increases which helps in increasing the monitoring (when counts reaches to 10cps) time by ex-core detector.

4. References

[1] "Handbook on Photonuclear data for applications cross-section and spectra", *IAEA Tech-doc-1178*, 1996-1999.

[2] ALLEN G. CROFF, "ORIGEN2: A Versatile Computer Code for Calculating the Nuclide Compositions and Characteristics of Nuclear Materials", *Nucl. Technol.* (March, 1983).

[3] "Reduction in ex-core counter reading during actuation of shutdown systems in 20mk subcritical core", NPCIL/FPS&S/01100/2021/M/103 (October, 2021).

SUPPLY OF Co-60 FROM PHWR TO MEET THE INCREASING DEMAND FOR SOCIETAL BENEFITS IN INDIA

Surendra Mishra[1] and Baltej Singh[2]

[1] Nuclear power Corporation of India Limited, Mumbai, India

[2] Department of Atomic Energy, Mumbai, India

[1]*e-mail: - smishra@npcil.co.in*

Abstract

The Cobalt-60 emits 1.17 and 1.33 MeV gamma rays which makes it useful for many societal applications (like food preservation through irradiation, sludge hygenization, sterilization, blood irradiation etc.) in daily life and its demand is in rising trend. The specific activity required for these applications is quite low (ranging from 50-100 Ci/g). One of the novel ways to irradiate Cobalt-59 in the adjusters of Pressurized Heavy Water Reactor (PHWR) produces high specific activity Cobalt-60 ranging from 250-300 Ci/g with irradiation period of 5-6 years for some limited applications. Looking at the increasing future demand of low specific activity of Cobalt-60, a 19 element PHWR bundle was designed to contain Cobalt-59 in its central element and remaining 18 elements contain Natural Uranium as usual fuel. The geometry of such bundle is identical to 19 element PHWR bundle. Depending on its location in the core, after irradiation for a period of about 2 years, the Cobalt-60 specific activity in the central element can range from 50-100 Ci/g. Moreover, the reactivity load due to loading of Cobalt is quite low (about 0.01-0.02 mK per bundle) in peripheral channels as compared to the central channels (0.05-0.06 mK per bundle). A complete study about designing and loading of such bundles in PHWR was carried out to provide uninterrupted supply of low activity Cobalt on regular basis. Under water cutting tool development to separate the irradiated central Cobalt element from remaining 18 fuel elements is in its advance stage. This paper describes about the details of the physics study.

1. Introduction

The Cobalt-60 emits 1.17 and 1.33 MeV gamma rays and it has various societal applications in daily life. Some of the facilities like blood irradiator, Medical & Pharmaceutical products Sterilization, Hygenization of sewage & sludge, Food Preservation and Polymerization & cross linking etc. use Cobalt-60 as gamma ray source. The specific activity required for these applications is quite low (ranging from 50-100 Ci/g). The annual requirement is about 1000 K Ci and it is expected to grow with increased demand of facilities listed above. Some applications like tele-therapy needs high specific activity (250 - 350 Ci/g) and its demand is being met through the Cobalt-60 presently being produced in nuclear reactors.

Conventionally, Cobalt-59 is irradiated at the adjuster locations in PHWRs to produce high grade / specific activity Cobalt-60. In order to get the desired grade of Cobalt-60, the residence period of the Cobalt-59 has to be about 5 years at least. The removal of Cobalt-60 from the adjusters has to be carried out in the shutdown state of the reactor and special arrangements are made to replace the adjusters. Also, the removal of Cobalt-60 along with the adjusters is high manrem consuming activity.

Looking at the future demand of low specific activity of Cobalt-60, a 19 element PHWR fuel bundle has been designed such that central fuel element of 19 element PHWR cluster is replaced by Cobalt-59 element and remaining 18 elements are unaltered to contain Natural Uranium (NU) as fuel. This

approach provides greater ease of loading and removal of the specially designed bundle as and when it is desired i.e. specially designed bundle can be loaded in the core and it can be removed from the core with the help of fuelling machine even when reactor is operating. After about 600 Full Power Days (FPD) of irradiation, these bundles will be taken out of the core. The central Cobalt element will be removed from bundle with the help of specially designed tools in the Spent Fuel Storage Bay (SFSB). The produced Cobalt-60 after 600 FPD of irradiation may vary from 50 to 100 Ci/g, depending on its loading in the core. As a trial irradiation, two such bundles have been loaded in KGS-3 reactor core at central position of peripheral fuel channels T07 and T15 in June 2021 and August 2021 respectively. The cross-sectional view of the specially designed Cobalt Natural Uranium bundle (referred as Co-NU fuel bundle) is shown in Figure 1.

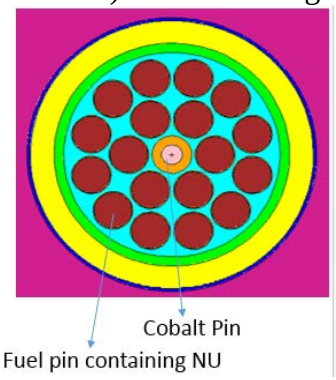


Figure 1: Co-NU Fuel bundle having central element as cobalt

2. Lattice Property of Co-NU bundle

Due to the presence of central Cobalt element, the effective multiplication factor at zero burnup of Co-NU bundle is 0.967 as compared to 1.044 of NU bundle in hot saturated Xenon condition as shown in Figure 2. The central element cobalt has radius 3 mm covered in the Zircoloy-4 element and the remaining 18 elements are identical to 19 element of 220 MWe PHWR bundle to keep bundle geometry identical. The outer element power ratio for Co-NU and NU bundle is same as given in Table 1. The lattice simulation has shown that thermal flux seen by the central cobalt element is about 0.28 times of cell averaged thermal flux (otherwise it is 0.5 for all 19 element NU bundle).

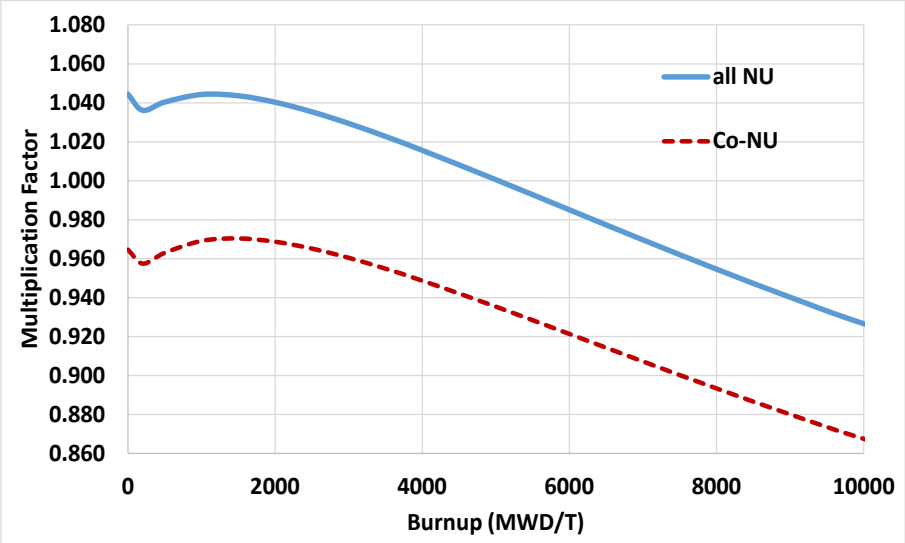


Figure 2: Effective multiplication factor variation with burnup for NU and Co-NU

Table 1: NU and Co-NU element power distribution

Burnup (GWD/T)	NU pin power distribution			Co-NU pin power distribution		
	Ring 1	Ring2	Ring3	Ring 1	Ring2	Ring3
0	0.82	0.89	1.07	0.00	0.87	1.07
1	0.82	0.88	1.07	0.00	0.87	1.07
4	0.83	0.89	1.07	0.00	0.87	1.06
8	0.84	0.89	1.07	0.00	0.88	1.06

3. Co-NU bundle properties in Reactor Core

Reactor core follow up study was carried out by employing 8 bundle shift scheme refueling in peripheral fuel channels A08, A10, T06 and T10 having one Co-NU bundle at 6th string position and remaining string positions of channel occupied by NU bundles. The core was followed up for a period of about 800 FPD.

When peripheral channel is refueled by loading all 8 fresh NU fuel bundles, the reactivity gain is about 0.1 mK to 0.2 mK. The reactivity loss due to loading of single Co-NU fuel bundle and rest 7 NU fuel bundle in a channel is 0.01-0.02 mK with respect to NU loading. Since due to loading of few Co-NU fuel bundle in peripheral fuel channels, change in core kinetic parameters and worth of PSS and SSS is found to be insignificant, hence all full core NU LORA, LOCA analysis results described in safety report do not require any re-evaluation. The cell averaged thermal neutron flux at Co-NU bundle location varies with FPD as shown in Figure 3. On the average, the cell averaged thermal neutron flux is about 0.95E+14 n/cm^2/s. As the Cobalt see about 0.28 times cell averaged flux, the thermal flux seen by Cobalt is about 0.27E+14 n/cm^2/s.

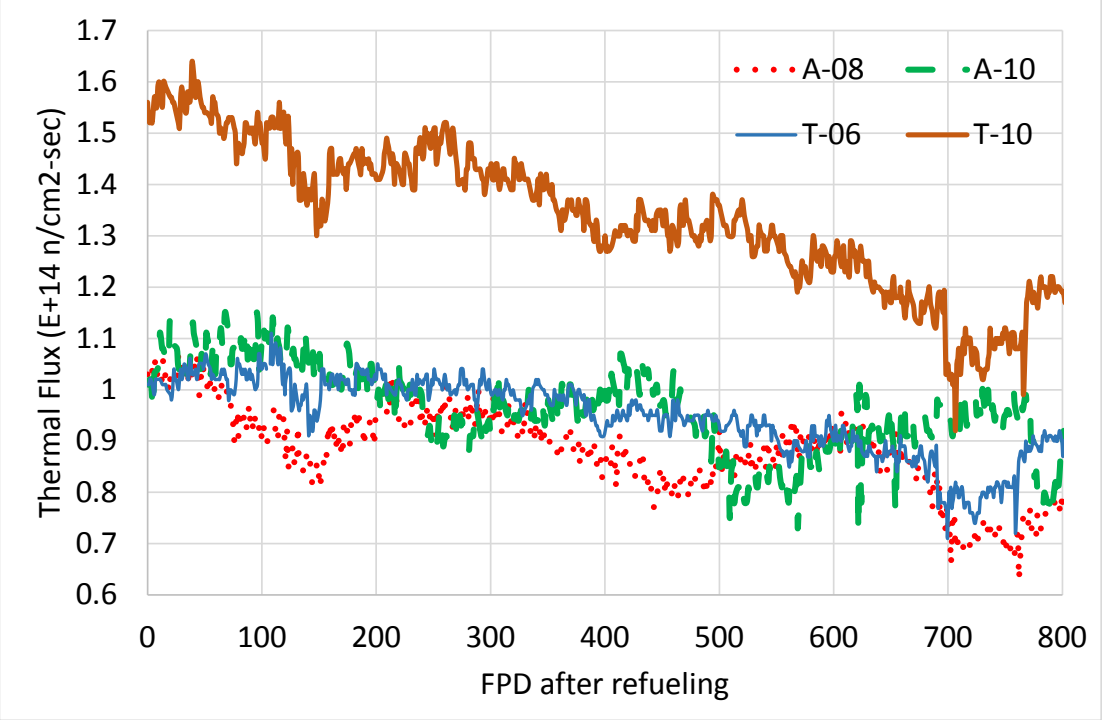


Figure 3: Thermal flux seen by Co-NU bundle with FPD after refueling

4. Cobalt Activity

The specific activity of Co-60 buildup during irradiation is shown in Figure 4. For the production of about 50 Ci/g specific activity of Co-60, about 600 FPD irradiation is required for peripheral channels.

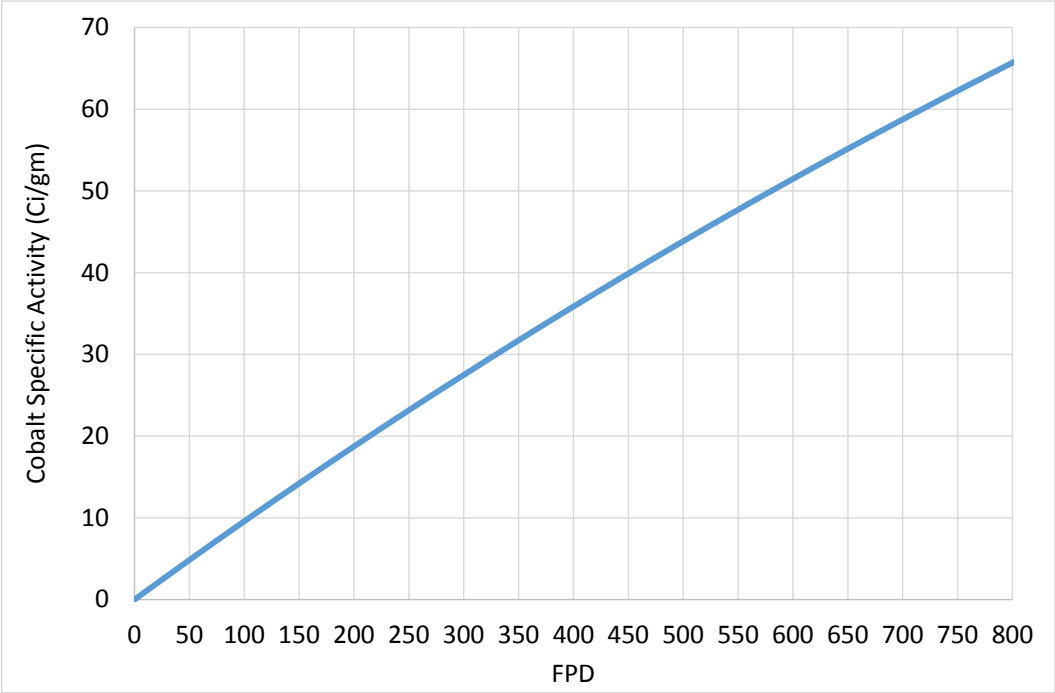


Figure 4: Cobalt-60 activity for 0.27E+14 n/cm^2/s thermal neutron irradiation

5. Conclusion

In 220 MWe PHWR, the peripheral fuel channels are refueled in about 350-400 FPD intervals, and during this period, channel achieves about 5500 MWD/T exit burnup. If these peripheral channels are refueled in 600 FPDs, the maximum burnup achieved by bundles remain less than 13000 MWD/T. For the production of about 50 Ci/g specific activity of Co-60, bundle having central element cobalt can be loaded in peripheral channels of 220 MWe reactor core and irradiated for about 600 FPD. Loading of few Co-NU bundles in 220 MWe PHWR peripheral fuel channels do not affect the core reactivity, the core kinetic parameters and reactivity worth of shutdown devices significantly, hence full core LORA and LOCA analysis results described in safety report do not require any re-evaluation.

6. References

[1] P. D. Krishnani, “CLUB-A Multigroup Integral Transport Theory Code for Lattice Calculations of PHWR cells”, BARC/1992/E-017.

[2] K. R. Srinivasan, “TAQUIL & TRIVENI- Computer Codes for Fuel Management of PHWRs”, PHWR-500/PHY/18 dated 30.01.1986.

FLUX PROFILE MEASUREMENTS THROUGH TRAVELING IN-CORE PROBE (TIP) SCAN AND LPFL READINGS FOR VARIOUS REACTIVITY DEVICE CONFIGURATIONS

Surabhi[1], Amritha Krishnan S[1], Rajarshi Das[1], P. B. Kamble[1] and Manojkumar Sonawani[2]
[1] Kakrapar Atomic Power Project, India
[2]Nuclear Power Corporation of India, Mumbai, India
[1]*e-mail: - surbhi@npcil.co.in*

Abstract

One of the most important activities carried out during Phase-B commissioning of KAPS-3 was the measurement of flux profile for different reactivity device configurations. This was carried out using Travelling In-core Probe (TIP) in selected Vertical and Horizontal Flux Units. Flux profiles obtained from the reactor physics codes were compared with the measured flux profiles.

1. Introduction

Physics experiments are carried out at low power (Phase B) for assessing the characteristics of the reactor core. Since KAPP#3 reactor is the first of the proposed fleet of indigenous 700MWe PHWRs, a large number of tests were carried out to provide a benchmark for the forthcoming reactors. Significant among these tests extensive flux profile measurements carried out primarily to [1]:

a) Compare the observed flux shape with estimations of the reactor follow-up code CFWARO and IQS3D.
b) Verify the Flux profile of reactor core and establish neutron sensitivity of SPNDs by TIP and LPFL system and comparing with the computed data.

The TIP detector is a miniature fission chamber (Figure.1) [2] having thermal neutron sensitivity of around 1.2 x 10^{-17} A/nv at low power range. The detector is 11.5cm in length having helical wire wrap arrangement for controlled movement and accurate position measurement within the VFUs and HFUs flux units.

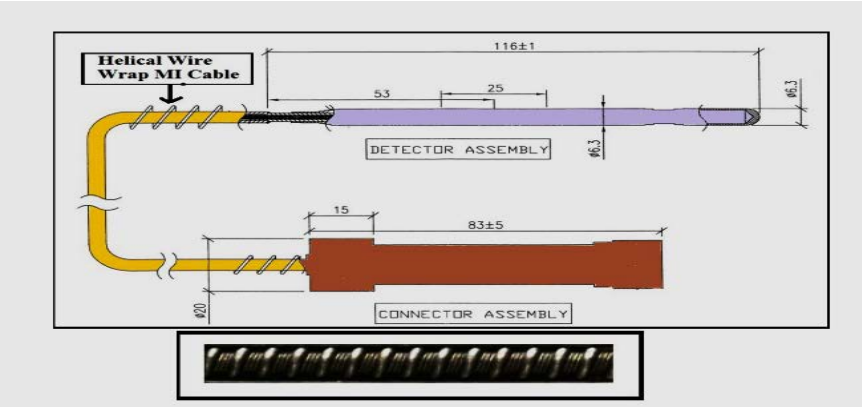


Figure-1**:** Illustrative diagram of a miniature fission chamber

2. TIP Drive Mechanism

The drive consists of a drum for winding and unwinding of detector cable. The gear mechanism ensures straightness and movement of cable. Absolute position encoder is provided to ensure the position of the detector within ± 5 mm accuracy. The TIP Dolly panel was provided at deck plate which enabled controlling of mechanism and position and flux data acquisition from each drive. The dolly pane is further interfaced with the Low Power Flux Logger (LPFL) system which ensured data storage during the Phase-B experiments. Refer Figure- 2 for a photograph of the TIP drive mechanism and schematic of the Interface with dolly panel and LPFL system [3].

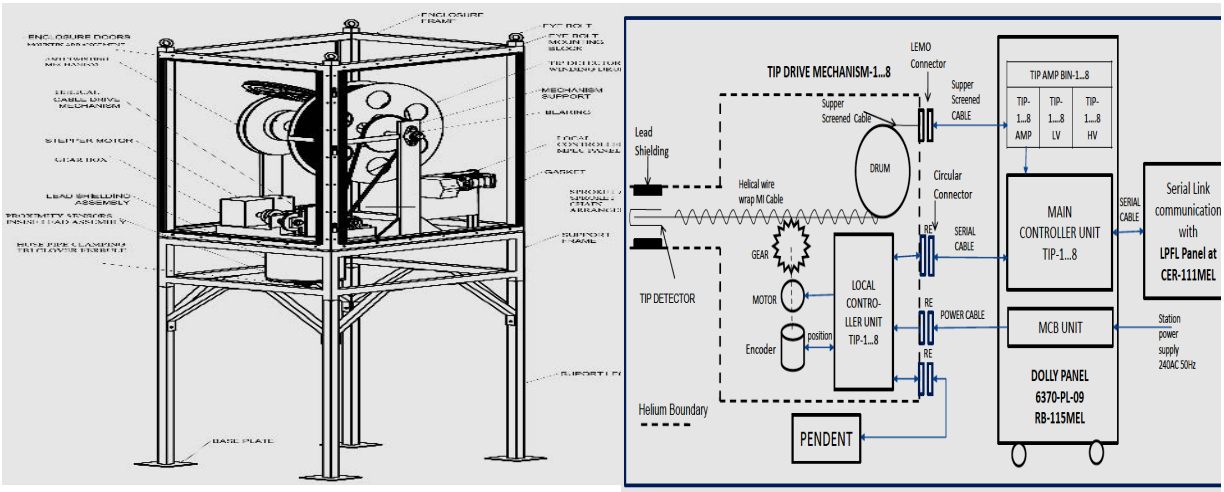


Figure-2**:** TIP drive mechanism and TIP Dolly panel Interface

The 6 number of TIP drives were installed in identified VFUs in the pump room at RB115 MEL whereas for the Horizontal Flux Units (HFUs) 2 numbers were placed at (Shutdown System-2) SDS-2 area inside the reactor building.

3. Experiment for the Flux Profile Measurements

Due to their small dimension (6mm diameter), the detectors were able to travel through Central Carrier Tube (CCT) of VFUs and HFUs capturing the thermal flux variation along the length of the carrier tube and at SPND locations in these flux units. The sensitivity (*S*) of a particular SPND housed in the flux unit was estimated by the relation,

$$S = \; _{I}\square_{SPND}\square \; \square \; 1\square(b-a)\square \; a\square b\square$$

$$S = \frac{I_{SPND}}{\frac{1}{(b-a)}\int_a^b \Phi(x)dx}$$

Where, I_{SPND} (Amperes) is the current measured by the SPND, S_v (Amperes/nv) is the sensitivity of the SPND, Φ(x) is the measured flux ("x" being the distance along the length of the SPND), a = start elevation, b = end elevation of SPND. Thus, (b-a) = length of the SPND[1].

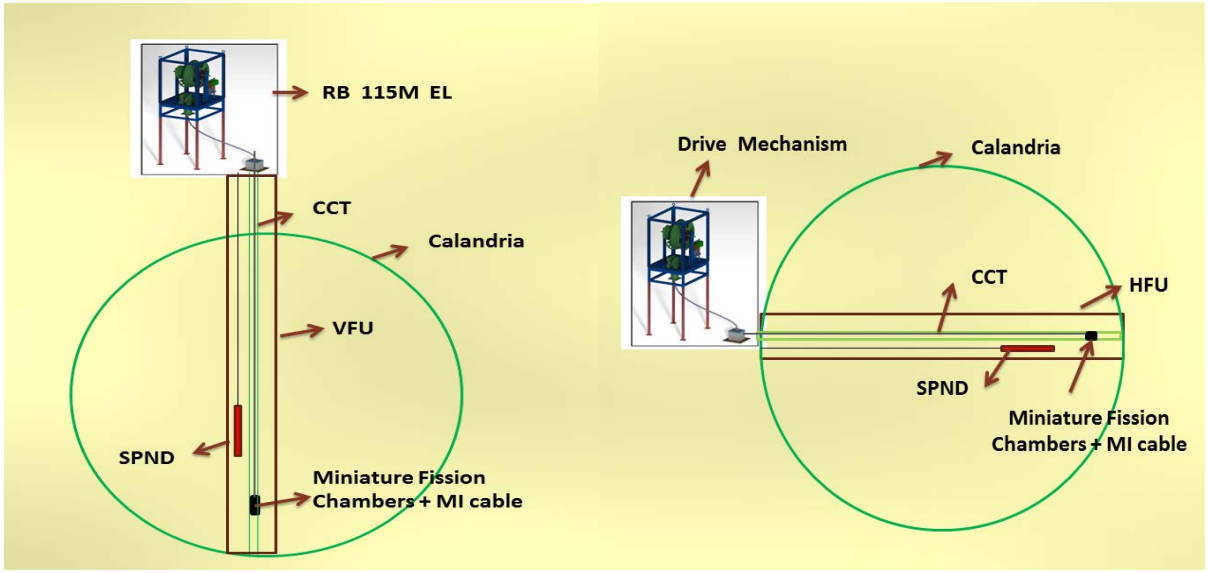


Figure-3**:** Representative diagram for flux profile measurements in a VFU and HFU

4. Results

TIP Scans for 22 cases of reactivity devices configurations [1] were carried out for flux measurement during low power physics experiments in total of 18 VFUs and 5 HFUs. Various parameters such as Ion Chamber readings, reactivity device positions, select SPND readings were recorded by system data recorder. TIP detectors were moved inside the core with speed of 1mm/s and Flux Profiles obtained from TIP detectors were compared with simulated flux profiles for all configurations. It is seen that the Observed Flux Profile matches well with the expected Flux Profile. A plot showing the flux profile comparison of TIP scan with V_SPND and IQS3D simulations in VFU-5 for Nominal Reactivity Device Configuration is given in Figure-4 [1]. The peaks and valleys in the TIP scan as shown in Figure-4 is due to the location of probe during scanning i.e. if the probe is nearby any fuel channel there is a dip due to greater absorption of thermal flux in the vicinity of fuel channel and if the probe is away from any fuel channel then there is a corresponding peak. Locations of reactivity devices as well as VFUs are shown in Figure-5.

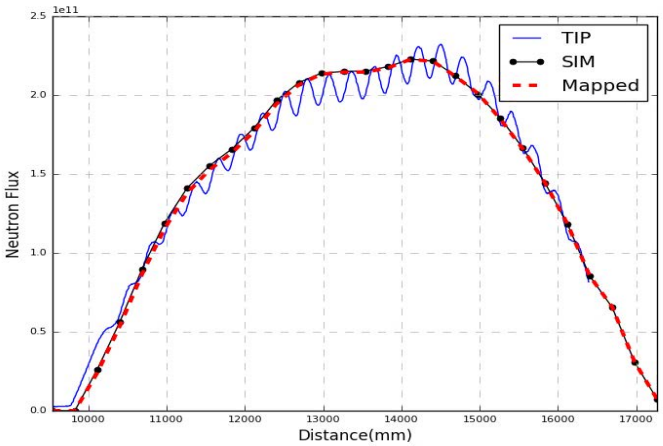


Figure-4: VFU 5 fluxes as measured by TIP 2 for Nominal Reactivity Device Configuration

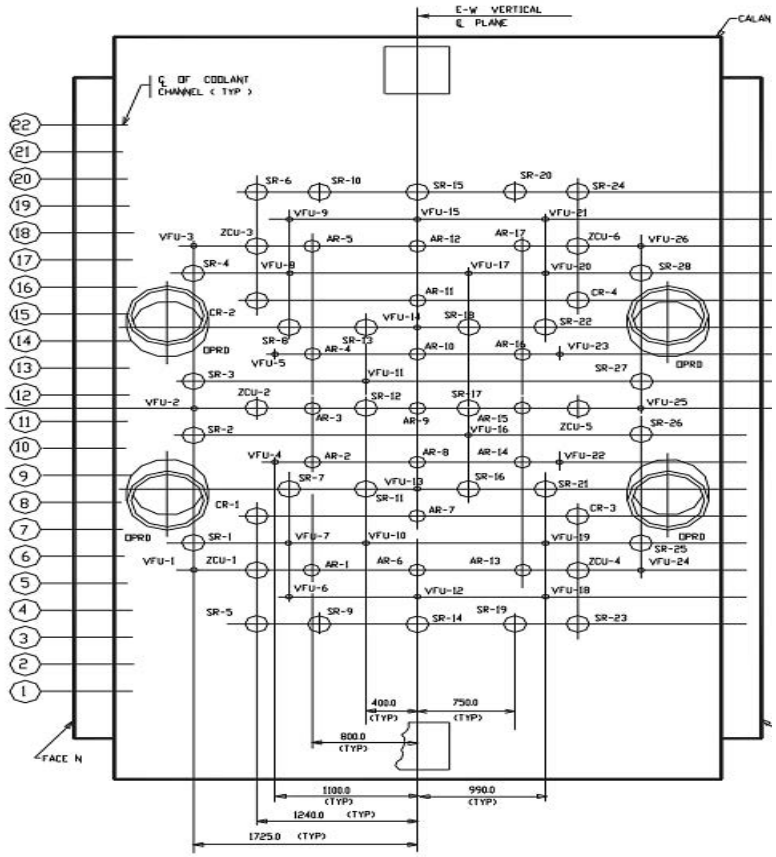


Figure-5: Top view of calandria showing locations of reactivity devices

5. Conclusion

In-core flux profile measurements were successfully carried out in selected flux units. Observed flux profile was compared with simulations of CFWARO and IQS-3D. In situ estimation of the sensitivity of SPNDs were also carried out. The V SPND sensitivity derived from TIP scan was close to the value of 1.05 x 10^{-20} A/nv as measured in KAMINI reactor at Kalpakkam.

From the comparison of TIP and ion chamber readings, it was inferred that the reactor power indicated by ion chambers were about 6.44 times lower than actual power. The gain of the ion chamber amplifiers was suitably corrected. The actual power level was confirmed after thermal power measurements starting from 5%FP after performing station heat balance [4]**.**

6. References

[1] *Commissioning report for low power physics experiments (Part-b)"*,Rev-0 , KAPP-3&4-01132-CR1

[2] *Report on Status of Low Power Flux Logging System and Travelling Incore Probe (TIP) System of KAPP-3, KAPP-3&4/60000/C&I/2020/183*

[3] *Design note on Low Power Flux Logger (LPFL) for 700 MWe PHWR,* 700MWe/DN/63715/0001/R1

[4] *Designer comments on CR for LPPE (Part-B) at KAPP-3,* NPCIL/ FPSS/2020/M/708

ESTIMATION OF DYNAMIC CHARACTERISTIC OF INCONEL DETECTORS IN KAPP-3

Suresh Kandpal [1], Rajarshi Das[2], M. P. S. Fernando[1]
[1]Nuclear Power Corporation of India Limited, Mumbai, India
[2]Kakrapar Atomic Power Project-3&4, Gujarat, India
[1]*e-mail: ksuresh@npcil.co.in*

Abstract

Self-powered neutron detectors (SPNDs) are used extensively in large PHWRs such as 540 MWe and 700 MWe for flux-mapping, control and protection. In Indian PHWR, various kinds of SPNDs are used for protection and control purpose such as Inconel, vanadium. All these detectors are prompt except vanadium which is delayed responding. For shut down system actuation, prompt responding detectors are used while on the other hand vanadium detectors are used in flux mapping system. In the present study, we discuss the methodology to find out dynamic response of In-conel detectors using measured detector signal, acquired during reactor shutdown at Kakrapar Atomic Power Project-3 (KAPP-3). The signals from the detectors as function of time following the trip are fitted using nonlinear regression to determine response. Results show that the dominant term in Inconel detector, due to prompt (n, γ, e) interaction, accounts for nearly 93 to 96% of the total detector signal.

1. Introduction

A typical self-powered neutron detector consists of three concentric cylindrical parts viz. a collector-sheath, an insulator and an emitter (Figure 1). The current induced in a SPND is mainly due to three main types of interactions (n, β-), (n, γ, e) and (γ, e). For a self-powered detector, the material and dimension are chosen so that one or two of these interactions will dominate thus producing a relatively large net current [1, 2]. The net current generated in the detector is the sum of all these components:

$$I = I_{(n,\,\beta-)} + I_{(n,\gamma,\,e)} + I_{(\gamma,\,e)}$$

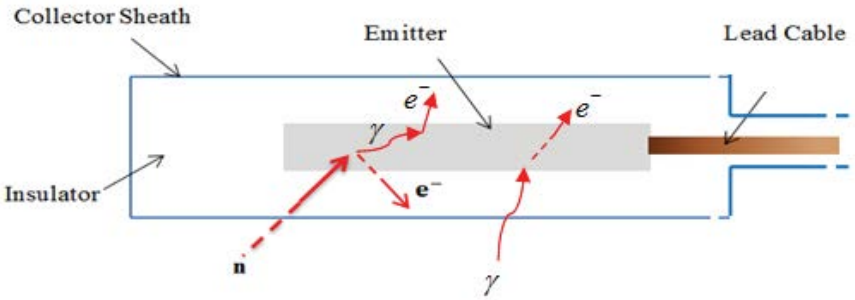


Figure 1: Schematic of SPND

Because the (n, γ, e) interaction produces a prompt signal, i.e. one which follows changes in neutron flux essentially instantaneously, while the (n, β-) and delayed (γ, e) interactions results in delayed signals. A detector in which the (n, γ, e) interaction dominates is preferred in many application, and particularly if the detector is to be used in a reactor safety system. A detector having Inconel emitter and Inconel sheath is such a device. The detector material Inconel is a nickel based alloy containing nominally 76% Nickel, 15.5% Chromium and 8% Iron. It is a prompt responding detector with the primary advantage of low burnout rate, lower activation field and lower (γ, e) sensitivity. The prompt and delayed components together decide the dynamic response of a SPND during varying flux at SPND location [3].

The main objective of this work is to develop a dynamic model for Inconel SPNDs based on measured time characteristic during reactor shutdown in KAPP-3 and to implement the model to simulate the dynamic response of SPNDs during neutron flux transient.

2. Methodology

The nonlinear regression model is

$$y_i = f(x_i; \theta) + \varepsilon_i \qquad i=1,2,\ldots,M \qquad (1)$$

where the observed values of the y_i's constitute the responses of the dependent variable, the known x_i's are the vectors of the values of the independent variables, θ is the vector of p regression parameters, M is the total number of data points and the ε_i's are independently distributed normal errors with mean zero and variance σ^2. For this model, a least squares estimate of θ is also a maximum likelihood estimate of θ.

The residuals for the model are

$$e_i(\theta) = y_i - f(x_i; \theta) \qquad i=1,2,\ldots\ldots,M \qquad (2)$$

A value of θ that minimizes $\sum_{i=1}^{M}[e_i(\theta)]^2$ is a least squares estimate of θ.

In order to determine the set of values for prompt and delayed fractions, the current from the detector as function of time following trip, is fitted to the equation (3) and (4).

$$\frac{I(t)}{I(0)} = F_P \frac{\emptyset(t)}{\emptyset(0)} + \sum_{j=1}^{N_d} \frac{I_j(t)}{I(0)} \qquad (3)$$

$$\frac{dI_j(t)}{dt} = \lambda_j I_j(0) \left[\frac{\emptyset(t)}{\emptyset(0)} - \frac{I_j(t)}{I(0)}\right] \qquad (4)$$

$$A_j = \frac{I_j(0)}{I(0)} \qquad (5)$$

Here, $I_j(t)$ is the current associated with j^{th} delayed component, having a decay constant λ_j, at a time t after the trip. F_P is prompt fraction of the total current and A_j is fraction of the total current corresponding to j^{th} delayed component. $\phi(t)$ is the time variation of the flux at detector location following reactor trip.

3. Results and Discussions

The current I(t) for in-conel detectors was obtained from fast recorder (sampling interval 20.0 ms) following KAPP-3 reactor trip by SDS-1 for 80 seconds. The time variation of the flux, $\phi(t)$ at each detector location during reactor trip was computed using in-house 3D space time neutron kinetic code, IQS3D [4].

3.1 Validation using synthetic signal:

The total detector signal has one prompt component and N_d delayed components. Each delayed component is proportional to the decay rate of an activated fission product. The current of the detector is simulated with known amount of prompt (F_P) and delayed (A_j) components using equations (3) and (4). The results with synthetic signal, Table 1, show that the method is able to reproduce the fraction of prompt and delayed components for different cases.

Table 1: Simulation results for synthetic signal

S. No.	No. of delayed component	Synthetic Signal			Non Linear Least Square Fitting Results		
		Prompt Fraction (F_P)	Delayed Fraction (A_j)	Decay constant (sec^{-1})	Prompt Fraction (F_P)	Delayed Fraction (A_j)	Decay constant (sec^{-1})
1.	1	0.083	a=0.917	λ=3.6e-3	0.082	a=0.918	λ=3.6e-3
2.	2	0.90	a_1=0.05 a_2=0.05	λ_1=3.33e-2 λ_2=3.75e-3	0.90	a_1=0.05 a_2=0.05	λ_1=3.33e-2 λ_2=3.75e-3
3.	3	0.90	a_1=0.02 a_2=0.04 a_3=0.04	λ_1=3.33e-2 λ_2=3.75e-4 λ_3=7.50e-5	0.90	a_1=0.02 a_2=0.04 a_3=0.04	λ_1=3.33e-2 λ_2=3.75e-4 λ_3=7.50e-5

3.2 Dynamic response using measured reactor trip data for in-conel detector:

The dynamic response (F_P and A_j) for in-conel detectors was measured by fitting the decay of the signal from the detector to the equations (3) and (4). Results show that the dynamic response of Inconel detector is dominated by (n, γ, e) interaction and have prompt fraction of nearly 0.93 to 0.96. The delayed response of the Inconel detector is described using two delayed components. The delayed components can be attributed to the combined effect of delayed reactor γ-rays, and to the β-decay of nuclides such as ^{55}Cr and ^{66}Cu (Table 2). The simulated dynamic response of Inconel detectors using determined parameters along with measured responses are shown in figure 2.

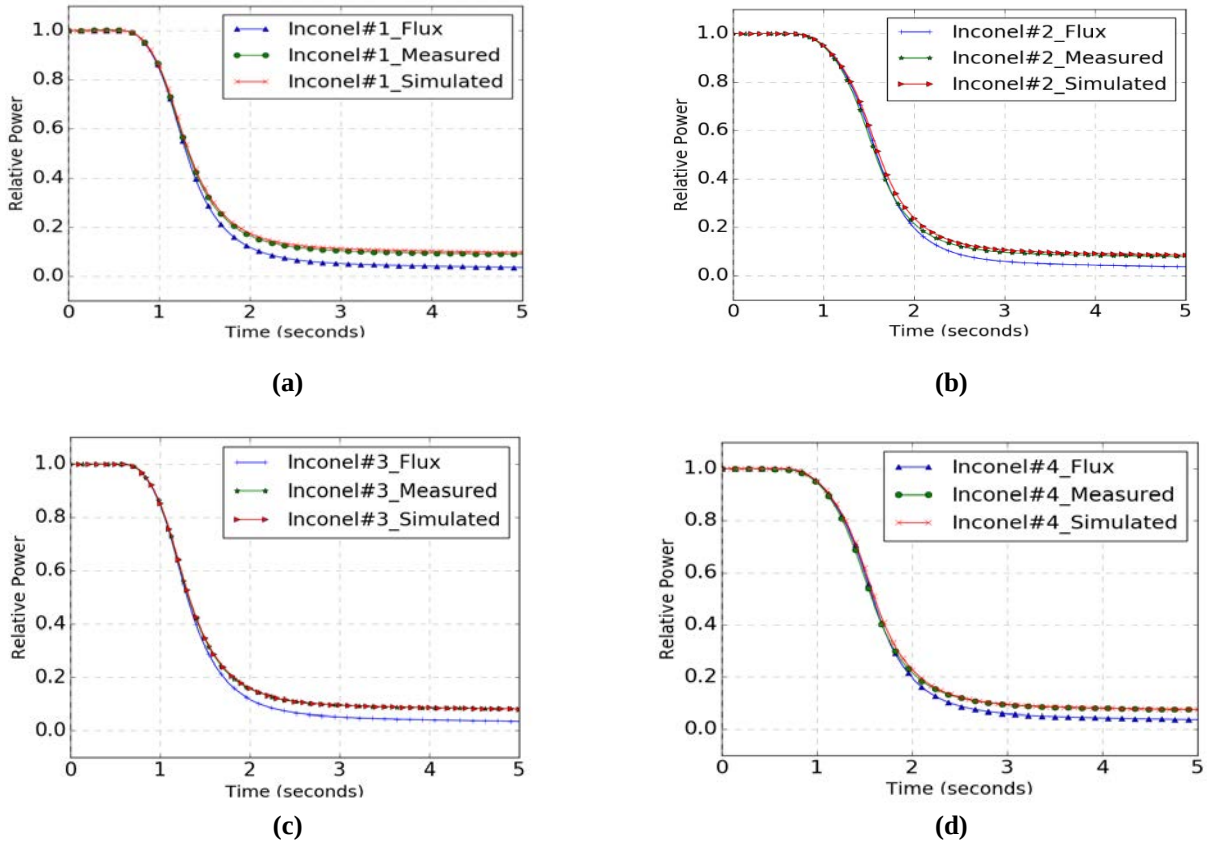


Figure 2: Simulation of Inconel SPNDs (no. 1 to 4) Dynamic Response

Table 2: Prompt and delayed fractions for Inconel detector

Parameter	Decay Constant (sec^{-1})	Amplitude of Parameter F_P or a_i			
		Inconel#1	Inconel#2	Inconel#3	Inconel#4
F_P	-	0.9355	0.9492	0.9527	0.9621
λ_1	1.05e-2	0.0246	0.0109	-0.0098	-0.0169
λ_2	6.50e-4	0.0399	0.0399	0.0571	0.0548
λ_3	7.50e-5	*	*	*	*

* The amplitude of λ_3 could not be determined as the measured data was available for only few minutes after reactor trip and the data recording is limited to 0 to 150%, resulting to the loss of information about negative signal.

4. Conclusion

Methodology to obtain the dynamic response of Inconel SPNDs using measured detector signal during reactor shutdown is developed. The signals from detector as function of time are fitted using nonlinear regression to determine the prompt and delayed fractions. The dynamic response of Inconel detectors, used for safety and control in the reactor, are modeled using one prompt and two delayed components. The Inconel detector's response is dominated by (n, γ, e) interaction and the detector is nearly 93% to 96% prompt.

5. References

[1] C.J. Allan, "A New Self-Powered Flux Detector", *Atomic Energy of Canada Ltd., Rep. AECL-6681*, 1979.

[2] C.J. Allan, "A Review of the dynamic response of self-powered flux detectors in CANDU reactors", *AECL. 2nd Annual Conference proceedings*, 1981.

[3] D.S. Hall and S. Shimoto, "A Computer-controlled travelling flux detector system for CANDU reactors", *IEEE transactions on Nuclear Science*, 31(1) 1984.

[4] M.P.S. Fernando, "Development of Space-time Kinetics Technique to analyse localized perturbations in PHWR", *PhD Thesis, IIT Bombay, 2003.*

MODIFIED SLOPE METHOD ANALYSIS OF DELAYED NEUTRON DATA FOR EARLY FUEL FAILURE IDENTIFICATION

A. Chiranjit Ghosh[1], B. Alok Kumar Jha[1] and C. Samiran Samanta[1]
[1]Tarapur Atomic Power Station,Tarapur, India
[1]*e-mail: - cghosh@npcil.co.in*

Abstract

TAPS#3&4 are twin 540MWe IPHWRs using 37elrment natural Uranium fuel bundles. Any loss in fuel-clad integrity in reactor is undesired; in such cases early detection and removal becomes priority. For identification of coolant channel having fuel failure, established system and method is in place. However operating experience shows that there is room for improvement in analysis method of DNM data. A new method "Modified Slope Method (MSM)" has been developed which can provide accurate identification in lesser time compared to standard 3σ method as well as trend method.

1. Introduction

Each 540Mwe PHWR core consists of 392 fuel channels and each channel has 13 natural Uranium (NU) bundles [1]. Early identification and removal of failed fuel [2, 3] is imperative since active fission products from failed fuel leads to enhanced corrosion in PHT loop, generates hotspots making maintenance job radiation dose intensive and elevates source term. Continued irradiation of failed fuel element may alter fuel geometry or dimension. This can impair fuel heat removal, coolant channel inner surface or fuelling machine during handling. Presence of failed fuel represented by PHT I^{131} activity and the expectation is to maintain PHT I^{131} activity <0.5 µCi/L; could be achieved only if there is no failure inside core. For higher I^{131} activity, DNM system scan data is used to identify the failed fuel channel.

2. DNM system data acquisition and analysis

The principle is based on comparative quantification of neutron counts in coolant samples from each channel where coolant sample carries delayed neutron precursors from leaky fuel. It has 28 BF3 gas filled detectors operating in proportional region. Each detector takes scan of a pre-selected group of 14 fuel channels; the grouping of channels is based on coolant flow direction (S/N), similar power and similar sample transport time. The system scans 28 coolant channel samples in one batch using the 28 detectors and collects all 392 DN data in 14 batches. After completion of the scan process, the collection of 392 signal readings (DN data) becomes available in Computerised Operator Information System (COIS) as detector Vs batch tabulation.

2.1 Analysis by 3σ method and trend method:

Consider n is the detector number, b is the batch number and $S_{b,n}$ is the DN count of the channel $C_{b,n}$. The DN ratio of this channel is obtained by the following expression

$$\text{DN ratio } (N_{b,n}) = \frac{\text{Individual DN count } (S_{b,n})}{\text{Detector average count } (K_n)} \text{ ; b =1 to 14; n = 1 to 28} \quad (1)$$

$$\text{Where, Detector average count } (K_n) = \frac{1}{14}\sum_{b=1}^{14} S_{b,n}$$

Standard deviation of the 392 DN ratio set is obtained by the following expression

$$\sigma = \sqrt{\frac{1}{bn-1}\sum_{b=1,n=1}^{b=14,n=28}(N_{b,n} - \bar{N})^2} \qquad \text{Where} \quad \bar{N} = \frac{1}{bn}\sum_{b=1,n=1}^{b=14,n=28} N_{b,n} \qquad (2)$$

Channels having DN ratio less than (1-3σ) and greater than (1+3σ) are segregated as odd ones. The channels with more than 3σ deviation in normalized reading from unity are suspected of having failed fuel, whereas channels with less than 3σ deviation are suspected to have sample blockage or deficient signal [2].

However the 3σ method was not giving correct identification with desired promptness (i.e. in early stage of failure) leading to refueling of channels as failure suspect without success. This incurred increase in refueling and loss in burnup. The inherited spread in DN ratio data set was the underlying cause of not getting desired result by 3σ method. As a solution, previously resorted to long term trending of DN data (counts and ratio) and analysis was based on picking up the channel rising above all other intra-detector channels. Identification based on synchronized rise in both DN count and DN ratio was successful and quicker compared to 3σ method as well as it restricted burnup loss. But being it a qualitative review method on collection of trend graphs for 14 channels in each of 28 detectors, it was cumbersome and lacks efficiency needed to meet expectation. *Operating experience also revealed scope for improvement in the data processing and analysis methodology*. This assertion is based on the following observations. When DN count of any individual channel inherently maintains lower value either due to higher sample delay or higher flow restriction compared to other channels of that detector, then it takes longer time to rise above other channels to get identified in case of failure. Similarly rise of an individual channel trend lacks attention if its count maintains higher values throughout, because of prevailing causes like low sample delay or contamination. So, here impact of values and visuals (trend plots) are not in synergy for all cases. The drawbacks of absolute signal trend analysis removed in new developed *Modified Slope Method (MSM)* analysis. It is quicker, accurate and the real life performance has been demonstrated by prompt identification of failed fuel channels. *In three months span this method identified 3 channels and failure confirmed afterwards, so far providing 100 % success rate*.

3. Modified slope method (MSM)

TAPS#3&4 reactors are in continuous full power operation, steady state equilibrium core condition is maintained with daily on power refueling. Channel refueling is primarily based on its burnout state and flux zone. Refueling replace the FP laden burnt fuel with FP free fresh fuel. In this process DN count and DN ratio of the channel reduces by certain magnitude depending on its position, irradiation and local perturbation. Though both DN count and DN ratio show similar phenomena in this case, DN ratio is preferred as effects from channel power and DN detector gets it nullified. With fuel irradiation FP gets accumulated and influence DN ratio to raise in steady proportion without any fuel failure, this is a normal phenomenon. Analysis past 15 years 540MWe actual data reveals that DN ratio increases by 25mili percent per FPD due to irradiation. For nominal fuel residence of 200 FPDs, irradiation contributes 5% increase in DN ratio. Apart from own irradiation contribution, neighboring perturbation leads to maximum 2% increase in DN ratio. So the DN ratio of any healthy channel increase up to 7% due to combined effect of irradiation and local perturbation as it becomes due for refueling. Fuel bundle having failure will contribute higher than nominal and increase the DN ratio. We trend the *% increase in DN ratio* values w.r.t. time. When the instantaneous *% increase in DN ratio* of any channel grows above 7%, the channel gets flagged. The novelty of MSM is in elimination of effects due to fuel irradiation rate, fuel residence time, local core perturbations as well as measurement variance by sample delay time spread or contamination, which is achieved by analyzing on % *increase* w.r.t. recent past.

3.1 MSM calculation methodology

Calculation of *% increase in DN ratio* is done over a specified time period. Based on the *% increase in DN ratio*, channels are short listed as failed fuel. For every detector a normal average DN count (K_n) is calculated. For a particular detector, if DN count of a batch is <80% of the *detector average count* (K_n) then the DN count of that batch is excluded. This exclusion rationalizes the data set by eliminating unhealthy /spurious DN readings. From this healthy reading, *eliminated average* and *ratio* are calculated by following expressions.

Eliminated average = Average of healthy DN counts of the detector (3)

Eliminated ratio = DN counts of the channel / Eliminated average (4)

This eliminated ratio is the *True DN ratio* if any batch count is less than 80% of average count otherwise $N_{b,n}$ is the true DN ratio. If *true DN ratio* is less than 0.8 then modified ratio for the particular date will be last healthy *true DN ratio* which is greater than 0.8 otherwise modified ratio is same as *true DN ratio*. Slope of this modified ratio is calculated within the date range (date1 to date2) as follows- If p is the number of days between two given dates, y_k is modified DN ratio on k^{th} day, where k = 1,2,…..p, then slope of modified DN ratio of the particular channel is found out by linear regression of data using formula-

$$\text{slope(b)} = \frac{\sum_{k=1}^{k=p}(k-\bar{k})(y_k-\bar{y})}{\sum_{k=1}^{k=p}(k-\bar{k})^2} \quad (5)$$

$$\text{Where, } \bar{k} = \frac{1}{p}\sum_{k=1}^{p} k \quad and \quad \bar{y} = \frac{1}{p}\sum_{k=1}^{p} y_k$$

Using the slope, % increase in DN ratio over the given period is calculated by formula-

$$\%\ \text{increase in DN ratio} = 100 * p * b \quad (6)$$

MSM method is summarized below using flow chart, data and result in Figures- 1, 2, 3.

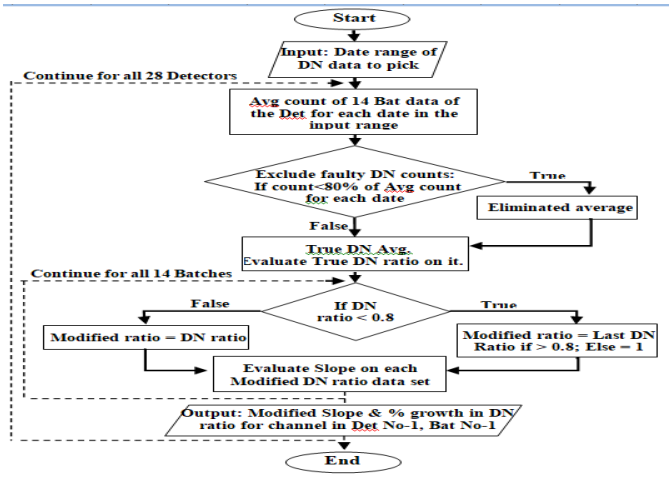


Figure 1: Flow chart showing MSM method.

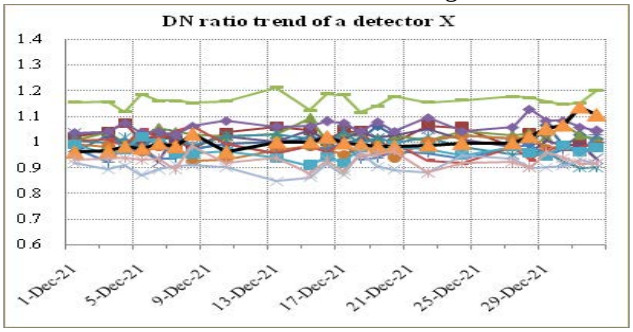


Figure 2: A normal DN ratio trend

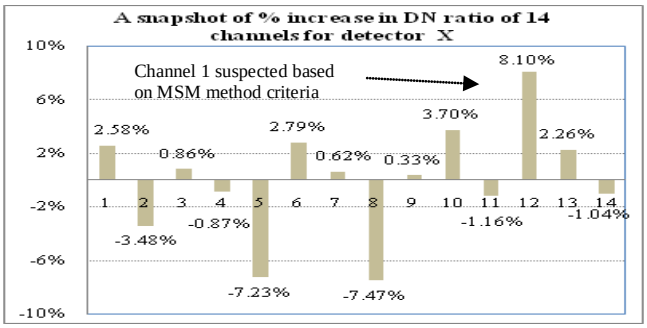


Figure 3: MSM output snapshot on same data

4. Results

Figure 4 shows the % increase in DN ratio over a month for channel 1. The instantaneous % increase crossed 7% mark on 30-Dec-21 and it was refuelled on 01-Jan-22 as failure suspect. The channel 1 burn up was 5331 MWD/TeU, DN count was 66cps whereas detector average was 62cps, DN ratio was 1.06; none of these parameters indicate presence of failed fuel. Channel 1 suspected and refueled based on outcome of MSM method only. Change in PHT I-131 concentration and DN ratio are given in Table-1. Sniffing result confirmed failure in two bundles of channel 1.

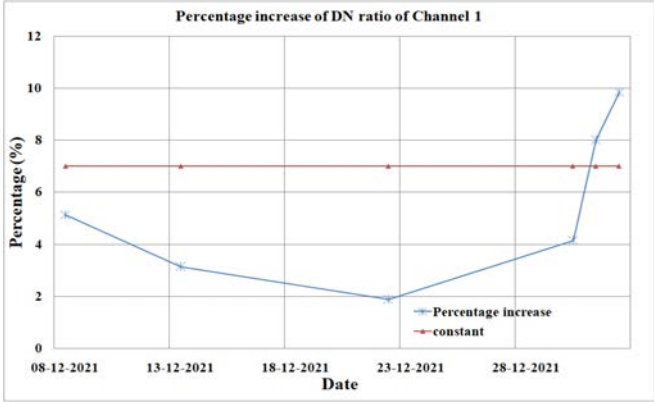


Figure 4: Percentage increase of DN ratio of channel 1

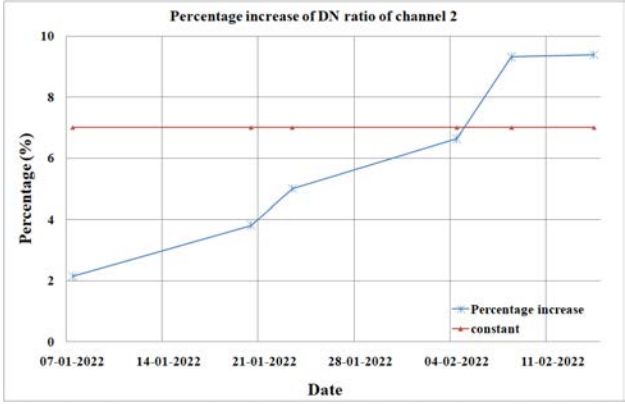


Figure 5: Percentage increase of DN ratio of channel 2

Figure 5 shows the trend of % increase in DN ratio for channel 2 over 6 weeks period. The instantaneous % increase crossed 7% mark on 08-Feb-22. It was refuelled on 16-Feb-22; the delay was due to refuelling constraint. The channel 2 burn up was 6218 MWD/TeU, DN count was 140cps, detector average was 128cps and DN ratio was 1.09; none of these parameters indicate presence of failed fuel. Change in PHT I-131 concentration and DN ratio are given in Table-2. Sniffing result confirmed failure in two bundles of channel 2.

Table-1: Before and after refueling of channel 1

DN counts (cps)		PHT I-131 (µCi/L)	
Before	After	Before	After
72	67	11.33	0.81

Table-2: Before and after refueling of channel 2

DN counts (cps)		PHT I-131 (µCi/L)	
Before	After	Before	After
140	130	0.99	0.76

5. Conclusion

Modified Slope Method (MSM) has been developed on DN ratio growth rate for early identification of failed channel. We present comprehensive data for two Identified failed fuel in this paper. The MSM method has been successful so far. The method is unique as it eliminates the error introduced due to fuel irradiation, neighboring perturbation and random loss or spread in DN data. Software tool developed for ease of data handling and short listing and trending as per user. We intend to add FPNG trend analysis in MSM for identification of failed fuel.

6. References

[1] Design Manual on Reactor Physics of TAPS#3&4. TAPP-3&4/DM/01100/01

[2] Design Manual on Failed fuel monitoring system.TAPP-3&4/DM/63132/01

[3] Reactor physics sectional procedure for identification andremoval of failed fuel from the core.TAPS- 3&4/ 01100/ RP/ 01

IMPROVEMENT IN FUEL FOLLOWUP SCHEME USING ONLINE INCORE VANADIUM DETECTOR READINGS OF FLUX MAPPING SYSTEM

Abhishek Chakraborty[1], AmrithaKrishnan S[2], Rajarshi Das[2], M. P. S. Fernando[1]
[1]Nuclear Power Corporation of India Limited, Mumbai, India
[2]Kakrapar Atomic Power Project-3&4, Gujarat, India
[1]*e-mail: abhishekc@npcil.co.in*

Abstract

The power distribution in the reactor core is determined by the fuel management code which solves the multi-group steady state neutron diffusion equation in 3 dimensions. The various lattice constants used for characterizing the diffusion, fission, absorption and scattering of neutrons depend on the composition of the fuel in each bundle. The power distribution in the core also depends on the reactivity device positions which vary continuously for maintaining steady power level. Since, the burnup change occurring due to reactor operation per day is a slow process, the core follow up is generally carried out on daily basis and is based on the steady state power distribution. This estimation is based on the assumption that the reactor flux shape remains invariant during the day. However, if we consider local changes in the reactor flux/power distribution during the day there will be improvement in burnup estimation. In this study, a new approach of burnup estimation based on vanadium SPND readings of the Flux Mapping System has been suggested which will have better accuracy.

1.0 Introduction

From the point of view of core irradiation, the operating life of a PHWR can be subdivided into four stages. The first four namely Fresh Core (0FPD), Samarium Dip (~5FPD), Plutonium Peak (~35 - 40 FPD) and Onset of refueling (~100-140 FPD) are short, transitional periods. The fourth stage is known as the equilibrium core and represents about 95% of the lifetime of the reactor. The Fresh core condition corresponds to the state when all fuel channels are loaded with fresh Natural Uranium (NU) bundles with Depleted Uranium (DU) bundles / Deeply Depleted Uranium (DDU) bundles for flux flattening purpose. The excess reactivity in this state is high (~90mk) and is compensated by adding neutron poison like Boron /Gadolinium in the moderator. In this state, the fuel temperature coefficient of reactivity is maximum (negative), coolant temperature coefficient is also negative, delayed neutron fraction and neutron prompt generation time are also maximum. However, with increase in burnup due to operation, the values of all these parameters decrease due to formation of Plutonium-239. Hence, the reactivity coefficients change with burnup of the fuel.

In the initial period of operation, i.e., from Fresh core to Onset of refueling the excess reactivity available in terms of neutron poison in the moderator is utilized for compensating for fuel burnup. Regular online refueling starts around the Onset of refueling and the refueling rate is high. After around 600FPDs, the refueling rate becomes constant and the values of all the parameters like reactivity coefficients and point kinetic parameters stabilizes. This state is known as equilibrium core and PHWRs operate the maximum portion of their life in this state.

The burnup database consisting of power extracted from each bundle is maintained and updated every full power day basis. This burnup distribution is used for determining the operating power distribution in the core, excess reactivity in the core, selection of refueling fuel channel and also determination of safety parameters like fuel, coolant, channel, void reactivity coefficient of reactivity and point kinetic parameters like effective delayed neutron fraction and neutron prompt generation time. These reactivity

feedback coefficients alongwith the point kinetic parameters govern the rate of power rise/fall during any reactivity initiated transient. Due to use of Natural Uranium as fuel, PHWRs operate with very less excess reactivity for most part of their lifetime and in core fuel management becomes very crucial.

2.0 Burnup Estimation using vanadium detector readings

The fresh core loading pattern was considered as the initial starting point for burnup estimation. Two approaches were used for estimation of burnup, one being the conventional method and the other being estimation using vanadium SPND readings. The conventional approach is carried out for intervals of 1 FPD and 0.5 FPD whereas the second method estimates the burnup at an interval of 1 second.

2.1 Mesh Powers estimation using vanadium detector readings

Using the 106 vanadium SPND readings the combining coefficient was estimated for each each second. For estimating 9408 (392 channels×24 axial meshes) mesh powers a new GGMatrix, "GG_mesh", was generated of dimension 9409×61 and the structure is given below:

$$\left[GG_mesh\right]_{9409\times 61} = \begin{bmatrix} tp_1 & tp_2 & \cdots & tp_{61} \\ mp_{1,1} & mp_{1,2} & \cdots & mp_{1,61} \\ \vdots & \vdots & \ddots & \vdots \\ mp_{9408,1} & mp_{9408,2} & \cdots & mp_{9408,61} \end{bmatrix}_{9408\times 61} \qquad (1)$$

tp_i = Component of i^{th} mode in total power,
$mp_{j,i}$ = Component of i^{th} mode in power of j^{th} mesh

The final output matrix, FF_mesh is obtained as

$$[FF_mesh] = [GG_mesh] \times [AA]$$

$$\Rightarrow \begin{bmatrix} tp \\ MP_1 \\ \vdots \\ \vdots \\ \vdots \\ \vdots \\ MP_{9408} \end{bmatrix}_{9409\times 1} = \begin{bmatrix} tp_1 & tp_2 & \cdots & tp_{61} \\ mp_{1,1} & mp_{1,2} & \cdots & mp_{1,61} \\ \vdots & \vdots & \ddots & \vdots \\ mp_{9408,1} & mp_{9408,2} & \cdots & mp_{9408,61} \end{bmatrix}_{9409\times 61} \begin{bmatrix} a_1 \\ a_2 \\ \vdots \\ \vdots \\ \vdots \\ \vdots \\ a_{61} \end{bmatrix}_{61\times 1} \qquad \ldots\ldots.(2)$$

tp_i = Component of i^{th} mode in total power,
$mp_{j,i}$ = Component of i^{th} mode in power of j^{th} mesh
tp = total reactor power (MWth)
MP_i = Mesh power (KWth)

2.2 Burnup estimation using the mesh powers

The burnup matrix was estimated by the following matrix multiplication

$$\Rightarrow \begin{bmatrix} Burnup_{1,t+\Delta t} \\ \vdots \\ Burnup_{9408,t+\Delta t} \end{bmatrix}_{9408\times1} = \begin{bmatrix} Burnup_{1,t} \\ \vdots \\ Burnup_{9408,t} \end{bmatrix}_{9408\times1} + \begin{bmatrix} MPF_1 \\ \vdots \\ MPF_{9408} \end{bmatrix}_{9408\times1} \frac{\Delta t}{Mass} \qquad (3)$$

$Burnup_{i,t+\Delta t}$ = Mesh Burnup for i^{th} mesh at time $t+\Delta t$
$Burnup_{i,t}$ = Mesh Burnup for i^{th} mesh at time t
MPF_i = Mesh power for i^{th} mesh normalized to fission power
Mass = Mass of Uranium in fuel mesh in Tonnes.

3.0 Results and discussions

The period of study is the initial operation for KAPS#3 from January 2021 to April 2021. The reactor has operated up to a maximum power of 50%FP and the operating history is shown in Figure 1. The reactor had crossed the Samarium Dip and was approaching the plutonium peak. Since, vanadium SPND readings are reliable for power levels greater than 1%FP, the duration of operation below 1%FP has not been considered for the analysis.

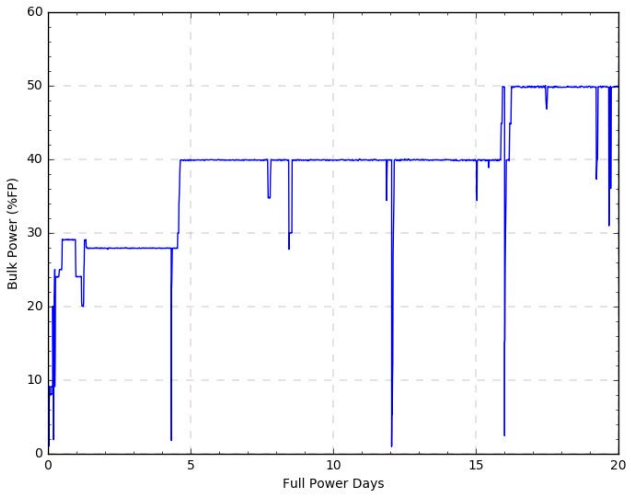
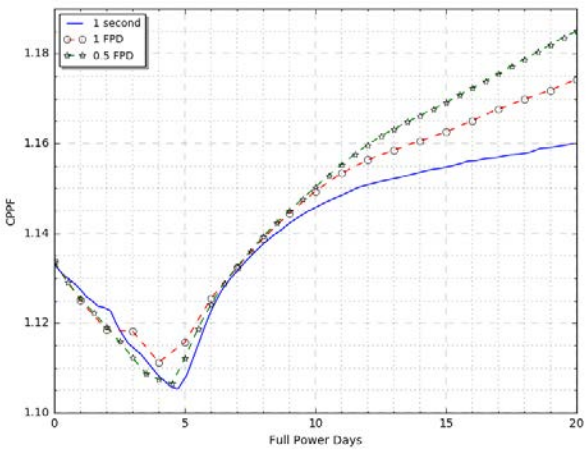


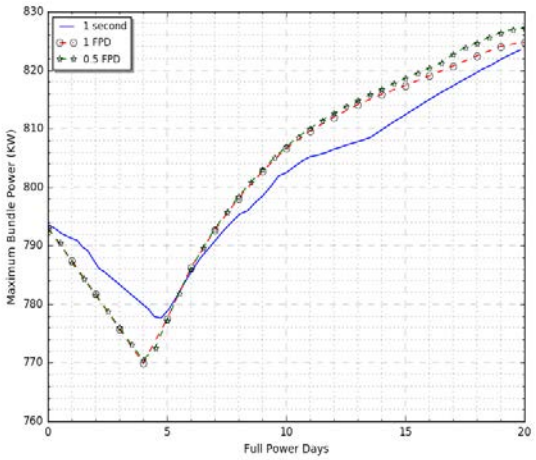
Figure 1 Operating Power History in KAPS#3

The variation of Channel Power Peaking Factor (CPPF) and Maximum bundle power has been compared and given in Figure 2. Core follow-up using intervals of 1 and 0.5FPD have been compared with FMS generated burnup distribution (referred to as 1 second). Since the follow-up is carried out at 100%FP with all ZCCs at 44%FL and All ARs 100%IN, the values of CPPF are greater than 1.1. However, the CPPF estimated up to 5 FPD using all the three methods are nearly the same. However,

beyond 8 FPDs, the CPPF is overestimated by follow-up simulations at 0.5 and 1 FPD. Maximum Bundle Power is underestimated by follow-up simulations at 0.5 and 1 FPD till 4.5 FPD and beyond that they are overestimated.



(a) Channel Power Peaking Factor



(b) Maximum Bundle power

Figure 2 Variation of Channel Power Peaking Factor and Maximum bundle power during core followup

4.0 Conclusions

In the present work, meshwise burnup estimation of all 4704 fuel bundles have been carried out for initial 20 FPD of operating for KAPS#3 using the Vanadium detector readings and compared with that using existing follow-up methodology. Various parameters like core excess reactivity, 14 zone powers, Channel Power Peaking Factor, Maximum bundle power have been compared for the duration with traditional approach. It is observed that, global parameter results are comparable where as there are some differences in the localized parameters such as few zone powers, CPPF and maximum bundle power which may be attributed to the local power variations. This core follow-up using vanadium SPND readings will be continued once KAPS#3 power operation is resumed. This approach will help in more accurate burnup estimation and hence better representation of the core status.

4.0 References

[1] Preliminary Safety Analysis Report for 700 MWe PHWR.

[2] Design Note on Improvement In Fuel Followup Scheme Using Online Incore Vanadium Detector Readings Of Flux Mapping System, 700MWE/DN/01100/00011.

FUEL MANAGEMENT TECHNIQUES ADOPTED AT RAPS-3&4

G. C. Chauthwani[1], Sumitra Kumari, L K Gupta
Rajasthan Atomic Power Station-3&4
Nuclear Power Corporation of India Limited, Mumbai, India
[1]*e-mail: -gcchauthwani@npcil.co.in*

Abstract

Rajasthan atomic power station-3&4 is a twin unit pressurized heavy water reactor (PHWR). Fuel management at nuclear power plant are the activities utilized to maintain the reactor in a critical state at rated power level by optimizing the fuel utilization and its performance without affecting the shut down and regulation system. To cater the aforesaid need, different fuel management techniques are adopted. These techniques include operating the reactor in peak flux mode and recycling the high burn-up bundles due to scarcity of fuel, utilizing the Depleted Uranium (DU) bundles for flattening the flux and changing the peak flux core to flat flux after the implementation of IAEA safeguard at RAPS-3&4. Wet quarantining of the channels at RAPS-3&4 imposed other challenges in fuel management. This paper aims to describe these challenges in detail and different techniques for better fuel management in these circumstances.

Keywords: Fuel management, PHWR, Peak Flux, Flat flux, Recycling.

1. Introduction

The Natural Uranium fueled Standard Indian PHWRs are designed to operate at rated thermal power of 801.9 MW (100%FP) on a continuous basis by employing 8-bundle shift scheme (8-BSS). The design burn-up with 12 mk excess reactivity at 100%FP is ~6364 MWd/te. In this standard operation, reactor is operated with flat flux distribution.

From August 2003, to conserve Natural Uranium all 220 MWe PHWRs in India were operating at lower power level than its rated capacity (From 100%FP to about 70%FP). During low power operation high burn-up bundles were recycled back to the core without any impact on fuel performance. In order to conserve the natural uranium bundles and raise reactor power, depleted uranium bundles were also used at RAPS-3&4. After the implementation of safeguard at RAPS-3&4, reactor power was raised back to the rated capacity in record time by changing the peak flux distribution to flat power distribution. In RAPS-3&4, some channels were wet quarantined due to operational problems, fuel management is being successfully carried out at RAPS-3&4 even in this mode of operation. To conserve the under-utilized fuel, a suitable recycling scheme is studied at RAPS-3&4 to be implemented before EMCCR of RAPS-3.

2. Low power operation

RAPS-3&4 was operating at 100%FP with excess reactivity about 12 mk in flat flux distribution since first synchronization. But due to the mismatch in demand and supply of nuclear fuel, following attempts were made to improve the burn-up and hence to reduce the refueling rate so as to conserve natural uranium [1].

(i) Operate the reactor at reduced power level

Since refueling rate is directly proportional to the reactor power so refueling rate will reduce directly. Negative load due to power co-efficient will reduce from 3.5 mk to 2.7 mk. It will improve the discharge burn-up by about 100 MWd/te, thus refueling rate will also reduce. Xenon negative load will also be reducing by about 1 mk and will improve the burn-up by about 120 MWd/te, thus refueling rate will also reduce.

(ii) Operate the reactor in peak flux mode

By operating the reactor in peak flux mode, neutron leakage will be reduced, it will improve the burn-up by about 1000 MWd/te. This will also help in reduction of refueling rate. Thus peak flux mode operation will also reduce the Refueling rate.

(iii) Operate the reactor with lower excess reactivity

By operating the reactor with about 3 -4 mk excess reactivity in adjuster rods, Fuel burn up can be improved by about 1000 MWd/te, leading to reduction in refueling rate. By taking these measures, the discharge burn-up in RAPS-3&4 reactors were improved from 6364 MWd/te to about 8600 MWd/te. With these measures we could have operated RAPS-3&4 at 70%FP with about 50 % Fuel requirement. This is because of reduced Xenon load and power coefficients coupled with peak power operation. To take advantage of low power in conserving Natural uranium, all PHWRs are operated with peak flux distribution as shown in figure 1 below.

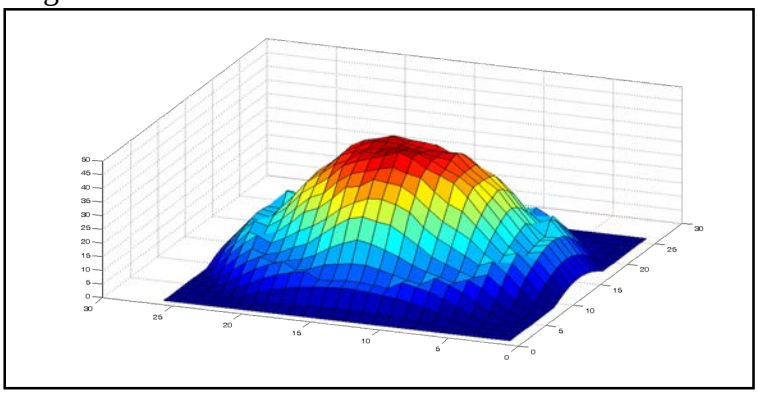


Figure 1: Radial flux distribution at 70%FP in peak flux mode

In this case, it must be noted that central bundles produce as much power as they were producing at 100% FP i.e. they are close to 100% FP. Therefore, trip set points for PSS and SSS were set as per the authorized power level rather than 100%FP.

3. High burn-up bundle recycling in peak flux distribution

Normally bundles with burnup <3000 MWd/te are recycled in the initial phase of reactor operation to utilize them more effectively. This practice is used in all PHWRs to make use of end bundles (11^{th}& 12^{th}or $9^{th}$to 12^{th}), which have very low burnup (<3000 MWd/te). Core, which is operating in equilibrium phase and need further increase in the fuel burnup requires recycling of bundles with considerably higher burnup in the range 5500- 7000 MWd/te from 9-12 location to 1-4 location of next channel. It was demonstrated that while recycling these high burn-up bundles and their subsequent refueling do not increase iodine in PHT system i.e. do not increase fuel failure rate. However, fuel consumption reduced significantly [2].

4. Use of depleted uranium bundles

As we have studied that in order to operate the reactor at 100%FP, flux in the central region has to be flattened. Thus if we use depleted uranium fuel (having less fissile content than natural uranium, U235 ~ 0.612%) in the central region of the core, we can achieve the radial flux flattening and reactor can be operated at 100%FP without crossing the bundle power envelope. This idea led towards the utilization of depleted uranium bundles in the equilibrium core of the PHWR. First time DU bundles were loaded in equilibrium core in RAPS-3&4 and reactor power was increased in phased manner from 70%FP to about 95%FP [3].

5. Changeover of peak flux distribution to flat power distribution

All NPCIL units including RAPS-3&4 were operating at reduced power level from August 2003 due to scarcity of the natural uranium. Flux profile of the core was modified from flat to peak profile by suitable refueling for better fuel utilization. RAPS-3&4 core was operating in this mode for about last 7 years. Excess reactivity was also reduced and maintained in the range of 3 mk to 4 mk to further conserve the fuel. RAPS-3&4 was brought under IAEA safeguard from 09.03.2010 and first imported fuel supply was received in May-2010. The initial IAEA inspection was completed on 04.05.2010 and RAPS-3&4 were allowed to use the imported fuel. RAPS-3&4 reactor power was raised from 70%FP to 100%FP within a period of three months adopting following methodology. [4]

- Refuel about 90 outer peripheral channels in one month to increase the outer flux and reduce inner zone flux to increase flux flattening.
- Refuel intermediate and inner channels suitably to operate the reactor and increase reactor power slowly from 90 to 100%FP in 2 months.

Flux profile along the central radial plane of the core in peaked flux (70 % FP) and in flat flux (100%FP) is shown in the figure-2. It can be seen from the figure that in peaked flux mode, maximum power is generated from the central core and outer core is producing negligible power. In flat flux mode, power is produced almost equally from all the quadrant of the core which makes it possible to operate the unit at 100 % FP.

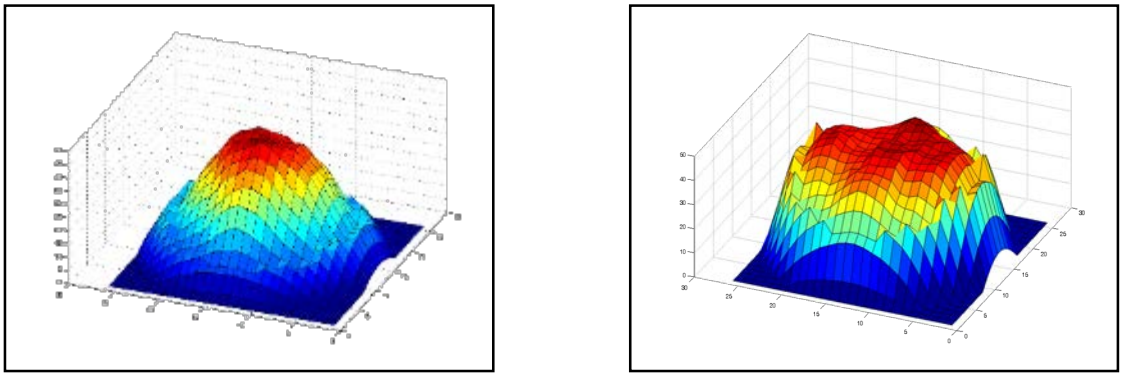


Figure 2: Radial flux profile of thermal neutrons at 70%FP and100%FP

6. Fuel management in wet quarantined condition

In RAPS-3&4 due to reduction in feeder to feeder gap, feeder to hardware gap and difficulty in fueling machine approach due to differential creep, a number of channels are wet quarantined. Due to the deviation from normal design, authorized power level changes. Change in authorized power level in this modified core condition is estimated based on core follow-up simulations using fuel management code TRIVENI [5]. Based on these simulations following rules are established.

S.N.	Number of Wet Quarantined channels	Power Reduction Requirement (%FP/Channel)
1.	5 to 7	0.8
2.	8-15	0.7
3.	16-20	0.6

Note: These rules are tested in different core conditions of RAPS-3&4. However, before implementing these rules, actual core condition should be reviewed thoroughly.

Therefore, if two channels are wet quarantined, authorized power level can be changed from 100%FP to about 88.4 %FP. In RAPS-3 currently 10 channels are wet quarantined and authorized power level is 93%FP and in RAPS-4 with 6 channels being out of service authorized power level is about 95.5 %FP.

7. Recycling scheme before EMCCR

RAPS-3 is scheduled for EMCCR in Oct-2022, to conserve natural uranium, it is necessary to recycle the low burn-up bundles of the core. Flux in the core at first two bundles (1^{st}& 2^{nd}) is very low. In 8BSS, first two bundle burn-up cannot be increased unless these bundles are shifted to next position (9^{th},10^{th}) by refueling. All channels cannot be pushed at one time and thus at the time of EMCCR, most of the channels will have fresh bundles at 1st and 2nd location. Two bundles (most probably 11^{th}, 12^{th}location) from each channel are to be recycled in the next channel (at 1^{st}, 2^{nd}position) so that fresh bundle wastage at 1^{st} and 2^{nd} location in the channel can be minimized before EMCCR. This scheme to be initiated about 6 months prior to EMCCR [6].

8. Power reduction requirement

There are several instances during reactor power operation when due to operational constraints reactor power is required to be reduced. PHWRs are operated with low excess reactivity of about 5-6 mk only and with this low reactivity margin, power reduction should be suitably planned so that reactor should be operated with regulating rods in operating range without getting poisoned out due to increase in xenon concentration during power reduction. Over the period of time of operating the reactor, xenon simulations suggest following set of rules.

8.1 One step power reduction

For one step power reduction from any power level P and excess reactivity $\boldsymbol{\rho}$, following formula can be used: $$\boldsymbol{One\ step\ power\ reduction}\ (\%\boldsymbol{FP}) = \mathbf{14} - \mathbf{3.3} * \boldsymbol{\rho} + \mathbf{.9} * \boldsymbol{P}\ (\%\boldsymbol{FP})$$

8.2 Planned power reduction

For working on some reactor or turbine components power reduction is required up to a specified level, Power reduction may be planned as 5%FP per 5 hours without poisoning out of the reactor. If power reduction is required due to unavailability of fuelling machine (F/M), power may be reduced as 1%FP per 3 hours without poisoning out of the reactor.

It is important to note that the rules of power reduction are based on xenon dynamics and should be followed when reactor is operating with saturated xenon condition.

9. Conclusion

Both the units of RAPS-3&4 have operated successfully in different conditions viz. peak flux mode, operation with depleted uranium bundles, on power changing the flux from peak to flat, operation with wet quarantined, PT removed conditions and with different operational constraints.

10. References

[1] Gupta L. K., “Present low power operation with respect to other low power operation” dated 17-11-2005, No. RAPS-3&4 / Stn Phy / 05/ S-86.

[2] Chowdhury S., L K Gupta and Hemant Kumar, “Impact of recycling on fuel performance”, CQCNF, Hyderabad.

[3] Chauthwani G.C., Mahawar S, Chowdhury S., “A report on core behavior with loading of DU bundles in RAPS-4 for first seven months”

[4] Chauthwani G. C., “A report on reactor power raise by modifying the flux shape”.

[5] Srinivasan K.R., “TAQUIL and TRIVENI – Computer Codes for Fuel Management of PHWRs”.

[6] Sumitra Kumar, Study of Limited Recycling Scheme for fuel saving before EMCCR in RAPS-3.

Fuel conservation during pre-equilibrium core operation of PHWR

Ravi Kumar Bansal[1], Amit Thakur[2], MPS Fernando[1]
[1]Nuclear Power Corporation of India Ltd, Mumbai, India
[2]Bhabha Atomic Research Center, Mumbai, India
[1]e-mail: ravibansal@npcil.co.in

Abstract

During pre-equilibrium phase of operation of PHWR, the average burn-up of the core has not achieved the equilibrium values thereby mandating to discharge fuel pre-maturely. Suitable recycling fuel management strategies have been developed to improve the fuel utilization during pre-equilibrium phase of refueling to increase the fuel utilization and saving of natural uranium. Heuristic based approach based on proportionality of dependent core parameters like burn-up and channel power is used to study the core operation with feasibility of recycling of fuel in pre-equilibrium phase These studies show that significant fuel can be saved while maintaining safe operation within the prescribed limits and without requirement of reduction of core overall power.

1. Introduction

Efficient fuel utilization is important in view of the fact that uranium resources are limited on the planet. At every stage of the reactor, incore fuel management has to be studied in details for optimum utilization of natural uranium in the PHWR core [1]. The initial core excess reactivity suffices the operational requirement of PHWR for around first 100 FPDs and no refueling in required during this period. However, further decrement in fissile content due to operation requires to be replenished with online-refueling in PHWR. During these initial 100 FPDs, the average core burn-up achieved is of the order of 2700 MWD/TeU where a large number of bundles at peripheral flux locations have not achieved even the average burn-up. Hence, lower gain in reactivity is expected with refueling per channel. While refueling such a channel in pre-equilibrium phase, the low burn-up bundles will have to be discharged to spent fuel bay. Instead some pairs with suitable burn-up can be planned to be recycled within the core to utilize the fuel more judiciously. This will not only save natural Uranium but also achieve early equilibrium core.
The present paper presents a heuristic approach to study the possible recycling that can be taken up during the pre-equilibrium phase and work out the possible savings in a PHWR-700 reactor [2].

2. Refuelling Scheme during normal operation

The PHWR-700 is upgradation of the existing 540 MWe reactor in India. The 540 MWe and 700 MWe reactors use 37 element bundles with natural uranium as fuel. Nominal state of regulating devices like Adjuster rods are maintained using the core excess reactivity. Since core excess reactivity is small, these reactors require online-bidirectional refueling to maintain the nominal state of reactivity devices required for reactor operation. Each channel of PHWR-700 [3] contains 12 bundles with the typical axial neutron flux profile as cosine shape. As a result, the initial and last four bundles at 1-4 and 9-12 locations respectively of the channel sees lesser irradiation than the middle four bundles at 5-8 locations in the channel. In PHWR-700, normally 8 bundle shift scheme for refuelling is followed along with 4 bundle shift scheme especially for channels in high flux zones. When a channel is refuelled with 8 bundle shift scheme, the last eight bundles of location 5-12 will be discharged from the channel with normal refueling scheme. However, the bundles at 9-12 will have lesser burn-up and can

be suitably recycled to another channel for utilization and the bundles of the next channel can be discharged. Hence in refueling of two channels, four fresh bundles will be saved.

3. Proposed refuelling scheme for enhanced fuel utilization

Heuristic approach refers to the practical approach based on proportionality of dependent parameters to estimate the overall variation in independent variable. In the present study, refueling factor (RF) [3] is devised which encapsulates the core dependent parameters like burn-up, channel powers and neighboring channel powers of the nearest neighbors in a single value. Accordingly, the highest refueling factor will provide the best channel to be refueled [3]. Based on the heuristic approach refueling factor (RF) for each channel at i^{th} row and j^{th} column is estimated as below [3,4]:

$$\left(\mathrm{R.F.(i,j)}\right) = \mu(P_1, P_2).\frac{\left(\text{Burn up of the Channel }\left(\mathrm{B(i,j)}\right)\right)}{\text{Channel Power}\left(\mathrm{C(i,j)}\right) * \text{Avg Power of First Neigbhors}\left(\mathrm{C1(i,j)}\right)} \quad (1)$$

Where μ (P_1, P_2) is known as skew factor dependent on the design burn-up (P1) and design zonal powers (P2) and accordingly polarizes the refuelling factor suitably in the deficit burn-up and power zone [3,4].

This refueling factor is suitable for equilibrium core refueling where a single channel is refuelled at a time by inserting few pairs of bundles from one channel end and discharging the exit pairs of bundles on the other end of the channel to spent fuel storage bay.
In pre-equilibrium core at around 100 FPDs of operation, the average burn-up of the core is pretty less. However, refuelling becomes a necessity to replenish fissile content in core for continuous operation. Since the burn-up of the channels is less, gain due to refuelling is expectedly less. Therefore, a greater number of channels are required to be refuelled for each FPD operation and this requires low burn-up bundles to be discharged to spent fuel storage bay. In present study, recycling of bundles is studied using recyclable factor (RCF) during pre-equilibrium core from 106 to 300 FPDs to conserve natural uranium.
The burn-up of various bundles are in the range may be varying from 0-10 GWD/TeU due to variation in irradiation at different locations. The channels, which are less than half of the design discharge burn-up are appropriate for recycling.

Further, even channels with burn-ups less than one-third of the design discharge burn-up are appropriate for recycling in high flux zone of central channels. However, channels with more than half of the average discharge burn-up (D) are not suitable for recycling so their recycling factor is zero. Therefore, the relationship for RCF that develops for a channel (i,j) is as follows:

$$RCF(i,j) = 0;\ if\ B > D \quad (2)$$

$$RCF(i,j) = \mathrm{RF(i,j)};\ \text{if } D/2 > B > 0 \quad (3)$$

The channels are categorized as group 1, 2, 3 channels which correspond with 0 <B< D/3, D/3<B<D/2 and B>D/2. The channels are arranged in descending order according to groups. According to channel selected for main refuelling, channels from Group 1 or Group 2 are selected to recycle bundles to the desired channel.

Initial Dummy core load of PHWR-700 is used to simulate the core up-to 106 FPDs, where the refueling requirement arises. The core is simulated from 106 FPDs to 300 FPDs using PARCUSH (Program for auto refueling and conservation of uranium strategy using heuristic approach) code with the help of refueling factor formulation [3,4].

Now using the concept of recycling factors as defined below, a new module has been developed and integrated in PARCUSH for pre-equilibrium phase refueling strategy. The core is simulated using this module of PARCUSH for recycling and various core parameters are observed. For comparison and completeness of study various reactor physics/operational parameters are generated, with the similar core configurations, by simulating the normal refueling scheme (without internal recycling of fuel).

4. Observations

Figure 1-4 shows the comparison of various parameters for special refueling scheme with internal recycling of U fuel and with normal refueling scheme, without internal re-cycling. The variation of in-core average burn-up and channel power peaking factors (CPPF) have been plotted in fig 1 & 2 from 106 FPDs to 300 FPDs in both normal single channel refueling and special recycling scheme. In this analysis, comparable excess reactivity of ~ 1mk has been maintained for both these studies. From fig 1&2, it is observed that similar incore burn-up and CPPF are observed in both the studies. This shows that 100%FP operation is possible for both the studies. The figure 3 shows the comparison for variation of average discharge burn-up during the same period for both these studies. It is observed that using special recycling scheme the average discharge burn-up has improved compared to the earlier case of normal refueling. This shows that the equilibrium core status is achieved faster with recycling.

Figure 4 shows the variation of bundles/FPD consumption in both cases. It is observed that if special refueling scheme with internal re-cycling is used, lesser number of bundles are loaded in the core for similar operational period and hence fresh fuel requirement is reduced. In a span of ~ 195 FPDs, ~650 fresh NU bundles can be saved if the proposed special refueling scheme is used where re-cycling of lesser burnt bundles is done. This turns out to be ~ 15% saving in NU fuel during this time.

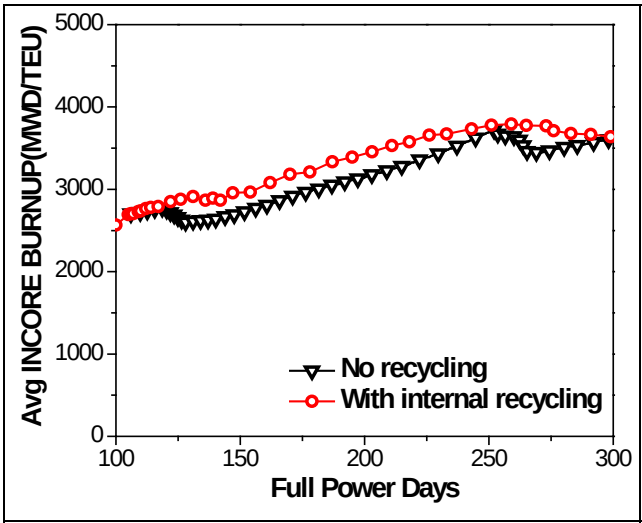


Fig 1: Incore burn-up Vs Full Power Days

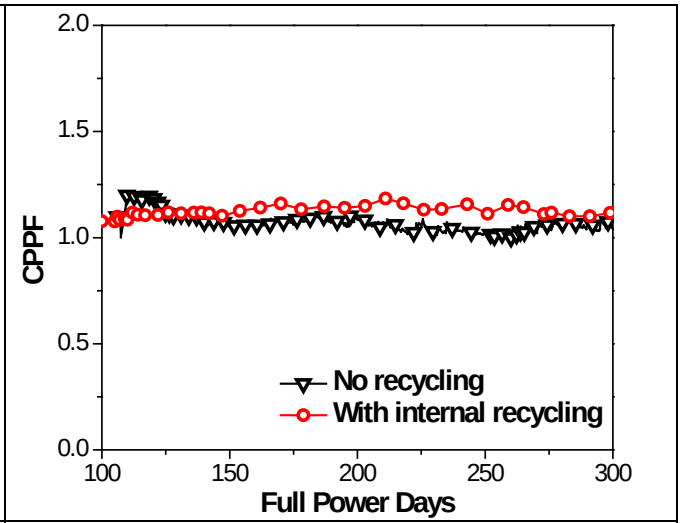


Fig 2: CPPF Vs Full Power Days

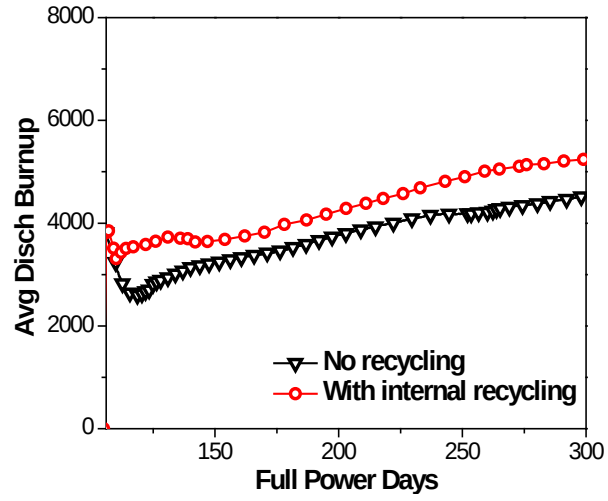


Fig 3: Avg discharge burn-up Vs Full Power Days

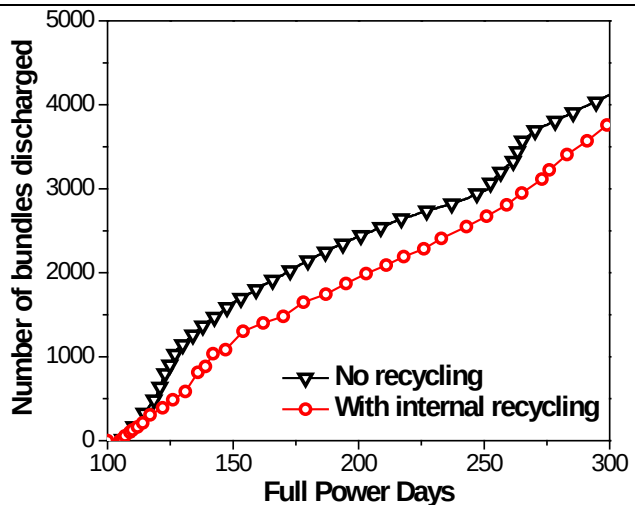


Fig 4: Number of bundles loaded Vs Full Power Days

5. Results and Conclusions

The refuelling scheme developed on the basis of refuelling factor and recycling factor during the pre-equilibrium core provides a plausible way for planning the refueling in PHWR core with auto channel selection system with code PARCUSH. The internal recycling of fuel during the pre-equilibrium core can help in saving of natural uranium. Also, the refuelling scheme helps to achieve the equilibrium core earlier which is important for a stabilized long-term operation. The proposed refuelling scheme is quite efficient; however, number of refuelling machine operations will increase if internal re-cycling is carried out. Further, only limited recycling of bundles can be done as excess recycling can limit the authorized power level due to flux peaking. As the operation continues beyond 300-400 FPDs, the average in core burnup and the average discharge burn-up will achieve the equilibrium values and there will be no visible gain due to recycling of fuel. Therefore, this scheme is practical and a comprehensive economics study can be carried out for deciding large scale implementation of this scheme.

It is observed that in normal operation, 3.5 refuelling machine operations / day is required. If special refuelling scheme is used, it increases to 4 to 5 operations/ day which is within the refueling capability of the fuelling machines.

6. References

[1] Bajaj, S.S. & Gore, A.R., 2006, “The Indian PHWR”, Nuclear Engineering and Design. 236, 701-722.

[2] Bhardwaj. S.A., 2006, “The future 700 MWe pressurized heavy water reactor.”, Nuclear Engineering and Design. 236, 861-871

[3] Bansal, Ravi Kumar et al, “An innovative scheme to conserve natural Uranium in Indian Pressurized Heavy Water Reactors”, Nuclear Engineering and Design, Volume 379, 2021, ISSN 0029-5493, https://doi.org/10.1016/j.nucengdes. 2021.111263.

[4] Bansal, Ravi & Thakur, Amit & Tejram, & Singh, Ram & Sharma, Har & Kannan, Umasankari. (2022), “Conservation of natural Uranium by inter unit transfer of fuel in PHWRs”, Annals of Nuclear Energy. 166. 108820. 10.1016/j.anucene.2021.108820.

STUDY OF ATWS MITIGATION FOR COOL DOWN AND HEAT UP EVENTS FOR VVER-1000 REACTORS

Manish Mehta[1], Anirban Biswangri[2], P Krishna Kumar[3] and Y.K. Pandey[4]
[1,2,3,4]Nabhikiya Urja Bhavan
Nuclear Power Corporation of India Limited, Mumbai, India
[1]*e-mail: -manishmehta@npcil.co.in*

Abstract

Anticipated Transients Without Scram (ATWS) is a Design Extension Condition that can occur due to failure of SCRAM after generation of signal for reactor trip. Kudankulam Nuclear Power Plant (KKNPP) has two operating VVER-1000 Pressurized Water Reactors. The mitigation of ATWS in KKNPP takes place by passive and active safety systems which injects borated coolant into the reactor core. The objective of this study is to evaluate the efficacy of ATWS mitigation systems during different functional categories. Two functional categories considered for the present study are cool down and heat up of primary circuit. During cool down of the primary circuit, there will be increase in the positive reactivity in the core while the opposite occurs for heat up. To analyse system Neutronic behaviour under ATWS scenarios a detailed Nodalization was developed for the core, primary system, secondary system and safety systems. Reactivity feedbacks due to fuel temperature, coolant density and boron concentration in the core are simulated using control parameters coupled with Neutronic point kinetics model.

1. Introduction

KKNPP VVER (Voda-Vodyanoi Energetichesky Reacktor, Water-Water Power Reactor) belongs to family of Pressurised Water. Kudankulam Nuclear Power Plant (KKNPP 1& 2) has 1000 MWe VVER-1000 Reactors. The reactor plant consists of four circulating loops and a pressurising system connected to the reactor with each loop containing a horizontal steam generator, a main circulating pump and passive part of emergency core cooling system (accumulators). KKNPP has two special safety systems i.e. Quick boron injection system (QBIS) and Emergency Boron Injection System (EBIS) for ATWS mitigation. Emergency Boron Injection System is an active system which takes suction of borated water from spent fuel pool and injects into cold leg of main coolant pipelines. QBIS is a passive system which has four high concentration boric acid solution tanks installed across each Reactor Coolant Pump (RCP) set. QBIS supplies boric acid into the primary circuit due to the differential pressure across RCP set suction and discharge during their operation and also during coast-down. To study the effectiveness of ATWS mitigation systems, two transients of different functional categories has been analysed. First transient is a cool down event of primary circuit initiated due to False Actuation of Steam generator emergency cooldown system (SGECD) without reactor scram. Second transient is heat up event of primary circuit caused by the Inadvertent closure of Main Steam Isolation Valve without reactor scram. This paper contains the modelling and verification aspect of the required systems and evaluation of the Neutronic parameters such as Neutronic power, core reactivity due to different feedbacks etc.

2. Calculation methodology and Modelling

ATWS transients has been analyzed using RELAP-5/MOD 3.2. RELAP5[1] code was developed to analyze the thermal-hydraulic behavior of light-water systems during postulated accidents. To

analyze system thermal-hydraulic behaviour under ATWS scenarios a detailed Nodalization of primary and secondary circuit has been developed for the reactor. In the modelling rector core consists of a Hot Fuel Assembly (FA), Average Power FA and By-pass. The primary circuit consists of four loops, each primary circuit loop consists of horizontal Steam Generator (SG), Reactor Coolant Pump (RCP) and Pressurizer is connected in any one of the hot leg. ATWS mitigation safety systems, QBIS and EBIS were also modelled and the rate of boron addition by these systems in the core during such events was also verified.
Other safety systems were also modelled. As a Single Failure Criteria (SFC), the failure of one Diesel Generator (DG) is assumed in the calculation, which results in failure of one channel of active safety systems. Besides, in the calculation the account is taken for bringing one DG into repair as a result of which another channel of active safety system is out of operation. Due to SFC, the failure of one train of passive safety system is also assumed in the calculation. Reactor point kinetics was also incorporated in the model with coolant density, boron concentration and fuel temperature feedback effects. In the analysis, loss of offsite power is assumed to occur before the reactor trip.

3. Results and discussion

3.1. Event progression for Cool down event with ATWS – The event progression has been provided in Table 1

Table 1

Time moment, s	Event
0.0	Actuation of ECDs on all SGs
34.0	Assumption of Loss of unit power supply which leads to trip of RCP sets , closure of turbine stop valve and feedwater supply valve
35.9	Arrival of the signal for CPS AR movement due to power increase but the CPS AR remain immovable
40.2	Signal generation for startup of QBIS and EBIS
74.0	Startup of system EBIS
119.0	Coastdown of RCP is completed.
200.0	End of calculation

As a result of the initiating event beginning from 0.0 s of the event the ECD on all SGs begin to operate. As a result, heat removal from the primary circuit is increased, the coolant temperature of the reactor coolant system decreases which results in rise of the reactor power. Scram signal is generated by the fact of increase in neutron reactor power, but control rod fails to drop. As the scram signal is generated, and the neutron flux is not reduced below 15 % within four seconds as shown in Figure 1, the signal for QBIS start-up and, simultaneously, for start-up of the EBIS is generated. As a result of supply of solution with temperature of 55 °C from QBIS into three loops, the temperature in these loops is significantly reduced. Injection of boron solution from QBIS inserts negative reactivity into coolant. This leads to decreases of fuel and coolant temperature which inserts positive reactivity in the core as shown in Figure 2. RCP set trips due to loss of

offsite power supply. During the RCP set coastdown the efficiency of QBIS decreases. After the termination of RCP coastdown, the natural coolant circulation would establish in the reactor coolant system The reactor power is reduced to residual power heat, after actuation of QBIS, which is removed by the SGECD.

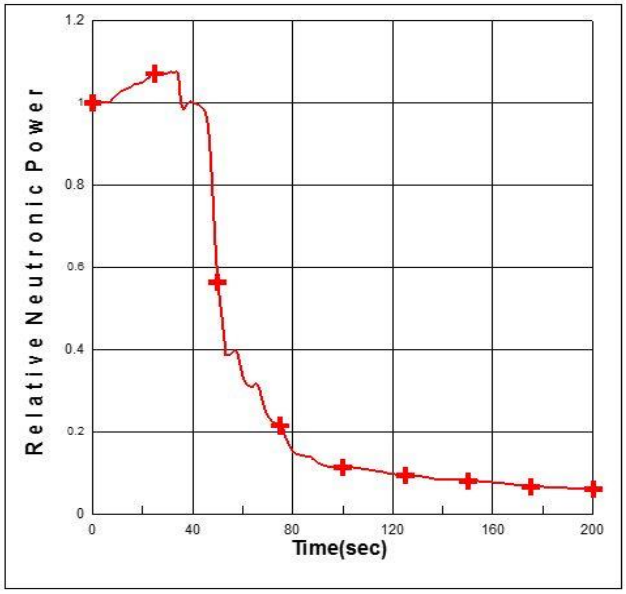


Figure 1.

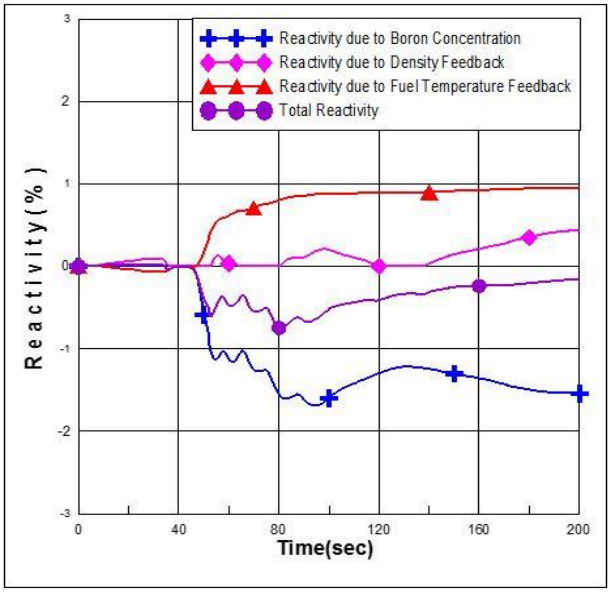


Figure 2.

3.2. Event progression for Heat up event with ATWS - The event progression has been provided in Table 2

Table 2

Moment of time, s	Event
0.00	MSIV closing on the steamline of loop 4
11.3	Assumption Loss of Unit power supply
13.2	Arrival of the signal for moving the CPS AR due to decrease in DNBR but the CPS ARs remain immovable.
17.5	Generation of signal for starting the QBIS and EBIS
51.3	Starting of EBIS
96.3	Coastdown of RCP is completed.
200.0	Termination of calculation

As a result of the initiating event from 0.0s of the process the main steam isolation valve in the SG loop 4 is closed. Simultaneously due to closing of the isolation valve and lack of the steamline break signal from 0.0s there occurs coastdown of the RCP set of loop 4. This leads to the increase

of primary coolant temperature which induces negative reactivity in the core. EP signal is generated by the fact of decreasing the DNBR.

As the EP signal has been generated, and reactor power is not reduced below 15 % for 4.0s as shown in Figure 3, a signal for start-up of the QBIS and EBIS is generated. Loss of offsite power supply is assumed before the actuation of QBIS. This leads to trip of RCP and reduction in the efficiency of QBIS. Injection of boron solution from QBIS inserts negative reactivity into coolant. This leads to decreases of fuel and coolant temperature which inserts positive reactivity in the core as shown in Figure 4. After completion of coast down of RCP, natural circulation is established in the primary circuit. Actuation of QBIS reduces the reactor power up to the decay heat level as shown in Figure 3. which is removed by SGECD in the secondary circuit.

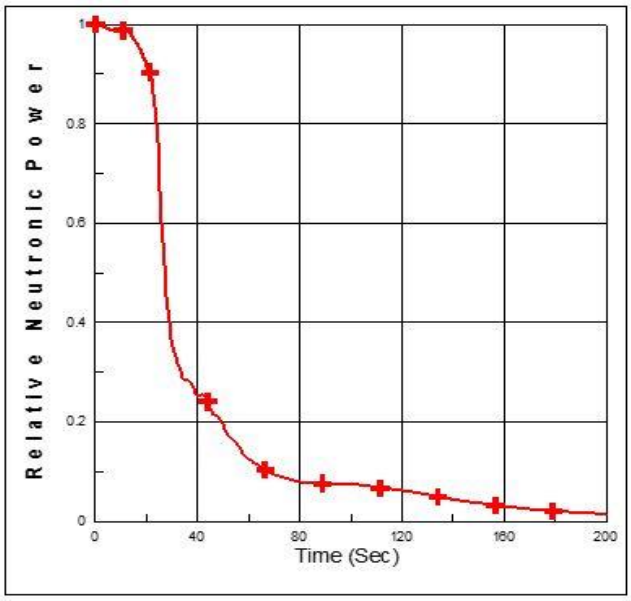


Figure 3.

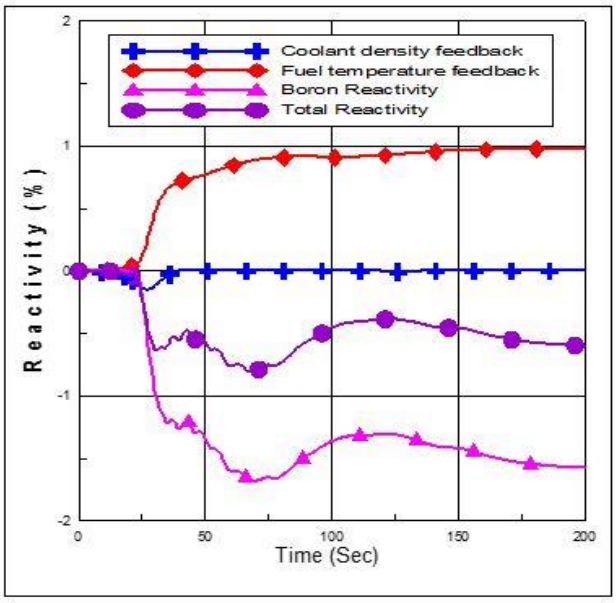


Figure 4.

4. Conclusion

Events of primary circuit cool down and heat up followed by ATWS was analyzed. It was found that the operation of QBIS and EBIS is sufficient to bring the reactor to sub critical state during cool down and heat up event without causing any DNBR. Even after termination of RCP coast down, Borated water supplied by QBIS is sufficient to bring the reactor power to decay heat level. Further, continuous operation of EBIS will maintain the reactor in prolonged sub critical state. Absence of DNB for all fuel rods was observed.

5. References

[1] V. H. Ransom et al., RELAP5/MOD2 Code Manual, Volume 1: Code Structure, System Models, and Solution Methods, NUREG/CR-4312, EGG-2396, August 1985.

REACTOR SAFETY ANALYSIS OF REACTIVITY EXCURSION EVENT OF WRONG START-UP OF INACTIVE REACTOR COOLANT PUMP FOR VVER-1000 REACTORS

Sanuj Chaudhary[1], S. K. Shukla[2], P. Krishna Kumar[3] and Y.K. Pandey [4]
[1, 2, 3 & 4] Nuclear Power Corporation of India Ltd, Mumbai, India
[1]*e-mail: - sanujc@npcil.co.in*

Abstract

In a VVER-1000 Nuclear Power Plant (NPP), fission heat generated in the fuel is removed from the core by forced circulation of coolant i.e. light water at high pressure and temperature using large Reactor Coolant Pump sets (RCPs). VVER-1000 reactor allows operation on partial running of RCP sets by decreasing power, in-order to match power to flow ratio. In the present event the reactor initially operates at reduced power with 3 RCP sets running, 4th RCP set is started without reactor power decrease to 30% against nominal as per operating procedures. This will result in supply of cold water into the reactor core leading to positive reactivity insertion due to negative coolant temperature coefficient of reactivity.

The objective of this study is to observe the extent of reactivity excursion and thermal hydraulic behaviour of the core during the event and check the capability of plant features/systems for mitigation of such an event.

1. Introduction

At present two power units of 1000 MWe each (KKNPP-1&2) are operational at the Kudankulam site. 4 more units (KKNPP 3-6) are under construction. In VVER-1000 Reactors, enriched uranium in oxide form is used as fuel with light water as moderator and coolant. Reactor is a two circuit system namely primary and secondary circuit. Primary circuit contains radioactive coolant. Heat is generated in the fuel due to fission reaction and is removed from the core by forced circulation of large Reactor Coolant Pump sets (RCPs). The primary circuit consists of a heterogeneous thermal neutron core, four main circulation loops. Each loop consists of a steam generators and the main circulation pump which are connected to reactor by cold and hot legs of the main circulation pipeline thus transferring the energy from the reactor to the Steam Generator (SG). The Fuel Assemblies are arranged in a hexagonal lattice in the core. The In/Out movements of the Control Rods, Integrated burnable absorber rods and boron control system control the nuclear fission energy generated in the Reactor.Planned connection of the inoperable RCP set in loop shall be carried out at decreased power. Under connection of the 4th loop to three loops already in operation, reactor power shall be decreased to 30% against nominal. The operator may carry out erroneous connection of the loop without preliminary power decrease under connection of the loop to three loops in operation. Wrong start-up of RCP leads to insertion of positive reactivity and increase in neutron power and reactor pressure. The plant features/systems shall prevent fuel melting, damage of fuel clad and reactor overpressure conditions.

2. Calculation Methodology & Modelling

The neutron kinetics and thermal-hydraulic behaviour during the event of wrong start-up of inactive RCP was analyzed using thermal hydraulic computer code RELAP-5/MOD 3.2 [1]. This model provides continuity, momentum, and energy equations for both the liquid and the vapour phases within a control volume. The energy equation contains source terms which couple the hydrodynamic model to

the heat structure conduction model by a convective heat transfer formulation. The code contains special process models for critical flow, abrupt area changes, branching, cross flow junctions, pumps, accumulators, valves, core neutronics, and control systems. A counter current flow limitation model can also be applied at vertical junctions.

The feedbacks due to fuel temperature and coolant temperature are simulated using control parameters coupled with Neutronic point kinetics model. Decay heat data is used from the 1979 standard data (American National Standard for Decay Heat Power in Light Water Reactors) for U-235 in light water reactors. Transient analysis was carried out using the developed RELAP model for VVER-1000 reactors.

2.1 Nodalization of Primary and Secondary Circuit

Nodalization of primary circuit involves reactor, four circulation loops and pressurizer. Nodalization scheme of Primary Circuit is shown in Figure 1. To describe the reactor, four elements are considered: reactor core, down comer, lower plenum and upper plenum. Reactor core is represented by a maximum power channel, average power channel and bypass path.

Nodalization of secondary circuit involves four steam generators; steam lines from each SG to main steam header (MSH) on which main steam isolation valves (MSIV's) are located. All four steam lines from SGs join MSH followed by turbine stop valve, governor valve and finally connecting to turbine. The relief devices like atmospheric steam discharge valves (BRU-A) and Steam generator relief valves (SG-PSD) are also modelled. The steam generator blowdown and emergency cool down (SGECD) safety system is also modelled. Nodalization of the secondary circuit is shown in Figure 2.

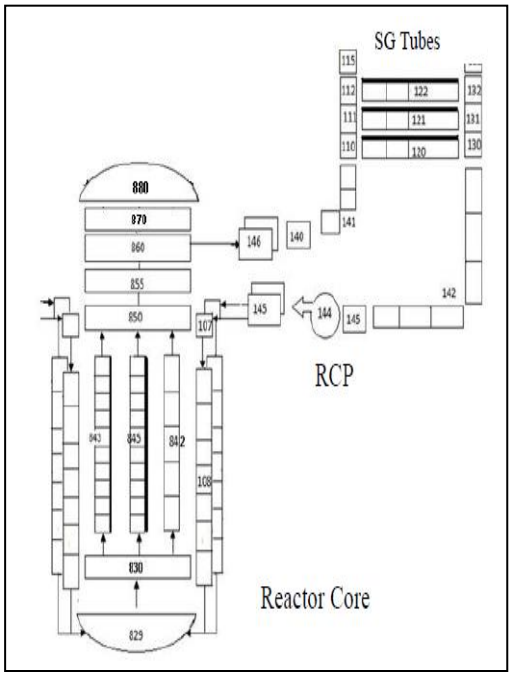


Figure 1: Primary circuit Nodalization

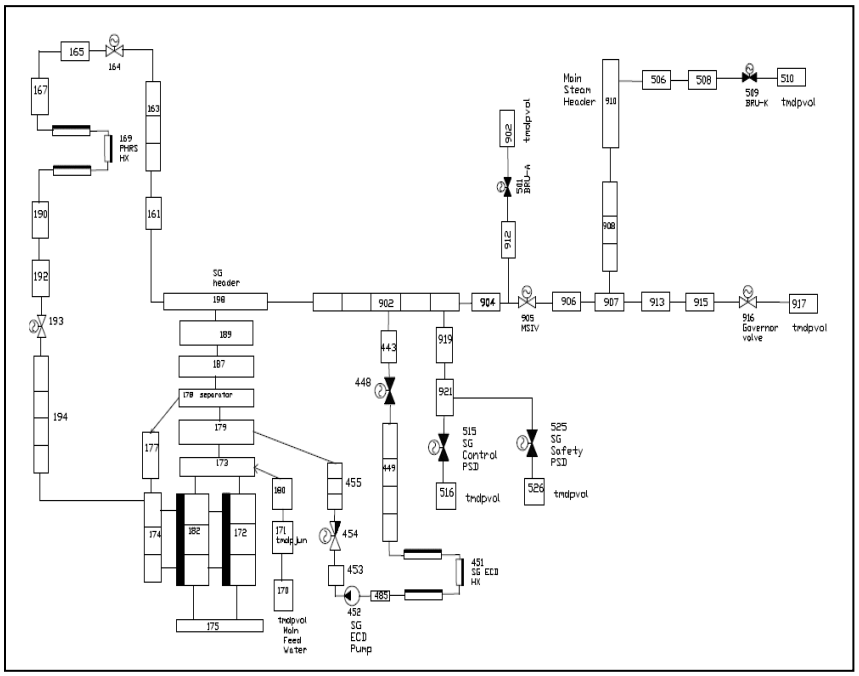


Figure 2: Secondary circuit Nodalization

3. Results and Discussion

The process initiates at 0 s, when inactive RCP is started in the 1st loop of the reactor coolant system. Start-up of RCP causes increase in coolant flow rate through the core (Figure 5) resulting in coolant temperature decrease. Coolant temperature decrease causes reactivity insertion (Figure 4) in the core due to negative coolant temperature feedback and reactor power starts increasing (Figure 3) resulting in sharp increase in primary pressure. As the reactor power increases to 107% of nominal power first reactor scram signal is generated but it is conservatively ignored as per safety analysis philosophy. Subsequent to this, departure from nucleate boiling ratio (DNBR) on the fuel rod surface less than its set point is observed and reactor scram takes place. As per safety analysis rule, complete loss of power at the station at the moment of 1.9s before beginning of control rods motion is also assumed. This results in trip of all RCP sets, turbine trip and closure of steam generator feed water system. After scram the reactor power decreases to the level of decay heat, the primary pressure also decreases and finally all the thermal hydraulic parameters are stabilized. The sequence of events during the event are presented in Tables 1

Table 1: Sequence of events

Time, s	Event	Cause
0.0	Beginning of start-up of RCP in the first loop	Initiating event
11.5	Generation of the first signal for scram (is not considered)	Set point for EP actuation is reached by power level of 107 % of nominal.
12.0	Generation of the second signal for scram	DNBR on the fuel rod surface is less than set point
13.6	Loss of NPP station service power	
15.5	Reactor scram	Control rods begin to move
18.5	Secondary side atmospheric steam dump valve operation	The steam generator header pressure is in-creased up to the set point
19.5	End of drop of control rods, reactor is in subcritical condition	
1200	The end of calculation	Parameters Stabilization

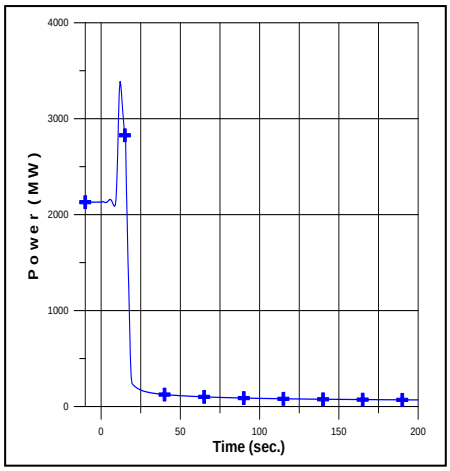
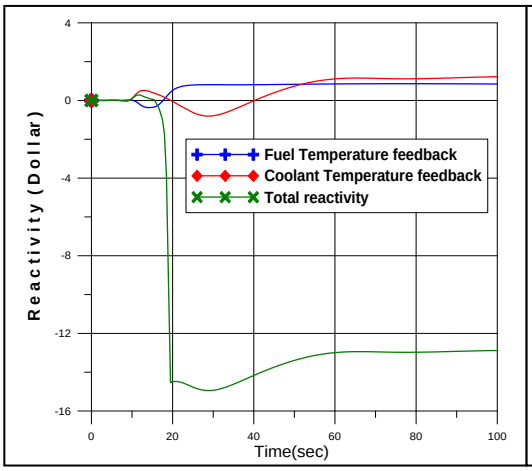


Figure 3: Reactor Power



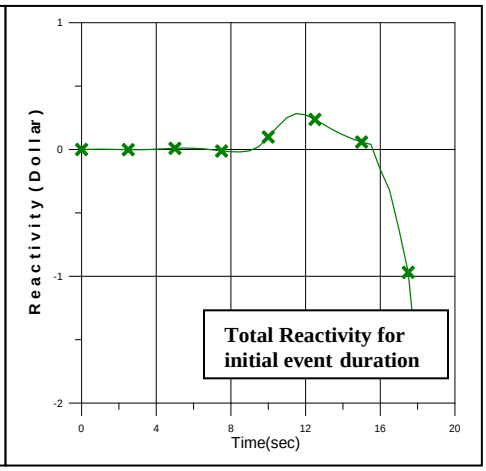


Figure 4: Reactivity

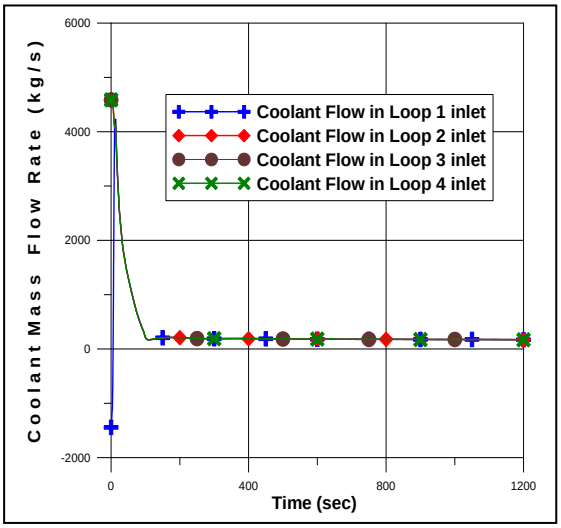


Figure 5: Coolant flow rate in each loop

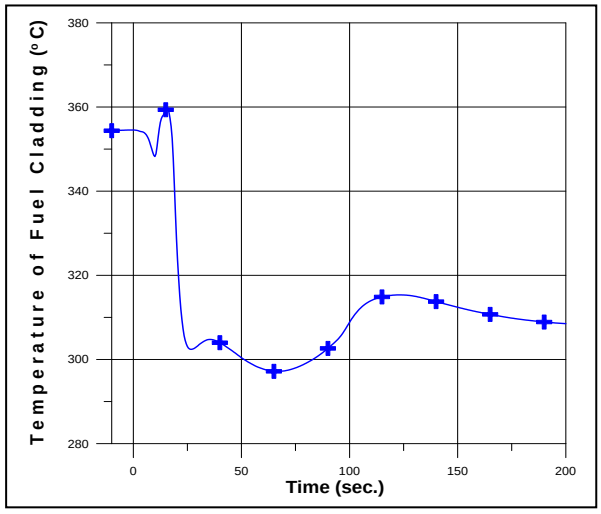


Figure 6: Maximum Clad temperature

4. Conclusion

An integrated study of reactor neutronic feedbacks and thermal hydraulics phenomenon during reactivity excursion event of wrong start-up of inactive reactor coolant pump for VVER-1000 reactors is carried out. Reactor power increase is observed due to coolant temperature feedback, resulting in sharp increase in primary pressure and fuel clad temperature. Analysis of this reactivity induced event was carried out without credit of any operator's action and calculation results showed that limiting values of all the important safety parameters are not reached throughout the event. Maximum fuel rod claddings temperature reached during the event indicate absence of any fuel clad damage (Figure 6). Absence of Departure from nucleate boiling (DNB) over fuel rod was observed. Temperature of the fuel rod during the transient was within limits so as to avoid any local fuel fragmentation and fuel damage.

5. References

[1] V. H. Ransom et al., RELAP5/MOD2 Code Manual, Volume 1: Code Structure, System Models, and Solution Methods, NUREG/CR-4312, EGG-2396, August 1985. , F.: Article title. Journal 2(5), 99–110 (2016).

Operational Aspects of loading of Cobalt-Natural Uranium (Co-NU) bundle in KGS-3 Reactor

Hardeep Singh, Hari Ram, S. K. Subramanya and Ashok Bhatia
Kaiga Generating Station-3&4, NPCIL, Kaiga
e-mail: - hsingh@npcil.co.in

Abstract

This paper discusses the operational experience while loading of Co-NU bundles in the reactor involving - measures taken at site prior to loading, checks before refueling, refueling of Co-NU bundles, changes in core parameters during loading, and monitoring of related parameters after loading.

1. Introduction

For majority of applications, low specific activity (30 Ci/g to 100 Ci/g) Cobalt-60 is required. For this purpose, on trial basis loading of Co-NU bundles (a bundle having central cobalt element and rest 18 fuel element of Natural Uranium) was planned. After regulatory approval, two of such Co-NU bundles were loaded in KGS-3 peripheral fuel channels, T-07 and T-15 at string position 6. The cobalt content in the central element of Co-NU fuel bundle is about 84 g and it can produce about 50 Ci/g specific activity, after about 600 Full Power Days (FPD) of irradiation.

2. Description of Co-NU bundle

The 19-element Co-NU Fuel Bundle (Figure-1) is similar to normal Natural Uranium (NU) fuel bundle being used in 220 MWe PHWRs except that NU pellets in the Central Fuel Element are replaced by 2 nos. of Cobalt slug filled Pencil Tubes and Zircaloy Sleeves and Plugs. The 6 inner and 12 outer NU fuel elements remain the same. The Central Fuel Element houses two Cobalt Pencil sub-assemblies.

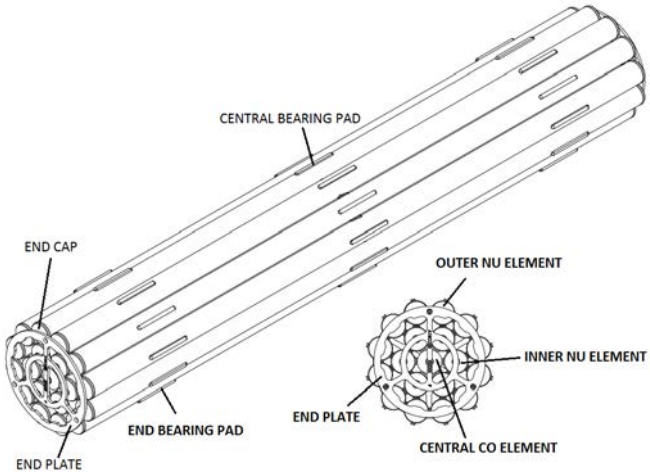


Figure-1: **19-element Co-NU Fuel Bundle**

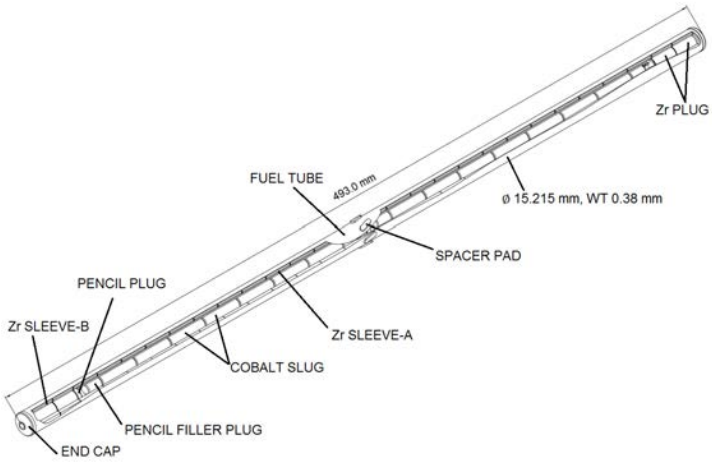


Figure-2: Central Fuel Tube

Each Cobalt Pencil sub-assembly (Figure-3) has seven Cobalt Slugs of 6 mm diameter and 25 mm length. Two Zr-4 pencil filler plugs are kept on either end of Pencil Tube, to keep the column of 7 Cobalt Slugs nearly equi-spaced from its centre. Helium is filled within the Central Fuel Tube and Pencil Tube to provide inert atmosphere. The annular space between the Cobalt Pencil Tube and Fuel Tube is filled by Zircaloy Sleeves-A. Rest of the length (after accounting for the length of 2 Pencils) within the Fuel tube is filled with Zircaloy Plugs (within Zircaloy Sleeves-B), leaving a marginal gap from the End Cap.

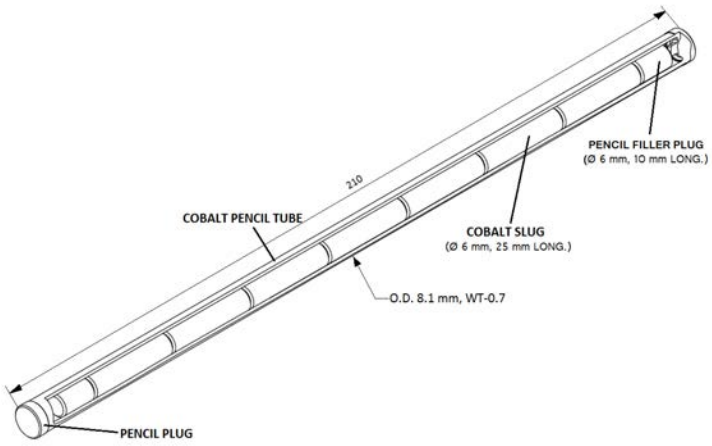


Figure-3: Cobalt Pencil Sub-assembly

3. Loading of Co-NU bundles in KGS-3

4 Co-NU bundles were received from fuel manufacturer. The bundles were kept on separate rack marked with "Co-NU bundles" tag to avoid intermixing. The nomenclature used for Co-NU bundle is B1H**CN** followed by year of manufacturing (for eg 21 for 2021) and five digit number. Weight of Co-NU bundle is about 16.2 kg, whereas weight of NU bundle is about 16.5 kg. As expected Co-NU bundle was lighter than NU bundle. The details are as given here:

Bundle ID	Bundle weight measured at site (kg)	Bundle ID	Bundle weight measured at site (kg)
B1HCN21-00001	16.230	B1HCN21-00003	16.177
B1HCN21-00002	16.197	B1HCN21-00004	16.185

Quality Assurance checks of Visual inspection, Kinked gauge check, Ring gauge test and Helium leak test were done for all Co-Nu bundles and were acceptable.

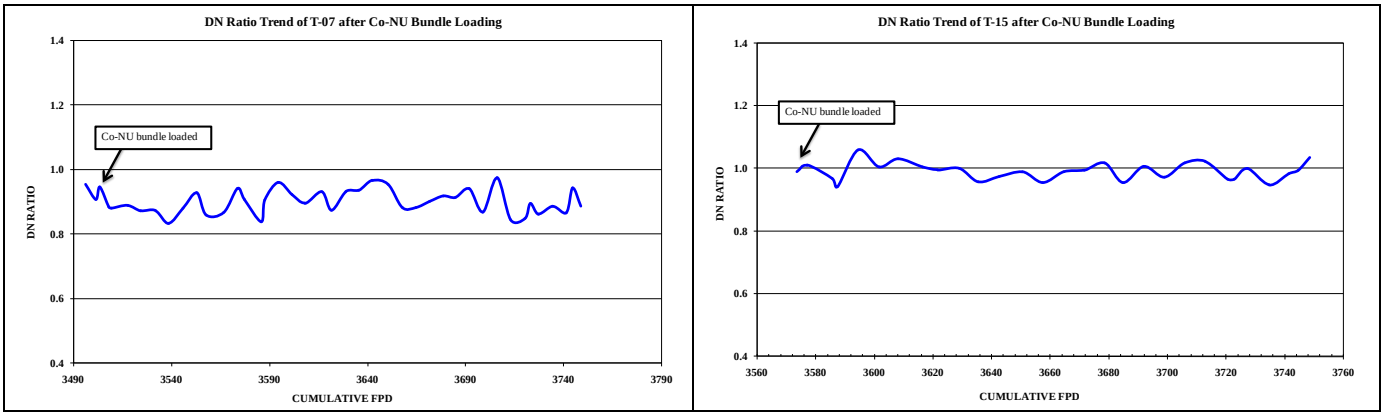
Loading of bundles was done by based on separate checklist with peer check. It was ensured that the bundles are loaded at 6^{th} location in the respective channel. Fuel change Order involving Co-NU bundle loading were highlighted specially along with 6^{th} string position for Co-NU bundle. One Co-NU bundle was loaded in T-07/S on 16/06/2021 (at 3505 FPD) and the second Co-NU bundle in T-15/S on 17/08/2021 (at 3567 FPD) at 6th location.

3.1 Operational parameters after loading of Co-NU bundles in T-07 & T-15

i) PHT I-131 & Co-60 activity:

I-131 and Co-60 activity in PHT system was maintaining at about 1 µCi/l and <0.5 µCi/l respectively before loading of Co-NU bundles and values are still maintaining after loading of Co-NU bundles.

ii) Delayed Neutron data and reactivity gain after refuelling of T-07 and T-15



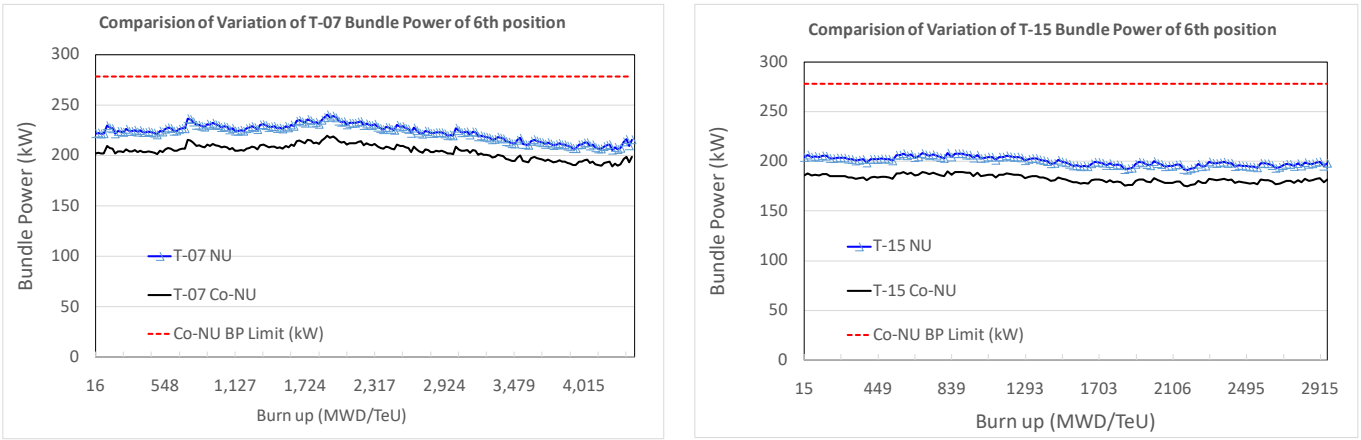
DN ratio data trend is normal.

iii) Reactivity gain after refuelling of T-07 and T-15

Type of Loading	Reactivity Gain (mk) due to refueling of	
	T-07	T-15
All 8 NU bundle loading	0.065	0.035
7 NU + 1 Co-NU bundle loading	0.05	0.022
Difference in reactivity gain	0.015	0.013

The reactivity loss due to loading of single Co-NU fuel bundle in a channel is about 0.015 mk in T-07 and 0.013 mk in T-15 with respect to that of all 8 NU bundles loading.

iv) Bundle Power Variation of Co-NU Bundle:



The Co-NU bundle power is maintaining well below the operating limit of 278 kW. Bundle powers of Co-NU bundle is about 18 kW lower than that of NU bundle.

4. Conclusion

Two Co-NU bundles were successfully loaded in KGS-3 reactor core and are being monitored. The changes in core reactivity and channel COT are as per expectation. The bundles are planned to be discharged from T-07 on 06-Feb-2023 and from T-15 on 09-Apr-2023.

5. References

[1] A report on Co-NU bundle loading in KGS-3 No KGS-3&4/RP/2022/Rep/1.

[2] Technical note on design of Central Cobalt Element of 19-element Co-NU fuel bundle No. NPCIL/F&FCM/37000/2020/M/08 dated 09 Dec 2020

BULK ADDITION OF MODERATOR AND FIRST APPROACH TO CRITICALITY (FAC) OF KAKRAPAR ATOMIC POWER PROJECT-3

Himanshu Mishra[1], Rimpi[1], R. Das[1] and Shankar Venkataramani[1]
[1]Kakrapar Atomic Power Project-3&4, Gujarat, India
[1]*e-mail: - hmishra@npcil.co.in*

Abstract

Kakrapar Atomic Power Project-3 (KAPP-3) is an Indian Pressurized Heavy Water Reactor (IPHWR) which is designed to produce 700MWe energy. Typically, in standard design of IPHWRs, First Approach to criticality (FAC) is carried out by modulating the neutron loss rate. At first, fuel is loaded, as per the approved fuel loading pattern, in a dry, clean core with many administrative and regulatory measures adequately met. Following this, bulk addition of moderator is carried out, wherein highly poisoned (strong neutron absorber) heavy water is added in pre-determined steps, till level in the calandria reaches about 96 %FT, with neutron counts monitored all through the activity. The extent of poisoning of heavy water ensures that reactor will remain subcritical under all circumstance during bulk addition i.e the core is maintained under Guaranteed Shutdown State (GSS). FAC is achieved by gradual removal of neutron poison from moderator in smaller steps. Boron coated counters are used to monitor the neutron counts.
In this paper, comparison of results obtained from estimation and observed during bulk addition of moderator and FAC of KAPP-3 core has been presented.

1. Introduction

Prior to initial fuel loading (IFL) In-core as well as out-core neutron monitoring instruments were installed. Four boron coated startup counters having sensitivity of ~4 cps/nv were installed in the core at VFU-8 location. Similarly, four boron coated counters were installed in the detector housing on the east side of calandria vault. Six ion chambers (ICs) were installed on the east side calandria vault housings, three each for Reactor regulation system and Reactor protection system (RPS-1). Three RPS-2 ion chambers were installed on the west side calandria vault housing.
A total of 248 DDU and 4456 NU fuel bundles were loaded into the core as first charge. DDU bundles are loaded at 7^{th} bundle position in 72 fuel channels and at 11^{th} & 12^{th} bundle position in 88 intermediate fuel channels [1]. The remaining bundle positions are occupied by NU fuel bundles. On completion of fuel loading, the PHT system was filled with heavy water. Neutron counts were negligible due to the absence of moderator D_2O.

2. Bulk addition of moderator into calandria

Around 65 Tonnes of D_2O with about 103 ppm of Boron and 10 ppm of Gadolinium was added to the moderator system to start with. With this heavy water inventory, the moderator level in calandria was about 10%FT which is just below the bottom-most row of fuel channels (W row) [2].
The four in-core startup counters were initially kept at the same elevations as during IFL, i.e. 14 %FT, 25 %FT, 36 %FT and 47 %FT (Figure-1). Subsequently, D_2O was added to the calandria in a controlled manner with pre-defined stop points. The count rate of in-core detectors was monitored continuously and 1/CR vs. moderator level was plotted for every 4%FT rise in moderator level. The moderator addition was stopped at every 8%FT level increase and after moderator samples were collected for poison analysis. Further addition of moderator was continued after reviewing the results.

At moderator level of 72% FT, the in-core startup counters were pulled up from their initial position to 47 % FT to 39 % FT, 50 % FT, 61 % FT and 72 % FT (Figure-1) [2].

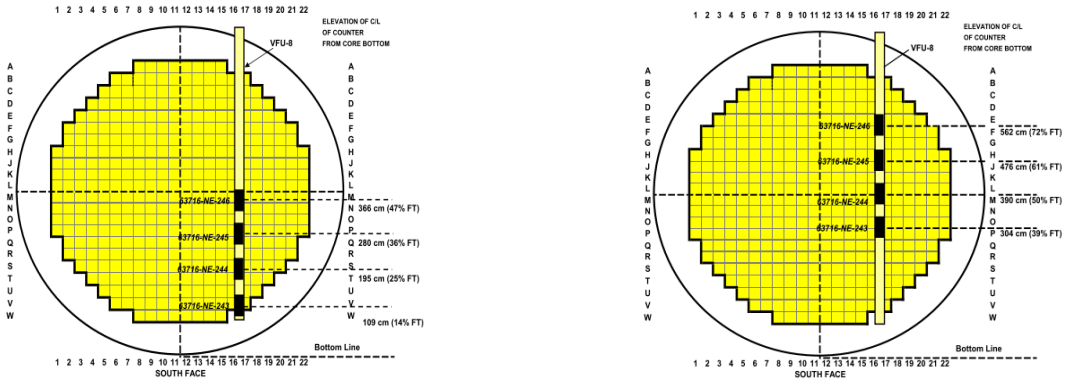


Figure 1: In-core detectors arranged before and after calandria level 72%FT

During heavy water addition, at each stop point the observed and estimated count rates were found to be in good agreement (Figure-2). The final moderator level at the end of bulk addition was 95.78%FT and the boron and gadolinium concentrations were 21.74 ppm and 2.35 ppm respectively.

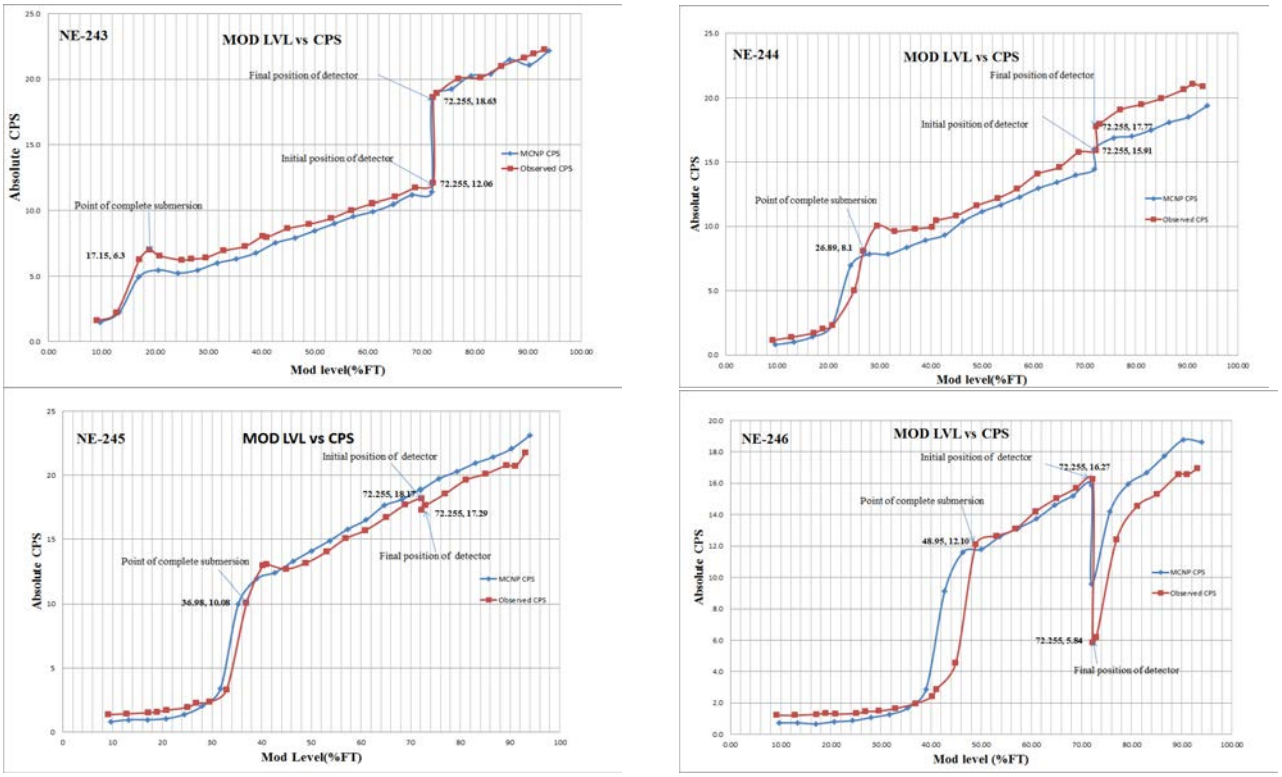


Figure 2: Response of in-core boron coated counters during bulk addition of moderator

During the entire bulk addition activity, all the reactivity devices (Shut off Rods (SRs), Control Rods (CRs), and Adjuster rods (ARs)) were kept fully IN and Zone Control Compartments (ZCCs) were completely filled. The final count rate after the end of the activity was ~ 22 to 23 cps, which was in good agreement with the estimations. Subsequent to the activity and before commencement of FAC, all the reactivity devices SRs, CRs, ARs were Fully IN and ZCCs were completely drained.

2.1 First Approach to Criticality (FAC)

First approach to criticality commenced with the withdrawal of the reactivity devices (SRs, CRs and ARs) manually in sequence except for AR Bank # 4 which was pulled to 50%OUT. The changes in count-rates during rod withdrawal were monitored.

Subsequently, Gadolinium was removed, to BDL (<40 ppb), followed by boron removal. At every step of poison removal, trip set points on all four in-core counters were set at one decade above the actual count rates. The high-count rate trip set point on out-core counters was set at 50 cps. The out-core counters remained below scale during the entire FAC.

During removal of Gadolinium and Boron from moderator, the observed count rates of all 4 in-core counters showed close matching with the estimated counts (Figure-3).

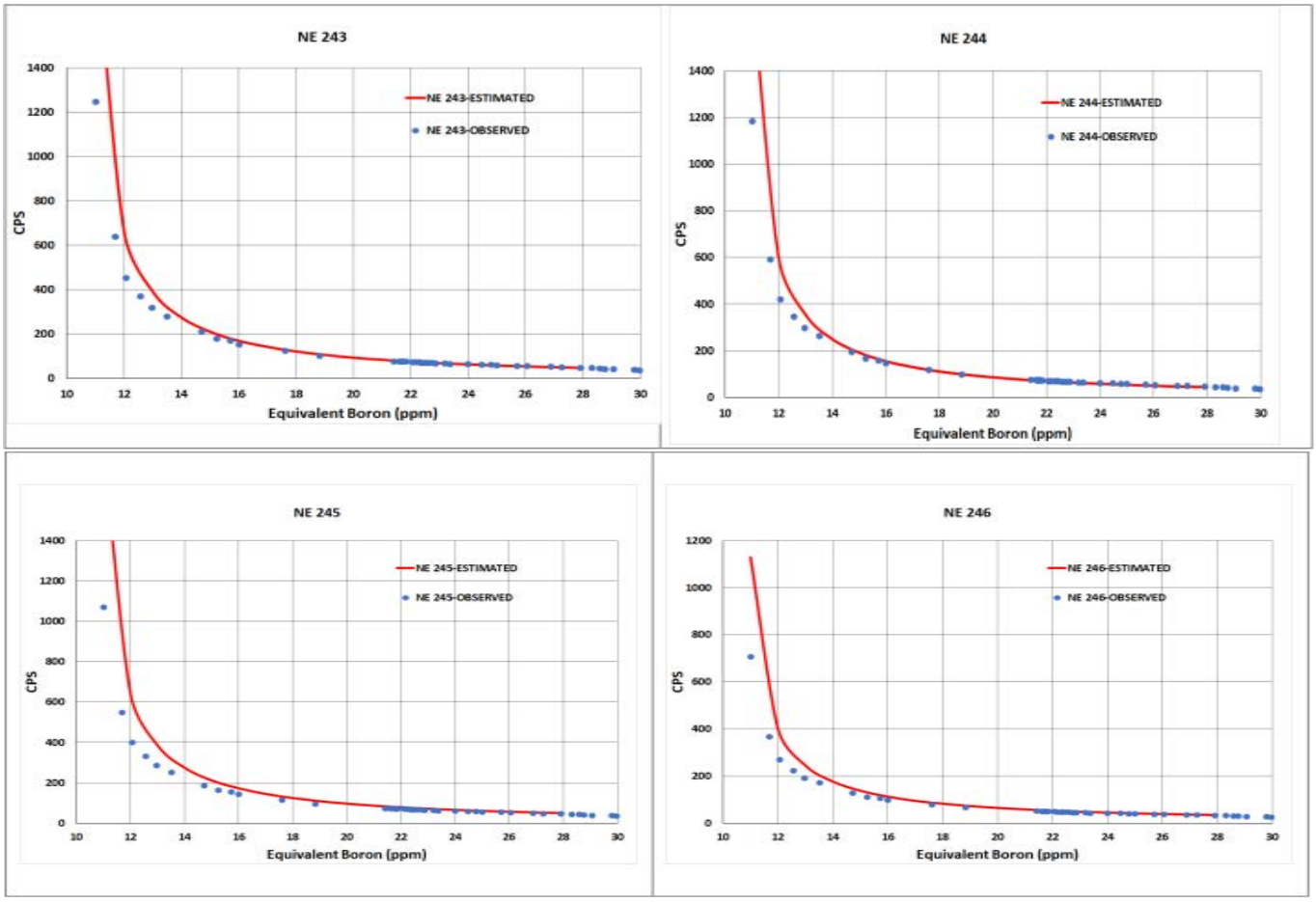


Figure 3: Estimated count rates Vs Observed count rates of NE-245 and NE-246 during poison removal

The count rate was monitored continuously and 1/CR vs. Boron equivalent was plotted (Figure-4). When boron concentration reached 11 ppm, rod cycling with AR BK#4 was commenced. KAPP-3 reactor core achieved first criticality at 09:36 hrs on 22 July 2020.

After observation of sustained positive reactor period (time period was 372 seconds), the reactor power was manually stabilized at around 33000 cps and maintained in that state for about one hour. Subsequently reactor was manually tripped.

The critical configuration corresponding to steady state operation was, AR bank-4:71%IN, boron in moderator: 10.1 ppm. Moderator and PHT IP were 99.91 % and 99.86 % w/w respectively. The difference between estimated and observed critical boron was 0.07 mk.

Response of the in-core counters was excellent and no unwanted fluctuations / spikes were observed during the whole process. Spikes seen in Figure-4 are due to channel trip tests carried during FAC.

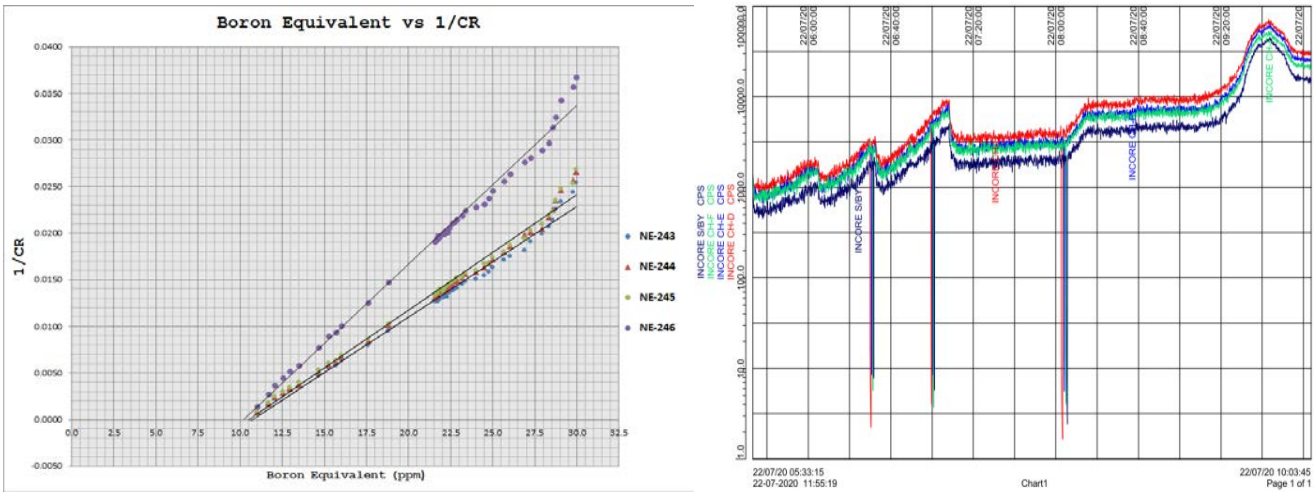


Figure 4: Plot of inverse count rates showing extrapolated critical boron and variation of count rates during cycling of AR bank#4

3. Conclusion

Fuel was successfully loaded manually in the core as per the approved fuel loading pattern. The calandria filling with moderator grade heavy water completed successfully. At every step of moderator filling, core was always in the GSS state. The in-core counters were responding satisfactorily for D_2O addition to calandria. The ex-core counters were below scale during this activity.

The point of criticality was predicted continuously and reactivity addition was made finer / smaller steps as the reactor comes closer to critical state. Critical configuration was taken after stabilizing reactor power. Operational procedures and calculation for prediction of criticality has been improved and predictions were more accurate as compared to earlier PHWRs.

4. References

[1] Commissioning Report for Initial Fuel Loading (IFL), KAPP-3&4-01160-CR-1 (Rev-0), March, 2020.

[2] Commissioning Report (Part B) for Bulk Heavy Water Addition, KAPP-3-32000-CR-07 (Rev 0), July 2020.

[3] Commissioning Report on First Approach to Criticality KAPP-3&4-01131-CR-01-(Rev-0), July 2020.

OPERATING EXPERIENCE OF SINGLE CHANNEL PULSE AMPLIFIER (SCPA) WITH FISSION COUNTERS IN KAPS-1

G.Rajarao[1], R.Goutam[2], R.Padhy[3], R.Das[4] and M.K.Sonavani[5]
[1,2,3,4] Kakrapar Atomic Power Station, Anumala, India
[5] Nuclear Power Corporation of India Limited, HQ, Mumbai, India
[1]*e-mail: -* *rajarao@npcil.co.in*

Abstract

Fission counters are used as special instrumentation for neutron power monitoring during reactor start-up after completion of EMCCR due to its high gamma radiation tolerance. In the past, many units of NPCIL have used the Fission counters (FCs) as start-up detectors for neutron flux monitoring after EMMCR, like MAPS 1&2, NAPS1&2 and KAPS-1. Both KAPS-1 and 2 reactors were shut down for EMCCR and up gradation of safety system. KAPS-2 was made critical in Sept-2018, while KAPS-1 made critical in May-2019 after completion of EMCCR. FCs were used in both the reactors for start-up activity. During criticality of KAPS-2, noise pick up in the Fission counter start up system had made neutron signal monitoring very difficult. Subsequently by changing the charge sensitive preamplifiers electronic of B-10 counters with current sensitive fast pulse preamplifiers electronic system which is called as single channel pulse amplifier (SCPA), a smooth first approach of criticality was achieved in KAPS-1. This report brings out the experience of FC's with two different electronics systems viz.. of Boron coated counters used in KAPS-2 and SCPA used in KAPS-1.

Key points: EMCCR- En-masse coolant channel replacement, FC –fission counter, FAC-First approach to criticality, SCPA- single channel pulse amplifier, TTL-transistor -transistor logic.

1. Introduction

Neutron flux during FAC (Fresh core) is monitored with in-core Boron coated proportional counters (B-10 detectors) operating in pulse mode having sensitivity of about 4 cps/nv with their associated charge sensitive pre amplifier electronics in triplicated channels. However after completion of EMCCR, first criticality is monitored by Fission counters due to high gamma field inside the reactor core. Both the reactors, KAPS-1 and KAPS-2, were underwent EMCCR. Same Fission counters were used in both the reactors for start-up activity. It was observed that during KAPS-2 start-up, the count rates in two out of three channels were not matching with expected count rate. Two channels were showing more counts which might be due to background gamma. The reason attributed to this mismatch is the use of electronics which is not compatible with Fission counters (Inadequate to process the fast pulses due to fission energy compared to B-10 pulses due to α interaction). The pre amplifier of existing B-10 counters is comparatively slow for fission counters. The B-10 counter pulses are **for about 100µs while the fission counter pulses are for about 100ns.**

Hence for approach to first criticality in KAPS-1 after EMCCR, Fission Counters along current sensitive amplifier - Single Channel Pulse Amplifiers (SCPA) is used in triplicated channels. Thermal neutron sensitivity found to be around 0.7cps/nv which is 2.5 times more than the value of FCs with B-10 electronics used in KAPS-2. The approach to criticality was very smooth when compared with KAPS-2 with same fission counters but with new electronics (SCPA).

2. Experience in KAPS-2 during first approach to criticality after EMCCR:

After completion of EMCCR and safety system upgradation jobs, KAPS-2 start up was taken up in Sep-2018. Three set of fission counters (NE-35, NE-36, NE-37) having sensitivity of 0.3CPS/nv along with B-10 electronic systems (old electronics) were used for approach to FAC. The prediction of critical boron was based on the variation of count rate reading with the poison concentration for the in-core start-up detectors. **It was observed that the detector readings on NE-35 and NE-37, 1/NE-35 and 1/NE-37 vs boron concentration graph was not consistent due to hunting in readings while on NE-36, 1/NE-36 reading was close to predicted critical boron. Moreover the count rates on NE-35 and NE-37 were more compared to that of NE-36**. This was attributed to contribution of back ground gamma. Variation of 1/CR vs boron concentration for all the detectors from 30 ppm to 20ppm is shown in Figure-1. Below 20 ppm to till criticality, 1/CR vs boron concentration graph for all the detectors were converging to a single point and predicting critical boron close to the design value. The hunting in readings was observed to be eliminated after the dominance of strong neutron source below 20 ppm. Variation of inverse count rate from 20 ppm to till criticality is shown in Figure-2.

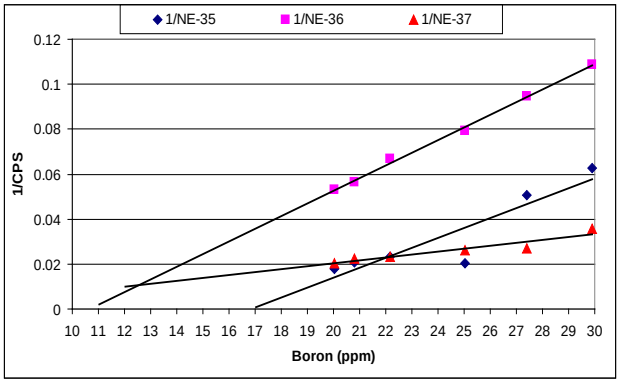


Figure-1: Prediction of critical boron based on inverse count rate Vs boron from30ppm-20ppm

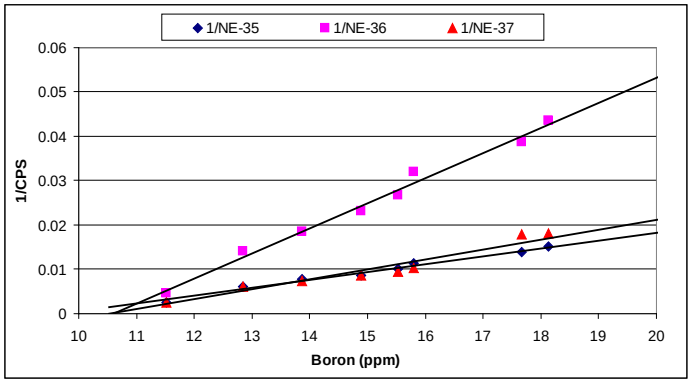


Figure-2: Prediction of critical boron based on Inverse count rate Vs boron from 20ppm.

It can be seen from the above figures that two channels were showing more counts which might be due to background gamma. The reason attributed to this mismatch was the use of electronics which was not fully compatible with Fission Counter detectors.

3. Implementation of SCPA in KAPS-1:

The SCPA electronics for Fission counters was developed by Electronics Division, BARC. The SCPA, Optical Transmitter, Optical Receiver and the Optical Fibre cables have been tested and qualified[1] . The existing Pre amplifier of B-10 counters is comparatively slow for FCs. The B-10 counter pulses are about 100µs while the fission counter pulses are about 100ns. Current sensitive trans impedance amplifier instead of charge sensitive preamplifiers are proposed to be used as in-core neutron monitoring purpose due to its fast response and better noise discrimination ability. For further improvement, In KAPS-1 start-up after EMCCR, Fission Counters (FCs) along with triplicate Single Channel Pulse Amplifiers (SCPA) are proposed to be used.

In existing B-10 detector electronics the signal from preamplifier are fed to pulse amplifier which are located in RB. The discrimination bias is set at pulse amplifier and TTL pulses were transmitted to control room for start-up dolly interface. While in SCPA there will be only one

amplifier and discriminator module and the output pulses are converted to optical pulses and transmitted through fibre optical cable. At receiving end, optical to TTL converter module is there for start-up dolly interface. The sensitivity and discrimination bias of fission counters were established with SCPA by calibration with neutron source before using in the start-up of KAPS-1. The value of sensitivity found to be around 0.7cps/nv which is 2.5 times higher than the value obtained with (B-10 detector electronics) in KAPS-2.

Integrated testing of four numbers of Fast Current Pulse Amplifier Channels with Optical Transmission Scheme was carried out at KAPS-1. The linearity of pulse channels was checked over the entire range of neutron monitoring, using a function generator and test box. Source response check of the pulse channels integrated along with fission counter was also carried out by using 5 Ci Am-Be source to ascertain the operating H.V. (~500V) and D.B. (-55mV) settings. Experience with SCPA in KAPS-1 first approach to criticality after EMCCR:

Neutron power monitoring during First approach to criticality with SCPA in KAPS-1 was done in two stages as given below.

3.1 KAPS-1 First approach to criticality from 34ppm to 20ppm

In core monitoring of neutron flux was carried out with two fission counter NE-35,NE-36 with old electronics(i.e B-10 electronics) and NE-37 with new electronics (SCPA) from 34ppm to 20ppm as per the approval of AERB safety committee **[2]**. The observed 1/CR vs Boron level is given below.

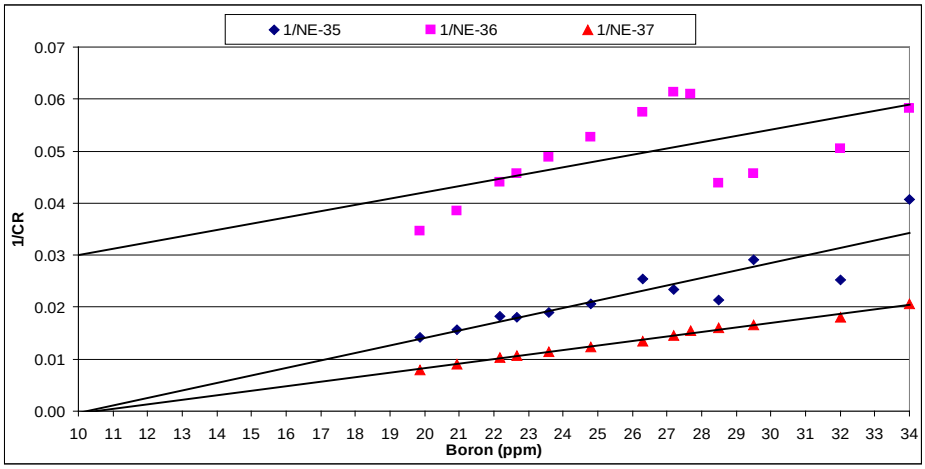


Figure-3: Prediction of critical boron based on inverse count rate Vs boron from 34ppm to 20ppm.

It can be seen from the above figure that the change in count rate is very consistent for NE-37 (new electronics) compared to detectors NE-35 and NE-36 (old electronics).

At 20 ppm of boron level PSS trip test was carried out and count rates was noted as per SARCOP recommendation to asses the performance of new electronics in comparison with old electronics. After assessing the performance of new electronics for NE-37, the electronics of NE-35 and NE-36 was also changed to new electronics. Before proceeding for further boron removal, again trip test was performed to assess the performance of all the three detectors. The readings obtained are given in the following table.

	INCORE COUNTERS		
	NE-35 (Ch-D) Old	NE-36 (Ch-E) Old	NE-37 (Ch-F) New
BEFORE PSS TRIP	71	29	125
AFTER PSS TRIP (PSS with all rods IN)	36	16	65
Ratio(>1.5)	1.97	1.81	1.92

	INCORE COUNTERS		
	NE-35 (Ch-D) New	NE-36 (Ch-E) New	NE-37 (Ch-F) New
BEFORE PSS TRIP	125	118	123
AFTER PSS TRIP (PSS with all rods IN)	67	65	65
Ratio(>1.5)	1.86	1.81	1.89

From the above two tables, the observed ratios due to PSS drop at about 20 ppm, with both old electronics and new electronics, were comparable and as per expectation.

3.2 Approach of criticality from 20ppm to till criticality:

Hence this point on wards the FAC was carried out with new electronics in all the three channels. 1/CR vs. boron concentration graphs were converging close to estimated critical boron concentration in all three counters. The estimated critical boron (11.18 ppm) matched well with the predicted critical boron (11.2 ppm with UE and UW at 80 % IN, moderator IP 99.90%). It can be seen from Figure-4, that there is a smooth convergence of all counters data in KAPS-1 with new electronics.

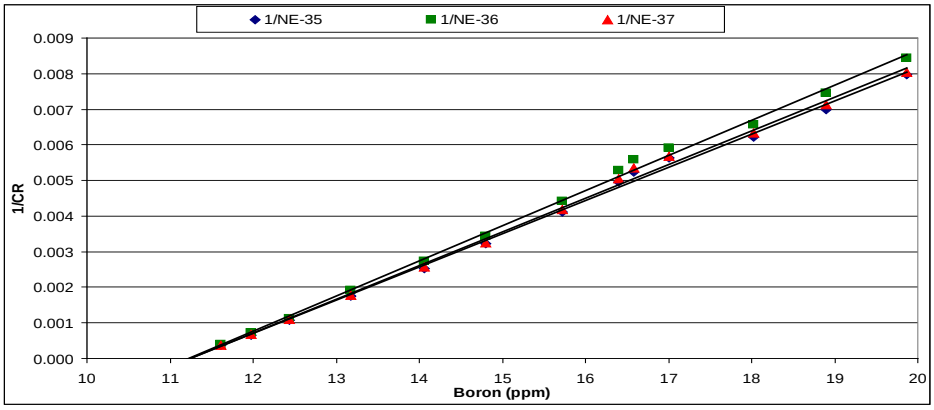


Figure-4: Prediction of critical boron based on inverse count rate Vs boron from 20ppm

5. Conclusion:

1. New electronics connected to Fission counter has shown higher sensitivity due to accounting of all the neutron pulses.

2. Smooth convergence of all counters data in KAPS-1 with SCPA is observed as compared to KAPS-2 criticality with B-10 electronics system.

3. The behaviour of all the counters with new electronics is very consistent due to dominance of neutron source even in presence of high gamma field. It is proposed to use Fission counter with new electronics for power monitoring during start up of an irradiated core.

6. References

[1] Report on integrated testing of fast current pulse amplifier channels with optical transmission scheme along with fission counter at KAPS-1.(BARC/ED/RIS/ KAPS-1/241 Date:14th MAY 2019).

[2] Safety proposal for use of triplicated Single channel Pulse Amplifiers (SCPA) with fission counter for In-core monitoring of neutron flux during restart of reactor after KAPS-1 EMCCR.(AERB/SARCOP/61022/2019/1136).

Comparison of theoretically estimated thermal neutron flux profile with TIP generated profile during Phase-B of KAPP-3

Gaurav Agarwal[1], Sherly Ray[1]
[1] Nuclear Power Corporation of India LTD., Mumbai, India
[1]*e-mail: - gagarwal@npcil.co.in*

Abstract

Many physics experiments are normally carried out as part of the commissioning activities and the results are compared with the estimated values. During low power Phase-B commissioning activities of KAPP-3, the first IPHWR of 700 MWe capacity, worth of various reactivity devices were measured and performance of control and protection systems were assessed. The measured worths and other relevant parameters were compared with the estimated values. Thermal neutron flux profiles were also measured along the flux units, in different configurations of reactivity devices, using traveling in-core probes (TIPs). The flux profile thus obtained were compared with theoretically estimated profile from cell average thermal fluxes generated by diffusion theory based fuel management code TRIVENI. The TIP generated and estimated profiles are in good agreement.

1. Introduction

Various physics related experiments were performed during the commissioning of KAPP-3 700 MWe PHWR. These experiments are necessary to validate the computer codes and to obtain the base line data to be useful for reactor operation. After first approach to criticality (FAC), Phase-B physics experiments were carried out at reactor power ≤ 0.1%FP. The Phase-B experiments also included the flux profile measurement using travelling in-core probe (TIP) to verify the flux shapes, in vertical flux units (VFU) as well as in horizontal flux units (HFU) estimated by computer codes. The travelling in-core probe (TIP) is a miniature fission chamber and it is used to scan the flux along VFUs and HFUs. There are 26 VFUs and 9 HFUs in 700 MWe PHWR core. Among these VFUs, six VFUs are chosen for installation of TIPs. Similarly 2 out of 9 HFUs are designated for insertion of TIP in horizontal direction.

Since the computer codes used to estimate the flux in the core give the average flux in cell (or mesh or node), the actual profile of flux within the cell (node or mesh) cannot be estimated by these codes. Monte Carlo method can be used to estimate the neutron flux variation within a VFU and using this information, flux profile can be generated from cell average flux. In this paper methodology to estimate the flux profile (similar to TIP generated profile) along the VFU has been presented. Also compression has been made with observations.

2. Analysis

Deterministic codes used for core simulation are based on neutron diffusion theory and uses homogenous few energy group cross-sections of the lattice (cell). However, lattice in the core is heterogeneous as shown in figure-1. The reactivity devises and flux units in the rector passes through moderator regions. The effect of these devices is taken care in core simulations by adding the incremental cross-section to the homogenous lattice cross sections. There will be flux variation along the flux unit within a lattice (cell). The flux within lattice cell is estimated by Monte-Carlo method based code and is used to get the flux profile, from the cell average flux, along the length of VFUs.

For estimation of flux variation along the flux unit, 37 element fuel bundle lattice with VFU located in the moderator is simulated and shown in figure-1.

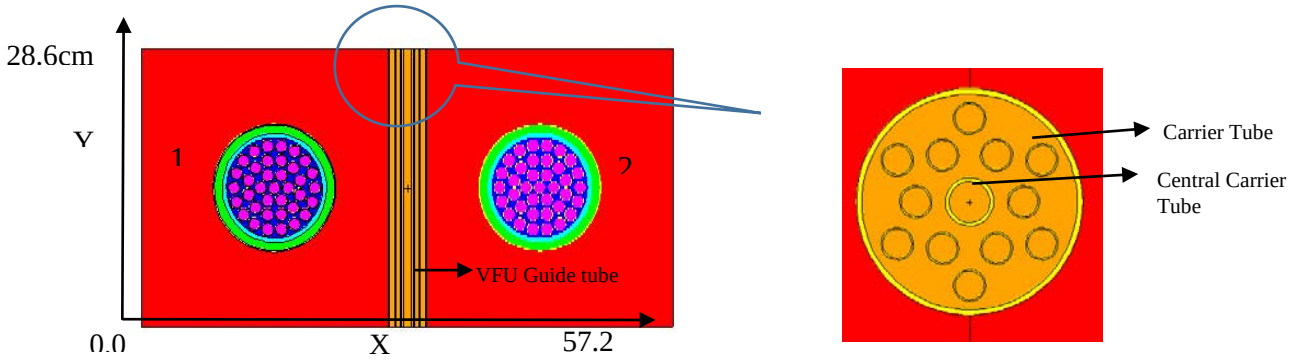


Figure-1: Simulated lattice with VFU

In the initial core, NU and DDU fuel bundles are loaded in the core (4456 NU and 248 DDU bundles) to achieve the full reactor power with flux flattening. Due to this, there could be different fuel types present in either side of VFU i.e. 1 and 2 number lattice could be either both NU or DDU or one could be NU and one DDU. There could be scenario when reactivity devices can be present near the flux units. All such scenarios were simulated and flux profile in central carrier tube (CCT) along the Y-axis is estimated with respect to cell (lattice) average thermal flux [1]. Typical variation of flux along the CCT relative to cell average flux is shown in figure-2.

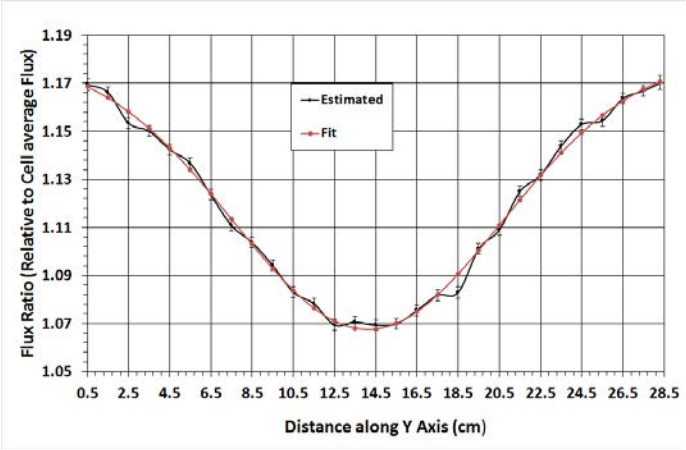


Figure-2 Flux profile along CCT for NU lattice

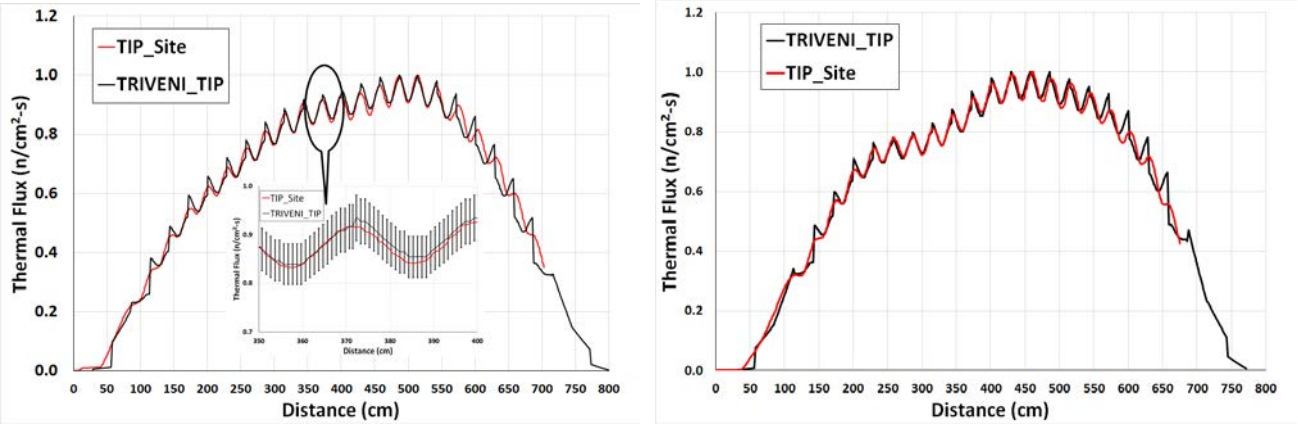
It can be noted from figure-2 that the flux is minimum at the cell center plane and it increases towards the cell boundary. Volume (of CCT) averaged thermal flux over 28.6cm long CCT is 1.12 times of the cell averaged thermal flux. Thermal flux near the boundary of the lattice along CCT is about 1.17 times of cell average thermal flux. Thermal flux at the center of CCT is about 1.07 times of cell average thermal flux.

2.1 Core Simulation

As part of Phase-B low power physics experiments, neutron flux distribution inside the core has been measured for different core configurations using Traveling In-core probe (TIP). To compare the measured flux with the estimation by diffusion theory code TRIVENI [2], core simulations have been

carried out in nominal core configuration and few off-nominal configuration using TRIVENI code. TRIVENI uses two group homogeneous cross-section generated using CLUB [3] code which uses ENDF-6.8 69 group nuclear data library. Variation of the flux profile along the flux units is generated using the TRIVENI estimated flux and flux profile along the CCT in a lattice.

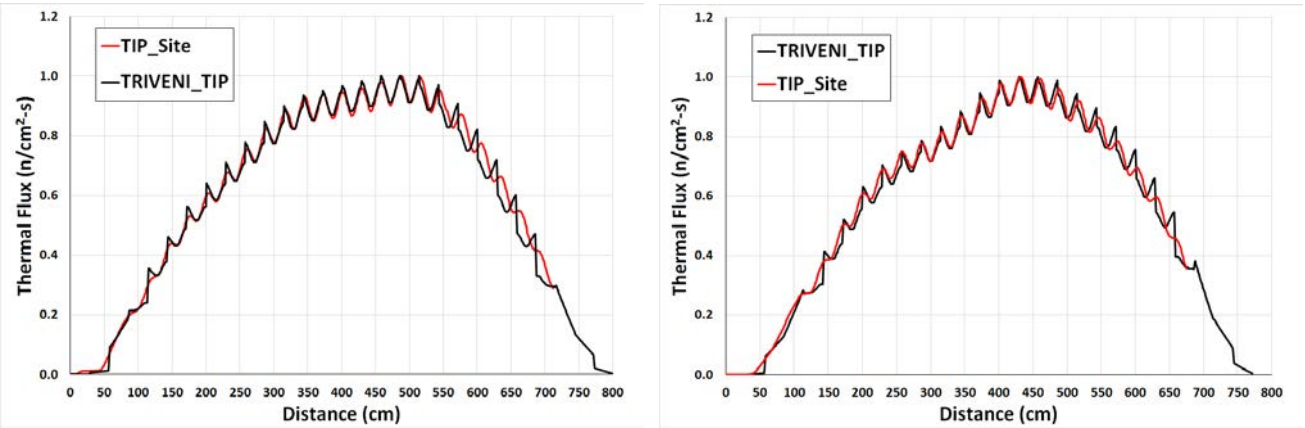
These flux profiles are given in figure-3 to figure-5. In figure-3 observed and estimated normalized thermal flux profile along the VFU-2 and VFU-19 is shown for nominal configuration (All ARs 100 % IN, CRs 100% OUT, AVZL 44%FL)



(a) (b)

Figure-3 Variation of normalized thermal flux along a) VFU-2 b) VFU-19 for nominal configuration

Figure-4 shows the observed and estimated normalized thermal flux profile along the VFU-2 and VFU-19 for all ARs OUT and AVZL at 44%FL.



(a) (b)

Figure-4 Variation of normalized thermal flux along a) VFU-2 b) VFU-19 for all ARs OUT and AVZL at 44%FL

Though ARs are always inside the core, but due to some reason they can be taken out in sequence. There could be case when AR bank can be in partially IN position which is very rare and practically eliminated by administrative control. ARs in partially IN configuration may create asymmetry in the flux. TIP measurement was carried out with different ARs in partially IN configuration. In figure-5

observed and estimated normalized thermal flux profile along the VFU-2 and VFU-19 is shown for AR bank-6 (AR-7 50%IN and AR-1 50%IN) partially IN configuration.

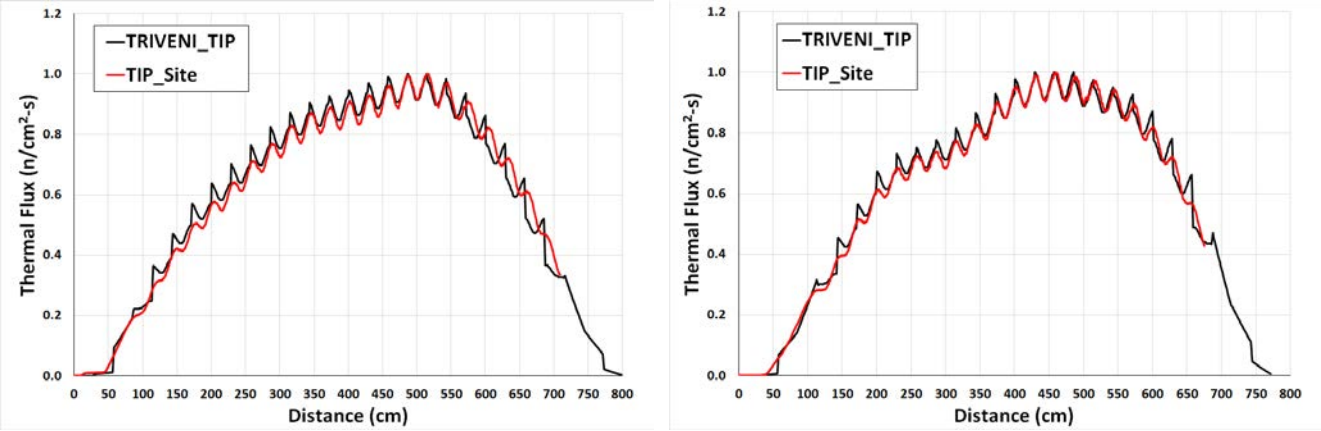


Figure-5 Variation of normalized thermal flux along a) VFU-2 b) VFU-19 for AR bank-6 partially IN

Estimated flux profiles along the CCT of VFUs are closely matching with observations. However, at the end of CCT there is a slight deviation in estimation and observation. This could be due to the error in distance recorded by TIP.

3. Conclusion

Simulation is carried out for different lattices such as NU, DU, DU+NU, with AR, with ZCCs to find the thermal flux profile along the CCT under different conditions. From the result it can be seen that there will be a dip in thermal flux in the CCT at central plane of lattice. Along the CCT in a cell, thermal flux is maximum near the boundary of a lattice. Thermal neutron flux profile in the CCT of VFU in the core peripheral region is also generated, to see the effect of neutron leakage from the core peripheral region on flux profile in CCT. These variations in flux profiles are used with TRIVENI generated cell average thermal fluxes to obtain flux profiles along CCT. The fluxes estimated by TRIVENI are matching well with measured fluxes. This approach of generating flux profile along CCT can be used to estimate the SPNDs flux installed in different CTs of same flux units. Also these comparisons give a confidence that bundle powers estimated by TRIVENI are quite accurate.

4. References

[1] Gaurav Agarwal, “Design calculation on estimation of thermal neutron flux variation along VFUs”, *700MWe/DC/01100/00018*.

[2] Surendra Mishra, “Manual on TRIVENI 700 a Fuel management computer code”, NPCIL/700MWE/RP&S/Report/DocumentType/2019/0001.

Start up source calculation for Tarapur BWR using monte-carlo methods

Pradeep Baraila[1], Rashmi Rai, A.K. Singh, K.P. Singh
Bhabha Atomic Research Centre, Mumbai, India
[1]*e-mail: - baraila@barc.gov.in*

Abstract

Present paper pertains to the start up source calculation for 160 MWe Tarapur Boiling Water Reactor (BWR) unit-1 cycle-27. External neutron sources of given source strengths are placed at specified geometric locations in the reactor core and counts at given source range monitor (SRM) locations are evaluated using monte-carlo methods. The paper describes the simulation of reactor core geometry and evaluation of detector counts using monte-carlo methods.

1. Introduction

The external neutron source being used in Tarapur BWR unit at the time of reactor start up is the Antimony-Beryllium (Sb-Be) photo-neutron source. Radioactive isotope of Antimony (Sb-124) emits gamma photon (1691 keV and 2091 keV) that interacts with Beryllium to produce photo neutrons. The objective of this analysis is to look for adequate external neutron source strength to predict proper neutron flux values at given SRM locations. Fission counting chambers are used as SRMs

2. Geometry

Table-1 provides the overall geometry details of the reactor core and individual core elements. Light water serves as coolant as well as moderator for the core. For radial and axial reflector, light water is used with thickness being equal to one or two assembly pitch. Reload-2 fresh fuel assembly is a 6X6 pin cluster arranged in a square lattice as shown in fig-1. Fresh fuel assembly contains fuel pins of different enrichments. Two fuel pins also contain 1.5 wt% Gd_2O_3 as burnable absorber. Fig-1 depicts the square lattice arrangement and enrichment of fuel pins in a fresh reload-2 fuel assembly. For a burnt fuel assembly, though the enrichment of different pins is different in general and different burnt assemblies would have undergone different burn-up, here we have assumed a constant average burn-up for each burnt assembly and accordingly the enrichment of each fuel pin has been assigned. Therefore, enrichment of each fuel pin of burnt assembly is assumed to be same and same assembly has been put wherever the burnt fuel is required. The average burn-up of each burnt fuel assembly is assumed to be 12.5 GWd/t. Control rod (CR) geometry is shown in fig-3. There are two types of water gaps between the fuel assemblies; one is called wide water gap and the other as narrow water gap. The cruciform control rod is placed in the wide water gap between the fuel assemblies as shown in fig-3. In the simulation of control rods, a solid stainless steel structure having cylindrical holes of dimensions fitting the dimension of the B_4C (absorber) rods, has been assumed. Each arm of cruciform control rod contains 17 absorber pins. Pin dimensions and the dimensions of control rod arms are given in table-1. In actual reactor core, B_4C pins used in the control rod arms are fresh as well as depleted. In our calculation, all pins are assumed to have same Boron-10 enrichment. It is assumed that all B_4C pins have undergone a same average depletion. Therefore, average Boron-

10 enrichment in a single pin has been taken to be same. The external neutron source is an antimony-beryllium photo-neutron source.

Source dimensions are tabulated in table-1. The source geometry is shown in fig-4. Beryllium cylinder surrounds antimony cylinder which is contained in a steel tube. Emitted gamma radiation from antimony interacts with beryllium to produce source neutrons. Various locations in the reactor core are specified to put neutron sources. There are five such locations in the core. To measure the neutron flux, three SRM locations are also specified. In our calculation, the source strength of a single neutron source is assumed to be 272 ci/sec which corresponds to $3.1x10^8$ neutrons per second. The x-y view of the core map showing schematic geometry locations of external neutron sources and SRM is given in fig-2 below.

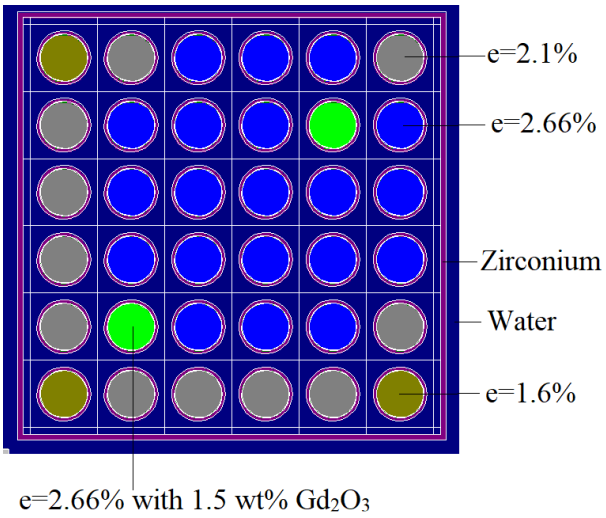


Fig-1 Reload-2 fresh fuel assembly

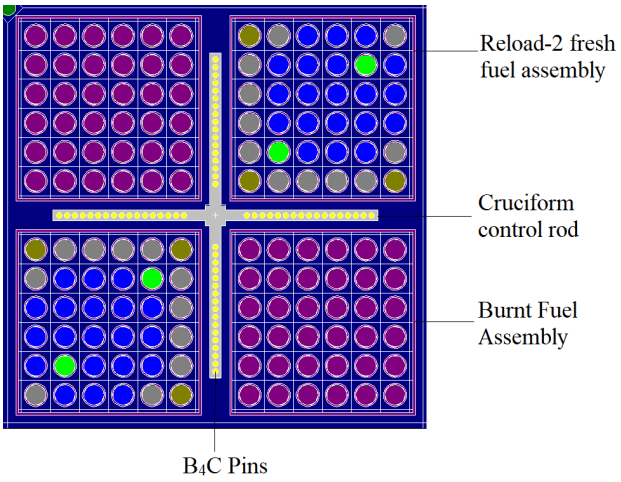


Fig-3 Cruciform control rod

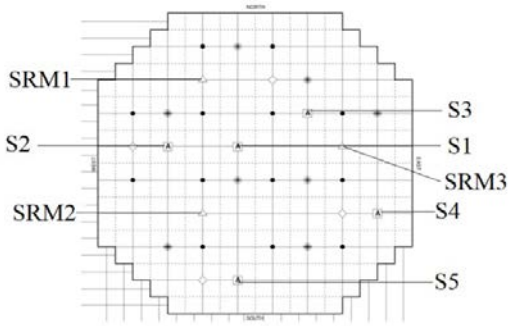


Fig-2 neutron source and SRM locations

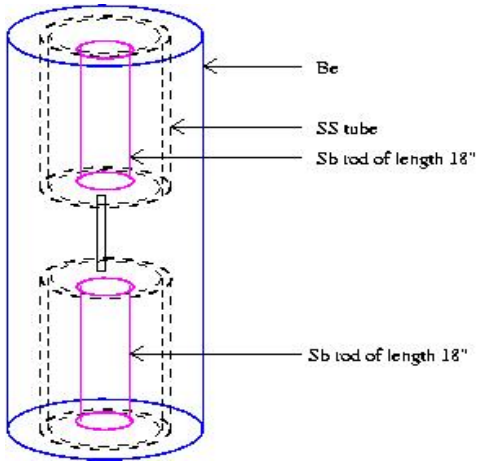


Fig-4 Sb-Be source geometry

3. Results and conclusion

The geometry of the reactor core is simulated using combinatorial geometry methods used in monte-carlo techniques. External neutron sources with prescribed geometry and prescribed locations in the core are simulated. Provided SRM locations are also simulated. We are interested in the detector counts when all CRs are fully IN. A fixed number of source particles

(10^7 particles) are transported with proper accounting of the neutron multiplication. A neutron is transported until it is leaked out of the reactor core or is absorbed by fuel or any other absorbing material. If a neutron is absorbed in the fuel material and it causes fission, the number of neutrons emitted in fission is also taken into account for tally estimation. For estimation of tallies at SRM locations, volume averaged cell flux tallies are given. The results of the analysis are given in table-2. S1, S2, S3, S4 and S5 are external neutron sources. The sensitivity of each SRM is 10^{-4} counts per second per unit neutron flux. At the time of first approach to criticality, when all control rods are IN, each SRM reading should at least be 3 counts per second (CPS); accordingly the required number of sources or source strength is decided. It is seen from table-4 that if two or more than two neutron sources with proper locations are used in the core, each SRM reading is above 3 CPS.

Table-1: Lattice and core data of TAPS-BWR unit-1 cycle-27

Parameter	Unit	Value
Enrichment of fuel	%	3 pins(1.6) 11pins (2.1) 20 pins (2.66) 2 pins (2.66 with 1.5 w/o Gd_2O_3)
Number of fuel pins in a fuel assembly		36 rods (6x6)
Pin pitch	cm	1.78054
Radius of fuel pellet	cm	0.61976
Inner radius of Zirconium cladding	cm	0.63373
Outer radius of Zr cladding	cm	0.71501
Assembly pitch	cm	12.7
Density of fuel (g/cc)		9.64522 (7 pins –corner/edge) 9.8558 (27 pins) 9.59477 (2 Gd pins)
Channel outer dimension	cm	11.35124
Channel thickness	cm	0.1524
Inner H_2O thickness	cm	0.1816
Wide water gap in fuel assembly	cm	0.8712
Narrow water gap in fuel assembly	cm	0.476
Assembly lattice pitch	cm	12.7
Saturated coolant density	g/cc	1.0
Active core radius	cm	131.0
Active core height	cm	365.8
B_4C tube radius	cm	0.17145
SS arm length	cm	9.95680
Sb pin length each	cm	45.72
Sb pin radius each	cm	0.35052

Air gap between SS tube and Sb pin	cm	0.0127
SS tube length each	cm	53.975
SS tube inner radius	cm	0.36322
SS tube outer radius	cm	0.40894
Be sleeve radius	cm	0.46482

Table-2: Results of analysis with different number of source

Number of sources	Counts per second (CPS) in SRMs		
	SRM1	SRM2	SRM3
1(S1)	5.0±0.44%	5.1±0.44%	2.3±0.65%
2(S1,S2)	10.0±0.44%	10.2±0.44%	2.7±0.85%
2(S1,S3)	7.0 ± 0.55%	5.8 ± 0.58%	15.0 ± 0.36%
2(S1,S4)	5.1 ± 0.61%	5.4 ± 0.60%	6.8 ± 0.53%
2(S1,S5)	5.1 ± 0.61%	10.0 ± 0.44%	2.6 ± 0.86%
2(S2,S3)	6.8 ± 0.53%	5.7 ± 0.59%	13.0 ± 0.39%
2(S2,S4)	4.9 ± 0.63%	5.4 ± 0.61%	4.9 ± 0.63%
2(S2,S5)	5.0 ± 0.62%	9.9 ± 0.45%	0.6 ± 1.72%
2(S3,S4)	2.0 ± 0.98%	1.0 ± 1.39%	17.0 ± 0.34%
2(S3,S5)	2.0 ± 0.97%	5.6 ± 0.59%	13.0 ± 0.39%
2(S4,S5)	0.1 ± 3.08%	5.2 ± 0.62%	4.8 ± 0.63%
3(S1,S2,S3)	11.9 ± 0.49%	10.8 ± 0.52%	15.4 ± 0.44%
3(S2,S3,S5)	7.1 ± 0.64%	10.7 ± 0.53%	15.2 ± 0.44%
3(S1,S3,S5)	7.0 ± 0.65%	10.6 ± 0.53%	13.2 ± 0.47%
4(S1,S2,S3,S4)	11.9 ± 0.57%	11.2 ± 0.59%	19.9 ± 0.44%
5(S1,S2,S3,S4,S5)	12.1 ± 0.63%	16.2 ± 0.55%	20.1 ± 0.49%

4. References

[1] Amandeep Singh, Soumen Koner, Dr. V. Jagannathan and Obaidurrahaman K., **"**Independent Analysis of TAPS BWR core using VISWAM code", *AERB/NSARG/TR/2019*

[2] Indrajeet Singh, Rashmi Rai, Pradeep Baraila, Anurag Gupta, K.P. Singh and Umasankari Kannan, "Development of monte carlo model of TARAPUR Boiling Water Reactor for K-eff calculations," *Report No: RPDD/GE/48/Sep-2021*

[3] Private communication with TAPS personals, "operational sources installed in the Tarapur Reactor"

COMPOSITE LOG-LINEAR AMPLIFIER FOR FULL POWER RANGE OPERATION OF NUCLEAR REACTORS

A. Shivam Tripathi[1], B. DM Nikhare, C. SP Borkar and D. Sadhana Bhattacharya
Bhabha Atomic Research Centre, Mumbai, India
[1]*e-mail: - shivamt@barc.gov.in*

Abstract

The control and monitoring of a nuclear reactor in current mode is done over a wide range of current inputs based on neutron flux levels. Conventionally this wide range of current input is required to be measured in log scale. A linear amplifier is additionally utilized over the last decade to allow precise control of power fluctuations in operating regions. . The paper describes the philosophy of the design, implementation and test results of a new composite log linear amplifier with 7 overlapping linear and 1 composite log power signal developed using current gain based log antilog approach.

1. INTRODUCTION

The output current from radiation detectors in the current mode of operation [1] can vary upto 7 decades or more based on neutron flux and current sensitivity of the detectors. Traditionally the input current from these detectors is measured in log scale for all decades of current inputs [2]. Since 7 decades of input current signal is compressed into 1 log power output, significant changes in power will result in only small changes in signal from the log amplifier. Using log scale for measurement of 7 decades of current input has disadvantages like low accuracies, low resolution and temperature sensitivity in power measurement. To overcome the limitation faced with log scale measurement, linear amplifier is utilized over the highest decades of current input to allow more precise and better control of power fluctuations [3]. However using a conventional approach of measuring voltage (produced due to detector current) across a series resistance can be used at most for 3-4 decades of large current input as gains become unfeasible due to instability of amplifiers and background noise.

A new scheme namely Log Antilog technique for processing upto 7 decades of detector current input (from 100 pA to 1 mA), generating 7 overlapping linear power signals and a consolidated log power signal using quad matched transistors has been discussed. The scheme also eliminates the need of high value resistors and reed relays which are used in conventional multidecade linear amplifiers thereby improving noise immunity of the system.

2. Design of log antilog amplifier using opamp and matched transistors

Traditional transistor based log antilog circuit is shown in figure 1:

Input current flows through transistor Qa and logarithmic voltage is generated at the emitter.

$V_{EB\text{-}Qa} = Vlog = -2.3\ (kT/q) \log \frac{I}{Io1}$ (where I_{o1} is emitter saturation current for transistor Qa) (1)

The current flowing through transistor Qb is given by:

$I_c = I_{o2} * 10^{(q/2.3kT) * V_{BE\text{-}Qb}}$ (where I_{o2} is emitter saturation current for transistor Qb) (2)

Since $V_{BE\text{-}Qb} = - Vlog$ & if Qa and Qb are matched transistors then $I_{o1} = I_{o2} = I_o$

$I_c = I_o * 10^{(q/2.3kT) * 2.3\ (kT/q) \log \frac{I}{Io}}$ (3)

Thus $I_c = I$ & $V_{antilog} = I*R$ (4)

It is extremely critical the opamp used for the log amplifier has ultra-low bias current (of the order of 15fA) to achieve good accuracy for low current inputs.

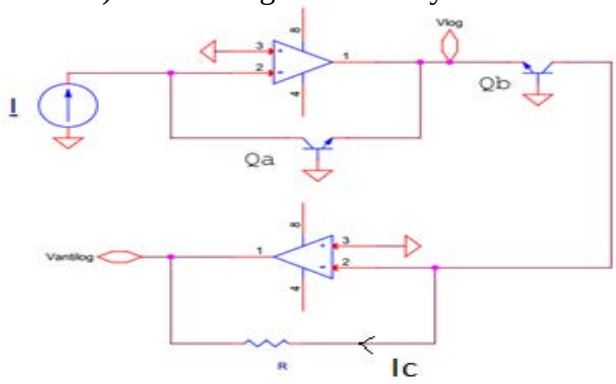


Figure 1 Traditional log antilog circuit using opamp and matched transistor pair

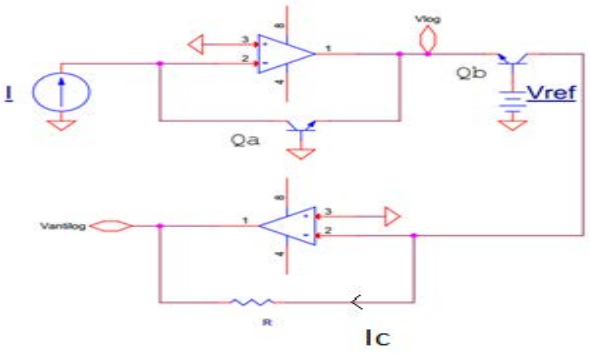


Figure 2 Log antilog circuit using opamp and matched transistor pair with current gain

In this log-antilog circuit, the base of the antilog transistor Qb was grounded hence the current flowing through the antilog transistor was same as the input current. If the base voltage of the antilog transistor is raised to a voltage level current flowing through the antilog transistor can be increased. This technique is shown in figure 2. The base of the antilog transistor Qb is biased at voltage Vref. The output of the log transistor is still given by-

From (1): $V_{EB\text{-}Qa} = Vlog = -2.3\ (kT/q) \log \frac{I}{Io}$ (5)

From (2): $I_c = I_o * 10^{(q/2.3kT) *(Vref - Vlog)}$ (Since $V_{BE\text{-}Qb} = Vref - Vlog$) (6)

From (3): $I_c = I * 10^{(q/2.3kT) *Vref}$ (7)

$I_c = I * 10^m$ & $V_{antilog} = R* I * 10$ (where Vref = m* 2.3(kT/q)) (8)

Thus, a current gain (of 10^m) can be achieved by biasing the base of the antilog transistor. This ensures that even for very low values of current 'I' relatively small resistances values (less than 100kohm) are sufficient for getting measurable voltage output. Hence high stability, highly accurate and ultra-low temperature coefficient resistances can be used for this purpose.

Since Vref = m*2.3KT/q and as KT/q is temperature dependent phenomenon, the reference voltage should also be temperature dependent. For achieving this, the temperature compensated reference voltage circuit is used as shown in Figure 3. Currents I_1 and I_2 flow through transistors Qc and Qd respectively (I_{o3} & I_{o4} are the emitter saturation current for transistor Qc & Qd respectively)

From (1): Voltage at emitter of Qc i.e. $V_{E\text{-}QC} = -2.3\ (kT/q) \log \frac{I1}{Io3}$ (9)

Since $V_{BE\text{-}QC} = V_{B\text{-}QD} - V_{E\text{-}QD} = V_{B\text{-}QD} - V_{E\text{-}QC}$ & if Qc and Qd are matched transistors $I_{o3} = I_{o4}$

From (7): $I_2 = I_1 * (10^{(q/2.3kT) *V_{B\text{-}Qd}})$ (10)

$\log (I_2 / I_1) = (q/2.3kT) * V_{B\text{-}Qd}$ (11)

Since $I_2 = 10i_1$ (as resistance values are chosen as R and 10R)

$V_{B\text{-}Qd} = 2.3(kT/q)$ (12)

Hence a temperature dependent voltage is developed at the base of Qd. This is scaled using R5 and R6 to get reference voltage Vref given by:

Vref = (1 + R5/R6) * 2.3(kT/q) (13)

Thus, a temperature dependent voltage Vref can be generated using two matched transistors. If these two matched transistors have same temperatures as that of log-antilog matched pair

transistors (in case of quad matched transistors), the antilog log output will have a current gain of 10^m and will be independent of temperature.

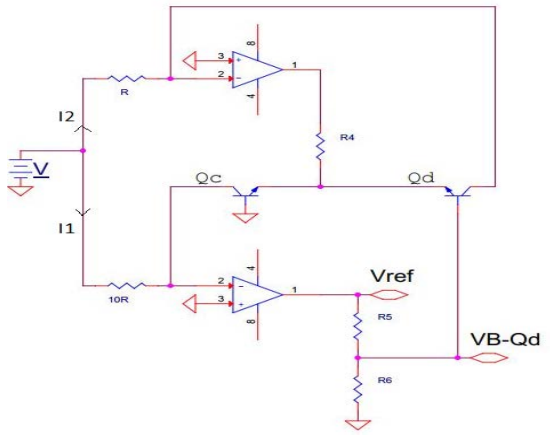


Figure 3 Temperature compensated reference voltage generation circuit

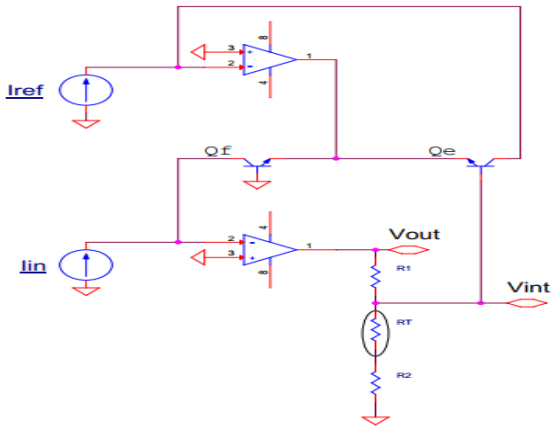


Figure 4 Thermal compensated log amplifier

The design of thermal compensated log amplifier using a matched pair transistor and sensistor (+ve temperature coefficient resistor) is given in [4]. The log amplifier circuit is shown in Figure 4. The output of the log amplifier is given by [4] -

$$V_{out} = -(1+\frac{R1}{R2+RT})* 2.3\,(kT/q) *(\log \frac{Iin}{Iref}) \quad \text{where } R_T \text{ is the sensistor} \qquad (14)$$

Hence with a matched transistor pair and a sensistor thermal compensated log power signal can be generated. It is extremely critical the opamp used for the log amplifier has ultra-low bias current (of the order of 15fA) to achieve good accuracy for low current inputs.

3. Design of 7 decade Composite Log Linear Amplifier using Quad matched transistor

From figures 2, 3 and 4 it can be noted that computing a thermal compensated log output requires 2 matched transistors, while computing log antilog output with a current gain requires 4 matched transistors. Octa-matched transistors though commercially available are very rare and expensive.
A composite log and linear amplifier based on current gain log antilog circuitry has been developed using a quad matched transistor. The scheme is shown in Figure 5.
The amplifier uses a novel design approach of using one common transistor for thermal compensation (of log output) and Vref (biasing voltage for base of antilog amplifier) generation. This allows the thermal compensated log output and current gain antilog output to be accommodated in a quad matched transistor configuration. One transistor (Q1) is used for log generation, one for antilog generation (Q4) and other two for base reference voltage generation (Q2, Q3) as well as thermal compensation of log output (Q2).
The log output generated from detector and reference current is fed through an instrumentation amplifier (INA) and passed through a gain stage involving sensistor R_T for thermal compensation. The voltage produced across series resistance 'Rseries' is fed to another INA and passed through amplification stage to provide 3 overlapping linear power output signals (N5-N7).
The base of antilog transistor Q4 is biased at 3*2.3kT/q (i.e. m=3) to get current gain of 10^3. The current gain based antilog voltage output across the resistor 'Rantilog' is passed through amplification stage to provide 4 overlapping linear power output signals (N1-N4). Since high

voltage gains (of 1000) is provided it is extremely critical that opamps used for gain and offset adjustment have ultra-low offset voltages (of the order 1uV) to have good output accuracy.

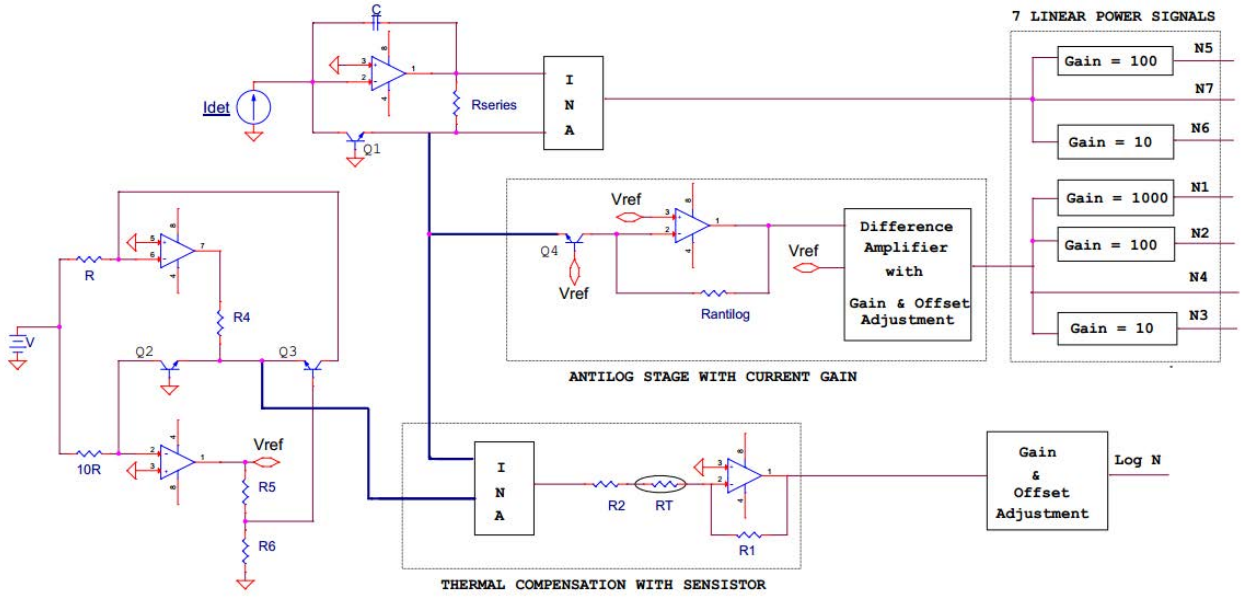


Figure 5 Scheme for composite log linear amplifier with quad matched transistor

4. Validation of Composite Log Linear Amplifier

Log and 7 Linear output signals of this composite Log- Linear amplifier for input currents from 100pA to 1mA are given in Table 1.

Table 1 Log & 7 Linear outputs for 7 decades of input current from 100pA to 1mA

Current	Log N	N1	N2	N3	N4	N5	N6	N7
100 pA	0.00	1.01	0.102	0.01	0.001	0.001	0.001	0.001
1 nA	1.43	10.04	1.005	0.102	0.017	0.001	0.001	0.001
10 nA	2.86	>13	10.00	1.01	0.107	0.01	0.001	0.001
100 nA	4.28	>13	>13	9.99	1.008	0.100	0.011	0.001
1 uA	5.72	>13	>13	>13	10.00	1.00	0.101	0.011
10 uA	7.14	>13	>13	>13	>13	9.99	1.00	0.101
100 uA	8.57	>13	>13	>13	>13	>13	9.99	1.00
1 mA	10	>13	>13	>13	>13	>13	>13	9.99

From Table 1, figure 6 and figure 7 it can be observed that for all 7-linear power and 1 log power signals error observed was less than 1% for entire 7 decades of current input (100 pA- 1mA). Also there is adequate overlap is available for consecutive linear power signals. Eg. When N5 is 1V, N4 is 10V and N6 shows 0.1V. This ensures continuity in linear power outputs.

Figure 8 shows pictures of a composite Log- Linear amplifier producing 7 overlapping linear power signals and 1 composite log power signal developed for GCIC signal conditioning.

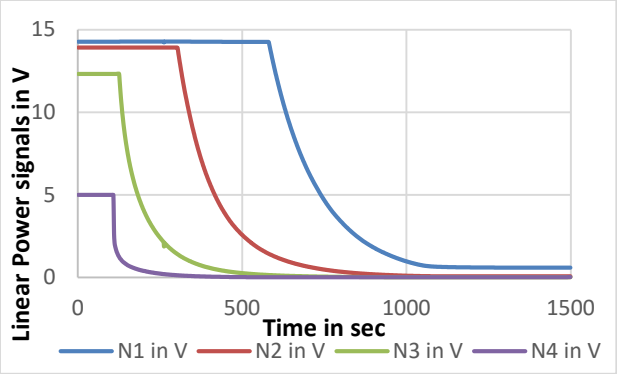


Figure 6 Current: 500 nA to 100 pA

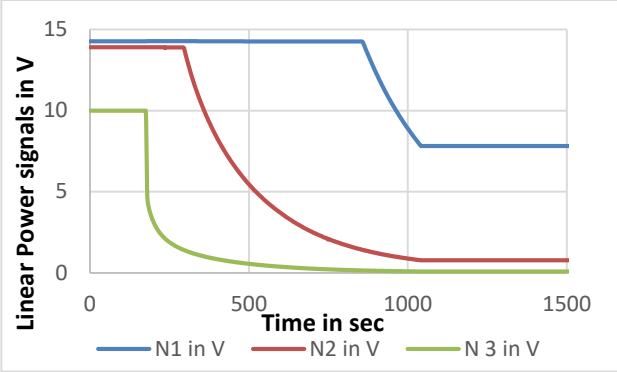


Figure 7 Current: 100 nA to 780 pA

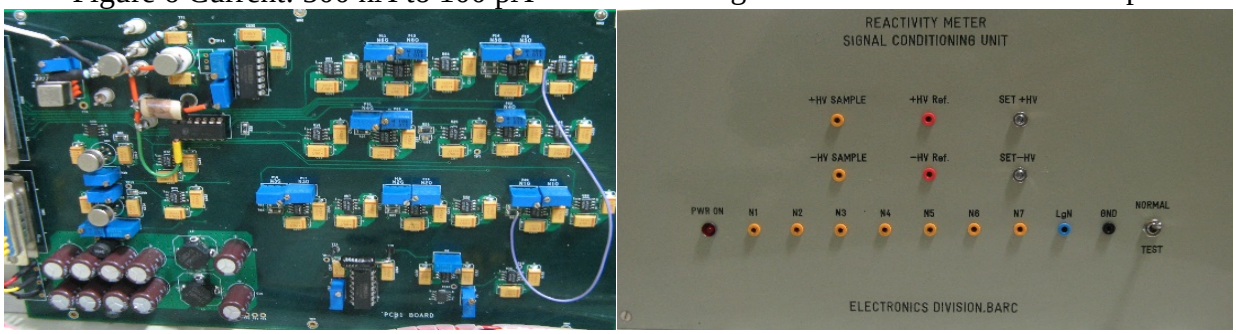


Figure 8 PCB & Facia of composite Log-Linear amplifier for processing 7 decades of current

5. Conclusion

The design of composite Log-Lin Amplifier with 7 overlapping linear power signals along with a consolidated log power signal using one quad matched transistor has been developed and tested. The availability of these linear power signals provides precise control of power in higher power range for even small changes in reactor power which is not possible with log power signal. The linear power output signals are immune to drifts due to variations in ambient temperature. The availability of overlap between consecutive linear power signals ensures continuity in reactor power output which is essential for computation of parameters like reactivity and reactor period (derived from reactor power signals). The implementation of the scheme will be used in Reactor Instrumentation in future generation or upcoming reactors.

6. Acknowledgement

I gratefully thank Shri PV Bhatnagar and wiring team for their contributions in development, wiring and testing of composite Log-Linear amplifier module.

7. References

[1] G. F. Knoll, Radiation Detection and Measurement. New York: Wiley, 4th edition, p. 107
[2] Ferrarini, M., et al. "A wide dynamic range BF3 neutron monitor with front-end electronics based on a logarithmic amplifier." Nuclear Instruments and Methods in Physics Research Section A: Accelerators, Spectrometers, Detectors and Associated Equipment 613.2 (2010): 272-276.
[3] Westinghouse Technology Systems Manual Section 9.1 Excore Nuclear Instrumentation
[4] Texas Instruments LOG101 Datasheet

XENON POISON MEASUREMENT IN APSARA-U INTERMEDIATE CORE

Shantanab Banerjee[1], Paritosh Pandey[1] and Tej Singh[1]
[1] Bhabha Atomic Research Centre, Mumbai, India
[1]*e-mail: - t_singh@barc.gov.in*

Abstract

Xenon poisoning is an important aspect of thermal reactor operation due to its reactivity implication. In Apsara-U reactor, that was commissioned in September, 2018 the effect of xenon-135 poisoning was studied for the 1.8 MW Intermediate core. This paper discusses the experiment carried out to obtain the xenon coefficients usefulness of which is in routine reactor operation.

1. Introduction

Apsara-U reactor is 2 MW thermal, swimming pool type reactor [1]. The intermediate core configuration of the same consists of 10 Standard Fuel Assemblies (SFAs), 4 Control Fuel Assemblies (CFAs), one dummy fuel assembly at core position E-6 and a Hollow Aluminium Plug (HAP) at core position D-5 (Figure 1) which was operated at maximum power of 1.8 MW. At this power level, flux in the fuel assemblies is > 10^{13} n/cm2/sec. This will cause buildup of Xe-135 poison. To aid day to day reactor operation, experiment was conducted to obtain the xenon parameters as discussed below.

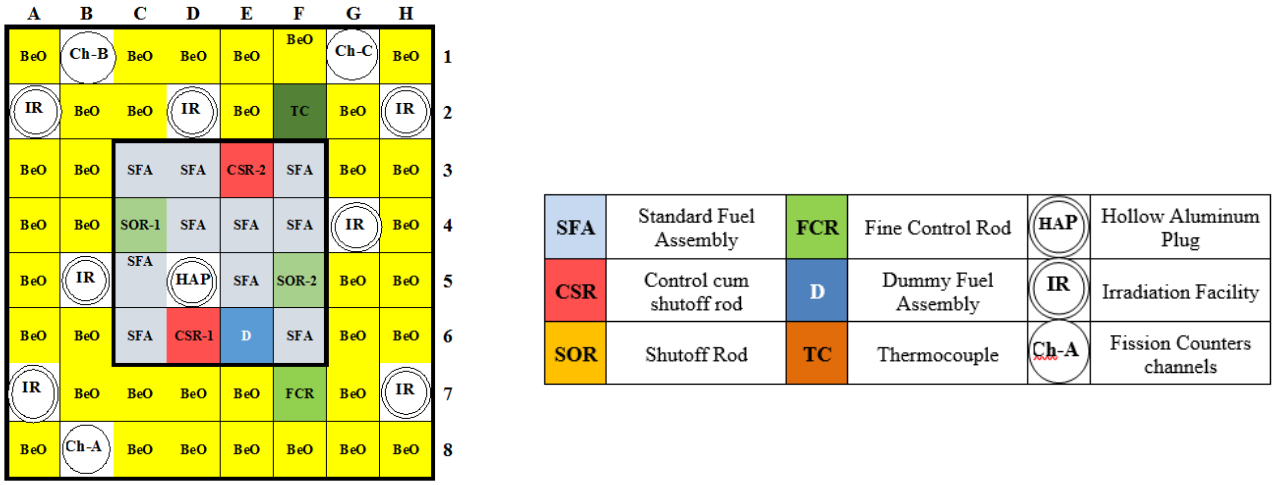


Figure 1: Core configuration of Apsara-U with intermediate core

2. Parameters regarding variation of Xenon

In nuclear reactor, Xenon-135 is produced from β-decay of Tellurium-135, which is a fission product. Reaction leading to the production and subsequent decay of Xenon-135 are as follows:

$$Te^{135} \xrightarrow{T_{1/2}<1\text{minutes}} I^{135} \xrightarrow{T_{1/2}\approx 6.7 hours} Xe^{135} \xrightarrow{T_{1/2}\approx 9.2 hours} Cs^{135} \xrightarrow{T_{1/2}\approx 2\times 10^{6} years} Ba^{135}(stable)$$

$$\downarrow \sigma_c$$

$$Xe^{136}(stable)$$

governing equations: $\frac{dI(t)}{dt} = \frac{aW}{n} - \frac{I(t)}{T_1}$ and $\frac{dX(t)}{dt} = \frac{I(t)}{T_1} - \left(\frac{X(t)}{T_0} + \frac{AW}{n}X(t)\right)$

I(t) = Concentration of Iodine-135 at time "t" in potential milli-k (mk) units
X(t) = Xenon-135 concentration at time "t" in mk

a = Iodine production coefficient
A = Xenon power destruction coefficient
W = Reactor power
T_0 = Mean life of Xenon-135, 13.28 Hrs.
T_1 = Mean life of Iodine-135, 9.66 Hrs.
n = No. of equivalent Standard Fuel Assemblies in core

These two equations can be solved for concentration of Iodine-135 and Xenon-135 at any time t:

$$I(t) = I_i\, e^{-\frac{t}{T_1}} + \frac{aWT_1}{n}\left(1 - e^{-\frac{t}{T_1}}\right) \tag{1}$$

$$X(t) = X_i\, \mathrm{e}^{-\left(\frac{1}{T_0}+\frac{AW}{n}\right)t} + \frac{\frac{aW}{n}}{\frac{1}{T_0}+\frac{AW}{n}}\left(1 - \mathrm{e}^{-\left(\frac{1}{T_0}+\frac{AW}{n}\right)t}\right) + \frac{\frac{I_i}{T_1} - \frac{aW}{n}}{\frac{1}{T_0} - \frac{1}{T_1} + \frac{AW}{n}}\left\{e^{-\frac{t}{T_1}} - \mathrm{e}^{-\left(\frac{1}{T_0}+\frac{AW}{n}\right)t}\right\} \tag{2}$$

Here, X_i and I_i represents the value of Xe-135 and I-135 corresponding to time t=0.
It can also be seen that the equilibrium concentration of Xe-135 (X_E) and I-135 (I_E) are given by:

$$X_E = \frac{\frac{aW}{n}}{\frac{1}{T_0}+\frac{AW}{n}} \quad , \; I_E = \frac{aWT_1}{n} \tag{3}$$

Now, a and A are reactor specific constants which can be calculated if reactivity loads of Xe-135 at multiple power levels are known. Note that Eq-5 above can be written as:

$$\frac{1}{X_E} = \left(\frac{n}{aT_0}\right)\frac{1}{W} + \frac{A}{a} \tag{4}$$

So, the variables $\frac{1}{X_E}$ and $\frac{1}{W}$ follows a linear relationship with each other, and least square fitting of the data points will yield a single slope and intercept value, which is equally valid for all operating power ranges. From Equation 4, it is clear that *a* and *A* can be derived from the slope and intercept.

3. Experimental observations

In Apsara-U, the reactor control is by two twin blade fork type hafnium blade with provision of movement in Control Fuel Assembly (CFA) namely Control cum Shout-off Rods (CSRs) and one single blade Fine Control Rod (FCR) also made of Hf. The reactivity load in the core can be gauzed by seeing the CSRs/FCR position (higher the rod position, higher the reactivity load in the core). For the experiment, reactor was operated at different power levels, and the equilibrium xenon concentration in reactivity unit was estimated by comparing the control rod positions with respect to the cold, xenon free critical height with identical core loading and fuel burnup condition, after taking into consideration the correction due to power. The reactor was made critical at cold, xenon free

condition on 16th July, 2019 at about 16:10 hrs, the critical position of control rods was noted (CSR-1/CSR-2 and FCR at 47.9/48.0 and 34.0% UP). This position is treated as reference xenon free position for future calculations. The equilibrium rod positions at different reactor power is given in Table-1.

Table-1: Observed equilibrium control rod positions at various power operation

Reactor Power (MW)		Observation approximately done on		Control Rod Position (%UP)		
Set Point	MRDC	Date	Time (hrs)	CSR-1	CSR-2	FCR
LP	0.015	16/07/2019	16:10	47.9	48.0	34.0
0.60	0.54	19/07/2019	16:00	54.2	57.4	63.1
1.00	0.90	24/07/2019	14:07	60.2	60.2	72.0
1.50	1.40	29/07/2019	11:28	64.8	64.8	59.1
1.80	1.65	31/07/2019	08:00	67.3	68.4	33.9

4. Calculation of Xenon reactivity load from observed data

The observed movement of critical control rod positions with power as mentioned in Table-1 can be used to calculate the equilibrium xenon loads at those respective power levels using the calibration curve of CSRs and FCR obtained previously (CSRs by rod drop and compensation method, while FCR by Period method). Observed movement in CSRs and FCR are mostly due to reactivity load from two sources – Xenon load and Power load. The power load is a prompt acting reactivity load which takes account of the cumulative load from the rise of reactor power, which in turn results in rise of fuel, clad and coolant temperature. The power load of Apsara-U has been measured to be around 0.5 mk/MW. Another thing to note is that although the two control rods are supposed to move as a bank, there may exist a disagreement among their position. This requires introduction of a small correction factor to account for difference in worth actually realized due to movement of the rods and the predicted worth obtained from calibration curve (which corresponds to the average control rod position. The final adjusted worth of the equilibrium xenon loads is provided at Table-2.

Intermediate core has been modelled using deterministic computer codes also. The four group space-homogenized cross-section dataset for all fuel assemblies was obtained using codes WIMS-D and TWOTRAN. The cross section data for two cases were generated for all of the aforementioned power levels: one without any xenon load (fresh fuel) and another with saturated xenon concentration (using SATURATE card option in the EDIT data section). The results of theoretically obtained and observed Xe-135 loads are compared in Table-3.

5. Estimation of Xenon Parameters

The xenon load, as obtained in the previous section at various power levels – was used to find a set of five points which lie on a straight line given by the Equation-6. The best-fit straight line through them was drawn and slope & intercept value of the same calculated. Solving for the coefficients *a* and *A*, using Equation 4 (slope=$\frac{n}{aT_0}$, intercept=$\frac{A}{a}$) and taking n=12.8 and T_0=13.28, we finally get *a*=30.9822 and *A*=0.7213. The buildup of Xe-135 with power and its variation after shutdown is calculated with these parameters (Figure 2) and it matches well with observation.

Table-2: Equilibrium xenon load at various power levels

Reactor Power (MRDC) (MW)	Control Rod Position (%UP)		Total reactivity load corresponding to rod (both CSR and FCR) position (mk)	Change in reactivity w.r.t cold, Xenon free state (mk)	Correction factors		Total Xenon load (mk)
	Average CSR	FCR			Due to CSR-2 disagreement (mk)	Correction due to power load (mk)	
0.0	47.95	34.0	46.66	-	-	-	0.0
0.54	55.8	63.1	58.68	12.01	0.62	-0.27	12.36
0.90	60.2	72.0	64.44	17.78	0.0	-0.45	17.33
1.40	64.8	59.1	69.18	22.52	0.0	-0.7	21.82
1.65	67.85	33.9	71.13	24.47	0.21	-0.83	23.86

Table-3: Comparison between theoretical (deterministic) and observed xenon loads

Reactor Power (MRDC) (MW)	Equilibrium Xenon load (mk)	
	Observed	Calculated
0.0	0.0	0.0
0.54	12.36	12.21
0.90	17.33	16.90
1.40	21.82	21.63
1.65	23.86	23.43

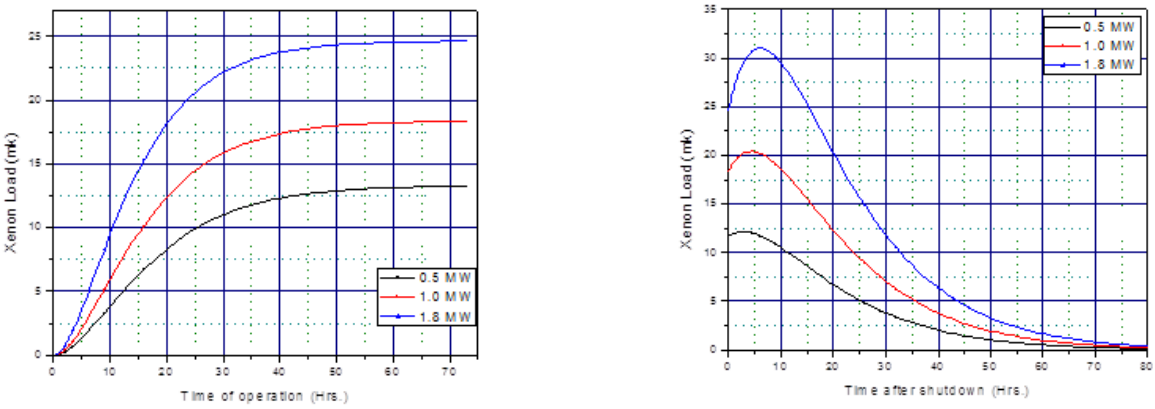


Figure 2: Xe load variation in operation and after shutdown at different power level

6. Conclusion

Experimental and theoretical estimation of xenon load at equilibrium for the intermediate core of Apsara-U has enabled us to define two xenon parameter constants which would make it possible to predict quickly the behaviour of xenon for any change in operating power level of Apsara-U.

7. References

[1] Tej Singh et al., "Physics Design of 2 MW upgraded Apsara research reactor, *Annals of Nuclear Energy*, Vol. 60, 2013, pp.141-156.